TECHNISCHE UNIVERSITÄT MÜNCHEN

Lehrstuhl für Flugsystemdynamik

Survivable Flight Control with Guaranteed Stability and Performance Characteristics

Dipl.-Ing. Christian David Heise

Vollständiger Abdruck der von der Fakultät für Maschinenwesen der Technischen Universität München zur Erlangung des akademischen Grades eines

Doktor-Ingenieurs

genehmigten Dissertation.

Vorsitzender:	Prof. Dr.-Ing. Harald Klein
Prüfer der Dissertation:	1. Prof. Dr.-Ing. Florian Holzapfel
	2. Prof. Dr.-Ing. habil. Boris Lohmann

Die Dissertation wurde am 19.01.2017 bei der Technischen Universität München eingereicht und durch die Fakultät für Maschinenwesen am 09.05.2017 angenommen.

Danksagung

Die vorliegende Arbeit wäre ohne die Unterstützung zahlreicher Personen nicht zu realisieren gewesen. Zunächst möchte ich meinem Doktorvater Prof. Dr.-Ing. Florian Holzapfel dafür danken, dass er mir die Möglichkeit zur Promotion an seinem Lehrstuhl eingeräumt und mich während der gesamten Promotionszeit stets unterstützt hat. Darüber hinaus gilt mein Dank auch den übrigen Mitgliedern der Prüfungskommission, Prof. Dr.-Ing. habil. Boris Lohmann und Prof. Dr.-Ing. Harald Klein.

Wesentlichen Anteil am Gelingen dieser Arbeit hatte mein von Munich Aerospace e.V. bewilligtes Stipendium. Dieses Stipendium gab mir den Freiraum, mich auf die Forschung und das Verfassen dieser Dissertation zu konzentrieren. Die unkomplizierte und unbürokratische Zusammenarbeit mit den Mitarbeiterinnen der Geschäftsführung von Munich Aerospace e.V. verdient dabei besondere Erwähnung.

Des Weiteren möchte ich mich bei den Mitarbeitern und Mitarbeiterinnen des Lehrstuhls für Flugsystemdynamik für das überaus angenehme Umfeld und die konstruktive Zusammenarbeit bedanken. Besonders hervorzuheben sind dabei Guillermo Falconí, Miguel Leitão, Maximilian Mühlegg und Simon Schatz sowie meine Kollegen aus dem Gute-Laune-Büro Nils Mumm, Volker Schneider und David Tromba. Unsere unzähligen spannenden Diskussionen und gemeinsam verfolgten Projekte haben immer wieder zu neuen Fragen und Ideen geführt, die diese Arbeit entscheidend bereichert haben.

Mein zutiefst empfundener Dank gilt meinen Eltern, Viola und Norbert, die mich während meiner gesamten Promotionszeit immer in meinem Vorhaben bestärkt haben und mir geholfen haben, auch die schwierigen Phasen dieser Arbeit zu meistern.

Der größte Dank gebührt jedoch meiner Freundin Vicky. Ohne ihren Rückhalt, ihr Verständnis und ihre schier endlose Geduld während der vergangenen fünf Jahre wäre diese Arbeit niemals zustande gekommen.

Abstract

In modern aircraft, flight control systems fulfill diverse tasks. These tasks range from the automation of routine maneuvers to the improvement of the handling qualities of the aircraft. The development of a flight control system requires a mathematical model of the aircraft physics. In practice, the structure as well as the parameters of this model are uncertain, that is, not precisely known. In order to comply with the high safety standards of aerospace industry, flight control systems must hence exhibit high robustness with respect to these uncertainties. For this purpose, conventional flight control systems are developed in such a way that they provide satisfactory performance despite the uncertainties. More recently, alternative approaches which actively compensate the uncertainties have started to raise (renewed) interest. The active compensation of uncertainties does not only admit to exploit the physical capabilities of the aircraft, but also increases safety in critical situations caused by damages or faults. Furthermore, they reduce the effort and the associated cost of a precise identification of the model parameters.

In order to deploy a flight control system in civil aviation, it must be certified (i.e. approved) by the authorities. Among other things, certification requires guarantees that the flight control system possesses sufficient robustness and yields satisfactory performance. That is why this thesis aims at the analysis and the development of control systems which actively compensate (even large) uncertainties and exhibit guaranteed robustness and performance characteristics. In order to meet this objective, this thesis follows two different strategies.

The first strategy relies on Model Reference Adaptive Control (MRAC). Adaptive controllers adjust themselves at runtime to the plant. They are hence well suited for the control of highly uncertain systems. However, adaptive approaches intrinsically lead to nonlinear controllers. As current certification standards derive from linear system theory, adaptive controllers may therefore not be used in civil aviation. In order to resolve this issue, novel measures (metrics) are required to allow evaluating the robustness and performance of an adaptive flight control system. Two metrics, which might be of use in a future certification process, are the time-delay margin as a measure of robustness and the largest tracking error as a measure of performance. In practice, the computation of these metrics constitutes a major difficulty. For this reason, the first strategy aims at the development of novel methods for the computation of the

time-delay margin and of the largest tracking error.

For the computation of the time-delay margin, this thesis proposes a novel method which relies on a proof of stability according to Lyapunov-Razumikhin and Sum-Of-Squares optimization. To the best of the author's knowledge, it is the first method for MRAC with σ-modification which considers the tracking case and does not require a-priori known bounds on the so-called regressor vector.

Conventional approaches for the computation of the largest tracking error only yield highly conservative upper bounds. Therefore, this thesis proposes novel computational methods for MRAC (with σ-modification). Due to the use of optimization subject to Linear Matrix Inequality constraints, the conservatism of the bounds reduces by nearly one order of magnitude.

In contrast to the first strategy, the second strategy follows an opposite approach. Instead of nonlinear adaptive controllers, this approach relies on methods from linear system theory which admit certification according to existing rules and requirements. In case of the second strategy, the challenge does not consist in certification but in the development of linear control approaches which actively compensate even large uncertainties. The result of the second strategy is the Modified Linear Extended State Observer (MLESO). As opposed to a conventional Luenberger observer, this observer estimates the disturbance signal which stems from the deviation between the plant and some desired plant response. It will be proven that MLESO-based control leads to the same closed-loop performance as $\mathcal{L}_1$ Adaptive Control.

Zusammenfassung

In modernen Flugzeugen erfüllen Regelungssysteme vielfältige Aufgaben, welche von der Entlastung des Piloten von Routineaufgaben bis hin zur Verbesserung der Flugeigenschaften reichen. Grundlage für den Entwurf von Flugregelungssystemen ist ein mathematisches Modell der Flugzeugphysik. Die Struktur als auch die Parameter eines solchen Modells sind naturgemäß unsicherheitsbehaftet, d.h. nicht exakt bekannt. Um den hohen Sicherheitsanforderungen in der Luftfahrt Rechnung zu tragen, müssen Flugregelungssysteme daher eine hohe Robustheit gegenüber Unsicherheiten aufweisen. Während klassische Flugregelungssysteme so entwickelt werden, dass sie trotz Unsicherheiten zufriedenstellend funktionieren, gilt das (erneute) Interesse in jüngerer Zeit auch Ansätzen, die den Unsicherheiten aktiv entgegen wirken. Dieses Vorgehen ermöglicht es nicht nur, die physikalischen Fähigkeiten des Flugzeugs auszureizen, sondern erhöht auch die Sicherheit in kritischen Situationen wie Ausfällen oder Schäden. Darüber hinaus reduzieren solche Ansätze auch den Aufwand und die damit verbundenen Kosten für eine präzise Identifikation des mathematischen Modells.

Der Einsatz eines Regelungssystems in der zivilen Luftfahrt erfordert eine Zulassung durch die Behörden. Hierfür muss u.A. der Nachweis erbracht werden, dass das Flugregelungssystem ausreichende Robustheits- und Performance-Eigenschaften aufweist. Ziel dieser Arbeit ist daher die Analyse und Entwicklung von Regelungssystemen, welche auch großen Unsicherheiten aktiv entgegen wirken können und garantierte Robustheits- und Performance-Eigenschaften aufweisen. Zu diesem Zweck verfolgt diese Arbeit zwei unterschiedliche Strategien.

Die erste Strategie basiert auf adaptiver Modellfolgeregelung (engl.: Model Reference Adaptive Control – MRAC). Adaptive Regler passen sich zur Laufzeit an die Strecke an und eignen sich daher sehr gut zur Regelung hochgradig unsicherer Systeme. Adaptive Ansätze führen jedoch i.A. zu nichtlinearen Reglern. Da die derzeitigen Vorschriften zur Zulassung von Flugregelungssystemen auf linearer Systemtheorie basieren, kommen adaptive Regler in der zivilen Luftfahrt derzeit nicht zum Einsatz. Zur Lösung dieses Problem sind u.A. neue Metriken zur Bewertung der Robustheit und Performance eines adaptiven Reglers erforderlich. Zwei potentielle Metriken, die in einem künftigen Zulassungsprozess adaptiver Regler zum Einsatz kommen könnten, sind der Time-Delay-Margin als Maß für die Robustheit und der größte Tracking Error als Maß für die Performance. Da sich diese Metriken in der Praxis bisher nur schwer

analytisch bestimmen lassen, zielt die erste Strategie auf die Entwicklung neuartiger Berechnungsmethoden ab.

Zur Berechnung des Time-Delay-Margins wird in dieser Arbeit eine neuartige Methode auf Basis eines Stabilitätsbeweises nach Lyapunov-Razumikhin und Sum-of-Squares-Optimierung vorgestellt. Nach bestem Wissen des Autors ist es die erste Methode für einen MRAC mit σ-Modifikation, welche den Kommandofolgefall betrachtet und keine a-priori bekannten Schranken für den sogenannten Regressorvektor benötigt.

Konventionelle Methoden zur Berechnung des größten Tracking Errors liefern nur äußerst konservative, obere Schranken. Daher werden in dieser Arbeit neuartige Berechnungsmethoden für MRAC (mit σ-Modifikation) entwickelt. Durch Nutzung von Optimierung auf Basis von linearen Matrixungleichungen kann die Konservativität der berechenbaren Schranken um nahezu eine Größenordnung reduziert werden.

Im Gegensatz zur ersten Strategie verfolgt die Zweite einen umgekehrten Weg. Anstelle eines nichtlinearen, adaptiven Ansatzes kommen hierbei lineare Methoden zum Einsatz, welche eine Zulassung nach existierenden Normen und Regularien erlauben. Im Falle der zweiten Strategie besteht die Herausforderung darin, mit Methoden der linearen Systemtheorie großen Unsicherheiten entgegenzuwirken. Das Ergebnis der zweiten Strategie ist der Modified Linear Extended State Observer (MLESO). Anders als konventionelle Luenberger-Beobachter schätzt dieser das Störsignal, welches von der Abweichung der Strecke von einem Wunschverhalten herrührt. Darüber hinaus wird nachgewiesen, dass die MLESO-basierte Regelung zur gleichen Performance des geschlossenen Regelkreises führt wie das weitverbreitete $\mathcal{L}_1$ Adaptive Control.

Contents

List of Figures

List of Tables

Acronyms

$\mathcal{L}_1$-AC	$\mathcal{L}_1$ Adaptive Control
$\mathcal{L}_1$-PUL	$\mathcal{L}_1$ Adaptive Control with Proportional Update Law
$\mathcal{L}_1$-PWC	$\mathcal{L}_1$ Adaptive Control with Piecewise Constant Update Law
AC	Advisory Circular
ADRC	Active Disturbance Rejection Control
ADS	Air Data System
AHRS	Attitude and Heading Reference System
AMC	Acceptable Means of Compliance
BIBO	Bounded Input Bounded Output
BIBS	Bounded Input Bounded State
CDF	Cumulative Density Function
CRM	Closed-Loop Reference Model
CS	Certification Specification
DOB	Disturbance Observer
EASA	European Aviation Safety Agency
ECEF	Earth-Centered Earth-Fixed
ECI	Earth-Centered Inertial
EOMs	Equations of Motion
ESO	Extended State Observer
FAA	Federal Aviation Administration
GEVP	Generalized Eigenvalue Problem
GPS	Global Positioning System
I&I-AC	Immersion and Invariance Adaptive Control
IMU	Inertial Measurement Unit
INDI	Incremental Nonlinear Dynamic Inversion
LAS	Linear Asymptotic System
LESO	Linear Extended State Observer
LMI	Linear Matrix Inequality
LPV	Linear Parameter Varying
LQR	Linear Quadratic Regulator
LTI	Linear Time Invariant
LTV	Linear Time Varying

M-MRAC	Modified Reference Model MRAC
MIMO	Multiple-Input Multiple-Output
MLESO	Modified Linear Extended State Observer
MM-LQR	Multiple-Model LQR
MRAC	Model Reference Adaptive Control
MRC	Model Reference Control
NDI	Nonlinear Dynamic Inversion
NED	North-East-Down
NN	Neural Network
NP	Nominal Performance
NS	Nominal Stability
PDF	Probability Density Function
PI	Proportional Integral
PINDI	Predictive Incremental Nonlinear Dynamic Inversion
RBF	Radial Basis Function
RCAC	Retrospective Cost Adaptive Control
RD	Relative Degree
RFDE	Retarded Functional Differential Equation
RLAS	Reduced Linear Asymptotic System
RMS	Root Mean Square
RP	Robust Performance
RS	Robust Stability
SDP	Semidefinite Program
SISO	Single-Input Single-Output
SOS	Sum-Of-Squares
SPR	Strictly Positive Real
SVD	Singular Value Decomposition
UAS	Unmanned Aerial System
UUB	Uniform Ultimate Boundedness

Symbols and Indices

Nomenclature

a	A scalar variable.
$\boldsymbol{a}$	A matrix- or vector-valued variable.
$\vec{\boldsymbol{a}}$	A vector in a (3-dimensional) Cartesian space.
$\boldsymbol{A}$	A matrix- or vector-valued variable.
a_{ij}	Element of the matrix $\boldsymbol{A}$ in the i-th row and the j-th column.
a_x	First element of the Cartesian vector $\vec{\boldsymbol{a}}$.
a_y	Second element of the Cartesian vector $\vec{\boldsymbol{a}}$.
a_z	Third element of the Cartesian vector $\vec{\boldsymbol{a}}$.
$\boldsymbol{A}^T$	The transpose of the matrix $\boldsymbol{A}$.
$\boldsymbol{A}^H$	The conjugate transpose of the matrix $\boldsymbol{A}$.
$\boldsymbol{A}^\#$	The pseudo inverse of the matrix $\boldsymbol{A}$.
$\mathcal{A}$	A set.
$\mathcal{A}\{\cdot\}$	A general operator.
$\bar{a}$	Upper bound of the scalar variable a.
$\bar{\boldsymbol{A}}$	The transformation of a vector or matrix $\boldsymbol{A}$ or a complementary matrix.
$\bar{\mathcal{A}}$	Superset of the set $\mathcal{A}$.
$\underline{a}$	Lower bound of the scalar variable a.
$\underline{\mathcal{A}}$	Subset of the set $\mathcal{A}$.
$\hat{a}$	Estimate of a variable a.
$\tilde{a}$	Deviation between variables a such as in $\tilde{a} = \hat{a} - a$.
δa	Deviation of a variable from its stationary (trim) value.
$\lambda_{\min}(\boldsymbol{A})$	Minimum eigenvalue of the square matrix $\boldsymbol{A}$.
$\lambda_{\max}(\boldsymbol{A})$	Maximum eigenvalue of the square matrix $\boldsymbol{A}$.
$\|\boldsymbol{a}\|_p$	Direct p-norm of a vector $\boldsymbol{a}$ or a matrix $\boldsymbol{A}$.
$\|\boldsymbol{a}\|_{p,i}$	Induced p-norm of a vector $\boldsymbol{a}$ or a matrix $\boldsymbol{A}$.
$\|\boldsymbol{a}(\cdot)\|_{\mathcal{L}_p}$	$\mathcal{L}_p$-norm of the signal $\boldsymbol{a}(\cdot)$.
$\|\boldsymbol{a}(\cdot)_\tau\|_{\mathcal{L}_p}$	Truncated $\mathcal{L}_p$-norm of the signal $\boldsymbol{a}(\cdot)$ as defined in (C.18).

$\operatorname{diag}\ \boldsymbol{a}$	The operator which turns the vector $\boldsymbol{a}$ into a diagonal matrix, whose diagonal entries correspond to the elements of the vector $\boldsymbol{a}$.
$\operatorname{rank} \boldsymbol{A}$	Returns the rank of the matrix $\boldsymbol{A}$.
$\operatorname{sat} a$	The saturation function, which is defined as $\operatorname{sat} a \triangleq \begin{cases} a, & \lvert a\rvert \leq 1 \\ 1, & \lvert a\rvert > 1 \end{cases}$.
$\operatorname{sgn} a$	The signum function, which is defined as $\operatorname{sgn} a \triangleq \begin{cases} 1, & a > 0 \\ 0, & a = 0 \\ -1, & a < 0 \end{cases}$.
$\operatorname{Tr}\ \boldsymbol{A}$	The trace of the square matrix $\boldsymbol{A}$ as defined in (B.150).
$\operatorname{vec} \boldsymbol{A}$	The vector representation of a matrix $\boldsymbol{A}$ as defined in (B.12).

Symbols

$\boldsymbol{\Delta}$	The extended state of a LESO or MLESO.
$\boldsymbol{\Gamma}$	The learning rate of an adaptive controller.
$\boldsymbol{\Lambda}$	Control effectiveness matrix.
Φ	Bank angle (Euler angle attitude representation of an aircraft).
Ψ	Yaw angle (Euler angle attitude representation of an aircraft).
$\Sigma(\boldsymbol{x})$	The set of all Sum-of-Squares polynomials in the variable $\boldsymbol{x}$.
Θ	Pitch angle (Euler angle attitude representation of an aircraft).
$\boldsymbol{\Theta}$	Adaptive parameter (direct MRAC) or parametric uncertainty (indirect approaches).
α	Angle-of-attack of an aircraft.
β	Angle-of-sideslip of an aircraft.
$\boldsymbol{\epsilon}$	Residual error of the parametrization of a nonlinearity.
η	Elevator deflection of an aircraft.
λ	Scalar uncertainty or uncertainty scaling factor.
λ	Geodetic longitude of an aircraft.
μ	Geodetic latitude of an aircraft.
ω	The eigenfrequency of a complex conjugate pair of poles / zeros.
ω	The angular frequency $\omega = 2\pi f$.
$\boldsymbol{\omega}$	Regressor vector of an adaptive controller.
$\vec{\boldsymbol{\omega}}$	Angular rate vector of an aircraft.
$\boldsymbol{\phi}$	Basis function for the parametrization of nonlinearities.
$\boldsymbol{\sigma}$	The modification gain of a σ-modification of MRAC.
$\boldsymbol{\sigma}(\cdot)$	The disturbance signal which results from the deviation between the actual plant response and the desired plant response in case of $\mathcal{L}_1$ Adaptive Control with Piecewise Constant Update Law.
τ_c	Delay at the plant input.
τ_m	Delay of the plant measurements.
τ	Alternative time variable (usually within integrals).

ξ	Aileron deflection of an aircraft.
ζ	The relative damping of a complex conjugate pair of poles / zeros.
ζ	Rudder deflection of an aircraft.
$\mathbf{0}^{n\times m}$	$n \times m$ matrix of zeros.
$\mathbf{0}$	Zero matrix of appropriate size.
$\boldsymbol{A}$	System matrix of a state space model.
$\vec{\boldsymbol{b}}$	Vector of normalized specific forces acting on an aircraft.
$\boldsymbol{B}$	Input matrix of a state space model.
c	The level set constant.
$\boldsymbol{C}$	Output matrix of a state space model.
$\boldsymbol{C}(s)$	A low-pass filter.
$\mathbb{C}$	The field of complex numbers.
$\mathbb{C}^n$	The n-dimensional vector space defined over the field of complex numbers $\mathbb{C}$.
$\mathbb{C}^{n\times m}$	The $n \times m$-dimensional vector space defined over the field of complex numbers $\mathbb{C}$.
$\boldsymbol{d}$	The disturbance signal which results from the deviation between the actual plant response and the desired plant response in case of signal-based approaches such as the MLESO.
$\boldsymbol{D}$	Feedthrough matrix of a state space model.
$\boldsymbol{D}(s)$	The design transfer function of a $\mathcal{L}_1$ Adaptive Controller or a MLESO.
δT	Thrust lever position of an aircraft.
$\boldsymbol{e}$	An error signal.
$\vec{\boldsymbol{f}}$	Vector of specific forces acting on an aircraft.
$\boldsymbol{f}(\cdot)$	A nonlinear function.
$\vec{\boldsymbol{F}}$	Vector of forces acting on an aircraft.
$\mathbb{F}$	A general field.
g	Earth gravitational acceleration.
$\vec{\boldsymbol{g}}$	Earth gravitational acceleration vector.
$\boldsymbol{g}(\cdot)$	A nonlinear function.
h	Altitude of an aircraft.
$\boldsymbol{h}(\cdot)$	A nonlinear function.
$\boldsymbol{I}$	Identity matrix of appropriate size.
$\boldsymbol{I}^{n\times n}$	$n \times n$ identity matrix.
$\boldsymbol{I}^{(\cdot)}$	Inertia tensor of the aircraft relative to the point $(\cdot)$.
K	A (state-dependent) Lipschitz constant.
$\boldsymbol{K}$	A controller gain.
$L^{(\cdot)}$	First element of the aircraft moment vector $\vec{\boldsymbol{M}}^{(\cdot)}$ around the point $(\cdot)$.
L	A (state-dependent) Lipschitz constant.
$\boldsymbol{L}$	Luenberger(-like) observer gain.

$\mathcal{L}\{\cdot\}$	The Laplace transform.
$\mathcal{L}^{-1}\{\cdot\}$	The inverse Laplace transform.
m	The mass (of an aircraft or of fuel).
$M^{(\cdot)}$	Second element of the aircraft moment vector $\vec{\boldsymbol{M}}^{(\cdot)}$ around the point $(\cdot)$.
$\boldsymbol{M}$	Output gain of a MLESO.
$\boldsymbol{M}_{(\cdot),(\cdot)}$	Transformation matrix between coordinate frames.
$\vec{\boldsymbol{M}}$	Vector of moments / torques vector acting on an aircraft.
$\mathcal{M}$	A level set of a Lyapunov(-like) function.
$N^{(\cdot)}$	Third element of the aircraft moment vector $\vec{\boldsymbol{M}}^{(\cdot)}$ around the point $(\cdot)$.
$\mathbb{N}$	The set of natural numbers including zero.
$\mathbb{N}_{++}$	The set of natural numbers without zero.
$\boldsymbol{P}$	A solution to a Lyapunov(-like) equation or inequality.
$\boldsymbol{Q}$	The design parameter of a Lyapunov(-like) equation or inequality such as in $\boldsymbol{A}_M^T\boldsymbol{P} + \boldsymbol{P}\boldsymbol{A}_M = -\boldsymbol{Q}$.
$\boldsymbol{r}$	Command signal issued by the user of the control system.
$\vec{\boldsymbol{r}}$	Position vector of an aircraft.
$\mathbb{R}$	The field of real numbers.
$\mathbb{R}_+$	The non-negative real numbers.
$\mathbb{R}_{++}$	The strictly positive real numbers.
$\mathbb{R}_-$	The non-positive real numbers.
$\mathbb{R}_{--}$	The strictly negative real numbers.
$\mathbb{R}^n$	The n-dimensional vector space defined over the field of real numbers $\mathbb{R}$.
$\mathbb{R}^{n\times m}$	The $n \times m$-dimensional vector space defined over the field of real numbers $\mathbb{R}$.
s	Complex frequency variable of a Laplace transform.
$\mathbb{S}^n$	The vector space of $n \times n$ symmetric matrices.
$\mathbb{S}^n_+$	The positive semidefinite, symmetric matrices.
$\mathbb{S}^n_{++}$	The positive definite, symmetric matrices.
$\mathbb{S}^n_-$	The negative semidefinite, symmetric matrices.
$\mathbb{S}^n_{--}$	The negative definite, symmetric matrices.
t	Time variable.
T_s	Sampling rate.
$u^{(\cdot)}$	First element of the aircraft velocity vector $\vec{\boldsymbol{V}}^{(\cdot)}$ of the point $(\cdot)$.
$\boldsymbol{u}$	Input (vector) of a state space model.
$v^{(\cdot)}$	Second element of the aircraft velocity vector $\vec{\boldsymbol{V}}^{(\cdot)}$ of the point $(\cdot)$.
$V(\cdot)$	A Lyapunov function (candidate).
V	Absolute velocity of an aircraft.
$\vec{\boldsymbol{V}}$	Velocity vector of an aircraft.
$w^{(\cdot)}$	Third element of the aircraft velocity vector $\vec{\boldsymbol{V}}^{(\cdot)}$ of the point $(\cdot)$.

$\boldsymbol{w}$	A disturbance signal that violates the assumptions of a controller (which results for example from unmodeled dynamics).
$x^{(\cdot)}$	First element of the aircraft position vector $\vec{\boldsymbol{r}}^{(\cdot)}$ of the point $(\cdot)$.
$\boldsymbol{x}$	State (vector) of a state space model.
$X^{(\cdot)}$	First element of the aircraft force vector $\vec{\boldsymbol{F}}^{(\cdot)}$ in the point $(\cdot)$.
$y^{(\cdot)}$	Second element of the aircraft position vector $\vec{\boldsymbol{r}}^{(\cdot)}$ of the point $(\cdot)$.
$\boldsymbol{y}$	Output (vector) of a state space model.
$Y^{(\cdot)}$	Second element of the aircraft force vector $\vec{\boldsymbol{F}}^{(\cdot)}$ in the point $(\cdot)$.
$z^{(\cdot)}$	Third element of the aircraft position vector $\vec{\boldsymbol{r}}^{(\cdot)}$ of the point $(\cdot)$.
$\boldsymbol{z}$	The state vector of unmodeled dynamics or a joint state vector.
$Z^{(\cdot)}$	Third element of the aircraft force vector $\vec{\boldsymbol{F}}^{(\cdot)}$ in the point $(\cdot)$.

Indices

$*$	Ideal / true value of a scalar, matrix or signal.
ϕ	Scalar, matrix or signal associated with the nonlinear function $\boldsymbol{\phi}(\boldsymbol{x}_P(t))$.
A	aerodynamic (A) frame, with • x-axis pointing in the direction of the aerodynamic velocity; • y-axis pointing right, completing an orthogonal right hand system; • z-axis lying in the plane spanned by the x_B-axis and the z_B-axis, pointing downwards, being orthogonal to the x_A-axis.
act	Scalar, matrix or signal associated to an actuator.
ad	Scalar, matrix or signal of an adaptive controller or augmentation.
B	Body-fixed (B) frame, with • x-axis pointing towards the nose of the aircraft within the aircraft's symmetry plane; • y-axis pointing towards the right wing; • z-axis pointing completes an orthogonal right-hand system and points downwards.
bl	Scalar, matrix or signal of a baseline controller.
C	Index of the control error in $\boldsymbol{e}_C(t)$.
cmd	Commanded value or signal such as α_{cmd}.
E	Earth-Centered Earth-Fixed (ECEF) frame, with • x-axis in the equatorial plane, pointing towards the Greenwich meridian; • y-axis in the equatorial plane, completing an orthogonal right hand system; • z-axis parallel to Earth's rotation axis, pointing north.

fb Feedback signal or transfer function such as $\boldsymbol{C}_{fb}(s)$.

ff Feedforward signal or transfer function such as $\boldsymbol{C}_{ff}(s)$.

G The center of gravity of the aircraft.

I Earth-Centered Inertial (ECI) frame, with
- x-axis in the ecliptic plane, pointing towards the vernal equinox;
- y-axis in the equatorial plane, completing an orthogonal right hand system;
- z-axis parallel to Earth's rotation axis, pointing north.

K kinematic (K) frame, with
- x-axis pointing in the direction of the kinematic velocity;
- y-axis pointing right, completing an orthogonal right hand system;
- z-axis lying in the plane spanned by the x_K-axis and the local surface normal of WGS-84 reference ellipsoid, pointing downwards, being orthogonal to the x_K-axis.

$\bar{K}$ kinematic frame rotated by flight-path bank angle μ_K^R about the x_K-axis

M Reference model state in expressions such as $\boldsymbol{x}_M(t)$.

M Mounting position of the AHRS in expressions of position, force, moments, etc. such as $\left(\vec{\boldsymbol{f}}^M\right)_B$.

m Matched uncertainty, signal or transfer function such as $\boldsymbol{d}_m(t)$.

max Maximum value of a scalar.

min Minimum value of a scalar.

nom Nominal value.

O North-East-Down (NED) frame, with
- x-axis parallel to the local geoid surface, pointing towards the geographic North Pole;
- y-axis parallel to the local geoid surface, pointing east;
- z-axis perpendicular to the local geoid surface, pointing downwards.

P Plant state or signal such as $\boldsymbol{x}_P(t)$.

P Index of the prediction error in $\boldsymbol{e}_P(t)$.

$Proj$ Indicates a projection of a vector or a set.

R Some known reference point within the aircraft.

r Scalar, matrix or signal associated with the reference signal $\boldsymbol{r}(t)$.

ref State or signal of the $\mathcal{L}_1$ *Reference Model* such as $\boldsymbol{x}_{\text{ref}}(t)$.

um Unmatched uncertainty, signal or transfer function such as $\boldsymbol{d}_{um}(t)$.

x Scalar, matrix or signal associated with the plant state $\boldsymbol{x}_P(t)$.

Chapter 1

Introduction

In modern aircraft, flight control systems fulfill diverse tasks. These tasks range from the improvement of the aircraft handling qualities over the automation of routine maneuvers to the alleviation of gust loads, which may severely stress the aircraft structure. Among these tasks, gust load alleviation is a good example of the complex interactions between control and aircraft design since an effective gust load alleviation also allows different sizing of the aircraft structure [20]. The latter may enable a reduction of the overall weight, leading to a more efficient aircraft. Irrespective of the precise control objective, the overarching goal of any flight control system is safety. In order to meet this goal, flight control systems must provide a high level of robustness.

The development of any flight control system relies on some mathematical model of the aircraft physics. The parameters of such a model have to be determined in experiments such as wind tunnel tests and hence, are uncertain. Furthermore, the structure of the model itself is uncertain since any mathematical model ultimately is an approximation of the true aircraft behavior. Based on such a model, the control system is usually designed using methods from linear system theory. In order to deal with the model uncertainty, the controller gains have to be chosen in such a way that the control objective is met for all expected uncertainties. This approach often requires an unsatisfactory tradeoff between safety (i.e. robustness) and other control objectives. A control design approach which admits a potentially more benign tradeoff between these diametral objectives is adaptive control. In contrast to traditional control design approaches, an adaptive controller adjusts its gains at runtime to the plant. This does not only enable the full exploitation of the physical capabilities of the plant, but also increases safety in critical situations such as damages or faults. Furthermore, adaptive control admits to reduce the effort, and thus the cost associated with a precise identification of the model parameters.

While the potential of adaptive control has been successfully demonstrated in several research programs such as RESTORE [19] or IRAC [76] by virtue of flight tests, adaptive control is not routinely used in civil aviation. This situation derives from the fact that today's adaptive controllers lack reliable guarantees for their robustness as

well as their performance. However, such guarantees are crucial for the application of adaptive control in safety critical applications such as aircraft. This aspect will be explained in more detail in the upcoming section. Afterwards, Sections 1.2 and 1.3 highlight the objectives and contributions of this thesis. Finally, Section 1.4 outlines the layout of the remainder of this thesis.

1.1 Background

Adaptive flight control has a long history which dates back well to the middle of the 20th century. One of the earliest examples of an aircraft featuring an adaptive flight control system was the hypersonic X-15-3 aircraft [46]. The use of an adaptive controller aimed at compensating the dramatic changes of the aircraft dynamics throughout the X15's envelope. In 1967, the X-15-3 crashed due to a failure of the adaptive flight control system. This event led to decreasing interest in adaptive flight control [46] and in adaptive control in general [89]. A major problem of these early adaptive controllers was "the lack of stability proofs and the lack of understanding of the properties of the proposed adaptive control schemes" [89]. As a result, the following decades saw the development of new adaptive control schemes which guarantee closed-loop stability. One of the most famous adaptive control approaches of this kind is Model Reference Adaptive Control (MRAC) [119, 89, 105]. This control scheme ensures that the plant asymptotically tracks a previously defined reference model which embeds the desired closed-loop performance specifications. While adaptive control schemes such as MRAC ensured stability for certain classes of uncertainty, they did not yet consider robustness. In the late 1970s and in the 1980s, several examples were published which demonstrated that small perturbations, which are not covered by the proof of stability, may render an adaptive controller unstable. One of the most famous examples of this kind was *Rohrs' counterexample* from 1985 [136] which demonstrated instability due to small unmodeled dynamics. The analysis of these examples led to the development of various so-called *robustness modifications*, which ensure boundedness of the adaptive controller even in the presence of such perturbations. Widely known robustness modifications of MRAC include the dead zone modification [130, 119], the σ-modification [88, 89], the e-modification [118, 119] or the projection algorithm [131, 105]. In conjunction with *Neural Networks* [158, 105, 63], the development of robust adaptive controllers led to new interest in adaptive flight control. In 1998, a *Neural Network*-based adaptive flight control system was successfully tested on the X-36 tailless aircraft within the RESTORE program [19]. Starting from this time on, various research programs successfully demonstrated the capabilities of adaptive flight control in simulations as well as flight tests (such as on a modified F-18 aircraft within the IRAC program [76]).

Although adaptive controllers have repeatedly demonstrated their beneficial capabilities, they are not yet routinely used in civil aviation since current norms and stan-

dards do not allow their certification. Informally, certification refers to the process of convincing the authorities that the aircraft and its components comply with governmental regulations. In order to show compliance, one usually resorts to established standards of (aerospace) industry. While there is no legal obligation to follow these standards, their use is advisable because it facilitates the certification process.

Established standards for the certification of any equipment aboard an aircraft, including flight control systems, are SAE ARP4754A *Guidelines for Development of Civil Aircraft and Systems*, SAE ARP4761 *Guidelines and Methods for Conducting the Safety Assessment Process on Civil Airborne Systems and Equipment* and RTCA DO-178B/C *Software Considerations in Airborne Systems and Equipment Certification*. These standards do not list specific requirements which must be met by the flight control system, but rather describe its development process. A central element of this process is *verification*. Roughly speaking, this means that the intended behavior of the flight control system is precisely defined before its development. The outcome of this step is a set of rigorous requirements. After the development of the flight control system, the satisfaction of these requirements is tested in order to demonstrate that it actually acts as previously defined.

For the specification of the intended behavior of a flight control system, one usually resorts to standards such as SAE AS94900 [140], SAE ARP94910 [142], MIL-F-8785C [41] or MIL-HDBK-1797 [42]. These documents formulate requirements which should be met by the flight control system in order to achieve satisfactory robustness and performance. These requirements may be roughly divided into time-domain and frequency-domain requirements. As examples of the latter, consider for example gain and phase margin, which serve as metrics (measures) of control system robustness. For both, SAE AS94900 specifies lower limits which the flight control system must exceed. Similarly, MIL-F-8785C requires that the flight control system ensures a minimal relative damping of the short-period motion, which may be seen as a metric for control system performance. In case of an adaptive controller, such frequency-domain requirements do not apply since an adaptive controller is inherently nonlinear and therefore, no frequency-domain representation exists. For this reason, new robustness and performance metrics are needed in order to formulate requirements for the robustness and performance of an adaptive flight control system. The absence of such robustness and performance metrics currently is a major hurdle for the certification of adaptive controllers [92, 161, 14].

Another certification challenge consists in testing whether the adaptive flight control system actually meets these novel requirements. This challenge derives from the highly nonlinear dependence of the behavior of an adaptive controller on the commands, the uncertainties, the disturbances as well as the design parameters. While the response of a conventional linear controller also depends on these factors, it is more easily predictable due to linearity. For example, if the commands are doubled,

the response will double as well. In contrast, a doubled command may lead to a fundamentally different response of an adaptive controller. In order to account for these nonlinear effects, ideal testing would have to cover all admissible commands, uncertainties and disturbances.

In practice, there exist several options for testing. In case of a linear control system and conventional frequency-domain requirements, an analytical computation (for example of gain and phase margins) suffices to check the satisfaction of the associated requirements. Consequently, *analytical methods* also represent an interesting solution in case of an adaptive flight control system. They usually rely on a proof of closed-loop stability and yield guaranteed results which hold for all suitably bounded commands, uncertainties and disturbances. In practice, however, analytical methods are often unavailable. Furthermore, even if appropriate methods exist, they mostly require simplifications of the mathematical model of the plant. Moreover, they often tend to substantially over- or underestimate the true value of the metric. Due to this conservatism, they are currently not appropriate for testing.

As an alternative to analytical methods, one may also resort to *simulation-based testing* using Monte-Carlo simulations or related methods. Simulation-based testing offers the advantage that no simplifications of the mathematical model of the plant are required. Furthermore, they do not over- or underestimate the metric and hence, are well suited for testing. However, since each simulation run only reflects the response to one specific command, uncertainty and disturbance, a huge number of simulations is required in order to cover a statistically significant number of responses. This disadvantage may be partially compensated using modern Monte-Carlo methods such as *Subset simulations* [7] or using *counter-proving* [169]. In case of the latter, numerical methods from optimal control are used to compute the worst-case value of the metric. If the worst-case value satisfies the requirement, then it is also expected to be satisfied for all other commands, uncertainties and disturbances. Similar to analytical methods, optimal control approaches often require simplified plant models. Furthermore, there is usually no guarantee for convergence to the global optimum. As another alternative, one may also consider *formal methods* such as model checking [9, 165, 132]. This method provides the appealing capability to prove correctness of finite state machines with respect to formally specified requirements. The application of these methods is however not straightforward because it requires an abstraction of the adaptive controller as a finite state machine [92, 132].

The preceding discussion of testing methods highlights that each method provides unique advantages and disadvantages. Since the former can effectively complement each other, it may be expected that only combinations of these methods will lead to a successful certification of adaptive controllers. Furthermore, it must be realized that the absence of suitable metrics and the difficulties with testing do not constitute the only challenges with respect to the certification of adaptive controllers. Other difficul-

ties derive for example from the lack of viable monitoring systems which can detect malfunctions of an adaptive controller during runtime.

More recently, a novel adaptive control approach, namely $\mathcal{L}_1$ Adaptive Control ($\mathcal{L}_1$-AC) [87], raised significant interest. While there is an ongoing discussion on the question as to whether this approach should be called adaptive or not (see for example [97, 126, 86, 127]), it certainly provides interesting features from an engineering point of view. One variant of $\mathcal{L}_1$-AC, so-called $\mathcal{L}_1$ Adaptive Control with Piecewise Constant Update Law ($\mathcal{L}_1$-PWC), leads to a linear control law. This approach has recently been successfully flight-tested on a Learjet 25D aircraft [1]. Due to linearity, one may actually certify $\mathcal{L}_1$-PWC according to existing rules and requirements without the need for novel robustness and performance metrics. With respect to the previous discussion about the certification of adaptive control, the latter results in a major advantage. While it is expected that a nonlinear approach such as MRAC outperforms a linear approach in suitable conditions [38], it nevertheless represents an interesting solution: If a linear approach such as $\mathcal{L}_1$-PWC solves a given control problem, there is no need to use a nonlinear, currently non-certifiable controller. Furthermore, such linear approaches may also be seen as a viable interim solution until the certification challenges of adaptive controllers have been solved.

1.2 Objective

The overall objective of this thesis consists in the development of control systems:

1. which can control highly uncertain plants;
2. which admit reliable robustness and performance guarantees that may be used in a certification process.

In order to achieve this overall goal, this thesis adopts two different strategies.

The *first strategy* resorts to adaptive control, namely MRAC. While MRAC is well suited for the control of highly uncertain plants, it lacks appropriate robustness and performance guarantees. In literature, several robustness and performance metrics have been suggested. The computation of these metrics however still represents a major difficulty. For this reason, the present thesis does not propose novel metrics, but aims at improving and developing methods for the computation of metrics.

The *second strategy*, which is adopted by this thesis, consists in the development and the analysis of *linear* control strategies which may control highly uncertain plants. In contrast to MRAC, these approaches may be analyzed with existing techniques and may be certified according to existing rules and requirements due to their linearity. In case of the *second strategy*, the challenge consists in handling highly uncertain plants.

1.3 Contribution

With respect to the previously defined objectives, this thesis makes the following contributions:

Consistent Derivations

MRAC (see e.g. [119, 89, 105]) and $\mathcal{L}_1$-AC (see [87]) represent two widely known branches of adaptive control. This may already be seen from the sheer amount of publications on these topics. Most publications do however only consider one of the two approaches. As a result, the introductions to these approaches usually rely on different nomenclatures and on different assumptions, obscuring their relations. For this reason, this thesis introduces all control approaches (MRAC, $\mathcal{L}_1$-AC and its variants, Modified Linear Extended State Observer (MLESO)) based on a common nomenclature and using common assumptions.

Classification into Signal-based and Parameter-based Approaches

All control approaches considered within this thesis aim at the control of highly uncertain systems. In order to deal with the uncertainty, they possess some uncertainty estimation mechanism. These mechanisms do, however, differ fundamentally. In case of MRAC and $\mathcal{L}_1$-AC (with Integral Update Law), the controller adjusts its *parameters / gains* to the plant. For this reason, these approaches are referred to as *parameter-based* approaches. In contrast, $\mathcal{L}_1$-PWC, MLESO-based controllers and several other approaches do not adjust their parameters. Instead, they estimate a *disturbance signal* which results from the deviation between a reference model and the true plant. These approaches are hence referred to as *signal-based* approaches. To the best of the author's knowledge, this classification has not yet been introduced in research.

In contrast to a classification as adaptive or non-adaptive, the distinction into *signal-based* and *parameter-based* approaches facilitates the discussion of their properties and limitations. This is because *signal-based* and *parameter-based* approaches may be clearly distinguished, whereas terms such as *adaptivity* are not uniquely defined in literature (see for example [119] for several definitions). An initial discussion on the properties and limitations of *signal-based* and *parameter-based* approaches will be presented.

Strategy 1: Systematic Review of Robustness and Performance Metrics

In literature, various robustness and performance metrics for adaptive controllers have been proposed. The need for new metrics has been highlighted in [92] and some solutions and metrics were gathered in [92, 161]. However, none of these previous works has provided a systematic review and a systematic classification of available approaches. For this reason, the current thesis presents such a systematic review. While there exist various adaptive control approaches and associated analysis techniques, this study mainly considers MRAC and $\mathcal{L}_1$-AC.

Strategy 1: Development of Novel Methods for the Computation of Robustness and Performance Metrics

The review of robustness and performance metrics identifies two promising metrics, which might be of use in a future certification process of adaptive controllers. These two metrics are the time-delay margin (as a measure of robustness) and bounds on the tracking error[1] components (as a measure of performance). While both metrics provide valuable insight into the robustness or the performance of an adaptive controller, their practical application is challenging due to the lack of methods for their computation. For this reason, this thesis develops novel analytical methods for the computation of these two metrics in case of a MRAC. Since the present thesis aims at obtaining robustness and performance guarantees, the analytical computation is preferred over other computational methods.

The analytical computation of the time-delay margin of an adaptive controller has been addressed in several publications. In order to prove stability of the resulting nonlinear delayed system, they usually resort to either the stability theorems of Lyapunov-Razumikhin or Lyapunov-Krasovskii [75, 73]. Ishihara et al. [90] compute the time-delay margin of an adaptive controller for a second order plant using the Lyapunov-Razumikhin theorem. The approach does, however, require the knowledge of an upper bound on the regressor vector[2], which is not always readily available. Matsutani et al. [112] determine the time-delay margin by showing robustness to unmodeled dynamics and using a Padé approximation of the time-delay. Due to the use of a Padé approximation, the approach does not yield a guaranteed bound. More recently, Matsutani et al. [113] inferred the time-delay margin of MRAC using an analysis of the trajectories using first principles and the Lyapunov-Razumikhin theorem. This method exploits the special properties of the projection algorithm [131, 105]. Dorobantu et al. [43] calculate the time-delay margin of MRAC with σ-modification in the stabilization case using the Lyapunov-Krasovsikii theorem and so-called Sum-Of-Squares (SOS) optimization. The use of SOS optimization enables the reduction of conservatism. Following a similar spirit, this thesis proposes a method for the computation of the time-delay margin of a MRAC with σ-modification which relies on the Lyapunov-Razumikhin theorem and SOS optimization. In contrast to Dorobantu et al. [43], the tracking case is considered.

Analytical methods for the computation of bounds on the tracking error immediately derive from the conventional proof of stability of MRAC. Essentially, all of these methods aim at the computation of an invariant set, i.e. a set which the trajectories of the closed-loop system cannot leave. The size and the shape of this set lead to a bound on the tracking error. The process of computing such an invariant set usually

[1] Control approaches such as MRAC aim at tracking a previously defined reference model. The error between the plant and the reference model is referred to as tracking error.

[2] Parameter-based approaches such as MRAC separate the uncertainties into an unknown parameter vector and a vector of known basis functions. The latter vector is commonly referred to as the regressor vector.

involves various upper and lower bounds on the Lyapunov function and its derivative (see for example [158]), which introduces significant conservatism. The emergence of conservatism will be analyzed systematically, which represents one contribution.

More recently, Fravolini et al. [55] replaced these upper and lower bounds by Linear Matrix Inequality (LMI) conditions. They used the resulting novel computational method to *synthesize* adaptive controllers which satisfy a-priori specified tracking error bounds. In a later publication, Fravolini et al. also used this idea for the *analysis* of adaptive controllers (see [56]). Furthermore, synthesis procedures for other MRAC variants have been proposed (see [61, 60, 58, 57]). In this thesis, a conceptually similar, but independent approach is developed. In contrast to Fravolini, this approach exclusively focuses on the analysis scenario. In order to mitigate conservatism, a slightly altered Lyapunov function candidate is proposed, which does not change the adaptive controller itself. Furthermore, a novel method is introduced to deal with statistically distributed uncertainties which adapts methods from probabilistic μ-analysis (see for example [11]). Moreover, a method is presented which allows the computation of tracking error bounds in case of unmatched parametric uncertainties. To the best of the author's knowledge, this case has not been addressed so far in literature.

Strategy 2: Development of the Modified Linear Extended State Observer

Although significantly improved methods have been recently proposed for the computation of robustness and performance metrics, their conservatism still prevents their use in a certification process. This raises the question as to whether the objective of controlling highly uncertain systems may also be achieved using linear, that is, certifiable control approaches. Following this line of thought, this thesis introduces the MLESO. In its simplest form, the MLESO is a Luenberger-like observer which estimates the disturbance signal that results from the plant uncertainties. In contrast to a conventional Linear Extended State Observer (LESO) [65, 27, 28], the MLESO follows a different paradigm. While a LESO is designed like a conventional Luenberger observer, the MLESO follows a signal-driven approach. The design of the MLESO ensures that the disturbance estimate closely follows the true disturbance signal. The lag of the disturbance estimate is described by a strictly proper filter, whose transfer function may be freely chosen. In contrast, a conventional LESO does not admit to realize arbitrary transfer functions.

Furthermore, it will be proven that the MLESO achieves the same closed-loop performance as a $\mathcal{L}_1$-AC or a $\mathcal{L}_1$-PWC. Hence, the MLESO may be seen as a viable alternative to these approaches. Its close relation to $\mathcal{L}_1$-AC and a $\mathcal{L}_1$-PWC also enables to establish connections to other signal-based approaches such as Disturbance Observers (DOBs). Moreover, similarities of MLESO-based controllers and Proportional Integral (PI) controllers as well as integral model inversion controllers [156] will be clarified.

Strategy 2: Application and Assessment of the Modified Linear Extended State Observer

In order to demonstrate the capabilities of the MLESO, it is applied to a challenging benchmark control problem: A fallback control system for the lateral motion of an Unmanned Aerial System (UAS) is developed which only relies on the measurements provided by the Attitude and Heading Reference System (AHRS). Thus, the controller may only resort to measurements of linear accelerations, angular rates and attitude angles. Nevertheless, the controller must operate throughout velocity and altitude ranges of interest. Since altitude and velocity are not available as measurements, conventional design strategies based on gain-scheduling are not applicable.

In order to assess the robustness and performance of the MLESO-based control law, a second control system is developed additionally. This second control system relies on an ad hoc modification of the Linear Quadratic Regulator (LQR) problem. The modification enables the LQR controller to simultaneously stabilize multiple plant models and hence, to stabilize the plant at various altitudes and velocities.

A comparison leads to the rather unexpected result that both controllers equally solve the control problem. Moreover, the LQR controller seems preferable due to its simpler structure. This observation initiates a discussion of the limitations of the control objective “model following”, which is pursued by most control approaches of this thesis including the MLESO.

1.4 Layout of the Thesis

The remainder of this thesis is structured as follows: Chapter 2 introduces two benchmark control problems. The first one consists in the control of the short-period motion of an UAS. Due to its simplicity, this control problem will be used recurrently throughout this thesis to demonstrate various control approaches and their properties. The second control problem aims at the development of a fallback controller for the lateral motion of the same UAS. Due to its complexity, it will not be treated recurrently. Instead, Chapter 6 is dedicated to this problem. Afterwards, Chapter 3 reviews the theory of MRAC and $\mathcal{L}_1$-AC, which represent two widely known adaptive control approaches. With respect to the *first strategy*, Chapter 4 then summarizes available robustness and performance metrics for MRAC and proposes novel methods for their computation. With respect to the *second strategy*, Chapter 5 introduces the MLESO as a Linear Time Invariant (LTI) control approach for highly uncertain systems. This novel control approach is applied to the lateral benchmark control problem in Chapter 6. Furthermore, Chapter 6 also introduces a slightly modified LQR control problem which is used to derive an alternative controller for the purpose of comparison. Finally, Chapter 7 concludes this thesis, highlights its achievements (and open problems) and proposes directions for future work.

The reader is expected to be familiar with linear and nonlinear system theory as covered in introductory textbooks such as [110, 111, 156, 96]. Furthermore, basic concepts from linear algebra and analysis are required. Some previous knowledge about LMIs and related concepts such as SOS polynomials are advantageous. While most of these topics will be briefly reviewed in Appendix B and C, these sections do not present them in a fully self-contained fashion.

Chapter 2

Benchmark Problem Description

This chapter introduces two benchmark control problems which will be considered within this thesis. The first problem is the control of the angle-of-attack of a linearized short-period approximation of the longitudinal dynamics of an Unmanned Aerial System (UAS). This control problem is used recurrently throughout this thesis in order to demonstrate the basic properties of the control approaches which will be introduced later on. The details of this control problem may be found in Section 2.2.

The second benchmark problem considers the lateral dynamics of the same UAS. A control system is to be developed that ensures tracking of a bank angle command, while keeping the angle-of-sideslip at small values. The benchmark problem features two additional challenges:

1. The controller should operate on a whole envelope of interest, that is, for a velocity range, altitude range and fuel mass range of interest.
2. Only measurements processed by the Attitude and Heading Reference System (AHRS) are available to the controller. That is, the controller may only resort to measurements of the angular rates, attitude angles and linear accelerations to complete its control task. Other measurements such as the altitude, the velocity, the angle-of-attack or the angle-of-sideslip are *not* available.

The details of the second control problem itself are presented in Section 2.3. Due to its complexity, the second control problem is not treated recurrently throughout the thesis. Instead, Chapter 6 is dedicated to the development of the controller and to the assessment of its robustness and performance.

Both control problems, which are introduced in this chapter, consider the same UAS. Before introducing the respective control problems, a suitable model of the UAS is required. To that end, Section 2.1 introduces the general nonlinear Equations of Motion (EOMs) of the UAS, their linearization and the modeling of further aircraft subsystems such as the actuators. Notice that the detailed modeling of the forces and moments acting on the UAS will not be presented since these details may not be published. In order to maintain reproducibility, a few linearized models of the UAS are nevertheless

provided for selected flight conditions with an extended landing gear. These linearized models are sufficient to reproduce most simulation results presented within this thesis.

Unlike the other chapters of this thesis, the explicit dependence on time is dropped in this chapter in order to improve readability. It should however be clear from the context that positions, velocities, etc. are time-varying quantities.

2.1 Modeling of the UAS

This section presents the general structure of the UAS model, which constitutes the basis for all later controller developments. The model comprises two major components. On the one side, there are the EOMs of the UAS itself. On the other side, there are aircraft subsystems such as actuators, digital processing, etc. From the perspective of the flight control system, these subsystems are also part of the aircraft dynamics. Their consideration is of uttermost importance as their presence can significantly limit the achievable control system performance.

The EOMs of the UAS are derived under the assumption of a rigid body. The states of such a rigid body in the three dimensional space are given by its velocity, its position, its angular rate and its attitude. The velocity, the position and the angular rate may be conveniently represented as three dimensional vectors. For the representation of attitude, one of the numerous available attitude representations (such as quaternions, Euler angles, Rodrigues parameters - see [154]) has to be chosen. For the sake of simplicity, an attitude representation in terms of Euler angles is convenient. Hence, the total number of states of the rigid body EOMs amounts to twelve. In addition, the states of the aircraft subsystems have to be considered as well. In this thesis, the only subsystem adding further states to the overall aircraft model is the actuation system. The UAS provides four independent control inputs, namely the elevator, the aileron, the rudder and the thrust lever position. The dynamics of the three control surfaces are modeled as second order lag elements and hence, the number of states of the overall aircraft model increases to 18. Since none of the controllers, which will be presented later on, alters the thrust lever position, the engine dynamics will not be modeled.

The EOMs of the rigid body (for the velocity and the angular rate) derive from the laws of conservation of translational and angular momentum. These physical laws may only be applied when modeling the aircraft in an inertial frame. In case of an aircraft moving in the atmosphere of the Earth, it is reasonable to assume that a coordinate system, whose origin is the center of the Earth, and which does not rotate while the Earth orbits the Sun, is approximately an inertial frame. Hence, the EOMs could be stated in this frame, which will be later on referred to as Earth-Centered Inertial (ECI) frame. However, the derivation of the EOMs ultimately serves the purpose of obtaining models which are suitable for the process of control design. Hence, the states of the model should represent measurable quantities. Since the velocity of the aircraft with

respect to the ECI frame is not easily measurable, modeling in a non-inertial (accelerating) frame is more appropriate. A measurable and more intuitive velocity is for example given by the velocity of the aircraft with respect to the (rotating) surface of the Earth, which represents a rotating reference frame. Modeling in such a frame comes at the cost that fictitious forces such as centrifugal forces have to be considered.

Subsequently, the required reference frames will be introduced first in Subsection 2.1.1. Furthermore, the general nomenclature for denoting positions, (angular) velocities, (angular) accelerations, forces and moments will be presented. With these prerequisites in place, the nonlinear EOMs are stated in Subsection 2.1.2. Based on the nonlinear EOMs, the general structure of the linearized model of the aircraft is presented in Subsection 2.1.3. Finally, Subsection 2.1.4 presents the modeling of the aircraft subsystems such as the actuators and the digital processing units.

2.1.1 Reference Frames and Nomenclature

This section presents the reference frames, which are important for the modeling of the UAS motion. Furthermore, transformations between the respective frames are presented, if they are required subsequently. Afterwards, the nomenclature for denoting positions, (angular) velocities, (angular) accelerations, forces and moments will be presented. This nomenclature is commonly used at the Institute of Flight System Dynamics.

The pictures within this section are taken from internal documents by courtesy of the Institute of Flight System Dynamics.

Earth-Centered Inertial Frame

The origin of the Earth-Centered Inertial (ECI) frame is the center of the Earth. Its x_I-axis lies within the ecliptic (the plane in which the Earth orbits the Sun) and points towards the vernal equinox. Its y_I-axis completes an orthonormal, right-handed coordinate system. Its z_I-axis is aligned with the Earth's rotational axis and points north. Figure 2.1(a) illustrates the ECI frame. The index associated with the ECI frame is I.

While the ECI frame does *not* rotate around the Earth's rotational axis, it moves on an elliptic orbit around the Sun. Nevertheless, it may be approximately (strictly speaking: locally) seen as an inertial frame. Hence, the laws of conservation of translational and angular momentum may be applied.

Earth-Centered Earth-Fixed Frame

Similar to the ECI frame, the origin of the Earth-Centered Earth-Fixed (ECEF) frame is the center of the Earth. Its x_E-axis lies within the equatorial plane and points from the Earth center towards the Greenwich meridian. Its y_E-axis also lies within the equatorial plane and completes an orthonormal, right-handed coordinate system. Its z_E-axis is equivalent to the z_I-axis. Due to the above definition of the x_E-axis, the ECEF frame

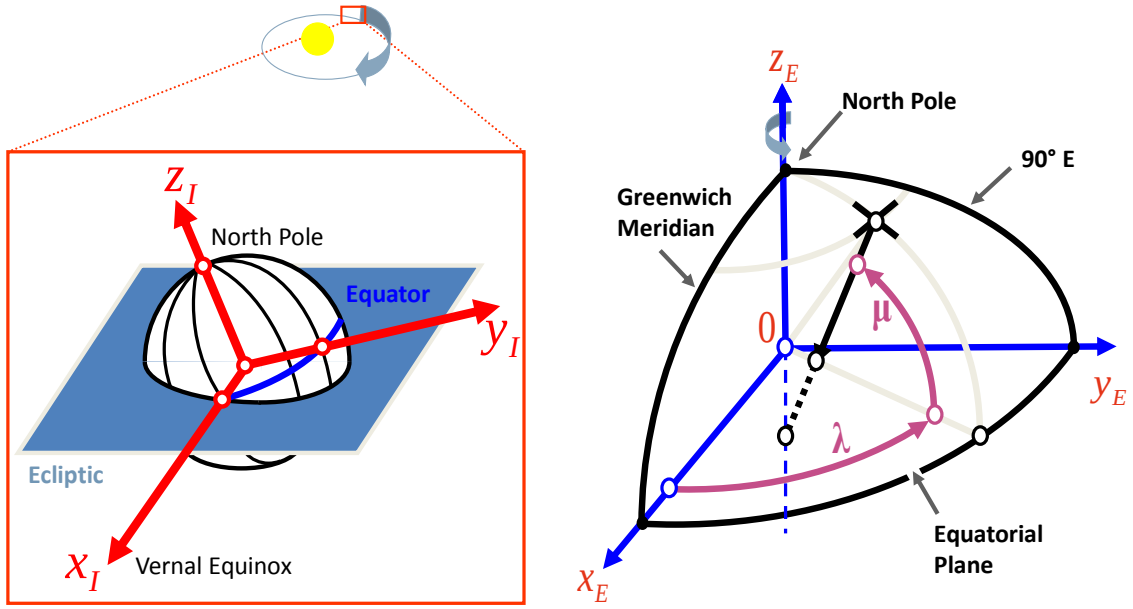

(a) ECI frame

(b) ECEF frame

Figure 2.1: Illustrations of the ECI frame and of the ECEF frame.

rotates with the Earth rotation rate $\left(\vec{\omega}^{IE}\right)$ with respect to the ECI frame. Figure 2.1(b) illustrates the ECEF frame. The index associated with the ECEF frame is E.

The ECEF frame is especially suited for the representation of the position and of the velocity of the aircraft relative to the Earth's surface.

North-East-Down Frame

The origin of the North-East-Down (NED) frame is the so-called reference point R, which is some known point within the aircraft. The x_O-axis is parallel to the local geoid surface, pointing towards the geographic North Pole. The y_O-axis is parallel to the local geoid surface and points east. The z_O-axis is perpendicular to the local geoid surface and points downwards. The NED frame is illustrated in Figure 2.2. The index associated with the NED frame is O.

Since the origin of the NED frame is within the aircraft, positions may not be represented in this frame. The NED frame is primarily used as a reference to indicate the attitude of the aircraft. Since the x_O-axis always points towards the geographic North Pole, the NED frame has to rotate with respect to the ECEF frame when the aircraft moves relative to the Earth's surface. This rotation is called transport rate and is denoted by $\left(\vec{\omega}^{EO}\right)$. The transport rate depends on the current position and velocity of the aircraft. A formula for its computation may for example be found in [173].

Body-Fixed Frame

Similar to the NED frame, the origin of the body-fixed frame is the reference point R of the aircraft. The x_B-axis points towards the nose of the aircraft within the aircraft's symmetry plane. The y_B-axis points towards the right wing. The z_B-axis completes an

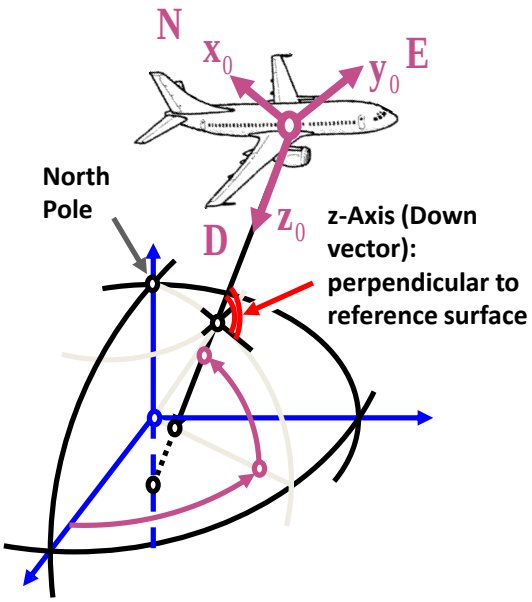

Figure 2.2: Illustration of the NED frame.

orthonormal right-hand system and points downwards within the aircraft's symmetry plane. The index associated with the body-fixed frame is B.

Since the axes of the body-fixed frame are aligned with the aircraft body, the body-fixed frame is the preferred frame for writing down forces and moments acting on the aircraft.

The orientation of the body-fixed frame with respect to the NED frame is specified with the help of three Euler angles, namely the bank angle Φ, the pitch angle Θ and the azimuth angle Ψ. The rotation matrix which transforms a vector from the NED frame to the body-fixed frame is given by ([20]):

$$\boldsymbol{M}_{BO} = \begin{bmatrix} 1 & 0 & 0 \\ 0 & \cos\Phi & \sin\Phi \\ 0 & -\sin\Phi & \cos\Phi \end{bmatrix} \cdot \begin{bmatrix} \cos\Theta & 0 & -\sin\Theta \\ 0 & 1 & 0 \\ \sin\Theta & 0 & \cos\Theta \end{bmatrix} \cdot \begin{bmatrix} \cos\Psi & \sin\Psi & 0 \\ -\sin\Psi & \cos\Psi & 0 \\ 0 & 0 & 1 \end{bmatrix}. \tag{2.1}$$

Kinematic Frame

Similar to the body-fixed frame, the origin of the kinematic frame is the reference point R of the aircraft. The x_K-axis however points in the direction of the *kinematic* velocity of the aircraft. The y_K-axis points right and completes an orthonormal right-hand system. The z_K-axis lies in the plane spanned by the x_K-axis and the local surface normal of WGS-84 reference ellipsoid, points downwards and is orthogonal to the x_K-axis. The index associated with the kinematic frame is K.

Since the x_K-axis points in the direction of the *kinematic* velocity, the latter velocity has an exceptionally simple representation in the kinematic frame.

The orientation of the kinematic frame with respect to the body-fixed frame is specified with the help of the flight-path angle-of-attack α_K^R, the flight-path angle-of-sideslip

β_K^R and the flight-path bank angle μ_K^R. The rotation matrix which transforms a vector from the kinematic frame to the body-fixed frame is given by:

$$\boldsymbol{M}_{BK} = \begin{bmatrix} \cos\alpha_K^R & 0 & -\sin\alpha_K^R \\ 0 & 1 & 0 \\ \sin\alpha_K^R & 0 & \cos\alpha_K^R \end{bmatrix} \cdot \begin{bmatrix} \cos\beta_K^R & -\sin\beta_K^R & 0 \\ \sin\beta_K^R & \cos\beta_K^R & 0 \\ 0 & 0 & 1 \end{bmatrix} \cdot \begin{bmatrix} 1 & 0 & 0 \\ 0 & \cos\mu_K^R & \sin\mu_K^R \\ 0 & -\sin\mu_K^R & \cos\mu_K^R \end{bmatrix}. \quad (2.2)$$

Modified Kinematic Frame

The modified kinematic frame is similar to the kinematic frame. It is however rotated by the flight-path bank angle μ_K^R around the x_K-axis. The index associated with the modified kinematic frame is $\bar{K}$. The rotation matrix which transforms a vector from the modified kinematic frame to the body-fixed frame is given by:

$$\boldsymbol{M}_{B\bar{K}} = \begin{bmatrix} \cos\alpha_K^R & 0 & -\sin\alpha_K^R \\ 0 & 1 & 0 \\ \sin\alpha_K^R & 0 & \cos\alpha_K^R \end{bmatrix} \cdot \begin{bmatrix} \cos\beta_K^R & -\sin\beta_K^R & 0 \\ \sin\beta_K^R & \cos\beta_K^R & 0 \\ 0 & 0 & 1 \end{bmatrix}. \quad (2.3)$$

Aerodynamic Frame

The aerodynamic frame is conceptually similar to the modified kinematic frame $\bar{K}$. Its origin is the reference point R of the aircraft. In contrast to the modified kinematic frame $\bar{K}$, the x_A-axis however points in the direction of the *aerodynamic* velocity.

The y_K-axis points right and completes an orthonormal right-hand system. The z_A-axis lies in the plane spanned by the x_B-axis and the z_B-axis, points downwards and is orthogonal to the x_A-axis. The index associated with the aerodynamic frame is A.

Since the x_A-axis points in the direction of the *aerodynamic* velocity, the latter velocity has an exceptional simple representation in the aerodynamic frame.

The orientation of the aerodynamic frame with respect to the body-fixed frame is specified with the help of the aerodynamic angle-of-attack α_A^R and the aerodynamic angle-of-sideslip β_A^R. The rotation matrix which transforms a vector from the aerodynamic frame to the body-fixed frame is given by:

$$\boldsymbol{M}_{BA} = \begin{bmatrix} \cos\alpha_A^R & 0 & -\sin\alpha_A^R \\ 0 & 1 & 0 \\ \sin\alpha_A^R & 0 & \cos\alpha_A^R \end{bmatrix} \cdot \begin{bmatrix} \cos\beta_A^R & -\sin\beta_A^R & 0 \\ \sin\beta_A^R & \cos\beta_A^R & 0 \\ 0 & 0 & 1 \end{bmatrix}. \quad (2.4)$$

Nomenclature

In addition to the definitions of the reference frames, a rigorous nomenclature for specifying vectors in these frames is required. The nomenclature is specific to the type of vector, i.e. depends on whether the vector represents a position, a velocity, etc. It is introduced by means of an example for any relevant vector type.

The position of a point G relative to the origin of the body-fixed (B) frame, denoted in the body-fixed (B) frame, is given by

$$\left(\vec{\boldsymbol{r}}^G\right)_B = \begin{bmatrix} x^G \\ y^G \\ z^G \end{bmatrix}_B. \quad (2.5)$$

Likewise, the position of a point P relative to a point G is specified as

$$\left(\vec{\boldsymbol{r}}^{GP}\right)_B = \left(\vec{\boldsymbol{r}}^{P}\right)_B - \left(\vec{\boldsymbol{r}}^{G}\right)_B = \begin{bmatrix} x^{GP} \\ y^{GP} \\ z^{GP} \end{bmatrix}_B . \tag{2.6}$$

For the differentiation of a vector, the so-called *Euler differentiation* will be frequently used, which allows the differentiation of a vector, noted in a reference frame B, with respect to another reference frame A. In case of the position vector $\left(\vec{\boldsymbol{r}}^{G}\right)_B$, the Euler differentiation with respect to a reference frame A is defined as [20]

$$\left(\frac{d}{dt}\right)^A \left(\vec{\boldsymbol{r}}^{G}\right)_B = \left(\dot{\vec{\boldsymbol{r}}}^{G}\right)_B^A \triangleq \left(\dot{\vec{\boldsymbol{r}}}^{G}\right)_B^B + \left(\vec{\boldsymbol{\omega}}^{AB}\right)_B \times \left(\vec{\boldsymbol{r}}^{G}\right)_B , \tag{2.7}$$

where $\left(\vec{\boldsymbol{\omega}}^{AB}\right)_B$ denotes the angular rate between the reference frames A and B (see below). The frame, with respect to which is differentiated, is indicated by the upper right index of the derivative $\dot{\vec{\boldsymbol{r}}}$ as well as the upper right index of the differential operator $(d/dt)^A$.

The kinematic (K) velocity of a point R relative to the ECEF (E) frame, denoted in the body-fixed (B) frame, is written as

$$\left(\vec{\boldsymbol{V}}_K^R\right)_B^E = \left(\frac{d}{dt}\right)^E \left(\vec{\boldsymbol{r}}^{R}\right)_B = \begin{bmatrix} u_K^R \\ v_K^R \\ w_K^R \end{bmatrix}_B^E . \tag{2.8}$$

Notice that the lower left index K indicates a kinematic velocity, but does not state that the velocity is given in the kinematic frame. Other types of velocities are aerodynamic (A) or wind (W). The upper right index E indicates that the Euler differentiation is performed with respect to the ECEF frame.

The kinematic (K) acceleration of a point R denoted in the body-fixed (B) frame, is given by

$$\left(\dot{\vec{\boldsymbol{V}}}_K^R\right)_B^{EB} = \left(\frac{d}{dt}\right)^B \left(\vec{\boldsymbol{V}}_K^R\right)_B^E = \begin{bmatrix} \dot{u}_K^R \\ \dot{v}_K^R \\ \dot{w}_K^R \end{bmatrix}_B^{EB} . \tag{2.9}$$

The upper right index EB indicates that the velocity of a point, which is defined relative to the ECEF frame, is differentiated in the body-fixed (B) frame.

Angular rates specify the rotation of reference frames with respect to each other. The angular rate of the body-fixed (B) frame with respect to the inertial (I) frame, noted in the body-fixed (B) frame, is written as

$$\left(\vec{\boldsymbol{\omega}}^{IB}\right)_B = \begin{bmatrix} \omega_x^{IB} \\ \omega_y^{IB} \\ \omega_z^{IB} \end{bmatrix}_B . \tag{2.10}$$

The angular acceleration (the derivative of the angular rate $\left(\vec{\boldsymbol{\omega}}^{IB}\right)_B$) with respect to the NED (O) frame is denoted as

$$\left(\dot{\vec{\boldsymbol{\omega}}}^{IB}\right)_B^O = \left(\frac{d}{dt}\right)^O \left(\vec{\boldsymbol{\omega}}^{IB}\right)_B = \begin{bmatrix} \dot{\omega}_x^{IB} \\ \dot{\omega}_y^{IB} \\ \dot{\omega}_z^{IB} \end{bmatrix}_B^O . \tag{2.11}$$

As before, the differential operator $(d/dt)^O$ indicates that the differentiation is actually performed in the NED (O) frame.

The total (T) force, which applies in the point G, noted in the body-fixed (B) frame, is written as

$$\left(\vec{\boldsymbol{F}}_T^G\right)_B = \begin{bmatrix} X_T^G \\ X_T^G \\ X_T^G \end{bmatrix}_B . \tag{2.12}$$

Similarly, the total (T) moment relative to the point R, noted in the body-fixed (B) frame, is denoted as

$$\left(\vec{\boldsymbol{M}}_T^R\right)_B = \begin{bmatrix} L_T^R \\ M_T^R \\ N_T^R \end{bmatrix}_B . \tag{2.13}$$

2.1.2 Equations of Motion

This section summarizes the EOMs of an aircraft, when assuming a rigid body with a quasi-stationary (distribution of) mass.

Translation

The EOMs of the translational motion derive from the law of conservation of translational momentum. According to [83], the translational EOMs of the point R are given by:

$$\begin{aligned} \left(\dot{\vec{\boldsymbol{V}}}_K^R\right)_B^{EB} = \frac{\left(\vec{\boldsymbol{F}}_T^G\right)_B}{m} &- \left(\vec{\boldsymbol{\omega}}^{EB}\right)_B \times \left(\vec{\boldsymbol{V}}_K^R\right)_B^E - 2 \cdot \left(\vec{\boldsymbol{\omega}}^{IE}\right)_B \times \left(\vec{\boldsymbol{V}}_K^R\right)_B^E \\ &- \left(\vec{\boldsymbol{\omega}}^{IE}\right)_B \times \left[\left(\vec{\boldsymbol{\omega}}^{IE}\right)_B \times \left(\vec{\boldsymbol{r}}^R\right)_B\right] \\ &- \left(\dot{\vec{\boldsymbol{\omega}}}^{IB}\right)_B^B \times \left(\vec{\boldsymbol{r}}^{RG}\right)_B - \left(\vec{\boldsymbol{\omega}}^{IB}\right)_B \times \left[\left(\vec{\boldsymbol{\omega}}^{IB}\right)_B \times \left(\vec{\boldsymbol{r}}^{RG}\right)_B\right], \end{aligned} \tag{2.14}$$

where m denotes the quasi-constant mass of the UAS, i.e. $\dot{m} \approx 0$, and G denotes the center of gravity.

In (2.14), the rotations of the body-fixed frame with respect to the inertial frame $\left(\vec{\boldsymbol{\omega}}^{IB}\right)$ and of the body-fixed frame with respect to the ECEF frame $\left(\vec{\boldsymbol{\omega}}^{EB}\right)$ appear. They are related by

$$\left(\vec{\boldsymbol{\omega}}^{IB}\right) = \left(\vec{\boldsymbol{\omega}}^{IE}\right) + \left(\vec{\boldsymbol{\omega}}^{EB}\right). \tag{2.15}$$

Rotation

The EOMs of the rotational motion derive from the law of conservation of rotational momentum. According to [83], they are given by:

$$\begin{aligned}\left(\boldsymbol{I}^R\right)_B \left(\dot{\vec{\boldsymbol{\omega}}}^{IB}\right)_B^B = \left(\vec{\boldsymbol{M}}_T^R\right)_B &- \left(\vec{\boldsymbol{\omega}}^{IB}\right)_B \times \left[\left(\boldsymbol{I}^R\right)_B \cdot \left(\vec{\boldsymbol{\omega}}^{IB}\right)_B\right] \\ &- m \cdot \left(\vec{\boldsymbol{r}}^{RG}\right)_B \times \left[\left(\dot{\vec{\boldsymbol{V}}}_K^R\right)_B^{EB} + \left(\vec{\boldsymbol{\omega}}^{EB}\right)_B \times \left(\vec{\boldsymbol{V}}_K^R\right)_B^E\right] \\ &- m \cdot \left(\vec{\boldsymbol{r}}^{RG}\right)_B \times \left[2 \cdot \left(\vec{\boldsymbol{\omega}}^{IE}\right)_B \times \left(\vec{\boldsymbol{V}}_K^R\right)_B^E\right] \\ &- m \cdot \left(\vec{\boldsymbol{r}}^{RG}\right)_B \times \left[\left(\vec{\boldsymbol{\omega}}^{IE}\right)_B \times \left[\left(\vec{\boldsymbol{\omega}}^{IE}\right)_B \times \left(\vec{\boldsymbol{r}}^R\right)_B\right]\right],\end{aligned} \tag{2.16}$$

where $\left(\boldsymbol{I}^R\right)_B$ denotes the quasi-constant inertia tensor with respect to the reference point R, given in body-fixed coordinates.

Attitude

The attitude of an aircraft is determined by the relative attitude of the body-fixed frame relative to the NED frame. In order to specify the relative attitude between these two frames, various representations such as Euler angles, quaternions, etc. have been proposed (see for example [154]). For reasons of simplicity, the Euler angles Φ, Θ, Ψ as defined in Section 2.1.1 are chosen here. The time derivatives of the Euler angles relate to the angular rate $\left(\vec{\boldsymbol{\omega}}^{OB}\right)_B$ by

$$\begin{bmatrix}\dot{\Phi}\\ \dot{\Theta}\\ \dot{\Psi}\end{bmatrix} = \begin{bmatrix}1 & \sin\Phi\tan\Theta & \cos\Phi\tan\Theta\\ 0 & \cos\Phi & -\sin\Phi\\ 0 & \frac{\sin\Phi}{\cos\Theta} & \frac{\cos\Phi}{\cos\Theta}\end{bmatrix} \cdot \left(\vec{\boldsymbol{\omega}}^{OB}\right)_B, \tag{2.17}$$

(see for example [20]). The angular rate $\left(\vec{\boldsymbol{\omega}}^{OB}\right)$ relates to $\left(\vec{\boldsymbol{\omega}}^{IB}\right)$ by

$$\begin{aligned}\left(\vec{\boldsymbol{\omega}}^{OB}\right) &= \left(\vec{\boldsymbol{\omega}}^{EB}\right) - \left(\vec{\boldsymbol{\omega}}^{EO}\right) \\ &= \left(\vec{\boldsymbol{\omega}}^{IB}\right) - \left(\vec{\boldsymbol{\omega}}^{IE}\right) - \left(\vec{\boldsymbol{\omega}}^{EO}\right).\end{aligned} \tag{2.18}$$

Position

Similar to the attitude, the position of an aircraft may be represented in several ways. For a short-range UAS, a local positioning with respect to some fixed point on the Earth may be sufficient. For a long-range UAS, a position representation with respect to the ECEF frame is however more appropriate. Such a representation is also considered here.

The position in the ECEF frame could be represented in Cartesian coordinates. In practice, a representation in terms of geodetic latitude μ, geodetic longitude λ and height h is however more intuitive. Such a representation requires a model of the shape of the Earth's surface. To that end, the WGS-84 model is underlain, which models the Earth as an ellipsoid. The parameters of this ellipsoid are specified in Table 2.1.

Description	Symbol	Value
Semi-major axis	a	6378137.0 m
Semi-minor axis	b	$b = a \cdot (1 - f)$
Flattening	f	$f = \frac{a-b}{a} = \frac{1}{298.257223563}$
Excentricity	e	$e = \sqrt{f \cdot (2 - f)}$
Normal curvature radius	$N(\mu)$	$N(\mu) = \frac{a}{\sqrt{1-e^2 \sin^2 \mu}}$
Meridian curvature radius	$M(\mu)$	$M(\mu) = \frac{a\left(1-e^2\right)}{\sqrt{\left(1-e^2 \sin^2 \mu\right)^3}}$

Table 2.1: Parameters of the WGS-84 Earth Model according to [50, 173].

In order to obtain a relation between the kinematic velocity $\left(\vec{\boldsymbol{V}}_K^R\right)_B^E$ and the rate of change of latitude μ, longitude λ and height h, the kinematic velocity is first transformed to the NED frame by $\left(\vec{\boldsymbol{V}}_K^R\right)_O^E = \boldsymbol{M}_{OB} \cdot \left(\vec{\boldsymbol{V}}_K^R\right)_B^E$. The components of the vector $\left(\vec{\boldsymbol{V}}_K^R\right)_O^E$ are denoted by

$$\left(\vec{\boldsymbol{V}}_K^R\right)_O^E \triangleq \begin{bmatrix} V_N \\ V_E \\ V_D \end{bmatrix}_O^E . \tag{2.19}$$

According to [173], the position differential equations are then given by

$$\begin{aligned} \dot{\lambda} &= \frac{V_E}{(N(\mu) + h) \cdot \cos \mu}, \\ \dot{\mu} &= \frac{V_N}{M(\mu) + h}, \\ \dot{h} &= -V_D, \end{aligned} \tag{2.20}$$

where $N(\mu)$ and $M(\mu)$ are defined in Table 2.1.

Alternative Representations

While the above EOMs fully describe the motion of the UAS, an alternative representation of the kinematic velocity $\left(\vec{\boldsymbol{V}}_K^R\right)^E$ is sometimes more convenient as it allows a more intuitive understanding of the aircraft motion. The kinematic velocity $\left(\vec{\boldsymbol{V}}_K^R\right)_B^E$, given in the body-fixed (B) frame, is more conveniently described in terms of the absolute velocity V_K^R, the flight-path angle-of-attack α_K^R and the flight-path angle-of-sideslip β_K^R. When denoting the components of $\left(\vec{\boldsymbol{V}}_K^R\right)_B^E$ by u_K, v_K, w_K, the relations

$$V_K^R = \sqrt{u_K^2 + v_K^2 + w_K^2}, \tag{2.21}$$

Control Surface	Primary Influence	Symbol	Lower Deflection Limit [°]	Upper Deflection Limit [°]	Rate Limit [$^\circ/s$]
Elevator	y_B-axis	η	-30	30	100
Aileron	x_B-axis	ξ	-30	30	100
Rudder	z_B-axis	ζ	-25	25	100

Table 2.2: Summary of the control surfaces, their axis of primary influence and their limits.

$$\alpha_K^R = \arctan_2\left(\frac{w_K}{u_K}\right), \tag{2.22}$$

$$\beta_K^R = \arcsin\left(\frac{v_K}{\sqrt{u_K^2 + v_K^2 + w_K^2}}\right) \tag{2.23}$$

hold [20].

Forces and Moments

The total forces and moments $\left(\vec{\boldsymbol{F}}_T^G\right)$ and $\left(\vec{\boldsymbol{M}}_T^R\right)$ acting on the aircraft can be divided into three groups. The first group are the forces and moments due to gravity, which are denoted by $\left(\vec{\boldsymbol{F}}_G^G\right)$ and $\left(\vec{\boldsymbol{M}}_G^R\right)$.

The second group are the forces and moments due to the propulsion system, which are denoted by $\left(\vec{\boldsymbol{F}}_P^G\right)$ and $\left(\vec{\boldsymbol{M}}_P^R\right)$. The propulsion forces and moments may be influenced by the control system with the help of the trust lever position δT, which is assumed to be normalized to the range from 0 to 1.

The third group are the forces and moments due to the aerodynamics, which are denoted by $\left(\vec{\boldsymbol{F}}_A^G\right)$ and $\left(\vec{\boldsymbol{M}}_A^R\right)$. The size of these forces and moments strongly depends on the aerodynamic velocity $\left(\vec{\boldsymbol{V}}_A^R\right)^E$, which relates to the kinematic velocity $\left(\vec{\boldsymbol{V}}_K^R\right)^E$ and the wind speed $\left(\vec{\boldsymbol{V}}_W^R\right)^E$ by

$$\left(\vec{\boldsymbol{V}}_A^R\right)^E \triangleq \left(\vec{\boldsymbol{V}}_K^R\right)^E - \left(\vec{\boldsymbol{V}}_W^R\right)^E. \tag{2.24}$$

The flight control system may influence the aerodynamic forces and moments by appropriate deflections of the control surfaces, namely the elevator η, the aileron ξ and the rudder ζ. A positive deflection of these control surfaces is defined such that it leads to a negative rotation around the primarily influenced axis, which is specified in Table 2.2. Furthermore, Table 2.2 also summarizes the control surface limitations.

The total forces and moments $\left(\vec{\boldsymbol{F}}_T^G\right)$ and $\left(\vec{\boldsymbol{M}}_T^R\right)$, which act on the aircraft, hence result from

$$\left(\vec{\boldsymbol{F}}_T^G\right) = \left(\vec{\boldsymbol{F}}_G^G\right) + \left(\vec{\boldsymbol{F}}_P^G\right) + \left(\vec{\boldsymbol{F}}_A^G\right), \tag{2.25}$$

$$\left(\vec{\boldsymbol{M}}_T^R\right) = \left(\vec{\boldsymbol{M}}_G^R\right) + \left(\vec{\boldsymbol{M}}_P^R\right) + \left(\vec{\boldsymbol{M}}_A^R\right). \tag{2.26}$$

According to [20], the specific force, which sums up all forces except gravity, is defined as:

$$\left(\vec{\boldsymbol{f}}^G\right) \triangleq \frac{\left(\vec{\boldsymbol{F}}_T^G\right) - \left(\vec{\boldsymbol{F}}_G^G\right)}{m} = \frac{\left(\vec{\boldsymbol{F}}_P^G\right) + \left(\vec{\boldsymbol{F}}_A^G\right)}{m}. \tag{2.27}$$

Since the details of the UAS model may not be published here, further details on the exact modeling of forces and moments are omitted.

Output Equations

The previously presented EOMs model the translational and rotational motion of the aircraft. The EOMs lead to a state space model with twelve states. For the purpose of control, these states (or appropriate transformations of these states) have to be measured. This section introduces the nonlinear output equations, which relate the states of the EOMs to the measurement outputs, if ideal sensors and ideal processing units for the sensor data were used. The actual sensor model, which leads to a distortion of these ideal read-outs, is not considered here.

As measurement devices, the considered UAS features an Inertial Measurement Unit (IMU), pitot tubes for static and dynamic pressure measurements and a Global Positioning System (GPS). The IMU data are processed by the AHRS. The ideal outputs of the AHRS are given by:

- the angular rates $\left(\vec{\boldsymbol{\omega}}^{IB}\right)_B$, given in body-fixed coordinates;
- the Euler angles Φ, Θ, Ψ;
- the specific force $\left(\vec{\boldsymbol{f}}^M\right)_B$ at the mounting point M of the IMU divided by the gravitational acceleration g, given in body-fixed coordinates:

$$\begin{aligned}\left(\vec{\boldsymbol{b}}^M\right)_B \triangleq \frac{\left(\vec{\boldsymbol{f}}^M\right)_B}{g} = \frac{\left(\vec{\boldsymbol{f}}^G\right)_B}{g} &+ \frac{\left(\dot{\vec{\boldsymbol{\omega}}}^{IB}\right)_B^B \times \left(\vec{\boldsymbol{r}}^{GM}\right)_B}{g} \\ &+ \frac{\left(\vec{\boldsymbol{\omega}}^{IB}\right)_B \times \left[\left(\vec{\boldsymbol{\omega}}^{IB}\right)_B \times \left(\vec{\boldsymbol{r}}^{GM}\right)_B\right]}{g}.\end{aligned} \tag{2.28}$$

In (2.28), the additional cross products account for the centrifugal and Euler accelerations of the IMU due to the rotation of the mounting point M relative to the center of gravity G.

Later on, the output equation (2.28) has to be linearized. The linearization simplifies significantly by deriving a kinematic relation for the output $\left(\vec{\boldsymbol{b}}^M\right)$. To that end, insert the

definition of the specific force (2.27) into the translational EOMs and solve for $\left(\vec{\boldsymbol{f}}^{G}\right)$, which yields:

$$\begin{aligned}\left(\vec{\boldsymbol{f}}^{G}\right)_{B} = \left(\dot{\vec{\boldsymbol{V}}}_{K}^{R}\right)_{B}^{EB} &- \left(\vec{\boldsymbol{g}}^{G}\right)_{B} + \left(\vec{\boldsymbol{\omega}}^{EB}\right)_{B} \times \left(\vec{\boldsymbol{V}}_{K}^{R}\right)_{B}^{E} + 2 \cdot \left(\vec{\boldsymbol{\omega}}^{IE}\right)_{B} \times \left(\vec{\boldsymbol{V}}_{K}^{R}\right)_{B}^{E} \\ &+ \left(\vec{\boldsymbol{\omega}}^{IE}\right)_{B} \times \left[\left(\vec{\boldsymbol{\omega}}^{IE}\right)_{B} \times \left(\vec{\boldsymbol{r}}^{R}\right)_{B}\right] \\ &+ \left(\dot{\vec{\boldsymbol{\omega}}}^{IB}\right)_{B}^{B} \times \left(\vec{\boldsymbol{r}}^{RG}\right)_{B} + \left(\vec{\boldsymbol{\omega}}^{IB}\right)_{B} \times \left[\left(\vec{\boldsymbol{\omega}}^{IB}\right)_{B} \times \left(\vec{\boldsymbol{r}}^{RG}\right)_{B}\right],\end{aligned} \tag{2.29}$$

where $\left(\vec{\boldsymbol{g}}^{G}\right) = \left(\vec{\boldsymbol{F}}_{G}^{G}\right)/m$ denotes the gravitational acceleration. Inserting the result into the output equation (2.28) leads to the kinematic relation

$$\begin{aligned}\left(\vec{\boldsymbol{b}}^{M}\right)_{B} = \frac{\left(\dot{\vec{\boldsymbol{V}}}_{K}^{R}\right)_{B}^{EB}}{g} &+ \frac{-\left(\vec{\boldsymbol{g}}^{G}\right)_{B} + \left(\vec{\boldsymbol{\omega}}^{EB}\right)_{B} \times \left(\vec{\boldsymbol{V}}_{K}^{R}\right)_{B}^{E} + 2 \cdot \left(\vec{\boldsymbol{\omega}}^{IE}\right)_{B} \times \left(\vec{\boldsymbol{V}}_{K}^{R}\right)_{B}^{E}}{g} \\ &+ \frac{\left(\vec{\boldsymbol{\omega}}^{IE}\right)_{B} \times \left[\left(\vec{\boldsymbol{\omega}}^{IE}\right)_{B} \times \left(\vec{\boldsymbol{r}}^{R}\right)_{B}\right]}{g} \\ &+ \frac{\left(\dot{\vec{\boldsymbol{\omega}}}^{IB}\right)_{B}^{B} \times \left(\vec{\boldsymbol{r}}^{RM}\right)_{B} + \left(\vec{\boldsymbol{\omega}}^{IB}\right)_{B} \times \left[\left(\vec{\boldsymbol{\omega}}^{IB}\right)_{B} \times \left(\vec{\boldsymbol{r}}^{RM}\right)_{B}\right]}{g}.\end{aligned} \tag{2.30}$$

The measurements of the pitot tubes are processed by the Air Data System (ADS). Assuming wind-free conditions, the ideal outputs of the ADS are:

- the absolute value of the kinematic velocity V_K^R;
- the flight-path angle-of-attack α_K^R;
- the flight-path angle-of-sideslip β_K^R.

In addition to these quantities, the ADS also yields further estimates such as barometric height, which are however not relevant for the control tasks to be presented later on.

The GPS yields estimates of the position of the aircraft in WGS-84 coordinates as well as an estimate of the kinematic velocity $\left(\vec{\boldsymbol{V}}_{K}^{R}\right)_{O}^{E}$. In ideal conditions, these estimates correspond to the true position and the true kinematic velocity.

2.1.3 Linearized Equations of Motion

For the development of a controller, the nonlinear EOMs are linearized. The linearization assumes wind-free conditions, i.e. $\left(\vec{\boldsymbol{V}}_{W}^{R}\right)^{E} = \boldsymbol{0}$. Hence, (2.24) implies that the kinematic velocity $\left(\vec{\boldsymbol{V}}_{K}^{R}\right)^{E}$ equals the aerodynamic velocity $\left(\vec{\boldsymbol{V}}_{A}^{R}\right)^{E}$.

Since the translational EOMs depend on the derivatives of the rotational EOMs and vice versa, the EOMs may be generally written as implicit differential equations:

$$\begin{aligned}\boldsymbol{f}\left(\boldsymbol{x}, \dot{\boldsymbol{x}}, \boldsymbol{u}\right) &= \boldsymbol{0}, \\ \boldsymbol{y} &= \boldsymbol{h}\left(\boldsymbol{x}, \dot{\boldsymbol{x}}, \boldsymbol{u}\right).\end{aligned} \tag{2.31}$$

In (2.31), the state, input and output vectors are defined as

$$\begin{aligned}\boldsymbol{x}^T \triangleq \Big[&\left(u_K^R\right)_B^E \quad \left(v_K^R\right)_B^E \quad \left(w_K^R\right)_B^E \quad \left(\omega_x^{IB}\right)_B \quad \left(\omega_y^{IB}\right)_B \quad \left(\omega_z^{IB}\right)_B \quad \Phi \quad \Theta \quad \Psi \quad \dots \\ &\lambda \quad \mu \quad h\Big]\end{aligned} \tag{2.32}$$

$$\boldsymbol{u}^T \triangleq \begin{bmatrix}\delta T & \eta & \xi & \zeta\end{bmatrix}, \tag{2.33}$$

$$\begin{aligned}\boldsymbol{y}^T \triangleq \Big[&V_K^R \quad \alpha_K^R \quad \beta_K^R \quad \left(\omega_x^{IB}\right)_B \quad \left(\omega_y^{IB}\right)_B \quad \left(\omega_z^{IB}\right)_B \quad \Phi \quad \Theta \quad \Psi \quad \dots \\ &\lambda \quad \mu \quad h \quad \left(b_x^M\right)_B \quad \left(b_y^M\right)_B \quad \left(b_z^M\right)_B\Big].\end{aligned} \tag{2.34}$$

All elements of the state vector $\boldsymbol{x}$ are given in m/s, rad/s, rad and m, respectively. The first element δT of the input vector $\boldsymbol{u}$ is normalized and dimensionless, whereas the other control surfaces are given in rad. The convention for units of the output vector corresponds to the convention of the state vector, except for the components $\left(b_x^M\right)_B$, $\left(b_y^M\right)_B$, $\left(b_z^M\right)_B$, which are normalized and hence, dimensionless.

For the linearization of the implicit differential equation (2.31), a trim condition $\boldsymbol{x}_0$, $\boldsymbol{u}_0$ has to be determined first, such that

$$\boldsymbol{f}\left(\boldsymbol{x}_0, \dot{\boldsymbol{x}}_{des,0}, \boldsymbol{u}_0\right) = \boldsymbol{0}, \tag{2.35}$$

holds. In (2.35), the vector $\dot{\boldsymbol{x}}_{des,0}$ specifies the desired derivatives of the state vector, i.e. $\dot{\boldsymbol{x}}$ should be equivalent to $\dot{\boldsymbol{x}}_{des,0}$. For a steady-state horizontal flight, almost all elements of $\dot{\boldsymbol{x}}_{des,0}$ should be zero. However, since the aircraft is moving, the position may not be constant and hence, $\dot{\mu} = 0$, $\dot{\lambda} = 0$ may not be enforced. Roughly speaking, the trim condition (2.35) only requires relevant state vector derivatives to be zero.

Eq. (2.35) defines a nonlinear system of equations with the unknowns $\boldsymbol{x}_0$, $\boldsymbol{u}_0$. In general, this system of equations possesses an infinite number of solutions, which describe different flight conditions (such as level flight, steady climb, etc.). These solutions vary for example with altitude, velocity and the mass of the aircraft. The trim condition, which is specifically considered subsequently, is steady-state, horizontal flight at a given altitude $h = h_0$, a given kinematic velocity $V_K^R = V_0$ and a given fuel mass $m_{fuel} = m_{fuel,0}$. The altitude h_0 and the velocity V_0 immediately constrain the states of the aircraft. In contrast, the fuel mass $m_{fuel,0}$ does not constrain any states. It nevertheless influences the solutions of the nonlinear system of equations (2.35) as it implies an alteration of the total mass m of the aircraft, of the position of the center of gravity G and of the inertia tensor $\boldsymbol{I}^R$.

The nonlinear system of equations (2.35) may be solved numerically. Once a trim condition $\boldsymbol{x}_0$, $\boldsymbol{u}_0$ has been determined, the EOMs (2.31) are linearized. To that end, the Taylor series expansions of $\boldsymbol{f}\left(\boldsymbol{x}, \dot{\boldsymbol{x}}, \boldsymbol{u}\right)$ and $\boldsymbol{h}\left(\boldsymbol{x}, \dot{\boldsymbol{x}}, \boldsymbol{u}\right)$ are computed:

$$\boldsymbol{f}\left(\boldsymbol{x}, \dot{\boldsymbol{x}}, \boldsymbol{u}\right) \approx \underbrace{\boldsymbol{f}\left(\boldsymbol{x}_0, \dot{\boldsymbol{x}}_{des,0}, \boldsymbol{u}_0\right)}_{\boldsymbol{0}} + \left.\frac{\partial \boldsymbol{f}\left(\boldsymbol{x}, \dot{\boldsymbol{x}}, \boldsymbol{u}\right)}{\partial \dot{\boldsymbol{x}}}\right|_0 \cdot \left(\dot{\boldsymbol{x}} - \dot{\boldsymbol{x}}_{des,0}\right)$$

$$+ \left.\frac{\partial \boldsymbol{f}\left(\boldsymbol{x}, \dot{\boldsymbol{x}}, \boldsymbol{u}\right)}{\partial \boldsymbol{x}}\right|_0 \cdot \left(\boldsymbol{x} - \boldsymbol{x}_0\right) \tag{2.36}$$
$$+ \left.\frac{\partial \boldsymbol{f}\left(\boldsymbol{x}, \dot{\boldsymbol{x}}, \boldsymbol{u}\right)}{\partial \boldsymbol{u}}\right|_0 \cdot \left(\boldsymbol{u} - \boldsymbol{u}_0\right)$$

as well as

$$\begin{aligned}\boldsymbol{h}\left(\boldsymbol{x}, \dot{\boldsymbol{x}}, \boldsymbol{u}\right) \approx \boldsymbol{h}\left(\boldsymbol{x}_0, \dot{\boldsymbol{x}}_{des,0}, \boldsymbol{u}_0\right) &+ \left.\frac{\partial \boldsymbol{h}\left(\boldsymbol{x}, \dot{\boldsymbol{x}}, \boldsymbol{u}\right)}{\partial \dot{\boldsymbol{x}}}\right|_0 \cdot \left(\dot{\boldsymbol{x}} - \dot{\boldsymbol{x}}_{des,0}\right) \\ &+ \left.\frac{\partial \boldsymbol{h}\left(\boldsymbol{x}, \dot{\boldsymbol{x}}, \boldsymbol{u}\right)}{\partial \boldsymbol{x}}\right|_0 \cdot \left(\boldsymbol{x} - \boldsymbol{x}_0\right) \\ &+ \left.\frac{\partial \boldsymbol{h}\left(\boldsymbol{x}, \dot{\boldsymbol{x}}, \boldsymbol{u}\right)}{\partial \boldsymbol{u}}\right|_0 \cdot \left(\boldsymbol{u} - \boldsymbol{u}_0\right).\end{aligned} \tag{2.37}$$

Assuming that the Jacobian matrix $\partial \boldsymbol{f}\left(\boldsymbol{x}, \dot{\boldsymbol{x}}, \boldsymbol{u}\right) / \partial \dot{\boldsymbol{x}} \mid_0$ is regular, the explicit linearized state space model

$$\delta \dot{\boldsymbol{x}} = \boldsymbol{A} \cdot \delta \boldsymbol{x} + \boldsymbol{B} \cdot \delta \boldsymbol{u} + \dot{\boldsymbol{x}}_{des,0} \tag{2.38}$$
$$\delta \boldsymbol{y} = \boldsymbol{C} \cdot \delta \boldsymbol{x} + \boldsymbol{D} \cdot \delta \boldsymbol{u} \tag{2.39}$$

with

$$\delta \boldsymbol{x} = \boldsymbol{x} - \boldsymbol{x}_0, \qquad \delta \boldsymbol{u} = \boldsymbol{u} - \boldsymbol{u}_0, \qquad \delta \boldsymbol{y} = \boldsymbol{y} - \boldsymbol{h}\left(\boldsymbol{x}_0, \dot{\boldsymbol{x}}_{des,0}, \boldsymbol{u}_0\right) \tag{2.40}$$

and

$$\boldsymbol{A} = \left(-\left.\frac{\partial \boldsymbol{f}\left(\boldsymbol{x}, \dot{\boldsymbol{x}}, \boldsymbol{u}\right)}{\partial \dot{\boldsymbol{x}}}\right|_0\right)^{-1} \cdot \left.\frac{\partial \boldsymbol{f}\left(\boldsymbol{x}, \dot{\boldsymbol{x}}, \boldsymbol{u}\right)}{\partial \boldsymbol{x}}\right|_0, \tag{2.41}$$

$$\boldsymbol{B} = \left(-\left.\frac{\partial \boldsymbol{f}\left(\boldsymbol{x}, \dot{\boldsymbol{x}}, \boldsymbol{u}\right)}{\partial \dot{\boldsymbol{x}}}\right|_0\right)^{-1} \cdot \left.\frac{\partial \boldsymbol{f}\left(\boldsymbol{x}, \dot{\boldsymbol{x}}, \boldsymbol{u}\right)}{\partial \boldsymbol{u}}\right|_0, \tag{2.42}$$

$$\boldsymbol{C} = \left.\frac{\partial \boldsymbol{h}\left(\boldsymbol{x}, \dot{\boldsymbol{x}}, \boldsymbol{u}\right)}{\partial \dot{\boldsymbol{x}}}\right|_0 \cdot \boldsymbol{A} + \left.\frac{\partial \boldsymbol{h}\left(\boldsymbol{x}, \dot{\boldsymbol{x}}, \boldsymbol{u}\right)}{\partial \boldsymbol{x}}\right|_0, \tag{2.43}$$

$$\boldsymbol{D} = \left.\frac{\partial \boldsymbol{h}\left(\boldsymbol{x}, \dot{\boldsymbol{x}}, \boldsymbol{u}\right)}{\partial \dot{\boldsymbol{x}}}\right|_0 \cdot \boldsymbol{B} + \left.\frac{\partial \boldsymbol{h}\left(\boldsymbol{x}, \dot{\boldsymbol{x}}, \boldsymbol{u}\right)}{\partial \boldsymbol{u}}\right|_0. \tag{2.44}$$

follows. Notice that the presence of $\dot{\boldsymbol{x}}_{des,0}$ in (2.38) is not an error, but results from the fact that not all state vector derivatives may be forced to zero. As an example, consider once again the position of the aircraft. Since the aircraft is moving at a non-zero velocity, the position state needs to change constantly. At the same time, it follows from the definition of the state vector $\delta \boldsymbol{x}$ that the linearized position state represents the deviation of the aircraft position from that position, where the aircraft was trimmed. This position deviation does however stem from the absolute velocity of the aircraft, which is the sum of the velocity at the trim condition and the deviation of the velocity from the trim condition due to the aircraft movement. This fact manifests itself in the term $\dot{\boldsymbol{x}}_{des,0}$ in (2.38).

In practice, a velocity representation in terms of δV_K^R, $\delta \alpha_K^R$ and $\delta \beta_K^R$ is more intuitive as compared to $\delta \left(u_K^R\right)_B^E$, $\delta \left(v_K^R\right)_B^E$ and $\delta \left(w_K^R\right)_B^E$. However, in the linearized state space

model (2.38) and (2.39), δV_K^R, $\delta\alpha_K^R$ and $\delta\beta_K^R$ are only outputs. In order to turn these outputs into states, the similarity transformation $\delta\boldsymbol{x} = \boldsymbol{T}^{-1} \cdot \delta\bar{\boldsymbol{x}}$ is applied to (2.38) and (2.39). The transformation matrix $\boldsymbol{T}$ is defined as

$$\begin{bmatrix} \boldsymbol{T} \\ * \end{bmatrix} \triangleq \boldsymbol{C}, \tag{2.45}$$

where $\boldsymbol{T} \in \mathbb{R}^{12\times 12}$ is the upper block of the output matrix $\boldsymbol{C}$. The resulting state space model takes the form

$$\delta\dot{\bar{\boldsymbol{x}}} = \boldsymbol{T}\boldsymbol{A}\boldsymbol{T}^{-1} \cdot \delta\bar{\boldsymbol{x}} + \boldsymbol{T}\boldsymbol{B} \cdot \delta\boldsymbol{u}, \tag{2.46}$$

$$\boldsymbol{y} = \boldsymbol{C}\boldsymbol{T}^{-1} \cdot \delta\bar{\boldsymbol{x}} + \boldsymbol{D} \cdot \delta\boldsymbol{u}, \tag{2.47}$$

whose state vector now possesses the desired states:

$$\delta\bar{\boldsymbol{x}}^T = \begin{bmatrix} V_K^R & \alpha_K^R & \beta_K^R & \left(\omega_x^{IB}\right)_B & \left(\omega_y^{IB}\right)_B & \left(\omega_z^{IB}\right)_B & \Phi & \Theta & \Psi \end{bmatrix}. \tag{2.48}$$

When neglecting small influences such as

1. the influence of the position dynamics $\delta\dot{\mu}$, $\delta\dot{\lambda}$, $\delta\dot{h}$ on the other states,
2. cross-coupling terms between the longitudinal and lateral motion,
3. the influences due to the rotation of the Earth with $\left(\vec{\boldsymbol{\omega}}^{IE}\right)$,
4. the influences of the transport rate $\left(\vec{\boldsymbol{\omega}}^{EO}\right)$,
5. the dependence of the aerodynamic forces on the derivatives of α_K^R and β_K^R,

the state space model takes the form (2.49) [162]. The nomenclature for the coefficients of (2.49) does however slightly deviate from [162]: The coefficients $X_{(\cdot)}$ denote the partial derivatives of the acceleration $((X_A^R)_{\bar{K}} + (X_P^R)_{\bar{K}})/m$ resulting from the aerodynamic and propulsion forces ($(X_A^R)_{\bar{K}}$ and $(X_P^R)_{\bar{K}}$) with respect to the elements of the state vector $\boldsymbol{x}$. Similarly, $Y_{(\cdot)}$ and $Z_{(\cdot)}$ represent the partial derivatives of the angular velocities resulting from the aerodynamic and propulsion forces ($(Y_A^R)_{\bar{K}}$, $(Y_P^R)_{\bar{K}}$ and $(Z_A^R)_{\bar{K}}$, $(Z_P^R)_{\bar{K}}$). In a similar fashion, $L_{(\cdot)}$, $M_{(\cdot)}$, $N_{(\cdot)}$ denote the partial derivatives of the angular accelerations resulting from the aerodynamic moments ($(L_A^R)_B$, $(M_A^R)_B$, $(N_A^R)_B$) and the propulsion moments ($(L_P^R)_B$, $(M_P^R)_B$, $(N_P^R)_B$). As the inertia tensor $\left(\boldsymbol{I}^R\right)_B$ is usually not diagonal, the roll rate ω_x^{IB} does not only result from the roll moment $(L_T^R)_B$, but also from the yaw moment $(N_T^R)_B$. Thus, $L_{(\cdot)}$ summarizes the effects of both $(L_T^R)_B$ and $(N_T^R)_B$. Nevertheless, since the roll rate ω_x^{IB} is primarily influenced by the roll moment $(L_T^R)_B$, the partial derivatives influencing the roll motion are denoted by the letter $L_{(\cdot)}$. Similar arguments also apply to $M_{(\cdot)}$ and $N_{(\cdot)}$.

Furthermore, since the influence of the position on the other states is neglected, the position states have been removed in (2.49). Moreover, notice that Θ_0 denotes the pitch angle Θ in trim conditions, which is equivalent to the flight-path angle-of-attack α_K^R

$$
\frac{d}{dt}\begin{bmatrix} \delta V_K^R \\ \delta\alpha_K^R \\ \delta\beta_K^R \\ \delta\left(\omega_x^{IB}\right)_B \\ \delta\left(\omega_y^{IB}\right)_B \\ \delta\left(\omega_z^{IB}\right)_B \\ \delta\Phi \\ \delta\Theta \\ \delta\Psi \end{bmatrix} = \begin{bmatrix} X_V & X_\alpha + g & 0 & 0 & X_q & 0 & 0 & -g & 0 \\ Z_V & Z_\alpha & 0 & 0 & 1 + Z_q & 0 & 0 & 0 & 0 \\ 0 & 0 & Y_\beta & Y_p + \sin\Theta_0 & 0 & Y_r - \cos\Theta_0 & \frac{g}{V_0}\cos\Theta_0 & 0 & 0 \\ 0 & 0 & L_\beta & L_p & 0 & L_r & 0 & 0 & 0 \\ M_V & M_\alpha & 0 & 0 & M_q & 0 & 0 & 0 & 0 \\ 0 & 0 & N_\beta & N_p & 0 & N_r & 0 & 0 & 0 \\ 0 & 0 & 0 & 1 & 0 & \tan\Theta_0 & 0 & 0 & 0 \\ 0 & 0 & 0 & 0 & 1 & 0 & 0 & 0 & 0 \\ 0 & 0 & 0 & 0 & 0 & \frac{1}{\cos\Theta_0} & 0 & 0 & 0 \end{bmatrix} \cdot \begin{bmatrix} \delta V_K^R \\ \delta\alpha_K^R \\ \delta\beta_K^R \\ \delta\left(\omega_x^{IB}\right)_B \\ \delta\left(\omega_y^{IB}\right)_B \\ \delta\left(\omega_z^{IB}\right)_B \\ \delta\Phi \\ \delta\Theta \\ \delta\Psi \end{bmatrix} + \begin{bmatrix} X_{\delta T} & X_\eta & 0 & 0 \\ Z_{\delta T} & Z_\eta & 0 & 0 \\ 0 & 0 & Y_\xi & Y_\zeta \\ 0 & 0 & L_\xi & L_\zeta \\ M_{\delta T} & M_\eta & 0 & 0 \\ 0 & 0 & N_\xi & N_\zeta \\ 0 & 0 & 0 & 0 \\ 0 & 0 & 0 & 0 \\ 0 & 0 & 0 & 0 \end{bmatrix} \cdot \begin{bmatrix} \delta T \\ \delta\eta \\ \delta\xi \\ \delta\zeta \end{bmatrix}
$$

$$
\begin{bmatrix} \delta V_K^R \\ \delta\alpha_K^R \\ \delta\beta_K^R \\ \delta\left(\omega_x^{IB}\right)_B \\ \delta\left(\omega_y^{IB}\right)_B \\ \delta\left(\omega_z^{IB}\right)_B \\ \delta\Phi \\ \delta\Theta \\ \delta\Psi \\ \delta\left(b_y^M\right)_B \end{bmatrix} = \begin{bmatrix} 1 & 0 & 0 & 0 & 0 & 0 & 0 & 0 & 0 \\ 0 & 1 & 0 & 0 & 0 & 0 & 0 & 0 & 0 \\ 0 & 0 & 1 & 0 & 0 & 0 & 0 & 0 & 0 \\ 0 & 0 & 0 & 1 & 0 & 0 & 0 & 0 & 0 \\ 0 & 0 & 0 & 0 & 1 & 0 & 0 & 0 & 0 \\ 0 & 0 & 0 & 0 & 0 & 1 & 0 & 0 & 0 \\ 0 & 0 & 0 & 0 & 0 & 0 & 1 & 0 & 0 \\ 0 & 0 & 0 & 0 & 0 & 0 & 0 & 1 & 0 \\ 0 & 0 & 0 & 0 & 0 & 0 & 0 & 0 & 1 \\ 0 & 0 & F_{y,\beta} & F_{y,p} & 0 & F_{y,r} & 0 & 0 & 0 \end{bmatrix} \cdot \begin{bmatrix} \delta V_K^R \\ \delta\alpha_K^R \\ \delta\beta_K^R \\ \delta\left(\omega_x^{IB}\right)_B \\ \delta\left(\omega_y^{IB}\right)_B \\ \delta\left(\omega_z^{IB}\right)_B \\ \delta\Phi \\ \delta\Theta \\ \delta\Psi \end{bmatrix} + \begin{bmatrix} 0 & 0 & 0 & 0 \\ 0 & 0 & 0 & 0 \\ 0 & 0 & 0 & 0 \\ 0 & 0 & 0 & 0 \\ 0 & 0 & 0 & 0 \\ 0 & 0 & 0 & 0 \\ 0 & 0 & 0 & 0 \\ 0 & 0 & 0 & 0 \\ 0 & 0 & 0 & 0 \\ 0 & 0 & F_{y,\xi} & F_{y,\zeta} \end{bmatrix} \cdot \begin{bmatrix} \delta T \\ \delta\eta \\ \delta\xi \\ \delta\zeta \end{bmatrix} \tag{2.49}
$$

Control Surface	Eigenfrequency $\omega_{0,act}$ [rad/s]	Relative Damping ζ_{act}
Elevator, Aileron, Rudder	40.84	0.5

Table 2.3: Parameters of the second order model of the actuator dynamics.

in trim conditions. Finally, notice that only the output for the lateral normalized specific force is retained in (2.49) as only that output will be required for the controller development. A linearization of the output equation (2.30) leads to the output coefficients

$$F_{y,(\cdot)} = \frac{V_0}{g} \cdot Y_{(\cdot)} + \frac{\left(x^{RM}\right)_B}{g} \cdot N_{(\cdot)} - \frac{\left(z^{RM}\right)_B}{g} \cdot L_{(\cdot)}, \tag{2.50}$$

where $\left(x^{RM}\right)_B$ and $\left(z^{RM}\right)_B$ are the x- and z-components of the position of the IMU relative to the reference point R.

2.1.4 Aircraft Subsystem Models

The EOMs model the motion of the aircraft itself. They do, however, not model further dynamics such as the actuator dynamics, which also contribute to the overall aircraft dynamics from the perspective of a flight control system. Due to the actuation system, the actual control surface deflections (for example of the aileron ξ) lag behind their commands (for example ξ_{cmd}). Similarly, the measurement instruments aboard the aircraft also exhibit dynamic behavior. In principle, an accelerometer is for example a mass which is connected to the aircraft body through a spring and hence, constitutes a dynamic system. Further dynamics, which have to be considered, are for example time-delays due to the discrete-time processing and transmission of signals within the flight control system. Hence, this section introduces simple models of these additional dynamics.

The actuators of the control surfaces are modeled as second order lag (PT2) elements. All control surface actuators exhibit the same eigenfrequency and the same relative damping, which are specified in Table 2.3. Furthermore, the actuators also respect the deflection limits given by Table 2.2. The overall structure of the actuator model for the control surfaces is exemplary shown in Figure 2.3 in case of the aileron.

The on-board processing of signals and their discrete-time transmission is modeled as a delay τ_m of the measurement signals and as a delay τ_c of the actuator command signals. The sensor dynamics are not explicitly modeled as it is assumed that the phase lag due to the measurement delay leads to adverse effects at much lower frequencies

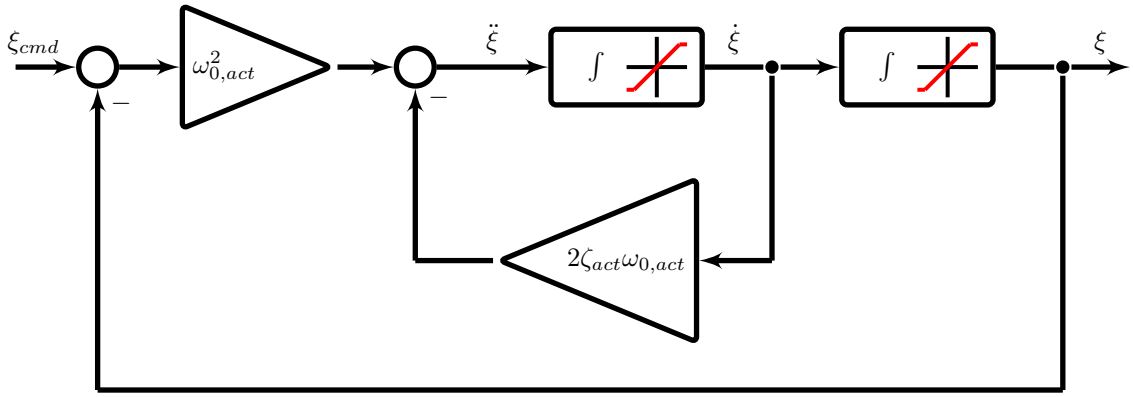

Figure 2.3: Second order model of the control surface actuator of the aileron with saturation of the deflection and the rate.

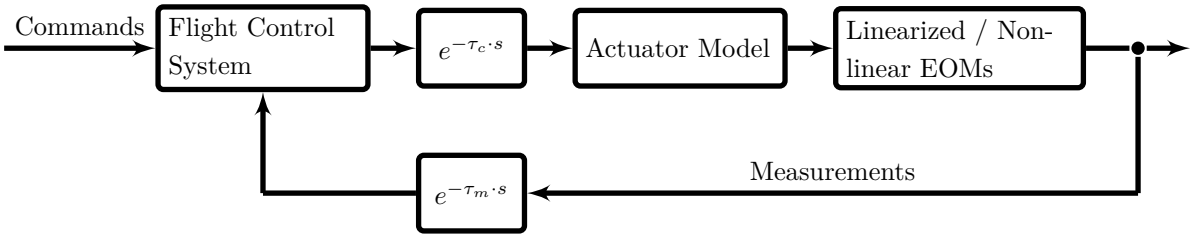

Figure 2.4: Overall control system model including the flight control system, delays, actuator models and the EOMs.

than the dynamics of the measurement devices. Further adverse effects of the sensors such as sensor bias, scaling errors, etc. are not considered either.

The overall control system structure including the flight control system to be developed, the actuator model, the delays and the EOMs is shown in Figure 2.4.

2.2 Control of the Short-Period Approximation

The first benchmark control problem considers the short-period approximation of the longitudinal motion of the UAS. The short-period approximation readily follows from the linearized EOMs (2.49).

The short-period benchmark control problem is used recurrently throughout this thesis in order to demonstrate the basic properties of different control approaches. In order to simplify these examples, the force generated by the elevator is neglected (i.e. $Z_\eta = 0$). Hence, the short-period approximation is given by

$$\begin{bmatrix} \dot{\alpha} \\ \dot{q} \end{bmatrix} = \begin{bmatrix} \lambda_{Z\alpha} \cdot Z_\alpha & 1 + \lambda_{Zq} \cdot Z_q \\ \lambda_\alpha \cdot M_\alpha & \lambda_q \cdot M_q \end{bmatrix} \cdot \begin{bmatrix} \alpha \\ q \end{bmatrix} + \begin{bmatrix} 0 \\ \lambda_\eta \cdot M_\eta \end{bmatrix} \cdot \eta. \tag{2.51}$$

Notice that (2.51) uses the simplified nomenclature $\alpha \triangleq \delta\alpha_K^R$, $q \triangleq \delta\left(\omega_y^{IB}\right)_B$, $\eta \triangleq \delta\eta$. Furthermore, (2.51) depends on the scalar coefficients $\lambda_{Z\alpha} \in \mathbb{R}$, $\lambda_{Zq} \in \mathbb{R}$, $\lambda_\alpha \in \mathbb{R}$,

Coefficient	Nominal Value	Uncertainty Range
Z_α	-2.42	$\lambda_{Z\alpha} \in [0.5, 1.5]$
Z_q	-0.09	$\lambda_{Zq} \in [0.5, 1.5]$
M_α	-29.04	$\lambda_\alpha \in [0.5, 1.5]$
M_q	-6.69	$\lambda_q \in [0.5, 1.5]$
M_η	-21.40	$\lambda_\eta \in [0.5, 1.5]$

Table 2.4: Coefficients of the short-period approximation for a linearization of the nonlinear EOMs at $V_K^R = 40\,m/s$, $h = 500\,m$, $m_{fuel} = 3.2\,kg$ with extended landing gear.

$\lambda_q \in \mathbb{R}$ and $\lambda_\eta \in \mathbb{R}$, which allow the introduction of parametric uncertainties. In nominal conditions, $\lambda_{Z\alpha} = \lambda_{Zq} = \lambda_\alpha = \lambda_q = \lambda_\eta = 1$ holds. When linearizing the nonlinear EOMs in case of an extended landing gear for a velocity $V_K^R = V_0 = 40\,m/s$, an altitude $h = h_0 = 500\,m$ and a fuel mass $m_{fuel} = m_{fuel,0} = 3.2\,kg$, the short-period coefficients in Table 2.4 result. Unless stated otherwise, the uncertainty ranges from Table 2.4 will be assumed. In nominal conditions, the poles of the short-period approximation are located at $-4.55 \pm 4.68j$ ($\omega_{0,SP} = 6.5\,rad/s$, $\zeta_{SP} = 0.7$).

Based on the above model of the short-period approximation, a controller is to be developed, which ensures stationary accurate tracking of an angle-of-attack command α_{cmd}. Furthermore, the controller shall ensure that the poles of the short-period approximation lie at $-2.19 \pm 2.19j$ ($\omega_{0,SP,des} = 3.1\,rad/s$, $\zeta_{SP,des} = 1/\sqrt{2}$). The controller may resort to state feedback with respect to the rigid body states, that is, $\delta\alpha_K^R$ and $\delta\left(\omega_y^{IB}\right)_B$ are available as measurements.

Within the various examples, which rely on the short-period benchmark control problem, the actuator model and the control delay τ_c will be considered or neglected. However, the measurement delay is always assumed to be zero, i.e. $\tau_m = 0\,ms$.

2.3 Control of the Lateral Dynamics

The objective of the second benchmark control problem is the development of a fallback controller for the lateral motion of the UAS. The controller shall ensure coordinated turns with a commanded bank angle Φ_{cmd}, while only relying on measurements provided by the AHRS. That is, the controller remains operational even if other measurement devices such as the ADS or the GPS have failed. The restriction to AHRS measurements implies that the controller does neither know the current velocity nor the current altitude of the UAS. For this reason, conventional flight control approaches,

which rely on gain-scheduling of the controller gains with velocity and altitude[1], can for example not be applied. Even though no information on velocity and altitude is available, the controller is expected to operate over the velocity range $V_K^R \in [35\,m/s, 50\,m/s]$, the altitude range $h \in [0\,m, 1000\,m]$ and the fuel mass range $m_{fuel} \in [0\,kg, 23\,kg]$. This envelope range covers a significant part of the overall UAS envelope.

For the development of the controller, the linearized lateral dynamics of the UAS are considered. They readily follow from the linearized EOMs (2.49) and are given by

$$\frac{d}{dt}\begin{bmatrix} \delta\left(\omega_z^{IB}\right)_B \\ \delta\beta_K^R \\ \delta\left(\omega_x^{IB}\right)_B \\ \delta\Phi \end{bmatrix} = \begin{bmatrix} N_r & N_\beta & N_p & 0 \\ Y_r - \cos\Theta_0 & Y_\beta & Y_p + \sin\Theta_0 & \frac{g}{V_0}\cos\Theta_0 \\ L_r & L_\beta & L_p & 0 \\ \tan\Theta_0 & 0 & 1 & 0 \end{bmatrix} \cdot \begin{bmatrix} \delta\left(\omega_z^{IB}\right)_B \\ \delta\beta_K^R \\ \delta\left(\omega_x^{IB}\right)_B \\ \delta\Phi \end{bmatrix} + \begin{bmatrix} N_\xi & N_\zeta \\ Y_\xi & Y_\zeta \\ L_\xi & L_\zeta \\ 0 & 0 \end{bmatrix} \cdot \begin{bmatrix} \delta\xi \\ \delta\zeta \end{bmatrix}. \tag{2.52}$$

When linearizing the nonlinear EOMs for a low velocity $V_K^R = V_0 = 35\,m/s$, a high altitude $h = h_0 = 1000\,m$ and a high fuel mass $m_{fuel} = m_{fuel,0} = 23\,kg$ in case of an extended landing gear, the lateral motion coefficients in Table 2.5 in Column 2 result. At this trim condition, the spiral pole is stable and lies at -0.001. The roll pole is given by -3.37, whereas the Dutch roll is weakly damped with a relative damping $\zeta_{DR} = 0.06$ and an eigenfrequency $\omega_{0,DR} = 3.60\,rad/s$. Conversely, the linearization at a high velocity $V_K^R = V_0 = 50\,m/s$, a low altitude $h = h_0 = 500\,m$ and a low fuel mass $m_{fuel} = m_{fuel,0} = 0\,kg$ in case of an extended landing gear leads to the coefficients in Column 3 of Table 2.5. At this trim condition, the spiral pole is unstable and lies at 0.001. The roll pole is given by -5.31, whereas the Dutch roll is weakly damped with a relative damping $\zeta_{DR} = 0.08$ and an eigenfrequency $\omega_{0,DR} = 5.05\,rad/s$.

Since only AHRS measurements are available, the output equation of the lateral motion reduces to

$$\begin{bmatrix} \delta\left(\omega_z^{IB}\right)_B \\ \delta\left(b_y^M\right)_B \\ \delta\left(\omega_x^{IB}\right)_B \\ \delta\Phi \end{bmatrix} = \begin{bmatrix} 1 & 0 & 0 & 0 \\ F_{y,r} & F_{y,\beta} & F_{y,p} & 0 \\ 0 & 0 & 1 & 0 \\ 0 & 0 & 0 & 1 \end{bmatrix} \cdot \begin{bmatrix} \delta\left(\omega_z^{IB}\right)_B \\ \delta\beta_K^R \\ \delta\left(\omega_x^{IB}\right)_B \\ \delta\Phi \end{bmatrix} + \begin{bmatrix} 0 & 0 \\ F_{y,\xi} & F_{y,\zeta} \\ 0 & 0 \\ 0 & 0 \end{bmatrix} \cdot \begin{bmatrix} \delta\xi \\ \delta\zeta \end{bmatrix}. \tag{2.53}$$

The coefficients $F_{y,(\cdot)}$ are computed from (2.50) with $\left(z^{RM}\right)_B = 0.42\,m$ and $\left(z^{RM}\right)_B = -0.147\,m$.

Besides precise tracking, a central task of any control system is the rejection or accommodation of exogenous disturbances. In case of a flight control system, gust and turbulence represent the most important sources of such exogenous disturbances. Since the linearized plant model (2.52), (2.53) has been derived under the assumption of wind-free conditions, it does not admit a proper analysis of such disturbances. In order to evaluate the capability of the flight control system to reject exogenous disturbances, an appropriate linear model is hence required. In case of small wind speed, i.e.

$$\left|\left(\vec{\boldsymbol{V}}_W^R\right)^E\right| \ll \left|\left(\vec{\boldsymbol{V}}_K^R\right)^E\right|, \tag{2.54}$$

[1] See [138] for a thorough introduction to gain scheduling.

a simple linear model may be easily derived from the kinematic linear model (2.52), (2.53). To that end, notice that the expressions $N_\beta \cdot \delta\beta_K^R$, $Y_\beta \cdot \delta\beta_K^R$, etc. reflect the influence of an angle-of-sideslip variation $\delta\beta_K^R$ on the respective states in case of wind-free conditions. The coefficients N_β, Y_β, etc. ultimately originate from the aerodynamic forces and moments, whose size actually depends on the aerodynamic velocity $\left(\vec{\boldsymbol{V}}_A^R\right)^E$. Hence, it is reasonable to replace $N_\beta \cdot \delta\beta_K^R$, $Y_\beta \cdot \delta\beta_K^R$, etc. by $N_\beta \cdot \delta\beta_A^R$, $Y_\beta \cdot \delta\beta_A^R$ in order to model the influence of small wind fields.

The aerodynamic angle-of-sideslip $\delta\beta_A^R$ is not a state of the linear state space model (2.52). Hence, it must be related to the flight-path angle-of-sideslip $\delta\beta_K^R$ and the wind speed. For this, notice that (2.24) implies that the lateral aerodynamic velocity $\left(v_A^R\right)_B^E$ relates to the lateral kinematic velocity $\left(v_K^R\right)_B^E$ and the lateral wind speed $\left(v_W^R\right)_B^E$ by

$$\left(v_A^R\right)_B^E = \left(v_K^R\right)_B^E - \left(v_W^R\right)_B^E. \tag{2.55}$$

The transformations of the kinematic velocity $\left(\vec{\boldsymbol{V}}_K^R\right)_K^E$ and the aerodynamic velocity $\left(\vec{\boldsymbol{V}}_A^R\right)_A^E$ to the B-frame using the transformation matrices (2.2) and (2.4) yields:

$$\left(v_K^R\right)_B^E = V_K^R \cdot \sin\beta_K^R, \tag{2.56}$$

$$\left(v_A^R\right)_B^E = V_A^R \cdot \sin\beta_A^R. \tag{2.57}$$

Inserting (2.56) and (2.57) into (2.55) leads to

$$V_A^R \cdot \sin\beta_A^R = V_K^R \cdot \sin\beta_K^R - \left(v_W^R\right)_B^E. \tag{2.58}$$

The linearization of (2.58) for horizontal, wind-free, steady-state flight ($V_K^R = V_A^R = V_0$, $\left(v_W^R\right)_B^E = 0$, $\beta_K^R = \beta_A^R = 0$) results in

$$V_0 \cdot \delta\beta_A^R = V_0 \cdot \delta\beta_K^R - \delta\left(v_W^R\right)_B^E. \tag{2.59}$$

With the definition

$$\beta_{W,cmd} \triangleq \frac{\delta\left(v_W^R\right)_B^E}{V_0}, \tag{2.60}$$

one obtains the desired relation between the aerodynamic angle-of-sideslip $\delta\beta_A^R$, the state $\delta\beta_K^R$ and the exogenous disturbance $\beta_{W,cmd}$:

$$\delta\beta_A^R = \delta\beta_K^R - \beta_{W,cmd}. \tag{2.61}$$

Replacing $N_\beta \cdot \delta\beta_K^R$, $Y_\beta \cdot \delta\beta_K^R$, etc. in (2.52) and (2.53) by $N_\beta \cdot (\delta\beta_K^R - \beta_{W,cmd})$, $Y_\beta \cdot (\delta\beta_K^R - \beta_{W,cmd})$, etc. finally leads to

$$\begin{bmatrix} \dot{r} \\ \dot{\beta}_K \\ \dot{p} \\ \dot{\Phi} \end{bmatrix} = \begin{bmatrix} N_r & N_\beta & N_p & 0 \\ Y_r - \cos\Theta_0 & Y_\beta & Y_p + \sin\Theta_0 & \frac{g}{V_0}\cos\Theta_0 \\ L_r & L_\beta & L_p & 0 \\ \tan\Theta_0 & 0 & 1 & 0 \end{bmatrix} \cdot \begin{bmatrix} r \\ \beta_K \\ p \\ \Phi \end{bmatrix} + \begin{bmatrix} N_\xi & N_\zeta & -N_\beta \\ Y_\xi & Y_\zeta & -Y_\beta \\ L_\xi & L_\zeta & -L_\beta \\ 0 & 0 & 0 \end{bmatrix} \cdot \begin{bmatrix} \xi \\ \zeta \\ \beta_{W,cmd} \end{bmatrix}, \tag{2.62}$$

$$\begin{bmatrix} r \\ b_y \\ p \\ \Phi \end{bmatrix} = \begin{bmatrix} 1 & 0 & 0 & 0 \\ F_{y,r} & F_{y,\beta} & F_{y,p} & 0 \\ 0 & 0 & 1 & 0 \\ 0 & 0 & 0 & 1 \end{bmatrix} \cdot \begin{bmatrix} r \\ \beta_K \\ p \\ \Phi \end{bmatrix} + \begin{bmatrix} 0 & 0 & 0 \\ F_{y,\xi} & F_{y,\zeta} & -F_{y,\beta} \\ 0 & 0 & 0 \\ 0 & 0 & 0 \end{bmatrix} \cdot \begin{bmatrix} \xi \\ \zeta \\ \beta_{W,cmd} \end{bmatrix}, \tag{2.63}$$

where $\beta_{W,cmd}$ is treated like a (disturbance) input to the state space model. Notice that (2.62) and (2.63) use the simplified nomenclature $r \triangleq \delta \left(\omega_z^{IB}\right)_B$, $\beta_K \triangleq \delta\beta_K^R$, $p \triangleq \delta \left(\omega_x^{IB}\right)_B$, $\Phi \triangleq \delta\Phi$, $\xi \triangleq \delta\xi$, $\zeta \triangleq \delta\zeta$ and $b_y \triangleq \delta \left(b_y^M\right)_B$.

For the controller development and linear simulations, the overall control system structure of Figure 2.4 is supposed. The control time-delay is given by $\tau_c = 50\,ms$ and the measurement time-delay by $\tau_m = 20\,ms$. As stated before, the actuators are modeled as second order filters according to Figure 2.3 with the parameters from Table 2.3. In case of nonlinear simulations, a high-fidelity plant model is used, which includes more accurate actuator models and also accounts for variable time-delays, sensor dynamics and several other effects.

Coefficient	Nominal Value (First Trim Condition)	Nominal Value (Second Trim Condition)	Uncertainty Range
L_r	0.43	0.61	$\pm 50\%$
L_p	-3.32	-5.16	$\pm 50\%$
L_β	-32.34	-43.07	$\pm 20\%$
L_ξ	-26.31	-56.11	$\pm 20\%$
L_ζ	-2.95	-4.88	$\pm 20\%$
N_r	-0.32	-0.52	$\pm 50\%$
N_p	-0.48	-0.42	$\pm 50\%$
N_β	5.61	20.91	$\pm 20\%$
N_ξ	-0.59	-2.50	$\pm 20\%$
N_ζ	-2.29	-5.91	$\pm 20\%$
Y_r	0.0035	0.0041	0%
Y_p	0.0056	0.0154	0%
Y_β	-0.20	-0.45	0%
Y_ξ	-0.0187	-0.0249	$\pm 20\%$
Y_ζ	0.0115	0.0265	$\pm 20\%$
Θ_0	12.35°	3.80°	N/A
g	9.8066 m/s^2	9.8066 m/s^2	N/A

Table 2.5: Coefficients of the lateral motion for a linearization of the nonlinear EOMs at $V_K^R = 35\,m/s$, $h = 1000\,m$, $m_{fuel} = 23\,kg$ (Column 2), $V_K^R = 50\,m/s$, $h = 500\,m$, $m_{fuel} = 0\,kg$ (Column 3), and their parametric uncertainty (Column 4) in case of an extended landing gear.

Chapter 3

Adaptive Model Following Control Approaches

Most of today's control design approaches rely on a mathematical model of the underlying physical process. However, due to the complexity of reality, no mathematical model is capable of exactly representing a physical process. Hence, any model is subject to uncertainty. These uncertainties may be roughly divided into *parametric* and *non-parametric* uncertainties [105]. *Parametric* uncertainties arise since physical parameters such as the mass of an aircraft are never known exactly. In contrast, *non-parametric* uncertainties stem, roughly speaking, from simplifications or approximations during the derivation of the model. In some cases, these simplifications are conducted deliberately in order to reduce model complexity - for example in order to ease the control design process [156]. Such an approach is sound, if the amplitude of the neglected dynamics is sufficiently small and its time constants are significantly smaller than those of the closed-loop control system. In the context of flight control, a typical example is the negligence of flexible modes if the aircraft structure is sufficiently rigid and the controller is sufficiently slow. In other cases, simplifications are inevitable since modeling has to be stopped at some level of detail. The unmodeled portion of the physical process is then treated as unmodeled dynamics or exogenous disturbance, depending of the control design approach and the interaction of the unmodeled portion with the plant model. An extreme example of such inevitable simplification are gusts. While gusts and their interaction with the aircraft could in theory be described by some complex mathematical model, their formation essentially depends on the weather conditions on the whole Earth. For this reason, gusts are usually treated as an exogenous disturbance.

Since any model is uncertain, any controller derived from a model has to exhibit a certain degree of robustness. In order to achieve robustness with respect to the modeling uncertainties, one may follow two major paradigms. In *Robust Control*, a controller of fixed gains is sought such that it achieves an adequate level of stability and performance for all expected uncertainties. For this, the controller gains are chosen such

that the performance requirements are met for the worst case uncertainty. Common robust control approaches include for example $\mathcal{H}_\infty$ control or μ-synthesis [156, 45]. In contrast, in *Adaptive Control*, the controller gains are not fixed and are adjusted at runtime to the plant using available measurements. The adjustment of controller gains offers several advantages: First of all, it allows for increased system performance as the controller gains are not chosen based on a worst-case argument. Furthermore, *Adaptive Control* may reduce the effort and the associated cost for system identification as the adaptation may counteract the increased level of parametric uncertainties of a low fidelity plant model. Finally, it also improves the overall system safety as the gains may adjust to unforeseen events such as damages or faults.

In literature, the term *Adaptive Control* encompasses various different control approaches. These approaches do not only differ in their respective control objectives but also in the way the adaptation to the plant uncertainty is achieved. With respect to their control objectives, *Adaptive Controllers* may stabilize highly uncertain systems at a given equilibrium. In contrast, extremum-seeking *Adaptive Controllers* [74] stabilize the plant at an a-priori unknown equilibrium, which optimizes a predefined objective function. Another common control objective is model following control. Here, the adjustment of controller gains aims at rendering the response of the closed-loop control system as close as possible to a predefined dynamical system - the so-called reference model [119, 89, 105]. In contrast to the previously mentioned stabilization problems, model following controllers admit an elegant solution of tracking control problems. Since many flight control problems involve tracking, *Adaptive Controllers* for model following are specifically considered in this chapter.

With respect to the adaptation of the controller to the uncertainties, various approaches have been proposed as well. In case of Retrospective Cost Adaptive Control (RCAC) [144, 145], the controller gains are adjusted based on the consecutive optimization of two cost functions. At each time step, the controller first computes a sequence of control inputs, which would have led from some past state to the present state in an optimal manner. Afterwards, a second optimization problem is solved to adjust the gains of the controller in such a way that the difference between the control input of the actual control law and the optimal control history is minimized. Other approaches for the design of the adaptation include for example Immersion and Invariance Adaptive Control (I&I-AC) [5, 125, 4]. While each of these approaches provides unique and intriguing features, the probably most widely known adaptive control approaches are Model Reference Adaptive Control (MRAC) and $\mathcal{L}_1$ Adaptive Control ($\mathcal{L}_1$-AC). These approaches have proven their maturity in various flight testing programs such as IRAC [76], RESTORE [19] or more recently, on a Learjet 25D aircraft [1]. For this reason, the present chapter focuses on the latter two approaches.

Ultimately, *Adaptive Controllers* such as MRAC adjust their controller gains in such a way that the parametric uncertainties are canceled. In comparison to *Robust Con-*

trollers, they do hence possess a significantly larger robustness with respect to parametric uncertainties. However, even small non-parametric uncertainties or deliberately neglected parametric uncertainties, which would hardly affect a *Robust Controller*, can endanger closed-loop stability. While appropriate counter-measures in the form of so-called robustness modifications are available, this raises the question about how an *Adaptive Controller* reacts to a deviation between the plant, which is used for control design, and the actual plant. While this question will be discussed in more detail later on, it is useful to introduce some terms in order to clearly distinguish the different plant models. These terms extend several definitions which are well-known in *Robust Control*. To that end, the plant model, which underlies the design of the adaptive controller, is referred to as the nominal plant (model). Since an *Adaptive Controller* exhibits intrinsic robustness to parametric uncertainties, the nominal plant is uncertain and features those parametric uncertainties, which the *Adaptive Controller* may deal with. Conversely, if the plant model deviates from the nominal plant in any way, this plant is referred to as off-nominal plant (model). The effects, which cause an off-nominal plant to differ from the nominal plant, are referred to as plant imperfection, since these effects usually destroy at least some ideal properties of the *Adaptive Controller*. The term *plant imperfections* includes non-parametric uncertainties, but is not limited to them. For example, parametric uncertainties which have been neglected during control design are also referred to as plant imperfections. Based on these definitions of nominal and off-nominal plants, important terms related to the stability of the closed-loop control system are introduced. The closed loop is said to provide

- **Nominal Stability (NS)**, if the controller stabilizes the nominal plant model;
- **Nominal Performance (NP)**, if the performance objectives are satisfied for the nominal plant model;
- **Robust Stability (RS)**, if the controller stabilizes the off-nominal plant model for some structurally known and appropriately bounded plant imperfections;
- **Robust Performance (RP)**, if the performance objectives are satisfied for the off-nominal plant model for some structurally known and appropriately bounded plant imperfections.

While these definitions read similar to those in *Robust Control* (see for example [156, 186, 45]), they differ in one important aspect. In the literature on *Robust Control*, the nominal plant is usually considered to be free of uncertainties, whereas the definitions above admit an uncertain nominal plant. This extended definition is required in order to account for the specific properties of *Adaptive Controllers*. However, when considering a Linear Time Invariant (LTI) closed-loop and when taking the nominal plant to be uncertainty-free, the above definitions reduce to the conventional definitions in the *Robust Control* literature. Finally, notice that any real physical system may be considered as an off-nominal plant. However, since no mathematical model can exactly represent the physical process, the structure of the plant imperfection and appropriate bounds

are never known exactly neither. Hence, one may never prove RS or RP with respect to the real physical system. Nevertheless, the consideration of high-fidelity plant models (i.e. high fidelity models of the plant imperfection) increases the confidence in the obtained controller design.

The remainder of this chapter is structured as follows: Since both MRAC and $\mathcal{L}_1$-AC aim at achieving model following control, the general Model Reference Control (MRC) problem is stated first in Section 3.1. Afterwards, Section 3.2 and Section 3.3 introduce to the theory of MRAC and $\mathcal{L}_1$-AC, respectively. Finally, Section 3.4 introduces a novel classification of the considered controllers. Furthermore, some specific properties and limitations are presented that will be of interest in the later course of the thesis.

3.1 Problem Statement

This section introduces the control objective of model following control. Notice that this thesis uses the terms *model following control* and *Model Reference Control (MRC)* interchangeably. The high level objective of any model following control system is to let the plant follow a predefined reference model. Using the reference model, the control system designer specifies the desired closed-loop response. That is, he designs the reference model in such a way that it satisfies the given performance objectives. If the controller is successful in driving the plant towards the reference model, the plant will also satisfy these performance objectives. In order to achieve model following control, numerous approaches have been proposed. Assuming a perfectly known minimum-phase plant, the objective of model following control could be achieved using pure feedforward control [20]. However, since no model exactly represents the physical process under control, this approach is extraordinary sensitive to uncertainties. For this reason, approaches based on feedback control are more appropriate. In case of LTI systems, model following control can for example be achieved using state feedback [20] and LTI control design techniques such pole placement. Furthermore, control designs based on feedback linearization [91, 146, 96] or backstepping [101] also often lead to model following control, since their reference trajectories are usually generated by a reference model. A common feature of each of the previously mentioned approaches is the fact that their performance will gracefully degrade in the presence of uncertainties. However, especially in case of highly uncertain plants, the objective of model following control is of high practical relevance as it promises a uniform response for all uncertainties. In order to recover a uniform response despite of uncertainties, one may resort to adaptive model following control approaches such as MRAC or $\mathcal{L}_1$-AC.

Throughout this thesis, different adaptive control approaches are presented which aim at achieving MRC. These approaches do not only differ in the way in which they achieve their control objective, but also differ in the precise definition of the control objective itself. For this reason, the remainder of this section is dedicated to showing

common features as well as highlighting fundamental differences.

Unless stated otherwise, let the nominal, nonlinear plant model be of the form

$$\begin{aligned} \dot{\boldsymbol{x}}_P(t) &= \boldsymbol{A}_P \boldsymbol{x}_P(t) + \boldsymbol{B}_P \boldsymbol{\Lambda} \boldsymbol{u}(t) + \boldsymbol{f}(\boldsymbol{x}_P(t), t), \\ \boldsymbol{y}_P(t) &= \boldsymbol{C}_P \boldsymbol{x}_P(t), \end{aligned} \tag{3.1}$$

where $\boldsymbol{x}_P : \mathbb{R}_+ \to \mathbb{R}^n$ is the state vector, $\boldsymbol{u} : \mathbb{R}_+ \to \mathbb{R}^m$ is the input (vector) and $\boldsymbol{y}_P : \mathbb{R}_+ \to \mathbb{R}^m$ is the output (vector). While the input matrix $\boldsymbol{B}_P \in \mathbb{R}^{n \times m}$ and the output matrix $\boldsymbol{C}_P \in \mathbb{R}^{m \times n}$ are assumed to be known, the system matrix $\boldsymbol{A}_P \in \mathbb{R}^{n \times n}$, the control effectiveness matrix $\boldsymbol{\Lambda} \in \mathbb{R}^{m \times m}$ and the nonlinear mapping $\boldsymbol{f} : \mathbb{R}^n \times \mathbb{R}_+ \to \mathbb{R}^n$ are unknown. Since $\boldsymbol{f}(\boldsymbol{x}_P(t), t)$ depends explicitly on time, this function also reflects exogenous disturbances entering (nonlinearly) into the plant. Furthermore, ($\boldsymbol{A}_P$, $\boldsymbol{B}_P\boldsymbol{\Lambda}$) is controllable.

The plant (3.1) is subject to the following assumptions:

Assumption 3.1 (State Feedback)**.** *The state vector $\boldsymbol{x}_P(t)$ is measurable.*

Assumption 3.2 (Positive Definite Control Effectiveness)**.** *The control effectiveness matrix $\boldsymbol{\Lambda}$ is positive definite, i.e. $\boldsymbol{\Lambda} > 0$, and hence, does not become singular.*

Assumption 3.3 (Lipschitz Condition)**.** *The nonlinear mapping $\boldsymbol{f}(\boldsymbol{x}_P(t), t)$ is semi-globally Lipschitz, i.e.*

$$\|\boldsymbol{f}(\boldsymbol{x}_1, t) - \boldsymbol{f}(\boldsymbol{x}_2, t)\| \leq K(r) \cdot \|\boldsymbol{x}_1 - \boldsymbol{x}_2\| \quad \forall \|\boldsymbol{x}_1\| \leq r,\ \|\boldsymbol{x}_2\| \leq r, \tag{3.2}$$

holds uniformly in t, where $K : \mathbb{R}_+ \to \mathbb{R}_+$ denotes the state-dependent Lipschitz constant. Furthermore, the nonlinear mapping satisfies the boundedness condition

$$\|\boldsymbol{f}(\boldsymbol{0}, t)\| \leq B \tag{3.3}$$

with $B \geq 0$.

Remark 3.1. *Due to Assumption 3.1, the state vector $\boldsymbol{x}_P(t)$ is available to the controller. The output vector $\boldsymbol{y}_P(t)$ only specifies a linear combination of the states that is to be controlled with stationary accuracy.*

On the one side, notice that most of the MRC approaches, which will be introduced throughout this thesis, are neither strictly limited to the plant (3.1) nor rely on (all of) the Assumptions 3.1-3.3. Nevertheless, the plant (3.1) and the associated assumptions were chosen to underlie the subsequent derivations in the interest of a simple and consistent introduction. Relaxations of certain assumptions (such as output feedback instead of state feedback) and extensions to broader classes of plants (such as non-input-affine plants) may be found in the respective literature. On the other side, notice that all of the particular approaches require additional assumptions, which are stated in their respective sections.

Roughly speaking, the plant (3.1) is to follow the LTI reference model

$$\begin{aligned} \dot{\boldsymbol{x}}_M(t) &= \boldsymbol{A}_M \boldsymbol{x}_M(t) + \boldsymbol{B}_M \boldsymbol{r}(t), \\ \boldsymbol{y}_M(t) &= \boldsymbol{C}_P \boldsymbol{x}_M(t) \end{aligned} \tag{3.4}$$

using an appropriate control law, where $\boldsymbol{x}_M : \mathbb{R}_+ \to \mathbb{R}^n$ is state vector of the reference model, and $\boldsymbol{r} : \mathbb{R}_+ \to \mathbb{R}^m$ is the command (vector) to be tracked by the output (vector) $\boldsymbol{y}_M : \mathbb{R}_+ \to \mathbb{R}^m$. In (3.4), $\boldsymbol{A}_M \in \mathbb{R}^{n \times n}$ is Hurwitz and specifies the desired system matrix, whereas $\boldsymbol{B}_M \in \mathbb{R}^{n \times m}$ denotes the desired command input matrix. Usually, $\boldsymbol{B}_M$ is chosen such that the reference model exhibits a DC gain of $\boldsymbol{I}$ from the command $\boldsymbol{r}(t)$ to the reference model output $\boldsymbol{y}_M(t)$.

The rough statement of the control objective shall now be stated more precisely. In principle, the control objective depends on two aspects. First of all, it depends on the type of adaptive model following control approach. On the one side, there are asymptotic MRC approaches such as MRAC, which may achieve asymptotic tracking of the reference model. On the other side, there are approximate MRC approaches including $\mathcal{L}_1$-AC or the Modified Linear Extended State Observer (MLESO) (see Chapter 5), which only achieve model following up to a certain precision. The precision depends on the chosen design parameters. Secondly, the control objective also depends on the uncertainties of the plant (3.1). These uncertainties may be divided into *matched* and *unmatched* uncertainties. If an uncertainty lies within the span of the input matrix $\boldsymbol{B}_P$, it is called *matched*. This is equivalent to saying that the uncertainty may be canceled by an appropriate control input $\boldsymbol{u}(t)$. If all uncertainties are *matched*, the objective of the adaptive controller is *state tracking*. Thus, the plant state $\boldsymbol{x}_P(t)$ shall track the states of the reference model $\boldsymbol{x}_M(t)$. The technical assumptions of this case will be discussed in Section 3.1.1. However, if at least one uncertainty of the nominal plant does not lie in the span of the input matrix, state tracking is no longer achievable. In this case, the control objective is shifted to *output tracking*, i.e. $\boldsymbol{y}_P(t)$ is to follow $\boldsymbol{y}_M(t)$, which will be discussed in Section 3.1.2. The different control objectives are summarized in Table 3.1. A mapping of these control objectives to some existing adaptive control approaches is shown in Table 3.2. Notice that Table 3.2 is by no means complete. In case of MRAC, there exist for example numerous modifications. Depending on the modification at hand, the achievable control objective also changes. In case of the so-called σ-modification, which will be introduced in Section 3.2.4, a MRAC may for example only achieve approximate MRC.

3.1.1 Matched Uncertainties Only

If the uncertainties lie in the span of the input matrix $\boldsymbol{B}_P$, the control law $\boldsymbol{u}(t)$ has to ensure that the states $\boldsymbol{x}_P(t)$ of the plant (3.1) asymptotically or approximately track the states $\boldsymbol{x}_M(t)$ of the reference model (3.4). In order to achieve this goal, the deviation

	Asymptotic MRC	Approximate MRC
Matched Uncertainties Only	$\lim_{t\to\infty} \|\boldsymbol{x}_P(t) - \boldsymbol{x}_M(t)\| = 0$	$\|\boldsymbol{x}_P(t) - \boldsymbol{x}_M(t)\| \leq \epsilon_x,\ \forall\, t \geq 0$
Matched and Unmatched Uncertainties	$\lim_{t\to\infty} \|\boldsymbol{y}_P(t) - \boldsymbol{y}_M(t)\| = 0$	$\|\boldsymbol{y}_P(t) - \boldsymbol{y}_M(t)\| \leq \epsilon_y,\ \forall\, t \geq 0$

Table 3.1: Overview of the pursued control objective depending on the uncertainty type and the type of MRC control approach.

	Asymptotic MRC	Approximate MRC
Matched Uncertainties Only	State-Feedback MRAC (see Section 3.2)	$\mathcal{L}_1$-AC (see Section 3.3), MLESO (see Chapter 5)
Matched and Unmatched Uncertainties	Output-Feedback MRAC, Adaptive Backstepping [101]	$\mathcal{L}_1$-AC (see Section 3.3), MLESO (see Chapter 5)

Table 3.2: Overview of the pursued control objectives of different adaptive control approaches.

between the plant (3.1) and the reference model (3.4) is parametrized as a fictitious control input which causes the latter deviation. This parametrization is also referred to as the matching condition. Depending on the control approach, two alternative matching conditions are commonly used, which differ in the way the control effectiveness $\boldsymbol{\Lambda}$ is accounted for.

Matching Condition

Assumption 3.4 (Matching Condition)**.** *The uncertain matrices and functions of the plant* (3.1) *satisfy the matching conditions*

$$\begin{aligned} \boldsymbol{A}_P &= \boldsymbol{A}_M - \boldsymbol{B}_P \boldsymbol{\Lambda} \boldsymbol{\Theta}_x^*, \\ \boldsymbol{B}_M &= \boldsymbol{B}_P \boldsymbol{\Lambda} \boldsymbol{\Theta}_r^*, \\ \boldsymbol{f}(\boldsymbol{x}_P(t), t) &= -\boldsymbol{B}_P \boldsymbol{\Lambda} \bar{\boldsymbol{f}}(\boldsymbol{x}_P(t), t), \end{aligned} \tag{3.5}$$

where $\boldsymbol{\Theta}_x^* \in \mathbb{R}^{m\times n}$ *and* $\boldsymbol{\Theta}_r^* \in \mathbb{R}^{m\times m}$ *are unknown, constant matrices and where* $\bar{\boldsymbol{f}} : \mathbb{R}^n \times \mathbb{R}_+ \to \mathbb{R}^m$ *is an unknown function.*

The matching condition (3.5) relates the plant uncertainties $\boldsymbol{A}_P$, $\boldsymbol{\Lambda}$, $\boldsymbol{f}(\boldsymbol{x}_P(t), t)$ to the reference model (3.4) and to the unknown matrices $\boldsymbol{\Theta}_x^*$, $\boldsymbol{\Theta}_r^*$ as well as the unknown

function $\bar{\boldsymbol{f}}\left(\boldsymbol{x}_P\left(t\right),t\right)$. In contrast to the original uncertainties $\boldsymbol{A}_P$, $\boldsymbol{\Lambda}$, $\boldsymbol{f}\left(\boldsymbol{x}_P\left(t\right),t\right)$, the newly defined quantities $\boldsymbol{\Theta}_x^*$, $\boldsymbol{\Theta}_r^*$, $\bar{\boldsymbol{f}}\left(\boldsymbol{x}_P\left(t\right),t\right)$ clearly lie in the span of the input matrix $\boldsymbol{B}_P$. Matrices such as $\boldsymbol{\Theta}_x^*$ and $\boldsymbol{\Theta}_r^*$ will be referred to as *ideal parameters* or *matched uncertainties*. Using the matching condition (3.5), the plant (3.1) may be equivalently represented as:

$$\dot{\boldsymbol{x}}_P\left(t\right)=\boldsymbol{A}_M\boldsymbol{x}_P\left(t\right)+\boldsymbol{B}_P\boldsymbol{\Lambda}\left(\boldsymbol{u}\left(t\right)-\boldsymbol{\Theta}_x^*\boldsymbol{x}_P\left(t\right)-\bar{\boldsymbol{f}}\left(\boldsymbol{x}_P\left(t\right),t\right)\right). \tag{3.6}$$

By adding and subtracting $\boldsymbol{B}_M=\boldsymbol{B}_P\boldsymbol{\Lambda}\boldsymbol{\Theta}_r^*$, (3.6) becomes:

$$\begin{aligned}\dot{\boldsymbol{x}}_P\left(t\right)=\boldsymbol{A}_M\boldsymbol{x}_P\left(t\right)+\boldsymbol{B}_M\boldsymbol{r}\left(t\right)\\+\boldsymbol{B}_P\boldsymbol{\Lambda}\left(\boldsymbol{u}\left(t\right)-\boldsymbol{\Theta}_x^*\boldsymbol{x}_P\left(t\right)-\boldsymbol{\Theta}_r^*\boldsymbol{r}\left(t\right)-\bar{\boldsymbol{f}}\left(\boldsymbol{x}_P\left(t\right),t\right)\right).\end{aligned} \tag{3.7}$$

Eq. (3.7) illustrates that the control objective of tracking the states of the reference model (3.4) is achieved, if the control law $\boldsymbol{u}\left(t\right)$ asymptotically or approximately cancels the unknown term $\boldsymbol{\Theta}_x^*\boldsymbol{x}_P\left(t\right)+\boldsymbol{\Theta}_r^*\boldsymbol{r}\left(t\right)+\bar{\boldsymbol{f}}\left(\boldsymbol{x}_P\left(t\right),t\right)$, i.e.

$$\lim_{t\to\infty}\left\|\boldsymbol{u}\left(t\right)-\boldsymbol{\Theta}_x^*\boldsymbol{x}_P\left(t\right)-\boldsymbol{\Theta}_r^*\boldsymbol{r}\left(t\right)-\bar{\boldsymbol{f}}\left(\boldsymbol{x}_P\left(t\right),t\right)\right\|=0 \tag{3.8}$$

or

$$\left\|\boldsymbol{u}\left(t\right)-\boldsymbol{\Theta}_x^*\boldsymbol{x}_P\left(t\right)-\boldsymbol{\Theta}_r^*\boldsymbol{r}\left(t\right)-\bar{\boldsymbol{f}}\left(\boldsymbol{x}_P\left(t\right),t\right)\right\|\approx 0. \tag{3.9}$$

In conjunction with an appropriate parametrization of the nonlinearity $\bar{\boldsymbol{f}}\left(\boldsymbol{x}_P\left(t\right),t\right)$, (3.7) is commonly used for the introduction of so-called direct MRAC (see Section 3.2.1).

Alternative Matching Condition

For the introduction of so-called predictor-based MRAC in Section 3.2.3, $\mathcal{L}_1$-AC in Section 3.3 and the (Modified) Linear Extended State Observer (LESO) in Chapter 5 (all in case of matched uncertainties), the control effectiveness matrix $\boldsymbol{\Lambda}$ has to be treated slightly different. This is expressed by the alternative matching condition:

Assumption 3.5 (Alternative Matching Condition)**.** *The uncertain matrices and functions of the plant* (3.1) *satisfy the matching conditions*

$$\begin{aligned}\boldsymbol{A}_P&=\boldsymbol{A}_M+\boldsymbol{B}_P\boldsymbol{\Theta}_{m,x}^*,\\\boldsymbol{B}_M&=\boldsymbol{B}_P\boldsymbol{K}_r,\\\boldsymbol{f}\left(\boldsymbol{x}_P\left(t\right),t\right)&=\boldsymbol{B}_P\boldsymbol{f}_m\left(\boldsymbol{x}_P\left(t\right),t\right),\end{aligned} \tag{3.10}$$

where the matched uncertainty $\boldsymbol{\Theta}_{m,x}^*\in\mathbb{R}^{m\times n}$ *is an unknown, constant matrix and where* $\boldsymbol{f}_m:\mathbb{R}^n\times\mathbb{R}_+\to\mathbb{R}^m$ *is an unknown function. Furthermore,* $\boldsymbol{K}_r\in\mathbb{R}^{m\times m}$ *is a known feedforward gain.*

Notice that Assumption 3.5 is equivalent to Assumption 3.4, since for any non-singular control effectiveness $\boldsymbol{\Lambda}$,

$$\begin{aligned}\boldsymbol{\Theta}_{m,x}^*&=-\boldsymbol{\Lambda}\boldsymbol{\Theta}_x^*,\\\boldsymbol{K}_r&=\boldsymbol{\Lambda}\boldsymbol{\Theta}_r^*,\\\boldsymbol{f}_m\left(\boldsymbol{x}_P\left(t\right),t\right)&=-\boldsymbol{\Lambda}\bar{\boldsymbol{f}}\left(\boldsymbol{x}_P\left(t\right),t\right)\end{aligned} \tag{3.11}$$

uniquely hold. Using (3.10), the plant (3.1) may also be expressed as:

$$\dot{\boldsymbol{x}}_P(t) = \boldsymbol{A}_M \boldsymbol{x}_P(t) + \boldsymbol{B}_P \left(\boldsymbol{\Lambda} \boldsymbol{u}(t) + \boldsymbol{\Theta}_{m,x}^{*} \boldsymbol{x}_P(t) + \boldsymbol{f}_m(\boldsymbol{x}_P(t), t) \right). \tag{3.12}$$

3.1.2 Matched and Unmatched Uncertainties

In case of matched uncertainties, all uncertainties lie in the span of the input matrix $\boldsymbol{B}_P$. Cancellation of these uncertainties by virtue of an appropriate control input leads to asymptotic or approximate tracking of the *states* of the reference model. However, if the uncertainties do not satisfy the matching condition anymore, parts of the uncertainties will be matched, whereas others will be unmatched. While a cancellation of the matched parts is still possible, this will not recover the desired response of the reference model. For the latter, the control signal, which is matched by definition, needs to be modified appropriately. This modification will inevitably lead to differences between the states of the reference model and the states of the plant. Hence, any controller for matched and unmatched uncertainties will only achieve *output tracking*.

In order to account for unmatched uncertainties, literature proposes numerous control approaches such as Adaptive Backstepping [101]. Furthermore, it is worth noting that some output-feedback control approaches such as output-feedback MRAC [89] do not even distinguish between matched and unmatched uncertainties. In either case, these approaches lead to rather complex control designs. Hence, in this thesis, unmatched uncertainties are dealt with in a rather simple way which requires the following assumption in addition to Assumptions 3.1-3.3:

Assumption 3.6. *The plant* (3.1) *is not over-actuated. Hence, it satisfies* $m \leq n$ *and the input matrix* $\boldsymbol{B}_P$ *has full column-rank, i.e.* $\operatorname{rank}(\boldsymbol{B}_P) = m$.

Remark 3.2. *If Assumption 3.6 holds, then there will exist a virtual input matrix* $\bar{\boldsymbol{B}}_P \in \mathbb{R}^{n \times (n-m)}$ *for the unmatched uncertainties, such that the joint matrix*

$$\boldsymbol{B} = \begin{bmatrix} \boldsymbol{B}_P & \bar{\boldsymbol{B}}_P \end{bmatrix}, \tag{3.13}$$

has full rank, i.e. $\operatorname{rank}(\boldsymbol{B}) = n$. *Notice that* $\bar{\boldsymbol{B}}_P$ *is a design parameter.*

If Assumption 3.6 holds, the following representation of the uncertainties is always feasible due to Remark 3.2:

$$\begin{aligned} \boldsymbol{A}_P &= \boldsymbol{A}_M + \begin{bmatrix} \boldsymbol{B}_P & \bar{\boldsymbol{B}}_P \end{bmatrix} \cdot \begin{bmatrix} \boldsymbol{\Theta}_{m,x}^{*} \\ \boldsymbol{\Theta}_{um,x}^{*} \end{bmatrix}, \\ \boldsymbol{f}(\boldsymbol{x}_P(t), t) &= \begin{bmatrix} \boldsymbol{B}_P & \bar{\boldsymbol{B}}_P \end{bmatrix} \cdot \begin{bmatrix} \boldsymbol{f}_m(\boldsymbol{x}_P(t), t) \\ \boldsymbol{f}_{um}(\boldsymbol{x}_P(t), t) \end{bmatrix}. \end{aligned} \tag{3.14}$$

In (3.14), $\boldsymbol{\Theta}_{m,x}^{*}$ and $\boldsymbol{f}_m(\boldsymbol{x}_P(t), t)$ are equivalently defined as in Assumption 3.5. Moreover, $\boldsymbol{\Theta}_{um,x}^{*} \in \mathbb{R}^{(n-m) \times n}$ denotes an unknown unmatched uncertainty and $\boldsymbol{f}_{um} : \mathbb{R}^n \times \mathbb{R}_+ \to \mathbb{R}^{n-m}$ is an unknown unmatched function.

Using (3.14), the plant (3.1) admits the following representation similar to (3.12):

$$\begin{aligned}\dot{\boldsymbol{x}}_P(t) = \boldsymbol{A}_M \boldsymbol{x}_P(t) + \boldsymbol{B}_P\left(\boldsymbol{\Lambda}\boldsymbol{u}(t) + \boldsymbol{\Theta}_{m,x}^{*}\boldsymbol{x}_P(t) + \boldsymbol{f}_m\left(\boldsymbol{x}_P(t), t\right)\right) \\ + \bar{\boldsymbol{B}}_P\left(\boldsymbol{\Theta}_{um,x}^{*}\boldsymbol{x}_P(t) + \boldsymbol{f}_{um}\left(\boldsymbol{x}_P(t), t\right)\right).\end{aligned} \tag{3.15}$$

Eq. (3.15) will be used for the derivation of $\mathcal{L}_1$ Adaptive Control with Piecewise Constant Update Law ($\mathcal{L}_1$-PWC) in Section 3.3.2 and of the MLESO in case of unmatched uncertainties in Chapter 5.

3.2 Model Reference Adaptive Control

Model Reference Adaptive Control [119, 89, 105] is one of the most widely known and most popular adaptive control approaches. This may already be seen by the sheer amount of technical papers, which have been published on the topic of MRAC, proposing numerous modifications and extensions. Using these extensions and modifications, MRAC may be tailored to a wide range of distinct plants and to a desirable closed-loop performance.

Similar to all MRC approaches, the overall objective of MRAC is to let the plant track a predefined reference model despite the presence of parametric uncertainties. For this, MRAC adjusts its controller gains at runtime in such a way that the effects of the uncertainties are mitigated. Subsequently, a short and by no-means complete overview / classification of MRAC and its numerous modifications follows. A more extensive review may for example be found in [15].

Direct and Indirect Approaches

Despite their vast literature, all MRAC-based controllers may be roughly divided into direct and indirect approaches. In direct approaches, the error between the reference model and the plant drives the so-called update law. Using for example gradient-descent or least-squares-like algorithms (see [89]), the update law immediately adjusts the controller gains such that the plant asymptotically tracks the reference model. The fundamentals of direct MRAC will be introduced in more detail in Section 3.2.1. An extension of direct MRAC, which may be used to augment an existing non-adaptive controller, is presented in Section 3.2.2.

In contrast to direct approaches, indirect MRAC relies on a two-step procedure. In the first step, the unknown system parameters are identified. For this purpose, an identification model with adjustable parameters mimics the structure of the nominal plant. The error between the identification model and the plant then drives the update law, which adjusts the parameters of the identification model. In the second step, algebraic or dynamic relationships are used to compute the required controller gains in order to achieve asymptotic tracking of the reference model. A special type of an indirect approach, the so-called predictor-based MRAC, is treated in Section 3.2.3.

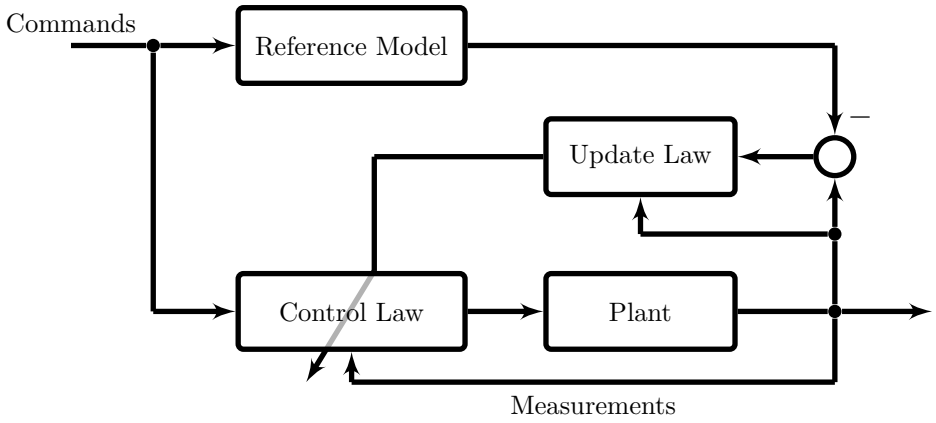

Figure 3.1: General structure of direct MRAC.

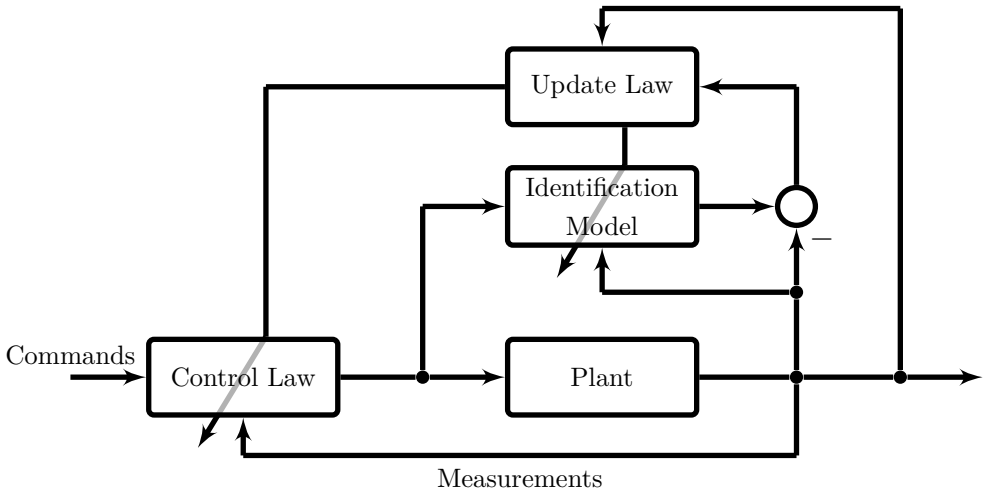

Figure 3.2: General structure of predictor-based MRAC.

Furthermore, there are also hybrid approaches, which result from combining direct and indirect MRAC [44]. In literature, they are referred to as combined or composite MRAC. For the sake of simplicity, this thesis will not cover these approaches and the reader is referred to the respective literature [44, 120, 102].

The general structure of direct and predictor-based (indirect) MRAC is illustrated in Figures 3.1 and 3.2, respectively.

State Feedback and Output Feedback

A second criterion for characterizing MRAC approaches is the type of employed feedback. On the one side, there are state-feedback approaches, which use measurements of the whole state vector in order to achieve asymptotic tracking of the *states* of the reference model. The update law of state-feedback MRAC may be conveniently derived using Lyapunov's second method, even in case of nonlinear plants [105, 15].

Apart from state-feedback MRAC, there are also output-feedback approaches that only use measurements of the plant outputs in order to achieve asymptotic tracking of

the *outputs* of the reference model. While the derivation of an appropriate update law is rather straight-forward in case of a plant with a Relative Degree (RD) of one and a Strictly Positive Real (SPR) reference model (see [96] for an introduction to positive real systems), the situation becomes significantly more complex in case of higher relative degrees [89]. In the latter case, one either has to sacrifice ideal properties (e.g. Uniform Ultimate Boundedness (UUB) instead of asymptotic tracking of the reference model [103, 26, 105]) or is mostly limited to LTI systems [89].

Since most of the states of an aircraft may be conveniently measured or may be replaced by appropriate surrogate measurements (e.g. accelerations instead of aerodynamic angles), this thesis focuses on state feedback. For an introduction to output-feedback MRAC, the reader is referred to the previously mentioned literature and references therein.

Parametrization of Uncertainties

The fundamental objective of any MRAC is the adjustment of the adaptive parameters, which are also known as adaptive controller gains, such that the response of the reference model is recovered. Ultimately, this requires that the update law adjusts the controller gains in such a way that the uncertain terms are canceled, as demonstrated in (3.8). Since the underlying principle is adjustment of parameters, this however presumes that all uncertain terms are appropriately parametrized. In case of the plant (3.1), the matching condition in Assumption 3.4 implicitly introduced a parametrization of the system matrix $\boldsymbol{A}_P$. However, the derivation of MRAC additionally requires a parametrization of the unknown nonlinear function $\bar{\boldsymbol{f}}\left(\boldsymbol{x}_P\left(t\right), t\right)$. The parametrization of the uncertainties represents a third criterion for classifying adaptive controllers.

On the one hand, one distinguishes linear and nonlinear parametrizations. In case of a linear parametrization, the nonlinear function $\bar{\boldsymbol{f}}\left(\boldsymbol{x}_P\left(t\right), t\right)$ may be represented by a linear combination of a finite number of known basis functions, i.e.

$$\bar{\boldsymbol{f}}\left(\boldsymbol{x}_P\left(t\right), t\right) \triangleq \boldsymbol{\Theta}_\phi^* \cdot \boldsymbol{\phi}\left(\boldsymbol{x}_P\left(t\right)\right), \tag{3.16}$$

where $\boldsymbol{\Theta}_\phi^* \in \mathbb{R}^{m \times n_\phi}$ is an unknown parameter matrix and $\boldsymbol{\phi} : \mathbb{R}^n \to \mathbb{R}^{n_\phi}$ is a vector of known basis functions. In contrast, in case of a nonlinear parametrization, the nonlinear function $\bar{\boldsymbol{f}}\left(\boldsymbol{x}_P\left(t\right), t\right)$ is represented by a general, known nonlinear function depending on a finite number of unknown parameters, i.e.

$$\bar{\boldsymbol{f}}\left(\boldsymbol{x}_P\left(t\right), t\right) \triangleq \boldsymbol{g}\left(\boldsymbol{x}_P\left(t\right), \boldsymbol{\Theta}_\phi^*\right), \tag{3.17}$$

where $\boldsymbol{\Theta}_\phi^* \in \mathbb{R}^{n_{\phi,1} \times n_{\phi,2}}$ is an unknown parameter matrix and $\boldsymbol{g} : \mathbb{R}^n \times \mathbb{R}^{n_{\phi,1} \times n_{\phi,2}} \to \mathbb{R}^m$ is a known function.

On the other side, the parametrization of a nonlinear function may also be characterized as exact or approximate. Eqs. (3.16) and (3.17) are examples of exact parametrizations. When modeling physical processes, appropriate basis functions $\boldsymbol{\phi}\left(\boldsymbol{x}_P\left(t\right)\right)$ often immediately derive from the modeled process. For this reason, an exact

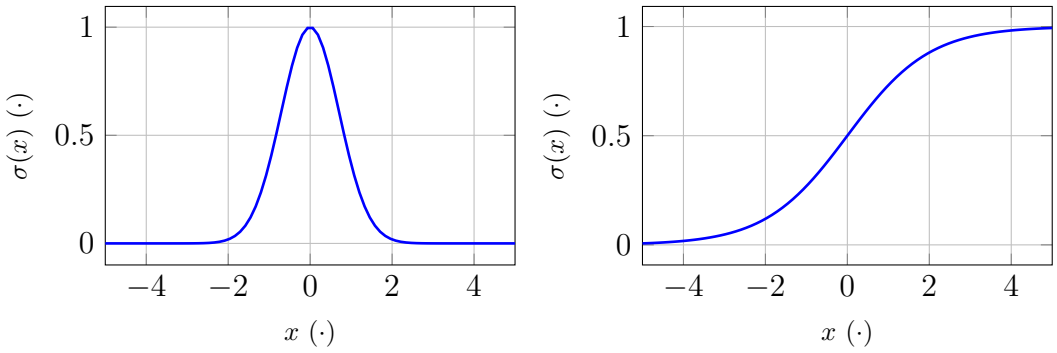

(a) Radial Basis Function $\sigma(x) = e^{-\frac{x^2}{\mu}}$ (b) Sigmoid $\sigma(x) = \frac{1}{1+e^{-x}}$

Figure 3.3: Typical Activation Functions (i.e. basis functions) in Single Hidden Layer Neural Network Adaptive Control

parametrization of $\bar{\boldsymbol{f}}\left(\boldsymbol{x}_P\left(t\right), t\right)$ is also referred to as a physically motivated parametrization. In contrast, an approximate parametrization represents $\bar{\boldsymbol{f}}\left(\boldsymbol{x}_P\left(t\right), t\right)$ with a residual error. Hence, in case of an approximate linear parametrization,

$$\bar{\boldsymbol{f}}\left(\boldsymbol{x}_P\left(t\right), t\right) \triangleq \boldsymbol{\Theta}_{\phi}^{*} \cdot \boldsymbol{\phi}\left(\boldsymbol{x}_P\left(t\right)\right) - \boldsymbol{\epsilon}\left(\boldsymbol{x}_P\left(t\right), t\right) \tag{3.18}$$

holds, whereas in case of an approximate nonlinear parametrization,

$$\bar{\boldsymbol{f}}\left(\boldsymbol{x}_P\left(t\right), t\right) \triangleq \boldsymbol{g}\left(\boldsymbol{x}_P\left(t\right), \boldsymbol{\Theta}_{\phi}^{*}\right) - \boldsymbol{\epsilon}\left(\boldsymbol{x}_P\left(t\right), t\right) \tag{3.19}$$

is satisfied. In either case, $\boldsymbol{\epsilon} : \mathbb{R}^n \times \mathbb{R}_+ \rightarrow \mathbb{R}^m$ denotes the parametrization error. A common example of approximate parametrizations are so-called Single Hidden Layer Neural Networks (NNs). It may be proven that these NNs possess a universal approximation property, that is, any continuous function $\bar{\boldsymbol{f}}\left(\boldsymbol{x}_P\left(t\right), t\right)$ may be approximated on a compact set with bounded parametrization error [64]. The basic elements of such NNs are weighted sums of so-called activation functions, which may be thought of as generic (not physically-motivated) basis functions. Typical activation functions are shown in Figure 3.3. Depending on the structure of the network and the choice of the activation function, Single Hidden Layer NNs may lead to linear or nonlinear parametrizations. For a detailed introduction to NN adaptive control, the reader is referred to [158, 105] or in a wider sense to [63].

In any case, the residual parametrization errors contribute to the plant imperfections as shown in Section 3.2.4. At this point, it has to be stressed that this thesis uses the terms *exact* and *approximate* to refer to the parametrization of a function. Since a real physical system may never be represented by (3.1), any parametrization of the plant will be approximate with respect to the true physical system. One could hence argue that any plant imperfection such as non-parametric uncertainties may be regarded as a parametrization error, which results from our inability to properly parametrize the true physics. For this reason, the parametrization error is sometimes used in literature

to represent plant imperfections such as unmodeled dynamics and exogenous disturbances. This notion of the parametrization error may however not be confused with the definition of the parametrization error in (3.18) and (3.19). In (3.18) and (3.19), the parametrization error is the difference between functions, whereas in the latter case, the parametrization error represents the difference between a nonlinear function and a nonlinear (infinite dimensional) dynamical system. In order to avoid confusions, the term *parametrization error* only refers to the difference between functions in this thesis.

Update Laws

With an appropriate parametrization in place, an algorithm is required to update the adaptive parameters or the adaptive controller gains, respectively. This algorithm is at the heart of the adaptive controller and greatly influences its robustness and performance. The most simple, but probably most widely known, update law readily follows from a Lyapunov stability analysis of the adaptive control system. This Lyapunov-based update law will be the only update law which is studied within this thesis. However, numerous other update laws have been proposed in literature, such as update laws which derive from a *Recursive Least Squares* argument [89]. More recently, an update law, which is inspired from machine learning [16], was proposed in the context of Gaussian Process MRAC [33]. Further update laws have been proposed in the context of RCAC [144, 145] or I&I-AC [5, 125, 4].

Modifications

The fifth (and last) criterion distinguishing different MRAC approaches is the set of chosen modifications. In general, modifications may be applied to the update law and/or to the reference model.

Roughly speaking, modifications of the update law alter the adaptation process itself. An important class of update law modifications are robustness modifications, which guarantee robustness of the closed-loop control system even in the presence of plant imperfections such as non-parametric uncertainties. Without modification, various instability phenomena such as *parameter drift* may occur [89]. One important robustness modification to overcome these difficulties is the so-called σ-modification, which is presented in Section 3.2.4.

Other modifications to the update law do not (only) aim at recovering robustness but at improving the adaptation performance. Numerous modifications of this kind have been proposed such as the Q-modification [171], the Multi-Model Q-modification [83] or *Concurrent Learning* [32, 34, 117]. While these approaches greatly benefit the overall control system performance, they are not covered in this thesis.

While modifications to the update law alter the adaptation process itself, modifications of the reference model essentially alter the desired closed-loop system response. Such modifications may for example be desirable, if control surfaces reach their deflection limit and hence, the prescribed closed-loop system response may not be physically

recovered by an appropriate control input. By adjusting the reference model to match the current physical capabilities of the plant, an erroneous adaptation trying to compensate the deflection limit may be avoided. The underlying modification is known as *hedging*. *Hedging* as well as several other modifications of the reference model will be covered in Section 3.2.5.

Outline

The remainder of this section is structured as follows: First of all, Subsection 3.2.1 introduces direct MRAC in its basic form. Subsection 3.2.2 then extends these results to the case, when a direct MRAC shall augment an existing non-adaptive baseline controller. Afterwards, predictor-based MRAC is introduced in Subsection 3.2.3. Since all methods, which will be presented later on in this thesis, depend on a linear parametrization, Subsections 3.2.1-3.2.3 are also limited to a linear parametrization:

Assumption 3.7 (Linear Parametrization)**.** *The nonlinear function $\bar{\boldsymbol{f}}(\boldsymbol{x}_P(t), t)$ may be linearly parametrized according to* (3.18)*, i.e. $\bar{\boldsymbol{f}}(\boldsymbol{x}_P(t), t) \triangleq \boldsymbol{\Theta}_\phi^* \cdot \boldsymbol{\phi}(\boldsymbol{x}_P(t)) - \boldsymbol{\epsilon}(\boldsymbol{x}_P(t), t)$, where $\boldsymbol{\Theta}_\phi^* \in \mathbb{R}^{m \times n_\phi}$ is the unknown, constant, ideal parameter and $\boldsymbol{\phi} : \mathbb{R}^n \to \mathbb{R}^{n_\phi}$ is a known vector-valued function.*

In terms of the nonlinear function $\boldsymbol{f}_m(\boldsymbol{x}_P(t), t)$, which relates to $\bar{\boldsymbol{f}}(\boldsymbol{x}_P(t), t)$ through (3.11)*, it may be equivalently stated that $\boldsymbol{f}_m(\boldsymbol{x}_P(t), t) \triangleq \boldsymbol{\Theta}_{m,\phi}^* \cdot \boldsymbol{\phi}(\boldsymbol{x}_P(t)) - \boldsymbol{\epsilon}_m(\boldsymbol{x}_P(t), t)$ with $\boldsymbol{\Theta}_{m,\phi}^* = -\boldsymbol{\Lambda}\boldsymbol{\Theta}_\phi^*$ and $\boldsymbol{\epsilon}_m(\boldsymbol{x}_P(t), t) = -\boldsymbol{\Lambda}\boldsymbol{\epsilon}(\boldsymbol{x}_P(t), t)$.*

Furthermore, in order to be able to prove asymptotic convergence of the plant towards the reference model, Subsections 3.2.1-3.2.3 will assume that there is no parametrization error:

Assumption 3.8 (Exact Parametrization)**.** *The parametrization of the nonlinear function $\bar{\boldsymbol{f}}(\boldsymbol{x}_P(t), t)$, or $\boldsymbol{f}_m(\boldsymbol{x}_P(t), t)$ respectively, is exact, that is, $\boldsymbol{\epsilon}(\boldsymbol{x}_P(t), t) = 0$ and $\boldsymbol{\epsilon}_m(\boldsymbol{x}_P(t), t) = 0$.*

This assumption will be alleviated in Section 3.2.4, where the effects of plant imperfections and appropriate counter-measures in the form of robustness modifications are discussed. Finally, Subsection 3.2.5 introduces several reference model modifications.

3.2.1 Direct Model Reference Adaptive Control

This section derives a direct MRAC for the plant (3.1) in case of matched uncertainties and an exact, linear parametrization of the nonlinearities. Thus, throughout this section, Assumptions 3.1 (state feedback), 3.2 (positive definite control effectiveness), 3.3 (Lipschitz condition), 3.4 (matching condition), 3.7 (linear parametrization) and 3.8 (exact parametrization) are assumed to hold. Starting from the plant representation (3.7), which was obtained using the matching condition of Assumption 3.4, the plant

may be rewritten as

$$\begin{aligned}\dot{\boldsymbol{x}}_P(t) = \boldsymbol{A}_M\boldsymbol{x}_P(t) + \boldsymbol{B}_M\boldsymbol{r}(t) + \boldsymbol{B}_P\boldsymbol{\Lambda}\boldsymbol{u}(t) \\ + \boldsymbol{B}_P\boldsymbol{\Lambda}\left(-\boldsymbol{\Theta}_x^*\boldsymbol{x}_P(t) - \boldsymbol{\Theta}_r^*\boldsymbol{r}(t) - \boldsymbol{\Theta}_\phi^*\cdot\boldsymbol{\phi}(\boldsymbol{x}_P(t))\right) \\ + \boldsymbol{B}_P\boldsymbol{\Lambda}\boldsymbol{\epsilon}(\boldsymbol{x}_P(t), t)\end{aligned} \tag{3.20}$$

by virtue of Assumption 3.7. Furthermore, since the parametrization is exact according to Assumption 3.8, i.e. $\boldsymbol{\epsilon}(\boldsymbol{x}_P(t), t) = 0$, the plant representation (3.20) simplifies to

$$\begin{aligned}\dot{\boldsymbol{x}}_P(t) = \boldsymbol{A}_M\boldsymbol{x}_P(t) + \boldsymbol{B}_M\boldsymbol{r}(t) + \boldsymbol{B}_P\boldsymbol{\Lambda}\boldsymbol{u}(t) \\ + \boldsymbol{B}_P\boldsymbol{\Lambda}\left(-\boldsymbol{\Theta}_x^*\boldsymbol{x}_P(t) - \boldsymbol{\Theta}_r^*\boldsymbol{r}(t) - \boldsymbol{\Theta}_\phi^*\cdot\boldsymbol{\phi}(\boldsymbol{x}_P(t))\right).\end{aligned} \tag{3.21}$$

In order to cancel the unknown parameters $\boldsymbol{\Theta}_x^*$, $\boldsymbol{\Theta}_r^*$ and $\boldsymbol{\Theta}_\phi^*$, the time-varying control law

$$\boldsymbol{u}(t) = \boldsymbol{\Theta}_x(t)\cdot\boldsymbol{x}_P(t) + \boldsymbol{\Theta}_r(t)\cdot\boldsymbol{r}(t) + \boldsymbol{\Theta}_\phi(t)\cdot\boldsymbol{\phi}(\boldsymbol{x}_P(t)) \tag{3.22}$$

is proposed, where $\boldsymbol{\Theta}_x : \mathbb{R}_+ \to \mathbb{R}^{m\times n}$, $\boldsymbol{\Theta}_r : \mathbb{R}_+ \to \mathbb{R}^{m\times m}$ and $\boldsymbol{\Theta}_\phi : \mathbb{R}_+ \to \mathbb{R}^{m\times n_\phi}$ are the adaptive controller gains, which are also called adaptive parameters. Using the definitions

$$\begin{aligned}\boldsymbol{\Theta}^* &\triangleq \begin{bmatrix}\boldsymbol{\Theta}_x^* & \boldsymbol{\Theta}_r^* & \boldsymbol{\Theta}_\phi^*\end{bmatrix}, \\ \boldsymbol{\omega}(\boldsymbol{x}_P(t), t) &\triangleq \begin{bmatrix}\boldsymbol{x}_P(t) \\ \boldsymbol{r}(t) \\ \boldsymbol{\phi}(\boldsymbol{x}_P(t))\end{bmatrix},\end{aligned} \tag{3.23}$$

the unknown parameters and the known signals may be summarized in one unknown parameter matrix $\boldsymbol{\Theta}^* \in \mathbb{R}^{m\times n_r}$ and one regressor vector $\boldsymbol{\omega} : \mathbb{R}^n \times \mathbb{R}_+ \to \mathbb{R}^{n_r}$, respectively. Here, $n_r = n + m + n_\phi$ denotes the size of the regressor vector. Similarly, the adaptive gains are summarized into one adaptive gain

$$\boldsymbol{\Theta}(t) \triangleq \begin{bmatrix}\boldsymbol{\Theta}_x(t) & \boldsymbol{\Theta}_r(t) & \boldsymbol{\Theta}_\phi(t)\end{bmatrix} \tag{3.24}$$

with $\boldsymbol{\Theta} : \mathbb{R}_+ \to \mathbb{R}^{m\times n_r}$. The definitions (3.23) and (3.24) allow to reformulate the plant (3.21) and the control law (3.22) more compactly as

$$\dot{\boldsymbol{x}}_P(t) = \boldsymbol{A}_M\boldsymbol{x}_P(t) + \boldsymbol{B}_M\boldsymbol{r}(t) + \boldsymbol{B}_P\boldsymbol{\Lambda}\left(\boldsymbol{u}(t) - \boldsymbol{\Theta}^*\boldsymbol{\omega}(\boldsymbol{x}_P(t), t)\right) \tag{3.25}$$

and

$$\boldsymbol{u}(t) = \boldsymbol{\Theta}(t)\cdot\boldsymbol{\omega}(\boldsymbol{x}_P(t), t), \tag{3.26}$$

respectively. By inserting (3.26) and using the definition of the parameter error

$$\tilde{\boldsymbol{\Theta}}(t) \triangleq \boldsymbol{\Theta}(t) - \boldsymbol{\Theta}^*, \tag{3.27}$$

(3.25) becomes

$$\dot{\boldsymbol{x}}_P(t) = \boldsymbol{A}_M\boldsymbol{x}_P(t) + \boldsymbol{B}_M\boldsymbol{r}(t) + \boldsymbol{B}_P\boldsymbol{\Lambda}\tilde{\boldsymbol{\Theta}}(t)\cdot\boldsymbol{\omega}(\boldsymbol{x}_P(t), t). \tag{3.28}$$

Since the overall objective of the control law is asymptotic tracking of the reference model, the tracking error $\boldsymbol{e}_C(t) \triangleq \boldsymbol{x}_P(t) - \boldsymbol{x}_M(t)$ is introduced in order to quantify the difference between the plant states and the reference model states. The tracking error $\boldsymbol{e}_C(t)$ evolves according to the differential equation

$$\dot{\boldsymbol{e}}_C(t) = \boldsymbol{A}_M \boldsymbol{e}_C(t) + \boldsymbol{B}_P \boldsymbol{\Lambda} \tilde{\boldsymbol{\Theta}}(t) \cdot \boldsymbol{\omega}(\boldsymbol{x}_P(t), t), \tag{3.29}$$

which results from differentiating the definition of $\boldsymbol{e}_C(t)$ and inserting (3.4) and (3.28), respectively. Intuitively, the error dynamics (3.29) indicate that the control objective may be achieved if for example the parameters converge, i.e. $\boldsymbol{\Theta}(t) = \boldsymbol{\Theta}^*$ or equivalently $\tilde{\boldsymbol{\Theta}}(t) = 0$. While the control objective seems to be achievable, the actual choice of the adaptive parameter $\boldsymbol{\Theta}(t)$ has not yet been addressed. One approach of deriving an update law for the adaptive parameter is based on a proof of stability of the tracking error dynamics $\dot{\boldsymbol{e}}_C(t)$ and the (not yet known) parameter error dynamics $\dot{\tilde{\boldsymbol{\Theta}}}(t)$. For this, consider the Lyapunov function candidate

$$V(t) = \frac{1}{2} \boldsymbol{e}_C(t)^T \boldsymbol{P} \boldsymbol{e}_C(t) + \frac{1}{2} \operatorname{Tr}\left\{ \tilde{\boldsymbol{\Theta}}(t) \boldsymbol{\Gamma}^{-1} \tilde{\boldsymbol{\Theta}}(t)^T \boldsymbol{\Lambda} \right\}. \tag{3.30}$$

In (3.30), $\boldsymbol{P} \in \mathbb{S}^n_{++}$ is the positive definite, unique solution of the Lyapunov equation

$$\boldsymbol{A}_M^T \boldsymbol{P} + \boldsymbol{P} \boldsymbol{A}_M = -\boldsymbol{Q}, \tag{3.31}$$

where $\boldsymbol{Q} \in \mathbb{S}^n_{++}$ is a positive definite design parameter. Notice that $\mathbb{S}^n_{++}$ denotes the set of all positive definite matrices in $\mathbb{R}^{n \times n}$. The so-called learning rate $\boldsymbol{\Gamma} \in \mathbb{S}^{n_r}_{++}$ is another positive definite design parameter. The interpretation of the design parameters $\boldsymbol{\Gamma}$ and $\boldsymbol{Q}$ will be clarified later on.

The direct method of Lyapunov (Theorem C.2) requires that the Lyapunov function candidate (3.30) is a positive definite function. The following lemma establishes that (3.30) satisfies this requirement.

Lemma 3.3. *If $\boldsymbol{P}$, $\boldsymbol{\Gamma}$ and $\boldsymbol{\Lambda}$ are positive definite, then the Lyapunov function candidate* (3.30) *is a positive definite function.*

Proof. Since $\boldsymbol{\Lambda}$ is symmetric and positive definite, its matrix square root exists, i.e. $\boldsymbol{\Lambda} = \boldsymbol{\Lambda}^{\frac{1}{2}} \cdot \boldsymbol{\Lambda}^{\frac{1}{2}}$, where $\boldsymbol{\Lambda}^{\frac{1}{2}}$ is symmetric as well. Using the cyclic property (B.154), the Lyapunov function candidate (3.30) becomes:

$$V(t) = \frac{1}{2} \boldsymbol{e}_C(t)^T \boldsymbol{P} \boldsymbol{e}_C(t) + \frac{1}{2} \operatorname{Tr}\left\{ \boldsymbol{\Lambda}^{\frac{1}{2}} \tilde{\boldsymbol{\Theta}}(t) \boldsymbol{\Gamma}^{-1} \tilde{\boldsymbol{\Theta}}(t)^T \boldsymbol{\Lambda}^{\frac{1}{2}T} \right\}. \tag{3.32}$$

By defining $\bar{\boldsymbol{\Theta}}(t) = \boldsymbol{\Lambda}^{\frac{1}{2}} \tilde{\boldsymbol{\Theta}}(t)$, (3.32) is compactly written as:

$$V(t) = \frac{1}{2} \boldsymbol{e}_C(t)^T \boldsymbol{P} \boldsymbol{e}_C(t) + \frac{1}{2} \operatorname{Tr}\left\{ \bar{\boldsymbol{\Theta}}(t) \boldsymbol{\Gamma}^{-1} \bar{\boldsymbol{\Theta}}(t)^T \right\}. \tag{3.33}$$

Using the quadratic form bounds (B.64) and (B.102), (3.33) may be bounded by:

$$\begin{aligned} &\frac{1}{2} \lambda_{\min}(\boldsymbol{P}) \cdot \|\boldsymbol{e}_C(t)\|_2^2 + \frac{1}{2} \lambda_{\min}(\boldsymbol{\Gamma}^{-1}) \cdot \|\bar{\boldsymbol{\Theta}}(t)\|_F^2 \leq V(t), \\ &V(t) \leq \frac{1}{2} \lambda_{\max}(\boldsymbol{P}) \cdot \|\boldsymbol{e}_C(t)\|_2^2 + \frac{1}{2} \lambda_{\max}(\boldsymbol{\Gamma}^{-1}) \cdot \|\bar{\boldsymbol{\Theta}}(t)\|_F^2. \end{aligned} \tag{3.34}$$

Since $\boldsymbol{\Gamma}$ is positive definite, it is invertible. For this reason, $\lambda_{\min}(\boldsymbol{\Gamma}^{-1}) = 1/\lambda_{\max}(\boldsymbol{\Gamma})$ and $\lambda_{\max}(\boldsymbol{\Gamma}^{-1}) = 1/\lambda_{\min}(\boldsymbol{\Gamma})$ hold. By applying the definition of the Frobenius norm (B.9) and resubstituting $\bar{\boldsymbol{\Theta}}(t) = \boldsymbol{\Lambda}^{\frac{1}{2}}\tilde{\boldsymbol{\Theta}}(t)$, one obtains:

$$\begin{aligned} &\frac{1}{2}\lambda_{\min}(\boldsymbol{P}) \cdot \|\boldsymbol{e}_C(t)\|_2^2 + \frac{1}{2 \cdot \lambda_{\max}(\boldsymbol{\Gamma})} \cdot \mathrm{Tr}\left\{\tilde{\boldsymbol{\Theta}}^T \boldsymbol{\Lambda} \tilde{\boldsymbol{\Theta}}(t)\right\} \leq V(t), \\ &V(t) \leq \frac{1}{2}\lambda_{\max}(\boldsymbol{P}) \cdot \|\boldsymbol{e}_C(t)\|_2^2 + \frac{1}{2 \cdot \lambda_{\min}(\boldsymbol{\Gamma})} \cdot \mathrm{Tr}\left\{\tilde{\boldsymbol{\Theta}}^T \boldsymbol{\Lambda} \tilde{\boldsymbol{\Theta}}(t)\right\}. \end{aligned} \tag{3.35}$$

Applying the quadratic form bound (B.102) once again yields

$$\begin{aligned} &\frac{1}{2}\lambda_{\min}(\boldsymbol{P}) \cdot \|\boldsymbol{e}_C(t)\|_2^2 + \frac{\lambda_{\min}(\boldsymbol{\Lambda})}{2 \cdot \lambda_{\max}(\boldsymbol{\Gamma})} \cdot \|\tilde{\boldsymbol{\Theta}}(t)\|_F^2 \leq V(t), \\ &V(t) \leq \frac{1}{2}\lambda_{\max}(\boldsymbol{P}) \cdot \|\boldsymbol{e}_C(t)\|_2^2 + \frac{\lambda_{\max}(\boldsymbol{\Lambda})}{2 \cdot \lambda_{\min}(\boldsymbol{\Gamma})} \cdot \|\tilde{\boldsymbol{\Theta}}(t)\|_F^2. \end{aligned} \tag{3.36}$$

Since $\boldsymbol{P}$, $\boldsymbol{\Gamma}$ and $\boldsymbol{\Lambda}$ are positive definite, the lower bound in (3.36) implies that $V(t)$ cannot become negative. Furthermore, $V = 0$ can only hold, if $\boldsymbol{e}_C = \mathbf{0}$ and $\tilde{\boldsymbol{\Theta}} = \mathbf{0}$ hold. Hence, $V(t)$ is positive definite. □

Differentiating the Lyapunov function candidate with respect to time yields:

$$\dot{V}(t) = \boldsymbol{e}_C(t)^T \boldsymbol{P}\dot{\boldsymbol{e}}_C(t) + \mathrm{Tr}\left\{\tilde{\boldsymbol{\Theta}}(t)\,\boldsymbol{\Gamma}^{-1}\dot{\tilde{\boldsymbol{\Theta}}}(t)^T \boldsymbol{\Lambda}\right\}. \tag{3.37}$$

By inserting the error dynamics (3.29), (3.37) becomes

$$\begin{aligned} \dot{V}(t) = \boldsymbol{e}_C(t)^T \boldsymbol{P}\boldsymbol{A}_M \boldsymbol{e}_C(t) + \boldsymbol{e}_C(t)^T \boldsymbol{P}\boldsymbol{B}_P \boldsymbol{\Lambda}\tilde{\boldsymbol{\Theta}}(t) \cdot \boldsymbol{\omega}(\boldsymbol{x}_P(t), t) \\ + \mathrm{Tr}\left\{\tilde{\boldsymbol{\Theta}}(t)\,\boldsymbol{\Gamma}^{-1}\dot{\tilde{\boldsymbol{\Theta}}}(t)^T \boldsymbol{\Lambda}\right\}. \end{aligned} \tag{3.38}$$

With the definition of the Lyapunov equation in (3.31) and due to $\boldsymbol{e}_C(t)^T \boldsymbol{P}\boldsymbol{A}_M \boldsymbol{e}_C(t) = \boldsymbol{e}_C(t)^T \boldsymbol{A}_M^T \boldsymbol{P}\boldsymbol{e}_C(t)$, one obtains:

$$\begin{aligned} \dot{V}(t) = -\frac{1}{2}\boldsymbol{e}_C(t)^T \boldsymbol{Q}\boldsymbol{e}_C(t) + \boldsymbol{e}_C(t)^T \boldsymbol{P}\boldsymbol{B}_P \boldsymbol{\Lambda} \cdot \tilde{\boldsymbol{\Theta}}(t)\,\boldsymbol{\omega}(\boldsymbol{x}_P(t), t) \\ + \mathrm{Tr}\left\{\tilde{\boldsymbol{\Theta}}(t)\,\boldsymbol{\Gamma}^{-1}\dot{\tilde{\boldsymbol{\Theta}}}(t)^T \boldsymbol{\Lambda}\right\}. \end{aligned} \tag{3.39}$$

Using the trace property (B.156), the second term in (3.39) can be moved into the trace:

$$\begin{aligned} \dot{V}(t) = &-\frac{1}{2}\boldsymbol{e}_C(t)^T \boldsymbol{Q}\boldsymbol{e}_C(t) \\ &+ \mathrm{Tr}\left\{\tilde{\boldsymbol{\Theta}}(t)\left(\boldsymbol{\Gamma}^{-1}\dot{\tilde{\boldsymbol{\Theta}}}(t)^T + \boldsymbol{\omega}(\boldsymbol{x}_P(t), t) \cdot \boldsymbol{e}_C(t)^T \boldsymbol{P}\boldsymbol{B}_P\right)\boldsymbol{\Lambda}\right\}. \end{aligned} \tag{3.40}$$

By choosing

$$\dot{\tilde{\boldsymbol{\Theta}}}(t)^T = -\boldsymbol{\Gamma}\boldsymbol{\omega}(\boldsymbol{x}_P(t), t) \cdot \boldsymbol{e}_C(t)^T \boldsymbol{P}\boldsymbol{B}_P, \tag{3.41}$$

the derivative of the Lyapunov function candidate may be rendered negative semidefinite, i.e.

$$\dot{V}(t) = -\frac{1}{2}\boldsymbol{e}_C(t)^T \boldsymbol{Q}\boldsymbol{e}_C(t) \leq 0 \quad \forall\, \boldsymbol{e}_C(t), \tilde{\boldsymbol{\Theta}}(t). \tag{3.42}$$

Hence, $\boldsymbol{e}_C = 0$ and $\tilde{\boldsymbol{\Theta}} = 0$ is the globally stable equilibrium of the tracking error dynamics (3.29) and the parameter error dynamics (3.41). Since $\boldsymbol{\Theta}^*$ is a constant by assumption, the definition of the parameter error in (3.27) finally admits to state the following update law for the adaptive gain $\boldsymbol{\Theta}(t)$:

$$\dot{\boldsymbol{\Theta}}(t)^T = -\boldsymbol{\Gamma}\boldsymbol{\omega}(\boldsymbol{x}_P(t), t) \cdot \boldsymbol{e}_C(t)^T \boldsymbol{P}\boldsymbol{B}_P. \tag{3.43}$$

Furthermore, since the command signal $\boldsymbol{r}(t)$ is bounded by definition, the reference model state $\boldsymbol{x}_M(t)$ will be bounded as well. Due to the global stability of the error dynamics, this implies boundedness of the plant state $\boldsymbol{x}_P(t)$. Thus, all signals of the closed-loop control system are bounded.

While the update law (3.43) ensures boundedness of the closed-loop control system, it does not yet prove asymptotic convergence of the plant states towards the reference model states. For this, notice that due to $\dot{V}(t) \leq 0$ and $V(t) \geq 0$, $0 \leq V(\infty) \leq V(0)$ holds. Thus, the integral

$$\int_0^\infty -\dot{V}(t)\, dt = \int_\infty^0 \dot{V}(t)\, dt = V(0) - V(\infty) \geq 0 \tag{3.44}$$

exists and is finite. Furthermore, since the command signal $\boldsymbol{r}(t)$ and the plant state $\boldsymbol{x}_P(t)$ are bounded, the Lipschitz condition in Assumption 3.3 implies boundedness of the regressor vector $\boldsymbol{\omega}(\boldsymbol{x}_P(t), t)$. Boundedness of the regressor vector $\boldsymbol{\omega}(\boldsymbol{x}_P(t), t)$ together with boundedness of $\boldsymbol{e}_C(t)$ and $\tilde{\boldsymbol{\Theta}}(t)$ due to the Lyapunov proof of stability then proves boundedness of $\dot{\boldsymbol{e}}_C(t)$, i.e. $\dot{\boldsymbol{e}}_C(t) \in \mathcal{L}_\infty$. The latter implies uniform continuity of $-\dot{V}(t)$ as $-\ddot{V}(t) = \boldsymbol{e}_C(t)^T \boldsymbol{Q}\dot{\boldsymbol{e}}_C(t)$ is bounded. Invoking Barbalat's Lemma (Lemma C.3) shows

$$\lim_{t\to\infty} -\dot{V}(t) = \frac{1}{2} \cdot \lim_{t\to\infty} \boldsymbol{e}_C(t)^T \boldsymbol{Q}\boldsymbol{e}_C(t) = 0, \tag{3.45}$$

implying $\lim_{t\to\infty} \|\boldsymbol{e}_C(t)\| = 0$. Thus, the tracking error asymptotically decreases to zero, which proves that the derived direct MRAC does indeed achieve asymptotic tracking of the reference model (3.4). The results of the preceding derivation are summarized in the following theorem:

Theorem 3.4 (Nominal Stability of Direct MRAC)**.** *Consider the plant* (3.1) *and let Assumptions 3.1 (state feedback), 3.2 (positive definite control effectiveness), 3.3 (Lipschitz condition), 3.4 (matching condition), 3.7 (linear parametrization) and 3.8 (exact parametrization) hold. Then, according to* (3.25)*, the plant admits the compact representation*

$$\dot{\boldsymbol{x}}_P(t) = \boldsymbol{A}_M\boldsymbol{x}_P(t) + \boldsymbol{B}_M\boldsymbol{r}(t) + \boldsymbol{B}_P\boldsymbol{\Lambda}\left(\boldsymbol{u}(t) - \boldsymbol{\Theta}^*\boldsymbol{\omega}(\boldsymbol{x}_P(t), t)\right),$$

where the true parameter matrix $\boldsymbol{\Theta}^*$ and the regressor vector $\boldsymbol{\omega}(\boldsymbol{x}_P(t), t)$ are defined in (3.23)*. Furthermore, let the learning rate $\boldsymbol{\Gamma} \in \mathbb{S}^{n_r}_{++}$ and the weighting matrix $\boldsymbol{Q} \in \mathbb{S}^n_{++}$ be chosen positive definite, and let $\boldsymbol{P} \in \mathbb{S}^n_{++}$ be the positive definite solution of the Lyapunov equation* (3.31)*. Then the control law*

$$\boldsymbol{u}(t) = \boldsymbol{\Theta}(t) \cdot \boldsymbol{\omega}(\boldsymbol{x}_P(t), t),$$

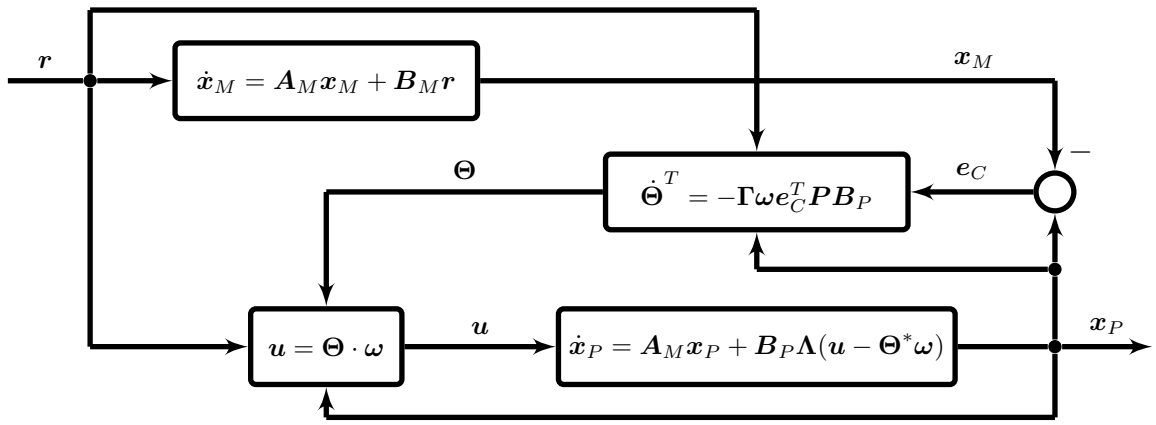

Figure 3.4: Illustration of direct MRAC.

$$\dot{\boldsymbol{\Theta}}\left(t\right)^T = -\boldsymbol{\Gamma}\boldsymbol{\omega}\left(\boldsymbol{x}_P\left(t\right), t\right)\cdot\boldsymbol{e}_C\left(t\right)^T\boldsymbol{P}\boldsymbol{B}_P,$$

proposed / derived in (3.26) *and* (3.43)*, will ensure that (*$\boldsymbol{e}_C = \boldsymbol{0}$*,* $\tilde{\boldsymbol{\Theta}} = \boldsymbol{0}$*) is a globally stable equilibrium of the error dynamics* (3.29) *and* (3.41)*. Furthermore, all signals of the closed-loop control system are bounded and the control law ensures asymptotic tracking of the reference model* (3.4)*, i.e.*

$$\lim_{t\to\infty}\left\|\boldsymbol{e}_C\left(t\right)\right\| = 0.$$

Proof. The proof relies on the Lyapunov candidate function (3.30) and amounts to the steps which have led from (3.30) to (3.45). □

Remark 3.5. *While Barbalat's Lemma shows asymptotic convergence of the tracking error* $\boldsymbol{e}_C\left(t\right)$*, it does not allow any conclusion on the parameter error* $\tilde{\boldsymbol{\Theta}}\left(t\right)$*. Thus, despite of asymptotic convergence of the tracking error, the parameter error is only stable, i.e. bounded to some neighborhood of the origin. In order for the parameters to converge exponentially, the regressor vectors* $\boldsymbol{\omega}\left(\boldsymbol{x}_P\left(t\right), t\right)$ *has to satisfy a so-called Persistency of Excitation condition. While the math associated with Persistency of Excitation is rather involved even in case of LTI plants, its idea is rather intuitive. Since adaptation is based on measurements of the input- / output map of the plant, some commands leading to changes of the regressor vector have to be issued to the plant. Conversely, if no commands are given to the plant, for example due to* $\boldsymbol{r}\left(t\right) = 0$*, no new output* $\boldsymbol{\omega}\left(\boldsymbol{x}_P\left(t\right), t\right)$ *is generated and hence, no information about the parameters may be inferred. Mathematically, Persistency of Excitation relates to uniform complete observability [89]. In case of LTI plants, it may be shown that parameter convergence relates to the number of sinusoids in the command signal* $\boldsymbol{r}\left(t\right)$*.*

The structure of direct MRAC is illustrated in Figure 3.4. Its application to the short-period example from Section 2.2 is demonstrated by the following example:

Example 3.6. *Consider the linearized short-period approximation* (2.51) *of the longitudinal motion of the UAS from Chapter 2 and assume* $\lambda_{Z\alpha} = \lambda_{Zq} = 1$*. Following the nomenclature introduced in the current chapter, the state vector and the input are defined as* $\boldsymbol{x}_P(t)^T \triangleq \begin{bmatrix}\alpha(t) & q(t)\end{bmatrix}$ *and* $u(t) \triangleq \eta(t)$*. Furthermore, the uncertain system matrix* $\boldsymbol{A}_P$*, the known input matrix* $\boldsymbol{B}_P$ *and the uncertain control effectiveness* Λ *are given by:*

$$\boldsymbol{A}_P = \begin{bmatrix} Z_\alpha & 1+Z_q \\ \lambda_\alpha \cdot M_\alpha & \lambda_q \cdot M_q \end{bmatrix}, \qquad \boldsymbol{B}_P = \begin{bmatrix} 0 \\ M_\eta \end{bmatrix}, \qquad \Lambda = \lambda_\eta. \tag{3.46}$$

The nominal system matrix $\boldsymbol{A}_{p,nom}$*, which represents the most likely value of the system matrix* $\boldsymbol{A}_P$*, results from* (2.51) *for* $\lambda_\alpha = \lambda_q = \lambda_\eta = 1$ *and is given by*

$$\boldsymbol{A}_{p,nom} = \begin{bmatrix} Z_\alpha & 1+Z_q \\ M_\alpha & M_q \end{bmatrix}. \tag{3.47}$$

As stated in Section 2.2, the controller for the plant (2.51) *shall ensure accurate tracking of angle-of-attack commands* $\alpha_{cmd}(t)$ *and closed-loop poles located at* $-2.19 \pm 2.19j$*. Since MRAC is a model following control approach, a suitable reference model has to be designed first, which satisfies these control objectives. To that end, consider the nominal system matrix* $\boldsymbol{A}_{p,nom}$*. Using pole placement [111], an ideal feedback gain* $\boldsymbol{K}_x$ *may be easily computed, such that* $\boldsymbol{A}_{p,nom} + \boldsymbol{B}_P \cdot \boldsymbol{K}_x$ *provides the desired pole locations. By choosing* $\boldsymbol{A}_M = \boldsymbol{A}_{p,nom} + \boldsymbol{B}_P \cdot \boldsymbol{K}_x$ *with* $\boldsymbol{K}_x = \begin{bmatrix}-1.11 & -0.22\end{bmatrix}$*, the desired system matrix is found:*

$$\boldsymbol{A}_M = \begin{bmatrix} Z_\alpha & 1+Z_q \\ M_{\alpha,des} & M_{q,des} \end{bmatrix} = \begin{bmatrix} -2.42 & 0.91 \\ -5.32 & -1.97 \end{bmatrix}, \tag{3.48}$$

where $M_{\alpha,des}$ *and* $M_{q,des}$ *specify the desired pitch stiffness and damping, respectively. Similarly, an ideal feedforward gain* K_r *is computed such that the reference model*

$$\dot{\boldsymbol{x}}_M(t) = \boldsymbol{A}_M \cdot \boldsymbol{x}_M(t) + \boldsymbol{B}_P K_r \cdot r(t) \tag{3.49}$$

with $\boldsymbol{x}_M(t)^T = \begin{bmatrix}\alpha_M(t) & q_M(t)\end{bmatrix}$ *provides a DC gain of* 1 *and hence, ensures stationary accurate tracking of angle-of-attack commands* $r(t) \triangleq \alpha_{cmd}(t)$*. With* $K_r = -0.49$*, the input matrix of the reference model becomes*

$$\boldsymbol{B}_M = \boldsymbol{B}_P \cdot K_r = \begin{bmatrix} 0 \\ 10.53 \end{bmatrix}. \tag{3.50}$$

With the above choice of the system matrix $\boldsymbol{A}_M$ *and the command input matrix* $\boldsymbol{B}_M$*, the reference model satisfies the control objectives.*

In the next step, the adaptive controller for the plant (2.51) *is designed. To that end, notice that the matching condition from Assumption 3.4 is satisfied for all uncertainties* λ_α*,* λ_q *and* λ_η *because* Z_η *has been neglected and* $\lambda_{Z\alpha} = \lambda_{Zq} = 1$ *have been assumed. Furthermore, the control effectiveness* $\Lambda = \lambda_\eta$ *is positive due to the assumed*

uncertainty range from Table 2.4 and thus, Assumption 3.2 is satisfied as well. Since the plant is LTI, Assumptions 3.3, 3.7 and 3.8 are irrelevant. Hence, all assumptions of state-feedback direct MRAC, as stated in Theorem 3.4, are satisfied. Since there are no nonlinearities, the regressor vector, the adaptive parameter $\boldsymbol{\Theta}(t)$ and the true parameter $\boldsymbol{\Theta}^*$ simplify to

$$\boldsymbol{\omega}\left(\boldsymbol{x}_P(t), t\right)^T = \begin{bmatrix}\boldsymbol{x}_P(t)^T & r(t)\end{bmatrix} = \begin{bmatrix}\alpha(t) & q(t) & \alpha_{cmd}(t)\end{bmatrix}, \tag{3.51}$$

$$\boldsymbol{\Theta}(t) = \begin{bmatrix}\boldsymbol{\Theta}_x(t) & \Theta_r(t)\end{bmatrix} = \begin{bmatrix}\Theta_\alpha(t) & \Theta_q(t) & \Theta_r(t)\end{bmatrix} \tag{3.52}$$

$$\boldsymbol{\Theta}^* = \begin{bmatrix}\boldsymbol{\Theta}_x^* & \Theta_r^*\end{bmatrix} = \begin{bmatrix}\Theta_\alpha^* & \Theta_q^* & \Theta_r^*\end{bmatrix}. \tag{3.53}$$

Using the matching condition (3.5)*, the value of the ideal parameter $\boldsymbol{\Theta}^*$ may be computed as:*

$$\Theta_\alpha^* = \frac{M_{\alpha,des} - M_\alpha \cdot \lambda_\alpha}{\lambda_\eta \cdot M_\eta}, \qquad \Theta_q^* = \frac{M_{q,des} - M_q \cdot \lambda_q}{\lambda_\eta \cdot M_\eta}, \qquad \Theta_r^* = \frac{K_r}{\lambda_\eta}. \tag{3.54}$$

The design parameters $\boldsymbol{Q}$ and $\boldsymbol{\Gamma}$ of the direct MRAC are chosen as

$$\boldsymbol{Q} = \boldsymbol{I}^{2\times 2}, \qquad \boldsymbol{\Gamma} > 0. \tag{3.55}$$

Thus, the conditions of Theorem 3.4 are satisfied and the adaptive control law (3.26)*,* (3.43) *ensures closed-loop stability.*

Figure 3.5 compares the performance of the direct MRAC for different values of the learning rate $\boldsymbol{\Gamma}$. One observes that all controllers meet the control objective after some time, when the adaptive parameters converged sufficiently close to their ideal values. The time to convergence does however depend on the learning rate. For a small learning rate $\boldsymbol{\Gamma} = 10 \cdot \boldsymbol{I}^{3\times 3}$, the adaptive controller significantly deviates from the reference model during the first step. It approximately takes until the third upward step until the performance of the reference model is recovered. For larger learning rates, the desired performance is recovered significantly faster. However, with increasing learning rate $\boldsymbol{\Gamma}$, low-amplitude, high-frequency oscillations appear in the adaptive parameters, in the elevator deflection $\eta(t)$ and in the pitch rate $q(t)$. This demonstrates the fundamental trade-off when designing an adaptive controller. On the one side, if the learning rate is chosen too small, the performance of the reference model is recovered too slowly. On the other side, overly large learning rates lead to high-frequency, low-amplitude oscillations at the beginning. These oscillations do not only wear out the actuator, but are also signs of a weakly damped, hardly robust control system during this transient phase.

The reference model (3.4) of an adaptive control system is one of the most important design parameters as it specifies the desired closed-loop system response. Since the tracking error $\boldsymbol{e}_C(t)$ quantifies the difference between the reference model and the plant, it is an intuitive measure for the success of adaptive control. If the tracking error is small, the plant approximately responds like the reference model and hence, the

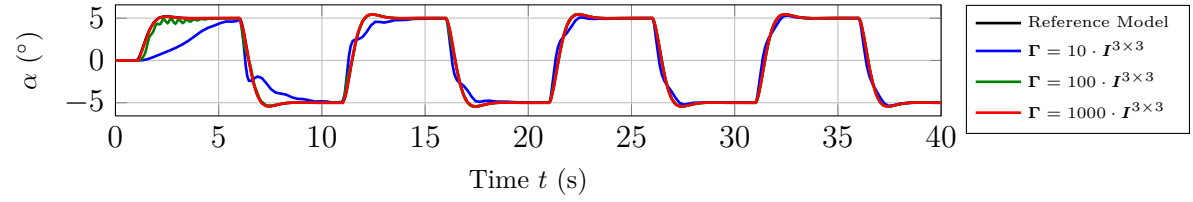

(a) Angle-Of-Attack α

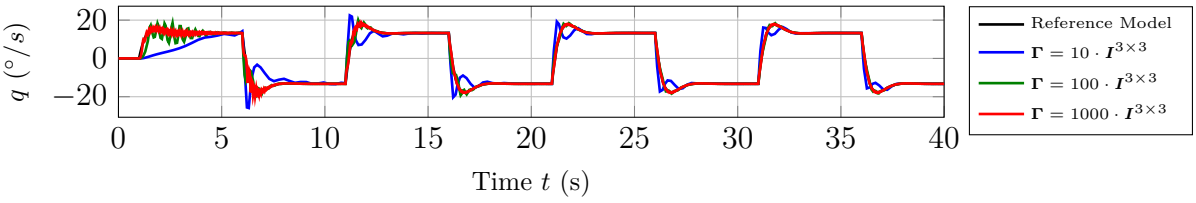

(b) Pitch Rate q

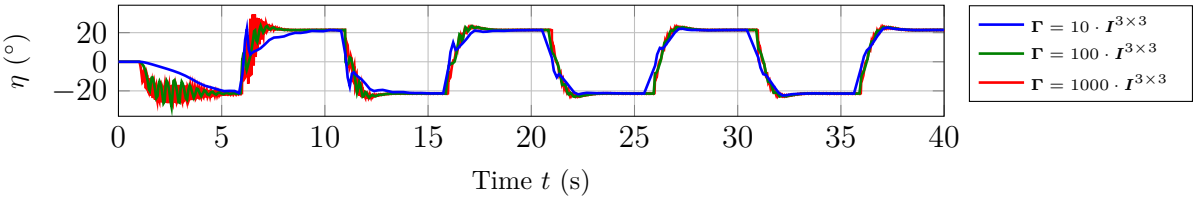

(c) Elevator Deflection η

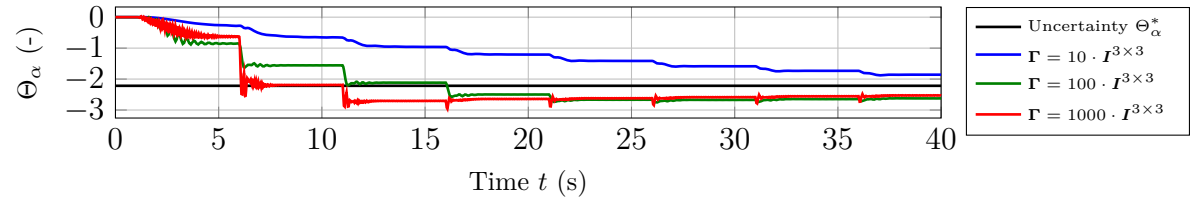

(d) Adaptive Parameter Θ_α

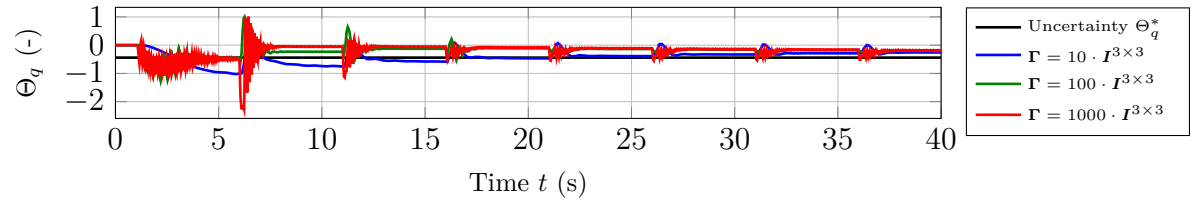

(e) Adaptive Parameter Θ_q

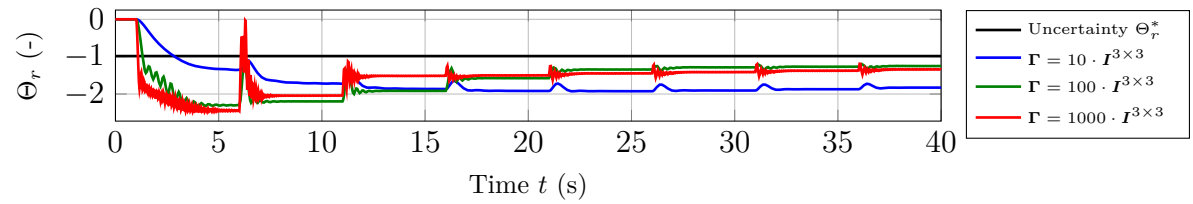

(f) Adaptive Parameter Θ_r

Figure 3.5: Performance of a direct MRAC for different values of the learning rate $\mathbf{\Gamma}$ for a 5° square wave command in case of $\lambda_\alpha = \lambda_q = 1$ and $\lambda_\eta = 0.5$.

desired closed-loop system response is recovered. While the size of tracking error is an important measure of performance, Theorem 3.4 only proves that the tracking error asymptotically decreases to zero. Even though asymptotic tracking of the reference model was the original control objective (see Section 3.1), it is also of significant interest to obtain insight into the tracking performance before the tracking error converges. Furthermore, Theorem 3.4 did not clarify the meaning of the other two design parameters of the adaptive controller, namely the learning rate $\boldsymbol{\Gamma}$ and the weighting matrix $\boldsymbol{Q}$. In order to shed light on these aspects, a guaranteed bound on the tracking error is derived subsequently. For reasons of simplicity, assume that the initial conditions of the reference model and of the plant are identical, i.e. $\boldsymbol{x}_P(0) = \boldsymbol{x}_M(0)$, and that the update law is initialized to zero, i.e. $\boldsymbol{\Theta}(0) = \mathbf{0}$. Due to these assumptions, the initial conditions of the tracking error and the parameter error become

$$\boldsymbol{e}_C(0) = \mathbf{0}, \qquad \tilde{\boldsymbol{\Theta}}(0) = -\boldsymbol{\Theta}^*. \tag{3.56}$$

Furthermore, assume that conservative bounds on the unknown parameter $\boldsymbol{\Theta}^*$ and the control effectiveness $\boldsymbol{\Lambda}$ are known such that

$$\|\boldsymbol{\Theta}^*\|_F \leq \Theta^*_{\max}, \qquad \lambda_{\max}(\boldsymbol{\Lambda}) = \|\boldsymbol{\Lambda}\|_{i,2} \leq \Lambda_{\max} \tag{3.57}$$

hold, where $\Theta^*_{\max}$ and $\Lambda_{\max}$ are known, positive scalars.

In order to derive a bound on the tracking error, consider the Lyapunov function (3.30). At $t = 0$, the Lyapunov function takes the value $V(0)$. Since Theorem 3.4 guarantees global stability, the Lyapunov function will be smaller than or equal to $V(0)$ for all times, i.e. $V(t) \leq V(0)$, due to $\dot{V}(t) \leq 0 \; \forall t \geq 0$. Using the lower bound for $V(t)$ derived in Lemma 3.3, the following relation follows immediately:

$$\frac{1}{2}\lambda_{\min}(\boldsymbol{P}) \cdot \|\boldsymbol{e}_C(t)\|_2^2 \leq V(t) \leq V(0) \quad \forall\, t \geq 0. \tag{3.58}$$

Solving (3.58) for $\|\boldsymbol{e}_C(t)\|_2$ yields a bound on the tracking error:

$$\|\boldsymbol{e}_C(t)\|_2 \leq \sqrt{\frac{2 \cdot V(0)}{\lambda_{\min}(\boldsymbol{P})}} \quad \forall\, t \geq 0. \tag{3.59}$$

While (3.59) is a viable bound for the tracking error, the value of the Lyapunov function at $t = 0$ may not be determined exactly as it depends on the initial conditions $\boldsymbol{e}_C(0)$ and $\tilde{\boldsymbol{\Theta}}(0)$, which are inherently uncertain (see (3.56)). However, an appropriate upper bound may be determined. For this, evaluate the upper bound for $V(t)$ from Lemma 3.3 at $t = 0$:

$$V(0) \leq \frac{1}{2}\lambda_{\max}(\boldsymbol{P}) \cdot \|\boldsymbol{e}_C(0)\|_2^2 + \frac{\lambda_{\max}(\boldsymbol{\Lambda})}{2 \cdot \lambda_{\min}(\boldsymbol{\Gamma})} \cdot \|\tilde{\boldsymbol{\Theta}}(0)\|_F^2. \tag{3.60}$$

With the initial conditions from (3.56) and the uncertainty bound from (3.57), the following upper bound for $V(0)$ results right away:

$$V(0) \leq \frac{\Lambda_{\max}}{2 \cdot \lambda_{\min}(\boldsymbol{\Gamma})} \cdot {\Theta^*_{\max}}^2. \tag{3.61}$$

Using the upper bound (3.61), the tracking error bound (3.59) becomes

$$\|\boldsymbol{e}_C(t)\|_2 \leq \sqrt{\frac{\Lambda_{\max} \cdot {\Theta^*_{\max}}^2}{\lambda_{\min}(\boldsymbol{P}) \cdot \lambda_{\min}(\boldsymbol{\Gamma})}} \quad \forall\, t \geq 0. \tag{3.62}$$

Eq. (3.62) shows that large uncertainties may lead to large tracking errors. This effect may only be compensated by choosing a large learning rate $\boldsymbol{\Gamma}$ or a large weighting matrix $\boldsymbol{Q}$. In order to see the latter, notice that the Lyapunov equation (3.31) yields a scaled $\boldsymbol{P}$, if $\boldsymbol{Q}$ is scaled by some factor. However, it is a well-known fact that overly large learning rates will decrease the robustness of MRAC with respect to plant imperfections and especially to non-parametric uncertainties such as time-delay [43] or unmodeled dynamics [136, 89]. Thus, the choice of the design parameters needs to trade off good tracking performance versus robustness to plant imperfections. Unfortunately, no precise rules for the selection of the design parameters exist so far.

Although the tracking error bound (3.62) indicates that both design parameters $\boldsymbol{\Gamma}$ and $\boldsymbol{Q}$ are similar in the sense that they may serve to reduce the transient tracking error, they have substantially different interpretations. In the first place, the learning rate $\boldsymbol{\Gamma}$ is a weighting of the regressor vector as is evident from the update law (3.43). Assuming a diagonal learning rate, the i-th element of the regressor vector is scaled by the i-th diagonal entry of the learning rate and leads to an update of the i-th column of $\boldsymbol{\Theta}(t)$ or i-th row of $\boldsymbol{\Theta}(t)^T$, respectively. Thus, the i-th diagonal entry of the learning rate determines how fast the parameters associated with the i-th regressor vector element are updated. In contrast, the matrix $\boldsymbol{Q}$ implicitly determines the relative weighting of the tracking error. Since the matrix $\boldsymbol{P}$ is computed from the Lyapunov equation (3.31), the relation between the choice of $\boldsymbol{Q}$ and the weighting of the tracking error by virtue of $\boldsymbol{P} \cdot \boldsymbol{B}_P$ is not as evident.

3.2.2 Direct Model Reference Adaptive Control with Baseline

The previous section introduced direct MRAC in its most basic form. The control law (3.22) is purely adaptive as it only depends on the time-varying adaptive parameter $\boldsymbol{\Theta}(t)$. In practice, adaptive controllers are usually not used as standalone controllers, but augment an existing baseline controller. In this scenario, the baseline controller is a conventional, non-adaptive controller, which satisfies all control design requirements for reasonably sized uncertainties. If the uncertainties grow larger (for example due to an unexpected malfunction or damage), then the baseline controller might not be able to maintain stability and performance. For this reason, the baseline controller is augmented with an additional adaptive control signal, which compensates the uncertainties. Due to the practical relevance of this scenario, this section extends the results of the previous section in such a way that a baseline controller may be accommodated.

To that end, let the baseline control law be given by

$$\boldsymbol{u}_{bl}(t) = \boldsymbol{K}_x \cdot \boldsymbol{x}_P(t) + \boldsymbol{K}_r \cdot \boldsymbol{r}(t). \tag{3.63}$$

This control law is augmented with an additional adaptive control signal, which is structurally equivalent to (3.22). The overall control law, including baseline controller and adaptive augmentation, is hence given by:

$$\boldsymbol{u}(t) = \boldsymbol{u}_{bl}(t) + \boldsymbol{\Psi}(t) \cdot \boldsymbol{\omega}(\boldsymbol{x}_P(t), t). \tag{3.64}$$

In (3.64), $\boldsymbol{\Psi}(t) \triangleq \begin{bmatrix} \boldsymbol{\Psi}_x(t) & \boldsymbol{\Psi}_r(t) & \boldsymbol{\Psi}_\phi(t) \end{bmatrix}$ represents the adaptive parameter. As compared to the previous section, the adaptive parameter is denoted by $\boldsymbol{\Psi}(t)$ instead of $\boldsymbol{\Theta}(t)$ in order to clearly distinguish the cases with and without baseline controller.

Due to the presence of a baseline controller, the matching conditions of the direct MRAC have to be slightly altered. The plant (3.1), the reference model (3.4) and the baseline controller (3.63) are required to satisfy:

Assumption 3.9 (Matching Condition with Baseline)**.** *The uncertain matrices and functions of the plant* (3.1) *satisfy the matching conditions*

$$\begin{aligned} \boldsymbol{A}_P &= \boldsymbol{A}_M - \boldsymbol{B}_P \boldsymbol{\Lambda} \cdot (\boldsymbol{\Psi}_x^* + \boldsymbol{K}_x), \\ \boldsymbol{B}_M &= \boldsymbol{B}_P \boldsymbol{\Lambda} \cdot (\boldsymbol{\Psi}_r^* + \boldsymbol{K}_r), \\ \boldsymbol{f}(\boldsymbol{x}_P(t), t) &= -\boldsymbol{B}_P \boldsymbol{\Lambda} \bar{\boldsymbol{f}}(\boldsymbol{x}_P(t), t), \end{aligned} \tag{3.65}$$

which relate the uncertain matrices and functions to the reference model (3.4) *and the baseline controller* (3.63)*.*

If the nonlinearity $\bar{\boldsymbol{f}}(\boldsymbol{x}_P(t), t)$ may be parametrized linearly and exactly, $\bar{\boldsymbol{f}}(\boldsymbol{x}_P(t), t) = \boldsymbol{\Psi}_\phi^* \cdot \boldsymbol{\phi}(\boldsymbol{x}_P(t))$ holds. The resulting ideal parameter is denoted by $\boldsymbol{\Psi}^* \triangleq \begin{bmatrix} \boldsymbol{\Psi}_x^* & \boldsymbol{\Psi}_r^* & \boldsymbol{\Psi}_\phi^* \end{bmatrix}$ instead of $\boldsymbol{\Theta}^*$ to clearly distinguish the cases with and without baseline controller. The modified matching condition (3.65) ensures that the baseline controller recovers the desired closed-loop response, if there are no parametric uncertainties (i.e. $\boldsymbol{\Psi}^* = \boldsymbol{0}$). Put another way, the control objective of the adaptive augmentation and of the baseline controller have to be compatible.

Following the same steps as in the previous section, the modified control law (3.64) and the modified matching conditions (3.65) may be used to rewrite the plant as

$$\dot{\boldsymbol{x}}_P(t) = \boldsymbol{A}_M \boldsymbol{x}_P(t) + \boldsymbol{B}_M \boldsymbol{r}(t) + \boldsymbol{B}_P \boldsymbol{\Lambda} \tilde{\boldsymbol{\Psi}}(t) \cdot \boldsymbol{\omega}(\boldsymbol{x}_P(t), t), \tag{3.66}$$

where $\tilde{\boldsymbol{\Psi}}(t) = \boldsymbol{\Psi}(t) - \boldsymbol{\Psi}^*$ denotes the parameter error. Since (3.66) is structurally equivalent to (3.28), the error dynamics and the proof of closed-loop stability are equivalent to the case without baseline controller. Hence, the update law

$$\dot{\boldsymbol{\Psi}}(t)^T = \dot{\tilde{\boldsymbol{\Psi}}}(t)^T = -\boldsymbol{\Gamma} \boldsymbol{\omega}(\boldsymbol{x}_P(t), t) \cdot \boldsymbol{e}_C(t)^T \boldsymbol{P} \boldsymbol{B}_P \tag{3.67}$$

results, which is structurally equivalent to the update law without baseline controller from (3.43).

Although the consideration of the baseline controller (3.63) does neither change the structure of the adaptive controller nor its proof of stability, the cases with and without

baseline controller are not equivalent. Due to the consideration of the baseline controller, the ideal value $\boldsymbol{\Psi}^*$ of the adaptive parameter is not equivalent to $\boldsymbol{\Theta}^*$. Likewise, the trajectories of the adaptive parameter $\boldsymbol{\Psi}(t)$ are not equivalent to $\boldsymbol{\Theta}(t)$. In fact, the cases with and without baseline controller are related by the variable substitutions

$$\boldsymbol{\Theta}_x^* = \boldsymbol{\Psi}_x^* + \boldsymbol{K}_x, \qquad \boldsymbol{\Theta}_x(t) = \boldsymbol{\Psi}_x(t) + \boldsymbol{K}_x, \tag{3.68}$$

$$\boldsymbol{\Theta}_r^* = \boldsymbol{\Psi}_r^* + \boldsymbol{K}_r, \qquad \boldsymbol{\Theta}_r(t) = \boldsymbol{\Psi}_r(t) + \boldsymbol{K}_r, \tag{3.69}$$

$$\boldsymbol{\Theta}_\phi^* = \boldsymbol{\Psi}_\phi^*, \qquad \boldsymbol{\Theta}_\phi(t) = \boldsymbol{\Psi}_\phi(t). \tag{3.70}$$

It is interesting to notice that the above substitutions imply that the consideration of a baseline controller is equivalent to initializing the parameters of a standalone adaptive controller to

$$\boldsymbol{\Theta}_x(0) = \boldsymbol{K}_x, \qquad \boldsymbol{\Theta}_r(0) = \boldsymbol{K}_r, \qquad \boldsymbol{\Theta}_\phi(0) = \mathbf{0}, \tag{3.71}$$

when assuming that the adaptive parameter $\boldsymbol{\Psi}(t)$ is initialized as $\boldsymbol{\Psi}(0) = \mathbf{0}$. Furthermore, while the consideration of the baseline controller leads to a different ideal parameter $\boldsymbol{\Psi}^*$ and a different adaptive parameter $\boldsymbol{\Psi}(t)$, it does not change the parameter error as $\tilde{\boldsymbol{\Theta}}_{(\cdot)}(t) = \tilde{\boldsymbol{\Psi}}_{(\cdot)}(t)$ holds.

Since the adaptive controller and its proof of stability in case of an additional baseline controller are structurally equivalent to the case without baseline controller, these two cases will not be specifically distinguished in the remainder of this thesis. Hence, $\boldsymbol{\Theta}(t)$ and $\boldsymbol{\Theta}^*$ (instead of $\boldsymbol{\Psi}(t)$ and $\boldsymbol{\Psi}^*$) will denote the adaptive and ideal parameter, even if a baseline controller is present. With respect to the objectives of this thesis, the most important difference between these two cases consists in the different computation of the ideal parameter $\boldsymbol{\Theta}^*$. If a baseline controller is present, the baseline controller gains $\boldsymbol{K}_x$ and $\boldsymbol{K}_r$ have to be considered according to (3.65).

3.2.3 Predictor-Based Model Reference Adaptive Control

In direct MRAC, the control law (3.26) and the adaptation are inseparably related, as the update law (3.43) immediately alters the controller gains. While direct approaches lead to a simple controller architecture, they are limited in the sense that a change in the control law requires a completely new proof of stability. In contrast, indirect approaches separate the adaptation from the control law by resorting to a two-step procedure. In the first step, the unknown plant parameters are identified using adaptation. In the second step, this information is used within an appropriate control law. Owing to this separation, stability of the identification may be proven independently from stability of the closed-loop control system. This separation is for example also exploited in $\mathcal{L}_1$-AC, which is based on an indirect approach.

Subsequently, a special class of indirect approaches is introduced, which is referred to as predictor-based MRAC in literature [104]. In contrast to classical indirect approaches, predictor-based MRAC parametrizes the uncertainties in an input-affine

way. Hence, the estimated parameters may be used immediately for control purposes. If the parametrization includes inputs for matched as well as unmatched uncertainties, then predictor-based MRAC will be algebraically equivalent to classical indirect MRAC [15]. This section will however focus on the case of matched uncertainties only. The derived control law depends on the same assumptions as direct MRAC, namely Assumptions 3.1 (state feedback), 3.2 (positive definite control effectiveness), 3.3 (Lipschitz condition), 3.5 (matching condition), 3.7 (linear parametrization) and 3.8 (exact parametrization).

For the first step, namely parameter identification, consider the plant representation (3.12), which results from the general plant (3.1) by virtue of the alternative matching condition of Assumption 3.5. Since the nonlinearity $\boldsymbol{f}_m\left(\boldsymbol{x}_P\left(t\right),t\right)$ admits an exact, linear parametrization due to Assumptions 3.7 and 3.8, (3.12) may be restated as

$$\dot{\boldsymbol{x}}_P\left(t\right)=\boldsymbol{A}_M\boldsymbol{x}_P\left(t\right)+\boldsymbol{B}_P\left(\boldsymbol{\Lambda}\boldsymbol{u}\left(t\right)+\boldsymbol{\Theta}_{m,x}^{*}\boldsymbol{x}_P\left(t\right)+\boldsymbol{\Theta}_{m,\phi}^{*}\cdot\boldsymbol{\phi}\left(\boldsymbol{x}_P\left(t\right)\right)\right). \tag{3.72}$$

The adaptive state predictor (identifier) for the plant (3.72) is given by:

$$\dot{\hat{\boldsymbol{x}}}_P\left(t\right)=\boldsymbol{A}_M\hat{\boldsymbol{x}}_P\left(t\right)+\boldsymbol{B}_P\left(\hat{\boldsymbol{\Lambda}}\left(t\right)\boldsymbol{u}\left(t\right)+\hat{\boldsymbol{\Theta}}_{m,x}\left(t\right)\boldsymbol{x}_P\left(t\right)+\hat{\boldsymbol{\Theta}}_{m,\phi}\left(t\right)\cdot\boldsymbol{\phi}\left(\boldsymbol{x}_P\left(t\right)\right)\right), \tag{3.73}$$

where $\hat{\boldsymbol{\Theta}}_{m,x}:\mathbb{R}_+\to\mathbb{R}^{m\times n}$, $\hat{\boldsymbol{\Lambda}}:\mathbb{R}_+\to\mathbb{R}^{m\times m}$ and $\hat{\boldsymbol{\Theta}}_{m,\phi}:\mathbb{R}_+\to\mathbb{R}^{m\times n_\phi}$ are the adaptive estimates of the plant parameters $\boldsymbol{\Theta}_{m,x}^{*}$, $\boldsymbol{\Lambda}$ and $\boldsymbol{\Theta}_{m,\phi}^{*}$, respectively. Similar to direct MRAC, the true parameters and the known signals may be summarized in a true parameter matrix and a regressor vector:

$$\begin{aligned}\boldsymbol{\Theta}_m^{*}&=\begin{bmatrix}\boldsymbol{\Theta}_{m,x}^{*} & \boldsymbol{\Lambda} & \boldsymbol{\Theta}_{m,\phi}^{*}\end{bmatrix},\\ \boldsymbol{\omega}\left(\boldsymbol{x}_P\left(t\right),t\right)&=\begin{bmatrix}\boldsymbol{x}_P\left(t\right)\\ \boldsymbol{u}\left(t\right)\\ \boldsymbol{\phi}\left(\boldsymbol{x}_P\left(t\right)\right)\end{bmatrix}\end{aligned} \tag{3.74}$$

with $\boldsymbol{\Theta}_m^{*}\in\mathbb{R}^{m\times n_r}$, $n_r=n+m+n_\phi$, and $\boldsymbol{\omega}:\mathbb{R}^n\times\mathbb{R}_+\to\mathbb{R}^{n_r}$. Notice that the definition of the regressor vector in (3.74) does not coincide with the definition in (3.23). As it should always be clear from the context, whether a direct or a predictor-based approach is in use, no confusion should arise. Similar to (3.74), the adaptive estimates may also be collected in a single adaptive parameter matrix:

$$\hat{\boldsymbol{\Theta}}_m\left(t\right)=\begin{bmatrix}\hat{\boldsymbol{\Theta}}_{m,x}\left(t\right) & \hat{\boldsymbol{\Lambda}}\left(t\right) & \hat{\boldsymbol{\Theta}}_{m,\phi}\left(t\right)\end{bmatrix} \tag{3.75}$$

with $\hat{\boldsymbol{\Theta}}_m:\mathbb{R}_+\to\mathbb{R}^{m\times n_r}$. Using (3.74) and (3.75), the plant (3.72) and the state predictor (3.73) become

$$\dot{\boldsymbol{x}}_P\left(t\right)=\boldsymbol{A}_M\boldsymbol{x}_P\left(t\right)+\boldsymbol{B}_P\boldsymbol{\Theta}_m^{*}\cdot\boldsymbol{\omega}\left(\boldsymbol{x}_P\left(t\right),t\right) \tag{3.76}$$

and

$$\dot{\hat{\boldsymbol{x}}}_P\left(t\right)=\boldsymbol{A}_M\hat{\boldsymbol{x}}_P\left(t\right)+\boldsymbol{B}_P\hat{\boldsymbol{\Theta}}_m\left(t\right)\cdot\boldsymbol{\omega}\left(\boldsymbol{x}_P\left(t\right),t\right), \tag{3.77}$$

respectively. The derivation of an update law for the estimate $\hat{\boldsymbol{\Theta}}_m(t)$ follows the same lines as in case of direct MRAC. It is based on a proof of stability of the prediction error dynamics and the yet unknown parameter error dynamics. The prediction error is defined as

$$\boldsymbol{e}_P(t) \triangleq \hat{\boldsymbol{x}}_P(t) - \boldsymbol{x}_P(t) \tag{3.78}$$

and evolves according to the differential equation

$$\dot{\boldsymbol{e}}_P(t) = \dot{\hat{\boldsymbol{x}}}_P(t) - \dot{\boldsymbol{x}}_P(t) = \boldsymbol{A}_M \boldsymbol{e}_P(t) + \boldsymbol{B}_P \tilde{\boldsymbol{\Theta}}_m(t) \cdot \boldsymbol{\omega}(\boldsymbol{x}_P(t), t), \tag{3.79}$$

where $\tilde{\boldsymbol{\Theta}}_m(t)$ denotes the parameter error, which is defined as

$$\tilde{\boldsymbol{\Theta}}_m(t) \triangleq \hat{\boldsymbol{\Theta}}_m(t) - \boldsymbol{\Theta}_m^*. \tag{3.80}$$

In order to prove stability of the error dynamics (3.79) and to derive an update law for the adaptive parameter $\hat{\boldsymbol{\Theta}}_m$, consider the Lyapunov function candidate

$$V(t) = \frac{1}{2}\boldsymbol{e}_P(t)^T \boldsymbol{P}\boldsymbol{e}_P(t) + \frac{1}{2}\operatorname{Tr}\left\{\tilde{\boldsymbol{\Theta}}_m(t)\,\boldsymbol{\Gamma}^{-1}\tilde{\boldsymbol{\Theta}}_m(t)^T\right\}, \tag{3.81}$$

where $\boldsymbol{P} \in \mathbb{S}_{++}^n$ is the positive definite, unique solution of the Lyapunov equation (3.31) and $\boldsymbol{\Gamma} \in \mathbb{S}_{++}^{n_r}$ is the positive definite learning rate. Differentiating (3.81) with respect to time, inserting the error dynamics (3.79), exploiting the Lyapunov equation (3.31) and using the trace property (B.156) yields:

$$\begin{aligned}\dot{V}(t) = &-\frac{1}{2}\boldsymbol{e}_P(t)^T \boldsymbol{Q}\boldsymbol{e}_P(t) \\ &+ \operatorname{Tr}\left\{\tilde{\boldsymbol{\Theta}}_m(t)\left(\boldsymbol{\Gamma}^{-1}\dot{\tilde{\boldsymbol{\Theta}}}_m(t)^T + \boldsymbol{\omega}(\boldsymbol{x}_P(t), t)\cdot \boldsymbol{e}_P(t)^T \boldsymbol{P}\boldsymbol{B}_P\right)\right\}.\end{aligned} \tag{3.82}$$

By choosing the parameter error dynamics as

$$\dot{\tilde{\boldsymbol{\Theta}}}_m(t)^T = -\boldsymbol{\Gamma}\boldsymbol{\omega}(\boldsymbol{x}_P(t), t)\cdot \boldsymbol{e}_P(t)^T \boldsymbol{P}\boldsymbol{B}_P, \tag{3.83}$$

the derivative of the Lyapunov function candidate may be rendered negative semidefinite, i.e.

$$\dot{V}(t) = -\frac{1}{2}\boldsymbol{e}_P(t)^T \boldsymbol{Q}\boldsymbol{e}_P(t) \leq 0 \quad \forall\, \boldsymbol{e}_P(t), \tilde{\boldsymbol{\Theta}}_m(t), \tag{3.84}$$

which proves global stability of the prediction error $\boldsymbol{e}_P(t)$ and the parameter error $\tilde{\boldsymbol{\Theta}}_m(t)$. Since $\boldsymbol{\Theta}_m^*$ is a constant by assumption, the definition of the parameter error in (3.80) admits to state the following update law for the adaptive parameter $\hat{\boldsymbol{\Theta}}_m(t)$:

$$\dot{\hat{\boldsymbol{\Theta}}}_m(t)^T = -\boldsymbol{\Gamma}\boldsymbol{\omega}(\boldsymbol{x}_P(t), t)\cdot \boldsymbol{e}_P(t)^T \boldsymbol{P}\boldsymbol{B}_P. \tag{3.85}$$

To conclude the first step of the derivation, the preceding results are summarized in the following lemma:

Lemma 3.7 (Nominal Stability of the Prediction Error and the Parameter Error)**.** *Consider the plant* (3.1) *and let Assumptions 3.1 (state feedback), 3.2 (positive definite control effectiveness), 3.3 (Lipschitz condition), 3.5 (matching condition), 3.7 (linear parametrization) and 3.8 (exact parametrization) hold. Then, according to* (3.76)*, the plant admits the compact representation*

$$\dot{\boldsymbol{x}}_P(t) = \boldsymbol{A}_M \boldsymbol{x}_P(t) + \boldsymbol{B}_P \boldsymbol{\Theta}_m^* \cdot \boldsymbol{\omega}(\boldsymbol{x}_P(t), t),$$

where the true parameter matrix $\boldsymbol{\Theta}_m^*$ and the regressor vector $\boldsymbol{\omega}(\boldsymbol{x}_P(t), t)$ are defined in (3.74)*. Furthermore, let the learning rate $\boldsymbol{\Gamma} \in \mathbb{S}_{++}^{n_r}$ and the weighting matrix $\boldsymbol{Q} \in \mathbb{S}_{++}^{n}$ be chosen positive definite, and let $\boldsymbol{P} \in \mathbb{S}_{++}^{n}$ be the positive definite solution of the Lyapunov equation* (3.31)*. Then, the error dynamics* (3.79) *and* (3.83) *of the adaptive state predictor*

$$\begin{aligned}\dot{\hat{\boldsymbol{x}}}_P(t) &= \boldsymbol{A}_M \hat{\boldsymbol{x}}_P(t) + \boldsymbol{B}_P \hat{\boldsymbol{\Theta}}_m(t) \cdot \boldsymbol{\omega}(\boldsymbol{x}_P(t), t), \\ \dot{\hat{\boldsymbol{\Theta}}}_m(t)^T &= -\boldsymbol{\Gamma} \boldsymbol{\omega}(\boldsymbol{x}_P(t), t) \cdot \boldsymbol{e}_P(t)^T \boldsymbol{P} \boldsymbol{B}_P,\end{aligned}$$

derived in (3.77) *and* (3.85)*, will have a globally stable equilibrium at $\boldsymbol{e}_P = \boldsymbol{0}$ and $\tilde{\boldsymbol{\Theta}}_m = 0$.*

Proof. The proof relies on the Lyapunov candidate function (3.81). It amounts to the steps which have led from (3.81) to (3.84), where the latter establishes stability of the error dynamics (3.79), (3.83). □

Remark 3.8. *Similar to the direct case, it is also possible to derive an explicit bound on the transient prediction error. To that end, let the initial conditions be such that*

$$\boldsymbol{e}_P(0) = 0, \qquad \hat{\boldsymbol{\Theta}}_m(0) = \boldsymbol{0} \tag{3.86}$$

hold and let a conservative bound on the uncertainties be known:

$$\|\boldsymbol{\Theta}_m^*\|_F \leq \Theta_{\max}^*. \tag{3.87}$$

Then, the following bound on the prediction error may be derived by following the same steps, which led to tracking error bound (3.62) *of direct MRAC:*

$$\|\boldsymbol{e}_P(t)\|_2 \leq \frac{\Theta_{\max}^*}{\sqrt{\lambda_{\min}(\boldsymbol{P}) \cdot \lambda_{\min}(\boldsymbol{\Gamma})}} \quad \forall\, t \geq 0. \tag{3.88}$$

When using the update law (3.85), Eq. (3.84) implies that the prediction error dynamics are stable irrespective of the actual control input $\boldsymbol{u}(t)$. However, since neither the plant (3.72) nor the state predictor (3.73) are known to be stable a-priori, boundedness of the other signals of the closed loop is not ensured. This is also the reason why Barbalat's Lemma (Lemma C.3) may not yet be applied at this point in order to conclude $\lim_{t\to\infty} -\dot{V}(t) = 0$. For this, the control law $\boldsymbol{u}(t)$, which usually is a function

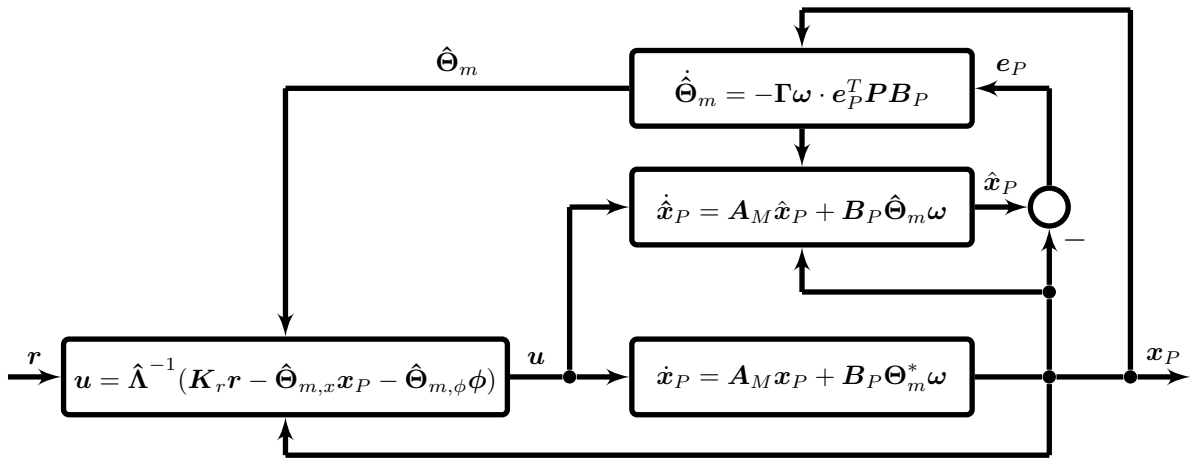

Figure 3.6: Illustration of predictor-based MRAC.

of either $\boldsymbol{x}_P(t)$ or $\hat{\boldsymbol{x}}_P(t)$, would have to be bounded in order to conclude that $\boldsymbol{e}_P(t)$ and hence $-\dot{V}(t)$ is uniformly continuous.

In order to prove asymptotic convergence of the prediction error $\boldsymbol{e}_P(t)$, the actual control law has to be chosen. Since the overall control objective is asymptotic tracking of the reference model (3.4), the control law is determined such that the predictor (3.73) turns into the reference model. This idea leads to the control law

$$\boldsymbol{u}(t) = \hat{\boldsymbol{\Lambda}}(t)^{-1} \left(\boldsymbol{K}_r \boldsymbol{r}(t) - \hat{\boldsymbol{\Theta}}_{m,x}(t) \boldsymbol{x}_P(t) - \hat{\boldsymbol{\Theta}}_{m,\phi}(t) \boldsymbol{\phi}(\boldsymbol{x}_P(t)) \right). \tag{3.89}$$

As expected, inserting the control law (3.89) into the predictor (3.73) yields

$$\dot{\hat{\boldsymbol{x}}}_P(t) = \boldsymbol{A}_M \hat{\boldsymbol{x}}_P(t) + \boldsymbol{B}_M \boldsymbol{r}(t). \tag{3.90}$$

The overall structure of the resulting predictor-based MRAC is shown in Figure 3.6. Its stability is proven in the following theorem:

Theorem 3.9 (Nominal Stability of Predictor-Based MRAC)**.** *Consider the plant* (3.1) *and let Lemma 3.7 hold. Then, the control law*

$$\boldsymbol{u}(t) = \hat{\boldsymbol{\Lambda}}(t)^{-1} \left(\boldsymbol{K}_r \boldsymbol{r}(t) - \hat{\boldsymbol{\Theta}}_{m,x}(t) \boldsymbol{x}_P(t) - \hat{\boldsymbol{\Theta}}_{m,\phi}(t) \boldsymbol{\phi}(\boldsymbol{x}_P(t)) \right),$$

defined in (3.89)*, will ensure boundedness of all closed-loop signals. Furthermore, the prediction error will asymptotically decrease to zero, i.e.*

$$\lim_{t \to \infty} \|\boldsymbol{e}_P(t)\| = 0,$$

which implies asymptotic tracking of the reference model (3.4)*.*

Proof. If the command signal $\boldsymbol{r}(t)$ is bounded, the state vector $\hat{\boldsymbol{x}}_P(t)$ of the state predictor will be bounded as well since the state predictor implicitly realizes the reference model, as shown in (3.90). Since the prediction error $\boldsymbol{e}_P(t)$ and the parameter error

$\tilde{\boldsymbol{\Theta}}_m(t)$ are bounded by virtue of Lemma 3.7, the Lyapunov proof of stability ensures boundedness of $\dot{\boldsymbol{e}}_P(t)$. Thus, following the same lines as in case of direct MRAC, Barbalat's Lemma (Lemma C.3) proves asymptotic convergence of the prediction error towards zero, i.e. $\lim_{t\to\infty} \|\boldsymbol{e}_P(t)\| = 0$. Since the latter implies asymptotic tracking of the reference model (3.4), this proves that the predictor-based MRAC actually achieves its control objective. □

Remark 3.10. *While the control law* (3.89) *seems to achieve the control objective, it has to be noted that* (3.89) *involves an explicit inversion of* $\hat{\boldsymbol{\Lambda}}(t)$*. Thus, in order to use* (3.89) *in practice, a modification of the update law such as the Singular Value Decomposition (SVD)-based projection algorithm from [83] is required in order to ensure that* $\hat{\boldsymbol{\Lambda}}(t)$ *does not become singular. Instead of using the estimates of the plant parameters in an explicit computation such as* (3.89)*, it has also been proposed to update the actual control law using an additional differential equation [119, 15]. This approach does not only bypass the need for an explicit inversion, but also introduces additional filtering into the control law, leading to smoother transient performance.*

3.2.4 Robustness Modifications

In the previous sections, direct and predictor-based MRAC have been derived for the nominal plant model (3.1). However, almost any control system shall be applied to some real physical system. As outlined at the beginning of this chapter, any mathematical model only is an approximation of the real physical system, even if it considers uncertainties. Thus, the proofs of stability, which have been derived in the previous sections for the plant model (3.1), do not hold for the real system. In order to study the effect of differences between the true physical system and the (uncertain) plant model, one commonly analyzes the stability of the controller in feedback with a more accurate plant model. While even the use of a more accurate plant model will not yield any guarantee with respect to the real physical system, stability with respect to a more realistic plant model increases confidence in the developed controller. Subsequently, this approach will be used to demonstrate that plant imperfections, even if they result from an inadequate parametrization, may cause instability of a direct MRAC. The same also holds true for indirect or predictor-based MRAC.

In order to deal with this problem, two general solutions are available. On the one side, one may require that the command $\boldsymbol{r}(t)$ is sufficiently exciting such that the regressor vector $\boldsymbol{\omega}(\boldsymbol{x}_P(t), t)$ becomes persistently exciting. In this case, MRAC becomes exponentially stable [89] and hence, robust to some plant imperfections [96]. On the other side, literature has proposed numerous robustness modifications which avoid the undesirable requirement for persistent excitation. Since the instability in case of plant imperfections results from a drift of the adaptive parameters, essentially all of the robustness modifications alter the update law. Widely known robustness modifi-

cations include the dead zone modification [130, 119], the σ-modification [88, 89], the e-modification [118, 119] or the projection algorithm [131, 105]. Due to its simplicity, this section will only introduce the σ-modification. For other modifications, the reader is referred to the respective literature.

In order to analyze stability of direct MRAC in the presence of a more realistic plant model, consider the off-nominal plant

$$\begin{aligned} \dot{\boldsymbol{x}}_P(t) &= \boldsymbol{A}_P \boldsymbol{x}_P(t) + \boldsymbol{B}_P \boldsymbol{\Lambda} \boldsymbol{u}(t) + \boldsymbol{f}(\boldsymbol{x}_P(t), t) + \boldsymbol{h}(\boldsymbol{z}_P(t)), \\ \dot{\boldsymbol{z}}_P(t) &= \boldsymbol{g}(\boldsymbol{x}_P(t), \boldsymbol{z}_P(t), \boldsymbol{u}(t), t), \\ \boldsymbol{y}_P(t) &= \boldsymbol{C}_P \boldsymbol{x}_P(t), \end{aligned} \tag{3.91}$$

where $\boldsymbol{z}_P : \mathbb{R}_+ \to \mathbb{R}^l$ is the state vector of some unmodeled dynamics with an uncertain dimension l. In (3.91), the functions $\boldsymbol{h} : \mathbb{R}^l \to \mathbb{R}^n$ and $\boldsymbol{g} : \mathbb{R}^n \times \mathbb{R}^l \times \mathbb{R}^m \times \mathbb{R}_+ \to \mathbb{R}^l$ are unknown. As the functions $\boldsymbol{f}(\boldsymbol{x}_P(t), t)$ and $\boldsymbol{g}(\boldsymbol{x}_P(t), \boldsymbol{z}_P(t), \boldsymbol{u}(t), t)$ explicitly depend on time, they may also model the effects of exogenous disturbances such as gusts. Notice that the plant model (3.1), which has underlain the derivation of MRAC in the previous sections, will result from (3.91), if $\boldsymbol{h}(\boldsymbol{z}_P(t)) = 0$ holds. While (3.91) represents a significantly larger class of plants, it still is a model of the true physical system and does for example not reflect the effects of measurement noise. In contrast to the previous sections, only Assumptions 3.1 (state feedback), 3.2 (positive definite control effectiveness), 3.3 (Lipschitz condition), 3.6 ($\operatorname{rank}(\boldsymbol{B}_P) = m$), 3.7 (linear parametrization) are assumed to hold. In this set of assumptions, Assumption 3.6 alleviates the matching condition and allows dealing with unmatched uncertainties in a simple way. Furthermore, notice that the parametrization of the nonlinear function $\boldsymbol{f}(\boldsymbol{x}_P(t), t)$ is not assumed to be exact anymore.

Since $\boldsymbol{B}_P$ has full rank due to Assumption 3.6, (3.91) may be represented as follows using (3.14):

$$\begin{aligned} \dot{\boldsymbol{x}}_P(t) &= \boldsymbol{A}_M \boldsymbol{x}_P(t) + \boldsymbol{B}_P \left(\boldsymbol{\Lambda} \boldsymbol{u}(t) + \boldsymbol{\Theta}_{m,x}^* \boldsymbol{x}_P(t) + \boldsymbol{f}_m(\boldsymbol{x}_P(t), t) \right) \\ &\quad + \bar{\boldsymbol{B}}_P \left(\boldsymbol{\Theta}_{um,x}^* \boldsymbol{x}_P(t) + \boldsymbol{f}_{um}(\boldsymbol{x}_P(t), t) \right) + \boldsymbol{h}(\boldsymbol{z}_P(t)), \\ \dot{\boldsymbol{z}}_P(t) &= \boldsymbol{g}(\boldsymbol{x}_P(t), \boldsymbol{z}_P(t), \boldsymbol{u}(t), t), \\ \boldsymbol{y}_P(t) &= \boldsymbol{C}_P \boldsymbol{x}_P(t). \end{aligned} \tag{3.92}$$

Using the relations in (3.11), (3.92) becomes:

$$\begin{aligned} \dot{\boldsymbol{x}}_P(t) &= \boldsymbol{A}_M \boldsymbol{x}_P(t) + \boldsymbol{B}_P \boldsymbol{\Lambda} \left(\boldsymbol{u}(t) - \boldsymbol{\Theta}_x^* \boldsymbol{x}_P(t) - \bar{\boldsymbol{f}}(\boldsymbol{x}_P(t), t) \right) \\ &\quad + \bar{\boldsymbol{B}}_P \left(\boldsymbol{\Theta}_{um,x}^* \boldsymbol{x}_P(t) + \boldsymbol{f}_{um}(\boldsymbol{x}_P(t), t) \right) + \boldsymbol{h}(\boldsymbol{z}_P(t)), \\ \dot{\boldsymbol{z}}_P(t) &= \boldsymbol{g}(\boldsymbol{x}_P(t), \boldsymbol{z}_P(t), \boldsymbol{u}(t), t), \\ \boldsymbol{y}_P(t) &= \boldsymbol{C}_P \boldsymbol{x}_P(t). \end{aligned} \tag{3.93}$$

By adding and subtracting $\boldsymbol{B}_M \cdot \boldsymbol{r}(t)$ and by replacing $\bar{\boldsymbol{f}}(\boldsymbol{x}_P(t), t)$ by its linear, non-exact parametrization $\boldsymbol{\Theta}_\phi^* \cdot \boldsymbol{\phi}(\boldsymbol{x}_P(t)) - \boldsymbol{\epsilon}(\boldsymbol{x}_P(t), t)$, the $\boldsymbol{x}_P$-dynamics in (3.93) may be

compactly rewritten as

$$\begin{aligned}\dot{\boldsymbol{x}}_P(t) = \boldsymbol{A}_M \boldsymbol{x}_P(t) + \boldsymbol{B}_M \boldsymbol{r}(t) + \boldsymbol{B}_P \boldsymbol{\Lambda}\left(\boldsymbol{u}(t) - \boldsymbol{\Theta}^* \boldsymbol{\omega}\left(\boldsymbol{x}_P(t), t\right)\right) \\ + \boldsymbol{w}\left(\boldsymbol{x}_P(t), \boldsymbol{z}_P(t), t\right).\end{aligned} \tag{3.94}$$

The function $\boldsymbol{w}\left(\boldsymbol{x}_P(t), \boldsymbol{z}_P(t), t\right)$ in (3.94) is defined as

$$\begin{aligned}\boldsymbol{w}\left(\boldsymbol{x}_P(t), \boldsymbol{z}_P(t), t\right) \triangleq \boldsymbol{h}\left(\boldsymbol{z}_P(t)\right) + \boldsymbol{B}_P \boldsymbol{\Lambda} \boldsymbol{\epsilon}\left(\boldsymbol{x}_P(t), t\right) \\ + \bar{\boldsymbol{B}}_P \left(\boldsymbol{\Theta}_{um,x}^* \boldsymbol{x}_P(t) + \boldsymbol{f}_{um}\left(\boldsymbol{x}_P(t), t\right)\right)\end{aligned} \tag{3.95}$$

and represents the plant imperfections resulting from unaccounted unmatched parametric uncertainties, approximate parametrization and non-parametric uncertainties such as unmodeled dynamics. When comparing the plant representation (3.94) derived from the extended plant model (3.91) to the plant representation (3.25) derived from the original plant model (3.1), one observes that these models only differ in the presence of the disturbance signal $\boldsymbol{w}\left(\boldsymbol{x}_P(t), \boldsymbol{z}_P(t), t\right)$. In order to demonstrate the effect of this disturbance, the same direct MRAC as derived in Section 3.2.1 will be applied to (3.94).

Throughout the following analysis, it will be assumed that the disturbance function $\boldsymbol{w}\left(\boldsymbol{x}_P(t), \boldsymbol{z}_P(t), t\right)$ is bounded according to

$$\left\|\boldsymbol{w}\left(\boldsymbol{x}_P(t), \boldsymbol{z}_P(t), t\right)\right\|_2 \leq w_0, \tag{3.96}$$

where $w_0 \in \mathbb{R}$ is a positive known constant. As $\boldsymbol{w}\left(\boldsymbol{x}_P(t), \boldsymbol{z}_P(t), t\right)$ depends on the states, such a bound may not be known a-priori without further analysis such as those demonstrated in Chapter 4. Nevertheless, treating $\boldsymbol{w}\left(\boldsymbol{x}_P(t), \boldsymbol{z}_P(t), t\right)$ like a bounded exogenous signal suffices to illustrate fundamental instability phenomena, which an adaptive controller may exhibit. However, in order to stress that the analysis actually only applies to bounded exogenous signals, $\boldsymbol{w}\left(\boldsymbol{x}_P(t), \boldsymbol{z}_P(t), t\right)$ will be denoted as $\boldsymbol{w}(t)$. Thus, (3.94) simplifies to

$$\dot{\boldsymbol{x}}_P(t) = \boldsymbol{A}_M \boldsymbol{x}_P(t) + \boldsymbol{B}_M \boldsymbol{r}(t) + \boldsymbol{B}_P \boldsymbol{\Lambda}\left(\boldsymbol{u}(t) - \boldsymbol{\Theta}^* \boldsymbol{\omega}\left(\boldsymbol{x}_P(t), t\right)\right) + \boldsymbol{w}(t). \tag{3.97}$$

Applying the adaptive control law (3.26) and using the definition of the parameter error in (3.27) leads to

$$\dot{\boldsymbol{x}}_P(t) = \boldsymbol{A}_M \boldsymbol{x}_P(t) + \boldsymbol{B}_M \boldsymbol{r}(t) + \boldsymbol{B}_P \boldsymbol{\Lambda} \tilde{\boldsymbol{\Theta}}(t) \boldsymbol{\omega}\left(\boldsymbol{x}_P(t), t\right) + \boldsymbol{w}(t). \tag{3.98}$$

Thus, the error dynamics between the plant (3.98) and the reference model (3.4) evolve according to the differential equation

$$\dot{\boldsymbol{e}}_C(t) = \boldsymbol{A}_M \boldsymbol{e}_C(t) + \boldsymbol{B}_P \boldsymbol{\Lambda} \tilde{\boldsymbol{\Theta}}(t) \boldsymbol{\omega}\left(\boldsymbol{x}_P(t), t\right) + \boldsymbol{w}(t). \tag{3.99}$$

In an attempt to prove stability of the tracking error dynamics (3.99) and the parameter error dynamics (3.41), the same Lyapunov function candidate (3.30) is used as in Section 3.2.1, which is

$$V(t) = \frac{1}{2} \boldsymbol{e}_C(t)^T \boldsymbol{P} \boldsymbol{e}_C(t) + \frac{1}{2} \operatorname{Tr}\left\{\tilde{\boldsymbol{\Theta}}(t) \boldsymbol{\Gamma}^{-1} \tilde{\boldsymbol{\Theta}}(t)^T \boldsymbol{\Lambda}\right\}.$$

Using the same update law (3.43) and the same simplifications as in Section 3.2.1, the derivative of the Lyapunov function candidate becomes

$$\dot{V}(t) = -\frac{1}{2}\boldsymbol{e}_C(t)^T \boldsymbol{Q}\boldsymbol{e}_C(t) + \boldsymbol{e}_C(t)^T \boldsymbol{P}\boldsymbol{w}(t). \tag{3.100}$$

Unlike Section 3.2.1, $\dot{V}(t)$ in (3.100) is not negative semidefinite due to the presence of the indefinite term $\boldsymbol{e}_C(t)^T \boldsymbol{P}\boldsymbol{w}(t)$. Thus, the Lyapunov function candidate (3.30) does not prove stability of the tracking/parameter error dynamics. Even worse, a simple example reveals that the closed-loop control system may actually become unstable:

Example 3.11. *Consider the plant and the direct MRAC from Example 3.6 for* $\boldsymbol{\Gamma} = 10 \cdot \boldsymbol{I}^{3\times 3}$*. In contrast to Example 3.6, the plant is extended to*

$$\dot{\boldsymbol{x}}_P(t) = \boldsymbol{A}_P\boldsymbol{x}_P(t) + \boldsymbol{B}_P\boldsymbol{\Lambda}\boldsymbol{u}(t) + \boldsymbol{w}(t), \tag{3.101}$$

where $\boldsymbol{w}(t)$ *models an exogenous, that is, not state-dependent, disturbance. The disturbance is defined as*

$$\boldsymbol{w}(t) = \begin{bmatrix} 2.42 \\ 29.04 \end{bmatrix} \cdot w_0(iT_s), \quad \forall\, i \cdot T_s \leq t < (i+1) \cdot T_s. \tag{3.102}$$

where w_0 *is drawn from a zero-mean Gaussian distribution with a variance* $\sigma^2 = 0.0001$ *at each sampling instant* $i \cdot T_s$ *with* $T_s = 0.01$*. In Figure 3.7, the response of the closed-loop system to this disturbance is shown in case of a single step command of* 5° *at* $t = 1\,s$*. While the adaptive controller is able to maintain the commanded angle-of-attack, the parameters slowly drift away. For even longer simulation times, the parameters would ultimately drift to infinity.*

The instability observed in Example 3.11 is known as parameter drift. The underlying effect may be explained with the help of the derivative of the Lyapunov function candidate (3.100). The first term in (3.100) is a negative definite, second order multivariate polynomial in $\boldsymbol{e}_C$. In contrast, the second term is an indefinite first order multivariate polynomial in $\boldsymbol{e}_C$. Thus, whenever $\boldsymbol{e}_C(t)$ is small, the value of the first order polynomial will exceed the value of the second order polynomial, implying that $\dot{V}(t) > 0$ may hold, if $\boldsymbol{e}_C(t)^T \boldsymbol{P}\boldsymbol{w}(t) > 0$. Hence, the Lyapunov function candidate may grow as long as $\boldsymbol{e}_C(t)$ is small, which admits arbitrary growth of the adaptive parameters. This intuitive reasoning may be stated more formally by deriving an upper bound for the derivative (3.100). For this, notice that the first term in (3.100) may be bounded from above using the quadratic form bound (B.64) and that the second term may be equivalently expressed as a scalar product:

$$\begin{aligned} \dot{V}(t) &= -\frac{1}{2}\boldsymbol{e}_C(t)^T \boldsymbol{Q}\boldsymbol{e}_C(t) + \boldsymbol{e}_C(t)^T \boldsymbol{P}\boldsymbol{w}(t) \\ &\leq -\frac{1}{2}\lambda_{\min}(\boldsymbol{Q}) \cdot \|\boldsymbol{e}_C(t)\|_2^2 + \langle\, \boldsymbol{e}_C(t), \boldsymbol{P}\boldsymbol{w}(t) \,\rangle. \end{aligned} \tag{3.103}$$

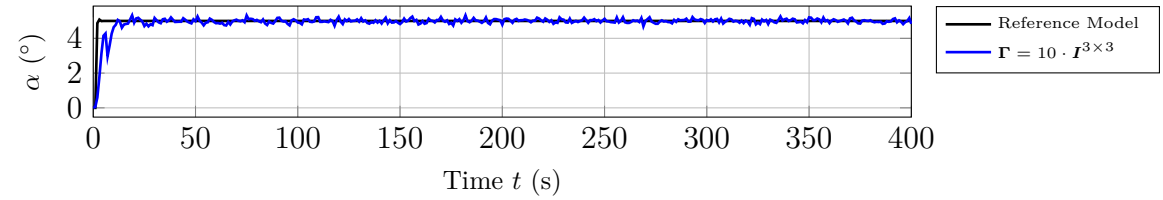

(a) Angle-Of-Attack α

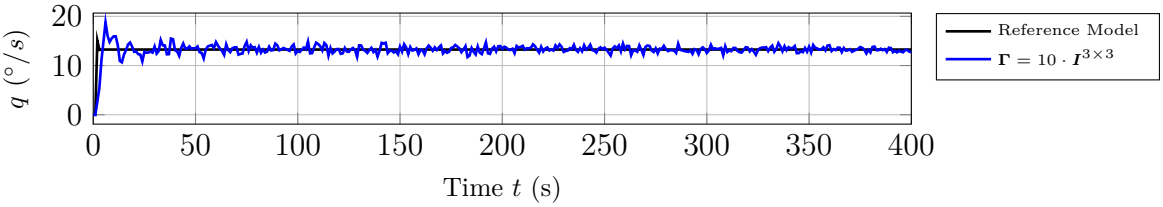

(b) Pitch Rate q

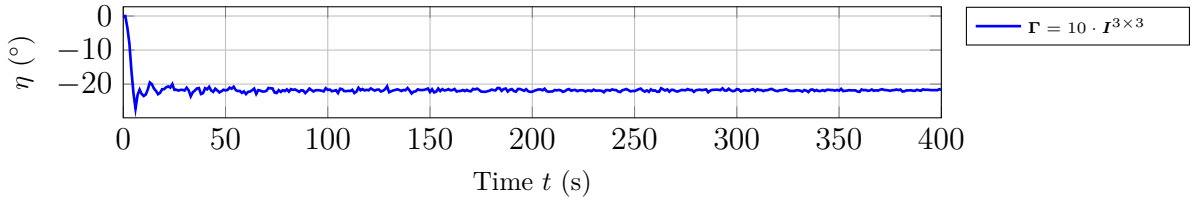

(c) Elevator Deflection η

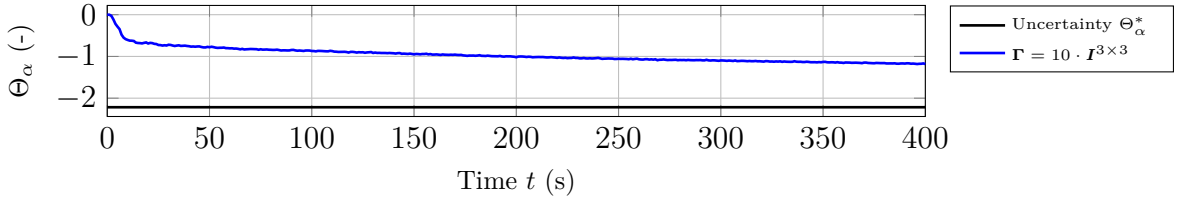

(d) Adaptive Parameter Θ_α

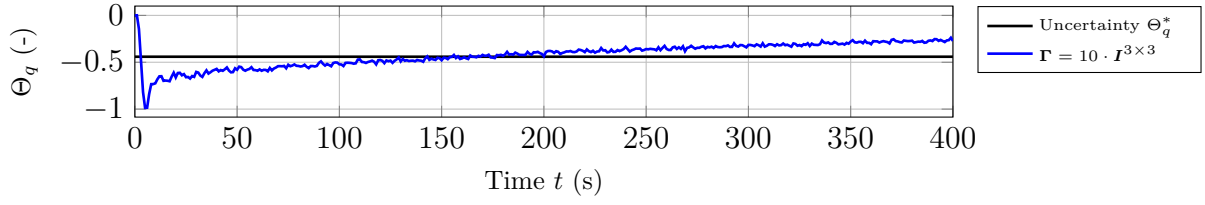

(e) Adaptive Parameter Θ_q

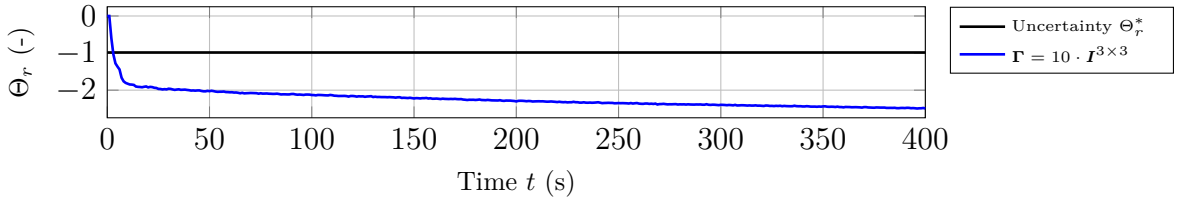

(f) Adaptive Parameter Θ_r

Figure 3.7: Demonstration of parameter drift in the presence of a disturbance $\boldsymbol{w}(t)$ for $\lambda_\alpha = \lambda_q = 1$ and $\lambda_\eta = 0.5$. For $t \to \infty$, the adaptive parameters diverge to infinity.

Using the Cauchy Schwarz inequality and the properties of induced norms, the upper bound may be refined to:

$$\dot{V}(t) \leq -\frac{1}{2}\lambda_{\min}(\boldsymbol{Q}) \cdot \|\boldsymbol{e}_C(t)\|_2^2 + \|\boldsymbol{P}\|_{2,i} \cdot \|\boldsymbol{e}_C(t)\|_2 \cdot \|\boldsymbol{w}(t)\|_2. \tag{3.104}$$

Inserting the bound (3.96) for $\boldsymbol{w}(t)$ then yields

$$\dot{V}(t) \leq -\frac{1}{2}\lambda_{\min}(\boldsymbol{Q}) \cdot \|\boldsymbol{e}_C(t)\|_2^2 + \|\boldsymbol{P}\|_{2,i} \cdot \|\boldsymbol{e}_C(t)\|_2 \cdot w_0. \tag{3.105}$$

Eq. (3.105) implies that $\dot{V}(t) \leq 0$ holds, if

$$\|\boldsymbol{e}_C(t)\|_2 \geq \frac{2 \cdot \|\boldsymbol{P}\|_{2,i} \cdot w_0}{\lambda_{\min}(\boldsymbol{Q})} = \frac{2 \cdot \sigma_{\max}(\boldsymbol{P}) \cdot w_0}{\lambda_{\min}(\boldsymbol{Q})} \triangleq e_0. \tag{3.106}$$

In contrast, if $\|\boldsymbol{e}_C(t)\|_2 < e_0$, the Lyapunov function candidate may grow unboundedly due to an unbounded growth of the parameter errors as $\dot{V}(t) > 0$ *might* hold. Since $\boldsymbol{\Theta}^*$ is constant, this implies unbounded growth of the adaptive parameters $\boldsymbol{\Theta}(t)$. An unbounded growth of the adaptive parameters may in turn cause arbitrary large control signals, causing saturation of any real control input $\boldsymbol{u}(t)$. To visualize the parameter drift, denote the upper bound, which has been derived in Lemma 3.3 for the Lyapunov function candidate (3.30), by $\bar{V}(t)$. Hence, one has:

$$V(t) \leq \bar{V}(t), \text{ where} \tag{3.107}$$

$$\bar{V}(t) \triangleq \frac{1}{2}\lambda_{\max}(\boldsymbol{P}) \cdot \|\boldsymbol{e}_C(t)\|_2^2 + \frac{\lambda_{\max}(\boldsymbol{\Lambda})}{2 \cdot \lambda_{\min}(\boldsymbol{\Gamma})} \cdot \|\tilde{\boldsymbol{\Theta}}(t)\|_F^2. \tag{3.108}$$

Due to (3.107), whenever $\bar{V}(t) \leq c$ holds for some $c \geq 0$, this implies $V(t) \leq c$ (but not vice versa). Hence, the set $\mathcal{M}_{\bar{V}} = \{\boldsymbol{e}_C, \tilde{\boldsymbol{\Theta}} |\ \bar{V}(\boldsymbol{e}_C, \tilde{\boldsymbol{\Theta}}) \leq c\}$ is a subset of $\mathcal{M}_V = \{\boldsymbol{e}_C, \tilde{\boldsymbol{\Theta}} |\ V(\boldsymbol{e}_C, \tilde{\boldsymbol{\Theta}}) \leq c\}$, i.e. $\mathcal{M}_{\bar{V}} \subseteq \mathcal{M}_V$. Thus, if the set $\mathcal{M}_{\bar{V}}$ grows due to growth of $\|\tilde{\boldsymbol{\Theta}}(t)\|_F^2$, the set $\mathcal{M}_V$ will grow as well. Conversely, if $\mathcal{M}_V$ grows due to $\dot{V}(t) > 0$, this implies growth of $\mathcal{M}_{\bar{V}}$ due to (3.107). Thus, (3.106) and (3.108) may be used to conveniently visualize the process of parameter drift in terms of the norms of the tracking error $\boldsymbol{e}_C(t)$ and the parameter error $\tilde{\boldsymbol{\Theta}}(t)$ as shown in Figure 3.8.

The foregoing discussion revealed that a bounded exogenous disturbance may cause instability of MRAC. In the first instance, this instability is characterized by diverging adaptive parameters, while the tracking error remains small. In order to avoid this parameter drift (without requiring the regressor vector to be *Persistently Exciting*), a modification of the update law seems promising. One of the simplest modifications in this direction is the σ-modification. By adding a damping term to the update law (3.43), the modification counteracts the divergence of the adaptive parameters. The modified update law is given by

$$\dot{\boldsymbol{\Theta}}(t)^T = -\boldsymbol{\Gamma}\left(\boldsymbol{\omega}(\boldsymbol{x}_P(t), t) \cdot \boldsymbol{e}_C(t)^T \boldsymbol{P}\boldsymbol{B}_P + \boldsymbol{\sigma} \cdot \boldsymbol{\Theta}(t)^T\right), \tag{3.109}$$

where $\boldsymbol{\sigma} \in \mathbb{S}_{++}^{n_r}$ is a positive definite design parameter. Using $\boldsymbol{\sigma}$, one may specify the rate of decay of the modified update law (3.109). In order to see this, assume

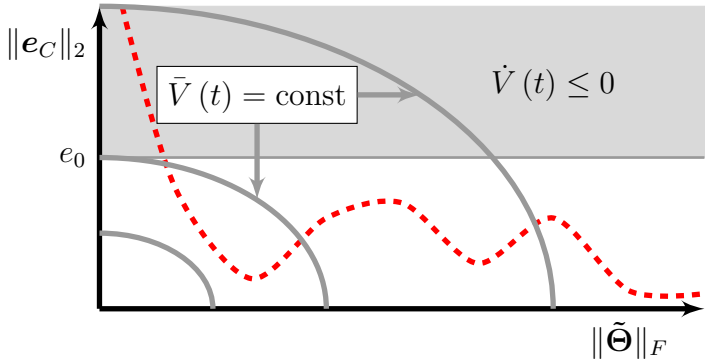

Figure 3.8: Visualization of Parameter Drift: Due to a decaying tracking error, the trajectory of $\bar{V}(t)$ (dashed) enters the indefinite region $\|\boldsymbol{e}_C\|_2 < e_0$. While within the indefinite region, $\bar{V}(t)$ may grow unboundedly due to the growth of the adaptive parameter $\tilde{\boldsymbol{\Theta}}(t)$.

that $\boldsymbol{e}_C(t) = 0$ would hold for all time. In this case, the update law would become $\dot{\boldsymbol{\Theta}}(t)^T = -\boldsymbol{\Gamma}\boldsymbol{\sigma}\boldsymbol{\Theta}(t)^T$, which decays to zero at the rate specified by $\boldsymbol{\Gamma} \cdot \boldsymbol{\sigma}$. Since the modification tries to drag $\boldsymbol{\Theta}(t)$ to zero and not towards $\boldsymbol{\Theta}^*$, it disturbs the adaptation. Therefore, $\boldsymbol{\sigma}$ should be chosen as small as possible. The modification in (3.109) is also referred to as *leakage modification* as it turns the integrator of the original update law (3.43) into a leaky, i.e. forgetting, integrator.

Using the modified update law (3.109), the instability due to parameter drift may be prevented, as shown in the following theorem:

Theorem 3.12 (Robust Stability of Direct MRAC with σ-Modification)**.** *Consider the plant* (3.1) *and let Assumptions 3.1 (state feedback), 3.2 (positive definite control effectiveness), 3.3 (Lipschitz condition), 3.6 (full-rank $\boldsymbol{B}_P$), 3.7 (linear parametrization) hold. Then, according to* (3.94)*, the plant admits the compact representation*

$$\begin{aligned}\dot{\boldsymbol{x}}_P(t) = \boldsymbol{A}_M\boldsymbol{x}_P(t) + \boldsymbol{B}_M\boldsymbol{r}(t) + \boldsymbol{B}_P\boldsymbol{\Lambda}\left(\boldsymbol{u}(t) - \boldsymbol{\Theta}^*\boldsymbol{\omega}\left(\boldsymbol{x}_P(t), t\right)\right) \\ + \boldsymbol{w}\left(\boldsymbol{x}_P(t), \boldsymbol{z}_P(t), t\right).\end{aligned}$$

where the true parameter matrix $\boldsymbol{\Theta}^*$ and the regressor vector $\boldsymbol{\omega}(\boldsymbol{x}_P(t), t)$ are defined in (3.23)*. Furthermore, let the learning rate $\boldsymbol{\Gamma} \in \mathbb{S}^{n_r}_{++}$, the modification gains $\boldsymbol{\sigma} \in \mathbb{S}^{n_r}_{++}$ and the weighting matrix $\boldsymbol{Q} \in \mathbb{S}^{n}_{++}$ be chosen positive definite, and let $\boldsymbol{P} \in \mathbb{S}^{n}_{++}$ be the positive definite solution of the Lyapunov equation* (3.31)*. If a bound $w_0 > 0$ is known such that the disturbance signal satisfies*

$$\|\boldsymbol{w}\left(\boldsymbol{x}_P(t), \boldsymbol{z}_P(t), t\right)\|_2 \leq w_0$$

and may hence be treated like an exogenous disturbance, then the adaptive control law with σ-modification

$$\begin{aligned}\boldsymbol{u}(t) &= \boldsymbol{\Theta}(t) \cdot \boldsymbol{\omega}\left(\boldsymbol{x}_P(t), t\right), \\ \dot{\boldsymbol{\Theta}}(t)^T &= -\boldsymbol{\Gamma}\left(\boldsymbol{\omega}\left(\boldsymbol{x}_P(t), t\right) \cdot \boldsymbol{e}_C(t)^T\boldsymbol{P}\boldsymbol{B}_P + \boldsymbol{\sigma} \cdot \boldsymbol{\Theta}(t)^T\right),\end{aligned}$$

originally proposed in (3.26) *and* (3.109)*, ensures UUB of the tracking error* $\boldsymbol{e}_C(t)$ *and the parameter error* $\tilde{\boldsymbol{\Theta}}(t)$ *and boundedness of all other closed-loop signals.*

Proof. Consider the modified update law (3.109) and notice that due to $\boldsymbol{\Theta}(t) = \tilde{\boldsymbol{\Theta}}(t) + \boldsymbol{\Theta}^*$, the parameter error dynamics evolve according to

$$\dot{\tilde{\boldsymbol{\Theta}}}(t)^T = -\boldsymbol{\Gamma}\left(\boldsymbol{\omega}(\boldsymbol{x}_P(t), t) \cdot \boldsymbol{e}_C(t)^T \boldsymbol{P}\boldsymbol{B}_P + \boldsymbol{\sigma} \cdot \tilde{\boldsymbol{\Theta}}(t)^T + \boldsymbol{\sigma} \cdot \boldsymbol{\Theta}^{*T}\right). \tag{3.110}$$

Now consider the same Lyapunov function candidate (3.30) used throughout the previous sections, namely

$$V(t) = \frac{1}{2}\boldsymbol{e}_C(t)^T \boldsymbol{P}\boldsymbol{e}_C(t) + \frac{1}{2}\operatorname{Tr}\left\{\tilde{\boldsymbol{\Theta}}(t)\boldsymbol{\Gamma}^{-1}\tilde{\boldsymbol{\Theta}}(t)^T\boldsymbol{\Lambda}\right\}.$$

Upon insertion of the tracking error dynamics (3.99) and the parameter error dynamics (3.110), and upon the same simplifications as in Section 3.2.1, the derivate of the Lyapunov function candidate becomes

$$\begin{aligned}\dot{V}(t) = -\frac{1}{2}\boldsymbol{e}_C(t)^T \boldsymbol{Q}\boldsymbol{e}_C(t) + \boldsymbol{e}_C(t)^T \boldsymbol{P}\boldsymbol{w}(t) - \operatorname{Tr}\left\{\tilde{\boldsymbol{\Theta}}(t)\boldsymbol{\sigma}\tilde{\boldsymbol{\Theta}}(t)^T\boldsymbol{\Lambda}\right\} \\ - \operatorname{Tr}\left\{\tilde{\boldsymbol{\Theta}}(t)\boldsymbol{\sigma}\boldsymbol{\Theta}^{*T}\boldsymbol{\Lambda}\right\}.\end{aligned} \tag{3.111}$$

Since $\boldsymbol{\Lambda}$ is symmetric and positive definite, its matrix square root $\boldsymbol{\Lambda} = \boldsymbol{\Lambda}^{\frac{1}{2}} \cdot \boldsymbol{\Lambda}^{\frac{1}{2}}$ exists. Using the cyclic property (B.154), the derivative of the Lyapunov function candidate becomes:

$$\begin{aligned}\dot{V}(t) = -\frac{1}{2}\boldsymbol{e}_C(t)^T \boldsymbol{Q}\boldsymbol{e}_C(t) + \boldsymbol{e}_C(t)^T \boldsymbol{P}\boldsymbol{w}(t) - \operatorname{Tr}\left\{\boldsymbol{\Lambda}^{\frac{1}{2}}\tilde{\boldsymbol{\Theta}}(t)\boldsymbol{\sigma}\tilde{\boldsymbol{\Theta}}(t)^T\boldsymbol{\Lambda}^{\frac{1}{2}}\right\} \\ - \operatorname{Tr}\left\{\tilde{\boldsymbol{\Theta}}(t)\boldsymbol{\sigma}\boldsymbol{\Theta}^{*T}\boldsymbol{\Lambda}\right\}.\end{aligned} \tag{3.112}$$

By virtue of the definition $\bar{\boldsymbol{\Theta}}(t) = \boldsymbol{\Lambda}^{\frac{1}{2}}\tilde{\boldsymbol{\Theta}}(t)$ as well as the definitions of the scalar product in (B.2) and (B.8), the derivative further simplifies to

$$\begin{aligned}\dot{V}(t) = -\frac{1}{2}\boldsymbol{e}_C(t)^T \boldsymbol{Q}\boldsymbol{e}_C(t) + \langle \boldsymbol{e}_C(t), \boldsymbol{P}\boldsymbol{w}(t)\rangle \\ - \operatorname{Tr}\left\{\bar{\boldsymbol{\Theta}}(t)\boldsymbol{\sigma}\bar{\boldsymbol{\Theta}}(t)^T\right\} - \langle \boldsymbol{\Lambda}\boldsymbol{\Theta}^*, \tilde{\boldsymbol{\Theta}}(t)\boldsymbol{\sigma}\rangle.\end{aligned} \tag{3.113}$$

Using the quadratic form bounds (B.64) and (B.102) and the Cauchy Schwarz inequality (B.1), one obtains the following upper bound:

$$\begin{aligned}\dot{V}(t) \leq -\frac{1}{2}\lambda_{\min}(\boldsymbol{Q}) \cdot \|\boldsymbol{e}_C(t)\|_2^2 + w_0 \cdot \|\boldsymbol{P}\|_{2,i} \cdot \|\boldsymbol{e}_C(t)\|_2 \\ - \lambda_{\min}(\boldsymbol{\sigma}) \cdot \|\bar{\boldsymbol{\Theta}}(t)\|_F^2 + \|\boldsymbol{\Lambda}\boldsymbol{\Theta}^*\|_F \cdot \|\boldsymbol{\sigma}\|_F \cdot \|\tilde{\boldsymbol{\Theta}}(t)\|_F.\end{aligned} \tag{3.114}$$

Resubstituting $\bar{\boldsymbol{\Theta}}(t)$ and using the definition of the Frobenius norm in (B.9) yields

$$\begin{aligned}\dot{V}(t) \leq -\frac{1}{2}\lambda_{\min}(\boldsymbol{Q}) \cdot \|\boldsymbol{e}_C(t)\|_2^2 + w_0 \cdot \|\boldsymbol{P}\|_{2,i} \cdot \|\boldsymbol{e}_C(t)\|_2 \\ - \lambda_{\min}(\boldsymbol{\sigma}) \cdot \operatorname{Tr}\left\{\tilde{\boldsymbol{\Theta}}(t)^T\boldsymbol{\Lambda}\tilde{\boldsymbol{\Theta}}(t)\right\} + \|\boldsymbol{\Lambda}\boldsymbol{\Theta}^*\|_F \cdot \|\boldsymbol{\sigma}\|_F \cdot \|\tilde{\boldsymbol{\Theta}}(t)\|_F.\end{aligned} \tag{3.115}$$

Applying the quadratic form bound (B.102) once again, leads to

$$\begin{aligned}\dot{V}(t) \leq &-\frac{1}{2}\lambda_{\min}(\boldsymbol{Q}) \cdot \|\boldsymbol{e}_C(t)\|_2^2 + w_0 \cdot \|\boldsymbol{P}\|_{2,i} \cdot \|\boldsymbol{e}_C(t)\|_2 \\ &- \lambda_{\min}(\boldsymbol{\sigma}) \cdot \lambda_{\min}(\boldsymbol{\Lambda}) \cdot \|\tilde{\boldsymbol{\Theta}}(t)\|_F^2 + \|\boldsymbol{\Lambda}\boldsymbol{\Theta}^*\|_F \cdot \|\boldsymbol{\sigma}\|_F \cdot \|\tilde{\boldsymbol{\Theta}}(t)\|_F,\end{aligned} \tag{3.116}$$

which may be further bounded by

$$\begin{aligned}\dot{V}(t) \leq &-\min\left\{\frac{1}{2}\lambda_{\min}(\boldsymbol{Q}),\ \ \lambda_{\min}(\boldsymbol{\sigma}) \cdot \lambda_{\min}(\boldsymbol{\Lambda})\right\} \cdot \left(\|\boldsymbol{e}_C(t)\|_2^2 + \|\tilde{\boldsymbol{\Theta}}(t)\|_F^2\right) \\ &+ \max\left\{w_0 \cdot \|\boldsymbol{P}\|_{2,i},\ \ \|\boldsymbol{\Lambda}\boldsymbol{\Theta}^*\|_F \cdot \|\boldsymbol{\sigma}\|_F\right\} \cdot \left(\|\boldsymbol{e}_C(t)\|_2 + \|\tilde{\boldsymbol{\Theta}}(t)\|_F\right).\end{aligned} \tag{3.117}$$

Using the definitions

$$c_1 = \min\left\{\frac{1}{2}\lambda_{\min}(\boldsymbol{Q}),\ \ \lambda_{\min}(\boldsymbol{\sigma}) \cdot \lambda_{\min}(\boldsymbol{\Lambda})\right\}, \tag{3.118}$$

$$c_2 = \sqrt{2} \cdot \max\left\{w_0 \cdot \|\boldsymbol{P}\|_{2,i},\ \ \|\boldsymbol{\Lambda}\boldsymbol{\Theta}^*\|_F \cdot \|\boldsymbol{\sigma}\|_F\right\}, \tag{3.119}$$

Eq. (3.117) may be written more compactly as

$$\dot{V}(t) \leq -c_1\left(\|\boldsymbol{e}_C(t)\|_2^2 + \|\tilde{\boldsymbol{\Theta}}(t)\|_F^2\right) + \frac{c_2}{\sqrt{2}}\left(\|\boldsymbol{e}_C(t)\|_2 + \|\tilde{\boldsymbol{\Theta}}(t)\|_F\right). \tag{3.120}$$

Due to $\|\boldsymbol{e}_C(t)\|_2 + \|\tilde{\boldsymbol{\Theta}}(t)\|_F \leq \sqrt{2} \cdot \sqrt{\|\boldsymbol{e}_C(t)\|_2^2 + \|\tilde{\boldsymbol{\Theta}}(t)\|_F^2}$, (3.120) may now be rewritten in terms of the squares of the norms:

$$\dot{V}(t) \leq -c_1\left(\|\boldsymbol{e}_C(t)\|_2^2 + \|\tilde{\boldsymbol{\Theta}}(t)\|_F^2\right) + c_2\sqrt{\|\boldsymbol{e}_C(t)\|_2^2 + \|\tilde{\boldsymbol{\Theta}}(t)\|_F^2}\,. \tag{3.121}$$

Now, let $\boldsymbol{x}(t)^T = \begin{bmatrix}\boldsymbol{e}_C(t)^T & \operatorname{vec}\tilde{\boldsymbol{\Theta}}(t)^T\end{bmatrix}$ denote the extended error dynamics vector. Due to $\|\tilde{\boldsymbol{\Theta}}(t)\|_F = \|\operatorname{vec}\tilde{\boldsymbol{\Theta}}(t)\|_2$, the upper bound in (3.121) may be simplified to

$$\dot{V}(t) \leq -c_1\|\boldsymbol{x}(t)\|_2^2 + c_2\|\boldsymbol{x}(t)\|_2. \tag{3.122}$$

By adding and subtracting $kc_1\|\boldsymbol{x}(t)\|_2^2$ with $0 < k < 1$, one finally obtains:

$$\dot{V}(t) \leq -c_1 \cdot (1-k) \cdot \|\boldsymbol{x}(t)\|_2^2 - kc_1\|\boldsymbol{x}(t)\|_2^2 + c_2\|\boldsymbol{x}(t)\|_2. \tag{3.123}$$

Thus,

$$\dot{V}(t) \leq -c_1 \cdot (1-k) \cdot \|\boldsymbol{x}(t)\|_2^2, \quad \forall\, \|\boldsymbol{x}(t)\|_2 \geq \frac{c_2}{k \cdot c_1}, \tag{3.124}$$

holds. Hence, all requirements of Theorem C.5 are satisfied and the tracking error $\boldsymbol{e}_C(t)$ and the parameter error $\tilde{\boldsymbol{\Theta}}(t)$ are globally UUB. If the command vector $\boldsymbol{r}(t)$ is bounded, then the states of the reference model $\boldsymbol{x}_M(t)$ will be bounded as well, which implies boundedness of the plant state $\boldsymbol{x}_P(t)$ due to UUB of $\boldsymbol{e}_C(t)$. Hence, all closed-loop signals are bounded. □

Remark 3.13. *Due to the use of a σ-modification, the adaptive controller loses some of its ideal properties. Even in the absence of a bounded exogenous disturbance, i.e. $\boldsymbol{w}(t) = 0$, Barbalat's Lemma may not be invoked to show asymptotic convergence of*

the tracking error. This is because the derivative of the Lyapunov function in (3.111) *always contains the indefinite term* $\tilde{\boldsymbol{\Theta}}(t)\,\boldsymbol{\sigma}\boldsymbol{\Theta}^{*T}\boldsymbol{\Lambda}$*. Due to the indefinite term, one cannot prove that* $\boldsymbol{e}_C(t) \in \mathcal{L}_2$ *holds. Furthermore, even in the presence of Persistent Excitation, parameter convergence cannot be shown. To some extent, these ideal properties may be recovered using other robustness modifications [89].*

Remark 3.14. *In many cases, a nominal value* $\boldsymbol{\Theta}_0^*$ *of the uncertainty* $\boldsymbol{\Theta}^*$ *is known. Assuming that the true uncertainty* $\boldsymbol{\Theta}^*$ *is rather close to* $\boldsymbol{\Theta}_0^*$*, it would improve the performance of the adaptive control system if the* σ*-modification would try to drag* $\boldsymbol{\Theta}$ *towards* $\boldsymbol{\Theta}_0^*$ *instead of* $\mathbf{0}$*. This may be achieved using a slight modification of the update law* (3.109)*:*

$$\dot{\boldsymbol{\Theta}}(t)^T = -\boldsymbol{\Gamma}\left(\boldsymbol{\omega}(\boldsymbol{x}_P(t), t)\cdot \boldsymbol{e}_C(t)^T \boldsymbol{P}\boldsymbol{B}_P + \boldsymbol{\sigma}\cdot\left(\boldsymbol{\Theta}(t)^T - \boldsymbol{\Theta}_0^{*T}\right)\right). \tag{3.125}$$

Using this modification, the stationary response of the modified update law is $\boldsymbol{\Theta} = \boldsymbol{\Theta}_0^*$*, if* $\boldsymbol{e}_C(t) = 0$*.*

Remark 3.15. *At the first glance, one might wonder whether a robustness modification is actually required in order to establish UUB of the closed-loop adaptive control system consisting of the reference model* (3.4)*, the disturbed plant* (3.98) *and the unmodified update law* (3.43)*. A key requirement for establishing UUB is however that the derivative of the Lyapunov function candidate may be bounded by a negative definite function* $-W_3(\boldsymbol{x}(t))$*, whenever the state vector* $\boldsymbol{x}(t)$ *exceeds some size. As the derivative* (3.100)*, which results from the application of the unmodified update law, only depends on* $\boldsymbol{e}_C(t)$*, one may only bound* $\dot{V}(t)$ *by a negative semidefinite function* $-W_3(\boldsymbol{e}_C(t))$*. Thus, UUB cannot be established using the unmodified update law* (3.43)*.*

3.2.5 Reference Model Modifications

One of the most important design parameters of any MRC approach is the reference model. Using the reference model, the control system designer specifies the desired response characteristics of the closed loop for the control problem at hand. While the desired response characteristics are often derived from some exogenous requirements and the reference model hence seems to be fixed, there exist several situations in which the reference model needs to be modified. Some common situations and the corresponding modifications will be exemplified subsequently in case of direct MRAC. Upon a proper adjustment, these modifications may also be applied to indirect or predictor-based MRAC (and sometimes even to other MRC approaches).

A common situation, which requires the modification of the reference model, is the control of plants with saturation. If the control surface deflections required to track the reference model, exceed the physical limits of the actuation system, the control objective of tracking the reference model is obviously not achievable anymore. Even more

importantly, the saturation will lead to a persistent disturbance in the error dynamics, which may cause windup (parameter-drift) of the adaptive controller gains. In order to prevent this situation, the reference model can be altered to account for the saturation in such a way that the original error dynamics are restored [115, 94]. That is, the persistent disturbance is hidden from the error dynamics, which also is the reason, why such an approach is referred to as *hedging* [93].

Another common situation, where the modification of a reference model is desirable, emerges if the error dynamics should decay at a different rate than the reference model. In standard MRAC, the error dynamics (3.29) and the reference model decay at the rate specified by $\boldsymbol{A}_M$. By adding a Luenberger-like feedback $-\boldsymbol{L} \cdot \boldsymbol{e}_C(t)$ to the reference model, the decay rate of the error dynamics may be altered. It has been shown in [160] that the feedback gain $\boldsymbol{L}$ determines the damping, whereas the learning rate $\boldsymbol{\Gamma}$ determines the speed (the "eigenfrequency") of the control signal $\boldsymbol{u}(t)$. Thus, the latter modification of the reference model leads to smoother, less oscillatory responses. This modification of the reference model is commonly referred to as Modified Reference Model MRAC (M-MRAC) [159, 160] or MRAC with *Closed-Loop Reference Model (CRM)* [69, 70].

Finally, a modification of the reference model may also be used to cancel the residual adaptation error $\boldsymbol{B}_P \boldsymbol{\Lambda} \tilde{\boldsymbol{\Theta}}(t) \cdot \boldsymbol{\omega}(\boldsymbol{x}_P(t), t) = \boldsymbol{B}_P \cdot \boldsymbol{d}_{ad}(\boldsymbol{x}_P(t), t)$ in (3.28). Using an estimate of $\boldsymbol{d}_{ad}(\boldsymbol{x}_P(t), t)$, the reference signal $\boldsymbol{r}(t)$ is altered in such a way that $\boldsymbol{d}_{ad}(\boldsymbol{x}_P(t), t)$ is approximately canceled. This modification of the reference model is known as the *Command Governor* [182, 183].

Subsequently, the reference model modifications *hedging*, *CRM* and the *Command Governor* will be presented. As the name suggests, a common feature of all reference model modifications is the alteration of the original reference model (3.4). Instead of tracking (3.4), the direct MRAC will track the modified reference model. Nevertheless, the overall control objective remains tracking of the original, unmodified reference model (as long as physically feasible). In order to clearly distinguish the modified reference model, which is tracked by the direct MRAC, from the original unmodified reference model, which prescribes the control objective, the original reference model is restated as

$$\dot{\boldsymbol{x}}_{M,0}(t) = \boldsymbol{A}_M \boldsymbol{x}_{M,0}(t) + \boldsymbol{B}_M \boldsymbol{r}_0(t). \tag{3.126}$$

Eq. (3.126) is structurally equivalent to the original reference model (3.4), except for the substitutions $\boldsymbol{x}_M(t) \to \boldsymbol{x}_{M,0}(t)$ and $\boldsymbol{r}(t) \to \boldsymbol{r}_0(t)$. Furthermore, notice that (3.126) will not be implemented, but is only required for the purpose of analysis. In (3.126), $\boldsymbol{x}_{M,0} : \mathbb{R}_+ \to \mathbb{R}^n$ denotes the state vector of the unmodified reference model and $\boldsymbol{r}_0 : \mathbb{R}_+ \to \mathbb{R}^m$ is the unmodified reference signal, i.e. the command issued by the pilot or another outer loop control system. In case of *hedging* and *CRM*, $\boldsymbol{r}_0(t) = \boldsymbol{r}(t)$ will hold. However, the *Command Governor* will alter $\boldsymbol{r}(t)$ and consequently, $\boldsymbol{r}_0(t) \neq \boldsymbol{r}(t)$ holds.

Hedging

While the term *hedging* generally refers to the idea of hiding the influence of certain known functions or dynamics from the error dynamics $\dot{\boldsymbol{e}}_C(t)$ [15], the case of known dynamics at the plant input is specifically considered here. For the introduction of *hedging*, let an off-nominal plant be given by

$$\dot{\boldsymbol{x}}_P(t) = \boldsymbol{A}_P\boldsymbol{x}_P(t) + \boldsymbol{B}_P\boldsymbol{\Lambda}\cdot\mathcal{F}\{\boldsymbol{u}(t)\} + \boldsymbol{f}(\boldsymbol{x}_P(t),t) \tag{3.127}$$

instead of (3.1). In (3.127), the operator $\mathcal{F}:\mathbb{R}^m\to\mathbb{R}^m$ is known and may represent various plant imperfections at the plant input such as

- Saturation:

  $$\mathcal{F}\{\boldsymbol{u}(t)\} = \left[u_{1,\max}\cdot\operatorname{sat}\left(\tfrac{u_1(t)}{u_{1,\max}}\right) \quad \dots \quad u_{m,\max}\cdot\operatorname{sat}\left(\tfrac{u_m(t)}{u_{m,\max}}\right)\right]^T,$$

  where $u_{i,\max}>0$, $i=1,\dots,m$ are the known control deflection limits;

- Delay:

  $$\mathcal{F}\{\boldsymbol{u}(t)\} = \boldsymbol{u}(t-\tau_c),$$

  where $\tau_c>0$ is the known input delay;

- Actuator Dynamics:

  $$\mathcal{F}\{\boldsymbol{u}(t)\} = \mathcal{L}^{-1}\{\boldsymbol{F}(s)\cdot\boldsymbol{u}(s)\},$$

  where $\boldsymbol{u}(s)$ is the Laplace transform of $\boldsymbol{u}(t)$, i.e. $\boldsymbol{u}(s)=\mathcal{L}\{\boldsymbol{u}(t)\}$, and $\boldsymbol{F}:\mathbb{C}\to\mathbb{C}^{m\times m}$ is a stable, known filter.

Following the same lines as in Section 3.2.1 with the same underlying assumptions, the plant (3.127) may be represented as

$$\dot{\boldsymbol{x}}_P(t) = \boldsymbol{A}_M\boldsymbol{x}_P(t) + \boldsymbol{B}_M\boldsymbol{r}(t) + \boldsymbol{B}_P\boldsymbol{\Lambda}\left(\mathcal{F}\{\boldsymbol{u}(t)\} - \boldsymbol{\Theta}^*\boldsymbol{\omega}(\boldsymbol{x}_P(t),t)\right). \tag{3.128}$$

By adding and subtracting $\boldsymbol{B}_P\boldsymbol{\Lambda}\cdot\boldsymbol{u}(t)$ and using the control law (3.22), the following closed-loop representation of the plant follows from (3.128):

$$\dot{\boldsymbol{x}}_P(t) = \boldsymbol{A}_M\boldsymbol{x}_P(t) + \boldsymbol{B}_M\boldsymbol{r}(t) + \boldsymbol{B}_P\boldsymbol{\Lambda}\left(\mathcal{F}\{\boldsymbol{u}(t)\} - \boldsymbol{u}(t) + \tilde{\boldsymbol{\Theta}}(t)\,\boldsymbol{\omega}(\boldsymbol{x}_P(t),t)\right). \tag{3.129}$$

When comparing (3.129) to (3.28), one observes the presence of the term $\Delta\boldsymbol{u}(t)\triangleq\mathcal{F}\{\boldsymbol{u}(t)\}-\boldsymbol{u}(t)$. The term $\Delta\boldsymbol{u}(t)$ represents the error between the true, but perturbed control input $\mathcal{F}\{\boldsymbol{u}(t)\}$ and the ideal control input $\boldsymbol{u}(t)$, which is expected by MRAC. For this reason, $\Delta\boldsymbol{u}(t)$ is referred to as the control deficiency. When forming the error dynamics

$$\dot{\boldsymbol{e}}_C(t) = \dot{\boldsymbol{x}}_P(t) - \dot{\boldsymbol{x}}_M(t) = \boldsymbol{A}_M\boldsymbol{e}_C(t) + \boldsymbol{B}_P\boldsymbol{\Lambda}\cdot\Delta\boldsymbol{u}(t) + \boldsymbol{B}_P\boldsymbol{\Lambda}\tilde{\boldsymbol{\Theta}}(t)\cdot\boldsymbol{\omega}(\boldsymbol{x}_P(t),t), \tag{3.130}$$

it becomes evident that the control deficiency $\Delta\boldsymbol{u}(t)$ resembles the bounded disturbance $\boldsymbol{w}(t)$ in (3.99) in Section 3.2.4. It may thus cause the adaptive parameters $\boldsymbol{\Theta}(t)$

to wind up, i.e., it may cause parameter drift. However, as this parameter drift is the result of the *known* disturbance $\Delta \boldsymbol{u}(t)$, it seems reasonable that a proper modification of the control system could eliminate $\Delta \boldsymbol{u}(t)$ from the error dynamics, which would in turn prevent the parameter drift. For this, the original reference model (3.4) is altered as follows:

$$\dot{\boldsymbol{x}}_M(t) = \boldsymbol{A}_M \boldsymbol{x}_M(t) + \boldsymbol{B}_M \boldsymbol{r}(t) + \boldsymbol{B}_P \hat{\boldsymbol{\Lambda}}(t) \cdot \Delta \boldsymbol{u}(t), \tag{3.131}$$

where $\hat{\boldsymbol{\Lambda}} : \mathbb{R}_+ \to \mathbb{R}^m$ is an estimate of $\boldsymbol{\Lambda}$. It is evident from (3.131) that the modified reference model only corresponds to the original reference model (3.4), if $\Delta \boldsymbol{u}(t) = \boldsymbol{0}$ holds. Using the modified reference model, the error dynamics now become

$$\dot{\boldsymbol{e}}_C(t) = \boldsymbol{A}_M \boldsymbol{e}_C(t) - \boldsymbol{B}_P \tilde{\boldsymbol{\Lambda}}(t) \cdot \Delta \boldsymbol{u}(t) + \boldsymbol{B}_P \boldsymbol{\Lambda} \tilde{\boldsymbol{\Theta}}(t) \cdot \boldsymbol{\omega}(\boldsymbol{x}_P(t), t), \tag{3.132}$$

with $\tilde{\boldsymbol{\Lambda}}(t) = \hat{\boldsymbol{\Lambda}}(t) - \boldsymbol{\Lambda}$. With the Lyapunov function candidate

$$V(t) = \frac{1}{2} \boldsymbol{e}_C(t)^T \boldsymbol{P} \boldsymbol{e}_C(t) + \frac{1}{2} \operatorname{Tr}\left\{\tilde{\boldsymbol{\Theta}}(t) \boldsymbol{\Gamma}^{-1} \tilde{\boldsymbol{\Theta}}(t)^T \boldsymbol{\Lambda}\right\} + \frac{1}{2} \operatorname{Tr}\left\{\tilde{\boldsymbol{\Lambda}}(t) \boldsymbol{\Gamma}_u^{-1} \tilde{\boldsymbol{\Lambda}}(t)^T\right\}, \tag{3.133}$$

the following update laws may be derived:

$$\dot{\boldsymbol{\Theta}}(t)^T = -\boldsymbol{\Gamma} \boldsymbol{\omega}(\boldsymbol{x}_P(t), t) \cdot \boldsymbol{e}_C(t)^T \boldsymbol{P} \boldsymbol{B}_P, \tag{3.134}$$

$$\dot{\hat{\boldsymbol{\Lambda}}}(t)^T = \boldsymbol{\Gamma}_u \Delta \boldsymbol{u}(t) \cdot \boldsymbol{e}_C(t)^T \boldsymbol{P} \boldsymbol{B}_P. \tag{3.135}$$

Lemma 3.16 (Bounded Error Dynamics of Direct MRAC with Hedging)**.** *Consider the plant* (3.127) *and let Assumptions 3.1 (state feedback), 3.2 (positive definite control effectiveness), 3.3 (Lipschitz condition), 3.4 (matching condition), 3.7 (linear parametrization) and 3.8 (exact parametrization) hold. Then, according to* (3.128)*, the plant admits the compact representation*

$$\dot{\boldsymbol{x}}_P(t) = \boldsymbol{A}_M \boldsymbol{x}_P(t) + \boldsymbol{B}_M \boldsymbol{r}(t) + \boldsymbol{B}_P \boldsymbol{\Lambda} \left(\mathcal{F}\{\boldsymbol{u}(t)\} - \boldsymbol{\Theta}^* \boldsymbol{\omega}(\boldsymbol{x}_P(t), t)\right),$$

where the true parameter matrix $\boldsymbol{\Theta}^*$ and the regressor vector $\boldsymbol{\omega}(\boldsymbol{x}_P(t), t)$ are defined in (3.23)*. Let the learning rates $\boldsymbol{\Gamma} \in \mathbb{S}_{++}^{n_r}$, $\boldsymbol{\Gamma}_u \in \mathbb{S}_{++}^m$ and the weighting matrix $\boldsymbol{Q} \in \mathbb{S}_{++}^n$ be chosen positive definite, and let $\boldsymbol{P} \in \mathbb{S}_{++}^n$ be the positive definite solution of the Lyapunov equation* (3.31)*. Then the control law*

$$\begin{aligned} \boldsymbol{u}(t) &= \boldsymbol{\Theta}(t) \cdot \boldsymbol{\omega}(\boldsymbol{x}_P(t), t), \\ \dot{\boldsymbol{\Theta}}(t)^T &= -\boldsymbol{\Gamma} \boldsymbol{\omega}(\boldsymbol{x}_P(t), t) \cdot \boldsymbol{e}_C(t)^T \boldsymbol{P} \boldsymbol{B}_P, \end{aligned}$$

from (3.22) *and* (3.134)*, respectively, and the modified reference model*

$$\begin{aligned} \dot{\boldsymbol{x}}_M(t) &= \boldsymbol{A}_M \boldsymbol{x}_M(t) + \boldsymbol{B}_M \boldsymbol{r}(t) + \boldsymbol{B}_P \hat{\boldsymbol{\Lambda}}(t) \cdot \Delta \boldsymbol{u}(t), \\ \dot{\hat{\boldsymbol{\Lambda}}}(t)^T &= \boldsymbol{\Gamma}_u \Delta \boldsymbol{u}(t) \cdot \boldsymbol{e}_C(t)^T \boldsymbol{P} \boldsymbol{B}_P \end{aligned}$$

from (3.131) *and* (3.135)*, respectively, will ensure that ($\boldsymbol{e}_C = \boldsymbol{0}$, $\tilde{\boldsymbol{\Theta}} = \boldsymbol{0}$, $\tilde{\boldsymbol{\Lambda}} = \boldsymbol{0}$) is a globally stable equilibrium of the error dynamics*

$$\dot{\boldsymbol{e}}_C(t) = \boldsymbol{A}_M \boldsymbol{e}_C(t) - \boldsymbol{B}_P \tilde{\boldsymbol{\Lambda}}(t) \cdot \Delta \boldsymbol{u}(t) + \boldsymbol{B}_P \boldsymbol{\Lambda} \tilde{\boldsymbol{\Theta}}(t) \cdot \boldsymbol{\omega}(\boldsymbol{x}_P(t), t),$$

$$\dot{\tilde{\boldsymbol{\Theta}}}\left(t\right)^{T} = \dot{\boldsymbol{\Theta}}\left(t\right)^{T} = -\boldsymbol{\Gamma\omega}\left(\boldsymbol{x}_{P}\left(t\right), t\right) \cdot \boldsymbol{e}_{C}\left(t\right)^{T} \boldsymbol{PB}_{P},$$
$$\dot{\tilde{\boldsymbol{\Lambda}}}\left(t\right)^{T} = \dot{\hat{\boldsymbol{\Lambda}}}\left(t\right)^{T} = \boldsymbol{\Gamma}_{u} \Delta\boldsymbol{u}\left(t\right) \cdot \boldsymbol{e}_{C}\left(t\right)^{T} \boldsymbol{PB}_{P}.$$

Proof. Consider the representation (3.128) of the plant (3.127). Adding and subtracting $\boldsymbol{B}_{P}\boldsymbol{\Lambda} \cdot \boldsymbol{u}\left(t\right)$ and inserting the control law (3.22) yields the closed-loop representation (3.129). Consequently, the tracking error dynamics evolve according to (3.132). Now consider the Lyapunov function candidate (3.133). Its derivative is

$$\dot{V}\left(t\right) = \boldsymbol{e}_{C}\left(t\right)^{T} \boldsymbol{P}\dot{\boldsymbol{e}}_{C}\left(t\right) + \mathrm{Tr}\left\{\tilde{\boldsymbol{\Theta}}\left(t\right)\boldsymbol{\Gamma}^{-1}\dot{\tilde{\boldsymbol{\Theta}}}\left(t\right)^{T}\boldsymbol{\Lambda}\right\} + \mathrm{Tr}\left\{\tilde{\boldsymbol{\Lambda}}\left(t\right)\boldsymbol{\Gamma}_{u}^{-1}\dot{\tilde{\boldsymbol{\Lambda}}}\left(t\right)^{T}\right\}. \tag{3.136}$$

Since $\tilde{\boldsymbol{\Theta}}\left(t\right) = \boldsymbol{\Theta}\left(t\right) - \boldsymbol{\Theta}^{*}$, $\tilde{\boldsymbol{\Lambda}}\left(t\right) = \hat{\boldsymbol{\Lambda}}\left(t\right) - \boldsymbol{\Lambda}$ hold and $\boldsymbol{\Theta}^{*}$, $\boldsymbol{\Lambda}$ are constant, $\dot{\tilde{\boldsymbol{\Theta}}}\left(t\right) = \dot{\boldsymbol{\Theta}}\left(t\right)$ and $\dot{\tilde{\boldsymbol{\Lambda}}}\left(t\right) = \dot{\hat{\boldsymbol{\Lambda}}}\left(t\right)$ follow. Inserting the error dynamics (3.132) and the update laws (3.134), (3.135) into (3.136) hence yields

$$\begin{aligned}\dot{V}\left(t\right) = \boldsymbol{e}_{C}\left(t\right)^{T}\boldsymbol{P}\Big(&\boldsymbol{A}_{M}\boldsymbol{e}_{C}\left(t\right) - \boldsymbol{B}_{P}\tilde{\boldsymbol{\Lambda}}\left(t\right)\cdot\Delta\boldsymbol{u}\left(t\right) + \boldsymbol{B}_{P}\boldsymbol{\Lambda}\tilde{\boldsymbol{\Theta}}\left(t\right)\cdot\boldsymbol{\omega}\left(\boldsymbol{x}_{P}\left(t\right),t\right)\Big)\\ &- \mathrm{Tr}\left\{\tilde{\boldsymbol{\Theta}}\left(t\right)\boldsymbol{\omega}\left(\boldsymbol{x}_{P}\left(t\right),t\right)\cdot\boldsymbol{e}_{C}\left(t\right)^{T}\boldsymbol{PB}_{P}\boldsymbol{\Lambda}\right\}\\ &+ \mathrm{Tr}\left\{\tilde{\boldsymbol{\Lambda}}\left(t\right)\Delta\boldsymbol{u}\left(t\right)\cdot\boldsymbol{e}_{C}\left(t\right)^{T}\boldsymbol{PB}_{P}\right\}.\end{aligned} \tag{3.137}$$

Using the relations $\boldsymbol{e}_{C}\left(t\right)^{T}\boldsymbol{PB}_{P}\tilde{\boldsymbol{\Lambda}}\left(t\right)\cdot\Delta\boldsymbol{u}\left(t\right) = \mathrm{Tr}\left\{\tilde{\boldsymbol{\Lambda}}\left(t\right)\Delta\boldsymbol{u}\left(t\right)\boldsymbol{e}_{C}\left(t\right)^{T}\boldsymbol{PB}_{P}\right\}$ as well as $\boldsymbol{e}_{C}\left(t\right)^{T}\boldsymbol{PB}_{P}\boldsymbol{\Lambda}\tilde{\boldsymbol{\Theta}}\left(t\right)\cdot\boldsymbol{\omega}\left(\boldsymbol{x}_{P}\left(t\right),t\right) = \mathrm{Tr}\left\{\tilde{\boldsymbol{\Theta}}\left(t\right)\boldsymbol{\omega}\left(\boldsymbol{x}_{P}\left(t\right),t\right)\boldsymbol{e}_{C}\left(t\right)^{T}\boldsymbol{PB}_{P}\boldsymbol{\Lambda}\right\}$, (3.137) becomes

$$\dot{V}\left(t\right) = \boldsymbol{e}_{C}\left(t\right)^{T}\boldsymbol{PA}_{M}\boldsymbol{e}_{C}\left(t\right) = -\frac{1}{2}\boldsymbol{e}_{C}\left(t\right)^{T}\boldsymbol{Q}\boldsymbol{e}_{C}\left(t\right) \leq 0, \tag{3.138}$$

which proves global stability of the equilibrium ($\boldsymbol{e}_{C} = \boldsymbol{0}$, $\tilde{\boldsymbol{\Theta}} = \boldsymbol{0}$, $\tilde{\boldsymbol{\Lambda}} = \boldsymbol{0}$). □

While Lemma 3.16 proves boundedness of $\boldsymbol{e}_{C}\left(t\right)$, $\boldsymbol{\Theta}\left(t\right)$ and $\hat{\boldsymbol{\Lambda}}\left(t\right)$, it does not ensure boundedness of the plant state $\boldsymbol{x}_{P}\left(t\right)$. This is because the modified reference model (3.131) depends on $\Delta\boldsymbol{u}\left(t\right)$, which is a function of $\boldsymbol{x}_{P}\left(t\right)$ by itself. In general, the question of stability of the overall closed-loop control system, when using *hedging*, is an open question and strongly depends on the operator $\mathcal{F}\left\{\boldsymbol{u}\left(t\right)\right\}$. For example, if $\mathcal{F}\left\{\boldsymbol{u}\left(t\right)\right\}$ only represents a saturation and the plant (3.127) is Bounded Input Bounded State (BIBS)-stable by itself, then boundedness of $\boldsymbol{x}_{P}\left(t\right)$ is intrinsically ensured. If the operator $\mathcal{F}\left\{\boldsymbol{u}\left(t\right)\right\}$ represents actuator dynamics, a more complex stability analysis is required. To that end, similarities between *hedging* and $\mathcal{L}_{1}$ Adaptive Control may be exploited in order to prove boundedness [15]. More recently, an analysis based on Linear Matrix Inequalities (LMIs) has also been proposed [72].

In any case, notice that tracking of the modified reference model (3.131) does not imply tracking of the unmodified reference model (3.126). Hence, satisfaction of the original design requirements, which are embedded into the unmodified reference model, is no longer guaranteed.

Closed-Loop Reference Models

The objective of MRAC with CRM is the alteration of the decay rate of the tracking error dynamics, as this admits smoother, less oscillatory transient responses [159, 70]. While the plant representation (3.25), the control law (3.26) and the update law (3.43) of direct MRAC remain *structurally unchanged*, a modification of the reference model is required in order to achieve the latter goal. To that end, consider the CRM

$$\dot{\boldsymbol{x}}_M(t) = \boldsymbol{A}_M \boldsymbol{x}_M(t) + \boldsymbol{B}_M \boldsymbol{r}(t) - \boldsymbol{L}\boldsymbol{e}_C(t) \tag{3.139}$$

instead of (3.4). The tracking error dynamics between the CRM (3.139) and the plant (3.25) become

$$\dot{\boldsymbol{e}}_C(t) = \dot{\boldsymbol{x}}_P(t) - \dot{\boldsymbol{x}}_M(t) = (\boldsymbol{A}_M + \boldsymbol{L}) \cdot \boldsymbol{e}_C(t) + \boldsymbol{B}_P \boldsymbol{\Lambda} \tilde{\boldsymbol{\Theta}}(t) \cdot \boldsymbol{\omega}(\boldsymbol{x}_P(t), t). \tag{3.140}$$

Obviously, the gain $\boldsymbol{L}$ may be used to arbitrarily shape the decay rate of the error dynamics. The stability of the tracking error dynamics (3.140) and the parameter error dynamics (3.41) may now be established with the help of the Lyapunov function candidate

$$V(t) = \frac{1}{2}\boldsymbol{e}_C(t)^T \boldsymbol{P}_L \boldsymbol{e}_C(t) + \frac{1}{2}\operatorname{Tr}\left\{\tilde{\boldsymbol{\Theta}}(t)\boldsymbol{\Gamma}^{-1}\tilde{\boldsymbol{\Theta}}(t)^T \boldsymbol{\Lambda}\right\}. \tag{3.141}$$

While (3.141) is structurally equivalent to the Lyapunov function (3.30) of direct MRAC, the matrix $\boldsymbol{P}_L$ is *not* the solution of the Lyapunov equation (3.31) anymore, but of the altered Lyapunov equation

$$(\boldsymbol{A}_M + \boldsymbol{L})^T \boldsymbol{P}_L + \boldsymbol{P}_L (\boldsymbol{A}_M + \boldsymbol{L}) = -\boldsymbol{Q}, \tag{3.142}$$

where $\boldsymbol{Q} \in \mathbb{S}^n_{++}$ is a positive definite design parameter.

Theorem 3.17 (Nominal Stability of Direct MRAC with CRM)**.** *Consider the plant* (3.1) *and let Assumptions 3.1 (state feedback), 3.2 (positive definite control effectiveness), 3.3 (Lipschitz condition), 3.4 (matching condition), 3.7 (linear parametrization) and 3.8 (exact parametrization) hold. Then, according to* (3.25)*, the plant admits the compact representation*

$$\dot{\boldsymbol{x}}_P(t) = \boldsymbol{A}_M \boldsymbol{x}_P(t) + \boldsymbol{B}_M \boldsymbol{r}(t) + \boldsymbol{B}_P \boldsymbol{\Lambda}\left(\boldsymbol{u}(t) - \boldsymbol{\Theta}^* \boldsymbol{\omega}(\boldsymbol{x}_P(t), t)\right),$$

where the true parameter matrix $\boldsymbol{\Theta}^*$ and the regressor vector $\boldsymbol{\omega}(\boldsymbol{x}_P(t), t)$ are defined in (3.23)*. Furthermore, the CRM is given by* (3.139)*, that is:*

$$\dot{\boldsymbol{x}}_M(t) = \boldsymbol{A}_M \boldsymbol{x}_M(t) + \boldsymbol{B}_M \boldsymbol{r}(t) - \boldsymbol{L}\boldsymbol{e}_C(t),$$

where $\boldsymbol{A}_M$ is Hurwitz. Let the learning rate $\boldsymbol{\Gamma} \in \mathbb{S}^{n_r}_{++}$ and the weighting matrix $\boldsymbol{Q} \in \mathbb{S}^n_{++}$ be chosen positive definite, and let $\boldsymbol{P}_L \in \mathbb{S}^n_{++}$ be the positive definite solution of the altered Lyapunov equation (3.142)*. Then the control law*

$$\begin{aligned} \boldsymbol{u}(t) &= \boldsymbol{\Theta}(t) \cdot \boldsymbol{\omega}(\boldsymbol{x}_P(t), t), \\ \dot{\boldsymbol{\Theta}}(t)^T &= -\boldsymbol{\Gamma}\boldsymbol{\omega}(\boldsymbol{x}_P(t), t) \cdot \boldsymbol{e}_C(t)^T \boldsymbol{P}_L \boldsymbol{B}_P \end{aligned}$$

from (3.26) *and* (3.43) *will ensure*

1. *that ($\boldsymbol{e}_C = \mathbf{0}$, $\tilde{\boldsymbol{\Theta}} = \mathbf{0}$) is a globally stable equilibrium of the tracking error dynamics* (3.140) *and the parameter error dynamics* (3.41)*;*
2. *that the CRM and all other closed-loop signals are bounded;*
3. *that the plant asymptotically tracks the closed-loop reference model* (3.139)*, i.e.*

$$\lim_{t\to\infty} \|\boldsymbol{e}_C(t)\| = 0;$$

4. *that the plant asymptotically tracks the unmodified reference model* (3.126)*, i.e.*

$$\lim_{t\to\infty} \|\boldsymbol{x}_P(t) - \boldsymbol{x}_{M,0}(t)\| = 0.$$

Proof. Consider the plant representation (3.25). Inserting the control law (3.26) yields

$$\dot{\boldsymbol{x}}_P(t) = \boldsymbol{A}_M \boldsymbol{x}_P(t) + \boldsymbol{B}_M \boldsymbol{r}(t) + \boldsymbol{B}_P \boldsymbol{\Lambda} \tilde{\boldsymbol{\Theta}}(t) \cdot \boldsymbol{\omega}(\boldsymbol{x}_P(t), t). \tag{3.143}$$

Hence, the error between the plant (3.143) and the CRM (3.139) evolves according to (3.140), that is

$$\dot{\boldsymbol{e}}_C(t) = (\boldsymbol{A}_M + \boldsymbol{L}) \cdot \boldsymbol{e}_C(t) + \boldsymbol{B}_P \boldsymbol{\Lambda} \tilde{\boldsymbol{\Theta}}(t) \cdot \boldsymbol{\omega}(\boldsymbol{x}_P(t), t).$$

Now consider the Lyapunov function candidate (3.141), where $\boldsymbol{P}_L$ is the solution of the Lyapunov equation (3.142). Its derivative is given by

$$\dot{V}(t) = \boldsymbol{e}_C(t)^T \boldsymbol{P}_L \dot{\boldsymbol{e}}_C(t) + \mathrm{Tr}\left\{\tilde{\boldsymbol{\Theta}}(t) \boldsymbol{\Gamma}^{-1} \dot{\tilde{\boldsymbol{\Theta}}}(t)^T \boldsymbol{\Lambda}\right\}. \tag{3.144}$$

Since $\tilde{\boldsymbol{\Theta}}(t) = \boldsymbol{\Theta}(t) - \boldsymbol{\Theta}^*$ holds and $\boldsymbol{\Theta}^*$ is constant, $\dot{\tilde{\boldsymbol{\Theta}}}(t) = \dot{\boldsymbol{\Theta}}(t)$ follows. Inserting the error dynamics (3.140) and the update law (3.43) into (3.144) yields

$$\begin{aligned}\dot{V}(t) = \boldsymbol{e}_C(t)^T \boldsymbol{P}_L \Big((\boldsymbol{A}_M + \boldsymbol{L}) \boldsymbol{e}_C(t) + \boldsymbol{B}_P \boldsymbol{\Lambda} \tilde{\boldsymbol{\Theta}}(t) \cdot \boldsymbol{\omega}(\boldsymbol{x}_P(t), t)\Big) \\ - \mathrm{Tr}\left\{\tilde{\boldsymbol{\Theta}}(t) \boldsymbol{\omega}(\boldsymbol{x}_P(t), t) \cdot \boldsymbol{e}_C(t)^T \boldsymbol{P}_L \boldsymbol{B}_P \boldsymbol{\Lambda}\right\}.\end{aligned} \tag{3.145}$$

Using $\boldsymbol{e}_C(t)^T \boldsymbol{P}_L \boldsymbol{B}_P \boldsymbol{\Lambda} \tilde{\boldsymbol{\Theta}}(t) \cdot \boldsymbol{\omega}(\boldsymbol{x}_P(t), t) = \mathrm{Tr}\left\{\tilde{\boldsymbol{\Theta}}(t) \boldsymbol{\omega}(\boldsymbol{x}_P(t), t) \boldsymbol{e}_C(t)^T \boldsymbol{P}_L \boldsymbol{B}_P \boldsymbol{\Lambda}\right\}$, the derivative (3.145) becomes

$$\dot{V}(t) = \boldsymbol{e}_C(t)^T \boldsymbol{P}_L (\boldsymbol{A}_M + \boldsymbol{L}) \boldsymbol{e}_C(t) = -\frac{1}{2} \boldsymbol{e}_C(t)^T \boldsymbol{Q} \boldsymbol{e}_C(t) \leq 0, \tag{3.146}$$

which proves global stability of the equilibrium ($\boldsymbol{e}_C = \mathbf{0}$, $\tilde{\boldsymbol{\Theta}} = \mathbf{0}$). Since $\boldsymbol{e}_C(t)$ is bounded, the CRM (3.139) is bounded as well as $\boldsymbol{A}_M$ is Hurwitz. Hence, $\boldsymbol{x}_P(t) = \boldsymbol{e}_C(t) + \boldsymbol{x}_M(t)$ is bounded as well. Furthermore, since the command signal $\boldsymbol{r}(t)$ is bounded by definition, the Lipschitz condition in Assumption 3.3 implies boundedness of the regressor vector $\boldsymbol{\omega}(\boldsymbol{x}_P(t), t)$ and hence, of all closed-loop signals. Boundedness of the regressor vector $\boldsymbol{\omega}(\boldsymbol{x}_P(t), t)$ together with boundedness of $\boldsymbol{e}_C(t)$ and $\tilde{\boldsymbol{\Theta}}(t)$ due to the Lyapunov proof of stability proves boundedness of $\dot{\boldsymbol{e}}_C(t)$, i.e. $\dot{\boldsymbol{e}}_C(t) \in \mathcal{L}_\infty$.

The latter implies uniform continuity of $-\dot{V}(t)$ as $-\ddot{V}(t) = \boldsymbol{e}_C(t)^T \boldsymbol{Q}\dot{\boldsymbol{e}}_C(t)$ is bounded. Invoking Barbalat's Lemma (Lemma C.3) shows

$$\lim_{t\to\infty} -\dot{V}(t) = \frac{1}{2} \cdot \lim_{t\to\infty} \boldsymbol{e}_C(t)^T \boldsymbol{Q}\boldsymbol{e}_C(t) = 0, \tag{3.147}$$

implying $\lim_{t\to\infty} \|\boldsymbol{e}_C(t)\| = 0$. Finally, consider the error $\boldsymbol{x}_P(t) - \boldsymbol{x}_{M,0}(t) = \boldsymbol{x}_P(t) - \boldsymbol{x}_M(t) + \boldsymbol{x}_M(t) - \boldsymbol{x}_{M,0}(t) = \boldsymbol{e}_C(t) + \boldsymbol{x}_M(t) - \boldsymbol{x}_{M,0}(t)$. Notice that the error $\boldsymbol{x}_M(t) - \boldsymbol{x}_{M,0}(t)$ between the CRM (3.139) and the unmodified reference model (3.126) evolves according to

$$\dot{\boldsymbol{x}}_M(t) - \dot{\boldsymbol{x}}_{M,0}(t) = \boldsymbol{A}_M \cdot (\boldsymbol{x}_M(t) - \boldsymbol{x}_{M,0}(t)) - \boldsymbol{L}\boldsymbol{e}_C(t). \tag{3.148}$$

Since $\|\boldsymbol{e}_C(t)\| \to 0$ holds as $t \to \infty$, $\|\boldsymbol{x}_M(t) - \boldsymbol{x}_{M,0}(t)\| \to 0$ holds as well as $t \to \infty$. Thus, one has $\|\boldsymbol{x}_P(t) - \boldsymbol{x}_{M,0}(t)\| \to 0$ as $t \to \infty$. □

Command Governor

When considering the direct MRAC of Section 3.2.1, one observes in the closed-loop plant representation (3.28) that the plant and the reference model (3.4) only differ in the term $\boldsymbol{B}_P \cdot \boldsymbol{d}_{ad}(\boldsymbol{x}_P(t), t)$ with

$$\boldsymbol{d}_{ad}(\boldsymbol{x}_P(t), t) \triangleq \boldsymbol{\Lambda}\tilde{\boldsymbol{\Theta}}(t) \cdot \boldsymbol{\omega}(\boldsymbol{x}_P(t), t). \tag{3.149}$$

The signal (3.149) may be considered as the disturbance, which results from residual parameter error $\tilde{\boldsymbol{\Theta}}(t)$, and is hence referred to as residual adaption error. In direct MRAC without further modifications, the residual adaptation error $\boldsymbol{d}_{ad}(\boldsymbol{x}_P(t), t)$ will only vanish asymptotically as the plant approaches the reference model. Thus, during transients, the plant and the reference model may display significantly different responses. Now assume that an estimate $\hat{\boldsymbol{d}}_{ad}(t)$ of $\boldsymbol{d}_{ad}(\boldsymbol{x}_P(t), t)$ was known. By choosing the command signal $\boldsymbol{r}(t)$ as

$$\boldsymbol{r}(t) = \boldsymbol{r}_0(t) - \boldsymbol{K}_r^{-1} \cdot \hat{\boldsymbol{d}}_{ad}(t), \tag{3.150}$$

where $\boldsymbol{B}_M = \boldsymbol{B}_P\boldsymbol{K}_r$ holds due to (3.10), the reference model (3.4) becomes

$$\dot{\boldsymbol{x}}_M(t) = \boldsymbol{A}_M\boldsymbol{x}_M(t) + \boldsymbol{B}_M\boldsymbol{r}_0(t) - \boldsymbol{B}_P\hat{\boldsymbol{d}}_{ad}(t). \tag{3.151}$$

Likewise, the plant representation (3.28) turns into

$$\dot{\boldsymbol{x}}_P(t) = \boldsymbol{A}_M\boldsymbol{x}_P(t) + \boldsymbol{B}_M\boldsymbol{r}_0(t) + \boldsymbol{B}_P\left(\boldsymbol{d}_{ad}(\boldsymbol{x}_P(t), t) - \hat{\boldsymbol{d}}_{ad}(t)\right). \tag{3.152}$$

Thus, if $\hat{\boldsymbol{d}}_{ad}(t) \approx \boldsymbol{d}_{ad}(\boldsymbol{x}_P(t), t)$ holds, then the plant will approximately respond like the unmodified reference model (3.126) - even in transients. Despite of the modification of $\boldsymbol{r}(t)$, the error dynamics between the modified reference model (3.151) and the modified plant (3.152) become:

$$\begin{aligned}\dot{\boldsymbol{e}}_C(t) &= \boldsymbol{A}_M\boldsymbol{e}_C(t) + \boldsymbol{B}_P \cdot \boldsymbol{d}_{ad}(\boldsymbol{x}_P(t), t) \\ &= \boldsymbol{A}_M\boldsymbol{e}_C(t) + \boldsymbol{B}_P\boldsymbol{\Lambda}\tilde{\boldsymbol{\Theta}}(t) \cdot \boldsymbol{\omega}(\boldsymbol{x}_P(t), t).\end{aligned} \tag{3.153}$$

Since these tracking error dynamics are structurally equivalent to the error dynamics (3.29) of direct MRAC, the same Lyapunov proof of stability as in case of direct MRAC establishes that $(\boldsymbol{e}_C, \tilde{\boldsymbol{\Theta}}) = \boldsymbol{0}$ is a globally stable equilibrium. Furthermore, this proof will lead to the same update laws for the adaptive parameter $\boldsymbol{\Theta}(t)$ as in case of direct MRAC.

So far, a modification of the command signal $\boldsymbol{r}(t)$ has been proposed, which uses an estimate of the residual adaptation error $\boldsymbol{d}_{ad}(\boldsymbol{x}_P(t), t)$, in order to approximately cancel it during steady state and, more importantly, during transients. However, is has not been explained how this estimate is obtained. While there exist numerous methods to estimate the signal $\boldsymbol{d}_{ad}(\boldsymbol{x}_P(t), t)$, the *Command Governor* publications [182, 183] specifically propose the filtered differentiation of the tracking error signal $\boldsymbol{e}_C(t)$. Using the filtered differentiation, the error dynamics (3.153) may be solved for $\boldsymbol{d}_{ad}(\boldsymbol{x}_P(t), t)$, yielding the desired estimate $\hat{\boldsymbol{d}}_{ad}(t)$. To that end, consider the LTI filter

$$\boldsymbol{F}(s) = \frac{\omega_0}{s + \omega_0} \cdot \boldsymbol{I}^{n \times n}, \tag{3.154}$$

where $\omega_0 > 0$ determines the bandwidth of the filtered differentiation. Assuming zero initial conditions,

$$\dot{\boldsymbol{e}}_C(t) \approx \mathcal{L}^{-1}\{s \cdot \boldsymbol{F}(s) \cdot \boldsymbol{e}_C(s)\} \tag{3.155}$$

approximately holds, where $\boldsymbol{e}_C(s) = \mathcal{L}\{\boldsymbol{e}_C(t)\}$ denotes the Laplace transform of $\boldsymbol{e}_C(t)$. If $\boldsymbol{B}_P$ has full rank, the error dynamics (3.153) may be uniquely solved for $\boldsymbol{d}_{ad}(\boldsymbol{x}_P(t), t)$:

$$\boldsymbol{d}_{ad}(\boldsymbol{x}_P(t), t) = \boldsymbol{B}_P^{\#}(\dot{\boldsymbol{e}}_C(t) - \boldsymbol{A}_M \boldsymbol{e}_C(t)), \tag{3.156}$$

where $\boldsymbol{B}_P^{\#}$ denotes the pseudo inverse of $\boldsymbol{B}_P$. By replacing $\dot{\boldsymbol{e}}_C(t)$ by its estimate (3.155), one obtains the following estimate of the signal $\boldsymbol{d}_{ad}(\boldsymbol{x}_P(t), t)$:

$$\hat{\boldsymbol{d}}_{ad}(t) \triangleq \boldsymbol{B}_P^{\#} \cdot \mathcal{L}^{-1}\{(s \cdot \boldsymbol{F}(s) - \boldsymbol{A}_M) \cdot \boldsymbol{e}_C(s)\}. \tag{3.157}$$

By noticing that

$$\begin{aligned} s \cdot \boldsymbol{F}(s) &= \frac{s \cdot \omega_0}{s + \omega_0} \cdot \boldsymbol{I}^{n \times n} = \frac{s \cdot \omega_0 + \omega_0^2 - \omega_0^2}{s + \omega_0} \cdot \boldsymbol{I}^{n \times n} \\ &= \frac{\omega_0 \cdot (s + \omega_0) - \omega_0^2}{s + \omega_0} \cdot \boldsymbol{I}^{n \times n} = \omega_0 \cdot (\boldsymbol{I} - \boldsymbol{F}(s)) \end{aligned} \tag{3.158}$$

holds, the transfer function relation (3.157) may be equivalently represented in the time-domain as

$$\begin{aligned} \dot{\boldsymbol{\xi}}(t) &= -\omega_0 \boldsymbol{I}^{n \times n} \cdot \boldsymbol{\xi}(t) + \omega_0 \boldsymbol{I}^{n \times n} \cdot \boldsymbol{e}_C(t), \\ \hat{\boldsymbol{d}}_{ad}(t) &= \boldsymbol{B}_P^{\#} \cdot \left(\left(\omega_0 \boldsymbol{I}^{n \times n} - \boldsymbol{A}_M \right) \boldsymbol{e}_C(t) - \omega_0 \boldsymbol{I}^{n \times n} \cdot \boldsymbol{\xi}(t) \right). \end{aligned} \tag{3.159}$$

The time-domain representation (3.159) may also be found in [183]. Depending on the bandwidth ω_0 of the filtered differentiation, the *Command Governor* (3.159) may amplify measurement noise. For this reason, a robust *Command Governor* has been proposed in [183], which adds another PT1 low-pass filter. In any case, the following stability theorem holds:

Theorem 3.18 (Nominal Stability of Direct MRAC with Command Governor)**.** *Consider the plant* (3.1) *and let Assumptions 3.1 (state feedback), 3.2 (positive definite control effectiveness), 3.3 (Lipschitz condition), 3.4 (matching condition), 3.6 (full-rank $\boldsymbol{B}_P$), 3.7 (linear parametrization) and 3.8 (exact parametrization) hold. Then, according to* (3.25)*, the plant admits the compact representation*

$$\dot{\boldsymbol{x}}_P(t) = \boldsymbol{A}_M \boldsymbol{x}_P(t) + \boldsymbol{B}_M \boldsymbol{r}(t) + \boldsymbol{B}_P \boldsymbol{\Lambda}\left(\boldsymbol{u}(t) - \boldsymbol{\Theta}^* \boldsymbol{\omega}\left(\boldsymbol{x}_P(t), t\right)\right),$$

where the true parameter matrix $\boldsymbol{\Theta}^*$ and the regressor vector $\boldsymbol{\omega}\left(\boldsymbol{x}_P(t), t\right)$ are defined in (3.23)*. Furthermore, the command signal $\boldsymbol{r}(t)$ is given by* (3.150)*, i.e.*

$$\boldsymbol{r}(t) = \boldsymbol{r}_0(t) - \boldsymbol{K}_r^{-1} \cdot \hat{\boldsymbol{d}}_{ad}(t),$$

where $\boldsymbol{r}_0 : \mathbb{R}_+ \to \mathbb{R}^m$ is the actual pilot command and $\hat{\boldsymbol{d}}_{ad} : \mathbb{R}_+ \to \mathbb{R}^m$ is an estimate of the residual adaptation error (3.149)*, which is computed using the filter* (3.159)*. Let the learning rate $\boldsymbol{\Gamma} \in \mathbb{S}_{++}^{n_r}$ and the weighting matrix $\boldsymbol{Q} \in \mathbb{S}_{++}^{n}$ be chosen positive definite, let $\boldsymbol{P} \in \mathbb{S}_{++}^{n}$ be the positive definite solution of the Lyapunov equation* (3.31) *and let the design parameter ω_0 of the filter* (3.159) *be positive. Then the control law*

$$\begin{aligned}
\boldsymbol{u}(t) &= \boldsymbol{\Theta}(t) \cdot \boldsymbol{\omega}\left(\boldsymbol{x}_P(t), t\right), \\
\dot{\boldsymbol{\Theta}}(t)^T &= -\boldsymbol{\Gamma} \boldsymbol{\omega}\left(\boldsymbol{x}_P(t), t\right) \cdot \boldsymbol{e}_C(t)^T \boldsymbol{P} \boldsymbol{B}_P,
\end{aligned}$$

from (3.26) *and* (3.43)*, will ensure*

1. *that ($\boldsymbol{e}_C = \boldsymbol{0}$, $\tilde{\boldsymbol{\Theta}} = \boldsymbol{0}$) is a globally stable equilibrium of the tracking error dynamics* (3.153) *and the parameter error dynamics* (3.41)*;*
2. *that all closed-loop signals are bounded;*
3. *that the plant asymptotically tracks the modified reference model* (3.151)*, i.e.*

$$\lim_{t \to \infty} \|\boldsymbol{e}_C(t)\| = 0;$$

4. *that the plant asymptotically tracks the unmodified reference model* (3.126)*, i.e.*

$$\lim_{t \to \infty} \|\boldsymbol{x}_P(t) - \boldsymbol{x}_{M,0}(t)\| = 0.$$

Proof. As the *Command Governor* is based on a modification of the command signal $\boldsymbol{r}(t)$, it does neither alter the tracking error dynamics nor the parameter error dynamics of direct MRAC. Hence, the first part of Theorem 3.4 may be invoked to conclude that ($\boldsymbol{e}_C = \boldsymbol{0}$, $\tilde{\boldsymbol{\Theta}} = \boldsymbol{0}$) is a globally stable equilibrium. This establishes the first assertion. Furthermore, since $\hat{\boldsymbol{d}}_{ad}(t)$ is bounded for any bounded tracking error $\boldsymbol{e}_C(t)$, the modified reference model (3.151) is bounded, which implies boundedness of $\boldsymbol{x}_P(t)$. Hence, all closed-loop signals are bounded, which establishes the second assertion. Since all closed-loop signals are bounded, the second part of Theorem 3.4 establishes asymptotic tracking of the modified reference model (3.151), i.e. the third assertion. Finally,

notice that asymptotic convergence of the tracking error $\boldsymbol{e}_C(t)$ implies $\hat{\boldsymbol{d}}_{ad}(t) \to \boldsymbol{0}$ as $t \to \infty$. Thus, the error $\boldsymbol{x}_M(t) - \boldsymbol{x}_{M,0}(t)$ between the modified reference model (3.151) and the unmodified reference model (3.126), which evolves according to

$$\dot{\boldsymbol{x}}_M(t) - \dot{\boldsymbol{x}}_{M,0}(t) = \boldsymbol{A}_M \cdot (\boldsymbol{x}_M(t) - \boldsymbol{x}_{M,0}(t)) - \boldsymbol{B}_P \hat{\boldsymbol{d}}_{ad}(t), \tag{3.160}$$

asymptotically decreases to zero. Due to $\boldsymbol{x}_P(t) - \boldsymbol{x}_{M,0}(t) = \boldsymbol{x}_P(t) - \boldsymbol{x}_M(t) + \boldsymbol{x}_M(t) - \boldsymbol{x}_{M,0}(t)$, this proves the fourth assertion. □

3.3 $\mathcal{L}_1$ Adaptive Control

In Section 3.2, direct and predictor-based MRAC have been introduced. It has been shown that this particular adaptive controller achieves asymptotic MRC under some idealistic assumptions on the plant. Since the reference model specifies the desired closed-loop system response, one is however not only interested in the asymptotic performance (for $t \to \infty$), but also in the transient performance. In this regard, the bound (3.62) enabled to conclude that the plant will closely follow the reference model if the learning rate $\boldsymbol{\Gamma}$ is chosen sufficiently high. In practice, high learning rates come at the price of oscillatory responses of the closed-loop system, which are highly undesirable as they indicate a weakly damped system of little robustness. In fact, it is well known that high learning rates will cause significant problems if the idealistic assumptions on the plant do not hold (even if robustness modifications are used). In case of aircraft, high learning rates may for example lead to the excitation of unmodeled structural dynamics [136, 89] or may reduce the time-delay margin [43]. Hence, MRAC (without further modifications) seems to possess an inversely proportional coupling between its transient performance and its robustness. Depending on the application at hand, a satisfactory trade-off between these two diametral objectives cannot be achieved. In an effort to obtain a more benign trade-off between robustness and performance, the $\mathcal{L}_1$-AC architecture was proposed [27, 28, 87].

In its original form, $\mathcal{L}_1$-AC is a modification of predictor-based MRAC. By inserting a low-pass filter in the control channel of predictor-based MRAC (see Figure 3.9), $\mathcal{L}_1$-AC prevents undesirable high-frequency signals from affecting the plant. By compensating uncertainties only within the bandwidth of this filter, $\mathcal{L}_1$-AC admits a more benign trade-off between robustness and the speed of adaptation. However, notice that the speed of adaptation does not immediately relate to the transient performance anymore as the state predictor will not turn into the reference model (3.4) upon insertion of the modified control law. Instead, the speed of adaptation determines the transient performance with respect to the so-called $\mathcal{L}_1$ *Reference Model*. The $\mathcal{L}_1$ *Reference Model* is the closed-loop system which would result if the unknown plant parameters were known. Due to its dependence on the unknown plant parameters, the $\mathcal{L}_1$ *Reference Model* will not be implemented in the controller and is only required for the purpose of stability

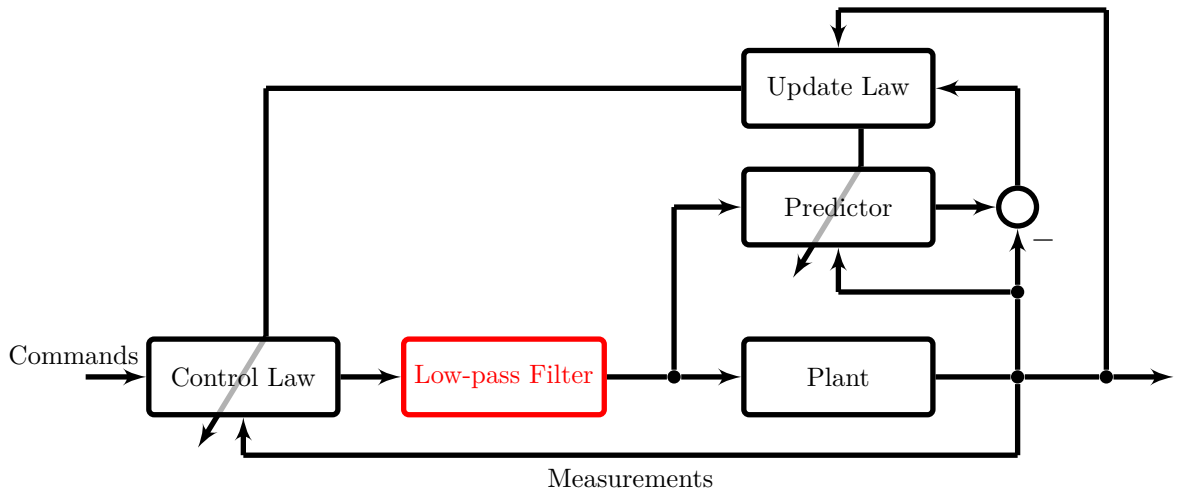

Figure 3.9: General structure of $\mathcal{L}_1$-AC with Integral Update Law.

and performance analysis. While the $\mathcal{L}_1$ *Reference Model* and the reference model (3.4) are substantially different, it is important to notice that $\mathcal{L}_1$ *Reference Model* will turn into the reference model (3.4), if the bandwidth of the low-pass filter in the control law tends to infinity. A sufficiently high bandwidth of the low-pass filter may hence render the $\mathcal{L}_1$ *Reference Model* arbitrarily close to the reference model (3.4). On the one hand, the latter point illustrates that $\mathcal{L}_1$-AC does not achieve asymptotic tracking of the reference model (3.4), but approximate tracking. On the other hand, it shows that an appropriate design of the low-pass filter is crucial for a successful control design. While an overly low filter bandwidth prevents all high frequency content from entering the plant, it also leads to bad tracking of the reference model (3.4). Conversely, a high filter bandwidth leads to close tracking of the reference model, but does hardly filter out any high-frequency content.

In Section 3.3.1, $\mathcal{L}_1$-AC in its original form will be introduced in case of matched uncertainties. Due to the use of the (integral) update law of predictor-based MRAC, this approach is also referred to as $\mathcal{L}_1$-AC with Integral Update Law. While the term $\mathcal{L}_1$ Adaptive Control ($\mathcal{L}_1$-AC) originally referred to approaches, which are closely related to predictor-based MRAC, it is nowadays often used as an umbrella term for several different controllers, which share certain properties and elements. These controllers range from nonlinear ones (such as the original $\mathcal{L}_1$-AC) to purely LTI controllers. The common elements of these controllers are

1. a state predictor with some uncertainty estimation approach;
2. a low-pass filtered control law, which makes use of the uncertainty estimates;
3. an uncertainty-dependent reference model, i.e. the $\mathcal{L}_1$ *Reference Model*, which determines the achievable closed-loop system performance if the uncertainties are only compensated within the filter bandwidth.

In Section 3.3.2, one of these other variants of $\mathcal{L}_1$-AC will be introduced, namely $\mathcal{L}_1$-AC with Piecewise Constant Update Law ($\mathcal{L}_1$-PWC) [25, 175]. A striking feature of this variant is its entire linearity. In the context of certification, which is the main driver of this thesis, linearity is a significant advantage. Ultimately, linearity enables the application of well-known tools from linear system theory to evaluate the robustness and performance of this $\mathcal{L}_1$-AC variant [152]. As to be discussed in Chapter 4, the absence of similar tools for nonlinear systems is a major hurdle for the certification of conventional, nonlinear adaptive controllers. Finally, the relation of $\mathcal{L}_1$-AC to other, well-established control approaches such as Disturbance Observers (DOBs) will be discussed in Section 3.3.3.

3.3.1 Matched Uncertainties with Integral Update Law

This section presents a $\mathcal{L}_1$ Adaptive Controller with Integral Update Law for the plant (3.1) in case of matched uncertainties and an exact, linear parametrization of the nonlinearities. The assumption of an exact, linear parametrization constitutes a major difference to the derivation of $\mathcal{L}_1$-AC in [87], where the nonlinearity of the plant is parametrized using a set of time-varying parameters. On the one side, an exact linear parametrization is advantageous as it leads to physically meaningful ideal parameters, whereas the time-varying ideal parameter in [87] may not be interpreted as easily. On the other side, the assumption of an exact, linear parametrization admits to reuse the exact same state predictor that has been derived in Section 3.2.3 in the context of MRAC. Since the derived controller essentially is a modification of the predictor-based MRAC of Section 3.2.3, the same Assumptions, namely Assumptions 3.1 (state feedback), 3.2 (positive definite control effectiveness), 3.3 (Lipschitz condition), 3.5 (matching condition), 3.7 (linear parametrization) and 3.8 (exact parametrization), are assumed to hold. Unlike the conventional predictor-based MRAC, stability of $\mathcal{L}_1$-AC can however not be established for uncertainties of an arbitrary size and for input matrices $\boldsymbol{B}_P$ of an arbitrary rank. For this reason, Assumption 3.6 (full-rank $\boldsymbol{B}_P$) and the following additional assumption are required:

Assumption 3.10. *The uncertainties $\boldsymbol{\Lambda}$, $\boldsymbol{\Theta}^*_{m,x}$ and $\boldsymbol{\Theta}^*_{m,\phi}$ are bounded. They are guaranteed to remain within the known compact sets Ω_Λ, $\Omega_{x,m}$ and $\Omega_{\phi,m}$, i.e.*

$$\boldsymbol{\Lambda} \in \Omega_\Lambda, \qquad \boldsymbol{\Theta}^*_{m,x} \in \Omega_{x,m}, \qquad \boldsymbol{\Theta}^*_{m,\phi} \in \Omega_{\phi,m}. \tag{3.161}$$

The sets Ω_Λ, $\Omega_{x,m}$ and $\Omega_{\phi,m}$ may be conservative in the sense that they are supersets of the sets, in which the uncertainties will remain in reality.

In order to ease the subsequent derivations, it is assumed that the initial conditions of all states are zero. For derivations, which respect non-zero initial conditions, the reader is referred to [87].

The derivation of a $\mathcal{L}_1$-AC for a nonlinear plant requires the knowledge of the Lipschitz constant of the nonlinearity. Roughly speaking, the Lipschitz constant admits to bound the "growth" of the nonlinearity. With the help of this bound, conditions for the stability of the $\mathcal{L}_1$ *Reference Model* and the closed-loop control system can be derived. However, Assumption 3.3 only requires the nonlinearity to be semi-globally Lipschitz. Roughly speaking, this means that there is a Lipschitz constant on any compact subset of the state space. The size of the constant does however depend on the distance from the origin. In essence, the semi-global character turns any stability result into a local one.

In order to ease the understanding, this section will be split into two parts. In the first part, the $\mathcal{L}_1$-AC will be derived, if the semi-global Lipschitz condition of Assumption 3.3 is strengthened to a global one. In this case, global stability results may be derived rather easily. In the second part, the restriction to globally Lipschitz nonlinearities will be alleviated leading to the final, local stability conditions.

Part One: Global Lipschitz condition

Throughout the first part, assume that the Lipschitz condition of Assumption 3.3 is strengthened to

$$\|\boldsymbol{f}(\boldsymbol{x}_1,t)-\boldsymbol{f}(\boldsymbol{x}_2,t)\| \leq K\cdot\|\boldsymbol{x}_1-\boldsymbol{x}_2\|, \tag{3.162}$$

where $K>0$ is some positive constant, independent of $\boldsymbol{x}_1$ and $\boldsymbol{x}_2$. Since the nonlinearity furthermore admits an exact, linear parametrization due to Assumptions 3.7 and 3.8, the regressor vector $\boldsymbol{\phi}\left(\boldsymbol{x}_P\left(t\right)\right)$ of the parametrization is subject to the following global Lipschitz condition:

$$\|\phi(\boldsymbol{x}_1)-\phi(\boldsymbol{x}_2)\|_\infty \leq L\cdot\|\boldsymbol{x}_1-\boldsymbol{x}_2\|_\infty. \tag{3.163}$$

In (3.163), $L>0$ is the global Lipschitz constant, which is known because the function $\phi(\boldsymbol{x})$ is known. Using the reverse triangle inequality, (3.163) especially yields a bound on the size of the nonlinearity, which depends linearly on $\|\boldsymbol{x}\|_\infty$, namely:

$$\|\phi(\boldsymbol{x})\|_\infty \leq L\cdot\|\boldsymbol{x}\|_\infty+\phi_0, \tag{3.164}$$

where $\phi_0 \geq \|\phi(\boldsymbol{0})\|_\infty$ with $\phi_0<\infty$ is a known constant.

Now consider the plant representation (3.12), which results from the general plant (3.1) by virtue of the alternative matching condition of Assumption 3.5. Since the nonlinearity $\boldsymbol{f}_m\left(\boldsymbol{x}_P\left(t\right),t\right)$ admits an exact, linear parametrization due to Assumptions 3.7 and 3.8, (3.12) may be restated as

$$\begin{aligned}\dot{\boldsymbol{x}}_P\left(t\right) &= \boldsymbol{A}_M\boldsymbol{x}_P\left(t\right)+\boldsymbol{B}_P\left(\boldsymbol{\Lambda}\boldsymbol{u}\left(t\right)+\boldsymbol{\Theta}_{m,x}^*\boldsymbol{x}_P\left(t\right)+\boldsymbol{\Theta}_{m,\phi}^*\cdot\boldsymbol{\phi}\left(\boldsymbol{x}_P\left(t\right)\right)\right)\\ &= \boldsymbol{A}_M\boldsymbol{x}_P\left(t\right)+\boldsymbol{B}_P\boldsymbol{\Theta}_m^*\boldsymbol{\omega}\left(\boldsymbol{x}_P\left(t\right),t\right),\end{aligned} \tag{3.165}$$

where $\boldsymbol{\Theta}_m^*$ and $\boldsymbol{\omega}\left(\boldsymbol{x}_P\left(t\right),t\right)$ have been defined in (3.74). According to Section 3.2.3, an adaptive state predictor for the plant (3.165) is given by:

$$\dot{\hat{\boldsymbol{x}}}_P\left(t\right)=\boldsymbol{A}_M\hat{\boldsymbol{x}}_P\left(t\right)+\boldsymbol{B}_P\left(\hat{\boldsymbol{\Lambda}}\left(t\right)\boldsymbol{u}\left(t\right)+\hat{\boldsymbol{\Theta}}_{m,x}\left(t\right)\boldsymbol{x}_P\left(t\right)+\hat{\boldsymbol{\Theta}}_{m,\phi}\left(t\right)\cdot\boldsymbol{\phi}\left(\boldsymbol{x}_P\left(t\right)\right)\right)$$

$$
\begin{aligned}
&= \boldsymbol{A}_M \hat{\boldsymbol{x}}_P(t) + \boldsymbol{B}_P \hat{\boldsymbol{\Theta}}_m(t) \cdot \boldsymbol{\omega}(\boldsymbol{x}_P(t), t), \\
\dot{\hat{\boldsymbol{\Theta}}}_m(t)^T &= -\boldsymbol{\Gamma}\boldsymbol{\omega}(\boldsymbol{x}_P(t), t) \cdot \boldsymbol{e}_P(t)^T \boldsymbol{P}\boldsymbol{B}_P,
\end{aligned} \tag{3.166}
$$

where $\boldsymbol{\Gamma} \in \mathbb{S}^{n_r}_{++}$ denotes the learning rate and $\boldsymbol{P} \in \mathbb{S}^{n}_{++}$ is the positive definite solution of the Lyapunov equation (3.31). The error dynamics of the prediction error $\boldsymbol{e}_P(t) = \hat{\boldsymbol{x}}_P(t) - \boldsymbol{x}_P(t)$ and the parameter error $\tilde{\boldsymbol{\Theta}}_m(t) = \hat{\boldsymbol{\Theta}}_m(t) - \boldsymbol{\Theta}^*_m$ evolve according to

$$
\begin{aligned}
\dot{\boldsymbol{e}}_P(t) &= \boldsymbol{A}_M \boldsymbol{e}_P(t) + \boldsymbol{B}_P \tilde{\boldsymbol{\Theta}}_m(t) \cdot \boldsymbol{\omega}(\boldsymbol{x}_P(t), t), \\
\dot{\tilde{\boldsymbol{\Theta}}}_m(t)^T &= -\boldsymbol{\Gamma}\boldsymbol{\omega}(\boldsymbol{x}_P(t), t) \cdot \boldsymbol{e}_P(t)^T \boldsymbol{P}\boldsymbol{B}_P.
\end{aligned} \tag{3.167}
$$

Lemma 3.7 guarantees global stability of the tracking error $\boldsymbol{e}_P(t)$ and the parameter error $\tilde{\boldsymbol{\Theta}}_m(t)$.

Using the estimate $\hat{\boldsymbol{\Theta}}_m(t)$ of the uncertainty $\boldsymbol{\Theta}^*_m$, a control law is to be derived which ensures approximate tracking of the reference model (3.4) and prevents the control law from feeding high-frequency signals to the plant. For the derivation of the control law, let's follow a certainty equivalence type of argument. That is, in a first step, an ideal control law is designed which assumes perfect knowledge of the true uncertainties and prevents high-frequency content in the control signal. This first step will also lead to the definition of the $\mathcal{L}_1$ *Reference Model*. In the second step, the real control law is obtained by replacing the true uncertainties by their adaptive estimates.
In order to derive the ideal control law and the $\mathcal{L}_1$ *Reference Model* within one step, rewrite the plant (3.165) as follows:

$$
\dot{\boldsymbol{x}}_{\text{ref}}(t) = \boldsymbol{A}_M \boldsymbol{x}_{\text{ref}}(t) + \boldsymbol{B}_P \left(\boldsymbol{\Lambda}\boldsymbol{u}_{\text{ref}}(t) + \boldsymbol{\Theta}^*_{m,x} \boldsymbol{x}_{\text{ref}}(t) + \boldsymbol{\Theta}^*_{m,\phi} \cdot \boldsymbol{\phi}(\boldsymbol{x}_{\text{ref}}(t)) \right), \tag{3.168}
$$

where $\boldsymbol{x}_{\text{ref}} : \mathbb{R}_+ \to \mathbb{R}^n$ is the state vector of the $\mathcal{L}_1$ *Reference Model* and $\boldsymbol{u}_{\text{ref}}(t) : \mathbb{R}_+ \to \mathbb{R}^m$ is the input vector. Notice that (3.168) is structurally equivalent to the plant (3.165) except for the substitutions $\boldsymbol{x}_P(t) \to \boldsymbol{x}_{\text{ref}}(t)$ and $\boldsymbol{u}(t) \to \boldsymbol{u}_{\text{ref}}(t)$. Now, let the ideal control law for the plant (3.168) (i.e. the control law assuming perfect knowledge of the uncertainties) be given in the frequency-domain by

$$
\boldsymbol{u}_{\text{ref}}(s) = \boldsymbol{K}\boldsymbol{D}(s) \left(\boldsymbol{K}_r \boldsymbol{r}(s) - \boldsymbol{\Lambda}\boldsymbol{u}_{\text{ref}}(s) - \boldsymbol{\Theta}^*_{m,x} \boldsymbol{x}_{\text{ref}}(s) - \boldsymbol{\Theta}^*_{m,\phi} \boldsymbol{\phi}_{\text{ref}}(s) \right), \tag{3.169}
$$

where $\boldsymbol{K}_r$ is the feedforward gain defined in (3.10) and $\boldsymbol{\phi}_{\text{ref}}(s)$ denotes the Laplace transform of $\boldsymbol{\phi}(\boldsymbol{x}_{\text{ref}}(t))$, i.e. $\boldsymbol{\phi}_{\text{ref}}(s) = \mathcal{L}\{\boldsymbol{\phi}(\boldsymbol{x}_{\text{ref}}(t))\}$. Notice that the index $(\cdot)_{ref}$ is required to indicate that the Laplace transform $\boldsymbol{\phi}_{\text{ref}}(s)$ depends on the state $\boldsymbol{x}_{\text{ref}}(t)$. In (3.169), the feedback gain $\boldsymbol{K} \in \mathbb{R}^{m \times m}$ and the strictly proper transfer function matrix $\boldsymbol{D} : \mathbb{C} \to \mathbb{C}^{m \times m}$, which has to contain an integrator, are the design parameters of the low-pass-filtered control law. In order to clarify how $\boldsymbol{D}(s)$ and $\boldsymbol{K}$ are used to create a low-pass filter, notice that the ideal control law (3.169) may be rewritten as

$$
(\boldsymbol{I} + \boldsymbol{K}\boldsymbol{D}(s)\boldsymbol{\Lambda}) \cdot \boldsymbol{u}_{\text{ref}}(s) = \boldsymbol{K}\boldsymbol{D}(s) \left(\boldsymbol{K}_r \boldsymbol{r}(s) - \boldsymbol{\Theta}^*_{m,x} \boldsymbol{x}_{\text{ref}}(s) - \boldsymbol{\Theta}^*_{m,\phi} \boldsymbol{\phi}_{\text{ref}}(s) \right). \tag{3.170}
$$

Multiplying by $(\boldsymbol{I} + \boldsymbol{K}\boldsymbol{D}(s)\boldsymbol{\Lambda})^{-1}$ from the left leads to

$$\boldsymbol{u}_{\text{ref}}(s) = (\boldsymbol{I} + \boldsymbol{K}\boldsymbol{D}(s)\boldsymbol{\Lambda})^{-1}\boldsymbol{K}\boldsymbol{D}(s)\left(\boldsymbol{K}_r\boldsymbol{r}(s) - \boldsymbol{\Theta}_{m,x}^{*}\boldsymbol{x}_{\text{ref}}(s) - \boldsymbol{\Theta}_{m,\phi}^{*}\boldsymbol{\phi}_{\text{ref}}(s)\right). \quad (3.171)$$

Multiplying (3.171) by $\boldsymbol{\Lambda}$ from the left and using the Searle identity (B.177), the ideal control law becomes

$$\boldsymbol{\Lambda}\boldsymbol{u}_{\text{ref}}(s) = (\boldsymbol{I}+\boldsymbol{\Lambda}\boldsymbol{K}\boldsymbol{D}(s))^{-1}\boldsymbol{\Lambda}\boldsymbol{K}\boldsymbol{D}(s)\left(\boldsymbol{K}_r\boldsymbol{r}(s) - \boldsymbol{\Theta}_{m,x}^{*}\boldsymbol{x}_{\text{ref}}(s) - \boldsymbol{\Theta}_{m,\phi}^{*}\boldsymbol{\phi}_{\text{ref}}(s)\right). \quad (3.172)$$

Using the definition of the low-pass filter

$$\boldsymbol{C}(s) \triangleq (\boldsymbol{I} + \boldsymbol{\Lambda}\boldsymbol{K}\boldsymbol{D}(s))^{-1}\boldsymbol{\Lambda}\boldsymbol{K}\boldsymbol{D}(s), \quad (3.173)$$

Eq. (3.172) may be compactly written as

$$\begin{aligned}\boldsymbol{\Lambda}\boldsymbol{u}_{\text{ref}}(s) &= \boldsymbol{C}(s)\left(\boldsymbol{K}_r\boldsymbol{r}(s) - \boldsymbol{\Theta}_{m,x}^{*}\boldsymbol{x}_{\text{ref}}(s) - \boldsymbol{\Theta}_{m,\phi}^{*}\boldsymbol{\phi}_{\text{ref}}(s)\right),\\ \boldsymbol{u}_{\text{ref}}(s) &= \boldsymbol{\Lambda}^{-1}\boldsymbol{C}(s)\left(\boldsymbol{K}_r\boldsymbol{r}(s) - \boldsymbol{\Theta}_{m,x}^{*}\boldsymbol{x}_{\text{ref}}(s) - \boldsymbol{\Theta}_{m,\phi}^{*}\boldsymbol{\phi}_{\text{ref}}(s)\right).\end{aligned} \quad (3.174)$$

The representation (3.174) illustrates that the ideal control law (3.169) effectively realizes a low-pass-filtered version of the ideal control law of predictor-based MRAC, which would be given by $\boldsymbol{u}_{\text{ref}}(t) = \boldsymbol{\Lambda}^{-1}\left(\boldsymbol{K}_r\boldsymbol{r}(s) - \boldsymbol{\Theta}_{m,x}^{*}\boldsymbol{x}_{\text{ref}}(t) - \boldsymbol{\Theta}_{m,\phi}^{*}\boldsymbol{\phi}(\boldsymbol{x}_{\text{ref}}(t))\right)$. Since the filter is defined as a feedback connection in (3.173), it will always be stationary accurate as $\boldsymbol{D}(s)$ is required to contain an integrator. Furthermore, upon an appropriate design of the filter, the ideal control law (3.169) may effectively prevent high-frequency signals from entering into the plant. However, depending on the structure of $\boldsymbol{D}(s)$, the design of the filter may become very challenging as the filter is dependent on the input uncertainty $\boldsymbol{\Lambda}$. In order to ensure a stable filter, the design parameters $\boldsymbol{K}$ and $\boldsymbol{D}(s)$ have to be chosen in such a way that the filter is Hurwitz for all $\boldsymbol{\Lambda} \in \Omega_{\Lambda}$. While an appropriate choice may be hard to obtain in general, the subsequent example highlights a convenient design choice:

Example 3.19. *Consider a plant with only one control input, i.e.* $m = 1$*. By choosing the design parameters according to*

$$D(s) = \frac{1}{s}, \qquad K > 0,$$

the filter $C(s)$ *turns into the PT1 (low-pass) filter*

$$C(s) = \frac{\Lambda K}{s + \Lambda K}.$$

This PT1 element is Hurwitz for all $K > 0$ *and* $\Lambda > 0$*. It is interesting to notice that the bandwidth decreases with decreasing control effectiveness. In case of multiple control inputs, this result generalizes to*

$$\boldsymbol{D}(s) = \frac{1}{s}\cdot\boldsymbol{I}, \qquad \boldsymbol{K} \in \mathbb{S}_{++}^{m},$$

which will ensure stability of the low-pass filter

$$\boldsymbol{C}(s) = (s\boldsymbol{I} + \boldsymbol{\Lambda}\boldsymbol{K})^{-1}\boldsymbol{\Lambda}\boldsymbol{K}$$

for all $\boldsymbol{\Lambda} > 0$ *and* $\boldsymbol{K} > 0$*. This fact can be proven using the Lyapunov function candidate* $V(t) = (1/2) \cdot \boldsymbol{x}_f^T(t)\boldsymbol{\Lambda}^{-1}\boldsymbol{x}_f(t)$*, where* $\boldsymbol{x}_f$ *denotes the state vector of the filter* $\boldsymbol{C}(s)$*.*

The plant (3.168) and the representation (3.174) of the ideal control law define the $\mathcal{L}_1$ *Reference Model*:

$$\begin{aligned} \dot{\boldsymbol{x}}_{\text{ref}}(t) &= \boldsymbol{A}_M\boldsymbol{x}_{\text{ref}}(t) + \boldsymbol{B}_P\left(\boldsymbol{\Lambda}\boldsymbol{u}_{\text{ref}}(t) + \boldsymbol{\Theta}_{m,x}^*\boldsymbol{x}_{\text{ref}}(t) + \boldsymbol{\Theta}_{m,\phi}^* \cdot \boldsymbol{\phi}(\boldsymbol{x}_{\text{ref}}(t))\right), \\ \boldsymbol{u}_{\text{ref}}(s) &= \boldsymbol{\Lambda}^{-1}\boldsymbol{C}(s)\left(\boldsymbol{K}_r\boldsymbol{r}(s) - \boldsymbol{\Theta}_{m,x}^*\boldsymbol{x}_{\text{ref}}(s) - \boldsymbol{\Theta}_{m,\phi}^*\boldsymbol{\phi}_{\text{ref}}(s)\right). \end{aligned} \tag{3.175}$$

The $\mathcal{L}_1$ *Reference Model* (3.175) represents the closed-loop performance which could be achieved by the ideal control law (3.169), if the true plant uncertainties $\boldsymbol{\Theta}_m^*$ were known. Notice that if the bandwidth of the filter $\boldsymbol{C}(s)$ tends to infinity, i.e. $\boldsymbol{C}(s) \to \boldsymbol{I}$, then the $\mathcal{L}_1$ *Reference Model* turns into the reference model (3.4). Hence, by a sufficiently fast filter $\boldsymbol{C}(s)$, the $\mathcal{L}_1$ *Reference Model* may be rendered arbitrarily close to the reference model (3.4). The latter implies that the ideal control law may indeed achieve its control objective of approximately tracking the reference model (3.4), given that the bandwidth of the filter is sufficiently high. At the same time, the filter should also prevent that high-frequency signals enter the plant. To that end, a filter of sufficiently low bandwidth is required. Hence, the filter is the crucial design parameter of the control law (3.169), which allows trading robustness versus performance.

Furthermore, the design of the filter also needs to ensure that the $\mathcal{L}_1$ *Reference Model* (3.175) is stable. Unlike the reference model (3.4), the $\mathcal{L}_1$ *Reference Model* depends on the true plant uncertainties. Hence, its stability is not ensured by $\boldsymbol{A}_M$ being Hurwitz. The question of stability will however be postponed at this time.

Having derived an ideal control law which may achieve the control objective, the real control law may now be stated. By replacing $\boldsymbol{\Lambda}$, $\boldsymbol{\Theta}_{m,x}^*$, $\boldsymbol{\Theta}_{m,\phi}^*$ by their adaptive estimates $\hat{\boldsymbol{\Lambda}}(t)$, $\hat{\boldsymbol{\Theta}}_{m,x}(t)$, $\hat{\boldsymbol{\Theta}}_{m,\phi}(t)$ in (3.169), the real control law for the plant (3.165) is obtained as:

$$\boldsymbol{u}(s) = \boldsymbol{K}\boldsymbol{D}(s)\left(\boldsymbol{K}_r\boldsymbol{r}(s) - \mathcal{L}\left\{\hat{\boldsymbol{\Lambda}}(t)\,\boldsymbol{u}(t) + \hat{\boldsymbol{\Theta}}_{m,x}(t)\,\boldsymbol{x}_P(t) + \hat{\boldsymbol{\Theta}}_{m,\phi}(t)\,\boldsymbol{\phi}(\boldsymbol{x}_P(t))\right\}\right). \tag{3.176}$$

In contrast to the ideal control law, the real control law (3.176) realizes a time-varying filter as the estimate $\hat{\boldsymbol{\Lambda}}(t)$ of the control effectiveness is time-varying. The time-varying character of the filter also is the reason why the real control law (3.176) is represented as a feedback interconnection instead of an explicit filter realization such as in (3.174).

The adaptive state predictor (3.166) together with the control law (3.176) constitute the $\mathcal{L}_1$ Adaptive Controller. While the structure of the $\mathcal{L}_1$-AC is known now, the stability of $\mathcal{L}_1$-AC has not been considered so far. The subsequent proof of boundedness of all closed-loop signals involves the following three steps:

1. Prove boundedness of the $\mathcal{L}_1$ *Reference Model* (3.175).
2. Prove boundedness of the error $\boldsymbol{e}_{\text{ref}}(t) = \boldsymbol{x}_P(t) - \boldsymbol{x}_{\text{ref}}(t)$ between the plant (3.165) and the $\mathcal{L}_1$ *Reference Model* (3.175).
3. Use the boundedness of the error $\boldsymbol{e}_{\text{ref}}(t)$ and of the $\mathcal{L}_1$ *Reference Model* to conclude that the plant state $\boldsymbol{x}_P(t)$ is bounded. Since the prediction error $\boldsymbol{e}_P(t)$ is bounded by virtue of Lemma 3.7, this implies boundedness of the adaptive state predictor (3.166). With this, all closed-loop signals are bounded.

Step 1: In order to be able to prove boundedness of the $\mathcal{L}_1$ *Reference Model*, assume that the design parameters of the filter (3.173) are chosen such that it is Hurwitz for all $\boldsymbol{\Lambda} \in \Omega_\Lambda$. By applying the definition

$$\boldsymbol{v}_{\text{ref}}(t) \triangleq \boldsymbol{\Lambda}\boldsymbol{u}_{\text{ref}}(t) + \boldsymbol{\Theta}^*_{m,x}\boldsymbol{x}_{\text{ref}}(t) + \boldsymbol{\Theta}^*_{m,\phi} \cdot \boldsymbol{\phi}(\boldsymbol{x}_{\text{ref}}(t)) \tag{3.177}$$

to the first equation in (3.175), the $\mathcal{L}_1$ *Reference Model* becomes

$$\dot{\boldsymbol{x}}_{\text{ref}}(t) = \boldsymbol{A}_M\boldsymbol{x}_{\text{ref}}(t) + \boldsymbol{B}_P \cdot \boldsymbol{v}_{\text{ref}}(t), \tag{3.178}$$

$$\boldsymbol{v}_{\text{ref}}(s) = \boldsymbol{\Lambda}\boldsymbol{u}_{\text{ref}}(s) + \boldsymbol{\Theta}^*_{m,x}\boldsymbol{x}_{\text{ref}}(s) + \boldsymbol{\Theta}^*_{m,\phi}\boldsymbol{\phi}_{\text{ref}}(s), \tag{3.179}$$

$$\boldsymbol{u}_{\text{ref}}(s) = \boldsymbol{\Lambda}^{-1}\boldsymbol{C}(s)\left(\boldsymbol{K}_r\boldsymbol{r}(s) - \boldsymbol{\Theta}^*_{m,x}\boldsymbol{x}_{\text{ref}}(s) - \boldsymbol{\Theta}^*_{m,\phi}\boldsymbol{\phi}_{\text{ref}}(s)\right). \tag{3.180}$$

Inserting the control law (3.180) into (3.179) then yields

$$\begin{aligned}\dot{\boldsymbol{x}}_{\text{ref}}(t) &= \boldsymbol{A}_M\boldsymbol{x}_{\text{ref}}(t) + \boldsymbol{B}_P \cdot \boldsymbol{v}_{\text{ref}}(t),\\ \boldsymbol{v}_{\text{ref}}(s) &= \boldsymbol{C}(s)\boldsymbol{K}_r\boldsymbol{r}(s) + (\boldsymbol{I} - \boldsymbol{C}(s)) \cdot \left(\boldsymbol{\Theta}^*_{m,x}\boldsymbol{x}_{\text{ref}}(s) + \boldsymbol{\Theta}^*_{m,\phi}\boldsymbol{\phi}_{\text{ref}}(s)\right).\end{aligned} \tag{3.181}$$

By virtue of the definition

$$\boldsymbol{G}_m(s) \triangleq (s\boldsymbol{I} - \boldsymbol{A}_M)^{-1}\boldsymbol{B}_P \tag{3.182}$$

and by assuming zero initial conditions, the $\mathcal{L}_1$ *Reference Model* may be represented entirely in the frequency-domain by:

$$\begin{aligned}\boldsymbol{x}_{\text{ref}}(s) &= \boldsymbol{G}_m(s) \cdot \boldsymbol{v}_{\text{ref}}(s),\\ \boldsymbol{v}_{\text{ref}}(s) &= \boldsymbol{C}(s)\boldsymbol{K}_r\boldsymbol{r}(s) + (\boldsymbol{I} - \boldsymbol{C}(s)) \cdot \left(\boldsymbol{\Theta}^*_{m,x}\boldsymbol{x}_{\text{ref}}(s) + \boldsymbol{\Theta}^*_{m,\phi}\boldsymbol{\phi}_{\text{ref}}(s)\right),\end{aligned} \tag{3.183}$$

or more compactly by

$$\begin{aligned}\boldsymbol{x}_{\text{ref}}(s) = \boldsymbol{G}_m(s)\boldsymbol{C}(s)\boldsymbol{K}_r \cdot \boldsymbol{r}(s)\\ + \boldsymbol{G}_m(s)(\boldsymbol{I} - \boldsymbol{C}(s)) \cdot \left(\boldsymbol{\Theta}^*_{m,x}\boldsymbol{x}_{\text{ref}}(s) + \boldsymbol{\Theta}^*_{m,\phi}\boldsymbol{\phi}_{\text{ref}}(s)\right).\end{aligned} \tag{3.184}$$

If the filter $\boldsymbol{C}(s)$ is Hurwitz, which implies that $\|\boldsymbol{C}(s)\|_{\mathcal{L}_1}$ exists, then the following norm inequality immediately results from the frequency-domain representation (3.184):

$$\begin{aligned}\|\boldsymbol{x}_{\text{ref}}(t)_\tau\|_{\mathcal{L}_\infty} \leq \|\boldsymbol{G}_m(s)\boldsymbol{C}(s)\boldsymbol{K}_r\|_{\mathcal{L}_1} \cdot \|\boldsymbol{r}(t)\|_{\mathcal{L}_\infty}\\ + \|\boldsymbol{G}_m(s)(\boldsymbol{I} - \boldsymbol{C}(s))\boldsymbol{\Theta}^*_{m,x}\|_{\mathcal{L}_1} \cdot \|\boldsymbol{x}_{\text{ref}}(t)_\tau\|_{\mathcal{L}_\infty}\\ + \|\boldsymbol{G}_m(s)(\boldsymbol{I} - \boldsymbol{C}(s))\boldsymbol{\Theta}^*_{m,\phi}\|_{\mathcal{L}_1} \cdot \|\boldsymbol{\phi}(\boldsymbol{x}_{\text{ref}}(t))_\tau\|_{\mathcal{L}_\infty}.\end{aligned} \tag{3.185}$$

Notice that truncated norms $\|(\cdot)_\tau\|_{\mathcal{L}}$ are used for all terms involving $\boldsymbol{x}_{\text{ref}}(t)$ as boundedness of these terms is not yet ensured. Hence, the $\mathcal{L}_\infty$-norm of $\boldsymbol{x}_{\text{ref}}(t)$ is not yet known to exist, which is required in order to establish boundedness of the $\mathcal{L}_1$ *Reference Model*. In order to conclude on boundedness from (3.185), one has to solve (3.185) for $\|\boldsymbol{x}_{\text{ref}}(t)_\tau\|_{\mathcal{L}_\infty}$. To that end, one may exploit that $\boldsymbol{\phi}(\boldsymbol{x}_{\text{ref}}(t))$ is assumed to be globally Lipschitz. Hence, the bound (3.164) may be used. Since the bound (3.164) holds for all $t = 0, \ldots, \tau$, it can be used to arrive at the following upper bound for (3.185):

$$\begin{aligned}\|\boldsymbol{x}_{\text{ref}}(t)_\tau\|_{\mathcal{L}_\infty} \leq\ & \|\boldsymbol{G}_m(s)\boldsymbol{C}(s)\boldsymbol{K}_r\|_{\mathcal{L}_1} \cdot \|\boldsymbol{r}(t)\|_{\mathcal{L}_\infty} \\ & + \|\boldsymbol{G}_m(s)(\boldsymbol{I} - \boldsymbol{C}(s))\boldsymbol{\Theta}^*_{m,x}\|_{\mathcal{L}_1} \cdot \|\boldsymbol{x}_{\text{ref}}(t)_\tau\|_{\mathcal{L}_\infty} \\ & + \|\boldsymbol{G}_m(s)(\boldsymbol{I} - \boldsymbol{C}(s))\boldsymbol{\Theta}^*_{m,\phi}\|_{\mathcal{L}_1} \cdot \phi_0 \\ & + \|\boldsymbol{G}_m(s)(\boldsymbol{I} - \boldsymbol{C}(s))\boldsymbol{\Theta}^*_{m,\phi}\|_{\mathcal{L}_1} \cdot L \cdot \|\boldsymbol{x}_{\text{ref}}(t)_\tau\|_{\mathcal{L}_\infty}.\end{aligned} \tag{3.186}$$

Solving (3.186) for $\|\boldsymbol{x}_{\text{ref}}(t)_\tau\|_{\mathcal{L}_\infty}$ yields:

$$\|\boldsymbol{x}_{\text{ref}}(t)_\tau\|_{\mathcal{L}_\infty} \leq \rho_r, \tag{3.187}$$

where

$$\rho_r \triangleq \frac{\|\boldsymbol{G}_m(s)\boldsymbol{C}(s)\boldsymbol{K}_r\|_{\mathcal{L}_1} \cdot \|\boldsymbol{r}(t)\|_{\mathcal{L}_\infty} + \|\boldsymbol{G}_m(s)(\boldsymbol{I} - \boldsymbol{C}(s))\boldsymbol{\Theta}^*_{m,\phi}\|_{\mathcal{L}_1} \cdot \phi_0}{1 - \|\boldsymbol{G}_m(s)(\boldsymbol{I} - \boldsymbol{C}(s))\boldsymbol{\Theta}^*_{m,x}\|_{\mathcal{L}_1} - \|\boldsymbol{G}_m(s)(\boldsymbol{I} - \boldsymbol{C}(s))\boldsymbol{\Theta}^*_{m,\phi}\|_{\mathcal{L}_1} \cdot L}. \tag{3.188}$$

Since $\boldsymbol{r}(t)$ and $\phi_0 \geq 0$ are bounded, the numerator of ρ_r is positive and bounded. However, the denominator may adopt positive or negative values. Hence, depending on the sign of the denominator, (3.187) yields an upper bound or a lower bound for $\|\boldsymbol{x}_{\text{ref}}(t)_\tau\|_{\mathcal{L}_\infty}$. Since an upper bound is desired in order to establish boundedness of $\|\boldsymbol{x}_{\text{ref}}(t)_\tau\|_{\mathcal{L}_\infty}$, the so-called $\mathcal{L}_1$-norm condition

$$\|\boldsymbol{G}_m(s)(\boldsymbol{I} - \boldsymbol{C}(s))\boldsymbol{\Theta}^*_{m,x}\|_{\mathcal{L}_1} + \|\boldsymbol{G}_m(s)(\boldsymbol{I} - \boldsymbol{C}(s))\boldsymbol{\Theta}^*_{m,\phi}\|_{\mathcal{L}_1} \cdot L < 1 \tag{3.189}$$

has to hold for all $\boldsymbol{\Lambda} \in \Omega_\Lambda$, $\boldsymbol{\Theta}^*_{m,x} \in \Omega_{x,m}$, $\boldsymbol{\Theta}^*_{m,\phi} \in \Omega_{\phi,m}$, implying $\rho_r \geq 0$. As shown in the next steps of the proof, the satisfaction of the $\mathcal{L}_1$-norm condition (3.189) is the central requirement to establish stability of $\mathcal{L}_1$-AC. Since ρ_r does not depend on τ, the bound (3.187) holds uniformly for all τ and one may conclude that

$$\|\boldsymbol{x}_{\text{ref}}(t)\|_{\mathcal{L}_\infty} \leq \rho_r \tag{3.190}$$

holds as well, if the $\mathcal{L}_1$-norm condition is satisfied. With (3.190), one can finally establish boundedness of the $\mathcal{L}_1$ *Reference Model*. The foregoing derivation is summarized in the following Lemma for stability of the $\mathcal{L}_1$ *Reference Model*:

Lemma 3.20 (Boundedness of the $\mathcal{L}_1$ *Reference Model*)**.** *Let Assumption 3.10 (i.e. bounded uncertainties) hold and assume that the semi-global Lipschitz condition of Assumption 3.3 is strengthened to a global one, such that*

$$\|\phi(\boldsymbol{x}_1) - \phi(\boldsymbol{x}_2)\|_\infty \leq L \cdot \|\boldsymbol{x}_1 - \boldsymbol{x}_2\|_\infty$$

holds, where $L > 0$ is a known constant. Consider the $\mathcal{L}_1$ Reference Model

$$\dot{\boldsymbol{x}}_{ref}(t) = \boldsymbol{A}_M \boldsymbol{x}_{ref}(t) + \boldsymbol{B}_P \left(\boldsymbol{\Lambda} \boldsymbol{u}_{ref}(t) + \boldsymbol{\Theta}^*_{m,x} \boldsymbol{x}_{ref}(t) + \boldsymbol{\Theta}^*_{m,\phi} \cdot \boldsymbol{\phi}\left(\boldsymbol{x}_{ref}(t)\right) \right),$$
$$\boldsymbol{u}_{ref}(s) = \boldsymbol{\Lambda}^{-1} \boldsymbol{C}(s) \left(\boldsymbol{K}_r \boldsymbol{r}(s) - \boldsymbol{\Theta}^*_{m,x} \boldsymbol{x}_{ref}(s) - \boldsymbol{\Theta}^*_{m,\phi} \boldsymbol{\phi}_{ref}(s) \right),$$

originally given in (3.175)*, and the filter from* (3.173)*, i.e.:*

$$\boldsymbol{C}(s) \triangleq (\boldsymbol{I} + \boldsymbol{\Lambda} \boldsymbol{K} \boldsymbol{D}(s))^{-1} \boldsymbol{\Lambda} \boldsymbol{K} \boldsymbol{D}(s),$$

where $\boldsymbol{K} \in \mathbb{R}^{m \times m}$ is a feedback gain and $\boldsymbol{D} : \mathbb{C} \to \mathbb{C}^{m \times m}$ is a strictly proper transfer function matrix containing an integrator. If the design parameters $\boldsymbol{K}$ and $\boldsymbol{D}(s)$ are chosen such that

1. *the filter $\boldsymbol{C}(s)$ is Hurwitz for all $\boldsymbol{\Lambda} \in \Omega_\Lambda$;*
2. *the $\mathcal{L}_1$-norm condition* (3.189) *is satisfied for all $\boldsymbol{\Lambda} \in \Omega_\Lambda$, $\boldsymbol{\Theta}^*_{m,x} \in \Omega_{x,m}$, $\boldsymbol{\Theta}^*_{m,\phi} \in \Omega_{\phi,m}$, i.e.*

$$\left\| \boldsymbol{G}_m(s) \left(\boldsymbol{I} - \boldsymbol{C}(s) \right) \boldsymbol{\Theta}^*_{m,x} \right\|_{\mathcal{L}_1} + \left\| \boldsymbol{G}_m(s) \left(\boldsymbol{I} - \boldsymbol{C}(s) \right) \boldsymbol{\Theta}^*_{m,\phi} \right\|_{\mathcal{L}_1} \cdot L < 1$$
$$\forall\, \boldsymbol{\Lambda} \in \Omega_\Lambda,\ \boldsymbol{\Theta}^*_{m,x} \in \Omega_{x,m},\ \boldsymbol{\Theta}^*_{m,\phi} \in \Omega_{\phi,m},$$

where $\boldsymbol{G}_m(s) \triangleq (s\boldsymbol{I} - \boldsymbol{A}_M)^{-1} \boldsymbol{B}_P$,

then the $\mathcal{L}_1$ Reference Model is bounded for $\boldsymbol{x}_{ref}(0) = \boldsymbol{0}$ and the bound is given by (3.190) *and* (3.188)*.*

Proof. The proof essentially repeats the derivation of *Step 1*, which has led from the *$\mathcal{L}_1$ Reference Model* (3.175) to the norm inequality (3.190). Since the design parameters $\boldsymbol{K}$ and $\boldsymbol{D}(s)$ are chosen such that the $\mathcal{L}_1$-norm condition (3.189) is satisfied, boundedness of the *$\mathcal{L}_1$ Reference Model* follows. □

Remark 3.21. *The derivation leading to Lemma 3.20 only establishes boundedness, if the initial condition $\boldsymbol{x}_{ref}(0)$ is zero. However, it may be easily shown that the conditions of Lemma 3.20 also suffice to show boundedness of the $\mathcal{L}_1$ Reference Model in case of bounded, non-zero initial conditions (see [87]).*

Remark 3.22. *The satisfaction of the conditions of Lemma 3.20 is rather challenging in general. However, by choosing $\boldsymbol{K}$ and $\boldsymbol{D}(s)$ according to Example 3.19, the first condition may always be satisfied. With respect to the second condition, notice that the transfer function $\boldsymbol{G}_m(s)$ always acts like a low-pass filter as it does not possess a direct feedthrough. Conversely, $(\boldsymbol{I} - \boldsymbol{C}(s))$ always acts like a high-pass filter. Thus, if the bandwidth of $\boldsymbol{C}(s)$ is chosen sufficiently high, then $\boldsymbol{G}_m(s)(\boldsymbol{I} - \boldsymbol{C}(s))$ will become a "no-pass" filter. Since the $\mathcal{L}_1$-norm of a "no-pass" filter vanishes, the second condition of Lemma 3.20 may also be always satisfied by an appropriate choice of the design parameters $\boldsymbol{K}$ and $\boldsymbol{D}(s)$.*

Step 2: Having established stability of the $\mathcal{L}_1$ *Reference Model*, boundedness of the error $\boldsymbol{e}_{\text{ref}}(t) = \boldsymbol{x}_P(t) - \boldsymbol{x}_{\text{ref}}(t)$ has to be proven in order to conclude on boundedness of $\boldsymbol{x}_P(t)$. To that end, notice that the plant (3.165) may be restated as

$$\begin{aligned} \dot{\boldsymbol{x}}_P(t) &= \boldsymbol{A}_M \boldsymbol{x}_P(t) + \boldsymbol{B}_P \cdot \boldsymbol{v}_P(t), \\ \boldsymbol{v}_P(s) &\triangleq \boldsymbol{\Lambda}\boldsymbol{u}(s) + \boldsymbol{\Theta}^*_{m,x}\boldsymbol{x}_P(s) + \boldsymbol{\Theta}^*_{m,\phi}\boldsymbol{\phi}_P(s), \end{aligned} \tag{3.191}$$

where $\boldsymbol{\phi}_P(s)$ denotes the Laplace transform of $\boldsymbol{\phi}(\boldsymbol{x}_P(t))$, i.e. $\boldsymbol{\phi}_P(s) = \mathcal{L}\{\boldsymbol{\phi}(\boldsymbol{x}_P(t))\}$. Here, the index $(\cdot)_P$ is used to indicate that the Laplace transform $\boldsymbol{\phi}_P(s)$ depends on the state $\boldsymbol{x}_P(t)$. The control law (3.176) may be rewritten as

$$\begin{aligned} \boldsymbol{u}(s) = \boldsymbol{K}\boldsymbol{D}(s)\Big(\boldsymbol{K}_r\boldsymbol{r}(s) - \boldsymbol{\Lambda}\boldsymbol{u}(s) - \boldsymbol{\Theta}^*_{m,x}\boldsymbol{x}_P(s) - \boldsymbol{\Theta}^*_{m,\phi}\boldsymbol{\phi}_P(s)\Big) \\ - \boldsymbol{K}\boldsymbol{D}(s)\mathcal{L}\Big\{\tilde{\boldsymbol{\Theta}}_m(t)\,\boldsymbol{\omega}(\boldsymbol{x}_P(t), t)\Big\} \end{aligned} \tag{3.192}$$

using $\hat{\boldsymbol{\Theta}}_m(t) = \boldsymbol{\Theta}^*_m + \tilde{\boldsymbol{\Theta}}_m(t)$. Applying the same steps to (3.192), which led from the ideal control law (3.169) to its alternative representation (3.174), yields

$$\begin{aligned} \boldsymbol{\Lambda}\boldsymbol{u}(s) = \boldsymbol{C}(s)\Big(\boldsymbol{K}_r\boldsymbol{r}(s) - \boldsymbol{\Theta}^*_{m,x}\boldsymbol{x}_P(s) - \boldsymbol{\Theta}^*_{m,\phi}\boldsymbol{\phi}_P(s)\Big) \\ - \boldsymbol{C}(s)\mathcal{L}\Big\{\tilde{\boldsymbol{\Theta}}_m(t)\,\boldsymbol{\omega}(\boldsymbol{x}_P(t), t)\Big\}. \end{aligned} \tag{3.193}$$

Inserting the control law representation (3.193) into (3.191) leads to the closed-loop system

$$\begin{aligned} \dot{\boldsymbol{x}}_P(t) &= \boldsymbol{A}_M\boldsymbol{x}_P(t) + \boldsymbol{B}_P \cdot \boldsymbol{v}_P(t), \\ \boldsymbol{v}_P(s) &= \boldsymbol{C}(s)\boldsymbol{K}_r\boldsymbol{r}(s) + (\boldsymbol{I} - \boldsymbol{C}(s)) \cdot \Big(\boldsymbol{\Theta}^*_{m,x}\boldsymbol{x}_P(s) + \boldsymbol{\Theta}^*_{m,\phi}\boldsymbol{\phi}_P(s)\Big) \\ &\quad - \boldsymbol{C}(s) \cdot \mathcal{L}\Big\{\tilde{\boldsymbol{\Theta}}_m(t)\,\boldsymbol{\omega}(\boldsymbol{x}_P(t), t)\Big\}. \end{aligned} \tag{3.194}$$

It follows from (3.181) and (3.194) that the error $\boldsymbol{e}_{\text{ref}}(t)$ evolves according to

$$\begin{aligned} \dot{\boldsymbol{e}}_{\text{ref}}(t) = \dot{\boldsymbol{x}}_P(t) - \dot{\boldsymbol{x}}_{\text{ref}}(t) = \boldsymbol{A}_M\boldsymbol{e}_{\text{ref}}(t) + \boldsymbol{B}_P(\boldsymbol{v}_P(t) - \boldsymbol{v}_{\text{ref}}(t)) \\ \boldsymbol{v}_P(s) - \boldsymbol{v}_{\text{ref}}(s) = (\boldsymbol{I} - \boldsymbol{C}(s)) \cdot \Big(\boldsymbol{\Theta}^*_{m,x}\boldsymbol{e}_{\text{ref}}(s) + \boldsymbol{\Theta}^*_{m,\phi}(\boldsymbol{\phi}_P(s) - \boldsymbol{\phi}_{\text{ref}}(s))\Big) \\ - \boldsymbol{C}(s) \cdot \mathcal{L}\Big\{\tilde{\boldsymbol{\Theta}}_m(t)\,\boldsymbol{\omega}(\boldsymbol{x}_P(t), t)\Big\}. \end{aligned} \tag{3.195}$$

Assuming zero initial conditions and using the definition of $\boldsymbol{G}_m(s)$ in (3.182), the error dynamics (3.195) may be represented in the frequency-domain as:

$$\begin{aligned} \boldsymbol{e}_{\text{ref}}(s) = \boldsymbol{G}_m(s)(\boldsymbol{I} - \boldsymbol{C}(s)) \cdot \Big(\boldsymbol{\Theta}^*_{m,x}\boldsymbol{e}_{\text{ref}}(s) + \boldsymbol{\Theta}^*_{m,\phi}(\boldsymbol{\phi}_P(s) - \boldsymbol{\phi}_{\text{ref}}(s))\Big) \\ - \boldsymbol{G}_m(s)\boldsymbol{C}(s) \cdot \mathcal{L}\Big\{\tilde{\boldsymbol{\Theta}}_m(t)\,\boldsymbol{\omega}(\boldsymbol{x}_P(t), t)\Big\}. \end{aligned} \tag{3.196}$$

Since $\boldsymbol{B}_P$ has full rank due to Assumption 3.6, Lemma D.1 admits to replace $\boldsymbol{C}(s) \cdot \mathcal{L}\Big\{\tilde{\boldsymbol{\Theta}}_m(t)\,\boldsymbol{\omega}(\boldsymbol{x}_P(t), t)\Big\}$ by $\boldsymbol{C}_{e_P}(s) \cdot \boldsymbol{e}_P(s)$, where $\boldsymbol{C}_{e_P}(s)$ is a stable and proper filter, if $\boldsymbol{C}(s)$ is Hurwitz. This leads to:

$$\begin{aligned} \boldsymbol{e}_{\text{ref}}(s) = \boldsymbol{G}_m(s)(\boldsymbol{I} - \boldsymbol{C}(s)) \cdot \Big(\boldsymbol{\Theta}^*_{m,x}\boldsymbol{e}_{\text{ref}}(s) + \boldsymbol{\Theta}^*_{m,\phi}(\boldsymbol{\phi}_P(s) - \boldsymbol{\phi}_{\text{ref}}(s))\Big) \\ - \boldsymbol{G}_m(s)\boldsymbol{C}_{e_P}(s) \cdot \boldsymbol{e}_P(s). \end{aligned} \tag{3.197}$$

If $\boldsymbol{C}(s)$ is Hurwitz for all $\boldsymbol{\Lambda} \in \Omega_\Lambda$, which implies that $\|\boldsymbol{C}(s)\|_{\mathcal{L}_1}$ and $\|\boldsymbol{C}_{e_P}(s)\|_{\mathcal{L}_1}$ exist, then the following inequality immediately results from the frequency-domain representation (3.197):

$$\begin{aligned}\|\boldsymbol{e}_{\text{ref}}(t)_\tau\|_{\mathcal{L}_\infty} \leq{}& \|\boldsymbol{G}_m(s)\,\boldsymbol{C}_{e_P}(s)\|_{\mathcal{L}_1} \cdot \|\boldsymbol{e}_P(t)\|_{\mathcal{L}_\infty} \\ &+ \|\boldsymbol{G}_m(s)\,(\boldsymbol{I}-\boldsymbol{C}(s))\,\boldsymbol{\Theta}^*_{m,x}\|_{\mathcal{L}_1} \cdot \|\boldsymbol{e}_{\text{ref}}(t)_\tau\|_{\mathcal{L}_\infty} \\ &+ \|\boldsymbol{G}_m(s)\,(\boldsymbol{I}-\boldsymbol{C}(s))\,\boldsymbol{\Theta}^*_{m,\phi}\|_{\mathcal{L}_1} \cdot \|(\boldsymbol{\phi}(\boldsymbol{x}_P(t)) - \boldsymbol{\phi}(\boldsymbol{x}_{\text{ref}}(t)))_\tau\|_{\mathcal{L}_\infty}.\end{aligned} \tag{3.198}$$

Since $\boldsymbol{\phi}(\boldsymbol{x}_P(t))$ is globally Lipschitz, the Lipschitz condition (3.163) leads to:

$$\begin{aligned}\|\boldsymbol{e}_{\text{ref}}(t)_\tau\|_{\mathcal{L}_\infty} \leq{}& \|\boldsymbol{G}_m(s)\,\boldsymbol{C}_{e_P}(s)\|_{\mathcal{L}_1} \cdot \|\boldsymbol{e}_P(t)\|_{\mathcal{L}_\infty} \\ &+ \|\boldsymbol{G}_m(s)\,(\boldsymbol{I}-\boldsymbol{C}(s))\,\boldsymbol{\Theta}^*_{m,x}\|_{\mathcal{L}_1} \cdot \|\boldsymbol{e}_{\text{ref}}(t)_\tau\|_{\mathcal{L}_\infty} \\ &+ \|\boldsymbol{G}_m(s)\,(\boldsymbol{I}-\boldsymbol{C}(s))\,\boldsymbol{\Theta}^*_{m,\phi}\|_{\mathcal{L}_1} \cdot L \cdot \|\boldsymbol{e}_{\text{ref}}(t)_\tau\|_{\mathcal{L}_\infty}.\end{aligned} \tag{3.199}$$

Solving for $\|\boldsymbol{e}_{\text{ref}}(t)_\tau\|_{\mathcal{L}_\infty}$ yields

$$\|\boldsymbol{e}_{\text{ref}}(t)_\tau\|_{\mathcal{L}_\infty} \leq \gamma_1, \tag{3.200}$$

where

$$\gamma_1 \triangleq \frac{\|\boldsymbol{G}_m(s)\,\boldsymbol{C}_{e_P}(s)\|_{\mathcal{L}_1} \cdot \|\boldsymbol{e}_P(t)\|_{\mathcal{L}_\infty}}{1 - \|\boldsymbol{G}_m(s)\,(\boldsymbol{I}-\boldsymbol{C}(s))\,\boldsymbol{\Theta}^*_{m,x}\|_{\mathcal{L}_1} - \|\boldsymbol{G}_m(s)\,(\boldsymbol{I}-\boldsymbol{C}(s))\,\boldsymbol{\Theta}^*_{m,\phi}\|_{\mathcal{L}_1} \cdot L}. \tag{3.201}$$

If the $\mathcal{L}_1$-norm condition (3.189) is satisfied, then $\gamma_1 \geq 0$ holds and (3.200) yields an upper bound on $\|\boldsymbol{e}_{\text{ref}}(t)_\tau\|_{\mathcal{L}_\infty}$. Furthermore, since the bound holds uniformly for all τ,

$$\|\boldsymbol{e}_{\text{ref}}(t)\|_{\mathcal{L}_\infty} \leq \gamma_1 \tag{3.202}$$

holds as well. Since $\boldsymbol{e}_P(t)$ is bounded by virtue of Lemma 3.7, (3.202) establishes boundedness of $\boldsymbol{e}_{\text{ref}}(t)$. On top of that, it is even possible to derive an explicit bound for $\boldsymbol{e}_{\text{ref}}(t)$. Since zero initial conditions are assumed throughout this section, the explicit bound (3.88) for $\boldsymbol{e}_P(t)$ may be used. Denoting that upper bound by γ_0, (3.88) implies $\|\boldsymbol{e}_P(t)\|_{\mathcal{L}_\infty} \leq \gamma_0$. Hence, (3.202) becomes

$$\|\boldsymbol{e}_{\text{ref}}(t)\|_{\mathcal{L}_\infty} \leq \bar{\gamma}_1, \tag{3.203}$$

where

$$\begin{aligned}\bar{\gamma}_1 &= \frac{\|\boldsymbol{G}_m(s)\,\boldsymbol{C}_{e_P}(s)\|_{\mathcal{L}_1}}{1 - \|\boldsymbol{G}_m(s)\,(\boldsymbol{I}-\boldsymbol{C}(s))\,\boldsymbol{\Theta}^*_{m,x}\|_{\mathcal{L}_1} - \|\boldsymbol{G}_m(s)\,(\boldsymbol{I}-\boldsymbol{C}(s))\,\boldsymbol{\Theta}^*_{m,\phi}\|_{\mathcal{L}_1} \cdot L} \cdot \gamma_0, \\ \gamma_0 &\triangleq \frac{\Theta^*_{\max}}{\sqrt{\lambda_{\min}(\boldsymbol{P}) \cdot \lambda_{\min}(\boldsymbol{\Gamma})}}.\end{aligned} \tag{3.204}$$

Eqs. (3.203) and (3.204) admit to conclude that the error $\boldsymbol{e}_{\text{ref}}(t)$ may be decreased arbitrarily (even in transients) by increasing the learning rate $\boldsymbol{\Gamma}$. Due to the presence of a filter in the control law (3.176), large learning rates $\boldsymbol{\Gamma}$ will not cause overly strong oscillations of the closed-loop response, if the bandwidth of the filter is sufficiently low. The preceding derivation is summarized in the following lemma:

Lemma 3.23 (Boundedness of the error $\boldsymbol{e}_{\text{ref}}(t) = \boldsymbol{x}_P(t) - \boldsymbol{x}_{\text{ref}}(t)$)**.** *Let Assumption 3.6 (full-rank $\boldsymbol{B}_P$) and the conditions of Lemma 3.7 and Lemma 3.20 hold. Then, the error $\boldsymbol{e}_{ref}(t) = \boldsymbol{x}_P(t) - \boldsymbol{x}_{ref}(t)$ between the plant* (3.165) *and the $\mathcal{L}_1$ Reference Model* (3.175) *is bounded, assuming $\boldsymbol{e}_{ref}(0) = \boldsymbol{0}$. If $\boldsymbol{e}_P(0) = \boldsymbol{0}$ holds as well, then an explicit bound on the error $\boldsymbol{e}_{ref}(t)$ is given by* (3.203) *and* (3.204)*, which shows that the error $\boldsymbol{e}_{ref}(t)$ may be arbitrarily decreased by increasing the learning rate $\boldsymbol{\Gamma}$.*

Proof. The proof essentially repeats the derivation of *Step 2*, which has led from the error dynamics (3.195) to the norm inequality (3.203). Since the $\mathcal{L}_1$-norm condition is satisfied due to Lemma 3.20 and since the prediction error is bounded due to Lemma 3.7, boundedness of the error $\boldsymbol{e}_{\text{ref}}(t)$ follows from (3.203). □

Step 3: Since the $\mathcal{L}_1$ *Reference Model* $\boldsymbol{x}_{\text{ref}}(t)$ is bounded by virtue of Lemma 3.20 and the error $\boldsymbol{e}_{\text{ref}}(t) = \boldsymbol{x}_P(t) - \boldsymbol{x}_{\text{ref}}(t)$ is bounded by virtue of Lemma 3.23, the plant state $\boldsymbol{x}_P(t)$ is bounded as well. As the prediction error $\boldsymbol{e}_P(t)$ is bounded due to Lemma 3.7, the predictor state $\hat{\boldsymbol{x}}_P(t)$ is also bounded. Finally, notice that due to Lemma D.1, the control law (3.193) may be rewritten as

$$\boldsymbol{\Lambda}\boldsymbol{u}(s) = \boldsymbol{C}(s)\left(\boldsymbol{K}_r\boldsymbol{r}(s) - \boldsymbol{\Theta}^*_{m,x}\boldsymbol{x}_P(s) - \boldsymbol{\Theta}^*_{m,\phi}\boldsymbol{\phi}_P(s)\right) - \boldsymbol{C}_{e_P}(s)\cdot\boldsymbol{e}_P(s), \tag{3.205}$$

where $\boldsymbol{C}_{e_P}(s)$ is stable and proper, if $\boldsymbol{C}(s)$ is Hurwitz. Since $\boldsymbol{x}_P(t)$, $\boldsymbol{r}(t)$ and $\boldsymbol{e}_P(t)$ are bounded, one may hence conclude that the control signal $\boldsymbol{u}(t)$ is bounded as well. Hence, all closed-loop signals are bounded, leading to the following theorem:

Theorem 3.24 (Nominal Stability of $\mathcal{L}_1$ Adaptive Control with Integral Update Law)**.** *Consider the plant* (3.1) *and let Assumptions 3.1 (state feedback), 3.2 (positive definite control effectiveness), 3.3 (Lipschitz condition), 3.5 (matching condition), 3.6 (full-rank $\boldsymbol{B}_P$), 3.7 (linear parametrization), 3.8 (exact parametrization), 3.10 (bounded uncertainties) hold. If the design parameters $\boldsymbol{\Gamma}$, $\boldsymbol{Q}$, $\boldsymbol{K}$ and $\boldsymbol{D}(s)$ of the $\mathcal{L}_1$ Adaptive Controller*

$$\begin{aligned}
\dot{\hat{\boldsymbol{x}}}_P(t) &= \boldsymbol{A}_M\hat{\boldsymbol{x}}_P(t) + \boldsymbol{B}_P\left(\hat{\boldsymbol{\Lambda}}(t)\,\boldsymbol{u}(t) + \hat{\boldsymbol{\Theta}}_{m,x}(t)\,\boldsymbol{x}_P(t) + \hat{\boldsymbol{\Theta}}_{m,\phi}(t)\cdot\boldsymbol{\phi}(\boldsymbol{x}_P(t))\right),\\
\dot{\hat{\boldsymbol{\Theta}}}_m(t)^T &= -\boldsymbol{\Gamma}\boldsymbol{\omega}(\boldsymbol{x}_P(t), t)\cdot\boldsymbol{e}_P(t)^T\boldsymbol{P}\boldsymbol{B}_P,\\
\boldsymbol{u}(s) &= \boldsymbol{K}\boldsymbol{D}(s)\left(\boldsymbol{K}_r\boldsymbol{r}(s) - \mathcal{L}\left\{\hat{\boldsymbol{\Lambda}}(t)\,\boldsymbol{u}(t) + \hat{\boldsymbol{\Theta}}_{m,x}(t)\,\boldsymbol{x}_P(t) + \hat{\boldsymbol{\Theta}}_{m,\phi}(t)\,\boldsymbol{\phi}(\boldsymbol{x}_P(t))\right\}\right)
\end{aligned}$$

and the initial conditions are chosen to satisfy the conditions of Lemma 3.7, Lemma 3.20 and Lemma 3.23, then all closed-loop signals are bounded. Furthermore, the states of the plant will track the $\mathcal{L}_1$ Reference Model (3.175)*, which by itself approximately tracks the reference model* (3.4)*. The error between the plant and the $\mathcal{L}_1$ Reference Model and the error between the $\mathcal{L}_1$ Reference Model and the reference model* (3.4) *can be arbitrarily decreased.*

Proof. See the derivation of *Step 3*. □

The overall structure of $\mathcal{L}_1$-AC with Integral Update Law is shown in Figure 3.10. The following example demonstrates its application:

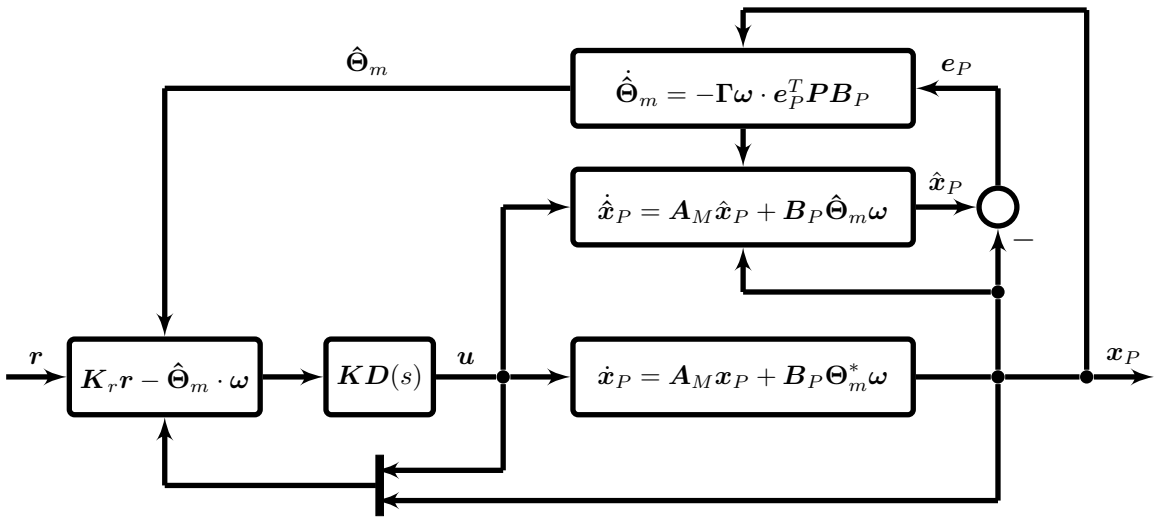

Figure 3.10: Illustration of $\mathcal{L}_1$-AC with Integral Update Law.

Example 3.25. *Consider the same short-period approximation and the same reference model as in Example 3.6. Since direct MRAC and $\mathcal{L}_1$-AC essentially suppose the same assumptions, whose satisfaction has been shown in Example 3.6, all assumptions of Theorem 3.24 are satisfied. Since there are no nonlinearities, the regressor vector, the adaptive parameter $\hat{\boldsymbol{\Theta}}_m(t)$ and the true parameter $\boldsymbol{\Theta}_m^*$ simplify to*

$$\boldsymbol{\omega}(\boldsymbol{x}_P(t), t)^T = \begin{bmatrix} \boldsymbol{x}_P(t)^T & u(t) \end{bmatrix} = \begin{bmatrix} \alpha(t) & q(t) & \eta(t) \end{bmatrix}, \tag{3.206}$$

$$\hat{\boldsymbol{\Theta}}_m(t) = \begin{bmatrix} \hat{\boldsymbol{\Theta}}_{m,x}(t) & \hat{\Lambda}(t) \end{bmatrix} = \begin{bmatrix} \hat{\Theta}_{m,\alpha}(t) & \hat{\Theta}_{m,q}(t) & \hat{\Lambda}(t) \end{bmatrix}, \tag{3.207}$$

$$\boldsymbol{\Theta}_m^* = \begin{bmatrix} \boldsymbol{\Theta}_{m,x}^* & \Lambda \end{bmatrix} = \begin{bmatrix} \Theta_{m,\alpha}^* & \Theta_{m,q}^* & \Lambda \end{bmatrix}. \tag{3.208}$$

Using the matching condition (3.10)*, the value of the true parameter $\boldsymbol{\Theta}_m^*$ may be computed as:*

$$\Theta_{m,\alpha}^* = \frac{M_\alpha \cdot \lambda_\alpha - M_{\alpha,des}}{M_\eta}, \qquad \Theta_{m,q}^* = \frac{M_q \cdot \lambda_q - M_{q,des}}{M_\eta}, \qquad \Lambda = \lambda_\eta. \tag{3.209}$$

The design parameters $\boldsymbol{Q}$ and $\boldsymbol{\Gamma}$ of the adaptive state predictor are chosen as

$$\boldsymbol{Q} = \boldsymbol{I}^{2\times 2}, \qquad \boldsymbol{\Gamma} = 100 \cdot \boldsymbol{I}^{3\times 3}. \tag{3.210}$$

Thus, the conditions of Lemma 3.7 are satisfied and the prediction error dynamics are globally stable. The design parameters of the filter are chosen as

$$D(s) = \frac{1}{s}, \qquad K > 0. \tag{3.211}$$

In case of $\lambda_\alpha = \lambda_q = 1$ and $\lambda_\eta = 0.5$, the true uncertainties evaluate to

$$\Theta_{m,\alpha}^* = 1.11, \qquad \Theta_{m,q}^* = 0.22, \qquad \Lambda = 0.5. \tag{3.212}$$

For these uncertainties, the $\mathcal{L}_1$-norm condition (3.189) *is satisfied for $K \gtrsim 100$.*

Figure 3.11 compares the performance of the $\mathcal{L}_1$-AC for different bandwidths K of the low-pass filter. For a high filter bandwidth $K = 100$, the response of the $\mathcal{L}_1$-AC shows significant oscillations in the pitch rate $q(t)$ as well as the elevator deflection $\eta(t)$. By decreasing the filter bandwidth K, these oscillations may be successfully suppressed. As compared to the direct MRAC of Example 3.6, the response of the $\mathcal{L}_1$-AC is clearly less oscillatory for low filter bandwidths K. This comes at the expense that the $\mathcal{L}_1$-AC never exactly recovers the performance of the reference model (3.4)*. Hence, the $\mathcal{L}_1$-AC never exactly satisfies the performance requirements that are embedded in the reference model.*

Part Two: Semi-Global Lipschitz condition

So far, stability of $\mathcal{L}_1$-AC was established, if the Lipschitz condition of Assumption 3.3 was strengthened from a semi-global to a global condition. Now, this additional restriction is dropped. By alleviating the assumption of a global Lipschitz condition, many more regressor vectors $\boldsymbol{\phi}(\boldsymbol{x}_P(t))$ are admissible, such as regressor vectors involving higher order polynomials. Fortunately, the change of the Lipschitz condition does not alter the structure of the $\mathcal{L}_1$-AC itself, but only requires a different proof of stability. Thus, the $\mathcal{L}_1$-AC and the $\mathcal{L}_1$ *Reference Model* are still given by Eqs. (3.166), (3.176) and Eq. (3.175), respectively. In Part 1, the proof of stability consisted of three steps. While the proof of stability in case of a semi-global Lipschitz condition does still involve three steps, the semi-global character requires to change several aspects of these steps. Subsequently, these differences will be highlighted.

Since the Lipschitz condition of Assumption 3.3 considers the nonlinear function $\boldsymbol{f}(\boldsymbol{x}_P(t), t)$, it needs to be translated into a Lipschitz condition on the regressor vector. To that end, notice that the regressor vector $\boldsymbol{\phi}(\boldsymbol{x}_P(t))$ is subject to the following semi-global Lipschitz condition as the nonlinearity $\boldsymbol{f}(\boldsymbol{x}_P(t), t)$ admits an exact linear parametrization due to Assumptions 3.7 and 3.8:

$$\|\phi(\boldsymbol{x}_1) - \phi(\boldsymbol{x}_2)\|_\infty \leq L(r) \cdot \|\boldsymbol{x}_1 - \boldsymbol{x}_2\|_\infty \quad \forall \|\boldsymbol{x}_1\|_\infty \leq r,\ \|\boldsymbol{x}_2\|_\infty \leq r. \tag{3.213}$$

In (3.213), $L : \mathbb{R}_+ \to \mathbb{R}_+$ denotes is the state-dependent Lipschitz constant, which is known because the function $\phi(\boldsymbol{x})$ is known. Using the reverse triangle inequality, (3.213) especially yields a bound on the size of the nonlinearity, which depends linearly on $\|\boldsymbol{x}\|_\infty$, namely:

$$\|\phi(\boldsymbol{x})\|_\infty \leq L(r) \cdot \|\boldsymbol{x}\|_\infty + \phi_0 \quad \forall \|\boldsymbol{x}\|_\infty \leq r, \tag{3.214}$$

where $\phi_0 \geq \|\phi(\boldsymbol{0})\|_\infty$ with $\phi_0 < \infty$ is a known constant.

Step 1: In this step, stability of the $\mathcal{L}_1$ *Reference Model* is proven. Exactly as in Part 1, one may derive the following norm inequality from the definition of the $\mathcal{L}_1$ *Reference Model* in (3.175):

$$\|\boldsymbol{x}_{\text{ref}}(t)_\tau\|_{\mathcal{L}_\infty} \leq \|\boldsymbol{G}_m(s)\boldsymbol{C}(s)\boldsymbol{K}_r\|_{\mathcal{L}_1} \cdot \|\boldsymbol{r}(t)\|_{\mathcal{L}_\infty}$$

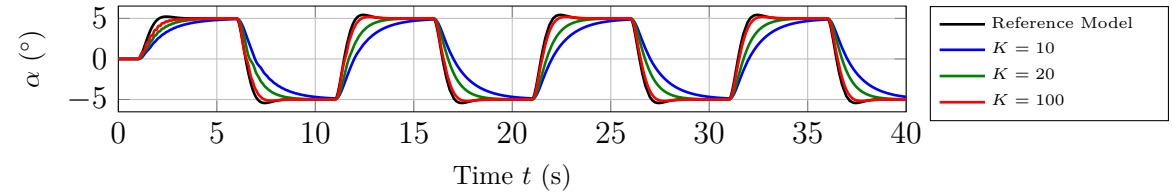

(a) Angle-Of-Attack α

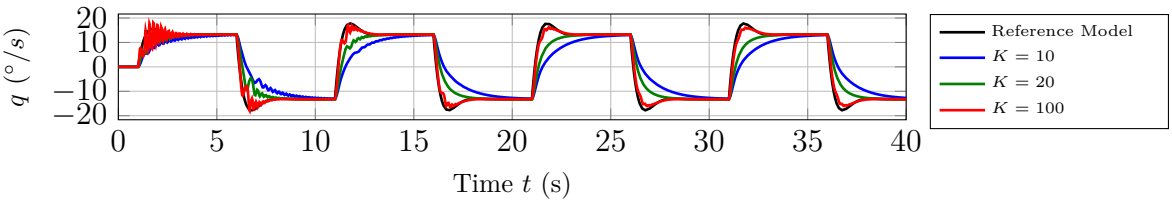

(b) Pitch Rate q

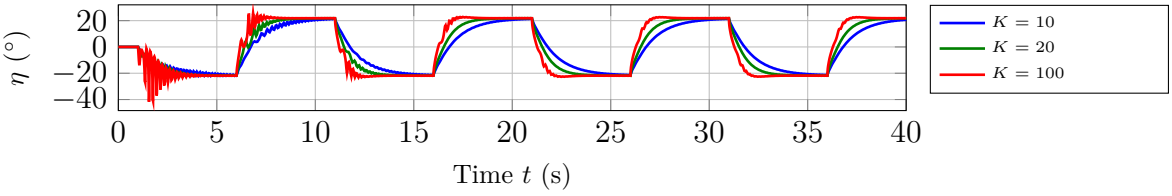

(c) Elevator Deflection η

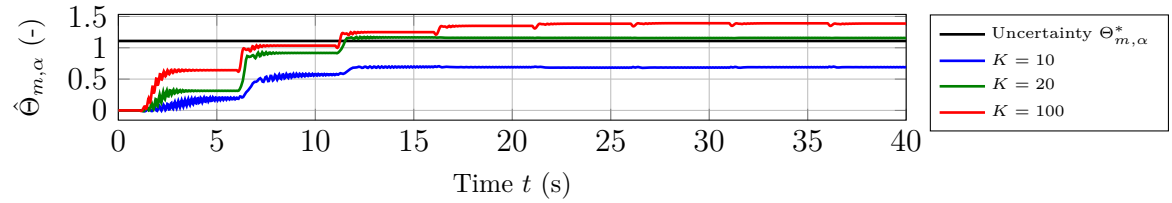

(d) Adaptive Parameter $\hat{\Theta}_{m,\alpha}$

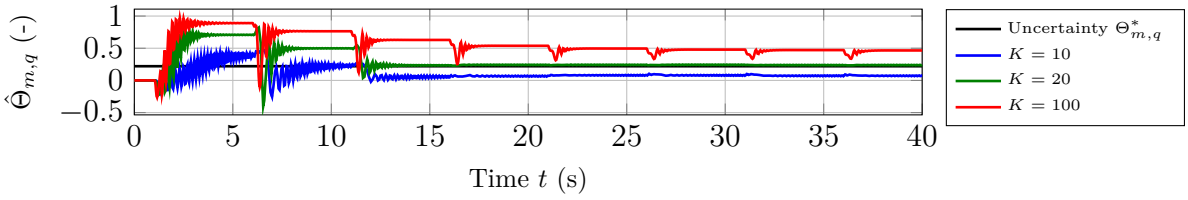

(e) Adaptive Parameter $\hat{\Theta}_{m,q}$

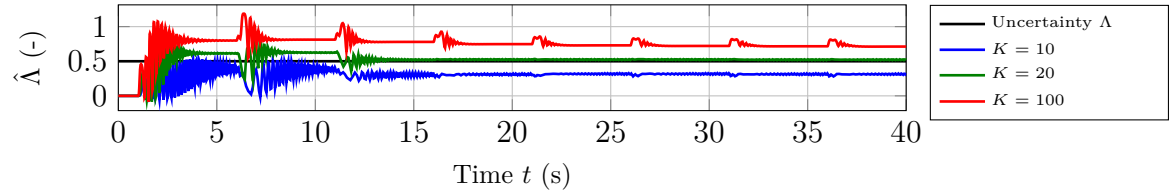

(f) Adaptive Parameter $\hat{\Lambda}$

Figure 3.11: Performance of a $\mathcal{L}_1$-AC with Integral Update Law for different values of the filter bandwidth K for a $5°$ square wave command in case of $\lambda_\alpha = \lambda_q = 1$ and $\lambda_\eta = 0.5$.

$$+ \|\boldsymbol{G}_m(s)\left(\boldsymbol{I} - \boldsymbol{C}(s)\right)\boldsymbol{\Theta}^*_{m,x}\|_{\mathcal{L}_1} \cdot \|\boldsymbol{x}_{\text{ref}}(t)_\tau\|_{\mathcal{L}_\infty}$$
$$+ \|\boldsymbol{G}_m(s)\left(\boldsymbol{I} - \boldsymbol{C}(s)\right)\boldsymbol{\Theta}^*_{m,\phi}\|_{\mathcal{L}_1} \cdot \|\boldsymbol{\phi}\left(\boldsymbol{x}_{\text{ref}}(t)\right)_\tau\|_{\mathcal{L}_\infty},$$

which is equivalent to (3.185). Notice that truncated norms are used since boundedness of $\boldsymbol{x}_{\text{ref}}(t)$ is not yet ensured. Due to the semi-global character of the Lipschitz condition, applying (3.214) yields a conditional bound:

$$\begin{aligned}\|\boldsymbol{x}_{\text{ref}}(t)_\tau\|_{\mathcal{L}_\infty} \leq\ & \|\boldsymbol{G}_m(s)\boldsymbol{C}(s)\boldsymbol{K}_r\|_{\mathcal{L}_1} \cdot \|\boldsymbol{r}(t)\|_{\mathcal{L}_\infty} \\ & + \|\boldsymbol{G}_m(s)\left(\boldsymbol{I} - \boldsymbol{C}(s)\right)\boldsymbol{\Theta}^*_{m,x}\|_{\mathcal{L}_1} \cdot \|\boldsymbol{x}_{\text{ref}}(t)_\tau\|_{\mathcal{L}_\infty} \\ & + \|\boldsymbol{G}_m(s)\left(\boldsymbol{I} - \boldsymbol{C}(s)\right)\boldsymbol{\Theta}^*_{m,\phi}\|_{\mathcal{L}_1} \cdot \left(L(r) \cdot \|\boldsymbol{x}_{\text{ref}}(t)_\tau\|_{\mathcal{L}_\infty} + \phi_0\right),\end{aligned} \tag{3.215}$$

which is *only* true if $\|\boldsymbol{x}_{\text{ref}}(t)_\tau\|_{\mathcal{L}_\infty} \leq r$ is satisfied. However, (3.215) does not ensure that $\|\boldsymbol{x}_{\text{ref}}(t)_\tau\|_\infty \leq r$ does actually hold. In order to deal with this circular dependence, assume that $\|\boldsymbol{x}_{\text{ref}}(t)_\tau\|_{\mathcal{L}_\infty} < \rho_r$ holds, where $\rho_r > 0$ specifies the hypercube in the state space, within which all trajectories of $\boldsymbol{x}_{\text{ref}}(t)$ will remain during the interval $t = [0, \tau]$. In this case, (3.215) becomes

$$\begin{aligned}\|\boldsymbol{x}_{\text{ref}}(t)_\tau\|_{\mathcal{L}_\infty} <\ & \|\boldsymbol{G}_m(s)\boldsymbol{C}(s)\boldsymbol{K}_r\|_{\mathcal{L}_1} \cdot \|\boldsymbol{r}(t)\|_{\mathcal{L}_\infty} \\ & + \|\boldsymbol{G}_m(s)\left(\boldsymbol{I} - \boldsymbol{C}(s)\right)\boldsymbol{\Theta}^*_{m,x}\|_{\mathcal{L}_1} \cdot \rho_r \\ & + \|\boldsymbol{G}_m(s)\left(\boldsymbol{I} - \boldsymbol{C}(s)\right)\boldsymbol{\Theta}^*_{m,\phi}\|_{\mathcal{L}_1} \cdot \left(L\left(\rho_r + \bar{\gamma}_1\right) \cdot \rho_r + \phi_0\right).\end{aligned} \tag{3.216}$$

In (3.216), the state-dependent Lipschitz constant is chosen larger than actually required (in this step) due to the constant $\bar{\gamma}_1 > 0$. The meaning of the constant $\bar{\gamma}_1$ will be clarified later during Step 2. In order to ensure that the assumption $\|\boldsymbol{x}_{\text{ref}}(t)_\tau\|_{\mathcal{L}_\infty} < \rho_r$ holds, the right hand side of (3.216) is required to satisfy

$$\begin{aligned}& \|\boldsymbol{G}_m(s)\boldsymbol{C}(s)\boldsymbol{K}_r\|_{\mathcal{L}_1} \cdot \|\boldsymbol{r}(t)\|_{\mathcal{L}_\infty} \\ & + \|\boldsymbol{G}_m(s)\left(\boldsymbol{I} - \boldsymbol{C}(s)\right)\boldsymbol{\Theta}^*_{m,x}\|_{\mathcal{L}_1} \cdot \rho_r \\ & + \|\boldsymbol{G}_m(s)\left(\boldsymbol{I} - \boldsymbol{C}(s)\right)\boldsymbol{\Theta}^*_{m,\phi}\|_{\mathcal{L}_1} \cdot \left(L\left(\rho_r + \bar{\gamma}_1\right) \cdot \rho_r + \phi_0\right) < \rho_r.\end{aligned} \tag{3.217}$$

Bringing the first term to the right hand side of the inequality yields

$$\begin{aligned}& \|\boldsymbol{G}_m(s)\left(\boldsymbol{I} - \boldsymbol{C}(s)\right)\boldsymbol{\Theta}^*_{m,x}\|_{\mathcal{L}_1} \cdot \rho_r \\ & + \|\boldsymbol{G}_m(s)\left(\boldsymbol{I} - \boldsymbol{C}(s)\right)\boldsymbol{\Theta}^*_{m,\phi}\|_{\mathcal{L}_1} \cdot \left(L\left(\rho_r + \bar{\gamma}_1\right) \cdot \rho_r + \phi_0\right) \\ & < \rho_r - \|\boldsymbol{G}_m(s)\boldsymbol{C}(s)\boldsymbol{K}_r\|_{\mathcal{L}_1} \cdot \|\boldsymbol{r}(t)\|_{\mathcal{L}_\infty}.\end{aligned} \tag{3.218}$$

Since the inequality (3.218) has been derived under the assumption that $\|\boldsymbol{x}_{\text{ref}}(t)_\tau\|_{\mathcal{L}_\infty} < \rho_r$ holds, its satisfaction does obviously not yet prove $\|\boldsymbol{x}_{\text{ref}}(t)_\tau\|_{\mathcal{L}_\infty} < \rho_r$, as this would be a circular argument. However, the latter implication can be proven to be true by virtue of a proof by contradiction as shown in the following lemma:

Lemma 3.26 (Boundedness of the $\mathcal{L}_1$ *Reference Model*)**.** *Let Assumptions 3.3 (Lipschitz condition) and 3.10 (bounded uncertainties) hold. Consider the $\mathcal{L}_1$ Reference Model*

$$\dot{\boldsymbol{x}}_{ref}(t) = \boldsymbol{A}_M \boldsymbol{x}_{ref}(t) + \boldsymbol{B}_P\left(\boldsymbol{\Lambda}\boldsymbol{u}_{ref}(t) + \boldsymbol{\Theta}^*_{m,x}\boldsymbol{x}_{ref}(t) + \boldsymbol{\Theta}^*_{m,\phi} \cdot \boldsymbol{\phi}\left(\boldsymbol{x}_{ref}(t)\right)\right),$$

$$\boldsymbol{u}_{ref}(s) = \boldsymbol{\Lambda}^{-1}\boldsymbol{C}(s)\left(\boldsymbol{K}_r\boldsymbol{r}(s) - \boldsymbol{\Theta}^*_{m,x}\boldsymbol{x}_{ref}(s) - \boldsymbol{\Theta}^*_{m,\phi}\boldsymbol{\phi}_{ref}(s)\right),$$

originally given in (3.175)*, and the filter from* (3.173)*, i.e.:*

$$\boldsymbol{C}(s) \triangleq (\boldsymbol{I} + \boldsymbol{\Lambda}\boldsymbol{K}\boldsymbol{D}(s))^{-1}\boldsymbol{\Lambda}\boldsymbol{K}\boldsymbol{D}(s),$$

where $\boldsymbol{K} \in \mathbb{R}^{m\times m}$ is a feedback gain and $\boldsymbol{D} : \mathbb{C} \to \mathbb{C}^{m\times m}$ is a strictly proper transfer function matrix containing an integrator. If the design parameters $\boldsymbol{K}$ and $\boldsymbol{D}(s)$ are chosen such that

1. *the filter $\boldsymbol{C}(s)$ is Hurwitz for all $\boldsymbol{\Lambda} \in \Omega_\Lambda$;*
2. *the $\mathcal{L}_1$-norm condition* (3.218) *is satisfied for some values of the design parameters $\rho_r > 0$, $\bar{\gamma}_1 > 0$ and for all $\boldsymbol{\Lambda} \in \Omega_\Lambda$, $\boldsymbol{\Theta}^*_{m,x} \in \Omega_{x,m}$, $\boldsymbol{\Theta}^*_{m,\phi} \in \Omega_{\phi,m}$, i.e.*

$$\begin{aligned}
&\|\boldsymbol{G}_m(s)\left(\boldsymbol{I} - \boldsymbol{C}(s)\right)\boldsymbol{\Theta}^*_{m,x}\|_{\mathcal{L}_1} \cdot \rho_r \\
&+ \|\boldsymbol{G}_m(s)\left(\boldsymbol{I} - \boldsymbol{C}(s)\right)\boldsymbol{\Theta}^*_{m,\phi}\|_{\mathcal{L}_1} \cdot \left(L\left(\rho_r + \bar{\gamma}_1\right)\cdot\rho_r + \phi_0\right) \\
&< \rho_r - \|\boldsymbol{G}_m(s)\boldsymbol{C}(s)\boldsymbol{K}_r\|_{\mathcal{L}_1} \cdot \|\boldsymbol{r}(t)\|_{\mathcal{L}_\infty}. \\
&\qquad \forall\ \boldsymbol{\Lambda} \in \Omega_\Lambda,\ \boldsymbol{\Theta}^*_{m,x} \in \Omega_{x,m},\ \boldsymbol{\Theta}^*_{m,\phi} \in \Omega_{\phi,m},
\end{aligned}$$

   where $\boldsymbol{G}_m(s) \triangleq (s\boldsymbol{I} - \boldsymbol{A}_M)^{-1}\boldsymbol{B}_P$,

then, for $\boldsymbol{x}_{ref}(0) = \boldsymbol{0}$, the $\mathcal{L}_1$ Reference Model is bounded and the bound is given by

$$\|\boldsymbol{x}_{ref}(t)\|_{\mathcal{L}_\infty} < \rho_r. \tag{3.219}$$

Proof. The proof of Lemma 3.26 is done by contradiction. To that end, assume that (3.219) was not true. In this case, due to $\boldsymbol{x}_{\text{ref}}(0) = \boldsymbol{0}$ and due to continuity, there must exist an interval $t \in [0, \tau]$ such that

$$\|\boldsymbol{x}_{\text{ref}}(t)\|_\infty < \rho_r \quad \forall\ t \in [0, \tau[\tag{3.220}$$

and

$$\|\boldsymbol{x}_{\text{ref}}(\tau)\|_\infty = \rho_r. \tag{3.221}$$

Hence, throughout the interval $[0, \tau]$,

$$\|\boldsymbol{x}_{\text{ref}}(t)_\tau\|_{\mathcal{L}_\infty} \leq \rho_r \tag{3.222}$$

holds. Due to (3.222) and Assumption 3.3 (Lipschitz condition), the norm inequality

$$\begin{aligned}
\|\boldsymbol{x}_{\text{ref}}(t)_\tau\|_{\mathcal{L}_\infty} \leq\ &\|\boldsymbol{G}_m(s)\boldsymbol{C}(s)\boldsymbol{K}_r\|_{\mathcal{L}_1} \cdot \|\boldsymbol{r}(t)\|_{\mathcal{L}_\infty} \\
&+ \|\boldsymbol{G}_m(s)\left(\boldsymbol{I} - \boldsymbol{C}(s)\right)\boldsymbol{\Theta}^*_{m,x}\|_{\mathcal{L}_1} \cdot \rho_r \\
&+ \|\boldsymbol{G}_m(s)\left(\boldsymbol{I} - \boldsymbol{C}(s)\right)\boldsymbol{\Theta}^*_{m,\phi}\|_{\mathcal{L}_1} \cdot \left(L(\rho_r)\cdot\rho_r + \phi_0\right)
\end{aligned} \tag{3.223}$$

follows from (3.215), where (3.215) only holds for $\boldsymbol{x}_{\text{ref}}(0) = \mathbf{0}$. By increasing the Lipschitz constant to $L(\rho_r + \bar{\gamma}_1) > L(\rho_r)$, one obtains the upper bound

$$\begin{aligned}\|\boldsymbol{x}_{\text{ref}}(t)_\tau\|_{\mathcal{L}_\infty} \leq\ & \|\boldsymbol{G}_m(s)\,\boldsymbol{C}(s)\boldsymbol{K}_r\|_{\mathcal{L}_1} \cdot \|\boldsymbol{r}(t)\|_{\mathcal{L}_\infty} \\ & + \|\boldsymbol{G}_m(s)\,(\boldsymbol{I} - \boldsymbol{C}(s))\,\boldsymbol{\Theta}^*_{m,x}\|_{\mathcal{L}_1} \cdot \rho_r \\ & + \|\boldsymbol{G}_m(s)\,(\boldsymbol{I} - \boldsymbol{C}(s))\,\boldsymbol{\Theta}^*_{m,\phi}\|_{\mathcal{L}_1} \cdot (L(\rho_r + \bar{\gamma}_1) \cdot \rho_r + \phi_0)\,.\end{aligned} \tag{3.224}$$

Since the $\mathcal{L}_1$-norm condition may be restated as (3.217), whose left hand side corresponds to the upper bound in (3.224), $\|\boldsymbol{x}_{\text{ref}}(t)_\tau\|_{\mathcal{L}_\infty} < \rho_r$ follows from (3.224). As the latter contradicts (3.221), no such instant of time τ can exist, at which (3.221) holds. Hence, the bound (3.219) is proven. □

Step 2: Within the second step, boundedness of the error $\boldsymbol{e}_{\text{ref}}(t)$ is proven. Exactly as in Part 1, one may derive the following norm inequality

$$\begin{aligned}\|\boldsymbol{e}_{\text{ref}}(t)_\tau\|_{\mathcal{L}_\infty} \leq\ & \|\boldsymbol{G}_m(s)\,\boldsymbol{C}_{e_P}(s)\|_{\mathcal{L}_1} \cdot \|\boldsymbol{e}_P(t)\|_{\mathcal{L}_\infty} \\ & + \|\boldsymbol{G}_m(s)\,(\boldsymbol{I} - \boldsymbol{C}(s))\,\boldsymbol{\Theta}^*_{m,x}\|_{\mathcal{L}_1} \cdot \|\boldsymbol{e}_{\text{ref}}(t)_\tau\|_{\mathcal{L}_\infty} \\ & + \|\boldsymbol{G}_m(s)\,(\boldsymbol{I} - \boldsymbol{C}(s))\,\boldsymbol{\Theta}^*_{m,\phi}\|_{\mathcal{L}_1} \cdot \|(\boldsymbol{\phi}(\boldsymbol{x}_P(t)) - \boldsymbol{\phi}(\boldsymbol{x}_{\text{ref}}(t)))_\tau\|_{\mathcal{L}_\infty},\end{aligned}$$

which is equivalent to (3.198) and holds in case of zero initial conditions. Due to the semi-global character of the Lipschitz condition, the application of (3.213) leads to the conditional bound

$$\begin{aligned}\|\boldsymbol{e}_{\text{ref}}(t)_\tau\|_{\mathcal{L}_\infty} \leq\ & \|\boldsymbol{G}_m(s)\,\boldsymbol{C}_{e_P}(s)\|_{\mathcal{L}_1} \cdot \|\boldsymbol{e}_P(t)\|_{\mathcal{L}_\infty} \\ & + \|\boldsymbol{G}_m(s)\,(\boldsymbol{I} - \boldsymbol{C}(s))\,\boldsymbol{\Theta}^*_{m,x}\|_{\mathcal{L}_1} \cdot \|\boldsymbol{e}_{\text{ref}}(t)_\tau\|_{\mathcal{L}_\infty} \\ & + \|\boldsymbol{G}_m(s)\,(\boldsymbol{I} - \boldsymbol{C}(s))\,\boldsymbol{\Theta}^*_{m,\phi}\|_{\mathcal{L}_1} \cdot L(r) \cdot \|\boldsymbol{e}_{\text{ref}}(t)_\tau\|_{\mathcal{L}_\infty},\end{aligned} \tag{3.225}$$

which *only* holds for $\|\boldsymbol{x}_P(t)_\tau\|_{\mathcal{L}_\infty} \leq r$ and $\|\boldsymbol{x}_{\text{ref}}(t)_\tau\|_{\mathcal{L}_\infty} \leq r$. However, as no bound is known for $\boldsymbol{x}_P(t)$, no suitable value for r is known either. In order to resolve this issue, assume that $\|\boldsymbol{e}_{\text{ref}}(t)_\tau\|_{\mathcal{L}_\infty} < \bar{\gamma}_1$ was known to hold, and let Lemma 3.26 be satisfied for that $\bar{\gamma}_1$. The satisfaction of Lemma 3.26 implies boundedness of $\boldsymbol{x}_{\text{ref}}(t)$ with the bound $\|\boldsymbol{x}_{\text{ref}}(t)_\tau\|_{\mathcal{L}_\infty} < \rho_r$. By virtue of the triangle inequality, one hence obtains a bound for $\boldsymbol{x}_P(t) = \boldsymbol{e}_P(t) + \boldsymbol{x}_{\text{ref}}(t)$:

$$\|\boldsymbol{x}_P(t)_\tau\|_{\mathcal{L}_\infty} \leq \|\boldsymbol{e}_{\text{ref}}(t)_\tau\|_{\mathcal{L}_\infty} + \|\boldsymbol{x}_{\text{ref}}(t)_\tau\|_{\mathcal{L}_\infty} < \bar{\gamma}_1 + \rho_r. \tag{3.226}$$

Hence, under the assumption $\|\boldsymbol{e}_{\text{ref}}(t)_\tau\|_{\mathcal{L}_\infty} < \bar{\gamma}_1$, a suitable Lipschitz constant may now be selected, which results for $r = \bar{\gamma}_1 + \rho_r$ and is defined as

$$L_{\rho_r} \triangleq L(\rho_r + \bar{\gamma}_1). \tag{3.227}$$

Hence, (3.225) becomes

$$\begin{aligned}\|\boldsymbol{e}_{\text{ref}}(t)_\tau\|_{\mathcal{L}_\infty} \leq\ & \|\boldsymbol{G}_m(s)\,\boldsymbol{C}_{e_P}(s)\|_{\mathcal{L}_1} \cdot \|\boldsymbol{e}_P(t)\|_{\mathcal{L}_\infty} \\ & + \|\boldsymbol{G}_m(s)\,(\boldsymbol{I} - \boldsymbol{C}(s))\,\boldsymbol{\Theta}^*_{m,x}\|_{\mathcal{L}_1} \cdot \|\boldsymbol{e}_{\text{ref}}(t)_\tau\|_{\mathcal{L}_\infty} \\ & + \|\boldsymbol{G}_m(s)\,(\boldsymbol{I} - \boldsymbol{C}(s))\,\boldsymbol{\Theta}^*_{m,\phi}\|_{\mathcal{L}_1} \cdot L_{\rho_r} \cdot \|\boldsymbol{e}_{\text{ref}}(t)_\tau\|_{\mathcal{L}_\infty},\end{aligned} \tag{3.228}$$

which holds for $\|\boldsymbol{x}_P(t)_\tau\|_{\mathcal{L}_\infty} < \rho_r + \bar{\gamma}_1$ and $\|\boldsymbol{x}_{\text{ref}}(t)_\tau\|_{\mathcal{L}_\infty} < \rho_r < \rho_r + \bar{\gamma}_1$. Solving for $\|\boldsymbol{e}_{\text{ref}}(t)_\tau\|_{\mathcal{L}_\infty}$ yields

$$\|\boldsymbol{e}_{\text{ref}}(t)_\tau\|_{\mathcal{L}_\infty} \leq \frac{\|\boldsymbol{G}_m(s)\boldsymbol{C}_{\boldsymbol{e}_P}(s)\|_{\mathcal{L}_1} \cdot \|\boldsymbol{e}_P(t)\|_{\mathcal{L}_\infty}}{1 - \|\boldsymbol{G}_m(s)(\boldsymbol{I} - \boldsymbol{C}(s))\boldsymbol{\Theta}^*_{m,x}\|_{\mathcal{L}_1} - \|\boldsymbol{G}_m(s)(\boldsymbol{I} - \boldsymbol{C}(s))\boldsymbol{\Theta}^*_{m,\phi}\|_{\mathcal{L}_1} \cdot L_{\rho_r}}. \tag{3.229}$$

In order to obtain an upper bound from (3.229), the denominator of the right hand side of (3.229) must be positive. To that end, notice that the $\mathcal{L}_1$-norm condition of Lemma 3.26 implies

$$\begin{aligned}
&\|\boldsymbol{G}_m(s)(\boldsymbol{I} - \boldsymbol{C}(s))\boldsymbol{\Theta}^*_{m,x}\|_{\mathcal{L}_1} + \|\boldsymbol{G}_m(s)(\boldsymbol{I} - \boldsymbol{C}(s))\boldsymbol{\Theta}^*_{m,\phi}\|_{\mathcal{L}_1} \cdot L(\rho_r + \bar{\gamma}_1) \\
&\quad < \frac{\rho_r - \|\boldsymbol{G}_m(s)\boldsymbol{C}(s)\boldsymbol{K}_r\|_{\mathcal{L}_1} \cdot \|\boldsymbol{r}(t)\|_{\mathcal{L}_\infty} - \|\boldsymbol{G}_m(s)(\boldsymbol{I} - \boldsymbol{C}(s))\boldsymbol{\Theta}^*_{m,\phi}\|_{\mathcal{L}_1} \cdot \phi_0}{\rho_r} \\
&\quad \leq \frac{\rho_r}{\rho_r} = 1.
\end{aligned}$$

Hence, (3.229) does actually yield a finite upper bound. This upper bound depends on the size of the prediction error $\boldsymbol{e}_P(t)$. In case of zero initial conditions, the explicit upper bound (3.88) for $\boldsymbol{e}_P(t)$ may be used. Denoting that upper bound by γ_0, (3.229) may be rewritten as

$$\|\boldsymbol{e}_{\text{ref}}(t)\|_{\mathcal{L}_\infty} \leq \gamma_1, \tag{3.230}$$

where

$$\gamma_1 \triangleq \frac{\|\boldsymbol{G}_m(s)\boldsymbol{C}_{\boldsymbol{e}_P}(s)\|_{\mathcal{L}_1} \cdot \gamma_0}{1 - \|\boldsymbol{G}_m(s)(\boldsymbol{I} - \boldsymbol{C}(s))\boldsymbol{\Theta}^*_{m,x}\|_{\mathcal{L}_1} - \|\boldsymbol{G}_m(s)(\boldsymbol{I} - \boldsymbol{C}(s))\boldsymbol{\Theta}^*_{m,\phi}\|_{\mathcal{L}_1} \cdot L_{\rho_r}}, \tag{3.231}$$

$$\gamma_0 \triangleq \frac{\Theta^*_{\max}}{\sqrt{\lambda_{\min}(\boldsymbol{P}) \cdot \lambda_{\min}(\boldsymbol{\Gamma})}}. \tag{3.232}$$

Notice that the bound γ_1 may be arbitrarily decreased by decreasing the bound γ_0, that is, by increasing the learning rate $\boldsymbol{\Gamma}$. Thus, the learning rate may also be chosen such that $\|\boldsymbol{e}_{\text{ref}}(t)_\tau\|_{\mathcal{L}_\infty}$ is slightly smaller than $\bar{\gamma}_1$, i.e. $\gamma_1 = \bar{\gamma}_1 - \beta$, where $\beta > 0$ is an arbitrary constant satisfying $\bar{\gamma}_1 - \beta > 0$. With this choice, the original assumption $\|\boldsymbol{e}_{\text{ref}}(t)_\tau\|_{\mathcal{L}_\infty} < \bar{\gamma}_1$, which still is not proven, is slightly strengthened. As shown in the next lemma, this strengthened condition allows to construct a contradiction in order to prove that $\|\boldsymbol{e}_{\text{ref}}(t)_\tau\|_{\mathcal{L}_\infty} < \bar{\gamma}_1$ holds uniformly for all τ.

Lemma 3.27 (Boundedness of the error $\boldsymbol{e}_{\text{ref}}(t) = \boldsymbol{x}_P(t) - \boldsymbol{x}_{\text{ref}}(t)$)**.** *Let Assumption 3.6 (full-rank $\boldsymbol{B}_P$) and Lemma 3.7 hold. If*

1. *the conditions of Lemma 3.26 hold for some $\bar{\gamma}_1 = \gamma_1 + \beta > 0$, where $\beta > 0$ is an arbitrary small design parameter;*
2. *the learning rate $\boldsymbol{\Gamma}$ is chosen such that*

$$\lambda_{\min}(\boldsymbol{\Gamma}) \geq \frac{{\Theta^*_{\max}}^2}{\lambda_{\min}(\boldsymbol{P}) \cdot \gamma_0^2} \tag{3.233}$$

holds, where $\gamma_1 > 0$ *and* $\gamma_0 > 0$ *are linked by* (3.231)*, i.e.*

$$\gamma_1 \triangleq \frac{\|\boldsymbol{G}_m(s)\,\boldsymbol{C}_{e_P}(s)\|_{\mathcal{L}_1} \cdot \gamma_0}{1 - \|\boldsymbol{G}_m(s)\,(\boldsymbol{I} - \boldsymbol{C}(s))\,\boldsymbol{\Theta}^*_{m,x}\|_{\mathcal{L}_1} - \|\boldsymbol{G}_m(s)\,(\boldsymbol{I} - \boldsymbol{C}(s))\,\boldsymbol{\Theta}^*_{m,\phi}\|_{\mathcal{L}_1} \cdot L_{\rho_r}};$$

3. the initial conditions of all states are zero,

then the error $\boldsymbol{e}_{ref}(t) = \boldsymbol{x}_P(t) - \boldsymbol{x}_{ref}(t)$ *between the plant* (3.165) *and the* $\mathcal{L}_1$ *Reference Model* (3.175) *is bounded by*

$$\|\boldsymbol{e}_{ref}(t)|_{\mathcal{L}_\infty} < \bar{\gamma}_1. \tag{3.234}$$

Proof. Lemma 3.27 is proven by contradiction. To that end, assume that the bound (3.234) would not hold. In this case, due to $\boldsymbol{e}_{\text{ref}}(0) = \boldsymbol{0}$ and due to continuity, there must exist an interval $t \in [0, \tau]$ such that

$$\|\boldsymbol{e}_{\text{ref}}(t)\|_\infty < \bar{\gamma}_1 \quad \forall\, t \in [0, \tau[\tag{3.235}$$

and

$$\|\boldsymbol{e}_{\text{ref}}(\tau)\|_\infty = \bar{\gamma}_1. \tag{3.236}$$

Hence, throughout the interval $[0, \tau]$,

$$\|\boldsymbol{e}_{\text{ref}}(t)_\tau\|_{\mathcal{L}_\infty} \leq \bar{\gamma}_1 \tag{3.237}$$

holds. Since Lemma 3.26 holds, the triangle inequality implies

$$\|\boldsymbol{x}_P(t)_\tau\|_{\mathcal{L}_\infty} \leq \|\boldsymbol{x}_{\text{ref}}(t)_\tau\|_{\mathcal{L}_\infty} + \|\boldsymbol{e}_{\text{ref}}(t)_\tau\|_{\mathcal{L}_\infty} < \rho_r + \bar{\gamma}_1. \tag{3.238}$$

Thus, throughout the interval, $\|\boldsymbol{x}_P(t)_\tau\|_{\mathcal{L}_\infty} < \rho_r + \bar{\gamma}_1$ and $\|\boldsymbol{x}_{\text{ref}}(t)_\tau\|_{\mathcal{L}_\infty} < \rho_r < \rho_r + \bar{\gamma}_1$ hold. Consequently, the semi-global Lipschitz condition (3.213) holds throughout the interval with $r = \rho_r + \bar{\gamma}_1$. Denoting $L_{\rho_r} \triangleq L(\rho_r + \bar{\gamma}_1)$, the norm inequality (3.229) hence holds throughout the interval, that is

$$\|\boldsymbol{e}_{\text{ref}}(t)_\tau\|_{\mathcal{L}_\infty} \leq \frac{\|\boldsymbol{G}_m(s)\,\boldsymbol{C}_{e_P}(s)\|_{\mathcal{L}_1} \cdot \|\boldsymbol{e}_P(t)\|_{\mathcal{L}_\infty}}{1 - \|\boldsymbol{G}_m(s)\,(\boldsymbol{I} - \boldsymbol{C}(s))\,\boldsymbol{\Theta}^*_{m,x}\|_{\mathcal{L}_1} - \|\boldsymbol{G}_m(s)\,(\boldsymbol{I} - \boldsymbol{C}(s))\,\boldsymbol{\Theta}^*_{m,\phi}\|_{\mathcal{L}_1} \cdot L_{\rho_r}}.$$

Since $\boldsymbol{\Gamma}$ is chosen according to (3.233) and the initial conditions are zero, $\|\boldsymbol{e}_P(t)\|_{\mathcal{L}_\infty} \leq \gamma_0$ holds (see (3.232) and (3.88)). With the definition of γ_1 in (3.231), this implies

$$\|\boldsymbol{e}_{\text{ref}}(t)_\tau\|_{\mathcal{L}_\infty} \leq \gamma_1 = \bar{\gamma}_1 - \beta < \bar{\gamma}_1, \tag{3.239}$$

which contradicts (3.236). Hence, no such instant of time τ can exist, in which (3.236) holds, which proves the bound (3.234). □

Step 3: Following the same lines as in Part 1, Lemma 3.26 and Lemma 3.27 imply boundedness of all closed-loop signals, leading to the following theorem:

Theorem 3.28 (Nominal Stability of $\mathcal{L}_1$ Adaptive Control with Integral Update Law)**.** *Consider the plant* (3.1) *and let Assumptions 3.1 (state feedback), 3.2 (positive definite control effectiveness), 3.3 (Lipschitz condition), 3.5 (matching condition), 3.6 (full-rank $\boldsymbol{B}_P$), 3.7 (linear parametrization), 3.8 (exact parametrization), 3.10 (bounded uncertainties) hold. If the design parameters $\boldsymbol{\Gamma}$, $\boldsymbol{Q}$, $\boldsymbol{K}$ and $\boldsymbol{D}(s)$ of the $\mathcal{L}_1$ Adaptive Controller*

$$\begin{aligned}
\dot{\hat{\boldsymbol{x}}}_P(t) &= \boldsymbol{A}_M \hat{\boldsymbol{x}}_P(t) + \boldsymbol{B}_P\left(\hat{\boldsymbol{\Lambda}}(t)\,\boldsymbol{u}(t) + \hat{\boldsymbol{\Theta}}_{m,x}(t)\,\boldsymbol{x}_P(t) + \hat{\boldsymbol{\Theta}}_{m,\phi}(t)\cdot\boldsymbol{\phi}(\boldsymbol{x}_P(t))\right),\\
\dot{\hat{\boldsymbol{\Theta}}}_m(t)^T &= -\boldsymbol{\Gamma}\boldsymbol{\omega}(\boldsymbol{x}_P(t),t)\cdot\boldsymbol{e}_P(t)^T\boldsymbol{P}\boldsymbol{B}_P,\\
\boldsymbol{u}(s) &= \boldsymbol{K}\boldsymbol{D}(s)\left(\boldsymbol{K}_r\boldsymbol{r}(s) - \mathcal{L}\left\{\hat{\boldsymbol{\Lambda}}(t)\,\boldsymbol{u}(t) + \hat{\boldsymbol{\Theta}}_{m,x}(t)\,\boldsymbol{x}_P(t) + \hat{\boldsymbol{\Theta}}_{m,\phi}(t)\,\boldsymbol{\phi}(\boldsymbol{x}_P(t))\right\}\right)
\end{aligned}$$

and the initial conditions are chosen to satisfy the conditions of Lemma 3.7, Lemma 3.26 and Lemma 3.27, then all closed-loop signals are bounded. Furthermore, the states of the plant will track the $\mathcal{L}_1$ Reference Model (3.175)*, which by itself approximately tracks the reference model* (3.4)*. The error between the plant and the $\mathcal{L}_1$ Reference Model and the error between the $\mathcal{L}_1$ Reference Model and the reference model* (3.4) *may be arbitrarily decreased.*

Proof. Similar to *Step 3* in case of a global Lipschitz condition, the satisfaction of Lemma 3.26 and Lemma 3.27 implies boundedness of all closed-loop signals. □

Remark 3.29. *Theorem 3.28 establishes stability of $\mathcal{L}_1$-AC, if the uncertainties satisfy a semi-global Lipschitz condition. Due to the cross-serial dependency between Lemma 3.26 and Lemma 3.27, on which Theorem 3.28 is based, the choice of the design parameters $\boldsymbol{\Gamma}$, $\boldsymbol{Q}$, $\boldsymbol{K}$, $\boldsymbol{D}(s)$ and the design constants ρ_r, $\bar{\gamma}_1$, β seems difficult. One approach to satisfy all the conditions is given by the following steps:*

1. *Choose some weighting matrix $\boldsymbol{Q}$ and solve the Lyapunov equation* (3.31) *in order to obtain $\boldsymbol{P}$.*
2. *Choose the design constant $\bar{\gamma}_1$, which specifies the largest error between the plant and the $\mathcal{L}_1$ Reference Model. Qualitatively, small desired errors imply large learning rates $\boldsymbol{\Gamma}$.*
3. *Choose the design constant $\beta > 0$ such that $\gamma_1 = \bar{\gamma}_1 - \beta$ is positive. As β only served to construct a contradiction in Lemma 3.27, it should be as small as possible.*
4. *Choose the design constant ρ_r, which specifies the hypercube, in which all states of the $\mathcal{L}_1$ Reference Model are to remain. This choice needs to ensure that the right hand side of the $\mathcal{L}_1$-norm condition* (3.218) *is positive. Qualitatively, small values of the right hand side of the $\mathcal{L}_1$-norm condition will lead to large filter bandwidths.*
5. *Since ρ_r and $\bar{\gamma}_1$ are chosen, the Lipschitz constant $L(\rho_r + \bar{\gamma}_1)$ may be computed explicitly. The design parameters $\boldsymbol{D}(s)$ and $\boldsymbol{K}$ of the filter may now be chosen*

such that the conditions of Lemma 3.26 are satisfied. These conditions may always be satisfied as a sufficiently fast filter turns $\boldsymbol{G}_m(s)(\boldsymbol{I}-\boldsymbol{C}(s))$ *into a "no-pass" filter, whose* $\mathcal{L}_1$*-norm vanishes.*

6. *As the filters and* γ_1 *are known,* (3.231) *may be solved to obtain the required value of* γ_0*.*
7. *Using* γ_0*, a sufficiently fast learning rate* Γ *is determined, which satisfies* (3.233)*.*

3.3.2 Matched and Unmatched Uncertainties with Piecewise Constant Update Law

The $\mathcal{L}_1$-AC with integral update law, as introduced in Section 3.3.1, is based on the state predictor and the update laws of predictor-based MRAC. The purpose of the state predictor and its accompanying update laws is the estimation of the uncertain plant *parameters*. In this section, a $\mathcal{L}_1$-AC is introduced, whose state-predictor follows a different philosophy. Instead of estimating uncertain *parameters*, the state predictor of $\mathcal{L}_1$-AC with piecewise constant update law ($\mathcal{L}_1$-PWC) aims at estimating the disturbance *signal*, which causes the state predictor to deviate from the plant. Due to this *signal-based* perspective, the $\mathcal{L}_1$-PWC does not require any assumptions on the parametrization of the uncertainties. In contrast to the $\mathcal{L}_1$-AC with Integral Update Law from Section 3.3.1, the $\mathcal{L}_1$-PWC will be introduced for the more complex case of matched and unmatched uncertainties [25, 175]. It has to be noted though that unmatched uncertainties may also be handled by $\mathcal{L}_1$-AC with Integral Update Law and other $\mathcal{L}_1$-AC variants. The scenario of unmatched uncertainties has only not been covered so far for reasons of clarity and brevity.

The $\mathcal{L}_1$-PWC will be introduced for the plant (3.1) under the Assumptions 3.1 (state feedback), 3.2 (positive definite control effectiveness), 3.3 (semi-global Lipschitz condition) and 3.6 (full-rank $\boldsymbol{B}_P$). Similar to $\mathcal{L}_1$-AC with Integral Update Law, stability of $\mathcal{L}_1$-PWC may not be established for uncertainties of an arbitrary size. For this reason, the following additional assumption is required:

Assumption 3.11. *The uncertainties* $\boldsymbol{\Lambda}$*,* $\boldsymbol{\Theta}^*_{m,x}$*,* $\boldsymbol{\Theta}^*_{um,x}$ *are bounded. They are guaranteed to remain within the known sets* Ω_Λ*,* $\Omega_{x,m}$ *and* $\Omega_{x,um}$*, i.e.*

$$\boldsymbol{\Lambda} \in \Omega_\Lambda, \qquad \boldsymbol{\Theta}^*_{m,x} \in \Omega_{x,m}, \qquad \boldsymbol{\Theta}^*_{um,x} \in \Omega_{x,um}, \tag{3.240}$$

with $\boldsymbol{I} \in \Omega_\Lambda$*. The sets* Ω_Λ*,* $\Omega_{x,m}$ *and* $\Omega_{x,um}$ *may be conservative in the sense that they are supersets of the sets, in which the uncertainties will remain in reality. Furthermore, the state-dependent Lipschitz constant* $K(r)$ *and the bound* B *of the exogenous disturbances of the nonlinear, uncertain function* $\boldsymbol{f}(\boldsymbol{x}_P(t), t)$ *are known.*

Since unmatched uncertainties are to be handled, the following assumption is required in addition:

Assumption 3.12. *The transfer function*

$$\boldsymbol{H}_m(s) \triangleq \boldsymbol{C}_P\left(s\boldsymbol{I}-\boldsymbol{A}_M\right)^{-1}\boldsymbol{B}_P \tag{3.241}$$

is minimum-phase, that is, its transmission zeros strictly lie in the left half-plane. Notice that this assumption affects the desired system matrix $\boldsymbol{A}_M$ and not the plant system matrix $\boldsymbol{A}_P$.

The remainder of this section is structured as follows: At first, the state predictor of $\mathcal{L}_1$-PWC will be derived. Afterwards, a suitable control law is developed, which ensures approximate tracking of the *output* of the reference model (3.4) in the presence of unmatched uncertainties. Finally, the stability of the closed-loop control system is proven.

State Predictor

Due to Assumption 3.6 (full-rank $\boldsymbol{B}_P$) and Remark 3.2, the plant (3.1) may be represented according to (3.15), that is

$$\begin{aligned}\dot{\boldsymbol{x}}_P(t) = \boldsymbol{A}_M\boldsymbol{x}_P(t) &+ \boldsymbol{B}_P\left(\boldsymbol{\Lambda}\boldsymbol{u}(t) + \boldsymbol{\Theta}_{m,x}^{*}\boldsymbol{x}_P(t) + \boldsymbol{f}_m\left(\boldsymbol{x}_P(t),t\right)\right)\\ &+ \bar{\boldsymbol{B}}_P\left(\boldsymbol{\Theta}_{um,x}^{*}\boldsymbol{x}_P(t) + \boldsymbol{f}_{um}\left(\boldsymbol{x}_P(t),t\right)\right).\end{aligned}$$

By gathering all uncertainties into the disturbance signals

$$\begin{aligned}\boldsymbol{\sigma}_m\left(\boldsymbol{x}_P(t),t\right) &\triangleq \left(\boldsymbol{\Lambda}-\boldsymbol{I}\right)\cdot\boldsymbol{u}(t) + \boldsymbol{\Theta}_{m,x}^{*}\boldsymbol{x}_P(t) + \boldsymbol{f}_m\left(\boldsymbol{x}_P(t),t\right),\\ \boldsymbol{\sigma}_{um}\left(\boldsymbol{x}_P(t),t\right) &\triangleq \boldsymbol{\Theta}_{um,x}^{*}\boldsymbol{x}_P(t) + \boldsymbol{f}_{um}\left(\boldsymbol{x}_P(t),t\right),\end{aligned} \tag{3.242}$$

the plant representation (3.15) may be rewritten more compactly as

$$\dot{\boldsymbol{x}}_P(t) = \boldsymbol{A}_M\boldsymbol{x}_P(t) + \boldsymbol{B}_P\cdot\boldsymbol{u}(t) + \begin{bmatrix}\boldsymbol{B}_P & \bar{\boldsymbol{B}}_P\end{bmatrix}\cdot\begin{bmatrix}\boldsymbol{\sigma}_m\left(\boldsymbol{x}_P(t),t\right)\\ \boldsymbol{\sigma}_{um}\left(\boldsymbol{x}_P(t),t\right)\end{bmatrix}. \tag{3.243}$$

Using the definitions of $\boldsymbol{B}$ in (3.13) and of

$$\boldsymbol{\sigma}\left(\boldsymbol{x}_P(t),t\right) \triangleq \begin{bmatrix}\boldsymbol{\sigma}_m\left(\boldsymbol{x}_P(t),t\right)\\ \boldsymbol{\sigma}_{um}\left(\boldsymbol{x}_P(t),t\right)\end{bmatrix}, \tag{3.244}$$

(3.243) becomes:

$$\dot{\boldsymbol{x}}_P(t) = \boldsymbol{A}_M\boldsymbol{x}_P(t) + \boldsymbol{B}_P\cdot\boldsymbol{u}(t) + \boldsymbol{B}\cdot\boldsymbol{\sigma}\left(\boldsymbol{x}_P(t),t\right). \tag{3.245}$$

For the plant representation (3.245), a state predictor and an update law are to be developed, which estimate the disturbance signal $\boldsymbol{\sigma}\left(\boldsymbol{x}_P(t),t\right)$. In the particular approach, which is introduced subsequently, a continuous time state predictor is used, for which a discrete-time update law is sought. The state predictor mimics the structure of (3.245) and is given by

$$\begin{aligned}\dot{\hat{\boldsymbol{x}}}_P(t) &= \boldsymbol{A}_M\hat{\boldsymbol{x}}_P(t) + \boldsymbol{B}_P\cdot\left(\boldsymbol{u}(t) + \hat{\boldsymbol{\sigma}}_m(t)\right) + \bar{\boldsymbol{B}}_P\hat{\boldsymbol{\sigma}}_{um}(t)\\ &= \boldsymbol{A}_M\hat{\boldsymbol{x}}_P(t) + \boldsymbol{B}_P\cdot\boldsymbol{u}(t) + \boldsymbol{B}\cdot\hat{\boldsymbol{\sigma}}(t)\end{aligned} \tag{3.246}$$

with

$$\hat{\boldsymbol{\sigma}}\left(t\right) \triangleq \begin{bmatrix} \hat{\boldsymbol{\sigma}}_m\left(t\right) \\ \hat{\boldsymbol{\sigma}}_{um}\left(t\right) \end{bmatrix}, \tag{3.247}$$

where $\hat{\boldsymbol{\sigma}}_m : \mathbb{R}_+ \to \mathbb{R}^m$ and $\hat{\boldsymbol{\sigma}}_{um} : \mathbb{R}_+ \to \mathbb{R}^{n-m}$ are the estimates of the matched and unmatched disturbance signals $\boldsymbol{\sigma}_m\left(\boldsymbol{x}_P\left(t\right), t\right)$ and $\boldsymbol{\sigma}_{um}\left(\boldsymbol{x}_P\left(t\right), t\right)$, respectively. In (3.246), the yet undefined, piecewise constant estimate $\hat{\boldsymbol{\sigma}}\left(t\right)$ of the uncertainty $\boldsymbol{\sigma}\left(\boldsymbol{x}_P\left(t\right), t\right)$ satisfies

$$\hat{\boldsymbol{\sigma}}\left(t\right) = \hat{\boldsymbol{\sigma}}(iT_s), \qquad t \in [i \cdot T_s,\ (i+1) \cdot T_s[, \tag{3.248}$$

where $T_s > 0$ is the sampling period of the discrete-time update law. The error dynamics between the plant (3.245) and the predictor (3.246) are given by:

$$\dot{\boldsymbol{e}}_P\left(t\right) = \dot{\hat{\boldsymbol{x}}}_P\left(t\right) - \dot{\boldsymbol{x}}_P\left(t\right) = \boldsymbol{A}_M \boldsymbol{e}_P\left(t\right) + \boldsymbol{B} \cdot \left(\hat{\boldsymbol{\sigma}}\left(t\right) - \boldsymbol{\sigma}\left(\boldsymbol{x}_P\left(t\right), t\right)\right). \tag{3.249}$$

For the derivation of an update law for the still undefined estimate $\hat{\boldsymbol{\sigma}}\left(t\right)$, notice that the solution of the differential equation (3.249) on the interval $t \in [i \cdot T_s,\ (i+1) \cdot T_s]$ is given by

$$\boldsymbol{e}_P(iT_s + \xi) = e^{\boldsymbol{A}_M \cdot \xi} \cdot \boldsymbol{e}_P(iT_s) + \int_{iT_s}^{iT_s+\xi} e^{\boldsymbol{A}_M(iT_s+\xi-\bar{\tau})} \boldsymbol{B}\left(\hat{\boldsymbol{\sigma}}\left(\bar{\tau}\right) - \boldsymbol{\sigma}\left(\boldsymbol{x}_P\left(\bar{\tau}\right), \bar{\tau}\right)\right) d\bar{\tau}, \tag{3.250}$$

where $\xi \in [0,\ T_s]$. Upon the transformation $\tau = \bar{\tau} - iT_s$, the integral becomes

$$\begin{aligned} \boldsymbol{e}_P(iT_s + \xi) = e^{\boldsymbol{A}_M \cdot \xi} \cdot \boldsymbol{e}_P(iT_s) &+ \int_0^{\xi} e^{\boldsymbol{A}_M(\xi-\tau)} \boldsymbol{B}\hat{\boldsymbol{\sigma}}\left(\tau + iT_s\right) d\tau \\ &- \int_0^{\xi} e^{\boldsymbol{A}_M(\xi-\tau)} \boldsymbol{B}\boldsymbol{\sigma}\left(\boldsymbol{x}_P\left(\tau + iT_s\right), \tau + iT_s\right) d\tau. \end{aligned} \tag{3.251}$$

Since the disturbance estimate $\hat{\boldsymbol{\sigma}}\left(t\right)$ is constant throughout the interval $[i \cdot T_s,\ (i+1) \cdot T_s[$ due to the definition (3.248), one obtains

$$\begin{aligned} \boldsymbol{e}_P(iT_s + \xi) = e^{\boldsymbol{A}_M \cdot \xi} \cdot \boldsymbol{e}_P(iT_s) &+ \int_0^{\xi} e^{\boldsymbol{A}_M(\xi-\tau)} \boldsymbol{B}\hat{\boldsymbol{\sigma}}(iT_s) d\tau \\ &- \int_0^{\xi} e^{\boldsymbol{A}_M(\xi-\tau)} \boldsymbol{B}\boldsymbol{\sigma}\left(\boldsymbol{x}_P\left(\tau + iT_s\right), \tau + iT_s\right) d\tau. \end{aligned} \tag{3.252}$$

At the instant of the next sampling period, i.e. $\xi = T_s$, (3.252) evaluates to

$$\begin{aligned} \boldsymbol{e}_P(iT_s + T_s) = e^{\boldsymbol{A}_M \cdot T_s} \cdot \boldsymbol{e}_P(iT_s) &+ \int_0^{T_s} e^{\boldsymbol{A}_M(T_s-\tau)} \boldsymbol{B}\hat{\boldsymbol{\sigma}}(iT_s) d\tau \\ &- \int_0^{T_s} e^{\boldsymbol{A}_M(T_s-\tau)} \boldsymbol{B}\boldsymbol{\sigma}\left(\boldsymbol{x}_P\left(\tau + iT_s\right), \tau + iT_s\right) d\tau. \end{aligned} \tag{3.253}$$

Eq. (3.253) shows how the prediction error evolves from one sampling instant to the next. The value of the prediction error at the next sampling instant depends on three quantities:

1. the prediction error at the current time instant (first term);

2. the effect of the uncertainty estimate $\hat{\boldsymbol{\sigma}}(t)$ during one sampling period (second term);
3. the effect of the uncertainty $\boldsymbol{\sigma}(\boldsymbol{x}_P(t), t)$ during one sampling period (third term).

Ideally, one would like to choose $\hat{\boldsymbol{\sigma}}(t)$ in such a way that $\boldsymbol{e}_P(iT_s + Ts) = 0$. Unfortunately, this would require the knowledge of the uncertainty $\boldsymbol{\sigma}(\boldsymbol{x}_P(t), t)$ throughout the considered sampling period. While the prediction error may hence not be driven to zero exactly, its growth from one sampling instant to the next may be limited. This can be achieved if the first and the second term on the right hand side of (3.253) cancel:

$$e^{\boldsymbol{A}_M \cdot T_s} \cdot \boldsymbol{e}_P(iT_s) + \int_0^{T_s} e^{\boldsymbol{A}_M (T_s - \tau)} \boldsymbol{B} \hat{\boldsymbol{\sigma}}(iT_s) d\tau = \boldsymbol{0}. \tag{3.254}$$

In this case, the prediction error at the next sampling instant is given by

$$\boldsymbol{e}_P(iT_s + T_s) = -\int_0^{T_s} e^{\boldsymbol{A}_M (T_s - \tau)} \boldsymbol{B} \boldsymbol{\sigma}\left(\boldsymbol{x}_P(\tau + iT_s), \tau + iT_s\right) d\tau. \tag{3.255}$$

Now assume that the control law, which is not yet defined, would lead to a stable closed loop. In this case, $\boldsymbol{x}_P(t)$ and $\boldsymbol{u}(t)$ are bounded and so is $\boldsymbol{\sigma}(\boldsymbol{x}_P(t), t)$. Thus, the prediction error may not grow unbounded during one sampling period. Furthermore, when the sampling period goes to zero, i.e. $T_s \to 0$, the value of the integral will vanish as well. Thus, the prediction error at the next sampling instant may be rendered arbitrarily small, which implies a small prediction error at all sampling instants iT_s, $i \geq 1$. It remains to show that the equation (3.254) can actually be solved. To that end, solving the integral in (3.254) yields the equation

$$\begin{aligned} &e^{\boldsymbol{A}_M \cdot T_s} \cdot \boldsymbol{e}_P(iT_s) + \left[-\boldsymbol{A}_M^{-1} e^{\boldsymbol{A}_M (T_s - \tau)} \boldsymbol{B} \hat{\boldsymbol{\sigma}}(iT_s)\right]_0^{T_s} = \\ &e^{\boldsymbol{A}_M \cdot T_s} \cdot \boldsymbol{e}_P(iT_s) + \boldsymbol{A}_M^{-1} \left(e^{\boldsymbol{A}_M T_s} - \boldsymbol{I}\right) \boldsymbol{B} \hat{\boldsymbol{\sigma}}(iT_s) = \boldsymbol{0}. \end{aligned} \tag{3.256}$$

Solving for $\hat{\boldsymbol{\sigma}}(iT_s)$ then yields the desired update law:

$$\hat{\boldsymbol{\sigma}}(iT_s) = -\boldsymbol{B}^{-1} \left(e^{\boldsymbol{A}_M T_s} - \boldsymbol{I}\right)^{-1} \boldsymbol{A}_M \cdot e^{\boldsymbol{A}_M \cdot T_s} \cdot \boldsymbol{e}_P(iT_s). \tag{3.257}$$

Notice that the update law (3.257) as well as the state predictor (3.246) are linear. Since the update law is discrete and the state predictor is continuous, the disturbance signal $\boldsymbol{\sigma}(\boldsymbol{x}_P(t), t)$ is hence estimated by the $\mathcal{L}_1$-PWC using a linear hybrid approach.

Control Law

Using the estimate $\hat{\boldsymbol{\sigma}}(t)$ of the disturbance signal $\boldsymbol{\sigma}(\boldsymbol{x}_P(t), t)$, a control law is to be developed, which ensures approximate tracking of the *output* $\boldsymbol{y}_M(t)$ of the reference model (3.4) and prevents high-frequency content from entering the plant. Similar to the derivation of $\mathcal{L}_1$-AC with Integral Update Law in case of matched uncertainties, the derivation of the control law follows a certainty-equivalence-like argument. Thus, at first, an ideal control law is derived assuming that the disturbance signal $\boldsymbol{\sigma}(\boldsymbol{x}_P(t), t)$

was known. By replacing the true disturbance by its estimate, the actual control law is obtained.
In order to derive the ideal control law and the $\mathcal{L}_1$ *Reference Model* within one step, rewrite the plant (3.243) as follows:

$$\begin{aligned}\dot{\boldsymbol{x}}_{\text{ref}}(t) &= \boldsymbol{A}_M \boldsymbol{x}_{\text{ref}}(t) + \boldsymbol{B}_P \cdot \boldsymbol{u}_{\text{ref}}(t) + \begin{bmatrix}\boldsymbol{B}_P & \bar{\boldsymbol{B}}_P\end{bmatrix} \cdot \begin{bmatrix}\boldsymbol{\sigma}_m(\boldsymbol{x}_{\text{ref}}(t), t) \\ \boldsymbol{\sigma}_{um}(\boldsymbol{x}_{\text{ref}}(t), t)\end{bmatrix}, \\ \boldsymbol{y}_{\text{ref}}(t) &= \boldsymbol{C}_P \cdot \boldsymbol{x}_{\text{ref}}(t),\end{aligned} \tag{3.258}$$

where $\boldsymbol{x}_{\text{ref}} : \mathbb{R}_+ \to \mathbb{R}^n$ is the state vector, $\boldsymbol{u}_{\text{ref}}(t) : \mathbb{R}_+ \to \mathbb{R}^m$ the input vector and $\boldsymbol{y}_{\text{ref}}(t) : \mathbb{R}_+ \to \mathbb{R}^m$ the output vector of the $\mathcal{L}_1$ *Reference Model*. Notice that (3.258) is structurally equivalent to the plant (3.243) except for the substitutions $\boldsymbol{x}_P(t) \to \boldsymbol{x}_{\text{ref}}(t)$ and $\boldsymbol{u}(t) \to \boldsymbol{u}_{\text{ref}}(t)$. Upon the definitions

$$\boldsymbol{G}_{um}(s) \triangleq (s\boldsymbol{I} - \boldsymbol{A}_M)^{-1} \bar{\boldsymbol{B}}_P, \tag{3.259}$$

$$\boldsymbol{\sigma}_{ref,m}(s) \triangleq \mathcal{L}\{\boldsymbol{\sigma}_m(\boldsymbol{x}_{\text{ref}}(t), t)\}, \tag{3.260}$$

$$\boldsymbol{\sigma}_{ref,um}(s) \triangleq \mathcal{L}\{\boldsymbol{\sigma}_{um}(\boldsymbol{x}_{\text{ref}}(t), t)\} \tag{3.261}$$

with $\boldsymbol{G}_m(s)$ as in (3.182) and assuming zero initial conditions, the $\mathcal{L}_1$ *Reference Model* (3.258) may be rewritten in the frequency-domain as

$$\begin{aligned}\boldsymbol{x}_{\text{ref}}(s) &= \boldsymbol{G}_m(s)(\boldsymbol{u}_{\text{ref}}(s) + \boldsymbol{\sigma}_{ref,m}(s)) + \boldsymbol{G}_{um}(s)\boldsymbol{\sigma}_{ref,um}(s), \\ \boldsymbol{y}_{\text{ref}}(s) &= \boldsymbol{C}_P \cdot \boldsymbol{x}_{\text{ref}}(s).\end{aligned} \tag{3.262}$$

Furthermore, using the definitions

$$\boldsymbol{H}_m(s) \triangleq \boldsymbol{C}_P(s\boldsymbol{I} - \boldsymbol{A}_M)^{-1}\boldsymbol{B}_P = \boldsymbol{C}_P \cdot \boldsymbol{G}_m(s), \tag{3.263}$$

$$\boldsymbol{H}_{um}(s) \triangleq \boldsymbol{C}_P(s\boldsymbol{I} - \boldsymbol{A}_M)^{-1}\bar{\boldsymbol{B}}_P = \boldsymbol{C}_P \cdot \boldsymbol{G}_{um}(s), \tag{3.264}$$

(3.262) becomes

$$\boldsymbol{y}_{\text{ref}}(s) = \boldsymbol{H}_m(s) \cdot (\boldsymbol{u}_{\text{ref}}(s) + \boldsymbol{\sigma}_{ref,m}(s)) + \boldsymbol{H}_{um}(s)\boldsymbol{\sigma}_{ref,um}(s). \tag{3.265}$$

Ideally, one would like that the output $\boldsymbol{y}_{\text{ref}}(t)$ exactly follows the output $\boldsymbol{y}_M(t)$ of the reference model (3.4). Equating $\boldsymbol{y}_{\text{ref}}(t)$ and $\boldsymbol{y}_M(t)$ in the frequency-domain yields

$$\boldsymbol{H}_m(s) \cdot (\boldsymbol{u}_{\text{ref}}(s) + \boldsymbol{\sigma}_{ref,m}(s)) + \boldsymbol{H}_{um}(s)\boldsymbol{\sigma}_{ref,um}(s) = \boldsymbol{H}_m(s)\boldsymbol{K}_r\boldsymbol{r}(s). \tag{3.266}$$

Unlike $\boldsymbol{G}_m(s)$, the transfer function $\boldsymbol{H}_m(s)$ is square and thus, invertible. Furthermore, due to Assumption 3.12, the poles of $\boldsymbol{H}_m^{-1}(s)$ are in the left half-plane. Thus, (3.266) may be solved for $\boldsymbol{u}_{\text{ref}}(s)$, yielding the non-causal control law

$$\boldsymbol{u}_{\text{ref}}(s) = \boldsymbol{K}_r\boldsymbol{r}(s) - \boldsymbol{\sigma}_{ref,m}(s) - \boldsymbol{H}_m^{-1}(s)\boldsymbol{H}_{um}(s)\boldsymbol{\sigma}_{ref,um}(s). \tag{3.267}$$

While (3.267) is non-causal due to the product $\boldsymbol{H}_m^{-1}(s)\boldsymbol{H}_{um}(s)$ (except for some rare cases), adding the filter

$$\boldsymbol{C}_m(s) \triangleq (\boldsymbol{I} + \boldsymbol{K}\boldsymbol{D}(s))^{-1}\boldsymbol{K}\boldsymbol{D}(s), \tag{3.268}$$

where $\boldsymbol{K}$ and $\boldsymbol{D}(s)$ are defined as in Section 3.3.1, may render (3.267) causal:

$$\boldsymbol{u}_{\text{ref}}(s) \triangleq \boldsymbol{C}_m(s)\left(\boldsymbol{K}_r\boldsymbol{r}(s) - \boldsymbol{\sigma}_{ref,m}(s) - \boldsymbol{H}_m^{-1}(s)\,\boldsymbol{H}_{um}(s)\,\boldsymbol{\sigma}_{ref,um}(s)\right). \tag{3.269}$$

For this, the filter $\boldsymbol{C}_m(s)$ has to ensure that the transfer function

$$\boldsymbol{C}_{um}(s) \triangleq \boldsymbol{C}_m(s)\boldsymbol{H}_m^{-1}(s)\,\boldsymbol{H}_{um}(s) \tag{3.270}$$

is proper. At this point, it is important to realize that the ideal control law (3.269) is not guaranteed to be stable, even if $\boldsymbol{C}_m(s)$ is Hurwitz. This is because the uncertainty $\boldsymbol{\sigma}_m(\boldsymbol{x}_{\text{ref}}(t), t)$ depends on $\boldsymbol{u}_{\text{ref}}(t)$. Hence, (3.269) contains a feedback connection, whose stability is not yet proven. Thus, even in case of bounded inputs into the ideal control law (3.269), its output could be unbounded. While the actually implemented control law derives from (3.269), the proof of stability uses an alternative representation, where this feedback connection is resolved. Nevertheless, using (3.258) and the causal control law (3.269), an initial representation of the $\mathcal{L}_1$ *Reference Model* is obtained:

$$\begin{aligned}
\dot{\boldsymbol{x}}_{\text{ref}}(t) &= \boldsymbol{A}_M\boldsymbol{x}_{\text{ref}}(t) + \boldsymbol{B}_P\cdot\left(\boldsymbol{u}_{\text{ref}}(t) + \boldsymbol{\sigma}_m(\boldsymbol{x}_{\text{ref}}(t), t)) + \bar{\boldsymbol{B}}_P\boldsymbol{\sigma}_{um}(\boldsymbol{x}_{\text{ref}}(t), t)\right),\\
\boldsymbol{u}_{\text{ref}}(s) &= \boldsymbol{C}_m(s)\left(\boldsymbol{K}_r\boldsymbol{r}(s) - \boldsymbol{\sigma}_{ref,m}(s) - \boldsymbol{H}_m^{-1}(s)\,\boldsymbol{H}_{um}(s)\,\boldsymbol{\sigma}_{ref,um}(s)\right),\\
\boldsymbol{y}_{\text{ref}}(t) &= \boldsymbol{C}_P\cdot\boldsymbol{x}_{\text{ref}}(t).
\end{aligned} \tag{3.271}$$

Moreover, by replacing $\boldsymbol{\sigma}_{ref,m}(s)$ and $\boldsymbol{\sigma}_{ref,um}(s)$ by their estimates $\hat{\boldsymbol{\sigma}}_m(s)$ and $\hat{\boldsymbol{\sigma}}_{um}(s)$, the actual control law for the plant (3.1) follows from the ideal control law (3.269):

$$\boldsymbol{u}(s) = \boldsymbol{C}_m(s)\left(\boldsymbol{K}_r\boldsymbol{r}(t) - \hat{\boldsymbol{\sigma}}_m(s) - \boldsymbol{H}_m^{-1}(s)\,\boldsymbol{H}_{um}(s)\,\hat{\boldsymbol{\sigma}}_{um}(s)\right). \tag{3.272}$$

Proof of Stability

The state predictor (3.246), the piecewise constant update law (3.257) and the control law (3.272) constitute the $\mathcal{L}_1$-PWC. While the structure of the $\mathcal{L}_1$-PWC is known now, its stability has not been established so far. The proof of stability follows similar lines as the one for $\mathcal{L}_1$-AC with Integral Update Law. However, as the boundedness of the prediction error $\boldsymbol{e}_P(t)$ cannot be established by virtue of a Lyapunov proof of stability independent of $\boldsymbol{u}(t)$ and $\boldsymbol{x}_P(t)$, an additional step is required. The subsequent proof of boundedness of all closed-loop signals hence involves the following four steps:

1. Prove boundedness of the $\mathcal{L}_1$ *Reference Model* (3.271).
2. Prove boundedness of the predictor (3.246) and the update law (3.257), assuming that $\boldsymbol{x}_P(t)$ and $\boldsymbol{u}(t)$ are bounded.
3. Using the boundedness results from Step 1 and 2, prove boundedness of the errors $\boldsymbol{e}_{\text{ref}}(t) = \boldsymbol{x}_P(t) - \boldsymbol{x}_{\text{ref}}(t)$ and $\boldsymbol{u}(t) - \boldsymbol{u}_{\text{ref}}(t)$ between the plant representation (3.243) and the $\mathcal{L}_1$ *Reference Model* (3.271).

4. Use the boundedness of the error $\boldsymbol{e}_{\text{ref}}(t)$ and of the $\mathcal{L}_1$ *Reference Model* to conclude that the plant state $\boldsymbol{x}_P(t)$ is bounded. Since the prediction error $\boldsymbol{e}_P(t)$ is bounded by virtue of Step 2, this implies boundedness of the state predictor (3.246). With this, all closed-loop signals are bounded.

As mentioned earlier, the ideal control law (3.269) and, as will be shown subsequently, the actual control law (3.272) contain an implicit feedback connection as the disturbance signal $\boldsymbol{\sigma}_m(\cdot, t)$ depends on the control input. As this feedback connection complicates statements about the Bounded Input Bounded Output (BIBO) stability of the control laws, alternative representations are required. These representations of the plant dynamics (3.243), the control law (3.272) and of the $\mathcal{L}_1$ *Reference Model* (3.271) separate the state-dependent uncertainties from the input uncertainty $\boldsymbol{\Lambda}$. The state-dependent uncertainties are defined as

$$\boldsymbol{\eta}_m(\boldsymbol{x}_P(t), t) \triangleq \boldsymbol{\Theta}_{m,x}^* \boldsymbol{x}_P(t) + \boldsymbol{f}_m(\boldsymbol{x}_P(t), t) \tag{3.273}$$

$$\boldsymbol{\eta}_{um}(\boldsymbol{x}_P(t), t) \triangleq \boldsymbol{\Theta}_{um,x}^* \boldsymbol{x}_P(t) + \boldsymbol{f}_{um}(\boldsymbol{x}_P(t), t) \tag{3.274}$$

The Laplace transforms of $\boldsymbol{\eta}_m(\boldsymbol{x}_P(t), t)$ and $\boldsymbol{\eta}_{um}(\boldsymbol{x}_P(t), t)$ are denoted as $\boldsymbol{\eta}_{P,m}(s) = \mathcal{L}\{\boldsymbol{\eta}_m(\boldsymbol{x}_P(t), t)\}$ and $\boldsymbol{\eta}_{P,um}(s) = \mathcal{L}\{\boldsymbol{\eta}_{um}(\boldsymbol{x}_P(t), t)\}$, where the index $(\cdot)_P$ indicates that $\boldsymbol{\eta}_{P,m}(s)$ and $\boldsymbol{\eta}_{P,um}(s)$ actually depend on $\boldsymbol{x}_P(t)$. With (3.273) and (3.274), the plant (3.243) becomes

$$\dot{\boldsymbol{x}}_P(t) = \boldsymbol{A}_M \boldsymbol{x}_P(t) + \boldsymbol{B}_P(\boldsymbol{\Lambda}\boldsymbol{u}(t) + \boldsymbol{\eta}_m(\boldsymbol{x}_P(t), t)) + \bar{\boldsymbol{B}}_P \boldsymbol{\eta}_{um}(\boldsymbol{x}_P(t), t). \tag{3.275}$$

Similarly, the control law (3.272) is rewritten in such a way that it depends on the state-dependent uncertainties. Since the control law (3.272) does not explicitly depend on $\boldsymbol{\sigma}_m(\boldsymbol{x}_P(t), t)$, $\boldsymbol{\eta}_m(\boldsymbol{x}_P(t), t)$, $\boldsymbol{\sigma}_{um}(\boldsymbol{x}_P(t), t)$ nor $\boldsymbol{\eta}_{um}(\boldsymbol{x}_P(t), t)$, adding and subtracting $\boldsymbol{C}_m(s) \cdot \boldsymbol{\sigma}_{P,m}(s)$ and $\boldsymbol{C}_m(s)\boldsymbol{H}_m^{-1}(s)\boldsymbol{H}_{um}(s)\boldsymbol{\sigma}_{P,um}(s)$ yields

$$\begin{aligned}\boldsymbol{u}(s) = \boldsymbol{C}_m(s)\Big(\boldsymbol{K}_r \boldsymbol{r}(s) - \boldsymbol{\sigma}_{P,m}(s) - \boldsymbol{H}_m^{-1}(s)\boldsymbol{H}_{um}(s)\boldsymbol{\sigma}_{P,um}(s)\Big) \\ - \boldsymbol{C}_m(s)(\hat{\boldsymbol{\sigma}}_m(s) - \boldsymbol{\sigma}_{P,m}(s)) \\ - \boldsymbol{C}_m(s)\boldsymbol{H}_m^{-1}(s)\boldsymbol{H}_{um}(s)(\hat{\boldsymbol{\sigma}}_{um}(s) - \boldsymbol{\sigma}_{P,um}(s)).\end{aligned} \tag{3.276}$$

In (3.276), the Laplace transforms of $\boldsymbol{\sigma}_m(\boldsymbol{x}_P(t), t)$ and $\boldsymbol{\sigma}_{um}(\boldsymbol{x}_P(t), t)$ are denoted as $\boldsymbol{\sigma}_{P,m}(s) \triangleq \mathcal{L}\{\boldsymbol{\sigma}_m(\boldsymbol{x}_P(t), t)\}$ and $\boldsymbol{\sigma}_{P,um}(s) \triangleq \mathcal{L}\{\boldsymbol{\sigma}_{um}(\boldsymbol{x}_P(t), t)\}$, where the index $(\cdot)_P$ indicates that $\boldsymbol{\sigma}_{P,m}(s)$ and $\boldsymbol{\sigma}_{P,um}(s)$ actually depend on $\boldsymbol{x}_P(t)$. Furthermore, notice that the following relation between the *output* $\boldsymbol{C}_P \cdot \boldsymbol{e}_P(s)$ of the prediction error dynamics (3.249) and the disturbance estimation errors $\hat{\boldsymbol{\sigma}}_m(t) - \boldsymbol{\sigma}_m(\boldsymbol{x}_P(t), t)$ and $\hat{\boldsymbol{\sigma}}_{um}(t) - \boldsymbol{\sigma}_{um}(\boldsymbol{x}_P(t), t)$ holds:

$$\boldsymbol{C}_P \cdot \boldsymbol{e}_P(s) = \boldsymbol{H}_m(s)(\hat{\boldsymbol{\sigma}}_m(s) - \boldsymbol{\sigma}_{P,m}(s)) + \boldsymbol{H}_{um}(s)(\hat{\boldsymbol{\sigma}}_{um}(s) - \boldsymbol{\sigma}_{P,um}(s)). \tag{3.277}$$

Multiplying by $\boldsymbol{H}_m^{-1}(s)$ yields:

$$\hat{\boldsymbol{\sigma}}_m(s) - \boldsymbol{\sigma}_{P,m}(s) + \boldsymbol{H}_m^{-1}(s)\boldsymbol{H}_{um}(s)(\hat{\boldsymbol{\sigma}}_{um}(s) - \boldsymbol{\sigma}_{P,um}(s)) = \boldsymbol{H}_m^{-1}(s)\boldsymbol{C}_P \cdot \boldsymbol{e}_P(s). \tag{3.278}$$

Substituting (3.278) into (3.276) gives

$$\begin{aligned}\boldsymbol{u}(s) = \boldsymbol{C}_m(s) \cdot \Big(\boldsymbol{K}_r \boldsymbol{r}(s) - \boldsymbol{\sigma}_{P,m}(s) - \boldsymbol{H}_m^{-1}(s)\, \boldsymbol{H}_{um}(s) \cdot \boldsymbol{\sigma}_{P,um}(s)\Big) \\ - \boldsymbol{C}_m(s) \boldsymbol{H}_m^{-1}(s)\, \boldsymbol{C}_P \cdot \boldsymbol{e}_P(s)\,.\end{aligned} \tag{3.279}$$

By applying the definitions of the state-dependent uncertainties (3.273) and (3.274), (3.279) becomes

$$\begin{aligned}\boldsymbol{u}(s) = \boldsymbol{C}_m(s) \cdot \Big(\boldsymbol{K}_r \boldsymbol{r}(s) - (\boldsymbol{\Lambda} - \boldsymbol{I}) \cdot \boldsymbol{u}(s) - \boldsymbol{\eta}_{P,m}(s)\Big) \\ - \boldsymbol{C}_m(s) \cdot \Big(\boldsymbol{H}_m^{-1}(s)\, \boldsymbol{H}_{um}(s) \cdot \boldsymbol{\eta}_{P,um}(s) + \boldsymbol{H}_m^{-1}(s)\, \boldsymbol{C}_P \cdot \boldsymbol{e}_P(s)\Big)\,.\end{aligned} \tag{3.280}$$

With the definition of the filter $\boldsymbol{C}_m(s)$ in (3.268), multiplying by $(\boldsymbol{I} + \boldsymbol{K}\boldsymbol{D}(s))$ from the left yields

$$\begin{aligned}(\boldsymbol{I} + \boldsymbol{K}\boldsymbol{D}(s)) \cdot \boldsymbol{u}(s) = \boldsymbol{K}\boldsymbol{D}(s) \cdot \Big(\boldsymbol{K}_r \boldsymbol{r}(s) - (\boldsymbol{\Lambda} - \boldsymbol{I}) \cdot \boldsymbol{u}(s) - \boldsymbol{\eta}_{P,m}(s)\Big) \\ - \boldsymbol{K}\boldsymbol{D}(s) \cdot \boldsymbol{H}_m^{-1}(s)\, \boldsymbol{H}_{um}(s) \cdot \boldsymbol{\eta}_{P,um}(s) \\ - \boldsymbol{K}\boldsymbol{D}(s) \cdot \boldsymbol{H}_m^{-1}(s)\, \boldsymbol{C}_P \cdot \boldsymbol{e}_P(s)\,,\end{aligned} \tag{3.281}$$

which is equivalent to

$$\begin{aligned}(\boldsymbol{I} + \boldsymbol{K}\boldsymbol{D}(s)\boldsymbol{\Lambda}) \cdot \boldsymbol{u}(s) = \boldsymbol{K}\boldsymbol{D}(s) \cdot \Big(\boldsymbol{K}_r \boldsymbol{r}(s) - \boldsymbol{\eta}_{P,m}(s)\Big) \\ - \boldsymbol{K}\boldsymbol{D}(s) \cdot \boldsymbol{H}_m^{-1}(s)\, \boldsymbol{H}_{um}(s) \cdot \boldsymbol{\eta}_{P,um}(s) \\ - \boldsymbol{K}\boldsymbol{D}(s) \cdot \boldsymbol{H}_m^{-1}(s)\, \boldsymbol{C}_P \cdot \boldsymbol{e}_P(s)\,.\end{aligned} \tag{3.282}$$

Using the Searle identity (B.177) and the definition of the filter $\boldsymbol{C}(s)$ in (3.173), one finally obtains a compact representation of the control law (3.272), which depends on the state-dependent uncertainties (and the prediction error $\boldsymbol{e}_P(t)$):

$$\begin{aligned}\boldsymbol{u}(s) = \boldsymbol{\Lambda}^{-1}\boldsymbol{C}(s) \cdot \Big(\boldsymbol{K}_r \boldsymbol{r}(s) - \boldsymbol{\eta}_{P,m}(s) - \boldsymbol{H}_m^{-1}(s)\, \boldsymbol{H}_{um}(s) \cdot \boldsymbol{\eta}_{P,um}(s)\Big) \\ - \boldsymbol{\Lambda}^{-1}\boldsymbol{C}(s) \cdot \boldsymbol{H}_m^{-1}(s)\, \boldsymbol{C}_P \cdot \boldsymbol{e}_P(s)\,.\end{aligned} \tag{3.283}$$

The inputs of the control law representation (3.283) are the signals $\boldsymbol{r}(t)$, $\boldsymbol{\eta}_m(\boldsymbol{x}_P(t), t)$, $\boldsymbol{\eta}_{um}(\boldsymbol{x}_P(t), t)$ and $\boldsymbol{e}_P(t)$. It is causal and BIBO-stable, if the filter $\boldsymbol{C}(s)$ is Hurwitz for all $\boldsymbol{\Lambda} \in \Omega_\Lambda$ and renders $\boldsymbol{C}(s)\boldsymbol{H}_m^{-1}(s)\, \boldsymbol{H}_{um}(s)$ proper for all $\boldsymbol{\Lambda} \in \Omega_\Lambda$. By repeating similar steps, which led to the representations (3.275) and (3.283) of the plant and the control law, the following representation of the $\mathcal{L}_1$ *Reference Model* (3.271) is obtained:

$$\begin{aligned}\dot{\boldsymbol{x}}_{\text{ref}}(t) &= \boldsymbol{A}_M \boldsymbol{x}_{\text{ref}}(t) + \boldsymbol{B}_P \cdot \Big(\boldsymbol{\Lambda}\boldsymbol{u}_{\text{ref}}(t) + \boldsymbol{\eta}_m(\boldsymbol{x}_{\text{ref}}(t), t)) + \bar{\boldsymbol{B}}_P \boldsymbol{\eta}_{um}(\boldsymbol{x}_{\text{ref}}(t), t)\Big)\,, \\ \boldsymbol{u}_{\text{ref}}(s) &= \boldsymbol{\Lambda}^{-1}\boldsymbol{C}(s)\Big(\boldsymbol{K}_r \boldsymbol{r}(s) - \boldsymbol{\eta}_{ref,m}(s) - \boldsymbol{H}_m^{-1}(s)\, \boldsymbol{H}_{um}(s)\, \boldsymbol{\eta}_{ref,um}(s)\Big)\,, \\ \boldsymbol{y}_{\text{ref}}(t) &= \boldsymbol{C}_P \cdot \boldsymbol{x}_{\text{ref}}(t)\,,\end{aligned} \tag{3.284}$$

which may also be found in [87]. In (3.284), $\boldsymbol{\eta}_{ref,m}(s)$ and $\boldsymbol{\eta}_{ref,um}(s)$ are the Laplace transforms of $\boldsymbol{\eta}_m(\boldsymbol{x}_{\text{ref}}(t), t)$ and $\boldsymbol{\eta}_{um}(\boldsymbol{x}_{\text{ref}}(t), t)$. The index $(\cdot)_{ref}$ is used to indicate that $\boldsymbol{\eta}_{ref,m}(s)$ and $\boldsymbol{\eta}_{ref,um}(s)$ actually depend on $\boldsymbol{x}_{\text{ref}}(s)$.

Throughout the different steps of the proof of stability, the semi-global Lipschitz condition and the boundedness condition of Assumption 3.3 are frequently used. In order to obtain a more compact notation, the semi-global Lipschitz condition is restated in terms of the state-dependent uncertainties $\boldsymbol{\eta}_m\left(\boldsymbol{x}_P\left(t\right),t\right)$ and $\boldsymbol{\eta}_{um}\left(\boldsymbol{x}_P\left(t\right),t\right)$:

$$\begin{aligned}\left\|\boldsymbol{\eta}_m\left(\boldsymbol{x}_1,t\right)-\boldsymbol{\eta}_m\left(\boldsymbol{x}_2,t\right)\right\|_\infty &\leq L_m\left(r\right)\cdot\left\|\boldsymbol{x}_1-\boldsymbol{x}_2\right\|_\infty\\ &\quad\forall\left\|\boldsymbol{x}_1\right\|_\infty\leq r,\ \left\|\boldsymbol{x}_2\right\|_\infty\leq r,\\ \left\|\boldsymbol{\eta}_{um}\left(\boldsymbol{x}_1,t\right)-\boldsymbol{\eta}_{um}\left(\boldsymbol{x}_2,t\right)\right\|_\infty &\leq L_{um}\left(r\right)\cdot\left\|\boldsymbol{x}_1-\boldsymbol{x}_2\right\|_\infty\\ &\quad\forall\left\|\boldsymbol{x}_1\right\|_\infty\leq r,\ \left\|\boldsymbol{x}_2\right\|_\infty\leq r,\end{aligned}\tag{3.285}$$

where $L_m:\mathbb{R}_+\rightarrow\mathbb{R}_+$ and $L_{um}:\mathbb{R}_+\rightarrow\mathbb{R}_+$ are the known, state-dependent Lipschitz constants. Similarly, the boundedness condition is restated as

$$\begin{aligned}\left\|\boldsymbol{\eta}_m\left(\boldsymbol{0},t\right)\right\|_\infty&\leq\phi_{m,0},\\ \left\|\boldsymbol{\eta}_{um}\left(\boldsymbol{0},t\right)\right\|_\infty&\leq\phi_{um,0},\end{aligned}\tag{3.286}$$

where $\phi_{m,0}$ and $\phi_{um,0}$ are known constants. If Assumptions 3.3 (Lipschitz condition) and 3.11 (known Lipschitz constant) hold, then the constants $L_m\left(r\right)$, $L_{um}\left(r\right)$, $\phi_{m,0}$ and $\phi_{um,0}$ always exist. Furthermore, they are known since $\boldsymbol{f}_m\left(\boldsymbol{x}_P\left(t\right),t\right)$ and $\boldsymbol{f}_{um}\left(\boldsymbol{x}_P\left(t\right),t\right)$ relate to $\boldsymbol{f}\left(\boldsymbol{x}_P\left(t\right),t\right)$ by a unique transformation and, since the linear uncertainties $\boldsymbol{\Theta}_{m,x}^*\cdot\boldsymbol{x}_P\left(t\right)$ and $\boldsymbol{\Theta}_{um,x}^*\cdot\boldsymbol{x}_P\left(t\right)$ in $\boldsymbol{\eta}_m\left(\boldsymbol{x}_P\left(t\right),t\right)$ and $\boldsymbol{\eta}_{um}\left(\boldsymbol{x}_P\left(t\right),t\right)$ are globally Lipschitz with a known bound. Using the reverse triangle inequality, Eqs. (3.285) and (3.286) especially yield bounds on the size of the state-dependent uncertainties, which depend linearly on $\left\|\boldsymbol{x}\right\|_\infty$, namely:

$$\begin{aligned}\left\|\boldsymbol{\eta}_m\left(\boldsymbol{x},t\right)\right\|_\infty&\leq L_m\left(r\right)\cdot\left\|\boldsymbol{x}\right\|_\infty+\phi_{m,0}\quad\forall\left\|\boldsymbol{x}\right\|_\infty\leq r,\\ \left\|\boldsymbol{\eta}_{um}\left(\boldsymbol{x},t\right)\right\|_\infty&\leq L_{um}\left(r\right)\cdot\left\|\boldsymbol{x}\right\|_\infty+\phi_{um,0}\quad\forall\left\|\boldsymbol{x}\right\|_\infty\leq r.\end{aligned}\tag{3.287}$$

Step 1: In order to be able to prove boundedness of the $\mathcal{L}_1$ *Reference Model*, assume that the design parameters $\boldsymbol{K}$ and $\boldsymbol{D}(s)$ of the filter $\boldsymbol{C}(s)$, defined in (3.173), are chosen such that $\boldsymbol{C}(s)$ is Hurwitz for all $\boldsymbol{\Lambda}\in\Omega_\Lambda$. Furthermore, the design parameters render the transfer function $\boldsymbol{C}(s)\boldsymbol{H}_m^{-1}\left(s\right)\boldsymbol{H}_{um}\left(s\right)$ proper. By applying the definition

$$\boldsymbol{v}_{\text{ref}}\left(t\right)\triangleq\boldsymbol{\Lambda}\boldsymbol{u}_{\text{ref}}\left(t\right)+\boldsymbol{\eta}_m\left(\boldsymbol{x}_{\text{ref}}\left(t\right),t\right)\tag{3.288}$$

to the first equation in (3.284), the $\mathcal{L}_1$ *Reference Model* becomes

$$\dot{\boldsymbol{x}}_{\text{ref}}\left(t\right)=\boldsymbol{A}_M\boldsymbol{x}_{\text{ref}}\left(t\right)+\boldsymbol{B}_P\cdot\boldsymbol{v}_{\text{ref}}\left(t\right)+\bar{\boldsymbol{B}}_P\boldsymbol{\eta}_{um}\left(\boldsymbol{x}_{\text{ref}}\left(t\right),t\right),\tag{3.289}$$

$$\boldsymbol{v}_{\text{ref}}\left(s\right)=\boldsymbol{\Lambda}\boldsymbol{u}_{\text{ref}}\left(s\right)+\boldsymbol{\eta}_{ref,m}\left(s\right),\tag{3.290}$$

$$\boldsymbol{u}_{\text{ref}}\left(s\right)=\boldsymbol{\Lambda}^{-1}\boldsymbol{C}(s)\left(\boldsymbol{K}_r\boldsymbol{r}\left(s\right)-\boldsymbol{\eta}_{ref,m}\left(s\right)-\boldsymbol{H}_m^{-1}\left(s\right)\boldsymbol{H}_{um}\left(s\right)\boldsymbol{\eta}_{ref,um}\left(s\right)\right).\tag{3.291}$$

Inserting the control law (3.291) into (3.290) then yields

$$\begin{aligned}\dot{\boldsymbol{x}}_{\text{ref}}\left(t\right)&=\boldsymbol{A}_M\boldsymbol{x}_{\text{ref}}\left(t\right)+\boldsymbol{B}_P\cdot\boldsymbol{v}_{\text{ref}}\left(t\right)+\bar{\boldsymbol{B}}_P\boldsymbol{\eta}_{um}\left(\boldsymbol{x}_{\text{ref}}\left(t\right),t\right),\\ \boldsymbol{v}_{\text{ref}}\left(s\right)&=\boldsymbol{C}(s)\boldsymbol{K}_r\boldsymbol{r}\left(s\right)+\left(\boldsymbol{I}-\boldsymbol{C}(s)\right)\cdot\boldsymbol{\eta}_{ref,m}\left(s\right)\\ &\quad-\boldsymbol{C}(s)\boldsymbol{H}_m^{-1}\left(s\right)\boldsymbol{H}_{um}\left(s\right)\boldsymbol{\eta}_{ref,um}\left(s\right).\end{aligned}\tag{3.292}$$

By virtue of the definitions of $\boldsymbol{G}_m(s)$ in (3.182) and of $\boldsymbol{G}_{um}(s)$ in (3.259) and by assuming zero initial conditions, the $\mathcal{L}_1$ *Reference Model* may be represented entirely in the frequency-domain by:

$$\begin{aligned}\boldsymbol{x}_{\text{ref}}(s) &= \boldsymbol{G}_m(s)\cdot\boldsymbol{v}_{\text{ref}}(s) + \boldsymbol{G}_{um}(s)\,\boldsymbol{\eta}_{ref,um}(s),\\ \boldsymbol{v}_{\text{ref}}(s) &= \boldsymbol{C}(s)\boldsymbol{K}_r\boldsymbol{r}(s) + (\boldsymbol{I}-\boldsymbol{C}(s))\cdot\boldsymbol{\eta}_{ref,m}(s)\\ &\quad - \boldsymbol{C}(s)\boldsymbol{H}_m^{-1}(s)\,\boldsymbol{H}_{um}(s)\,\boldsymbol{\eta}_{ref,um}(s)\end{aligned} \tag{3.293}$$

or more compactly by

$$\begin{aligned}\boldsymbol{x}_{\text{ref}}(s) = \boldsymbol{G}_m(s)\,\boldsymbol{C}(s)\boldsymbol{K}_r\cdot\boldsymbol{r}(s) + \boldsymbol{G}_m(s)\,(\boldsymbol{I}-\boldsymbol{C}(s))\cdot\boldsymbol{\eta}_{ref,m}(s)\\ + \left(\boldsymbol{I}-\boldsymbol{G}_m(s)\,\boldsymbol{C}(s)\boldsymbol{H}_m^{-1}(s)\,\boldsymbol{C}_P\right)\cdot\boldsymbol{G}_{um}(s)\cdot\boldsymbol{\eta}_{ref,um}(s),\end{aligned} \tag{3.294}$$

where $\boldsymbol{H}_{um}(s) = \boldsymbol{C}_P\cdot\boldsymbol{G}_{um}(s)$ was used. Since $\boldsymbol{H}_m(s)$ is minimum-phase due to Assumption 3.12 and since $\boldsymbol{C}(s)$ and $\boldsymbol{C}(s)\boldsymbol{H}_m^{-1}(s)\,\boldsymbol{H}_{um}(s)$ are assumed to be causal and Hurwitz by virtue of an appropriate choice of the design parameters, the following norm inequality immediately results from the frequency-domain representation (3.294):

$$\begin{aligned}\|\boldsymbol{x}_{\text{ref}}(t)_\tau\|_{\mathcal{L}_\infty} \le\ & \|\boldsymbol{G}_m(s)\,\boldsymbol{C}(s)\boldsymbol{K}_r\|_{\mathcal{L}_1}\cdot\|\boldsymbol{r}(t)\|_{\mathcal{L}_\infty}\\ &+ \|\boldsymbol{G}_m(s)\,(\boldsymbol{I}-\boldsymbol{C}(s))\|_{\mathcal{L}_1}\cdot\|\boldsymbol{\eta}_m(\boldsymbol{x}_{\text{ref}}(t),t)_\tau\|_{\mathcal{L}_\infty}\\ &+ \|\left(\boldsymbol{I}-\boldsymbol{G}_m(s)\,\boldsymbol{C}(s)\boldsymbol{H}_m^{-1}(s)\,\boldsymbol{C}_P\right)\cdot\boldsymbol{G}_{um}(s)\|_{\mathcal{L}_1}\cdot\|\boldsymbol{\eta}_{um}(\boldsymbol{x}_{\text{ref}}(t),t)_\tau\|_{\mathcal{L}_\infty}.\end{aligned} \tag{3.295}$$

Notice that truncated norms are used since boundedness of $\boldsymbol{x}_{\text{ref}}(t)$ is not yet ensured. Due to the semi-global character of the Lipschitz condition, applying (3.287) yields a conditional bound:

$$\begin{aligned}&\|\boldsymbol{x}_{\text{ref}}(t)_\tau\|_{\mathcal{L}_\infty}\\ &\quad\le \|\boldsymbol{G}_m(s)\,\boldsymbol{C}(s)\boldsymbol{K}_r\|_{\mathcal{L}_1}\cdot\|\boldsymbol{r}(t)\|_{\mathcal{L}_\infty}\\ &\qquad+ \|\boldsymbol{G}_m(s)\,(\boldsymbol{I}-\boldsymbol{C}(s))\|_{\mathcal{L}_1}\cdot(L_m(r)\cdot\|\boldsymbol{x}_{\text{ref}}(t)_\tau\|_{\mathcal{L}_\infty}+\phi_{m,0})\\ &\qquad+ \|\left(\boldsymbol{I}-\boldsymbol{G}_m(s)\,\boldsymbol{C}(s)\boldsymbol{H}_m^{-1}(s)\,\boldsymbol{C}_P\right)\cdot\boldsymbol{G}_{um}(s)\|_{\mathcal{L}_1}\cdot L_{um}(r)\cdot\|\boldsymbol{x}_{\text{ref}}(t)_\tau\|_{\mathcal{L}_\infty}\\ &\qquad+ \|\left(\boldsymbol{I}-\boldsymbol{G}_m(s)\,\boldsymbol{C}(s)\boldsymbol{H}_m^{-1}(s)\,\boldsymbol{C}_P\right)\cdot\boldsymbol{G}_{um}(s)\|_{\mathcal{L}_1}\cdot\phi_{um,0},\end{aligned} \tag{3.296}$$

which is *only* true if $\|\boldsymbol{x}_{\text{ref}}(t)_\tau\|_{\mathcal{L}_\infty}\le r$ is satisfied. However, (3.296) does not ensure that $\|\boldsymbol{x}_{\text{ref}}(t)_\tau\|_{\infty}\le r$ does actually hold. In order to deal with this circular dependence, assume that $\|\boldsymbol{x}_{\text{ref}}(t)_\tau\|_{\mathcal{L}_\infty}<\rho_r$ holds, where $\rho_r>0$ specifies the hypercube in the state space, within which all trajectories of $\boldsymbol{x}_{\text{ref}}(t)$ will remain during the interval $t=[0,\tau]$. By defining

$$L_{m,\rho_r} \triangleq L_m(\rho_r+\bar{\gamma}_1), \tag{3.297}$$

$$L_{um,\rho_r} \triangleq L_{um}(\rho_r+\bar{\gamma}_1), \tag{3.298}$$

(3.296) becomes

$$\|\boldsymbol{x}_{\text{ref}}(t)_\tau\|_{\mathcal{L}_\infty} \le \|\boldsymbol{G}_m(s)\,\boldsymbol{C}(s)\boldsymbol{K}_r\|_{\mathcal{L}_1}\cdot\|\boldsymbol{r}(t)\|_{\mathcal{L}_\infty}$$

$$
\begin{aligned}
&+ \|\boldsymbol{G}_m(s)\left(\boldsymbol{I}-\boldsymbol{C}(s)\right)\|_{\mathcal{L}_1} \cdot \left(L_{m,\rho_r}\cdot\rho_r+\phi_{m,0}\right) \\
&+ \|\Big(\boldsymbol{I}-\boldsymbol{G}_m(s)\,\boldsymbol{C}(s)\boldsymbol{H}_m^{-1}(s)\,\boldsymbol{C}_P\Big)\cdot\boldsymbol{G}_{um}(s)\|_{\mathcal{L}_1}\cdot\left(L_{um,\rho_r}\cdot\rho_r+\phi_{um,0}\right).
\end{aligned}
\tag{3.299}
$$

Exactly as in Section 3.3.1, the Lipschitz constants are chosen to hold on a larger area of the state space than actually required due to the use of $\bar{\gamma}_1 > 0$ in the definitions (3.297) and (3.298). This choice will ensure boundedness of the error $\boldsymbol{e}_{\text{ref}}(t)$ in Step 3. For the same reason, the upper bound in (3.299) is further bounded by

$$
\begin{aligned}
\|\boldsymbol{x}_{\text{ref}}(t)_\tau\|_{\mathcal{L}_\infty} \leq\ & \|\boldsymbol{G}_m(s)\,\boldsymbol{C}(s)\boldsymbol{K}_r\|_{\mathcal{L}_1}\cdot\|\boldsymbol{r}(t)\|_{\mathcal{L}_\infty} \\
&+ \|\boldsymbol{G}_m(s)\left(\boldsymbol{I}-\boldsymbol{C}(s)\right)\|_{\mathcal{L}_1}\cdot\left(L_{m,\rho_r}\cdot\rho_r+\phi_0\right) \\
&+ \|\Big(\boldsymbol{I}-\boldsymbol{G}_m(s)\,\boldsymbol{C}(s)\boldsymbol{H}_m^{-1}(s)\,\boldsymbol{C}_P\Big)\cdot\boldsymbol{G}_{um}(s)\|_{\mathcal{L}_1}\cdot\frac{L_{um,\rho_r}}{L_{m,\rho_r}}\left(L_{m,\rho_r}\cdot\rho_r+\phi_0\right),
\end{aligned}
\tag{3.300}
$$

where

$$
\phi_0 \triangleq \max\left\{\phi_{m,0},\ \frac{L_{m,\rho_r}}{L_{um,\rho_r}}\cdot\phi_{um,0}\right\}. \tag{3.301}
$$

In order to ensure that the assumption $\|\boldsymbol{x}_{\text{ref}}(t)_\tau\|_{\mathcal{L}_\infty} < \rho_r$ holds, the upper bound in (3.300) is required to satisfy

$$
\begin{aligned}
&\|\boldsymbol{G}_m(s)\,\boldsymbol{C}(s)\boldsymbol{K}_r\|_{\mathcal{L}_1}\cdot\|\boldsymbol{r}(t)\|_{\mathcal{L}_\infty} \\
&\quad+ \|\boldsymbol{G}_m(s)\left(\boldsymbol{I}-\boldsymbol{C}(s)\right)\|_{\mathcal{L}_1}\cdot\left(L_{m,\rho_r}\cdot\rho_r+\phi_0\right) \\
&\quad+ \|\Big(\boldsymbol{I}-\boldsymbol{G}_m(s)\,\boldsymbol{C}(s)\boldsymbol{H}_m^{-1}(s)\,\boldsymbol{C}_P\Big)\cdot\boldsymbol{G}_{um}(s)\|_{\mathcal{L}_1}\cdot\frac{L_{um,\rho_r}}{L_{m,\rho_r}}\left(L_{m,\rho_r}\cdot\rho_r+\phi_0\right) < \rho_r.
\end{aligned}
\tag{3.302}
$$

Bringing the first term to the right hand side of the inequality and dividing by $L_{m,\rho_r}\cdot\rho_r+\phi_0$ yields the $\mathcal{L}_1$-norm condition

$$
\begin{aligned}
&\|\boldsymbol{G}_m(s)\left(\boldsymbol{I}-\boldsymbol{C}(s)\right)\|_{\mathcal{L}_1} + \|\Big(\boldsymbol{I}-\boldsymbol{G}_m(s)\,\boldsymbol{C}(s)\boldsymbol{H}_m^{-1}(s)\,\boldsymbol{C}_P\Big)\cdot\boldsymbol{G}_{um}(s)\|_{\mathcal{L}_1}\cdot\frac{L_{um,\rho_r}}{L_{m,\rho_r}} \\
&\quad< \frac{\rho_r - \|\boldsymbol{G}_m(s)\,\boldsymbol{C}(s)\boldsymbol{K}_r\|_{\mathcal{L}_1}\cdot\|\boldsymbol{r}(t)\|_{\mathcal{L}_\infty}}{L_{m,\rho_r}\cdot\rho_r+\phi_0}.
\end{aligned}
\tag{3.303}
$$

Since the inequality (3.303) has been derived under the assumption that $\|\boldsymbol{x}_{\text{ref}}(t)_\tau\|_{\mathcal{L}_\infty} < \rho_r$ holds, its satisfaction does obviously not yet prove $\|\boldsymbol{x}_{\text{ref}}(t)_\tau\|_{\mathcal{L}_\infty} < \rho_r$, as this would be a circular argument. However, the latter implication may be proven to be true by virtue of a proof by contradiction as shown in the following lemma:

Lemma 3.30 (Boundedness of the $\mathcal{L}_1$ *Reference Model*)**.** *Let Assumptions 3.3 (semi-global Lipschitz condition), 3.6 (full-rank $\boldsymbol{B}_P$), 3.11 (bounded uncertainties) and 3.12 (minimum-phase reference model) hold. Consider the $\mathcal{L}_1$ Reference Model*

$$
\begin{aligned}
\dot{\boldsymbol{x}}_{\textit{ref}}(t) &= \boldsymbol{A}_M\boldsymbol{x}_{\textit{ref}}(t) + \boldsymbol{B}_P\cdot\Big(\boldsymbol{\Lambda}\boldsymbol{u}_{\textit{ref}}(t) + \boldsymbol{\eta}_m\left(\boldsymbol{x}_{\textit{ref}}(t),t\right) + \bar{\boldsymbol{B}}_P\boldsymbol{\eta}_{um}\left(\boldsymbol{x}_{\textit{ref}}(t),t\right)\Big), \\
\boldsymbol{u}_{\textit{ref}}(s) &= \boldsymbol{\Lambda}^{-1}\boldsymbol{C}(s)\Big(\boldsymbol{K}_r\boldsymbol{r}(s) - \boldsymbol{\eta}_{ref,m}(s) - \boldsymbol{H}_m^{-1}(s)\,\boldsymbol{H}_{um}(s)\,\boldsymbol{\eta}_{ref,um}(s)\Big), \\
\boldsymbol{y}_{\textit{ref}}(t) &= \boldsymbol{C}_P\cdot\boldsymbol{x}_{\textit{ref}}(t).
\end{aligned}
$$

originally given in (3.284)*, and the filter from* (3.173)*, i.e.:*

$$\boldsymbol{C}(s) \triangleq (\boldsymbol{I} + \boldsymbol{\Lambda}\boldsymbol{K}\boldsymbol{D}(s))^{-1}\boldsymbol{\Lambda}\boldsymbol{K}\boldsymbol{D}(s),$$

where $\boldsymbol{K} \in \mathbb{R}^{m\times m}$ is a feedback gain and $\boldsymbol{D} : \mathbb{C} \to \mathbb{C}^{m\times m}$ is a strictly proper transfer function matrix containing an integrator. If the design parameters $\boldsymbol{K}$ and $\boldsymbol{D}(s)$ are chosen such that

1. *the filter $\boldsymbol{C}(s)$ is Hurwitz for all $\boldsymbol{\Lambda} \in \Omega_\Lambda$;*
2. *the transfer functions $\boldsymbol{C}(s)\boldsymbol{H}_m^{-1}(s)\,\boldsymbol{H}_{um}(s)$ is proper for all $\boldsymbol{\Lambda} \in \Omega_\Lambda$;*
3. *the $\mathcal{L}_1$-norm condition* (3.303) *is satisfied for some values of the design parameters $\rho_r > 0$, $\bar{\gamma}_1 > 0$ and for all $\boldsymbol{\Lambda} \in \Omega_\Lambda$, i.e.*

$$\begin{aligned}\|\boldsymbol{G}_m(s)(\boldsymbol{I} - \boldsymbol{C}(s))\|_{\mathcal{L}_1} + \|\Big(\boldsymbol{I} - \boldsymbol{G}_m(s)\boldsymbol{C}(s)\boldsymbol{H}_m^{-1}(s)\boldsymbol{C}_P\Big)\cdot\boldsymbol{G}_{um}(s)\|_{\mathcal{L}_1}\cdot\frac{L_{um,\rho_r}}{L_{m,\rho_r}}\\ < \frac{\rho_r - \|\boldsymbol{G}_m(s)\boldsymbol{C}(s)\boldsymbol{K}_r\|_{\mathcal{L}_1}\cdot\|\boldsymbol{r}(t)\|_{\mathcal{L}_\infty}}{L_{m,\rho_r}\cdot\rho_r + \phi_0} \quad \forall\ \boldsymbol{\Lambda} \in \Omega_\Lambda,\end{aligned}$$

where $\boldsymbol{G}_m(s)$, $\boldsymbol{G}_{um}(s)$, L_{m,ρ_r}, L_{um,ρ_r} and ϕ_0 have been defined in (3.182)*,* (3.259)*,* (3.297)*,* (3.298)*,* (3.301)*, respectively,*

then, for $\boldsymbol{x}_{ref}(0) = \boldsymbol{0}$, the $\mathcal{L}_1$ Reference Model is bounded and the bound is given by

$$\|\boldsymbol{x}_{ref}(t)\|_{\mathcal{L}_\infty} < \rho_r. \tag{3.304}$$

Proof. The proof of Lemma 3.30 is done by contradiction. To that end, assume that (3.304) was not true. In this case, due to $\boldsymbol{x}_{\text{ref}}(0) = \boldsymbol{0}$ and due to continuity, there must exist an interval $t \in [0, \tau]$ such that

$$\|\boldsymbol{x}_{\text{ref}}(t)\|_\infty < \rho_r \quad \forall\ t \in [0, \tau[\tag{3.305}$$

and

$$\|\boldsymbol{x}_{\text{ref}}(\tau)\|_\infty = \rho_r. \tag{3.306}$$

Hence, throughout the interval $[0, \tau]$,

$$\|\boldsymbol{x}_{\text{ref}}(t)_\tau\|_{\mathcal{L}_\infty} \leq \rho_r \tag{3.307}$$

holds. Due to (3.307) and Assumptions 3.3 (semi-global Lipschitz condition), 3.11 (bounded uncertainties) and 3.12 (minimum-phase reference model), the norm inequality (3.300) holds for $\boldsymbol{x}_{\text{ref}}(0) = \boldsymbol{0}$, that is

$$\begin{aligned}\|\boldsymbol{x}_{\text{ref}}(t)_\tau\|_{\mathcal{L}_\infty} \leq\ & \|\boldsymbol{G}_m(s)\boldsymbol{C}(s)\boldsymbol{K}_r\|_{\mathcal{L}_1}\cdot\|\boldsymbol{r}(t)\|_{\mathcal{L}_\infty}\\ &+ \|\boldsymbol{G}_m(s)(\boldsymbol{I} - \boldsymbol{C}(s))\|_{\mathcal{L}_1}\cdot(L_{m,\rho_r}\cdot\rho_r + \phi_0)\\ &+ \|\Big(\boldsymbol{I} - \boldsymbol{G}_m(s)\boldsymbol{C}(s)\boldsymbol{H}_m^{-1}(s)\boldsymbol{C}_P\Big)\cdot\boldsymbol{G}_{um}(s)\|_{\mathcal{L}_1}\cdot\frac{L_{um,\rho_r}}{L_{m,\rho_r}}(L_{m,\rho_r}\cdot\rho_r + \phi_0).\end{aligned} \tag{3.308}$$

Since the $\mathcal{L}_1$-norm condition may be restated as (3.302), whose left hand side corresponds to the upper bound in (3.308), $\|\boldsymbol{x}_{\text{ref}}(t)_\tau\|_{\mathcal{L}_\infty} < \rho_r$ follows from (3.308), which contradicts (3.306). Hence, no such instant of time τ can exist, in which (3.306) holds, which proves the bound (3.304). □

Since $\boldsymbol{C}(s)$ and $\boldsymbol{C}(s)\boldsymbol{H}_m^{-1}(s)\,\boldsymbol{H}_{um}(s)$ are proper and Hurwitz, their $\mathcal{L}_1$-norms exists. Hence, the boundedness of $\boldsymbol{x}_{\text{ref}}(t)$ immediately implies boundedness of $\boldsymbol{u}_{\text{ref}}(t)$:

$$\|\boldsymbol{u}_{\text{ref}}(t)\|_{\mathcal{L}_\infty} < \rho_{ur} \tag{3.309}$$

with

$$\begin{aligned}\rho_{ur} \triangleq\ & \|\boldsymbol{\Lambda}^{-1}\boldsymbol{C}(s)\boldsymbol{K}_r\|_{\mathcal{L}_1} \cdot \|\boldsymbol{r}(t)\|_{\mathcal{L}_\infty} + \|\boldsymbol{\Lambda}^{-1}\boldsymbol{C}(s)\|_{\mathcal{L}_1} \cdot (L_{m,\rho_r} \cdot \rho_r + \phi_{m,0}) \\ & + \|\boldsymbol{\Lambda}^{-1}\boldsymbol{C}(s)\boldsymbol{H}_m^{-1}(s)\,\boldsymbol{H}_{um}(s)\|_{\mathcal{L}_1} \cdot (L_{um,\rho_r} \cdot \rho_r + \phi_{um,0})\,.\end{aligned} \tag{3.310}$$

In case of the piecewise constant update law, bounds on the control signals are required in order to prove stability. This is because the prediction error depends on the size of the control signal, as will become evident in the next step.

Step 2: During the derivation of the piecewise constant update law, it has already been noted qualitatively that the prediction error $\boldsymbol{e}_P(iT_s)$ at the sampling instants may be rendered arbitrarily small, if the sampling time T_s is sufficiently small and if the plant state $\boldsymbol{x}_P(t)$ and the input $\boldsymbol{u}(t)$ are bounded (see (3.255)). This statement is formalized and extended to time instants between the sampling instants in the following lemma adapted from [87]:

Lemma 3.31. *Let the sampling rate T_s be chosen such that*

$$\gamma_0(T_s) < \bar{\gamma}_0 \tag{3.311}$$

holds for some given $\bar{\gamma}_0 > 0$, where the function $\gamma_0(T_s) > 0$ is defined in reference [87, Eq. 3.138]. Consider the plant in (3.15) *and the $\mathcal{L}_1$ adaptive controller defined via* (3.246)*,* (3.257)*,* (3.272)*, subject to the $\mathcal{L}_1$-norm condition in* (3.302)*. If*

$$\|\boldsymbol{x}_P(t)_\tau\|_{\mathcal{L}_\infty} \leq \rho, \qquad \|\boldsymbol{u}(t)_\tau\|_{\mathcal{L}_\infty} \leq \rho_u \tag{3.312}$$

hold from some $\rho > 0$ and $\rho_u > 0$, then

$$\|\boldsymbol{e}_P(t)_\tau\| < \bar{\gamma}_0. \tag{3.313}$$

Proof. See [87, Lemma 3.3.3]. □

Step 3: Having established boundedness of the $\mathcal{L}_1$ *Reference Model*, the boundedness of the errors $\boldsymbol{e}_{\text{ref}}(t) = \boldsymbol{x}_P(t) - \boldsymbol{x}_{\text{ref}}(t)$ and $\boldsymbol{u}(t) - \boldsymbol{u}_{\text{ref}}(t)$ is proven in order to conclude on boundedness of $\boldsymbol{x}_P(t)$ and $\boldsymbol{u}(t)$. For this purpose, norm inequalities will be derived for the errors $\boldsymbol{e}_{\text{ref}}(t)$ and $\boldsymbol{u}(t) - \boldsymbol{u}_{\text{ref}}(t)$. Upon an appropriate choice of the design

parameters of the $\mathcal{L}_1$-PWC, a proof by contradiction then establishes boundedness of these errors.

In order to derive a norm inequality for the error $\boldsymbol{e}_{\text{ref}}(t)$, notice that the plant representation (3.275) may be rewritten as

$$\begin{aligned}\dot{\boldsymbol{x}}_P(t) &= \boldsymbol{A}_M\boldsymbol{x}_P(t) + \boldsymbol{B}_P\boldsymbol{v}_P(t) + \bar{\boldsymbol{B}}_P\boldsymbol{\eta}_{um}(\boldsymbol{x}_P(t), t),\\ \boldsymbol{v}_P(s) &\triangleq \boldsymbol{\Lambda}\boldsymbol{u}(s) + \boldsymbol{\eta}_{P,m}(s).\end{aligned} \tag{3.314}$$

Inserting the control law representation (3.283) yields

$$\begin{aligned}\dot{\boldsymbol{x}}_P(t) &= \boldsymbol{A}_M\boldsymbol{x}_P(t) + \boldsymbol{B}_P\boldsymbol{v}_P(t) + \bar{\boldsymbol{B}}_P\boldsymbol{\eta}_{um}(\boldsymbol{x}_P(t), t),\\ \boldsymbol{v}_P(s) &= \boldsymbol{C}(s)\boldsymbol{K}_r\boldsymbol{r}(s) + (\boldsymbol{I} - \boldsymbol{C}(s))\cdot\boldsymbol{\eta}_{P,m}(s)\\ &\quad - \boldsymbol{C}(s)\boldsymbol{H}_m^{-1}(s)\boldsymbol{H}_{um}(s)\cdot\boldsymbol{\eta}_{P,um}(s) - \boldsymbol{C}(s)\boldsymbol{H}_m^{-1}(s)\boldsymbol{C}_P\cdot\boldsymbol{e}_P(s).\end{aligned} \tag{3.315}$$

It follows from (3.292) and (3.315) that the error $\boldsymbol{e}_{\text{ref}}(t)$ evolves according to

$$\begin{aligned}\dot{\boldsymbol{e}}_{\text{ref}}(t) &= \boldsymbol{A}_M\boldsymbol{e}_{\text{ref}}(t) + \boldsymbol{B}_P(\boldsymbol{v}_P(t) - \boldsymbol{v}_{\text{ref}}(t))\\ &\quad + \bar{\boldsymbol{B}}_P(\boldsymbol{\eta}_{um}(\boldsymbol{x}_P(t), t) - \boldsymbol{\eta}_{um}(\boldsymbol{x}_{\text{ref}}(t), t)),\\ \boldsymbol{v}_P(s) - \boldsymbol{v}_{\text{ref}}(s) &= (\boldsymbol{I} - \boldsymbol{C}(s))\cdot\Big(\boldsymbol{\eta}_{P,m}(s) - \boldsymbol{\eta}_{ref,m}(s)\Big)\\ &\quad - \boldsymbol{C}(s)\boldsymbol{H}_m^{-1}(s)\boldsymbol{H}_{um}(s)\cdot\Big(\boldsymbol{\eta}_{P,um}(s) - \boldsymbol{\eta}_{ref,um}(s)\Big)\\ &\quad - \boldsymbol{C}(s)\boldsymbol{H}_m^{-1}(s)\boldsymbol{C}_P\cdot\boldsymbol{e}_P(s).\end{aligned} \tag{3.316}$$

Assuming zero initial conditions, the error dynamics (3.316) may be compactly represented in the frequency-domain by

$$\begin{aligned}\boldsymbol{e}_{\text{ref}}(s) = &-\boldsymbol{G}_m(s)\boldsymbol{C}(s)\boldsymbol{H}_m^{-1}(s)\boldsymbol{C}_P\cdot\boldsymbol{e}_P(s)\\ &+\boldsymbol{G}_m(s)(\boldsymbol{I} - \boldsymbol{C}(s))\cdot\Big(\boldsymbol{\eta}_{P,m}(s) - \boldsymbol{\eta}_{ref,m}(s)\Big)\\ &+\Big(\boldsymbol{I} - \boldsymbol{G}_m(s)\boldsymbol{C}(s)\boldsymbol{H}_m^{-1}(s)\boldsymbol{C}_P\Big)\cdot\boldsymbol{G}_{um}(s)\cdot\Big(\boldsymbol{\eta}_{P,um}(s) - \boldsymbol{\eta}_{ref,um}(s)\Big),\end{aligned} \tag{3.317}$$

where $\boldsymbol{H}_{um}(s) = \boldsymbol{C}_P\cdot\boldsymbol{G}_{um}(s)$ was used. Since $\boldsymbol{H}_m(s)$ is minimum-phase due to Assumption 3.12 and since $\boldsymbol{C}(s)$ and $\boldsymbol{C}(s)\boldsymbol{H}_m^{-1}(s)\boldsymbol{H}_{um}(s)$ are assumed to be causal and Hurwitz by virtue of an appropriate choice of the design parameters, the following norm inequality immediately results from the frequency-domain representation (3.317):

$$\begin{aligned}\|\boldsymbol{e}_{\text{ref}}(t)_\tau\|_{\mathcal{L}_\infty} \leq &\|\boldsymbol{G}_m(s)\boldsymbol{C}(s)\boldsymbol{H}_m^{-1}(s)\boldsymbol{C}_P\|_{\mathcal{L}_1}\cdot\|\boldsymbol{e}_P(t)_\tau\|_{\mathcal{L}_\infty}\\ &+\|\boldsymbol{G}_m(s)(\boldsymbol{I} - \boldsymbol{C}(s))\|_{\mathcal{L}_1}\cdot\\ &\quad\|(\boldsymbol{\eta}_m(\boldsymbol{x}_P(t), t) - \boldsymbol{\eta}_m(\boldsymbol{x}_{\text{ref}}(t), t))_\tau\|_{\mathcal{L}_\infty}\\ &+\|\Big(\boldsymbol{I} - \boldsymbol{G}_m(s)\boldsymbol{C}(s)\boldsymbol{H}_m^{-1}(s)\boldsymbol{C}_P\Big)\cdot\boldsymbol{G}_{um}(s)\|_{\mathcal{L}_1}\cdot\\ &\quad\|(\boldsymbol{\eta}_{um}(\boldsymbol{x}_P(t), t) - \boldsymbol{\eta}_{um}(\boldsymbol{x}_{\text{ref}}(t), t))_\tau\|_{\mathcal{L}_\infty}.\end{aligned} \tag{3.318}$$

The application of the Lipschitz condition (3.285) leads to the conditional bound

$$\|\boldsymbol{e}_{\text{ref}}(t)_\tau\|_{\mathcal{L}_\infty} \leq \|\boldsymbol{G}_m(s)\boldsymbol{C}(s)\boldsymbol{H}_m^{-1}(s)\boldsymbol{C}_P\|_{\mathcal{L}_1}\cdot\|\boldsymbol{e}_P(t)_\tau\|_{\mathcal{L}_\infty}$$

$$
\begin{aligned}
&+ \|\boldsymbol{G}_m(s)(\boldsymbol{I}-\boldsymbol{C}(s))\|_{\mathcal{L}_1} \cdot L_m(r) \cdot \|\boldsymbol{e}_{\text{ref}}(t)_\tau\|_{\mathcal{L}_\infty} \\
&+ \|\Big(\boldsymbol{I}-\boldsymbol{G}_m(s)\boldsymbol{C}(s)\boldsymbol{H}_m^{-1}(s)\boldsymbol{C}_P\Big)\cdot\boldsymbol{G}_{um}(s)\|_{\mathcal{L}_1} \cdot L_{um}(r) \cdot \|\boldsymbol{e}_{\text{ref}}(t)_\tau\|_{\mathcal{L}_\infty},
\end{aligned}
\tag{3.319}
$$

which *only* holds for $\|\boldsymbol{x}_P(t)_\tau\|_{\mathcal{L}_\infty} \leq r$ and $\|\boldsymbol{x}_{\text{ref}}(t)_\tau\|_{\mathcal{L}_\infty} \leq r$. However, as no bound is known for $\boldsymbol{x}_P(t)$, no suitable value for r is known either. In order to resolve this issue, assume that

$$
\begin{aligned}
\|\boldsymbol{e}_{\text{ref}}(t)_\tau\|_{\mathcal{L}_\infty} &< \bar{\gamma}_1, \\
\|\boldsymbol{u}(t)-\boldsymbol{u}_{\text{ref}}(t)\|_{\mathcal{L}_\infty} &< \gamma_u
\end{aligned}
\tag{3.320}
$$

were known to hold, and let Lemma 3.30 be satisfied for that $\bar{\gamma}_1$. The satisfaction of Lemma 3.30 implies boundedness of $\boldsymbol{x}_{\text{ref}}(t)$ and $\boldsymbol{u}_{\text{ref}}(t)$ with the bounds $\|\boldsymbol{x}_{\text{ref}}(t)_\tau\|_{\mathcal{L}_\infty} < \rho_r$ and $\|\boldsymbol{u}_{\text{ref}}(t)_\tau\|_{\mathcal{L}_\infty} < \rho_{ur}$ (see (3.309)). By virtue of the triangle inequality, one obtains bounds for $\boldsymbol{x}_P(t)$ and $\boldsymbol{u}_{\text{ref}}(t)$:

$$
\begin{aligned}
\|\boldsymbol{x}_P(t)_\tau\|_{\mathcal{L}_\infty} &\leq \|\boldsymbol{e}_{\text{ref}}(t)_\tau\|_{\mathcal{L}_\infty} + \|\boldsymbol{x}_{\text{ref}}(t)_\tau\|_{\mathcal{L}_\infty} < \bar{\gamma}_1 + \rho_r, \\
\|\boldsymbol{u}(t)\|_{\mathcal{L}_\infty} &\leq \|\boldsymbol{u}(t)-\boldsymbol{u}_{\text{ref}}(t)\|_{\mathcal{L}_\infty} + \|\boldsymbol{u}_{\text{ref}}(t)\|_{\mathcal{L}_\infty} < \gamma_u + \rho_{ur}.
\end{aligned}
\tag{3.321}
$$

Under the foregoing assumptions, a suitable Lipschitz constant may be chosen, which results for $r = \bar{\gamma}_1 + \rho_r$. Using the definitions of L_{m,ρ_r} in (3.297) and of L_{um,ρ_r} in (3.298), (3.319) becomes

$$
\begin{aligned}
\|\boldsymbol{e}_{\text{ref}}(t)_\tau\|_{\mathcal{L}_\infty} \leq\ & \|\boldsymbol{G}_m(s)\boldsymbol{C}(s)\boldsymbol{H}_m^{-1}(s)\boldsymbol{C}_P\|_{\mathcal{L}_1} \cdot \|\boldsymbol{e}_P(t)_\tau\|_{\mathcal{L}_\infty} \\
&+ \|\boldsymbol{G}_m(s)(\boldsymbol{I}-\boldsymbol{C}(s))\|_{\mathcal{L}_1} \cdot L_{m,\rho_r} \cdot \|\boldsymbol{e}_{\text{ref}}(t)_\tau\|_{\mathcal{L}_\infty} \\
&+ \|\Big(\boldsymbol{I}-\boldsymbol{G}_m(s)\boldsymbol{C}(s)\boldsymbol{H}_m^{-1}(s)\boldsymbol{C}_P\Big)\cdot\boldsymbol{G}_{um}(s)\|_{\mathcal{L}_1} \cdot L_{um,\rho_r} \cdot \|\boldsymbol{e}_{\text{ref}}(t)_\tau\|_{\mathcal{L}_\infty},
\end{aligned}
\tag{3.322}
$$

which holds for $\|\boldsymbol{x}_P(t)_\tau\|_{\mathcal{L}_\infty} < \rho_r + \bar{\gamma}_1$ and $\|\boldsymbol{x}_{\text{ref}}(t)_\tau\|_{\mathcal{L}_\infty} < \rho_r < \rho_r + \bar{\gamma}_1$. Solving for $\|\boldsymbol{e}_{\text{ref}}(t)_\tau\|_{\mathcal{L}_\infty}$ yields

$$
\begin{aligned}
&\|\boldsymbol{e}_{\text{ref}}(t)_\tau\|_{\mathcal{L}_\infty} \\
&\quad\leq \frac{\|\boldsymbol{G}_m(s)\boldsymbol{C}(s)\boldsymbol{H}_m^{-1}(s)\boldsymbol{C}_P\|_{\mathcal{L}_1} \cdot \|\boldsymbol{e}_P(t)_\tau\|_{\mathcal{L}_\infty}}{1-\|\boldsymbol{G}_m(s)(\boldsymbol{I}-\boldsymbol{C}(s))\|_{\mathcal{L}_1} \cdot L_{m,\rho_r} - \|\Big(\boldsymbol{I}-\boldsymbol{G}_m(s)\boldsymbol{C}(s)\boldsymbol{H}_m^{-1}(s)\boldsymbol{C}_P\Big)\cdot\boldsymbol{G}_{um}(s)\|_{\mathcal{L}_1} \cdot L_{um,\rho_r}}.
\end{aligned}
\tag{3.323}
$$

In order to obtain an upper bound from (3.323), the denominator of the right hand side of (3.323) must be positive. To that end, notice that the $\mathcal{L}_1$-norm condition of Lemma 3.30 implies

$$
\begin{aligned}
&\|\boldsymbol{G}_m(s)(\boldsymbol{I}-\boldsymbol{C}(s))\|_{\mathcal{L}_1} \cdot L_{m,\rho_r} + \Big\|\Big(\boldsymbol{I}-\boldsymbol{G}_m(s)\boldsymbol{C}(s)\boldsymbol{H}_m^{-1}(s)\boldsymbol{C}_P\Big)\cdot\boldsymbol{G}_{um}(s)\Big\|_{\mathcal{L}_1} \cdot L_{um,\rho_r} \\
&\quad< L_{m,\rho_r} \cdot \frac{\rho_r - \|\boldsymbol{G}_m(s)\boldsymbol{C}(s)\boldsymbol{K}_r\|_{\mathcal{L}_1} \cdot \|\boldsymbol{r}(t)\|_{\mathcal{L}_\infty}}{L_{m,\rho_r}\cdot\rho_r + \phi_0} \\
&\quad= \underbrace{\frac{L_{m,\rho_r}\cdot\rho_r}{L_{m,\rho_r}\cdot\rho_r+\phi_0}}_{\leq 1} - \underbrace{\frac{L_{m,\rho_r}\cdot\|\boldsymbol{G}_m(s)\boldsymbol{C}(s)\boldsymbol{K}_r\|_{\mathcal{L}_1}\cdot\|\boldsymbol{r}(t)\|_{\mathcal{L}_\infty}}{L_{m,\rho_r}\cdot\rho_r+\phi_0}}_{\geq 0} \leq 1.
\end{aligned}
$$

Hence, (3.323) does actually yield a finite upper bound, which depends on the size of the prediction error $\boldsymbol{e}_P(t)$. Due to the assumption of bounded errors in (3.320) and the

triangle inequalities in (3.321), $\boldsymbol{x}_P(t)$ and $\boldsymbol{u}(t)$ are bounded. Thus, one may invoke Lemma 3.31 to conclude that $\|\boldsymbol{e}_P(t)_\tau\| < \bar{\gamma}_0$ holds, where $\bar{\gamma}_0$ is the desired bound on the prediction error $\boldsymbol{e}_P(t)$. Hence,

$$\|\boldsymbol{e}_{\text{ref}}(t)_\tau\| \leq \gamma_1 \tag{3.324}$$

with

$$\gamma_1 \triangleq \frac{\|\boldsymbol{G}_m(s)\boldsymbol{C}(s)\boldsymbol{H}_m^{-1}(s)\boldsymbol{C}_P\|_{\mathcal{L}_1} \cdot \bar{\gamma}_0}{1 - \|\boldsymbol{G}_m(s)(\boldsymbol{I} - \boldsymbol{C}(s))\|_{\mathcal{L}_1} \cdot L_{m,\rho_r} - \|\big(\boldsymbol{I} - \boldsymbol{G}_m(s)\boldsymbol{C}(s)\boldsymbol{H}_m^{-1}(s)\boldsymbol{C}_P\big) \cdot \boldsymbol{G}_{um}(s)\|_{\mathcal{L}_1} \cdot L_{um,\rho_r}} \tag{3.325}$$

follows from (3.323).

Next, a norm inequality for the error $\boldsymbol{u}(t) - \boldsymbol{u}_{\text{ref}}(t)$ is derived by noticing that subtracting (3.291) from (3.283) yields

$$\begin{aligned} \boldsymbol{u}(s) - \boldsymbol{u}_{\text{ref}}(s) = & -\boldsymbol{\Lambda}^{-1}\boldsymbol{C}(s) \cdot \Big(\boldsymbol{\eta}_{P,m}(s) - \boldsymbol{\eta}_{ref,m}(s)\Big) \\ & -\boldsymbol{\Lambda}^{-1}\boldsymbol{C}(s)\boldsymbol{H}_m^{-1}(s)\boldsymbol{H}_{um}(s) \cdot \Big(\boldsymbol{\eta}_{P,um}(s) - \boldsymbol{\eta}_{ref,um}(s)\Big) \\ & -\boldsymbol{\Lambda}^{-1}\boldsymbol{C}(s)\boldsymbol{H}_m^{-1}(s)\boldsymbol{C}_P \cdot \boldsymbol{e}_P(s). \end{aligned} \tag{3.326}$$

Consequently, the following norm inequality holds

$$\begin{aligned} \|(\boldsymbol{u}(t) - \boldsymbol{u}_{\text{ref}}(t))_\tau\|_{\mathcal{L}_\infty} \leq & \|\boldsymbol{\Lambda}^{-1}\boldsymbol{C}(s)\|_{\mathcal{L}_1} \cdot \|(\boldsymbol{\eta}_m(\boldsymbol{x}_P(t), t) - \boldsymbol{\eta}_m(\boldsymbol{x}_{\text{ref}}(t), t))_\tau\|_{\mathcal{L}_\infty} \\ & + \|\boldsymbol{\Lambda}^{-1}\boldsymbol{C}(s)\boldsymbol{H}_m^{-1}(s)\boldsymbol{H}_{um}(s)\|_{\mathcal{L}_1} \cdot \\ & \quad \|(\boldsymbol{\eta}_{um}(\boldsymbol{x}_P(t), t) - \boldsymbol{\eta}_{um}(\boldsymbol{x}_{\text{ref}}(t), t))_\tau\|_{\mathcal{L}_\infty} \\ & + \|\boldsymbol{\Lambda}^{-1}\boldsymbol{C}(s)\boldsymbol{H}_m^{-1}(s)\boldsymbol{C}_P\|_{\mathcal{L}_1} \cdot \|\boldsymbol{e}_P(t)_\tau\|_{\mathcal{L}_\infty}. \end{aligned} \tag{3.327}$$

Due to the assumption of $\|\boldsymbol{e}_{\text{ref}}(t)_\tau\|_{\mathcal{L}_\infty} < \bar{\gamma}_1$, the application of the Lipschitz condition (3.285) yields:

$$\begin{aligned} \|(\boldsymbol{u}(t) - \boldsymbol{u}_{\text{ref}}(t))_\tau\|_{\mathcal{L}_\infty} < & \|\boldsymbol{\Lambda}^{-1}\boldsymbol{C}(s)\|_{\mathcal{L}_1} \cdot L_{m,\rho_r} \cdot \bar{\gamma}_1 \\ & + \|\boldsymbol{\Lambda}^{-1}\boldsymbol{C}(s)\boldsymbol{H}_m^{-1}(s)\boldsymbol{H}_{um}(s)\|_{\mathcal{L}_1} \cdot L_{um,\rho_r} \cdot \bar{\gamma}_1 \\ & + \|\boldsymbol{\Lambda}^{-1}\boldsymbol{C}(s)\boldsymbol{H}_m^{-1}(s)\boldsymbol{C}_P\|_{\mathcal{L}_1} \cdot \|\boldsymbol{e}_P(t)_\tau\|_{\mathcal{L}_\infty}. \end{aligned} \tag{3.328}$$

Since the assumption of bounded errors in (3.320) implies $\|\boldsymbol{e}_P(t)_\tau\| < \bar{\gamma}_0$ due to Lemma 3.31, the norm inequalities

$$\|\boldsymbol{e}_{\text{ref}}(t)_\tau\| \leq \gamma_1, \tag{3.329}$$

$$\|(\boldsymbol{u}(t) - \boldsymbol{u}_{\text{ref}}(t))_\tau\|_{\mathcal{L}_\infty} < \gamma_u \tag{3.330}$$

with

$$\begin{aligned} \gamma_u \triangleq & \|\boldsymbol{\Lambda}^{-1}\boldsymbol{C}(s)\|_{\mathcal{L}_1} \cdot L_{m,\rho_r} \cdot \bar{\gamma}_1 \\ & + \|\boldsymbol{\Lambda}^{-1}\boldsymbol{C}(s)\boldsymbol{H}_m^{-1}(s)\boldsymbol{H}_{um}(s)\|_{\mathcal{L}_1} \cdot L_{um,\rho_r} \cdot \bar{\gamma}_1 \\ & + \|\boldsymbol{\Lambda}^{-1}\boldsymbol{C}(s)\boldsymbol{H}_m^{-1}(s)\boldsymbol{C}_P\|_{\mathcal{L}_1} \cdot \bar{\gamma}_0 \end{aligned} \tag{3.331}$$

follow from (3.324) and (3.328). Notice that the bound γ_1 may be arbitrarily decreased by decreasing the bound $\bar{\gamma}_0$, that is, by decreasing the sampling rate T_s. Thus, the sampling rate T_s may also be chosen such that $\|\boldsymbol{e}_{\text{ref}}(t)_\tau\|_{\mathcal{L}_\infty}$ is slightly smaller than $\bar{\gamma}_1$, i.e. $\gamma_1 = \bar{\gamma}_1 - \beta$, where $\beta > 0$ is an arbitrary constant satisfying $\bar{\gamma}_1 - \beta > 0$. With this choice, the original assumption $\|\boldsymbol{e}_{\text{ref}}(t)_\tau\|_{\mathcal{L}_\infty} < \bar{\gamma}_1$, which still is not proven, is slightly strengthened. As shown in the next lemma, this strengthened condition allows to construct a contradiction in order to prove that $\|\boldsymbol{e}_{\text{ref}}(t)_\tau\|_{\mathcal{L}_\infty} < \bar{\gamma}_1$ holds uniformly for all τ.

Lemma 3.32 (Boundedness of the error $\boldsymbol{e}_{\text{ref}}(t) = \boldsymbol{x}_P(t) - \boldsymbol{x}_{\text{ref}}(t)$)**.** *Consider the plant representation* (3.275)*, the $\mathcal{L}_1$ Reference Model* (3.284) *and the $\mathcal{L}_1$ adaptive controller defined by* (3.246)*,* (3.257) *and* (3.272)*. If*

1. *the conditions of Lemma 3.30 hold for some freely chosen design parameter $\bar{\gamma}_1 = \gamma_1 + \beta > 0$, where $\beta > 0$ is an arbitrary small constant;*
2. *the sampling rate T_s is chosen such that Lemma 3.31 holds for*
   - *$\bar{\gamma}_0 > 0$, which is the solution of the equation* (3.325)*;*
   - *$\rho = \bar{\gamma}_1 + \rho_r$, where $\bar{\gamma}_1$ is a freely chosen design parameter and ρ_r results from Lemma 3.30;*
   - *$\rho_u = \gamma_u + \rho_{ur}$, where γ_u and ρ_{ur} are defined in* (3.331) *and* (3.310)*, which are functions of the other design parameters and constants;*
3. *the initial conditions of all states are zero,*

then

1. *the error $\boldsymbol{e}_{ref}(t) = \boldsymbol{x}_P(t) - \boldsymbol{x}_{ref}(t)$ between the plant* (3.275) *and the $\mathcal{L}_1$ Reference Model* (3.284) *is bounded by*

$$\|\boldsymbol{e}_{ref}(t)|_{\mathcal{L}_\infty} < \bar{\gamma}_1; \tag{3.332}$$

2. *the error $\boldsymbol{u}(t) - \boldsymbol{u}_{ref}(t)$ is bounded by*

$$\|\boldsymbol{u}(t) - \boldsymbol{u}_{ref}(t)\|_{\mathcal{L}_\infty} < \gamma_u, \tag{3.333}$$

   where γ_u is defined in (3.331)*.*

Proof. Lemma 3.32 is proven by contradiction. To that end, assume that one or both of the bounds (3.332), (3.333) would not hold. In this case, due to $\boldsymbol{e}_{\text{ref}}(0) = \boldsymbol{0}$, $\boldsymbol{u}(0) = \boldsymbol{0}$, $\boldsymbol{u}_{\text{ref}}(0) = \boldsymbol{0}$ and due to continuity, there must exist an interval $t \in [0, \tau]$ such that

$$\begin{aligned} \|\boldsymbol{e}_{\text{ref}}(t)\|_\infty &< \bar{\gamma}_1 \quad \forall\, t \in [0, \tau[\\ \|\boldsymbol{u}(t) - \boldsymbol{u}_{\text{ref}}(t)\|_{\mathcal{L}_\infty} &< \gamma_u \quad \forall\, t \in [0, \tau[\end{aligned} \tag{3.334}$$

and either

$$\|\boldsymbol{e}_{\text{ref}}(\tau)\|_\infty = \bar{\gamma}_1. \tag{3.335}$$

or

$$\|\boldsymbol{u}(\tau) - \boldsymbol{u}_{\text{ref}}(\tau)\|_\infty = \gamma_u. \tag{3.336}$$

or both hold. Hence, throughout the interval $[0, \tau]$,

$$\begin{aligned} \|\boldsymbol{e}_{\text{ref}}(t)_\tau\|_{\mathcal{L}_\infty} &\leq \bar{\gamma}_1, \\ (\|(\boldsymbol{u}(t) - \boldsymbol{u}_{\text{ref}}(t))_\tau\|_{\mathcal{L}_\infty} &\leq \gamma_u \end{aligned} \tag{3.337}$$

holds. Since Lemma 3.30 holds, the triangle inequality and (3.309) imply

$$\begin{aligned} \|\boldsymbol{x}_P(t)_\tau\|_{\mathcal{L}_\infty} &\leq \|\boldsymbol{x}_{\text{ref}}(t)_\tau\|_{\mathcal{L}_\infty} + \|\boldsymbol{e}_{\text{ref}}(t)_\tau\|_{\mathcal{L}_\infty} < \rho_r + \bar{\gamma}_1, \\ \|\boldsymbol{u}(t)_\tau\| &\leq \|\boldsymbol{u}_{\text{ref}}(t)_\tau\|_{\mathcal{L}_\infty} + (\|(\boldsymbol{u}(t) - \boldsymbol{u}_{\text{ref}}(t))_\tau\|_{\mathcal{L}_\infty} < \rho_{ur} + \gamma_u. \end{aligned} \tag{3.338}$$

Thus, throughout the interval, $\|\boldsymbol{x}_P(t)_\tau\|_{\mathcal{L}_\infty} < \rho_r + \bar{\gamma}_1$ and $\|\boldsymbol{x}_{\text{ref}}(t)_\tau\|_{\mathcal{L}_\infty} < \rho_r < \rho_r + \bar{\gamma}_1$ hold. Consequently, the semi-global Lipschitz condition (3.285) holds throughout the interval with $r = \rho_r + \bar{\gamma}_1$. Hence, the norm inequality (3.323) holds throughout the interval, that is

$$\|\boldsymbol{e}_{\text{ref}}(t)_\tau\|_{\mathcal{L}_\infty} \leq \frac{\|\boldsymbol{G}_m(s)\boldsymbol{C}(s)\boldsymbol{H}_m^{-1}(s)\boldsymbol{C}_P\|_{\mathcal{L}_1} \cdot \|\boldsymbol{e}_P(t)_\tau\|_{\mathcal{L}_\infty}}{1 - \|\boldsymbol{G}_m(s)(\boldsymbol{I} - \boldsymbol{C}(s))\|_{\mathcal{L}_1} \cdot L_{m,\rho_r} - \|\left(\boldsymbol{I} - \boldsymbol{G}_m(s)\boldsymbol{C}(s)\boldsymbol{H}_m^{-1}(s)\boldsymbol{C}_P\right) \cdot \boldsymbol{G}_{um}(s)\|_{\mathcal{L}_1} \cdot L_{um,\rho_r}}.$$

Due to (3.338) and the choice of the sampling rate T_s, Lemma 3.31 implies that the prediction error bound $\|\boldsymbol{e}_P(t)_\tau\|_{\mathcal{L}_\infty} < \bar{\gamma}_0$ holds. With the definition of γ_1 in (3.325), this implies

$$\|\boldsymbol{e}_{\text{ref}}(t)_\tau\|_{\mathcal{L}_\infty} < \gamma_1 = \bar{\gamma}_1 - \beta < \bar{\gamma}_1, \tag{3.339}$$

which contradicts (3.335).

Similarly, the non-strict norm inequality

$$\begin{aligned} \|(\boldsymbol{u}(t) - \boldsymbol{u}_{\text{ref}}(t))_\tau\|_{\mathcal{L}_\infty} \leq\ & \|\boldsymbol{\Lambda}^{-1}\boldsymbol{C}(s)\|_{\mathcal{L}_1} \cdot L_{m,\rho_r} \cdot \|\boldsymbol{e}_{\text{ref}}(t)_\tau\|_{\mathcal{L}_\infty} \\ &+ \|\boldsymbol{\Lambda}^{-1}\boldsymbol{C}(s)\boldsymbol{H}_m^{-1}(s)\boldsymbol{H}_{um}(s)\|_{\mathcal{L}_1} \cdot L_{um,\rho_r} \cdot \|\boldsymbol{e}_{\text{ref}}(t)_\tau\|_{\mathcal{L}_\infty} \\ &+ \|\boldsymbol{\Lambda}^{-1}\boldsymbol{C}(s)\boldsymbol{H}_m^{-1}(s)\boldsymbol{C}_P\|_{\mathcal{L}_1} \cdot \|\boldsymbol{e}_P(t)_\tau\|_{\mathcal{L}_\infty}, \end{aligned}$$

follows from (3.327). With Lemma 3.31 and (3.339), one obtains the strict inequality

$$\begin{aligned} \|(\boldsymbol{u}(t) - \boldsymbol{u}_{\text{ref}}(t))_\tau\|_{\mathcal{L}_\infty} <\ & \|\boldsymbol{\Lambda}^{-1}\boldsymbol{C}(s)\|_{\mathcal{L}_1} \cdot L_{m,\rho_r} \cdot \gamma_1 \\ &+ \|\boldsymbol{\Lambda}^{-1}\boldsymbol{C}(s)\boldsymbol{H}_m^{-1}(s)\boldsymbol{H}_{um}(s)\|_{\mathcal{L}_1} \cdot L_{um,\rho_r} \cdot \gamma_1 \\ &+ \|\boldsymbol{\Lambda}^{-1}\boldsymbol{C}(s)\boldsymbol{H}_m^{-1}(s)\boldsymbol{C}_P\|_{\mathcal{L}_1} \cdot \bar{\gamma}_0. \end{aligned} \tag{3.340}$$

The definitions of γ_u in (3.331) and of $\gamma_1 = \bar{\gamma}_1 - \beta$ lead to

$$\begin{aligned} \|(\boldsymbol{u}(t) - \boldsymbol{u}_{\text{ref}}(t))_\tau\|_{\mathcal{L}_\infty} <\ & \gamma_u - \|\boldsymbol{\Lambda}^{-1}\boldsymbol{C}(s)\|_{\mathcal{L}_1} \cdot L_{m,\rho_r} \cdot \beta \\ &- \|\boldsymbol{\Lambda}^{-1}\boldsymbol{C}(s)\boldsymbol{H}_m^{-1}(s)\boldsymbol{H}_{um}(s)\|_{\mathcal{L}_1} \cdot L_{um,\rho_r} \cdot \beta < \gamma_u, \end{aligned} \tag{3.341}$$

which contradicts (3.336). Hence, due to (3.339) and (3.341), no such instant of time τ can exist, in which (3.335) or (3.336) hold, which proves the bounds (3.332) and (3.333). □

Step 4: With Lemmas 3.30 (bounded $\mathcal{L}_1$ *Reference Model*), 3.31 (bounded prediction error $\boldsymbol{e}_P(t)$) and 3.32 (bounded error $\boldsymbol{e}_{\text{ref}}(t)$), the following theorem results:

Theorem 3.33 (Nominal Stability of $\mathcal{L}_1$ Adaptive Control with Piecewise Constant Update Law)**.** *Consider the plant* (3.1) *and let Assumptions 3.1 (state feedback), 3.2 (positive definite control effectiveness), 3.3 (semi-global Lipschitz condition), 3.6 (full-rank $\boldsymbol{B}_P$), 3.11 (bounded uncertainties) and 3.12 (minimum-phase reference model) hold. If the design parameters T_s, $\boldsymbol{K}$ and $\boldsymbol{D}(s)$ of the $\mathcal{L}_1$ Adaptive Controller*

$$\begin{aligned}\dot{\hat{\boldsymbol{x}}}_P(t) &= \boldsymbol{A}_M\hat{\boldsymbol{x}}_P(t) + \boldsymbol{B}_P\cdot(\boldsymbol{u}(t) + \hat{\boldsymbol{\sigma}}_m(t)) + \bar{\boldsymbol{B}}_P\hat{\boldsymbol{\sigma}}_{um}(t),\\ \begin{bmatrix}\hat{\boldsymbol{\sigma}}_m(iT_s)\\ \hat{\boldsymbol{\sigma}}_{um}(iT_s)\end{bmatrix} &= -\boldsymbol{B}^{-1}\left(e^{\boldsymbol{A}_M T_s} - \boldsymbol{I}\right)^{-1}\boldsymbol{A}_M\cdot e^{\boldsymbol{A}_M\cdot T_s}\cdot\boldsymbol{e}_P(iT_s),\\ \boldsymbol{u}(s) &= \boldsymbol{C}_m(s)\left(\boldsymbol{K}_r\boldsymbol{r}(t) - \hat{\boldsymbol{\sigma}}_m(s) - \boldsymbol{H}_m^{-1}(s)\boldsymbol{H}_{um}(s)\hat{\boldsymbol{\sigma}}_{um}(s)\right)\end{aligned}$$

and the initial conditions are chosen to satisfy the conditions of Lemma 3.30, Lemma 3.31 and Lemma 3.32, then all closed-loop signals are bounded. Furthermore, the states $\boldsymbol{x}_P(t)$ of the plant will track the states $\boldsymbol{x}_{\text{ref}}(t)$ of the $\mathcal{L}_1$ Reference Model (3.284)*, which by itself approximately tracks the outputs $\boldsymbol{y}_M(t)$ of the reference model* (3.4)*. The error between the states $\boldsymbol{x}_P(t)$ of the plant and the states $\boldsymbol{x}_{\text{ref}}(t)$ of the $\mathcal{L}_1$ Reference Model and the error between the outputs $\boldsymbol{y}_{\text{ref}}(t)$ of the $\mathcal{L}_1$ Reference Model and the outputs $\boldsymbol{y}_M(t)$ of the reference model* (3.4) *may be arbitrarily decreased.*

Proof. Due to Lemma 3.30, the $\mathcal{L}_1$ *Reference Model* is bounded, implying boundedness of $\boldsymbol{x}_{\text{ref}}(t)$ and $\boldsymbol{u}_{\text{ref}}(t)$. It follows from Lemma 3.32 that the errors $\boldsymbol{e}_{\text{ref}}(t) = \boldsymbol{x}_P(t) - \boldsymbol{x}_{\text{ref}}(t)$ and $\boldsymbol{u}(t) - \boldsymbol{u}_{\text{ref}}(t)$ are bounded. Hence, the plant state $\boldsymbol{x}_P(t)$ and the control signal $\boldsymbol{u}(t)$ are bounded. Invoking Lemma 3.31 then shows that the prediction error $\boldsymbol{e}_P(t) = \hat{\boldsymbol{x}}_P(t) - \boldsymbol{x}_P(t)$ is bounded, which implies boundedness of the predictor state $\hat{\boldsymbol{x}}_P(t)$. Thus, all closed-loop signals are bounded. □

The following example demonstrates the application of $\mathcal{L}_1$-PWC:

Example 3.34. *Consider the same reference model as in Example 3.6. In contrast to Example 3.6, $\lambda_{Z\alpha} = \lambda_{Zq} = 1$ are* no longer assumed*. Hence, the system matrix of the plant is given by*

$$\boldsymbol{A}_P = \begin{bmatrix}\lambda_{Z\alpha}\cdot Z_\alpha & 1 + \lambda_{Zq}\cdot Z_q\\ \lambda_\alpha\cdot M_\alpha & \lambda_q\cdot M_q\end{bmatrix}. \tag{3.342}$$

This alternative definition admits the introduction of unmatched uncertainties by virtue of the coefficients $\lambda_{Z\alpha}$ and λ_{Zq}, whose uncertainty ranges are given in Table 2.4. Apart from this difference, the plant is equivalently defined as in Example 3.6. The transfer functions $H_m(s)$ and $H_{um}(s)$ are given by

$$H_m(s) = \frac{-19.52}{s^2 + 4.384s + 9.61}, \tag{3.343}$$

$$H_{um}(s) = \frac{s + 1.967}{s^2 + 4.384s + 9.61}. \tag{3.344}$$

Clearly, $H_m(s)$ is minimum-phase and hence, satisfies Assumption 3.12. The remaining assumptions of Theorem 3.33 can also be verified easily. If the input matrix for unmatched uncertainties $\bar{\boldsymbol{B}}_P$ is chosen as $\bar{\boldsymbol{B}}_P^T = \begin{bmatrix} 1 & 0 \end{bmatrix}$, it follows from (3.14) *that the values of the true parameters $\boldsymbol{\Theta}_{m,x}^* \triangleq \left[\, \Theta_{m,\alpha}^* \;\; \Theta_{m,q}^* \,\right]$ and $\boldsymbol{\Theta}_{um,x}^* \triangleq \left[\, \Theta_{um,\alpha}^* \;\; \Theta_{um,q}^* \,\right]$ are given by*

$$\Theta_{m,\alpha}^* = \frac{M_\alpha \cdot \lambda_\alpha - M_{\alpha,des}}{M_\eta}, \qquad \Theta_{m,q}^* = \frac{M_q \cdot \lambda_q - M_{q,des}}{M_\eta}, \tag{3.345}$$

$$\Theta_{um,\alpha}^* = Z_\alpha \cdot \lambda_{Z\alpha} - Z_\alpha, \qquad \Theta_{um,q}^* = Z_q \cdot \lambda_{Zq} - Z_q. \tag{3.346}$$

The above plant is to be controlled by a $\mathcal{L}_1$-PWC, given by the predictor (3.246)*, the update law* (3.257) *and the control law* (3.272)*. The sample rate T_s, which determines the speed of adaptation, is selected as $T_s = 0.01\,s$. The filter $C_m(s)$ is chosen as*

$$C_m(s) = \frac{\omega_0^2}{s^2 + 2\zeta\omega_0 \cdot s + \omega_0^2}, \tag{3.347}$$

where the damping $\zeta = 0.5$ is fixed, whereas $\omega_0 > 0$ scales the bandwidth of the filter.

Figure 3.12 compares the performance of the $\mathcal{L}_1$-PWC for different bandwidths ω_0 of the low-pass filter $C_m(s)$. Despite the presence of unmatched uncertainties, the $\mathcal{L}_1$-PWC tracks the reference model (3.4)*. As in case of $\mathcal{L}_1$-AC with Integral Update Law, the filter bandwidth ω_0 is the crucial parameter, which determines how close the $\mathcal{L}_1$-PWC tracks the reference model* (3.4)*.*

With respect to the estimation of the uncertainty signals $\sigma_m(t)$ and $\sigma_{um}(t)$, one may observe that the estimate $\hat{\sigma}_m(t)$ closely tracks the matched uncertainty signal $\sigma_m(t)$ in all cases. At the same time, the estimate $\hat{\sigma}_{um}(t)$ displays a significant offset from the unmatched uncertainty signal $\sigma_{um}(t)$. This offset may be reduced by decreasing the sample rate T_s for example to $T_s = 0.001\,s$. Since further simulations reveal that the offset does not deteriorate the tracking performance in case of the considered uncertainties, such a high sample rate is however not required in practice.

3.3.3 Limiting Behavior and Hedging

Even though the $\mathcal{L}_1$ *Reference Model* is not implemented within the controller, it constitutes a central element of the $\mathcal{L}_1$-AC architecture. It reflects the closed-loop performance, which may be expected from the $\mathcal{L}_1$-AC, if the uncertainties are only compensated within the bandwidth of a filter. By an appropriate design of the filter parameters $\boldsymbol{K}$ and $\boldsymbol{D}(s)$, the critical trade-off between robustness and performance can be resolved. While a fast filter may render the $\mathcal{L}_1$ *Reference Model* arbitrarily close to the reference model (3.4), it will lead to a design of little robustness, for example with respect to time-delay. Conversely, a design based on a slow filter will be robust to larger

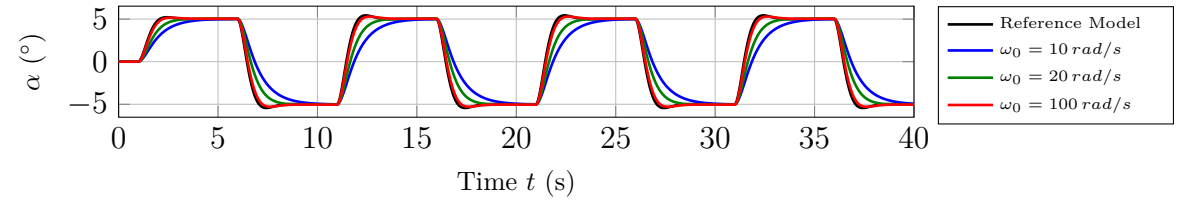

(a) Angle-Of-Attack α

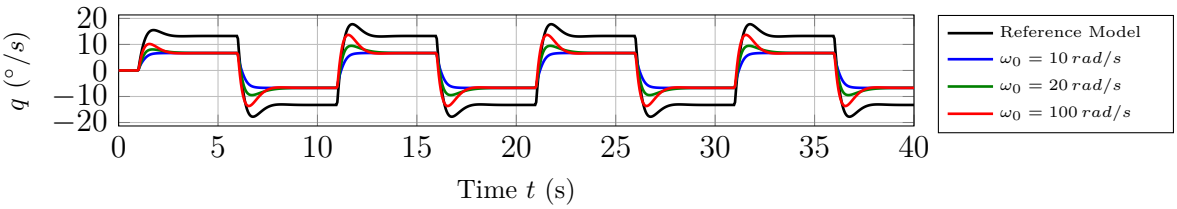

(b) Pitch Rate q

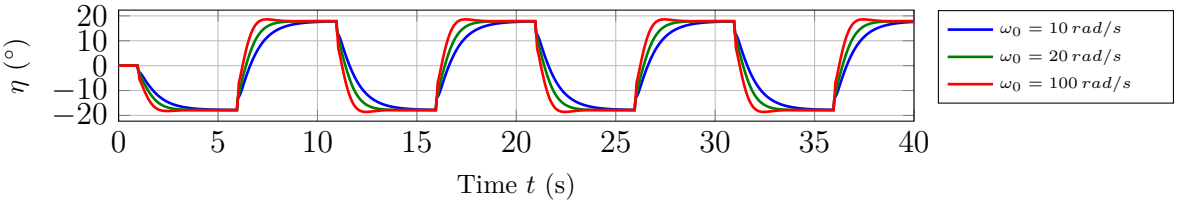

(c) Elevator Deflection η

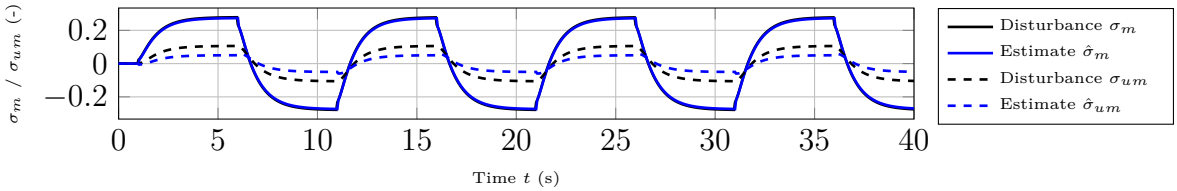

(d) Uncertainty Estimation for $\omega_0 = 10\,rad/s$

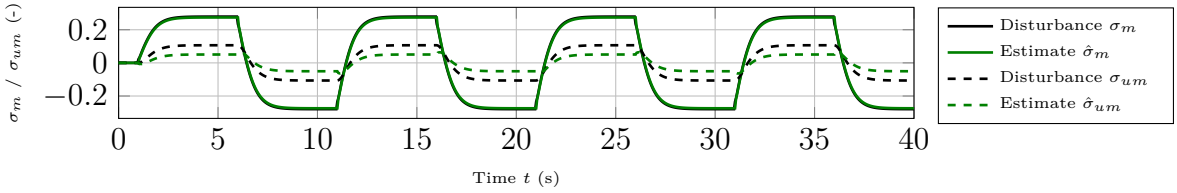

(e) Uncertainty Estimation for $\omega_0 = 20\,rad/s$

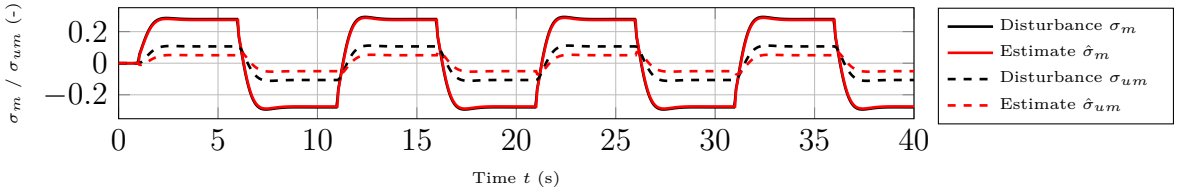

(f) Uncertainty Estimation for $\omega_0 = 100\,rad/s$

Figure 3.12: Performance of the $\mathcal{L}_1$-PWC from Example 3.34 for different values of the filter bandwidth ω_0 in case of $\lambda_\alpha = \lambda_q = \lambda_{Zq} = 1$ and $\lambda_{Z\alpha} = \lambda_\eta = 0.5$.

time-delays at the expense of a less precise tracking of the reference model (3.4). If an appropriate trade-off has been determined, the parameters of the adaptation may be chosen in such a way that the plant tracks the $\mathcal{L}_1$ *Reference Model* with any desired precision. To that end, the learning rate $\boldsymbol{\Gamma}$ of the integral update law needs to be sufficiently high or the sampling rate T_s of the piecewise constant update law has to be chosen sufficiently small. In the limit, that is for $\lambda_{\min}(\boldsymbol{\Gamma}) \to \infty$ or $T_s \to 0$, the error $\boldsymbol{e}_{\text{ref}}(t)$ between the plant and $\mathcal{L}_1$ *Reference Model* will approach zero. Thus, the plant will respond like the $\mathcal{L}_1$ *Reference Model*. As the $\mathcal{L}_1$ *Reference Model* reflects the desired trade-off between robustness and performance, the performance in the limit may be seen as the "best-case" performance, which may be expected from the $\mathcal{L}_1$-AC.

While $\mathcal{L}_1$-AC achieves its "best-case" performance only in the limit, the ideal control law (second equation in (3.175) or second equation in (3.284), respectively) would also achieve this performance. While the ideal control law itself is not implementable as it depends on the unknown uncertainties, a simple transformation has been proposed in [98], which renders the ideal control law implementable. This transformation will be exemplified for the ideal control law of $\mathcal{L}_1$-AC with Integral Update Law in case of matched uncertainties and for the ideal control law of $\mathcal{L}_1$-PWC in case of matched and unmatched uncertainties. As the implementable representations of the ideal control laws recover the performance of $\mathcal{L}_1$-AC in the limit, these representations are also referred to as limiting control laws. Their existence raises the question as to whether adaptation is needed at all. An answer to this question will be given after the derivation of the limiting control laws. It relates to the possibility of hedging in case of $\mathcal{L}_1$-AC, which is not available for the limiting control laws.

Matched Uncertainties

Consider the $\mathcal{L}_1$ *Reference Model* (3.175) of Section 3.3.1 in case of a plant with one input, i.e. $m = 1$:

$$\dot{\boldsymbol{x}}_{\text{ref}}(t) = \boldsymbol{A}_M \boldsymbol{x}_{\text{ref}}(t) + \boldsymbol{B}_P \left(\Lambda u_{\text{ref}}(t) + \boldsymbol{\Theta}^*_{m,x} \boldsymbol{x}_{\text{ref}}(t) + \boldsymbol{\Theta}^*_{m,\phi} \cdot \boldsymbol{\phi}(\boldsymbol{x}_{\text{ref}}(t)) \right), \tag{3.348}$$

$$\boldsymbol{u}_{\text{ref}}(s) = \Lambda^{-1} C(s) \left(K_r r(s) - \boldsymbol{\Theta}^*_{m,x} \boldsymbol{x}_{\text{ref}}(s) - \boldsymbol{\Theta}^*_{m,\phi} \boldsymbol{\phi}_{\text{ref}}(s) \right). \tag{3.349}$$

With the definition of $\boldsymbol{G}_m(s)$ in (3.182), the following frequency-domain representation follows from (3.348):

$$\boldsymbol{x}_{\text{ref}}(s) = \boldsymbol{G}_m(s) \cdot \left(\Lambda u_{\text{ref}}(s) + \boldsymbol{\Theta}^*_{m,x} \boldsymbol{x}_{\text{ref}}(s) + \boldsymbol{\Theta}^*_{m,\phi} \cdot \boldsymbol{\phi}_{\text{ref}}(s) \right). \tag{3.350}$$

Now consider the artificial plant output

$$y_{art}(t) = \boldsymbol{B}_P^T \boldsymbol{P} \cdot \boldsymbol{x}_{\text{ref}}(t), \tag{3.351}$$

where $\boldsymbol{P}$ is the solution of the Lyapunov equation (3.31). It follows from the Kalman-Yakubovich-Popov Lemma [96] that the transfer function $\boldsymbol{B}_P^T \boldsymbol{P} \boldsymbol{G}_m(s)$ is SPR, which implies that the transfer function has $RD \leq 1$ and its zeros lie in the left half-plane.

Furthermore, since $\boldsymbol{B}_P^T\boldsymbol{P}\boldsymbol{G}_m(s)$ is square, it is invertible. With respect to the artificial plant output, (3.350) becomes

$$y_{art}(s) = \boldsymbol{B}_P^T\boldsymbol{P}\boldsymbol{G}_m(s)\cdot\left(\Lambda u_{\text{ref}}(s) + \boldsymbol{\Theta}_{m,x}^*\boldsymbol{x}_{\text{ref}}(s) + \boldsymbol{\Theta}_{m,\phi}^*\cdot\boldsymbol{\phi}_{\text{ref}}(s)\right). \tag{3.352}$$

On the other side, it has been shown in Section 3.3.1 that the ideal control law (3.349) admits the alternative representation (3.169), which is

$$u_{\text{ref}}(s) = KD(s)\left(K_r r(s) - \Lambda u_{\text{ref}}(s) - \boldsymbol{\Theta}_{m,x}^*\boldsymbol{x}_{\text{ref}}(s) - \boldsymbol{\Theta}_{m,\phi}^*\boldsymbol{\phi}_{\text{ref}}(s)\right). \tag{3.353}$$

Solving the plant representation (3.352) for $\Lambda u_{\text{ref}}(s) + \boldsymbol{\Theta}_{m,x}^*\boldsymbol{x}_{\text{ref}}(s) + \boldsymbol{\Theta}_{m,\phi}^*\cdot\boldsymbol{\phi}_{\text{ref}}(s)$ and inserting the result into the control law (3.353) yields

$$u_{\text{ref}}(s) = KD(s)\left(K_r r(s) - \left(\boldsymbol{B}_P^T\boldsymbol{P}\boldsymbol{G}_m(s)\right)^{-1}\boldsymbol{B}_P^T\boldsymbol{P}\cdot\boldsymbol{x}_{\text{ref}}(s)\right). \tag{3.354}$$

Since $D(s)$ is strictly proper and $\boldsymbol{B}_P^T\boldsymbol{P}\boldsymbol{G}_m(s)$ is minimum-phase with $RD \leq 1$, the limiting control law (3.354) is causal and stable. In order to shed further light onto the structure of the control law, factor out $\left(\boldsymbol{B}_P^T\boldsymbol{P}\boldsymbol{G}_m(s)\right)^{-1}$, yielding

$$u_{\text{ref}}(s) = KD(s)\left(\boldsymbol{B}_P^T\boldsymbol{P}\boldsymbol{G}_m(s)\right)^{-1}\cdot\left(\boldsymbol{B}_P^T\boldsymbol{P}\boldsymbol{G}_m(s)K_r r(s) - \boldsymbol{B}_P^T\boldsymbol{P}\cdot\boldsymbol{x}_{\text{ref}}(s)\right). \tag{3.355}$$

Thus, the limiting control law (3.354) realizes an integral, model-inversion-type control law since $D(s)$ contains an integrator. In general, integral model-inversion control laws are well-known in robust control [156]. A comparison of the limiting control law (3.355) with the classical loop-shaping designs proposed in [156, specifically Sections 2.6.4 and 3.4.4] admits some interesting observations:

- Using the matching condition (and further assumptions), the original, uncertain plant representation (3.1) is transformed into a representation in terms of the desired dynamics $\boldsymbol{G}_m(s)$ and (state-dependent) disturbances entering at the plant input (see for example (3.352)). For this reason, the model-inversion controller (3.355) inverts the *desired* plant dynamics $\boldsymbol{B}_P^T\boldsymbol{P}\boldsymbol{G}_m(s)$. In contrast, the classical loop-shaping design from [156] would invert the *nominal* plant dynamics $\boldsymbol{C}_P(s\boldsymbol{I} - \boldsymbol{A}_P)^{-1}\boldsymbol{B}_P$.
- As noted in [156], an inverse-based design is a reasonable choice for reference tracking and for rejection of disturbances at the plant output. Interestingly, it is not the preferred choice for disturbances entering at the plant input!

Besides of its relation to integral model-inversion types of control laws, it has been shown in [98] that the limiting control law (3.354) of $\mathcal{L}_1$-AC is algebraically equivalent to a Disturbance Observer (DOB) [153]. Although no further details on DOBs will be presented subsequently, it should be noted that DOB-based control and $\mathcal{L}_1$-AC both aim at the same control objective [98]. While DOBs require an explicit plant inversion similar to (3.355) in order to achieve their control objective, such inversion is not required in case of $\mathcal{L}_1$-AC. As to be shown later on, the latter fact constitutes a major advantage of the $\mathcal{L}_1$-AC architecture over DOBs.

Matched and Unmatched Uncertainties

Consider the $\mathcal{L}_1$ *Reference Model* (3.271) of Section 3.3.2, given by:

$$\dot{\boldsymbol{x}}_{\text{ref}}(t) = \boldsymbol{A}_M \boldsymbol{x}_{\text{ref}}(t) + \boldsymbol{B}_P \cdot \left(\boldsymbol{\Lambda}\boldsymbol{u}_{\text{ref}}(t) + \boldsymbol{\eta}_m\left(\boldsymbol{x}_{\text{ref}}(t), t\right)\right) + \bar{\boldsymbol{B}}_P \boldsymbol{\eta}_{um}\left(\boldsymbol{x}_{\text{ref}}(t), t\right)\Big), \tag{3.356}$$

$$\boldsymbol{u}_{\text{ref}}(s) = \boldsymbol{\Lambda}^{-1}\boldsymbol{C}(s)\left(\boldsymbol{K}_r \boldsymbol{r}(s) - \boldsymbol{\eta}_{ref,m}(s) - \boldsymbol{H}_m^{-1}(s)\boldsymbol{H}_{um}(s)\boldsymbol{\eta}_{ref,um}(s)\right), \tag{3.357}$$

$$\boldsymbol{y}_{\text{ref}}(t) = \boldsymbol{C}_P \cdot \boldsymbol{x}_{\text{ref}}(t), \tag{3.358}$$

with the signals $\boldsymbol{\eta}_m\left(\boldsymbol{x}_{\text{ref}}(t), t\right) = \mathcal{L}^{-1}\left\{\boldsymbol{\eta}_{ref,m}(s)\right\} = \boldsymbol{\Theta}_{m,x}^{*}\boldsymbol{x}_{\text{ref}}(t) + \boldsymbol{f}_m\left(\boldsymbol{x}_{\text{ref}}(t), t\right)$ and $\boldsymbol{\eta}_{um}\left(\boldsymbol{x}_{\text{ref}}(t), t\right) = \mathcal{L}^{-1}\left\{\boldsymbol{\eta}_{ref,um}(s)\right\} = \boldsymbol{\Theta}_{um,x}^{*}\boldsymbol{x}_{\text{ref}}(t) + \boldsymbol{f}_{um}\left(\boldsymbol{x}_{\text{ref}}(t), t\right)$. With the definitions of $\boldsymbol{H}_m(s)$ and $\boldsymbol{H}_{um}(s)$ in (3.241) and (3.264), respectively, the following frequency-domain representation follows from (3.356) with respect to the output $\boldsymbol{y}_{\text{ref}}(t)$:

$$\boldsymbol{y}_{\text{ref}}(s) = \boldsymbol{H}_m(s) \cdot \left(\boldsymbol{\Lambda}\boldsymbol{u}_{\text{ref}}(s) + \boldsymbol{\eta}_{ref,m}(s)\right) + \boldsymbol{H}_{um}(s) \cdot \boldsymbol{\eta}_{ref,um}(s). \tag{3.359}$$

Notice that $\boldsymbol{H}_m(s)$ is square and thus, invertible. One hence obtains

$$\boldsymbol{H}_m^{-1}(s)\,\boldsymbol{y}_{\text{ref}}(s) = \boldsymbol{\Lambda}\boldsymbol{u}_{\text{ref}}(s) + \boldsymbol{\eta}_{ref,m}(s) + \boldsymbol{H}_m^{-1}(s)\boldsymbol{H}_{um}(s)\boldsymbol{\eta}_{ref,um}(s). \tag{3.360}$$

At the same time, the definition of the filter $\boldsymbol{C}(s)$ in (3.173) admits to represent the ideal control law (3.357) as:

$$\begin{aligned}\boldsymbol{u}_{\text{ref}}(s) = {} & \boldsymbol{K}\boldsymbol{D}(s)\boldsymbol{K}_r\boldsymbol{r}(s) \\ & - \boldsymbol{K}\boldsymbol{D}(s)\left(\boldsymbol{\Lambda}\boldsymbol{u}_{\text{ref}}(s) + \boldsymbol{\eta}_{ref,m}(s) + \boldsymbol{H}_m^{-1}(s)\boldsymbol{H}_{um}(s)\boldsymbol{\eta}_{ref,um}(s)\right).\end{aligned} \tag{3.361}$$

Replacing $\boldsymbol{\Lambda}\boldsymbol{u}_{\text{ref}}(s) + \boldsymbol{\eta}_{ref,m}(s) + \boldsymbol{H}_m^{-1}(s)\boldsymbol{H}_{um}(s)\boldsymbol{\eta}_{ref,um}(s)$ by the left hand side of (3.360) hence yields the causal and stable control law

$$\boldsymbol{u}_{\text{ref}}(s) = \boldsymbol{K}\boldsymbol{D}(s)\left(\boldsymbol{K}_r\boldsymbol{r}(s) - \boldsymbol{H}_m^{-1}(s)\,\boldsymbol{y}_{\text{ref}}(s)\right). \tag{3.362}$$

Similar to the case of matched uncertainties only, factoring $\boldsymbol{H}_m^{-1}(s)$ out shows that the limiting control law (3.362) is an integral, model-inversion-type control law:

$$\boldsymbol{u}_{\text{ref}}(s) = \boldsymbol{K}\boldsymbol{D}(s)\boldsymbol{H}_m^{-1}(s)\left(\boldsymbol{H}_m(s)\,\boldsymbol{K}_r\boldsymbol{r}(s) - \boldsymbol{y}_{\text{ref}}(s)\right). \tag{3.363}$$

Hence, the same observations stated in case of matched uncertainties apply as well. While the limiting control laws in case of matched (3.355) and unmatched uncertainties (3.363) are structurally similar, they differ in the fact that (3.355) employs state feedback, whereas (3.363) is an output-feedback control law.

$\mathcal{L}_1$ Adaptive Control and Hedging

As the limiting control laws (3.355) and (3.363) are transformations of the respective ideal control laws, they achieve the "best-case" performance, which is to be expected from a $\mathcal{L}_1$-AC, without resorting to adaptation. This raises the fundamental question as to whether adaptation is necessary at all, if a $\mathcal{L}_1$-AC control law is used. An answer to this question has been proposed in [98] as well. To that end, assume that

the plant possesses a known imperfection such as a saturating control input and/or a delayed control input. From the limiting control laws' point of view, these imperfections constitute an additional disturbance, which they will try to compensate. However, as the disturbance resulting from a saturated or delayed control input may not be compensated using an increased control effort, the integrator of the limiting control law will wind-up, ultimately leading to instability. For this reason, some anti-windup measure is required in order to prevent the integrator from diverging. While there exist well-known anti-windup measures in case of saturating control inputs [6], appropriate anti-windup strategies in case of other plant imperfections such as delays are hardly available [98]. When considering the unmodified $\mathcal{L}_1$-AC control laws, it is well known that the previously mentioned plant imperfections may also lead to instability. In contrast to the limiting control laws, there does however exist a simple and systematic procedure in order to prevent the windup, which is hedging. Since $\mathcal{L}_1$-AC is an indirect approach, hedging of a known plant imperfection amounts to simply mimicking the imperfection in the predictor, which is shown in the next example.

Example 3.35. *Consider a $\mathcal{L}_1$-AC with Integral Update Law in case of matched uncertainties. Let the plant representation* (3.165) *possess a known imperfection at the plant input:*

$$\dot{\boldsymbol{x}}_P(t) = \boldsymbol{A}_M \boldsymbol{x}_P(t) + \boldsymbol{B}_P\left(\boldsymbol{\Lambda}\mathcal{F}\left\{\boldsymbol{u}(t)\right\} + \boldsymbol{\Theta}_{m,x}^{*}\boldsymbol{x}_P(t) + \boldsymbol{\Theta}_{m,\phi}^{*}\cdot\boldsymbol{\phi}\left(\boldsymbol{x}_P(t)\right)\right), \tag{3.364}$$

where the operator $\mathcal{F}\left\{\boldsymbol{u}(t)\right\}$ has been introduced in the context of hedging for direct MRAC. By redefining the regressor vector as

$$\boldsymbol{\omega}\left(\boldsymbol{x}_P(t), t\right) \triangleq \begin{bmatrix} \boldsymbol{x}_P(t) \\ \mathcal{F}\left\{\boldsymbol{u}(t)\right\} \\ \boldsymbol{\phi}\left(\boldsymbol{x}_P(t)\right) \end{bmatrix}, \tag{3.365}$$

the plant (3.364) *may be compactly written as*

$$\dot{\boldsymbol{x}}_P(t) = \boldsymbol{A}_M \hat{\boldsymbol{x}}_P(t) + \boldsymbol{B}_P\boldsymbol{\Theta}_m^{*}\cdot\boldsymbol{\omega}\left(\boldsymbol{x}_P(t), t\right). \tag{3.366}$$

An appropriate modification of the adaptive state predictor (3.166)*, which mimics the imperfection, is then given by:*

$$\begin{aligned}\dot{\hat{\boldsymbol{x}}}_P(t) &= \boldsymbol{A}_M\hat{\boldsymbol{x}}_P(t) + \boldsymbol{B}_P\left(\hat{\boldsymbol{\Lambda}}(t)\mathcal{F}\left\{\boldsymbol{u}(t)\right\} + \hat{\boldsymbol{\Theta}}_{m,x}(t)\boldsymbol{x}_P(t) + \hat{\boldsymbol{\Theta}}_{m,\phi}(t)\cdot\boldsymbol{\phi}\left(\boldsymbol{x}_P(t)\right)\right) \\ &= \boldsymbol{A}_M\hat{\boldsymbol{x}}_P(t) + \boldsymbol{B}_P\hat{\boldsymbol{\Theta}}_m(t)\cdot\boldsymbol{\omega}\left(\boldsymbol{x}_P(t), t\right), \\ \dot{\hat{\boldsymbol{\Theta}}}_m(t)^T &= -\boldsymbol{\Gamma}\boldsymbol{\omega}\left(\boldsymbol{x}_P(t), t\right)\cdot\boldsymbol{e}_P(t)^T\boldsymbol{P}\boldsymbol{B}_P.\end{aligned} \tag{3.367}$$

Notice that the update law does not change since the hedging of $\mathcal{F}\left\{\boldsymbol{u}(t)\right\}$ leads to the same error dynamics (3.79) *that would appear in case of no imperfection at the plant input. Apart from the modification of the adaptive state predictor, no further structural modification of the $\mathcal{L}_1$-AC controller is required.*

3.4 Discussion

In the previous sections, two important branches of adaptive model following control, namely MRAC and $\mathcal{L}_1$-AC, have been introduced. The derivations of these two approaches (in their basic forms) were based on the assumption that the plant is exactly represented by the mathematical model (3.1). Even when neglecting the fact that no practically feasible mathematical model may exactly represent the physical process under control, the structure (3.1) is restrictive. This is because common plant imperfections such as time-delays or neglected (actuator) dynamics may not be represented by (3.1) - at least not without violating the assumption of state feedback. Even if these imperfections are known, the analysis of Section 3.2.5 shows that they may cause instability of the adaptive controller. However, by using a modification of the reference model, namely *hedging*, stability of the tracking/prediction error dynamics may be recovered. Nevertheless, even if these imperfections are known and *hedging* is used, plant imperfections substantially limit the capabilities of the adaptive controller. This aspect will be discussed in Section 3.4.1.

While MRAC and $\mathcal{L}_1$-AC with Integral Update Law differ significantly with respect to their control laws and their proofs of stability, they are similar in the sense that both approaches rely on the same adaptive state predictor. In contrast, other approaches of the $\mathcal{L}_1$-AC family, such as $\mathcal{L}_1$-PWC, resort to a fundamentally different approach for estimating the plant uncertainties. Instead of estimating individual parameters, these approaches estimate the disturbance signal, which results from the uncertain plant parameters. The importance of this difference will be discussed in detail in Section 3.4.2, where a novel classification of these controllers is proposed.

3.4.1 Limitations Imposed by Plant Imperfections

One of the most important design parameters of any model following control system is the reference model. Using the reference model, the control system designer specifies the desired closed-loop response characteristics. When considering the idealistic plant model (3.1), the choice of the reference model (3.4) is essentially arbitrary and is only restricted by the technical assumption of the respective adaptive control approach.

While (3.1) is suitable for the derivation of many adaptive control approaches, it neglects common plant imperfections such as saturation or delay. Without further modifications of the adaptive controller, these imperfections may lead to instability of the closed-loop system. However, if the imperfections are (approximately) known, *hedging* approaches such as those of Sections 3.2.5 and 3.3.3 may be used. Using *hedging*, stability of the tracking error dynamics and of the parameter error dynamics is recovered. Nevertheless, plant imperfections fundamentally limit the achievable closed-loop performance (despite the use of *hedging*). Subsequently, this will be demonstrated in

case of a direct MRAC and a control time-delay, but analogous results also hold for other MRC approaches and other imperfections. In Section 6.5, this observation will help to explain why a conventional PI controller outperforms an adaptive(-like) MRC approach in certain situations.

For the purpose of illustration, consider the special case of a scalar, linear, delayed plant with known control effectiveness. In this case, the plant (3.127) becomes

$$\dot{x}_P(t) = A_P \cdot x_P(t) + B_P \cdot u(t - \tau_c), \tag{3.368}$$

where $A_P \in \mathbb{R}$ is unknown, whereas $B_P \in \mathbb{R}$ and $\tau_c \in \mathbb{R}_+$ are known. By using the "matching condition" $A_P = A_M - B_P \cdot \Theta_x^*$ and by adding and subtracting $B_P \cdot u(t)$, (3.368) turns into

$$\dot{x}_P(t) = A_M \cdot x_P(t) + B_P \cdot (u\,(t) - \Theta_x^* \cdot x_P\,(t)) + B_P \cdot (u\,(t - \tau_c) - u\,(t))\,, \tag{3.369}$$

where $A_M \in \mathbb{R}_{--}$ specifies the desired dynamics. The control law is given by

$$u(t) = K_r \cdot r(t) + \Theta_x(t) \cdot x_P(t), \tag{3.370}$$

where K_r satisfies $B_M = B_P \cdot K_r$ analogously to (3.10) and $\Theta_x : \mathbb{R}_+ \to \mathbb{R}$ is the adaptive parameter. Inserting the control law (3.370) into (3.369) yields

$$\dot{x}_P(t) = A_M \cdot x_P(t) + B_M \cdot r(t) + B_P \tilde{\Theta}_x(t) \cdot x_P(t) + B_P \cdot (u\,(t - \tau_c) - u\,(t)) \tag{3.371}$$

with $\tilde{\Theta}_x(t) = \Theta_x(t) - \Theta_x^*$. In order to hide the effect of the known delay τ_c from the error dynamics, the reference model is modified analogously to (3.131), yielding the reference model dynamics

$$\dot{x}_M(t) = A_M \cdot x_M(t) + B_M \cdot r(t) + B_P \cdot (u\,(t - \tau_c) - u\,(t)) \tag{3.372}$$

and the error dynamics

$$\dot{e}_C(t) = A_M \cdot e_C(t) + B_P \tilde{\Theta}_x(t) \cdot x_P(t). \tag{3.373}$$

Due to the use of *hedging*, the delay τ_c does not influence the error dynamics (3.373) and the conventional update law of direct MRAC results from a Lyapunov proof of stability.

While the Lyapunov proof of stability ensures boundedness of the tracking error $e_C(t)$ and the parameter $\Theta_x(t)$, there is no guarantee for the stability of the overall control system since neither $x_P(t)$ nor $x_M(t)$ are known to be bounded. Nevertheless, a necessary condition for stability may be derived when considering the special case of converged parameters, i.e. $\Theta_x(t) = \Theta_x^*$. While this condition does not guarantee stability of the overall control system, its violation implies instability. In case of converged parameters, the control law (3.370) becomes

$$u(t) = K_r \cdot r(t) + \Theta_x^* \cdot x_P(t). \tag{3.374}$$

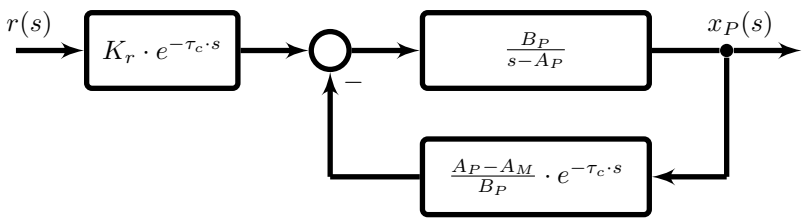

Figure 3.13: Illustration of the feedback connection in Eq. (3.377).

Inserting (3.374) into the plant (3.368) yields

$$\dot{x}_P(t) = A_P \cdot x_P(t) + B_P \left(K_r \cdot r\left(t - \tau_c\right) + \Theta_x^* \cdot x_P\left(t - \tau_c\right) \right). \tag{3.375}$$

With the "matching condition" $\Theta_x^* = (A_M - A_P)/B_P$, (3.375) becomes

$$\dot{x}_P(t) = A_P \cdot x_P(t) + B_P \left(K_r \cdot r\left(t - \tau_c\right) + \frac{A_M - A_P}{B_P} \cdot x_P\left(t - \tau_c\right) \right). \tag{3.376}$$

Thus, in case of converged parameters, the plant and the overall control system are only stable if A_M is chosen such that the delayed feedback connection in (3.376) is stable. In case of no delay, the feedback connection is trivially stable for any stable, desired dynamics $A_M < 0$. However, for $\tau_c > 0$, the delay limits the set of admissible values of A_M, i.e. $\underline{a}_M(\tau_c) \leq A_M < 0$. In order to obtain further insight into these limits, consider the frequency-domain representation of (3.376).

$$x_P(s) = \frac{B_P}{s - A_P} \cdot \left(K_r e^{-\tau_c \cdot s} \cdot r(s) - \frac{A_P - A_M}{B_P} e^{-\tau_c \cdot s} \cdot x_P(s) \right), \tag{3.377}$$

which is illustrated in Figure 3.13. The loop transfer function of this feedback connection from $x_P(s)$ to $x_P(s)$ in case of negative feedback is given by

$$L(s) = \frac{A_P - A_M}{s - A_P} \cdot e^{-\tau_c \cdot s}. \tag{3.378}$$

In case of a stable plant, i.e. $A_P < 0$, the Nyquist criterion implies that the feedback connection is stable, independent of the delay, if $|L(j\omega)| \leq 1$ holds for all ω. However, $|L(j\omega)| \leq 1 \ \forall\omega$ only holds for $2 \cdot A_P \leq A_M < 0$. In case of an unstable plant, i.e. $A_P \geq 0$, or for $A_M < 2 \cdot A_P < 0$, the loop transfer function does not satisfy $|L(j\omega)| \leq 1 \ \forall\omega$ anymore. Hence, $L(j\omega)$ will cross the 0 dB line in the Bode diagram at some frequency $\omega_c > 0$, which implies a finite phase margin and a finite time-delay margin. The dependence of the largest admissible delay $\tau_{c,\max}$ (the time-delay margin) on A_M in case of the loop transfer function $L(s)$ is depicted in Figure 3.14 for two exemplary values of A_P. For a given delay τ_c, only those values of A_M will lead to a stable closed-loop, which satisfy $\tau_{c,\max}(A_M) \geq \tau_c$. Thus, with increasing delay τ_c, the set of admissible values of A_M is shrinking. Conversely, Figure 3.14 implies that a high demand on the plant in the form of a fast reference model inevitably implies little robustness to time-delay. Thus, even with *hedging*, the control system designer has to carefully weigh the

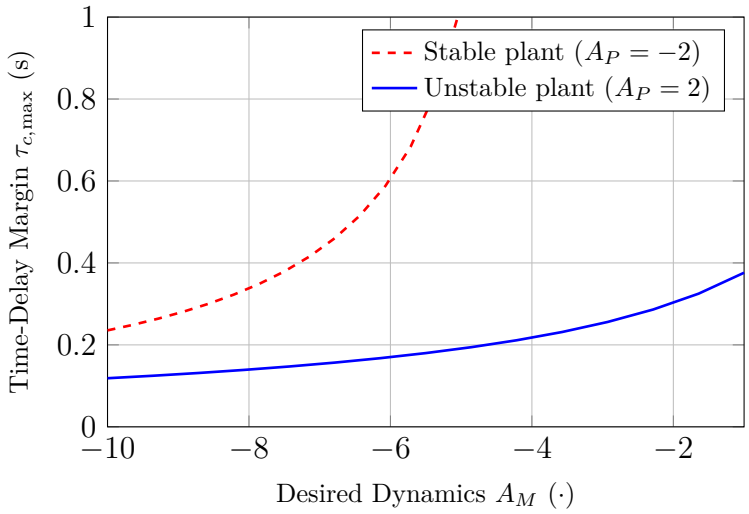

Figure 3.14: Dependence of the largest admissible delay $\tau_{c,\max}$ on the choice of the reference model dynamics A_M. For $A_P = -2$, the closed-loop (3.376) is stable, independent of the delay, for $-4 \leq A_M < 0$.

choice of the reference model dynamics A_M with the robustness of the overall control system to plant imperfections such as a known time-delay τ_c.

In case of converged parameters, the preceding discussion highlighted that the delay τ_c substantially limits the choice of the desired plant dynamics A_M. However, one might wonder whether this limitation entails any consequences for the transient phase and for the overall adaptive control system. To that end, assume that a (fictitious) proof of stability would hold for the overall control system. Now, consider the special case that the parameters have converged at some time $t_0 \geq 0$, where parameter convergence is defined as $\Theta_x(t) = \Theta_x^* \ \ \forall\, t \geq t_0$ and $\dot{\Theta}_x(t) = 0 \ \ \forall\, t \geq t_0$. Due to $\dot{\Theta}_x(t) = 0 \ \ \forall\, t \geq t_0$, the plant is fully represented by (3.376) for all times $t \geq t_0$. Since the overall control system is stable and, since the (fictitious) proof also covers the special case of converged parameters, this implies stability of (3.376). As (3.376) is stable, if and only if the desired reference dynamics A_M ensures its stability, the following implication holds

"Stability of the overall control system" $\rightarrow$ "A_M ensures stability of (3.376)".

Hence, an appropriate choice of A_M is a necessary condition for the stability of the overall control system. Conversely, if A_M is not chosen appropriately, this implies instability of the overall control system. Thus, any feasible design has to ensure stability of the plant (3.368) in feedback with the ideal control law (3.374). As this only constitutes a necessary condition, a feasible design requires some safety margin.

In practice, the plant dynamics A_P is uncertain. For two exemplary values of A_M, Figure 3.15 shows the dependence of the largest admissible delay $\tau_{c,\max}$ on the plant dynamics A_P. Clearly, the delay margin $\tau_{c,\max}$ decreases to zero for $A_P \rightarrow \infty$. Since the stability of (3.376) is a necessary condition for the stability of the closed-loop system,

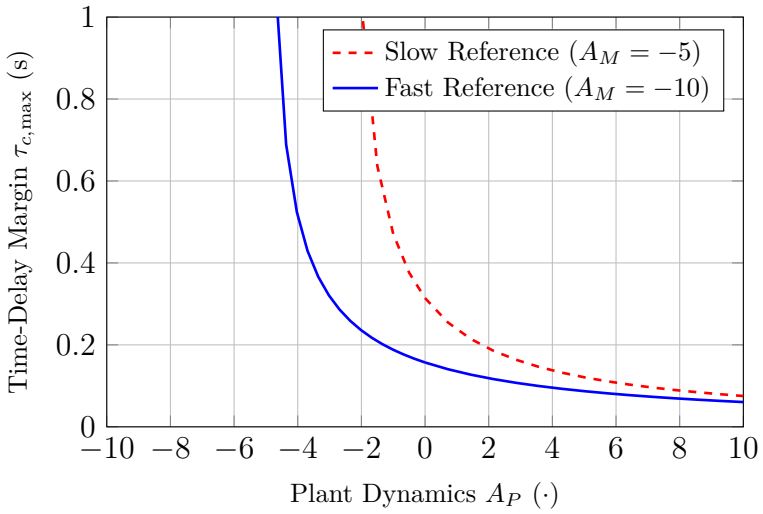

Figure 3.15: Dependence of the largest admissible delay $\tau_{c,\max}$ on the plant dynamics A_P. For $A_P \leq A_M/2$, the closed loop (3.376) is stable independent of the delay.

a MRAC with *hedging* hence loses the ideal property of stabilizing all plants (i.e. A_P is arbitrary) for $\tau_c > 0$. As bounds on the plant dynamics A_P are usually known (e.g. $A_P \in \Omega$), the necessary condition for stability allows some insight into the trade-off between the reference model dynamics A_M and the size of the uncertainty set Ω. To that end, notice that the necessary condition for stability amounts to the robust control problem:

> "Find A_M such that the performance requirements are met and (3.376) is stable for the known delay τ_c and for all $A_P \in \Omega$."

If no solution to this robust control problem exists, then the MRAC with *hedging* will be unstable. In this case, the uncertainty set Ω is too large and/or the performance requirements are overly high. In contrast, if a solution exists, then the adaptive controller may be stable, but there is no guarantee whatsoever.

The preceding discussion specifically considered a time-delay at the plant input. However, similar necessary conditions for stability of the adaptive control system are expected to hold in case of other plant imperfections such as unmodeled actuator dynamics. Furthermore, the result extends to *hedging* in case of predictor-based MRAC as the closed-loop plant in case of converged parameters is the same. Upon an appropriate modification, a similar necessary condition should also hold for $\mathcal{L}_1$-AC. Finally, the result should remain valid for non-scalar plants.

To conclude this section, a remark on *hedging* (and other reference model modifications) is in place. As noted earlier, the *hedging* of a known plant imperfection will lead to the loss of the ideal property of MRAC of stabilizing arbitrary plants. Hence, one might wonder whether *hedging* is a good idea at all. To that end, assume that no *hedging* would be used. In this case, it is for example well known that the time-delay margin depends on the size of the uncertainty and on the size of the learning

rate $\boldsymbol{\Gamma}$ [43]. Thus, in addition to the dependence of the time-delay margin on the size of the uncertainties, an additional coupling between the learning rate $\boldsymbol{\Gamma}$ and the time-delay margin appears. The latter coupling is not present in case of *hedging*. Hence, *hedging* admits fast "learning" - even in the presence of delay. For this, *hedging* decouples the adaptation from the delay by virtue of a modification of the reference model. When viewing the reference model as the demand, with which the plant has to comply, *hedging* may be viewed as a means to reduce this demand to a feasible level. A similar property may also be attributed to CRMs. By dragging the reference model towards the plant, the CRM reduces the demand in transients. This does not only lead to smoother responses of the closed-loop system [159, 70], but also to an increased robustness to unmodeled dynamics (i.e. unknown plant imperfections) [189]. The examples of *hedging* and CRM highlight that a static demand, which follows from an unmodified reference (3.4), may lead to unsatisfactory results. By dynamically adjusting the reference model to the plant, an improved closed-loop performance may be obtained. Such modifications do however come at the price of a reference model which does not guarantee a-priori the satisfaction of the design requirements.

3.4.2 Signal-based vs. Parameter-based Approaches

Throughout this chapter, two important branches of adaptive control have been introduced, namely MRAC and $\mathcal{L}_1$-AC. While $\mathcal{L}_1$-AC with Integral Update Law and predictor-based MRAC differ significantly with respect to their control laws and their proofs of stability, they may be considered to be similar in the sense that both approaches rely on the same adaptive state predictor. In both approaches, the adaptive state predictor estimates the unknown plant parameters $\boldsymbol{\Theta}_m^* \triangleq \begin{bmatrix}\boldsymbol{\Theta}_{m,x}^* & \boldsymbol{\Lambda} & \boldsymbol{\Theta}_{m,\phi}^*\end{bmatrix}$. The resulting estimate $\hat{\boldsymbol{\Theta}}_m(t)$ is used in the respective control laws to cancel the parametric plant uncertainties. The other member of the $\mathcal{L}_1$-AC family, which has been introduced in this chapter, namely $\mathcal{L}_1$-PWC, relies on a profoundly different approach. Here, the plant is represented in terms of the desired dynamics and a disturbance signal $\boldsymbol{\sigma}_m(\boldsymbol{x}_P(t), t)$ (and $\boldsymbol{\sigma}_{um}(\boldsymbol{x}_P(t), t)$, respectively) which represents the deviation between the real dynamics and the desired dynamics. By estimating and feeding back this disturbance signal, the plant is forced to approximately follow the reference model. Thus, $\mathcal{L}_1$-PWC does not estimate individual plant parameters.

Owing to this fundamentally different way of operating, the approaches introduced within this thesis are classified as *parameter-based* and *signal-based* approaches. An approach is referred to as *parameter-based*, if

1. individual plant parameters are estimated;
2. the estimated parameters lead to persistent knowledge about the plant which admits to treat the uncertainties proactively (at least locally in the state space).

While the reason for the first criterion is evident from term *parameter-based*, the second criterion requires further discussion. To that end, consider for example a LTI plant whose parameters are perfectly known except for the control effectiveness $\boldsymbol{\Lambda}$. This plant is to be controlled by a LTI baseline controller. Furthermore, a $\mathcal{L}_1$-PWC augmentation shall counteract the uncertainty of the control effectiveness $\boldsymbol{\Lambda}$. Now, consider a step of the command $\boldsymbol{r}(t)$. In response to this command, the baseline controller will first provide some control input $\boldsymbol{u}(t)$. As $\boldsymbol{u}(t)$ does not account for the control effectiveness uncertainty, the closed loop will start to deviate from the reference model, leading to $\boldsymbol{\sigma}(\boldsymbol{x}_P(t), t) \neq \mathbf{0}$. The $\mathcal{L}_1$-PWC will estimate this deviation and computes an appropriate control increment. This process repeats if further step commands are issued. Thus, the $\mathcal{L}_1$-PWC reacts to the control effectiveness uncertainty each time when its effect becomes measurable. The $\mathcal{L}_1$-PWC does hence not lead to persistent knowledge. In contrast, if an (indirect) MRAC or a $\mathcal{L}_1$-AC augmentation had been used instead of the $\mathcal{L}_1$-PWC, the estimate $\hat{\boldsymbol{\Lambda}}$ of the control effectiveness would adjust during the first step of $\boldsymbol{r}(t)$. After some more steps, $\hat{\boldsymbol{\Lambda}}$ would equal $\boldsymbol{\Lambda}$. For all subsequent step commands, no deviation between the plant and the reference model would be observed. Hence, MRAC or $\mathcal{L}_1$-AC augmentations generate persistent knowledge which admits to account for the uncertainties before the control signal $\boldsymbol{u}(t)$ is issued to the plant. Thus, both are said to treat the uncertainty proactively. Consequently, MRAC and $\mathcal{L}_1$-AC with Integral Update Law of Section 3.3.1 are parameter-based approaches.

In contrast to *parameter-based* approaches, a controller is considered as *signal-based*, if its primary intention is the estimation of a time-varying (disturbance) signal. The underlying estimation scheme crucially depends on measurements and hence, can only react to uncertainties once their effect becomes measurable. Consequently, $\mathcal{L}_1$-PWC and the limiting controllers of $\mathcal{L}_1$-AC (see Section 3.3.3) are *signal-based* approaches.

A common feature of all *signal-based* approaches is the presence of some high-gain control law and/or some high-gain observer: The control laws of *all* $\mathcal{L}_1$-AC variants are high-gain in the sense that the filter parameters $\boldsymbol{K}$ and $\boldsymbol{D}(s)$ have to grow with increasing size of the uncertainties in order to satisfy the $\mathcal{L}_1$-norm condition. Interestingly, this also includes $\mathcal{L}_1$-AC with Integral Update Law. Consequently, the limiting control laws (3.355) and (3.363) of $\mathcal{L}_1$-AC, which result from a transformation of the $\mathcal{L}_1$ *Reference Model*, are high-gain control laws as well. In addition, the state-predictors of *all* $\mathcal{L}_1$-AC variants are high-gain in the sense that a large learning rate $\boldsymbol{\Gamma}$ or a small sampling rate T_s, corresponding to a large feedback gain in (3.257), are required in order to achieve good tracking of the $\mathcal{L}_1$ *Reference Model*.

Less obviously, the Command Governor introduced in Section 3.2.5 is a *signal-based* approach as well since it estimates a disturbance signal and compensates it using an appropriate feedback. Unlike the other *signal-based* approaches, the Command Governor does however estimate the residual adaptation error $\boldsymbol{d}_{ad}(\boldsymbol{x}_P(t), t) \triangleq$

$\boldsymbol{\Lambda}\tilde{\boldsymbol{\Theta}}(t) \cdot \boldsymbol{\omega}(\boldsymbol{x}_P(t), t)$ instead of the effect of the plant uncertainty alone. By feeding back this estimate, the response of MRAC may be improved even in transients. This illustrates that *signal-based* and *parameter-based* approaches are not diametrically opposed, but may be advantageously combined. While *signal-based* approaches quickly yield estimates of the uncertainties, they do not lead to persistent knowledge about the plant. Conversely, a *parameter-based* approach admits to gain persistent knowledge. However, in order to obtain this knowledge, some time is required if undesirable effects of fast learning such as significant oscillations are to be avoided. By combining fast *signal-based* approaches and slowly learning *parameter-based* approaches, the advantages of both approaches may be combined in one design.

Chapter 4

Robustness and Performance Guarantees for Parameter-Based Approaches

As compared to a *conventional* flight control system, an *adaptive* flight control system provides several key advantages: First of all, it allows for increased system performance as the controller gains are not chosen based on a worst-case argument. Furthermore, adaptive control may reduce the effort and the associated cost for system identification as the adaptation may counteract the increased level of parametric uncertainties of a low fidelity plant model. Finally, it can also improve the overall system safety as the gains may adjust to unforeseen events such as damages or faults. While adaptive control has proven its maturity in various flight testing programs such as IRAC [76] or RESTORE [19], it has not yet been deployed in civil, commercial applications. The largest hurdle for the commercial application of adaptive control in safety critical applications such as aircraft is its certification.

Formally, certification may be defined as follows (RTCA DO-178C [134]):

> "Legal recognition by the certification authority that a product, service, organization or person complies with the requirements. Such certification comprises the activity of technically checking the product, service, organization or person and the formal recognition of compliance with the applicable requirements by issue of a certificate, license, approval or other documents as required by national laws and procedures."

In case of civil aviation, the European Aviation Safety Agency (EASA) is the European certification authority, whereas the Federal Aviation Administration (FAA) represents the respective US authority. Informally, the above definition means that certification of an aircraft (or its components) refers to the process of convincing the certification authority that the aircraft complies with the respective governmental regulations. Ultimately, this amounts to convincing the certification authority that all measures have

been taken to ensure aircraft safety, reliability and integrity [14].

In Europe, the legal requirements for the certification of an aircraft derive from the Regulation No. 216/2008 of the European Parliament and the Commission Regulation No. 748/2012 of the European Commission. Among other things, these regulations govern the European agency EASA and provide general requirements for airworthiness of an aircraft. The regulations require that the EASA provides Certification Specifications (CSs) for the certification of an aircraft. Furthermore, the agency has to establish Acceptable Means of Compliance (AMCs), which is legally non-binding guidance material that shows how to comply with the CSs as well as other legal requirements. In case of normal, utility, acrobatic, and commuter category airplanes, the EASA Certification Specification 23 (CS23) [51] does for example apply, whereas in case of large airplanes, the airplane must adhere to the CS25.

The CSs such as CS23 are divided into two books. The first book contains the so-called airworthiness code, which specifies the legally binding requirements that the aircraft and its components have to satisfy. In contrast to common expectation, the airworthiness code only contains rather vague, high level requirements for the aircraft functionality and for its safety. The so-called safety paragraph §1309 of the CS23 does for example state:

> "The occurrence of any failure condition that would prevent the continued safe flight and landing of the aeroplane must be extremely improbable."

Clearly, this requirement is vague as it does not specify a probability or any other tangible quantity. Consequently, satisfaction of this requirement may not be easily shown in practice. For this reason, the second book of each CS provides AMCs.

The CS23 only contains a few requirements which immediately affect the development of a flight control system, such as CS23 §171, which requires the aircraft to be statically stable. Essentially, a flight control system is considered as an equipment and hence, mainly has to satisfy the conditions of the safety paragraph CS23 §1309. Roughly speaking, the latter paragraph requires that each system, upon which the aircraft depends for proper functioning, must perform its intended functionality under any foreseeable operating condition. As cited above, the occurrence of any failure condition that would prevent the continued safe flight and landing of the aircraft must be extremely improbable. In contrast to the second book of the CS25, the second book of the CS23 does not list any AMC for the safety paragraph CS23 §1309. One may however resort to the Advisory Circular (AC) 23.1309-1E [52] of the FAA.

The AC23.1309-1E quantitatively specifies probabilities for the failure of aircraft equipment. Here, the term *failure* refers to a malfunction as well as a loss of a function. The specified probabilities depend on the aircraft class and on the severity of the failure. The severity of the failure ranges from "no effect" to a catastrophic effect, where the latter means a full loss of the aircraft and multiple fatalities. For example,

in case of a commuter class aircraft, the probability of a failure leading to catastrophic effects must be below 10^{-9} per flight hour. In order to show compliance with these requirements, the AC23.1309-1E proposes the development of the aircraft equipment according to established standards, which include:

- SAE ARP4754A (*Guidelines for Development of Civil Aircraft and Systems*) [141];
- SAE ARP4761 (*Guidelines and Methods for Conducting the Safety Assessment Process on Civil Airborne Systems and Equipment*) [139];
- RTCA DO-254 (*Design Assurance Guidance for Airborne Electronic Hardware*) [133];
- RTCA DO-178B/C (*Software Considerations in Airborne Systems and Equipment Certification*) [134].

While these standards do not provide any requirement which is specific to a flight control system, they establish an appropriate development process. A central element of this development process is the precise specification of the intended functionality of the aircraft equipment in terms of suitable requirements. These requirements must "be written in a manner that allows them to be tested" [92] after the development and must ensure that there is no unintended functionality.

Advanced flight control systems such as adaptive ones are ultimately implemented as software. The development of the hardware, on which this software is intended to run, usually follows RTCA DO-254 (as well as SAE ARP4754A, SAE ARP4761 and other standards). The software itself is developed according to RTCA DO-178B/C. Furthermore, in order to comply with the above mentioned development process, suitable requirements for the control algorithm itseld are required. Such requirements may for example be found in the standard SAE AS94900 [140] or in the handbook MIL-HDBK-1797 [42] of the Department of Defense of the United States of America. While there is no legal obligation to follow these standards, their use is advisable as they have been frequently used to specify the robustness and performance properties of a flight control system.

Ultimately, standards such as SAE AS94900 rely on linear system theory. The SAE AS94900 specifies for example requirements for the robustness of the flight control system in terms of phase and gain margin. Since parameter-based adaptive controllers such as MRAC are inherently nonlinear, such frequency-domain requirements cannot be applied. Thus, new robustness and performance metrics have to be developed, which admit to formulate requirements on the robustness and the performance of an adaptive flight control system. These requirements have to be engineered in such a way that they admit to replace the frequency-domain requirements of typical standards such as SAE AS94900 and provide an equivalent level of safety.

In this chapter, the development and the choice of such novel robustness and performance metrics is addressed. Section 4.1 provides a review of available robustness and performance metrics for adaptive controllers. Among these metrics, two promising

metrics are identified, which might be of use in a future certification process of adaptive control. These two metrics are the time-delay margin (as a measure of robustness) and the $\mathcal{L}_\infty$-norm of the tracking error components (as a measure of performance). Their practical application is however challenging due to the lack of methods for their computation. For this reason, Sections 4.2 and 4.3 propose novel analytical computational methods. Finally, Section 4.4 discusses the achieved results and identifies current limitations.

4.1 Review of Robustness and Performance Metrics

This section provides an overview of available robustness and performance metrics for parameter-based, nonlinear adaptive controllers. While there exist many metrics to evaluate a flight control system's performance, this section specifically focuses on metrics that are suited for the assessment of adaptive controllers. Furthermore, this review mainly deals with the adaptive control approaches MRAC and $\mathcal{L}_1$-AC. In similar work, the need for new metrics has been highlighted [92] and some solutions and metrics were suggested [92, 161]. However, none of these provided a systematic review and classification of available approaches. The present section is largely based on previous work [80] by the author of this thesis.

The reviewed robustness and performance metrics represent potential candidates which might be used in a future certification process to replace LTI robustness and performance metrics. For their use in a certification process, the metrics have to satisfy some basic properties. First of all, they have to provide an equivalent level of safety as compared to the LTI metrics that they shall replace. Secondly, they have to be useable to specify requirements before actually developing the controller and to later on verify these requirements [92]. Consequently, admissible values of the metrics have to be known beforehand. Thirdly, the metrics should be physically meaningful and be understandable without excessive mathematical training [92]. Fourthly, generality of the metrics is desirable in order to allow the objective comparison of different adaptive controllers. As the aim of this section is an overview of available metrics, some metrics that do not fulfill all of these four basic requirements will also be presented.

Within the following review, the metrics are classified according to their purpose. Here, stability, robustness, performance, and learning metrics are distinguished. Stability metrics are indicators of stability of a nominal or off-nominal closed-loop control system. In case of a LTI control system, the *largest* real part of the eigenvalues of the closed-loop system may for example serve as a stability metric. Obviously, the closed-loop system is stable if this metric is smaller than zero.

Robustness metrics specifically consider off-nominal plant models. They serve as indicators whether the given control system is likely to work if the plant deviates from the nominal plant model. To that end, robustness metrics usually consider the nominal

plant model and introduce some specific plant imperfection. Hence, they are measures of RS for the particular kind of plant imperfection. In order to draw meaningful conclusions, the particular imperfection should be representative of a large class of practically relevant imperfections. Well-known robustness metrics in linear system theory include the phase margin. In this case, the considered plant imperfection is an artificial phase lag. Since phase lag typically results from parametric as well as non-parametric uncertainties, the phase margin may serve as a meaningful indicator for robustness - at least in case of Single-Input Single-Output (SISO) systems [156].

Any control system has to meet certain performance requirements. Thus, performance metrics are required to rigorously specify and check these requirements. While NS is usually guaranteed by the control design, NP is not necessarily ensured. Furthermore, even if NP guarantees are available, these guarantees do not have to be easily interpretable, increasing the need of alternative performance metrics. As an example of the latter case, consider the quadratic cost functional of a Linear Quadratic Regulator (LQR) as a performance metric. Even though LQR guarantees minimization of this cost functional, this metric does not easily relate to conventional performance requirements such as overshoot and rise time. For this reason, performance metrics are required to evaluate both RP as well as NP.

Learning metrics consider the adaptation itself and provide information about the quality of the adaptive parameters and the convergence properties of the adaptation. Typical examples include the guaranteed speed of convergence of Concurrent Learning [32] or the covariance of Kalman Filter based adaptive control [149]. While learning metrics are important to properly specify the functionality of an adaptive controller, this section will focus on metrics that allow replacing existing LTI metrics. Since conventional flight control systems do not provide the ability to “learn”, there are no metrics that may be replaced. Hence, learning metrics will not be considered subsequently.

While the replacement of established robustness and performance metrics constitutes one challenge, the testing of the requirements specified in terms of these metrics represents another one. For the purpose of testing, the values of the metrics have to be computed. To that end, one may resort to analytical, simulation-based, optimization-based or formal methods.

Analytical methods usually rely on a proof of closed-loop stability and yield guaranteed results which hold for all suitably bounded commands, uncertainties and disturbances. In practice, however, they are usually limited to a specific plant model such as the nominal plant. Moreover, they often tend to substantially over- or underestimate the true value of the metric and hence, lead to conservative bounds.

As an alternative, one may also resort to simulation-based testing using Monte-Carlo simulations or related methods. Here, the nonlinear, possibly functional, differential equations of a (high-fidelity) closed-loop plant model are numerically solved for various realizations of the commands, uncertainties and exogenous disturbances. As

the metric is computed using these numerical solutions, simulation-based methods do not over- or underestimate the metric and thus, are well suited for testing. However, since each simulation run only reflects the response to one specific command, uncertainty and disturbance, a huge number of simulations is required in order to cover a statistically significant number of responses. This disadvantage may be partially compensated using modern Monte-Carlo methods such as Subset simulations [7] or using counter-proving [169]. In case of the latter, numerical methods from optimal control are used to compute the worst-case value of the metric. If the worst-case value satisfies the requirement, then it is also expected to be satisfied for all other commands, uncertainties and disturbances. Similar to analytical methods, optimal control approaches often require simplified plant models. Furthermore, there is usually no guarantee for convergence to the global optimum.

As another alternative, one may also consider formal methods such as model checking [9, 165, 132]. This method provides the appealing capability to prove correctness of finite state machines with respect to formally specified requirements. The application of these methods is, however, not straightforward because it requires an abstraction of the adaptive controller as a finite state machine [92, 132]. For this reason, formal methods are not considered any further.

While some metrics can be computed in several ways, others are limited to certain computational methods. For this reason, the subsequent review also deals with the computational aspects of the metrics. To that end, available analytical and simulation-based methods will be presented.

4.1.1 Stability Metrics

The stability of an adaptive controller in feedback with its nominal plant is usually guaranteed by a Lyapunov-based proof. Even in case of an off-nominal plant, stability in terms of Uniform Ultimate Boundedness (UUB) may be proven. This has for example been shown in Section 3.2.4. Further examples may be found in Section 4.2.3 or references [112, 55, 59]. Thus, Lyapunov (-like) proofs of stability represent powerful analytical stability indicators. However, they are usually limited to simplified plant models. Hence, simulations represent the only possibility of evaluating the response of an adaptive control system in feedback with a high-fidelity plant model. Due to the absence of a proof of stability, there exists no a-priori guarantee for the stability and hence, for the boundedness of the trajectories of the simulated system. For this reason, stability metrics are required to assess whether a single simulation run shall be deemed *stable* or not.

One of the simplest measures of stability is boundedness of all system states. In order to assess boundedness, one may for example resort to truncated $\mathcal{L}_p$ signal norms (see Appendix C.2). Notice that any signal norm, which is determined in simulations,

is truncated by definition since any simulation has a finite duration. Especially the truncated $\mathcal{L}_\infty$-norm seems well suited as its existence implies boundedness of the trajectories. In a similar spirit, one may also resort to the Lyapunov function that underlay the derivation of the adaptive controller. In case of a nominal plant model, a non-increasing trajectory of $V(\boldsymbol{e}_C(t), \tilde{\boldsymbol{\Theta}}(t))$ indicates stability. Furthermore, small values indicate that the adaptive controller is close to its ideal response since small values of $V(\boldsymbol{e}_C, \tilde{\boldsymbol{\Theta}})$ qualitatively indicate small tracking errors and small parameter errors. In case of an off-nominal plant model, the Lyapunov function is no longer guaranteed to be non-increasing. Nevertheless, the Lyapunov function may serve as a stability metric and has to remain bounded. Furthermore, large values of the Lyapunov function indicate stability problems as the adaptive controller does not properly satisfy its control objective of tracking the reference model.

Stability metrics, which relate to the boundedness of the trajectories, face difficulties when it comes to marginally stable or marginally unstable systems. The trajectories of these systems may diverge slowly towards infinity. Since simulation durations are finite, the trajectories might be deemed *stable*, even though they would escape to infinity for a large simulation duration. In order to grasp slowly diverging trajectories, one may resort to the mean convergence rate of the absolute value of the states on some interval $[T_0, T_1]$ with $T_1 \geq T_0$. Consider for example the tracking error $\boldsymbol{e}_C(t)^T = \begin{bmatrix} e_{C,1}(t) & \dots & e_{C,n}(t) \end{bmatrix}$. Assuming exponential convergence / divergence, the following relation holds on the considered interval:

$$|e_{C,k}(T_1)| = |e_{C,k}(T_0)| \cdot e^{\bar{\lambda} \cdot (T_1 - T_0)}. \tag{4.1}$$

Solving for $\bar{\lambda}$ then yields the mean convergence rate

$$\bar{\lambda} = \frac{\ln|e_{C,k}(T_1)| - \ln|e_{C,k}(T_0)|}{T_1 - T_0}. \tag{4.2}$$

Note that by using

$$\frac{d}{dt}\left(\ln|e_{C,k}(t)|\right) = \frac{\dot{e}_{C,k}(t)}{e_{C,k}(t)}, \tag{4.3}$$

Eq. (4.2) may be rewritten as

$$\bar{\lambda} = \frac{1}{T_1 - T_0} \cdot \int_{T_0}^{T_1} \frac{\dot{e}_{C,k}(\tau)}{e_{C,k}(\tau)} d\tau. \tag{4.4}$$

The quantity (4.4) is also called short-term departure index [84, 13]. Taking $T_1 = t$ and $T_0 = 0$, (4.4) yields the mean convergence on the interval $[0, t]$ and is also called a long-term departure index. If $\bar{\lambda}$ is smaller than zero, the respective state $e_{C,k}(t)$ decayed on average during the time-interval, which indicates stability, whereas for $\bar{\lambda} > 0$, the state grew, which may be seen as an indicator for instability. Originally, both quantities have been motivated as windowed versions of the Lyapunov exponent [84, 13].

Another potential stability metric is the projection activity measure [71] and applies to adaptive laws using a projection operator [131, 105]. It assesses the activity of

the projection operator by taking the truncated $\mathcal{L}_\infty$-norm of the correction term which prevents the adaptive parameter from growing beyond a predefined convex set. If the projection operator is highly active, then this may be seen as an indicator of stability problems. Furthermore, stability metrics based on passivity theory [84] have been proposed.

4.1.2 Robustness Metrics

Subsequently, several robustness metrics, which have been proposed for adaptive control systems, are presented.

Phase Margin

In case of LTI SISO systems, the phase margin quantifies the largest amount of pure phase lag, which may be introduced into the open-loop transfer function, before instability occurs. Since phase lag results from various kinds of uncertainties, the phase margin is commonly used to characterize the robustness of control systems. While it is well known that the significance of the phase margin vanishes for Multiple-Input Multiple-Output (MIMO) systems, its use as a robustness metric is wide-spread even in MIMO flight control applications. This is because common standards in aerospace industry such as SAE AS94900 [140] state explicit requirements for this robustness metrics. Hence, applying LTI concepts such as the phase margin to adaptive controllers is appealing since this would significantly ease the certification process. In order to compute the phase margin for an adaptive control system, various approaches have been proposed.

Analytical Computation

Consider for example the simplified direct MRAC

$$\begin{aligned} \dot{\boldsymbol{x}}_P(t) &= \boldsymbol{A}_M \boldsymbol{x}_P(t) + \boldsymbol{B}_P \boldsymbol{\Lambda}\left(\boldsymbol{u}(t) - \boldsymbol{\Theta}_x^* \boldsymbol{x}_P(t)\right), \\ \boldsymbol{u}(t) &= \boldsymbol{\Theta}_x(t) \cdot \boldsymbol{x}_P(t) + \boldsymbol{\Theta}_r(t) \cdot \boldsymbol{r}(t), \end{aligned} \tag{4.5}$$

which follows from the plant representation (3.6) and the control law (3.22), assuming $\bar{\boldsymbol{f}}\left(\boldsymbol{x}_P(t), t\right) = 0$. A straightforward approach to the application of LTI metrics is the frozen weight analysis of (4.5), which amounts to the computation of LTI margins when $\boldsymbol{\Theta}_x(t)$ and $\boldsymbol{\Theta}_r(t)$ are held constant. This approach is however not admissible since a frozen weight analysis does not even allow to draw (necessary) conclusions on the stability of the feedback system (4.5) with time-varying $\boldsymbol{\Theta}_x(t)$ and $\boldsymbol{\Theta}_r(t)$ [84]. While a frozen-weight analysis does hence not yield reliable results during transients, it may well be used to analyze steady-state conditions. If it was known that after some time $\boldsymbol{\Theta}_x(t) = \boldsymbol{\Theta}_{x,0}$ and $\boldsymbol{\Theta}_r(t) = \boldsymbol{\Theta}_{r,0}$ hold for all $t \geq T$, the phase margin of the adaptive control system in steady state may be determined. This result is useful in the sense that if the steady-state system does not fulfill a given phase margin requirement, then the time-varying adaptive control system will not meet this requirement, either.

Since a frozen-weight analysis completely neglects the dynamics of the update law, another approach is the linearization. To that end, consider for example the error dynamics (3.29), (3.41) and the reference model (3.4) of a direct MRAC. Furthermore, assume that:

1. the plant only has one control input (i.e. $m = 1$);
2. there is no nonlinear uncertainty (i.e. $\boldsymbol{\Theta}_\phi(t) = \boldsymbol{\Theta}_\phi^* = \mathbf{0}$);
3. the learning rate $\boldsymbol{\Gamma}$ has block diagonal form, i.e.

$$\boldsymbol{\Gamma} = \begin{bmatrix} \boldsymbol{\Gamma}_x & \mathbf{0} \\ \mathbf{0} & \Gamma_r \end{bmatrix}, \tag{4.6}$$

   where $\boldsymbol{\Gamma}_x \in \mathbb{S}_{++}^n$ and $\Gamma_r \in \mathbb{R}_{++}$ are the learning rates associated with the state-dependent uncertainty $\boldsymbol{\Theta}_x^*$ and the input uncertainty $\boldsymbol{\Theta}_r^*$, respectively.

In this case, the error dynamics (3.29), (3.41) become

$$\begin{aligned} \dot{\boldsymbol{e}}_C(t) &= \boldsymbol{A}_M \boldsymbol{e}_C(t) + \boldsymbol{B}_P \Lambda \tilde{\boldsymbol{\Theta}}_x(t) \cdot \boldsymbol{x}_P(t) + \boldsymbol{B}_P \Lambda \tilde{\Theta}_r(t) \cdot r(t), \\ \dot{\tilde{\boldsymbol{\Theta}}}_x(t)^T &= -\boldsymbol{\Gamma}_x \boldsymbol{x}_P(t) \cdot \boldsymbol{e}_C(t)^T \boldsymbol{P} \boldsymbol{B}_P, \\ \dot{\tilde{\Theta}}_r(t) &= -\Gamma_r r(t) \cdot \boldsymbol{e}_C(t)^T \boldsymbol{P} \boldsymbol{B}_P. \end{aligned} \tag{4.7}$$

For the linearization of (4.7), an equilibrium has to be determined first. Since the reference model (3.4) will only settle on a constant value $\boldsymbol{x}_{M,0}$, if the reference signal remains constant, $r(t) = r_0$ is chosen, leading to $\boldsymbol{x}_{M,0} = -\boldsymbol{A}_M^{-1} \boldsymbol{B}_M r_0$. It has been noted in [150] that for a constant reference signal r_0, the parameter errors $\tilde{\boldsymbol{\Theta}}_x(t)$ and $\tilde{\boldsymbol{\Theta}}_r(t)$ settle on unknown, but constant values $\tilde{\boldsymbol{\Theta}}_{x,0}$ and $\tilde{\Theta}_{r,0}$, which may for example be determined in simulations. Since Barbalat's Lemma ensures convergence of the tracking error towards zero, the equilibrium of the tracking error is given by $\boldsymbol{e}_{C,0} = \mathbf{0}$. For an equilibrium $\boldsymbol{x}_{M,0}$, $\boldsymbol{e}_{C,0} = \mathbf{0}$, $\tilde{\boldsymbol{\Theta}}_{x,0}$ and $\tilde{\Theta}_{r,0}$, the linearization of the reference model (3.4) and the error dynamics (4.7) is then given by:

$$\begin{aligned} \begin{bmatrix} \delta\dot{\boldsymbol{x}}_M(t) \\ \delta\dot{\boldsymbol{e}}_C(t) \\ \delta\dot{\tilde{\boldsymbol{\Theta}}}_x(t)^T \\ \delta\dot{\tilde{\Theta}}_r(t) \end{bmatrix} &= \begin{bmatrix} \boldsymbol{A}_M & \mathbf{0}^{n\times n} & \mathbf{0}^{n\times n} & \mathbf{0}^{n\times 1} \\ \boldsymbol{B}_P \Lambda \tilde{\boldsymbol{\Theta}}_{x,0} & \boldsymbol{A}_M + \boldsymbol{B}_P \Lambda \tilde{\boldsymbol{\Theta}}_{x,0} & \boldsymbol{B}_P \Lambda \boldsymbol{x}_{M,0}^T & \boldsymbol{B}_P \Lambda r_0 \\ \mathbf{0}^{n\times n} & -\boldsymbol{\Gamma}_x \boldsymbol{x}_{M,0} \boldsymbol{B}_P^T \boldsymbol{P} & \mathbf{0}^{n\times n} & \mathbf{0}^{n\times 1} \\ \mathbf{0}^{1\times n} & -\gamma_r r_0 \boldsymbol{B}_P^T \boldsymbol{P} & \mathbf{0}^{1\times n} & 0 \end{bmatrix} \cdot \begin{bmatrix} \delta\boldsymbol{x}_M(t) \\ \delta\boldsymbol{e}_C(t) \\ \delta\tilde{\boldsymbol{\Theta}}_x(t)^T \\ \delta\tilde{\Theta}_r(t) \end{bmatrix} \\ &\quad + \begin{bmatrix} \boldsymbol{B}_M \\ \boldsymbol{B}_P \Lambda \tilde{\Theta}_{r,0} \\ \mathbf{0}^{n\times 1} \\ 0 \end{bmatrix} \cdot \delta r(t), \end{aligned} \tag{4.8}$$

where $\delta\boldsymbol{x}_M(t) \triangleq \boldsymbol{x}_M(t) - \boldsymbol{x}_{M,0}$, $\delta\boldsymbol{e}_C(t) \triangleq \boldsymbol{e}_C(t) - \boldsymbol{e}_{C,0}$, $\delta\tilde{\boldsymbol{\Theta}}_x(t) \triangleq \tilde{\boldsymbol{\Theta}}_x(t) - \tilde{\boldsymbol{\Theta}}_{x,0}$, $\delta\tilde{\Theta}_r(t) \triangleq \tilde{\Theta}_r(t) - \tilde{\Theta}_{r,0}$ and $\delta r(t) \triangleq r(t) - r_0$ denote the deviations from the equilibrium condition. The linearization (4.8) is also referred to as Linear Asymptotic System (LAS) as it

approximates the dynamics to which the direct MRAC asymptotically converges in case of a constant reference signal $r(t)$. The LAS possesses $3n + 1$ states. Ref. [150] shows that n of these states, which are associated with the parameter errors, are free integrators and hence, their associated eigenvalues are zero. Thus, the closed-loop only exhibits marginal stability and any robustness margin becomes zero. By virtue of an appropriate model order reduction, the n free integrators may however be eliminated, leading to the so-called Reduced Linear Asymptotic System (RLAS). Using the RLAS and by cutting the loop for example at the control input, the phase margin (and the gain margin) may be computed for the considered equilibrium condition [47].

The foregoing approach allows the application of classical LTI robustness metrics to adaptive control systems. It is however important to stress that the linearized representation is only valid asymptotically, i.e. after the adaptive control system enters the domain within which the linearization approximates the nonlinear control system reasonably well. Hence, the obtained metrics are only valid asymptotically and do not allow assessing robustness during transients.

Simulation-based Computation

Since the phase margin essentially is a frequency-domain quantity, it may not be readily computed in simulations. In order to deal with this challenge, several methods have been proposed.

In [100], the performance of an adaptive controller is compared to the performance of a suitably chosen LTI system in Monte-Carlo simulations. If the performance of both systems matches according to some criteria in the presence of artificially introduced gain- and delay variations, the authors assign the robustness margins of the LTI system to the adaptive control system. Since the choice of a suitable LTI system and suitable metrics for comparison, which ensure that both systems actually have similar robustness properties, is non-trivial, this method requires further theoretical justification.

Alternatively, one may resort to the *Bounded Linear Analysis*, which has been proposed in [120, 121, 123]. Following a conceptually similar line of thought as in case of the analytical linearization, the *Bounded Linear Analysis* approximates the adaptive control system by a series of LTI systems, each of which is valid during some time window. The parameters of these LTI systems are determined during simulation. These LTI systems finally admit the computation of the phase margin and other LTI metrics for each time window. In contrast to the analytical linearization, the LTI systems, which result from the *Bounded Linear Analysis*, are intended to be valid also during transients, i.e. before the adaptive parameters settled to some stationary value. For the purpose of illustration, consider for example the error dynamics (3.29) and (3.41) of a direct MRAC. Furthermore, assume that:

1. the plant only has one control input (i.e. $m = 1$);
2. there is no input uncertainty (i.e. $\Lambda = 1$) and hence no adaptation of the feedforward gain $\boldsymbol{\Theta}_r(t)$ (i.e. $\boldsymbol{\Theta}_r(0) = \boldsymbol{K}_r$ and $\boldsymbol{\Gamma}_r = 0$);

3. there is no nonlinear uncertainty (i.e. $\boldsymbol{\Theta}_{\phi}(t) = \boldsymbol{\Theta}_{\phi}^{*} = \mathbf{0}$).

In this case, the error dynamics (3.29), (3.41) simplify to

$$\begin{aligned} \dot{\boldsymbol{e}}_C(t) &= \boldsymbol{A}_M \boldsymbol{e}_C(t) + \boldsymbol{B}_P \tilde{\boldsymbol{\Theta}}_x(t) \cdot \boldsymbol{x}_P(t), \\ \dot{\tilde{\boldsymbol{\Theta}}}_x(t)^T &= -\boldsymbol{\Gamma}_x \boldsymbol{x}_P(t) \cdot \boldsymbol{e}_C(t)^T \boldsymbol{P} \boldsymbol{B}_P, \end{aligned} \tag{4.9}$$

where $\boldsymbol{\Gamma}_x \in \mathbb{S}_{++}^n$ is the learning rate associated with the state-dependent uncertainty $\boldsymbol{\Theta}_x^*$. Using $\dot{\tilde{\boldsymbol{\Theta}}}_x(t) = \dot{\boldsymbol{\Theta}}_x(t)$, $u_{ad}(t) \triangleq \boldsymbol{\Theta}_x(t) \cdot \boldsymbol{x}_P(t)$ and $\boldsymbol{x}_P(t) = \boldsymbol{e}_C(t) + \boldsymbol{x}_M(t)$, (4.9) may be rewritten as

$$\begin{aligned} \dot{\boldsymbol{e}}_C(t) &= \boldsymbol{A}_M \boldsymbol{e}_C(t) + \boldsymbol{B}_P \cdot u_{ad}(t) - \boldsymbol{B}_P \boldsymbol{\Theta}_x^* \cdot (\boldsymbol{e}_C(t) + \boldsymbol{x}_M(t)), \\ u_{ad}(t) &= \boldsymbol{\Theta}_x(t) \cdot \boldsymbol{x}_P(t), \\ \dot{\boldsymbol{\Theta}}_x(t) &= -\boldsymbol{B}_P^T \boldsymbol{P} \boldsymbol{e}_C(t) \cdot \boldsymbol{x}_P(t)^T \boldsymbol{\Gamma}_x. \end{aligned} \tag{4.10}$$

Differentiating $u_{ad}(t)$ with respect to time and inserting the update law yields

$$\begin{aligned} \dot{\boldsymbol{e}}_C(t) &= \boldsymbol{A}_M \boldsymbol{e}_C(t) + \boldsymbol{B}_P \cdot u_{ad}(t) - \boldsymbol{B}_P \boldsymbol{\Theta}_x^* \cdot (\boldsymbol{e}_C(t) + \boldsymbol{x}_M(t)), \\ \dot{u}_{ad}(t) &= -\boldsymbol{B}_P^T \boldsymbol{P} \boldsymbol{e}_C(t) \cdot \boldsymbol{x}_P(t)^T \boldsymbol{\Gamma}_x \boldsymbol{x}_P(t) + \boldsymbol{\Theta}_x(t) \cdot (\dot{\boldsymbol{e}}_C(t) + \dot{\boldsymbol{x}}_M(t)). \end{aligned} \tag{4.11}$$

Now consider the time window $[(i-1) \cdot T, i \cdot T[$ with $i \in \mathbb{N}_{++}$ and $T > 0$. The objective of the *Bounded Linear Analysis* is the approximation of (4.11) by a LTI system during that time window. In contrast to [123], the subsequent derivation follows a different approach, which nevertheless leads to the same result. To that end, it is assumed that the adaptive parameter $\boldsymbol{\Theta}_x(t)$ hardly changes throughout the time window and is hence considered to be constant throughout the interval. Similarly, $\boldsymbol{x}_P(t)^T \boldsymbol{\Gamma}_x \boldsymbol{x}_P(t)$ is assumed to be approximately equivalent to its mean value during the considered interval, i.e.

$$\boldsymbol{x}_P(t)^T \boldsymbol{\Gamma}_x \boldsymbol{x}_P(t) \approx \frac{1}{T} \int_{(i-1)\cdot T}^{i \cdot T} \boldsymbol{x}_P^T(\tau) \boldsymbol{\Gamma}_x \boldsymbol{x}_P(\tau) d\tau \tag{4.12}$$

approximately holds for $(i-1) \cdot T \leq t < i \cdot T$. Upon the definitions

$$\alpha_i \triangleq \frac{1}{T} \int_{(i-1)\cdot T}^{i \cdot T} \boldsymbol{x}_P^T(\tau) \boldsymbol{\Gamma}_x \boldsymbol{x}_P(\tau) d\tau, \tag{4.13}$$

$$\boldsymbol{\Theta}_{x,i} \triangleq \boldsymbol{\Theta}_x(i \cdot T), \tag{4.14}$$

(4.11) is approximated by the LTI system

$$\dot{\boldsymbol{e}}_C(t) = \boldsymbol{A}_M \boldsymbol{e}_C(t) + \boldsymbol{B}_P \cdot u_{ad}(t) - \boldsymbol{B}_P \boldsymbol{\Theta}_x^* \cdot (\boldsymbol{e}_C(t) + \boldsymbol{x}_M(t)), \tag{4.15}$$

$$\dot{u}_{ad}(t) = -\alpha_i \boldsymbol{B}_P^T \boldsymbol{P} \cdot \boldsymbol{e}_C(t) + \boldsymbol{\Theta}_{x,i} \cdot (\dot{\boldsymbol{e}}_C(t) + \dot{\boldsymbol{x}}_M(t)) \tag{4.16}$$

for $t \in [(i-1) \cdot T, i \cdot T[$, where α_i and $\boldsymbol{\Theta}_{x,i}$ are computed from simulation data. By appropriately cutting the loop, the approximation (4.15), (4.16) allows to retrospectively evaluate the robustness as well as the performance of the adaptive control system at each instant of time $i \cdot T$ [123]. The parameters α_i and $\boldsymbol{\Theta}_{x,i}$ crucially depend on

the initial conditions, the matched uncertainty $\boldsymbol{\Theta}_x^*$ and the command signal $r(t)$. For this reason, the *Bounded Linear Analysis* has to be combined with some simulation technique such as Monte Carlo simulations in order to draw meaningful conclusions.

Subsequently, the relation between the stability of the LTI system (4.15), (4.16) and the error dynamics (4.9) shall be analyzed in some more detail. To that end, assume for simplicity that the reference signal $r(t)$ is constant and the initial conditions of the reference model are chosen such that $\dot{\boldsymbol{x}}_M(t) = 0$ holds for all $t \geq 0$. Differentiating (4.15) with respect to time and inserting (4.16) leads to the state space model

$$\frac{d}{dt}\begin{bmatrix}\boldsymbol{e}_C(t)\\ \dot{\boldsymbol{e}}_C(t)\end{bmatrix} = \begin{bmatrix}\boldsymbol{0} & \boldsymbol{I}\\ -\alpha_i \boldsymbol{B}_P \boldsymbol{B}_P^T \boldsymbol{P} & \boldsymbol{A}_P + \boldsymbol{B}_P \boldsymbol{\Theta}_{x,i}\end{bmatrix} \cdot \begin{bmatrix}\boldsymbol{e}_C(t)\\ \dot{\boldsymbol{e}}_C(t)\end{bmatrix}. \tag{4.17}$$

Depending on the size T of the time window, the size of the command $r(t)$ and the learning rate $\boldsymbol{\Gamma}_x$, the quantities $\boldsymbol{\Theta}_{x,i}$ and α_i may still be small for small i. Hence, if the plant is unstable (i.e. $\boldsymbol{A}_P$ is not Hurwitz), then the LTI system (4.17) may be unstable as well. Consequently, any computed robustness metric such as the phase margin would indicate an unstable loop. This illustrates that the stability of the approximation (4.15), (4.16) does not necessarily relate to the stability of the adaptive control system (4.9), which is known to be stable from the Lyapunov proof of stability. Consequently, robustness properties of the linear approximation do not transfer to the adaptive control system, either. While the windowed analysis may provide valuable insight about the behavior of an adaptive control system, the preceding example highlights that the *Bounded Linear Analysis* requires further research to rigorously relate the robustness properties of the series of LTI systems to the robustness properties of the adaptive control system.

Gain Margin

Previously, several methods have been reviewed that allow the approximate computation of the phase margin of an adaptive controller. Although these methods only lead to meaningful results in special occasions (if at all), it is obvious that the same approaches could also be used to compute the gain margin of an adaptive controller. However, for most adaptive control schemes, even stronger results hold.

In linear system theory, the gain margin quantifies the largest variation of the gain of the open-loop transfer function before instability occurs. Assuming that the gain variation is introduced at the plant input and considering the direct or predictor-based MRAC of Section 3.2.1 or Section 3.2.3, respectively, the gain variation may be incorporated into the control effectiveness matrix $\boldsymbol{\Lambda}$. Since stability of direct and predictor-based MRAC is established using the Lyapunov proof of stability independent of the actual control effectiveness $\boldsymbol{\Lambda}$ (except for the assumption $\boldsymbol{\Lambda} > 0$), admissible variations of the gain are within the interval $]0, \infty[$. Hence, the gain margin is infinity [143]. For MRAC with robustness modifications such as the σ-modification, the same result holds [158]. When using the projection algorithm [131], the size of the adaptive parameter

$\boldsymbol{\Theta}$ is limited and so is the gain margin [143]. In case of the projection operator, it is reasonable to consider the gain margin as a design parameter rather than a robustness metric since the largest admissible size of the adaptive parameter $\boldsymbol{\Theta}$ is a design parameter. For $\mathcal{L}_1$-AC, the gain margin is also finite [30]. This is because stability of the $\mathcal{L}_1$ *Reference Model* is only established for some compact set $\boldsymbol{\Lambda} \in \Omega_\Lambda$.

Computational Aspects

Since the gain margin essentially is a design parameter (or is infinity), no specific algorithms for its computation are required.

Time-Delay Margin

The time-delay margin is defined as the largest time-delay which a closed-loop control system may tolerate without becoming unstable [161]. Usually, the time-delay margin is either determined at the plant input or at the plant output. For reasons of simplicity, the subsequent considerations are limited to a time-delay τ_c at the plant input.

The time-delay margin is commonly seen as a potential successor to the phase margin [122]. First of all, this is because time-delay is a fundamental property of any flight control system and robustness to a certain amount of time-delay is an important prerequisite. Furthermore, for SISO LTI systems, phase and time-delay margin are closely related. This connection to a well-known metric might be advantageous in a certification process. Thirdly, robustness to time-delay also indicates robustness to unmodeled dynamics [187].

While the time-delay margin of a LTI system is readily computable, the computation for a nonlinear system such as an adaptive controller becomes significantly more challenging. The computation depends on the adaptive control architecture and the employed modifications. Furthermore, it has to account for the complex dependency of the time-delay margin on design parameters such as the learning rate $\boldsymbol{\Gamma}$, the uncertainties and the reference signal $\boldsymbol{r}\,(t)$. For a direct MRAC, it is for example well-known that the time-delay margin decreases to zero if $\lambda_{\min}(\boldsymbol{\Gamma}) \to \infty$ [123]. Similarly, large command signals $\boldsymbol{r}\,(t)$ lead to large plant states, which may effectively act like an increased learning rate $\boldsymbol{\Gamma}$ [148].

Analytical Computation

For the analytical computation of the time-delay margin, various tools have been proposed. For general nonlinear systems, the analytical computation usually relies on either the method of Lyapunov-Krasovskii or the method of Lyapunov-Razumikhin [75, 73]. A general problem of these techniques is that they require to determine a suitable Lyapunov-like functional or function, respectively, whose choice is crucial for obtaining less conservative results [122]. Alternatively, the time-delay margin may also be determined using a Padé approximation [110] of the time-delay. While the methods of Lyapunov-Krasovskii and Lyapunov-Razumikhin yield guaranteed lower bounds, the Padé approximation is not guaranteed to obtain lower bounds (see for example [123]).

Ref.	Control Scheme	Method	Approach / Limitations
[43]	MRAC with σ-modification	Lyapunov-Krasovskii	• Sum-Of-Squares (SOS) polynomial optimization of the Lyapunov-Krasovskii functional; • Requires a polynomial representation of the plant and the adaptive controller; • Only considers the adaptive stabilization problem.
[90]	MRAC with σ-modification	Lyapunov-Razumikhin	• Iterative manual procedure for determining Lyapunov functions to obtain less conservative time-delay margin estimates; • Requires knowledge of an upper-bound on the regressor vector.
[113]	MRAC with projection	Lyapunov-Razumikhin	• Presents an argument, which relies on first principles instead of Lyapunov analysis; • Lyapunov-Razumikhin is employed at some intermediate step.
[112]	MRAC with projection	Padé approximation	• Proves robustness to dynamic uncertainties at the plant input; • Padé approximation is used to estimate the time-delay margin.
[29]	$\mathcal{L}_1$-AC	Comparison with suitable LTI system	• Establishes equivalence of state and control trajectories of the $\mathcal{L}_1$-AC and a specifically designed LTI system in the presence of the same time-delay; • The time-delay margin of the LTI system constitutes the time-delay margin of the $\mathcal{L}_1$-AC.
[106]	$\mathcal{L}_1$-AC	Gap Metric Techniques	• Establishes a robust stability margin based on gap metric techniques; • The gap stability margin is used to estimate the time-delay margin; • Only considers the adaptive stabilization problem.

Table 4.1: Analytical methods for the computation of the time-delay margin.

Table 4.1 provides a list of some relevant publications, which address the problem of the analytical computation of the time-delay margin, and comments on features as well as limitations of the respective approaches.

Simulation-based Computation

For the simulation-based computation of the time-delay margin, one could resort to the simulation-based techniques for the computation of the phase margin. Using these techniques, the time-delay margin is for example readily obtained by computing both the phase margin and the gain crossover frequency. This approach does however suffer from the fact that the robustness properties of the LTI approximations do not

rigorously relate to the robustness properties of the adaptive controller.

Since a time-delay can be easily modeled in simulations, a more direct approach for the computation of the time-delay margin is favorable. To that end, the nominal plant model is considered and time-delay is additionally introduced at the position(s) of interest such as the plant input. Then, in an outer optimization loop, a simple bisection algorithm adjusts the time-delay, while in an inner simulation loop, a Monte Carlo simulation iterates over the uncertainties of the nominal plant model and the command signals $\boldsymbol{r}(t)$. For a single simulation run, stability (and performance) metrics assess whether the numerical solution should be considered stable or not. The largest value of the time-delay, for which the system maintained stability in terms of the employed stability or performance metrics, is then called the time-delay margin.

It should be noted that the obtained time-delay margin crucially depends on the simulated uncertainties and the simulated command signals $\boldsymbol{r}(t)$. Furthermore, it also depends on the stability and performance metrics which assess whether the particular simulation runs are considered to be stable. First of all, this illustrates the complex relationship between robustness, stability and performance metrics, where the latter two are used within the computation of the first ones. Secondly, this also implies that the stability criteria, according to which a simulation run is deemed to be stable, have to be clearly stated in order to ensure reproducibility. Finally, it follows from these observations that the time-delay margin determined in simulations only is an upper bound for the true time-delay margin. This is because there might exist uncertainty and command signal combinations which lead to a smaller time-delay margin.

While the presented approach specifically considered the nominal plant model, it may also serve to determine the time-delay margin in the presence of other plant imperfections such as actuator dynamics, etc. In this case, the respective off-nominal plant model has to be used instead of the nominal one.

$\mathcal{L}_2$-Gain

Adaptive controllers are inherently stable in the presence of matched parametric uncertainties. Other uncertainties such as unmatched parametric or non-parametric uncertainties may however endanger the closed-loop stability (see Section 3.2.4). Proving stability in the presence of these uncertainties becomes significantly more challenging (see for example [112]) as boundedness of the disturbance signal resulting from these uncertainties may not be assumed a-priori. When specifically considering unmodeled dynamics, the notion of *finite gain $\mathcal{L}$-stability* and the *small-gain theorem* (see Appendix C.2) constitute an appropriate framework. In general, the small-gain theorem admits the stability analysis of feedback configurations such as the one in Figure C.1, where both systems $\mathcal{G}_1\{\boldsymbol{w}_1\}$ and $\mathcal{G}_2\{\boldsymbol{z}_2\}$ are assumed to be finite-gain $\mathcal{L}$-stable. While the small-gain theorem holds for signals $\boldsymbol{w}_i(t) \in \mathcal{L}_e$, $\boldsymbol{z}_i(t) \in \mathcal{L}_e$, which are elements of arbitrary extended function spaces, a natural choice is the space $\mathcal{L}_{2,e}$ of signals with finite energy (for finite time).

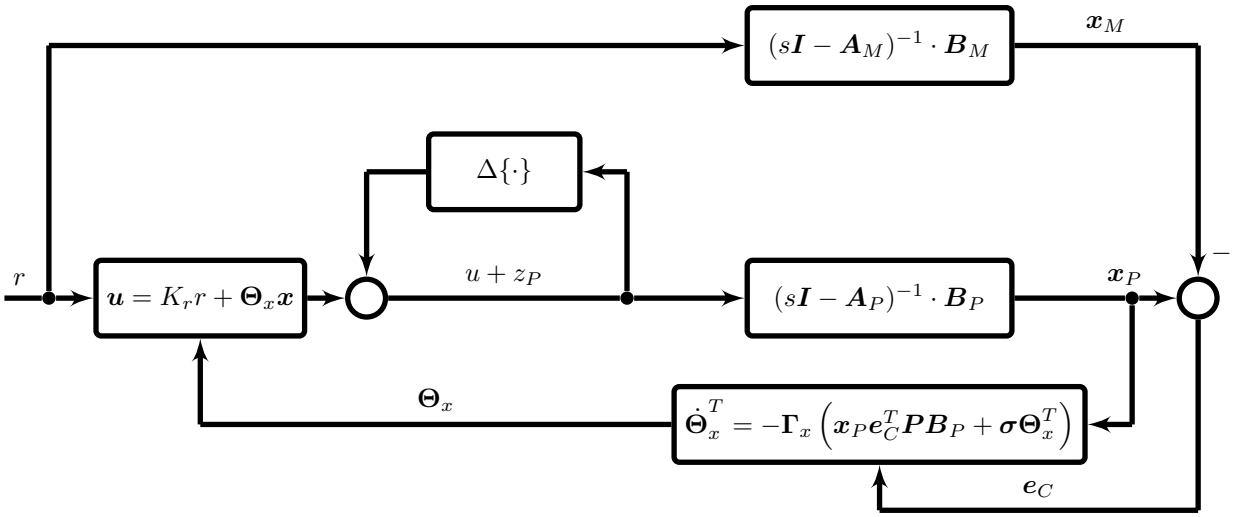

Figure 4.1: Overall control system with input uncertainty $\Delta\{\cdot\}$.

The feedback configuration in Figure C.1 may be used to analyze the stability of adaptive controllers facing various types of unmodeled dynamics. For the purpose of illustration, specifically consider the plant (3.94), which has been introduced during the introduction of the robustness modifications in Section 3.2.4, with unmodeled dynamics at the plant input [178]. Let this unmodeled dynamics be defined as

$$\boldsymbol{w}\left(\boldsymbol{x}_P\left(t\right), \boldsymbol{z}_P\left(t\right), t\right) \triangleq \boldsymbol{B}_P \cdot \boldsymbol{z}_P\left(t\right), \tag{4.18}$$

$$\boldsymbol{z}_P\left(t\right) \triangleq \Delta\left\{\boldsymbol{u}\left(t\right) + \boldsymbol{z}_P\left(t\right)\right\}, \tag{4.19}$$

where $\Delta\{\cdot\}$ is a finite-gain $\mathcal{L}_2$-stable operator. For the sake of simplicity, assume that

1. the plant only has one control input (i.e. $m = 1$);
2. there is no input uncertainty (i.e. $\Lambda = 1$) and thus, no adaptation of the feedforward gain $\boldsymbol{\Theta}_r\left(t\right)$ is required;
3. there is no nonlinear uncertainty (i.e. $\boldsymbol{\Theta}_\phi\left(t\right) = \boldsymbol{\Theta}_\phi^* = \boldsymbol{0}$).

In this case, the plant (3.94) becomes

$$\dot{\boldsymbol{x}}_P\left(t\right) = \boldsymbol{A}_M \boldsymbol{x}_P\left(t\right) + \boldsymbol{B}_P\left(u\left(t\right) + z_P\left(t\right) - \boldsymbol{\Theta}_x^* \cdot \boldsymbol{x}_P\left(t\right)\right). \tag{4.20}$$

For the control of the plant (4.20), a direct MRAC with σ-modification is used. Due to the foregoing assumptions, the control law (3.26) and the update law (3.109) simplify to:

$$\begin{aligned} u\left(t\right) &= K_r \cdot r\left(t\right) + \boldsymbol{\Theta}_x\left(t\right) \cdot \boldsymbol{x}_P\left(t\right), \\ \dot{\boldsymbol{\Theta}}_x\left(t\right)^T &= -\boldsymbol{\Gamma}_x \left(\boldsymbol{x}_P\left(t\right) \cdot \boldsymbol{e}_C\left(t\right)^T \boldsymbol{P} \boldsymbol{B}_P + \boldsymbol{\sigma} \cdot \boldsymbol{\Theta}_x\left(t\right)^T \right), \end{aligned} \tag{4.21}$$

where $\boldsymbol{\Gamma}_x \in \mathbb{S}_{++}^n$ is the learning rate associated with the state-dependent uncertainty $\boldsymbol{\Theta}_x^*$. The structure of the overall control system is shown in Figure 4.1.

In order to analyze the robustness to unmodeled dynamics using the small-gain theorem, the structure of the adaptive control system according to Figure 4.1 has to

match Figure C.1. To that end, notice that the preceding assumptions simplify the error dynamics (3.99), (3.110) as follows:

$$\begin{aligned} \dot{\boldsymbol{e}}_C(t) &= \boldsymbol{A}_M \boldsymbol{e}_C(t) + \boldsymbol{B}_P \left(\tilde{\boldsymbol{\Theta}}_x(t) \cdot \boldsymbol{x}_P(t) + \boldsymbol{z}_P(t) \right), \\ \dot{\tilde{\boldsymbol{\Theta}}}_x(t)^T &= -\boldsymbol{\Gamma}_x \left(\boldsymbol{x}_P(t) \cdot \boldsymbol{e}_C(t)^T \boldsymbol{P} \boldsymbol{B}_P + \boldsymbol{\sigma} \cdot \tilde{\boldsymbol{\Theta}}_x(t)^T + \boldsymbol{\sigma} \cdot \boldsymbol{\Theta}_x^{*T} \right). \end{aligned} \tag{4.22}$$

To arrive at a structure according to Figure C.1, choose $w_0(t) = 0$ and define

$$w_1(t) \triangleq z_P(t) = \Delta\{u(t) + z_P(t)\} = \Delta\{u(t) + w_1(t)\} = -w_2(t). \tag{4.23}$$

By defining

$$z_2(t) \triangleq u(t) + z_P(t) = u(t) + w_1(t), \tag{4.24}$$

the system $w_2(t) = \mathcal{G}_2\{z_2(t)\}$ has to be chosen as

$$\mathcal{G}_2\{z_2(t)\} = -\Delta\{u(t) + w_1(t)\} \tag{4.25}$$

in order to comply with Figure C.1. Furthermore, $z_2(t) = z_0(t) - z_1(t)$ has to hold. Hence, the signal $z_2(t)$, which has been defined in (4.24), needs to be appropriately partitioned. For this, the signal $z_2(t)$ is separated into one part $z_0(t)$, which is known to be bounded, and a second part, whose boundedness needs to be shown using the small-gain theorem. For this, the control signal $u(t)$ is inserted into the definition (4.24):

$$\begin{aligned} z_2(t) &= K_r r(t) + \boldsymbol{\Theta}_x(t) \cdot \boldsymbol{x}_P(t) + w_1(t) \\ &= K_r r(t) + \left(\tilde{\boldsymbol{\Theta}}_x(t) + \boldsymbol{\Theta}_x^* \right) \cdot \left(\boldsymbol{e}_C(t) + \boldsymbol{x}_M(t) \right) + w_1(t) \\ &= \underbrace{K_r r(t) + \boldsymbol{\Theta}_x^* \boldsymbol{x}_M(t)}_{z_0(t)} + \underbrace{\tilde{\boldsymbol{\Theta}}_x(t) \boldsymbol{x}_P(t) + \boldsymbol{\Theta}_x^* \cdot \boldsymbol{e}_C(t) + w_1(t)}_{-z_1(t)}. \end{aligned} \tag{4.26}$$

Since $r(t)$ is bounded, the signal $z_0(t)$ is bounded as well. Hence, the system $z_1(t) = \mathcal{G}_1\{w_1(t)\}$ is defined as follows:

$$\begin{aligned} \dot{\boldsymbol{e}}_C(t) &= \boldsymbol{A}_M \boldsymbol{e}_C(t) + \boldsymbol{B}_P \left(\tilde{\boldsymbol{\Theta}}_x(t) \cdot \boldsymbol{x}_P(t) + w_1(t) \right), \\ \dot{\tilde{\boldsymbol{\Theta}}}_x(t)^T &= -\boldsymbol{\Gamma}_x \left(\boldsymbol{x}_P(t) \cdot \boldsymbol{e}_C(t)^T \boldsymbol{P} \boldsymbol{B}_P + \boldsymbol{\sigma} \cdot \tilde{\boldsymbol{\Theta}}_x(t)^T + \boldsymbol{\sigma} \cdot \boldsymbol{\Theta}_x^{*T} \right), \\ z_1(t) &= -\left(\tilde{\boldsymbol{\Theta}}_x(t) \boldsymbol{x}_P(t) + \boldsymbol{\Theta}_x^* \cdot \boldsymbol{e}_C(t) + w_1(t) \right). \end{aligned} \tag{4.27}$$

Using the $\mathcal{L}_2$-gain γ_1 of the system (4.27) from the input $w_1(t)$ to the output $z_1(t)$, the small-gain theorem states that the feedback connection of $\mathcal{G}_1\{\cdot\}$ and $\mathcal{G}_2\{\cdot\}$ is finite-gain $\mathcal{L}_2$-stable, if the $\mathcal{L}_2$-gain γ_2 of $\mathcal{G}_2\{\cdot\}$ satisfies:

$$\gamma_2 < \frac{1}{\gamma_1}. \tag{4.28}$$

The $\mathcal{L}_2$-gain γ_1 therefore is a robustness metric for an adaptive controller and quantifies the largest admissible input uncertainty in terms of its $\mathcal{L}_2$-gain γ_2 [179]. For other types of unmodeled dynamics or unmatched parametric uncertainties, the error dynamics may be transformed to the structure of Figure C.1 in an analogous way [180].

Analytical Computation

In general, the $\mathcal{L}_2$-gain of a nonlinear system may be computed using the *Hamilton-Jacobi inequality* [96]. However, [178] proposes to obtain a Linear Parameter Varying (LPV) representation of the nonlinear system (4.27) first. This LPV representation follows from a linear differential inclusion [17]. For this, the plant state $\boldsymbol{x}_P(t)$ in (4.27) is treated as a bounded, time-varying parameter $\boldsymbol{\rho}(t)$ and the uncertainty $\boldsymbol{\Theta}_x^*$ in the parameter error differential equation is viewed as an exogenous, bounded disturbance. The LPV representation of $\mathcal{G}_1\{\cdot\}$ is then given by:

$$\begin{aligned}\begin{bmatrix}\dot{\boldsymbol{e}}_C(t)\\ \dot{\tilde{\boldsymbol{\Theta}}}_x(t)^T\end{bmatrix} &= \begin{bmatrix}\boldsymbol{A}_M & \boldsymbol{B}_P\boldsymbol{\rho}(t)^T\\ -\boldsymbol{\Gamma}_x\boldsymbol{\rho}(t)\boldsymbol{B}_P^T\boldsymbol{P} & -\boldsymbol{\Gamma}_x\boldsymbol{\sigma}\end{bmatrix}\cdot\begin{bmatrix}\boldsymbol{e}_C(t)\\ \tilde{\boldsymbol{\Theta}}_x(t)^T\end{bmatrix} + \begin{bmatrix}\boldsymbol{B}_P & \boldsymbol{0}\\ \boldsymbol{0} & -\boldsymbol{\Gamma}_x\boldsymbol{\sigma}\end{bmatrix}\cdot\begin{bmatrix}w_1(t)\\ \boldsymbol{\Theta}_x^{*T}\end{bmatrix}\\ z_1(t) &= \begin{bmatrix}-\boldsymbol{\Theta}_x^* & -\boldsymbol{\rho}(t)^T\end{bmatrix}\cdot\begin{bmatrix}\boldsymbol{e}_C(t)\\ \tilde{\boldsymbol{\Theta}}_x(t)^T\end{bmatrix} + \begin{bmatrix}-1 & \boldsymbol{0}\end{bmatrix}\cdot\begin{bmatrix}w_1(t)\\ \boldsymbol{\Theta}_x^{*T}\end{bmatrix}\end{aligned} \tag{4.29}$$

Using the LPV representation of $\mathcal{G}_1\{\cdot\}$, one may resort to the Bounded Real Lemma for LPV systems (see for example [2]) in order to compute the $\mathcal{L}_2$-gain [178]. An implementation is readily available in the Robust Control Toolbox of MATLAB®.

When computing the $\mathcal{L}_2$-gain based on a LPV representation of the nonlinear system as proposed in [178, 179], special attention has to be given to the choice of the bounds for the parameter $\boldsymbol{\rho}(t)$. While the LPV representation does indeed exhibit the computed $\mathcal{L}_2$-gain, these results do only hold as long as $\boldsymbol{\rho}(t)$ remains within its predefined bounds. Since $\boldsymbol{\rho}(t)$ actually represents the plant state $\boldsymbol{x}_P(t)$, there is however no guarantee for the parameter $\boldsymbol{\rho}(t)$ to stay within these bounds. A detailed explanation of this problem, which is common when using linear differential inclusions, may for example be found in [21]. Notice that this difficulty is not solved by the use of general regressors such as Radial Basis Functions (RBFs). While the regressor in case of RBFs is bounded by definition, the LPV analysis does not ensure that $\boldsymbol{x}_P(t)$ remains in the respective area of the state space, where the RBF centers have been placed. For this reason, the LPV-based computation of the $\mathcal{L}_2$-gain requires further research, in order to prevent either situation.

Simulation-based Computation

In case of LTI systems, the $\mathcal{L}_2$-gain may also be estimated in simulations using data-driven methods [12, 167]. However, neither an extension of these results to continuous time nonlinear systems nor an application of simulation-based $\mathcal{L}_2$-gain estimation for the robustness analysis of adaptive controllers are known to the author.

Gap Metric

The (ν)-gap metric was originally introduced in the context of LTI control loops [49, 170]. Roughly speaking, it is a measure for the similarity of the trajectories of a nominal LTI plant model and an off-nominal LTI plant model, both of which are controlled by the same LTI controller. Associated with this metric is a stability margin, which determines

the largest admissible gap metric between the nominal and the off-nominal plant that the controller is guaranteed to stabilize. This margin may be computed from the nominal plant model and the controller. As this concept may be generalized to nonlinear systems [68], it is possible to assess the robustness of an adaptive controller using the generalized gap stability margin concept. While it is shown that an unmodified MRAC without robustness modifications and persistent excitation has a zero gap stability margin [68], $\mathcal{L}_1$-ACs are shown to have a non-zero gap stability margin [106]. Having established a non-zero gap stability margin admits computing the largest gap between the nominal plant and a delayed plant, yielding an alternative way of computing the time-delay margin. Adaptive controllers may also be specifically designed to achieve non-zero gap stability margins [62].

Computational Aspects

To the best of the author's knowledge, the gap stability margin may only be computed analytically. It ultimately leads to the problem of computing the (incremental) $\mathcal{L}_p$-gain of an operator, which arises during the gap stability analysis [68].

Parametric Safety Margin

The parametric safety margin is a general methodology for the robust stability and robust performance assessment of arbitrary control systems [35]. The general idea is to determine the largest set (of a given shape) in the space of parametric uncertainties, for which all stability and/or performance requirements are satisfied. To that end, let all parametric uncertainties of the considered plant model be gathered in the vector $\boldsymbol{p}$ and let all controller parameters be gathered in the vector $\boldsymbol{d}$. Furthermore, let the vector $\bar{\boldsymbol{p}}$ denote the nominal values of the uncertainties. The stability and performance requirements (for example in terms of stability and performance metrics like those of Sections 4.1.1 and 4.1.3) are specified such that if all requirements are satisfied, the component-wise inequality

$$\boldsymbol{g}(\boldsymbol{p}, \boldsymbol{d}) < \boldsymbol{0} \Leftrightarrow g_j(\boldsymbol{p}, \boldsymbol{d}) < 0,\ j = 1, \ldots, N \tag{4.30}$$

holds.

To compute the largest set in the space of parameters $\boldsymbol{p}$, where inequality (4.30) holds, a parametrization of the shape of the set is required. For the purpose of illustration, consider a hyper-rectangular set centered on the nominal parameter value $\bar{\boldsymbol{p}}$:

$$\mathcal{R}(\bar{\boldsymbol{p}}, \boldsymbol{n}) = \{\boldsymbol{p} \mid \bar{\boldsymbol{p}} - \boldsymbol{n} \leq \boldsymbol{p} \leq \bar{\boldsymbol{p}} + \boldsymbol{n}\}, \tag{4.31}$$

where $\boldsymbol{n}$ denotes the semi-diagonal of the hyperrectangle and the inequality once again represents a component-wise inequality. The resulting shape of the set is shown in Figure 4.2. The set (4.31) is also called the Reference Set.

Ref. [35] then proposes to compute the largest set, for which all requirements are satisfied, in two steps. First of all, the smallest scaling factor $\alpha \cdot \boldsymbol{n}$ with $\alpha > 0$, for which

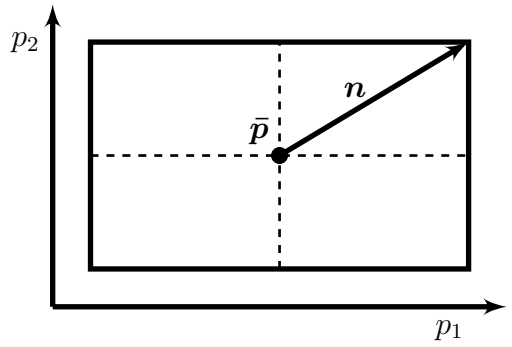

Figure 4.2: Illustration of the Reference Set in case of a parameter vector $\boldsymbol{p}$ with two components.

the j-th requirement $g_j(\boldsymbol{p}, \boldsymbol{d})$ is violated, is computed for each $j = 1, \ldots, N$, leading to:

$$\tilde{\alpha}_j = \arg\min_{\alpha, \boldsymbol{p}} \alpha, \qquad \text{s.t. } g_j(\boldsymbol{p}, \boldsymbol{d}) \geq 0,\ \bar{\boldsymbol{p}} - \alpha \cdot \boldsymbol{n} \leq \boldsymbol{p} \leq \bar{\boldsymbol{p}} - \alpha \cdot \boldsymbol{n} \tag{4.32}$$

The factor α is also called Similitude Ratio. Since the factor $\tilde{\alpha}_j$ denotes the smallest Similitude Ratio, for which the j-th requirement is violated, it is referred to as Critical Similitude Ratio for the j-th requirement. In the second step, the overall Critical Similitude Ratio $\tilde{\alpha}$ is determined by choosing the smallest $\tilde{\alpha}_j$, i.e. $\tilde{\alpha} = \min_j \tilde{\alpha}_j$. The Parametric Safety Margin ρ is then defined as

$$\rho \triangleq \tilde{\alpha} \cdot \|\boldsymbol{n}\|_2 \tag{4.33}$$

and is proportional to the largest size of the rectangular set, for which the requirements are at the verge of satisfaction.

Computational Aspects

For the computation of the Parametric Safety Margin, numerical methods have been proposed [36], which rely on the numerical solution of the optimization problem (4.32). It is interesting to note that this optimization problem may be solved using standard optimization algorithms. In general, the function $\boldsymbol{g}(\boldsymbol{p}, \boldsymbol{d})$ is however highly nonlinear (and non-convex) since its value results from the simulation of the closed-loop system for the uncertainties $\boldsymbol{p}$ and the controller gain $\boldsymbol{d}$. Thus, although the optimization problem (4.32) is a standard one, it may not be guaranteed that $\tilde{\alpha}_j$ and hence $\tilde{\alpha}$ are global minima. Thus, there exists the possibility that the true value of the Parametric Safety Margin is considerably smaller.

4.1.3 Performance Metrics

The reference model of a model following adaptive control system specifies the desired closed-loop performance which is to be achieved by the adaptive controller. In case of the nominal plant and an exact parametrization, a MRAC will asymptotically converge

to this reference model (see for example Theorem 3.4). During transients, the closed-loop performance may however deviate significantly from the reference model [188]. Hence, performance metrics are required in order to assess NP. In case of an off-nominal plant or a non-exact parametrization, a MRAC does no longer converge to the reference model since the adaptive parameters only converge to some vicinity of their ideal values. Thus, performance metrics are also necessary in order to evaluate RP.

Performance requirements for conventional, LTI flight control systems originate for example from the handbook MIL-HDBK-1797 [42]. The performance requirements therein may be roughly divided into frequency-domain requirements and time-domain requirements. While time-domain requirements may also apply to adaptive controllers, frequency-domain requirements may not be employed since adaptive controllers are inherently nonlinear. In some cases, corresponding time-domain criteria may however be derived [15]. Consider for example a requirement on the relative damping of the short-period approximation of the longitudinal motion. This frequency-domain requirement relates to the overshoot of the corresponding step response. It is hence natural to translate the frequency-domain requirement on the relative damping into a time-domain requirement on the step-response [15]. At this point, it is important to notice that the relative damping also relates to the tendency of observing oscillations in the closed-loop response. While a small overshoot of a second-order LTI system always implies high relative damping and little oscillations, a higher-order (nonlinear) system may also exhibit small overshoots and fast oscillations at the same time. This illustrates that the transformation of a frequency-domain requirement into corresponding time-domain requirements is a challenging task due to the nonlinearity of adaptive controllers.

In the remainder of this section, performance metrics for adaptive controllers are presented. At first, the usage of general time-domain performance metrics is discussed, which are not specific to adaptive controllers. Afterwards, specific performance metrics for adaptive controllers are presented.

General Time-Domain Performance Metrics

For the assessment of the performance of a nonlinear control system, one may resort to various time-domain criteria and methods such as

- step response characteristics such as overshoot, rise time, settling time;
- Fourier analysis to evaluate the spectral content of a signal of interest;
- the time-domain Neal-Smith criteria [10] to evaluate the handling qualities of a manned aircraft.

In several publications [159, 161, 37], various other quantities have been suggested. Since there exists a multitude of potential time-domain criteria and since the choice of suitable quantities largely depends on the flight control problem at hand, no complete list will be provided here.

Computational Aspects

A common feature of the previously mentioned performance metrics is that one has to resort to simulation-based techniques in order to compute their value.

Tracking Error Signal Norms

If the adaptive parameters converge, the plant will perfectly track its reference model. Thus, given a properly designed reference model satisfying the closed-loop flight control system requirements, the closed-loop adaptive control system also satisfies these requirements after parameter convergence. However, even in case of the nominal plant, the plant significantly deviates from the reference model during transients. Thus, the $\mathcal{L}_p$-norms of the tracking error (or its individual components) are intuitive metrics for NP of an adaptive controller. In case of an off-nominal plant, unmatched parametric uncertainties, unmodeled dynamics or noise will lead to a non-vanishing tracking error and again, the $\mathcal{L}_p$-norms of the tracking error may be used in order to assess RP of an adaptive controller.

A metric to measure the largest deviation of the closed-loop system from the reference model is given by the $\mathcal{L}_\infty$-norm of the tracking error:

$$M_{e,\mathcal{L}_\infty} = \|\boldsymbol{x}_P(t) - \boldsymbol{x}_M(t)\|_{\mathcal{L}_\infty}. \tag{4.34}$$

For the metric to scale with different sizes of the command $\boldsymbol{r}(t)$, it may be furthermore normalized according to:

$$\bar{M}_{e,\mathcal{L}_\infty} = \frac{\|\boldsymbol{x}_P(t) - \boldsymbol{x}_M(t)\|_{\mathcal{L}_\infty}}{\|\boldsymbol{x}_M(t)\|_{\mathcal{L}_\infty}}. \tag{4.35}$$

While the $\mathcal{L}_\infty$-norm characterizes the largest deviation between the plant and the reference model, the $\mathcal{L}_2$-norm reflects the energy of the tracking error signal. Similar to the $\mathcal{L}_\infty$-norm, unnormalized and normalized metrics may be defined:

$$M_{e,\mathcal{L}_2} = \|\boldsymbol{x}_P(t) - \boldsymbol{x}_M(t)\|_{\mathcal{L}_2}, \tag{4.36}$$

$$\bar{M}_{e,\mathcal{L}_2} = \frac{\|\boldsymbol{x}_P(t) - \boldsymbol{x}_M(t)\|_{\mathcal{L}_2}}{\|\boldsymbol{x}_M(t)\|_{\mathcal{L}_2}}. \tag{4.37}$$

Notice however that the $\mathcal{L}_2$-norm is only guaranteed to be bounded in case of the nominal plant model [89]. For off-nominal plants, the $\mathcal{L}_2$-norm may be infinite. In this case, the related Root Mean Square (RMS) of the tracking error may be used instead:

$$M_{e,RMS} = \lim_{T\to\infty} \frac{1}{T} \cdot \int_0^T \|\boldsymbol{x}_P(\tau) - \boldsymbol{x}_M(\tau)\|_2^2 \, d\tau. \tag{4.38}$$

Notice that a small value of the RMS of the tracking error does not exclude undesirable phenomena such as bursting [89]. Bursting describes an effect, where “the tracking error, after reaching a steady-state behavior, bursts into oscillations of large amplitude over short intervals of time” [89]. Similarly, a small value of the $M_{e,\mathcal{L}_2}$ does not exclude oscillations of the tracking error.

Analytical Computation

Bounds on the previously mentioned tracking error norms may be computed analytically. When considering NP, a conservative bound on $M_{e,\mathcal{L}_\infty}$ for a direct MRAC and zero initial tracking error ($\boldsymbol{e}_C(0) = \mathbf{0}$) follows for example from (3.62) and the equivalence of vector norms:

$$M_{e,\mathcal{L}_\infty} \leq \sqrt{\frac{\Lambda_{\max} \cdot {\Theta^*_{\max}}^2}{\lambda_{\min}(\boldsymbol{P}) \cdot \lambda_{\min}(\boldsymbol{\Gamma})}}. \tag{4.39}$$

The bound (4.39) is highly conservative. For this reason, a novel method for the computation of less conservative bounds has been recently proposed [56, 61, 58]. A similar development may also be found in this thesis, which will be discussed in detail in Section 4.2.

In case of an off-nominal plant, i.e. when considering RP, a similar bound to (4.39) may be derived as well. Similar to the bound in case of NP, this bound suffers from significant conservatism. In case of bounded plant imperfections (see (3.96)), Ref. [55, 57] describe a novel method, which admit the computation of less conservative upper bounds. A similar development may also be found in Section 4.2 of this thesis. More recently, the approach from [55, 57] was extended to the analysis of unmodeled actuator dynamics [60].

When considering NP, a bound on $M_{e,\mathcal{L}_2}$ may also be derived from the Lyapunov proof of stability. To that end, consider the direct MRAC of Section 3.2.1. The following relationship between the Lyapunov function and its derivative holds:

$$\int_0^T \dot{V}(\tau) d\tau = V(T) - V(0) \tag{4.40}$$

for all $T \geq 0$. Multiplying by -1 yields

$$-\int_0^T \dot{V}(\tau) d\tau = V(0) - V(T). \tag{4.41}$$

Inserting the actual value of $\dot{V}(t)$ from (3.42) then leads to

$$\int_0^T \boldsymbol{e}_C(\tau)^T \boldsymbol{Q} \boldsymbol{e}_C(\tau) d\tau = V(0) - V(T). \tag{4.42}$$

By using the quadratic form bound (B.64), Eq. (4.42) is bounded from below by

$$\lambda_{\min}(\boldsymbol{Q}) \cdot \int_0^T \|\boldsymbol{e}_C(\tau)\|_2^2 \, d\tau \leq V(0) - V(T). \tag{4.43}$$

Since $V(t)$ is positive definite and $\dot{V}(t) \leq 0$ holds for all times, the value of $V(T)$ is confined to the interval $0 \leq V(T) \leq V(0)$. Hence, the right hand side of (4.43) is bounded by $V(0)$:

$$\lambda_{\min}(\boldsymbol{Q}) \cdot \int_0^T \|\boldsymbol{e}_C(\tau)\|_2^2 \, d\tau \leq V(0). \tag{4.44}$$

The value $V(0)$ represents the initial level set, in which the adaptive controller will remain for all times. When assuming the initial conditions from (3.56) ($\boldsymbol{e}_C(0) = \mathbf{0}$ and

$\tilde{\boldsymbol{\Theta}}(0) = -\boldsymbol{\Theta}^*$) and the uncertainty bounds from (3.57) ($\|\boldsymbol{\Theta}^*\|_F \leq \Theta^*_{\max}$ and $\lambda_{\max}(\boldsymbol{\Lambda}) = \|\boldsymbol{\Lambda}\|_{i,2} \leq \Lambda_{\max}$), then Eq. (3.61) states that

$$V(0) \leq \frac{\Lambda_{\max}}{2 \cdot \lambda_{\min}(\boldsymbol{\Gamma})} \cdot {\Theta^*_{\max}}^2$$

holds. Inserting the latter relation into (4.44) yields

$$\lambda_{\min}(\boldsymbol{Q}) \cdot \int_0^T \|\boldsymbol{e}_C(\tau)\|_2^2 \, d\tau \leq \frac{\Lambda_{\max}}{2 \cdot \lambda_{\min}(\boldsymbol{\Gamma})} \cdot {\Theta^*_{\max}}^2 \tag{4.45}$$

For $T \to \infty$, the left hand side of (4.45) corresponds to the square of the definition of the $\mathcal{L}_2$-norm. The following bound for $M_{e,\mathcal{L}_2}$ results:

$$M_{e,\mathcal{L}_2} \leq \sqrt{\frac{\Lambda_{\max} \cdot {\Theta^*_{\max}}^2}{2 \cdot \lambda_{\min}(\boldsymbol{\Gamma}) \cdot \lambda_{\min}(\boldsymbol{Q})}}. \tag{4.46}$$

Since the $\mathcal{L}_2$-norm is finite due to (4.46), the metric $M_{e,RMS}$ will be zero for any direct MRAC in case of the nominal plant. However, when considering an off-nominal plant, that is when considering RP, $M_{e,\mathcal{L}_2}$ usually is not finite [89] as $\dot{V}(t)$ depends on the non-vanishing disturbance $\boldsymbol{w}(t) \in \mathcal{L}_\infty$. In case of a direct MRAC with σ-modification, this can be seen in (3.111). While $M_{e,\mathcal{L}_2}$ tends to infinity then, $M_{e,RMS}$ will take on non-negative, finite values [158].

Simulation-based Computation

Using simulations, the above performance metrics may be easily computed. Since a simulation run has a finite duration T_f, only truncated norms may be determined in practice.

Instead of applying the above norms to the signals of a whole simulation run, they may also be applied separately to the transient and the steady-state phases [161]. To distinguish the steady-state from the transient phases, the distance of the adaptive parameter $\boldsymbol{\Theta}(t)$ from its final value $\boldsymbol{\Theta}(T_f)$, learning metrics, or a-priori knowledge of the optimal adaptive parameters $\boldsymbol{\Theta}^*$ may be used.

Control Signal Norms

While tracking error norms assess the deviation between the plant and the reference model, the difference between the ideal control signal $\boldsymbol{u}^*(t) = \boldsymbol{\Theta}^* \cdot \boldsymbol{\omega}(\boldsymbol{x}_P(t), t)$ and the adaptive control signal $\boldsymbol{u}(t) = \boldsymbol{\Theta}(t) \cdot \boldsymbol{\omega}(\boldsymbol{x}_P(t), t)$ admits conclusions on the quality of the control signal. Based on the $\mathcal{L}_\infty$-norm, the following control signal metrics may be defined

$$M_{\mathcal{L}_\infty} = \|\boldsymbol{u}(t) - \boldsymbol{u}^*(t)\|_{\mathcal{L}_\infty}, \tag{4.47}$$

$$\bar{M}_{\mathcal{L}_\infty} = \frac{\|\boldsymbol{u}(t) - \boldsymbol{u}^*(t)\|_{\mathcal{L}_\infty}}{\|\boldsymbol{u}^*(t)\|_{\mathcal{L}_\infty}}. \tag{4.48}$$

In addition, the energy of the deviation between ideal and real control signal may also be used to define a normalized and an unnormalized metric for the control signal:

$$M_{\mathcal{L}_2} = \|\boldsymbol{u}(t) - \boldsymbol{u}^*(t)\|_{\mathcal{L}_2}, \tag{4.49}$$

$$\bar{M}_{\mathcal{L}_2} = \frac{\|\boldsymbol{u}(t) - \boldsymbol{u}^*(t)\|_{\mathcal{L}_2}}{\|\boldsymbol{u}^*(t)\|_{\mathcal{L}_2}}. \tag{4.50}$$

Analytical Computation

Compared to the analytical bounds on the tracking error, the computation of bounds on the control signal is more challenging. This is because the error $\boldsymbol{u}(t) - \boldsymbol{u}^*(t) = \tilde{\boldsymbol{\Theta}}(t) \cdot \boldsymbol{\omega}(\boldsymbol{x}_M(t) + \boldsymbol{e}_C(t), t)$ depends on the parameter error and the tracking error at the same time. More details on the computation of bounds on $\mathcal{L}_p$-norms of the control signal $\boldsymbol{u}(t) = \boldsymbol{\Theta}(t) \cdot \boldsymbol{\omega}(\boldsymbol{x}_P(t), t)$ can be found in [63].

Simulation-based Computation

With respect to the simulation-based computation, the same comments apply as in case of $\mathcal{L}_p$-norms of the tracking error.

4.1.4 Discussion

The previous subsections presented various robustness and performance metrics, which are applicable to an adaptive control system. The computation of these metrics may be carried out using simulations, analytically or both. Judging from the above review of robustness and performance metrics, the simulation-based computation is most versatile since almost all metrics (except for the $\mathcal{L}_2$-gain and the gap metric) can be computed in that way. Especially the general time-domain performance metrics enable a detailed assessment of the performance of an adaptive control system (see for example [15]). Furthermore, the simulation-based bounds on the metrics of interest are tight for the simulated trajectories. The confidence in the simulation-based metrics does however strongly depend on the number of conducted simulations. Even after a large number of simulations, there is no guarantee that there does not exist another combination of uncertainties and command signals, for which the metric of interest takes on a worse value. If the number of simulations is sufficiently high, the probability of such an event is small. In contrast to the simulation-based computation, the analytical computation yields guaranteed bounds on the metric of interest, which hold for all considered uncertainties and all considered command signals. However, as demonstrated in Sections 4.2 and 4.3, the conservatism of these bounds often limits their practical utility. Furthermore, analytical methods usually require the use of simplified plant models.

When comparing the properties of analytical and simulation-based computations, one observes that both approaches complement each other. This can be demonstrated best with the help of an example. For this, consider the time-delay margin of a direct

MRAC and notice that the time-delay margin can be computed in either way. Since a direct MRAC leads to a nonlinear closed loop, the true value $\tau_{c,\max}$ of the time-delay margin is unknown. Analytically, a bound $\tau_{c,ana}$ is computed, which is guaranteed to hold for all considered uncertainties $\boldsymbol{\Theta}^*$ and for all suitably bounded command signals $\boldsymbol{r}\,(t)$. A computational method to that end will be presented in Section 4.3. Since analytical bounds are conservative, $\tau_{c,ana}$ constitutes a lower bound on the true time-delay margin. Conversely, the time-delay margin, which is determined in simulations, will be denoted by $\tau_{c,sim}$. Strictly speaking, it only holds for the simulated trajectories, that is, for the simulated parametric uncertainties $\boldsymbol{\Theta}^*$ and the simulated command signals $\boldsymbol{r}\,(t)$. Hence, there might exist other combinations of the uncertainties and the command signal, for which the time-delay margin is lower. Consequently, the simulation-based time-delay margin represents an upper bound on the true time-delay margin. By increasing the number of simulation runs, the probability of a worse combination can be decreased. In any case, the following inequality holds, which relates simulation-based and analytical computations:

$$\tau_{c,ana} \leq \tau_{c,\max} \leq \tau_{c,sim}. \tag{4.51}$$

With respect to a future certification process, those metrics seem favorable whose bounds complement each other according to a relation such as (4.51): Since an analytical bound exists, the time-delay margin in (4.51) is guaranteed to be non-zero. At the same time, less conservative values of the time-delay margin follow from the simulation-based computation. Since the simulation-based bound only holds with a certain confidence, it could become zero. Due to the existence of a complementary analytical bound, this case is excluded.

Eq. (4.51) may also serve as an indicator of reliability. If the gap $\tau_{c,sim} - \tau_{c,ana}$ becomes small, then the analytical and simulation-based bounds closely approximate the unknown true time-delay margin $\tau_{c,\max}$. In order to decrease the gap between analytical and simulation-based computations, research has to address different aspects. In case of the analytical computation, the conservatism of the computed bounds needs to be reduced. For the simulation-based computation, research has to focus on a reduction of the computational effort, which is required in order to obtain reliable bounds. To that end, modern Monte-Carlo methods such as Subset simulations [7] or optimization techniques such as counter-proving [169] can be used. Notice that the same argument also holds for other metrics, which can be determined analytically and using simulations.

When only considering those metrics, which can be computed analytically *and* in simulations, the number of available robustness and performance metrics shrinks significantly. In case of robustness metrics, the time-delay margin represents the only metric that admits both computations. The other robustness metrics are either not computable in both ways ($\mathcal{L}_2$-gain, gap metric, parametric safety margin) or do not lead

to a reliable assessment of robustness in the transient phase (metrics, which rely on linearization). In case of performance metrics, only the $\mathcal{L}_p$-norms of the tracking error and the control signal remain. General time-domain performance metrics such as rise time and overshoot do not allow an analytical computation.

As noted at the beginning of this chapter, the robustness and performance metrics should satisfy basic criteria in order to be useful in a future certification process. When applying these criteria to the remaining metrics, one observes that the time-delay margin and the $\mathcal{L}_\infty$-norm of the tracking error *components* satisfy all of these requirements. Other metrics, such as the energy (i.e. the $\mathcal{L}_2$-norm) of the tracking error or the $\mathcal{L}_\infty$-norm of the *whole tracking error vector* $\boldsymbol{e}_C(t)$ violate at least some of these requirements. In case of the $\mathcal{L}_2$-norm of the tracking error, it is for example difficult to specify admissible values in advance. This is because the size of the $\mathcal{L}_2$-norm depends on the energy, which is inserted into the closed loop by plant imperfections. Similarly, a bound for the $\mathcal{L}_\infty$-norm of the *whole tracking error state vector* does not impose a physically meaningful requirement for *individual aircraft states* such as the angle-of-attack. Instead, the $\mathcal{L}_\infty$-norm of the *whole tracking error state vector* imposes a requirement on all states, even though each state represents a different physical quantity (with a different unit).

For this reason, the time-delay margin and the $\mathcal{L}_\infty$-norm of the tracking error *components* will be specifically considered in the subsequent sections. As this thesis focuses on adaptive control theory rather than simulation techniques, the improvement of simulation techniques is not considered any further.

4.2 Tracking Error Norms

In the previous section, the $\mathcal{L}_\infty$-norm of the tracking error components has been identified as a performance metric that might be suitable for a future certification process. While the specification of admissible bounds seems feasible, the verification of such requirements assumes efficient methods for the computation of tracking error bounds. However, conventional analytical bounds for the tracking error components are highly conservative.

In order to address this problem, this section proposes novel methods for the computation of less conservative bounds in case of a direct MRAC. First of all, the nominal plant is considered. In Section 4.2.1, a less conservative NP bound on the $\mathcal{L}_\infty$-norm of the components of the tracking error is derived. This bound is derived following a worst-case paradigm, in which all uncertainties $\boldsymbol{\Theta}^*$ and all amplitudes of the command signal $\boldsymbol{r}(t)$ are equally probable. In practice, the uncertainties $\boldsymbol{\Theta}^*$ are often distributed according to some a-priori known distribution. Hence, some uncertainty combinations are more probable than others. For this reason, Section 4.2.2 proposes a simple method to account for this fact. Finally, off-nominal plants are considered. Since an off-nominal

plant may lead to parameter drift, a direct MRAC with σ-modification is used. Section 4.2.3 derives RP bounds on the $\mathcal{L}_\infty$-norm of the tracking error components in case of neglected unmatched parametric uncertainties and bounded exogenous disturbances. Similar to Section 4.2.1, this derivation follows a worst-case paradigm.

4.2.1 Computation of Tracking Error Norms

In Section 4.1.3, the NP bound (4.39) for the $\mathcal{L}_\infty$-norm of the tracking error $\boldsymbol{e}_C(t)$ of a direct MRAC has been presented, which is highly conservative. This shall be demonstrated by the following example:

Example 4.1. *Consider the plant and the direct MRAC of Example 3.6. In order to apply the tracking error bound* (4.39)*, the minimum eigenvalues of $\boldsymbol{P}$ and $\boldsymbol{\Gamma}$ as well as the uncertainty bound $\Lambda_{\max}$ and the ideal parameter bound $\Theta^*_{\max}$ have to be determined first.*

Since the design parameters of the MRAC are chosen as $\boldsymbol{Q} = \boldsymbol{I}^{2\times 2}$ and $\boldsymbol{\Gamma} = \gamma \cdot \boldsymbol{I}^{3\times 3}$, where $\gamma > 0$ is some positive constant, $\lambda_{\min}(\boldsymbol{P}) = 0.1442$ and $\lambda_{\min}(\boldsymbol{\Gamma}) = \gamma$ result. With respect to the uncertainty bounds, $\Lambda_{\max} = \lambda_{\max}(\boldsymbol{\Lambda}) = \max \lambda_\eta = 1.5$ holds due to the uncertainty bounds of the plant, given in Table 2.4. In order to compute the ideal parameter bound $\Theta^*_{\max} = \|\boldsymbol{\Theta}^*\|_F$, all admissible values of the ideal parameter $\boldsymbol{\Theta}^*$, which result from the uncertainty bounds in Table 2.4 (assuming $\lambda_{Z\alpha} = \lambda_{Zq} = 1$), have to be computed first. To that end, notice that the matching condition implies that the ideal parameter $\boldsymbol{\Theta}^*$ relates to the plant uncertainties through (3.54)*. The ideal parameter Θ^*_r is hence confined to the interval*

$$-0.98 = \frac{K_r}{\min \lambda_\eta} \leq \Theta^*_r \leq \frac{K_r}{\max \lambda_\eta} = -0.33. \tag{4.52}$$

The computation of the ideal parameter $\boldsymbol{\Theta}^*_x$ is slightly more difficult. For each value of the control effectiveness $\Lambda = \lambda_\eta$, (3.54) *represents a shape-preserving transformation. Hence, the rectangular uncertainty set $0.5 \leq \lambda_\alpha \leq 1.5$ and $0.5 \leq \lambda_q \leq 1.5$ is mapped to a rectangular set in the $\boldsymbol{\Theta}^*_x$-space. The center and the size of these rectangles however vary with Λ. This situation is visualized in Figure 4.3 for three different values of the control effectiveness Λ. The extremal value of $\boldsymbol{\Theta}^*$ in terms of the Frobenius norm (2-norm) is hence reached at the point (-3.57, -0.75, -0.98), leading to $\Theta^*_{\max} = 3.78$.*

Figure 4.3 and Eq. (4.52) *show that the set of admissible ideal parameters lies entirely in the (-,-,-)-octant of the three-dimensional space of ideal parameters. Since the ball $\|\boldsymbol{\Theta}^*\|_F \leq 3.78$ covers a significantly larger volume, it is expected that a tracking error bound inferred from the uncertainty bound $\|\boldsymbol{\Theta}^*\|_F \leq 3.78$ is overly conservative. A simple solution to alleviate this problem is the use of a baseline controller. To that end, consider the baseline controller* (3.63)*. Suitable controller gains $\boldsymbol{K}_x$ and K_r have already been derived in Example 3.6 during the design of the reference model. Since a*

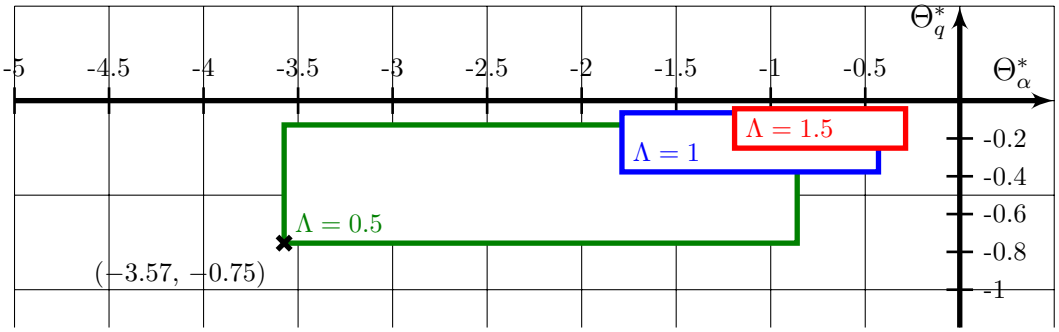

Figure 4.3: Mapping of the uncertainty set $0.5 \leq \lambda_\alpha \leq 1.5$, $0.5 \leq \lambda_q \leq 1.5$ to its corresponding ideal parameters Θ_α^*, Θ_q^* for three different values of the control effectiveness Λ, if no baseline controller is used.

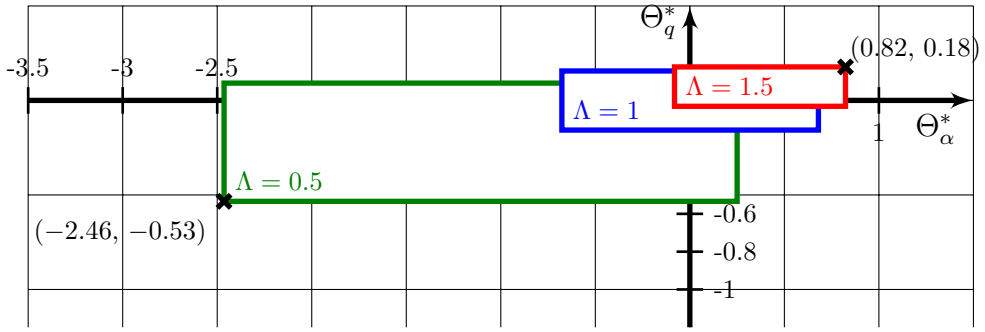

Figure 4.4: Mapping of the uncertainty set $0.5 \leq \lambda_\alpha \leq 1.5$, $0.5 \leq \lambda_q \leq 1.5$ to its corresponding ideal parameters Θ_α^*, Θ_q^* for three different values of the control effectiveness Λ, if a baseline controller is used.

baseline controller is used, the altered matching conditions from Assumption 3.9 have to be used to compute the ideal parameter $\boldsymbol{\Theta}^*$, leading to:

$$\Theta_\alpha^* = \frac{M_{\alpha,des} - M_\alpha \cdot \lambda_\alpha}{\lambda_\eta \cdot M_\eta} - K_\alpha, \quad \Theta_q^* = \frac{M_{q,des} - M_q \cdot \lambda_q}{\lambda_\eta \cdot M_\eta} - K_q, \quad \Theta_r^* = \frac{K_r}{\lambda_\eta} - K_r, \tag{4.53}$$

where the partition $\boldsymbol{K}_x = \begin{bmatrix} K_\alpha & K_q \end{bmatrix}$ is used. When a baseline controller is used, the ideal parameter Θ_r^* is confined to the interval

$$-0.49 \leq \Theta_r^* \leq 0.16. \tag{4.54}$$

The mapping of the rectangular uncertainty set $0.5 \leq \lambda_\alpha \leq 1.5$ and $0.5 \leq \lambda_q \leq 1.5$ to the resulting set in the $\boldsymbol{\Theta}_x^*$-space is visualized in Figure 4.4. The extremal value of $\boldsymbol{\Theta}^*$ in terms of the Frobenius norm (2-norm) is hence reached at the point (-2.46, -0.53, -0.49), leading to $\Theta_{\max}^* = 2.57$.

Since the accommodation of a baseline controller does neither change the error dynamics of the adaptive controller nor its proof of stability, the tracking error bound (4.39) *also holds in case of an adaptive augmentation of a baseline controller. In Figure 4.5, the results of the tracking error bound* (4.39) *are compared to the largest*

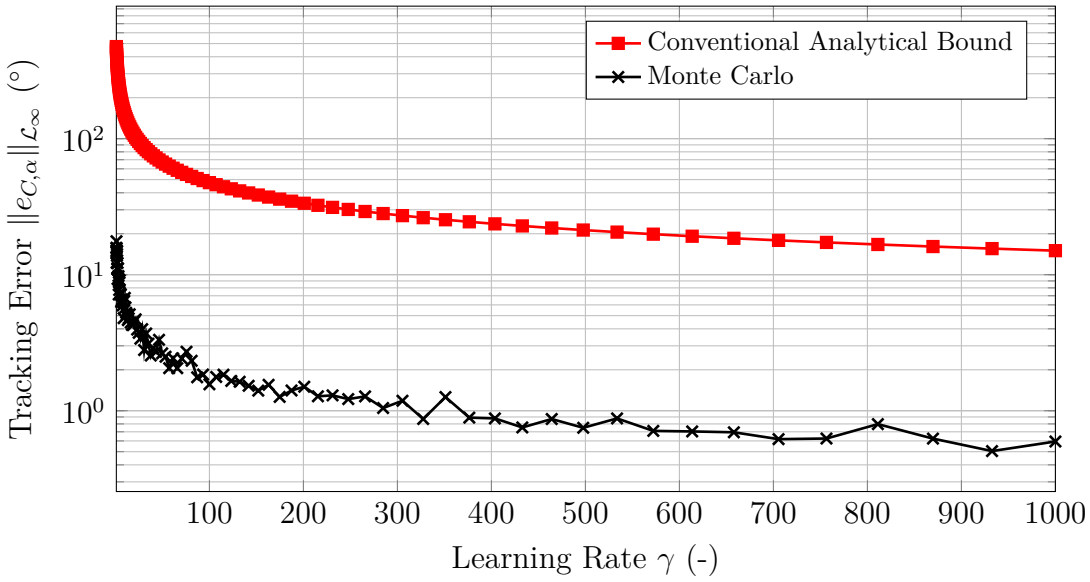

Figure 4.5: Comparison of the conventional analytical tracking error bound of Eq. (4.39) with the largest tracking error $\|e_{C,\alpha}(t)_\tau\|_{\mathcal{L}_\infty}$ observed in simulations for different values of the learning rate γ.

tracking error observed in Monte Carlo simulations for different values of the learning rate $\boldsymbol{\Gamma} = \gamma \cdot \boldsymbol{I}^{3\times 3}$. *For Figure 4.5, the analytical tracking error bound was computed using* (4.39) *for each value of* γ. *For the simulation-based tracking error bound, a Monte Carlo simulation with 1000 runs was carried out for each value of* γ. *This Monte Carlo simulation did not only vary the plant uncertainties* λ_α, λ_q *and* λ_η, *but also varied the size and the type of the command signal* $r(t)$. *It may be clearly observed that the analytical tracking error bound is by far larger than the largest tracking error* $e_{C,\alpha}(t) = \alpha(t) - \alpha_M(t)$, *which may be observed in simulations. Even for a high learning rate* $\gamma = 1000$, *the analytical bound exceeds the largest tracking error observed in simulations by 2400%.*

In order to use analytical bounds on the tracking error within a certification process, the conservatism of these bound needs to be reduced significantly. Subsequently, a novel method for the computation is presented, which leads to tighter bounds on the tracking error. In order to motivate this novel approach, the reasons for conservatism have to be analyzed first.

Sources of Conservatism

Two major aspects lead to the conservatism of the bound (4.39). The first contribution derives from the fact that the tracking error bound is derived from a Lyapunov proof of stability. The central elements of any Lyapunov proof of stability are the scalar, energy-like Lyapunov function and its derivative. By virtue of the Lyapunov theorem (e.g. Theorem C.2), the stability analysis of the original, n-dimensional system reduces to the analysis of the 1-dimensional Lyapunov function and its derivative. In this way,

the explicit analytical solution of the differential equations of the n-dimensional system is avoided. Since no explicit solution is available, one has to resort to the level sets of the 1-dimensional Lyapunov function in order to infer bounds on the states of the n-dimensional system. Except for some rare cases, these level sets do not describe individual state trajectories, but describe areas in the state space, which a multitude of different trajectories may not leave. Hence, the process of analyzing the n-dimensional system with the help of a scalar, auxiliary system and inferring bounds on the trajectories from its level sets leads to a loss of information and does hence introduce conservatism. The only way of mitigating this source of conservatism would be an alternative approach to the stability analysis of a MRAC. Since no appropriate alternative method is known to the author, this source of conservatism seems to be inevitable for the time being.

The second contribution for conservatism stems from the way, the bound on the tracking error is derived. In order to understand these sources of conservatism, a geometric derivation of the tracking error bound (4.39) is helpful. The derivation comprises two major steps:

1. A level set constant $c \geq 0$ is determined such that the level set

$$\mathcal{M}_c \triangleq \left\{ \boldsymbol{e}_C, \tilde{\boldsymbol{\Theta}} \mid V(\boldsymbol{e}_C, \tilde{\boldsymbol{\Theta}}) \leq c \right\} \tag{4.55}$$

   surrounds the set of all admissible initial conditions $\mathcal{M}_i$, i.e. $\mathcal{M}_i \subseteq \mathcal{M}_c$. Since level sets are invariant, all trajectories which start in $\mathcal{M}_i \subseteq \mathcal{M}_c$ will remain in $\mathcal{M}_c$ for all times:

$$\left(\boldsymbol{e}_C(t), \tilde{\boldsymbol{\Theta}}(t) \right) \in \mathcal{M}_c, \ \forall\, t \geq 0. \tag{4.56}$$

2. A bound on the tracking error is derived from the level set $\mathcal{M}_c$.

The definition of the set $\mathcal{M}_c$ in (4.55) neglects the dependence of the Lyapunov function on time. Furthermore, the Lyapunov function is expressed as $V(\boldsymbol{e}_C, \tilde{\boldsymbol{\Theta}})$ instead of $V(t)$. On the one side, this stresses the dependence of V on $\boldsymbol{e}_C$ and $\tilde{\boldsymbol{\Theta}}$. On the other side, the shape and size of the set $\mathcal{M}_c$ do not depend on time. For this reason, sets are defined in terms $\boldsymbol{e}_C$ and $\tilde{\boldsymbol{\Theta}}$ instead of $\boldsymbol{e}_C(t)$ and $\tilde{\boldsymbol{\Theta}}(t)$.

Geometrically, the level set $\mathcal{M}_c$ of the quadratic Lyapunov function (3.30) describes an ellipsoid in $\mathbb{R}^{n+m\cdot n_r}$. For further details on such quadratic forms, see Appendix B.2.1. The derivation of the tracking error bound (4.39) assumes the initial conditions from (3.56) (i.e. $\boldsymbol{e}_C(0) = \boldsymbol{0}$ and $\tilde{\boldsymbol{\Theta}}(0) = -\boldsymbol{\Theta}^*$) and the uncertainty bound from (3.57) (i.e. $\|\boldsymbol{\Theta}^*\|_F \leq \Theta^*_{\max}$). Hence, the set of admissible initial conditions is given by:

$$\mathcal{M}_i \triangleq \left\{ \boldsymbol{e}_C, \tilde{\boldsymbol{\Theta}} \mid \boldsymbol{e}_C = \boldsymbol{0} \wedge \|\tilde{\boldsymbol{\Theta}}\|_F \leq \Theta^*_{\max} \right\}. \tag{4.57}$$

Geometrically, $\mathcal{M}_i$ is a degenerate sphere in $\mathbb{R}^{n+m\cdot n_r}$. That is, it is a sphere in $\operatorname{vec}\tilde{\boldsymbol{\Theta}}$-direction due to $\|\tilde{\boldsymbol{\Theta}}\|_F = \|\operatorname{vec}\tilde{\boldsymbol{\Theta}}\|_2$ and has no extension in all $\boldsymbol{e}_C$-directions (see Figure 4.6).

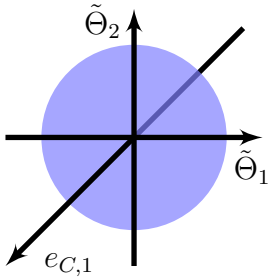

Figure 4.6: Illustration of a degenerate sphere in $\mathbb{R}^3$ with no extension in $e_{C,1}$-direction.

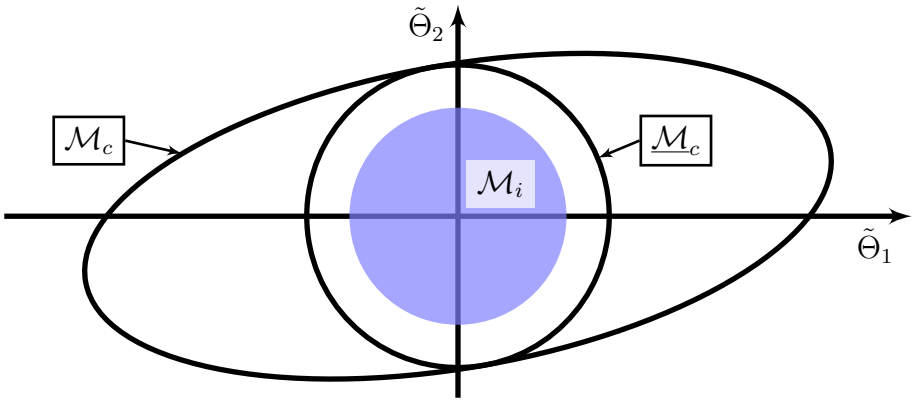

Figure 4.7: Plane section in $\operatorname{vec}\tilde{\boldsymbol{\Theta}}$-direction ($\boldsymbol{e}_C = \mathbf{0}$): The smallest level set constant c, for which $\mathcal{M}_c$ surrounds $\mathcal{M}_i$, is computed by equating the radius of initial condition set $\mathcal{M}_i$ and the inner approximation of $\mathcal{M}_c$.

The first step amounts to determining an appropriate level set constant c such that $\mathcal{M}_i \subseteq \mathcal{M}_c$ holds. For that, it is important to notice that $\mathcal{M}_c$ exhibits its largest extension in $\operatorname{vec}\tilde{\boldsymbol{\Theta}}$-direction for $\boldsymbol{e}_C = \mathbf{0}$. This is because as soon as $\boldsymbol{e}_C \neq \mathbf{0}$ holds, the admissible values of $\tilde{\boldsymbol{\Theta}}$ have to decrease in order to still satisfy the ellipsoid equation $V(\boldsymbol{e}_C, \tilde{\boldsymbol{\Theta}}) = c$. Formally, this can also be verified by projecting the ellipsoid $\mathcal{M}_c$ onto the $\operatorname{vec}\tilde{\boldsymbol{\Theta}}$-subspace. In order to compute c, an inner approximation $\underline{\mathcal{M}}_c$ of the ellipsoid $\mathcal{M}_c$ is determined, which is spherical in $\operatorname{vec}\tilde{\boldsymbol{\Theta}}$-direction. Matching the radius of $\underline{\mathcal{M}}_c$ and of the sphere $\mathcal{M}_i$ for $\boldsymbol{e}_C = \mathbf{0}$ then yields the desired level set constant c. This is illustrated in Figure 4.7.

According to Appendix B.2, the largest sphere, which fits into an ellipsoid, results from bounding the respective quadratic form from above as shown in (B.64). In case of the quadratic form $V(\boldsymbol{e}_C, \tilde{\boldsymbol{\Theta}})$, an appropriate upper bound follows from Lemma 3.3:

$$V(\boldsymbol{e}_C, \tilde{\boldsymbol{\Theta}}) \leq \frac{1}{2}\lambda_{\max}(\boldsymbol{P}) \cdot \|\boldsymbol{e}_C\|_2^2 + \frac{\lambda_{\max}(\boldsymbol{\Lambda})}{2 \cdot \lambda_{\min}(\boldsymbol{\Gamma})} \cdot \|\tilde{\boldsymbol{\Theta}}\|_F^2.$$

Since $\boldsymbol{\Lambda}$ is uncertain, the upper bound from (3.57) (i.e. $\lambda_{\max}(\boldsymbol{\Lambda}) \leq \Lambda_{\max}$) is used. This leads to

$$V(\boldsymbol{e}_C, \tilde{\boldsymbol{\Theta}}) \leq \frac{1}{2}\lambda_{\max}(\boldsymbol{P}) \cdot \|\boldsymbol{e}_C\|_2^2 + \frac{\Lambda_{\max}}{2 \cdot \lambda_{\min}(\boldsymbol{\Gamma})} \cdot \|\tilde{\boldsymbol{\Theta}}\|_F^2. \tag{4.58}$$

The inner approximation of $\mathcal{M}_c$ is hence given by

$$\underline{\mathcal{M}}_c = \left\{ \boldsymbol{e}_C, \tilde{\boldsymbol{\Theta}} \mid \frac{1}{2}\lambda_{\max}(\boldsymbol{P}) \cdot \|\boldsymbol{e}_C\|_2^2 + \frac{\Lambda_{\max}}{2 \cdot \lambda_{\min}(\boldsymbol{\Gamma})} \cdot \|\tilde{\boldsymbol{\Theta}}\|_F^2 \leq c \right\}. \tag{4.59}$$

For $\boldsymbol{e}_C = \boldsymbol{0}$, $\underline{\mathcal{M}}_c$ is the largest sphere, which fits into $\mathcal{M}_c$. For $\boldsymbol{e}_C = \boldsymbol{0}$, the radius of the sphere defined by $\underline{\mathcal{M}}_c$ is given by

$$r_c = \sqrt{\frac{2 \cdot c \cdot \lambda_{\min}(\boldsymbol{\Gamma})}{\Lambda_{\max}}}, \tag{4.60}$$

whereas the radius of $\mathcal{M}_i$ is

$$r_i = \Theta_{\max}^*. \tag{4.61}$$

Equating the radius of $\underline{\mathcal{M}}_c$ and $\mathcal{M}_i$ for $\boldsymbol{e}_C = \boldsymbol{0}$ leads to the level set constant

$$c = \frac{\Lambda_{\max}}{2 \cdot \lambda_{\min}(\boldsymbol{\Gamma})} \cdot {\Theta_{\max}^*}^2. \tag{4.62}$$

In case of the initial conditions from (3.56) and the uncertainty bound from (3.57), the invariant set $\mathcal{M}_c$, which no trajectory starting in $\mathcal{M}_i$ may leave, is given by:

$$\mathcal{M}_c = \left\{ \boldsymbol{e}_C, \tilde{\boldsymbol{\Theta}} \mid V(\boldsymbol{e}_C, \tilde{\boldsymbol{\Theta}}) \leq \frac{\Lambda_{\max}}{2 \cdot \lambda_{\min}(\boldsymbol{\Gamma})} \cdot {\Theta_{\max}^*}^2 \right\}. \tag{4.63}$$

In the second step, a bound on the tracking error is inferred from the invariant set (4.63). To that end, notice that the largest extension of the ellipsoid $\mathcal{M}_c$ in $\boldsymbol{e}_C$-direction results for $\tilde{\boldsymbol{\Theta}} = \boldsymbol{0}$. The orthogonal projection of $\mathcal{M}_c$ onto the $\boldsymbol{e}_C$-subspace ("shadow of $\mathcal{M}_c$ on the $\boldsymbol{e}_C$-plane") hence results from the plane section $\tilde{\boldsymbol{\Theta}} = \boldsymbol{0}$:

$$\mathcal{M}_{c,\boldsymbol{e}_C} = \left\{ \boldsymbol{e}_C \mid \frac{1}{2} \cdot \boldsymbol{e}_C^T \boldsymbol{P} \boldsymbol{e}_C \leq \frac{\Lambda_{\max}}{2 \cdot \lambda_{\min}(\boldsymbol{\Gamma})} \cdot {\Theta_{\max}^*}^2 \right\}. \tag{4.64}$$

The smallest sphere surrounding $\mathcal{M}_{c,\boldsymbol{e}_C}$ follows from bounding $(1/2) \cdot \boldsymbol{e}_C^T \boldsymbol{P} \boldsymbol{e}_C$ from below (see (B.64)):

$$\bar{\mathcal{M}}_{c,\boldsymbol{e}_C} = \left\{ \boldsymbol{e}_C \mid \frac{1}{2} \cdot \lambda_{\min}(\boldsymbol{P}) \cdot \|\boldsymbol{e}_C\|_2^2 \leq \frac{\Lambda_{\max}}{2 \cdot \lambda_{\min}(\boldsymbol{\Gamma})} \cdot {\Theta_{\max}^*}^2 \right\}. \tag{4.65}$$

The relation of $\mathcal{M}_{c,\boldsymbol{e}_C}$ and $\bar{\mathcal{M}}_{c,\boldsymbol{e}_C}$ is shown in Figure 4.8. Since $\mathcal{M}_c$ is invariant and $\bar{\mathcal{M}}_{c,\boldsymbol{e}_C}$ surrounds the projection of $\mathcal{M}_c$ onto the $\boldsymbol{e}_C$-plane, the tracking error bound

$$\|\boldsymbol{e}_C(t)\|_2 \leq \sqrt{\frac{\Lambda_{\max} \cdot {\Theta_{\max}^*}^2}{\lambda_{\min}(\boldsymbol{P}) \cdot \lambda_{\min}(\boldsymbol{\Gamma})}} \quad \forall\, t \geq 0 \tag{4.66}$$

results, which is equivalent to (3.62). Since (4.66) holds for all times, the tracking error bound (4.39) follows due to the equivalence of vector norms:

$$\|\boldsymbol{e}_C(t)\|_{\mathcal{L}_\infty} \leq \sqrt{\frac{\Lambda_{\max} \cdot {\Theta_{\max}^*}^2}{\lambda_{\min}(\boldsymbol{P}) \cdot \lambda_{\min}(\boldsymbol{\Gamma})}}. \tag{4.67}$$

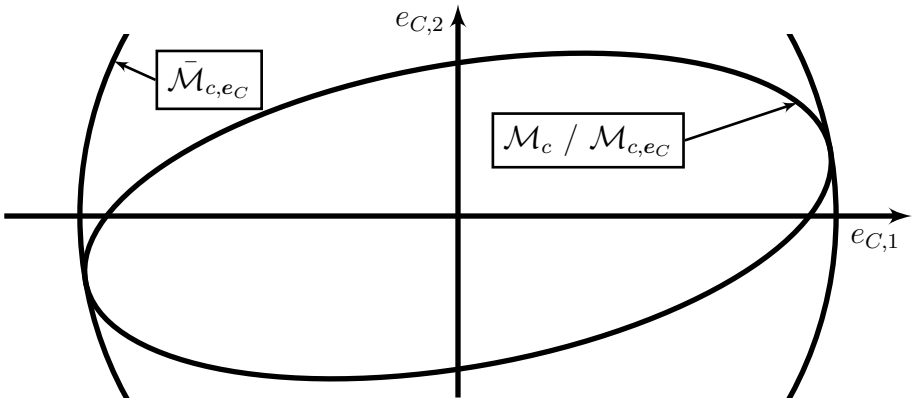

Figure 4.8: Plane section in $\boldsymbol{e}_C$-direction ($\tilde{\boldsymbol{\Theta}} = \mathbf{0}$): The tracking error bound (4.66) is derived by determining the largest sphere which surrounds the projection of the invariant set $\mathcal{M}_c$ onto the $\boldsymbol{e}_C$-plane.

From a geometric point of view, each of the two steps leading to the bound (4.39) ((4.67), respectively) may introduce conservatism. In the first step, an interior spherical approximation of the ellipsoid $\mathcal{M}_c$ is constructed in order to compute the level set constant c. If the uncertainties actually lie in a sphere, i.e. $\|\boldsymbol{\Theta}^*\|_F \leq \Theta^*_{\max}$, then this step will not introduce any conservatism since for $\boldsymbol{e}_C = \mathbf{0}$, the largest sphere within $\mathcal{M}_c$ is exactly given by $\underline{\mathcal{M}}_c$ with the level set constant c from (4.62). In practice, the uncertainties are usually not bounded by a sphere, but are rather bounded in terms of component-wise inequalities:

$$|\Theta^*_{ij}| \leq \Theta^*_{ij,\max}, \quad i = 1, \ldots, m, \quad j = 1, \ldots, n_r. \tag{4.68}$$

Here, Θ^*_{ij} is the component of $\boldsymbol{\Theta}^*$ in the i-th row and the j-th column and $\Theta^*_{ij,\max} \geq 0$ is a known bound. For the initial conditions from (3.56) (i.e. $\boldsymbol{e}_C(0) = \mathbf{0}$ and $\tilde{\boldsymbol{\Theta}}(0) = -\boldsymbol{\Theta}^*$), the set of initial conditions hence becomes

$$\mathcal{M}_i \triangleq \left\{ \boldsymbol{e}_C, \tilde{\boldsymbol{\Theta}} \mid \boldsymbol{e}_C = \mathbf{0} \wedge |\tilde{\Theta}_{ij}| \leq \Theta^*_{ij,\max},\ i = 1, \ldots, m,\ j = 1, \ldots, n_r \right\}, \tag{4.69}$$

where $\tilde{\Theta}_{ij}$ is the component of $\tilde{\boldsymbol{\Theta}}$ in the i-th row and the j-th column. Geometrically, (4.69) represents a degenerate hyperrectangle. In order to apply the bound (4.39), a sphere surrounding this hyperrectangle has to be computed by

$$\Theta^*_{\max} = \| \begin{bmatrix} \Theta^*_{11,\max} & \cdots & \Theta^*_{1n_r,\max} \\ \vdots & \ddots & \vdots \\ \Theta^*_{m1,\max} & \cdots & \Theta^*_{mn_r,\max} \end{bmatrix} \|_F. \tag{4.70}$$

Especially if the uncertainties have different scaling, this approximation will introduce significant conservatism as seen in Figure 4.9. In order to mitigate this source of conservatism, the level set constant c should be determined in such a way that $\mathcal{M}_c$ is the smallest level set, which surrounds $\mathcal{M}_i$, without resorting to an interior spherical approximation.

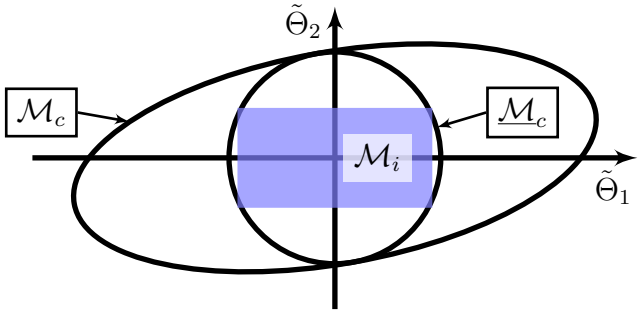

(a) Smallest level set constant c with circular inner approximation of $\mathcal{M}_c$.

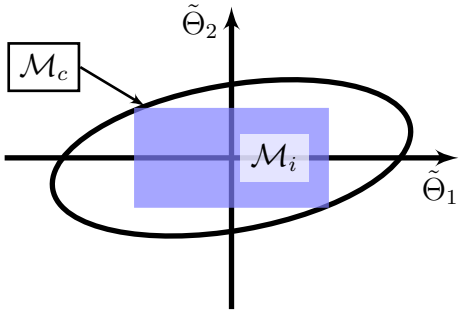

(b) Smallest level set constant c without circular inner approximation of $\mathcal{M}_c$.

Figure 4.9: Plane section in $\operatorname{vec}\tilde{\boldsymbol{\Theta}}$-direction ($\boldsymbol{e}_C = \mathbf{0}$): Computation of the level set constant c, if the set of initial conditions $\mathcal{M}_i$ is given by a hyperrectangle.

In the second step, a sphere surrounding the projection of $\mathcal{M}_c$ onto the $\boldsymbol{e}_C$-plane is determined. In case of the example in Figure 4.8, it is obvious that the resulting tracking error bound is little conservative in $e_{C,1}$-direction, whereas it is highly conservative in $e_{C,2}$-direction. In order to mitigate the conservatism, the largest extensions of the ellipsoid $\mathcal{M}_c$ in the $\boldsymbol{e}_C$-plane should be determined individually for each direction $e_{C,k}$.

Improved Tracking Error Bounds

In order to arrive at improved bounds for the tracking error of a direct MRAC, the two sources of conservatism have to be mitigated. The improved bounds are derived under the following additional assumptions on the direct MRAC of Section 3.2.1:

Assumption 4.1. *The control effectiveness matrix $\boldsymbol{\Lambda}$ is diagonal.*

Assumption 4.2. *The components of the uncertainty $\boldsymbol{\Theta}^*$ are known to remain within the hyperrectangle*

$$|\Theta^*_{ij} - \bar{\Theta}^*_{ij}| \leq \Theta^*_{ij,\max}, \quad i = 1, \ldots, m, \quad j = 1, \ldots, n_r, \tag{4.71}$$

where $\Theta^*_{ij,\max} > 0$ and $\bar{\Theta}^*_{ij} \in \mathbb{R}$ are known constants. Similarly, the diagonal elements of the control effectiveness matrix $\boldsymbol{\Lambda}$ remain within the hyperrectangle

$$0 < \Lambda_{i,\min} \leq \Lambda_i \leq \Lambda_{i,\max}, \quad i = 1, \ldots, m, \tag{4.72}$$

where Λ_i denotes the i-th diagonal element of $\boldsymbol{\Lambda}$ and $\Lambda_{i,\min}$, $\Lambda_{i,\max}$ denote known lower and upper bounds, respectively.

Assumption 4.3. *The initial conditions of the adaptive control system are given by $\boldsymbol{e}_C(0) = \mathbf{0}$ (i.e. $\boldsymbol{x}_M(0) = \boldsymbol{x}_P(0)$) and $\tilde{\boldsymbol{\Theta}}(0) = -\boldsymbol{\Theta}^*$ (i.e. $\boldsymbol{\Theta}(0) = \mathbf{0}$).*

Assumption 4.2 specifies component-wise bounds for the respective uncertainties. In order to arrive at a more compact notation and in order to improve readability, differ-

ent representations of the parameter error $\tilde{\boldsymbol{\Theta}}$, of its bounds and of the control effectiveness $\boldsymbol{\Lambda}$ are required. The parameter error $\tilde{\boldsymbol{\Theta}}$ may be partitioned row-wise:

$$\tilde{\boldsymbol{\Theta}} \triangleq \begin{bmatrix} \tilde{\boldsymbol{\theta}}_1 \\ \vdots \\ \tilde{\boldsymbol{\theta}}_m \end{bmatrix} = \begin{bmatrix} \tilde{\Theta}_{11} & \dots & \tilde{\Theta}_{1n_r} \\ \vdots & & \vdots \\ \tilde{\Theta}_{m1} & \dots & \tilde{\Theta}_{mn_r} \end{bmatrix}. \tag{4.73}$$

A row $\tilde{\boldsymbol{\theta}}_i \in \mathbb{R}^{1\times n_r}$ represents the parameter errors associated with the i-th plant input. A representation of the parameter error $\tilde{\boldsymbol{\Theta}}$ as a single column vector follows readily:

$$\tilde{\boldsymbol{\theta}}^T \triangleq \begin{bmatrix} \tilde{\boldsymbol{\theta}}_1 & \dots & \tilde{\boldsymbol{\theta}}_m \end{bmatrix} \tag{4.74}$$

with $\tilde{\boldsymbol{\theta}} \in \mathbb{R}^{m\cdot n_r}$. Similarly, the uncertainty bounds $\Theta^*_{ij,\max}$ and $\bar{\Theta}^*_{ij}$ are gathered in row vectors

$$\boldsymbol{\theta}^*_{i,\max} \triangleq \begin{bmatrix} \Theta^*_{i1,\max} & \dots & \Theta^*_{in_r,\max} \end{bmatrix}, \tag{4.75}$$

$$\bar{\boldsymbol{\theta}}^*_i \triangleq \begin{bmatrix} \bar{\Theta}^*_{i1} & \dots & \bar{\Theta}^*_{in_r} \end{bmatrix}, \tag{4.76}$$

each of which is associated with the i-th plant input for $i = 1, \dots, m$. A representation in terms of a single column vector is then given by

$${\boldsymbol{\theta}^*_{\max}}^T \triangleq \begin{bmatrix} \boldsymbol{\theta}^*_{1,\max} & \dots & \boldsymbol{\theta}^*_{m,\max} \end{bmatrix}, \tag{4.77}$$

$${\bar{\boldsymbol{\theta}}^*}^T \triangleq \begin{bmatrix} \bar{\boldsymbol{\theta}}^*_1 & \dots & \bar{\boldsymbol{\theta}}^*_m \end{bmatrix}. \tag{4.78}$$

Geometrically, $\bar{\boldsymbol{\theta}}^* \in \mathbb{R}^{m\cdot n_r}$ represents the center of the uncertainty rectangle, whereas $\boldsymbol{\theta}^*_{\max} \in \mathbb{R}^{m\cdot n_r}$ specifies the largest deviation from the center. Furthermore, the diagonal elements λ_i of the control effectiveness matrix $\boldsymbol{\Lambda}$ are summarized in the input uncertainty vector

$$\boldsymbol{\lambda}^T \triangleq \begin{bmatrix} \Lambda_1 & \dots & \Lambda_m \end{bmatrix}. \tag{4.79}$$

Improved Computation of the Level Set Constant

Due to Assumption 4.2, the uncertainty $\boldsymbol{\Theta}^*$ is known to remain within a hyperrectangle. As highlighted in Figure 4.9, a hyper-rectangular uncertainty set introduces significant conservatism, when using the conventional tracking error bound (4.39). This is because the level set constant c, which ensures $\mathcal{M}_i \subseteq \mathcal{M}_c$, is computed using an interior spherical approximation of $\mathcal{M}_c$. In order to overcome this source of conservatism, an approach based on the S-Procedure from Lemma B.7 is derived subsequently. In general, the S-Procedure allows solving many set containment problems in a less conservative way and leads to LMI conditions.

In order to apply the S-Procedure, the set containment problem $\mathcal{M}_i \subseteq \mathcal{M}_c$ has to be reformulated first. To that end, notice that Assumption 4.2 and Assumption 4.3 lead to the following set of initial conditions due to $\tilde{\boldsymbol{\Theta}}(0) = -\boldsymbol{\Theta}^*$:

$$\mathcal{M}_i \triangleq \left\{ \boldsymbol{e}_C, \tilde{\boldsymbol{\Theta}} \mid \boldsymbol{e}_C = \boldsymbol{0} \wedge |\tilde{\Theta}_{ij} + \bar{\Theta}^*_{ij}| \leq \Theta^*_{ij,\max},\ i = 1, \dots, m,\ j = 1, \dots, n_r \right\}. \tag{4.80}$$

Due to $\boldsymbol{e}_C = \mathbf{0}$, the set $\mathcal{M}_i$ is degenerate. Since $\mathcal{M}_i$ has no extension in $\boldsymbol{e}_C$-direction, the set containment problem $\mathcal{M}_i \subseteq \mathcal{M}_c$ may also be solved by first projecting the sets $\mathcal{M}_c$ and $\mathcal{M}_i$ orthogonally onto the $\tilde{\boldsymbol{\Theta}}$-subspace, leading to the projected sets $\mathcal{M}_{c,\tilde{\Theta}}$ and $\mathcal{M}_{i,\tilde{\Theta}}$. In the projected space, the level set constant c is then determined using the S-Procedure such that $\mathcal{M}_{i,\tilde{\Theta}} \subseteq \mathcal{M}_{c,\tilde{\Theta}}$ holds, which implies $\mathcal{M}_i \subseteq \mathcal{M}_c$.

Since $\mathcal{M}_i$ is degenerate in $\boldsymbol{e}_C$-directions, its projection onto the $\tilde{\boldsymbol{\Theta}}$-subspace is given by

$$\mathcal{M}_{i,\tilde{\Theta}} = \left\{ \tilde{\boldsymbol{\Theta}} \mid \quad |\tilde{\Theta}_{ij} + \bar{\Theta}^*_{ij}| \leq \Theta^*_{ij,\max},\ i = 1, \ldots, m,\ j = 1, \ldots, n_r \right\}. \tag{4.81}$$

For the projection of $\mathcal{M}_c$, one may resort to the ellipsoid projection from (B.95), which projects ellipsoids specified by quadratic forms of the structure $\boldsymbol{x}^T \boldsymbol{A} \boldsymbol{x}$. Since the Lyapunov function $V(\boldsymbol{e}_C, \tilde{\boldsymbol{\Theta}})$, whose arguments are the vector $\boldsymbol{e}_C$ and the *matrix* $\tilde{\boldsymbol{\Theta}}$, does not comply with this structure, it has to be reformulated as a function with vector-valued arguments. To that end, notice that the cyclic property (B.154) implies

$$\mathrm{Tr}\left\{ \tilde{\boldsymbol{\Theta}}(t)\, \boldsymbol{\Gamma}^{-1} \tilde{\boldsymbol{\Theta}}(t)^T \boldsymbol{\Lambda} \right\} = \mathrm{Tr}\left\{ \tilde{\boldsymbol{\Theta}}(t)^T \boldsymbol{\Lambda} \tilde{\boldsymbol{\Theta}}(t)\, \boldsymbol{\Gamma}^{-1} \right\}. \tag{4.82}$$

Since $\boldsymbol{\Lambda}$ is diagonal due to Assumption 4.1, it follows with the partition of $\tilde{\boldsymbol{\Theta}}$ in (4.73):

$$\tilde{\boldsymbol{\Theta}}(t)^T \boldsymbol{\Lambda} = \begin{bmatrix} \tilde{\boldsymbol{\theta}}_1^T & \ldots & \tilde{\boldsymbol{\theta}}_m^T \end{bmatrix} \cdot \begin{bmatrix} \Lambda_1 & \ldots & 0 \\ \vdots & \ddots & \vdots \\ 0 & \ldots & \Lambda_m \end{bmatrix} = \begin{bmatrix} \Lambda_1 \tilde{\boldsymbol{\theta}}_1^T & \ldots & \Lambda_m \tilde{\boldsymbol{\theta}}_m^T \end{bmatrix}. \tag{4.83}$$

Furthermore,

$$\tilde{\boldsymbol{\Theta}}(t)\, \boldsymbol{\Gamma}^{-1} = \begin{bmatrix} \tilde{\boldsymbol{\theta}}_1 \\ \vdots \\ \tilde{\boldsymbol{\theta}}_m \end{bmatrix} \cdot \boldsymbol{\Gamma}^{-1} = \begin{bmatrix} \tilde{\boldsymbol{\theta}}_1 \boldsymbol{\Gamma}^{-1} \\ \vdots \\ \tilde{\boldsymbol{\theta}}_m \boldsymbol{\Gamma}^{-1} \end{bmatrix} \tag{4.84}$$

holds. Hence, (4.82) becomes

$$\mathrm{Tr}\left\{ \tilde{\boldsymbol{\Theta}}(t)\, \boldsymbol{\Gamma}^{-1} \tilde{\boldsymbol{\Theta}}(t)^T \boldsymbol{\Lambda} \right\} = \mathrm{Tr}\left\{ \begin{bmatrix} \Lambda_1 \tilde{\boldsymbol{\theta}}_1^T & \ldots & \Lambda_m \tilde{\boldsymbol{\theta}}_m^T \end{bmatrix} \cdot \begin{bmatrix} \tilde{\boldsymbol{\theta}}_1 \boldsymbol{\Gamma}^{-1} \\ \vdots \\ \tilde{\boldsymbol{\theta}}_m \boldsymbol{\Gamma}^{-1} \end{bmatrix} \right\}. \tag{4.85}$$

Upon application of the trace identity (B.157), the right hand side may be represented as a sum of scalar products, yielding:

$$\mathrm{Tr}\left\{ \tilde{\boldsymbol{\Theta}}(t)\, \boldsymbol{\Gamma}^{-1} \tilde{\boldsymbol{\Theta}}(t)^T \boldsymbol{\Lambda} \right\} = \sum_{i=1}^{m} \Lambda_i \tilde{\boldsymbol{\theta}}_i \boldsymbol{\Gamma}^{-1} \tilde{\boldsymbol{\theta}}_i^T. \tag{4.86}$$

Hence, the Lyapunov function (3.30) admits the following representation:

$$V(\boldsymbol{e}_C, \tilde{\boldsymbol{\Theta}}) = \frac{1}{2} \boldsymbol{e}_C^T \boldsymbol{P} \boldsymbol{e}_C + \frac{1}{2} \sum_{i=1}^{m} \Lambda_i \tilde{\boldsymbol{\theta}}_i \boldsymbol{\Gamma}^{-1} \tilde{\boldsymbol{\theta}}_i^T. \tag{4.87}$$

With the vectorial representation $\tilde{\boldsymbol{\theta}}$ of the parameter error $\tilde{\boldsymbol{\Theta}}$ from (4.74) and the joint state vector

$$\boldsymbol{x}^T \triangleq \begin{bmatrix} \boldsymbol{e}_C^T & \tilde{\boldsymbol{\theta}}^T \end{bmatrix}, \tag{4.88}$$

the Lyapunov function (4.87) becomes

$$V(\boldsymbol{x}) = \frac{1}{2}\boldsymbol{e}_C^T \boldsymbol{P} \boldsymbol{e}_C + \frac{1}{2}\tilde{\boldsymbol{\theta}}^T \boldsymbol{M}_{\tilde{\Theta}}(\boldsymbol{\lambda})\tilde{\boldsymbol{\theta}} = \boldsymbol{x}^T \begin{bmatrix} \frac{1}{2}\boldsymbol{P} & \boldsymbol{0}^{n\times(m\cdot n_r)} \\ \boldsymbol{0}^{(m\cdot n_r)\times n} & \frac{1}{2}\boldsymbol{M}_{\tilde{\Theta}}(\boldsymbol{\lambda}) \end{bmatrix} \boldsymbol{x}. \tag{4.89}$$

In (4.89), the matrix $\boldsymbol{M}_{\tilde{\Theta}}(\boldsymbol{\lambda})$ is defined as

$$\boldsymbol{M}_{\tilde{\Theta}}(\boldsymbol{\lambda}) \triangleq \begin{bmatrix} \Lambda_1 \boldsymbol{\Gamma}^{-1} & \dots & \boldsymbol{0}^{n_r\times n_r} \\ \vdots & \ddots & \vdots \\ \boldsymbol{0}^{n_r\times n_r} & \dots & \Lambda_m \boldsymbol{\Gamma}^{-1} \end{bmatrix} \tag{4.90}$$

and depends on the input uncertainty vector $\boldsymbol{\lambda}$. With the orthonormal basis

$$\boldsymbol{C} = \begin{bmatrix} \boldsymbol{0}^{n\times(m\cdot n_r)} \\ \boldsymbol{I}^{(m\cdot n_r)\times(m\cdot n_r)} \end{bmatrix} \tag{4.91}$$

of the $\tilde{\boldsymbol{\theta}}$-subspace, the orthogonal projection of the ellipsoid $\mathcal{M}_c$ onto the $\tilde{\boldsymbol{\theta}}$-subspace follows from (B.94) and (B.95) and yields:

$$\mathcal{M}_{c,\tilde{\Theta}} = \left\{ \tilde{\boldsymbol{\theta}} \mid \frac{1}{2}\tilde{\boldsymbol{\theta}}^T \boldsymbol{M}_{\tilde{\Theta}}(\boldsymbol{\lambda})\tilde{\boldsymbol{\theta}} \leq c \right\}. \tag{4.92}$$

In order to use the S-Procedure for the solution of the set containment problem $\mathcal{M}_{i,\tilde{\Theta}} \subseteq \mathcal{M}_{c,\tilde{\Theta}}$, the sets $\mathcal{M}_{i,\tilde{\Theta}}$ and $\mathcal{M}_{c,\tilde{\Theta}}$ have to be reformulated as 0-sublevel sets of the structure $\mathcal{M}_{(\cdot)} = \{\boldsymbol{z} \mid \boldsymbol{z}^T \boldsymbol{M}_{(\cdot)} \boldsymbol{z} \leq 0\}$. Upon definition of the extended parameter vector

$$\boldsymbol{z}^T \triangleq \begin{bmatrix} \tilde{\boldsymbol{\theta}}^T & 1 \end{bmatrix}, \tag{4.93}$$

the set $\mathcal{M}_{c,\tilde{\Theta}}$ may be represented as

$$\mathcal{M}_{c,\tilde{\Theta}} = \{\boldsymbol{z} \mid g_0(\boldsymbol{z}) \leq 0\} \tag{4.94}$$

with

$$g_0(\boldsymbol{z}) = \boldsymbol{z}^T \underbrace{\begin{bmatrix} \boldsymbol{M}_{\tilde{\Theta}}(\boldsymbol{\lambda}) & \boldsymbol{0}^{(m\cdot n_r)\times 1} \\ \boldsymbol{0}^{1\times(m\cdot n_r)} & -2c \end{bmatrix}}_{\boldsymbol{M}_0(\boldsymbol{\lambda})} \boldsymbol{z}. \tag{4.95}$$

Similarly, the set $\mathcal{M}_{i,\tilde{\Theta}}$ is represented as

$$\mathcal{M}_{i,\tilde{\Theta}} = \{\boldsymbol{z} \mid g_{ij}(\boldsymbol{z}) \leq 0,\ \forall\, i = 1,\dots,m,\ j = 1,\dots,n_r\}, \tag{4.96}$$

where

$$g_{ij}(\boldsymbol{z}) = \boldsymbol{z}^T \underbrace{\begin{bmatrix} \boldsymbol{0}^{k_1\times k_1} & \boldsymbol{0}^{k_1\times 1} & \boldsymbol{0}^{k_1\times k_2} & \boldsymbol{0}^{k_1\times 1} \\ \boldsymbol{0}^{1\times k_1} & 1 & \boldsymbol{0}^{1\times k_2} & \bar{\Theta}_{ij}^* \\ \boldsymbol{0}^{k_2\times k_1} & \boldsymbol{0}^{k_2\times 1} & \boldsymbol{0}^{k_2\times k_2} & \boldsymbol{0}^{k_2\times 1} \\ \boldsymbol{0}^{1\times k_1} & \bar{\Theta}_{ij}^* & \boldsymbol{0}^{1\times k_2} & (\bar{\Theta}_{ij}^*)^2 - (\Theta_{ij,\max}^*)^2 \end{bmatrix}}_{\boldsymbol{M}_{ij}} \boldsymbol{z} \tag{4.97}$$

with $k_1 = (i-1) \cdot n_r + j - 1$ and $k_2 = m \cdot n_r - k_1 - 1$. According to the S-Procedure (Lemma B.7), the set $\mathcal{M}_{i,\tilde{\Theta}}$ is a subset of $\mathcal{M}_{c,\tilde{\Theta}}$, if there exist non-negative multipliers $l_{ij} \geq 0$ such that the LMI

$$\boldsymbol{M}_0(\boldsymbol{\lambda}) - \sum_{i=1}^{m} \sum_{j=1}^{n_r} l_{ij} \cdot \boldsymbol{M}_{ij} \leq 0 \tag{4.98}$$

is feasible. A more convenient representation of the LMI (4.98) results when lumping all multipliers l_{ij} into a diagonal matrix:

$$\boldsymbol{D} = \operatorname{diag} \begin{bmatrix} l_{11} & \dots & l_{1n_r} & \dots & l_{m1} & \dots & l_{mn_r} \end{bmatrix}. \tag{4.99}$$

Using $\boldsymbol{D} \in \mathbb{S}_+^{m \cdot n_r}$, $\boldsymbol{\theta}^*_{\max} \in \mathbb{R}^{m \cdot n_r}$ from (4.77) and $\bar{\boldsymbol{\theta}}^* \in \mathbb{R}^{m \cdot n_r}$ from (4.78), the sum in (4.98) admits the compact representation

$$\sum_{i=1}^{m} \sum_{j=1}^{n_r} l_{ij} \cdot \boldsymbol{M}_{ij} = \begin{bmatrix} \boldsymbol{D} & \boldsymbol{D}\bar{\boldsymbol{\theta}}^* \\ (\bar{\boldsymbol{\theta}}^*)^T \boldsymbol{D} & (\bar{\boldsymbol{\theta}}^*)^T \boldsymbol{D} \bar{\boldsymbol{\theta}}^* - (\boldsymbol{\theta}^*_{\max})^T \boldsymbol{D} \boldsymbol{\theta}^*_{\max} \end{bmatrix}. \tag{4.100}$$

The feasibility problem (4.98) becomes

$$\begin{bmatrix} \boldsymbol{M}_{\tilde{\Theta}}(\boldsymbol{\lambda}) - \boldsymbol{D} & -\boldsymbol{D}\bar{\boldsymbol{\theta}}^* \\ -(\bar{\boldsymbol{\theta}}^*)^T \boldsymbol{D} & (\boldsymbol{\theta}^*_{\max})^T \boldsymbol{D} \boldsymbol{\theta}^*_{\max} - (\bar{\boldsymbol{\theta}}^*)^T \boldsymbol{D} \bar{\boldsymbol{\theta}}^* - 2c \end{bmatrix} \leq 0, \quad \boldsymbol{D} \geq 0. \tag{4.101}$$

The feasibility problem (4.101) depends on the unknown input uncertainty $\boldsymbol{\Lambda}$. Thus, its solution requires the knowledge of a particular value of $\boldsymbol{\lambda}$, which is not available in practice. Due to Assumption 4.2, $\boldsymbol{\lambda}$ is however known to remain within a m-dimensional hyperrectangle. Any $\boldsymbol{\lambda}$ within such a hyperrectangle may be expressed in terms of the 2^m vertices $\boldsymbol{\lambda}_v$ of the hyperrectangle [3] according to

$$\boldsymbol{\lambda} = \sum_{v=1}^{2^m} \alpha_v \boldsymbol{\lambda}_v \tag{4.102}$$

with $\alpha_v \geq 0$ and

$$\sum_{v=1}^{2^m} \alpha_v = 1. \tag{4.103}$$

Now assume that the feasibility problem (4.101) holds on all vertices $\boldsymbol{\lambda}_v$:

$$\begin{bmatrix} \boldsymbol{M}_{\tilde{\Theta}}(\boldsymbol{\lambda}_v) - \boldsymbol{D} & -\boldsymbol{D}\bar{\boldsymbol{\theta}}^* \\ -(\bar{\boldsymbol{\theta}}^*)^T \boldsymbol{D} & (\boldsymbol{\theta}^*_{\max})^T \boldsymbol{D} \boldsymbol{\theta}^*_{\max} - (\bar{\boldsymbol{\theta}}^*)^T \boldsymbol{D} \bar{\boldsymbol{\theta}}^* - 2c \end{bmatrix} \leq 0 \quad \forall\, v = 1, \dots, 2^m, \quad \boldsymbol{D} \geq 0. \tag{4.104}$$

Due to the linearity of $\boldsymbol{M}_{\tilde{\Theta}}(\boldsymbol{\lambda})$ with respect to $\boldsymbol{\lambda}$, the feasibility problem will also hold for all intermediate values $\boldsymbol{\lambda}$ as shown below:

$$\begin{bmatrix} \boldsymbol{M}_{\tilde{\Theta}}(\boldsymbol{\lambda}) - \boldsymbol{D} & -\boldsymbol{D}\bar{\boldsymbol{\theta}}^* \\ -(\bar{\boldsymbol{\theta}}^*)^T \boldsymbol{D} & (\boldsymbol{\theta}^*_{\max})^T \boldsymbol{D} \boldsymbol{\theta}^*_{\max} - (\bar{\boldsymbol{\theta}}^*)^T \boldsymbol{D} \bar{\boldsymbol{\theta}}^* - 2c \end{bmatrix}$$

$$
\begin{aligned}
&= \begin{bmatrix} \boldsymbol{M}_{\tilde{\Theta}}(\sum_{v=1}^{2^m} \alpha_v \boldsymbol{\lambda}_v) - \boldsymbol{D} & -\boldsymbol{D}\bar{\boldsymbol{\theta}}^* \\ -(\bar{\boldsymbol{\theta}}^*)^T \boldsymbol{D} & (\boldsymbol{\theta}^*_{\max})^T \boldsymbol{D} \boldsymbol{\theta}^*_{\max} - (\bar{\boldsymbol{\theta}}^*)^T \boldsymbol{D} \bar{\boldsymbol{\theta}}^* - 2c \end{bmatrix} \\
&= \sum_{v=1}^{2^m} \alpha_v \cdot \underbrace{\begin{bmatrix} \boldsymbol{M}_{\tilde{\Theta}}(\boldsymbol{\lambda}_v) - \boldsymbol{D} & -\boldsymbol{D}\bar{\boldsymbol{\theta}}^* \\ -(\bar{\boldsymbol{\theta}}^*)^T \boldsymbol{D} & (\boldsymbol{\theta}^*_{\max})^T \boldsymbol{D} \boldsymbol{\theta}^*_{\max} - (\bar{\boldsymbol{\theta}}^*)^T \boldsymbol{D} \bar{\boldsymbol{\theta}}^* - 2c \end{bmatrix}}_{\leq 0} \leq 0.
\end{aligned} \tag{4.105}
$$

If the feasibility problem (4.104) may be solved, then $\mathcal{M}_{i,\tilde{\Theta}} \subseteq \mathcal{M}_{c,\tilde{\Theta}}$ holds. Since these sets represent orthogonal projections of $\mathcal{M}_i$ and $\mathcal{M}_c$ and since $\mathcal{M}_i$ is degenerate in $\boldsymbol{e}_C$-direction, the feasibility of (4.104) implies $\mathcal{M}_i \subseteq \mathcal{M}_c$. In order to solve the feasibility problem (4.104), the level set constant c has to be known. By introducing the level set constant c as an additional decision variable of the LMI problem and by extending the feasibility problem to a Semidefinite Program (SDP), the smallest level set constant may be determined. The following lemma results readily from (4.104):

Lemma 4.2. *Consider a direct MRAC according to Section 3.2.1, which satisfies the conditions for NS of Theorem 3.4. Furthermore, let the additional Assumptions 4.1 (diagonal control effectiveness), 4.2 (hyper-rectangular uncertainty sets) and 4.3 (initial conditions $\boldsymbol{e}_C(0) = \boldsymbol{0}$ and $\tilde{\boldsymbol{\Theta}}(0) = -\boldsymbol{\Theta}^*$) hold. Denote the minimizer of the following SDP by c^*:*

$$
\begin{aligned}
&\min_{c, \boldsymbol{D}} c \quad \textit{s.t.} \\
&\begin{bmatrix} \boldsymbol{M}_{\tilde{\Theta}}(\boldsymbol{\lambda}_v) - \boldsymbol{D} & -\boldsymbol{D}\bar{\boldsymbol{\theta}}^* \\ -(\bar{\boldsymbol{\theta}}^*)^T \boldsymbol{D} & (\boldsymbol{\theta}^*_{\max})^T \boldsymbol{D} \boldsymbol{\theta}^*_{\max} - (\bar{\boldsymbol{\theta}}^*)^T \boldsymbol{D} \bar{\boldsymbol{\theta}}^* - 2c \end{bmatrix} \leq 0 \quad \forall\, v = 1, \ldots, 2^m, \\
&\boldsymbol{D} \geq 0, \\
&c \geq 0,
\end{aligned} \tag{4.106}
$$

where the decision variable $\boldsymbol{D} \in \mathbb{S}^{m \cdot n_r}$ is diagonal and where $\boldsymbol{M}_{\tilde{\Theta}} : \mathbb{R}^m \to \mathbb{S}^{m \cdot n_r}$ is defined in (4.90)*. Due to Assumption 4.2, the diagonal components $\boldsymbol{\lambda}$ of the control effectiveness matrix $\boldsymbol{\Lambda}$, defined in* (4.79)*, remain within a hyperrectangle. The vectors $\boldsymbol{\lambda}_v$, $v = 1, \ldots, 2^m$, denote the vertices of this hyperrectangle. Similarly, the uncertainties $\boldsymbol{\Theta}^*$ are assumed to remain within a hyperrectangle. While the vector $\bar{\boldsymbol{\theta}}^*$ specifies the center of this hyperrectangle, the vector $\boldsymbol{\theta}^*_{\max}$, defined in* (4.77)*, summarizes the component-wise deviations from the center.*

For $\boldsymbol{e}_C(0) = \boldsymbol{0}$ and $\tilde{\boldsymbol{\Theta}}(0) = -\boldsymbol{\Theta}^*$, the minimizer c^* of the SDP (4.106) *guarantees that the trajectories of the adaptive control system remain within the invariant set*

$$
\mathcal{M}_c = \left\{ \boldsymbol{e}_C, \tilde{\boldsymbol{\Theta}} \mid V(\boldsymbol{e}_C, \tilde{\boldsymbol{\Theta}}) \leq c^* \right\} \tag{4.107}
$$

for all times, i.e.

$$
\left(\boldsymbol{e}_C(t), \tilde{\boldsymbol{\Theta}}(t) \right) \in \mathcal{M}_c, \ \forall\, t \geq 0. \tag{4.108}
$$

Proof. The subsequent proof essentially reverses the derivation of Lemma 4.2: Consider the solutions $c = c^*$ and $\boldsymbol{D}$ of the SDP (4.106). As the solutions hold on all vertices

$\boldsymbol{\lambda}_v$, the LMIs (4.101) are feasible as well for all intermediate values $\boldsymbol{\lambda}$ due to (4.105) and because Assumption 4.2 ensures that the diagonal components $\boldsymbol{\lambda}$ of the control effectiveness matrix $\boldsymbol{\Lambda}$ remain within a hyperrectangle. Due to (4.99) and (4.100), the first LMI of (4.101) is equivalent to (4.98), where $\boldsymbol{M}_0(\boldsymbol{\lambda})$ and $\boldsymbol{M}_{ij}$ are defined in (4.95) and (4.97), respectively. Due to $\boldsymbol{D} > 0$ and the S-Procedure (Lemma B.7), (4.98) implies $\mathcal{M}_{i,\tilde{\Theta}} \subseteq \mathcal{M}_{c,\tilde{\Theta}}$, where $\mathcal{M}_{i,\tilde{\Theta}}$ and $\mathcal{M}_{c,\tilde{\Theta}}$ are given by (4.96) and (4.94). Notice that (4.96) is equivalent to (4.81) ($\mathcal{M}_{i,\tilde{\Theta}} = \left\{\tilde{\boldsymbol{\Theta}} \mid |\tilde{\Theta}_{ij} + \bar{\Theta}^*_{ij}| \leq \Theta^*_{ij,\max},\ i = 1,\ldots,m,\ j = 1,\ldots,n_r\right\}$). At the same time, (4.94) is equivalent to (4.92) (i.e. $\mathcal{M}_{c,\tilde{\Theta}} = \left\{\tilde{\boldsymbol{\theta}} \mid \frac{1}{2}\tilde{\boldsymbol{\theta}}^T \boldsymbol{M}_{\tilde{\Theta}}(\boldsymbol{\lambda})\tilde{\boldsymbol{\theta}} \leq c\right\}$. With the definitions of $\tilde{\boldsymbol{\theta}}$ in (4.74) and of $\boldsymbol{M}_{\tilde{\Theta}}(\boldsymbol{\lambda})$ in (4.90) as well as the identity (4.86), $\mathcal{M}_{c,\tilde{\Theta}} = \left\{\tilde{\boldsymbol{\Theta}} \mid \frac{1}{2}\operatorname{Tr}\left\{\tilde{\boldsymbol{\Theta}}(t)\,\boldsymbol{\Gamma}^{-1}\tilde{\boldsymbol{\Theta}}(t)^T\,\boldsymbol{\Lambda}\right\} \leq c\right\}$ follows. Hence, the following set containment is ensured by the SDP (4.106):

$$\begin{aligned}\left\{\tilde{\boldsymbol{\Theta}} \mid\ |\tilde{\Theta}_{ij} + \bar{\Theta}^*_{ij}| \leq \Theta^*_{ij,\max},\ i = 1,\ldots,m,\ j = 1,\ldots,n_r\right\}& \\ \subseteq \left\{\tilde{\boldsymbol{\Theta}} \mid \frac{1}{2}\operatorname{Tr}\left\{\tilde{\boldsymbol{\Theta}}(t)\,\boldsymbol{\Gamma}^{-1}\tilde{\boldsymbol{\Theta}}(t)^T\,\boldsymbol{\Lambda}\right\} \leq c\right\}.&\end{aligned} \tag{4.109}$$

For $\boldsymbol{e}_C = \boldsymbol{0}$, the latter implies $\mathcal{M}_i \subseteq \mathcal{M}_c$, i.e.

$$\begin{aligned}\left\{\boldsymbol{e}_C, \tilde{\boldsymbol{\Theta}} \mid \boldsymbol{e}_C = \boldsymbol{0} \wedge |\tilde{\Theta}_{ij} + \bar{\Theta}^*_{ij}| \leq \Theta^*_{ij,\max},\ i = 1,\ldots,m,\ j = 1,\ldots,n_r\right\}& \\ \subseteq \left\{\boldsymbol{e}_C, \tilde{\boldsymbol{\Theta}} \mid V(\boldsymbol{e}_C, \tilde{\boldsymbol{\Theta}}) \leq c\right\}.&\end{aligned} \tag{4.110}$$

As the initial conditions satisfy $\boldsymbol{e}_C(0) = \boldsymbol{0}$ and $\tilde{\boldsymbol{\Theta}}(0) = -\boldsymbol{\Theta}^*$ due to Assumption 4.3 and as the uncertainties are bounded according to Assumption 4.2, the set of all admissible initial conditions $\boldsymbol{e}_C(0)$ and $\tilde{\boldsymbol{\Theta}}(0)$ is given by $\mathcal{M}_i$. Since $\mathcal{M}_i \subseteq \mathcal{M}_c$ holds at $t = 0$ for $\boldsymbol{e}_C(0) = \boldsymbol{0}$ and $\mathcal{M}_c$ is an invariant (level) set, the trajectories of $\boldsymbol{e}_C(t)$ and $\tilde{\boldsymbol{\Theta}}(t)$ may never leave $\mathcal{M}_c$. □

Improved Tracking Error Bound

The SDP of Lemma 4.2 yields an improved level set constant c. With the help of the involved optimization problem, the conservatism of the first step is significantly reduced. In order to reduce the conservatism of the second step, notice that the extension of the ellipsoid $\mathcal{M}_c$ in the directions of the unit vectors (of the state space) corresponds to the largest tracking or parameter error $e_{C,k}(t)$, $\tilde{\Theta}_{ij}(t)$. The largest extension of an ellipsoid $\mathcal{M}_c$ in any desired direction of the state space may be readily computed by projecting the ellipsoid onto a 1-dimensional subspace (a line) as shown in Figure 4.10. Hence, the largest tracking error of the state $e_{C,k}(t)$ results from the orthogonal projection of the ellipsoid $\mathcal{M}_c$ onto the respective unit vector.

Consider the ellipsoid $\mathcal{M}_c$ and the representation (4.89) of the Lyapunov function. The unit vector $\boldsymbol{c}_k \in \mathbb{R}^{n+(m\cdot n_r)}$, $k \in [1,\ldots,n]$, associated with the state $e_{C,k}(t)$ is given by

$$\boldsymbol{c}_k^T = \begin{bmatrix}\boldsymbol{b}_k^T & \boldsymbol{0}^{1\times(m\cdot n_r)}\end{bmatrix} \quad \text{with} \quad \boldsymbol{b}_k^T = \begin{bmatrix}\boldsymbol{0}^{1\times(k-1)} & 1 & \boldsymbol{0}^{1\times(n-k)}\end{bmatrix}. \tag{4.111}$$

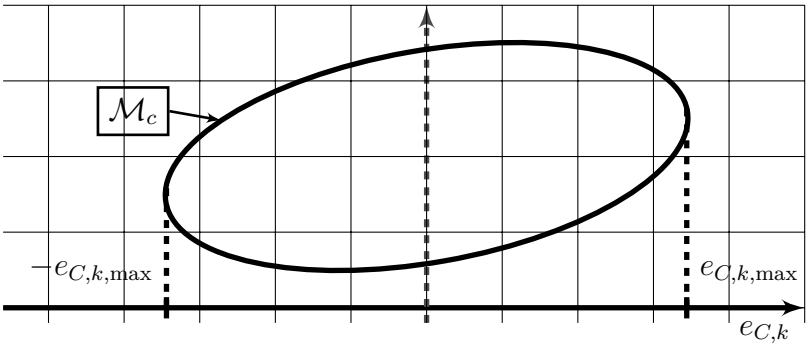

Figure 4.10: Illustration of the orthogonal projection for computing the tracking error bound for the state $e_{C,k}(t)$. Notice that the ellipsoid $\mathcal{M}_c$ and the $e_{C,k}$-axis pass through the origin. They have been separated for the purpose of illustration.

According to (B.94) and (B.95), the projection of $\mathcal{M}_c$ onto the subspace spanned by $\boldsymbol{c}_k$ is given by

$$\mathcal{M}_{c,Proj} = \left\{ e_{C,k} \mid \frac{1}{\boldsymbol{b}_k^T \left(\frac{1}{2}\boldsymbol{P}\right)^{-1} \boldsymbol{b}_k} \cdot e_{C,k}^2 \leq c \right\}. \tag{4.112}$$

Since $\mathcal{M}_c$ is invariant, a less conservative tracking error bound for the state $e_{C,k}(t)$ immediately follows:

$$\|e_{C,k}(t)\|_{\mathcal{L}_\infty} \leq \sqrt{2 \cdot c \cdot \boldsymbol{b}_k^T \boldsymbol{P}^{-1} \boldsymbol{b}_k}\,. \tag{4.113}$$

Similar bounds can also be derived for the parameter error $\tilde{\Theta}_{ij}(t)$.

The benefits of the improved method for the computation of a tracking error bound are demonstrated by the following example:

Example 4.3. *Consider the same plant and the same adaptive control system with baseline controller as in Example 4.1.*

In order to apply Lemma 4.2, an appropriate description of the set of admissible ideal parameters Θ^* is required first. Lemma 4.2 assumes that the set of admissible ideal parameters Θ^* is a hyperrectangle. This hyperrectangle is parametrized in terms of its center $\bar{\boldsymbol{\theta}}^*$ and the deviation from the center $\boldsymbol{\theta}^*_{\max}$. In case of the plant and the reference model from Example 4.1, the extremal values of this hyperrectangle ("lower left corner" / "upper right corner") are given by $\begin{bmatrix}-2.46 & -0.53 & -0.49\end{bmatrix}$ and $\begin{bmatrix}0.82 & 0.18 & 0.16\end{bmatrix}$ (see (4.54) *and Figure 4.4). The center point and the largest deviation are hence given by*

$$\begin{aligned} \bar{\boldsymbol{\theta}}^* &= \frac{1}{2} \cdot \left(\begin{bmatrix}0.82 & 0.18 & 0.16\end{bmatrix}^T + \begin{bmatrix}-2.46 & -0.53 & -0.49\end{bmatrix}^T \right), \\ \boldsymbol{\theta}^*_{\max} &= \frac{1}{2} \cdot \left(\begin{bmatrix}0.82 & 0.18 & 0.16\end{bmatrix}^T - \begin{bmatrix}-2.46 & -0.53 & -0.49\end{bmatrix}^T \right). \end{aligned} \tag{4.114}$$

Figure 4.11 compares the improved analytical tracking error bound computed using Lemma 4.2 and (4.113) *with the largest tracking error $\|e_{C,\alpha}(t)_\tau\|_{\mathcal{L}_\infty}$ observed in simulations for different values of the learning rate γ. While Figure 4.11 shows that the*

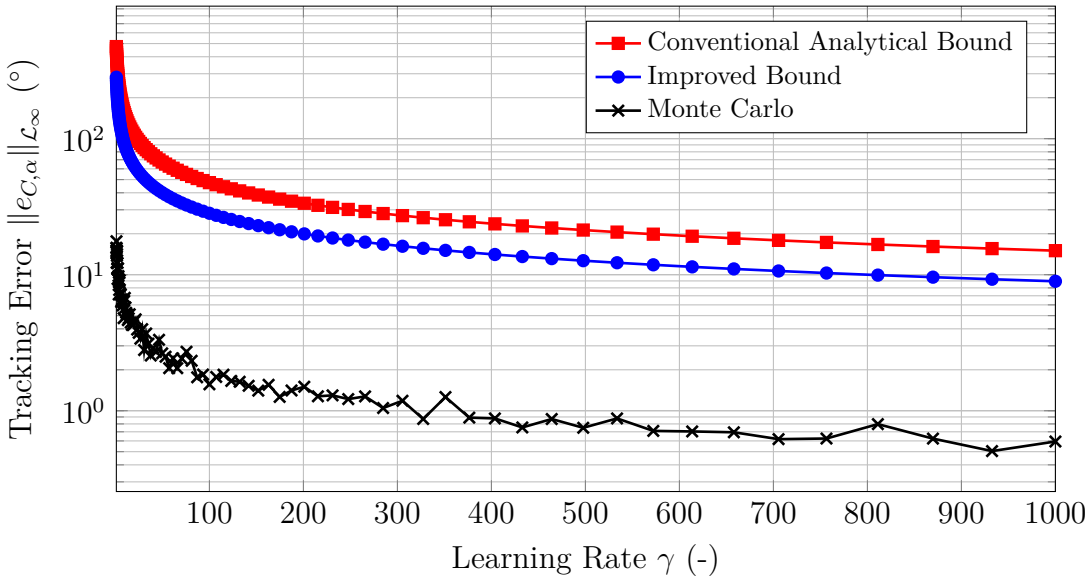

Figure 4.11: Comparison of the improved analytical tracking error bound computed using Lemma 4.2 and (4.113) with the largest tracking error $\|e_{C,\alpha}(t)_\tau\|_{\mathcal{L}_\infty}$ observed in simulations for different values of the learning rate γ.

tracking error bound for the angle-of-attack is significantly improved, it is still by far too conservative. For $\gamma = 1000$, the improved analytical bound exceeds the largest tracking error observed in simulations by 1400%.

Relation to Other Approaches in the Literature

While the previously presented approach has been derived independently, it is conceptually similar to [56, 61, 58].

Ref. [56] considers a MRAC with *Low Frequency Learning* [181]. In case of a nominal single-input plant and no input uncertainty $\mathbf{\Lambda}$, a set of LMIs is derived, which ensures the satisfaction of prescribed bounds on the tracking error. The approach differs from the approach of this section in several ways. First of all, [56] does not solve the set containment $\mathcal{M}_i \subseteq \mathcal{M}_c$ using the S-Procedure. Instead, it is shown that each vertex of the uncertainty hyperrectangle $\mathcal{M}_i$ lies within the ellipsoid $\mathcal{M}_c$, which implies that all points within the hyperrectangle are within $\mathcal{M}_c$ as well. Secondly, [56] assumes a scalar learning rate and scalar modification gains. Most importantly, [56] optimizes the design parameters of the *Low Frequency Learning* adaptive controller, including the matrix $\boldsymbol{P}$. This implies that [56] does not consider a pure analysis scenario, but a controller synthesis scenario since $\boldsymbol{P}$ is an important design parameter.

Refs. [61, 58] apply the same concept to a MRAC with *frequency-limited* learning [184] and to a MRAC with CRMs [159, 69], respectively. In contrast to [56], both references consider a nominal single-input plant with input uncertainty $\mathbf{\Lambda}$. Since there are no other conceptual differences, Refs. [61, 58] differ from the approach of this section in the same way as [56].

Further Improvement

While Example 4.3 demonstrates significant improvements over the conventional tracking error bounds, the question arises whether these bounds may be improved any further.

Since the tracking error bounds crucially depend on the design parameters $\boldsymbol{P}$ and $\boldsymbol{\Gamma}$ of the adaptive controller, the optimization of these parameters may lead to less conservative tracking error bounds. The feasibility of this approach has for example been demonstrated in [56, 61, 58] and also in a publication of the author of this thesis [79]. However, this chapter focuses on a pure analysis scenario. Hence, modifications of the design parameters are no admissible solution.

In order to find further directions for improvement, it is important to notice that the presented approach for the computation of tracking error bounds amounts to two *independent* steps. In the first step, an invariant set is determined such that it surrounds the set of admissible initial conditions. Afterwards, the tracking error bound derives from the largest extension of this invariant set in the direction of interest. These steps are independent in the sense that the level set constant c computed according to the conventional bound (4.62) may be combined with the improved computation of the tracking error according to (4.113) and vice versa.

Since the design parameter $\boldsymbol{\Gamma}$ may not be altered, further improvements of the first step may result from an appropriate consideration of the shape of the uncertainty set. In case of a circular uncertainty set, i.e. $\|\boldsymbol{\Theta}^*\|_F \leq \Theta^*_{\max}$, the level set constant computed according to (4.62) is preferable. Conversely, in case of a hyper-rectangular uncertainty set, the level set constant computed by Lemma 4.2 is less conservative. If the uncertainty set takes other shapes such as a polytopic or ellipsoidal shape, different methods for the computation of the level set constant may lead to less conservative level set constants.

At the first glance, further improvements of the second step seem to be impossible since any improvement of (4.113) either requires the reduction of the level set constant c from the first step or an alteration of the design parameter $\boldsymbol{P}$. At this point, it is important to recall the structure of the update law (3.41):

$$\dot{\tilde{\boldsymbol{\Theta}}}\left(t\right)^T = -\boldsymbol{\Gamma}\boldsymbol{\omega}\left(\boldsymbol{x}_P\left(t\right), t\right) \cdot \boldsymbol{e}_C\left(t\right)^T \boldsymbol{P}\boldsymbol{B}_P.$$

In order to avoid any change to the dynamic response of the adaptive controller, the matrices $\boldsymbol{\Gamma}$ and $\boldsymbol{P}$ may not be altered. However, notice that the design parameter $\boldsymbol{P}$ is multiplied by the matrix $\boldsymbol{B}_P$. For $m < n$, $\boldsymbol{B}_P$ will have a null space. Hence, the update law

$$\dot{\tilde{\boldsymbol{\Theta}}}\left(t\right)^T = -\boldsymbol{\Gamma}\boldsymbol{\omega}\left(\boldsymbol{x}_P\left(t\right), t\right) \cdot \boldsymbol{e}_C\left(t\right)^T \left(\boldsymbol{P} + \tilde{\boldsymbol{P}}\right) \boldsymbol{B}_P \tag{4.115}$$

will lead to the same dynamics as (3.41), if

$$\tilde{\boldsymbol{P}}\boldsymbol{B}_P = \boldsymbol{0}^{n\times m} \tag{4.116}$$

holds. This motivates a stability analysis of the adaptive controller with the help of the novel Lyapunov function candidate

$$V(t) = \frac{1}{2}\boldsymbol{e}_C(t)^T \boldsymbol{P}_0 \boldsymbol{e}_C(t) + \frac{1}{2}\operatorname{Tr}\left\{\tilde{\boldsymbol{\Theta}}(t)\,\boldsymbol{\Gamma}^{-1}\tilde{\boldsymbol{\Theta}}(t)^T\,\boldsymbol{\Lambda}\right\} \tag{4.117}$$

with $\boldsymbol{P}_0 = \boldsymbol{P} + \tilde{\boldsymbol{P}}$. While $\boldsymbol{P}$ is the fixed design parameter of the MRAC and adheres to the Lyapunov equation (3.31), the matrix $\tilde{\boldsymbol{P}} \in \mathbb{S}^n$, subject to the equality constraint (4.116), is an additional degree of freedom. In order to ensure stability of the adaptive controller, the parameter $\boldsymbol{P}_0$ of the novel Lyapunov function candidate (4.117) has to satisfy the LMI conditions

$$\boldsymbol{P}_0 = \boldsymbol{P} + \tilde{\boldsymbol{P}} > 0, \tag{4.118}$$

$$\boldsymbol{A}_M^T\boldsymbol{P}_0 + \boldsymbol{P}_0\boldsymbol{A}_M = \boldsymbol{A}_M^T(\boldsymbol{P} + \tilde{\boldsymbol{P}}) + (\boldsymbol{P} + \tilde{\boldsymbol{P}})\boldsymbol{A}_M < 0. \tag{4.119}$$

The first LMI condition ensures that $V(t)$ is positive definite, whereas the second condition ensures that $\dot{V}(t)$ is negative semidefinite.

Following the same steps as in Section 3.2.1, one arrives at

$$\begin{aligned}\dot{V}(t) = \frac{1}{2}\boldsymbol{e}_C(t)^T &\left(\boldsymbol{A}_M^T\boldsymbol{P}_0 + \boldsymbol{P}_0\boldsymbol{A}_M\right)\boldsymbol{e}_C(t) \\ &+ \boldsymbol{e}_C(t)^T\,\boldsymbol{P}_0\boldsymbol{B}_P\boldsymbol{\Lambda}\cdot\tilde{\boldsymbol{\Theta}}(t)\,\boldsymbol{\omega}\left(\boldsymbol{x}_P(t), t\right) \\ &+ \operatorname{Tr}\left\{\tilde{\boldsymbol{\Theta}}(t)\,\boldsymbol{\Gamma}^{-1}\dot{\tilde{\boldsymbol{\Theta}}}(t)^T\,\boldsymbol{\Lambda}\right\}.\end{aligned} \tag{4.120}$$

Due to the equality constraint (4.116), $\boldsymbol{P}_0\boldsymbol{B}_P = \tilde{\boldsymbol{P}}\boldsymbol{B}_P + \boldsymbol{P}\boldsymbol{B}_P = \boldsymbol{P}\boldsymbol{B}_P$ holds. Hence, insertion of the original update law (3.41) yields

$$\dot{V}(t) = \frac{1}{2}\boldsymbol{e}_C(t)^T\left(\boldsymbol{A}_M^T\boldsymbol{P}_0 + \boldsymbol{P}_0\boldsymbol{A}_M\right)\boldsymbol{e}_C(t). \tag{4.121}$$

Due to the LMI condition (4.119), $\dot{V}(t) \leq 0$ holds. Hence, the novel Lyapunov function (4.117) establishes stability of the tracking error dynamics (3.29) and the parameter error dynamics (3.41).

Since the novel Lyapunov function (4.117) establishes stability, its invariant level sets may be used in the exact same way as those of the original Lyapunov function (3.30) in order to analyze the error dynamics. Since the proof of stability using the novel Lyapunov function does not alter the error dynamics, both Lyapunov functions admit the computation of tracking error bounds for the same error dynamics. In contrast to the original Lyapunov function, the additional degree of freedom $\tilde{\boldsymbol{P}}$ of the novel Lyapunov function admits to alter the shape of the ellipsoid $\mathcal{M}_c$, as long as the equality constraint (4.116) is satisfied. Hence, an analysis based on the novel Lyapunov function offers the opportunity of less conservatism.

Due to the choice of the initial conditions from Assumption 4.3, the use of the novel Lyapunov function candidate within the first step does not alter the conditions for set

containment, namely $\mathcal{M}_i \subseteq \mathcal{M}_c$. This is because the projection of $\mathcal{M}_c$ onto the $\tilde{\boldsymbol{\theta}}$-subspace is independent of the matrix $\boldsymbol{P}$ or $\boldsymbol{P}_0$, respectively, as can be seen in (4.92). Since the LMI condition (4.104) derives from the projections of $\mathcal{M}_c$ and $\mathcal{M}_i$ onto the $\tilde{\boldsymbol{\theta}}$-subspace, its implication, namely $\mathcal{M}_i \subseteq \mathcal{M}_c$, also holds regardless of whether the Lyapunov function is defined in terms of $\boldsymbol{P}$ or $\boldsymbol{P}_0$.

Now assume that the level set constant c satisfies the LMI condition (4.104). When using the novel Lyapunov function, the tracking error bound

$$\|e_{C,k}(t)\|_{\mathcal{L}_\infty} \leq \sqrt{2 \cdot c \cdot \boldsymbol{b}_k^T \boldsymbol{P}_0^{-1} \boldsymbol{b}_k}\,. \tag{4.122}$$

for the state $e_{C,k}(t)$ follows immediately. The additional degree of freedom due to the use of $\boldsymbol{P}_0$ instead of $\boldsymbol{P}$ shall now be used to minimize this tracking error bound. Hence, a matrix $\tilde{\boldsymbol{P}}$ and a level set constant c are sought, which

1. minimize $2 \cdot c \cdot \boldsymbol{b}_k^T \boldsymbol{P}_0^{-1} \boldsymbol{b}_k$;
2. satisfy the equality constraint (4.116);
3. satisfy the LMI conditions (4.118) (positive definiteness of $V(t)$), (4.119) (negative definiteness of $\dot{V}(t)$) and (4.104) ($\mathcal{M}_i \subseteq \mathcal{M}_c$).

Unfortunately, the above objective function is not linear and hence, the optimization problem subject to LMI and equality constraints does not constitute a SDP. By an appropriate reformulation of the problem, this difficulty may be circumvented.

To that end, consider a slightly different problem. Instead of minimizing $2 \cdot c \cdot \boldsymbol{b}_k^T \boldsymbol{P}_0^{-1} \boldsymbol{b}_k$, assume that it is to be shown that the tracking error of the state $e_{C,k}(t)$ remains below the threshold $e_{C,k,\max}$, i.e. $|e_{C,k}(t)|^2 \leq e_{C,k,\max}^2 \ \forall t \geq 0$. This is equivalent to saying that the invariant set $\mathcal{M}_c$ should lie within the set $\mathcal{M}_k = \{\boldsymbol{e}_C, \tilde{\boldsymbol{\Theta}} \mid |e_{C,k}(t)|^2 \leq e_{C,k,\max}^2\}$. In terms of the joint state vector $\boldsymbol{x}$, which was defined in (4.88), the set $\mathcal{M}_k$ may be represented as

$$\mathcal{M}_k = \left\{\boldsymbol{x} \mid \boldsymbol{x}^T \cdot \boldsymbol{c}_k \boldsymbol{c}_k^T \cdot \boldsymbol{x} \leq e_{C,k,\max}^2\right\}, \tag{4.123}$$

where $\boldsymbol{c}_k$ still represents the unit vector associated with the state $e_{C,k}(t)$ as defined in (4.111). For the derivation of (4.123), the fact $e_{C,k} = \boldsymbol{c}_k^T \boldsymbol{x}$ was used, which leads to the dyadic product $\boldsymbol{c}_k \boldsymbol{c}_k^T$. In order to apply the S-Procedure, the sets $\mathcal{M}_c$ and $\mathcal{M}_k$ have to be represented as 0-sublevel sets. Upon definition of the new extended state vector

$$\boldsymbol{z}^T = \begin{bmatrix}\boldsymbol{x}^T & 1\end{bmatrix} = \begin{bmatrix}\boldsymbol{e}_C^T & \tilde{\boldsymbol{\theta}}^T & 1\end{bmatrix}, \tag{4.124}$$

the 0-sublevel set representations of $\mathcal{M}_c$ and $\mathcal{M}_k$ are

$$\mathcal{M}_k = \{\boldsymbol{z} \mid g_k(\boldsymbol{z}) \leq 0\}, \tag{4.125}$$

$$\mathcal{M}_c = \{\boldsymbol{z} \mid g_c(\boldsymbol{z}) \leq 0\} \tag{4.126}$$

with

$$g_k(\boldsymbol{z}) = \boldsymbol{z}^T \begin{bmatrix} \boldsymbol{b}_k \boldsymbol{b}_k^T & \boldsymbol{0}^{n\times(m\cdot n_r)} & \boldsymbol{0}^{n\times 1} \\ \boldsymbol{0}^{(m\cdot n_r)\times n} & \boldsymbol{0}^{(m\cdot n_r)\times(m\cdot n_r)} & \boldsymbol{0}^{(m\cdot n_r)\times 1} \\ \boldsymbol{0}^{1\times n} & \boldsymbol{0}^{1\times(m\cdot n_r)} & -e_{C,k,\max}^2 \end{bmatrix} \boldsymbol{z}, \tag{4.127}$$

$$g_c(\boldsymbol{z}) = \boldsymbol{z}^T \begin{bmatrix} \boldsymbol{P}_0 & \boldsymbol{0}^{n\times(m\cdot n_r)} & \boldsymbol{0}^{n\times 1} \\ \boldsymbol{0}^{(m\cdot n_r)\times n} & \boldsymbol{M}_{\tilde{\Theta}}(\boldsymbol{\lambda}) & \boldsymbol{0}^{(m\cdot n_r)\times 1} \\ \boldsymbol{0}^{1\times n} & \boldsymbol{0}^{1\times(m\cdot n_r)} & -2c \end{bmatrix} \boldsymbol{z}. \tag{4.128}$$

According to the S-Procedure, $\mathcal{M}_c \subset \mathcal{M}_k$ holds, if there exists a multiplier $\bar{l}_k \geq 0$ such that the matrix inequality conditions

$$\boldsymbol{b}_k \boldsymbol{b}_k^T - \bar{l}_k \boldsymbol{P}_0 \leq 0, \tag{4.129}$$

$$-\bar{l}_k \boldsymbol{M}_{\tilde{\Theta}}(\boldsymbol{\lambda}) \leq 0, \tag{4.130}$$

$$-e_{C,k,\max}^2 + \bar{l}_k 2c \leq 0 \tag{4.131}$$

are satisfied. Since $\boldsymbol{M}_{\tilde{\Theta}}(\boldsymbol{\lambda})$ is positive definite by definition, the LMI (4.130) always holds and may be discarded. As $\boldsymbol{P}_0$, c and $\bar{l}_k$ are decision variables, neither (4.129) nor (4.131) are LMIs. However, by dividing by $\bar{l}_k$ and upon definition of $l_k = 1/\bar{l}_k$, the LMIs

$$l_k \cdot \boldsymbol{b}_k \boldsymbol{b}_k^T - \boldsymbol{P}_0 \leq 0, \tag{4.132}$$

$$2c - l_k \cdot e_{C,k,\max}^2 \leq 0 \tag{4.133}$$

result. In order to prevent a division by zero, this step requires $l_k > 0$. Combining the stability condition derived from the novel Lyapunov function (4.117), the set containment conditions for $\mathcal{M}_i \subseteq \mathcal{M}_c$ and the above set containment conditions for $\mathcal{M}_c \subset \mathcal{M}_k$ gives rise to the following lemma:

Lemma 4.4. *Consider a direct MRAC according to Section 3.2.1, which satisfies the conditions for NS of Theorem 3.4. In addition, let Assumptions 4.1 (diagonal control effectiveness), 4.2 (hyper-rectangular uncertainty sets) and 4.3 (initial conditions $\boldsymbol{e}_C(0) = \boldsymbol{0}$ and $\tilde{\boldsymbol{\Theta}}(0) = -\boldsymbol{\Theta}^*$) hold. Let $e_{C,k,\max}$ be a given bound for the state $e_{C,k}(t)$ and let $\boldsymbol{b}_k \in \mathbb{R}^n$ denote the unit vector associated with the state $e_{C,k}(t)$. If there exist a level set constant $c > 0$, a multiplier $l_k > 0$, a diagonal positive semidefinite matrix $\boldsymbol{D} \in \mathbb{S}^{m\cdot n_r}$ and a symmetric matrix $\tilde{\boldsymbol{P}} \in \mathbb{S}^n$ such that the LMIs*

$$\begin{bmatrix} \boldsymbol{M}_{\tilde{\Theta}}(\boldsymbol{\lambda}_v) - \boldsymbol{D} & -\boldsymbol{D}\bar{\boldsymbol{\theta}}^* \\ -(\bar{\boldsymbol{\theta}}^*)^T \boldsymbol{D} & (\boldsymbol{\theta}_{\max}^*)^T \boldsymbol{D} \boldsymbol{\theta}_{\max}^* - (\bar{\boldsymbol{\theta}}^*)^T \boldsymbol{D} \bar{\boldsymbol{\theta}}^* - 2c \end{bmatrix} \leq 0 \quad \forall\, v = 1, \ldots, 2^m, \tag{4.134}$$

$$l_k \cdot \boldsymbol{b}_k \boldsymbol{b}_k^T - (\boldsymbol{P} + \tilde{\boldsymbol{P}}) \leq 0, \tag{4.135}$$

$$2c - l_k \cdot e_{C,k,\max}^2 \leq 0, \tag{4.136}$$

$$\boldsymbol{P} + \tilde{\boldsymbol{P}} > 0, \tag{4.137}$$

$$\boldsymbol{A}_M^T(\boldsymbol{P}+\tilde{\boldsymbol{P}})+(\boldsymbol{P}+\tilde{\boldsymbol{P}})\boldsymbol{A}_M<0 \tag{4.138}$$

and the equality constraint

$$\tilde{\boldsymbol{P}}\boldsymbol{B}_P=\boldsymbol{0}^{n\times m} \tag{4.139}$$

are feasible, then the state $e_{C,k}(t)$ *satisfies*

$$\|e_{C,k}(t)\|_{\mathcal{L}_\infty}\leq e_{C,k,\max}. \tag{4.140}$$

Proof. If the LMIs of Lemma 4.4 are feasible, then the novel Lyapunov function candidate (4.117) is positive definite due to (4.137). Furthermore, (4.138) and (4.139) establish that the derivative $\dot{V}(t)$ (upon insertion of the error dynamics of the adaptive controller) is negative semidefinite (see (4.120) and (4.121)). The latter proves stability of the adaptive controller (see Theorem 3.4).

As the condition (4.134) is satisfied, one may repeat the proof of Lemma 4.2 to show that the trajectories of $\boldsymbol{e}_C(t)$ and $\tilde{\boldsymbol{\Theta}}(t)$ are confined to the invariant set $\mathcal{M}_c$. Thus,

$$\left(\boldsymbol{e}_C(t),\tilde{\boldsymbol{\Theta}}(t)\right)\in\mathcal{M}_c,\ \forall\, t\geq 0 \tag{4.141}$$

holds, where $\mathcal{M}_c=\left\{\boldsymbol{e}_C,\tilde{\boldsymbol{\Theta}}\mid V(\boldsymbol{e}_C,\tilde{\boldsymbol{\Theta}})\leq c\right\}$ is now defined in terms of the novel Lyapunov function (4.117) as can be seen in (4.126).

Finally, notice that (4.135) and (4.136) imply (4.129)-(4.131) with $\bar{l}_k=1/l_k$ since $l_k>0$ and $\boldsymbol{M}_{\tilde{\Theta}}(\boldsymbol{\lambda})>0$ hold by definition. Due to the S-Procedure (Lemma B.7), (4.129)-(4.131) imply $\mathcal{M}_c\subset\mathcal{M}_k$, where $\mathcal{M}_k$ is defined in (4.123). Thus,

$$\mathcal{M}_c=\left\{\boldsymbol{e}_C,\tilde{\boldsymbol{\Theta}}\mid V(\boldsymbol{e}_C,\tilde{\boldsymbol{\Theta}})\leq c\right\}\subset\{\boldsymbol{e}_C,\tilde{\boldsymbol{\Theta}}\mid|e_{C,k}(t)|^2\leq e_{C,k,\max}^2\} \tag{4.142}$$

holds. Since the trajectories of $\boldsymbol{e}_C(t)$ and $\tilde{\boldsymbol{\Theta}}(t)$ may never leave the set $\mathcal{M}_c$, the latter proves (4.140). □

If the feasibility problem of Lemma 4.4 admits a solution, then the state $e_{C,k}(t)$ is guaranteed to remain below the given threshold $e_{C,k,\max}$. In practice, an appropriate value of $e_{C,k,\max}$ is however not known a-priori. Furthermore, one is usually interested in the smallest value of $e_{C,k,\max}$, which satisfies the conditions of Lemma 4.4. Hence, $e_{C,k,\max}^2$ is subsequently introduced as a decision variable, which is to be minimized. The following theorem results:

Theorem 4.5. *Consider a direct MRAC according to Section 3.2.1, which satisfies the conditions for NS of Theorem 3.4. In addition, let Assumptions 4.1 (diagonal control effectiveness), 4.2 (hyper-rectangular uncertainty sets) and 4.3 (initial conditions* $\boldsymbol{e}_C(0)=\boldsymbol{0}$ *and* $\tilde{\boldsymbol{\Theta}}(0)=-\boldsymbol{\Theta}^*$*) hold. Let* $\boldsymbol{b}_k\in\mathbb{R}^n$ *denote the unit vector associated with the state* $e_{C,k}(t)$*. If there exist a level set constant* $c>0$*, a multiplier* $l_k>0$*, a diagonal positive semidefinite matrix* $\boldsymbol{D}\in\mathbb{S}^{m\cdot n_r}$ *and a symmetric matrix* $\tilde{\boldsymbol{P}}\in\mathbb{S}^n$*, which minimize*

$$\min_{c,l_k,e_{C,k,\max}^2,\boldsymbol{D},\tilde{\boldsymbol{P}}}\quad e_{C,k,\max}^2, \tag{4.143}$$

subject to the matrix inequality constraints

$$\begin{bmatrix} \boldsymbol{M}_{\tilde{\Theta}}(\boldsymbol{\lambda}_v) - \boldsymbol{D} & -\boldsymbol{D}\bar{\boldsymbol{\theta}}^* \\ -(\bar{\boldsymbol{\theta}}^*)^T\boldsymbol{D} & (\boldsymbol{\theta}^*_{\max})^T\boldsymbol{D}\boldsymbol{\theta}^*_{\max} - (\bar{\boldsymbol{\theta}}^*)^T\boldsymbol{D}\bar{\boldsymbol{\theta}}^* - 2c \end{bmatrix} \leq 0 \quad \forall\, v = 1, \ldots, 2^m, \tag{4.144}$$

$$l_k \cdot \boldsymbol{b}_k\boldsymbol{b}_k^T - (\boldsymbol{P} + \tilde{\boldsymbol{P}}) \leq 0, \tag{4.145}$$

$$2c - l_k \cdot e^2_{C,k,\max} \leq 0, \tag{4.146}$$

$$\boldsymbol{P} + \tilde{\boldsymbol{P}} > 0, \tag{4.147}$$

$$\boldsymbol{A}_M^T(\boldsymbol{P} + \tilde{\boldsymbol{P}}) + (\boldsymbol{P} + \tilde{\boldsymbol{P}})\boldsymbol{A}_M < 0 \tag{4.148}$$

and the equality constraint

$$\tilde{\boldsymbol{P}}\boldsymbol{B}_P = \boldsymbol{0}^{n\times m}, \tag{4.149}$$

then the state $e_{C,k}(t)$ satisfies

$$\|e_{C,k}(t)\|_{\mathcal{L}_\infty} \leq e^*_{C,k,\max}, \tag{4.150}$$

where $e^*_{C,k,\max}$ denotes the minimizer of the above optimization problem.

Proof. If the optimization problem of Theorem 4.5 is feasible, Lemma 4.4 immediately proves the assertion (4.150). Since $e^*_{C,k,\max}$ is the minimizer of the optimization problem of Theorem 4.5, $e^*_{C,k,\max}$ represents the smallest value $e_{C,k,\max}$, for which Lemma 4.4 holds. □

Remark 4.6. *Due to the product $l_k \cdot e^2_{C,k,\max}$ in* (4.146)*, the optimization problem of Theorem 4.5 is no SDP, but a so-called Generalized Eigenvalue Problem (GEVP). GEVPs are similar to SDPs. In contrast to SDPs, they allow for one bilinear matrix inequality constraint which contains a product of a matrix valued decision variable and a single scalar decision variable, which is minimized. They are quasi-convex optimization problems and may be solved in polynomial time [17]. Appropriate solvers are for example available in the Robust Control Toolbox of MATLAB®.*

The benefits of the further improved method for the computation of a tracking error bound are demonstrated by the following example:

Example 4.7. *Consider the same plant and the same adaptive control system with baseline controller as in Examples 4.1 and 4.3.*

As in Example 4.3, the set of admissible ideal parameters is given by (4.114)*.*

Figure 4.12 compares the further improved analytical tracking error bound computed using Theorem 4.5 to the largest tracking error $\|e_{C,\alpha}(t)_\tau\|_{\mathcal{L}_\infty}$ observed in simulations for different values of the learning rate γ. Furthermore, the results of the previous analyses from Examples 4.1 and 4.3 are included. Figure 4.12 shows that the use of Theorem 4.5 leads to another significant improvement. For $\gamma = 1000$, the improved analytical bound exceeds the largest tracking error observed in simulations only by 361%. Such improvement is also achieved at lower learning rates. At $\gamma = 100$, the improved analytical bound exceeds the largest tracking error observed in simulations by 366%, whereas the conventional bound would lead to 2940%.

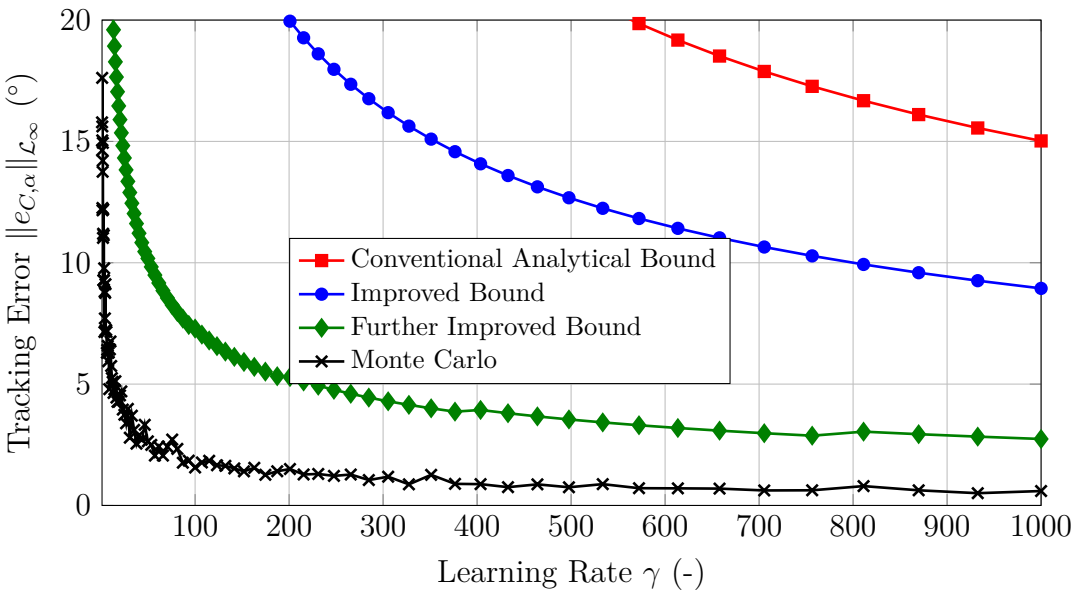

Figure 4.12: Comparison of the even further improved analytical tracking error bound computed using Theorem 4.5 with the largest tracking error $\|e_{C,\alpha}(t)_\tau\|_{\mathcal{L}_\infty}$ observed in simulations for different values of the learning rate γ.

4.2.2 Computation of Tracking Error Norms in Case of Statistically Distributed Uncertainties

From a probabilistic point of view, the uncertainties $\boldsymbol{\Theta}^*$ and $\boldsymbol{\Lambda}$ may be considered as random variables. If both $\boldsymbol{\Theta}^*$ and $\boldsymbol{\Lambda}$ are distributed uniformly, then any realization of the uncertainties is equally probable. However, if the uncertainties adhere to some other a-priori known Probability Density Function (PDF), then some realizations of the uncertainties are more likely than others. Hence, the tracking error bounds of the previous section consider a worst-case scenario as they hold for all uncertainties $\boldsymbol{\Theta}^*$ and $\boldsymbol{\Lambda}$ lying in sets of known shape and size. If those uncertainties, which contribute most to the size of the tracking error bounds, are highly unlikely, then a worst-case analysis will introduce unnecessary conservatism. For this reason, this section proposes a probabilistic approach to mitigate this conservatism.

To that end, let the same assumptions as in case of Theorem 4.5 hold, namely diagonal control effectiveness (Assumption 4.1), hyper-rectangular uncertainty sets (Assumption 4.2) and initial conditions $\boldsymbol{e}_C(0) = \boldsymbol{0}$, $\tilde{\boldsymbol{\Theta}}(0) = -\boldsymbol{\Theta}^*$ (Assumption 4.3). Let the joint uncertainty vector be defined as

$$\boldsymbol{\delta}^T \triangleq \begin{bmatrix} \boldsymbol{\theta}^{*T} & \boldsymbol{\lambda}^T \end{bmatrix}, \tag{4.151}$$

where the vectorial representations $\boldsymbol{\theta}^*$ and $\boldsymbol{\lambda}$ of $\boldsymbol{\Theta}^*$ and $\boldsymbol{\Lambda}$ have been used. In terms of the joint uncertainty vector $\boldsymbol{\delta}$, the set of admissible uncertainties is given by

$$\mathcal{Q} \triangleq \left\{ \boldsymbol{\delta} \;\middle|\; \begin{matrix} |\Theta^*_{ij} - \bar{\Theta}^*_{ij}| & \leq \Theta^*_{ij,\max}, & i = 1,\ldots,m, & j = 1,\ldots,n_r \\ \Lambda_{i,\min} \leq \Lambda_i & \leq \Lambda_{i,\max}, & & i = 1,\ldots,m \end{matrix} \right\}. \tag{4.152}$$

Furthermore, the uncertainties are assumed to be distributed according to some known PDF. Hence, $\boldsymbol{\delta}$ is a realization of the random variable $\boldsymbol{\Delta}$, which is assumed to satisfy

$$\Pr\{\mathcal{Q}\} = 1. \tag{4.153}$$

Each realization $\boldsymbol{\delta}$ of the random variable $\boldsymbol{\Delta}$ will lead to some largest tracking error

$$|e_{C,k}(t)| \leq \bar{e}_{C,k}(\boldsymbol{\delta}) \quad \forall\, t \geq 0. \tag{4.154}$$

Obviously, the size of the largest tracking error $\bar{e}_{C,k}(\boldsymbol{\delta})$ depends on the respective realization of the uncertainty $\boldsymbol{\delta}$. Since $\boldsymbol{\Delta}$ is a random variable, the tracking error bound $E_k \triangleq \bar{e}_{C,k}(\boldsymbol{\Delta})$ is a random variable as well. Using its Cumulative Density Function (CDF) $F_{E_k}(e_k) = \Pr\{E_k \leq e_k\}$, the probability of the event "the largest tracking error $\bar{e}_{C,k}$ stays below e_k" may be computed. Subsequently, this probabilistic notion of the largest tracking error is considered. At this point, it is important to stress that this notion concerns the *largest tracking error* $\bar{e}_{C,k}$ and not the tracking error $e_{C,k}(t)$ itself. Furthermore, notice that $\bar{e}_{C,k}$ is not equivalent to tracking error bound $e_{C,k,\max}$, which was introduced in Lemma 4.4 and Theorem 4.5. While $\bar{e}_{C,k}$ denotes the tight upper bound $\bar{e}_{C,k} = \|e_{C,k}(t)\|_{\mathcal{L}_\infty}$, the tracking error bound $e_{C,k,\max}$ only satisfies $\|e_{C,k}(t)\|_{\mathcal{L}_\infty} \leq e_{C,k,\max}$.

While a probabilistic notion of the tracking error bound would be helpful in practice, the computation of the CDF of the random variable E_k faces a major challenge: the map $\bar{e}_{C,k} : \mathbb{R}^{(m\cdot n_r)+m} \to \mathbb{R}_+$ is not known exactly. That is, for some given realization $\boldsymbol{\delta}$, the exact value of the largest tracking error $\bar{e}_{C,k}(\boldsymbol{\delta})$ is unknown. While analytical methods such as the Lyapunov-based methods from the previous section yield upper bounds on the largest tracking error, i.e.

$$\bar{e}_{C,k}(\boldsymbol{\delta}) \leq e_{C,k,\max}(\boldsymbol{\delta}), \tag{4.155}$$

simulations yield lower bounds $e_{C,k,\min}(\boldsymbol{\delta})$. The latter follows from the fact that the response of an adaptive controller depends upon the reference signal $\boldsymbol{r}\,(t)$. Since there exist infinitely many reference signals, there always remains the chance of another reference signal, which will lead to an even larger tracking error than the simulated reference signals. Hence,

$$e_{C,k,\min}(\boldsymbol{\delta}) \leq \bar{e}_{C,k}(\boldsymbol{\delta}) \tag{4.156}$$

holds. Since the map $\bar{e}_{C,k}(\boldsymbol{\delta})$ is unknown, the CDF of E_k may not be computed by simply transforming the random variable $\boldsymbol{\Delta}$ using the map $\bar{e}_{C,k}(\boldsymbol{\delta})$ [107]. While an exact computation of the CDF of E_k is hence not feasible, upper and lower bounds for the CDF of E_k may however be determined with the help of the upper and lower bounds $e_{C,k,\max}(\boldsymbol{\delta})$ and $e_{C,k,\min}(\boldsymbol{\delta})$.

The underlying idea of the proposed approach is closely inspired by the probabilistic computation of the *Structured Singular Value* μ, which has for example been demonstrated in [11]. While the technical details of the *Structured Singular Value* μ are not

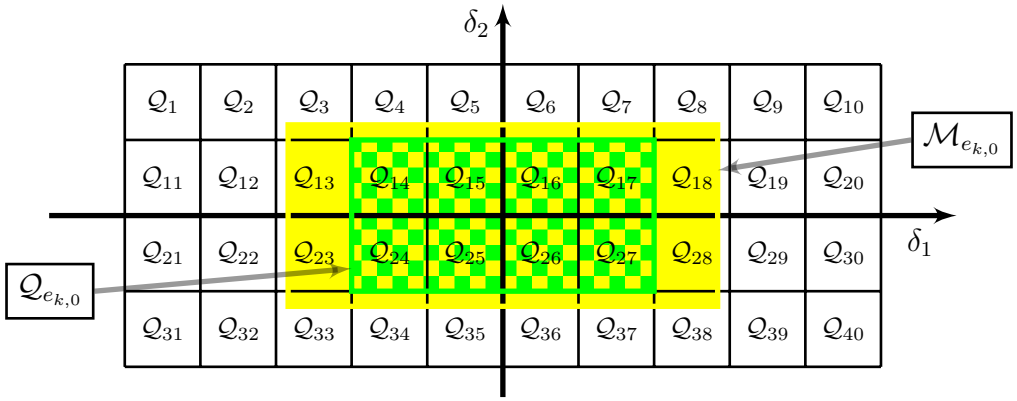

Figure 4.13: Partition of the uncertainty set $\mathcal{Q}$ into smaller subsets $\mathcal{Q}_v$. The set $\mathcal{M}_{e_{k,0}}$ surrounds all uncertainties which lead to a tracking error $\bar{e}_{C,k}$ smaller than $e_{k,0}$. The set $\mathcal{Q}_{e_{k,0}}$ (checkered) is the union of all subsets $\mathcal{Q}_v$, whose upper bound satisfies $e_{C,k,\max}(\mathcal{Q}_v) \leq e_{k,0}$.

important here, it is important to notice that its non-probabilistic computation considers a worst-case scenario and that only upper and lower bounds on μ may be computed in practice. The probabilistic computation of μ exhibits two intriguing features:

1. it reuses the existing worst-case computation methods;
2. it only requires the knowledge of upper and lower bounds of the worst-case value of μ in order to draw conclusions on the CDF of $\mu(\boldsymbol{\Delta})$.

Since upper and lower bounds for $\bar{e}_{C,k}$ are known, the probabilistic computation of tracking error bounds following the same lines as in [11] seems feasible.

Consider a partition of the uncertainty set $\mathcal{Q}$ into N smaller uncertainty subsets $\mathcal{Q}_v,\ v = 1, \ldots, N$ as shown in Figure 4.13. The uncertainty subsets $\mathcal{Q}_v$ are assumed to be disjoint, i.e.

$$\Pr\{\mathcal{Q}_v \cap \mathcal{Q}_w\} = 0, \quad v \neq w. \tag{4.157}$$

For each of the uncertainty subsets $\mathcal{Q}_v$, a worst-case upper bound $e_{C,k,\max}(\mathcal{Q}_v)$ and a worst-case lower bound $e_{C,k,\min}(\mathcal{Q}_v)$ may be computed using analytical techniques (such as those proposed in the previous section) and simulations, respectively. The following relation hence holds:

$$e_{C,k,\min}(\mathcal{Q}_v) \leq \bar{e}_{C,k}(\mathcal{Q}_v) \leq e_{C,k,\max}(\mathcal{Q}_v). \tag{4.158}$$

Now assume that appropriate bounds $e_{C,k,\min}(\mathcal{Q}_v),\ e_{C,k,\max}(\mathcal{Q}_v)$ have been computed for each subset $\mathcal{Q}_v,\ v = 1, \ldots, N$. The objective of the subsequent derivations is the computation of upper and lower bounds for the CDF $F_{E_k}(e_{k,0}) = \Pr\{E_k \leq e_{k,0}\}$ for one specific value $e_k = e_{k,0}$. To that end, consider the set

$$\mathcal{M}_{e_{k,0}} \triangleq \{\boldsymbol{\delta} \mid \bar{e}_{C,k}(\boldsymbol{\delta}) \leq e_{k,0}\} \tag{4.159}$$

of all uncertainties, which lead to a tracking error below $e_{k,0}$ (see Figure 4.13). In practice, the shape and the size of the set $\mathcal{M}_{e_{k,0}}$ is unknown since the map $\bar{e}_{C,k}(\boldsymbol{\delta})$ is unknown. However, all subsets $\mathcal{Q}_v$, whose upper bound lies below $e_{k,0}$, i.e. $e_{C,k,\max}(\mathcal{Q}_v) \leq e_{k,0}$, are subsets of $\mathcal{M}_{e_{k,0}}$, i.e. $\mathcal{Q}_v \subseteq \mathcal{M}_{e_{k,0}}$, due to $\bar{e}_{C,k}(\mathcal{Q}_v) \leq e_{C,k,\max}(\mathcal{Q}_v) \leq e_{k,0}$. The union of all of these sets is denoted as

$$\mathcal{Q}_{e_{k,0}} \triangleq \bigcup_{v:\, e_{C,k,\max}(\mathcal{Q}_v) \leq e_{k,0}} \mathcal{Q}_v. \tag{4.160}$$

In Figure 4.13, the set $\mathcal{Q}_{e_{k,0}}$ is indicated by the checkered rectangle. As PDFs are non-negative by definition [107] and as $\mathcal{Q}_{e_{k,0}} \subseteq \mathcal{M}_{e_{k,0}}$ holds, the probability of the set $\mathcal{Q}_{e_{k,0}}$ is lower than the probability of the set $\mathcal{M}_{e_{k,0}}$:

$$\Pr\{\mathcal{M}_{e_{k,0}}\} \geq \Pr\{\mathcal{Q}_{e_{k,0}}\} = \sum_{v:\, e_{C,k,\max}(\mathcal{Q}_v) \leq e_{k,0}} \Pr\{\mathcal{Q}_v\}. \tag{4.161}$$

While the exact shape and size of the set $\mathcal{M}_{e_{k,0}}$ is unknown, its probability $\Pr\{\mathcal{M}_{e_{k,0}}\}$ is exactly equivalent to $\Pr\{E_k \leq e_{k,0}\}$, since both quantities specify the probability that the largest tracking error $\bar{e}_{C,k}$ stays below $e_{k,0}$. Hence, (4.161) constitutes a lower bound for the CDF of E_k at $e_k = e_{k,0}$:

$$F_{E_k}(e_{k,0}) = \Pr\{\mathcal{M}_{e_{k,0}}\} \geq \sum_{v:\, e_{C,k,\max}(\mathcal{Q}_v) \leq e_{k,0}} \Pr\{\mathcal{Q}_v\}. \tag{4.162}$$

Since the probability of the sets $\mathcal{Q}_v$ may be easily determined from the PDF of $\boldsymbol{\Delta}$, the lower bound for the CDF of E_k may be readily computed.

While the upper bounds $e_{C,k,\max}(\mathcal{Q}_v)$ lead to a lower bound on the CDF of E_k, the lower bounds $e_{C,k,\min}(\mathcal{Q}_v)$ lead to an upper bound for the CDF of E_k. This is shown next. To that end, consider the set

$$\bar{\mathcal{M}}_{e_{k,0}} \triangleq \{\boldsymbol{\delta} \mid \bar{e}_{C,k}(\boldsymbol{\delta}) > e_{k,0}\} \tag{4.163}$$

of all uncertainties, which lead to a largest tracking error larger than $e_{k,0}$ (see Figure 4.14). In practice, the shape and the size of the set $\bar{\mathcal{M}}_{e_{k,0}}$ is unknown since the map $\bar{e}_{C,k}(\boldsymbol{\delta})$ is unknown. However, all subsets $\mathcal{Q}_v$, whose lower bound lies above $e_{k,0}$, i.e. $e_{C,k,\min}(\mathcal{Q}_v) > e_{k,0}$, are subsets of $\bar{\mathcal{M}}_{e_{k,0}}$, i.e. $\mathcal{Q}_v \subseteq \bar{\mathcal{M}}_{e_{k,0}}$, due to $e_{k,0} < e_{C,k,\min}(\mathcal{Q}_v) \leq \bar{e}_{C,k}(\mathcal{Q}_v)$. The union of all of these sets is denoted as

$$\bar{\mathcal{Q}}_{e_{k,0}} \triangleq \bigcup_{v:\, e_{C,k,\min}(\mathcal{Q}_v) > e_{k,0}} \mathcal{Q}_v. \tag{4.164}$$

In Figure 4.14, the set $\bar{\mathcal{Q}}_{e_{k,0}}$ is indicated as checkered. As PDFs are non-negative by definition and as $\bar{\mathcal{Q}}_{e_{k,0}} \subseteq \bar{\mathcal{M}}_{e_{k,0}}$ holds, the probability of the set $\bar{\mathcal{Q}}_{e_{k,0}}$ is lower than the probability of the set $\bar{\mathcal{M}}_{e_{k,0}}$:

$$\Pr\{\bar{\mathcal{M}}_{e_{k,0}}\} \geq \Pr\{\bar{\mathcal{Q}}_{e_{k,0}}\} = \sum_{v:\, e_{C,k,\min}(\mathcal{Q}_v) > e_{k,0}} \Pr\{\mathcal{Q}_v\}. \tag{4.165}$$

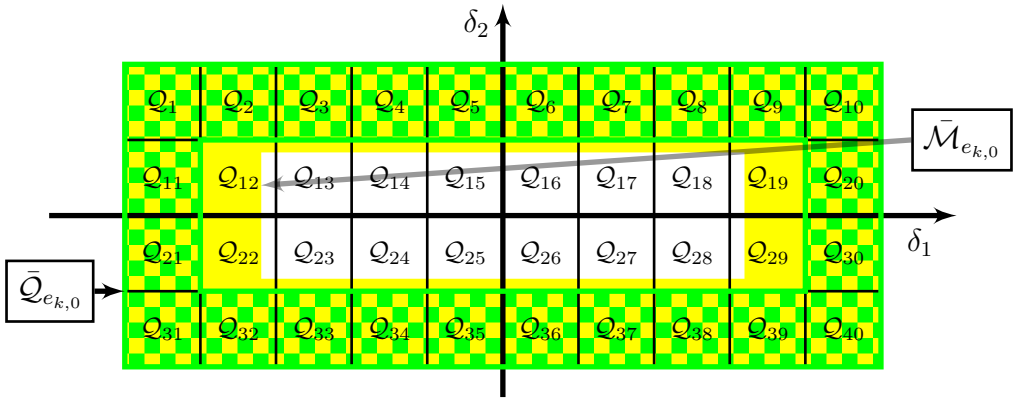

Figure 4.14: Partition of the uncertainty set $\mathcal{Q}$ into smaller subsets $\mathcal{Q}_v$. The set $\bar{\mathcal{M}}_{e_{k,0}}$ surrounds all uncertainties which lead to a tracking error $\bar{e}_{C,k}$ larger than $e_{k,0}$. The set $\bar{\mathcal{Q}}_{e_{k,0}}$ (checkered) is the union of all subsets $\mathcal{Q}_v$, whose lower bound satisfies $e_{C,k,\min}(\mathcal{Q}_v) > e_{k,0}$.

While the exact shape and size of the set $\bar{\mathcal{M}}_{e_{k,0}}$ is unknown, its probability $\Pr\{\bar{\mathcal{M}}_{e_{k,0}}\}$ is exactly equivalent to $\Pr\{E_k > e_{k,0}\} = 1 - \Pr\{E_k \leq e_{k,0}\}$, since both quantities specify the probability that the largest tracking error $\bar{e}_{C,k}$ stays above $e_{k,0}$. Hence, (4.165) constitutes a lower bound for the complementary CDF of E_k at $e_k = e_{k,0}$:

$$1 - F_{E_k}(e_{k,0}) = \Pr\{\bar{\mathcal{M}}_{e_{k,0}}\} \geq \sum_{v:\, e_{C,k,\min}(\mathcal{Q}_v) > e_{k,0}} \Pr\{\mathcal{Q}_v\}. \tag{4.166}$$

Rearranging then yields an upper bound for the CDF of E_k at $e_k = e_{k,0}$:

$$\begin{aligned} F_{E_k}(e_{k,0}) &\leq 1 - \sum_{v:\, e_{C,k,\min}(\mathcal{Q}_v) > e_{k,0}} \Pr\{\mathcal{Q}_v\} \\ &= \sum_{v:\, e_{C,k,\min}(\mathcal{Q}_v) \leq e_{k,0}} \Pr\{\mathcal{Q}_v\}. \end{aligned} \tag{4.167}$$

By iteratively computing upper and lower bounds according to (4.167) and (4.162) for different values of $e_{k,0}$, the CDF of E_k may be approximated. This procedure is summarized in the following algorithm:

Algorithm 4.8 (Approximation of $F_{E_k}(e_{k,0})$)**.** Pseudo-Code:

Input: CdfArguments = { Array of V different arguments of $F_{E_k}(e_{k,0})$ }

Output: CdfUpperBound, CdfLowerBound = { Arrays of upper and lower bounds for $F_{E_k}(e_{k,0})$ }

1: Grid uncertainty set $\mathcal{Q}$ into N subsets $\mathcal{Q}_v$
2: Probabilities = { Probabilities of each subset $\mathcal{Q}_v$, $v = 1, \ldots, N$ }
3: **for** $v = 1$ to N **do**
4: LowerBounds(v) = { $e_{C,k,\min}(\mathcal{Q}_v)$, computed in simulations }
5: UpperBounds(v) = { $e_{C,k,\max}(\mathcal{Q}_v)$, computed analytically using Theorem 4.5 }
6: **end for**

```
for i = 1 to V do
    CdfLowerBound(i) = 0
    CdfUpperBound(i) = 0
    for v = 1 to N do
        if LowerBounds(v) ≤ CdfArguments(i) then
            CdfUpperBound(i) = CdfUpperBound(i) + Probabilities(v)
        end if
        if UpperBounds(v) ≤ CdfArguments(i) then
            CdfLowerBound(i) = CdfLowerBound(i) + Probabilities(v)
        end if
    end for
end for
```

Remark 4.9. *The upper and lower bounds $e_{C,k,\max}(\mathcal{Q}_v)$ and $e_{C,k,\min}(\mathcal{Q}_v)$ do not have to satisfy any specific requirement except for being an upper or a lower bound, respectively. Hence, the number of simulations to determine $e_{C,k,\min}(\mathcal{Q}_v)$ may be very low or even one. Conversely, the upper bound $e_{C,k,\max}(\mathcal{Q}_v)$ is allowed to be highly conservative. However, if the gaps $e_{C,k,\max}(\mathcal{Q}_v) - e_{C,k,\min}(\mathcal{Q}_v)$ are large for all $v = 1, \ldots, N$, then the gap between the lower bound and the upper bound of the CDF of E_k will be large as well. For this reason, the use of efficient simulation algorithms to maximize $e_{C,k,\min}(\mathcal{Q}_v)$ and the use of more powerful analytical results such as Theorem 4.5 to minimize $e_{C,k,\max}(\mathcal{Q}_v)$ are advisable. For the maximization of $e_{C,k,\min}(\mathcal{Q}_v)$, approaches such as subset simulations [7] or counter-proving [169] seem to be promising.*

Remark 4.10. *In the above algorithm, a static partition of the uncertainty set $\mathcal{Q}$ is used. While such an approach might be reasonable for a low-dimensional uncertainty $\boldsymbol{\delta}$, it will certainly become computationally intractable for a high-dimensional uncertainty. In case of the probabilistic computation of the Structured Singular Value μ, the use of Branch-and-Bound techniques was suggested [177, 99, 176]. A similar extension also seems reasonable in case of the probabilistic computation of the largest tracking error.*

The benefits of the probabilistic computation of the tracking error are demonstrated by the following example:

Example 4.11. *Consider the plant and the adaptive control system with baseline controller from Example 4.1. In contrast to the previous examples, only state dependent uncertainties are accommodated, that is, λ_η is not uncertain and satisfies $\lambda_\eta = 1$. Since there is no control effectiveness uncertainty, the overall control law* (3.64) *may be simplified to*

$$\begin{aligned} \boldsymbol{u}(t) &= \boldsymbol{K}_x \cdot \boldsymbol{x}_P(t) + K_r \cdot r(t) + \boldsymbol{\Theta}_x(t) \cdot \boldsymbol{x}_P(t), \\ \dot{\hat{\boldsymbol{\Theta}}}_x(t) &= -\boldsymbol{\Gamma}_x \boldsymbol{x}_P(t) \boldsymbol{e}_C(t)^T \boldsymbol{P} \boldsymbol{B}_P. \end{aligned} \tag{4.168}$$

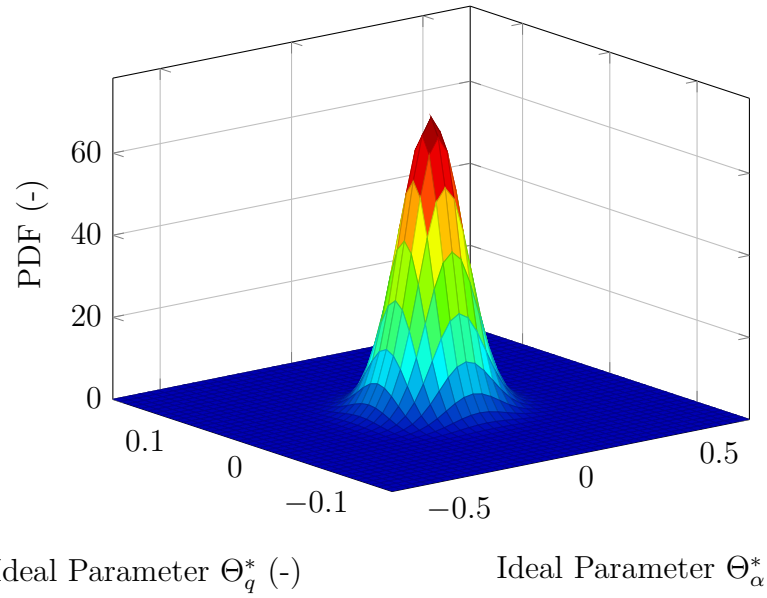

Figure 4.15: Illustration of the PDF of the state-dependent ideal parameter $\boldsymbol{\Theta}_x^*$.

It follows from (4.53) *that the state-dependent ideal parameter* $\boldsymbol{\Theta}_x^* = \begin{bmatrix}\Theta_\alpha^* & \Theta_q^*\end{bmatrix}$ *is confined to the rectangle*

$$\mathcal{Q} = \left\{\boldsymbol{\Theta}_x^* \mid -0.68 \leq \Theta_\alpha^* \leq 0.68, \qquad -0.16 \leq \Theta_q^* \leq 0.16\right\}. \tag{4.169}$$

The state-dependent ideal parameter $\boldsymbol{\Theta}_x^*$ *is assumed to be distributed by a zero-mean Gaussian distribution with the covariance matrix*

$$\Sigma = \begin{bmatrix}0.0100 & 0\\ 0 & 0.0005\end{bmatrix}. \tag{4.170}$$

The distribution over $\mathcal{Q}$ *is shown in Figure 4.15. Note that* $\Pr\{\mathcal{Q}\} \approx 1$ *holds.*

For the probabilistic computation of the tracking error, the design parameters of the direct MRAC are set to $\boldsymbol{Q} = \boldsymbol{I}^{2\times 2}$ *and* $\boldsymbol{\Gamma}_x = 10 \cdot \boldsymbol{I}^{2\times 2}$*. In case of these design parameters, Theorem 4.5 guarantees the worst-case tracking error bound* $\|e_{C,\alpha}(t)\|_{\mathcal{L}_\infty} \leq 5.26°$*. For the probabilistic analysis, the rectangle* $\mathcal{Q}$ *is divided into* $N = 4352$ *squares with an edge length of* 0.01*. For each of these squares, an analytical tracking error bound is computed using Theorem 4.5 and a simulation-based tracking error bound is inferred from 200 Monte Carlo simulation runs. These Monte Carlo simulations sample from a uniform distribution, which is limited to the respective square. Since the only requirement on the simulation-based data is that they represent a lower bound on the tracking error, a simple gridding would also be sufficient. Based on these data, Algorithm 4.8 is invoked for* $V = 20$ *CDF levels* $e_{k,0}$*, which are evenly spaced from* $0°$ *to* $5.26°$*. The results of this analysis are shown in Figure 4.16.*

Figure 4.16 displays the worst-case analytical bound, which holds if the known PDF of the ideal parameter $\boldsymbol{\Theta}_x^*$ *is neglected. Furthermore, the lower and the upper bound on the CDF of the tracking error bound* $\bar{e}_{C,\alpha}(\boldsymbol{\Delta}) = E_\alpha$ *are shown. The true CDF is known*

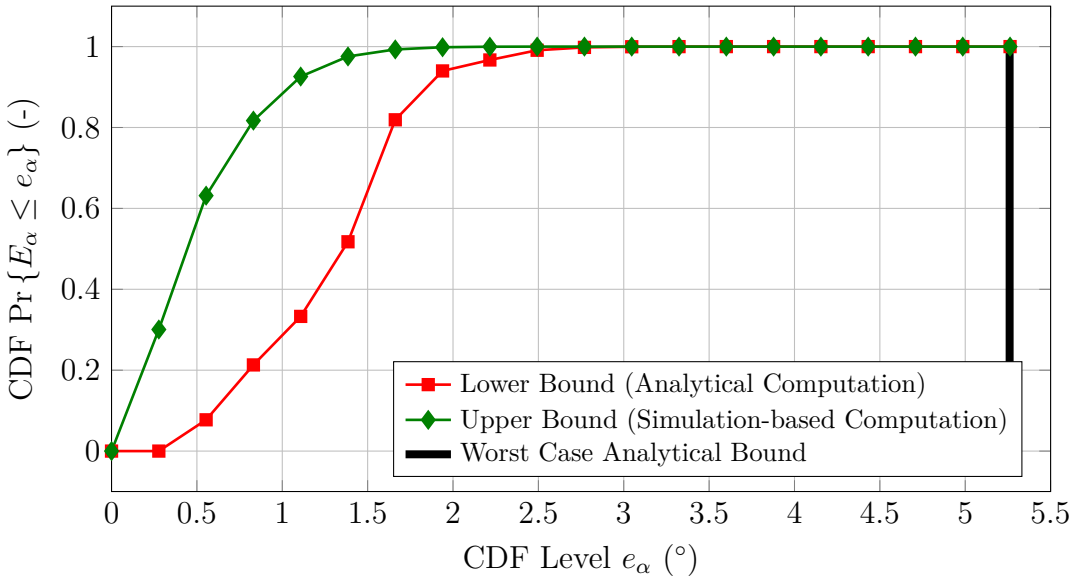

Figure 4.16: Results of the probabilistic tracking error analysis using Algorithm 4.8.

to lie somewhere in between these bounds. Figure 4.16 shows that the probability, that the tracking error satisfies $\|e_{C,\alpha}(t)\|_{\mathcal{L}_\infty} \leq 2.5°$*, is approximately 99% since the lower and the upper bound almost coincide. Hence, for an ideal parameter* $\boldsymbol{\Theta}_x^*$*, which is distributed according to Figure 4.15, the worst-case tracking error bound is overly conservative and at least halves with a 99% probability. In other words, the probability of encountering a tracking error* $\|e_{C,\alpha}(t)\|_{\mathcal{L}_\infty} > 2.5°$ *is about 1%.*

For smaller CDF levels, the upper and lower bound exhibit a significant gap. The upper bound, which is computed from simulations, suggests that the probability of encountering a tracking error $\|e_{C,\alpha}(t)\|_{\mathcal{L}_\infty} \leq 1°$ *is approximately 90%. On the other side, the lower bound only assigns a 30% probability to the latter event. Since the true value of the CDF lies somewhere in between these values, one should only rely on the smaller probability provided by the lower bound. This is because the lower bound is computed analytically and hence, is guaranteed to hold under the given assumptions.*

Figure 4.16 admits yet another interpretation. The previous considerations fixed a certain CDF level and evaluated the resulting probabilities. However, it is also possible to first choose a desired probability such as 90%. Then, Figure 4.16 implies that the largest tracking error, which is encountered with a 90% probability, is somewhere between $1.1°$ *and* $1.9°$*. Thus, Figure 4.16 does not only assign probability intervals to a certain tracking error bound but also assigns a tracking error bound interval to a given probability. Since the true value of the CDF lies somewhere in between these two values of the tracking error bound, one should only rely on the larger value provided by the lower CDF bound.*

The preceding discussion highlights that reliable information may only be inferred from the lower, guaranteed bound on the CDF. One might hence wonder why the upper bound is computed at all. While the upper bound is not strictly required to obtain

information about guaranteed probabilities or guaranteed tracking error bounds, it may serve as an indicator of conservativeness. If the lower and the upper bound are close, then only little conservatism will be present.

Remark 4.12. *It follows from* (4.162) *that the upper bounds* $e_{C,k,\max}(\mathcal{Q}_v)$ *for the tracking error lead to a lower bound for the CDF of* E_k*. At the first glance, this may seem counter-intuitive. However, notice that for a specific value* $e_{k,0}$*, the lower bound of the CDF yields the smallest probability that the largest tracking error is below* $e_{k,0}$*. Hence, the guaranteed upper bounds for the largest tracking errors lead to a guaranteed minimum probability.*

Relation to Other Approaches in the Literature

Algorithm 4.8 allows the computation of the CDF of the largest tracking error $\bar{e}_{C,k}$. In literature, a conceptually similar approach has been presented in [59]. Similar to the approach of this section, [59] aims at reusing worst-case analysis tools within a probabilistic analysis. The worst-case analysis in [59] considers a MRAC with projection operator and σ-modification in the presence of unmodeled actuator dynamics. A set of LMI conditions ensures that the tracking error remains below a predefined bound. In order to account for the stochastic nature of the uncertainties, a so-called *Scenario Approach* is taken. To that end, a set of LMI conditions is derived which ensures that the tracking error remains below the predefined bound *for one specific realization* of the uncertainties. The *Scenario Approach* then amounts to simultaneously solving this LMI for several realizations of the uncertainties. This set of realizations represents the *Scenario*. If the number of realizations is sufficiently high, then the probability of a violation of the predefined bounds is sufficiently low. The latter point also highlights the main difference to the approach of the present section. While the *Scenario Approach* of [59] guarantees that the probability of satisfying some tracking error bound is sufficiently high, the approach of this section explicitly computes the CDF of the largest tracking error. This difference also manifests itself in different computations. In the *Scenario Approach*, the worst-case analysis is slightly changed to account only for one realization of the uncertainties. The resulting set of LMIs is then solved simultaneously for several realizations of the uncertainties. In contrast, the approach of this section requires the iterated solution of the unmodified worst-case analysis LMIs on small subsets of the uncertainty space.

4.2.3 Computation of Tracking Error Norms in the Presence of Unmatched Uncertainties

In the previous sections, bounds for the tracking error have been derived under the assumption that the plant is exactly given by the nominal plant model from (3.25). As no plant model may perfectly represent the physical process under consideration, any

controller faces an off-nominal plant in practice. In order to evaluate the performance of an adaptive controller under more realistic conditions, this section derives RP tracking error bounds for a specific off-nominal plant model.

Consider the off-nominal plant model from (3.94)

$$\begin{aligned}\dot{\boldsymbol{x}}_P(t) = \boldsymbol{A}_M \boldsymbol{x}_P(t) + \boldsymbol{B}_M \boldsymbol{r}(t) + \boldsymbol{B}_P \boldsymbol{\Lambda}\left(\boldsymbol{u}(t) - \boldsymbol{\Theta}^* \boldsymbol{\omega}\left(\boldsymbol{x}_P(t), t\right)\right) \\ + \boldsymbol{w}\left(\boldsymbol{x}_P(t), \boldsymbol{z}_P(t), t\right),\end{aligned}$$

which formed the basis for the derivation of the σ-modification in Section 3.2.4. In (3.94), the term $\boldsymbol{w}\left(\boldsymbol{x}_P(t), \boldsymbol{z}_P(t), t\right)$ represents the plant imperfections resulting from unaccounted unmatched uncertainties and non-parametric uncertainties. As the disturbance signal $\boldsymbol{w}\left(\boldsymbol{x}_P(t), \boldsymbol{z}_P(t), t\right)$ may lead to parameter drift in case of an unmodified MRAC, a direct MRAC with σ-modification is considered subsequently. Due to the use of a σ-modification, neither stability nor asymptotic convergence of the tracking error may be proven. One may however prove UUB of the tracking error and the parameter error.

The proof of UUB in Section 3.2.4 assumed that the disturbance $\boldsymbol{w}\left(\boldsymbol{x}_P(t), \boldsymbol{z}_P(t), t\right)$ is known to be bounded a-priori. In practice, such a bound is not available since the disturbance $\boldsymbol{w}\left(\boldsymbol{x}_P(t), \boldsymbol{z}_P(t), t\right)$ is state-dependent. For this reason, an alternative UUB condition is derived in this section. Similar to Section 4.2.1, the novel UUB condition relies on LMIs and quadratic forms.

The subsequent results are based on the publication [79] of the author of this thesis. In contrast to [79], the results of the present section also account for an input uncertainty $\boldsymbol{\Lambda}$. While derived independently, the approach of this section is conceptually similar to [55, 57, 60]. Refs. [55, 57] derive LMI conditions for UUB of a direct MRAC with projection operator in the presence of bounded disturbances. In [60], this result is extended to the case of unmodeled actuator dynamics. In contrast to the approach of the present section, [55, 57, 60] assume that the uncertainties are confined to a spherical set. In case of uncertainties, which are known to remain within a hyper-rectangular set, this may introduce additional conservatism. Even more importantly, [55, 57, 60] consider a controller synthesis scenario, that is, they optimize the design parameters $\boldsymbol{P}$ and $\boldsymbol{\Gamma}$ of the adaptive controller, whereas the present section focuses on an analysis scenario. Finally, notice that the approach of this section also differs from [55, 57, 60] in a different usage of the S-Procedure. This different usage results since [55, 57, 60] consider the uncertainties / adaptive parameters to be norm-bounded [2] in terms of the 2-norm.

The derivation of the novel UUB condition assumes that the disturbance signal $\boldsymbol{w}\left(\boldsymbol{x}_P(t), \boldsymbol{z}_P(t), t\right)$ takes the form

$$\boldsymbol{w}\left(\boldsymbol{x}_P(t), \boldsymbol{z}_P(t), t\right) = \bar{\boldsymbol{B}}_P \boldsymbol{\Theta}^*_{um,x} \boldsymbol{x}_P(t) + \boldsymbol{B}_P \boldsymbol{\Lambda} \boldsymbol{\epsilon}\left(\boldsymbol{x}_P(t), t\right). \tag{4.171}$$

Hence, the novel UUB condition accounts for unmatched parametric, linearly state-dependent uncertainties and the matched parametrization error $\boldsymbol{\epsilon}\left(\boldsymbol{x}_P(t), t\right)$. Inserting

this definition of the disturbance into (3.94) yields

$$\begin{aligned}\dot{\boldsymbol{x}}_P(t) = \boldsymbol{A}_M\boldsymbol{x}_P(t) + \boldsymbol{B}_M\boldsymbol{r}(t) + \boldsymbol{B}_P\boldsymbol{\Lambda}\left(\boldsymbol{u}(t) - \boldsymbol{\Theta}^*\boldsymbol{\omega}\left(\boldsymbol{x}_P(t),t\right) + \boldsymbol{\epsilon}\left(\boldsymbol{x}_P(t),t\right)\right) \\ + \bar{\boldsymbol{B}}_P\boldsymbol{\Theta}^*_{um,x}\boldsymbol{x}_P(t).\end{aligned} \tag{4.172}$$

A direct MRAC with σ-modification for the plant (4.172) is given by the reference model (3.4), the control law (3.26) and the update law (3.109). Inserting the control law (3.26) yields

$$\begin{aligned}\dot{\boldsymbol{x}}_P(t) = \boldsymbol{A}_M\boldsymbol{x}_P(t) + \boldsymbol{B}_M\boldsymbol{r}(t) + \boldsymbol{B}_P\boldsymbol{\Lambda}\left(\tilde{\boldsymbol{\Theta}}(t)\,\boldsymbol{\omega}\left(\boldsymbol{x}_P(t),t\right) + \boldsymbol{\epsilon}\left(\boldsymbol{x}_P(t),t\right)\right) \\ + \bar{\boldsymbol{B}}_P\boldsymbol{\Theta}^*_{um,x}\boldsymbol{x}_P(t).\end{aligned} \tag{4.173}$$

The dynamics of the tracking error $\boldsymbol{e}_C(t) = \boldsymbol{x}_P(t) - \boldsymbol{x}_M(t)$ become

$$\begin{aligned}\dot{\boldsymbol{e}}_C(t) = \boldsymbol{A}_M\boldsymbol{e}_C(t) + \boldsymbol{B}_P\boldsymbol{\Lambda}\left(\tilde{\boldsymbol{\Theta}}(t)\,\boldsymbol{\omega}\left(\boldsymbol{x}_P(t),t\right) + \boldsymbol{\epsilon}\left(\boldsymbol{x}_P(t),t\right)\right) \\ + \bar{\boldsymbol{B}}_P\boldsymbol{\Theta}^*_{um,x}\boldsymbol{x}_P(t),\end{aligned} \tag{4.174}$$

whereas the dynamics of the parameter error $\tilde{\boldsymbol{\Theta}}(t) = \boldsymbol{\Theta}(t) - \boldsymbol{\Theta}^*$ are still given by (3.110), i.e.

$$\dot{\tilde{\boldsymbol{\Theta}}}(t)^T = -\boldsymbol{\Gamma}\left(\boldsymbol{\omega}\left(\boldsymbol{x}_P(t),t\right)\cdot\boldsymbol{e}_C(t)^T\boldsymbol{P}\boldsymbol{B}_P + \boldsymbol{\sigma}\cdot\tilde{\boldsymbol{\Theta}}(t)^T + \boldsymbol{\sigma}\cdot\boldsymbol{\Theta}^{*T}\right). \tag{4.175}$$

For reasons of simplicity, the plant (4.172) is subsequently assumed to have only one input, i.e. $m = 1$. Similar to Section 4.2.1, all uncertainties are supposed to be bounded as stated in the following assumption:

Assumption 4.4. *For all times, the parametrization error $\Lambda\cdot\epsilon(\boldsymbol{x}_P(t),t)$ is bounded, i.e.*

$$|\Lambda\cdot\epsilon(\boldsymbol{x}_P(t),t)| \leq \epsilon_0,\ \ \forall t \geq 0,$$

where $\epsilon_0 \geq 0$ is a known, conservative bound. The reference signal $r(t)$ satisfies

$$|r(t)| \leq r_0,\ \ \forall t \geq 0,$$

where $r_0 > 0$ is a known bound. Furthermore, the entries of the ideal parameter vector $\boldsymbol{\Theta}^* = \begin{bmatrix}\Theta^*_1 & \dots & \Theta^*_{n_r}\end{bmatrix}$ lie within a hyperrectangle:

$$\Theta^*_{i,\min} \leq \Theta^*_i \leq \Theta^*_{i,\max},\ i = 1,\dots,n_p,$$

where $\Theta^*_{i,\min} \in \mathbb{R}$ and $\Theta^*_{i,\max} \in \mathbb{R}$ are known conservative bounds. Similarly, the entries of the unmatched uncertainty matrix

$$\boldsymbol{\Theta}^*_{um,x} \triangleq \begin{bmatrix}\boldsymbol{\theta}^*_{um,1}\\ \vdots \\ \boldsymbol{\theta}^*_{um,n-1}\end{bmatrix}$$

with $\boldsymbol{\theta}^*_{um,k} = \begin{bmatrix}\Theta^*_{um,k,1} & \dots & \Theta^*_{um,k,n}\end{bmatrix},\ k = 1,\dots,n-1$ *lie in another hyperrectangle given by*

$$\Theta^*_{um,k,i,\min} \leq \Theta^*_{um,k,i} \leq \Theta^*_{um,k,i,\max},\ k = 1,\dots,n-1,\ i = 1,\dots,n,$$

where $\Theta^*_{um,k,i,\min} \in \mathbb{R}$, $\Theta^*_{um,k,i,\max} \in \mathbb{R}$ *are known conservative bounds. Similarly, the control effectiveness* $\Lambda \triangleq \Lambda_1$ *is bounded by*

$$0 < \Lambda_{1,\min} \leq \Lambda \leq \Lambda_{1,\max}, \tag{4.176}$$

where $\Lambda_{1,\min}$, $\Lambda_{1,\max}$ *denote known lower and upper bounds, respectively.*

From Assumption 4.4 follows that the joint vector

$$\boldsymbol{\xi}^T(t) = \begin{bmatrix}\Lambda \cdot \epsilon(\boldsymbol{x}_P(t), t) & r(t) & \Lambda & \boldsymbol{\Theta}^* & \boldsymbol{\theta}^*_{um,1} & \dots & \boldsymbol{\theta}^*_{um,n-1}\end{bmatrix} \tag{4.177}$$

lies within a q-dimensional hyperrectangle with 2^q vertices $\boldsymbol{\xi}_v$, where $v = 1,\dots,q$ and $q = (3 + n_r + (n-1)\cdot n)$. Any $\boldsymbol{\xi}$ within such a hyperrectangle can be expressed in terms of the vertices

$$\boldsymbol{\xi}^T_v = \begin{bmatrix}\epsilon_v & r_v & \Lambda_v & \boldsymbol{\Theta}^*_v & \boldsymbol{\theta}^*_{um,1,v} & \dots & \boldsymbol{\theta}^*_{um,n-1,v}\end{bmatrix} \tag{4.178}$$

of the hyperrectangle according to [3]:

$$\boldsymbol{\xi} = \sum_{v=1}^{2^q} \alpha_v \cdot \boldsymbol{\xi}_v \qquad \text{with } \alpha_v \geq 0, \quad \sum_{v=1}^{2^q} \alpha_v = 1. \tag{4.179}$$

In order to prove UUB of the error dynamics (4.174), (4.175), a suitable Lyapunov function candidate is required. Due to the unmatched uncertainty $\boldsymbol{\Theta}^*_{um,x}$, the tracking error dynamics (4.174) contain the term $\bar{\boldsymbol{B}}_P \boldsymbol{\Theta}^*_{um,x} \boldsymbol{x}_P(t)$, which depends on the plant state $\boldsymbol{x}_P(t)$. Since the unmatched uncertainty is not adapted, this term will not cancel with the update law in a Lyapunov analysis. Furthermore, since it is state-dependent, the term is not known to be bounded a-priori. For this reason, the Lyapunov function candidate (3.30) is enhanced by the additional term $(1/2)\cdot \boldsymbol{x}_M(t)^T \boldsymbol{P}_M \boldsymbol{x}_M(t)$, which accounts for the reference model. Using $\boldsymbol{x}_P(t) = \boldsymbol{e}_C(t) + \boldsymbol{x}_M(t)$, the unmatched uncertainty $\bar{\boldsymbol{B}}_P \boldsymbol{\Theta}^*_{um,x} \boldsymbol{x}_P(t)$ may be expressed in terms of the reference model state $\boldsymbol{x}_M(t)$ and the tracking error $\boldsymbol{e}_C(t)$. The Lyapunov function candidate is given by

$$V(t) = \frac{1}{2}\boldsymbol{e}_C(t)^T \boldsymbol{P} \boldsymbol{e}_C(t) + \frac{\Lambda}{2} \cdot \tilde{\boldsymbol{\Theta}}(t) \boldsymbol{\Gamma}^{-1} \tilde{\boldsymbol{\Theta}}(t)^T + \frac{1}{2}\boldsymbol{x}_M(t) \boldsymbol{P}_M \boldsymbol{x}_M(t), \tag{4.180}$$

where $\boldsymbol{P}_M \in \mathbb{S}^n_{++}$ is an additional design parameter. Differentiating the Lyapunov function candidate with respect to time yields

$$\dot{V}(t) = \boldsymbol{e}_C(t)^T \boldsymbol{P} \dot{\boldsymbol{e}}_C(t) + \Lambda \cdot \tilde{\boldsymbol{\Theta}}(t) \boldsymbol{\Gamma}^{-1} \dot{\tilde{\boldsymbol{\Theta}}}(t)^T + \boldsymbol{x}_M(t) \boldsymbol{P}_M \dot{\boldsymbol{x}}_M(t). \tag{4.181}$$

Upon insertion of (3.4), (4.174), (4.175), $\dot{V}(t)$ becomes:

$$\begin{aligned}\dot{V} = {} & \boldsymbol{e}_C(t)^T \boldsymbol{P} \Big(\boldsymbol{A}_M \boldsymbol{e}_C(t) + \boldsymbol{B}_P \Lambda \cdot \Big(\tilde{\boldsymbol{\Theta}}(t) \boldsymbol{\omega}(\boldsymbol{x}_P(t), t) + \epsilon(\boldsymbol{x}_P(t), t)\Big)\Big) \\ & + \boldsymbol{e}_C(t)^T \boldsymbol{P} \bar{\boldsymbol{B}}_P \boldsymbol{\Theta}^*_{um,x} \boldsymbol{x}_P(t), \\ & - \Lambda \cdot \tilde{\boldsymbol{\Theta}}(t) \Big(\boldsymbol{\omega}(\boldsymbol{x}_P(t), t) \cdot \boldsymbol{e}_C(t)^T \boldsymbol{P} \boldsymbol{B}_P + \boldsymbol{\sigma} \cdot \tilde{\boldsymbol{\Theta}}(t)^T + \boldsymbol{\sigma} \cdot \boldsymbol{\Theta}^{*T}\Big) \\ & + \boldsymbol{x}_M(t)^T \boldsymbol{P}_M (\boldsymbol{A}_M \boldsymbol{x}_M(t) + \boldsymbol{B}_M \cdot r(t)).\end{aligned} \tag{4.182}$$

Using $\boldsymbol{x}_P(t) = \boldsymbol{e}_C(t) + \boldsymbol{x}_M(t)$, (4.182) may be rearranged as

$$\begin{aligned}\dot{V}(t) = &-\frac{1}{2}\boldsymbol{e}_C(t)^T \boldsymbol{Q}_P \boldsymbol{e}_C(t) + \boldsymbol{e}_C(t)\boldsymbol{P}\boldsymbol{B}_P\Lambda\cdot\epsilon(\boldsymbol{x}_P(t),t)\\ &+\boldsymbol{e}_C(t)^T\boldsymbol{P}\bar{\boldsymbol{B}}_P\boldsymbol{\Theta}^*_{um,x}\boldsymbol{x}_M(t) - \Lambda\cdot\tilde{\boldsymbol{\Theta}}(t)\boldsymbol{\sigma}\tilde{\boldsymbol{\Theta}}(t)^T - \Lambda\cdot\tilde{\boldsymbol{\Theta}}(t)\boldsymbol{\sigma}\boldsymbol{\Theta}^{*T}\\ &-\frac{1}{2}\boldsymbol{x}_M(t)^T\boldsymbol{Q}_M\boldsymbol{x}_M(t) + \boldsymbol{x}_M(t)^T\boldsymbol{P}_M\boldsymbol{B}_M\cdot r(t)\end{aligned} \tag{4.183}$$

with

$$(\boldsymbol{A}_M + \bar{\boldsymbol{B}}_P\boldsymbol{\Theta}^*_{um,x})^T\boldsymbol{P} + \boldsymbol{P}(\boldsymbol{A}_M + \bar{\boldsymbol{B}}_P\boldsymbol{\Theta}^*_{um,x}) \triangleq -\boldsymbol{Q}_P, \tag{4.184}$$

$$\boldsymbol{A}_M^T\boldsymbol{P}_M + \boldsymbol{P}_M\boldsymbol{A}_M \triangleq -\boldsymbol{Q}_M. \tag{4.185}$$

Roughly speaking, proving UUB amounts to the computation of an invariant set $\mathcal{M}_c = \{\boldsymbol{e}_C, \boldsymbol{x}_M, \tilde{\boldsymbol{\Theta}} \mid V(\boldsymbol{e}_C, \boldsymbol{x}_M, \tilde{\boldsymbol{\Theta}}) \leq c\}$, which surrounds the set of all states, for which $\dot{V}(t) \geq 0$ holds. The latter set is given by $\mathcal{M}_i = \{\boldsymbol{e}_C, \boldsymbol{x}_M, \tilde{\boldsymbol{\Theta}} \mid \dot{V}(\boldsymbol{e}_C, \boldsymbol{x}_M, \tilde{\boldsymbol{\Theta}}) \geq 0\}$. Hence, any trajectory starting in $\mathcal{M}_i$ will remain in $\mathcal{M}_c$ for all times. Furthermore, it has to be ensured that any trajectory starting outside of $\mathcal{M}_i$ will enter $\mathcal{M}_c$ in finite time.

For the computation of an appropriate invariant set $\mathcal{M}_c$, a geometric point of view is once again helpful. Similar to the set $\mathcal{M}_c$ of Section 4.2.1, the above set $\mathcal{M}_c$ geometrically represents an ellipsoid. Interestingly, the set $\mathcal{M}_i$ also represents an ellipsoid. In order to see this, define the joint state vector

$$\boldsymbol{x}^T = \begin{bmatrix}\boldsymbol{e}_C^T & \boldsymbol{x}_M^T & \tilde{\boldsymbol{\Theta}}\end{bmatrix}. \tag{4.186}$$

In terms of the joint state vector, the inequality, which defines $\mathcal{M}_i$, admits the representation

$$\boldsymbol{x}^T\begin{bmatrix}\boldsymbol{Q}_P & -\boldsymbol{P}\bar{\boldsymbol{B}}_P\boldsymbol{\Theta}^*_{um,x} & \boldsymbol{0}\\ -\boldsymbol{\Theta}^{*,T}_{x,um}\bar{\boldsymbol{B}}_P^T\boldsymbol{P} & \boldsymbol{Q}_M & \boldsymbol{0}\\ \boldsymbol{0} & \boldsymbol{0} & 2\Lambda\boldsymbol{\sigma}\end{bmatrix}\boldsymbol{x} + 2\boldsymbol{x}^T\begin{bmatrix}-\boldsymbol{P}\boldsymbol{B}_P\Lambda\epsilon(\boldsymbol{x}_P(t),t)\\ -\boldsymbol{P}_M\boldsymbol{B}_M r(t)\\ \Lambda\boldsymbol{\sigma}\boldsymbol{\Theta}^{*T}\end{bmatrix} \leq 0. \tag{4.187}$$

It follows from (B.74) that (4.187) represents an ellipsoid if its first term is positive definite. Since $2\Lambda\boldsymbol{\sigma}$ is positive definite by definition, this is equivalent to the satisfaction of the stability condition

$$\begin{bmatrix}(\boldsymbol{A}_M + \bar{\boldsymbol{B}}_P\boldsymbol{\Theta}^*_{um,x})^T\boldsymbol{P} + \boldsymbol{P}(\boldsymbol{A}_M + \bar{\boldsymbol{B}}_P\boldsymbol{\Theta}^*_{um,x}) & \boldsymbol{P}\bar{\boldsymbol{B}}_P\boldsymbol{\Theta}^*_{um,x}\\ \boldsymbol{\Theta}^{*,T}_{x,um}\bar{\boldsymbol{B}}_P^T\boldsymbol{P} & \boldsymbol{A}_M^T\boldsymbol{P}_M + \boldsymbol{P}_M\boldsymbol{A}_M\end{bmatrix} < 0. \tag{4.188}$$

The center of the ellipsoid (4.187) is however not at the origin, but depends on the uncertainties $\boldsymbol{\Theta}^*_{um,x}$, $\boldsymbol{\Theta}^*$, Λ and the bounded signals $r(t)$ and $\epsilon(\boldsymbol{x}_P(t),t)$. The sets $\mathcal{M}_c$ and $\mathcal{M}_i$ are illustrated in Figure 4.17.

Since both sets $\mathcal{M}_c$ and $\mathcal{M}_i$ are ellipsoids, the set containment $\mathcal{M}_i \subseteq \mathcal{M}_c$ could be shown using the S-Procedure and LMIs in a similar fashion to Section 4.2.1. However, in order to ensure a minimum decay rate κ such that $\dot{V}(t) \leq -\kappa V(t)$ holds outside of

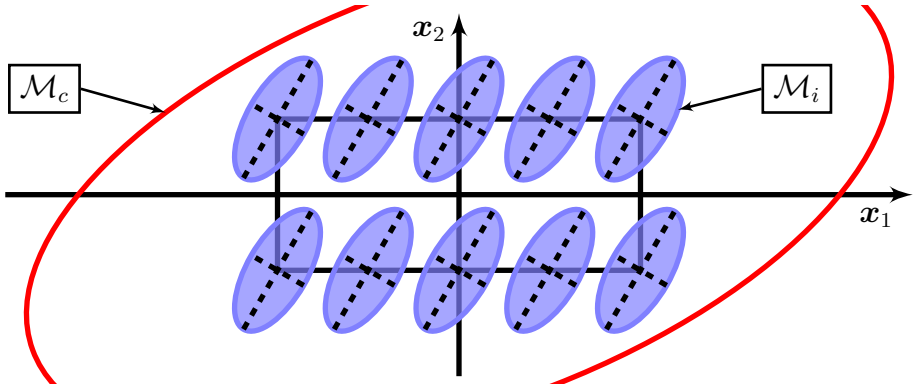

Figure 4.17: Geometric interpretation of UUB: For each uncertainty $\boldsymbol{\Theta}^*_{um,x}$, $\boldsymbol{\Theta}^*$, Λ and each r and ϵ, the set $\dot{V}(\boldsymbol{e}_C, \boldsymbol{x}_M, \tilde{\boldsymbol{\Theta}}) \geq 0$ is an ellipsoid. All of these ellipsoids have to remain within the invariant set $\mathcal{M}_c$.

the ultimate bound, a set containment problem in terms of the complementary sets of $\mathcal{M}_c$ and $\mathcal{M}_i$ is shown, namely

$$\{\boldsymbol{e}_C, \boldsymbol{x}_M, \tilde{\boldsymbol{\Theta}} \mid V \geq c\} \subseteq \{\boldsymbol{e}_C, \boldsymbol{x}_M, \tilde{\boldsymbol{\Theta}} \mid \dot{V} \leq -\kappa V\}. \tag{4.189}$$

This idea leads to the following theorem:

Theorem 4.13. *Consider the off-nominal plant* (4.172) *and the direct MRAC with σ-modification given by the reference model* (3.4)*, the control law* (3.26) *and the update law* (3.109)*.*

Let $\kappa > 0$ be a given constant. Let $\boldsymbol{P} \in \mathbb{S}^n_{++}$, $\boldsymbol{P}_M \in \mathbb{S}^n_{++}$, $\boldsymbol{\Gamma} \in \mathbb{S}^{n_r}_{++}$ and $\boldsymbol{\sigma} \in \mathbb{S}^{n_r}_{++}$ be the given design parameters of the adaptive controller and let Assumption 4.4 hold. If there exist constants $l > 0$ and $l_c > 0$, such that the LMIs

$$\begin{bmatrix} (\kappa+l)\boldsymbol{P}-\boldsymbol{Q}_{P,v} & \boldsymbol{P}\bar{\boldsymbol{B}}_P\boldsymbol{\Theta}^*_{x,um,v} & \boldsymbol{0} & \boldsymbol{P}\boldsymbol{B}_{P\cdot\epsilon_v} \\ \boldsymbol{\Theta}^{*,T}_{x,um,v}\bar{\boldsymbol{B}}^T_P\boldsymbol{P} & (\kappa+l)\boldsymbol{P}_M-\boldsymbol{Q}_M & \boldsymbol{0} & \boldsymbol{P}_M\boldsymbol{B}_{M\cdot r_v} \\ \boldsymbol{0} & \boldsymbol{0} & \Lambda_v\big((\kappa+l)\boldsymbol{\Gamma}^{-1}-2\boldsymbol{\sigma}\big) & -\Lambda_v\boldsymbol{\sigma}\boldsymbol{\Theta}^{*T}_v \\ \epsilon_v\cdot\boldsymbol{B}^T_P\boldsymbol{P} & r_v\cdot\boldsymbol{B}^T_M\boldsymbol{P}_M & -\Lambda_v\boldsymbol{\Theta}^*_v\boldsymbol{\sigma} & -2l_c \end{bmatrix} \leq 0, \tag{4.190}$$

$$-\boldsymbol{Q}_{P,v} \triangleq \left(\boldsymbol{A}_M + \bar{\boldsymbol{B}}_P\boldsymbol{\Theta}^*_{x,um,v}\right)^T\boldsymbol{P} + \boldsymbol{P}\left(\boldsymbol{A}_M + \bar{\boldsymbol{B}}_P\boldsymbol{\Theta}^*_{x,um,v}\right) \tag{4.191}$$
$$\forall\, v = 1, \ldots, 2^q,$$

with $\boldsymbol{Q}_M$ defined as in (4.185) *are jointly feasible, then the adaptive controller* (3.4)*,* (4.174)*,* (4.175) *is UUB. Furthermore, let the initial conditions be given by $\boldsymbol{e}_C(0) = \boldsymbol{e}_{C,0}$, $\boldsymbol{x}_M(0) = \boldsymbol{x}_{M,0}$ and $\tilde{\boldsymbol{\Theta}}(0) = \tilde{\boldsymbol{\Theta}}_0$. Then, the trajectories satisfy $(\boldsymbol{e}_C(t), \boldsymbol{x}_M(t), \tilde{\boldsymbol{\Theta}}(t)) \in \mathcal{M}_c\ \forall\, t \geq T$, where $\mathcal{M}_c = \left\{\boldsymbol{e}_C, \boldsymbol{x}_M, \tilde{\boldsymbol{\Theta}} \mid V(\boldsymbol{e}_C, \boldsymbol{x}_M, \tilde{\boldsymbol{\Theta}}) \leq c\right\}$ is an invariant set, $c = l_c/l$ is the ultimate bound and*

$$T = \begin{cases} 0, & \text{if } (\boldsymbol{e}_{C,0}, \boldsymbol{x}_{M,0}, \tilde{\boldsymbol{\Theta}}_0) \in \mathcal{M}_c, \\ -\frac{1}{\kappa}\ln\left(c/V(\boldsymbol{e}_{C,0}, \boldsymbol{x}_{M,0}, \tilde{\boldsymbol{\Theta}}_0)\right), & \text{if } (\boldsymbol{e}_{C,0}, \boldsymbol{x}_{M,0}, \tilde{\boldsymbol{\Theta}}_0) \notin \mathcal{M}_c. \end{cases} \tag{4.192}$$

Proof. Let l, l_c be solutions of the LMI problem of Theorem 4.13. Due to the negative semi-definiteness of (4.190) for all $v = 1, \ldots, 2^q$, the weighted sum

$$\sum_{v=1}^{2^q} \alpha_v \begin{bmatrix} (\kappa+l)\boldsymbol{P}-\boldsymbol{Q}_{P,v} & \boldsymbol{P}\bar{\boldsymbol{B}}_P\boldsymbol{\Theta}^*_{x,um,v} & \boldsymbol{0} & \boldsymbol{P}\boldsymbol{B}_P\cdot\epsilon_v \\ \boldsymbol{\Theta}^{*,T}_{x,um,v}\bar{\boldsymbol{B}}_P^T\boldsymbol{P} & (\kappa+l)\boldsymbol{P}_M-\boldsymbol{Q}_M & \boldsymbol{0} & \boldsymbol{P}_M\boldsymbol{B}_M\cdot r_v \\ \boldsymbol{0} & \boldsymbol{0} & \Lambda_v\big((\kappa+l)\boldsymbol{\Gamma}^{-1}-2\boldsymbol{\sigma}\big) & -\Lambda_v\boldsymbol{\sigma}\boldsymbol{\Theta}^{*T}_v \\ \epsilon_v\cdot\boldsymbol{B}_P^T\boldsymbol{P} & r_v\cdot\boldsymbol{B}_M^T\boldsymbol{P}_M & -\Lambda_v\boldsymbol{\Theta}^*_v\boldsymbol{\sigma} & -2l_c \end{bmatrix} \leq 0, \tag{4.193}$$

is negative semidefinite, too, for $\alpha_v \geq 0$. Due to (4.179), any

$$\boldsymbol{\xi}^T(t) = \begin{bmatrix} \Lambda\cdot\epsilon(\boldsymbol{x}_P(t),t) & r(t) & \Lambda & \boldsymbol{\Theta}^* & \boldsymbol{\theta}^*_{um,1} & \ldots & \boldsymbol{\theta}^*_{um,n-1} \end{bmatrix}$$

may be expressed in terms of the edges $\boldsymbol{\xi}_v$ of a q-dimensional hyperrectangle. Using (4.179), Eq. (4.193) implies negative semi-definiteness of

$$\begin{bmatrix} (\kappa+l)\boldsymbol{P}-\boldsymbol{Q}_P & \boldsymbol{P}\bar{\boldsymbol{B}}_P\boldsymbol{\Theta}^*_{um,x} & \boldsymbol{0} & \boldsymbol{P}\boldsymbol{B}_P\Lambda\cdot\epsilon(\boldsymbol{x}_P(t),t) \\ \boldsymbol{\Theta}^{*,T}_{x,um}\bar{\boldsymbol{B}}_P^T\boldsymbol{P} & (\kappa+l)\boldsymbol{P}_M-\boldsymbol{Q}_M & \boldsymbol{0} & \boldsymbol{P}_M\boldsymbol{B}_M\cdot r(t) \\ \boldsymbol{0} & \boldsymbol{0} & \Lambda\big((\kappa+l)\boldsymbol{\Gamma}^{-1}-2\boldsymbol{\sigma}\big) & -\Lambda\boldsymbol{\sigma}\boldsymbol{\Theta}^{*T} \\ \epsilon(\boldsymbol{x}_P(t),t)\cdot\Lambda\boldsymbol{B}_P^T\boldsymbol{P} & r(t)\cdot\boldsymbol{B}_M^T\boldsymbol{P}_M & -\Lambda\boldsymbol{\Theta}^*\boldsymbol{\sigma} & -2l_c \end{bmatrix} \leq 0 \tag{4.194}$$

for all $\Lambda\cdot\epsilon(\boldsymbol{x}_P(t),t)$, Λ, $r(t)$, $\boldsymbol{\Theta}^*$, $\boldsymbol{\Theta}^*_{um,x}$ satisfying Assumption 4.4. Since $l > 0$, $l_c > 0$ hold by definition, there exists a level set constant $c > 0$ such that $l_c = l\cdot c$ holds. After multiplying (4.194) by $1/2$, (4.194) may be rewritten as:

$$\frac{1}{2}\cdot\boldsymbol{M}_0 - \frac{1}{2}\cdot l\cdot\boldsymbol{M}_1 \leq 0 \text{ with}$$

$$\boldsymbol{M}_0 \triangleq \begin{bmatrix} -\boldsymbol{Q}_P & \boldsymbol{P}\bar{\boldsymbol{B}}_P\boldsymbol{\Theta}^*_{um,x} & \boldsymbol{0} & \boldsymbol{P}\boldsymbol{B}_P\Lambda\cdot\epsilon(\boldsymbol{x}_P(t),t) \\ \boldsymbol{\Theta}^{*,T}_{x,um}\bar{\boldsymbol{B}}_P^T\boldsymbol{P} & -\boldsymbol{Q}_M & \boldsymbol{0} & \boldsymbol{P}_M\boldsymbol{B}_M\cdot r(t) \\ \boldsymbol{0} & \boldsymbol{0} & -2\Lambda\boldsymbol{\sigma} & -\Lambda\boldsymbol{\sigma}\boldsymbol{\Theta}^{*T} \\ \epsilon(\boldsymbol{x}_P(t),t)\cdot\Lambda\boldsymbol{B}_P^T\boldsymbol{P} & r(t)\cdot\boldsymbol{B}_M^T\boldsymbol{P}_M & -\Lambda\boldsymbol{\Theta}^*\boldsymbol{\sigma} & 0 \end{bmatrix} + \kappa\begin{bmatrix} \boldsymbol{P} & 0 & 0 & 0 \\ 0 & \boldsymbol{P}_M & 0 & 0 \\ 0 & 0 & \Lambda\cdot\boldsymbol{\Gamma}^{-1} & 0 \\ 0 & 0 & 0 & 0 \end{bmatrix},$$

$$\boldsymbol{M}_1 \triangleq \begin{bmatrix} -\boldsymbol{P} & 0 & 0 & 0 \\ 0 & -\boldsymbol{P}_M & 0 & 0 \\ 0 & 0 & -\Lambda\cdot\boldsymbol{\Gamma}^{-1} & 0 \\ 0 & 0 & 0 & 2c \end{bmatrix}.$$

Notice that $(1/2)\cdot\boldsymbol{z}^T\boldsymbol{M}_0\boldsymbol{z} = \dot{V}(\boldsymbol{e}_C,\boldsymbol{x}_M,\tilde{\boldsymbol{\Theta}}) + \kappa V(\boldsymbol{e}_C,\boldsymbol{x}_M,\tilde{\boldsymbol{\Theta}})$ and $(1/2)\cdot\boldsymbol{z}^T\boldsymbol{M}_1\boldsymbol{z} = c - V(\boldsymbol{e}_C,\boldsymbol{x}_M,\tilde{\boldsymbol{\Theta}})$ with $\boldsymbol{z}^T = \begin{bmatrix} \boldsymbol{e}_C^T & \boldsymbol{x}_M^T & \tilde{\boldsymbol{\Theta}} & 1 \end{bmatrix}$ hold. Hence, the S-Procedure implies the set containment

$$\underbrace{\{\boldsymbol{e}_C,\boldsymbol{x}_M,\tilde{\boldsymbol{\Theta}} \mid V \geq c\}}_{\mathcal{M}_1} \subseteq \underbrace{\{\boldsymbol{e}_C,\boldsymbol{x}_M,\tilde{\boldsymbol{\Theta}} \mid \dot{V} \leq -\kappa V\}}_{\mathcal{M}_0}. \tag{4.195}$$

In order to show UUB, it has to be proven that

1. $(\boldsymbol{e}_{C,0},\boldsymbol{x}_{M,0},\tilde{\boldsymbol{\Theta}}_0) \in \mathcal{M}_c$ implies $(\boldsymbol{e}_C(t),\boldsymbol{x}_M(t),\tilde{\boldsymbol{\Theta}}(t)) \in \mathcal{M}_c\ \forall\, t \geq 0$;
2. $(\boldsymbol{e}_{C,0},\boldsymbol{x}_{M,0},\tilde{\boldsymbol{\Theta}}_0) \notin \mathcal{M}_c$ implies $(\boldsymbol{e}_C(t),\boldsymbol{x}_M(t),\tilde{\boldsymbol{\Theta}}(t)) \in \mathcal{M}_c\ \forall\, t \geq T > 0$.

To prove the first part, notice that due to the positive definiteness of $V(\boldsymbol{e}_C,\boldsymbol{x}_M,\tilde{\boldsymbol{\Theta}})$, (4.195) especially implies $\dot{V}(\boldsymbol{e}_C,\boldsymbol{x}_M,\tilde{\boldsymbol{\Theta}}) < 0\ \forall\ (\boldsymbol{e}_C,\boldsymbol{x}_M,\tilde{\boldsymbol{\Theta}}) \in \partial\mathcal{M}_1$, where $\partial\mathcal{M}_1 = \partial\mathcal{M}_c = \{\boldsymbol{e}_C,\boldsymbol{x}_M,\tilde{\boldsymbol{\Theta}} \mid V(\boldsymbol{e}_C,\boldsymbol{x}_M,\tilde{\boldsymbol{\Theta}}) = c\}$ denotes the boundary of $\mathcal{M}_1$, $\mathcal{M}_c$. Hence, $\mathcal{M}_c$ is an invariant set and any trajectory starting in $\mathcal{M}_c$ cannot leave this set, which concludes the proof of part 1.

In order to prove the second part, notice that (4.195) also implies $\dot{V}(\boldsymbol{e}_C, \boldsymbol{x}_M, \tilde{\boldsymbol{\Theta}}) \leq -\kappa \cdot V(\boldsymbol{e}_C, \boldsymbol{x}_M, \tilde{\boldsymbol{\Theta}}) \ \forall \ (\boldsymbol{e}_C, \boldsymbol{x}_M, \tilde{\boldsymbol{\Theta}}) \ \in \mathcal{M}_1$. By virtue of the comparison lemma [96], $V(\boldsymbol{e}_C, \boldsymbol{x}_M, \tilde{\boldsymbol{\Theta}})$ hence satisfies

$$V(\boldsymbol{e}_C(t), \boldsymbol{x}_M(t), \tilde{\boldsymbol{\Theta}}(t)) \leq c_0 \cdot e^{-\kappa \cdot t} \tag{4.196}$$

for $(\boldsymbol{e}_C, \boldsymbol{x}_M, \tilde{\boldsymbol{\Theta}}) \ \in \mathcal{M}_1$, where $c_0 = V(\boldsymbol{e}_{C,0}, \boldsymbol{x}_{M,0}, \tilde{\boldsymbol{\Theta}}_0)$ denotes the level set associated with the initial conditions. Eq. (4.196) guarantees that $V(t)$ decreases from the initial level set c_0 to the ultimate bound c during the interval $0 \leq t \leq T$, where $T = -(1/\kappa)\ln(c/c_0)$. Since $\mathcal{M}_c$ is invariant, the trajectories are guaranteed to never leave this set any time thereafter, which concludes the proof of part 2.

Due to parts 1 and 2, the trajectories of the adaptive control system (3.4), (4.174), (4.175) are UUB and (4.192) follows from the proofs of part 1 and 2. □

Remark 4.14. *While Theorem 4.13 has been derived for single-input plants, i.e.* $m = 1$*, it can be easily extended to MIMO plants, when assuming that* $\boldsymbol{\Lambda}$ *is diagonal. In this case, the trace operator used by the Lyapunov function* (3.30) *admits a representation as a sum of scalar products as shown in* (4.87)*. An appropriate Lyapunov function to establish UUB of the error dynamics* (4.174)*,* (4.175) *is then given by*

$$V(t) = \frac{1}{2}\boldsymbol{e}_C(t)^T \boldsymbol{P}\boldsymbol{e}_C(t) + \frac{1}{2}\sum_{i=1}^{m} \Lambda_i \tilde{\boldsymbol{\theta}}_i \boldsymbol{\Gamma}^{-1} \tilde{\boldsymbol{\theta}}_i^T + \frac{1}{2}\boldsymbol{x}_M(t)\boldsymbol{P}_M\boldsymbol{x}_M(t). \tag{4.197}$$

By applying the arguments of Theorem 4.13 to each input, a MIMO UUB condition follows.

While Theorem 4.13 yields conditions for UUB of a direct MRAC in the presence of unmatched parametric uncertainties and parametrization errors, the size of the tracking error has not yet been addressed. To that end, let the initial conditions be given by $\boldsymbol{e}_C(0) = \boldsymbol{0}$, $\boldsymbol{x}_M(0) = \boldsymbol{0}$ and $\tilde{\boldsymbol{\Theta}}(0) = -\boldsymbol{\Theta}^*$. Inserting these initial conditions into the derivative of the Lyapunov function yields $\dot{V}(\boldsymbol{e}_C(0), \boldsymbol{x}_M(0), \tilde{\boldsymbol{\Theta}}(0)) = 0$. Since Theorem 4.13 guarantees the set containment (4.195), the negation is true as well:

$$\{\boldsymbol{e}_C, \boldsymbol{x}_M, \tilde{\boldsymbol{\Theta}} \mid \dot{V} > -\kappa V\} \subseteq \{\boldsymbol{e}_C, \boldsymbol{x}_M, \tilde{\boldsymbol{\Theta}} \mid V < c\}. \tag{4.198}$$

Since the above initial conditions satisfy $\dot{V}(\boldsymbol{e}_C, \boldsymbol{x}_M, \tilde{\boldsymbol{\Theta}}) = 0$, they do hence lie within the set $\mathcal{M}_c$. Since $\mathcal{M}_c$ is an invariant set and furthermore an ellipsoid, the ellipsoid projection of Section 4.2.1 may be readily applied to obtain a bound on the tracking error. To that end, let $\boldsymbol{c}_k \in \mathbb{R}^{2n+n_r}$, $k \in [1, \ldots, n]$ denote the unit vector associated with the state $e_{C,k}(t)$:

$$\boldsymbol{c}_k^T = \begin{bmatrix} \boldsymbol{b}_k^T & \boldsymbol{0}^{1\times n} & \boldsymbol{0}^{1\times n_r} \end{bmatrix} \quad \text{with} \quad \boldsymbol{b}_k^T = \begin{bmatrix} \boldsymbol{0}^{1\times(k-1)} & 1 & \boldsymbol{0}^{1\times(n-k)} \end{bmatrix}. \tag{4.199}$$

According to (B.94) and (B.95), the projection of $\mathcal{M}_c$ onto the subspace spanned by $\boldsymbol{c}_k$ is given by:

$$\mathcal{M}_{c,Proj} = \left\{ e_{C,k} \mid \frac{1}{\boldsymbol{b}_k^T \left(\frac{1}{2}\boldsymbol{P}\right)^{-1} \boldsymbol{b}_k} \cdot e_{C,k}^2 \leq c \right\}. \tag{4.200}$$

The tracking error bound for the state $e_{C,k}(t)$ becomes

$$\|e_{C,k}(t)\|_{\mathcal{L}_\infty} \leq \sqrt{2 \cdot c \cdot \boldsymbol{b}_k^T \boldsymbol{P}^{-1} \boldsymbol{b}_k} \tag{4.201}$$

with $c = l_c/l$.

The LMI problem of Theorem 4.13 is a feasibility problem. Hence, the level set constant c, which crucially determines the size of the tracking error bound (4.201), may be significantly larger than the smallest level set constant c^*, for which the LMIs (4.190) are feasible. By solving the GEVP [17]:

$$\begin{aligned}
&\min_{l,c} \; c \\
&\begin{bmatrix}
(\kappa+l)\boldsymbol{P}-\boldsymbol{Q}_{P,v} & \boldsymbol{P}\bar{\boldsymbol{B}}_P\boldsymbol{\Theta}^*_{x,um,v} & \boldsymbol{0} & \boldsymbol{P}\boldsymbol{B}_P\cdot\epsilon_v \\
\boldsymbol{\Theta}^{*,T}_{x,um,v}\bar{\boldsymbol{B}}_P^T\boldsymbol{P} & (\kappa+l)\boldsymbol{P}_M-\boldsymbol{Q}_M & \boldsymbol{0} & \boldsymbol{P}_M\boldsymbol{B}_M\cdot r_v \\
\boldsymbol{0} & \boldsymbol{0} & \Lambda_v\big((\kappa+l)\boldsymbol{\Gamma}^{-1}-2\boldsymbol{\sigma}\big) & -\Lambda_v\boldsymbol{\sigma}\boldsymbol{\Theta}_v^{*T} \\
\epsilon_v\cdot\boldsymbol{B}_P^T\boldsymbol{P} & r_v\cdot\boldsymbol{B}_M^T\boldsymbol{P}_M & -\Lambda_v\boldsymbol{\Theta}_v^*\boldsymbol{\sigma} & -2cl
\end{bmatrix} \leq 0, \qquad (4.202) \\
&-\boldsymbol{Q}_{P,v} = \Big(\boldsymbol{A}_M + \bar{\boldsymbol{B}}_P\boldsymbol{\Theta}^*_{x,um,v}\Big)^T\boldsymbol{P} + \boldsymbol{P}\Big(\boldsymbol{A}_M + \bar{\boldsymbol{B}}_P\boldsymbol{\Theta}^*_{x,um,v}\Big) \qquad (4.203) \\
&\qquad\qquad \forall\; v = 1,\ldots,2^q,
\end{aligned}$$

the smallest level set constant $c^* = \arg\min c$ can be computed.

The application of Theorem 4.13 is demonstrated by the following example:

Example 4.15. *Consider the linearized short-period approximation* (2.51) *of the longitudinal motion of the UAS from Chapter 2. In contrast to the previous examples such as Example 3.6 or Example 4.1,* $\lambda_{Z\alpha} = \lambda_{Zq} = 1$ *are* no longer assumed*. Hence, the system matrix of the plant is now given by*

$$\boldsymbol{A}_P = \begin{bmatrix} Z_\alpha \cdot \lambda_{Z\alpha} & 1 + Z_q \cdot \lambda_{Zq} \\ \lambda_\alpha \cdot M_\alpha & \lambda_q \cdot M_q \end{bmatrix}. \tag{4.204}$$

This alternative definition admits the introduction of unmatched uncertainties by virtue of the coefficients $\lambda_{Z\alpha}$ *and* λ_{Zq}*. For the remainder of this example, the uncertainties are assumed to adhere to Table 4.2. Apart from these differences, the plant is equivalently defined as in Example 3.6.*

In order to control this plant, the adaptive controller with baseline from Example 4.1 is used. Due to the plant uncertainties from Table 4.2, the ideal parameters and the unmatched uncertainty are confined to the hyperrectangle

$$\begin{aligned}
&-1.0569 \leq \Theta^*_\alpha \leq 0.5691, && -0.2285 \leq \Theta^*_q \leq 0.1230, \\
&-0.2110 \leq \Theta^*_r \leq 0.1136, && \\
&-0.7253 \leq \Theta^*_{um,1} \leq 0.7253, && -0.0263 \leq \Theta^*_{um,2} \leq 0.0263.
\end{aligned}$$

Since unmatched uncertainties have to be considered, the update law of the direct MRAC is enhanced by a σ*-modification. The design parameters of the adaptive controller are chosen as*

$$\boldsymbol{P} = \begin{bmatrix} 0.5447 & 0.0142 \\ 0.0142 & 0.0934 \end{bmatrix}, \qquad \boldsymbol{\Gamma} = \gamma \cdot \boldsymbol{I}^{3\times3}, \qquad \boldsymbol{\sigma} = 0.001 \cdot \boldsymbol{I}^{3\times3}. \tag{4.205}$$

Coefficient	Nominal Value	Uncertainty Range
Z_α	-2.42	$\lambda_{Z\alpha} \in [0.7, 1.3]$
Z_q	-0.09	$\lambda_{Zq} \in [0.7, 1.3]$
M_α	-29.04	$\lambda_\alpha \in [0.7, 1.3]$
M_q	-6.69	$\lambda_q \in [0.7, 1.3]$
M_η	-21.40	$\lambda_\eta \in [0.7, 1.3]$

Table 4.2: Coefficients of the short-period approximation for a linearization of the non-linear EOMs at $V_K^R = 40\,m/s$, $h = 500\,m$, $m_{fuel} = 3.2\,kg$.

While the design parameters Γ and $\boldsymbol{\sigma}$ have been chosen in an ad hoc manner, the matrix $\boldsymbol{P}$ maximizes the decay rate of the error dynamics in the presence of unmatched uncertainties. The largest decay rate κ_e and the corresponding matrix $\boldsymbol{P}$ follow from the GEVP

$$\max_{\boldsymbol{P},\kappa_e} \kappa_e$$
$$\left(\boldsymbol{A}_M + \bar{\boldsymbol{B}}_P \boldsymbol{\Theta}^*_{x,um,v}\right)^T \boldsymbol{P} + \boldsymbol{P}\left(\boldsymbol{A}_M + \bar{\boldsymbol{B}}_P \boldsymbol{\Theta}^*_{x,um,v}\right) + \kappa_e \boldsymbol{P} \leq 0.$$

The rationale of this choice becomes clear when revisiting the LMI condition of Theorem 4.13. By determining $\boldsymbol{P}$ such that it maximizes the decay rate, the upper left block of the LMI (4.190) *is rendered as negative as possible, assuming $\kappa_e \gg (\kappa + l)$.*

In Figure 4.18, the performance of the control system to a 5° square wave is shown. For this simulation, the uncertainties have been chosen as $\lambda_\alpha = \lambda_q = \lambda_\eta = \lambda_{Zq} = 1$ and $\lambda_{Z\alpha} = 0.7$. The learning rate is set to $\gamma = 10$. While there is only an unmatched uncertainty associated with Z_α, this uncertainty leads to a significant deviation from the reference model. The effect of this uncertainty could for example be compensated by a baseline controller with integrator. Nevertheless, no such modification of the baseline controller is applied here since this example focuses on the tracking error analysis.

Similar to the case of a direct MRAC without modification and without unmatched uncertainties, the baseline controller does not alter the error dynamics. Hence, Theorem 4.13 may be used to analyze the tracking error in the presence of unmatched uncertainties. In order to obtain a minimal tracking error bound, the GEVP (4.202), (4.203) *is solved and afterwards,* (4.201) *yields the desired tracking error bound. The matrix $\boldsymbol{P}_M$ is chosen as*

$$\boldsymbol{P}_M = \begin{bmatrix} 0.5439 & -0.0231 \\ -0.0231 & 0.0933 \end{bmatrix}$$

and also follows from a decay rate maximization problem. The decay rate outside of

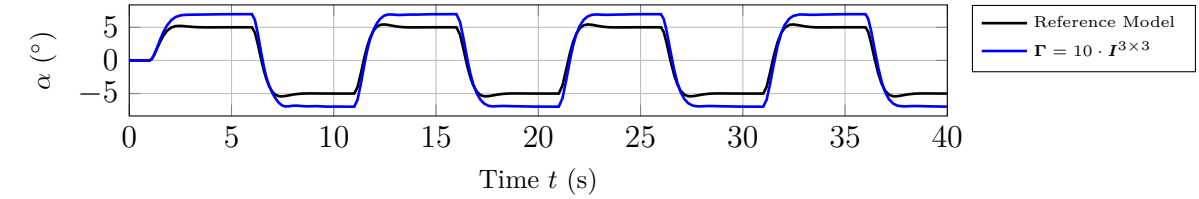

(a) Angle-Of-Attack α

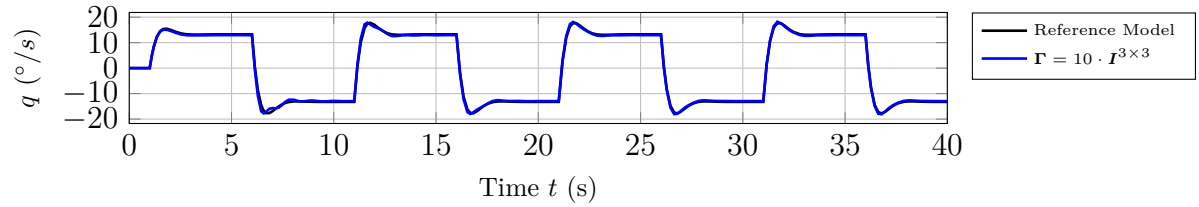

(b) Pitch Rate q

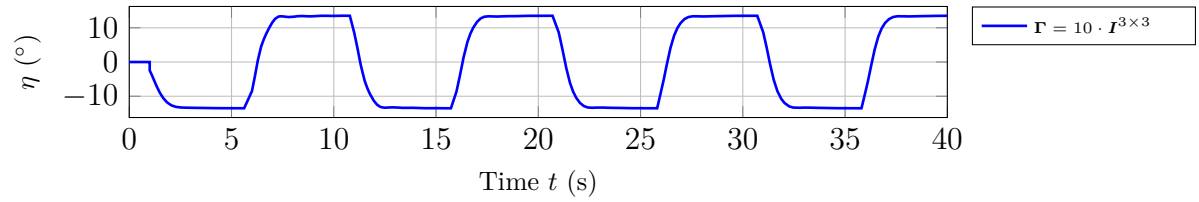

(c) Elevator Deflection η

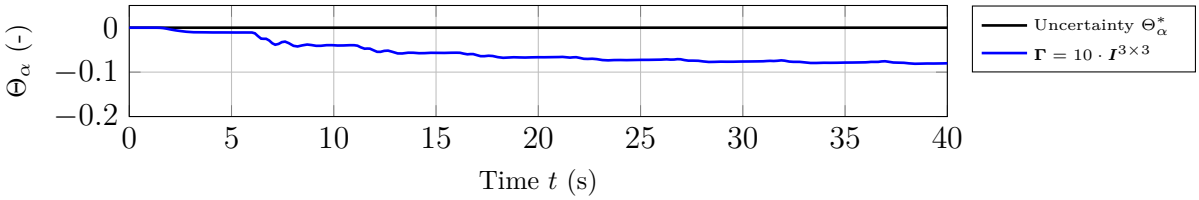

(d) Adaptive Parameter Θ_α

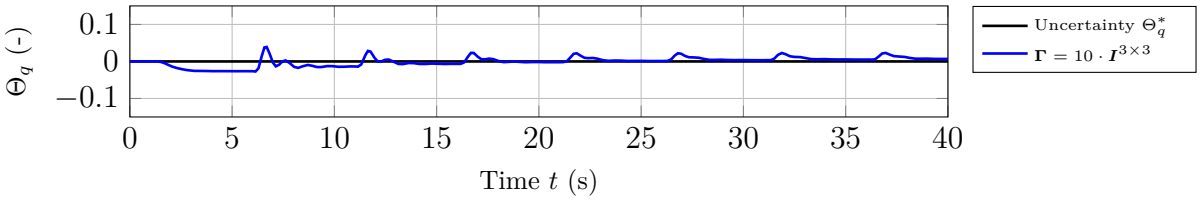

(e) Adaptive Parameter Θ_q

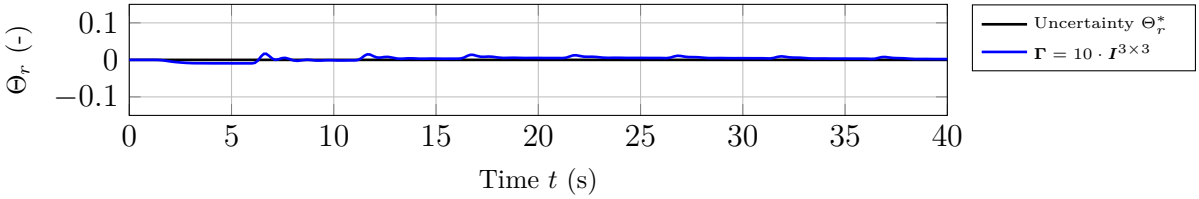

(f) Adaptive Parameter Θ_r

Figure 4.18: Exemplary response of the adaptive controller from Example 4.15 for $\lambda_\alpha = \lambda_q = \lambda_\eta = \lambda_{Zq} = 1$ and $\lambda_{Z\alpha} = 0.7$ to a $5°$ square wave command.

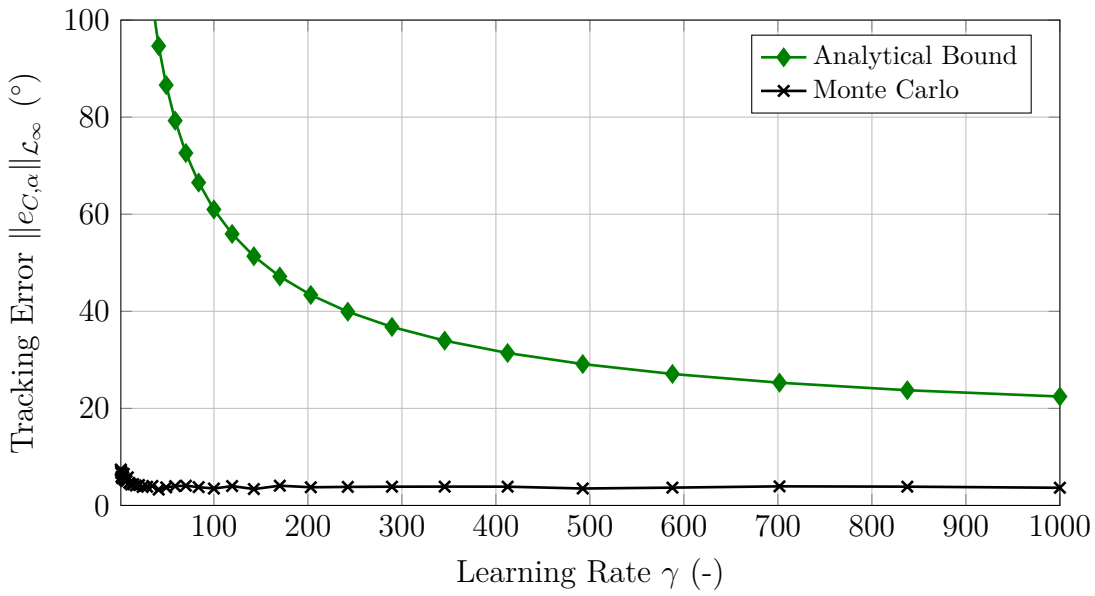

Figure 4.19: Comparison of the analytical tracking error bound in the presence of unmatched parametric uncertainty with the largest tracking error $\|e_{C,\alpha}(t)_\tau\|_{\mathcal{L}_\infty}$ observed in simulations for different values of the learning rate γ.

the ultimate bound κ, which should neither be confused with the decay rate of the error dynamics κ_e or the decay rate of the reference model dynamics, is chosen as $\kappa = 0.001$.

Figure 4.19 compares the resulting tracking error bound with the largest tracking error observed in Monte Carlo simulations for different values of the learning rate. First of all, one notices that the analytical tracking error bound decreases with increasing learning rate γ. Further simulations show that for $\gamma \gg 1000$ the tracking error bound approaches a constant, non-zero value. Second, it is interesting to notice that the simulation-based tracking error bound hardly shows any improvement with increasing learning rate. However, as the considered MRAC does not possess any means to account for the unmatched uncertainty, and as the uncertainty sizes are comparatively small, such trend was to be expected. Upon comparison of the analytical bound and the simulation-based evidence, one clearly observes that the analytical bound is conservative. Even for a high learning rate $\gamma = 1000$, the analytical bound exceeds the largest tracking error observed in simulations by 500%.

Finally, notice that a similar computation, where $\boldsymbol{P}$ and $\boldsymbol{P}_M$ are the results of the Lyapunov equation for $\boldsymbol{Q} = \boldsymbol{I}^{2\times 2}$, yields approximately four times worse tracking error bounds. This highlights that an appropriate choice of the matrices $\boldsymbol{P}$ and $\boldsymbol{P}_M$ is crucial in order to prove reasonably small tracking error bounds.

Example 4.15 highlights the ability of Theorem 4.13 to proof stability of a MRAC in the presence of unmatched parametric uncertainties and bounded disturbances. Despite the use of LMI-based optimization and ellipsoid projection, the resulting tracking error bound is conservative, especially for low learning rates. In order to mitigate this

conservatism, an optimization of the design parameters $\boldsymbol{P}$, $\boldsymbol{\Gamma}$ and $\boldsymbol{\sigma}$ of the adaptive controller might be considered. The feasibility of this approach has been demonstrated in the publication [79] of the author of this thesis. The required LMI conditions readily follow from Theorem 4.13 by introducing the design parameters as additional optimization variables. It has been demonstrated in the latter publication that this optimization may lead to significant improvements. Since the optimization of design parameters disagrees with the analysis scenario of this chapter, this idea is not pursued any further here. Apart from optimizing the design parameters, further improvements of the tracking error bound could also result from analyzing the adaptive control system with a Lyapunov function similar to (4.117) from Section 4.2.1. As (4.117) introduces an additional degree of freedom, less conservative analysis results seem feasible. Furthermore, a probabilistic analysis based on Section 4.2.2 might admit further improvements.

4.3 Time-Delay Margin

Among the robustness metrics introduced in Section 4.1.2, the time-delay margin is of special interest as it represents a physically meaningful, easily understandable robustness metric, which also applies to nonlinear systems. Furthermore, it seems to provide an equivalent level of safety as compared to the phase margin. Due to these properties, the time-delay margin seems suitable for a future certification process.

In literature, adaptive control of time-delay systems has been tackled in two distinct ways. One approach is the explicit modification of an adaptive controller such that it accommodates for the time-delay (see e.g. [124] and references therein). The second approach, which is also taken in this section, is to prove robustness of an existing adaptive control scheme (like MRAC) to time-delays. The largest time-delay, for which stability can be proven, may then serve as a lower bound on the true time-delay margin.

This section is largely based on a publication by the author of this thesis [78]. It specifically considers the computation of the time-delay margin of the MRAC with baseline controller, which was introduced in Section 3.2.2, in case of a single-input, LTI plant in the tracking case. The use of a baseline controller is beneficial as it shifts the set of ideal parameters closer to the origin, as demonstrated in Example 4.1. Furthermore, a σ-modification is used in order to prevent parameter drift due to the time-delay.

In order to proof stability of the adaptive controller in the presence of time-delay, a quadratic Lyapunov function is constructed that resembles the well-known Lyapunov function used in the proof of UUB in Section 3.2.4 in the delay-free case. Due to the time-delay, the derivative of this Lyapunov function is however not a quadratic form but a multivariate polynomial. Hence, SOS optimization [128] and an extension of the S-Procedure [17] are used to show that the Lyapunov function and its derivative satisfy the conditions of the Lyapunov-Razumikhin theorem for UUB (Theorem C.9) from [75].

To that end, consider the plant (3.1) and let its input be delayed by $\tau_c > 0$. Suppose that Assumptions 3.1 (state feedback), 3.2 (positive definite control effectiveness), 3.3 (Lipschitz condition), 3.9 (matching condition) hold. Due to these assumptions, the plant (3.1) becomes

$$\dot{\boldsymbol{x}}_P(t) = \boldsymbol{A}_M \boldsymbol{x}_P(t) + \boldsymbol{B}_P \boldsymbol{\Lambda} \left(\boldsymbol{u}(t-\tau_c) - (\boldsymbol{\Theta}_x^* + \boldsymbol{K}_x) \cdot \boldsymbol{x}_P(t) - \bar{\boldsymbol{f}}(\boldsymbol{x}_P(t), t) \right). \quad (4.206)$$

Furthermore, let the following additional assumptions hold:

Assumption 4.5. *There is no input uncertainty, i.e.* $\boldsymbol{\Lambda} = \boldsymbol{I}$.

Assumption 4.6. *The plant* (4.206) *is LTI and not subject to exogenous disturbances, i.e.* $\bar{\boldsymbol{f}}(\boldsymbol{x}_P(t), t) = \boldsymbol{0}$.

Assumption 4.7. *The plant only has one control input, i.e.* $m = 1$.

Assumption 4.8. *The command signal* $r(t)$ *is bounded, i.e.* $\|r(t)\|_{\mathcal{L}_\infty} \leq r_0$, $r_0 > 0$. *Furthermore, the first derivative of the command signal is bounded as well, i.e.* $\|\dot{r}(t)\|_{\mathcal{L}_\infty} \leq \bar{r}_0$, $\bar{r}_0 > 0$.

The true matched uncertainties $\boldsymbol{\Theta}_x^* \in \mathbb{R}^{1\times n}$ *with* $\boldsymbol{\Theta}_x^* = \begin{bmatrix} \Theta_{x,1}^* & \dots & \Theta_{x,n}^* \end{bmatrix}$ *are known to remain within a* n*-dimensional hyperrectangle* $\Omega_x = \{\boldsymbol{\Theta}_x^* \mid |\Theta_{x,k}^*| \leq \Theta_{x,k,\max}^*,\ k = 1,\dots,n\}$.

Furthermore, the baseline controller quadratically stabilizes the uncertain plant in the absence of time-delay (see [2] for an introduction of quadratic stability). Thus, it satisfies the Lyapunov LMI

$$(\boldsymbol{A}_P + \boldsymbol{B}_P \cdot \boldsymbol{K}_x)^T \boldsymbol{P} + \boldsymbol{P}(\boldsymbol{A}_P + \boldsymbol{B}_P \cdot \boldsymbol{K}_x) \leq -\boldsymbol{Q} \qquad \forall\, \boldsymbol{A}_P, \quad (4.207)$$

which is equivalent to

$$(\boldsymbol{A}_M - \boldsymbol{B}_P \cdot \boldsymbol{\Theta}_x^*)^T \boldsymbol{P} + \boldsymbol{P}(\boldsymbol{A}_M - \boldsymbol{B}_P \cdot \boldsymbol{\Theta}_x^*) \leq -\boldsymbol{Q} \qquad \forall\, \boldsymbol{\Theta}_x^* \in \Omega_x \quad (4.208)$$

due to the matching condition (3.65)*. In both equations,* $\boldsymbol{Q} \in \mathbb{S}_{++}^n$ *is a design parameter.*

Due to the additional assumptions, the plant (4.206) simplifies to

$$\dot{\boldsymbol{x}}_P(t) = \boldsymbol{A}_M \boldsymbol{x}_P(t) + \boldsymbol{B}_P \left(u(t-\tau_c) - (\boldsymbol{\Theta}_x^* + \boldsymbol{K}_x) \cdot \boldsymbol{x}_P(t) \right), \quad (4.209)$$

where $\boldsymbol{A}_M \in \mathbb{R}^{n\times n}$, $\boldsymbol{B}_P \in \mathbb{R}^{n\times 1}$ are known matrices, whereas the constant vector $\boldsymbol{\Theta}_x^* \in \mathbb{R}^{1\times n}$ represents the matched plant uncertainties. The plant (4.209) is to be controlled by the adaptive control law with baseline (3.64). Due to Assumptions 4.5-4.7, the control law (3.64) simplifies to

$$u(t) = \boldsymbol{K}_x \cdot \boldsymbol{x}_P(t) + K_r \cdot r(t) + \boldsymbol{\Theta}_x(t) \cdot \boldsymbol{x}_P(t). \quad (4.210)$$

Consequently, the error dynamics $\dot{\boldsymbol{e}}_C(t) = \dot{\boldsymbol{x}}_P(t) - \dot{\boldsymbol{x}}_M(t)$ become

$$\dot{\boldsymbol{e}}_C(t) = \boldsymbol{A}_M \boldsymbol{x}_P(t) + \boldsymbol{B}_P \left(u(t-\tau_c) - (\boldsymbol{K}_x + \boldsymbol{\Theta}_x^*) \boldsymbol{x}_P(t) \right) - \boldsymbol{A}_M \boldsymbol{x}_M(t) - \boldsymbol{B}_M r(t). \quad (4.211)$$

By adding and subtracting $\boldsymbol{B}_P \cdot u\,(t)$ and using the definition $\tilde{\boldsymbol{\Theta}}_x\,(t) \triangleq \boldsymbol{\Theta}_x\,(t) - \boldsymbol{\Theta}_x^*$, the error dynamics may be rewritten as

$$\dot{\boldsymbol{e}}_C\,(t) = \boldsymbol{A}_M \boldsymbol{e}_C\,(t) + \boldsymbol{B}_P \tilde{\boldsymbol{\Theta}}_x\,(t)\,\boldsymbol{x}_P\,(t) + \boldsymbol{B}_P\,(u(t-\tau_c) - u\,(t))\,. \tag{4.212}$$

It follows from (4.212), that even if the parameter estimation error $\tilde{\boldsymbol{\Theta}}_x\,(t)$ is driven to zero, a disturbance $u(t-\tau_c) - u\,(t)$ is still acting on the error dynamics. For this reason, the update law for $\boldsymbol{\Theta}_x\,(t)$ is enhanced by a σ-modification to avoid parameter drift (see Section 3.2.4). The update law is given by

$$\dot{\boldsymbol{\Theta}}_x\,(t)^T = -\boldsymbol{\Gamma}_x \left(\boldsymbol{x}_P\,(t)\,\boldsymbol{e}_C\,(t)^T\,\boldsymbol{P}\boldsymbol{B}_P + \boldsymbol{\sigma}\boldsymbol{\Theta}_x\,(t)^T\right), \tag{4.213}$$

where $\boldsymbol{\Gamma}_x \in \mathbb{S}_{++}^n$ is the learning rate and $\boldsymbol{\sigma} \in \mathbb{S}_{++}^n$ is the modification gain. In contrast to the proof of UUB from Section 3.2.4 in the delay-free case, $\boldsymbol{P} \in \mathbb{S}_{++}^n$ is not the solution of the Lyapunov equation (3.31), but of the Lyapunov LMI (4.208).

4.3.1 Model Transformation

In order to let (4.212) explicitly depend on the time-delay, a model-transformation is applied [73]. For this, notice that

$$\begin{aligned} u(t-\tau_c) - u\,(t) &= -\int_{t-\tau_c}^{t} \dot{u}(\bar{\xi}) d\bar{\xi} \quad \text{with} \\ \dot{u}(\bar{\xi}) &= \left.\frac{du\,(t)}{dt}\right|_{t=\bar{\xi}} \end{aligned} \tag{4.214}$$

holds. Upon substitution of $\bar{\xi} = \xi + t$, (4.214) becomes:

$$u(t-\tau_c) - u\,(t) = -\int_{-\tau_c}^{0} \dot{u}(t+\xi) d\xi. \tag{4.215}$$

The tracking error dynamics (4.212) may hence be written as:

$$\dot{\boldsymbol{e}}_C\,(t) = \boldsymbol{A}_M \boldsymbol{e}_C\,(t) + \boldsymbol{B}_P \cdot \tilde{\boldsymbol{\Theta}}_x\,(t)\,\boldsymbol{x}_P\,(t) - \boldsymbol{B}_P \int_{-\tau_c}^{0} \dot{u}(t+\xi) d\xi. \tag{4.216}$$

Using $\boldsymbol{A} \triangleq \boldsymbol{A}_M - \boldsymbol{B}_P \cdot \boldsymbol{\Theta}_x^*$, the derivative $\dot{u}\,(t)$ is given by:

$$\begin{aligned} \frac{du\,(t)}{dt} &= \dot{\boldsymbol{\Theta}}_x\,(t)\,\boldsymbol{x}_P\,(t) + (\boldsymbol{\Theta}_x\,(t) + \boldsymbol{K}_x) \cdot \dot{\boldsymbol{x}}_P\,(t) + K_r \dot{r}(t) \\ &= -\boldsymbol{B}_P^T \boldsymbol{P} \boldsymbol{e}_C\,(t) \cdot \boldsymbol{x}_P\,(t)^T\,\boldsymbol{\Gamma}_x \boldsymbol{x}_P\,(t) - \boldsymbol{\Theta}_x\,(t)\,\boldsymbol{\sigma}\boldsymbol{\Gamma}_x \boldsymbol{x}_P\,(t) \\ &\quad + (\boldsymbol{\Theta}_x\,(t) + \boldsymbol{K}_x) \cdot \dot{\boldsymbol{x}}_P\,(t) + K_r \dot{r}(t) \end{aligned} \tag{4.217}$$

with

$$\begin{aligned} \dot{\boldsymbol{x}}_P\,(t) = \boldsymbol{A} \cdot \boldsymbol{x}_P\,(t) + \boldsymbol{B}_P \boldsymbol{K}_x \cdot (\boldsymbol{x}_P\,(t-\tau_c) - \boldsymbol{x}_P\,(t)) + \boldsymbol{B}_M \cdot r(t-\tau_c) \\ + \boldsymbol{B}_P \cdot \boldsymbol{\Theta}_x(t-\tau_c) \boldsymbol{x}_P(t-\tau_c). \end{aligned} \tag{4.218}$$

$\boldsymbol{x}_P = \boldsymbol{x}_P(t)$	$\boldsymbol{x}_{P,\xi} = \boldsymbol{x}_P(t+\xi)$	$\boldsymbol{x}_{P,\tau} = \boldsymbol{x}_P(t+\xi-\tau_c)$
$\boldsymbol{x}_M = \boldsymbol{x}_M(t)$	$\boldsymbol{x}_{M,\xi} = \boldsymbol{x}_M(t+\xi)$	$\boldsymbol{x}_{M,\tau} = \boldsymbol{x}_M(t+\xi-\tau_c)$
$\boldsymbol{e}_C = \boldsymbol{e}_C(t)$	$\boldsymbol{e}_{C,\xi} = \boldsymbol{e}_C(t+\xi)$	$\boldsymbol{e}_{C,\tau} = \boldsymbol{e}_C(t+\xi-\tau_c)$
$\boldsymbol{\Theta}_x = \boldsymbol{\Theta}_x(t)$	$\boldsymbol{\Theta}_{x,\xi} = \boldsymbol{\Theta}_x(t+\xi)$	$\boldsymbol{\Theta}_{x,\tau} = \boldsymbol{\Theta}_x(t+\xi-\tau_c)$
$r = r(t)$	$r_\xi = r(t+\xi)$	$r_\tau = r(t+\xi-\tau_c)$
$\boldsymbol{z} = \boldsymbol{z}(t)$	$\boldsymbol{z}_\xi = \boldsymbol{z}(t+\xi)$	$\boldsymbol{z}_\tau = \boldsymbol{z}(t+\xi-\tau_c)$

Table 4.3: Compact notation for the time-delay margin analysis of MRAC with σ-modification.

In order to simplify the subsequent derivations, the compact notation according to Table 4.3 is used. Hence, $\dot{u}(t+\xi)$ in compact notation is given by:

$$\begin{aligned}\dot{u}(t+\xi) = &- \boldsymbol{B}_P^T \boldsymbol{P} \boldsymbol{e}_{C,\xi} \cdot \boldsymbol{x}_{P,\xi}^T \boldsymbol{\Gamma}_x \boldsymbol{x}_{P,\xi} - \boldsymbol{\Theta}_{x,\xi} \boldsymbol{\sigma} \boldsymbol{\Gamma}_x \boldsymbol{x}_{P,\xi} + K_r \dot{r}_\xi \\ &+ (\boldsymbol{\Theta}_{x,\xi} + \boldsymbol{K}_x) \cdot (\boldsymbol{A} \cdot \boldsymbol{x}_{P,\xi} + \boldsymbol{B}_P \boldsymbol{K}_x (\boldsymbol{x}_{P,\tau} - \boldsymbol{x}_{P,\xi})) \\ &+ (\boldsymbol{\Theta}_{x,\xi} + \boldsymbol{K}_x) \cdot (\boldsymbol{B}_M \cdot r_\tau + \boldsymbol{B}_P \cdot \boldsymbol{\Theta}_{x,\tau} \cdot \boldsymbol{x}_{P,\tau}) .\end{aligned} \tag{4.219}$$

4.3.2 Proof of Ultimate Boundedness

In this section, UUB of the time-delayed adaptive control system is proven. Similar to the delay-free case, a quadratic Lyapunov function candidate is chosen:

$$V(t) = \frac{1}{2} \boldsymbol{e}_C^T \boldsymbol{P} \boldsymbol{e}_C + \frac{1}{2} \boldsymbol{x}_M^T \boldsymbol{P}_M \boldsymbol{x}_M + \frac{1}{2} \boldsymbol{\Theta}_x \boldsymbol{\Gamma}_x^{-1} \boldsymbol{\Theta}_x^T, \tag{4.220}$$

where $\boldsymbol{P}_M \in \mathbb{S}_{++}^n$ solves the Lyapunov equation

$$\boldsymbol{A}_M^T \boldsymbol{P}_M + \boldsymbol{P}_M \boldsymbol{A}_M = -\boldsymbol{Q}_M. \tag{4.221}$$

In (4.221), $\boldsymbol{Q}_M \in \mathbb{S}_{++}^n$ is a design parameter. Unlike the delay-free case, the Lyapunov function candidate (4.220) also considers the reference model state $\boldsymbol{x}_M$. This is because the tracking error dynamics (4.216) contain a bounded disturbance depending on $\boldsymbol{x}_P = \boldsymbol{e}_C + \boldsymbol{x}_M$. Furthermore, the Lyapunov function candidate (4.220) does not depend on the parameter estimation error $\tilde{\boldsymbol{\Theta}}_x(t)$, but on the parameter estimation $\boldsymbol{\Theta}_x$. While this significantly simplifies the subsequent derivations, it is also the reason why $\boldsymbol{P}$ has to satisfy (4.208) (i.e. the plant is quadratically stable).

For the subsequent derivations, let $\|\boldsymbol{z}\|_W$ denote the weighted 2-norm of the vector $\boldsymbol{z}^T \triangleq \begin{bmatrix} \boldsymbol{e}_C^T & \boldsymbol{x}_M^T & \boldsymbol{\Theta}_x \end{bmatrix}$, satisfying $\|\boldsymbol{z}\|_W^2 = \boldsymbol{z}^T \boldsymbol{W} \boldsymbol{z},\ \boldsymbol{W} \in \mathbb{S}_{++}^{3n}$. With

$$\boldsymbol{W} = \frac{1}{2} \begin{bmatrix} \boldsymbol{P} & 0 & 0 \\ 0 & \boldsymbol{P}_M & 0 \\ 0 & 0 & \boldsymbol{\Gamma}_x^{-1} \end{bmatrix}, \tag{4.222}$$

the Lyapunov function candidate may be written as $V(\boldsymbol{z}) = \|\boldsymbol{z}\|_W^2$. Hence, using $u(s) = s^2$ and $v(s) = s^2$, the conditions of Theorem C.9 concerning the functions $u(s)$ and $v(s)$ are met and $u(\|\boldsymbol{z}\|_W) = V(\boldsymbol{z}) = v(\|\boldsymbol{z}\|_W)$ holds. Differentiating the Lyapunov function candidate (4.220) along the solutions of the Retarded Functional Differential Equation (RFDE) (4.216), (4.213) and (3.4) yields:

$$\begin{aligned}\dot{V}(\boldsymbol{z}) = \boldsymbol{e}_C^T \boldsymbol{P} \left(\boldsymbol{A}_M \boldsymbol{e}_C + \boldsymbol{B}_P \tilde{\boldsymbol{\Theta}}_x \boldsymbol{x}_P - \boldsymbol{B}_P \int_{-\tau_c}^{0} \dot{u}(t+\xi) d\xi \right) \\ + \boldsymbol{x}_M^T \boldsymbol{P}_M \left(\boldsymbol{A}_M \boldsymbol{x}_M + \boldsymbol{B}_M \cdot r \right) - \boldsymbol{\Theta}_x \left(\boldsymbol{x}_P \boldsymbol{e}_C^T \boldsymbol{P} \boldsymbol{B}_P + \boldsymbol{\sigma} \boldsymbol{\Theta}_x^T \right).\end{aligned} \tag{4.223}$$

Using $\tilde{\boldsymbol{\Theta}}_x = \boldsymbol{\Theta}_x - \boldsymbol{\Theta}_x^*$ and (4.208), (4.223) may be upper-bounded by:

$$\begin{aligned}\dot{V}(\boldsymbol{z}) \leq & -\frac{1}{2} \boldsymbol{e}_C^T \boldsymbol{Q} \boldsymbol{e}_C - \boldsymbol{e}_C^T \boldsymbol{P} \boldsymbol{B}_P \boldsymbol{\Theta}_x^* \boldsymbol{x}_M \\ & - \boldsymbol{e}_C^T \boldsymbol{P} \boldsymbol{B}_P \int_{-\tau_c}^{0} \dot{u}(t+\xi) d\xi \\ & - \frac{1}{2} \boldsymbol{x}_M^T \boldsymbol{Q}_M \boldsymbol{x}_M + \boldsymbol{x}_M^T \boldsymbol{P}_M \boldsymbol{B}_M r - \boldsymbol{\Theta}_x \boldsymbol{\sigma} \boldsymbol{\Theta}_x^T.\end{aligned} \tag{4.224}$$

In order to comply with condition (C.35) of Theorem C.9, $V(\boldsymbol{z}) \leq -w(\|\boldsymbol{z}\|_W)$ with $w(s) = \epsilon s^2$, $\epsilon > 0$, (if (C.36), (C.37) hold) will be proven in Theorem 4.16. To simplify the subsequent derivations, $w(\|\boldsymbol{z}\|_W) = \kappa V(\boldsymbol{z})$ is added and subtracted in (4.224):

$$\begin{aligned}\dot{V}(\boldsymbol{z}) \leq & -\kappa V(\boldsymbol{z}) - \frac{1}{2} \boldsymbol{e}_C^T \boldsymbol{Q} \boldsymbol{e}_C - \boldsymbol{e}_C^T \boldsymbol{P} \boldsymbol{B}_P \boldsymbol{\Theta}_x^* \boldsymbol{x}_M \\ & - \boldsymbol{e}_C^T \boldsymbol{P} \boldsymbol{B}_P \int_{-\tau_c}^{0} \dot{u}(t+\xi) d\xi - \frac{1}{2} \boldsymbol{x}_M^T \boldsymbol{Q}_M \boldsymbol{x}_M \\ & + \boldsymbol{x}_M^T \boldsymbol{P}_M \boldsymbol{B}_M r - \boldsymbol{\Theta}_x \boldsymbol{\sigma} \boldsymbol{\Theta}_x^T + \kappa V(\boldsymbol{z}).\end{aligned} \tag{4.225}$$

Since the integration in (4.225) is performed over ξ, the upper bound on $\dot{V}(\boldsymbol{z})$ may be rewritten as

$$\dot{V}(\boldsymbol{z}) \leq -\kappa V(\boldsymbol{z}) + \int_{-\tau_c}^{0} v(\boldsymbol{x}) d\xi \tag{4.226}$$

with

$$\begin{aligned}v(\boldsymbol{x}) = & \frac{1}{\tau_c} \left(\kappa V(\boldsymbol{z}) - \frac{1}{2} \left(\boldsymbol{e}_C^T \boldsymbol{Q} \boldsymbol{e}_C + \boldsymbol{x}_M^T \boldsymbol{Q}_M \boldsymbol{x}_M \right) - \boldsymbol{e}_C^T \boldsymbol{P} \boldsymbol{B}_P \boldsymbol{\Theta}_x^* \boldsymbol{x}_M \right) \\ & + \frac{1}{\tau_c} \left(\boldsymbol{x}_M^T \boldsymbol{P}_M \boldsymbol{B}_M r - \boldsymbol{\Theta}_x \boldsymbol{\sigma} \boldsymbol{\Theta}_x^T \right) - \boldsymbol{e}_C^T \boldsymbol{P} \boldsymbol{B}_P \dot{u}(t+\xi),\end{aligned} \tag{4.227}$$

where $\boldsymbol{x}^T = \begin{bmatrix} \boldsymbol{z}^T & \boldsymbol{z}_\xi^T & \boldsymbol{z}_\tau^T & r & r_\tau & \dot{r}_\xi & \boldsymbol{\Theta}_x^* \end{bmatrix}$. In (4.226), the vector $\boldsymbol{x}$ is chosen such that it contains all variables of a SOS optimization problem, which is going to be presented in Theorem 4.16. Using $\kappa_c \triangleq 1/\tau_c$, $v(\boldsymbol{x})$ becomes

$$\begin{aligned}v(\boldsymbol{x}) = & \kappa_c \left(\kappa V(\boldsymbol{z}) - \frac{1}{2} \boldsymbol{e}_C^T \boldsymbol{Q} \boldsymbol{e}_C - \frac{1}{2} \boldsymbol{x}_M^T \boldsymbol{Q}_M \boldsymbol{x}_M \right) \\ & + \kappa_c \left(-\boldsymbol{e}_C^T \boldsymbol{P} \boldsymbol{B}_P \boldsymbol{\Theta}_x^* \boldsymbol{x}_M + \boldsymbol{x}_M^T \boldsymbol{P}_M \boldsymbol{B}_M r - \boldsymbol{\Theta}_x \boldsymbol{\sigma} \boldsymbol{\Theta}_x^T \right) \\ & - \boldsymbol{e}_C^T \boldsymbol{P} \boldsymbol{B}_P \dot{u}(t+\xi).\end{aligned} \tag{4.228}$$

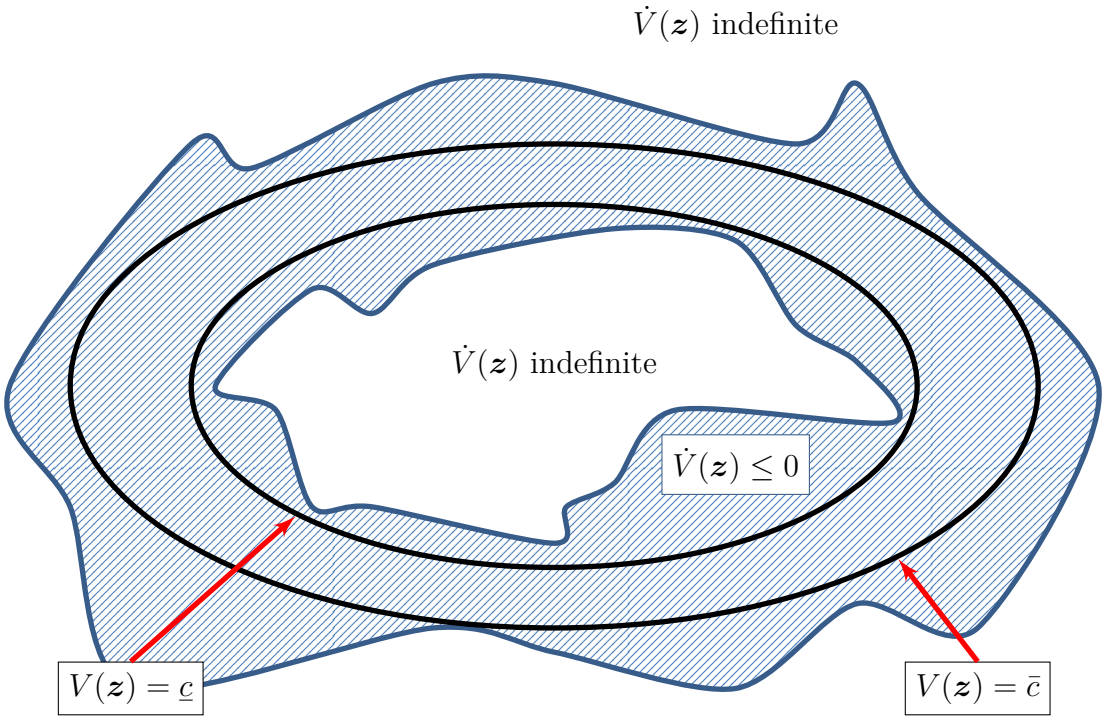

Figure 4.20: Illustration of the level sets: The derivative of the Lyapunov function $V(\boldsymbol{z})$ is indefinite inside the invariant set $V(\boldsymbol{z}) \leq \underline{c}$ and outside the invariant set $V(\boldsymbol{z}) \leq \bar{c}$.

By inspecting (4.226), a general idea about the sets involved in the proof of UUB may be obtained. In order to ensure $\dot{V}(\boldsymbol{z}) \leq -\kappa V(\boldsymbol{z})$, it suffices to show $v(\boldsymbol{x}) \leq 0$. Due to the reference signal r, the polynomial $v(\boldsymbol{x})$ is indefinite inside a level set $V(\boldsymbol{z}) \leq \underline{c}$ with $\underline{c} > 0$. Hence, $\dot{V}(\boldsymbol{z})$ is indefinite in this level set, too. Similarly, $v(\boldsymbol{x})$ is indefinite outside a level set $V(\boldsymbol{z}) \geq \bar{c}$ with $\bar{c} > 0$, since $v(\boldsymbol{x})$ is a polynomial of degree 4 and the largest negative definite terms in $v(\boldsymbol{x})$ are of degree 2. This is illustrated in Figure 4.20. One arrives at the following theorem:

Theorem 4.16. *Consider the transformed adaptive control system* (4.216), (4.213), (3.4) *and let* $p_0 > 1$, $\epsilon > 0$, $\underline{c} > 0$, $\bar{c} > \underline{c}$ *be given constants. Consider the polynomial* $f(\boldsymbol{x})$ *with*

$$f(\boldsymbol{x}) \triangleq v(\boldsymbol{x}) + \alpha_1 \left(p_0 V(\boldsymbol{z}) - V(\boldsymbol{z}_\xi)\right) + \alpha_2 \left(p_0 V(\boldsymbol{z}) - V(\boldsymbol{z}_\tau)\right), \tag{4.229}$$

where $v(\boldsymbol{x})$ *is defined in* (4.228). *Let the initial condition satisfy*

$$\|\boldsymbol{\phi}(\zeta)\|_c^2 = \sup_{-2\tau_c \leq \zeta \leq 0} \|\boldsymbol{\phi}(\zeta)\|_W^2 \leq \bar{c}.$$

If there are multipliers $\lambda_1(\boldsymbol{x})$, $\lambda_2(\boldsymbol{x}) \in \Sigma(\boldsymbol{x})$, λ_3, λ_4, λ_5, $\ldots$, $\lambda_{5+n} \in \mathbb{R}_{++}$ *and constants* α_1, $\alpha_2 \in \mathbb{R}_{++}$ *such that the SOS optimization problem*

$$\min_{\lambda_i, \alpha_1, \alpha_2} \kappa_c \quad i = 1, \ldots, 5+n;\ \kappa_c > 0 \qquad s.t. \tag{4.230}$$

$$
\begin{aligned}
-f(\boldsymbol{x}) + \lambda_1(\boldsymbol{x})\left(\underline{c} - V(\boldsymbol{z})\right) + \lambda_2(\boldsymbol{x})\left(V(\boldsymbol{z}) + V(\boldsymbol{z}_\xi) + V(\boldsymbol{z}_\tau) - 3\bar{c}\right) + \lambda_3(r^2 - r_0^2) \\
+ \lambda_4(r_\tau^2 - r_0^2) + \lambda_5(\dot{r}_\xi^2 - \bar{r}_0^2) + \sum_{k=1}^{n} \lambda_{(5+k)} \left({\Theta_{x,k}^*}^2 - {\Theta_{x,k,\max}^*}^2\right) \in \Sigma(\boldsymbol{x})
\end{aligned} \tag{4.231}
$$

is feasible, then the adaptive control system (4.216)*,* (4.213)*,* (3.4) *is UUB with a guaranteed time-delay margin of* $\tau_c^* = 1/\kappa_c^*$*. Furthermore, the ultimate bound is given by* $H^2 \triangleq \underline{c}$*.*

Proof. Let κ_c^* be the minimizer of the optimization problem. Then, its inverse $\tau_c^* = 1/\kappa_c^*$ is the largest time-delay for which (4.231) is satisfied and for which the Polynomial S-Procedure (Lemma B.11) proves the implication:

$$
\begin{aligned}
V(\boldsymbol{z}) \geq \underline{c} \wedge V(\boldsymbol{z}) \leq \bar{c} \wedge\ & V(\boldsymbol{z}_\xi) \leq \bar{c} \wedge\ V(\boldsymbol{z}_\tau) \leq \bar{c} \\
& \wedge r^2 \leq r_0^2 \quad \wedge\ r_\tau^2 \leq r_0^2 \quad \wedge\ \dot{r}_\xi^2 \leq \bar{r}_0^2 \\
& \wedge {\Theta_{x,k}^*}^2 \leq {\Theta_{x,k,\max}^*}^2,\ k = 1, \ldots, n\ \Rightarrow f \leq 0.
\end{aligned} \tag{4.232}
$$

Thus, one has $f(\boldsymbol{x}) \leq 0\ \forall\, \boldsymbol{x} \in \mathcal{M}_c$ with

$$
\begin{aligned}
\mathcal{M}_c = \{\boldsymbol{x} \mid\ & \underline{c} \leq V(\boldsymbol{z}) \leq \bar{c},\ V(\boldsymbol{z}_\xi) \leq \bar{c},\ V(\boldsymbol{z}_\tau) \leq \bar{c} \\
& r^2 \leq r_0^2,\ r_\tau^2 \leq r_0^2,\ \dot{r}_\xi^2 \leq \bar{r}_0^2 \\
& {\Theta_{x,k}^*}^2 \leq {\Theta_{x,k,\max}^*}^2,\ k = 1, \ldots, n\}.
\end{aligned} \tag{4.233}
$$

Now let $w(s) \triangleq \epsilon s^2$. According to Theorem C.9, $\dot{V}(\boldsymbol{z}) \leq -w(\|\boldsymbol{z}\|_W) = -\kappa V(\boldsymbol{z})$ has to hold, whenever

$$
\|\boldsymbol{z}\|_W^2 \geq H^2,\ H^2 = \underline{c}, \tag{4.234}
$$

$$
p_0 V(\boldsymbol{z}) - V(\boldsymbol{e}_C(t+\zeta), \boldsymbol{x}_M(t+\zeta), \boldsymbol{\Theta}_x(t+\zeta)) > 0 \tag{4.235}
$$

are satisfied for $\zeta \in [-2\tau_c, 0]$. Eq. (4.235) is however true if and only if

$$
p_0 V(\boldsymbol{z}) - V(\boldsymbol{z}_\xi) > 0, \tag{4.236}
$$

$$
p_0 V(\boldsymbol{z}) - V(\boldsymbol{z}_\tau) > 0 \tag{4.237}
$$

hold for $\xi = [-\tau_c, 0]$. Thus, $f(\boldsymbol{x}) \leq 0\ \forall x \in \mathcal{M}_c$ implies $v(\boldsymbol{x}) \leq 0\ \forall \boldsymbol{x} \in \mathcal{M}_c$, if (4.235) is satisfied. Furthermore, note that (4.234) is satisfied as well, since (4.232) ensures $V(\boldsymbol{z}) \geq \underline{c}$. Because of

1. Assumption 4.8, the bounds on the reference signal r, its delayed version r_τ, its delayed derivative $\dot{r}_\xi$ and the bounds on the true matched uncertainties $\Theta_{x,k}^*$ are always satisfied.
2. Remark C.10 and the boundedness of the initial conditions (i.e. $\|\boldsymbol{\phi}(\zeta)\|_c^2 \leq \bar{c}$), the Lyapunov function will never exceed the level set $V(\boldsymbol{z}) = \|\boldsymbol{z}\|_W^2 \leq \bar{c}$. Hence, the delayed states satisfy $\|\boldsymbol{z}_\xi\|_W^2 \leq \bar{c}$, $\|\boldsymbol{z}_\tau\|_W^2 \leq \bar{c}$.

Due to the preceding two remarks, $v(\boldsymbol{x}) \leq 0\ \forall x \in \mathcal{M}_c$ implies without loss of generality $\dot{V}(\boldsymbol{z}) \leq -\kappa V(\boldsymbol{z}),\ \forall \boldsymbol{z} \in \{\boldsymbol{z} \mid \bar{c} \geq \|\boldsymbol{z}\|_W^2 \geq \underline{c}\}$, if (4.235) is true. Hence, all conditions of Theorem C.9 are satisfied and the adaptive control system (4.216), (4.213), (3.4) is UUB with a time-delay margin τ_c^* and an ultimate bound $H^2 = \underline{c}$. □

Remark 4.17. *In Theorem 4.16, the multipliers $\lambda_i(\boldsymbol{x})$ with $i = 1, \ldots, 5+n$ have been chosen such that the computational burden is kept small. Other choices of the multipliers, like separate polynomial multipliers for each inequality on the left hand side of* (4.232)*, are also admissible and may lead to larger estimates of the time-delay margin at the price of an increased computational complexity.*

Remark 4.18. *For the application of Theorem 4.16, the question whether a time-delay may always be computed is of great importance. In order to obtain an insight into this question, consider* (4.225) *and denote the upper bound of $\dot{V}(\boldsymbol{z})$ as $\dot{V}_u(\boldsymbol{z})$. For $\tau_c \to 0$, it follows that $\dot{V}_u(\boldsymbol{z}) \to -\frac{1}{2}\boldsymbol{e}_C^T\boldsymbol{Q}\boldsymbol{e}_C - \boldsymbol{e}_C^T\boldsymbol{P}\boldsymbol{B}_P\boldsymbol{\Theta}_x^*\boldsymbol{x}_M - \frac{1}{2}\boldsymbol{x}_M^T\boldsymbol{Q}_M\boldsymbol{x}_M + \boldsymbol{x}_M^T\boldsymbol{P}_M\boldsymbol{B}_M r - \boldsymbol{\Theta}_x\boldsymbol{\sigma}\boldsymbol{\Theta}_x^T$. Thus, the upper bound converges to a second order polynomial, which is only indefinite inside of $V(\boldsymbol{z}) \leq \underline{c}$, but not outside of $V(\boldsymbol{z}) \leq \bar{c}$. Due to continuity, this implies that the outer limit $\bar{c}$ of the invariant region may diverge to infinity as $\tau_c \to 0$. This however implies that for sufficiently large $\underline{c}$, the set containment condition of Theorem 4.16 is always solvable if τ_c is sufficiently small.*

4.3.3 Numerical Example

The application of Theorem 4.16 is demonstrated by the following example:

Example 4.19. *Consider the plant $(\boldsymbol{A}_P, \boldsymbol{B}_P \cdot \Lambda)$ from Example 3.6. Due to the limitations of Theorem 4.16, only state dependent uncertainties are accommodated, that is, λ_η is not uncertain and satisfies $\Lambda = \lambda_\eta = 1$. The state-dependent, matched uncertainties are assumed to satisfy $0.9 \leq \lambda_\alpha \leq 1.1$ and $0.9 \leq \lambda_q \leq 1.1$. This size of the uncertainty set has been chosen as numerical problems occurred in case of larger sets.*

The plant is to be controlled by the adaptive control system with baseline controller (4.210)*,* (4.213)*. Suitable gains $\boldsymbol{K}_x$, K_r of the baseline controller have already been derived in Example 3.6. It follows from the matching condition (Assumption 3.9) that the ideal parameter $\boldsymbol{\Theta}_x^* = \begin{bmatrix}\Theta_\alpha^* & \Theta_q^*\end{bmatrix}$ is hence confined to the interval*

$$-0.14 \leq \Theta_\alpha^* \leq 0.14, \qquad -0.03 \leq \Theta_q^* \leq 0.03. \tag{4.238}$$

The design parameters of the adaptive controller are chosen as

$$\begin{aligned} \boldsymbol{P} &= \begin{bmatrix} 0.5381 & -0.0563 \\ -0.0563 & 0.0923 \end{bmatrix},\ \boldsymbol{\Gamma} = \gamma \cdot \boldsymbol{I}^{2\times 2},\ \boldsymbol{\sigma} = \boldsymbol{\Gamma}^{-1}, \\ \boldsymbol{P}_M &= \begin{bmatrix} 0.5439 & -0.0231 \\ -0.0231 & 0.0933 \end{bmatrix}, \end{aligned} \tag{4.239}$$

where $\gamma > 0$ scales the learning rate. Similar to Example 4.15, the matrices $\boldsymbol{P}$ and $\boldsymbol{P}_M$ are the results of decay rate maximization problems:

$$\begin{aligned}&\max_{\boldsymbol{P},\kappa_e} \kappa_e\\&\left(\boldsymbol{A}_M - \boldsymbol{B}_P\boldsymbol{\Theta}_x^*\right)^T\boldsymbol{P} + \boldsymbol{P}\left(\boldsymbol{A}_M - \boldsymbol{B}_P\boldsymbol{\Theta}_x^*\right) + \kappa_e\boldsymbol{P} \leq 0, \quad \forall\, \boldsymbol{\Theta}_x^* \in \Omega_x,\end{aligned}$$

and

$$\begin{aligned}&\max_{\boldsymbol{P},\kappa_m} \kappa_m\\&\boldsymbol{A}_M^T\boldsymbol{P} + \boldsymbol{P}\boldsymbol{A}_M + \kappa_m\boldsymbol{P} \leq 0,\end{aligned}$$

respectively. The matrices $\boldsymbol{Q}$ and $\boldsymbol{Q}_M$ are hence given by

$$\boldsymbol{Q} = \kappa_e \cdot \boldsymbol{P} = \begin{bmatrix} 2.6603 & -0.2783 \\ -0.2783 & 0.4565 \end{bmatrix}, \tag{4.240}$$

$$\boldsymbol{Q}_M = -\left(\boldsymbol{A}_M^T\boldsymbol{P}_M + \boldsymbol{P}_M\boldsymbol{A}_M\right) = \begin{bmatrix} 2.3846 & -0.1011 \\ -0.1011 & 0.4089 \end{bmatrix}. \tag{4.241}$$

Furthermore, the reference signal is assumed to satisfy $\|r\|_{\mathcal{L}_\infty} \leq 0.1\,rad = 5.7°$ and $\|\dot{r}\|_{\mathcal{L}_\infty} \leq 0.5\,rad/s = 28.7\,°/s$.

Since an adaptive controller is volatile to time-delay even in the absence of matched parametric uncertainties, at first $\boldsymbol{\Theta}_x^* = \boldsymbol{0}$ is assumed. Hence, the Lyapunov inequality (4.208) *may be replaced by the respective Lyapunov equality. The matrix $\boldsymbol{Q}$ is thus given by the matrix*

$$\boldsymbol{Q} = -\left(\boldsymbol{A}_M^T\boldsymbol{P} + \boldsymbol{P}\boldsymbol{A}_M\right) = \begin{bmatrix} 2.0026 & -0.2464 \\ -0.2464 & 0.4659 \end{bmatrix}. \tag{4.242}$$

Using these design parameters, Theorem 4.16 is invoked to compute the time-delay margin for different values of the learning rate γ. The optimization problem of Theorem 4.16 is formulated using the modeling language YALMIP [109] and solved by SDPT3 [166]. In order to isolate the effect of the learning rate, the modification gain $\boldsymbol{\sigma}$ has been chosen such that the leakage in the update law (4.213) *remains constant, i.e. $\boldsymbol{\Gamma\sigma} = \boldsymbol{I}^{2\times 2}$. Since the choice of the level set constants $\underline{c}$ and $\bar{c}$ also affects the provable time-delay margin, the optimization problem of Theorem 4.16 is additionally solved for different values of the level set constant $\underline{c}$. When considering the initial conditions $\boldsymbol{e}_C(\zeta) = 0$, $\boldsymbol{x}_M(\zeta) = 0$, $\boldsymbol{\Theta}_x(\zeta) = 0$ with $\zeta = [-2\tau_c, 0]$, these initial conditions lie within the level set $V(\boldsymbol{z}) \leq \underline{c}$. Hence, the remaining level set constant $\bar{c}$ is arbitrarily chosen slightly larger than $\underline{c}$, i.e. $\bar{c} = \underline{c} + 0.01$. In order to keep the computational complexity small, the multipliers $\lambda_1(\boldsymbol{x})$ and $\lambda_2(\boldsymbol{x})$ are restricted to polynomials of degree 2.*

In Figure 4.21(a), the analytically computed time-delay margin (for different choices of the level set constant $\underline{c}$) is compared to the time-delay margin determined in simulations. For the simulation-based computation, a Monte Carlo simulation with 1000 iterations was performed for each value of the learning rate γ, which only varied the command signal $r\,(t)$. Since the analytical results ensure that $V(\boldsymbol{e}_C\,(t)\,, \boldsymbol{x}_M\,(t)\,, \boldsymbol{\Theta}_x\,(t)) \leq \bar{c}$

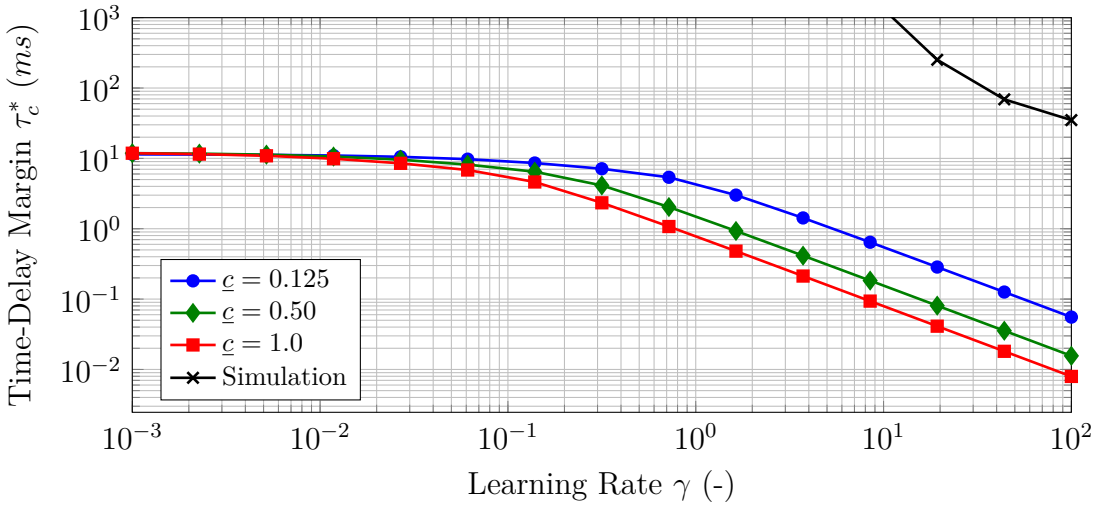

(a) Comparison of the provable time-delay margin with the time-delay margin determined in simulation

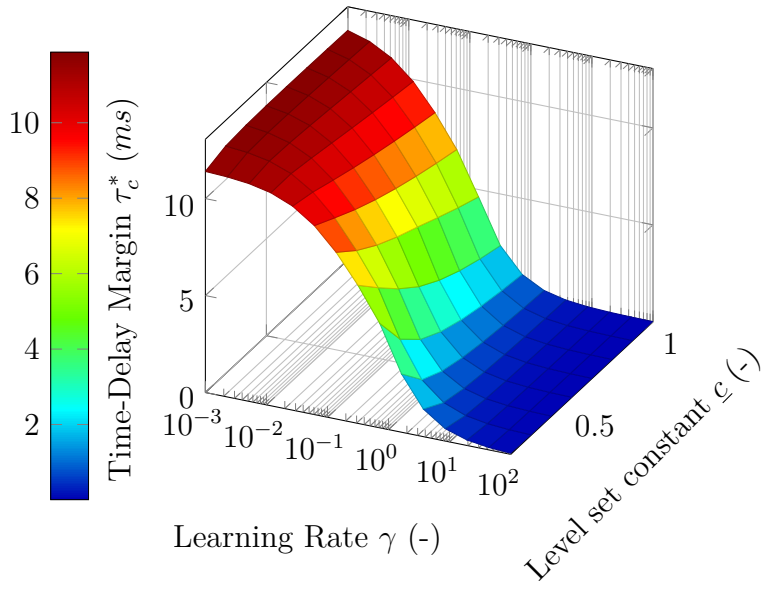

(b) Dependence of the provable time-delay margin on γ and $\underline{c}$

Figure 4.21: Dependence of the time-delay margin on the learning rate γ in the absence of parametric uncertainties.

holds for all $t \geq 0$, a simulation run was considered to be stable if the evaluation of the Lyapunov function $V(\boldsymbol{e}_C(t), \boldsymbol{x}_M(t), \boldsymbol{\Theta}_x(t))$ remained below 1.01 for all times. Notice that 1.01 represents the largest value of $\bar{c}$, for which Theorem 4.16 is solved.

As expected, Figure 4.21(a) shows that the time-delay margin decreases with increasing learning rate. Despite of the use of SOS programming, the gap between the analytically computed time-delay margin and the simulation-based time-delay margin remains considerable. At $\gamma = 19.3$, the provable time-delay margin for example amounts to 0.1% of the simulation evidence. Although increasing the degree of the multipliers might reduce conservatism, further research is required to substantially re-

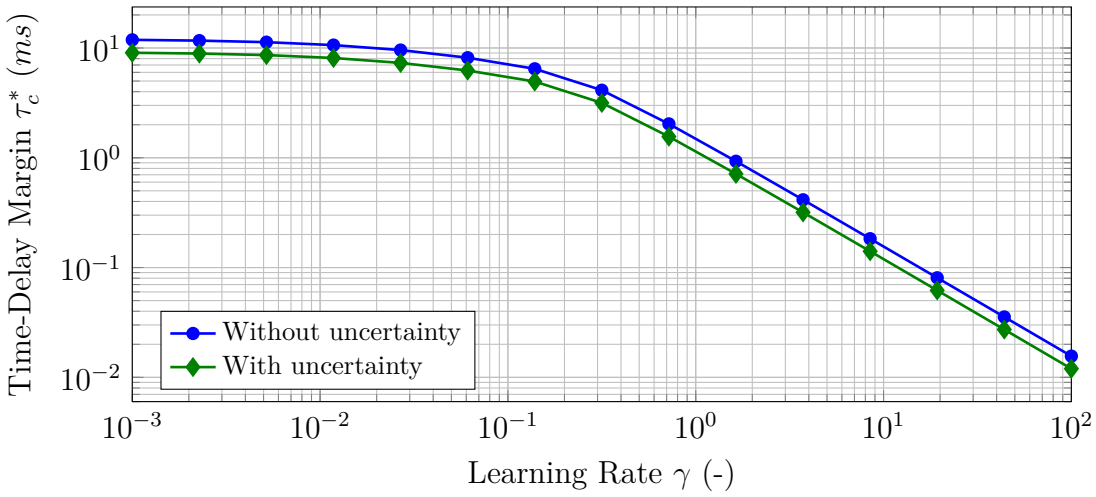

Figure 4.22: Dependence of the time-delay margin on the learning rate γ in case of 10% matched parametric uncertainties for $\underline{c} = 0.5$.

duce this gap. The influence of the level set constant $\underline{c}$ may be seen best in Figure 4.21(b). At first, the time-delay margin increases with an increasing value of the level set constant $\underline{c}$. After reaching a maximum, the time-delay margin begins to decrease again. This illustrates that the choice of an appropriate level set constant $\underline{c}$ is crucial for determining the largest value of the time-delay margin.

Next, the time-delay margin in the presence of 10% matched uncertainties is analyzed. Hence, $\boldsymbol{Q}$ from (4.240) *and $\boldsymbol{Q}_M$ from* (4.241) *are used. For $\underline{c} = 0.5$, Figure 4.19 compares the dependence of the time-delay margin on the learning rate γ with and without 10% matched uncertainty. It may be observed that the provable time-delay margin with uncertainties amounts to 76.3% at $\gamma = 10^{-3}$ and to 76.8% at $\gamma = 8.5$ of the value, which may be proven in case of no matched uncertainties.*

Example 4.19 highlighted the capability of Theorem 4.16 to compute a time-delay margin of a MRAC with σ-modification. In contrast to other work, the presented approach allows the computation of a time-delay margin for a single-input LTI plant in the tracking case. Furthermore, the resulting time-delay margin is valid for all matched uncertainties of admissible size. Since level set constants are explicitly used within the approach, the largest tracking error that may occur due to the time-delay can also be estimated. Although the explicit use of level set constants is advantageous, further research is required to quickly determine initial level set constants that solve the optimization problem of Theorem 4.16. Moreover, research is required to mitigate the conservatism that is introduced by using a Lyapunov function whose parameters have been determined beforehand. Another aspect that requires further attention is the SOS optimization problem itself. On the one side, its size often causes numerical difficulties, which are also the reason why the uncertainty set Ω_x had to be chosen very small. On the other side, the size of the problem is also limited by the capabilities of today's LMI

solvers as discussed in [43]. For this reason, only small-scale problems involving a few states can be solved.

4.4 Discussion

In this chapter, robustness and performance metrics for adaptive control have been reviewed, which may become part of a future certification process of adaptive controllers. The review came to the conclusion that the time-delay margin and bounds on the tracking error are useful metrics, which allow the evaluation of the robustness as well as of the performance of an adaptive controller. Since existing techniques for the analytical computation of these metrics led to overly conservative bounds on these metrics, novel techniques for their computation have been developed.

Despite all improvements, the computable bounds on these metrics still remain too conservative. In case of the time-delay margin, this has been demonstrated in Example 4.19. Even for a simple adaptive control problem, the gap between the analytical lower bound and the simulation-based upper bound remains considerably large. Even in good cases, the analytical bound only guarantees 0.1% of the time-delay margin which is observed in simulations. As compared to the analytical lower bounds on the time-delay margin, the analytical upper bounds on the tracking error seem to be more mature. Nevertheless, a significant gap between the analytical upper bound and the simulation-based lower bound is observed. In Example 4.7, the analytical bound exceeds the numerical evidence by roughly 400%. Consequently, this raises the question of how to improve these bounds even further.

The performance of an adaptive controller and also the size of the computable bounds crucially depend on the design parameters of the adaptive controller, such as $\boldsymbol{P}$, $\boldsymbol{\Gamma}$ and $\boldsymbol{\sigma}$. It is hence reasonable to go from the analysis scenario, which was considered in this chapter, to a controller synthesis scenario, where these design parameters are optimized in such a way that the respective bounds are maximized or minimized, respectively. In case of the time-delay margin, this approach has to overcome serious limitations. While a synthesis SOS program readily follows from Theorem 4.16, it is important to notice that this program would be bilinear. Since the linear SOS program from Theorem 4.16 already leads to a significant computational burden [78] and is sensitive to numerical problems, such a synthesis SOS program seems to be too demanding for the time being. To alleviate this difficulty, more efficient formulations of the analysis SOS program would be required first, which for example rely on appropriately simplified multipliers.

In case of the tracking error, the controller synthesis scenario has been addressed in a publication of the author by this thesis [79] as well as several other publications [55, 56, 61, 58, 57]. Since all of these approaches only rely on quadratic forms instead of SOS polynomials, the computational complexity is significantly lower. Hence,

even if the synthesis program is bilinear and hence, nonconvex, the computation of a suboptimal solution seems feasible. While technically feasible, the synthesis does not yet account for an important aspect: It is well known that the tracking error may be decreased almost arbitrarily by increasing the learning rate $\mathbf{\Gamma}$. Thus, minimizing the tracking error bound will lead to large learning rates $\mathbf{\Gamma}$. However, large learning rates are known to increase the likelihood of oscillatory closed-loop responses and are known to decrease the time-delay margin. Hence, additional constraints are required which prevent the optimization from increasing the learning rate. An ad hoc solution is the introduction of upper limits for $\mathbf{\Gamma}$ as shown in [79]. However, suitable upper bounds are just as hardly known as suitable values for the learning rate $\mathbf{\Gamma}$ itself. A potential solution to address this problem is the analysis of the linearization of the adaptive controller for its various equilibrium conditions (see for example (4.8)). While the linearization does not allow any conclusion on the transient response, the absence of weakly damped modes in the linearization is a necessary condition for the absence of weakly damped responses of the nonlinear system. This is because any (fictitious) method, which could detect oscillations of the closed-loop system, would also detect the weakly damped modes at the equilibrium conditions. By minimizing the tracking error bound whilst ensuring a lower bound for the relative damping would hence prevent the optimization from increasing the learning rate to overly large values.

All of the analytical methods, which have been presented in this chapter, ultimately relied on Lyapunov or Lyapunov-like arguments. As highlighted in Section 4.2.1, the use of Lyapunov theory also is an intrinsic source of conservatism. This is because Lyapunov theory reduces the stability analysis of a n-dimensional system to the analysis of a one-dimensional, energy-like Lyapunov function and its derivative. While this step is central, it also leads to a loss of information since the Lyapunov function does not admit precise conclusions on the individual trajectories. Since bounds on the tracking error or the time-delay margin are derived from the one-dimensional Lyapunov function, they are hence intrinsically conservative. To overcome this source of conservatism, a stability analysis using alternative approaches would be required.

In contrast to nonlinear systems such as adaptive control systems, the analysis of LTI systems is significantly more mature. To some extent, this is because LTI systems admit the analytical solution of their underlying differential equations. Obviously, less conservative bounds on the tracking error could be computed, if an analytical solution to the MRAC differential equations was available. For this reason, Appendix D.2 demonstrates the analytical solution of the MRAC differential equations in case of a scalar plant with one uncertain parameter and in case of stabilization. While the approach from Appendix D.2 is not relevant from a practical point of view, an extension to more complex classes of plants could yield important insights.

Following a similar line of thought, the analysis of adaptive controllers using a Wiener-Volterra representation [137, 146] might allow to overcome the inherent limi-

tation of a Lyapunov based analysis. Unlike Lyapunov theory, the Wiener-Volterra approach focuses on the input / output map of a nonlinear system. Roughly speaking, the input / output map of the nonlinear system is represented in terms of a generalization of the convolution integral known from LTI system theory.

The previous two ideas might also allow addressing another problem, which has not been mentioned so far. With respect to the certification of an adaptive flight control system, bounds on the time-delay margin and the tracking error are by far not sufficient to replace all of the existing LTI requirements with an equivalent level of safety. As an example, consider the performance specification in terms of the $\mathcal{L}_\infty$-norm of the tracking error components. Even if the latter norm is guaranteed to be small and the reference model is non-oscillatory, the nonlinearity of an adaptive controller may induce low amplitude, high-frequency oscillations. These oscillations may in turn excite typically neglected dynamics such as structural modes. No analytically computable metric is known to the author which reliably detects such oscillations.

All of the previously presented ideas assumed that certification of an adaptive controller requires a-priori guarantees on its robustness and performance. Since the computation of suitable guarantees is still an open problem, the paradigm of a-priori guarantees has to be questioned as well. Instead of aiming at the computation of a-priori guarantees, extensive online monitoring of the adaptive controller might be a viable alternative. In this paradigm, the adaptive controller is constantly monitored by a suitable algorithm. If the monitor detects an undesirable behavior of the adaptive controller, it arranges the deactivation of the adaptive control system and will hence prevent the adaptive controller from harming flight safety. On the one side, this approach reduces the need for a-priori guarantees for the adaptive controller. On the other side, a-priori guarantees are required for the monitoring algorithm, which ensure that the monitor reliably detects malfunctions of the adaptive controller. Thus, monitoring-based certification of adaptive control shifts the need for a-priori guarantees from the adaptive controller to the monitoring system.

Chapter 5

Modified Linear Extended State Observer

In the previous chapter, novel techniques for the computation of robustness and performance guarantees for certain MRAC schemes have been introduced. Even though these techniques admit the computation of significantly improved bounds on the tracking error and the time-delay margin, these bounds remain by far too conservative for usage in a certification process. Furthermore, bounds on the tracking error and the time-delay margin do not suffice to fully replace the existing LTI robustness and performance requirements such as stated in SAE AS94900 [140]. The damping coefficients of a LTI system allow for example a conclusion on the presence of oscillations in the transient response. In contrast, no similar analytical metric is known to the author, which admits a comparable conclusion for an adaptive control scheme.

The lack of widely accepted and reliable guarantees is a major obstacle to the certification of classical adaptive control schemes. Hence, it is natural to ask whether the objective of model following control in the presence of uncertainties may be achieved by alternative means, which are certifiable without major modifications of current certification standards. Following this line of thought, the deviation between desired and real rotational dynamics of an aircraft may for example be estimated and compensated using measurements of the angular accelerations. In conjunction with Nonlinear Dynamic Inversion (NDI), this idea forms the basis of Incremental Nonlinear Dynamic Inversion (INDI) [157], [8][1]. Furthermore, the dependence on angular acceleration measurements may be alleviated by introducing a specialized linear filter, which yields a prediction of the angular accelerations based on delayed measurements. The resulting control approach is consequently named Predictive Incremental Nonlinear Dynamic Inversion (PINDI) [155]. Assuming that the aircraft is sufficiently well described by a LTI system, the overall control system may be analyzed using tools from linear system theory. Hence, conventional requirements for certification may be examined. In

[1] The authors of [157], [8] did not refer to their approach as INDI. This name was introduced later on [155].

a similar spirit, a filtered differentiation of the pitch rate to estimate the modeling error has been proposed [40]. Since the filtered differentiation is achieved using a LTI filter, conventional certification requirements may be checked as well. While the previously mentioned approaches are rather specific to aircraft applications, one may also resort to more general ideas such as DOBs (see e.g. [153]). The rational of DOBs is the estimation and compensation of the disturbance at the plant input, which causes the plant to deviate from a nominal or desired model. For this, the transfer function of the desired plant response is explicitly inverted. By adding additional filters, a causal control law results. As highlighted in Section 3.3.3, an explicit inversion is however not desirable as there is no systematic approach for the incorporation of anti-windup mechanisms. To circumvent this difficulty, one has to resort to indirect approaches such as $\mathcal{L}_1$-AC. In $\mathcal{L}_1$-AC, a state predictor with an appropriate update law indirectly estimates the disturbances, which cause the plant to deviate from its desired model. Anti-windup measures may then be implemented by simply mimicking those plant dynamics, which cause windup, in the predictor. While $\mathcal{L}_1$-AC in its original form employs nonlinear update laws similar to MRAC [27, 28] (see also Section 3.3.1), later extensions introduced linear hybrid [25, 175] (see also Section 3.3.2) as well as linear continuous time update laws [168].

The common feature of each of the previously mentioned approaches is the estimation of the *disturbance signal*, which causes the plant to deviate from its desired response. Following the terminology, which has been introduced in the discussion of Section 3.4.2, these approaches are hence referred to as *signal-based*. This is in sharp contrast to traditional adaptive control approaches such as MRAC or $\mathcal{L}_1$-AC (with integral update law [27, 28]), which ultimately estimate the *parameters* that cause the plant to deviate from its desired response. In this chapter, yet another signal-based approach is introduced, which is based upon a LESO. The ESO [67], [66] forms the basis of Active Disturbance Rejection Control (ADRC). ADRC is an output-feedback control approach for nonlinear systems and seeks to control a plant solely based upon basic knowledge about the underlying physical process (like the order of the governing differential equation). For this, all uncertainties are lumped into a disturbance signal. By treating this signal as an additional state of the plant (by differentiation of the signal), conventional observer theory may be invoked for the estimation of the plant states and the additional disturbance state. Hence, the ESO transforms the problem of uncertainty estimation into a problem of state estimation. Originally, ESOs used nonlinear observer gains. However, even with linear observer gains, the objective of simultaneous state and disturbance estimation may be achieved [65]. The resulting observer is called LESO and is appealing from a certification point of view due to its linearity.

When comparing the LESO to the $\mathcal{L}_1$-PWC introduced in Section 3.3.2, one observes that both approaches follow an indirect approach for the estimation of the disturbances, which is desirable as it admits the simple realization of anti-windup measures.

The $\mathcal{L}_1$-PWC does however resort to a linear hybrid approach, which complicates the analysis. In contrast, the LESO may be realized as a simple LTI system. On the other hand, it was already observed in the context of $\mathcal{L}_1$-AC that the choice of the low-pass filter, which shapes the frequency content of the disturbance estimate, is of crucial importance for a successful control design. Using $\mathcal{L}_1$-PWC, there is large degree of freedom with respect to the choice of this filter. As to be demonstrated in Section 5.1, the LESO also realizes a low-pass filter. Its choice is however implicit in the observer design. In order to combine the advantages of $\mathcal{L}_1$-PWC, namely precise shaping of the low-pass filter, and LESO, namely realization as a continuous time LTI system, a slight modification of the LESO is proposed in this chapter. By adding an additional degree of freedom, a MLESO is obtained which allows the explicit realization of an arbitrary low-pass filter structure. The concept of the MLESO was originally proposed in [77, 81] by the author of this thesis and will be extended in this chapter to accommodate a larger class of plants.

A conceptually similar approach, which provides the same benefits as the MLESO, is $\mathcal{L}_1$ Adaptive Control with Proportional Update Law ($\mathcal{L}_1$-PUL) [168]. Similar to the MLESO, $\mathcal{L}_1$-PUL leads to a continuous time LTI controller and follows an indirect approach. Furthermore, the filter may be freely chosen. The relation of these approaches will be clarified later on (Section 5.3.3). In fact, it will be shown that the closed-loop response of the $\mathcal{L}_1$-PUL (and any other $\mathcal{L}_1$-AC as well) approximates the closed-loop response of the MLESO.

To conclude this introduction, it should be noted that all linear signal-based approaches including the MLESO and the $\mathcal{L}_1$-PWC ultimately realize a filtered differentiation in order to estimate the disturbance signal. The bandwidth of this filter is the main tuning parameter, which allows trading off performance in the presence of parametric uncertainties against sensitivity to non-parametric uncertainties such as time-delays, unmodeled dynamics and noise. Roughly speaking, large bandwidths admit the estimation and compensation of large parametric uncertainties. At the same time, robustness, for example to delays, is decreased. In essence, all of these approaches hence constitute a special class of linear fixed-gain controllers, which are based on high-gain feedback. Due to their inherent robustness (to parametric uncertainties), they may also be seen as a special class of robust controllers, even though approaches such as $\mathcal{L}_1$-PWC and the MLESO are derived from an adaptive control point of view.

The remainder of this chapter is organized as follows: In Section 5.1, "classical" LESO control is exemplified in case of state feedback for the general plant (3.1) introduced in Chapter 3. Following up on these results, Section 5.2 introduces the MLESO, which is used to estimate the deviation between the desired plant response and the actual plant response. Using this disturbance estimate, Section 5.3 proposes a control law, if there are only matched uncertainties. This section also highlights the intrinsic relationship between MLESO-based control and conventional Proportional Integral

(PI) control as well as $\mathcal{L}_1$-AC. Afterwards, the more general case of matched and unmatched uncertainties is considered in Section 5.4 and an appropriate control law is derived. To conclude this chapter, Section 5.5 discusses the obtained results and relates the MLESO to other *signal-based* and *parameter-based* approaches.

5.1 Linear Extended State Observer Control

ADRC is a conceptually simple control approach, which tries to control an uncertain plant solely based on limited information about the underlying physical process and on a limited number of measurements. For this, all uncertainties are lumped into disturbance signals, which are subsequently treated as additional states of the plant. By applying conventional observer theory to this extended plant model, an observer may be designed, which achieves state and disturbance estimation at the same time. Due to the introduction of additional states, this observer is called ESO. By feeding back the uncertainty estimates, the uncertainties are approximately canceled and the nominal plant response is approximately recovered. Despite its intriguing capabilities and its simplicity, ESOs and ADRC are hardly known in the control community [164]. To some extent, this derives from the fact that early papers such as [67] doubted the need of an appropriate model in order to achieve good control performance. While it is true that a low quality model suffices in theory to achieve good performance, this comes at the price of excessively high feedback gains. Such high gains render the controller infeasible in practice due to plant imperfections such as time-delay. In order to reduce the controller gains, additional plant knowledge needs to be incorporated in order to reduce the work load of the disturbance estimation scheme. This may for example be achieved with the use of a baseline controller.

In the following, a special class of ESOs, namely the LESO, is introduced. The derivation of the LESO is exemplified for the plant (3.1), which is subject to Assumptions 3.1 (state feedback), 3.2 (positive definite control effectiveness), 3.3 (Lipschitz condition), 3.5 (matching condition). In general, the LESO may accommodate a larger class of plants than specified by (3.1) and is not limited to state feedback. These restrictions are only introduced to ensure consistency throughout this thesis and to easily motivate the MLESO in the upcoming sections.

Consider the plant (3.1). If the matching conditions hold, the plant (3.1) admits the alternative representation (3.12). By adding and subtracting $\boldsymbol{B}_P \cdot \boldsymbol{u}(t)$, (3.12) becomes

$$\begin{aligned} \dot{\boldsymbol{x}}_P(t) &= \boldsymbol{A}_M \boldsymbol{x}_P(t) + \boldsymbol{B}_P \boldsymbol{u}(t) + \boldsymbol{B}_P \cdot \boldsymbol{d}_m(\boldsymbol{x}_P(t), t), \\ \boldsymbol{d}_m(\boldsymbol{x}_P(t), t) &= (\boldsymbol{\Lambda} - \boldsymbol{I})\boldsymbol{u}(t) + \boldsymbol{\Theta}^*_{m,x} \boldsymbol{x}_P(t) + \boldsymbol{f}_m(\boldsymbol{x}_P(t), t), \end{aligned} \tag{5.1}$$

where all uncertainties are lumped into the signal $\boldsymbol{d}_m : \mathbb{R}^n \times \mathbb{R}_+ \to \mathbb{R}^m$. Subsequently, this signal is treated like an exogenous, i.e. not state-dependent, disturbance. In order to stress this important idea, $\boldsymbol{d}_m(t)$ will be used to refer to the signal $\boldsymbol{d}_m(\boldsymbol{x}_P(t), t)$. By

differentiating $\boldsymbol{d}_m(t)$ with respect to time and denoting its derivative as $\dot{\boldsymbol{\Delta}}(t) \triangleq \dot{\boldsymbol{d}}_m(t)$, (5.1) becomes

$$\begin{aligned} \dot{\boldsymbol{x}}_P(t) &= \boldsymbol{A}_M \boldsymbol{x}_P(t) + \boldsymbol{B}_P \boldsymbol{u}(t) + \boldsymbol{B}_P \boldsymbol{\Delta}(t), \\ \dot{\boldsymbol{\Delta}}(t) &= \dot{\boldsymbol{d}}_m(t), \end{aligned} \tag{5.2}$$

where $\boldsymbol{\Delta} : \mathbb{R}_+ \to \mathbb{R}^m$ denotes the so-called extended state. Since the extended state may not be measured, ADRC proposes the usage of a conventional observer to estimate the state $\boldsymbol{\Delta}(t)$. Since the derivative $\dot{\boldsymbol{d}}_m(t)$ of the unknown disturbance signal $\boldsymbol{d}_m(t)$ is not known either, $\dot{\boldsymbol{d}}_m(t)$ is assumed to be zero during the observer design process. A rough motivation for this approach may be derived from the *internal model principle* [54, 105]: If the commands $\boldsymbol{r}(t)$ and the exogenous disturbances may be modeled as step functions, then the state- and input-dependent disturbance signal $\boldsymbol{d}_m(\boldsymbol{x}_P(t), t)$ will also be a step-like function. Thus, by designing an observer for (5.2) with $\dot{\boldsymbol{d}}_m(t) = \boldsymbol{0}$, this step-like disturbance characteristic may be appropriately considered within the observer. In case of state feedback, the resulting observer is given by

$$\begin{aligned} \dot{\hat{\boldsymbol{x}}}_P(t) &= \boldsymbol{A}_M \hat{\boldsymbol{x}}_P(t) + \boldsymbol{B}_P \boldsymbol{u}(t) + \boldsymbol{B}_P \hat{\boldsymbol{\Delta}}(t) + \boldsymbol{L}_1 \cdot \boldsymbol{e}_P(t), \\ \dot{\hat{\boldsymbol{\Delta}}}(t) &= \boldsymbol{L}_2 \cdot \boldsymbol{e}_P(t), \end{aligned} \tag{5.3}$$

where $\hat{\boldsymbol{x}}_P : \mathbb{R}_+ \to \mathbb{R}^n$ and $\boldsymbol{e}_P(t) = \hat{\boldsymbol{x}}_P(t) - \boldsymbol{x}_P(t)$ denote the observer state vector and the observer error, respectively. Since the observer (5.3) possesses the additional state $\hat{\boldsymbol{\Delta}} : \mathbb{R}_+ \to \mathbb{R}^m$ and uses the linear observer gains $\boldsymbol{L}_1 \in \mathbb{R}^{n \times n}$ and $\boldsymbol{L}_2 \in \mathbb{R}^{m \times n}$, it is called a LESO. Even though the plant (5.2) is nonlinear by definition, any LTI observer design technique such as pole placement or Kalman filtering may be applied, since the design model of the observer, which results from (5.2) for $\dot{\boldsymbol{d}}_m(t) = \boldsymbol{0}$, is LTI.

The observer (5.3) yields an estimate of the disturbance signal $\boldsymbol{d}_m(t)$. Using this signal, a control law to achieve approximate tracking of the states of the reference model (3.4) is given by

$$\boldsymbol{u}(t) = \boldsymbol{K}_r \boldsymbol{r}(t) - \hat{\boldsymbol{\Delta}}(t), \tag{5.4}$$

where $\boldsymbol{K}_r$ was introduced in Section 3.1. Since the LESO assumes a step function as the internal model of the disturbance $\boldsymbol{d}_m(t)$, the internal model principle suggests that $\hat{\boldsymbol{\Delta}}(t)$ tracks $\boldsymbol{d}_m(t)$ only asymptotically. From an engineering point of view, it is however intuitive that $\hat{\boldsymbol{\Delta}}(t) \approx \boldsymbol{d}_m(t)$ will hold if the observer gains $\boldsymbol{L}_1$ and $\boldsymbol{L}_2$ are chosen sufficiently high. To shed light on this aspect, a different perspective is chosen, which will lead to the introduction of the MLESO later on: Instead of considering $\boldsymbol{d}_m(t)$ as an additional state, $\boldsymbol{d}_m(t)$ will subsequently be treated as a signal. Now, consider the error dynamics derived from (5.1) and (5.3):

$$\begin{aligned} \dot{\boldsymbol{e}}_P(t) &= (\boldsymbol{A}_M + \boldsymbol{L}_1) \cdot \boldsymbol{e}_P(t) + \boldsymbol{B}_P \cdot \left(\hat{\boldsymbol{\Delta}}(t) - \boldsymbol{d}_m(t) \right), \\ \dot{\hat{\boldsymbol{\Delta}}}(t) &= \boldsymbol{L}_2 \cdot \boldsymbol{e}_P(t). \end{aligned} \tag{5.5}$$

Since $\boldsymbol{d}_m(t)$ is treated as an exogenous signal, (5.5) constitutes a strictly proper LTI filter with input $\boldsymbol{d}_m(t)$ and output $\hat{\boldsymbol{\Delta}}(t)$. Furthermore, since (5.5) is strictly proper, it acts like a low-pass filter. To gain additional insight into the structure of the filter, notice that (5.5) admits the equivalent representation

$$\begin{aligned} \dot{\boldsymbol{e}}_P(t) &= (\boldsymbol{A}_M + \boldsymbol{L}_1) \cdot \boldsymbol{e}_P(t) + \boldsymbol{B} \cdot \begin{bmatrix} \hat{\boldsymbol{\Delta}}(t) - \boldsymbol{d}_m(t) \\ 0 \end{bmatrix}, \\ \dot{\hat{\boldsymbol{\Delta}}}(t) &= \boldsymbol{L}_2 \cdot \boldsymbol{e}_P(t), \end{aligned} \tag{5.6}$$

where $\boldsymbol{B} = \begin{bmatrix} \boldsymbol{B}_P & \bar{\boldsymbol{B}}_P \end{bmatrix}$ was defined in (3.13). Next, apply the transformation $\boldsymbol{e}_P(t) = -\boldsymbol{B} \cdot \bar{\boldsymbol{e}}_P(t)$. Eq. (5.6) becomes

$$\begin{aligned} \dot{\bar{\boldsymbol{e}}}_P(t) &= \boldsymbol{B}^{-1}(\boldsymbol{A}_M + \boldsymbol{L}_1)\boldsymbol{B} \cdot \bar{\boldsymbol{e}}_P(t) + \boldsymbol{K}\left(\boldsymbol{d}_m(t) - \hat{\boldsymbol{\Delta}}(t)\right), \\ \dot{\hat{\boldsymbol{\Delta}}}(t) &= -\boldsymbol{L}_2\boldsymbol{B} \cdot \bar{\boldsymbol{e}}_P(t), \end{aligned} \tag{5.7}$$

where $\boldsymbol{K}^T = \begin{bmatrix} \boldsymbol{I}^{m\times m} & \boldsymbol{0}^{m\times(n-m)} \end{bmatrix}$. Since $\boldsymbol{L}_1$ and $\boldsymbol{L}_2$ are the only design parameters of the filter, (5.7) may not realize arbitrary strictly proper filters. To see this, consider the following example:

Example 5.1. *Let* (3.1) *describe a SISO plant with one state, i.e.* $n = m = 1$*. In this case,* (5.7) *simplifies to*

$$\begin{aligned} \dot{\bar{e}}_P(t) &= B_P^{-1}(A_M + L_1)B_P \cdot \bar{e}_P - \hat{\Delta}(t) + d_m(t), \\ \dot{\hat{\Delta}}(t) &= -L_2 B_P \cdot \bar{e}_P(t). \end{aligned} \tag{5.8}$$

Upon the transformation $\hat{\Delta}(t) = -L_2 B_P \bar{\Delta}(t)$*,* (5.8) *becomes:*

$$\begin{aligned} \dot{\bar{e}}_P(t) &= B_P^{-1}(A_M + L_1)B_P \cdot \bar{e}_P + L_2 B_P \cdot \bar{\Delta}(t) + d_m(t), \\ \dot{\bar{\Delta}}(t) &= \bar{e}_P(t), \\ \hat{\Delta}(t) &= -L_2 B_P \cdot \bar{\Delta}(t). \end{aligned} \tag{5.9}$$

By defining $a_0 = -L_2 B_P$ *and* $a_1 = -B_P^{-1}(A_M + L_1)B_P$*, one observes that* (5.9) *establishes the following relation in the frequency-domain between the input* $d_m(t)$ *and the output* $\hat{\Delta}(t)$*:*

$$\hat{\Delta}(s) = \frac{a_0}{s^2 + a_1 s + a_0} \cdot d_m(s). \tag{5.10}$$

Even though a_0 *and* a_1 *may be freely chosen by choosing* L_1 *and* L_2 *, this implies that the LESO may only realize the transfer function characteristics of a PT2 element.*

The preceding example showed that the LESO may not in general realize an arbitrary transfer function characteristic between the input $\boldsymbol{d}_m(t)$ and the disturbance estimate $\hat{\boldsymbol{\Delta}}(t)$. For the first-order example, this does not seem overly restrictive. However, similar results also hold in case of a plant with more than one state and one input ($n \geq 2$ and $m = 1$), as shown in the next example:

Example 5.2. *For the demonstration of the capabilities of the LESO, consider the same short-period approximation* $(\boldsymbol{A}_P, \boldsymbol{B}_P \cdot \Lambda)$ *and the same reference model* $(\boldsymbol{A}_M, \boldsymbol{B}_P \cdot \boldsymbol{K}_r)$ *as in Example 3.6.*

In order to achieve approximate MRC, the LESO (5.3) *and the control law* (5.4) *are used. A suitable value of the feedforward gain* K_r *has already been determined during the derivation of the reference model in Example 3.6. The observer gains* $\boldsymbol{L}_1$ *and* $\boldsymbol{L}_2$ *are determined by pole placement using the* `place` *command of the Control System Toolbox of MATLAB® 2014a. The desired pole locations are chosen as* -20 *and* $-14.14 \pm 14.14j$*, leading to the observer gains*

$$\boldsymbol{L}_1 = \begin{bmatrix} -17.5825 & -0.9125 \\ 5.3217 & -26.3135 \end{bmatrix}, \qquad \boldsymbol{L}_2 = \begin{bmatrix} 0.0000 & 18.6894 \end{bmatrix}. \tag{5.11}$$

Figure 5.1 exemplary shows the response of this controller to a $5°$ *square wave command. Clearly, the LESO-based controller achieves approximate MRC. This performance is due to the capability of the LESO to correctly estimate the true disturbance signal* $d_m(t)$*. By speeding up the LESO, closer-tracking of the reference model is also possible. For that, the eigenfrequencies of the poles have to be further increased.*

The transfer function relation between the true disturbance $d_m(t)$ *and its disturbance estimate* $\hat{\Delta}(t)$ *follows from the error dynamics* (5.6) *and is given by*

$$\hat{\Delta}(s) = \frac{399.88 \cdot (s+20)}{(s+20) \cdot (s^2 + 28.28s + 399.9)} \cdot d_m(s). \tag{5.12}$$

It is interesting to notice that this transfer function possesses a zero, which exactly cancels one of the poles of the error dynamics. Hence, the LESO effectively realizes a PT2 relation between the true disturbance $d_m(t)$ *and its estimate* $\hat{\Delta}(t)$*.*

The previous example highlighted that the LESO design leads to zeros in the transfer function form the true disturbance $d_m(t)$ to its estimate $\hat{\Delta}(t)$. This zero was benign in the sense that it canceled with a pole of the latter transfer function. For this reason, the LESO again realized a PT2 relation between the true disturbance $d_m(t)$ and its estimate $\hat{\Delta}(t)$. Notice however that the location of the zero depends on the observer design technique and is not guaranteed to cancel with a pole of the error dynamics.

In the subsequent example, a similar analysis is conducted in case of a MIMO uncertainty, in which case the latter transfer function becomes a transfer function matrix.

Example 5.3. *In order to demonstrate the effects in case of a MIMO uncertainty, a LESO is to be designed which may also estimate unmatched uncertainties. Nevertheless, the plant and the reference model are equivalently chosen as in Example 5.2.*

In order to estimate unmatched uncertainties, assume that the input matrix $\boldsymbol{B}_P$ *has full rank (Assumption 3.6). Hence, a complementary matrix* $\bar{\boldsymbol{B}}_P$ *exists due to Remark 3.2 such that* $\boldsymbol{B} = \begin{bmatrix} \boldsymbol{B}_P & \bar{\boldsymbol{B}}_P \end{bmatrix}$ *has full rank. Following the same argument as during the*

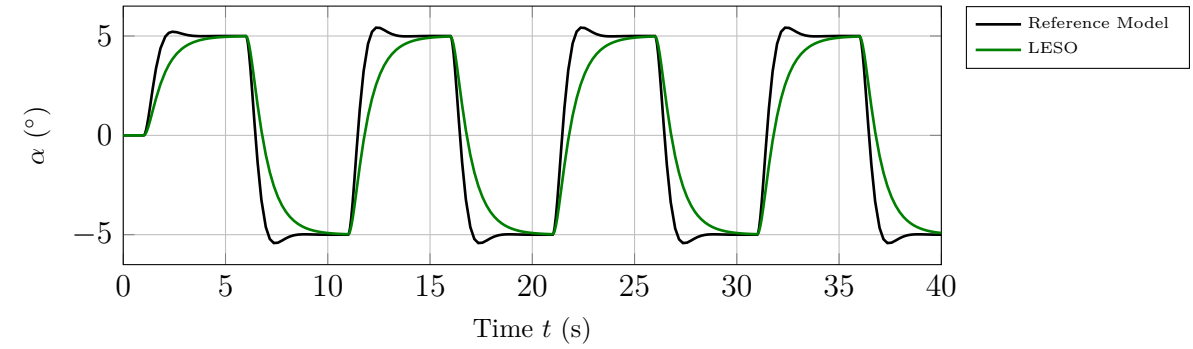

(a) Angle-Of-Attack α

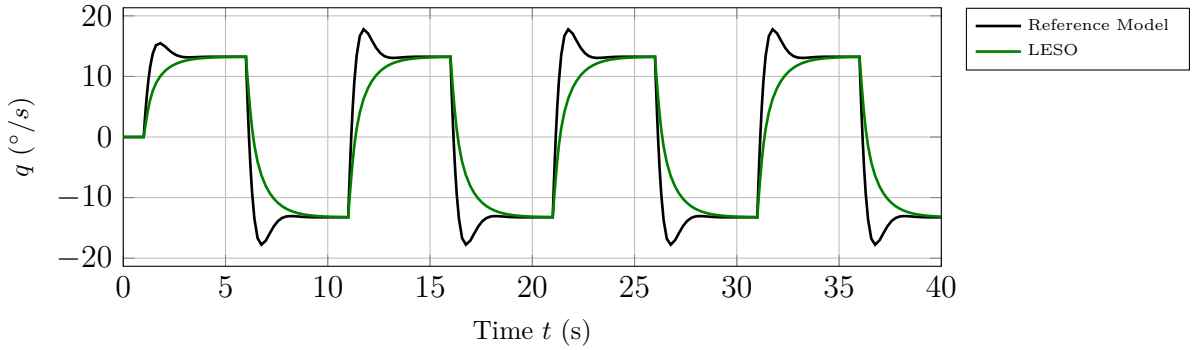

(b) Pitch Rate q

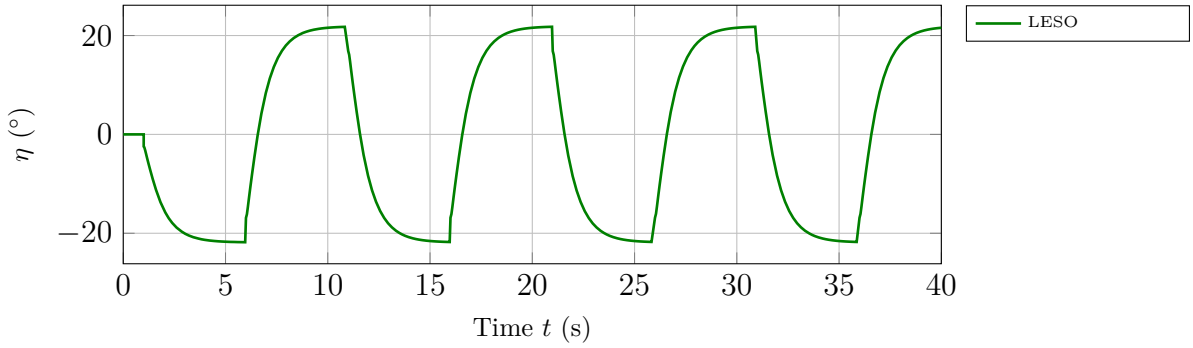

(c) Elevator Deflection η

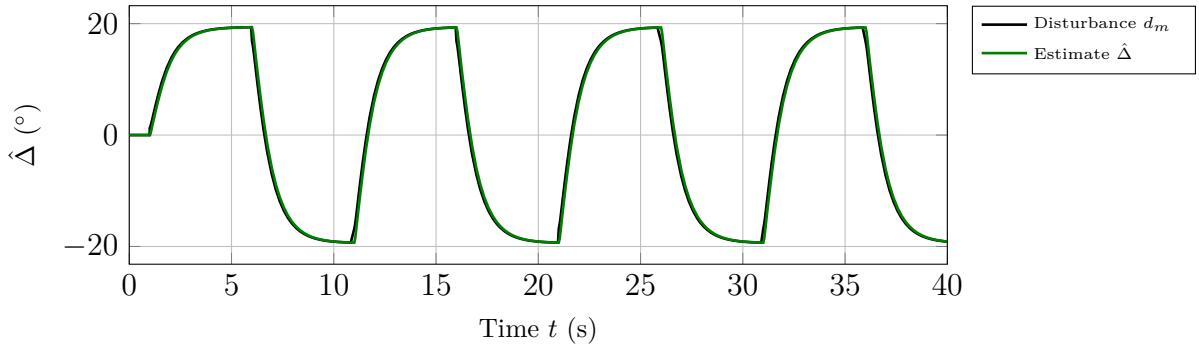

(d) Uncertainty Estimation

Figure 5.1: Exemplary response of the LESO from Example 5.2 for $\lambda_\alpha = \lambda_q = 1$ and $\lambda_\eta = 0.5$ to a $5°$ square wave command.

derivation of the LESO for matched uncertainties, the plant representation

$$\begin{aligned} \dot{\boldsymbol{x}}_P(t) &= \boldsymbol{A}_M \boldsymbol{x}_P(t) + \boldsymbol{B}_P \boldsymbol{u}(t) + \boldsymbol{B} \cdot \boldsymbol{d}(\boldsymbol{x}_P(t), t), \\ \boldsymbol{d}(\boldsymbol{x}_P(t), t) &= \boldsymbol{B}^{-1}\left(\boldsymbol{B}_P(\boldsymbol{\Lambda} - \boldsymbol{I})\boldsymbol{u}(t) + (\boldsymbol{A}_P - \boldsymbol{A}_M) \cdot \boldsymbol{x}_P(t)\right) \end{aligned} \tag{5.13}$$

and the LESO

$$\begin{aligned} \dot{\hat{\boldsymbol{x}}}_P(t) &= \boldsymbol{A}_M \hat{\boldsymbol{x}}_P(t) + \boldsymbol{B}_P \boldsymbol{u}(t) + \boldsymbol{B}\hat{\boldsymbol{\Delta}}(t) + \boldsymbol{L}_1 \cdot \boldsymbol{e}_P(t), \\ \dot{\hat{\boldsymbol{\Delta}}}(t) &= \boldsymbol{L}_2 \cdot \boldsymbol{e}_P(t), \end{aligned} \tag{5.14}$$

follow, where $\boldsymbol{L}_1 \in \mathbb{R}^{n\times n}$ and $\boldsymbol{L}_2 \in \mathbb{R}^{n\times n}$ are the observer gains.

Choose $\bar{\boldsymbol{B}}_P^T = \begin{bmatrix} 1 & 0 \end{bmatrix}$. The observer gains $\boldsymbol{L}_1$ and $\boldsymbol{L}_2$ are once again determined using pole placement using the `place` *command of the Control System Toolbox of MATLAB® 2014a. The desired pole locations are chosen as $-14.14 \pm 14.14j$ and $-15 \pm 15j$, leading to the observer gains*

$$\boldsymbol{L}_1 = \begin{bmatrix} -26.4113 & -1.4776 \\ 4.1842 & -27.4846 \end{bmatrix}, \qquad \boldsymbol{L}_2 = \begin{bmatrix} 1.5492 & 20.2845 \\ -415.8727 & -16.4672 \end{bmatrix}. \tag{5.15}$$

The transfer function matrix from $\boldsymbol{d}(\boldsymbol{x}_P(t), t)$ to $\hat{\boldsymbol{\Delta}}(t)$ follows from the error dynamics $\dot{\boldsymbol{e}}_P(t) = \dot{\hat{\boldsymbol{x}}}_P(t) - \dot{\boldsymbol{x}}_P(t)$ and is now given by

$$\hat{\boldsymbol{\Delta}}(s) = \frac{\begin{bmatrix} 434.01 \cdot (s^2 + 28.79s + 414.6) & -1.5492 \cdot s \cdot (s + 14.56) \\ -352.33 \cdot s \cdot (s + 14.56) & 415.87 \cdot (s^2 + 29.41s + 432.7) \end{bmatrix}}{(s^2 + 28.28s + 399.9) \cdot (s^2 + 30s + 450)} \cdot \boldsymbol{d}(s). \tag{5.16}$$

Clearly, the channels of this transfer function matrix are not decoupled. That is, the first component of $\boldsymbol{d}(\boldsymbol{x}_P(t), t)$ influences the estimate of the second component and vice versa. Especially the channel from the first component of $\boldsymbol{d}(\boldsymbol{x}_P(t), t)$ (matched uncertainty) to the second component of $\hat{\boldsymbol{\Delta}}$ (unmatched uncertainty estimate) shows a strong cross-coupling.

The previous example has shown that a LESO design may lead to undesirable cross-couplings between different disturbance estimate channels. Ideally, one would like to choose the zeros of the transfer functions associated with the cross-coupling channels in such a way that they cancel with the poles (of the error dynamics), leading to perfectly decoupled disturbance estimates. An appropriate design of the observer gains $\boldsymbol{L}_1$ and $\boldsymbol{L}_2$ is however non-trivial. This problem motivates the Modified LESO, which will be introduced in the upcoming section. By adding an additional degree of freedom, cross-couplings may be easily avoided. Furthermore, an appropriate modification is presented which realizes a strictly proper transfer function of *arbitrary degree* between the disturbance signal and its estimate.

5.2 The Modified Linear Extended State Observer

In the previous section, the classical LESO has been introduced. Together with the simple control law (5.4), the LESO achieves MRC in the presence of parametric uncertainties without resorting to nonlinear control methods such as MRAC. For this, the conventional LESO transforms the problem of disturbance estimation to a problem of state estimation, which is solved using classical Luenberger observer theory. By shifting the perspective from state estimation to transfer function properties, one may recognize the filter structure, which is implicitly realized by the LESO, as shown in (5.7). Examples 5.1-5.3 demonstrate that the LESO may only realize certain strictly proper low-pass filters. However, it has already been noted in the context of $\mathcal{L}_1$-AC that the choice of the low-pass filter, which shapes the frequency content of the disturbance estimate, is of crucial importance. In case of flight control problems, it might for example be desirable to obtain a disturbance estimate, which attenuates the frequencies of the structural modes of the aircraft. Since the filter transfer function of a LESO is implicitly determined by the observer design and only some low-pass filter transfer functions may be realized, such a design is hard to obtain.

To overcome these limitations, the MLESO is introduced in this section. As compared to the LESO, the MLESO exploits an additional design parameter at the disturbance estimate output of the observer. Using this design parameter, arbitrary strictly-proper low-pass transfer functions may be realized between the unknown disturbance input and the known disturbance estimate output. Similar to the LESO, this section proposes a MLESO, which is well suited for the approximate MRC problem.

Consider the plant (3.1) and let Assumptions 3.1 (state feedback), 3.2 (positive definite control effectiveness), 3.3 (Lipschitz condition), 3.6 (full-rank $\boldsymbol{B}_P$) hold. Due to Assumption 3.6, the plant (3.1) admits the alternative representation (3.15):

$$\begin{aligned}\dot{\boldsymbol{x}}_P(t) = \boldsymbol{A}_M \boldsymbol{x}_P(t) + \boldsymbol{B}_P\left(\boldsymbol{\Lambda}\boldsymbol{u}(t) + \boldsymbol{\Theta}_{m,x}^{*}\boldsymbol{x}_P(t) + \boldsymbol{f}_m(\boldsymbol{x}_P(t),t)\right) \\ + \bar{\boldsymbol{B}}_P\left(\boldsymbol{\Theta}_{um,x}^{*}\boldsymbol{x}_P(t) + \boldsymbol{f}_{um}(\boldsymbol{x}_P(t),t)\right).\end{aligned} \tag{5.17}$$

Adding and subtracting $\boldsymbol{B}_P \cdot \boldsymbol{u}(t)$ enables to separate (5.17) into a desired plant model and an unknown disturbance $\boldsymbol{d}(\boldsymbol{x}_P(t),t)$:

$$\dot{\boldsymbol{x}}_P(t) = \boldsymbol{A}_M \boldsymbol{x}_P(t) + \boldsymbol{B}_P \cdot \boldsymbol{u}(t) + \boldsymbol{B} \cdot \boldsymbol{d}(\boldsymbol{x}_P(t),t), \tag{5.18}$$

$$\begin{aligned}\boldsymbol{d}(\boldsymbol{x}_P(t),t) &\triangleq \begin{bmatrix}\boldsymbol{d}_m(\boldsymbol{x}_P(t),t)\\ \boldsymbol{d}_{um}(\boldsymbol{x}_P(t),t)\end{bmatrix} \\ &\triangleq \begin{bmatrix}(\boldsymbol{\Lambda}-\boldsymbol{I})\cdot\boldsymbol{u}(t) + \boldsymbol{\Theta}_{m,x}^{*}\boldsymbol{x}_P(t) + \boldsymbol{f}_m(\boldsymbol{x}_P(t),t)\\ \boldsymbol{\Theta}_{um,x}^{*}\boldsymbol{x}_P(t) + \boldsymbol{f}_{um}(\boldsymbol{x}_P(t),t)\end{bmatrix},\end{aligned} \tag{5.19}$$

where $\boldsymbol{B}$ was defined in (3.13) and, where $\boldsymbol{d}_m : \mathbb{R}^n \times \mathbb{R}_+ \to \mathbb{R}^m$ and $\boldsymbol{d}_{um} : \mathbb{R}^n \times \mathbb{R}_+ \to \mathbb{R}^{n-m}$ are the matched and unmatched disturbance signals, respectively. Even though

$\boldsymbol{d}_m(\boldsymbol{x}_P(t), t)$ and $\boldsymbol{d}_{um}(\boldsymbol{x}_P(t), t)$ are state-dependent by definition, they will subsequently be treated like exogenous, i.e. not state-dependent, disturbances. In order to stress this important idea, $\boldsymbol{d}_m(t) \triangleq \boldsymbol{d}_m(\boldsymbol{x}_P(t), t)$, $\boldsymbol{d}_{um}(t) \triangleq \boldsymbol{d}_{um}(\boldsymbol{x}_P(t), t)$ as well as $\boldsymbol{d}(t) \triangleq \boldsymbol{d}(\boldsymbol{x}_P(t), t)$ will be used to refer to these signals. Furthermore, notice that $\boldsymbol{d}_{um}(\boldsymbol{x}_P(t), t) = 0 \ \ \forall t \geq 0$ will hold, if the matching condition of Assumption 3.5 is satisfied.

Subsequently, Sections 5.2.1 and 5.2.2 propose the first order and the higher order MLESO, respectively, for the plant (5.17). Here, the order of the MLESO specifies the order of the strictly proper LTI transfer function that the MLESO realizes (for each disturbance channel).

Notice that the remainder of this section (namely Subsections 5.2.1 and 5.2.2) focuses on the MLESO itself. Thus, they only derive the disturbance estimator. For the respective control laws, which make use of the disturbance estimates, please refer to Sections 5.3 and 5.4. If the matching condition of Assumption 3.5 is satisfied, Section 5.3 presents a control law in order to achieve approximate tracking of the *states* of the reference model (3.4). Since the matching conditions hold, this control law only makes use of the estimate of the matched disturbance signal $\boldsymbol{d}_m(\boldsymbol{x}_P(t), t)$. If the matching conditions do *not* hold (see Section 3.1.2), an appropriately modified control law is given in Section 5.4, which achieves approximate tracking of the *outputs* of the reference model (3.4).

5.2.1 First Order MLESO

This section introduces the first order MLESO. Unlike the conventional LESO, this observer is derived from a signal-based point of view and does not require an extended state. Even though the term "extended" state observer may be misleading in the first order case, this terminology is introduced since extended states will appear in case of MLESOs of order $k \geq 2$.

Now, let $\boldsymbol{L}_0 \in \mathbb{R}^{n \times n}$ and $\boldsymbol{M}_0 \in \mathbb{R}^{n \times n}$ be an observer gain and an output gain, respectively. Then, the first order MLESO for the plant (5.18) is given by:

$$\begin{aligned} \dot{\hat{\boldsymbol{x}}}_P(t) &= \boldsymbol{A}_M \cdot \boldsymbol{x}_P(t) + \boldsymbol{B}_P \cdot \boldsymbol{u}(t) + \boldsymbol{L}_0 \cdot \boldsymbol{e}_P(t), \\ \hat{\boldsymbol{d}}(t) &= \boldsymbol{M}_0 \cdot \boldsymbol{e}_P(t), \end{aligned} \tag{5.20}$$

where $\hat{\boldsymbol{x}}_P : \mathbb{R}_+ \to \mathbb{R}^n$, $\boldsymbol{e}_P(t) \triangleq \hat{\boldsymbol{x}}_P(t) - \boldsymbol{x}_P(t)$ and $\hat{\boldsymbol{d}} : \mathbb{R}_+ \to \mathbb{R}^n$ denote the observer state vector, the observer error and the observer output (the disturbance estimate output), respectively. Furthermore, assume that the MLESO is initialized such that $\hat{\boldsymbol{x}}_P(0) = \boldsymbol{x}_P(0)$ holds. While the structure of (5.20) is rather general, the subsequent derivation will present a methodology for choosing the design parameters $\boldsymbol{L}_0$ and $\boldsymbol{M}_0$ of the MLESO in such a way that the output $\hat{\boldsymbol{d}}(t)$ of the MLESO provides an estimate of the unknown disturbance $\boldsymbol{d}(t)$.

For this, consider the error dynamics of the MLESO:

$$\begin{aligned} \dot{\boldsymbol{e}}_P(t) &= \dot{\hat{\boldsymbol{x}}}_P(t) - \dot{\boldsymbol{x}}_P(t) = \boldsymbol{L}_0 \cdot \boldsymbol{e}_P(t) - \boldsymbol{B} \cdot \boldsymbol{d}(t), \\ \hat{\boldsymbol{d}}(t) &= \boldsymbol{M}_0 \cdot \boldsymbol{e}_P(t). \end{aligned} \tag{5.21}$$

Utilizing the transformation $\boldsymbol{e}_P(t) = -\boldsymbol{B} \cdot \bar{\boldsymbol{e}}_P(t)$, the error dynamics become

$$\begin{aligned} \dot{\bar{\boldsymbol{e}}}_P(t) &= \boldsymbol{B}^{-1}\boldsymbol{L}_0\boldsymbol{B} \cdot \bar{\boldsymbol{e}}_P(t) + \boldsymbol{d}(t), \\ \hat{\boldsymbol{d}}(t) &= -\boldsymbol{M}_0\boldsymbol{B} \cdot \bar{\boldsymbol{e}}_P(t). \end{aligned} \tag{5.22}$$

Clearly, the error dynamics (5.22) may realize the structure of a n-dimensional, first-order lag element with input $\boldsymbol{d}(t)$ and output $\hat{\boldsymbol{d}}(t)$. Since $\boldsymbol{B}$ has full rank, the dynamics and the DC gain of this lag element may be arbitrarily chosen. Usually, one is interested in a decoupled estimate of the uncertainties, i.e. the i-th component of $\boldsymbol{d}(t)$ should only influence the i-th component of the disturbance estimate $\hat{\boldsymbol{d}}(t)$. Furthermore, the estimate should have a DC gain of one. Thus, a natural choice for the design parameters $\boldsymbol{L}_0$ and $\boldsymbol{M}_0$ of the first order MLESO is such that

$$\begin{aligned} \boldsymbol{B}^{-1}\boldsymbol{L}_0\boldsymbol{B} &= -\boldsymbol{A}_0, \\ -\boldsymbol{M}_0\boldsymbol{B} &= \boldsymbol{A}_0 \end{aligned} \tag{5.23}$$

hold, where

$$\boldsymbol{A}_0 \triangleq \begin{bmatrix} a_{0,11} & \dots & 0 \\ \vdots & \ddots & \vdots \\ 0 & \dots & a_{0,nn} \end{bmatrix} \tag{5.24}$$

is a positive definite, diagonal matrix. The elements $a_{0,ii},\ i = 1, ..., n$ of $\boldsymbol{A}_0$ specify the bandwidth with which the MLESO estimates the disturbance $\boldsymbol{d}(t)$. Solving (5.23) for $\boldsymbol{L}_0$ and $\boldsymbol{M}_0$ yields

$$\begin{aligned} \boldsymbol{L}_0 &= -\boldsymbol{B}\boldsymbol{A}_0\boldsymbol{B}^{-1}, \\ \boldsymbol{M}_0 &= -\boldsymbol{A}_0\boldsymbol{B}^{-1}. \end{aligned} \tag{5.25}$$

Using the design parameters (5.25) and due to the assumption $\boldsymbol{e}_P(0) = \hat{\boldsymbol{x}}_P(0) - \boldsymbol{x}_P(0) = \boldsymbol{0}$, the first-order MLESO establishes the following relationship between the uncertainty $\boldsymbol{d}(t)^T = \begin{bmatrix} d_1(t) & \dots & d_n(t) \end{bmatrix}$ and its estimate $\hat{\boldsymbol{d}}(t)^T = \begin{bmatrix} \hat{d}_1(t) & \dots & \hat{d}_n(t) \end{bmatrix}$:

$$\begin{aligned} \hat{d}_i(s) &= C_{d,i}(s) \cdot d_i(s) \quad \text{with} \\ C_{d,i}(s) &= \frac{a_{0,ii}}{s + a_{0,ii}}, \qquad i = 1, ..., n. \end{aligned} \tag{5.26}$$

Even though (5.26) holds, it has to be stressed that the observer (5.20) does not rely on the knowledge of the unknown signal $\boldsymbol{d}(t)$, but only uses measurements of the state vector $\boldsymbol{x}_P(t)$. Furthermore, since $(-\boldsymbol{A}_0)$ is Hurwitz, the MLESO will yield a bounded estimate $\hat{\boldsymbol{d}}(t)$, if $\boldsymbol{d}(t)$ is bounded. However, notice that boundedness of $\boldsymbol{d}(t)$ has not yet been proven.

5.2.2 Second and Higher Order MLESO

The first order MLESO establishes the relationship (5.26) between the uncertainty $\boldsymbol{d}(t)$ and its estimate $\hat{\boldsymbol{d}}(t)$. Depending on the application, higher filter orders may however be desirable. These can be achieved using a higher order MLESO, where the observer is augmented with additional states. A k-th order MLESO for the plant (5.18) is given by:

$$\begin{aligned}
\dot{\hat{\boldsymbol{\Delta}}}_0(t) &= \hat{\boldsymbol{\Delta}}_1(t), \\
\dot{\hat{\boldsymbol{\Delta}}}_1(t) &= \hat{\boldsymbol{\Delta}}_2(t), \\
&\vdots \\
\dot{\hat{\boldsymbol{\Delta}}}_{k-2}(t) &= \boldsymbol{e}_P(t), \\
\dot{\hat{\boldsymbol{x}}}_P(t) &= \boldsymbol{A}_M \cdot \boldsymbol{x}_P(t) + \boldsymbol{B}_P \cdot \boldsymbol{u}(t) + \boldsymbol{L}_0 \cdot \hat{\boldsymbol{\Delta}}_0(t) + \ldots + \boldsymbol{L}_{k-2} \cdot \hat{\boldsymbol{\Delta}}_{k-2}(t) + \boldsymbol{L}_{k-1} \cdot \boldsymbol{e}_P(t), \\
\hat{\boldsymbol{d}}(t) &= \boldsymbol{M}_0 \cdot \hat{\boldsymbol{\Delta}}_0(t) + \ldots + \boldsymbol{M}_{k-2} \cdot \hat{\boldsymbol{\Delta}}_{k-2}(t) + \boldsymbol{M}_{k-1} \cdot \boldsymbol{e}_P(t),
\end{aligned} \tag{5.27}$$

where $\hat{\boldsymbol{\Delta}}_j : \mathbb{R}_+ \to \mathbb{R}^n,\ j = 0, \ldots, k-2$ are the additional states and where $\boldsymbol{L}_j \in \mathbb{R}^{n \times n}$ and $\boldsymbol{M}_j \in \mathbb{R}^{n \times n},\ j = 0, ..., k-1$ are the design parameters of the MLESO. Furthermore, assume that the MLESO is initialized such that $\hat{\boldsymbol{x}}_P(0) = \boldsymbol{x}_P(0)$ and $\hat{\boldsymbol{\Delta}}_j(0) = \boldsymbol{0}$ hold. The error dynamics become:

$$\begin{aligned}
\dot{\hat{\boldsymbol{\Delta}}}_0(t) &= \hat{\boldsymbol{\Delta}}_1(t), \\
\dot{\hat{\boldsymbol{\Delta}}}_1(t) &= \hat{\boldsymbol{\Delta}}_2(t), \\
&\vdots \\
\dot{\hat{\boldsymbol{\Delta}}}_{k-2}(t) &= \boldsymbol{e}_P(t), \\
\dot{\boldsymbol{e}}_P(t) &= \boldsymbol{L}_0 \cdot \hat{\boldsymbol{\Delta}}_0(t) + \ldots + \boldsymbol{L}_{k-2} \cdot \hat{\boldsymbol{\Delta}}_{k-2}(t) + \boldsymbol{L}_{k-1} \cdot \boldsymbol{e}_P(t) - \boldsymbol{B} \cdot \boldsymbol{d}(t), \\
\hat{\boldsymbol{d}}(t) &= \boldsymbol{M}_0 \cdot \hat{\boldsymbol{\Delta}}_0(t) + \ldots + \boldsymbol{M}_{k-2} \cdot \hat{\boldsymbol{\Delta}}_{k-2}(t) + \boldsymbol{M}_{k-1} \cdot \boldsymbol{e}_P(t).
\end{aligned} \tag{5.28}$$

Utilizing the transformations $\boldsymbol{e}_P(t) = -\boldsymbol{B} \cdot \bar{\boldsymbol{e}}_P(t)$ and $\hat{\boldsymbol{\Delta}}_j(t) = -\boldsymbol{B} \cdot \bar{\boldsymbol{\Delta}}_j(t),\ j = 0, ..., k-2$, the error dynamics become

$$\begin{aligned}
\dot{\bar{\boldsymbol{\Delta}}}_0(t) &= \bar{\boldsymbol{\Delta}}_1(t), \\
\dot{\bar{\boldsymbol{\Delta}}}_1(t) &= \bar{\boldsymbol{\Delta}}_2(t), \\
&\vdots \\
\dot{\bar{\boldsymbol{\Delta}}}_{k-2}(t) &= \bar{\boldsymbol{e}}_P(t), \\
\dot{\bar{\boldsymbol{e}}}_P(t) &= \boldsymbol{B}^{-1}\boldsymbol{L}_0\boldsymbol{B} \cdot \bar{\boldsymbol{\Delta}}_0(t) + \ldots + \boldsymbol{B}^{-1}\boldsymbol{L}_{k-2}\boldsymbol{B} \cdot \bar{\boldsymbol{\Delta}}_{k-2}(t) + \boldsymbol{B}^{-1}\boldsymbol{L}_{k-1}\boldsymbol{B} \cdot \bar{\boldsymbol{e}}_P(t) + \boldsymbol{d}(t), \\
\hat{\boldsymbol{d}}(t) &= -\boldsymbol{M}_0\boldsymbol{B} \cdot \bar{\boldsymbol{\Delta}}_0(t) - \ldots - \boldsymbol{M}_{k-2}\boldsymbol{B} \cdot \bar{\boldsymbol{\Delta}}_{k-2}(t) - \boldsymbol{M}_{k-1}\boldsymbol{B} \cdot \bar{\boldsymbol{e}}_P(t).
\end{aligned} \tag{5.29}$$

Notice that the structure of (5.29) resembles the controllability canonical form of a strictly proper filter with input $\boldsymbol{d}(t)$ and output $\hat{\boldsymbol{d}}(t)$. Since $\boldsymbol{B}$ has full rank and since

$\boldsymbol{e}_P(0) = \hat{\boldsymbol{x}}_P(0) - \boldsymbol{x}_P(0) = \boldsymbol{0}$ and $\hat{\boldsymbol{\Delta}}_j(0) = \boldsymbol{0}$ are assumed, one may choose the design parameters of the MLESO such that the following relationship between the uncertainty $\boldsymbol{d}(t)$ and its estimate $\hat{\boldsymbol{d}}(t)$ holds:

$$\begin{aligned} \hat{d}_i(s) &= C_{d,i}(s) \cdot d_i(s) \quad \text{with} \\ C_{d,i}(s) &= \frac{b_{k-1,ii} \cdot s^{k-1} + ... + b_{1,ii} \cdot s + b_{0,ii}}{s^k + a_{k-1,ii} \cdot s^{k-1} + ... + a_{1,ii} \cdot s + a_{0,ii}}, \qquad i = 1, ..., n. \end{aligned} \tag{5.30}$$

In order to ensure a DC gain of one, the choice of the filter has to satisfy $b_{0,ii} = a_{0,ii}$. Furthermore, the coefficients $a_{j,ii},\ j = 0, ..., k-1, i = 1, ..., n$ in (5.30) have to be chosen such that the denominator polynomial is Hurwitz for each $i = 1, ..., n$. Define the diagonal matrices

$$\boldsymbol{A}_j \triangleq \begin{bmatrix} a_{j,11} & \dots & 0 \\ \vdots & \ddots & \vdots \\ 0 & \dots & a_{j,nn} \end{bmatrix}, \quad j = 0, ..., k-1, \tag{5.31}$$

$$\boldsymbol{B}_j \triangleq \begin{bmatrix} b_{j,11} & \dots & 0 \\ \vdots & \ddots & \vdots \\ 0 & \dots & b_{j,nn} \end{bmatrix}, \quad j = 1, ..., k-1. \tag{5.32}$$

For (5.30) to hold (with $b_{0,ii} = a_{0,ii}$), the design parameters $\boldsymbol{L}_j$ and $\boldsymbol{M}_j$ have to be chosen such that

$$\boldsymbol{B}^{-1}\boldsymbol{L}_j\boldsymbol{B} = -\boldsymbol{A}_j, \quad j = 0, ..., k-1, \tag{5.33}$$

$$-\boldsymbol{M}_j\boldsymbol{B} = \boldsymbol{B}_j, \quad j = 1, ..., k-1, \tag{5.34}$$

$$-\boldsymbol{M}_0\boldsymbol{B} = \boldsymbol{A}_0 \tag{5.35}$$

are satisfied. Since $\boldsymbol{A}_j$ and $\boldsymbol{B}_j$ are diagonal matrices, (5.29) may be equivalently represented in the frequency-domain by

$$\begin{aligned} \hat{\boldsymbol{d}}(s) &= \boldsymbol{C}_d(s) \cdot \boldsymbol{d}(s), \\ \boldsymbol{C}_d(s) &= \begin{bmatrix} C_{d,1}(s) & \dots & 0 \\ \vdots & \ddots & \vdots \\ 0 & \dots & C_{d,n}(s) \end{bmatrix} \\ &= (\boldsymbol{B}_{k-1} \cdot s^{k-1} + \ldots + \boldsymbol{B}_1 s + \boldsymbol{A}_0) \cdot (\boldsymbol{I} \cdot s^k + \boldsymbol{A}_{k-1} \cdot s^{k-1} + \ldots + \boldsymbol{A}_1 \cdot s + \boldsymbol{A}_0)^{-1}. \end{aligned} \tag{5.36}$$

Since the coefficients of the transfer function in (5.30) are chosen to be Hurwitz, the MLESO will yield a bounded estimate $\hat{\boldsymbol{d}}(t)$, if the true uncertainty $\boldsymbol{d}(t)$ is bounded. However, notice that boundedness of $\boldsymbol{d}(t)$ has not yet been proven.

5.3 Control Law for Matched Uncertainties

The MLESO yields an estimate $\hat{\boldsymbol{d}}(t)$ of matched as well as unmatched uncertainties. Similar to (5.19), $\hat{\boldsymbol{d}}(t)$ may be partitioned into a matched and an unmatched portion by

$\hat{\boldsymbol{d}}(t)^T = \begin{bmatrix}\hat{\boldsymbol{d}}_m(t)^T & \hat{\boldsymbol{d}}_{um}(t)^T\end{bmatrix}$ with $\hat{\boldsymbol{d}}_m : \mathbb{R}_+ \to \mathbb{R}^m$ and $\hat{\boldsymbol{d}}_{um} : \mathbb{R}_+ \to \mathbb{R}^{n-m}$. Based on the partition introduced for $\boldsymbol{d}(t)$ and $\hat{\boldsymbol{d}}(t)$, (5.36) admits the partition:

$$\begin{aligned}\hat{\boldsymbol{d}}_m(s) &= \boldsymbol{C}_m(s) \cdot \boldsymbol{d}_m(s),\\ \hat{\boldsymbol{d}}_{um}(s) &= \boldsymbol{C}_{um}(s) \cdot \boldsymbol{d}_{um}(s),\end{aligned} \tag{5.37}$$

where

$$\begin{aligned}\boldsymbol{C}_m(s) &= \begin{bmatrix} C_{d,1}(s) & \dots & 0 \\ \vdots & \ddots & \vdots \\ 0 & \dots & C_{d,m}(s)\end{bmatrix} \\ &= (\boldsymbol{B}_{k-1,m} \cdot s^{k-1} + \ldots + \boldsymbol{B}_{1,m}s + \boldsymbol{A}_{0,m}) \cdot \ldots \\ &\qquad (\boldsymbol{I} \cdot s^k + \boldsymbol{A}_{k-1,m} \cdot s^{k-1} + \ldots + \boldsymbol{A}_{1,m} \cdot s + \boldsymbol{A}_{0,m})^{-1},\end{aligned} \tag{5.38}$$

$$\begin{aligned}\boldsymbol{C}_{um}(s) &= \begin{bmatrix} C_{d,m+1}(s) & \dots & 0 \\ \vdots & \ddots & \vdots \\ 0 & \dots & C_{d,n}(s)\end{bmatrix} \\ &= (\boldsymbol{B}_{k-1,um} \cdot s^{k-1} + \ldots + \boldsymbol{B}_{1,um}s + \boldsymbol{A}_{0,um}) \cdot \ldots \\ &\qquad (\boldsymbol{I} \cdot s^k + \boldsymbol{A}_{k-1,um} \cdot s^{k-1} + \ldots + \boldsymbol{A}_{1,um} \cdot s + \boldsymbol{A}_{0,um})^{-1}\end{aligned} \tag{5.39}$$

are the transfer function matrices associated with matched and unmatched uncertainties. In (5.38) and (5.39), the matrices $\boldsymbol{A}_{j,m}, \boldsymbol{B}_{j,m} \in \mathbb{R}^{m\times m}$, $\boldsymbol{A}_{j,um}, \boldsymbol{B}_{j,um} \in \mathbb{R}^{(n-m)\times(n-m)}$ are partitions of (5.31) and (5.32), respectively:

$$\begin{aligned}\boldsymbol{A}_j &= \begin{bmatrix}\boldsymbol{A}_{j,m} & \boldsymbol{0} \\ \boldsymbol{0} & \boldsymbol{A}_{j,um}\end{bmatrix}, \quad j = 0, ..., k-1,\\ \boldsymbol{B}_j &= \begin{bmatrix}\boldsymbol{B}_{j,m} & \boldsymbol{0} \\ \boldsymbol{0} & \boldsymbol{B}_{j,um}\end{bmatrix}, \quad j = 1, ..., k-1.\end{aligned} \tag{5.40}$$

Now, let the matching condition of Assumption 3.5 hold. In this case, $\boldsymbol{d}_{um}(t) = \boldsymbol{0}$ holds and hence, (5.37) implies $\hat{\boldsymbol{d}}_{um}(t) = \boldsymbol{0}$. For this reason, the outputs of the MLESO associated with the unmatched uncertainties may be safely ignored. Similar to the conventional LESO, a control law to approximately solve the model following problem is given by

$$\boldsymbol{u}(t) = \boldsymbol{K}_r \cdot \boldsymbol{r}(t) - \hat{\boldsymbol{d}}_m(t). \tag{5.41}$$

The application of the control law (5.41) yields the overall control system structure displayed in Figure 5.2. By inserting the control law (5.41) into the plant representation (5.18) and exploiting $\boldsymbol{d}_{um}(t) = \boldsymbol{0}$, one obtains:

$$\dot{\boldsymbol{x}}_P(t) = \boldsymbol{A}_M \cdot \boldsymbol{x}_P(t) + \boldsymbol{B}_P\boldsymbol{K}_r \cdot \boldsymbol{r}(t) + \boldsymbol{B}_P \cdot (\boldsymbol{d}_m(t) - \hat{\boldsymbol{d}}_m(t)). \tag{5.42}$$

Clearly, the closed-loop plant dynamics are driven by the mismatch between the estimated and the actual matched uncertainty, whereas $\hat{\boldsymbol{d}}_{um}(t)$ has no influence. Given a

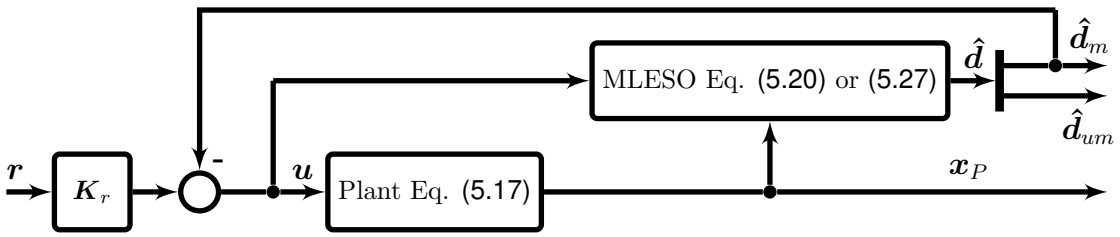

Figure 5.2: Structure of the closed-loop system with MLESO controller

sufficiently high bandwidth of the MLESO, the difference between $\boldsymbol{d}_m(t)$ and $\hat{\boldsymbol{d}}_m(t)$ will become small and hence, the plant will approximately follow the reference model (3.4). This intuitive idea is also exploited within the subsequent proof of BIBS stability, which is similar to the proof of BIBS stability of the $\mathcal{L}_1$ *Reference Model* presented in Section 3.3.1.

In order to establish closed-loop stability, the following assumption is required in addition to Assumptions 3.1, 3.2, 3.3 and 3.6, which have already been required during the derivation of the MLESO:

Assumption 5.1. *The uncertainties $\boldsymbol{\Lambda}$ and $\boldsymbol{\Theta}^*_{m,x}$ are bounded. They are guaranteed to remain within the known compact sets Ω_Λ and $\Omega_{x,m}$, i.e.*

$$\boldsymbol{\Lambda} \in \Omega_\Lambda, \qquad \boldsymbol{\Theta}^*_{m,x} \in \Omega_{x,m}. \tag{5.43}$$

The sets Ω_Λ and $\Omega_{x,m}$ may be conservative in the sense that they are supersets of the sets, in which the uncertainties will remain in reality. Furthermore, the state-dependent Lipschitz constant $K(r)$ and the bound on exogenous disturbances B, defined in Assumption 3.3, are known.

Assumption 5.1 implies that the uncertain, nonlinear function $\boldsymbol{f}_m\left(\boldsymbol{x}_P\left(t\right), t\right)$ satisfies the semi-global Lipschitz condition

$$\|\boldsymbol{f}_m(\boldsymbol{x}_1, t) - \boldsymbol{f}_m(\boldsymbol{x}_2, t)\|_\infty \leq L_m\left(r\right) \cdot \|\boldsymbol{x}_1 - \boldsymbol{x}_2\|_\infty \quad \forall\, \|\boldsymbol{x}_1\| \leq r,\ \|\boldsymbol{x}_2\| \leq r, \tag{5.44}$$

and

$$\|\boldsymbol{f}_m(\boldsymbol{0}, t)\|_\infty \leq \phi_{m,0}, \tag{5.45}$$

where $L_m\left(r\right)$ and $\phi_{m,0}$ are known constants. Similar to the proof of stability of $\mathcal{L}_1$-AC, the semi-global character of the Lipschitz condition significantly complicates the stability analysis. For this reason, Section 5.3.1 will first introduce stability conditions for the simpler case of a global Lipschitz condition. Afterwards, the more general case of a semi-global Lipschitz condition is considered in Section 5.3.2. Since the proof of BIBS stability of the MLESO is very similar to the proof of BIBS stability of the $\mathcal{L}_1$ *Reference Model*, Section 5.3.3 will comment on the relation between $\mathcal{L}_1$-AC and MLESO-based control. Furthermore, an intrinsic relation of MLESO-based control to PI control will be highlighted in Section 5.3.4.

5.3.1 Stability in Case of a Global Lipschitz Condition

In this section, assume that the semi-global Lipschitz condition of Assumption 3.3 is strengthened to a global Lipschitz condition. Consequently, the uncertain, nonlinear function $\boldsymbol{f}_m(\boldsymbol{x}_P(t), t)$ satisfies the global Lipschitz condition

$$\|\boldsymbol{f}_m(\boldsymbol{x}_1, t) - \boldsymbol{f}_m(\boldsymbol{x}_2, t)\|_\infty \leq L_m \cdot \|\boldsymbol{x}_1 - \boldsymbol{x}_2\|_\infty \tag{5.46}$$

and

$$\|\boldsymbol{f}_m(\boldsymbol{0}, t)\|_\infty \leq \phi_{m,0}, \tag{5.47}$$

where L_m and $\phi_{m,0}$ are known constants due to Assumption 5.1. Using the reverse triangle inequality, (5.46) especially yields a bound on the size of the nonlinearity, which depends linearly on $\|\boldsymbol{x}\|_\infty$, namely:

$$\|\boldsymbol{f}_m(\boldsymbol{x}, t)\|_\infty \leq L_m \cdot \|\boldsymbol{x}\|_\infty + \phi_{m,0}. \tag{5.48}$$

Using the global Lipschitz condition and following similar steps, which led to Lemma 3.20 in case of $\mathcal{L}_1$-AC, one arrives at the following theorem for BIBS:

Theorem 5.4 (BIBS Stability in Case of Matched Uncertainties and a Global Lipschitz Condition)**.** *Consider the plant* (3.1) *and let Assumptions 3.1 (state feedback), 3.2 (positive definite control effectiveness), 3.3 (Lipschitz condition), 3.5 (matching condition), 3.6 (full-rank $\boldsymbol{B}_P$) and 5.1 (bounded uncertainties) hold. Furthermore, assume that the Lipschitz condition of Assumption 3.3 has been strengthened to a global one such that* (5.46) *and* (5.47) *are satisfied. Let the initial conditions of the MLESO* (5.27) *(or* (5.20)*, respectively) be chosen such that*

$$\hat{\boldsymbol{x}}_P(0) = \boldsymbol{x}_P(0), \qquad \hat{\boldsymbol{\Delta}}_j(0) = \boldsymbol{0},\ j = 1, ..., k-1 \tag{5.49}$$

with $\|\boldsymbol{x}_P(0)\|_\infty < \infty$ hold.

If the design parameters $\boldsymbol{A}_j,\ j = 0, ...k-1$ and $\boldsymbol{B}_j,\ j = 1, ..., k-1$ of the MLESO (5.27) *(or* (5.20)*, respectively) are chosen such that*

1. *the filter $\boldsymbol{C}_m(s)$, defined in* (5.38)*, may be represented by the feedback connection*

$$\boldsymbol{C}_m(s) = (\boldsymbol{I} + \boldsymbol{K}\boldsymbol{D}(s))^{-1}\boldsymbol{K}\boldsymbol{D}(s), \tag{5.50}$$

   where $\boldsymbol{K} \in \mathbb{R}^{m\times m}$ is a feedback gain and $\boldsymbol{D} : \mathbb{C} \to \mathbb{C}^{m\times m}$ is a strictly proper transfer function matrix containing an integrator;

2. *the feedforward and feedback filters $\boldsymbol{C}_{ff}(s)$ and $\boldsymbol{C}_{fb}(s)$, defined as*

$$\begin{aligned} \boldsymbol{C}_{ff}(s) &\triangleq (\boldsymbol{I} + \boldsymbol{\Lambda}\boldsymbol{K}\boldsymbol{D}(s))^{-1}\boldsymbol{\Lambda}(\boldsymbol{I} + \boldsymbol{K}\boldsymbol{D}(s)), \\ \boldsymbol{C}_{fb}(s) &\triangleq (\boldsymbol{I} + \boldsymbol{\Lambda}\boldsymbol{K}\boldsymbol{D}(s))^{-1}\boldsymbol{\Lambda}\boldsymbol{K}\boldsymbol{D}(s), \end{aligned} \tag{5.51}$$

   are Hurwitz for all $\boldsymbol{\Lambda} \in \Omega_\Lambda$;

3. the $\mathcal{L}_1$-norm condition

$$\|\boldsymbol{G}_m(s)\cdot(\boldsymbol{I}-\boldsymbol{C}_{fb}(s))\cdot\boldsymbol{\Theta}^*_{m,x}\|_{\mathcal{L}_1}+\|\boldsymbol{G}_m(s)\cdot(\boldsymbol{I}-\boldsymbol{C}_{fb}(s))\|_{\mathcal{L}_1}\cdot L_m<1 \tag{5.52}$$

is satisfied for all $\boldsymbol{\Lambda}\in\Omega_\Lambda$, $\boldsymbol{\Theta}^*_{m,x}\in\Omega_{x,m}$, where

$$\boldsymbol{G}_m(s)\triangleq(s\boldsymbol{I}-\boldsymbol{A}_M)^{-1}\boldsymbol{B}_P, \tag{5.53}$$

then the control law (5.41) *ensures BIBS stability of the closed-loop control system consisting of the plant* (3.1)*, the control law* (5.41) *and the MLESO* (5.27) *or* (5.20)*, respectively.*

Proof. Due to Assumption 3.5, the plant (3.1) may be expressed as

$$\dot{\boldsymbol{x}}_P(t)=\boldsymbol{A}_M\boldsymbol{x}_P(t)+\boldsymbol{B}_P\left(\boldsymbol{\Lambda}\boldsymbol{u}(t)+\boldsymbol{\Theta}^*_{m,x}\boldsymbol{x}_P(t)+\boldsymbol{f}_m(\boldsymbol{x}_P(t),t)\right) \tag{5.54}$$

Since Assumption 3.5 ensures the absence of unmatched uncertainties, eq. (5.54) is equivalent to the plant representation (5.17), for which the MLESO (5.27) or (5.20) has been designed. By defining the signal

$$\boldsymbol{v}_P(t)\triangleq\boldsymbol{\Lambda}\boldsymbol{u}(t)+\boldsymbol{\Theta}^*_{m,x}\boldsymbol{x}_P(t)+\boldsymbol{f}_m(\boldsymbol{x}_P(t),t), \tag{5.55}$$

the plant (5.54) becomes

$$\dot{\boldsymbol{x}}_P(t)=\boldsymbol{A}_M\boldsymbol{x}_P(t)+\boldsymbol{B}_P\cdot\boldsymbol{v}_P(t). \tag{5.56}$$

Due to Assumptions 3.1 and 3.6, a state-feedback MLESO exists for the plant (3.1). It follows from the first condition of Theorem 5.4 and (5.37) that the MLESO ensures the relation

$$\hat{\boldsymbol{d}}_m(s)=(\boldsymbol{I}+\boldsymbol{K}\boldsymbol{D}(s))^{-1}\boldsymbol{K}\boldsymbol{D}(s)\cdot\boldsymbol{d}_m(s) \tag{5.57}$$

with $\boldsymbol{d}_m(t)$ defined in (5.19), if the initial conditions satisfy (5.49). Upon insertion of the above relation, the control law (5.41) becomes (in the frequency-domain):

$$\begin{aligned}\boldsymbol{u}(s)=\boldsymbol{K}_r\cdot\boldsymbol{r}(s)&-(\boldsymbol{I}+\boldsymbol{K}\boldsymbol{D}(s))^{-1}\boldsymbol{K}\boldsymbol{D}(s)\cdot(\boldsymbol{\Lambda}-\boldsymbol{I})\cdot\boldsymbol{u}(s)\\&-(\boldsymbol{I}+\boldsymbol{K}\boldsymbol{D}(s))^{-1}\boldsymbol{K}\boldsymbol{D}(s)\cdot\boldsymbol{\Theta}^*_{m,x}\cdot\boldsymbol{x}_P(s)\\&-(\boldsymbol{I}+\boldsymbol{K}\boldsymbol{D}(s))^{-1}\boldsymbol{K}\boldsymbol{D}(s)\cdot\mathcal{L}\{\boldsymbol{f}_m(\boldsymbol{x}_P(t),t)\}.\end{aligned} \tag{5.58}$$

Multiplying by $(\boldsymbol{I}+\boldsymbol{K}\boldsymbol{D}(s))$ from the left yields

$$\begin{aligned}(\boldsymbol{I}+\boldsymbol{K}\boldsymbol{D}(s))\cdot\boldsymbol{u}(s)=(\boldsymbol{I}+\boldsymbol{K}\boldsymbol{D}(s))\boldsymbol{K}_r\cdot\boldsymbol{r}(s)&-\boldsymbol{K}\boldsymbol{D}(s)\cdot(\boldsymbol{\Lambda}-\boldsymbol{I})\cdot\boldsymbol{u}(s)\\&-\boldsymbol{K}\boldsymbol{D}(s)\cdot\boldsymbol{\Theta}^*_{m,x}\cdot\boldsymbol{x}_P(s)\\&-\boldsymbol{K}\boldsymbol{D}(s)\cdot\mathcal{L}\{\boldsymbol{f}_m(\boldsymbol{x}_P(t),t)\}.\end{aligned} \tag{5.59}$$

Adding $\boldsymbol{K}\boldsymbol{D}(s)\cdot(\boldsymbol{\Lambda}-\boldsymbol{I})\cdot\boldsymbol{u}(s)$ on both sides leads to

$$\begin{aligned}(\boldsymbol{I}+\boldsymbol{K}\boldsymbol{D}(s)\boldsymbol{\Lambda})\cdot\boldsymbol{u}(s)=(\boldsymbol{I}+\boldsymbol{K}\boldsymbol{D}(s))\boldsymbol{K}_r\cdot\boldsymbol{r}(s)&-\boldsymbol{K}\boldsymbol{D}(s)\cdot\boldsymbol{\Theta}^*_{m,x}\cdot\boldsymbol{x}_P(s)\\&-\boldsymbol{K}\boldsymbol{D}(s)\cdot\mathcal{L}\{\boldsymbol{f}_m(\boldsymbol{x}_P(t),t)\}.\end{aligned} \tag{5.60}$$

Upon multiplication with $(\boldsymbol{I}+\boldsymbol{K}\boldsymbol{D}(s)\boldsymbol{\Lambda})^{-1}$ from the left, one obtains

$$\begin{aligned}\boldsymbol{u}(s) = &(\boldsymbol{I}+\boldsymbol{K}\boldsymbol{D}(s)\boldsymbol{\Lambda})^{-1}(\boldsymbol{I}+\boldsymbol{K}\boldsymbol{D}(s))\boldsymbol{K}_r\cdot\boldsymbol{r}(s)\\ &-(\boldsymbol{I}+\boldsymbol{K}\boldsymbol{D}(s)\boldsymbol{\Lambda})^{-1}\boldsymbol{K}\boldsymbol{D}(s)\cdot\boldsymbol{\Theta}^*_{m,x}\cdot\boldsymbol{x}_P(s)\\ &-(\boldsymbol{I}+\boldsymbol{K}\boldsymbol{D}(s)\boldsymbol{\Lambda})^{-1}\boldsymbol{K}\boldsymbol{D}(s)\cdot\mathcal{L}\left\{\boldsymbol{f}_m\left(\boldsymbol{x}_P(t),t\right)\right\}.\end{aligned} \tag{5.61}$$

Multiplying (5.61) by $\boldsymbol{\Lambda}$ and using the matrix identity (B.177) admits the compact representation

$$\boldsymbol{\Lambda}\cdot\boldsymbol{u}(s) = \boldsymbol{C}_{ff}(s)\boldsymbol{K}_r\cdot\boldsymbol{r}(s) - \boldsymbol{C}_{fb}(s)\cdot\left(\boldsymbol{\Theta}^*_{m,x}\cdot\boldsymbol{x}_P(s)+\mathcal{L}\left\{\boldsymbol{f}_m\left(\boldsymbol{x}_P(t),t\right)\right\}\right), \tag{5.62}$$

where $\boldsymbol{C}_{ff}(s)$ and $\boldsymbol{C}_{fb}(s)$ are defined in (5.51). Eq. (5.62) represents the effective MLESO control law, which is realized by the MLESO as it ensures the relation (5.57).

Combining the plant representation (5.56) and the control law representation (5.62) admits to state the closed-loop control system as the feedback interconnection

$$\begin{aligned}\boldsymbol{x}_P(s) &= \boldsymbol{G}_m(s)\cdot\boldsymbol{v}_P(s)+\boldsymbol{x}_0(s)\\ \boldsymbol{v}_P(s) &= \boldsymbol{C}_{ff}(s)\boldsymbol{K}_r\cdot\boldsymbol{r}(s)+(\boldsymbol{I}-\boldsymbol{C}_{fb}(s))\cdot\left(\boldsymbol{\Theta}^*_{m,x}\cdot\boldsymbol{x}_P(s)+\mathcal{L}\left\{\boldsymbol{f}_m\left(\boldsymbol{x}_P(t),t\right)\right\}\right),\end{aligned} \tag{5.63}$$

where $\boldsymbol{x}_0(s) = (s\boldsymbol{I}-\boldsymbol{A}_M)^{-1}\cdot\boldsymbol{x}_P(0)$ denotes response of the plant due to its initial condition $\boldsymbol{x}_P(0)$. Since the feedforward filter $\boldsymbol{C}_{ff}(s)$ and the feedback filter $\boldsymbol{C}_{fb}(s)$ are Hurwitz due to the second condition of Theorem 5.4, their $\mathcal{L}_1$-norms exist. Hence, the following norm inequality immediately results from (5.63):

$$\begin{aligned}\|\boldsymbol{x}_P(t)_\tau\|_{\mathcal{L}_\infty} \le &\|\boldsymbol{G}_m(s)\boldsymbol{C}_{ff}(s)\boldsymbol{K}_r\|_{\mathcal{L}_1}\cdot\|\boldsymbol{r}(t)\|_{\mathcal{L}_\infty}+\|\boldsymbol{x}_0(t)\|_{\mathcal{L}_\infty}\\ &+\|\boldsymbol{G}_m(s)(\boldsymbol{I}-\boldsymbol{C}_{fb}(s))\cdot\boldsymbol{\Theta}^*_{m,x}\|_{\mathcal{L}_1}\cdot\|\boldsymbol{x}_P(t)_\tau\|_{\mathcal{L}_\infty}\\ &+\|\boldsymbol{G}_m(s)(\boldsymbol{I}-\boldsymbol{C}_{fb}(s))\|_{\mathcal{L}_1}\cdot\|\boldsymbol{f}_m\left(\boldsymbol{x}_P(t),t\right)_\tau\|_{\mathcal{L}_\infty}.\end{aligned} \tag{5.64}$$

Notice that truncated norms $\|(\cdot)_\tau\|_{\mathcal{L}}$ are used for all terms involving $\boldsymbol{x}_P(t)$ as boundedness of $\boldsymbol{x}_P(t)$ has not yet been ensured. Since the nonlinearity $\boldsymbol{f}_m\left(\boldsymbol{x}_P(t),t\right)$ is globally Lipschitz, (5.48) holds. Thus, (5.64) becomes

$$\begin{aligned}\|\boldsymbol{x}_P(t)_\tau\|_{\mathcal{L}_\infty} \le &\|\boldsymbol{G}_m(s)\boldsymbol{C}_{ff}(s)\boldsymbol{K}_r\|_{\mathcal{L}_1}\cdot\|\boldsymbol{r}(t)\|_{\mathcal{L}_\infty}+\|\boldsymbol{x}_0(t)\|_{\mathcal{L}_\infty}\\ &+\|\boldsymbol{G}_m(s)(\boldsymbol{I}-\boldsymbol{C}_{fb}(s))\cdot\boldsymbol{\Theta}^*_{m,x}\|_{\mathcal{L}_1}\cdot\|\boldsymbol{x}_P(t)_\tau\|_{\mathcal{L}_\infty}\\ &+\|\boldsymbol{G}_m(s)(\boldsymbol{I}-\boldsymbol{C}_{fb}(s))\|_{\mathcal{L}_1}\cdot\left(L_m\cdot\|\boldsymbol{x}_P(t)_\tau\|_{\mathcal{L}_\infty}+\phi_{m,0}\right).\end{aligned} \tag{5.65}$$

Solving for $\|\boldsymbol{x}_P(t)_\tau\|_{\mathcal{L}_\infty}$ yields

$$\begin{aligned}&\|\boldsymbol{x}_P(t)_\tau\|_{\mathcal{L}_\infty}\\ &\le\frac{\|\boldsymbol{G}_m(s)\boldsymbol{C}_{ff}(s)\boldsymbol{K}_r\|_{\mathcal{L}_1}\|\boldsymbol{r}(t)\|_{\mathcal{L}_\infty}+\|\boldsymbol{G}_m(s)(\boldsymbol{I}-\boldsymbol{C}_{fb}(s))\|_{\mathcal{L}_1}\phi_{m,0}+\|\boldsymbol{x}_0(t)\|_{\mathcal{L}_\infty}}{1-\|\boldsymbol{G}_m(s)(\boldsymbol{I}-\boldsymbol{C}_{fb}(s))\cdot\boldsymbol{\Theta}^*_{m,x}\|_{\mathcal{L}_1}-\|\boldsymbol{G}_m(s)(\boldsymbol{I}-\boldsymbol{C}_{fb}(s))\|_{\mathcal{L}_1}\cdot L_m}.\end{aligned} \tag{5.66}$$

The numerator of (5.66) is bounded for bounded command signals $\boldsymbol{r}(t)$, bounded exogenous disturbances and bounded initial condition $\boldsymbol{x}_P(0)$. Due to the third condition of

Theorem 5.4, the denominator of (5.66) is larger than zero. Hence, (5.66) implies that the state $\boldsymbol{x}_P(t)$ is bounded for all τ. Since the bound does not depend on τ, it holds uniformly in τ, which implies that the plant state $\boldsymbol{x}_P(t)$ is bounded. Since the plant state is bounded, it follows from (5.62) that the control signal $\boldsymbol{u}(t)$ is bounded as well, which in turn implies boundedness of the disturbance $\boldsymbol{d}(t)$. As the latter implies boundedness of the error dynamics (5.28) (or (5.21), respectively), the states of the MLESO (5.27) (or (5.20), respectively) are bounded as well, which concludes the proof. □

Remark 5.5. *In the proof of Theorem 5.4, the feedforward filter $\boldsymbol{C}_{ff}(s)$ and the feedback filter $\boldsymbol{C}_{fb}(s)$ appear, which depend on the unknown control effectiveness matrix $\boldsymbol{\Lambda}$. Hence, these filters may not be implemented. They are, however, only used for the stability analysis of the closed-loop MLESO control system.*

Remark 5.6. *Depending on the order of the MLESO (and hence, on the order of the filter $\boldsymbol{C}_m(s)$), the conditions of Theorem 5.4 are hard to verify. For this reason, hints on cases, where the conditions are more easily verified, are helpful.*

If the filter $\boldsymbol{C}_m(s)$ is a PTk element, i.e. $\boldsymbol{B}_{j,m} = 0,\ j = 1, ..., k-1$, the first condition (5.50) *may always be satisfied by the choice*

$$\begin{aligned} \boldsymbol{D}(s) &= (s^k \cdot \boldsymbol{I} + s^{k-1} \cdot \boldsymbol{A}_{k-1,m} + \ldots + s \cdot \boldsymbol{A}_{1,m})^{-1}, \\ \boldsymbol{K} &= \boldsymbol{A}_{0,m}, \end{aligned} \tag{5.67}$$

since $\boldsymbol{A}_{j,m},\ j = 0, ..., k-1$ and $\boldsymbol{C}_m(s)$ are diagonal.

If the filter $\boldsymbol{C}_m(s)$ is a PT1 element (i.e. a first order MLESO is used), then Example 3.19 shows that the second condition (5.51) *may also be verified easily, since $\boldsymbol{\Lambda}$ is positive definite.*

Since the plant (5.17) *is strictly proper by definition, it ultimately represents a low-pass filter. Conversely, the filter $(\boldsymbol{I} - \boldsymbol{C}_{fb}(s))$ is a high-pass, since $\boldsymbol{C}_{fb}(s)$ is a low-pass filter. As already noted in the context of $\mathcal{L}_1$-AC (see Remark 3.22), $\boldsymbol{G}_m(s) \cdot (\boldsymbol{I} - \boldsymbol{C}_{fb}(s))$ will hence become a "no-pass" filter, if the bandwidth of $\boldsymbol{C}_{fb}(s)$ is sufficiently high. This observation implies that the $\mathcal{L}_1$-norm condition may always be satisfied, if the design parameters of the MLESO are appropriately chosen.*

The assumption of a global Lipschitz condition for the uncertainty $\boldsymbol{f}_m(\boldsymbol{x}_P(t), t)$ is restrictive in the sense that common nonlinearities such as second- or higher-order polynomials do not satisfy this condition. However, Theorem 5.4 suffices to show BIBS stability of a MLESO-based control system in case of a LTI plant. This is shown in the following example:

Example 5.7. *Consider the same plant and the same reference model as in the respective example on $\mathcal{L}_1$ Adaptive Control (Example 3.25) - namely the short-period approximation of the UAS introduced in Section 2.2. It may be easily verified that all assumptions of Theorem 5.4 are satisfied. It follows from $\lambda_{Z\alpha} = \lambda_{Zq} = 1$, the matching*

condition (3.10) *and Table 2.4 that the matched uncertainty* $\boldsymbol{\Theta}_m^* = \begin{bmatrix}\Theta_{m,\alpha}^* & \Theta_{m,q}^* & \Lambda\end{bmatrix}$ *is bounded by*

$$|\Theta_{m,\alpha}^*| \leq 1.78, \qquad |\Theta_{m,q}^*| \leq 0.38, \qquad 0.5 \leq \Lambda \leq 1.5. \tag{5.68}$$

For the estimation of the matched uncertainties, a first-order MLESO is used. The design parameters are chosen as $\bar{\boldsymbol{B}}_P^T = \begin{bmatrix}1 & 0\end{bmatrix}$ *and* $\boldsymbol{A}_0 = \omega_0 \cdot \boldsymbol{I}^{2\times 2}$*, where* $\omega_0 > 0$ *scales the bandwidth of the disturbance estimation. The resulting observer gains* $\boldsymbol{L}_0$ *and* $\boldsymbol{M}_0$ *may be computed using* (5.25)*, yielding for example for* $\omega_0 = 20$*:*

$$\boldsymbol{L}_0 = -20 \cdot \boldsymbol{I}^{2\times 2}, \qquad \boldsymbol{M}_0 = \begin{bmatrix} 0 & 0.93 \\ -20 & 0 \end{bmatrix}. \tag{5.69}$$

Based on this structure of the MLESO-based controller, closed-loop BIBS stability shall be investigated first. More precisely, the smallest bandwidth ω_0 *shall be computed for which the closed loop is stable according to Theorem 5.4. To that end, notice that the first and the second condition of Theorem 5.4 are easily satisfied due to Remark 5.6 since the first-order MLESO automatically ensures that* $\boldsymbol{C}_m(s)$ *is a PT1 filter, and since* Λ *is positive. For the third condition of Theorem 5.4, the satisfaction of the* $\mathcal{L}_1$*-norm condition* (5.52) *has to be established. Since a LTI plant is considered, the* $\mathcal{L}_1$*-norm condition simplifies to*

$$\|\boldsymbol{G}_m(s) \cdot (\boldsymbol{I} - \boldsymbol{C}_{fb}(s)) \cdot \boldsymbol{\Theta}_{m,x}^*\|_{\mathcal{L}_1} < 1. \tag{5.70}$$

Furthermore, notice that

$$\|\boldsymbol{G}_m(s) \cdot (\boldsymbol{I} - \boldsymbol{C}_{fb}(s)) \cdot \boldsymbol{\Theta}_{m,x}^*\|_{\mathcal{L}_1} \leq \|\boldsymbol{G}_m(s) \cdot (\boldsymbol{I} - \boldsymbol{C}_{fb}(s))\|_{\mathcal{L}_1} \cdot \|\boldsymbol{\Theta}_{m,x}^*\|_{\infty,i} \tag{5.71}$$

holds, where $\|\boldsymbol{\Theta}_{m,x}^*\|_{\infty,i}$ *is the* $\mathcal{L}_1$*-norm of the "transfer function"* $\boldsymbol{\Theta}_{m,x}^*$*. In case of the short-period example, the induced* ∞*-norm of the row vector* $\boldsymbol{\Theta}_{m,x}^* = \begin{bmatrix}\Theta_{m,\alpha}^* & \Theta_{m,q}^*\end{bmatrix}$ *is simply given by*

$$\|\boldsymbol{\Theta}_{m,x}^*\|_{\infty,i} = |\Theta_{m,\alpha}^*| + |\Theta_{m,q}^*|. \tag{5.72}$$

It follows from the uncertainty bounds given in (5.68)*, that*

$$\|\boldsymbol{\Theta}_{m,x}^*\|_{\infty,i} \leq \Theta_{m,x,\max}^* \tag{5.73}$$

with

$$\Theta_{m,x,\max}^* = \max|\Theta_{m,\alpha}^*| + \max|\Theta_{m,q}^*| = 2.16 \tag{5.74}$$

holds. Thus, if the strengthened $\mathcal{L}_1$*-norm condition*

$$\|\boldsymbol{G}_m(s) \cdot (\boldsymbol{I} - \boldsymbol{C}_{fb}(s))\|_{\mathcal{L}_1} \cdot \Theta_{m,x,\max}^* < 1 \tag{5.75}$$

is satisfied, then the original $\mathcal{L}_1$*-norm condition holds for all uncertainties* $\boldsymbol{\Theta}_{m,x}^*$*. By computing the* $\mathcal{L}_1$*-norm of* $\boldsymbol{G}_m(s) \cdot (\boldsymbol{I} - \boldsymbol{C}_{fb}(s))$ *for* $\Lambda = 0.5$*, one obtains that the* $\mathcal{L}_1$ *norm condition is satisfied for* $\omega_0 \gtrsim 182\, rad/s$*. Since the bandwidth of* $\boldsymbol{C}_{fb}(s)$ *monotonically*

increases with increasing values of Λ, it is also ensured that the $\mathcal{L}_1$-norm condition holds for all $\Lambda > 0.5$.

While the $\mathcal{L}_1$-norm condition suggests stability for rather high bandwidths ω_0, the time-domain performance of the MLESO is evaluated at lower bandwidths. In Figure 5.3, the performance of the MLESO is compared for different disturbance estimation bandwidths ω_0. Clearly, the closed loop is stable even at lower bandwidths. This comes as no surprise since the small-gain theorem, implicitly used in Theorem 5.4, is highly conservative. Furthermore, one observes that the MLESO approximates the reference model (3.4) *with increasing accuracy for increasing bandwidth ω_0. This correlates with Figures 5.3(d) to 5.3(f), which compare the true value of the matched uncertainty $d_m(t)$, computed using* (5.19)*, to its estimate $\hat{d}_m(t)$. Clearly, the increase in bandwidth admits a better estimation of the matched uncertainty and hence, leads to an improved tracking performance. Notice that the true value $d_m(t)$ is input-dependent and does hence differ for different bandwidths ω_0, as the control signal $u(t)$ varies as well (Figure 5.3(c)). Furthermore, the estimate $\hat{d}_{um}(t)$ of the unmatched uncertainties remains zero for all times irrespective of the chosen bandwidth ω_0, as shown in Figures 5.3(d) to 5.3(f).*

While the preceding time-domain analysis of the MLESO indicates that the closed loop approximates the reference model (3.4) *up to an arbitrary precision, this may be verified by virtue of a generalized root locus analysis. By applying a Linear Fractional Transformation (LFT, see for example [156]) to the closed-loop system consisting of the plant* (5.17)*, the control law* (5.41) *and the MLESO* (5.20)*, the closed-loop system may be represented by the feedback connection*

$$\begin{aligned} u_{\omega_0}(s) &= \omega_0 \cdot y_{\omega_0}(s), \\ \begin{bmatrix} y_{\omega_0}(s) \\ \boldsymbol{x}_P(s) \end{bmatrix} &= \begin{bmatrix} M_{11}(s) & M_{12}(s) \\ \boldsymbol{M}_{21}(s) & \boldsymbol{M}_{22}(s) \end{bmatrix} \cdot \begin{bmatrix} u_{\omega_0}(s) \\ r(s) \end{bmatrix}, \end{aligned} \tag{5.76}$$

where ω_0 has been "pulled out". Notice that a representation according to (5.76) *is for example easily computed using MATLAB®. The positive root locus of $(-M_{11}(s))$ then shows the location of the closed-loop poles when varying ω_0, and is depicted in Figure 5.4. Although plausible from an engineering point of view, it is interesting to notice that the zeros of $M_{11}(s)$ coincide with the poles of the reference model* (3.4)*. Thus, by increasing the bandwidth ω_0, the short-period poles of the closed-loop system may be moved arbitrarily close to the poles of the reference model.*

The preceding example showed that the MLESO essentially is a high-gain control architecture since an infinite bandwidth of the filter $\boldsymbol{C}_m(s)$ would be required to perfectly track the reference model (3.4). This is also in accordance with Remark 5.6, which stated that the $\mathcal{L}_1$-norm condition may always be satisfied if the bandwidth of the filter $\boldsymbol{C}_{fb}(s)$ (and hence of $\boldsymbol{C}_m(s)$) is sufficiently high. While the bandwidth of $\boldsymbol{C}_{fb}(s)$ may be

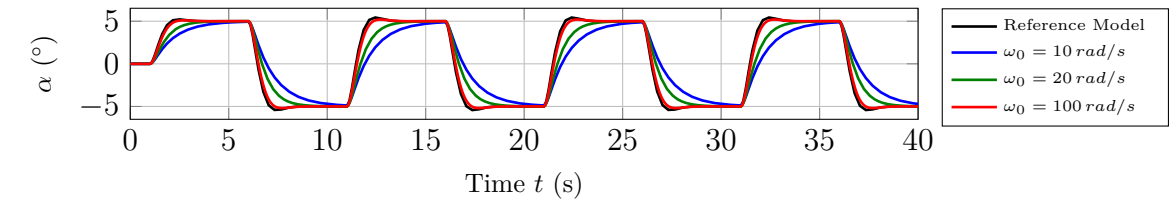

(a) Angle-Of-Attack α

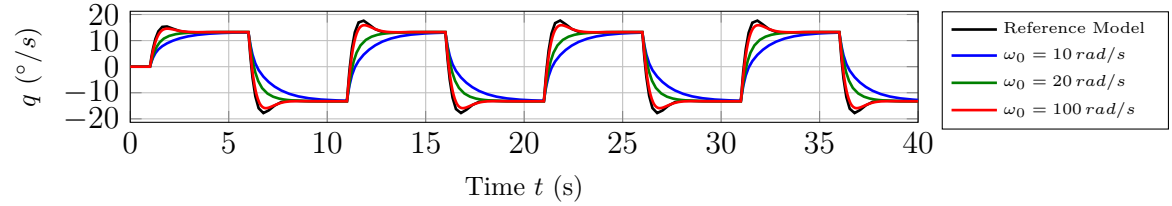

(b) Pitch Rate q

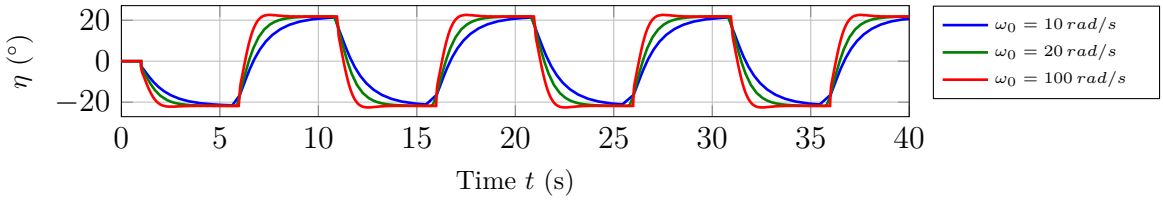

(c) Elevator Deflection η

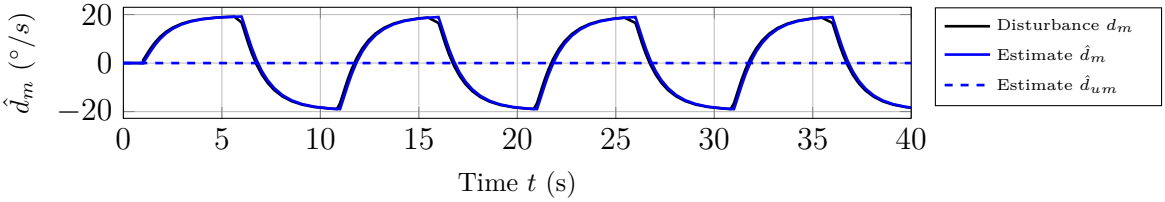

(d) Uncertainty Estimation for $\omega_0 = 10\,rad/s$

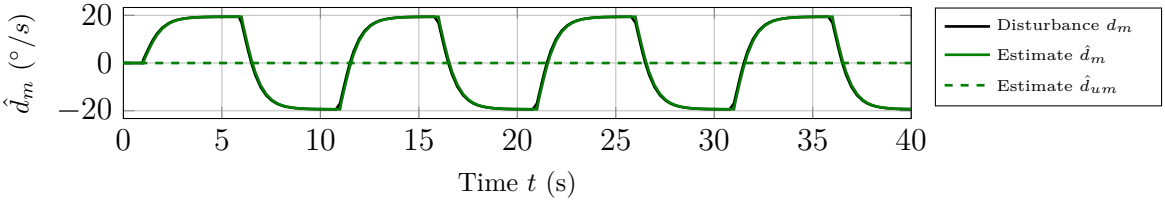

(e) Uncertainty Estimation for $\omega_0 = 20\,rad/s$

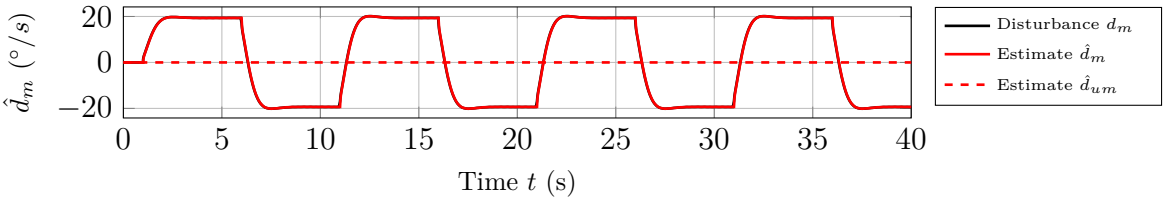

(f) Uncertainty Estimation for $\omega_0 = 100\,rad/s$

Figure 5.3: Performance of the MLESO for different values of the filter bandwidth ω_0 for a $5°$ square wave command in case of $\lambda_\alpha = \lambda_q = 1$ and $\lambda_\eta = 0.5$.

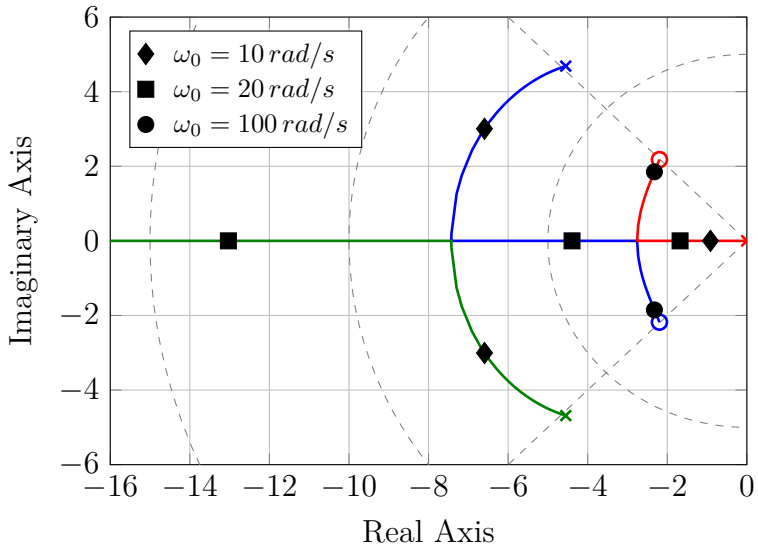

Figure 5.4: Generalized root locus analysis of the first-order MLESO from Example 5.7 for $\lambda_\alpha = \lambda_q = 1$ and $\lambda_\eta = 0.5$, when varying the filter bandwidth ω_0.

arbitrarily increased in theory, in practice time-delays, noise, unmodeled dynamics, etc. limit the admissible bandwidth. This is to be demonstrated by the following example.

Example 5.8. *Consider the same plant and the same MLESO-based controller as in the previous Example 5.7. Figure 5.5 shows the dependence of the phase margin and the time-delay margin on the filter bandwidth ω_0, when cutting the loop at the plant input $u(t)$. The gain margin is not shown here since it is larger than $300\,dB$ at all bandwidths ω_0.*

For all filter bandwidths ω_0, the phase margin is sufficiently high and remains above $90°$. Nevertheless, it is interesting to notice that the phase margin first increases until it reaches a maximum, after which it decreases. This effect may be explained as follows: At low filter bandwidths, the MLESO is slower than the plant dynamics. At these bandwidths, the MLESO neither achieves appropriate tracking nor disturbance rejection. Since the MLESO is too slow, its control action may even hamper robustness. Thus, with increasing filter bandwidth, the overall robustness of the closed loop increases first, leading to an increasing phase margin. At the same time, the increasing bandwidth renders the closed loop more and more sensitive to phase shifts at the plant input (e.g. due to actuator dynamics). At some filter bandwidth, this effect becomes dominating and hence, the phase margin decreases.

In contrast to the phase margin, the time-delay margin monotonically decreases. This also holds at low bandwidths, for which Figure 5.5 does not show any data. Thus, increasing the filter bandwidth of the MLESO will inevitably lead to a decreasing time-delay margin. Hence, any MLESO-design must trade-off robustness to parametric uncertainties, which is improved with increasing bandwidth, with robustness to non-parametric uncertainties, which deteriorates with increasing bandwidth.

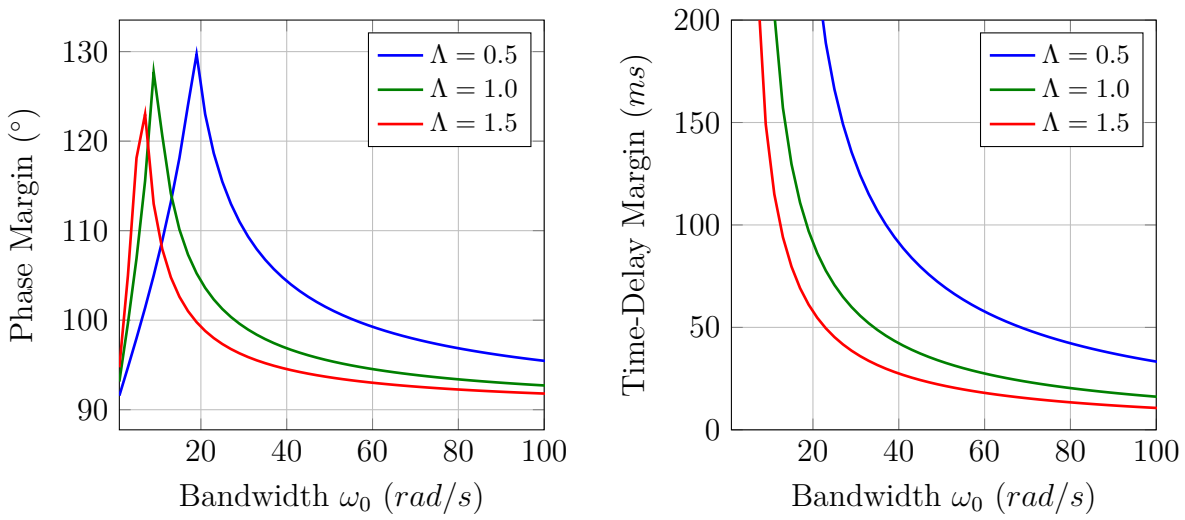

(a) Phase Margin

(b) Time-Delay Margin

Figure 5.5: Dependence of the phase and time-delay margins of the first-order MLESO from Example 5.8 for $\lambda_\alpha = \lambda_q = 1$, when varying the filter bandwidth ω_0.

With respect to the control effectiveness Λ, one observes in both plots that small values of the control effectiveness lead to the largest values of phase and time-delay margin. This effect is to be expected since a small control effectiveness reduces the effective bandwidth of the filter $\boldsymbol{C}_{fb}(s)$, which is implicitly realized by the MLESO. For this reason, the Nichols plots in Figure 5.6 depict the case of least robustness, i.e. for $\Lambda = 1.5$.

5.3.2 Stability in Case of a Semi-Global Lipschitz Condition

The assumption of a global Lipschitz condition for the nonlinearity $\boldsymbol{f}_m\left(\boldsymbol{x}_P\left(t\right), t\right)$ is restrictive as it excludes common nonlinearities such as second- or higher-order polynomials. Consider for example a second order polynomial $f_m(\boldsymbol{x}_P\left(t\right)) = x_{P,1}^2$. Obviously, (5.46) may not hold on $\mathbb{R}^n$ since the second order polynomial may not be bounded by a linear function on the whole $\mathbb{R}^n$. However, one may find a linear function, which bounds the second order polynomial, on any compact subset of $\mathbb{R}^n$. Thus, by resorting to the semi-global Lipschitz condition (5.44), nonlinearities such as polynomials can also be handled.

A semi-global Lipschitz condition complicates the proof of BIBS stability of the closed-loop MLESO control system. This is because the norm of the nonlinearity $\boldsymbol{f}_m\left(\boldsymbol{x}_P\left(t\right), t\right)$ has to be bounded (see (5.64) and (5.65) in the proof of Theorem 5.4). However, a subset $\{\boldsymbol{x}_P \in \mathbb{R}^n \mid \|\boldsymbol{x}_P\|_\infty \leq r\}$, in which the state $\boldsymbol{x}_P\left(t\right)$ remains for all times, is not known a-priori. For this reason, a slight modification of the proof is developed.

The idea of this modification is as follows: assume that we would know that the

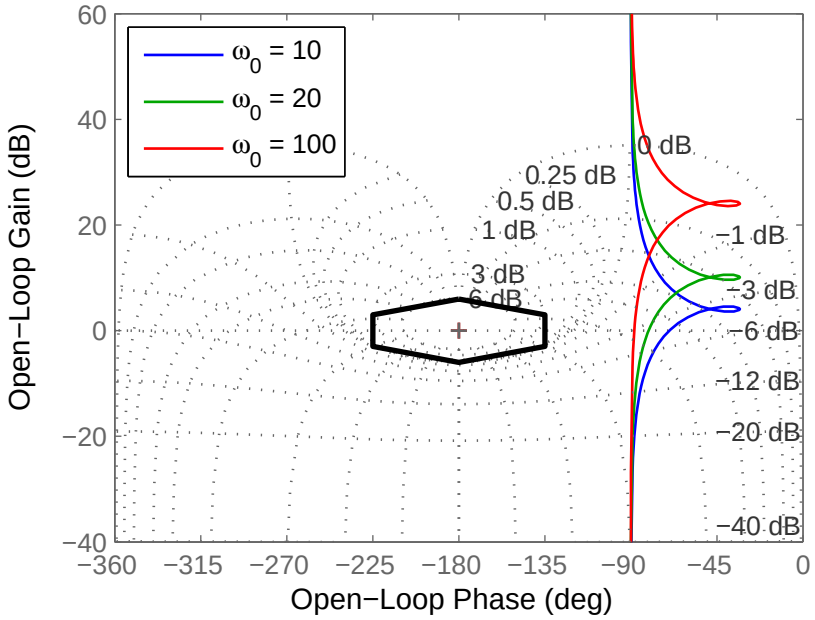

Figure 5.6: Nichols plots of the first-order MLESO from Example 5.8 for $\lambda_\alpha = \lambda_q = 1$ and $\lambda_\eta = 1.5$, when varying the filter bandwidth ω_0.

state $\boldsymbol{x}_P(t)$ is bounded by

$$\|\boldsymbol{x}_P(t)\|_{\mathcal{L}_\infty} \leq \rho_r, \tag{5.77}$$

where $\rho_r > 0$ is some known constant. Due to this assumption, the semi-global Lipschitz condition (5.44) and the boundedness condition (5.45) imply

$$\|\boldsymbol{f}_m(\boldsymbol{x}_P(t), t)\|_{\mathcal{L}_\infty} \leq L_m(\rho_r) \cdot \rho_r + \phi_{m,0}. \tag{5.78}$$

At the same time, $\boldsymbol{x}_P(t)$ is also known to be bounded by (5.64). Inserting the assumed bounds (5.77) and (5.78) into (5.64) yields

$$\begin{aligned}\|\boldsymbol{x}_P(t)_\tau\|_{\mathcal{L}_\infty} \leq\ & \|\boldsymbol{G}_m(s)\boldsymbol{C}_{ff}(s)\boldsymbol{K}_r\|_{\mathcal{L}_1} \cdot \|\boldsymbol{r}(t)\|_{\mathcal{L}_\infty} + \|\boldsymbol{x}_0(t)\|_{\mathcal{L}_\infty} \\ & + \|\boldsymbol{G}_m(s)(\boldsymbol{I} - \boldsymbol{C}_{fb}(s)) \cdot \boldsymbol{\Theta}^*_{m,x}\|_{\mathcal{L}_1} \cdot \rho_r \\ & + \|\boldsymbol{G}_m(s)(\boldsymbol{I} - \boldsymbol{C}_{fb}(s))\|_{\mathcal{L}_1} \cdot (L_m(\rho_r) \cdot \rho_r + \phi_{m,0}).\end{aligned} \tag{5.79}$$

In order to "ensure" that the assumed bound (5.77) actually holds, the upper bound in (5.79) has to be smaller than ρ_r. As will become clear later on, a strict inequality is required here, which leads to the new $\mathcal{L}_1$-norm condition:

$$\begin{aligned}&\|\boldsymbol{G}_m(s)(\boldsymbol{I} - \boldsymbol{C}_{fb}(s)) \cdot \boldsymbol{\Theta}^*_{m,x}\|_{\mathcal{L}_1} \cdot \rho_r \\ &\quad + \|\boldsymbol{G}_m(s)(\boldsymbol{I} - \boldsymbol{C}_{fb}(s))\|_{\mathcal{L}_1} \cdot (L_m(\rho_r) \cdot \rho_r + \phi_{m,0}) \\ &\quad < \rho_r - \|\boldsymbol{G}_m(s)\boldsymbol{C}_{ff}(s)\boldsymbol{K}_r\|_{\mathcal{L}_1} \cdot \|\boldsymbol{r}(t)\|_{\mathcal{L}_\infty} - \|\boldsymbol{x}_0(t)\|_{\mathcal{L}_\infty}.\end{aligned} \tag{5.80}$$

Even if the parameters of the MLESO are chosen to satisfy the $\mathcal{L}_1$-norm condition (5.80), it is not yet justified to claim that the plant state $\boldsymbol{x}_P(t)$ is bounded. This is because the $\mathcal{L}_1$-norm condition (5.80) has initially been derived under the assumption that

$\boldsymbol{x}_P(t)$ is bounded. Hence, the argument leading to (5.80) is circular. Nevertheless, the subsequent theorem will show by virtue of a proof by contradiction that $\|\boldsymbol{x}_P(t)\|_{\mathcal{L}_\infty} < \rho_r$ actually holds if ρ_r satisfies the $\mathcal{L}_1$-norm condition (5.80). This in turn implies BIBS stability of the closed-loop MLESO control system.

Theorem 5.9 (BIBS Stability in Case of Matched Uncertainties and a Semiglobal Lipschitz Condition)**.** *Consider the plant* (3.1) *and let Assumptions 3.1 (state feedback), 3.2 (positive definite control effectiveness), 3.3 (Lipschitz condition), 3.5 (Matching condition), 3.6 (full-rank $\boldsymbol{B}_P$) and 5.1 (bounded uncertainties) hold. Let the initial conditions of the MLESO* (5.27) *(or* (5.20)*, respectively) be chosen such that*

$$\hat{\boldsymbol{x}}_P(0) = \boldsymbol{x}_P(0), \qquad \hat{\boldsymbol{\Delta}}_j(0) = \boldsymbol{0},\ j = 1, ..., k-1 \tag{5.81}$$

with $\|\boldsymbol{x}_P(0)\|_\infty < \rho_r$ hold.

If the design parameters $\boldsymbol{A}_j,\ j = 0, ...k-1$ and $\boldsymbol{B}_j,\ j = 1, ..., k-1$ of the MLESO (5.27) *(or* (5.20)*, respectively) are chosen such that*

1. *the filter $\boldsymbol{C}_m(s)$, defined in* (5.38)*, may be represented by the feedback connection*

$$\boldsymbol{C}_m(s) = (\boldsymbol{I} + \boldsymbol{K}\boldsymbol{D}(s))^{-1}\boldsymbol{K}\boldsymbol{D}(s), \tag{5.82}$$

   where $\boldsymbol{K} \in \mathbb{R}^{m\times m}$ is a feedback gain and $\boldsymbol{D} : \mathbb{C} \to \mathbb{C}^{m\times m}$ is a strictly proper transfer function matrix containing an integrator;

2. *the feedforward and feedback filters $\boldsymbol{C}_{ff}(s)$ and $\boldsymbol{C}_{fb}(s)$, defined as*

$$\begin{aligned} \boldsymbol{C}_{ff}(s) &\triangleq (\boldsymbol{I} + \boldsymbol{\Lambda}\boldsymbol{K}\boldsymbol{D}(s))^{-1}\boldsymbol{\Lambda}(\boldsymbol{I} + \boldsymbol{K}\boldsymbol{D}(s)), \\ \boldsymbol{C}_{fb}(s) &\triangleq (\boldsymbol{I} + \boldsymbol{\Lambda}\boldsymbol{K}\boldsymbol{D}(s))^{-1}\boldsymbol{\Lambda}\boldsymbol{K}\boldsymbol{D}(s), \end{aligned} \tag{5.83}$$

   are Hurwitz for all $\boldsymbol{\Lambda} \in \Omega_\Lambda$;

3. *the $\mathcal{L}_1$-norm condition*

$$\begin{aligned} &\|\boldsymbol{G}_m(s)\,(\boldsymbol{I} - \boldsymbol{C}_{fb}(s)) \cdot \boldsymbol{\Theta}^*_{m,x}\|_{\mathcal{L}_1} \cdot \rho_r \\ &\quad + \|\boldsymbol{G}_m(s)\,(\boldsymbol{I} - \boldsymbol{C}_{fb}(s))\|_{\mathcal{L}_1} \cdot (L_m(\rho_r) \cdot \rho_r + \phi_{m,0}) \\ &\quad < \rho_r - \|\boldsymbol{G}_m(s)\,\boldsymbol{C}_{ff}(s)\boldsymbol{K}_r\|_{\mathcal{L}_1} \cdot \|\boldsymbol{r}(t)\|_{\mathcal{L}_\infty} - \|\boldsymbol{x}_0(t)\|_{\mathcal{L}_\infty}. \end{aligned} \tag{5.84}$$

   is satisfied for some $\rho_r > 0$ and all $\boldsymbol{\Lambda} \in \Omega_\Lambda$, $\boldsymbol{\Theta}^*_{m,x} \in \Omega_{x,m}$, where

$$\boldsymbol{G}_m(s) \triangleq (s\boldsymbol{I} - \boldsymbol{A}_M)^{-1}\boldsymbol{B}_P, \tag{5.85}$$

then the control law (5.41) *ensures that the plant state is bounded by*

$$\|\boldsymbol{x}_P(t)\|_{\mathcal{L}_\infty} < \rho_r. \tag{5.86}$$

Furthermore, the closed-loop control system consisting of the plant (3.1)*, the control law and the MLESO* (5.27) *(or* (5.20)*, respectively) is BIBS stable.*

Proof. The proof of Theorem 5.9 is done by contradiction. To that end, assume that (5.86) was not true. In this case, due to $\|\boldsymbol{x}_P(0)\|_\infty < \rho_r$ and due to continuity, there must exist an interval $t \in [0, \tau]$ such that

$$\|\boldsymbol{x}_P(t)\|_\infty < \rho_r \quad \forall\, t \in [0, \tau[\tag{5.87}$$

and

$$\|\boldsymbol{x}_P(\tau)\|_\infty = \rho_r. \tag{5.88}$$

Hence, throughout the interval $[0, \tau]$,

$$\|\boldsymbol{x}_P(t)_\tau\|_{\mathcal{L}_\infty} \leq \rho_r \tag{5.89}$$

holds. Following the same steps as in the proof of Theorem 5.4, one obtains the norm inequality

$$\begin{aligned}\|\boldsymbol{x}_P(t)_\tau\|_{\mathcal{L}_\infty} \leq\ & \|\boldsymbol{G}_m(s)\boldsymbol{C}_{ff}(s)\boldsymbol{K}_r\|_{\mathcal{L}_1} \cdot \|\boldsymbol{r}(t)\|_{\mathcal{L}_\infty} + \|\boldsymbol{x}_0(t)\|_{\mathcal{L}_\infty} \\ & + \|\boldsymbol{G}_m(s)(\boldsymbol{I} - \boldsymbol{C}_{fb}(s)) \cdot \boldsymbol{\Theta}^*_{m,x}\|_{\mathcal{L}_1} \cdot \|\boldsymbol{x}_P(t)_\tau\|_{\mathcal{L}_\infty} \\ & + \|\boldsymbol{G}_m(s)(\boldsymbol{I} - \boldsymbol{C}_{fb}(s))\|_{\mathcal{L}_1} \cdot \|\boldsymbol{f}_m(\boldsymbol{x}_P(t), t)_\tau\|_{\mathcal{L}_\infty}.\end{aligned} \tag{5.90}$$

Due to (5.89) and (5.78), the norm inequality (5.79) follows from (5.90), i.e.:

$$\begin{aligned}\|\boldsymbol{x}_P(t)_\tau\|_{\mathcal{L}_\infty} \leq\ & \|\boldsymbol{G}_m(s)\boldsymbol{C}_{ff}(s)\boldsymbol{K}_r\|_{\mathcal{L}_1} \cdot \|\boldsymbol{r}(t)\|_{\mathcal{L}_\infty} + \|\boldsymbol{x}_0(t)\|_{\mathcal{L}_\infty} \\ & + \|\boldsymbol{G}_m(s)(\boldsymbol{I} - \boldsymbol{C}_{fb}(s)) \cdot \boldsymbol{\Theta}^*_{m,x}\|_{\mathcal{L}_1} \cdot \rho_r \\ & + \|\boldsymbol{G}_m(s)(\boldsymbol{I} - \boldsymbol{C}_{fb}(s))\|_{\mathcal{L}_1} \cdot (L_m(\rho_r) \cdot \rho_r + \phi_{m,0}).\end{aligned} \tag{5.91}$$

Since the satisfaction of the $\mathcal{L}_1$-norm condition (5.84) implies

$$\begin{aligned}& \|\boldsymbol{G}_m(s)\boldsymbol{C}_{ff}(s)\boldsymbol{K}_r\|_{\mathcal{L}_1} \cdot \|\boldsymbol{r}(t)\|_{\mathcal{L}_\infty} + \|\boldsymbol{x}_0(t)\|_{\mathcal{L}_\infty} \\ & \quad + \|\boldsymbol{G}_m(s)(\boldsymbol{I} - \boldsymbol{C}_{fb}(s)) \cdot \boldsymbol{\Theta}^*_{m,x}\|_{\mathcal{L}_1} \cdot \rho_r \\ & \quad + \|\boldsymbol{G}_m(s)(\boldsymbol{I} - \boldsymbol{C}_{fb}(s))\|_{\mathcal{L}_1} \cdot (L_m(\rho_r) \cdot \rho_r + \phi_{m,0}) < \rho_r,\end{aligned} \tag{5.92}$$

it follows from (5.91) that

$$\|\boldsymbol{x}_P(t)_\tau\|_{\mathcal{L}_\infty} < \rho_r \tag{5.93}$$

holds. As the latter contradicts (5.88), no such interval $[0, \tau]$ can exist such that (5.88) holds, which proves the bound (5.86). Following the same argument as in the proof of Theorem 5.4, boundedness of the plant state $\boldsymbol{x}_P(t)$ then implies BIBS stability of the closed-loop MLESO control system. □

5.3.3 Relation to $\mathcal{L}_1$ Adaptive Control

The fundamental idea of the MLESO architecture for MRC is the estimation of the disturbance signal, which causes the real plant to deviate from a desired plant model. By feeding back this signal and hence, canceling this disturbance, model following is

achieved. Since the proof of stability of the MLESO architecture shares many elements with the proof of stability of the $\mathcal{L}_1$ *Reference Model*, it is natural to ask, whether and, in which way, these approaches are related.

To that end, consider the plant (3.1) and let Assumptions 3.1 (state feedback), 3.2 (positive definite control effectiveness), 3.3 (Lipschitz condition), 3.5 (Matching condition), 3.6 (full-rank $\boldsymbol{B}_P$) and 3.10 (bounded uncertainties) hold. Notice that the $\mathcal{L}_1$-AC for matched uncertainties from Section 3.3.1 has been derived under the assumption that the nonlinear function $\boldsymbol{f}_m\left(\boldsymbol{x}_P\left(t\right),t\right)$ admits an exact, linear parametrization (see Theorem 3.28 and Assumptions 3.7, 3.8). Due to its signal-based character, the MLESO does not require any special assumption with respect to the parametrization of the nonlinearity. Nevertheless, in order to enable a comparison, the latter two assumptions are supposed as well. Consequently, the matched disturbance signal $\boldsymbol{d}_m(t)$, originally defined in (5.19), simplifies to

$$\boldsymbol{d}_m\left(\boldsymbol{x}_P\left(t\right),t\right) = \left(\boldsymbol{\Lambda}-\boldsymbol{I}\right)\cdot\boldsymbol{u}\left(t\right)+\boldsymbol{\Theta}_{m,x}^{*}\boldsymbol{x}_P\left(t\right)+\boldsymbol{\Theta}_{m,\phi}^{*}\cdot\boldsymbol{\phi}\left(\boldsymbol{x}_P\left(t\right)\right). \tag{5.94}$$

In order to recognize the connection between $\mathcal{L}_1$-AC and the MLESO-based controller, notice that the particular $\mathcal{L}_1$-AC of Section 3.3.1 also filters the feedforward command signal (see (3.176)). For this reason, the control law (5.41) of the MLESO is modified accordingly, leading to:

$$\boldsymbol{u}\left(s\right) = \boldsymbol{C}_m(s)\boldsymbol{K}_r\cdot\boldsymbol{r}\left(s\right)-\hat{\boldsymbol{d}}_m(s), \tag{5.95}$$

where $\boldsymbol{C}_m(s)$ satisfies (5.82). By repeating the same transformations from the proof of Theorem 5.4, which led from (5.41) to (5.62), the new control law (5.95) becomes

$$\boldsymbol{u}\left(s\right) = \boldsymbol{\Lambda}^{-1}\boldsymbol{C}_{fb}(s)\cdot\left(\boldsymbol{K}_r\cdot\boldsymbol{r}\left(s\right)-\boldsymbol{\Theta}_{m,x}^{*}\cdot\boldsymbol{x}_P\left(s\right)-\boldsymbol{\Theta}_{m,\phi}^{*}\cdot\boldsymbol{\phi}_P\left(s\right)\right), \tag{5.96}$$

where $\boldsymbol{\phi}_P\left(s\right)=\mathcal{L}\{\boldsymbol{\phi}\left(\boldsymbol{x}_P\left(t\right)\right)\}$ denotes the Laplace transform of $\boldsymbol{\phi}\left(\boldsymbol{x}_P\left(t\right)\right)$ and where $\boldsymbol{C}_{fb}(s)$ was defined in (5.83). Eq. (5.96) represents the effective MLESO control law, if the matched disturbance is given by (5.94). Inserting (5.96) into the plant representation (5.18) and exploiting $\boldsymbol{d}_{um}(t)=\boldsymbol{0}$ yields

$$\begin{aligned}\dot{\boldsymbol{x}}_P\left(t\right) &= \boldsymbol{A}_M\boldsymbol{x}_P\left(t\right)+\boldsymbol{B}_P\left(\boldsymbol{\Lambda}\boldsymbol{u}\left(t\right)+\boldsymbol{\Theta}_{m,x}^{*}\boldsymbol{x}_P\left(t\right)+\boldsymbol{\Theta}_{m,\phi}^{*}\cdot\boldsymbol{\phi}\left(\boldsymbol{x}_P\left(t\right)\right)\right)\\ \boldsymbol{u}\left(s\right) &= \boldsymbol{\Lambda}^{-1}\cdot\boldsymbol{C}_{fb}(s)\cdot\left(\boldsymbol{K}_r\cdot\boldsymbol{r}\left(s\right)-\boldsymbol{\Theta}_{m,x}^{*}\cdot\boldsymbol{x}_P\left(s\right)-\boldsymbol{\Theta}_{m,\phi}^{*}\cdot\boldsymbol{\phi}_P\left(s\right)\right).\end{aligned} \tag{5.97}$$

Eq. (5.97) represents the effective closed-loop response, which is ensured by the MLESO control law (5.95).

When comparing (5.97) to the $\mathcal{L}_1$ *Reference Model* (3.175), one observes that both systems are structurally equivalent except for the different filters $\boldsymbol{C}(s)$ and $\boldsymbol{C}_{fb}(s)$. Notice, however, that $\boldsymbol{C}(s)$ and $\boldsymbol{C}_{fb}(s)$ are defined equivalently, which can be seen in (3.173) and (5.83), respectively. Thus, if the design parameters $\boldsymbol{D}(s)$ and $\boldsymbol{K}$ are chosen equivalently, $\boldsymbol{C}(s)=\boldsymbol{C}_{fb}(s)$ holds and hence, the MLESO-based closed loop is an

actual implementation of the $\mathcal{L}_1$ *Reference Model*. It needs to be stressed that this is in contrast to $\mathcal{L}_1$-AC, which only approximates the $\mathcal{L}_1$ *Reference Model* (up to an arbitrary precision). Thus, the performance of the $\mathcal{L}_1$-AC from Section 3.3.1 cannot be superior to the performance of the MLESO-based controller from this section. This aspect shall be illustrated by a simple example:

Example 5.10. *Consider the $\mathcal{L}_1$-AC with Integral Update Law from Example 3.25 and the MLESO from Example 5.7. Notice that the choice of the design parameters in Example 5.7 leads to the filter*

$$\boldsymbol{C}_m(s) = \frac{\omega_0}{s + \omega_0}, \tag{5.98}$$

which relates the matched uncertainty $d_m(t)$ to its estimate $\hat{d}_m(t)$. Hence, the feedback filter $\boldsymbol{C}_{fb}(s)$ is given by

$$\boldsymbol{C}_{fb}(s) = \frac{\Lambda \cdot \omega_0}{s + \Lambda \cdot \omega_0}. \tag{5.99}$$

At the same time, the choice of the design parameters of the $\mathcal{L}_1$-AC in Example 3.25 leads to the filter

$$\boldsymbol{C}(s) = \frac{\Lambda \cdot K}{s + \Lambda \cdot K}. \tag{5.100}$$

Thus, for $K = \omega_0$, the $\mathcal{L}_1$ Reference Model (3.175) *and the MLESO closed loop are equivalent, if the control law of the MLESO is enhanced as shown in* (5.95)*.*

Figure 5.7 compares the performance of the $\mathcal{L}_1$-AC and the MLESO for $\omega_0 = K = 20$. In case of the MLESO, the control law (5.95) *is used. Clearly, the $\mathcal{L}_1$-AC converges to the closed-loop response of the MLESO, once its parameters have converged to a vicinity of their ideal values.*

The relation between $\mathcal{L}_1$-AC and MLESO-based control has another interesting implication. It has already been demonstrated in Section 3.3.3 (and originally in [98]) that the $\mathcal{L}_1$ *Reference Model* may be implemented by a linear, integral, model-inversion type of control law. This control law was referred to as the limiting control law. Since the MLESO also implements the $\mathcal{L}_1$ *Reference Model*, it is yet another implementation of the limiting control law. Furthermore, [98] showed that the limiting control law is equivalent to a DOB [153]. Thus, the MLESO may be seen as an alternative implementation of a DOB. In contrast to a DOB, the MLESO is however an indirect approach, which does not rely on explicit model inversion. Following the same argument as in Section 3.3.3 or [98], a MLESO may hence systematically account for additional knowledge about the plant such as input saturation or time-delay at the control input. With the help of hedging, this additional knowledge admits the realization of effective anti-windup strategies, which are not readily available for direct approaches that rely on inversion of the (desired) plant dynamics.

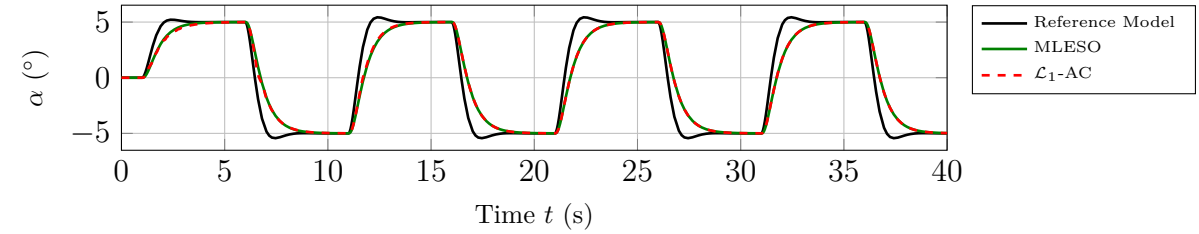

(a) Angle-Of-Attack α

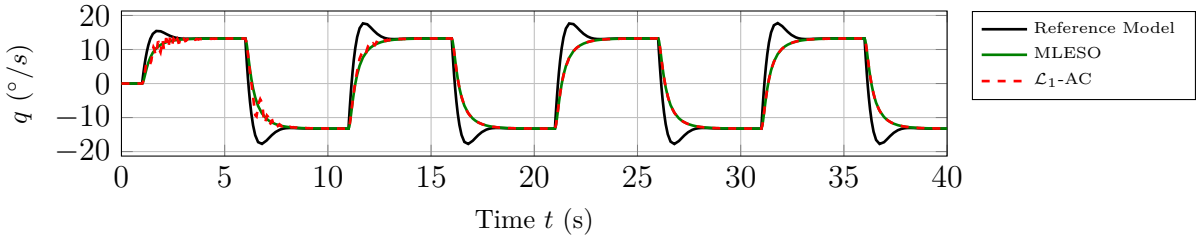

(b) Pitch Rate q

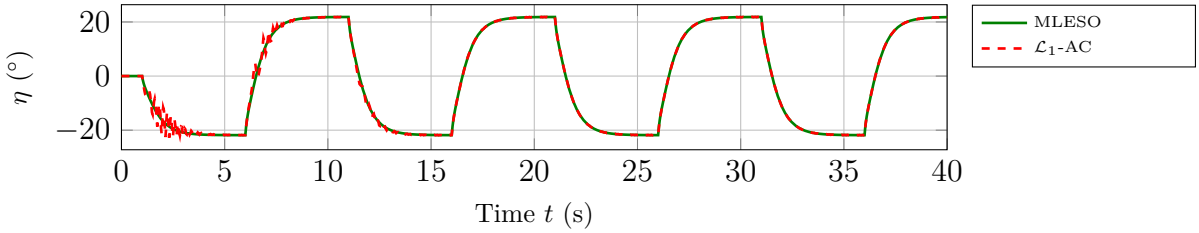

(c) Elevator Deflection η

Figure 5.7: Comparison of the MLESO from Example 5.10 with the $\mathcal{L}_1$-AC from Example 3.25 for a $5°$ square wave command in case of $\lambda_\alpha = \lambda_q = 1$ and $\lambda_\eta = 0.5$.

5.3.4 Relation to PI Control

This section will show that the control law (5.41) may be represented as a multivariable PI controller, if a first order MLESO estimates the matched disturbance signal $\boldsymbol{d}_m(t)$. In order to demonstrate this, a first step aims at obtaining a reduced MLESO, which only estimates matched uncertainties. In a second step, it is then shown that the reduced MLESO effectively degrades to a PI controller.

For the first step, consider the first order MLESO (5.20). Upon insertion of the design parameters (5.25), one obtains:

$$\begin{aligned} \dot{\hat{\boldsymbol{x}}}_P(t) &= \boldsymbol{A}_M \cdot \boldsymbol{x}_P(t) + \boldsymbol{B}_P \cdot \boldsymbol{u}(t) - \boldsymbol{B}\boldsymbol{A}_0\boldsymbol{B}^{-1} \cdot (\hat{\boldsymbol{x}}_P(t) - \boldsymbol{x}_P(t)) \\ \hat{\boldsymbol{d}}(t) &= -\boldsymbol{A}_0\boldsymbol{B}^{-1} \cdot (\hat{\boldsymbol{x}}_P(t) - \boldsymbol{x}_P(t)) \end{aligned} \tag{5.101}$$

Now, define the state transformation $\hat{\boldsymbol{x}}_P(t) = \boldsymbol{B} \cdot \bar{\boldsymbol{x}}_P(t)$. Eq. (5.101) becomes:

$$\begin{aligned} \dot{\bar{\boldsymbol{x}}}_P(t) &= \boldsymbol{B}^{-1}\boldsymbol{A}_M \cdot \boldsymbol{x}_P(t) + \boldsymbol{B}^{-1}\boldsymbol{B} \cdot \begin{bmatrix} \boldsymbol{u}(t) \\ \boldsymbol{0} \end{bmatrix} - \boldsymbol{A}_0 \cdot \bar{\boldsymbol{x}}_P(t) + \boldsymbol{A}_0\boldsymbol{B}^{-1} \cdot \boldsymbol{x}_P(t), \\ \hat{\boldsymbol{d}}(t) &= -\boldsymbol{A}_0 \cdot \bar{\boldsymbol{x}}_P(t) + \boldsymbol{A}_0\boldsymbol{B}^{-1} \cdot \boldsymbol{x}_P(t). \end{aligned} \tag{5.102}$$

Using the partitions

$$\boldsymbol{A}_0 = \begin{bmatrix} \boldsymbol{A}_{0,m} & \boldsymbol{0}^{m\times(n-m)} \\ \boldsymbol{0}^{(n-m)\times m} & \boldsymbol{A}_{0,um} \end{bmatrix} \text{ with } \boldsymbol{A}_{0,m} \in \mathbb{R}^{m\times m},\ \boldsymbol{A}_{0,um} \in \mathbb{R}^{(n-m)\times(n-m)}, \tag{5.103}$$

$$\boldsymbol{I}^{n\times n} = \begin{bmatrix} \boldsymbol{S}_m \\ \boldsymbol{S}_{um} \end{bmatrix} \text{ with } \boldsymbol{S}_m \in \mathbb{R}^{m\times n},\ \boldsymbol{S}_{um} \in \mathbb{R}^{(n-m)\times n}, \tag{5.104}$$

$$\bar{\boldsymbol{x}}_P(t) = \begin{bmatrix} \bar{\boldsymbol{x}}_{P,m}(t) \\ \bar{\boldsymbol{x}}_{P,um}(t) \end{bmatrix} \text{ with } \bar{\boldsymbol{x}}_{P,m} : \mathbb{R}_+ \to \mathbb{R}^m,\ \bar{\boldsymbol{x}}_{P,um} : \mathbb{R}_+ \to \mathbb{R}^{n-m}, \tag{5.105}$$

Eq. (5.102) may be equivalently written as:

$$\begin{aligned} \dot{\bar{\boldsymbol{x}}}_{P,m}(t) &= \boldsymbol{S}_m\boldsymbol{B}^{-1}\boldsymbol{A}_M \cdot \boldsymbol{x}_P(t) + \boldsymbol{u}(t) - \boldsymbol{A}_{0,m} \cdot \bar{\boldsymbol{x}}_{P,m}(t) + \boldsymbol{S}_m\boldsymbol{A}_0\boldsymbol{B}^{-1} \cdot \boldsymbol{x}_P(t), \\ \dot{\bar{\boldsymbol{x}}}_{P,um}(t) &= \boldsymbol{S}_{um}\boldsymbol{B}^{-1}\boldsymbol{A}_M \cdot \boldsymbol{x}_P(t) - \boldsymbol{A}_{0,um} \cdot \bar{\boldsymbol{x}}_{P,um}(t) + \boldsymbol{S}_{um}\boldsymbol{A}_0\boldsymbol{B}^{-1} \cdot \boldsymbol{x}_P(t), \\ \hat{\boldsymbol{d}}_m(t) &= -\boldsymbol{A}_{0,m} \cdot \bar{\boldsymbol{x}}_{P,m}(t) + \boldsymbol{S}_m\boldsymbol{A}_0\boldsymbol{B}^{-1} \cdot \boldsymbol{x}_P(t), \\ \hat{\boldsymbol{d}}_{um}(t) &= -\boldsymbol{A}_{0,um} \cdot \bar{\boldsymbol{x}}_{P,um}(t) + \boldsymbol{S}_{um}\boldsymbol{A}_0\boldsymbol{B}^{-1} \cdot \boldsymbol{x}_P(t). \end{aligned} \tag{5.106}$$

In (5.106), the estimation for matched and unmatched uncertainties is fully decoupled. Since the estimate for the unmatched uncertainties is not used in the MLESO control law (5.41), this part of the transformed MLESO (5.106) may be neglected and one obtains the reduced MLESO, which only estimates matched uncertainties.

For the second step, it suffices to insert the control law (5.41) in (5.106). The reduced MLESO and the control law become:

$$\begin{aligned} \dot{\bar{\boldsymbol{x}}}_{P,m}(t) &= \boldsymbol{K}_r \cdot \boldsymbol{r}(t) + \boldsymbol{S}_m\boldsymbol{B}^{-1}\boldsymbol{A}_M \cdot \boldsymbol{x}_P(t), \\ \boldsymbol{u}(t) &= \boldsymbol{K}_r \cdot \boldsymbol{r}(t) + \boldsymbol{A}_{0,m} \cdot \bar{\boldsymbol{x}}_{P,m}(t) - \boldsymbol{S}_m\boldsymbol{A}_0\boldsymbol{B}^{-1} \cdot \boldsymbol{x}_P(t). \end{aligned} \tag{5.107}$$

Utilizing the transformation $\boldsymbol{x}_i(t) = \boldsymbol{A}_{0,m} \cdot \bar{\boldsymbol{x}}_{P,m}(t)$, one arrives at a representation of the MLESO as a multivariable PI controller:

$$\begin{aligned} \dot{\boldsymbol{x}}_i(t) &= \underbrace{\boldsymbol{A}_{0,m}\boldsymbol{K}_r}_{\boldsymbol{K}_{i,r}} \cdot \boldsymbol{r}(t) + \underbrace{\boldsymbol{A}_{0,m}\boldsymbol{S}_m\boldsymbol{B}^{-1}\boldsymbol{A}_M}_{\boldsymbol{K}_{i,x}} \cdot \boldsymbol{x}_P(t), \\ \boldsymbol{u}(t) &= \boldsymbol{x}_i(t) + \underbrace{\boldsymbol{K}_r}_{\boldsymbol{K}_{p,r}} \cdot \boldsymbol{r}(t) \ \underbrace{-\boldsymbol{S}_m\boldsymbol{A}_0\boldsymbol{B}^{-1}}_{\boldsymbol{K}_{p,x}} \cdot \boldsymbol{x}_P(t). \end{aligned} \tag{5.108}$$

Even though the MLESO-based controller may be represented as a PI controller, in practice, a realization of the controller as a (reduced) state observer might be more desirable. Thanks to this representation, additional knowledge about the plant such as input saturation or time-delay at the control input may be systematically accounted for in the observer in order to prevent controller windup. This is illustrated in the following example:

Example 5.11. *Consider the plant, the reference model and the MLESO of Example 5.7. In contrast to Example 5.7, the plant now exhibits a saturation of the plant input:*

$$\dot{\boldsymbol{x}}_P(t) = \boldsymbol{A}_P\boldsymbol{x}_P(t) + \boldsymbol{B}_P\Lambda \cdot \eta_{\max} \cdot \operatorname{sat}\left(\frac{u(t)}{\eta_{\max}}\right), \tag{5.109}$$

where $\eta_{\max} = 30°$ denotes the largest admissible elevator deflection according to Table 2.2. Similar to $\mathcal{L}_1$-AC, the imperfection at the plant input may be accounted for by means of hedging (see also Section 3.3.3). Hence, it suffices to mimic the plant imperfection in the first order MLESO (5.20)*, leading to*

$$\begin{aligned} \dot{\hat{\boldsymbol{x}}}_P(t) &= \boldsymbol{A}_M \cdot \boldsymbol{x}_P(t) + \boldsymbol{B}_P \cdot \eta_{\max} \cdot \operatorname{sat}\left(\frac{u(t)}{\eta_{\max}}\right) + \boldsymbol{L}_0 \cdot \boldsymbol{e}_P(t), \\ \hat{\boldsymbol{d}}(t) &= \boldsymbol{M}_0 \cdot \boldsymbol{e}_P(t). \end{aligned} \tag{5.110}$$

Figure 5.8 compares the performance with and without hedging, if the disturbance estimation bandwidth is chosen as $\omega_0 = 20\,rad/s$. Regardless of whether hedging is used or not, the tracking performance does not differ between the two controllers. However, due to the saturation of the plant input, the commanded angle-of-attack $\alpha_{cmd}(t)$ may not be reached.

The difference between the cases with and without hedging can be seen in the commanded control signal $u(t) = \eta(t)$ and the disturbance estimate $\hat{d}_m(t)$. If hedging is used, the MLESO correctly estimates the matched uncertainty. In contrast, if no hedging is used, the disturbance estimate $\hat{d}_m(t)$ winds up.

5.4 Control Law for Matched and Unmatched Uncertainties

The MLESO-based control law (5.41) only uses the estimate $\hat{\boldsymbol{d}}_m(t)$ of the matched uncertainty. Due to the ability of the MLESO to estimate the unmatched uncertainty $\hat{\boldsymbol{d}}_{um}(t)$ as well, the question arises how this information may be used for control. To that end, notice that a control law for matched and unmatched uncertainties has been derived in Section 3.3.2, if the uncertainties are estimated using a $\mathcal{L}_1$-AC. When furthermore recalling the close relation between MLESO-based control and $\mathcal{L}_1$-AC, it seems reasonable to adapt this control law for the MLESO.

Consider the plant (3.1) and let Assumptions 3.1 (state feedback), 3.2 (positive definite control effectiveness), 3.3 (Lipschitz condition), 3.6 (full-rank $\boldsymbol{B}_P$) hold. As the novel control law is to be derived from the control law for unmatched uncertainties of $\mathcal{L}_1$-AC, the same additional assumptions are supposed, namely Assumptions 3.11 (bounded uncertainties) and 3.12 (minimum-phase desired dynamics).

The control law for unmatched uncertainties of $\mathcal{L}_1$-AC is derived by following a certainty-equivalence type of approach. That is, first of all, an ideal control law is developed, which ensures approximate tracking of the *output* $\boldsymbol{y}_M(t)$ of the reference model (3.4), if the uncertainties are perfectly known. By replacing the true uncertainties by their estimates, the actual control law results. Since this section supposes the same plant and the same assumptions as the $\mathcal{L}_1$-AC control law of Section 3.3.2, the

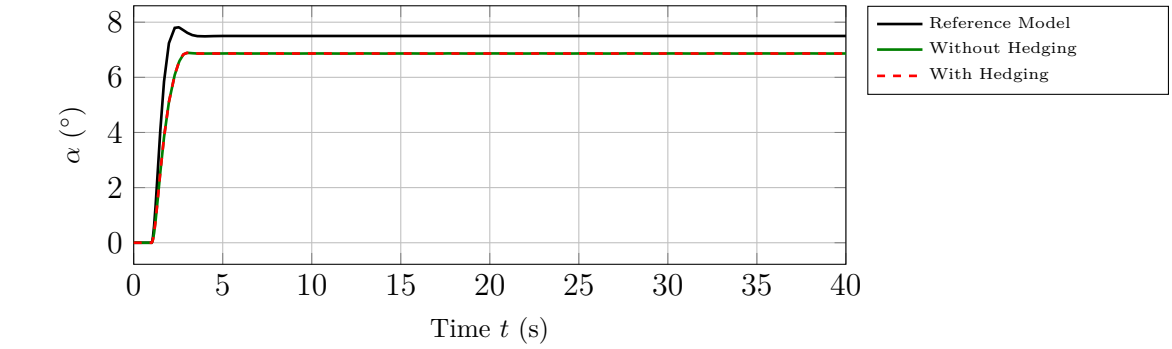

(a) Angle-Of-Attack α

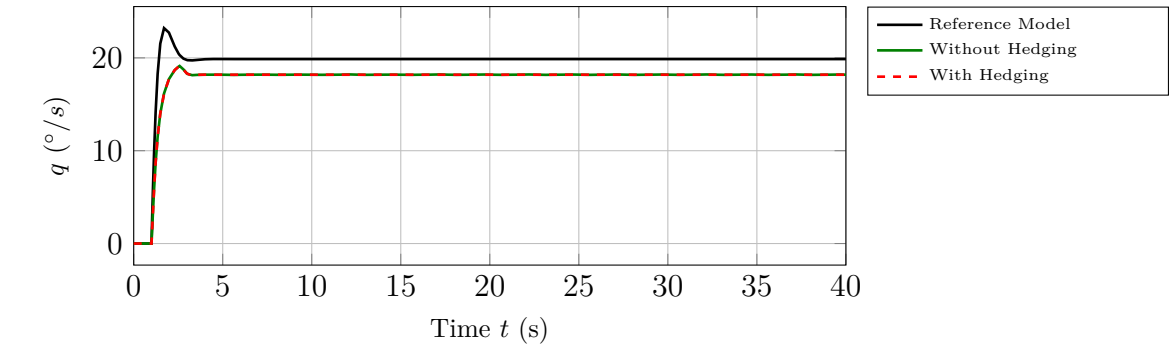

(b) Pitch Rate q

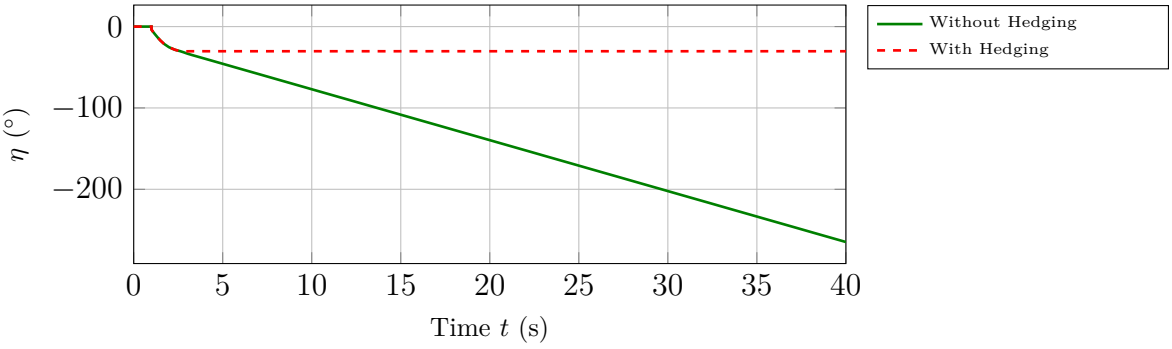

(c) Elevator Deflection η

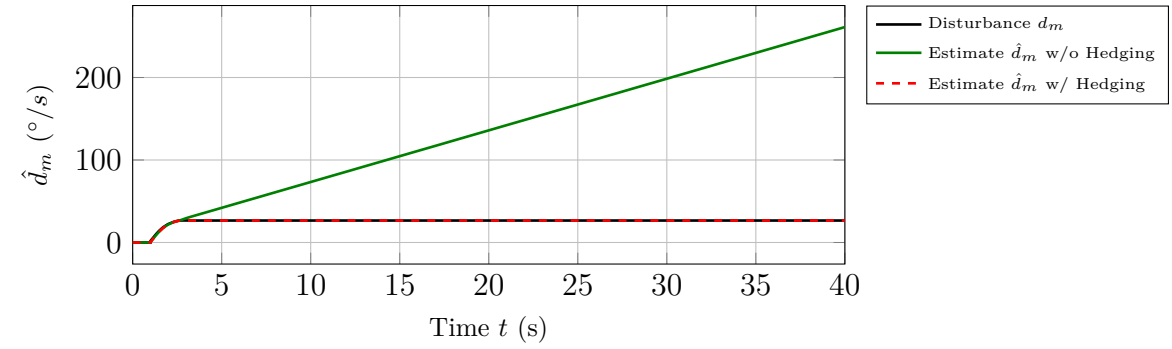

(d) Uncertainty Estimation

Figure 5.8: Comparison of the response of the MLESO with and without hedging for a $7.5°$ step command at $t = 1\,s$ in case of $\lambda_\alpha = \lambda_q = 1$ and $\lambda_\eta = 0.5$.

MLESO-based control law for unmatched uncertainties is derived in the same manner. Under the foregoing assumptions, the ideal control law for unmatched uncertainties of $\mathcal{L}_1$-AC is given by (3.269). In terms of the plant state $\boldsymbol{x}_P(t)$, the ideal control may be written as

$$\boldsymbol{u}(s) = \boldsymbol{C}_m(s)\left(\boldsymbol{K}_r\boldsymbol{r}(s) - \boldsymbol{\sigma}_{P,m}(s) - \boldsymbol{H}_m^{-1}(s)\,\boldsymbol{H}_{um}(s)\,\boldsymbol{\sigma}_{P,um}(s)\right). \tag{5.111}$$

Notice that (5.111) results from the ideal control law (3.269) of $\mathcal{L}_1$-AC with the substitutions $\boldsymbol{x}_{\text{ref}}(t) \rightarrow \boldsymbol{x}_P(t)$ and $\boldsymbol{u}_{\text{ref}}(t) \rightarrow \boldsymbol{u}(t)$. In contrast to $\mathcal{L}_1$-AC, the filter $\boldsymbol{C}_m(s)$ is subsequently required to ensure that $\boldsymbol{C}_m(s)\boldsymbol{H}_m^{-1}(s)\,\boldsymbol{H}_{um}(s)$ is *strictly* proper (instead of just proper). The reason for this slightly stronger requirement will be explained later on.

The ideal control law (5.111) depends on the disturbance signals $\boldsymbol{\sigma}_m(\boldsymbol{x}_P(t), t)$ and $\boldsymbol{\sigma}_{um}(\boldsymbol{x}_P(t), t)$. When comparing the definitions of $\boldsymbol{\sigma}_m(\boldsymbol{x}_P(t), t)$ and $\boldsymbol{\sigma}_{um}(\boldsymbol{x}_P(t), t)$ in (3.242) to the definitions of $\boldsymbol{d}_m(\boldsymbol{x}_P(t), t)$ and $\boldsymbol{d}_{um}(\boldsymbol{x}_P(t), t)$ in (5.19), one observes that they are equivalent. Hence, (5.111) may also be written as

$$\boldsymbol{u}(s) = \boldsymbol{C}_m(s)\left(\boldsymbol{K}_r\boldsymbol{r}(s) - \boldsymbol{d}_m(s) - \boldsymbol{H}_m^{-1}(s)\,\boldsymbol{H}_{um}(s)\,\boldsymbol{d}_{um}(s)\right). \tag{5.112}$$

Now, let the filter $\boldsymbol{C}_m(s)$ satisfy

$$\boldsymbol{C}_m(s) = \frac{k \cdot d(s)}{1 + k \cdot d(s)} \cdot \boldsymbol{I}^{m\times m} = c_m(s) \cdot \boldsymbol{I}^{m\times m}, \tag{5.113}$$

where k is a feedback gain and $d(s)$ is a strictly proper transfer function containing an integrator. Due to this definition, the ideal control law may be expressed as

$$\begin{aligned}\boldsymbol{u}(s) = c_m(s)\,\boldsymbol{I}^{m\times m} \cdot \boldsymbol{K}_r \cdot \boldsymbol{r}(s) - c_m(s)\,\boldsymbol{I}^{m\times m}\boldsymbol{d}_m(s) \\ - \boldsymbol{H}_m^{-1}(s)\,\boldsymbol{H}_{um}(s)\,c_m(s)\,\boldsymbol{I}^{(n-m)\times(n-m)} \cdot \boldsymbol{d}_{um}(s).\end{aligned} \tag{5.114}$$

If the design parameters $\boldsymbol{A}_j,\ j = 0, \ldots k-1$ and $\boldsymbol{B}_j,\ j = 1, \ldots, k-1$ of the MLESO are chosen such that

$$\begin{bmatrix}\hat{\boldsymbol{d}}_m(s) \\ \hat{\boldsymbol{d}}_{um}(s)\end{bmatrix} = c_m(s)\begin{bmatrix}\boldsymbol{I}^{m\times m} & \boldsymbol{0} \\ \boldsymbol{0} & \boldsymbol{I}^{(n-m)\times(n-m)}\end{bmatrix} \cdot \begin{bmatrix}\boldsymbol{d}_m(s) \\ \boldsymbol{d}_{um}(s)\end{bmatrix} \tag{5.115}$$

holds, the MLESO-based control law for unmatched uncertainties readily results:

$$\boldsymbol{u}(s) = \left(c_m(s)\,\boldsymbol{I}^{m\times m}\right)\boldsymbol{K}_r \cdot \boldsymbol{r}(s) - \hat{\boldsymbol{d}}_m(s) - \boldsymbol{H}_m^{-1}(s)\,\boldsymbol{H}_{um}(s)\,\hat{\boldsymbol{d}}_{um}(s). \tag{5.116}$$

At the first glance, the control law (5.116) seems to be non-causal. While this is certainly true when viewing the MLESO (5.27) and the control law (5.116) independently, it should be noted that a causal realization may always be obtained by viewing the MLESO and the control law simultaneously. In order to see this, recall that the filter

$\boldsymbol{C}_m(s)$ has to ensure that $\boldsymbol{C}_m(s)\boldsymbol{H}_m^{-1}(s)\,\boldsymbol{H}_{um}(s)$ is strictly proper and denote the RD of $\boldsymbol{C}_m(s)$ by r. Furthermore, let

$$\hat{\boldsymbol{d}}(s) = \begin{bmatrix} \hat{\boldsymbol{d}}_m(s) \\ \hat{\boldsymbol{d}}_{um}(s) \end{bmatrix} = \begin{bmatrix} \boldsymbol{F}_{MLESO,m}(s) \\ \boldsymbol{F}_{MLESO,um}(s) \end{bmatrix} \cdot \begin{bmatrix} \boldsymbol{x}_P(s) \\ \boldsymbol{u}(s) \end{bmatrix} \tag{5.117}$$

denote the transfer function representation of the MLESO (5.27). If the design parameters of the MLESO (5.27) satisfy (5.115), then the MLESO will possess $RD = r - 1$. In order to see this, notice that $\boldsymbol{M}_i \neq \boldsymbol{0}$ only holds for $i = 0, ..., k - r$. The latter implies that the output $\hat{\boldsymbol{d}}(t)$ has to be differentiated $r - 1$ times with respect to time until the inputs $\boldsymbol{u}(t)$ and $\boldsymbol{x}_P(t)$ of the MLESO appear. Hence, the transfer function $\boldsymbol{H}_m^{-1}(s)\,\boldsymbol{H}_{um}(s)\,\boldsymbol{F}_{MLESO,um}(s)$ will be proper, whereas $\boldsymbol{C}_m(s)\boldsymbol{H}_m^{-1}(s)\,\boldsymbol{H}_{um}(s)$ is strictly proper by definition. Thus, a proper realization of the MLESO and the control law (5.116) may always be obtained. Notice that a proper realization is not possible, if the filter $\boldsymbol{C}_m(s)$ only ensures that $\boldsymbol{C}_m(s)\boldsymbol{H}_m^{-1}(s)\,\boldsymbol{H}_{um}(s)$ is proper (instead of strictly proper). In the latter case, the MLESO would not provide a sufficient excess of poles to render $\boldsymbol{H}_m^{-1}(s)\,\boldsymbol{H}_{um}(s)\,\boldsymbol{F}_{MLESO,um}(s)$ proper.

For the above control law, the following theorem for closed-loop stability holds:

Theorem 5.12 (BIBS Stability in Case of Unmatched Uncertainties and a Semiglobal Lipschitz Condition)**.** *Consider the plant* (3.1) *and let Assumptions 3.1 (state feedback), 3.2 (positive definite control effectiveness), 3.3 (Lipschitz condition), 3.6 (full-rank $\boldsymbol{B}_P$), 3.11 (bounded uncertainties) and 3.12 (minimum-phase desired dynamics) hold. Consider the MLESO* (5.27) *and the control law* (5.116)

If the design parameters $\boldsymbol{A}_j,\ j = 0, ...k-1$ and $\boldsymbol{B}_j,\ j = 1, ..., k-1$ of the MLESO (5.27) *are chosen such that*

1. *the filter $\boldsymbol{C}_d(s)$, defined in* (5.36)*, may be represented by the feedback connection*

$$\boldsymbol{C}_d(s) = c_m(s) \cdot \boldsymbol{I}^{n\times n} \quad \textit{with} \quad c_m(s) = \frac{k \cdot d(s)}{1 + k \cdot d(s)} \tag{5.118}$$

   where $k \in \mathbb{R}$ is a feedback gain and $d(s) : \mathbb{C} \to \mathbb{C}$ is a strictly proper transfer function containing an integrator;

2. *the feedback filter $\boldsymbol{C}_{fb}(s)$, defined as*

$$\boldsymbol{C}_{fb}(s) = (\boldsymbol{I} + \boldsymbol{\Lambda} \cdot k \cdot d(s))^{-1}\,\boldsymbol{\Lambda} \cdot k \cdot d(s), \tag{5.119}$$

   is Hurwitz for all $\boldsymbol{\Lambda} \in \Omega_\Lambda$;

3. *the transfer functions $\boldsymbol{C}_{fb}(s)\boldsymbol{H}_m^{-1}(s)\,\boldsymbol{H}_{um}(s)$ is strictly proper for all $\boldsymbol{\Lambda} \in \Omega_\Lambda$;*

4. *the $\mathcal{L}_1$-norm condition*

$$\begin{aligned} &\|\boldsymbol{G}_m(s)\,(\boldsymbol{I} - \boldsymbol{C}_{fb}(s))\|_{\mathcal{L}_1} \\ &\quad + \|\Big(\boldsymbol{I} - \boldsymbol{G}_m(s)\,\boldsymbol{C}_{fb}(s)\boldsymbol{H}_m^{-1}(s)\,\boldsymbol{C}_P\Big) \cdot \boldsymbol{G}_{um}(s)\|_{\mathcal{L}_1} \cdot \frac{L_{um,\rho_r}}{L_{m,\rho_r}} \\ &\quad < \frac{\rho_r - \|\boldsymbol{G}_m(s)\,\boldsymbol{C}_{fb}(s)\boldsymbol{K}_r\|_{\mathcal{L}_1} \cdot \|\boldsymbol{r}(t)\|_{\mathcal{L}_\infty}}{L_{m,\rho_r} \cdot \rho_r + \phi_0} \quad \forall\ \boldsymbol{\Lambda} \in \Omega_\Lambda, \end{aligned} \tag{5.120}$$

is satisfied for some $\rho_r > 0$ *and some* $\bar{\gamma}_1 > 0$ *and for all* $\boldsymbol{\Lambda} \in \Omega_\Lambda$*, where* $\boldsymbol{G}_m(s)$*,* $\boldsymbol{G}_{um}(s)$*,* L_{m,ρ_r}*,* L_{um,ρ_r} *and* ϕ_0 *have been defined in* (3.182)*,* (3.259)*,* (3.297)*,* (3.298)*,* (3.301)*, respectively;*

then the control law (5.116) *ensures that for zero initial conditions, the plant state is bounded by*

$$\|\boldsymbol{x}_P(t)\|_{\mathcal{L}_\infty} < \rho_r. \tag{5.121}$$

Furthermore, the closed-loop control system consisting of the plant (3.1)*, the control law and the MLESO* (5.27) *is BIBS stable.*

Proof. The proof of Theorem 5.12 aims at representing the closed-loop MLESO control system in such a way that is structurally equivalent to the $\mathcal{L}_1$ *Reference Model* (3.284). Afterwards, the proof invokes Lemma 3.30 to show BIBS stability.

Due to Assumption 3.6, the plant (3.1) admits the alternative representation (5.17), which underlies the derivation of the MLESO (5.28). Using the definitions of the signals $\boldsymbol{\eta}_m(\boldsymbol{x}_P(t), t)$ and $\boldsymbol{\eta}_{um}(\boldsymbol{x}_P(t), t)$ in (3.273) and (3.274), the plant (5.17) becomes

$$\begin{aligned} \dot{\boldsymbol{x}}_P(t) &= \boldsymbol{A}_M \boldsymbol{x}_P(t) + \boldsymbol{B}_P\left(\boldsymbol{\Lambda}\boldsymbol{u}(t) + \boldsymbol{\eta}_m(\boldsymbol{x}_P(t), t)\right) + \bar{\boldsymbol{B}}_P \boldsymbol{\eta}_{um}(\boldsymbol{x}_P(t), t), \\ \boldsymbol{y}_P(t) &= \boldsymbol{C}_P \boldsymbol{x}_P(t). \end{aligned} \tag{5.122}$$

On the other hand, the first condition of Theorem 5.12 ensures that the control law (5.116) may be represented as

$$\begin{aligned} \boldsymbol{u}(s) &= c_m(s)\,\boldsymbol{K}_r \cdot \boldsymbol{r}(s) - c_m(s)\,\boldsymbol{d}_m(s) - \boldsymbol{H}_m^{-1}(s)\,\boldsymbol{H}_{um}(s)\,c_m(s)\,\boldsymbol{d}_{um}(s) \\ &= \frac{k \cdot d(s)}{1 + k \cdot d(s)}\left(\boldsymbol{K}_r \cdot \boldsymbol{r}(s) - \boldsymbol{d}_m(s) - \boldsymbol{H}_m^{-1}(s)\,\boldsymbol{H}_{um}(s)\,\boldsymbol{d}_{um}(s)\right). \end{aligned} \tag{5.123}$$

Multiplying by $(1 + k \cdot d(s))$ and using the definitions of $\boldsymbol{\eta}_m(\boldsymbol{x}_P(t), t)$ and $\boldsymbol{\eta}_{um}(\boldsymbol{x}_P(t), t)$ in (3.273) and (3.274) yields:

$$\begin{aligned} (1 + k \cdot d(s)) \cdot \boldsymbol{u}(s) = k \cdot d(s) \cdot \Big(&\boldsymbol{K}_r \cdot \boldsymbol{r}(s) - (\boldsymbol{\Lambda} - \boldsymbol{I}) \cdot \boldsymbol{u}(s) - \boldsymbol{\eta}_{P,m}(s)\Big) \\ &- k \cdot d(s) \cdot \boldsymbol{H}_m^{-1}(s)\,\boldsymbol{H}_{um}(s)\,\boldsymbol{\eta}_{P,um}(s). \end{aligned} \tag{5.124}$$

Adding $k \cdot d(s) \cdot (\boldsymbol{\Lambda} - \boldsymbol{I}) \cdot \boldsymbol{u}(s)$ on both sides leads to

$$\begin{aligned} (\boldsymbol{I} + k \cdot d(s) \cdot \boldsymbol{\Lambda}) \cdot \boldsymbol{u}(s) = k \cdot d(s) \cdot \Big(&\boldsymbol{K}_r \cdot \boldsymbol{r}(s) - \boldsymbol{\eta}_{P,m}(s)\Big) \\ &- k \cdot d(s) \cdot \boldsymbol{H}_m^{-1}(s)\,\boldsymbol{H}_{um}(s)\,\boldsymbol{\eta}_{P,um}(s). \end{aligned} \tag{5.125}$$

Upon multiplication with $(\boldsymbol{I} + k \cdot d(s) \cdot \boldsymbol{\Lambda})^{-1}$ from the left, one obtains

$$\begin{aligned} \boldsymbol{u}(s) = (\boldsymbol{I} + k \cdot d(s) \cdot \boldsymbol{\Lambda})^{-1} \cdot k \cdot d(s) \cdot &\Big(\boldsymbol{K}_r \cdot \boldsymbol{r}(s) - \boldsymbol{\eta}_{P,m}(s)\Big) \\ - (\boldsymbol{I} + k \cdot d(s) \cdot \boldsymbol{\Lambda})^{-1} \cdot k \cdot d(s) \cdot &\boldsymbol{H}_m^{-1}(s)\,\boldsymbol{H}_{um}(s)\,\boldsymbol{\eta}_{P,um}(s). \end{aligned} \tag{5.126}$$

Multiplying by $\boldsymbol{\Lambda}$ and using the matrix identity (B.177) admits the compact representation

$$\boldsymbol{u}(s) = \boldsymbol{\Lambda}^{-1}\boldsymbol{C}_{fb}(s) \cdot \Big(\boldsymbol{K}_r \cdot \boldsymbol{r}(s) - \boldsymbol{\eta}_{P,m}(s) - \boldsymbol{H}_m^{-1}(s)\,\boldsymbol{H}_{um}(s)\,\boldsymbol{\eta}_{P,um}(s)\Big), \tag{5.127}$$

which resorts to the definition of $\boldsymbol{C}_{fb}(s)$ in the second condition of Theorem 5.12.

When comparing (5.122) and (5.127) to the $\mathcal{L}_1$ *Reference Model* (3.284), one observers that both systems are structurally equivalent. Furthermore, it follows from Assumptions 3.3 and 3.11, that the Lipschitz condition (3.287) is satisfied, where $L_m(r)$ and $L_{um}(r)$ are known functions. Since Lemma 3.30 and Theorem 5.12 suppose the same assumptions and since satisfaction of conditions 2-4 of Theorem 5.12 implies satisfaction of conditions 1-3 of Lemma 3.30, the latter implies that the assertion (5.121) is satisfied.

Since the plant state $\boldsymbol{x}_P(t)$ is bounded, it follows from (5.127) that the control signal $\boldsymbol{u}(t)$ is bounded as well, which in turn implies boundedness of the disturbance $\boldsymbol{d}(t)$. As the latter implies boundedness of the error dynamics (5.28), the states of the MLESO (5.27) are bounded as well, which concludes the proof. □

Remark 5.13. *When comparing the conditions of Theorem 5.12 to those of Lemma 3.30, one observers that Theorem 5.12 is more restrictive. First of all, the filter $\boldsymbol{C}_{fb}(s)$ has to ensure that $\boldsymbol{C}_{fb}(s)\boldsymbol{H}_m^{-1}(s)\boldsymbol{H}_{um}(s)$ is strictly proper instead of just proper. Secondly, Theorem 5.12 requires a scalar gain k and a scalar function $d(s)$ to satisfy all of its conditions instead of a matrix $\boldsymbol{K}$ and a matrix-valued transfer function $\boldsymbol{D}(s)$. Thus, in case of unmatched uncertainties and a MIMO plant, $\mathcal{L}_1$-AC offers more degrees of freedom as compared to the MLESO.*

In order to address this limitation, several solutions might be feasible. A first, rather simple solution consists in using a very fast disturbance estimation. In order to limit the bandwidth of the control law, additional filters are used as proposed in [81]. It is interesting to notice that this approach essentially mimics the behavior of $\mathcal{L}_1$-PWC since the predictor of $\mathcal{L}_1$-PWC may also be seen as a very fast disturbance estimator. A second approach, which involves an extension of the MLESO design philosophy, also seems reasonable. The idea amounts to ensuring that the MLESO itself realizes the transfer function $\boldsymbol{C}_{um}(s) = \boldsymbol{C}_m(s)\boldsymbol{H}_m^{-1}(s)\boldsymbol{H}_{um}(s)$. Since the transfer function $\boldsymbol{H}_m^{-1}(s)\boldsymbol{H}_{um}(s)$ is neither scalar nor diagonal in general, this idea would require that the MLESO also admits non-diagonal transfer functions from $\boldsymbol{d}(t)$ to $\hat{\boldsymbol{d}}(t)$. The latter is currently not possible as to be seen from (5.36)*.*

The applicability of the control law (5.116) is demonstrated in the following example:

Example 5.14. *Consider the same plant and the same reference model as in the respective example on $\mathcal{L}_1$ Adaptive Control with Piecewise Constant Update law (Example 3.34) - namely the short-period approximation of the UAS introduced in Section 2.2. The transfer functions $H_m(s)$ and $H_{um}(s)$ are given by*

$$H_m(s) = \frac{-19.52}{s^2 + 4.384s + 9.61}, \tag{5.128}$$

$$H_{um}(s) = \frac{s + 1.967}{s^2 + 4.384s + 9.61}. \tag{5.129}$$

Clearly, $H_m(s)$ is minimum-phase and hence, satisfies Assumption 3.12. The remaining assumptions of Theorem 5.12 may also be verified easily.

For the estimation of the matched uncertainties, a second-order MLESO is used. The design parameters are chosen as $\bar{\boldsymbol{B}}_P^T = [\,1\;0\,]$, $\boldsymbol{A}_0 = \boldsymbol{B}_0 = \omega_0^2 \cdot \boldsymbol{I}^{2\times 2}$, $\boldsymbol{A}_1 = 2\zeta\omega_0 \cdot \boldsymbol{I}^{2\times 2}$. Here, $\zeta = 0.5$ is fixed and $\omega_0 > 0$ scales the bandwidth of the disturbance estimation. Hence, the transfer function $\boldsymbol{C}_d(s)$ is given by

$$\boldsymbol{C}_d(s) = \frac{\omega_0^2}{s^2 + 2\zeta\omega_0 \cdot s + \omega_0^2} \cdot \boldsymbol{I}^{2\times 2}. \tag{5.130}$$

Since $\boldsymbol{C}_d(s)$ is a PT2 element, it follows from Remark 5.6 that $\boldsymbol{C}_d(s)$ may be represented as a feedback connection. Hence, the first condition of Theorem 5.12 is satisfied.

In order to implement the control law (5.116)*, notice that the product $H_m^{-1}(s)\, H_{um}(s)$ yields the non-causal transfer function*

$$H_m^{-1}(s)\, H_{um}(s) = \frac{s + 1.967}{-19.52}. \tag{5.131}$$

Hence, the control term associated with the unmatched uncertainty is given by:

$$H_m^{-1}(s)\, H_{um}(s) \cdot \hat{d}_{um}(s) = \frac{1}{-19.52} \cdot s \cdot \hat{d}_{um}(s) + \frac{1.967}{-19.52} \cdot \hat{d}_{um}(s)\,. \tag{5.132}$$

Since a second order MLESO is used, the signal $s \cdot \hat{d}_{um}(s) = \mathcal{L}\{\dot{\hat{d}}_{um}(t)\}$ is available in the controller. Thus, the control law (5.116) *may be implemented.*

Figure 5.9 compares the performance of the MLESO for different bandwidths ω_0 of the low-pass filter $\boldsymbol{C}_d(s)$. Despite the presence of unmatched uncertainties, the MLESO tracks the reference model (3.4)*. As before, the filter bandwidth ω_0 is the crucial parameter, which determines how close the MLESO tracks the reference model* (3.4)*.*

With respect to the estimation of the uncertainty signals $d_m(t)$ and $d_{um}(t)$, one may observe that both $\hat{d}_m(t)$ and $\hat{d}_{um}(t)$ closely track their respective true uncertainty signals $d_m(t)$ and $d_{um}(t)$. This is in contrast to the $\mathcal{L}_1$-PWC from Example 3.34, where an offset between the estimate $\hat{\sigma}_{um}(t)$ and the true unmatched uncertainty signal $\sigma_{um}(t)$ was observed.

5.5 Discussion

In this chapter, the MLESO has been introduced as a viable tool for estimating the disturbance signal that causes the plant to deviate from a desired system response. By feeding back this estimate to cancel the disturbance signal, approximate MRC is achieved. To that end, two different types of control laws have been developed - one control law for the case of matched uncertainties only and one for the case of matched

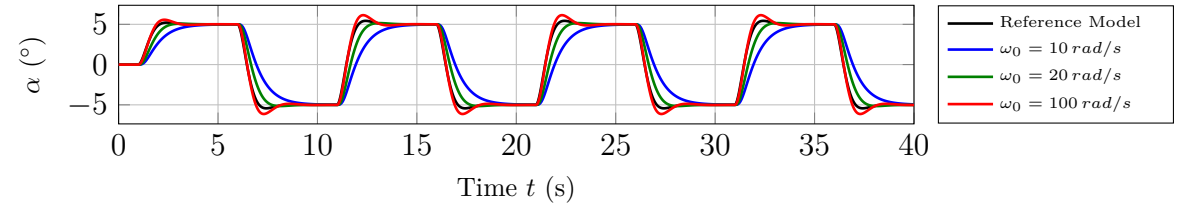

(a) Angle-Of-Attack α

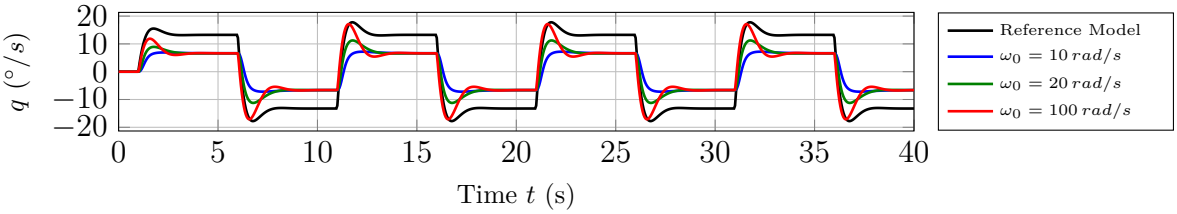

(b) Pitch Rate q

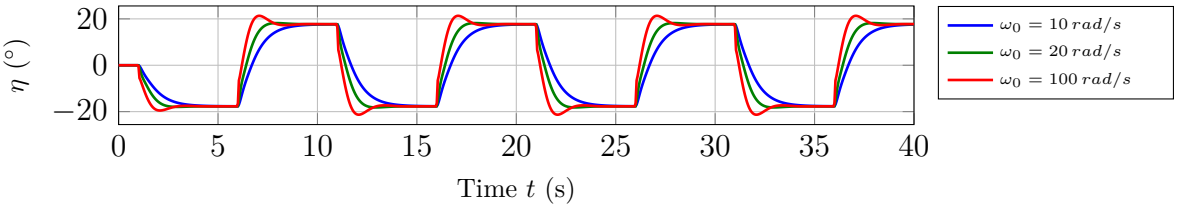

(c) Elevator Deflection η

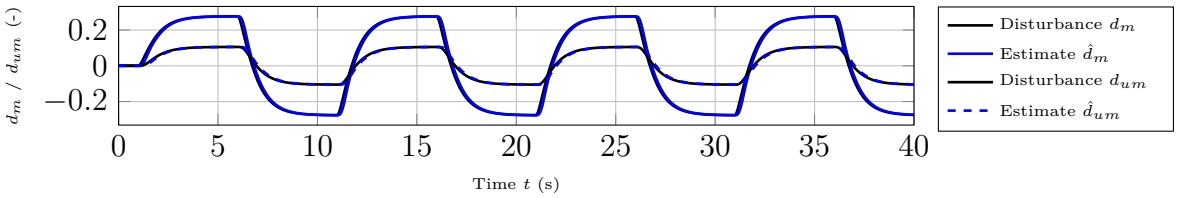

(d) Uncertainty Estimation for $\omega_0 = 10\,rad/s$

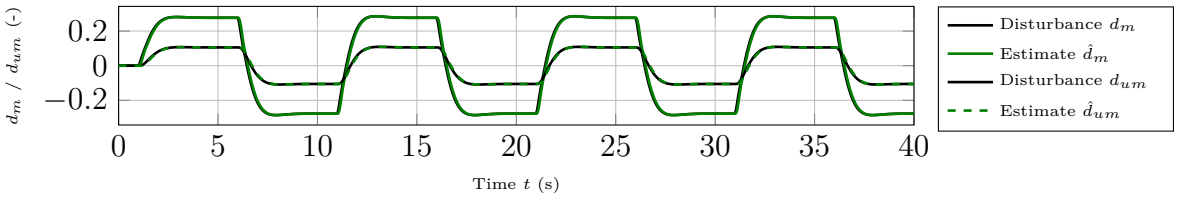

(e) Uncertainty Estimation for $\omega_0 = 20\,rad/s$

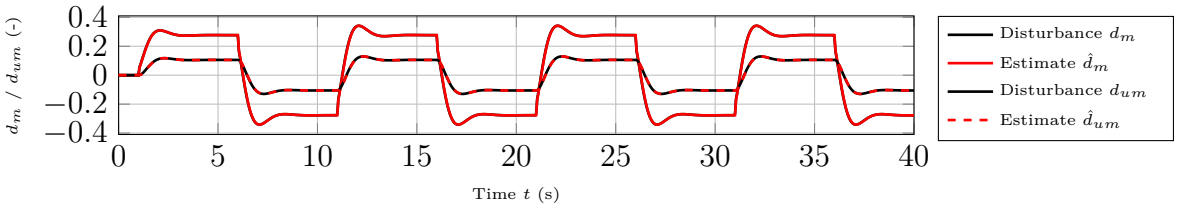

(f) Uncertainty Estimation for $\omega_0 = 100\,rad/s$

Figure 5.9: Performance of the MLESO from Example 5.14 for different values of the filter bandwidth ω_0 in case of $\lambda_\alpha = \lambda_q = \lambda_{Zq} = 1$ and $\lambda_{Z\alpha} = \lambda_\eta = 0.5$.

and unmatched uncertainties. The derivation of the MLESO and of the associated control laws applies to a rather general class of plants and mostly relies on assumptions, which are little restrictive. With respect to the MLESO itself, it has to be noted that the disturbance estimation requires state feedback. Since the state vector is not (entirely) measurable in many applications, an extension towards output feedback would be desirable. As conventional LESOs may also be derived easily in case of output feedback, an appropriate extension is expected to be feasible. The main challenge of such an extension consists in designing the MLESO in such a way that it admits the choice of arbitrary transfer functions between the disturbance and its estimate. With respect to the control laws, it has already been noted in Remark 5.13 that the design parameters of the MLESO have to adhere to rather restrictive requirements in case of unmatched uncertainties. For this reason, future research should also focus on mitigating these restrictions.

In Section 3.4.2, the MRC approaches have been classified as *signal-based* or *parameter-based*. As already noted at the beginning of this chapter, the MLESO is a signal-based approach since the MLESO aims at estimating a disturbance signal. This classification raises two major questions: First of all, how does the MLESO relate to other signal-based approaches? Secondly, how does the MLESO (and other signal-based approaches) relate and compare to parameter-based approaches?

With respect to the *first question*, the derivations and observations of this thesis admit at least a partial answer. In this thesis, the signal-based approaches $\mathcal{L}_1$-PWC, LESO and MLESO have been considered. Depending on the point of view, the MLESO may be seen as a generalization of the LESO. The MLESO admits to realize the relation $\hat{\boldsymbol{d}}(s) = \boldsymbol{C}_d(s) \cdot \boldsymbol{d}(s)$ between the true disturbance signal $\boldsymbol{d}(s)$ and its estimate $\hat{\boldsymbol{d}}(s)$ for any strictly proper, diagonal transfer function $\boldsymbol{C}_d(s)$. As demonstrated in Example 5.1, this is not possible in case of the conventional LESO. Thus, the MLESO is more general with respect to this property. However, with respect to other criteria such as the availability of output feedback, the conventional LESO is more general. Furthermore, Section 5.3.3 has shown that the MLESO is an implementation of the $\mathcal{L}_1$ *Reference Model* in case of matched uncertainties. Thus, any state-feedback $\mathcal{L}_1$-AC for matched uncertainties may also be equivalently implemented as a MLESO. A similar conclusion also holds in case of unmatched uncertainties. The latter follows from the fact that the proof of Theorem 5.12 essentially transformed the closed loop into the respective $\mathcal{L}_1$ *Reference Model*. Since the requirements on the filters are more restrictive for the MLESO than for the $\mathcal{L}_1$-AC, one may however not replace any state-feedback $\mathcal{L}_1$-AC for unmatched uncertainties by a MLESO.

The close relation between the MLESO and $\mathcal{L}_1$-AC has another implication. Since the $\mathcal{L}_1$ *Reference Model* may be implemented by virtue of a DOB (see Section 3.3.3), the MLESO and the DOB are also closely related and may be transformed into each other. More recently, it has been shown that the Command Governor, which had been

introduced in Section 3.2.5 as a modification of MRAC, may also operate independently of MRAC [39]. In the light of the discussion of Section 3.4.2, the resulting controller is a signal-based approach. Its relation to the MLESO has been clarified in [147], where it was observed that the command governor-based control law may also be represented as a MLESO.

The preceding discussion has highlighted that many signal-based approaches are closely related and may be transformed into each other. For this reason, it seems reasonable that similar relations also hold for other signal-based approaches. Consider for example PINDI [155]. In this approach, the derivative of the state vector is estimated using a linear filter. When looking at a plant representation such as (5.18), it is obvious that knowledge of the state vector derivative $\dot{\boldsymbol{x}}_P(t)$ implies knowledge of the disturbance $\boldsymbol{d}(t)$ and vice versa. Thus, PINDI is a signal-based approach and a relation to the MLESO is expected to exist. However, this expectation has to be confirmed by further research. In general, future research, which clarifies the relations between different signal-based approaches, offers two main advantages. On the one side, it allows finding unique features of the respective approaches. The knowledge of such features is of great practical relevance as it simplifies the choice of a suitable signal-based approach for the control problem at hand. On the other side, different signal-based approaches are often derived from fundamentally different points of view. Once their relations are clear, knowledge and observations, which hold for one signal-based approach, may be easily transferred to other approaches. Furthermore, such future research should also address the open-loop properties of the different approaches. This is because two controllers, which achieve the same closed-loop performance, do not necessarily have the same open-loop (robustness) characteristics.

With respect to the *second question* - the relation between parameter-based approaches and the MLESO -, a simple answer in the sense of a transformation is not available. For this reason, one has to resort to case studies, which compare the robustness and performance of the respective approaches. One such case study may be found in [15], where MRAC and $\mathcal{L}_1$-PWC have been compared. In the considered cases, the MRAC outperformed the $\mathcal{L}_1$-PWC with respect to RP. At the same time, the $\mathcal{L}_1$-PWC offered a higher time-delay margin. Due to the close relation between $\mathcal{L}_1$-AC and MLESO-based control, similar results are expected if the same study would have compared MRAC and MLESO. Notice however that single case studies do not allow a general answer to the relation between MLESO-based control and parameter-based approaches.

A more abstract answer to the *second question* results from an analysis of the underlying uncertainty estimation mechanisms. Section 3.4.2 outlined that parameter-based approaches (e.g. MRAC) admit a proactive treatment of uncertainties, whereas a MLESO only reacts to the uncertainties once their effect become measurable. For this reason, a MRAC may outperform a MLESO from an abstract point of view. Nev-

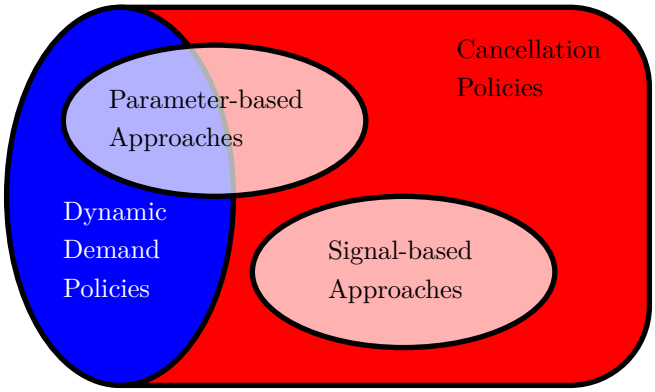

Figure 5.10: Relation of signal-based and parameter-based approaches with respect to the pursued policy. It is expected that only parameter-based approaches will enable to dynamically adjust the demand (the control objective) to the current plant capabilities.

ertheless, it should be noted that this possibly superior performance of MRAC comes at the price of a nonlinear and non-uniform closed-loop behavior. As no appropriate robustness and performance guarantees are available for MRAC (see Chapter 4), the MLESO and other signal-based approaches appear to be viable (interim) solutions until appropriate guarantees are available. In case of the MLESO, this (interim) solution combines robust MRC with reliable robustness and performance guarantees from linear system theory.

While parameter-based approaches such as MRAC and signal-based approaches such as the MLESO differ significantly with respect to the way of uncertainty estimation, they are similar in the way the uncertainty estimate is used. In either case, the estimated uncertain parameters or the estimated disturbance signal, respectively, are used to cancel the deviation between the plant and the reference model. For this reason, both approaches will be said to pursue a cancellation policy. This cancellation policy is an immediate consequence of the pursued control objective, namely MRC. As already highlighted in Section 3.4.1, the reference model of a MRC approach may be interpreted as the demand, which the controller tries to satisfy for the given uncertain plant. While this demand may always be satisfied in case of the nominal plant, which has underlain the derivation of MRAC or MLESO, it may become unrealizable in the presence of plant imperfections such as delay or unmodeled dynamics (see also Section 3.4.1). In this case, a policy, which dynamically manages the demand (i.e. adjusts the reference model at runtime), may be required in order to prevent instability. Such a purposeful modification of the reference model does however require the knowledge of some estimates of the physical parameters of the plant and ideally, of their reliability. While current parameter-based approaches such as MRAC do usually not manage their demand dynamically, their parameter-based nature seems well suited to achieve this goal. To some extent, RCAC for MRC [145] achieves this goal as it dynamically weighs reference model tracking and control effort. In contrast, signal-based

approaches, which do not acquire knowledge at runtime, seem less suited. Notice that reference model modifications such as *hedging* do not suffice for this purpose. While hedging manages the demand in such a way that controller wind-up is prevented, it does not alter the actual control objective such that it becomes achievable in the presence of the plant imperfections (see Section 3.4.1). The overall situation is visualized in Figure 5.10.

Chapter 6

Application to the Benchmark Problem

In this chapter, the MLESO theory, which has been developed in Chapter 5 is applied to the lateral control problem introduced in Section 2.3. This control problem aims at the development of a fallback controller for the lateral motion, which only relies on AHRS measurements. The unavailability of all other measurements constitutes the major challenge of the control problem. Since no measurements of the ADS or the GPS are available, the controller does neither know the current velocity nor the current altitude of the aircraft. Thus, the controller does not possess any information about the dynamic pressure $\bar{q} = (\rho/2) \cdot V^2$. Since all aerodynamic forces and moments depend on the dynamic pressure, an important measurement for any model-based control design is missing. In case of a *conventional control design* relying on gain-scheduling, the unavailability of the velocity and the altitude implies that its typical scheduling variables are unavailable. For a *nonlinear control design* such as Nonlinear Dynamic Inversion (NDI), the dynamic pressure is needed to cancel the plant dynamics in order to achieve feedback linearization.

With respect to the MRC approaches introduced throughout this thesis, the unavailability of the dynamic pressure has another important consequence. It is well known that the aircraft performance scales with the dynamic pressure, i.e. at low dynamic pressure, the aircraft is less agile than at high dynamic pressure. Thus, when designing a reference model for an aircraft, this reference model should account for the varying agility of the aircraft throughout its envelope. At high dynamic pressures, a fast reference model may be prescribed, whereas at low dynamic pressures, only a slow reference model is achievable. If no knowledge of the dynamic pressure is available, then the reference model may not be appropriately adjusted to the current flight condition. Thus, a reference model has to be sought which is achievable throughout the whole envelope, which is another challenge.

The controller, which is to be developed, should meet the following design requirements, which derive from SAE AS94900 [140] and SAE ARP94910 [142]:

1. Stability and Robustness: The flight control system must be stable. It must provide a phase margin $PM \geq 45^\circ$ and a gain margin $GM \geq 6\,dB$ in each control loop. These requirements must be satisfied for all expected parametric uncertainties. For the computation of the margins, the overall flight control system structure according to Figure 2.4 shall be considered.
2. Steady, horizontal flight: In level flight, the (aerodynamic) angle-of-sideslip $|\beta_A^R(t)|$ shall remain below 1° and the lateral acceleration $|b_y(t) \cdot g|$ below $0.02 \cdot g$;
3. Turn coordination: In steady banked turns, the (aerodynamic) angle-of-sideslip $|\beta_A^R(t)|$ must not exceed 2° and the lateral acceleration $|b_y(t) \cdot g|$ shall remain below $0.03 \cdot g$;
4. Roll performance: While rolling, the lateral acceleration $|b_y(t) \cdot g|$ shall not exceed $0.1 \cdot g$;
5. Tracking performance[1]: Steps of the bank angle command $\Phi_{cmd}(t)$ are to be tracked with steady-state accuracy. Rise time and settling time shall be rendered as small as possible without violating the other requirements. The overshoot should be kept as small as possible.

The remainder of this chapter is organized as follows: In Section 6.1, the overall plant as seen from the controller's perspective is derived. Furthermore, a transformation of the plant will be introduced to eliminate the non-measurable state $\beta_K(t)$. Based on this plant representation, Section 6.2 will introduce the MLESO-based control law. This control law combines principles of NDI with the MLESO from Chapter 5. Afterwards, a controller for the purpose of comparison will be derived which results from a slightly modified LQR control problem. Finally, Section 6.4 evaluates the controllers with respect to their stability, robustness and performance.

6.1 Plant Model

In this section, the overall plant model of the UAS, as seen from the control system's perspective, is derived. The plant consists of the linearized rigid-body EOMs (2.52), (2.53), the actuators according to Figure 2.3 and the control and measurement delays τ_c and τ_m.

In the remainder of this chapter, the rigid-body EOMs (2.52), (2.53) are denoted as

$$\begin{aligned} \dot{\boldsymbol{x}}_{lat}(t) &= \boldsymbol{A}_{lat} \cdot \boldsymbol{x}_{lat}(t) + \boldsymbol{B}_{lat} \cdot \boldsymbol{u}(t), \\ \boldsymbol{y}_{lat}(t) &= \boldsymbol{C}_{lat} \cdot \boldsymbol{x}_{lat}(t) + \boldsymbol{D}_{lat} \cdot \boldsymbol{u}(t), \end{aligned} \tag{6.1}$$

[1] This requirement actually states an optimization problem. This way of formulating the requirement has been chosen since the controller to be developed is a fallback controller for emergency situations. Hence, one may not expect the same level of performance as in nominal conditions. Furthermore, in case of an emergency, safe flight has priority over high agility.

where the state vector $\boldsymbol{x}_{lat}(t)$, the input vector $\boldsymbol{u}(t)$ and the output vector $\boldsymbol{y}_{lat}(t)$ are defined as

$$\begin{aligned} \boldsymbol{x}_{lat}(t)^T &\triangleq \begin{bmatrix} r(t) & \beta_K(t) & p(t) & \Phi(t) \end{bmatrix}, \\ \boldsymbol{u}(t)^T &\triangleq \begin{bmatrix} \xi(t) & \zeta(t) \end{bmatrix}, \\ \boldsymbol{y}_{lat}(t)^T &\triangleq \begin{bmatrix} r(t) & b_y(t) & p(t) & \Phi(t) \end{bmatrix}. \end{aligned} \tag{6.2}$$

As explained in Section 2.1.3, the state vector $\boldsymbol{x}_{lat}(t)$, the input vector $\boldsymbol{u}(t)$ and the output vector $\boldsymbol{y}_{lat}(t)$ actually represent deviations from their respective value at the trim condition. Since the trim value of each state, input and output is zero in case of a linearization for horizontal steady-state flight, this chapter will not specifically distinguish between absolute values of the states (the sum of trim value $\boldsymbol{x}_0$, $\boldsymbol{u}_0$ and deviation $\delta\boldsymbol{x}$, $\delta\boldsymbol{u}$) and deviations $\delta\boldsymbol{x}$, $\delta\boldsymbol{u}$ only.

The state space matrices of the EOMs (6.1) are given by

$$\boldsymbol{A}_{lat} = \begin{bmatrix} N_r & N_\beta & N_p & 0 \\ Y_r - \cos\Theta_0 & Y_\beta & Y_p + \sin\Theta_0 & \frac{g}{V_0}\cos\Theta_0 \\ L_r & L_\beta & L_p & 0 \\ \tan\Theta_0 & 0 & 1 & 0 \end{bmatrix}, \qquad \boldsymbol{B}_{lat} = \begin{bmatrix} N_\xi & N_\zeta \\ Y_\xi & Y_\zeta \\ L_\xi & L_\zeta \\ 0 & 0 \end{bmatrix}, \tag{6.3}$$

$$\boldsymbol{C}_{lat} = \begin{bmatrix} 1 & 0 & 0 & 0 \\ F_{y,r} & F_{y,\beta} & F_{y,p} & 0 \\ 0 & 0 & 1 & 0 \\ 0 & 0 & 0 & 1 \end{bmatrix}, \qquad \boldsymbol{D}_{lat} = \begin{bmatrix} 0 & 0 \\ F_{y,\xi} & F_{y,\zeta} \\ 0 & 0 \\ 0 & 0 \end{bmatrix}. \tag{6.4}$$

In order to accommodate the actuator in the plant model, a state space model of the actuator shown in Figure 2.3 is required first. Such a model is given by

$$\begin{aligned} \dot{\boldsymbol{x}}_{act}(t) &= \boldsymbol{A}_{act} \cdot \boldsymbol{x}_{act}(t) + \boldsymbol{B}_{act} \cdot \boldsymbol{u}_{cmd}(t), \\ \boldsymbol{u}(t) &= \boldsymbol{C}_{act} \cdot \boldsymbol{x}_{act}(t), \end{aligned} \tag{6.5}$$

where the state vector is defined as $\boldsymbol{x}_{act}(t)^T = \begin{bmatrix} \xi(t) & \zeta(t) & \dot{\xi}(t) & \dot{\zeta}(t) \end{bmatrix}$ and $\boldsymbol{u}_{cmd}(t)^T = \begin{bmatrix} \xi_{cmd}(t) & \zeta_{cmd}(t) \end{bmatrix}$ denotes the control surface deflections, which are commanded by the control system. The state space matrices of the actuator model (6.5) are given by

$$\begin{aligned} \boldsymbol{A}_{act} &= \begin{bmatrix} \boldsymbol{0}^{2\times2} & \boldsymbol{I}^{2\times2} \\ -\omega_{0,act}^2 \cdot \boldsymbol{I}^{2\times2} & -2\zeta_{act}\omega_{0,act} \cdot \boldsymbol{I}^{2\times2} \end{bmatrix}, \qquad \boldsymbol{B}_{act} = \begin{bmatrix} \boldsymbol{0}^{2\times2} \\ \omega_{0,act}^2 \cdot \boldsymbol{I}^{2\times2} \end{bmatrix}, \\ \boldsymbol{C}_{act} &= \begin{bmatrix} \boldsymbol{I}^2 & \boldsymbol{0}^{2\times2} \end{bmatrix}, \end{aligned} \tag{6.6}$$

where $\omega_{0,act}$ and ζ_{act} are specified in Table 2.3. Combining (6.1) and (6.5) yields the overall plant model

$$\begin{aligned} \dot{\boldsymbol{x}}(t) &= \boldsymbol{A} \cdot \boldsymbol{x}(t) + \boldsymbol{B} \cdot \boldsymbol{u}_{cmd}(t), \\ \boldsymbol{y}(t) &= \boldsymbol{C} \cdot \boldsymbol{x}(t), \\ \boldsymbol{y}_{lat}(t) &= \boldsymbol{C}_{meas} \cdot \boldsymbol{x}(t), \end{aligned} \tag{6.7}$$

where $\boldsymbol{x}(t)^T \triangleq [\,\boldsymbol{x}_{lat}(t)^T \quad \boldsymbol{x}_{act}(t)^T\,]$ denotes the overall state vector and $\boldsymbol{y}(t)^T \triangleq [\,\boldsymbol{y}_{lat}(t)^T \quad \boldsymbol{x}_{act}(t)^T\,]$ denotes the overall output vector. The state space matrices of the overall plant model (6.7) are defined as

$$\boldsymbol{A} \triangleq \begin{bmatrix} \boldsymbol{A}_{lat} & \boldsymbol{B}_{lat} \cdot \boldsymbol{C}_{act} \\ \boldsymbol{0}^{4\times4} & \boldsymbol{A}_{act} \end{bmatrix}, \qquad \boldsymbol{B} \triangleq \begin{bmatrix} \boldsymbol{0}^{4\times2} \\ \boldsymbol{B}_{act} \end{bmatrix}, \tag{6.8}$$

$$\boldsymbol{C} = \begin{bmatrix} \boldsymbol{C}_{lat} & \boldsymbol{D}_{lat} \cdot \boldsymbol{C}_{act} \\ \boldsymbol{0}^{4\times4} & \boldsymbol{I}^{4\times4} \end{bmatrix}, \qquad \boldsymbol{C}_{meas} \triangleq \begin{bmatrix} \boldsymbol{C}_{lat} & \boldsymbol{D}_{lat} \cdot \boldsymbol{C}_{act} \end{bmatrix}. \tag{6.9}$$

The controllers to be developed later on may only rely on the output $\boldsymbol{y}_{lat}(t)$. However, the control approaches introduced in this thesis depend on state feedback. For this reason, the plant model (6.7) is transformed to replace the non-measurable state $\beta_K(t)$ by a lateral acceleration state. To that end, notice that the output matrix $\boldsymbol{C}$, introduced in (6.9) is square and has full rank. Applying the similarity transformation $\boldsymbol{y}(t) = \boldsymbol{C} \cdot \boldsymbol{x}(t)$ to (6.7) hence yields

$$\begin{aligned} \dot{\boldsymbol{y}}(t) &= \boldsymbol{C}\boldsymbol{A}\boldsymbol{C}^{-1} \cdot \boldsymbol{y}(t) + \boldsymbol{C}\boldsymbol{B} \cdot \boldsymbol{u}_{cmd}(t), \\ \boldsymbol{y}_{lat}(t) &= \begin{bmatrix} \boldsymbol{I}^{4\times4} & \boldsymbol{0}^{4\times4} \end{bmatrix} \cdot \boldsymbol{y}(t), \end{aligned} \tag{6.10}$$

where the new rigid-body states $\boldsymbol{y}_{lat}(t)^T = \begin{bmatrix} r(t) & b_y(t) & p(t) & \Phi(t) \end{bmatrix}$ are measurable.

Finally, control and measurement delays may be incorporated to the plant model. The vector of measurements $\boldsymbol{y}_{meas}(t)^T = \begin{bmatrix} r_{meas}(t) & b_{y,meas}(t) & p_{meas}(t) & \Phi_{meas}(t) \end{bmatrix}$ is hence given by

$$\boldsymbol{y}_{meas}(t) = \boldsymbol{y}_{lat}(t - \tau_m). \tag{6.11}$$

Similarly, $\boldsymbol{u}_{cmd}(t)$ may be replaced by $\boldsymbol{u}_{cmd}(t - \tau_c)$ in all of the above plant representations to model the input delay.

6.2 MLESO Control

This section presents the MLESO-based control law for the lateral motion of the UAS from Chapter 2. For the development of the controller, one should first remember that the MLESO-based control, as introduced in Chapter 5, is a MRC approach. Hence, an appropriate reference model is required. If the controller would only have to operate at a single trim condition, the reference model could be designed similar to Example 3.6, where the reference model of the recurrent example was designed. That is, it would suffice to determine appropriate feedback and feedforward gains $\boldsymbol{K}_x$ and $\boldsymbol{K}_r$ for the nominal plant, which satisfy the control objectives. By closing the loop consisting of the nominal plant and these gains, the reference model would follow. Since the desired controller has to operate on a whole envelope of interest, this approach suffers from an important drawback: While such a reference model is an appropriate reference model

at some trim condition, it may be non-achievable at other trim conditions. For this reason, a different approach is taken in this section, which relies on principles of NDI.

Roughly speaking, NDI is a two-step procedure for controller development for nonlinear plants. In a first step, the nonlinear plant is transformed to a chain of integrators by virtue of an appropriate control law and by virtue of the definition of a virtual plant input. The control law, which turns the plant into a chain of integrators, is also referred to as *linearizing state feedback*. In the second step, a controller is designed for the transformed plant using any control design technique available for LTI plants. The theory of NDI is rather involved and will not be presented subsequently. For details on NDI, the reader is referred to [96], [146] or [91]. However, as the plant under consideration is approximately LTI, the NDI design steps significantly simplify and will be explained alongside with the derivation of the control law.

The NDI-based controller takes on a cascaded structure, which is composed of an inner rate control loop and an outer attitude control loop. While a non-cascaded structure would have also been possible and is advantageous in terms of the achievable closed-loop performance, a cascaded structure is nevertheless chosen. The reason for this will be explained shortly.

The objective of the inner rate control loop is to let the roll rate p and the yaw rate r follow the trajectories of a given inner loop reference model. Since the NDI-based controller already achieves MRC, the objective of the MLESO is different from Chapter 5. Instead of enforcing a reference model, the MLESO essentially supports the *linearizing state feedback* in turning the plant into a chain of integrators.

The outer attitude loop aims at letting the plant states $b_y(t)$ and $\Phi(t)$ follow an outer loop reference model. Unlike the bank angle $\Phi(t)$, the lateral acceleration $b_y(t)$ is clearly not an attitude state. In contrast to attitude states, the lateral acceleration is for example immediately influenced by the control surface deflections $\xi(t)$, $\zeta(t)$. However, for the purpose of control design, the lateral acceleration is *treated* like an attitude state. That is, the outer b_y-loop controls the lateral acceleration by issuing appropriate roll rate and yaw rate commands $p_{cmd}(t)$, $r_{cmd}(t)$ to the inner rate control loop. This structure of the attitude loop is also the reason why a cascaded structure has been chosen. In case of a non-cascaded structure, it would not be easily possible to treat $b_y(t)$ like an attitude state. This is because $b_y(t)$ possesses a feedthrough from ξ and ζ and hence, a $RD = 0$, which would prevent the application of non-cascaded NDI.

In the attitude loop, no MLESO augmentation is employed. In case of the bank angle $\Phi(t)$, a simple proportional controller is sufficient since the bank angle $\Phi(t)$ relates to the roll rate $p(t)$ and the yaw rate $r(t)$ only through kinematic relations, which are not uncertain. For the lateral acceleration, a slow PI controller is preferred over a MLESO. This is because the lateral acceleration state $b_y(t)$ also depends on the fast actuator states. In order to prevent undesirable cross-couplings between the attitude loop and the fast actuator dynamics, the outer attitude loop should be slow,

which prohibits a high-gain controller such as the MLESO.

In the following two subsections, the rate control loop and the attitude control loop are developed. Notice that measurement delays τ_m will not be accounted for during the controller development. They will only be accounted for during gain design, which is the topic of Section 6.2.3.

6.2.1 Rate Control Loop

The rate control loop aims at ensuring that the rate states $\boldsymbol{x}_1(t)^T = [\, p(t) \quad r(t) \,]$ follow the states $\boldsymbol{x}_{1,RM} : \mathbb{R}_+ \to \mathbb{R}^2$ of the reference model

$$\dot{\boldsymbol{x}}_{1,RM}(t) = -\boldsymbol{\Omega}_{1,RM} \cdot \boldsymbol{x}_{1,RM}(t) + \boldsymbol{\Omega}_{1,RM} \cdot \boldsymbol{x}_{1,cmd}(t)\,, \tag{6.12}$$

where $\boldsymbol{x}_{1,cmd}(t)^T = [\, p_{cmd}(t) \quad r_{cmd}(t) \,]$ denotes the rate commands, which will be issued by the outer attitude loop. In (6.12), the matrix $\boldsymbol{\Omega}_{1,RM} \in \mathbb{R}^{2\times 2}$ is a diagonal, positive definite design parameter, which allows to specify the desired bandwidth (or the desired rise time, respectively) of the rate states $\boldsymbol{x}_1(t)$.

The development of the rate control loop starts from the plant representation (6.1). It follows from (6.1) that the dynamics of the rate loop are given by

$$\dot{\boldsymbol{x}}_1(t) = \boldsymbol{F}_1 \cdot \boldsymbol{x}_{lat}(t) + \boldsymbol{G}_1 \cdot \boldsymbol{u}(t)\,, \tag{6.13}$$

where the matrices $\boldsymbol{F}_1$ and $\boldsymbol{G}_1$ are defined as

$$\boldsymbol{F}_1 \triangleq \begin{bmatrix} L_r & L_\beta & L_p & 0 \\ N_r & N_\beta & N_p & 0 \end{bmatrix}, \qquad \boldsymbol{G}_1 \triangleq \begin{bmatrix} L_\xi & L_\zeta \\ N_\xi & N_\zeta \end{bmatrix}. \tag{6.14}$$

Since the EOMs (6.1) are uncertain, the matrices $\boldsymbol{F}_1$ and $\boldsymbol{G}_1$ are uncertain as well. For this reason, let

$$\boldsymbol{F}_{1,nom} \triangleq \begin{bmatrix} L_{r,nom} & L_{\beta,nom} & L_{p,nom} & 0 \\ N_{r,nom} & N_{\beta,nom} & N_{p,nom} & 0 \end{bmatrix}, \qquad \boldsymbol{G}_{1,nom} \triangleq \begin{bmatrix} L_{\xi,nom} & L_{\zeta,nom} \\ N_{\xi,nom} & N_{\zeta,nom} \end{bmatrix}, \tag{6.15}$$

denote the nominal values of $\boldsymbol{F}_1$ and $\boldsymbol{G}_1$, respectively. With $\boldsymbol{F}_{1,nom}$ and $\boldsymbol{G}_{1,nom}$, the rate loop dynamics (6.13) may be reformulated as

$$\dot{\boldsymbol{x}}_1(t) = \boldsymbol{F}_{1,nom}\cdot\boldsymbol{x}_{lat}(t) + \boldsymbol{G}_{1,nom}\cdot\boldsymbol{u}(t) + (\boldsymbol{F}_1 - \boldsymbol{F}_{1,nom})\cdot\boldsymbol{x}_{lat}(t) + (\boldsymbol{G}_1 - \boldsymbol{G}_{1,nom})\cdot\boldsymbol{u}(t)\,. \tag{6.16}$$

The first two terms in (6.16) denote the nominal plant dynamics assumed by the controller, whereas the last two terms represent the plant uncertainties. The development of the NDI controller will rely on the nominal plant dynamics. Later on, a MLESO will be designed to accommodate the plant uncertainties.

If there were no uncertainties ($\boldsymbol{F}_1 = \boldsymbol{F}_{1,nom}$ and $\boldsymbol{G}_1 = \boldsymbol{G}_{1,nom}$) and no actuators, a "linearizing" state feedback, which turns (6.16) into two integrators, would be given by

$$\boldsymbol{u}_{cmd}(t) = \boldsymbol{G}_{1,nom}^{-1} \cdot (\boldsymbol{\nu}_1(t) - \boldsymbol{F}_{1,nom} \cdot \boldsymbol{x}_{lat}(t))\,, \tag{6.17}$$

where $\boldsymbol{\nu}_1 : \mathbb{R}_+ \rightarrow \mathbb{R}^2$ denotes the virtual *alternative control input*. In practice, the "linearizing" state feedback (6.17) may not be implemented as the state $\beta_K(t)$ is not available as a measurement. However, since a MLESO will be available to compensate for the plant uncertainties, it suffices to redefine the nominal plant model in order to obtain an implementable "linearizing" state feedback. To that end, let

$$\bar{\boldsymbol{F}}_{1,nom} \triangleq \begin{bmatrix} L_{r,nom} & 0 & L_{p,nom} & 0 \\ N_{r,nom} & 0 & N_{p,nom} & 0 \end{bmatrix} \tag{6.18}$$

denote the portion of the nominal plant dynamics, which does not depend on the non-measurable state $\beta_K(t)$. Similar to (6.16), the rate dynamics can now be rewritten as

$$\dot{\boldsymbol{x}}_1(t) = \bar{\boldsymbol{F}}_{1,nom} \cdot \boldsymbol{x}_{lat}(t) + \boldsymbol{G}_{1,nom} \cdot \boldsymbol{u}(t) + \boldsymbol{d}_m(t), \tag{6.19}$$

where

$$\boldsymbol{d}_m(t) \triangleq (\boldsymbol{F}_1 - \bar{\boldsymbol{F}}_{1,nom}) \cdot \boldsymbol{x}_{lat}(t) + (\boldsymbol{G}_1 - \boldsymbol{G}_{1,nom}) \cdot \boldsymbol{u}(t) \tag{6.20}$$

denotes a disturbance signal. Later on, a MLESO will be designed, which estimates $\boldsymbol{d}_m(t)$. An implementable "linearizing" state feedback is hence given by

$$\boldsymbol{u}_{cmd}(t) = \boldsymbol{G}_{1,nom}^{-1} \cdot \left(\boldsymbol{\nu}_1(t) - \bar{\boldsymbol{F}}_{1,nom} \cdot \boldsymbol{x}_{lat}(t) \right). \tag{6.21}$$

The "linearizing" state feedback (6.21) cannot directly influence the rate dynamics, but is delayed by τ_c and passes through the actuator. To reflect this fact, add and subtract $\boldsymbol{G}_{1,nom} \cdot \boldsymbol{u}_{cmd}(t)$ in (6.19), which yields:

$$\dot{\boldsymbol{x}}_1(t) = \bar{\boldsymbol{F}}_{1,nom} \cdot \boldsymbol{x}_{lat}(t) + \boldsymbol{G}_{1,nom} \cdot \boldsymbol{u}_{cmd}(t) + \boldsymbol{G}_{1,nom} \cdot (\boldsymbol{u}(t) - \boldsymbol{u}_{cmd}(t)) + \boldsymbol{d}_m(t). \tag{6.22}$$

Eq. (6.22) represents the rate dynamics in terms of the nominal rate dynamics (first two terms), a disturbance due to the actuator and the time-delay (third term) and a disturbance due to the plant uncertainties (fourth term).

Inserting the "linearizing" state feedback (6.21) into (6.22) yields

$$\dot{\boldsymbol{x}}_1(t) = \boldsymbol{\nu}_1(t) + \boldsymbol{G}_{1,nom} \cdot (\boldsymbol{u}(t) - \boldsymbol{u}_{cmd}(t)) + \boldsymbol{d}_m(t). \tag{6.23}$$

Clearly, if there was no actuator, no time-delay (i.e. $\boldsymbol{u}(t) = \boldsymbol{u}_{cmd}(t)$) and no uncertainty (i.e. $\boldsymbol{d}_m(t) = \boldsymbol{0}$), the "linearizing" state feedback turns the rate dynamics into two integrators. In the disturbance-free case, the pure feedforward control law $\boldsymbol{\nu}_1(t) = \boldsymbol{\nu}_{1,RM}(t)$ with

$$\boldsymbol{\nu}_{1,RM}(t) = -\boldsymbol{\Omega}_{1,RM} \cdot \boldsymbol{x}_{1,RM}(t) + \boldsymbol{\Omega}_{1,RM} \cdot \boldsymbol{x}_{1,cmd}(t) \tag{6.24}$$

would suffice to achieve tracking of the reference model (6.12). However, in the presence of disturbances, the reference model and the plant will deviate quickly. For this reason, the control law is extended to

$$\boldsymbol{\nu}_1(t) = \boldsymbol{\nu}_{1,RM}(t) + \boldsymbol{\nu}_{1,BL}(t) + \boldsymbol{\nu}_{1,MLESO}(t), \tag{6.25}$$

where $\boldsymbol{\nu}_{1,BL}(t)$ is the control signal of a conventional feedback and $\boldsymbol{\nu}_{1,MLESO}(t)$ is the control signal of the MLESO augmentation. In order to prevent wind-up due to the time-delay and the actuator dynamics, the reference model (6.12) is altered to

$$\begin{aligned}\dot{\boldsymbol{x}}_{1,RM}(t) &= -\boldsymbol{\Omega}_{1,RM}\cdot\boldsymbol{x}_{1,RM}(t) + \boldsymbol{\Omega}_{1,RM}\cdot\boldsymbol{x}_{1,cmd}(t) + \boldsymbol{G}_{1,nom}\cdot(\hat{\boldsymbol{u}}(t) - \boldsymbol{u}_{cmd}(t)),\\ \boldsymbol{\nu}_{1,RM}(t) &= -\boldsymbol{\Omega}_{1,RM}\cdot\boldsymbol{x}_{1,RM}(t) + \boldsymbol{\Omega}_{1,RM}\cdot\boldsymbol{x}_{1,cmd}(t),\end{aligned} \tag{6.26}$$

where $\hat{\boldsymbol{u}}(t)$ is an estimate of the control surface deflections $\boldsymbol{u}(t)$. The reason for this modification becomes evident, when considering the error between the modified reference model (6.26) and the rate dynamics (6.23), which is defined as $\boldsymbol{e}_1(t) \triangleq \boldsymbol{x}_{1,RM}(t) - \boldsymbol{x}_1(t)$. The error dynamics become

$$\begin{aligned}\dot{\boldsymbol{e}}_1(t) = \dot{\boldsymbol{x}}_{1,RM}(t) - \dot{\boldsymbol{x}}_1(t) = &\boldsymbol{G}_{1,nom}\cdot(\hat{\boldsymbol{u}}(t) - \boldsymbol{u}_{cmd}(t)) - \boldsymbol{\nu}_{1,BL}(t) - \boldsymbol{\nu}_{1,MLESO}(t)\\ &- \boldsymbol{G}_{1,nom}\cdot(\boldsymbol{u}(t) - \boldsymbol{u}_{cmd}(t)) - \boldsymbol{d}_m(t).\end{aligned} \tag{6.27}$$

Obviously, if $\hat{\boldsymbol{u}}(t) \approx \boldsymbol{u}(t)$ holds, then the error dynamics simplify to

$$\dot{\boldsymbol{e}}_1(t) = -\boldsymbol{\nu}_{1,BL}(t) - \boldsymbol{\nu}_{1,MLESO}(t) - \boldsymbol{d}_m(t). \tag{6.28}$$

Hence, any controller, which relies on the error $\boldsymbol{e}_1(t)$, will not "see" the influence of the actuator and the control delay τ_c. The actuator model, which is used within the controller to generate the estimate $\hat{\boldsymbol{u}}(t)$, will be presented later on in Section 6.2.3.

In order to stabilize the error dynamics, the conventional feedback $\boldsymbol{\nu}_{1,BL}(t)$ is chosen as

$$\boldsymbol{\nu}_{1,BL}(t) = \boldsymbol{K}_1\cdot\boldsymbol{e}_1(t), \tag{6.29}$$

where $\boldsymbol{K}_1 \in \mathbb{R}^{2\times2}$ is a diagonal, positive definite design parameter, which specifies the decay rate of the error dynamics. The error dynamics (6.28) become

$$\dot{\boldsymbol{e}}_1(t) = -\boldsymbol{K}_1\cdot\boldsymbol{e}_1(t) - \boldsymbol{\nu}_{1,MLESO}(t) - \boldsymbol{d}_m(t). \tag{6.30}$$

In order to estimate the disturbance $\boldsymbol{d}_m(t)$, a first-order MLESO is applied to the error dynamics (6.30). According to Chapter 5, it is given by

$$\begin{aligned}\dot{\hat{\boldsymbol{e}}}_1(t) &= -\boldsymbol{K}_1\cdot\boldsymbol{e}_1(t) - \boldsymbol{\nu}_{1,MLESO}(t) + \boldsymbol{L}_0\cdot(\hat{\boldsymbol{e}}_1(t) - \boldsymbol{e}_1(t)),\\ \hat{\boldsymbol{d}}_m(t) &= \boldsymbol{M}_0\cdot(\hat{\boldsymbol{e}}_1(t) - \boldsymbol{e}_1(t)).\end{aligned} \tag{6.31}$$

Upon definition of the error $\tilde{\boldsymbol{e}}_1(t) \triangleq \hat{\boldsymbol{e}}_1(t) - \boldsymbol{e}_1(t)$ between the MLESO and the NDI error state $\boldsymbol{e}_1(t)$, one obtains the error dynamics

$$\begin{aligned}\dot{\tilde{\boldsymbol{e}}}_1 &= \boldsymbol{L}_0\cdot\tilde{\boldsymbol{e}}_1(t) - \boldsymbol{d}_m(t),\\ \hat{\boldsymbol{d}}_m(t) &= \boldsymbol{M}_0\cdot\tilde{\boldsymbol{e}}_1(t).\end{aligned} \tag{6.32}$$

In order to obtain a disturbance estimate $\hat{\boldsymbol{d}}_m(t)$ with unit DC gain, the gains of the MLESO are chosen as $\boldsymbol{L}_0 = \boldsymbol{M}_0 = -\boldsymbol{\Omega}_{1,MLESO}$. The matrix $\boldsymbol{\Omega}_{1,MLESO} \in \mathbb{R}^{2\times2}$ is a

diagonal, positive definite design parameter that specifies the disturbance estimation bandwidth.

In order to cancel the disturbance $\boldsymbol{d}_m(t)$, the control signal of the MLESO is chosen as $\boldsymbol{\nu}_{1,MLESO}(t) = -\hat{\boldsymbol{d}}_m(t)$. Hence, the overall control law (6.25) becomes

$$\boldsymbol{\nu}_1(t) = \boldsymbol{\nu}_{1,RM}(t) - \boldsymbol{K}_1 \cdot \boldsymbol{e}_1(t) - \hat{\boldsymbol{d}}_m(t), \tag{6.33}$$

which turns the error dynamics (6.30) into

$$\dot{\boldsymbol{e}}_1(t) = -\boldsymbol{K}_1 \cdot \boldsymbol{e}_1(t) + \hat{\boldsymbol{d}}_m(t) - \boldsymbol{d}_m(t). \tag{6.34}$$

Clearly, if the MLESO is successful in estimating $\boldsymbol{d}_m(t)$, its influence on the rate error dynamics vanishes, which implies tracking of the reference model (6.26).

When reviewing the control law derived so far, one observes that it depends on the nominal plant coefficients through the matrices $\bar{\boldsymbol{F}}_{1,nom}$ and $\boldsymbol{G}_{1,nom}$. Since the controller shall operate on a whole envelope of interest, the question arises which coefficients shall be used. Since the aircraft is least agile at low dynamic pressures (high altitude / low velocity), it is reasonable to use the coefficients at $V_K^R = 35\,m/s$, $h = 1000\,m$, $m_{fuel} = 23\,kg$ in order to prevent the controller from overstraining the plant. Now consider the "linearizing" state feedback (6.21), which depends on the matrix $\boldsymbol{G}_{1,nom}$. When using the coefficients at $V_K^R = 35\,m/s$, $h = 1000\,m$, $m_{fuel} = 23\,kg$, the matrix $\boldsymbol{G}_{1,nom}$ is small due to the low dynamic pressure and hence, $\boldsymbol{G}_{1,nom}^{-1}$ is large. When applying this "linearizing" state feedback at a high dynamic pressure trim condition (low altitude / high velocity), a control signal $\boldsymbol{\nu}_1(t)$ is mapped to overly large control surface deflections, since $\boldsymbol{G}_{1,nom}^{-1}$ is larger than required at this trim condition. Thus, the matrix $\boldsymbol{G}_{1,nom}^{-1}$ acts similar to a gain uncertainty in the control channel, which may cause a significant reduction of the time-delay margin at high dynamic pressures. In order to prevent this situation, the matrix $\boldsymbol{G}_{1,nom}$ is artificially enlarged, which means that the control effectiveness of the control surfaces at low dynamic pressure is overestimated. This in turn reduces $\boldsymbol{G}_{1,nom}^{-1}$. Since a MLESO is available to estimate the disturbances, the use of an artificially enlarged matrix $\boldsymbol{G}_{1,nom}$ does neither endanger stability nor performance. Subsequently, the artificially enlarged matrix $\boldsymbol{G}_{1,nom}$ will be denoted by $\bar{\boldsymbol{G}}_{1,nom}$. The derivation of the rate control loop with an overestimation of the control effectiveness is exactly equivalent to the derivation presented before, with the only difference that $\boldsymbol{G}_{1,nom}$ has to be replaced by $\bar{\boldsymbol{G}}_{1,nom}$. For this reason, the derivation is not repeated here, but the resulting control laws are summarized in Table 6.1. Details on the choice of $\bar{\boldsymbol{G}}_{1,nom}$ will be presented during the gain design in Section 6.2.3.

6.2.2 Attitude Loop

The attitude control loop shall ensure that the "attitude states" $\boldsymbol{x}_2(t)^T = [\,\Phi(t) \quad b_y(t)\,]$ follow the states $\boldsymbol{x}_{2,RM} : \mathbb{R}_+ \to \mathbb{R}^2$ of the reference model

$$\dot{\boldsymbol{x}}_{2,RM} = -\boldsymbol{\Omega}_{2,RM} \cdot \boldsymbol{x}_{2,RM}(t) + \boldsymbol{\Omega}_{2,RM} \cdot \boldsymbol{x}_{2,cmd}(t), \tag{6.35}$$

where $\boldsymbol{x}_{2,cmd}\left(t\right)^T = \left[\,\Phi_{cmd}\left(t\right) \quad b_{y,cmd}\left(t\right)\,\right]$ denotes the attitude commands. In (6.35), the matrix $\boldsymbol{\Omega}_{2,RM} \in \mathbb{R}^{2\times 2}$ is a diagonal, positive definite design parameter, which allows to specify the desired bandwidth (or the desired rise time, respectively) of the attitude states $\boldsymbol{x}_2\left(t\right)$.

The development of the attitude control loop starts from the plant representation (6.10). It follows from (6.10) that the dynamics of the attitude loop are given by

$$\dot{\boldsymbol{x}}_2\left(t\right) = \boldsymbol{F}_2 \cdot \boldsymbol{y}\left(t\right) + \boldsymbol{G}_2 \cdot \boldsymbol{x}_1\left(t\right), \tag{6.36}$$

where the matrices $\boldsymbol{F}_2$ and $\boldsymbol{G}_2$ are defined as

$$\boldsymbol{F}_2 \triangleq \begin{bmatrix} 0 & 0 & 0 & 0 & 0 & 0 & 0 & 0 \\ 0 & \bar{Y}_{by} & 0 & \bar{Y}_{\Phi} & \bar{Y}_{\xi} & \bar{Y}_{\zeta} & \bar{Y}_{\dot{\xi}} & \bar{Y}_{\dot{\zeta}} \end{bmatrix}, \qquad \boldsymbol{G}_2 \triangleq \begin{bmatrix} 1 & \tan\Theta_0 \\ \bar{Y}_p & \bar{Y}_r \end{bmatrix}. \tag{6.37}$$

In (6.37), the coefficients $\bar{Y}_{(\cdot)}$ denote the coefficients of (6.10), which are associated with the state $b_y\left(t\right)$ (i.e. the coefficients of the second line of $\boldsymbol{CAC}^{-1}$).

Since the EOMs (6.1) are uncertain, the matrices $\boldsymbol{F}_2$ and $\boldsymbol{G}_2$ are uncertain as well. For this reason, let

$$\begin{aligned} \boldsymbol{F}_{2,nom} &\triangleq \begin{bmatrix} 0 & 0 & 0 & 0 & 0 & 0 & 0 & 0 \\ 0 & \bar{Y}_{by,nom} & 0 & \bar{Y}_{\Phi,nom} & \bar{Y}_{\xi,nom} & \bar{Y}_{\zeta,nom} & \bar{Y}_{\dot{\xi},nom} & \bar{Y}_{\dot{\zeta},nom} \end{bmatrix}, \\ \boldsymbol{G}_{2,nom} &\triangleq \begin{bmatrix} 1 & \tan\Theta_0 \\ \bar{Y}_{p,nom} & \bar{Y}_{r,nom} \end{bmatrix} \end{aligned} \tag{6.38}$$

denote the nominal values of $\boldsymbol{F}_2$ and $\boldsymbol{G}_2$, respectively. With $\boldsymbol{F}_{2,nom}$ and $\boldsymbol{G}_{2,nom}$, the attitude loop dynamics (6.36) may be reformulated as

$$\begin{aligned} \dot{\boldsymbol{x}}_2\left(t\right) = \boldsymbol{F}_{2,nom} \cdot \boldsymbol{y}\left(t\right) + \boldsymbol{G}_{2,nom} \cdot \boldsymbol{x}_1\left(t\right) + \left(\boldsymbol{F}_2 - \boldsymbol{F}_{2,nom}\right) \cdot \boldsymbol{y}\left(t\right) \\ + \left(\boldsymbol{G}_2 - \boldsymbol{G}_{2,nom}\right) \cdot \boldsymbol{x}_1\left(t\right). \end{aligned} \tag{6.39}$$

The first two terms in (6.39) denote the nominal plant dynamics assumed by the controller, whereas the last two terms represent the plant uncertainties.

The representation (6.39) of the attitude dynamics is not yet suitable for the development of an attitude control law, because:

1. the nominal matrix $\boldsymbol{F}_{2,nom}$, which would be used in the "linearizing" state feedback, would cause a coupling between the fast actuator state derivatives $\dot{\xi}(t)$ and $\dot{\zeta}(t)$ and the slow attitude loop;
2. (6.39) depends on the actuator states $\boldsymbol{x}_{act}\left(t\right)$, which are not measurable;
3. the plant state $\boldsymbol{x}_1\left(t\right)$ may not be directly commanded.

In order to address the first problem, let $\bar{\boldsymbol{F}}_{2,nom}$ denote the portion of $\boldsymbol{F}_{2,nom}$, which does not depend on $\dot{\xi}(t)$ and $\dot{\zeta}(t)$:

$$\bar{\boldsymbol{F}}_{2,nom} \triangleq \begin{bmatrix} 0 & 0 & 0 & 0 & 0 & 0 & 0 & 0 \\ 0 & \bar{Y}_{by,nom} & 0 & \bar{Y}_{\Phi,nom} & \bar{Y}_{\xi,nom} & \bar{Y}_{\zeta,nom} & 0 & 0 \end{bmatrix}. \tag{6.40}$$

To address the second problem, the matrix $\bar{\boldsymbol{F}}_{2,nom}$ is furthermore partitioned as follows

$$\bar{\boldsymbol{F}}_{2,nom} = \begin{bmatrix} \bar{\boldsymbol{F}}_{2,nom,lat} & \bar{\boldsymbol{F}}_{2,nom,act} \end{bmatrix}, \tag{6.41}$$

with $\bar{\boldsymbol{F}}_{2,nom,lat} \in \mathbb{R}^{2\times 4}$ and $\bar{\boldsymbol{F}}_{2,nom,act} \in \mathbb{R}^{2\times 4}$. For the third problem, notice that $\boldsymbol{x}_1(t) = \boldsymbol{x}_1(t) + \boldsymbol{x}_{1,cmd}(t) - \boldsymbol{x}_{1,cmd}(t)$ holds, where $\boldsymbol{x}_{1,cmd}(t)$ is the command signal for the rate control loop. The attitude dynamics may hence be written as

$$\begin{aligned} \dot{\boldsymbol{x}}_2(t) = \bar{\boldsymbol{F}}_{2,nom,lat} \cdot \boldsymbol{y}_{lat}(t) + \bar{\boldsymbol{F}}_{2,nom,act} \cdot \boldsymbol{x}_{act}(t) + \boldsymbol{G}_{2,nom} \cdot \boldsymbol{x}_{1,cmd}(t) \\ + \boldsymbol{G}_{2,nom} \cdot (\boldsymbol{x}_1(t) - \boldsymbol{x}_{1,cmd}(t)) + \boldsymbol{d}_{um}(t). \end{aligned} \tag{6.42}$$

In (6.42), $\boldsymbol{d}_{um}(t)$ denotes the uncertainties of the attitude control loop, which are defined as

$$\boldsymbol{d}_{um}(t) = \left(\boldsymbol{F}_2 - \bar{\boldsymbol{F}}_{2,nom}\right) \cdot \boldsymbol{y}(t) + (\boldsymbol{G}_2 - \boldsymbol{G}_{2,nom}) \cdot \boldsymbol{x}_1(t). \tag{6.43}$$

For the development of the attitude control law, consider the rate command $\boldsymbol{x}_{1,cmd}(t)$ as control input. If the rates $\boldsymbol{x}_1(t)$ would perfectly follow the rate commands $\boldsymbol{x}_{1,cmd}(t)$ (i.e. $\boldsymbol{x}_1(t) = \boldsymbol{x}_{1,cmd}(t)$) and if there were no uncertainties (i.e. $\boldsymbol{d}_{um}(t) = \boldsymbol{0}$), the "linearizing" state feedback of the attitude loop would be given by

$$\boldsymbol{x}_{1,cmd}(t) = \boldsymbol{G}_{2,nom}^{-1} \cdot \left(\boldsymbol{\nu}_2(t) - \bar{\boldsymbol{F}}_{2,nom,lat} \cdot \boldsymbol{y}_{lat}(t) - \bar{\boldsymbol{F}}_{2,nom,act} \cdot \boldsymbol{x}_{act}(t)\right). \tag{6.44}$$

Since the actuator state $\boldsymbol{x}_{act}(t)$ may not be measured, it is replaced by an estimate $\hat{\boldsymbol{x}}_{act}(t)$. The actuator model, which outputs the estimate $\hat{\boldsymbol{x}}_{act}(t)$, will be introduced in Section 6.2.3. The "linearizing" state feedback is hence defined as

$$\boldsymbol{x}_{1,cmd}(t) = \boldsymbol{G}_{2,nom}^{-1} \cdot \left(\boldsymbol{\nu}_2(t) - \bar{\boldsymbol{F}}_{2,nom,lat} \cdot \boldsymbol{y}_{lat}(t) - \bar{\boldsymbol{F}}_{2,nom,act} \cdot \hat{\boldsymbol{x}}_{act}(t)\right). \tag{6.45}$$

Inserting (6.45) into the attitude dynamics (6.42) yields

$$\begin{aligned} \dot{\boldsymbol{x}}_2(t) = \boldsymbol{\nu}_2(t) + \bar{\boldsymbol{F}}_{2,nom,act}(\boldsymbol{x}_{act}(t) - \hat{\boldsymbol{x}}_{act}(t)) \\ + \boldsymbol{G}_{2,nom} \cdot (\boldsymbol{x}_1(t) - \boldsymbol{x}_{1,cmd}(t)) + \boldsymbol{d}_{um}(t). \end{aligned} \tag{6.46}$$

Clearly, if there was no rate control loop dynamics, no actuator dynamics and no uncertainty, the "linearizing" state feedback (6.45) would turn the attitude dynamics into two integrators. However, since these disturbances have to be considered, the control law

$$\boldsymbol{\nu}_2(t) = \boldsymbol{\nu}_{2,RM}(t) + \boldsymbol{\nu}_{2,BL}(t) \tag{6.47}$$

is used. Similar to the rate loop, the reference model of the attitude loop outputs the feedforward signal $\boldsymbol{\nu}_{2,RM}(t)$. In order to prevent controller wind-up, the reference model for the attitude loop (6.35) is altered in order to hide the influence from the rate loop from the error dynamics of the attitude loop. The reference model and the feedforward control signal are hence given by

$$\begin{aligned} \dot{\boldsymbol{x}}_{2,RM} &= -\boldsymbol{\Omega}_{2,RM} \cdot \boldsymbol{x}_{2,RM}(t) + \boldsymbol{\Omega}_{2,RM} \cdot \boldsymbol{x}_{2,cmd}(t) \\ &\quad + \boldsymbol{G}_{2,nom} \cdot (\boldsymbol{x}_1(t) - \boldsymbol{x}_{1,cmd}(t)), \\ \boldsymbol{\nu}_{2,RM}(t) &= -\boldsymbol{\Omega}_{2,RM} \cdot \boldsymbol{x}_{2,RM}(t) + \boldsymbol{\Omega}_{2,RM} \cdot \boldsymbol{x}_{2,cmd}(t). \end{aligned} \tag{6.48}$$

The error between the attitude state $\boldsymbol{x}_2(t)$ and the reference model state $\boldsymbol{x}_{2,RM}(t)$ is defined as $\boldsymbol{e}_2(t) \triangleq \boldsymbol{x}_{2,RM}(t) - \boldsymbol{x}_2(t)$. With (6.46), (6.47) and (6.48), the error dynamics become

$$\dot{\boldsymbol{e}}_2(t) = -\boldsymbol{\nu}_{2,BL}(t) - \bar{\boldsymbol{F}}_{2,nom,act}\left(\boldsymbol{x}_{act}(t) - \hat{\boldsymbol{x}}_{act}(t)\right) - \boldsymbol{d}_{um}(t). \tag{6.49}$$

In order to stabilize the attitude loop error dynamics, the PI controller

$$\boldsymbol{\nu}_{2,BL}(t) = \boldsymbol{K}_{P,2} \cdot \boldsymbol{e}_2(t) + \boldsymbol{K}_{I,2} \cdot \int_0^t \boldsymbol{e}_2(\tau) d\tau \tag{6.50}$$

is chosen. Inserting (6.50) and differentiating (6.49) with respect to time yields the second order error dynamics

$$\ddot{\boldsymbol{e}}_2(t) = -\boldsymbol{K}_{I,2} \cdot \boldsymbol{e}_2(t) - \boldsymbol{K}_{P,2} \cdot \dot{\boldsymbol{e}}_2(t) - \frac{d}{dt}\left(\bar{\boldsymbol{F}}_{2,nom,act}\left(\boldsymbol{x}_{act}(t) - \hat{\boldsymbol{x}}_{act}(t)\right) + \boldsymbol{d}_{um}(t)\right). \tag{6.51}$$

The decay rate of the attitude loop error dynamics may be specified with the help of the controller gains $\boldsymbol{K}_{I,2}$ and $\boldsymbol{K}_{P,2}$.

6.2.3 Final Control Law and Gain Design

This section assembles the final control law consisting of the rate control loop and the attitude control loop. Furthermore, the actuator model, which is required by both loops, is presented. After that, the gains of the controller are presented.

The rate control loop as well as the attitude control loop require estimates of the control surface deflections $\hat{\boldsymbol{u}}(t)$ or even of the whole actuator state vector $\hat{\boldsymbol{x}}_{act}(t)$. The model of the actuator, which is embedded into the final controller, is given by

$$\begin{aligned} \dot{\hat{\boldsymbol{x}}}_{act}(t) &= \hat{\boldsymbol{A}}_{act} \cdot \hat{\boldsymbol{x}}_{act}(t) + \boldsymbol{B}_{act} \cdot \boldsymbol{u}_{cmd}(t - \tau_c), \\ \hat{\boldsymbol{u}}(t) &= \hat{\boldsymbol{C}}_{act} \cdot \hat{\boldsymbol{x}}_{act}(t), \end{aligned} \tag{6.52}$$

where $\hat{\boldsymbol{x}}_{act} : \mathbb{R}_+ \to \mathbb{R}^4$ denotes the state vector of the actuator model. The state space matrices of the actuator model (6.52) are given by

$$\begin{aligned} \hat{\boldsymbol{A}}_{act} &= \begin{bmatrix} \boldsymbol{0}^{2\times2} & \boldsymbol{I}^{2\times2} \\ -\hat{\omega}_{0,act}^2 \cdot \boldsymbol{I}^{2\times2} & -2\hat{\zeta}_{act}\hat{\omega}_{0,act} \cdot \boldsymbol{I}^{2\times2} \end{bmatrix}, \qquad \hat{\boldsymbol{B}}_{act} = \begin{bmatrix} \boldsymbol{0}^{2\times2} \\ \hat{\omega}_{0,act}^2 \cdot \boldsymbol{I}^{2\times2} \end{bmatrix}, \\ \hat{\boldsymbol{C}}_{act} &= \begin{bmatrix} \boldsymbol{I}^{2\times2} & \boldsymbol{0}^{2\times2} \end{bmatrix}, \end{aligned} \tag{6.53}$$

where $\hat{\omega}_{0,act}$ and $\hat{\zeta}_{act}$ are the best available guesses of the eigenfrequency and the relative damping of the actuator (see Table 2.3).

The control laws of the rate loop and the attitude loop are summarized in Table 6.1 and Table 6.2, respectively. Furthermore, Figure 6.1 illustrates the overall structure. The controller from Table 6.1 and Table 6.2 is designed at the low dynamic pressure trim condition $V_K^R = 35\,m/s$, $h = 1000\,m$, $m_{fuel} = 23\,kg$. The nominal plant coefficients of this trim condition are given in Table 2.5. Is has been outlined at the end of Section

Description	Value
Control Variable	$\boldsymbol{x}_1(t)^T = \begin{bmatrix} p(t) & r(t) \end{bmatrix}$, $\boldsymbol{x}_{1,cmd}(t)^T = \begin{bmatrix} p_{cmd}(t) & r_{cmd}(t) \end{bmatrix}$
Reference Model	$\dot{\boldsymbol{x}}_{1,RM}(t) = -\boldsymbol{\Omega}_{1,RM} \cdot \boldsymbol{x}_{1,RM}(t) + \boldsymbol{\Omega}_{1,RM} \cdot \boldsymbol{x}_{1,cmd}(t) + \bar{\boldsymbol{G}}_{1,nom} \cdot (\hat{\boldsymbol{u}}(t) - \boldsymbol{u}_{cmd}(t))$ $\boldsymbol{\nu}_{1,RM}(t) = -\boldsymbol{\Omega}_{1,RM} \cdot \boldsymbol{x}_{1,RM}(t) + \boldsymbol{\Omega}_{1,RM} \cdot \boldsymbol{x}_{1,cmd}(t)$
"Linearizing" State Feedback	$\boldsymbol{u}_{cmd}(t) = \bar{\boldsymbol{G}}_{1,nom}^{-1} \cdot \left(\boldsymbol{\nu}_1(t) - \bar{\boldsymbol{F}}_{1,nom} \cdot \boldsymbol{x}_{lat}(t)\right)$
Error Definition	$\boldsymbol{e}_1(t) \triangleq \boldsymbol{x}_{1,RM}(t) - \boldsymbol{x}_1(t)$
Control Law	$\boldsymbol{\nu}_1(t) = \boldsymbol{\nu}_{1,RM}(t) + \boldsymbol{\nu}_{1,BL}(t) + \boldsymbol{\nu}_{1,MLESO}(t) = \boldsymbol{\nu}_{1,RM}(t) + \boldsymbol{K}_1 \cdot \boldsymbol{e}_1(t) - \hat{\boldsymbol{d}}_m(t)$
MLESO	$\dot{\hat{\boldsymbol{e}}}_1(t) = -\boldsymbol{K}_1 \cdot \boldsymbol{e}_1(t) - \boldsymbol{\nu}_{1,MLESO}(t) + \boldsymbol{L}_0 \cdot (\hat{\boldsymbol{e}}_1(t) - \boldsymbol{e}_1(t))$ $\hat{\boldsymbol{d}}_m(t) = \boldsymbol{M}_0 \cdot (\hat{\boldsymbol{e}}_1(t) - \boldsymbol{e}_1(t))$

Table 6.1: Summary of the rate loop control law.

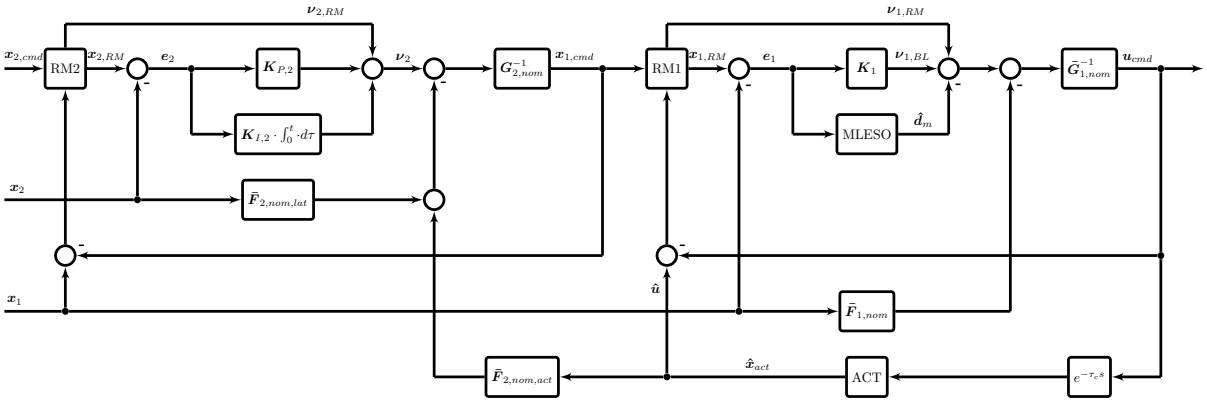

Figure 6.1: Overall structure of the MLESO-based controller. Acronyms: RM1 / RM2: Reference Model of the rate and attitude control loops; ACT: Actuator model from (6.52); MLESO: Augmentation from (6.31).

6.2.1 that the control effectiveness of the UAS at low dynamic pressure should be overestimated in order to avoid robustness problems of the controller at high dynamic pressures. To that end, notice that $\boldsymbol{G}_{1,nom}$ maps the control surface deflections $\xi(t)$ and $\zeta(t)$ to their resulting angular accelerations. The matrix $\boldsymbol{G}_{1,nom}$ may be partitioned as follows

$$\boldsymbol{G}_{1,nom} = \begin{bmatrix} \boldsymbol{g}_\xi & \boldsymbol{g}_\zeta \end{bmatrix}. \tag{6.54}$$

The vector $\boldsymbol{g}_\xi$ specifies the angular accelerations caused by the aileron, whereas $\boldsymbol{g}_\zeta$ specifies the angular acceleration of the rudder. At the low dynamic pressure trim condition, for which the controller is designed, it follows from Table 2.5 that $\boldsymbol{g}_{\xi,35} \triangleq \boldsymbol{g}_\xi$

Description	Value
Control Variable	$\boldsymbol{x}_2(t)^T = \begin{bmatrix}\Phi(t) & b_y(t)\end{bmatrix}$, $\boldsymbol{x}_{2,cmd}(t)^T = \begin{bmatrix}\Phi_{cmd}(t) & b_{y,cmd}(t)\end{bmatrix}$
Reference Model	$\dot{\boldsymbol{x}}_{2,RM} = -\boldsymbol{\Omega}_{2,RM}\cdot\boldsymbol{x}_{2,RM}(t)+\boldsymbol{\Omega}_{2,RM}\cdot\boldsymbol{x}_{2,cmd}(t)+\boldsymbol{G}_{2,nom}\cdot(\boldsymbol{x}_1(t)-\boldsymbol{x}_{1,cmd}(t))$ $\boldsymbol{\nu}_{2,RM}(t) = -\boldsymbol{\Omega}_{2,RM}\cdot\boldsymbol{x}_{2,RM}(t)+\boldsymbol{\Omega}_{2,RM}\cdot\boldsymbol{x}_{2,cmd}(t)$
"Linearizing" State Feedback	$\boldsymbol{x}_{1,cmd}(t) = \boldsymbol{G}_{2,nom}^{-1}\cdot\left(\boldsymbol{\nu}_2(t)-\bar{\boldsymbol{F}}_{2,nom,lat}\cdot\boldsymbol{y}_{lat}(t)-\bar{\boldsymbol{F}}_{2,nom,act}\cdot\hat{\boldsymbol{x}}_{act}(t)\right)$
Error Definition	$\boldsymbol{e}_2(t) \triangleq \boldsymbol{x}_{2,RM}(t)-\boldsymbol{x}_2(t)$
Control Law	$\boldsymbol{\nu}_2(t) = \boldsymbol{\nu}_{2,RM}(t)+\boldsymbol{\nu}_{2,BL}(t)$
PI Controller	$\boldsymbol{\nu}_{2,BL}(t) = \boldsymbol{K}_{P,2}\cdot\boldsymbol{e}_2(t)+\boldsymbol{K}_{I,2}\cdot\int_0^t\boldsymbol{e}_2(\tau)d\tau$

Table 6.2: Summary of the attitude loop control law.

and $\boldsymbol{g}_{\zeta,35} \triangleq \boldsymbol{g}_\zeta$ are given by

$$\boldsymbol{g}_{\xi,35} = \begin{bmatrix}-26.31\\-0.59\end{bmatrix}, \qquad \boldsymbol{g}_{\zeta,35} = \begin{bmatrix}-2.95\\-2.29\end{bmatrix}. \tag{6.55}$$

At the high dynamic pressure trim condition $V_K^R = 50\,m/s$, $h = 500\,m$, $m_{fuel} = 0\,kg$, the respective vectors are given by

$$\boldsymbol{g}_{\xi,50} = \begin{bmatrix}-56.11\\-2.50\end{bmatrix}, \qquad \boldsymbol{g}_{\zeta,50} = \begin{bmatrix}-4.88\\-5.91\end{bmatrix}. \tag{6.56}$$

For these two trim conditions, the vectors $\boldsymbol{g}_\xi$ and $\boldsymbol{g}_\zeta$ are depicted in Figure 6.2. One observes that the control effectiveness at a high dynamic pressure does not only increase, but also changes its direction. The overestimated input matrix $\bar{\boldsymbol{G}}_{1,nom}$ should not reflect this change in direction, but only the change in amplitude. For this reason, $\bar{\boldsymbol{G}}_{1,nom}$ is chosen as

$$\bar{\boldsymbol{G}}_{1,nom} = \boldsymbol{G}_{1,nom}\cdot\begin{bmatrix}\frac{\|\boldsymbol{g}_{\xi,50}\|_2}{\|\boldsymbol{g}_{\xi,35}\|_2} & 0\\ 0 & \frac{\|\boldsymbol{g}_{\zeta,50}\|_2}{\|\boldsymbol{g}_{\zeta,35}\|_2}\end{bmatrix}, \tag{6.57}$$

where $\boldsymbol{G}_{1,nom} = [\,\boldsymbol{g}_\xi \quad \boldsymbol{g}_\zeta\,] = [\,\boldsymbol{g}_{\xi,35} \quad \boldsymbol{g}_{\zeta,35}\,]$ is the nominal coefficient matrix at the design trim condition. Using (6.57), the length of the vectors $\boldsymbol{g}_\xi$ and $\boldsymbol{g}_\zeta$ is altered to match the length at high velocities without changing their direction. In simulations, this approach has proven to be advantageous as it avoids unnecessary artificial couplings between the aileron ξ and the rudder ζ at low velocities.

The parameters of the controller have been chosen in an iterated procedure, which involved the optimization of the controller gains with the `systune` command of the

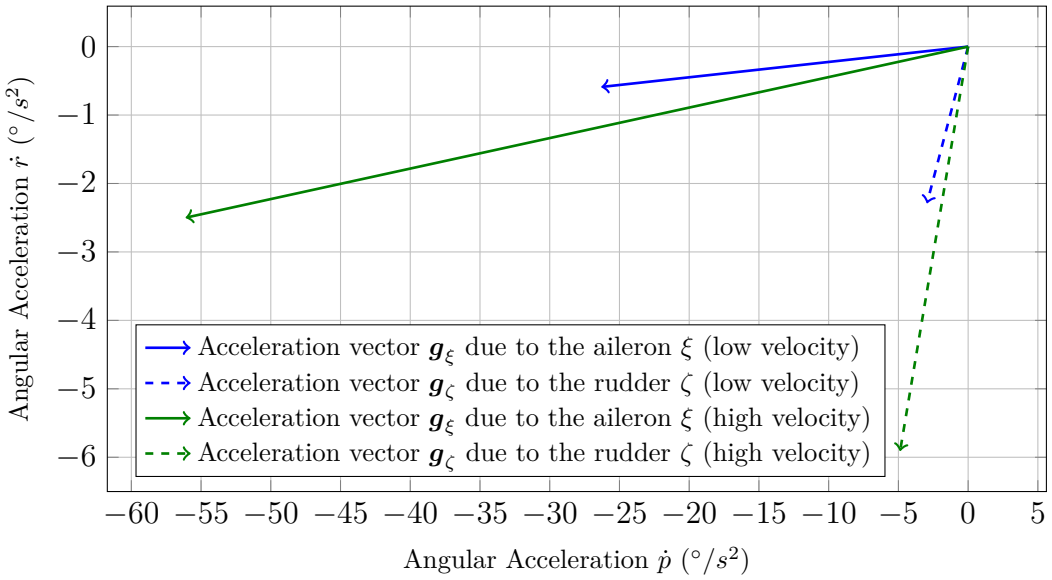

Figure 6.2: Illustration of the input directions for a 1° aileron / rudder deflection at the low dynamic pressure trim condition $V_K^R = 35\,m/s$, $h = 1000\,m$, $m_{fuel} = 23\,kg$ and the high dynamic pressure trim condition $V_K^R = 50\,m/s$, $h = 500\,m$, $m_{fuel} = 0\,kg$.

Robust Control Toolbox of MATLAB® 2014a and manual tuning. The gains in Table 6.3 yield stability and (mostly) adequate tracking performance for the whole envelope of interest.

6.3 Multiple-Model LQR Control

In the previous section, a MLESO-based control law for the lateral motion has been derived, which aims at ensuring satisfactory robustness and performance on a whole envelope of interest, while only using the measurements provided by the AHRS. Since there exists no similar controller, with which the MLESO-based control law could be compared, this section presents an alternative solution to the lateral control problem of Section 2.3.

Since the MLESO-based controller is LTI, another LTI control design is sought for the purpose of comparison. However, conventional LTI control design techniques such as pole placement or LQR are not suited to develop a controller which operates on a whole envelope of interest without scheduling. As a solution to this problem, a slightly modified LQR controller is used in this section. This solution is based on the fact that the standard LQR problem may not only be solved using the algebraic Riccati equation [105], but also using LMIs. By a slight change to these LMI conditions, a LQR-like controller is obtained, which simultaneously stabilizes the aircraft at low as well as high dynamic pressure trim conditions. Notice that this approach is an *ad hoc solution*. Hence, neither extensive research nor extensive literature studies have been

Description	Symbol	Value
Rate Loop Reference Model	$\boldsymbol{\Omega}_{1,RM}$	$\begin{bmatrix} 5 & 0 \\ 0 & 0.75 \end{bmatrix}$
Rate Loop Feedback Gain	$\boldsymbol{K}_1$	$\begin{bmatrix} 6 & 0 \\ 0 & 1 \end{bmatrix}$
Rate Loop MLESO Bandwidth	$\boldsymbol{\Omega}_{1,MLESO}$	$\begin{bmatrix} 4 & 0 \\ 0 & 2 \end{bmatrix}$
Attitude Loop Reference Model	$\boldsymbol{\Omega}_{2,RM}$	$\begin{bmatrix} 1 & 0 \\ 0 & 6 \end{bmatrix}$
Attitude Loop Proportional Gain	$\boldsymbol{K}_{P,2}$	$\begin{bmatrix} 2 & 0 \\ 0 & 2.8 \end{bmatrix}$
Attitude Loop Integrator Gain	$\boldsymbol{K}_{I,2}$	$\begin{bmatrix} 0 & 0 \\ 0 & 1.96 \end{bmatrix}$

Table 6.3: Controller gains of the MLESO-based control law.

conducted to validate the approach.

Subsequently, the LMI conditions for the LQR design are presented first for the case of a single plant. Afterwards, modified LMI conditions are proposed which may stabilize multiple plants. This design is referred to as Multiple-Model LQR (MM-LQR). With this design technique at hand, a MM-LQR controller is developed for the lateral control problem.

6.3.1 MM-LQR Control Design

Consider the plant

$$\dot{\boldsymbol{x}}(t) = \boldsymbol{A} \cdot \boldsymbol{x}(t) + \boldsymbol{B} \cdot \boldsymbol{u}(t). \tag{6.58}$$

where $\boldsymbol{x} : \mathbb{R}_+ \to \mathbb{R}^n$ is the state vector and $\boldsymbol{u} : \mathbb{R}_+ \to \mathbb{R}^m$ is the control input. The matrix $\boldsymbol{A} \in \mathbb{R}^{n \times n}$ denotes the known system matrix and $\boldsymbol{B} \in \mathbb{R}^{n \times m}$ is the known input matrix. The objective of the LQR design problem is to find a control input $\boldsymbol{u}(t) = \boldsymbol{K} \cdot \boldsymbol{x}(t)$, which minimizes the cost functional

$$J = \int_0^\infty \boldsymbol{x}(t)^T \cdot \boldsymbol{Q} \cdot \boldsymbol{x}(t) + \boldsymbol{u}(t)^T \cdot \boldsymbol{R} \cdot \boldsymbol{u}(t)\, dt. \tag{6.59}$$

In (6.59), $\boldsymbol{Q} \in \mathbb{S}_+^n$ and $\boldsymbol{R} \in \mathbb{S}_+^m$ are symmetric, positive semidefinite weighting matrices, which are chosen by the control system designer. For further details on LQR and its

properties, the reader is referred to [105] or [156].

Let the weighting matrices $\boldsymbol{Q}$ and $\boldsymbol{R}$ satisfy

$$\boldsymbol{C}_z^T \boldsymbol{C}_z = \boldsymbol{Q}, \qquad \boldsymbol{D}_z^T \boldsymbol{D}_z = \boldsymbol{R}, \tag{6.60}$$

such that the concatenation $\begin{bmatrix} \boldsymbol{C}_z & \boldsymbol{D}_z \end{bmatrix} \in \mathbb{S}_+^{n+m}$ of the matrices $\boldsymbol{C}_z \in \mathbb{R}^{(n+m)\times n}$ and $\boldsymbol{D}_z \in \mathbb{R}^{(n+m)\times m}$ is positive semidefinite. If $\boldsymbol{Q}$ and $\boldsymbol{R}$ are positive definite instead of positive semidefinite, the matrices $\boldsymbol{C}_z$ and $\boldsymbol{D}_z$ are for example given by

$$\boldsymbol{C}_z = \begin{bmatrix} \boldsymbol{Q}^{\frac{1}{2}} \\ \boldsymbol{0}^{m\times n} \end{bmatrix}, \qquad \boldsymbol{D}_z = \begin{bmatrix} \boldsymbol{0}^{n\times m} \\ \boldsymbol{R}^{\frac{1}{2}} \end{bmatrix}. \tag{6.61}$$

By reformulating the LQR problem as a $\mathcal{H}_2$-norm minimization problem [156] and using its LMI solution [48], the following SDP results (see also [135]):

$$\begin{aligned} &\min_{\boldsymbol{P},\boldsymbol{W},\boldsymbol{Z}} \operatorname{Tr} \boldsymbol{W}, \\ &\begin{bmatrix} \boldsymbol{P} & (\boldsymbol{C}_z \cdot \boldsymbol{P} + \boldsymbol{D}_z \cdot \boldsymbol{Z})^T \\ \boldsymbol{C}_z \cdot \boldsymbol{P} + \boldsymbol{D}_z \cdot \boldsymbol{Z} & \boldsymbol{W} \end{bmatrix} > 0, \\ &(\boldsymbol{A} \cdot \boldsymbol{P} + \boldsymbol{B} \cdot \boldsymbol{Z})^T + (\boldsymbol{A} \cdot \boldsymbol{P} + \boldsymbol{B} \cdot \boldsymbol{Z}) \leq -\boldsymbol{I}^{n\times n}, \end{aligned} \tag{6.62}$$

where $\boldsymbol{P} \in \mathbb{S}_{++}^n$, $\boldsymbol{W} \in \mathbb{S}_{++}^{n+m} \geq 0$ and $\boldsymbol{Z} \in \mathbb{R}^{m\times n}$ are the decision variables.

Using the solutions of the LMI problem, the controller is computed from

$$\boldsymbol{K} = \boldsymbol{Z} \cdot \boldsymbol{P}^{-1}. \tag{6.63}$$

The LMI problem (6.62) exhibits an interesting structure. The first LMI condition is specific to the LQR performance objective. The second LMI condition is however nothing but a Lyapunov condition, which ensures stability of the closed-loop system matrix $\boldsymbol{A} + \boldsymbol{B} \cdot \boldsymbol{K}$. This may for example be seen by substituting (6.63) into the second LMI condition of (6.62). In order to let the controller stabilize multiple plant models, the stability condition is simply repeated for each plant model, which should be stabilized. To that end, let the plant models be given by

$$\dot{\boldsymbol{x}}(t) = \boldsymbol{A}_i \cdot \boldsymbol{x}(t) + \boldsymbol{B}_i \cdot \boldsymbol{u}(t), \quad i = 1, \ldots, N. \tag{6.64}$$

A LMI optimization problem, which ensures that the LQR controller stabilizes multiple plants, is hence given by

$$\begin{aligned} &\min_{\boldsymbol{P},\boldsymbol{W},\boldsymbol{Z}} \operatorname{Tr} \boldsymbol{W}, \\ &\begin{bmatrix} \boldsymbol{P} & (\boldsymbol{C}_z \cdot \boldsymbol{P} + \boldsymbol{D}_z \cdot \boldsymbol{Z})^T \\ \boldsymbol{C}_z \cdot \boldsymbol{P} + \boldsymbol{D}_z \cdot \boldsymbol{Z} & \boldsymbol{W} \end{bmatrix} > 0, \\ &(\boldsymbol{A}_i \cdot \boldsymbol{P} + \boldsymbol{B}_i \cdot \boldsymbol{Z})^T + (\boldsymbol{A}_i \cdot \boldsymbol{P} + \boldsymbol{B}_i \cdot \boldsymbol{Z}) \leq -\boldsymbol{I}^{n\times n}, \quad \forall\, i = 1, \ldots, N. \end{aligned} \tag{6.65}$$

Despite the altered LMI condition (6.65), the controller gain $\boldsymbol{K}$ is still computed from (6.63).

6.3.2 Gain Design

For the design of the MM-LQR controller, appropriate plant models are required first, which represent the aircraft dynamics sufficiently well throughout the whole envelope. Subsequently, only two plant models will be used, namely one plant model for low dynamic pressure and one for high dynamic pressure. The rationale of this approach is as follows: The main difference between the two trim conditions stems from the variation of the dynamic pressure. By designing a controller for two extreme dynamic pressure conditions, a controller is expected to result that is also capable of stabilizing other trim conditions, whose dynamic pressures lie in between these extremes.

As low and high dynamic pressure trim conditions, the two trim conditions are chosen for which Table 2.5 provides data (i.e. $V_K^R = 35\,m/s$, $h = 1000\,m$, $m_{fuel} = 23\,kg$ and $V_K^R = 50\,m/s$, $h = 500\,m$, $m_{fuel} = 0\,kg$). Both plant models are expanded and transformed as explained in Section 6.1 in order to obtain a model according to (6.10). Due to the transformation, these plant models do not contain the non-measurable state $\beta_K(t)$ anymore, but the lateral acceleration state $b_y(t)$. The system matrix and the input matrix of the *transformed plant* at $V_K^R = 35\,m/s$, $h = 1000\,m$, $m_{fuel} = 23\,kg$ are denoted as $\boldsymbol{A}_1$ and $\boldsymbol{B}_1$. Likewise, the system matrix and the input matrix at $V_K^R = 50\,m/s$, $h = 500\,m$, $m_{fuel} = 0\,kg$ are denoted as $\boldsymbol{A}_2$ and $\boldsymbol{B}_2$.

The two plant models ($\boldsymbol{A}_1$, $\boldsymbol{B}_1$) and ($\boldsymbol{A}_2$, $\boldsymbol{B}_2$) will subsequently be used to develop a MM-LQR controller. Since the MM-LQR relies on state feedback, it will be assumed at first that the entire state vector including the actuator states is available for control. Later on, the actuator state measurements are replaced by suitable estimates.

Using the MM-LQR LMI (6.65), a state-feedback controller may be determined, which simultaneously stabilizes ($\boldsymbol{A}_1$, $\boldsymbol{B}_1$) and ($\boldsymbol{A}_2$, $\boldsymbol{B}_2$), whilst minimizing the objective functional (6.59). The lateral control problem is however not a stabilization problem, but a tracking problem. For this reason, the tracking problem has to be reformulated as a stabilization problem. For this purpose, a so-called *robust servomechanism* design [105] is chosen.

The objective of the lateral controller is stationary accurate tracking of bank angle *step commands* $\Phi_{cmd}(t)$, whilst keeping the lateral acceleration $b_y(t)$ close to zero in order to ensure a coordinated turn. Since step-like commands and disturbances are to be tracked / rejected, the *robust servomechanism* design amounts to enhancing the plant models ($\boldsymbol{A}_1$, $\boldsymbol{B}_1$) and ($\boldsymbol{A}_2$, $\boldsymbol{B}_2$) by integrators for $\Phi(t)$ and $b_y(t)$. For this, the commands, which are to be tracked, are summarized in the command vector $\boldsymbol{r}(t)^T = [\,\Phi_{cmd}(t) \quad b_y(t)\,]$. The states $\Phi(t)$, $b_y(t)$, which shall be tracked with stationary accuracy, are selected by the matrix $\boldsymbol{C}_{cmd} \in \mathbb{R}^{2\times 8}$:

$$\begin{bmatrix} \Phi(t) \\ b_y(t) \end{bmatrix} = \boldsymbol{C}_{cmd} \cdot \boldsymbol{y}(t) = \begin{bmatrix} 0 & 0 & 0 & 1 & 0 & 0 & 0 & 0 \\ 0 & 1 & 0 & 0 & 0 & 0 & 0 & 0 \end{bmatrix} \cdot \boldsymbol{y}(t)\,. \tag{6.66}$$

Furthermore, the states of the integrators are denoted by $\boldsymbol{e}_I : \mathbb{R}_+ \to \mathbb{R}^2$. With these

definitions, the extended plant models may be written as

$$\begin{bmatrix} \dot{\boldsymbol{e}}_I(t) \\ \dot{\boldsymbol{y}}(t) \end{bmatrix} = \begin{bmatrix} \boldsymbol{0}^{2\times 2} & -\boldsymbol{C}_{cmd} \\ \boldsymbol{0}^{8\times 2} & \boldsymbol{A}_i \end{bmatrix} \cdot \begin{bmatrix} \boldsymbol{e}_I(t) \\ \boldsymbol{y}(t) \end{bmatrix} + \begin{bmatrix} \boldsymbol{I}^{2\times 2} \\ \boldsymbol{0}^{8\times 2} \end{bmatrix} \cdot \boldsymbol{r}(t) + \begin{bmatrix} \boldsymbol{0}^{2\times 2} \\ \boldsymbol{B}_i \end{bmatrix} \cdot \boldsymbol{u}_{cmd}(t),\ i = 1, 2. \quad (6.67)$$

Using the MM-LQR approach, a state-feedback controller

$$\boldsymbol{u}_{cmd}(t) = \boldsymbol{K} \cdot \begin{bmatrix} \boldsymbol{e}_I(t) \\ \boldsymbol{y}(t) \end{bmatrix} = \begin{bmatrix} \boldsymbol{K}_I & \boldsymbol{K}_p \end{bmatrix} \cdot \begin{bmatrix} \boldsymbol{e}_I(t) \\ \boldsymbol{y}(t) \end{bmatrix} \quad (6.68)$$

is determined, which stabilizes the extended plant models (6.67). Due to the extension by an integrator, this control law also ensures stationary accurate tracking.

The weighting matrices $\boldsymbol{Q}$ and $\boldsymbol{R}$ have been determined manually. The choice

$$\begin{aligned} \boldsymbol{Q} &= \mathrm{diag}\ \begin{bmatrix} 20 & 40 & 15 & 20 & 0 & 1 & 0 & 0 & 0 & 0 \end{bmatrix}, \\ \boldsymbol{R} &= \mathrm{diag}\ \begin{bmatrix} 40 & 20 \end{bmatrix} \end{aligned} \quad (6.69)$$

has shown to yield mostly satisfactory robustness and performance throughout the whole envelope. The solution of the MM-LQR LMI problem (6.65) leads to the controller gains:

$$\begin{aligned} \boldsymbol{K}_I &= \begin{bmatrix} -0.6109 & 0.4966 \\ -0.4971 & -1.2249 \end{bmatrix}, \\ \boldsymbol{K}_P &= \begin{bmatrix} 0.0232 & 0.2470 & 0.1522 & 0.7325 & -0.4484 & -0.0837 & -0.0099 & -0.0018 \\ 0.9365 & 0.4289 & -0.0037 & 0.5076 & 0.0502 & -0.0589 & -0.0036 & -0.0023 \end{bmatrix}. \end{aligned} \quad (6.70)$$

The control law (6.68) may not be directly implemented, as it depends on the non-measurable actuator state $\boldsymbol{x}_{act}(t)$. While the conventional LQR theory would propose the design of a Kalman filter to estimate the non-measurable states, a more simple approach is taken here. Since the actuator dynamics are usually rather well known, an estimate of $\boldsymbol{x}_{act}(t)$ is simply computed from the actuator model (6.52), (6.53), assuming $\tau_c = 0$. Partitioning the feedback matrix $\boldsymbol{K}_P$ according to $\boldsymbol{K}_P = [\,\boldsymbol{K}_{P,lat} \quad \boldsymbol{K}_{P,act}\,]$, the implementable control law

$$\boldsymbol{u}_{cmd}(t) = \begin{bmatrix} \boldsymbol{K}_I & \boldsymbol{K}_{P,lat} & \boldsymbol{K}_{P,act} \end{bmatrix} \cdot \begin{bmatrix} \boldsymbol{e}_I(t) \\ \boldsymbol{y}_{meas}(t) \\ \hat{\boldsymbol{x}}_{act}(t) \end{bmatrix} \quad (6.71)$$

results from (6.68).

6.4 Assessment of the Controllers

In the previous two sections, two different fallback controllers for the lateral motion of the UAS from Chapter 2 have been developed. This section aims at evaluating the stability, robustness and performance of these controllers over the envelope. Furthermore, the controllers will also be compared to each other. In order to maintain clarity,

this section will only present some analysis results, which are considered to be important and representative. A detailed analysis of the developed controllers at the two representative trim conditions $V_K^R = 35\,m/s$, $h = 1000\,m$, $m_{fuel} = 23\,kg$ and $V_K^R = 50\,m/s$, $h = 500\,m$, $m_{fuel} = 0\,kg$, for which Section 2.3 provides data, may be found in Appendix E. The analyses there include step, doublet, gust, as well as Dryden responses with the linear and the nonlinear UAS model, open- and closed-loop Bode plots and Nichols plots.

All of the subsequent analyses, which rely on the linear plant model, consider the overall control system structure from Figure 2.4. Thus, the plant model includes the linearized rigid-body equations of motion (2.62), (2.63), actuator dynamics as well as control and measurement delays ($\tau_c = 50\,ms$ and $\tau_m = 20\,ms$). The nonlinear plant model, which is used within some other analyses, features the nonlinear, rigid-body equations of motions from Section 2.1, a precise model of the UAS environment and the resulting forces and moments, a detailed actuator model as well as a model of the onboard processing units. In case of nonlinear simulations, the UAS model is initialized to the respective trim condition. This especially includes the elevator deflection η and the thrust lever positions δT, which are held constant at their trim value throughout the simulation.

The central task of the developed controllers is precise tracking and disturbance rejection throughout the envelope of interest. For this reason, several of the subsequent analyses compare the stability, robustness or performance of the controllers at different trim conditions. The considered trim conditions include the two trim conditions, for which Section 2.3 provides data (namely $V_K^R = 35\,m/s$, $h = 1000\,m$, $m_{fuel} = 23\,kg$ and $V_K^R = 50\,m/s$, $h = 500\,m$, $m_{fuel} = 0\,kg$). Furthermore, the controllers are evaluated at two intermediate trim conditions ($V_K^R = 40\,m/s$, $h = 1000\,m$, $m_{fuel} = 13\,kg$ and $V_K^R = 45\,m/s$, $h = 500\,m$, $m_{fuel} = 3.2\,kg$). The rational of this choice is that these trim conditions range from low dynamic pressure and low agility (high fuel mass) to high dynamic pressure and high agility (low fuel mass). Since these four trim conditions feature different trim velocities V_K^R, they will sometimes simply be referred to by their trim velocity V_K^R. That is, when speaking about the trim condition $V_K^R = 40\,m/s$, this actually refers to the trim condition $V_K^R = 40\,m/s$, $h = 1000\,m$, $m_{fuel} = 13\,kg$.

6.4.1 Stability

The most fundamental property of any control system is its stability. Since neither the design of the MLESO nor of the MM-LQR intrinsically ensures stability at each trim condition, their stability has to be analyzed first. For this, a μ-analysis [156] is conducted. The *Structured Singular Value* μ is a general measure of RS of an uncertain LTI system. For its (rough) definition, consider a LTI system with uncertain coefficients (i.e. parametric uncertainty), which are known to lie in some predefined intervals. Then,

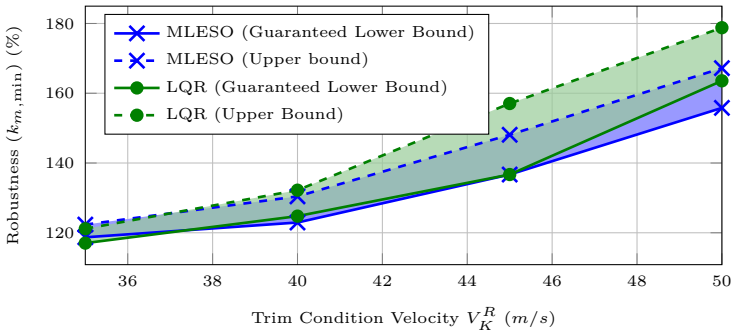

Figure 6.3: Results of μ-analyses of the MLESO and MM-LQR controllers at different trim conditions.

μ is defined as the reciprocal value $\mu \triangleq 1/k_{m,\min}$ of the smallest factor $k_{m,\min}$, by which these intervals must be scaled (simultaneously), such that the system is at the verge of stability. If the smallest scaling factor satisfies $k_{m,\min} > 1$ (which is equivalent to $\mu < 1$), then the LTI system is robustly stable for the modeled uncertainty (intervals). Furthermore, the uncertainty intervals may be scaled by $k_{m,\min} = 1/\mu$ and the system remains robustly stable. While the *Structured Singular Value* μ may not be computed exactly, efficient algorithms for the computation of upper and lower bounds exist.

For the μ-analyses of the MLESO-based controller and the MM-LQR controller, the closed-loop LTI state space model corresponding to Figure 2.4 is computed first. The coefficients of the rigid-body LTI plant model (2.62), (2.63) are confined to the uncertainty intervals specified in Table 2.5. Since the closed-loop system contains several time-delays, which may not be handled by the μ-analysis, the delays are replaced by their respective second order Padé approximations. The actual analysis is performed using the `robuststab` command of the Robust Control Toolbox of MATLAB® 2014a.

The results of the μ-analyses of the MLESO-based controller and the MM-LQR controller at four trim conditions are shown in Figure 6.3. Clearly, both controllers are robustly stable to the uncertainties specified in Table 2.5 at each considered trim condition. Furthermore, one observes that the robustness of the controllers to parametric uncertainty increases with increasing dynamic pressure and increasing agility. This result is to be expected since the effectiveness of the aileron and the rudder increases with increasing dynamic pressure. At the same time, inertia decreases due to the decreasing fuel mass. Finally, Figure 6.3 also illustrates that the robust stability results of the μ-analysis are not overly conservative since the upper and lower bounds on $k_{m,min}$, which derive from the lower and upper bound for the *Structured Singular Value* μ, are close.

When comparing the MLESO-based controller to the MM-LQR controller, the latter seems to be slightly more robust to parametric uncertainty. Since the true value of $k_{m,\min}$ is only known to lie somewhere in between the depicted upper and lower bounds, no definite conclusion may be inferred from Figure 6.3.

6.4.2 Robustness to Non-Parametric Uncertainty

The μ-analysis of the previous section revealed that both controllers are (robustly) stable at each considered trim condition. While the μ-analysis provides valuable insight into the robustness with respect to parametric uncertainties, it only admits limited conclusions on the robustness with respect to non-parametric uncertainties (such as unmodeled dynamics). For this reason, this section analyzes the robustness of both controllers with the help of phase, gain and time-delay margin. While it is well known that the "loop-by-loop" evaluation of these robustness metrics may lead to erroneous conclusions in case of MIMO systems (see for example [156, Section 3.7]), these metrics are nevertheless used here. This is because the widely accepted standard SAE ARP94910 specifies requirements for these robustness metrics. More precisely, SAE ARP94910 requires that the phase margin must be larger than 45° and that the gain margin must be larger than $6\,dB$.

For the computation of the margins, the control system structure according to Figure 2.4 is considered. The open-loop transfer function is computed by opening the loop in front of the control time-delay τ_c in either the ξ-channel or the ζ-channel. Afterwards, the margins may be inferred from the respective open-loop Bode plots. While the open-loop Bode plots are not shown here in order to maintain clarity, they may be found in Appendix E. Notice that the open-loop transfer functions are computed for non-zero control delay τ_c and non-zero measurement delay τ_m. Furthermore, since the coefficients of the linearized rigid-body EOMs (2.62), (2.63) are uncertain, the margins are computed for 1000 random samples of the parametric uncertainties. For this, each uncertain plant coefficient is assumed to be distributed uniformly within the uncertainty intervals specified in Table 2.5.

Figure 6.4 shows box plots[2] of the minimal phase margin, the minimal gain margin and the minimal time-delay margin of the MLESO-based controller at the four different trim conditions. Here, the minimal phase margin $PM_{\min}$ is defined as

$$PM_{\min} \triangleq \min\{PM_\xi, PM_\zeta\}, \tag{6.72}$$

where PM_ξ, PM_ζ denote the phase margin of the ξ-channel and the ζ-channel, respectively. Analogous definitions apply to the minimal gain margin and the minimal

[2] A box plot is a simple and convenient way to display realizations of a random variable (i.e. data), whose distribution is unknown. The box plot relies on the partition of the data in quartiles. The horizontal line within the box represents the median. That is, 50% of the data lies below the indicated value. The lower limit of the box indicates the end of the first quartile, that is, 25% of the data lies below this value. Likewise, the upper limit of the box indicates the end of the third quartile, that is, 75% of the data lies below the indicated value. Hence, the box covers 50% of all data. The range of the box (its height) is referred to as Interquartile Range (IQR). The antenna-like lines above and beneath the box are referred to as lower and upper whisker. The lower whisker indicates the last data point of the first quartile, whose distance to the lower box limit is smaller than $1.5 \cdot$ IQR. All other data in the first quartile is considered as outlier and is represented by separate crosses. An analogous definition holds for the upper whisker.

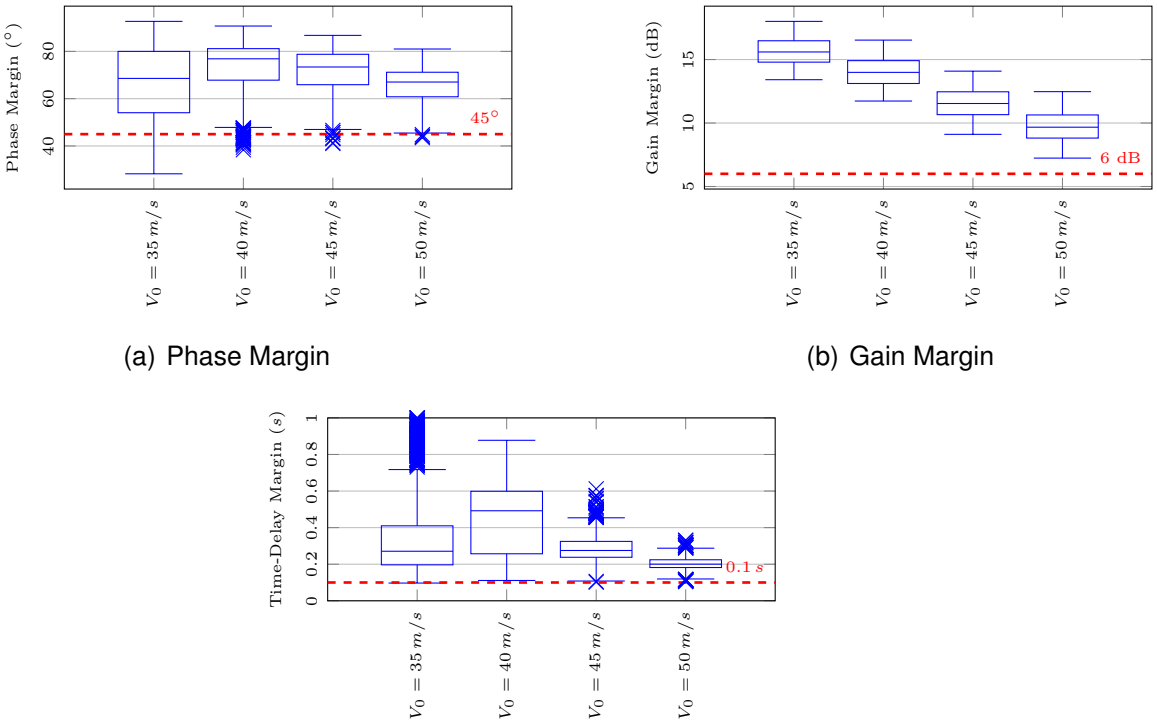

(a) Phase Margin

(b) Gain Margin

(c) Time-Delay Margin

Figure 6.4: Comparison of minimal phase, gain and time-delay margin of the MLESO controller at different trim conditions.

time-delay margin. For the margins PM_ξ, PM_ζ of the MLESO-based controller in a specific channel, the reader is referred to Figures E.2 and E.16, respectively.

Figure 6.4 illustrates that the MLESO-based controller does not fully satisfy the phase margin requirements of SAE ARP94910. At low velocity ($V_K^R = 35\,m/s$), the phase margin requirement is violated for a significant number of uncertainty combinations since the lower whisker crosses the $45°$-line. At higher velocities, the lower whisker does no longer cross the $45°$-line. Nevertheless, some uncertainty combinations still lead to a violation of the phase margin requirement, which can be seen from several outliers. These behavior is caused by a peak in the open-loop transfer function of the ξ-channel. At low velocity ($V_K^R = 35\,m/s$, see Figure E.1), the upper envelope of the open-loop transfer function exhibits two strong peaks. The first peak correlates with the control system. The second peak (at roughly $4\,rad/s$) correlates with the Dutch roll eigenfrequency and leads to a high gain crossover frequency. Since the phase has already dropped significantly at this frequency, a low phase margin results. With increasing velocity ($V_K^R = 40\,m/s$ or $V_K^R = 45\,m/s$), the amplitude of the second peak decreases continuously. Furthermore, its gain starts to drop below $0\,dB$. For this reason, the effect of the peak reduces and the phase margins begin to increase. Hence, only outliers violate the phase margin requirement. At high velocity ($V_K^R = 50\,m/s$, see Figure E.15), the second peak has vanished entirely.

While the MLESO-based controller does not satisfy the phase margin requirements

of SAE ARP94910, Figure 6.4 shows that it satisfies the gain margin requirements. It may be observed that the gain margin decreases with increasing dynamic pressure / agility. This behavior is caused by the fact that a non-scheduled controller operates over the whole envelope. With increasing dynamic pressure, the open-loop gain of the plant increases since the aileron and the rudder become more effective. Since the open-loop gain contributed by the MLESO-based controller remains constant, the gain margin decreases.

In case of the time-delay margin, SAE ARP94910 does not specify any requirement. Figure 6.4 illustrates that the MLESO-based controller may tolerate another $100\,ms$ time-delay in addition to the control delay τ_c and the measurement delay τ_m in either the ξ-channel or the ζ-channel at any velocity without becoming unstable.

The phase, gain and time-delay margins of the MM-LQR controller at the four different trim conditions are shown in Figure 6.5. Notice that the same realizations of the plant uncertainties, which have been used during the computation of the margins of the MLESO-based controller, have also been used for the computation of the margins of the MM-LQR controller. Figure 6.5 shows that similar comments, which have been raised in case of the MLESO-based controller, also apply to the MM-LQR controller. The most noticeable difference consists in the absence of outliers in the phase margin plots at intermediate trim conditions.

Finally, Figure 6.6 compares the robustness margins of both controllers at low velocity ($V_K^R = 35\,m/s$) and high velocity ($V_K^R = 50\,m/s$). It may be observed that in most situations, the MLESO-based controller provides slightly higher phase and time-delay margins than the MM-LQR controller. At the same time, the MM-LQR controller provides a slightly higher gain margin. Since the robustness of both controllers is rather similar, it is expected that an appropriate retuning of the MM-LQR controller will yield higher phase margins. Likewise, a retuning of the MLESO-based controller is expected to yield higher gain margins.

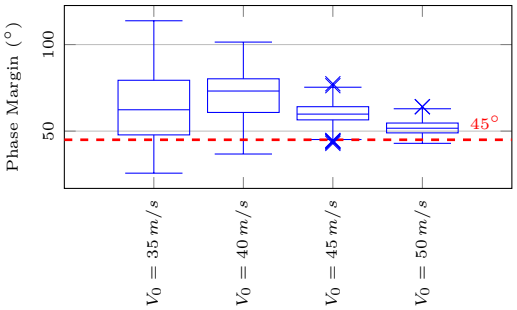

(a) Phase Margin

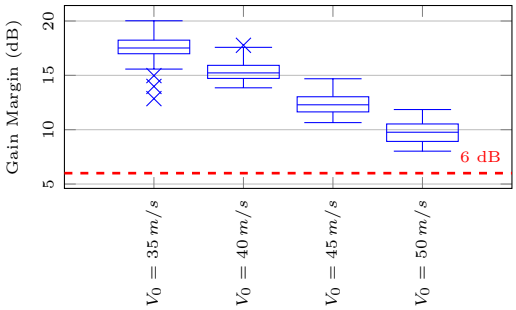

(b) Gain Margin

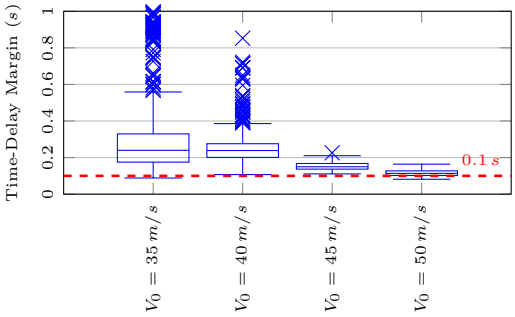

(c) Time-Delay Margin

Figure 6.5: Comparison of minimal phase, gain and time-delay margin of the MM-LQR controller at different trim conditions.

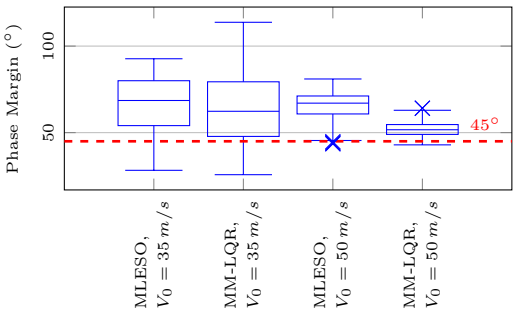

(a) Phase Margin

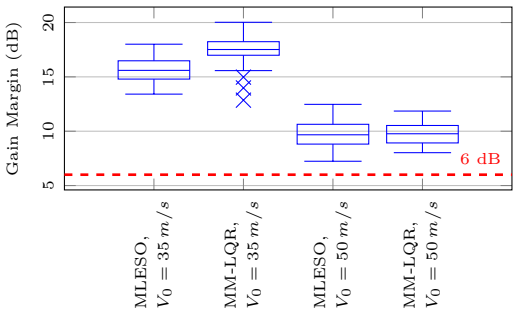

(b) Gain Margin

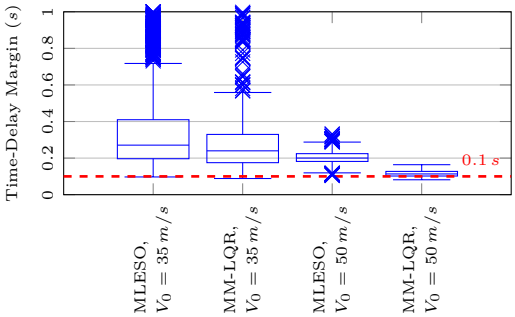

(c) Time-Delay Margin

Figure 6.6: Comparison of minimal phase, gain and time-delay margin of the MLESO controller with the MM-LQR controller.

6.4.3 Tracking Performance

This section analyzes the tracking performance of the developed controllers in linear as well as nonlinear simulations. As an exemplary maneuver, a 30° doublet command $\Phi_{cmd}(t)$ is issued to the controller. The responses of the developed controllers to a 30° step command as well as closed-loop Bode plots may be found in Appendix E. Furthermore, all time-domain simulations in this section are restricted to the nominal response, that is, the response if the uncertain plant coefficients take their nominal values. For the responses of the plant in case of uncertain plant coefficients, the reader is once again referred to Appendix E.

Since time-domain simulations only admit a qualitative assessment of the performance, this section also provides box plots of the rise time, settling time and overshoot in response to a 30° step command. In this thesis, the rise time is defined as the time, which is required by the step response to go from 10% of the steady-state value to 90%. The settling time is defined as the time, which is required by the step response to enter and remain within a 2% band around the steady-state value. Rise time, settling time and overshoot are determined from the step responses of the uncertain plant, which are shown in Appendix E. Notice that the simulations of these step responses rely on the same realizations of the uncertainties, which have also been used to compute the robustness margins in the previous section.

Figures 6.7 and 6.8 show the doublet response of the MLESO-based controller at the four trim conditions in case of the linearized rigid-body EOMs. Figure 6.7 illustrates that the controller is able to precisely track the commanded bank angle $\Phi_{cmd}(t)$ and that the response is rather uniform throughout the envelope. However, at low velocities, some overshoot appears, which decreases with increasing velocity.

Throughout the envelope, the MLESO-based controller ensures a coordinated turn. Figure 6.7 demonstrates that it requires roughly three seconds to regulate the lateral acceleration $b_y(t)$ close to zero, leading to a small, but non-zero aerodynamic/flight-path angle-of-sideslip $\beta_A(t) = \beta_K(t)$. Even during transients, the lateral acceleration $b_y(t) \cdot g$ remains below $0.1 \cdot g$ and the aerodynamic angle-of-sideslip $\beta_A(t)$ does not exceed 10% of the commanded bank angle $\Phi_{cmd}(t)$.

Figure 6.8 highlights that the controller does not command aileron and rudder deflections beyond the physical limitations of the actuator. However, during the step from $\Phi_{cmd} = 30^\circ$ to $\Phi_{cmd} = -30^\circ$, the required rate of the aileron slightly exceeds the physical capabilities of the actuator.

In order to quantitatively assess the tracking performance of the MLESO-based controller, Figure 6.9 depicts box plots of rise time, settling time and overshoot at the four trim conditions in case of the linearized rigid-body EOMs. Throughout the envelope, the median of the rise time remains close to $1.6\,s$. Furthermore, the box, which represents 50% of all step responses, stays within the interval $[1.5\,s, 1.8\,s]$. Thus, the step responses are rather uniform with respect to the rise time. In contrast to the rise

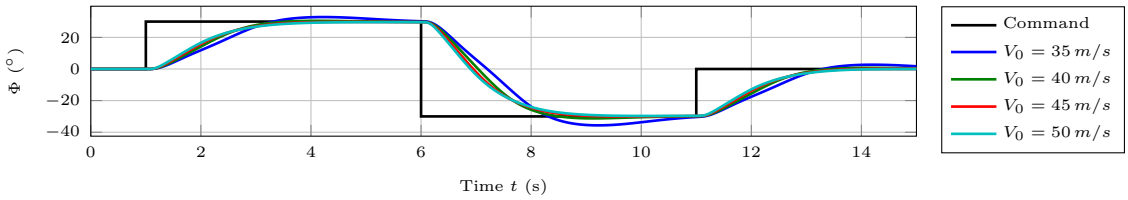

(a) Bank Angle

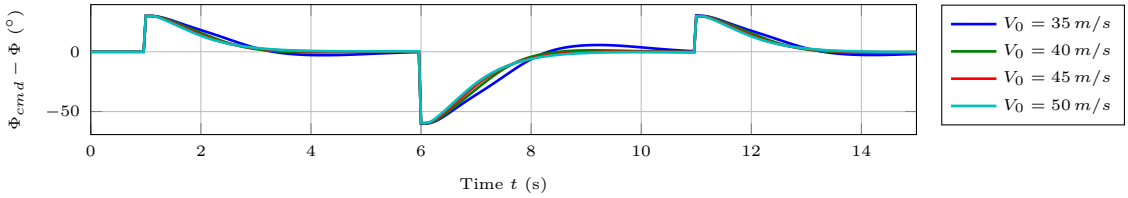

(b) Tracking Error

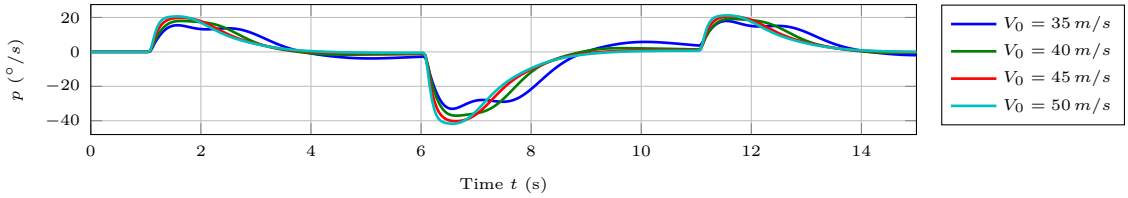

(c) Roll Rate

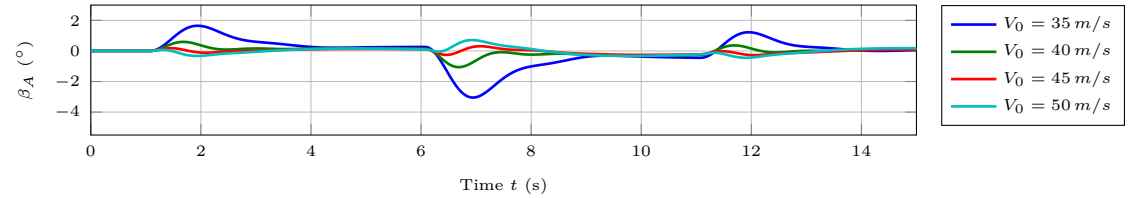

(d) Angle-of-sideslip

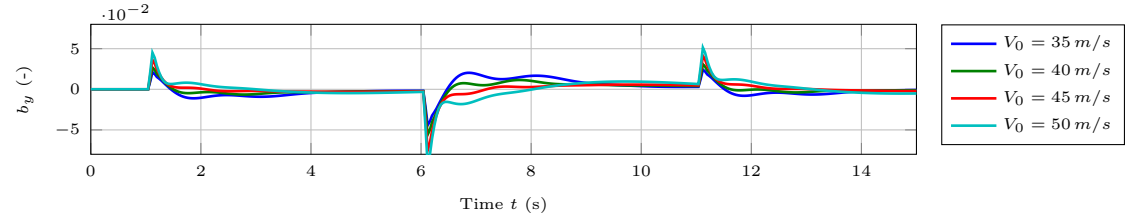

(e) Lateral Acceleration

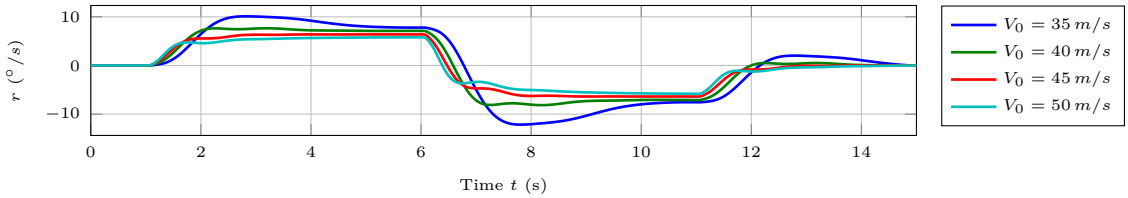

(f) Yaw Rate

Figure 6.7: Comparison of the response of the LTI plant model with MLESO controller to a $30°$ doublet command $\Phi_{cmd}\,(t)$ at different trim conditions.

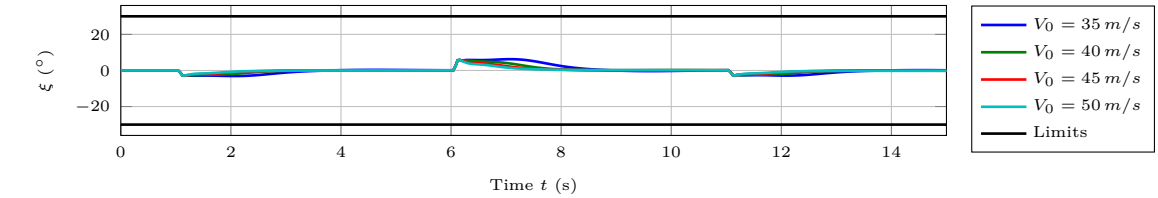

(a) Aileron Deflection

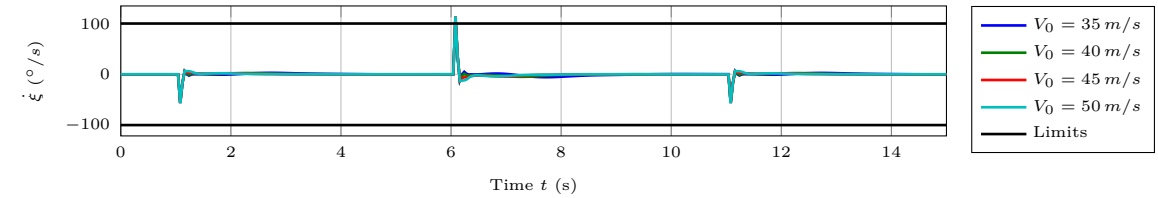

(b) Aileron Rate

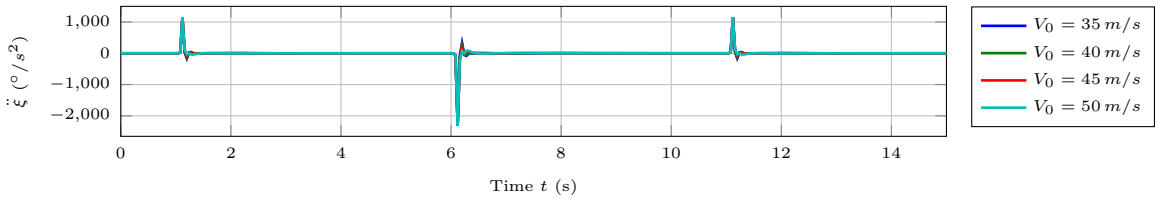

(c) Aileron Acceleration

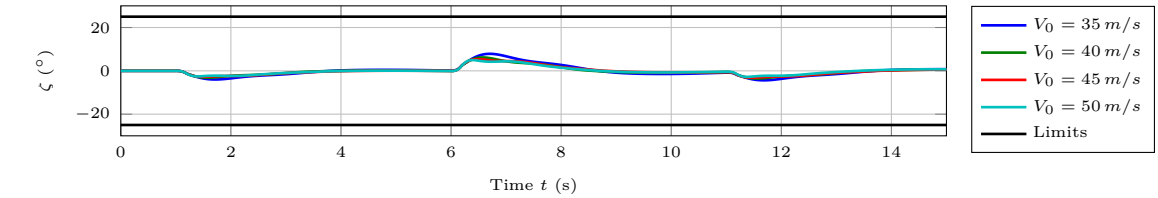

(d) Rudder Deflection

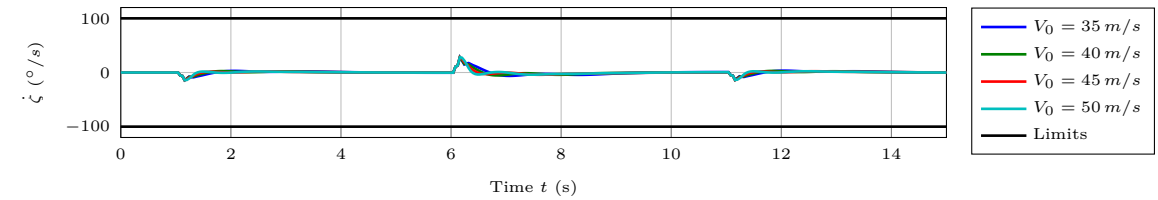

(e) Rudder Rate

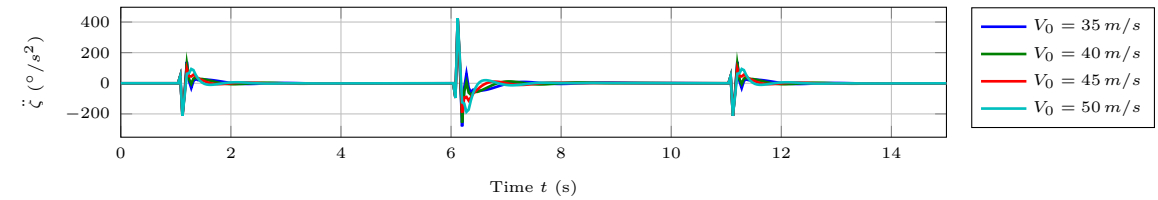

(f) Rudder Acceleration

Figure 6.8: Comparison of the response of the LTI plant model with MLESO controller to a $30°$ doublet command $\Phi_{cmd}(t)$ at different trim conditions.

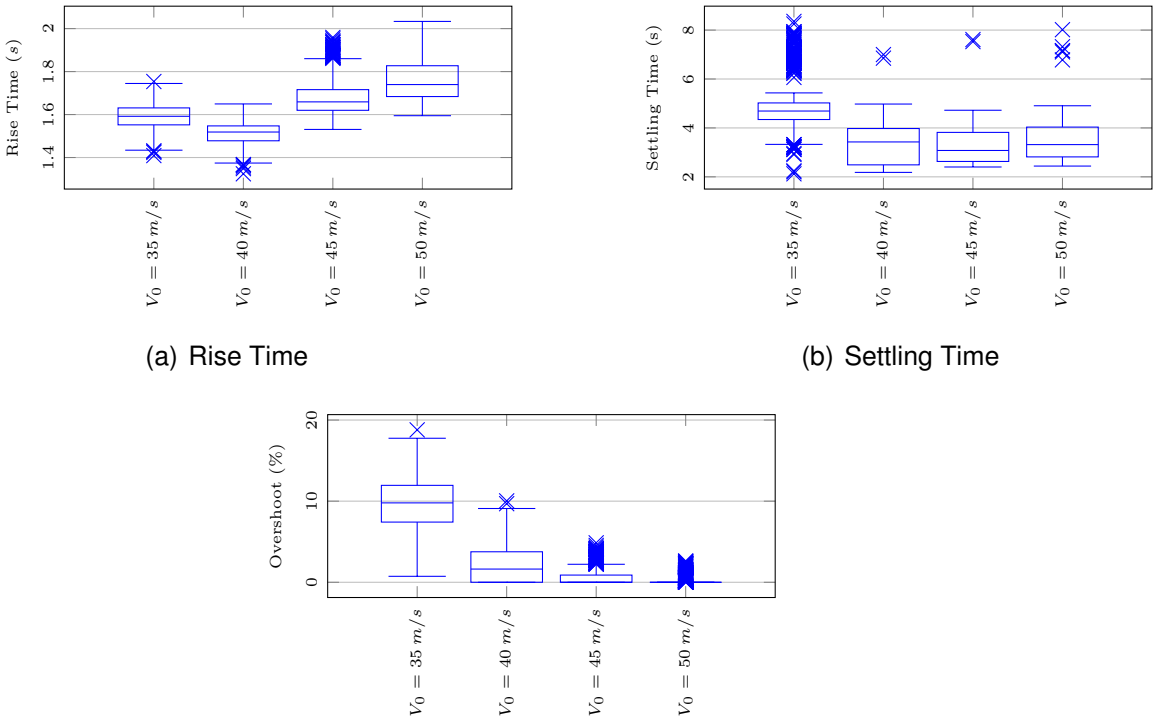

(a) Rise Time

(b) Settling Time

(c) Overshoot

Figure 6.9: Comparison of rise time, settling time and overshoot of the MLESO controller at different trim conditions.

time, the settling time is not as uniform throughout the envelope. On the one side, the median of the settling time decreases from $4.5\,s$ at low velocities to roughly $3.2\,s$ at high velocities. Furthermore, for all velocities $V_K^R \geq 40\,m/s$, the box, which represents 50% of all step responses, spans the rather large interval $[2.5\,s, 4.0\,s]$. In case of the overshoot, one may observe a decrease from approximately 18% at low velocities to less than 5% at high velocities. This trend has already been observed in the time-domain simulations of Figure 6.7.

So far, all simulation results considered the linearized rigid-body EOMs. In order to demonstrate the capabilities of the MLESO-based controller to work in the full, nonlinear simulation, the response of the linearized model is compared to the response of the nonlinear model in Figures 6.10 and 6.11 at $V_K^R = 35\,m/s$, $h = 1000\,m$, $m_{fuel} = 23\,kg$. It may be clearly seen that the responses with the linear and the nonlinear models are very similar. This demonstrates that the performance of the MLESO-based controller does not deteriorate in the nonlinear model.

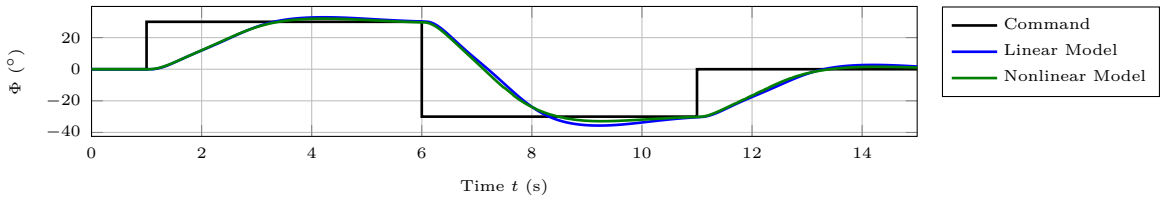

(a) Bank Angle

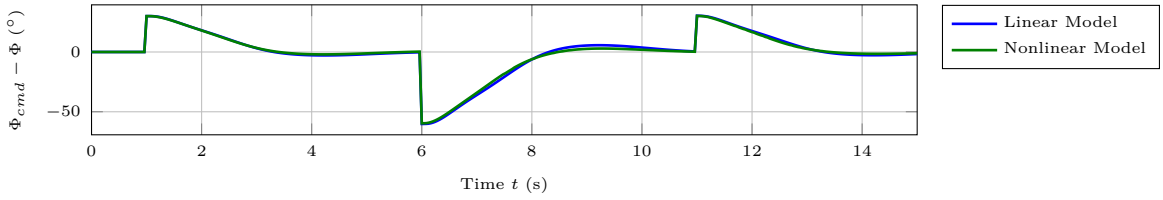

(b) Tracking Error

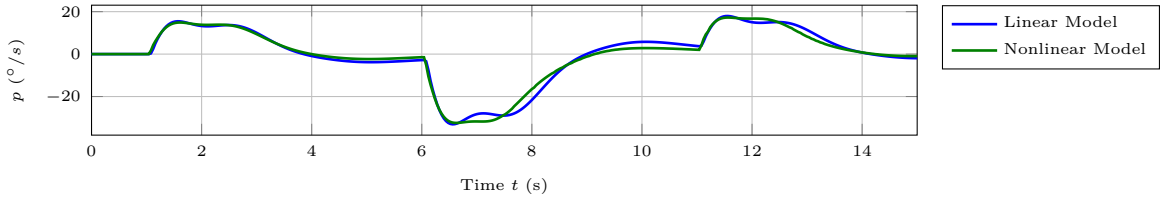

(c) Roll Rate

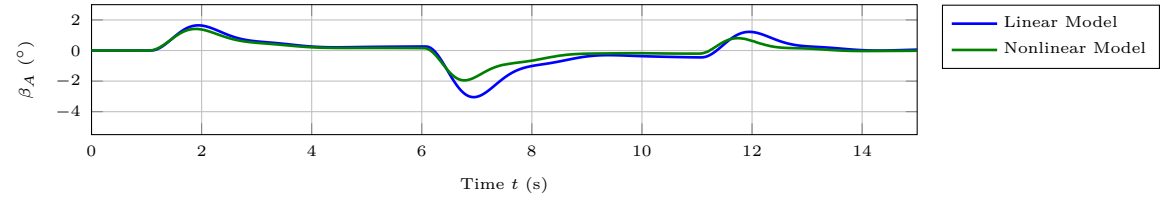

(d) Angle-of-sideslip

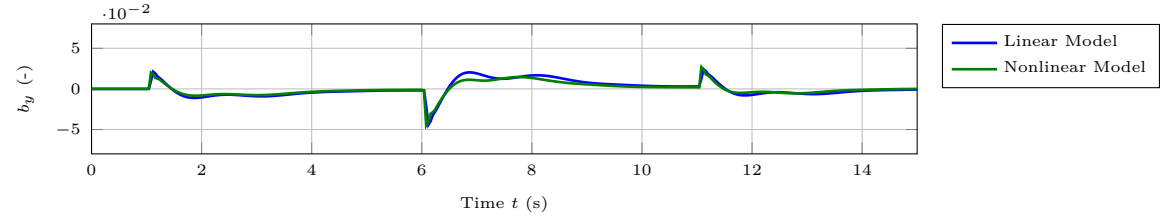

(e) Lateral Acceleration

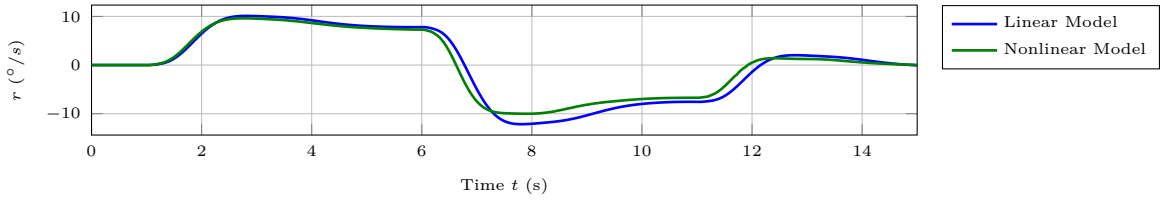

(f) Yaw Rate

Figure 6.10: Comparison of the response of the LTI plant model and the nonlinear plant model with MLESO controller to a $30°$ doublet command $\Phi_{cmd}(t)$ at $V_K^R = 35\,m/s$, $h = 1000\,m$, $m_{fuel} = 23\,kg$.

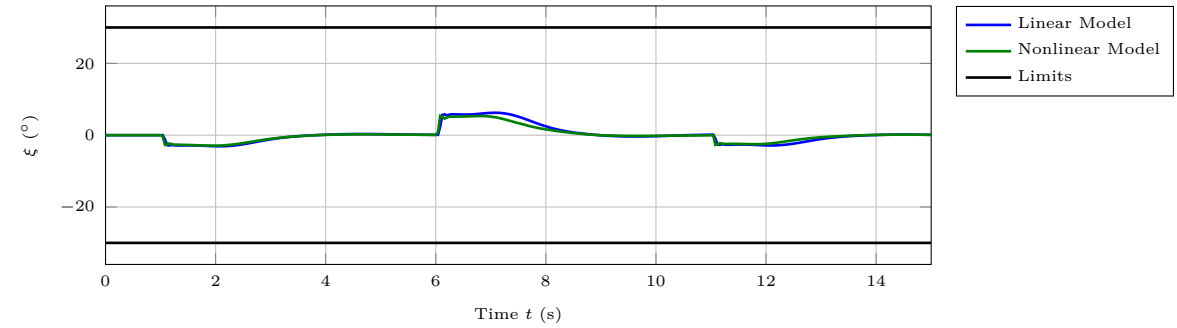

(a) Aileron Deflection

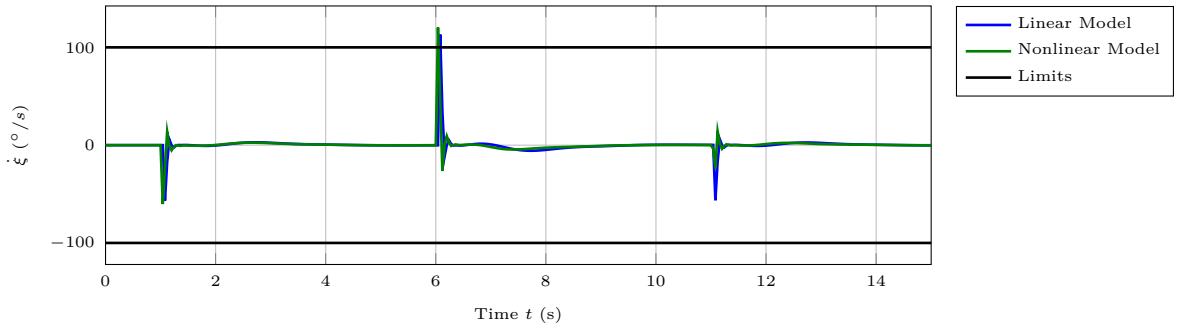

(b) Aileron Rate

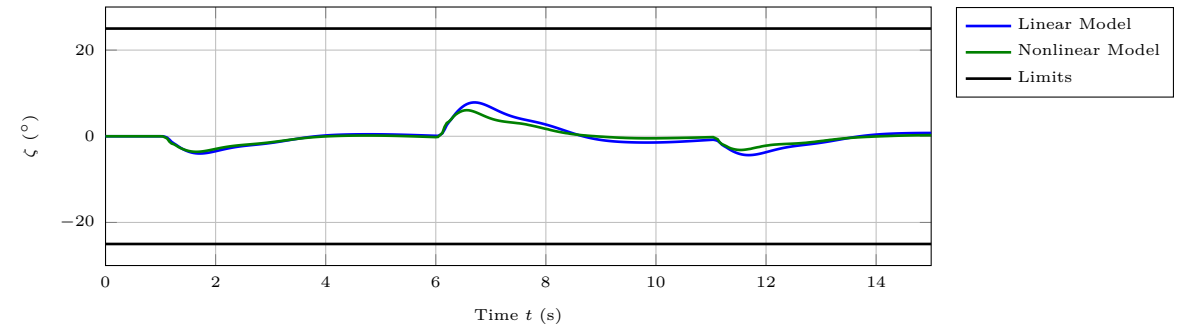

(c) Rudder Deflection

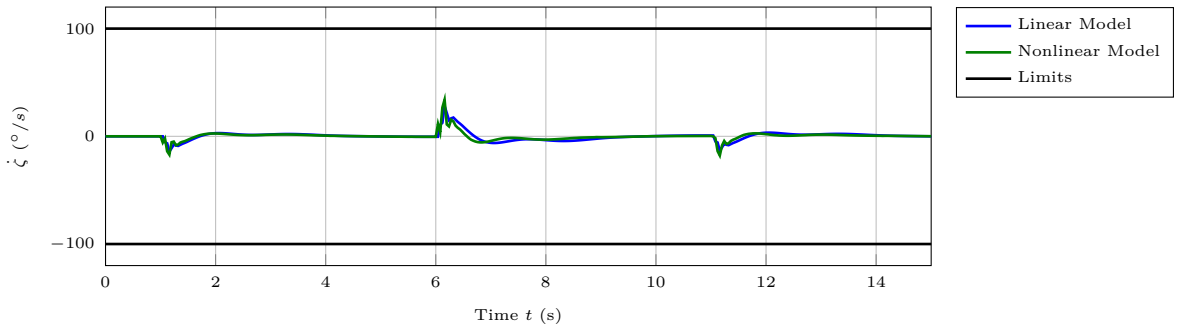

(d) Rudder Rate

Figure 6.11: Comparison of the response of the LTI plant model and the nonlinear plant model with MLESO controller to a 30° doublet command $\Phi_{cmd}(t)$ at $V_K^R = 35\,m/s$, $h = 1000\,m$, $m_{fuel} = 23\,kg$.

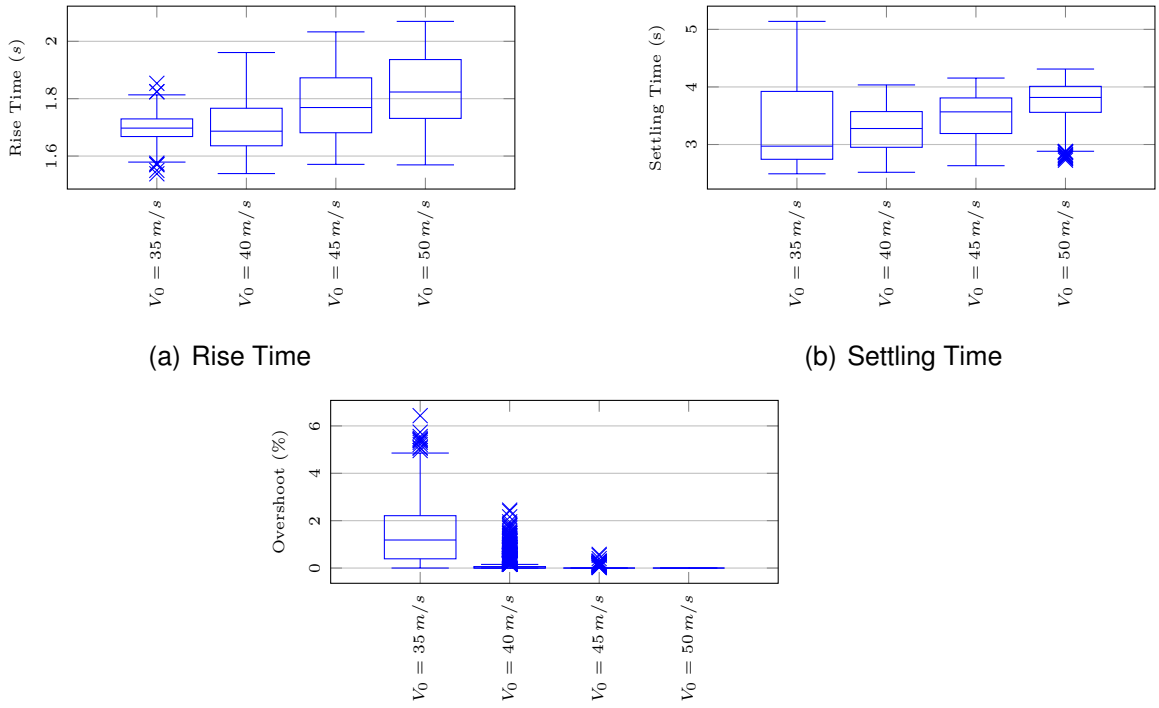

(a) Rise Time

(b) Settling Time

(c) Overshoot

Figure 6.12: Comparison of rise time, settling time and overshoot of the MM-LQR controller at different trim conditions.

Next, the MM-LQR controller is evaluated. Figures 6.13 and 6.14 show the doublet response of the MM-LQR controller at the four trim conditions in case of the linearized rigid-body EOMs. Similar to the MLESO-based controller, Figure 6.13 illustrates that the MM-LQR controller is able to precisely track the commanded bank angle $\Phi_{cmd}(t)$. The response is uniform throughout the envelope and only shows little overshoot.

Furthermore, the MM-LQR controller also ensures a coordinated turn. Figure 6.13 demonstrates that it requires roughly three seconds to regulate the lateral acceleration $b_y(t)$ close to zero, leading to a small, but non-zero aerodynamic/flight-path angle-of-sideslip $\beta_A(t) = \beta_K(t)$. Even during transients, the lateral acceleration $b_y(t) \cdot g$ remains below $0.1 \cdot g$ and the aerodynamic angle-of-sideslip $\beta_A(t)$ does not exceed 10% of the commanded bank angle $\Phi_{cmd}(t)$.

Figure 6.14 highlights that the MM-LQR controller does not command aileron and rudder deflections (or rates) beyond the physical limitations of the actuator.

In order to quantitatively assess the tracking performance of the MM-LQR controller, Figure 6.12 depicts box plots of rise time, settling time and overshoot at the four trim conditions in case of the linearized rigid-body EOMs. Similar to the MLESO-based controller, the rise time is uniform throughout the envelope. The box, which represents 50% of all step responses, roughly stays within the interval $[1.6\,s, 1.95\,s]$. In contrast to the MLESO-based controller, the settling time of the MM-LQR controller is more uniform. For velocities $V_K^R \geq 40\,m/s$, the box, which represents 50% of all step responses,

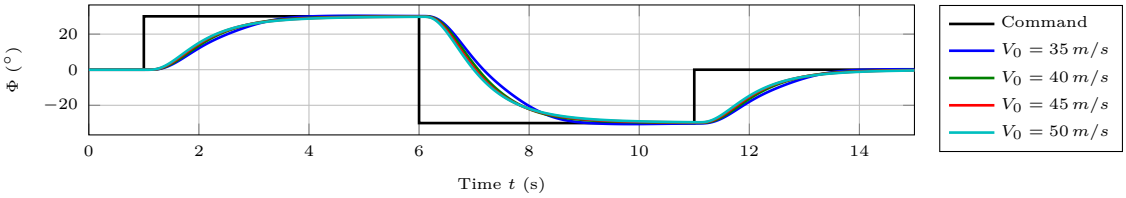

(a) Bank Angle

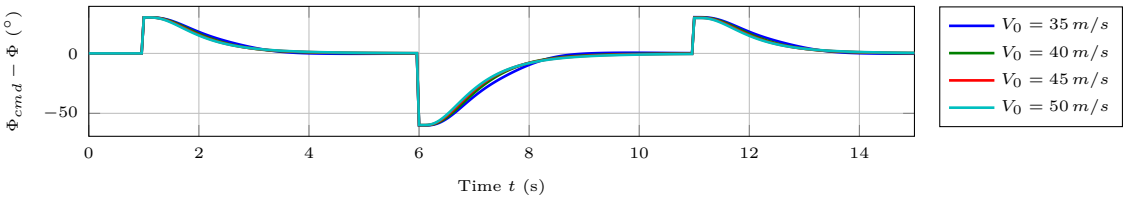

(b) Tracking Error

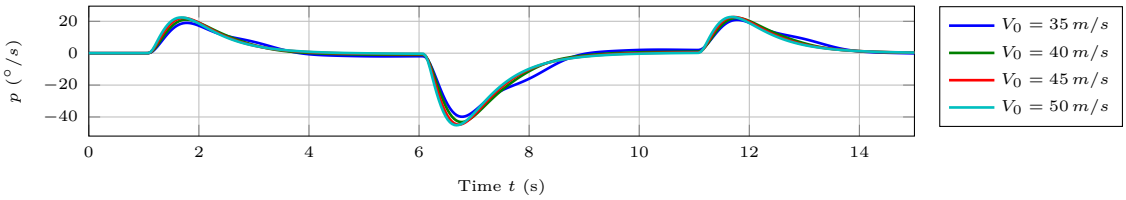

(c) Roll Rate

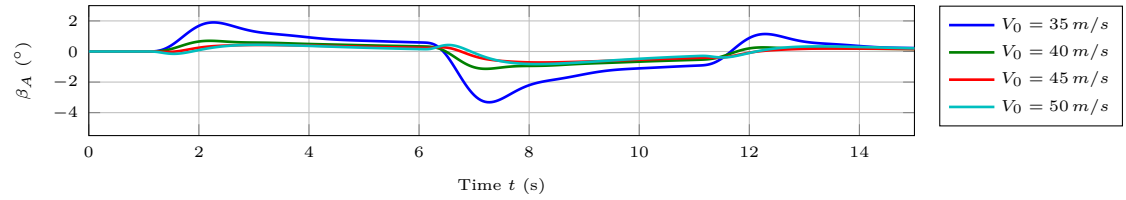

(d) Angle-of-sideslip

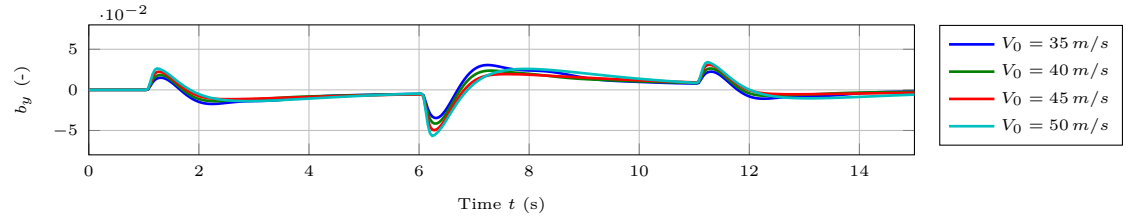

(e) Lateral Acceleration

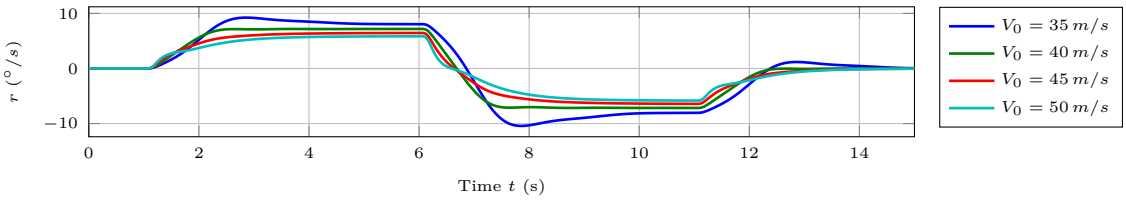

(f) Yaw Rate

Figure 6.13: Comparison of the response of the LTI plant model with MM-LQR controller to a 30° doublet command $\Phi_{cmd}(t)$ at different trim conditions.

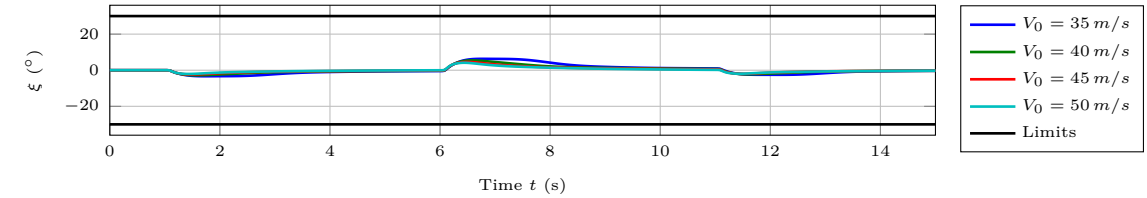

(a) Aileron Deflection

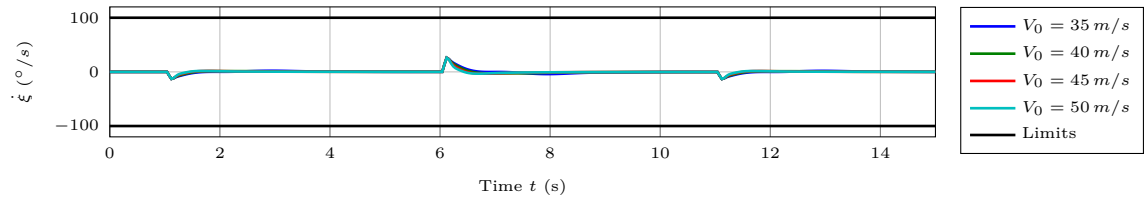

(b) Aileron Rate

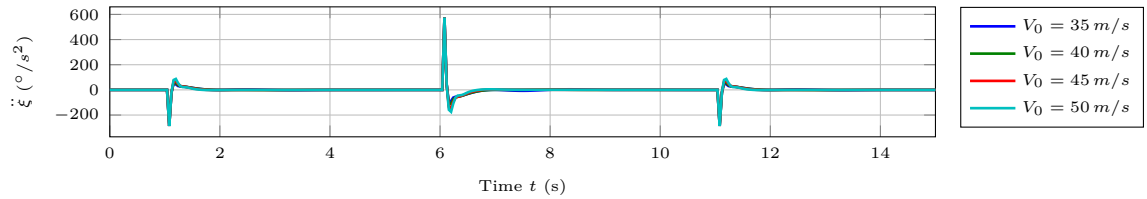

(c) Aileron Acceleration

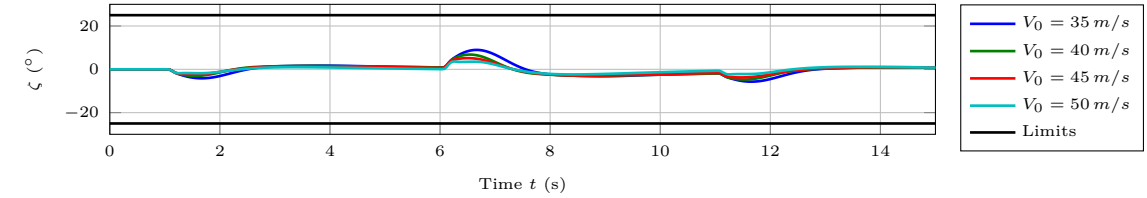

(d) Rudder Deflection

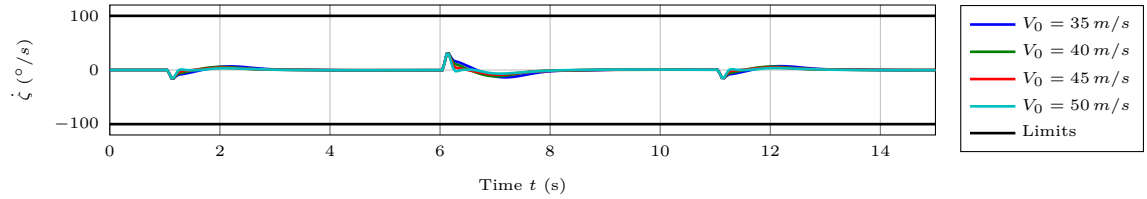

(e) Rudder Rate

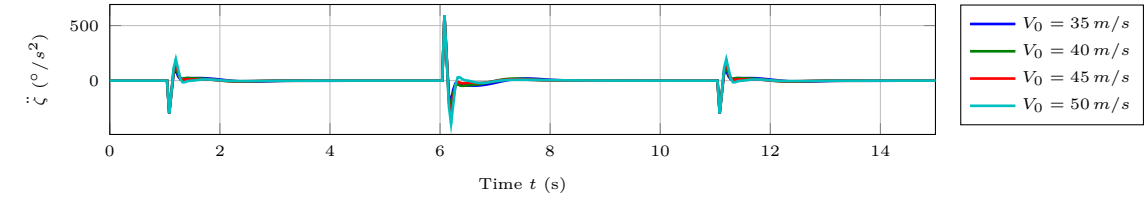

(f) Rudder Acceleration

Figure 6.14: Comparison of the response of the LTI plant model with MM-LQR controller to a $30°$ doublet command $\Phi_{cmd}(t)$ at different trim conditions.

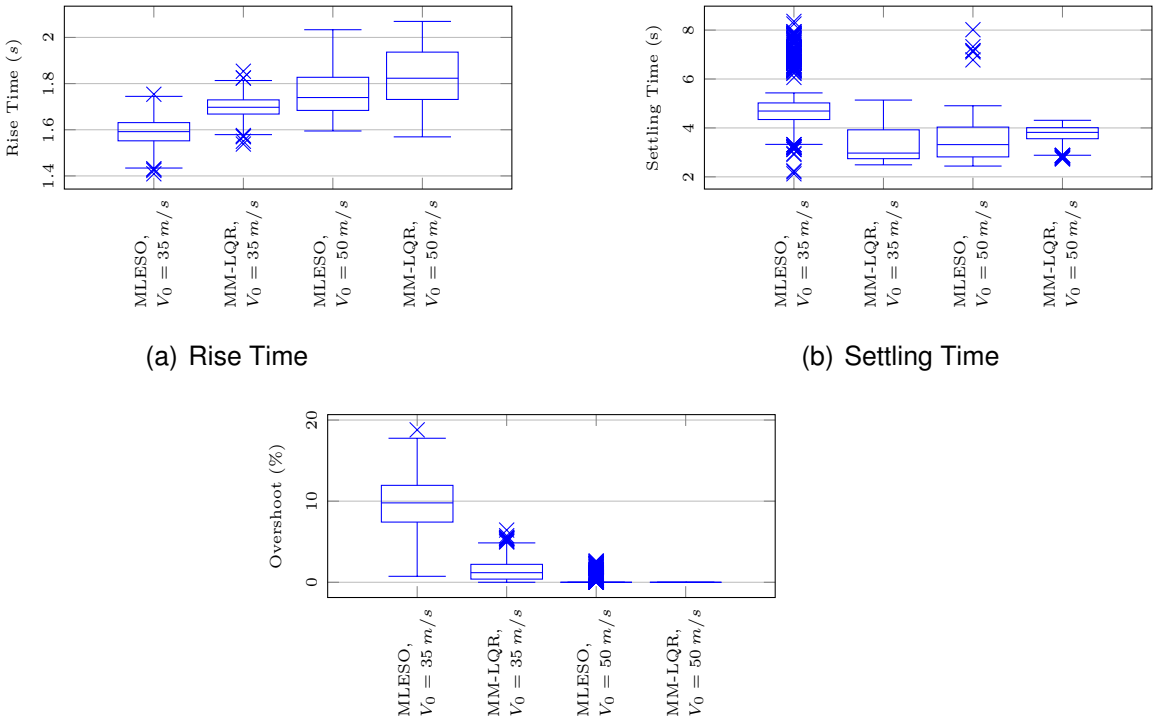

(a) Rise Time

(b) Settling Time

(c) Overshoot

Figure 6.15: Comparison of rise time, settling time and overshoot of the MLESO controller with the MM-LQR controller.

roughly lies within the interval $[3\,s, 4\,s]$. At all velocities, the largest, observed overshoot is small and decreases from 6.5% at low velocities to approximately 0% at high velocities.

As in case of the MLESO-based controller, the MM-LQR controller yields similar performance in nonlinear simulations. This is shown in Figures 6.16 and 6.17, which compare the performance of the MM-LQR controller in a linear simulation to the performance in a nonlinear simulation at $V_K^R = 35\,m/s$, $h = 1000\,m$, $m_{fuel} = 23\,kg$.

To conclude the assessment of the tracking performance, the responses of the MLESO-based controller and the MM-LQR controller are compared to each other in case of the linearized rigid-body EOMs. On the one side, Figure 6.15 highlights that the MLESO-based controller leads to slightly smaller rise times. On the other side, the MM-LQR controller provides more uniform settling times and less overshoot. All in all, the MM-LQR controllers leads to a slightly more uniform tracking of bank angle commands $\Phi_{cmd}(t)$. As can be seen in Figure 6.18, the MM-LQR controller however requires somewhat longer to regulate the lateral acceleration $b_y(t)$ to zero and hence, leads to a aerodynamically less efficient turn as compared to the MLESO-based controller. With respect to the aileron and rudder deflections, Figure 6.19 shows that the MLESO-based controller leads to more aggressive control surface deflections, especially of the aileron.

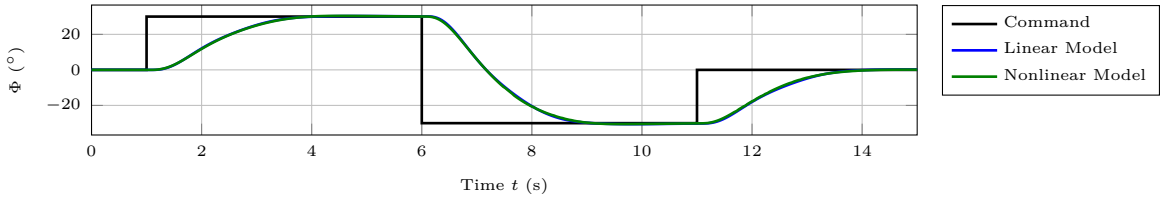

(a) Bank Angle

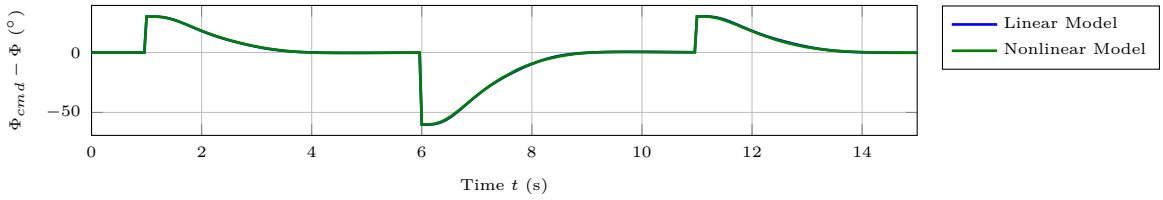

(b) Tracking Error

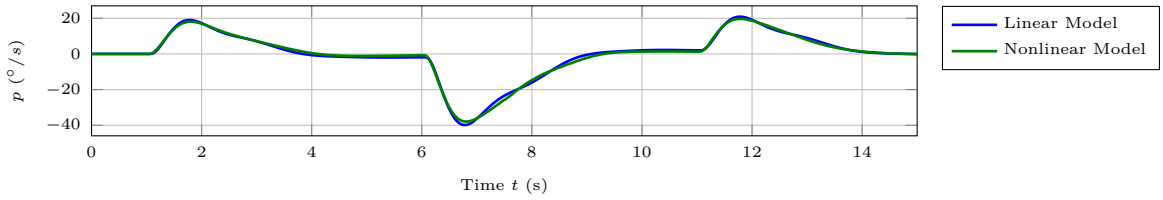

(c) Roll Rate

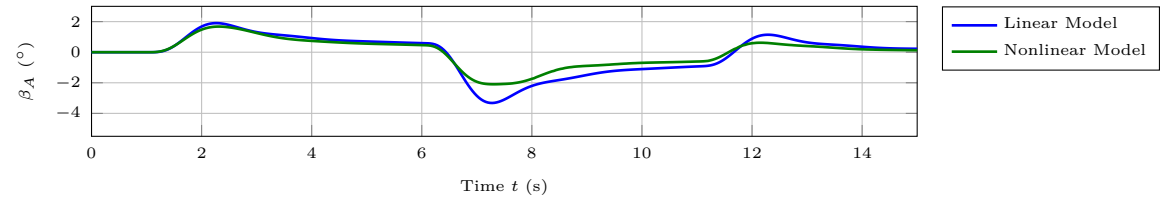

(d) Angle-of-sideslip

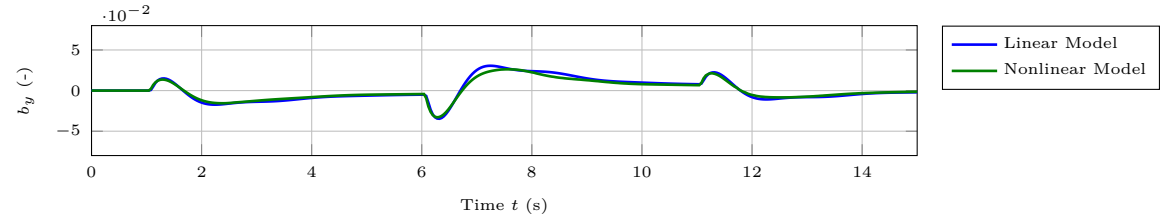

(e) Lateral Acceleration

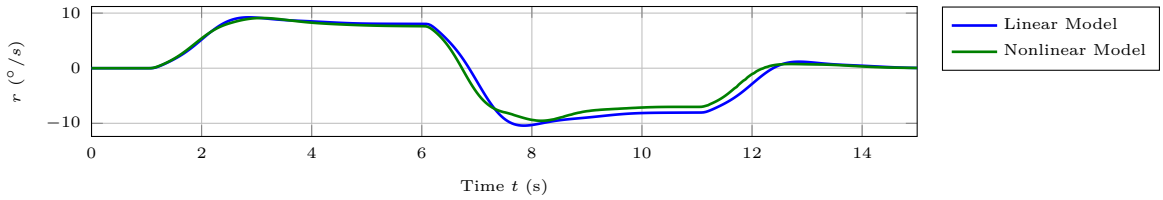

(f) Yaw Rate

Figure 6.16: Comparison of the response of the LTI plant model and the nonlinear plant model with MM-LQR controller to a $30°$ doublet command $\Phi_{cmd}(t)$ at $V_K^R = 35\,m/s$, $h = 1000\,m$, $m_{fuel} = 23\,kg$.

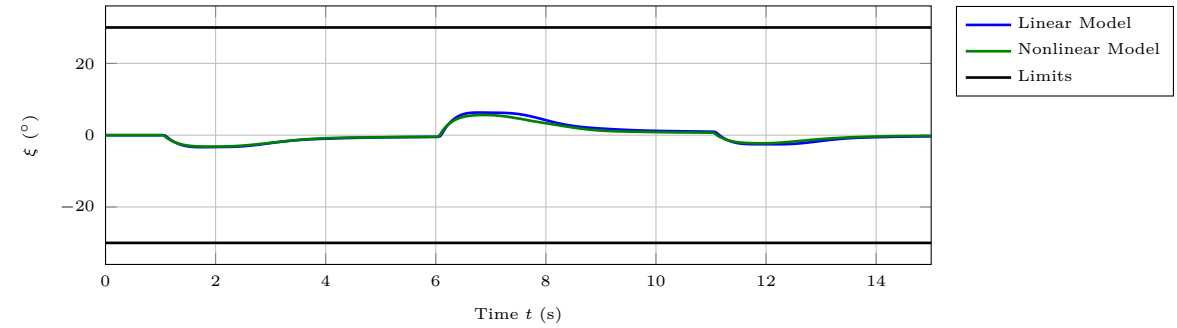

(a) Aileron Deflection

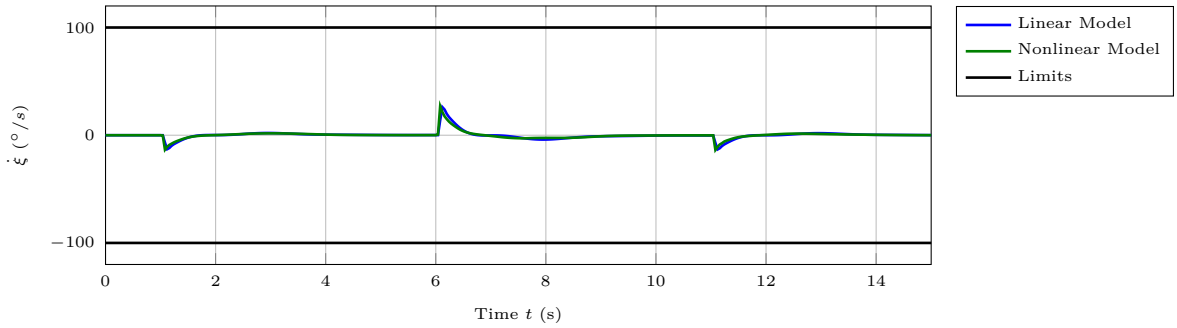

(b) Aileron Rate

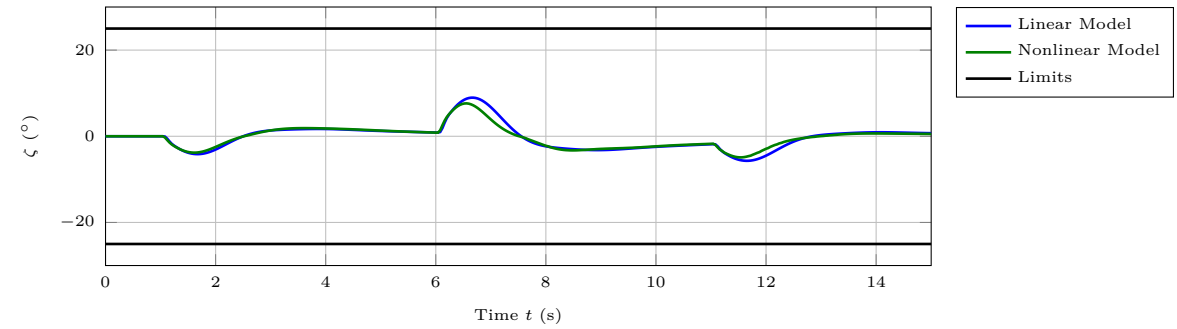

(c) Rudder Deflection

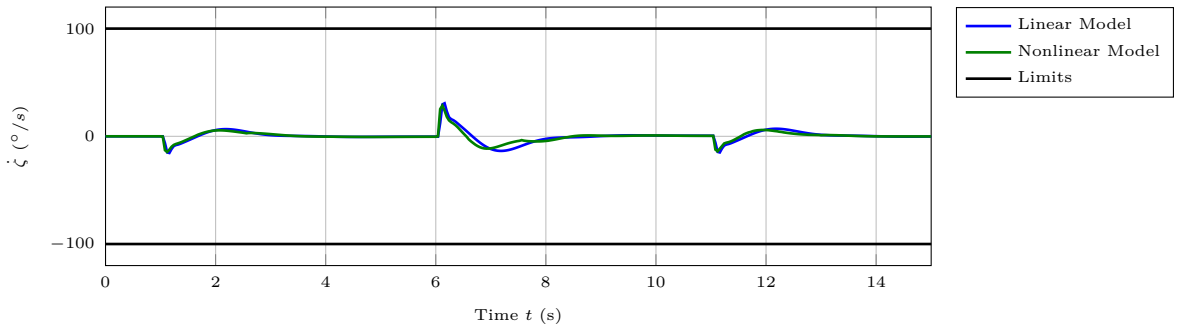

(d) Rudder Rate

Figure 6.17: Comparison of the response of the LTI plant model and the nonlinear plant model with MM-LQR controller to a $30°$ doublet command $\Phi_{cmd}(t)$ at $V_K^R = 35\,m/s$, $h = 1000\,m$, $m_{fuel} = 23\,kg$.

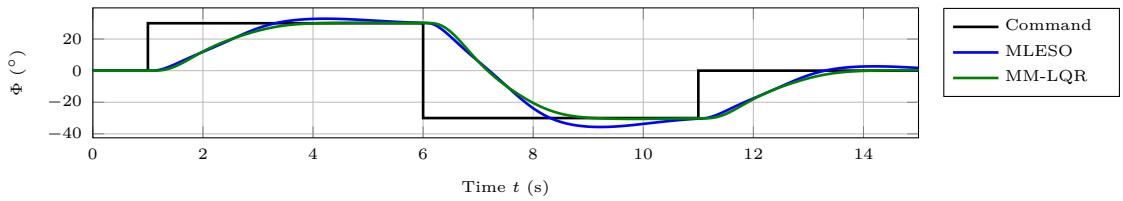

(a) Bank Angle

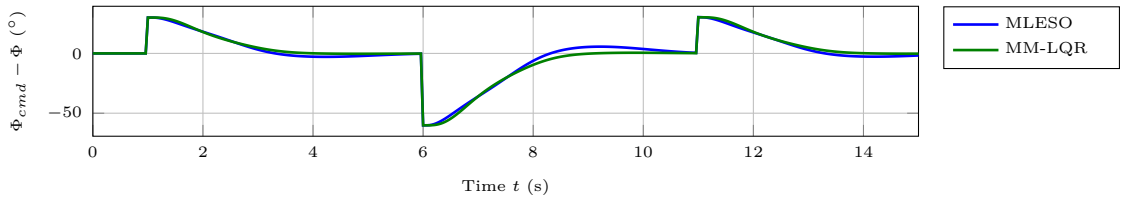

(b) Tracking Error

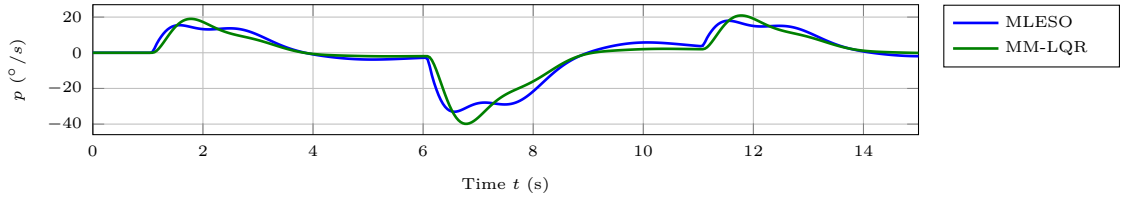

(c) Roll Rate

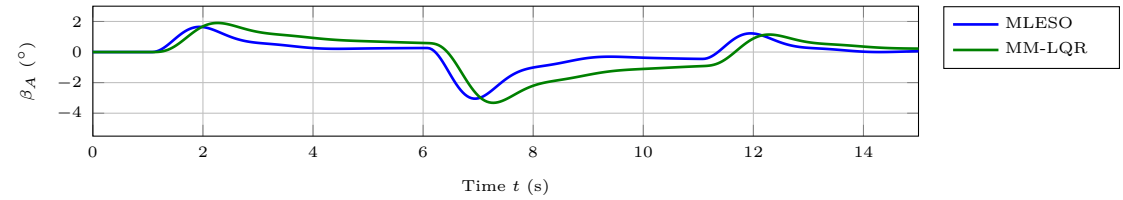

(d) Angle-of-sideslip

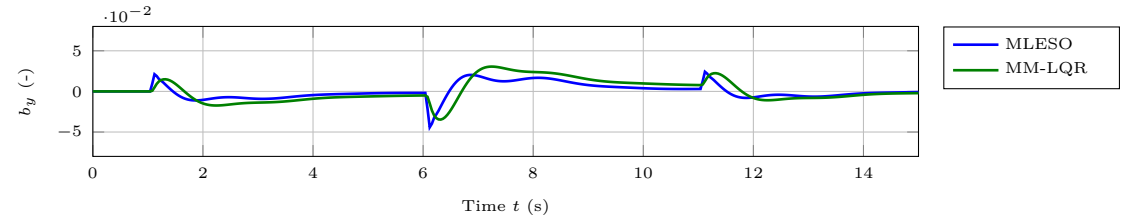

(e) Lateral Acceleration

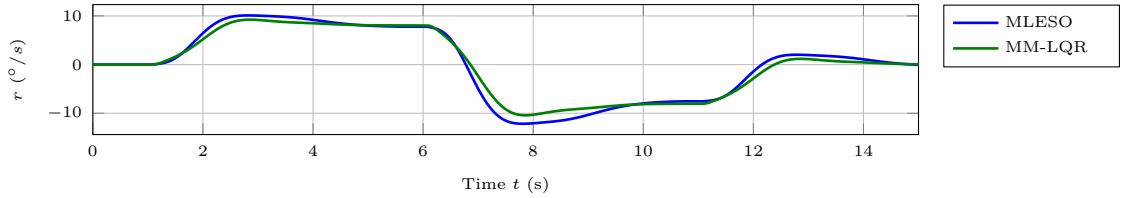

(f) Yaw Rate

Figure 6.18: Comparison of the MLESO controller and the MM-LQR controller (with LTI plant model at $V_K^R = 35\,m/s$, $h = 1000\,m$, $m_{fuel} = 23\,kg$) in response to a $30°$ doublet command $\Phi_{cmd}\,(t)$.

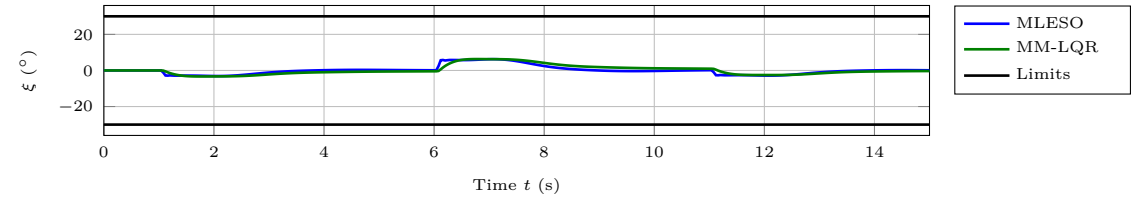

(a) Aileron Deflection

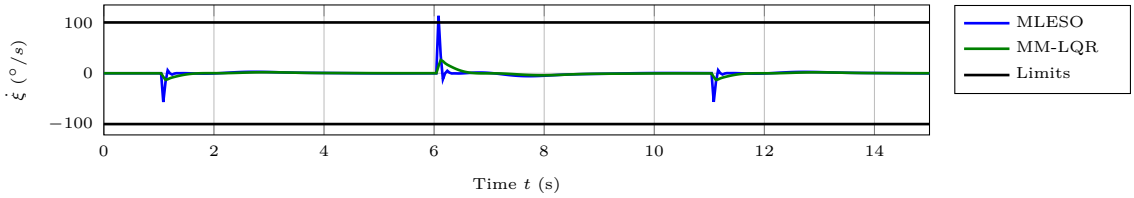

(b) Aileron Rate

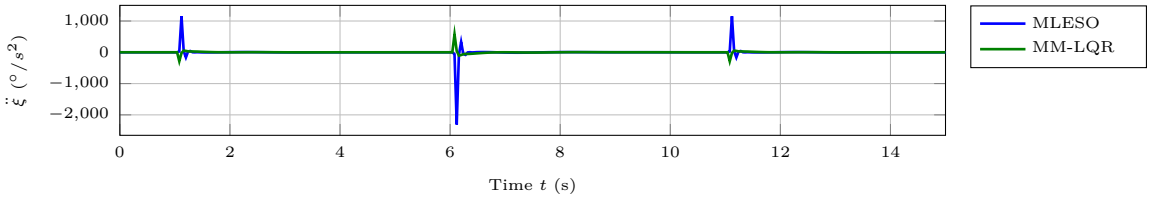

(c) Aileron Acceleration

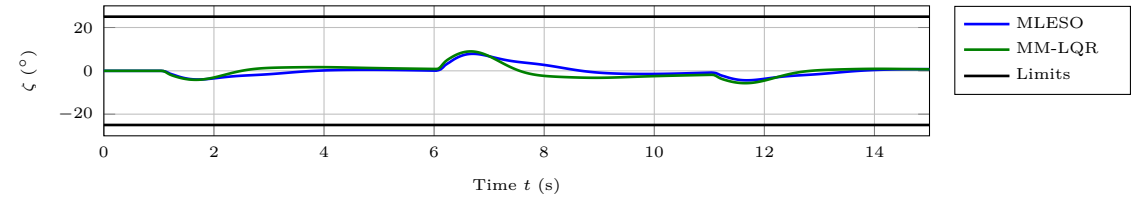

(d) Rudder Deflection

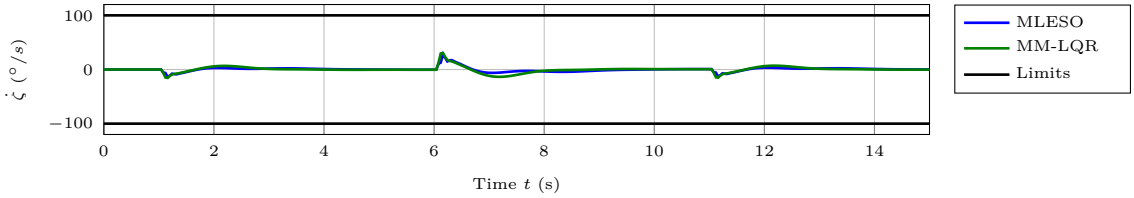

(e) Rudder Rate

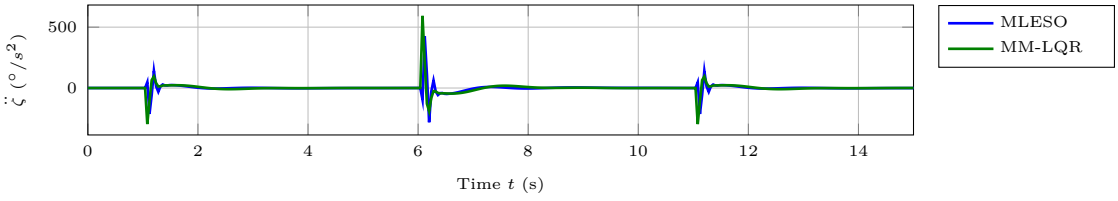

(f) Rudder Acceleration

Figure 6.19: Comparison of the MLESO controller and the MM-LQR controller (with LTI plant model at $V_K^R = 35\,m/s$, $h = 1000\,m$, $m_{fuel} = 23\,kg$) in response to a $30°$ doublet command $\Phi_{cmd}(t)$.

6.4.4 Disturbance Rejection

This section assesses the disturbance rejection capabilities of the developed controllers. As an exemplary disturbance, a discrete gust according to MIL-F-8785C [41] has been chosen. For reasons of clarity, the responses of the control systems to moderate Dryden turbulence have been postponed to Appendix E.

According to MIL-F-8785C [41], a discrete gust has a "1-cosine"-shape:

$$\delta\left(v_W^R\right)_B^E = \begin{cases} 0, & x < 0, \\ \frac{V_m}{2} \cdot \left(1 - \cos\frac{\pi x}{d_m}\right), & 0 \leq x \leq d_m, \\ V_m, & x > d_m. \end{cases} \tag{6.73}$$

In (6.73), V_m denotes the gust amplitude, d_m the gust length and x denotes the distance traveled into the wind field. MIL-F-8785C states that the gust shape (6.73) "may be used singly or in multiples". For the remainder of this thesis, the following gust shape is hence used, which constitutes a sequence of two gusts according to (6.73):

$$\delta\left(v_W^R\right)_B^E = \begin{cases} \frac{V_m}{2} \cdot \left(1 - \cos\frac{\pi x}{d_m}\right), & 0 \leq x \leq 2 \cdot d_m, \\ 0, & \text{otherwise}. \end{cases} \tag{6.74}$$

According to [116], this sequence is useful "to determine the control authority needed to recover from a large disturbance".

MIL-F-8785C states that multiple gust lengths d_m shall be chosen, which excite the natural frequencies of the aircraft and its flight control system. For reasons of simplicity, a single gust length of $d_m = 20\,m$ is used for all subsequent analyses. In MIL-F-8785C, the gust amplitude V_m is specified as function of the gust length, the altitude of the aircraft and the turbulence intensity. When choosing a moderate turbulence intensity, the gust amplitudes $V_m = 1.79\,m/s$ and $V_m = 2.04\,m/s$ result for $h = 500\,m$ and $h = 1000\,m$, respectively.

In order to apply the gust model (6.74) to the linearized, rigid-body EOMs, the *distance traveled into the wind field* x has to be determined. In case of steady-state, horizontal flight and when neglecting small velocity changes due to the gust, $x = V_0 \cdot (t - t_0)$ approximately holds for a gust starting at t_0. Using the definition of $\beta_{W,cmd}(t)$ in (2.60), the gust "commands" in Figure 6.20 result.

Figures 6.21 and 6.22 compare the disturbance rejection of the MLESO-based controller and the MM-LQR controller at the low dynamic pressure / low agility trim condition $V_K^R = 35\,m/s$, $h = 1000\,m$, $m_{fuel} = 23\,kg$ in linear as well as nonlinear simulations. Since hardly any difference between their responses may be observed, the disturbance rejection at this velocity is discussed for both controllers at once. Both controllers require approximately three seconds to regulate the bank angle $\Phi(t)$ and the lateral acceleration $b_y(t)$ to zero. During transients, the aerodynamic angle-of-sideslip remains below $2.5°$ and the lateral acceleration $b_y(t) \cdot g$ stays well below $0.1 \cdot g$. Furthermore,

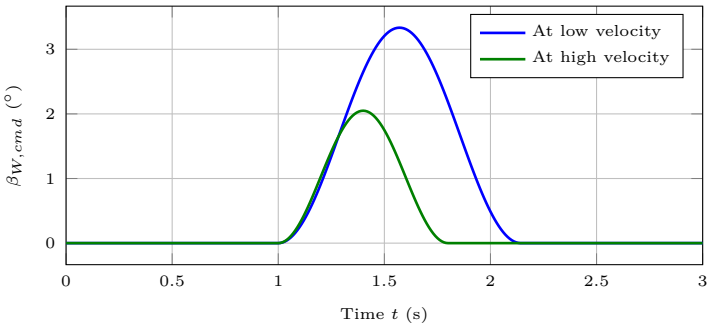

Figure 6.20: Gust command $\beta_{W,cmd}(t)$ at low velocity ($V_K^R = 35\,m/s$, $h = 1000\,m$, $m_{fuel} = 23\,kg$) and high velocity ($V_K^R = 50\,m/s$, $h = 500\,m$, $m_{fuel} = 0\,kg$) corresponding to a $20\,m$ discrete gust with an amplitude $V_m = 2.04\,m/s$ (low velocity) or $V_m = 1.79\,m/s$ (high velocity).

both controllers make moderate use of the control surfaces such that all deflection and rate limits are met.

Next, the performance of the controllers is evaluated at the high dynamic pressure / high agility trim condition $V_K^R = 50\,m/s$, $h = 500\,m$, $m_{fuel} = 0\,kg$, as shown in Figures 6.23 and 6.24. In contrast to the low dynamic pressure trim condition, both controllers only require approximately $2\,s$ to regulate the bank angle $\Phi(t)$ and the lateral acceleration $b_y(t)$ to zero. Furthermore, the excursions of the bank angle $\Phi(t)$ and the aerodynamic angle-of-sideslip $\beta_A(t)$ are smaller. This behavior is to be expected since the gust amplitudes V_m at both trim conditions are similar, which implies that the gust at high velocity is weaker relative to the kinematic velocity of the UAS. With respect to the roll motion, the MM-LQR controller provides a qualitatively better response as its bank angle excursion is smaller and it exhibits less oscillations. At the same time, the yaw responses of both controllers hardly show any difference.

While the disturbance rejection capabilities of both controllers are rather similar, the MM-LQR controller provides slightly better responses, especially with respect to the roll motion. Due to the similarity of the responses, it is however expected that the performance of the MLESO may be improved such that it meets the performance of the MM-LQR controller. This retuning may however lower the robustness margins of the MLESO-based controller to the level of the MM-LQR controller (see Section 6.4.2).

6.5 Discussion

The analysis of Section 6.4 revealed that the MLESO-based controller and the MM-LQR controller approximately achieve the same level of robustness and performance. With respect to the controller complexity, the MM-LQR controller is significantly simpler than the MLESO-based controller. While the MLESO-based controller requires in total 11 states (4 actuator model states, 4 reference model states, 2 MLESO states, 1 inte-

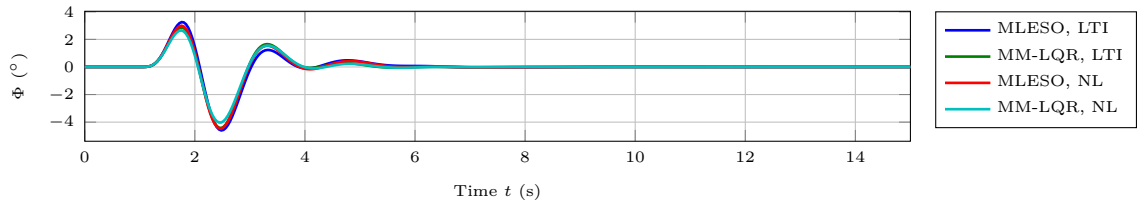

(a) Bank Angle

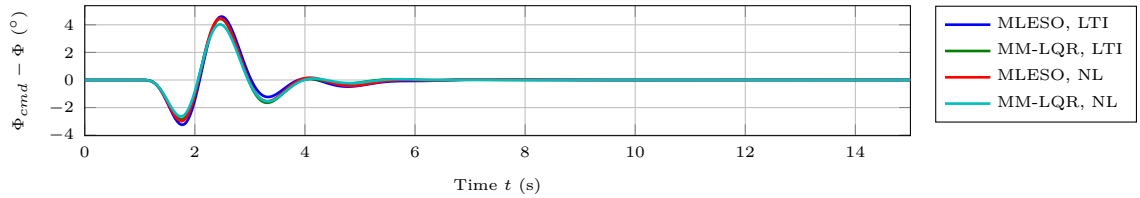

(b) Tracking Error

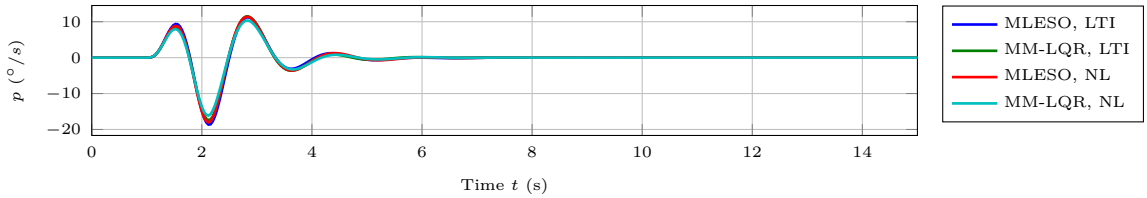

(c) Roll Rate

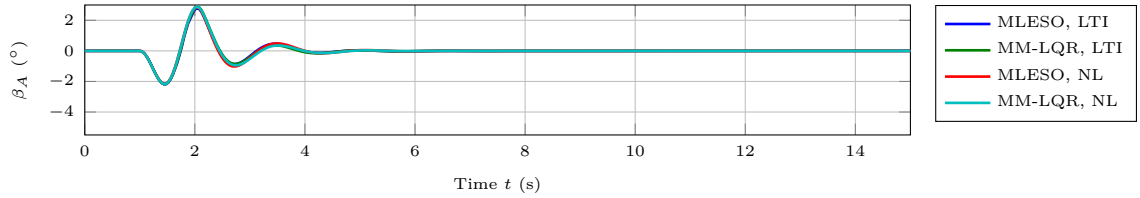

(d) Angle-of-sideslip

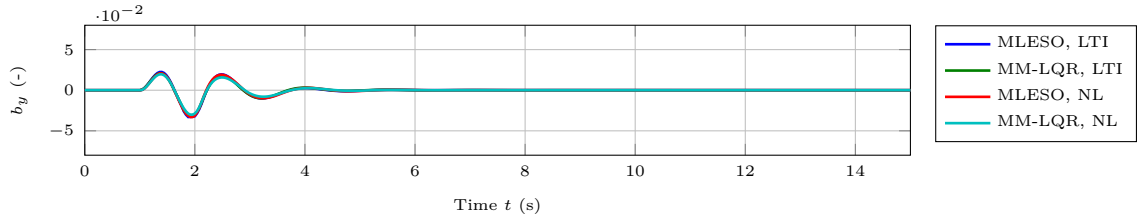

(e) Lateral Acceleration

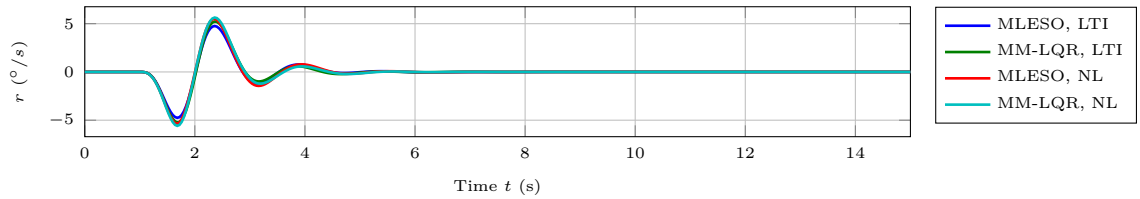

(f) Yaw Rate

Figure 6.21: Comparison of the MLESO controller and the MM-LQR controller (with LTI and nonlinear (NL) plant model at $V_K^R = 35\,m/s$, $h = 1000\,m$, $m_{fuel} = 23\,kg$) in response to a 20m discrete gust with amplitude $2.04\,m/s$.

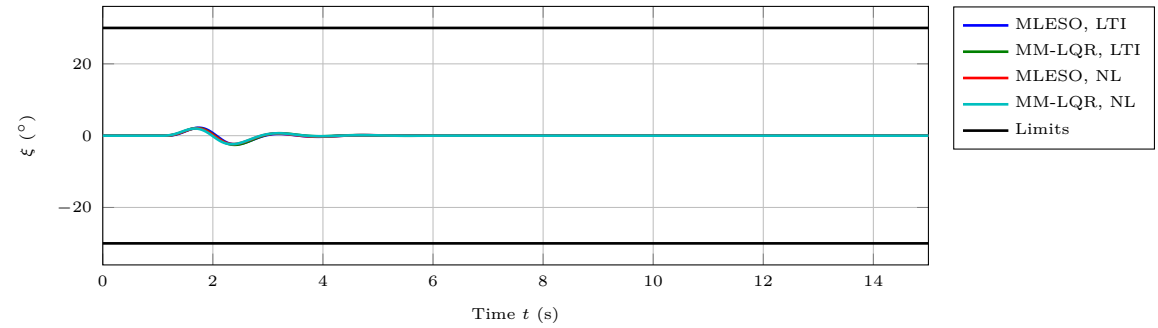

(a) Aileron Deflection

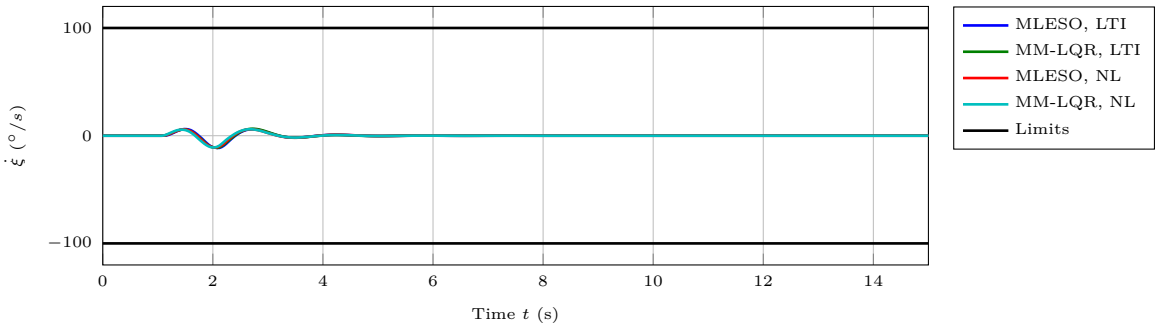

(b) Aileron Rate

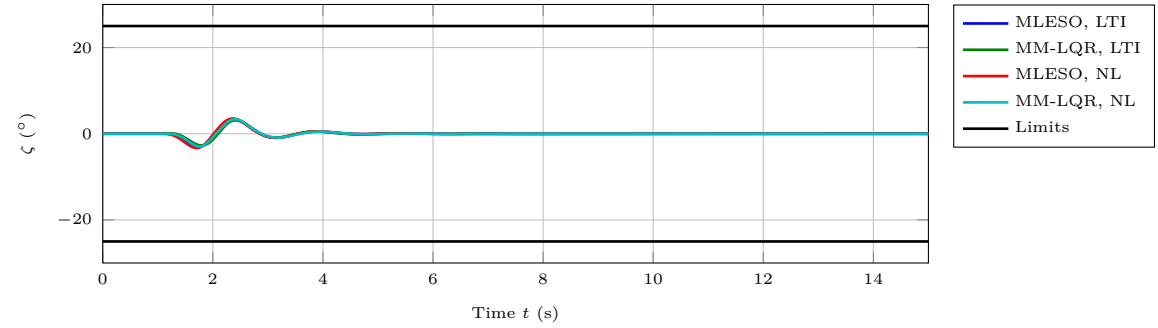

(c) Rudder Deflection

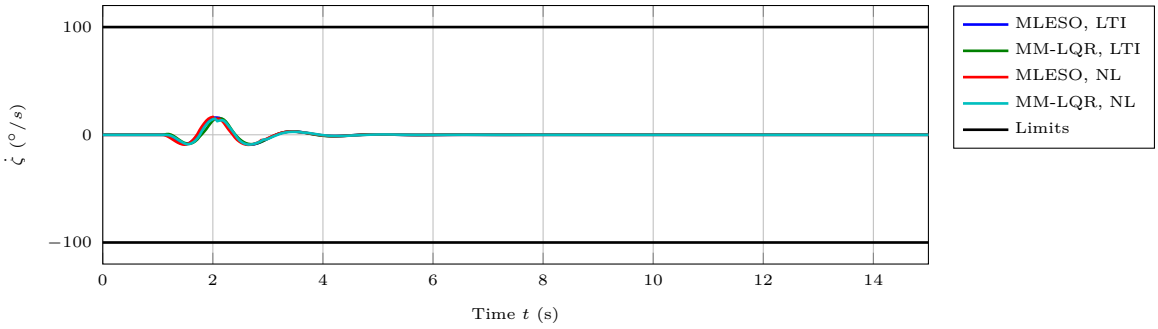

(d) Rudder Rate

Figure 6.22: Comparison of the MLESO controller and the MM-LQR controller (with LTI and nonlinear (NL) plant model at $V_K^R = 35\,m/s$, $h = 1000\,m$, $m_{fuel} = 23\,kg$) in response to a 20m discrete gust with amplitude $2.04\,m/s$.

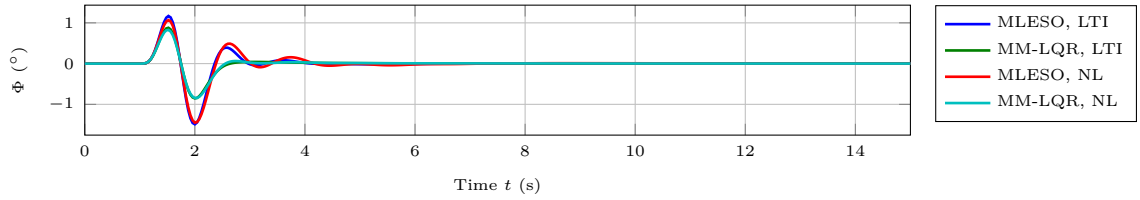

(a) Bank Angle

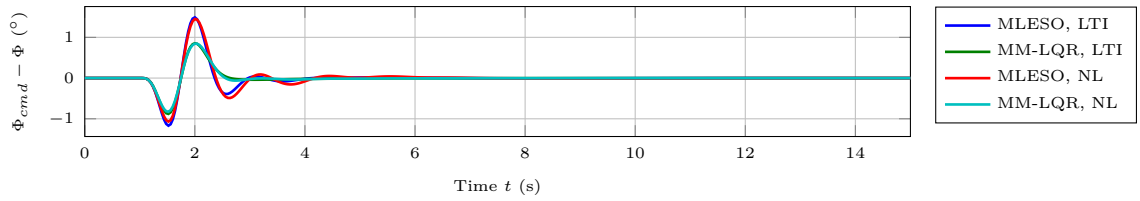

(b) Tracking Error

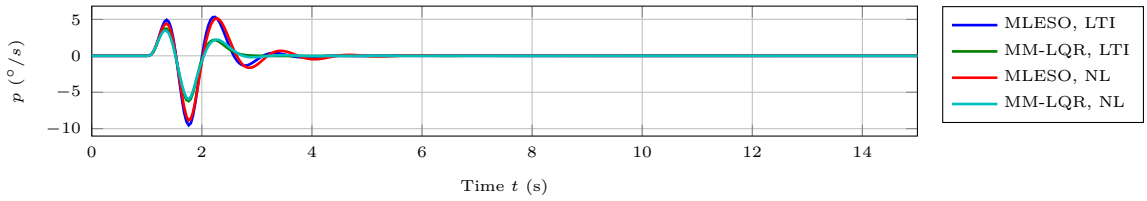

(c) Roll Rate

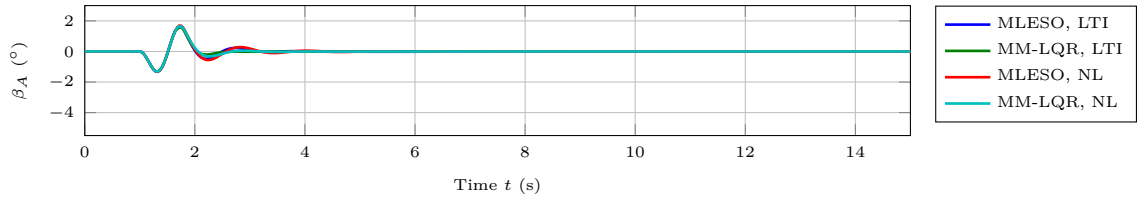

(d) Angle-of-sideslip

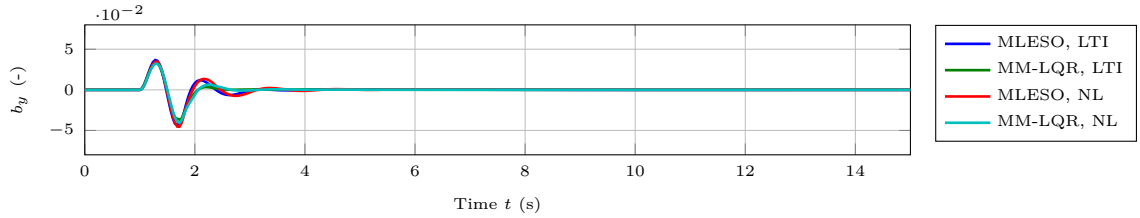

(e) Lateral Acceleration

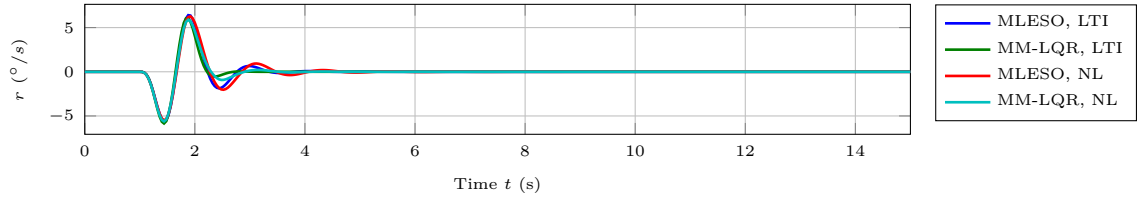

(f) Yaw Rate

Figure 6.23: Comparison of the MLESO controller and the MM-LQR controller (with LTI and nonlinear (NL) plant model at $V_K^R = 50\,m/s$, $h = 500\,m$, $m_{fuel} = 0\,kg$) in response to a 20m discrete gust with amplitude $1.79\,m/s$.

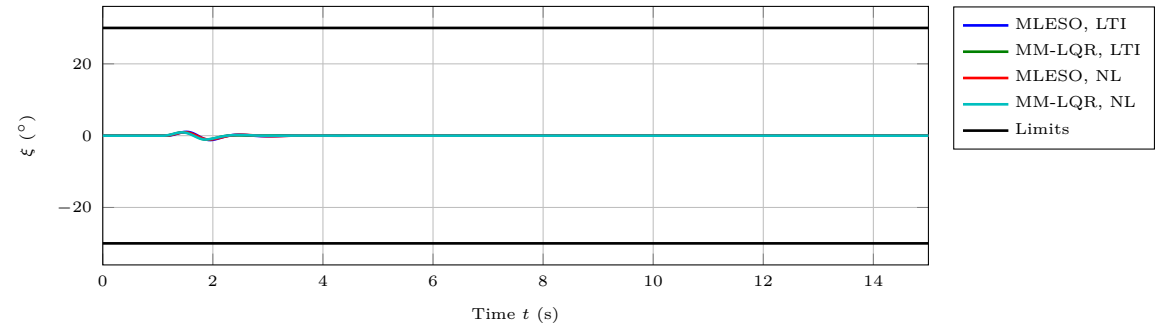

(a) Aileron Deflection

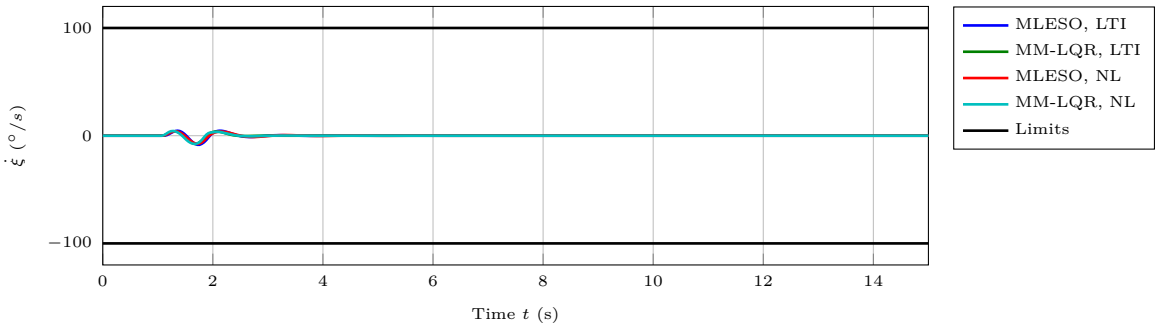

(b) Aileron Rate

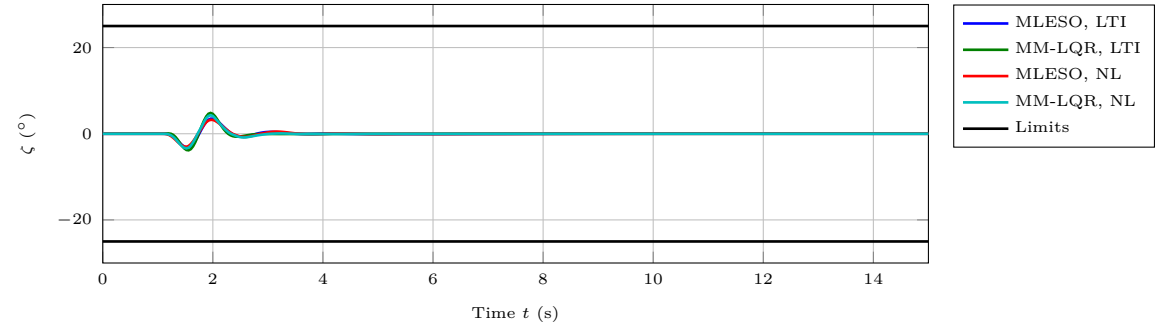

(c) Rudder Deflection

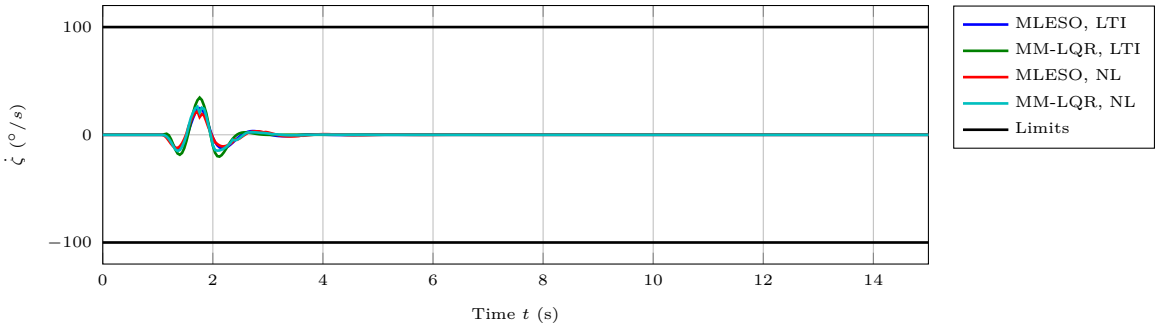

(d) Rudder Rate

Figure 6.24: Comparison of the MLESO controller and the MM-LQR controller (with LTI and nonlinear (NL) plant model at $V_K^R = 50\,m/s$, $h = 500\,m$, $m_{fuel} = 0\,kg$) in response to a 20m discrete gust with amplitude $1.79\,m/s$.

grator state), only 6 states suffice for the MM-LQR controller (4 actuator model states, 2 integrator states). Furthermore, the gain design process of the MM-LQR is substantially simpler as it amounts to the conventional choice of LQR weighting matrices. Due to a similar level of performance and less complexity, the MM-LQR controller seems to be more appropriate for the control design task at hand.

This rather surprising result raises the question why the MLESO-based controller does not outperform the MM-LQR controller. To answer this question, it has to be noticed first that the performance of the MLESO-based controller could in theory be improved almost arbitrarily by increasing the controller gains. This would however lower the time-delay margin to an unacceptable level. The problem that the actual choice of the design parameters is limited by the plant imperfections such as time-delay has already been discussed in Section 3.4.1 in the context of MRAC with hedging. Another limitation of the MLESO-based design derives from the fact that the available knowledge about the plant is only partially exploited. The MLESO-based controller is essentially developed for the low dynamic pressure trim condition. The knowledge about the high dynamic pressure trim condition is only exploited insofar as it admits to compute an overestimation of the control effectiveness. In contrast, the MM-LQR approach uses all of the available information, namely both the low and the high dynamic pressure trim conditions, to obtain an optimal feedback gain $\boldsymbol{K}$. It should be no surprise that a controller, which may resort to detailed knowledge about the plant, may achieve superior performance. Notice however that even the MM-LQR controller ultimately resorts to some sort of high-gain feedback in order to stabilize two plants simultaneously. This high-gain feedback is however specifically tailored to the available plant information. This is in sharp contrast to the MLESO, whose capability to estimate and compensate plant uncertainties is not tailored to a specific uncertainty model. This observation leads to the hypothesis that a model-based approach such as the MM-LQR will lead to superior performance if a suitable model is available. In case of malfunctions or damages, such a model is however often unavailable. In these situations, a MLESO-based controller (or other high-gain or adaptive control approaches) seem more appropriate. Since this hypothesis is derived from a single example, it needs further confirmation.

To conclude this section, notice that the performance of the controller is not expected to improve if for example a MRAC was used in place of the MLESO. This is because the limiting factors of the MLESO-based controller is not the estimation of the uncertainty, but plant imperfections such as the time-delay. These imperfections would affect the MRAC in a similar fashion as the MLESO since both controllers try to enforce model following without considering the inherent limitations that are imposed by these imperfections.

Chapter 7

Conclusion and Perspectives

7.1 Summary

This thesis considers the control of highly uncertain dynamical systems with guaranteed robustness and performance characteristics. In case of safety critical systems such as aircraft, these guarantees are urgently required for the certification, i.e. approval by the authorities. Without certification, no flight control system may operate in non-segregated airspace. In order to achieve this overall objective, the thesis follows two different *strategies*.

The *first strategy* relies on adaptive control, namely Model Reference Adaptive Control (MRAC). Adaptive controllers adjust their gains at runtime to the plant. Due to this principle of operation, adaptive controllers are intrinsically well suited for the control of highly uncertain systems. However, even today, adaptive controllers may not yet be certified. One important obstacle for certification is the lack of robustness and performance guarantees in the form of suitable metrics (measures). That is why the present thesis considers two metrics which might be of use in a future certification process. These metrics are the time-delay margin as a measure of robustness and the largest tracking error as a measure of performance. In practice, the analytical computation of these metrics constitutes a major challenge since only few methods for their computation are currently available. Furthermore, most available methods tend to substantially over- or underestimate the metrics and thus, are highly conservative. For this reason, the *first strategy* amounts to the development of novel methods for the analytical computation of robustness and performance metrics.

The *second strategy* possesses opposite properties as compared to the first one. The strategy relies on a linear control approach. Since current certification standards have been derived with linear system theory in mind, a linear controller is intrinsically certifiable. However, linear control approaches usually face difficulties when it comes to the control of highly uncertain plants. For this reason, the *second strategy* aims at the analysis and the development of linear control approaches which may control

such plants. The result of the *second strategy* is the Modified Linear Extended State Observer (MLESO). The MLESO is a Luenberger-like observer which estimates the deviation between a desired plant model and the true, unknown plant model.

The novel computational methods, which are derived while following the *first strategy*, lead to significant improvements (or represent the first methods of their kind). Nevertheless, they do not yet suffice for a certification process as they are still too conservative. In contrast, the MLESO, which has been developed while following the *second strategy*, is intrinsically certifiable due to its linearity. Furthermore, it possesses the capacity to control highly uncertain plants. Hence, for the time being, the *second strategy* seems more mature with respect to robustness and performance guarantees. Nevertheless, it has to be stressed that there exist situations where nonlinear approaches such as MRAC will outperform linear approaches such as the MLESO. Thus, MLESO-based control may not replace adaptive control. However, on the one side, it constitutes an interesting solution for control problems where both approaches yield similar performance. On the other side, MLESO-based control also is an interesting interim solution until the certification challenges of adaptive control have been solved.

7.2 Contributions

Consistent Derivations

In this thesis, several control approaches for highly uncertain systems are presented, namely MRAC, $\mathcal{L}_1$ Adaptive Control ($\mathcal{L}_1$-AC) with Integral Update Law, $\mathcal{L}_1$ Adaptive Control with Piecewise Constant Update Law ($\mathcal{L}_1$-PWC) and the MLESO. For reasons of clarity and comparability, all these approaches are introduced for the same plant, using a consistent nomenclature and underlying the same assumptions. If assumptions differed due to technical reasons, this has been clearly indicated.

When comparing the required assumptions, one notices a few expected, but nevertheless interesting differences. If matching conditions hold, MRAC is the only control approach that admits an arbitrary rank of the input matrix $\boldsymbol{B}_P$. All other approaches exclude over-actuated plants as they require a full-rank input matrix $\boldsymbol{B}_P$. Notice that this observation only applies to the respective approaches in their basic form. Thus, there might exist modifications which alleviate this restriction. Furthermore, signal-based and parameter-based approaches require different assumptions. In case of parameter-based approaches such as MRAC, nonlinearities must admit a parametrization in terms of known basis functions. In contrast, the signal-based approaches $\mathcal{L}_1$-PWC and MLESO do not require this assumption. Instead, they require the uncertainties to be bounded in some sense (for example in terms of a known Lipschitz constant).

Classification into Signal-based and Parameter-based Approaches

Within this thesis, a new classification of control approaches has been introduced. This classification distinguishes signal-based and parameter-based approaches. In case of parameter-based approaches such as MRAC or $\mathcal{L}_1$-AC, the controller adjusts its *parameters / gains* to account for the deviation between the uncertain plant and the reference model. In contrast, signal-based approaches such as $\mathcal{L}_1$-PWC and the MLESO estimate the *disturbance signal* which results from the deviation between the uncertain plant and the reference model.

The novel classification enables a general discussion of the properties and limitations of parameter-based and signal-based approaches: While both approaches differ fundamentally with respect to the way in which the uncertainty is estimated, they are often similar in the way this body of information is used. All parameter-based and signal-based approaches, which have been introduced within this thesis, use the information about the uncertainty to cancel the deviation between the plant and the reference model. While this approach is reasonable due to the control objective of model following, it may cause significant problems in case of real-world problems. This is because time-delay, actuator dynamics or sensor dynamics fundamentally limit the set of achievable reference models. If a reference model is non-achievable, instability may occur. In order to prevent such instability, the reference model would have to be adjusted in such a way that it remains achievable despite time-delays or sensor dynamics. For this purpose, parameter-based approaches seem more appropriate as they lead to persistent knowledge about the plant which in turn would allow adjusting the reference model. In case of signal-based approach, no such knowledge is generated.

Strategy 1: Systematic Review of Robustness and Performance Metrics

For the control of highly uncertain systems, parameter-based approaches such as MRAC are well suited due to their ability to adjust to the plant at runtime. The certification of these approaches is however currently prevented by the lack of reliable, well-established robustness and performance metrics. For this reason, this thesis presents a systematic review of available metrics which have been proposed in literature. The review classifies all metrics according to their purpose. To that end, stability, robustness and performance metrics are distinguished. Furthermore, the computational aspects are assessed, where analytical and simulation-based computations are distinguished.

Strategy 1: Development of Novel Methods for the Computation of Robustness and Performance Metrics

The review of robustness and performance metrics identifies two promising metrics which might be of use in a future certification process of adaptive controllers. These two metrics are the time-delay margin (as a measure of robustness) and bounds on the tracking error components (as a measure of performance). While both metrics provide valuable insight into the robustness or the performance of an adaptive controller, their

practical application is challenging due to the lack of methods for their computation. For this reason, this thesis developed novel analytical methods for the computation of these two metrics in case of a MRAC.

For the computation of the time-delay margin, a novel analytical method is developed for direct MRAC with σ-modification which relies on the stability theorem of Lyapunov-Razumikhin and Sum-Of-Squares (SOS) optimization. The method enables to compute a bound for the time-delay margin which holds for all bounded command signals and all bounded uncertainties, assuming that suitable bounds for the command and the uncertainties are known a-priori. To the best of the author's knowledge, it is the first method for direct MRAC with σ-modification, which:

- considers the tracking case;
- does not require a-priori bounds on the regressor vector.

Despite the use of SOS optimization, the developed method is highly conservative. In case of the recurring flight control example from Section 2.2, Example 4.19 shows that the analytically guaranteed time-delay margin only amounts to 0.1% of the time-delay margin which is observed in simulations.

In case of the tracking error, a novel analytical method is developed for direct MRAC. With the help of Linear Matrix Inequalities (LMIs) and a slightly modified Lyapunov function candidate, which does not alter the adaptive controller, the conservatism reduces significantly. In case of the recurring flight control example from Section 2.2, the guaranteed bound on the tracking error almost drops by one order of magnitude (see Example 4.7). For a learning rate of $\boldsymbol{\Gamma} = 100 \cdot \boldsymbol{I}^{3\times 3}$, the guaranteed tracking error in the angle-of-attack for example amounts to 7.3° and exceeds the simulation evidence by 366%. Further improvements are achieved when assuming that the plant uncertainties are distributed according to some a-priori known Probability Density Function (PDF). For this purpose, a novel method is developed which approximates the Cumulative Density Function (CDF) of the tracking error bound. This method enables to draw conclusions such as: "The tracking error bound of the angle-of-attack remains below 1° with 90% probability". Moreover, another novel method is developed to compute a tracking error bound in case of bounded exogenous disturbances and unmatched uncertainties. Due to the presence of the latter, a σ-modification is employed additionally. Despite the use of LMI optimization, the method leads to conservative results.

While the developed methods lead to significant improvements (or represent the first methods of their kind), they do not yet suffice for a certification process as they still lead to overly conservative results. One explanation for this observation derives from the fact that a Lyapunov-based analysis is conducted. This implies that the n-dimensional trajectories of the adaptive control system are analyzed using a scalar, energy-like function. This function is in turn used to infer bounds on the tracking error or the time-delay margin. The reduction to a one-dimensional system does however inevitably lead to a loss of information which in turn causes conservatism.

Strategy 2: Development of the Modified Linear Extended State Observer

Although the methods, which are derived while following the *first strategy*, lead to significant improvements, their conservatism still prevents their use in a certification process. For this reason, the MLESO is introduced in this thesis. The MLESO is a Luenberger-like observer which estimates the matched and unmatched disturbance signals resulting from the deviation between the plant and the reference model. In order to achieve model following control, two different control laws are proposed - one for the case of matched uncertainties only and one for the case of matched and unmatched uncertainties. As both control laws lead to Linear Time Invariant (LTI) controllers, MLESO-based control is intrinsically certifiable. Furthermore, linearity enables the use of powerful robustness and performance analysis tools from LTI system theory such as μ-analysis. Thus, the MLESO achieves control of highly uncertain plants with guaranteed robustness and performance characteristics.

In addition to the introduction of the MLESO, this thesis has also evaluated the relation of MLESO-based control to other approaches. Roughly speaking, it is shown that the MLESO-based control law leads to the same closed-loop performance as a $\mathcal{L}_1$-AC or a $\mathcal{L}_1$-PWC. More precisely, the MLESO-based control law actually implements the so-called $\mathcal{L}_1$ *Reference Model*, whereas $\mathcal{L}_1$-AC or $\mathcal{L}_1$-PWC only approximate the latter. However, it has to be noticed that $\mathcal{L}_1$-AC or $\mathcal{L}_1$-PWC provide more degrees of freedom in case of unmatched uncertainties. This means that every MLESO-based control law for unmatched uncertainties may be equivalently implemented as $\mathcal{L}_1$-AC or $\mathcal{L}_1$-PWC, but not vice versa. The relation between MLESO-based control and $\mathcal{L}_1$-AC is of great practical interest as $\mathcal{L}_1$-AC approaches have already proven their maturity in flight-tests on manned aircraft [1].

Due to its connection to $\mathcal{L}_1$-AC, MLESO-based control also relates to other signal-based approaches. In [98], it has been demonstrated that the $\mathcal{L}_1$ *Reference Model* may be equivalently implemented as a Disturbance Observer (DOB). Therefore, the MLESO is equivalent to a DOB under suitable assumptions. Moreover, as the DOB control law is similar to classical inverse-based loop-shaping designs (see for example [156]), the MLESO-based control law is also related to these controllers. Finally, this thesis proves that the MLESO-based control law in case of a matched uncertainties and a first order MLESO can be equivalently implemented as a special Proportional Integral (PI) controller. In contrast to DOBs, inverse-based loop-shaping designs and PI controllers, the MLESO possesses the advantage of being an indirect approach. For this reason, controller windup (for example due to saturations or time-delays) can be systematically prevented using hedging.

Strategy 2: Application and Assessment of the Modified Linear Extended State Observer

In order to demonstrate the capabilities of the MLESO, it is applied to a challenging benchmark control problem. This problem aims at the development of a fallback con-

trol system for the lateral motion of an Unmanned Aerial System (UAS) which may only rely on the measurements provided by the Attitude and Heading Reference System (AHRS) (i.e. linear accelerations, angular rates and attitude angles). Despite limited measurement information, the MLESO-based controller successfully stabilizes the plant for all velocities / altitudes and for all modeled uncertainties. With respect to robustness, the MLESO-based controller mostly satisfies the gain and phase margin requirements from SAE ARP94910. However, especially at low velocities, there exist several uncertainty combinations which lead to violations. In terms of performance, the controller achieves a rather uniform response which exhibits overshoots up to 20% at low velocities.

In order to assess the robustness and performance of the MLESO-based control law, a second control system has been developed additionally. This second controller relies on an *ad hoc modification* of the Linear Quadratic Regulator (LQR) problem. The modification enables to simultaneously stabilize multiple plant models and hence, to stabilize the plant at various altitudes and velocities. Similar to the MLESO-based control system, the LQR control system stabilizes the plant at all trim conditions and for all modeled uncertainties. With respect to robustness, the controller provides slightly lower phase and gain margins than the MLESO-based controller. At the same time, it provides a slightly more uniform tracking response with less overshoot.

When comparing both controllers, one comes to the conclusion that both equally solve the control problem. While there exist minor differences with respect to robustness and performance, it is expected that these differences vanish upon appropriate retuning. Thus, the LQR controller seems preferable for the control task at hand due to its simpler structure. This result was unexpected as MLESO-based control seems more appropriate for the control of highly uncertain plants. In order to explain this result, one has to recall that the MLESO enforces model following by canceling all deviations between a desired plant response and the actual plant response. While this approach is sound in case of an idealistic plant model, it is fundamentally limited in practice by time-delays, actuator dynamics, etc. For this reason, the bandwidth of the MLESO and the bandwidth of the reference model had to be chosen rather small in order to maintain stability (despite the use of hedging). In contrast to the MLESO, the LQR approach does not enforce model following but optimizes a cost function. Since the modification of the LQR design allows considering several operating points at the same time, the LQR approach leads to an optimal compromise between these points. Most importantly, this compromise also accounts for the actuator dynamics. Notice however that this compromise requires a model of the uncertainty. In case of unexpected uncertainties (for example due to malfunctions or damages), no such optimal compromise may be computed a-priori. Hence, it is expected that in case of such events, a MLESO might yield preferable results as it is not optimized to a certain model of the uncertainty.

7.3 Perspectives and Future Work

With respect to the *first strategy*, this thesis has developed novel approaches for the assessment of robustness and performance of adaptive controllers. These approaches rely on Lyapunov(-like) analyses and advanced optimization techniques such as LMIs and SOS programs. Despite the use of optimization, the results are still overly conservative. As this conservatism derives (at least to some extent) from the use of a Lyapunov(-like) analysis, this raises the question as to whether the limits of Lyapunov-based analysis have been reached. For this reason, future work should consider alternative means of proving stability of adaptive control systems. One solution would for example consist in the development of analytical solutions to the differential equations of a closed-loop MRAC control system. Using such solutions, bounds on the tracking error could for example immediately be inferred. The feasibility of this idea is demonstrated in Section D.2. Another solution might consist in a representation of the closed-loop adaptive control system as Wiener-Volterra series [137, 146]. Roughly speaking, a Wiener-Volterra series represents the input / output map of a nonlinear system using a generalization of the convolution integral.

The analytical computation of robustness and performance metrics is appealing as it leads to guaranteed bounds. In practice, however, only few metrics may be computed analytically (see Section 4.1). As these metrics do not suffice to fully specify the intended behavior of an adaptive controller, one might doubt whether analytical computations are actually suited for a certification process. This doubt strengthens when recalling the mathematical effort which is required to compute analytical bounds. For this reason, future work should focus on alternative computational techniques such as simulations or optimization. Due to their high flexibility, it is expected that this focus will facilitate the derivation of novel metrics which allow replacing traditional (frequency-domain) requirements from SAE AS94900 or MIL-HDBK-1997.

The response of an adaptive control system crucially depends on the uncertainty, the command (history) and the disturbance (history). Hence, the excessive use of simulations or optimization entails the challenge of covering all these factors. As neither simulations nor (most) optimization techniques lead to guaranteed bounds (i.e. cover all uncertainties, commands, and disturbances), future work should also focus on online monitoring systems for adaptive flight control systems. If the monitor detects an undesirable behavior of the adaptive controller, it arranges the deactivation of the adaptive control system and will hence prevent the adaptive controller from harming flight safety. On the one side, this approach reduces the need for a-priori guarantees for the adaptive controller. On the other side, a-priori guarantees are required for the monitoring algorithm which ensure that the monitor reliably detects malfunctions of the adaptive controller. Thus, monitoring shifts the need for a-priori guarantees from the adaptive controller to the monitoring system. To that end, it will become an interesting

question how much confidence in a simulation-based assessment is required relative to the confidence in a monitoring system.

With respect to the *second strategy*, this thesis has developed the MLESO. It has been demonstrated that MLESO-based control (mostly) achieves the same closed-loop performance as $\mathcal{L}_1$-AC. Furthermore, this thesis established connections to other signal-based approaches such as DOBs. Future research should try to establish similar connections with other approaches such as Predictive Incremental Nonlinear Dynamic Inversion (PINDI). The knowledge of such relations offers two main advantages. On the one side, it allows finding unique features of the respective approaches. The knowledge of such features is of great practical relevance as it simplifies the choice of a suitable signal-based approach for the control problem at hand. On the other side, different signal-based approaches are often derived from fundamentally different points of view. Once their relations are clear, knowledge and observations, which hold for one signal-based approach, may be easily transferred to other approaches. Such research should also address the open-loop (robustness) properties.

Finally, future work should also investigate ways of combining signal-based and parameter-based approaches. Since signal-based approaches do not care about the intrinsic structure of the uncertainty, they may quickly react to deviations between the plant and the reference model. They do, however, not lead to persistent knowledge about the plant. In contrast, parameter-based approaches admit to gain persistent knowledge. In order to obtain this knowledge, some time is required if undesired effects of fast learning such as significant oscillations are to be avoided. By using fast signal-based approaches and slowly learning parameter-based approaches, the advantages of both approaches may be combined in one design. Such an approach is for example realized by the Command Governor modification [182, 183] of direct MRAC. Here, the Command Governor is used to counteract the effect of fast uncertainties. Similar approaches which rely on a MLESO or $\mathcal{L}_1$-PWC instead of the Command Governor should also be feasible.

Bibliography

[1] Kasey Ackerman, Enric Xargay, Ronald Choe, Naira Hovakimyan, M. Christopher Cotting, Robert B. Jeffrey, Margaret P. Blackstun, Timothy P. Fulkerson, Timothy R. Lau, and Shawn S. Stephens. $\mathcal{L}_1$ Stability Augmentation System for Calspan's Variable-Stability Learjet. In *AIAA Guidance, Navigation, and Control Conference*, 2016.

[2] Francesco Amato. *Robust control of linear systems subject to uncertain time-varying parameters*, volume 325 of *Lecture notes in control and information sciences*. Springer-Verlag, Berlin and Heidelberg, 2006.

[3] Pierre Apkarian, Pascal Gahinet, and Greg Becker. Self-scheduled $\mathcal{H}_\infty$ control of linear parameter-varying systems: a design example. *Automatica*, 31(9):1251–1261, 1995.

[4] A. Astolfi, D. Karagiannis, and Romeo Ortega. *Nonlinear and adaptive control with applications*. Communications and control engineering. Springer-Verlag, London, 2008.

[5] A. Astolfi and Romeo Ortega. Immersion and invariance: a new tool for stabilization and adaptive control of nonlinear systems. *IEEE Transactions on Automatic Control*, 48(4):590–606, 2003.

[6] Karl J. Åström and Tore Hägglund. *Advanced PID control*. ISA - The Instrumentation, Systems, and Automation Society, Research Triangle Park, NC, 2006.

[7] Siu-Kui Au and James L. Beck. Estimation of small failure probabilities in high dimensions by subset simulation. *Probabilistic Engineering Mechanics*, 2001(16):262–277, 2001.

[8] Barton Bacon and Aaron Ostroff. Reconfigurable flight control using nonlinear dynamic inversion with a special accelerometer implementation. In *AIAA Guidance, Navigation, and Control Conference and Exhibit*, 2000.

[9] Christel Baier and Joost-Pieter Katoen. *Principles of model checking*. MIT Press, Cambridge, MA, 2008.

[10] Randall E. Bailey and Timothy J. Bidlack. Unified Pilot-Induced Oscillation Theory. Volume 4. Time-Domain Neal-Smith Criterion. Technical Report WL-TR-96-3031, Air Force Wright Laboratory, 1995.

[11] Gary J. Balas, Peter Seiler, and Andrew Packard. Analysis of an UAV Flight Control System Using Probabilistic μ. In *AIAA Guidance, Navigation, and Control Conference*, 2012.

[12] Märta Barenthin, Bo Wahlberg, Håkan Hjalmarsson, and Mathias Barkhagen. Data-Driven Methods for $\mathcal{L}_2$-Gain Estimation. *IFAC Proceedings Volumes*, 42(10):1597–1602, 2009.

[13] Eric Best, Tony Adami, and Jianchao Zhu. Instability Detection for Nonlinear Time-Varying Systems Using Lyapunov Exponent. In *AIAA Guidance, Navigation, and Control Conference and Exhibit*, 2003.

[14] Siddhartha Bhattacharyya, Darren Cofer, David J. Musliner, Joseph Mueller, and Eric Engstrom. Certification Considerations for Adaptive Systems. Technical Report NASA/CR-2015-218702, NASA Langley Research Center, Hampton, VA, 2015.

[15] Thomas Bierling. *Comparative Analysis of Adaptive Control Techniques for Improved Robust Performance*. PhD thesis, Technische Universität München, München, 2014.

[16] Christopher M. Bishop. *Pattern recognition and machine learning*. Information science and statistics. Springer-Verlag, New York, 2006.

[17] Stephen P. Boyd. *Linear matrix inequalities in system and control theory*. SIAM, Philadelphia, PA, 1994.

[18] Stephen P. Boyd and Lieven Vandenberghe. *Convex optimization*. Cambridge University Press, Cambridge, UK, 2004.

[19] Joseph S. Brinker and Kevin A. Wise. Flight Testing of Reconfigurable Control Law on the X-36 Tailless Aircraft. *Journal of Guidance, Control, and Dynamics*, 24(5):903–909, 2001.

[20] Rudolf Brockhaus, Wolfgang Alles, and Robert Luckner. *Flugregelung*. Springer-Verlag, Berlin and Heidelberg, 3rd edition, 2010.

[21] Fredrik Bruzelius. *Linear parameter-varying systems: An approach to gain scheduling*. PhD thesis, Chalmers University of Technology, Göteborg, 2004.

[22] Klemens Burg, Herbert Haf, Friedrich Wille, and Andreas Meister. *Partielle Differentialgleichungen und funktionalanalytische Grundlagen: Höhere Mathematik für Ingenieure, Naturwissenschaftler und Mathematiker*. Vieweg+Teubner Verlag, Wiesbaden, 5th edition, 2010.

[23] Klemens Burg, Herbert Haf, Friedrich Wille, and Andreas Meister. *Lineare Algebra*, volume 2 of *Höhere Mathematik für Ingenieure*. Springer Vieweg, Wiesbaden, 7th edition, 2012.

[24] Klemens Burg, Herbert Haf, Friedrich Wille, and Andreas Meister. *Analysis*, volume 1 of *Höhere Mathematik für Ingenieure*. Springer Vieweg, Wiesbaden, 10th edition, 2013.

[25] Chengyu Cao and Naira Hovakimyan. $\mathcal{L}_1$ Adaptive Output-Feedback Controller for Non-Strictly-Positive-Real Reference Systems: Missile Longitudinal Autopilot Design. *Journal of Guidance, Control, and Dynamics*, 32(3):717–726, 2009.

[26] Rajeev Chandramohan and Anthony J. Calise. Output Feedback Adaptive Control in the Presence of Unmodeled Dynamics. In *AIAA Guidance, Navigation, and Control Conference*, 2013.

[27] Chengyu Cao and Naira Hovakimyan. Design and Analysis of a Novel $\mathcal{L}_1$ Adaptive Controller, Part I: Control Signal and Asymptotic Stability. In *American Control Conference*, pages 3397–3402, 2006.

[28] Chengyu Cao and Naira Hovakimyan. Design and Analysis of a Novel $\mathcal{L}_1$ Adaptive Controller, Part II: Guaranteed Transient Performance. In *American Control Conference*, pages 3403–3408, 2006.

[29] Chengyu Cao and Naira Hovakimyan. Stability Margins of $\mathcal{L}_1$ Adaptive Controller: Part II. In *American Control Conference*, pages 3931–3936, 2007.

[30] Chengyu Cao and Naira Hovakimyan. Stability Margins of $\mathcal{L}_1$ Adaptive Control Architecture. *IEEE Transactions on Automatic Control*, 55(2):480–487, 2010.

[31] M. D. Choi, T. Y. Lam, and B. Reznick. Sums of Squares of Real Polynomials. *Proceedings of Symposia in Pure Mathematics*, 58(2):103–126, 1995.

[32] Girish Chowdhary. *Concurrent learning for convergence in adaptive control without persistency of excitation*. PhD thesis, Georgia Institute of Technology, Atlanta, GA, 2010.

[33] Girish Chowdhary, Jonathan How, and Hassan Kingravi. Model Reference Adaptive Control using Nonparametric Adaptive Elements. In *AIAA Guidance, Navigation, and Control Conference*, 2012.

[34] Girish Chowdhary, Tansel Yucelen, Maximilian Mühlegg, and Eric N. Johnson. Concurrent learning adaptive control of linear systems with exponentially convergent bounds. *International Journal of Adaptive Control and Signal Processing*, 2012.

[35] Luis G. Crespo, Sean P. Kenny, and Daniel P. Giesy. Figures of Merit for Control Verification. In *AIAA Guidance, Navigation and Control Conference and Exhibit*, 2008.

[36] Luis G. Crespo, Sean P. Kenny, and Daniel P. Giesy. A computational framework to control verification and robustness analysis. Technical Report NASA/TP-2010-216189, NASA, 2010.

[37] Luis G. Crespo, Megumi Matsutani, Jinho Jang, Travis E. Gibson, and Anuradha M. Annaswamy. Design and Verification of an Adaptive Controller for the Generic Transport Model. In *AIAA Guidance, Navigation, and Control Conference*, 2009.

[38] S. J. Cusumano and K. Poolla. Nonlinear feedback vs. linear feedback for robust stabilization. In *27th IEEE Conference on Decision and Control*, pages 1776–1780, 1988.

[39] De La Torre, Gerardo, Tansel Yucelen, and Eric N. Johnson. A new model reference control architecture: Stability, performance, and robustness. *International Journal of Robust and Nonlinear Control*, 2015.

[40] Stéphane Delannoy and Simon Oudin. Longitudinal control law for modern long range civil aircrafts. In *Proceedings of the EuroGNC 2013, 2nd CEAS Specialist Conference on Guidance, Navigation & Control*, 2013.

[41] Department of Defense. Flying Qualities of Piloted Airplanes. Military Specification MIL-F-8785C, Washington, 1980.

[42] Department of Defense. Flying Qualities of Piloted Aircraft. Military Handbook MIL-HDBK-1797, Washington, 1997.

[43] Andrei Dorobantu, Peter Seiler, and Gary J. Balas. Time-Delay Margin Analysis for an Adaptive Controller. *Journal of Guidance, Control, and Dynamics*, 35(5):1418–1425, 2012.

[44] M. A. Duarte and Kumpati S. Narendra. Combined direct and indirect approach to adaptive control. *IEEE Transactions on Automatic Control*, 34(10):1071–1075, 1989.

[45] Geir E. Dullerud and Fernando G. Paganini. *A course in robust control theory: A convex approach*, volume 36 of *Texts in applied mathematics*. Springer-Verlag, New York, 2000.

[46] Zachary Thompson Dydek, Anuradha M. Annaswamy, and Eugene Lavretsky. Adaptive Control and the NASA X-15-3 Flight Revisited. *IEEE Control Systems Magazine*, 30(3):32–48, 2010.

[47] Zachary Thompson Dydek, Himani Jain, Jinho Jang, Anuradha M. Annaswamy, and Eugene Lavretsky. Theoretically Verifiable Stability Margins for an Adaptive Controller. In *AIAA Guidance, Navigation, and Control Conference and Exhibit*, 2006.

[48] Laurent El Ghaoui and Silviu-Iulian Niculescu. *Advances in linear matrix inequality methods in control*. Advances in design and control. SIAM, Philadelphia, PA, 1999.

[49] A. El-Sakkary. The gap metric: Robustness of stabilization of feedback systems. *IEEE Transactions on Automatic Control*, 30(3):240–247, 1985.

[50] EUROCONTROL and University FAF Munich, Institute of Geodesy and Navigation. WGS84 Implementation Manual. Technical Report Version 2.4, 1998.

[51] European Aviation Safety Agency. EASA Certification Specifications for Normal, Utility, Aerobatic, and Commuter Category Aeroplanes. Certification Specifications 23 (CS23), 2015.

[52] Federal Aviation Administration. System Safety Analysis and Assessment for Part 23 Airplanes. Advisory Circular 23.1309-1E, 2011.

[53] Helmut Fischer. *Mathematik für Physiker Band 2*. Teubner-Studienbücher : Mathematik, Physik. Springer Spektrum, Wiesbaden, 4th edition, 2014.

[54] B. A. Francis and W. M. Wonham. The internal model principle of control theory. *Automatica*, 12(5):457–465, 1976.

[55] Mario Luca Fravolini and Giampiero Campa. Integrated design of a linear/neuro-adaptive controller in the presence of norm-bounded uncertainties. *International Journal of Control*, 84(10):1664–1677, 2011.

[56] Mario Luca Fravolini, Tansel Yucelen, and Giampiero Campa. Performance verification of low-frequency learning adaptive controllers. In *American Control Conference*, pages 5091–5096, 2014.

[57] Mario Luca Fravolini, Tansel Yucelen, and Giampiero Campa. Set theoretic performance verification of low-frequency learning adaptive controllers. *International Journal of Adaptive Control and Signal Processing*, 29(10):1243–1258, 2015.

[58] Mario Luca Fravolini, Tansel Yucelen, Benjamin C. Gruenwald, Nhan T. Nguyen, and Wagner Daniel. A Design, Analysis and Verification Framework for Adaptive Flight Control. In *AIAA Guidance, Navigation, and Control Conference*, 2015.

[59] Mario Luca Fravolini, Tansel Yucelen, Benjamin C. Gruenwald, Daniel Wagner, and Marcello R. Napolitano. Comparison of Robust and Probabilistic LMI-Based Design of Adaptive Flight Controllers with Uncertain Input Dynamics. In *AIAA Guidance, Navigation, and Control Conference*, 2016.

[60] Mario Luca Fravolini, Tansel Yucelen, Jonathan A. Muse, and Paolo Valigi. Analysis and design of adaptive control systems with unmodeled input dynamics via multiobjective convex optimization. In *American Control Conference*, pages 1579–1584, 2015.

[61] Mario Luca Fravolini, Tansel Yucelen, Daniel Wagner, Ali Albattat, and Paolo Valigi. Verifiable frequency-limited adaptive control performance based on linear matrix inequalities. In *IEEE Conference on Decision and Control*, pages 6641–6646, 2014.

[62] Mark French. Adaptive Control and Robustness in the Gap Metric. *IEEE Transactions on Automatic Control*, 53(2):461–478, 2008.

[63] Mark French, Csaba Szepesvári, and Eric Rogers. *Performance of nonlinear approximate adaptive controllers*. Wiley, Chichester, UK, 2003.

[64] Ken-Ichi Funahashi. On the approximate realization of continuous mappings by neural networks. *Neural Networks*, 2(3):183–192, 1989.

[65] Zhiqiang Gao. Scaling and bandwidth-parameterization based controller tuning. In *American Control Conference*, pages 4989–4996, 2003.

[66] Zhiqiang Gao. Active disturbance rejection control: a paradigm shift in feedback control system design. In *American Control Conference*, 2006.

[67] Zhiqiang Gao, Yi Huang, and Jingqing Han. An alternative paradigm for control system design. In *40th Conference on Decision and Control*, pages 4578–4585, 2001.

[68] T.T Georgiou and M.C Smith. Robustness analysis of nonlinear feedback systems: an input-output approach. *IEEE Transactions on Automatic Control*, 42(9):1200–1221, 1997.

[69] Travis E. Gibson, Anuradha M. Annaswamy, and Eugene Lavretsky. Improved Transient Response in Adaptive Control Using Projection Algorithms and Closed Loop Reference Models. In *AIAA Guidance, Navigation, and Control Conference*, 2012.

[70] Travis E. Gibson, Anuradha M. Annaswamy, and Eugene Lavretsky. Adaptive systems with closed-loop reference-models, part I: Transient performance. In *American Control Conference*, pages 3376–3383, 2013.

[71] Travis E. Gibson, Luis G. Crespo, Sean P. Kenny, and David E. Cox. Internal Algorithm Monitors for Adaptive Systems. Technical Report AAC/TM-2010-0001, Active Adaptive Controls Laboratory, 2010.

[72] Benjamin C. Gruenwald, Daniel Wagner, Tansel Yucelen, and Jonathan A. Muse. An LMI-Based Hedging Approach to Adaptive Control with Actuator Dynamics in the Presence of Unknown Control Effectiveness. In *AIAA Guidance, Navigation, and Control Conference*, 2016.

[73] Keqin Gu, Vladimir Kharitonov, and Jie Chen. *Stability of time-delay systems*. Birkhäuser, Boston, MA, 2003.

[74] M. Guay and T. Zhang. Adaptive extremum seeking control of nonlinear dynamic systems with parametric uncertainties. *Automatica*, 39(7):1283–1293, 2003.

[75] Jack K. Hale and S. M. Verduyn Lunel. *Introduction to functional differential equations*, volume 99 of *Applied mathematical sciences*. Springer-Verlag, New York, 1993.

[76] Curt Hanson, Marcus Johnson, Jacob Schaefer, Nhan T. Nguyen, and John Burken. Handling Qualities Evaluations of Low Complexity Model Reference Adaptive Controllers for Reduced Pitch and Roll Damping Scenarios. In *AIAA Guidance, Navigation, and Control Conference*, 2011.

[77] Christian D. Heise, Guillermo P. Falconí, and Florian Holzapfel. Hexacopter Outdoor Flight Test Results of an Extended State Observer based Controller. In *IEEE International Conference on Aerospace Electronics and Remote Sensing Technology*, 2014.

[78] Christian D. Heise and Florian Holzapfel. Time-Delay Margin Computation of Model Reference Adaptive Control using the Razumikhin Theorem. In *IEEE Conference on Decision and Control*, 2014.

[79] Christian D. Heise and Florian Holzapfel. Uniform ultimate boundedness of a Model Reference Adaptive Controller in the presence of unmatched parametric uncertainties. In *6th International Conference on Automation, Robotics and Applications*, 2015.

[80] Christian D. Heise, Miguel Leitão, and Florian Holzapfel. Performance and Robustness Metrics for Adaptive Flight Control – Available Approaches. In *AIAA Guidance, Navigation, and Control Conference*, 2013.

[81] Christian D. Heise, Simon P. Schatz, and Florian Holzapfel. Modified Extended State Observer Control of Linear Systems. In *AIAA Guidance, Navigation, and Control Conference*, 2016.

[82] H. V. Henderson and S. R. Searle. On Deriving the Inverse of a Sum of Matrices. *SIAM Review*, 23(1):53–60, 1981.

[83] Leonhard Höcht. *Advances in Stability Analysis for Model Reference Adaptive Control Systems and Application to Unmanned Aerial Systems*. PhD thesis, Technische Universität München, München, 2014.

[84] A. Hodel, Mark Whorton, and J. Jim Zhu. Stability Metrics for Simulation and Flight-Software Assessment and Monitoring of Adaptive Control Assist Compensators. In *AIAA Guidance, Navigation and Control Conference and Exhibit*, 2008.

[85] Roger A. Horn and Charles R. Johnson. *Matrix analysis, second edition*. Cambridge University Press, Cambridge, UK, 2nd edition, 2013.

[86] Naira Hovakimyan. $\mathcal{L}_1$ Adaptive Control, 2014. `http://mechsenaira.web.engr.illinois.edu/wp-content/uploads/2012/05/L1AC_response.pdf` (visited: 25.10.2016).

[87] Naira Hovakimyan and Chengyu Cao. *$\mathcal{L}_1$ adaptive control theory: Guaranteed robustness with fast adaptation*. SIAM, Philadelphia, 2010.

[88] P. A. Ioannou and Petar V. Kokotović. Instability analysis and improvement of robustness of adaptive control. *Automatica*, 20(5):583–594, 1984.

[89] P. A. Ioannou and Jing Sun. *Robust adaptive control*. Prentice Hall, Upper Saddle River, NJ, 1996.

[90] Abraham K. Ishihara, Shahar Ben-Menahem, and Nhan T. Nguyen. Time Delay Margin Computation via the Razumikhin Method for an Adaptive Control System. In *AIAA Guidance, Navigation, and Control Conference*, 2009.

[91] Alberto Isidori. *Nonlinear control systems*. Springer-Verlag, London, 3rd edition, 1995.

[92] Stephen A. Jacklin. Closing the Certification Gaps in Adaptive Flight Control Software. In *AIAA Guidance, Navigation and Control Conference and Exhibit*, 2008.

[93] Eric N. Johnson and Anthony J. Calise. Limited Authority Adaptive Flight Control for Reusable Launch Vehicles. *Journal of Guidance, Control, and Dynamics*, 26(6):906–913, 2003.

[94] S. P. Karason and Anuradha M. Annaswamy. Adaptive control in the presence of input constraints. *IEEE Transactions on Automatic Control*, 39(11):2325–2330, 1994.

[95] W. C. Karl, G. C. Verghese, and A. S. Willsky. Reconstructing Ellipsoids from Projections. *CVGIP: Graphical Models and Image Processing*, 56(2):124–139, 1994.

[96] Hassan K. Khalil. *Nonlinear systems*. Prentice Hall, Upper Saddle River, NJ, 3rd edition, 2002.

[97] Evgeny Kharisov, Naira Hovakimyan, and Karl J. Åström. Comparison of architectures and robustness of model reference adaptive controllers and $\mathcal{L}_1$ adaptive controllers. *International Journal of Adaptive Control and Signal Processing*, 28(7-8):633–663, 2014.

[98] Evgeny Kharisov, Kwang Ki Kevin Kim, Xiaofeng Wang, and Naira Hovakimyan. Limiting Behavior of $\mathcal{L}_1$ Adaptive Controllers. In *AIAA Guidance, Navigation, and Control Conference*, 2011.

[99] S. Khatri and Pablo A. Parrilo. Guaranteed bounds for probabilistic μ. In *37th IEEE Conference on Decision and Control*, pages 3349–3354, 1998.

[100] Michael Kimbrell, Eric N. Johnson, Girish Chowdhary, Anthony J. Calise, and Rajeev Chandramohan. A Process to Obtain Robustness Metrics for Adaptive Flight Controllers. In *AIAA Guidance, Navigation, and Control Conference*, 2009.

[101] Miroslav Krstić, Ioannis Kanellakopoulos, and Petar V. Kokotović. *Nonlinear and adaptive control design*. Adaptive and learning systems for signal processing, communications, and control. Wiley, New York, 1995.

[102] Eugene Lavretsky. Combined/Composite Model Reference Adaptive Control. *IEEE Transactions on Automatic Control*, 54(11):2692–2697, 2009.

[103] Eugene Lavretsky. Adaptive Output Feedback Design Using Asymptotic Properties of LQG/LTR Controllers. *IEEE Transactions on Automatic Control*, 57(6):1587–1591, 2012.

[104] Eugene Lavretsky, Ross Gadient, and Irene M. Gregory. Predictor-Based Model Reference Adaptive Control. *Journal of Guidance, Control, and Dynamics*, 33(4):1195–1201, 2010.

[105] Eugene Lavretsky and Kevin A. Wise. *Robust and adaptive control: With aerospace applications*. Advanced textbooks in control and signal processing. Springer-Verlag, London, 2013.

[106] Dapeng Li, Naira Hovakimyan, and T.T Georgiou. Robustness of $\mathcal{L}_1$ Adaptive Controllers in the Gap Metric. In *American Control Conference*, 2010.

[107] Lothar Litz. *Wahrscheinlichkeitstheorie für Ingenieure: Grundlagen, Anwendungen, Übungen*. Hüthig, Heidelberg, 2001.

[108] J. Lofberg. YALMIP: A toolbox for modeling and optimization in MATLAB. *IEEE International Symposium on Computer Aided Control System Design*, pages 284–289, 2004.

[109] J. Lofberg. Pre- and Post-Processing Sum-of-Squares Programs in Practice. *IEEE Transactions on Automatic Control*, 54(5):1007–1011, 2009.

[110] Jan Lunze. *Regelungstechnik 1: Systemtheoretische Grundlagen, Analyse und Entwurf einschleifiger Regelungen*. Springer-Verlag, Berlin and Heidelberg, 6th edition, 2007.

[111] Jan Lunze. *Regelungstechnik 2: Mehrgrößensysteme, Digitale Regelung*. Springer-Lehrbuch. Springer-Verlag, Berlin and Heidelberg, 5th edition, 2008.

[112] Megumi Matsutani, Anuradha M. Annaswamy, Travis E. Gibson, and Eugene Lavretsky. Trustable autonomous systems using adaptive control. In *50th IEEE Conference on Decision and Control and European Control Conference*, pages 6760–6764, 2011.

[113] Megumi Matsutani, Anuradha M. Annaswamy, and Eugene Lavretsky. Guaranteed Delay Margins for Adaptive Systems with State Variables Accessible. In *American Control Conference*, pages 3362–3369, 2013.

[114] A. Megretski and A. Rantzer. System analysis via integral quadratic constraints. *IEEE Transactions on Automatic Control*, 42(6):819–830, 1997.

[115] Richard Monopoli. Adaptive control for systems with hard saturation. In *IEEE Conference on Decision and Control including the 14th Symposium on Adaptive Processes*, pages 841–843, 1975.

[116] David J. Moorhouse and Robert J. Woodcock. Background Information and User Guide for MIL-F-8785C, Military Specification - Flying Qualities of Piloted Airplanes. Technical Report AFWAL-TR-81-3109, Flight Dynamics Laboratory, AF Wright Aeronautical Laboratories, 1982.

[117] Maximilian Mühlegg, Girish Chowdhary, and Eric N. Johnson. Concurrent Learning Adaptive Control of Linear Systems with Noisy Measurements. In *AIAA Guidance, Navigation, and Control Conference*, 2012.

[118] Kumpati S. Narendra and Anuradha M. Annaswamy. A new adaptive law for robust adaptation without persistent excitation. *IEEE Transactions on Automatic Control*, 32(2):134–145, 1987.

[119] Kumpati S. Narendra and Anuradha M. Annaswamy. *Stable adaptive systems*. Prentice Hall, Englewood Cliffs, NJ, 1989.

[120] Nhan T. Nguyen, Maryam Bakhtiari-Nejad, and Yong Huang. Hybrid Adaptive Flight Control with Bounded Linear Stability Analysis. In *AIAA Guidance, Navigation and Control Conference and Exhibit*, 2007.

[121] Nhan T. Nguyen and Jovan D. Boskovic. Bounded linear stability margin analysis of nonlinear hybrid adaptive control. In *American Control Conference*, pages 3638–3643, 2008.

[122] Nhan T. Nguyen, Abraham K. Ishihara, Kalmanje Krishnakumar, and Maryam Bakhtiari-Nejad. Bounded Linear Stability Analysis - A Time Delay Margin Estimation Approach for Adaptive Control. In *AIAA Guidance, Navigation, and Control Conference*, 2009.

[123] Nhan T. Nguyen and Erin Summers. On Time Delay Margin Estimation for Adaptive Control and Robust Modification Adaptive Laws. In *AIAA Guidance, Navigation, and Control Conference*, 2011.

[124] Silviu-Iulian Niculescu. *Delay effects on stability: A control perspective*, volume 269 of *Lecture notes in control and information sciences*. Springer-Verlag, London, 2001.

[125] Romeo Ortega, A. Astolfi, and L. Hsu. Immersion and invariance model reference adaptive control: new parameterizations for the problem. In *42nd IEEE International Conference on Decision and Control*, pages 3239–3243, 2003.

[126] Romeo Ortega and Elena Panteley. Comments on $\mathcal{L}_1$-adaptive control: stabilisation mechanism, existing conditions for stability and performance limitations. *International Journal of Control*, 87(3):581–588, 2014.

[127] Romeo Ortega, Elena Panteley, and Alexey Bobtsov. Comments on 'comparison of architectures and robustness of model reference adaptive controllers and L1-adaptive controllers'. *International Journal of Adaptive Control and Signal Processing*, 30(1):125–127, 2016.

[128] Pablo A. Parrilo. *Structured Semidefinite Programs and Semialgebraic Geometry Methods in Robustness and Optimization*. PhD thesis, California Institute of Technology, Pasadena, CA, 2000.

[129] Kaare Brandt Petersen and Michael Syskind Pedersen. The Matrix Cookbook, 2012. `http://www2.imm.dtu.dk/pubdb/views/edoc_download.php/3274/pdf/imm3274.pdf` (visited: 15.11.2016).

[130] B. Peterson and Kumpati S. Narendra. Bounded error adaptive control. *IEEE Transactions on Automatic Control*, 27(6):1161–1168, 1982.

[131] J.-B. Pomet and L. Praly. Adaptive nonlinear regulation: estimation from the Lyapunov equation. *IEEE Transactions on Automatic Control*, 37(6):729–740, 1992.

[132] Laura Pullum, Xiaohui Cui, Emil Vassev, Michael Hinchey, Christopher Rouff, and Richard Buskens. Verification of Adaptive Systems. In *Infotech@Aerospace*, 2012.

[133] Radio Technical Commission for Aeronautics. Design Assurance Guidance for Airborne Electronic Hardware. Standard DO-254 (RTCA DO-254), 2000.

[134] Radio Technical Commission for Aeronautics. Software Considerations in Airborne Systems and Equipment Certification. Standard DO-178C (RTCA DO-178C), 2011.

[135] Sebastian Rapp. Development and Analysis of a Novel Adaptive Control Architecture. Master's thesis, Technische Universität München, München, 2015.

[136] C. Rohrs, L. Valavani, M. Athans, and G. Stein. Robustness of continuous-time adaptive control algorithms in the presence of unmodeled dynamics. *IEEE Transactions on Automatic Control*, 30(9):881–889, 1985.

[137] Wilson J. Rugh. *Nonlinear system theory: The Volterra/Wiener approach*. Johns Hopkins University Press, Baltimore, MD, 1981.

[138] Wilson J. Rugh and Jeff S. Shamma. Research on gain scheduling. *Automatica*, 36(10):1401–1425, 2000.

[139] SAE International. Guidelines and Methods for Conducting the Safety Assessment Process on Civil Airborne Systems and Equipment. Aerospace Recommended Practices 4761 (SAE ARP4761), 1996.

[140] SAE International. Aerospace - Flight Control Systems - Design, Installation and Test of Piloted Military Aircraft, General Specification for,. Aerospace Standard 94900 (SAE AS94900), 2007.

[141] SAE International. Guidelines for Development of Civil Aircraft and Systems. Aerospace Recommended Practices 4754A (SAE ARP4754A), 2010.

[142] SAE International. Aerospace - Vehicle Management Systems - Flight Control Design, Installation and Test of, Military Unmanned Aircraft, Specification Guide For. Aerospace Recommended Practices 94910 (SAE ARP94910), 2012.

[143] Qian Sang and Gang Tao. Gain Margins of Adaptive Control Systems. *IEEE Transactions on Automatic Control*, 55(1):104–115, 2010.

[144] Mario A. Santillo. *Adaptive Control Based on Retrospective Cost Optimization*. PhD thesis, The University of Michigan, 2009.

[145] Mario A. Santillo and Dennis S. Bernstein. Adaptive Control Based on Retrospective Cost Optimization. *Journal of Guidance, Control, and Dynamics*, 33(2):289–304, 2010.

[146] Shankar Sastry. *Nonlinear system: Analysis, stability, and control*. Springer-Verlag, New York, 1999.

[147] Simon P. Schatz, Christian D. Heise, and Florian Holzapfel. Comparison of Command Governor Augmentation and Modified Linear Extended State Observers for Uncertain Dynamical Systems. In *The 24th Mediterranean Conference on Control and Automation*, 2016.

[148] Simon P. Schatz, Tansel Yucelen, Benjamin C. Gruenwald, and Florian Holzapfel. Application of a Novel Scalability Notion in Adaptive Control to Various Adaptive Control Frameworks. In *AIAA Guidance, Navigation, and Control Conference*, 2015.

[149] Johann Schumann and Yan Liu. Tools and Methods for the Verification and Validation of Adaptive Aircraft Control Systems. In *IEEE Aerospace Conference*, pages 1–8, 2007.

[150] Mac Schwager, Himani Jain, Anuradha M. Annaswamy, and Eugene Lavretsky. Towards Verifiable Adaptive Flight Control for Safety Critical Applications. In *AIAA Guidance, Navigation, and Control Conference and Exhibit*, 2005.

[151] Peter Seiler, Gary J. Balas, Andrew Packard, and Ufuk Topcu. Analytical Validation Tools for Safety Critical Systems. In *AIAA Infotech@Aerospace Conference and AIAA Unmanned Unlimited Conference*, 2009.

[152] Peter Seiler, Andrei Dorobantu, and Gary J. Balas. Robustness Analysis of an L1 Adaptive Controller. In *AIAA Guidance, Navigation, and Control Conference*, 2012.

[153] Hyungbo Shim and Young-Jun Joo. State space analysis of disturbance observer and a robust stability condition. In *46th IEEE Conference on Decision and Control*, pages 2193–2198, 2007.

[154] Malcom D. Shuster. A Survey of Attitude Representations. *The Journal of the Astronautical Sciences*, 41(4):439–517, 1993.

[155] S. Sieberling, Q. P. Chu, and J. A. Mulder. Robust Flight Control Using Incremental Nonlinear Dynamic Inversion and Angular Acceleration Prediction. *Journal of Guidance, Control, and Dynamics*, 33(6):1732–1742, 2010.

[156] Sigurd Skogestad and Ian Postlethwaite. *Multivariable feedback control: Analysis and design*. Wiley, Chichester, UK, 1996.

[157] P. Smith. A simplified approach to nonlinear dynamic inversion based flight control. In *23rd Atmospheric Flight Mechanics Conference*, 1998.

[158] Jeffrey Spooner. *Stable adaptive control and estimation for nonlinear systems: Neural and fuzzy approximator techniques*. Wiley, New York, 2002.

[159] Vahram Stepanyan and Kalmanje Krishnakumar. MRAC Revisited: Guaranteed Performance with Reference Model Modification. In *American Control Conference*, pages 93–98, 2010.

[160] Vahram Stepanyan and Kalmanje Krishnakumar. M-MRAC for Nonlinear Systems with Bounded Disturbances. In *50th IEEE Conference on Decision and Control and European Control Conference*, pages 5419–5424, 2011.

[161] Vahram Stepanyan, Kalmanje Krishnakumar, Nhan T. Nguyen, and Laurens van Eykeren. Stability and Performance Metrics for Adaptive Flight Control. In *AIAA Guidance, Navigation, and Control Conference*, 2009.

[162] Brian L. Stevens, Frank L. Lewis, and Eric N. Johnson. *Aircraft control and simulation: Dynamics, controls design, and autonomous systems*. Wiley, Hoboken, NJ, 3rd edition, 2016.

[163] Jos F. Sturm. Implementation of interior point methods for mixed semidefinite and second order cone optimization problems. *Optimization Methods and Software*, 17(6):1105–1154, 2002.

[164] Gang Tian and Zhiqiang Gao. From Poncelet's invariance principle to Active Disturbance Rejection. In *American Control Conference*, pages 2451–2457, 2009.

[165] Ashish Tiwari. Bounded Verification of Adaptive Flight Control Systems. In *AIAA Infotech@Aerospace*, 2010.

[166] R. H. Tütüncü, K. C. Toh, and M. J. Todd. Solving semidefinite-quadratic-linear programs using SDPT3. *Mathematical Programming*, 95(2):189–217, 2003.

[167] Klaske van Heusden, Alireza Karimi, and Dominique Bonvin. Data-driven estimation of the infinity norm of a dynamical system. In *46th IEEE Conference on Decision and Control*, pages 4889–4894, 2007.

[168] J. Vanness, Evgeny Kharisov, and Naira Hovakimyan. $\mathcal{L}_1$ adaptive control with proportional adaptation law. In *American Control Conference*, pages 1919–1924, 2012.

[169] Andreas Varga. *Optimization based clearance of flight control laws: A civil aircraft application*, volume 416 of *Lecture notes in control and information sciences*. Springer-Verlag, Berlin and Heidelberg, 2012.

[170] Glenn Vinnicombe. *Measuring robustness of feedback systems*. PhD thesis, University of Cambridge, Cambridge, UK, 1992.

[171] K. Y. Volyanskyy, Anthony J. Calise, and Bong-Jun Yang. A novel Q-modification term for adaptive control. In *American Control Conference*, page 5 pp, 2006.

[172] Rolf Walter. *Lineare Algebra und analytische Geometrie*. Vieweg-Lehrbuch Mathematik. Vieweg, Braunschweig and Wiesbaden, 2nd edition, 1993.

[173] Jan Wendel. *Integrierte Navigationssysteme: Sensordatenfusion, GPS und Inertiale Navigation*. Oldenbourg, München, 2nd edition, 2011.

[174] Dirk Werner. *Funktionalanalysis*. Springer-Lehrbuch. Springer-Verlag, Berlin and Heidelberg, 2011.

[175] Enric Xargay, Naira Hovakimyan, and Chengyu Cao. $\mathcal{L}_1$ adaptive controller for multi-input multi-output systems in the presence of nonlinear unmatched uncertainties. In *American Control Conference*, pages 874–879, 2010.

[176] Xiaoyun Zhu. Improved bounds computation for probabilistic μ. In *American Control Conference*, pages 4336–4340 vol.6, 2000.

[177] Xiaoyun Zhu, Yun Huang, and John Comstock Doyle. Soft vs. hard bounds in probabilistic robustness analysis. In *35th IEEE Conference on Decision and Control*, pages 3412–3417, 1996.

[178] Bong-Jun Yang, Tansel Yucelen, Anthony J. Calise, and Jong-Yeob Shin. LMI-Based Analysis for Stability Margins of Adaptive Flight Control. In *AIAA Guidance, Navigation, and Control Conference*, 2009.

[179] Bong-Jun Yang, Tansel Yucelen, Jong-Yeob Shin, and Anthony J. Calise. An LMI-based Analysis for Adaptive Flight Control with Unmodeled Input Dynamics. In *AIAA Guidance, Navigation, and Control Conference*, 2010.

[180] Bong-Jun Yang, Tansel Yucelen, Jong-Yeob Shin, and Anthony J. Calise. LMI-Based Analysis of An Adaptive Flight Control System with Unmatched Uncertainty. In *AIAA Infotech@Aerospace*, 2010.

[181] Tansel Yucelen and Wassim M. Haddad. Low-Frequency Learning and Fast Adaptation in Model Reference Adaptive Control. *IEEE Transactions on Automatic Control*, 58(4):1080–1085, 2013.

[182] Tansel Yucelen and Eric N. Johnson. Command Governor-Based Adaptive Control. In *AIAA Guidance, Navigation, and Control Conference*, 2012.

[183] Tansel Yucelen and Eric N. Johnson. A new command governor architecture for transient response shaping. *International Journal of Adaptive Control and Signal Processing*, 27(12):1065–1085, 2013.

[184] Tansel Yucelen, Gerardo de La Torre, and Eric N. Johnson. Frequency-limited adaptive control architecture for transient response improvement. In *American Control Conference*, pages 6631–6636, 2013.

[185] Eberhard Zeidler. *Springer-Taschenbuch der Mathematik*. Springer Spektrum, Wiesbaden, 2013.

[186] Kemin Zhou, John Comstock Doyle, and K. Glover. *Robust and optimal control*. Prentice Hall, Upper Saddle River, NJ, 1996.

[187] J. Jim Zhu, Xiaojing Yang, and A. Hodel. A Singular Perturbation Approach for Time-Domain Assessment of Phase Margin. In *American Control Conference*, pages 315–322, 2010.

[188] Zhuquan Zang and Robert R. Bitmead. Transient bounds for adaptive control systems. *IEEE Transactions on Automatic Control*, 39(1):171–175, 1994.

[189] Alexander W. Zollitsch, Florian Holzapfel, and Anuradha M. Annaswamy. Application of adaptive control with closed-loop reference models to a model aircraft with actuator dynamics and input uncertainty. In *American Control Conference*, pages 3848–3853, 2015.

Appendix A

Scientific Publications

Several papers have been published by the author of this thesis, whose results constitute an integral part of this thesis. These publications are:

- Christian D. Heise, Miguel Leitão, and Florian Holzapfel. Performance and Robustness Metrics for Adaptive Flight Control – Available Approaches. In *AIAA Guidance, Navigation, and Control Conference*, 2013
- Christian D. Heise, Guillermo P. Falconí, and Florian Holzapfel. Hexacopter Outdoor Flight Test Results of an Extended State Observer based Controller. In *IEEE International Conference on Aerospace Electronics and Remote Sensing Technology*, 2014
- Christian D. Heise and Florian Holzapfel. Time-Delay Margin Computation of Model Reference Adaptive Control using the Razumikhin Theorem. In *IEEE Conference on Decision and Control*, 2014
- Christian D. Heise and Florian Holzapfel. Uniform ultimate boundedness of a Model Reference Adaptive Controller in the presence of unmatched parametric uncertainties. In *6th International Conference on Automation, Robotics and Applications*, 2015
- Christian D. Heise, Simon P. Schatz, and Florian Holzapfel. Modified Extended State Observer Control of Linear Systems. In *AIAA Guidance, Navigation, and Control Conference*, 2016

Appendix B

Mathematical Preliminaries

This chapter provides a short summary of several branches of mathematics which are relevant for this thesis. Section B.1 will first review some important elements of analysis, linear algebra and functional analysis. Afterwards, Section B.2 puts special emphasis on positive definite functions and their associated (sub-)level sets. These definitions are key to the understanding of several geometric problems which may be conveniently solved using LMIs and Semidefinite Programs (SDPs). The latter are briefly introduced in Section B.3. Finally, Section B.4 will summarize several useful facts about matrices, including their traces, symmetric matrices and inverses.

B.1 Elements of Analysis and Linear Algebra

This section reviews some elements of analysis, linear algebra and functional analysis, which are important for the understanding of this thesis. This review is largely based on the excellent summary of these topics in [45], which specifically covers topics relevant for control theory. Due to the brevity of the present review, the reader is referred to the respective literature such as [22, 23, 24, 174, 172] for a more detailed introduction.

B.1.1 Normed Spaces and Inner Product Spaces

Subsequently, it is assumed that the reader is familiar with the concept of linear spaces (vector spaces) $\mathcal{V}$ (see for example [23, 45]) such as

- the vector spaces of real $\mathbb{R}^n$ or complex $\mathbb{C}^n$ vectors defined over the field of real $\mathbb{R}$ or complex numbers $\mathbb{C}$, respectively;
- the vector spaces of real $\mathbb{R}^{l\times m}$ or complex $\mathbb{C}^{l\times m}$ matrices defined over the field of real $\mathbb{R}$ or complex numbers $\mathbb{C}$, respectively;
- the vector space of symmetric matrices $\mathbb{S}^n$ defined over the field of real numbers $\mathbb{R}$;
- the vector space of functions $\mathcal{F}(\mathbb{R}, \mathbb{C}^n)$ mapping variables of $\mathbb{R}$ to variables in $\mathbb{C}^n$.

While every vector space defines some basic operations such as addition or multiplication by a scalar, it does not possess an intrinsic notion of *size* of its elements. For this, the concept of a norm is required. Formally, a norm $\|\cdot\|$ is a function, which maps an element of a vector space $\mathcal{V}$ onto a non-negative real number, i.e. $\|\cdot\| : \mathcal{V} \to \mathbb{R}_+$, and which satisfies the following *norm axioms* ([45, 174], [22, p. 34]):

1. Positive Definiteness: $\|v\| \geq 0$ for all $v \in \mathcal{V}$; $\|v\| = 0$, if and only if $v = 0$;
2. Homogenity: $\|\alpha \cdot v\| = |\alpha| \cdot \|v\|$ for all scalars $\alpha \in \mathbb{F}$ and all $v \in \mathcal{V}$;
3. Triangle Inequality: $\|u + v\| \leq \|u\| + \|v\|$ for all $u,\ v \in \mathcal{V}$.

A vector space together with a suitable norm is a called a *normed space*.

While the concept of a norm captures the notion of size, it does not capture the notion of *direction*. Such notion may be introduced by the definition of an inner product $\langle \cdot, \cdot \rangle$ between two elements of a vector space. Formally, an inner product is a function which maps two elements of a vector space $\mathcal{V}$ onto the field $\mathbb{F}$, over which the vector space is defined, i.e. $\langle \cdot, \cdot \rangle : \mathcal{V} \times \mathcal{V} \to \mathbb{F}$, and which satisfies the following *inner product axioms* [22, p. 42]:

1. Positive Definiteness: $\langle v, v \rangle \geq 0$ for all $v \in \mathcal{V}$; $\langle v, v \rangle = 0$, if and only if $v = 0$;
2. Conjugate symmetry: $\langle u, v \rangle = \langle v, u \rangle^*$ for all $u, v \in \mathcal{V}$;
3. $\langle \alpha \cdot u, v \rangle = \alpha \cdot \langle u, v \rangle$ for all $u, v \in \mathcal{V}$ and scalars $\alpha \in \mathbb{F}$;
4. $\langle u_1 + u_2, v \rangle = \langle u_1, v \rangle + \langle u_2, v \rangle$ for all $u_1, u_2, v \in \mathcal{V}$.

In case of a real vector space, i.e. $\mathbb{F} = \mathbb{R}$, the last two axioms imply linearity. A vector space with an inner product is called an *inner product space*. It may be proven that any inner product defines a norm by $\|v\| \triangleq \sqrt{\langle v, v \rangle}$ [22, p. 43]. Thus, any *inner product space* is a *normed space*. Furthermore, the *Cauchy Schwarz inequality* holds on any inner product space [22, p. 43]:

$$|\langle u, v \rangle| \leq \|u\| \cdot \|v\| \tag{B.1}$$

for all $u, v \in \mathcal{V}$, where the norms are those defined by the inner product.

Using the notion of size, which any *normed space* possesses, it is natural to define a measure of distance by $d(u, v) = \|u - v\|$. Now let v_k be a sequence. The sequence will be referred to as a *Cauchy sequence*, if there exists a sequence index $M \geq 0$ for every $\epsilon > 0$, such that $\|v_i - v_j\| \leq \epsilon$ for all $i, j \geq M$. Intuitively, this definition states that a sequence is *Cauchy*, if for any given distance ϵ, one may find an index M, such that the distance between any two sequence elements $i \geq M$, $j \geq M$ is below ϵ. While it may be shown that any convergent sequence is *Cauchy*, the converse is not necessarily true [45], [22, p. 13]. Thus, there might exist *Cauchy sequences*, for which no limit value exists. However, if it may be proven that any *Cauchy sequence* in

a vector space will converge to a limit value in that vector space, then the same holds for all convergent sequences. Such a vector space, in which all *Cauchy sequences* converge, will be denoted as *complete*. A *complete normed space* is also referred to as a *Banach space* and a *complete inner product space* is also referred to as a *Hilbert space*. To conclude this section, the properties of some vector spaces are presented, which are important for this thesis.

The Vector Spaces $\mathbb{R}^n$ and $\mathbb{C}^n$

The vector spaces $\mathbb{R}^n$ and $\mathbb{C}^n$ of real or complex vectors are *complete inner product spaces* (*Hilbert spaces*) [45]. Their inner product is the scalar product

$$\langle \boldsymbol{a}, \boldsymbol{b} \rangle = \boldsymbol{a}^H \boldsymbol{b}, \tag{B.2}$$

which naturally defines the Euclidean norm (2-norm) by

$$\|\boldsymbol{a}\|_2 = \sqrt{\langle \boldsymbol{a}, \boldsymbol{a} \rangle} = \sqrt{\sum_{i=1}^{n} |a_i|^2}, \tag{B.3}$$

where $\boldsymbol{a}^T = \begin{bmatrix} a_1 & \dots & a_n \end{bmatrix}$. The 2-norm is a special case of the p-norms, which are generally defined as

$$\|\boldsymbol{a}\|_p = \left(\sum_{i=1}^{n} |a_i|^p \right)^{\frac{1}{p}} \tag{B.4}$$

for $p \leq 1 \leq \infty$. In the limit, i.e. $p = \infty$, the p-norm becomes

$$\|\boldsymbol{a}\|_\infty = \max_{i=1,\dots n} |a_i|. \tag{B.5}$$

It may be proven that the p-norms are equivalent [22, p. 20]. That is, for any two p-norms p_1 and p_2, constants $c_1 > 0$, $c_2 > 0$ can be found such that

$$c_1 \cdot \|\boldsymbol{a}\|_{p_1} \leq \|\boldsymbol{a}\|_{p_2} \leq c_2 \cdot \|\boldsymbol{a}\|_{p_1} \tag{B.6}$$

holds for all $\boldsymbol{a} \in \mathbb{R}^n$ or $\boldsymbol{a} \in \mathbb{C}^n$, respectively. For the commonly used 2-norm and the ∞-norm, the following relations may be derived with the help of Figure B.1:

$$\begin{aligned} \|\boldsymbol{a}\|_\infty \leq \|\boldsymbol{a}\|_2 &\leq \sqrt{n} \cdot \|\boldsymbol{a}\|_\infty, \\ \frac{1}{\sqrt{n}} \cdot \|\boldsymbol{a}\|_2 \leq \|\boldsymbol{a}\|_\infty &\leq \|\boldsymbol{a}\|_2. \end{aligned} \tag{B.7}$$

The Vector Spaces $\mathbb{R}^{l \times m}$ and $\mathbb{C}^{l \times m}$

The vector spaces $\mathbb{R}^{l \times m}$ and $\mathbb{C}^{l \times m}$ of real or complex matrices are *complete inner product spaces* (*Hilbert spaces*) as well [45]. Their inner product is the Frobenius scalar product [85, Section 5.2]

$$\langle \boldsymbol{A}, \boldsymbol{B} \rangle = \mathrm{Tr}\left\{ \boldsymbol{A}^H \boldsymbol{B} \right\} = \mathrm{Tr}\left\{ \boldsymbol{B} \boldsymbol{A}^H \right\}, \tag{B.8}$$

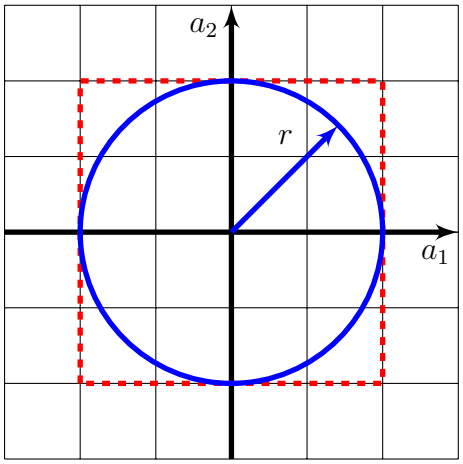

(a) Every point on the circle $\|\boldsymbol{a}\|_2 = r$ lies within the dashed square $\|\boldsymbol{a}\|_\infty \leq r$. Thus, $\|\boldsymbol{a}\|_\infty \leq \|\boldsymbol{a}\|_2 = r$.

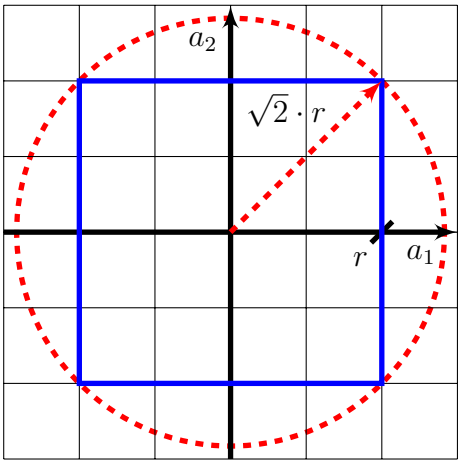

(b) Every point on the square $\|\boldsymbol{a}\|_\infty = r$ lies within the dashed circle $\|\boldsymbol{a}\|_2 \leq \sqrt{2} \cdot r$. Thus, $\|\boldsymbol{a}\|_2 / \sqrt{2} \leq \|\boldsymbol{a}\|_\infty = r$.

Figure B.1: Equivalence of direct 2-norm and direct ∞-norm.

where the trace operator $\mathrm{Tr}\,\{\cdot\}$ is used. Further details on traces may be found in Section B.4.1. The Frobenius scalar product naturally defines the Frobenius norm by

$$\|\boldsymbol{A}\|_F = \sqrt{\langle \boldsymbol{A}, \boldsymbol{A} \rangle} = \sqrt{\mathrm{Tr}\left\{\boldsymbol{A}^H \boldsymbol{A}\right\}}. \tag{B.9}$$

Due to the definition of the trace operator, it may be verified that the Frobenius norm of the matrix $\boldsymbol{A}$ is equivalent to the 2-norm of its vector representation [85, Section 5.6]:

$$\|\boldsymbol{A}\|_F = \|\mathrm{vec}\,\boldsymbol{A}\|_2, \tag{B.10}$$

where $\mathrm{vec}\,(\cdot)$ of the matrix

$$\boldsymbol{A} = \begin{bmatrix} \boldsymbol{a}_1 & \dots & \boldsymbol{a}_m \end{bmatrix} \tag{B.11}$$

with $\boldsymbol{a}_i \in \mathbb{R}^l$ for $i = 1, \dots, m$ is defined as

$$\mathrm{vec}\,\boldsymbol{A} \triangleq \begin{bmatrix} \boldsymbol{a}_1 \\ \vdots \\ \boldsymbol{a}_m \end{bmatrix}. \tag{B.12}$$

The $\mathcal{L}_p^n$ Vector Spaces

Let $\mathcal{L}_p^n$ with $p \geq 1$ denote the vector space $\mathcal{F}(\mathbb{R}, \mathbb{C}^n)$ of functions that map $\mathbb{R}$ to $\mathbb{C}^n$ and which satisfy

$$\int_{-\infty}^{\infty} \|\boldsymbol{u}(t)\|_p^p \, dt < \infty, \tag{B.13}$$

for all $\boldsymbol{u}(t) \in \mathcal{L}_p^n$. Strictly speaking, notice that the integration in (B.13) is to be understood in the sense of *Lebesgue*. While all functions that are integrable in the sense of *Riemann* are also integrable in the sense of *Lebesgue*, the converse is not true [53]. Since most functions encountered in this thesis are integrable the sense of *Riemann*,

the details of $\mathcal{L}_p$ spaces associated with integration in the sense of *Lebesgue* and measure theory will not be specifically covered here. It may be proven that the vector space $\mathcal{L}_p^n$ is a *complete normed space* (*Banach space*) [45], whose norm is defined as:

$$\|\boldsymbol{u}\|_{\mathcal{L}_p} = \left(\int_{-\infty}^{\infty} \|\boldsymbol{u}(t)\|_p^p \, dt \right)^{\frac{1}{p}}. \tag{B.14}$$

In case of $p = \infty$, the norm becomes

$$\|\boldsymbol{u}\|_{\mathcal{L}_\infty} = \operatorname{ess\,sup}_{t \in \mathbb{R}} \|\boldsymbol{u}\|_\infty. \tag{B.15}$$

The use of the essential supremum in (B.15) relates to measure theory and may be thought of as a conventional supremum in most cases, which are considered in this thesis [45]. Furthermore, notice that the function space $\mathcal{L}_2^n$ for $p = 2$ is a *complete inner product space* (*Hilbert space*) [45] with the inner product

$$\langle \boldsymbol{u}, \boldsymbol{v} \rangle = \int_{-\infty}^{\infty} \boldsymbol{u}(t)^H \boldsymbol{v}(t) \, dt, \tag{B.16}$$

which naturally leads to the definition of the $\mathcal{L}_2$-norm

$$\|\boldsymbol{u}\|_{\mathcal{L}_2} = \sqrt{\int_{-\infty}^{\infty} \|\boldsymbol{u}(t)\|_2^2 \, dt}, \tag{B.17}$$

which equals (B.14) for $p = 2$.

B.1.2 Subsets of Vector Spaces

Throughout this thesis, subsets of vector spaces (such as subsets of $\mathbb{R}^n$) are often encountered. It is assumed that the reader is familiar with common terminology with respect to sets such as the empty set $\emptyset$, the union of sets ($\mathcal{A} \cup \mathcal{B}$), the intersection of sets ($\mathcal{A} \cap \mathcal{B}$) or the difference of sets ($\mathcal{A} \backslash \mathcal{B}$) [24]. Furthermore, common set relations such as $\mathcal{A} \subset \mathcal{B}$ to denote that $\mathcal{A}$ is a subset of $\mathcal{B}$, $\mathcal{A} \subseteq \mathcal{B}$ to denote that $\mathcal{A}$ is a subset of $\mathcal{B}$ or is equivalent to $\mathcal{B}$ are assumed to be known [24]. While a detailed treatment of set theory (and its axiomatic introduction) is beyond the scope of this thesis, the following definitions with respect to subsets $\mathcal{S}$ of the vector space $\mathbb{R}^n$ are useful: A subset $\mathcal{S} \subset \mathbb{R}^n$ is:

- *open*, "if, for every vector $\boldsymbol{x} \in \mathcal{S}$, one can find an ϵ-neighborhood of $\boldsymbol{x}$

  $$\mathcal{N}(\boldsymbol{x}, \epsilon) = \{\boldsymbol{z} \in \mathbb{R}^n \mid \|\boldsymbol{z} - \boldsymbol{x}\| < \epsilon\}$$

  such that $\mathcal{N}(\boldsymbol{x}, \epsilon) \subset \mathcal{S}$ " [96]. Roughly speaking, this definition states that one may always find a point nearby $\boldsymbol{x}$, which is also part of $\mathcal{S}$.
- *closed*, "if its complement in $\mathbb{R}^n$ is open" [96].
- *bounded*, "if there is $r > 0$ such that $\|\boldsymbol{x}\| \leq r$ for all $\boldsymbol{x} \in \mathcal{S}$" [96].

- *compact*, "if it is closed and bounded" [96].
- *connected*, "if every pair of points in $\mathcal{S}$ can be joined by an arc lying in $\mathcal{S}$" [96].
- a *domain*, if it is open and connected.
- *convex*, "if, for every $\boldsymbol{x}, \boldsymbol{y} \in \mathcal{S}$ and every real number θ, $0 < \theta < 1$, the point satisfies $\theta\boldsymbol{x} + (1-\theta) \cdot \boldsymbol{y} \in \mathcal{S}$ " [96]. This is to say that every pair of points in a convex set $\mathcal{S}$ may be connected with a line, which entirely lies within the set $\mathcal{S}$.

Furthermore, "a point $\boldsymbol{x}$ is a *boundary point* of a set $\mathcal{S}$ if every neighborhood of $\boldsymbol{x}$ contains at least one point of $\mathcal{S}$ and one point not belonging to $\mathcal{S}$ " [96]. $\partial\mathcal{S}$ will be used to denote all boundary points of $\mathcal{S}$.

In this thesis, subsets of $\mathbb{R}^n$ will frequently arise in the form of so-called sublevel sets. Let $f : D \to \mathbb{R}$ be a scalar function defined on a subset of $\mathbb{R}^n$, i.e. $\mathcal{D} \subseteq \mathbb{R}^n$. Then, the α-sublevel set of the function f is defined as [18]:

$$\mathcal{M}_\alpha \triangleq \{\boldsymbol{x} \in \mathcal{D} \mid f(\boldsymbol{x}) \leq \alpha\}. \tag{B.18}$$

In (B.18), the parameter $\alpha \in \mathbb{R}$ is a scaling parameter, which determines the size of the set. Furthermore, if $f(\boldsymbol{x})$ is a convex function, then its α-sublevel sets will be convex [18]. A convex function is a function, where the line connecting any two points on its graph lies above the graph of the function [18]. In case of a positive definite function $f(\boldsymbol{x})$ (see Section B.2), $\alpha \geq 0$ may be thought of as a generalization of the radius of a circle. That is, for $0 \leq \alpha \leq \beta < \infty$, the relation

$$\underbrace{\{\boldsymbol{x} \in \mathcal{D} \mid f(\boldsymbol{x}) \leq \alpha\}}_{\mathcal{M}_\alpha} \subseteq \underbrace{\{\boldsymbol{x} \in \mathcal{D} \mid f(\boldsymbol{x}) \leq \beta\}}_{\mathcal{M}_\beta} \tag{B.19}$$

holds.

Proof. (B.19) is proven by contradiction. Assume that (B.19) does not hold. Then, there must exist an element $\boldsymbol{x}_0 \in \mathcal{D}$, which is contained in $\mathcal{M}_\alpha$ and but not in $\mathcal{M}_\beta$ (i.e. it must lie in the complementary set of $\mathcal{M}_\beta$), i.e.

1. $\boldsymbol{x}_0 \in \mathcal{M}_\alpha$, implying $f(\boldsymbol{x}_0) \leq \alpha$;
2. $\boldsymbol{x}_0 \in \bar{\mathcal{M}}_\beta$ with $\bar{\mathcal{M}}_\beta = \{\boldsymbol{x} \in \mathcal{D} \mid f(\boldsymbol{x}) > \beta\}$, implying $f(\boldsymbol{x}_0) > \beta$.

Bullet points 1 and 2 would however imply $\alpha \geq f(\boldsymbol{x}_0) > \beta$ implying $\alpha > \beta$, which contradicts $\alpha \leq \beta$. Hence, no such point $\boldsymbol{x}_0$ may exist, which proves (B.19). □

Another common task when dealing with sublevel sets is to show set containment. For this, let $g : \mathcal{D} \to \mathbb{R}$ be another scalar function defined on the same set $\mathcal{D}$ as f. If the functions f and g satisfy $f(\boldsymbol{x}) \leq g(\boldsymbol{x})\ \forall\ \boldsymbol{x} \in \mathcal{D}$, then the following set containment condition holds:

$$\underbrace{\{\boldsymbol{x} \in \mathcal{D} \mid g(\boldsymbol{x}) \leq \alpha\}}_{\mathcal{M}_g} \subseteq \underbrace{\{\boldsymbol{x} \in \mathcal{D} \mid f(\boldsymbol{x}) \leq \alpha\}}_{\mathcal{M}_f}. \tag{B.20}$$

Proof. (B.20) is proven by contradiction. Assume that (B.20) does not hold. Then, there must exist an element $\boldsymbol{x}_0 \in \mathcal{D}$, which is contained in $\mathcal{M}_g$ and but not in $\mathcal{M}_f$, i.e.

1. $\boldsymbol{x}_0 \in \mathcal{M}_g$, implying $g(\boldsymbol{x}_0) \leq \alpha$;
2. $\boldsymbol{x}_0 \in \bar{\mathcal{M}}_f$ with $\bar{\mathcal{M}}_f = \{\boldsymbol{x} \in \mathcal{D} |\ f(\boldsymbol{x}) > \alpha\}$, implying $\alpha < f(\boldsymbol{x}_0)$.

Bullet points 1 and 2 would however imply $g(\boldsymbol{x}_0) < f(\boldsymbol{x}_0)$, which contradicts $f(\boldsymbol{x}) \leq g(\boldsymbol{x}) \ \forall\ \boldsymbol{x} \in \mathcal{D}$. Hence, no such point $\boldsymbol{x}_0$ may exist, which proves (B.20). □

Similar to (B.18), a level set of the function $f(\boldsymbol{x})$ is defined as

$$\partial\mathcal{M}_\alpha \triangleq \{\boldsymbol{x} \in \mathcal{D} |\ f(\boldsymbol{x}) = \alpha\} \tag{B.21}$$

and represents the boundary of the sublevel set $\mathcal{M}_\alpha$. Throughout this thesis, the terms *level set* and *sublevel set* are not always clearly distinguished as it is usually clear from the context whether the boundary or the interior of the set are meant.

B.1.3 Subspaces

A subspace $\mathcal{S}$ of a vector space $\mathcal{V}$ is a subset of $\mathcal{V}$, which is also a vector space with respect to the same field and operations [45]. Common examples include planes in $\mathbb{R}^3$ (two-dimensional subspace) or lines in $\mathbb{R}^2$ (one-dimensional subspace).

An important operation is the orthogonal projection of a point $\boldsymbol{x} \in \mathcal{V}$ onto a subspace $\mathcal{S}$. For the purpose of this thesis, this operation is only introduced in case of the vector space $\mathcal{V} = \mathbb{R}^n$ and a m-dimensional subspace $m < n$. To that end, let

$$\boldsymbol{C} = \begin{bmatrix} (\boldsymbol{c}_1)_\mathcal{V} & \dots & (\boldsymbol{c}_m)_\mathcal{V} \end{bmatrix} \tag{B.22}$$

with $(\boldsymbol{c}_i)_\mathcal{V} \in \mathcal{V},\ i = 1, \dots, m$ denote an orthonormal basis of the subspace, i.e.

$$\langle (\boldsymbol{c}_i)_\mathcal{V}\,,\, (\boldsymbol{c}_j)_\mathcal{V} \rangle = 0, \quad \forall\, i \neq j, \tag{B.23}$$

$$\|(\boldsymbol{c}_i)_\mathcal{V}\|_2 = 1, \quad \forall\, i = 1, \dots, m. \tag{B.24}$$

Using orthogonal projection, a point $(\boldsymbol{y})_\mathcal{V}$ in the subspace $\mathcal{S}$ is to be determined such that $(\boldsymbol{y})_\mathcal{V} - (\boldsymbol{x})_\mathcal{V}$ is orthogonal to all basis vectors of the subspace as shown in Figure B.2. Since $\boldsymbol{y}$ should lie in the subspace $\mathcal{S}$, it has to satisfy

$$(\boldsymbol{y})_\mathcal{V} = \boldsymbol{C} \cdot (\boldsymbol{y})_\mathcal{S}. \tag{B.25}$$

Since the line connecting $(\boldsymbol{y})_\mathcal{V}$ and $(\boldsymbol{x})_\mathcal{V}$ should be orthogonal to the basis vectors, the point $\boldsymbol{y}$ has to satisfy

$$\langle\, (\boldsymbol{y})_\mathcal{V} - (\boldsymbol{x})_\mathcal{V},\ (\boldsymbol{c}_i)_\mathcal{V} \,\rangle = 0, \quad i = 1, \dots, m. \tag{B.26}$$

Inserting (B.25) into (B.26) yields

$$\langle\, \boldsymbol{C} \cdot (\boldsymbol{y})_\mathcal{S} - (\boldsymbol{x})_\mathcal{V},\ (\boldsymbol{c}_i)_\mathcal{V} \,\rangle = 0, \quad i = 1, \dots, m. \tag{B.27}$$

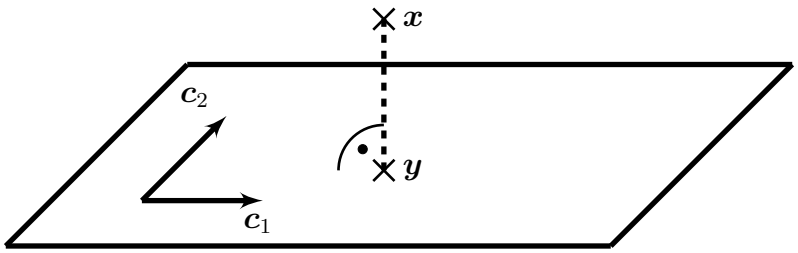

Figure B.2: Orthogonal projection of $\boldsymbol{x} \in \mathcal{V},\ \mathcal{V} = \mathbb{R}^3$ onto a two-dimensional subspace $\mathcal{S}$ specified by its basis vectors $\boldsymbol{c}_1$ and $\boldsymbol{c}_2$. The projection is denotes as $\boldsymbol{y} \in \mathcal{S}$.

Using the properties and the definition of the scalar product, one obtains the equation

$$(\boldsymbol{c}_i)_{\mathcal{V}}^T \cdot \boldsymbol{C} \cdot (\boldsymbol{y})_{\mathcal{S}} = (\boldsymbol{c}_i)_{\mathcal{V}}^T \cdot (\boldsymbol{x})_{\mathcal{V}} \quad i = 1, \ldots, m. \tag{B.28}$$

Since the basis vectors $(\boldsymbol{c}_i)_{\mathcal{V}}$ are orthonormal, the term

$$\begin{aligned} (\boldsymbol{c}_i)_{\mathcal{V}}^T \cdot \boldsymbol{C} &= (\boldsymbol{c}_i)_{\mathcal{V}}^T \cdot \begin{bmatrix} (\boldsymbol{c}_1)_{\mathcal{V}} & \ldots & (\boldsymbol{c}_m)_{\mathcal{V}} \end{bmatrix} \\ &= \begin{bmatrix} 0 & \ldots & (\boldsymbol{c}_i)_{\mathcal{V}}^T \cdot (\boldsymbol{c}_i)_{\mathcal{V}} & \ldots & 0 \end{bmatrix} \\ &= \begin{bmatrix} 0 & \ldots & 1 & \ldots & 0 \end{bmatrix} \end{aligned} \tag{B.29}$$

selects the i-th component from the vector $(\boldsymbol{y})_{\mathcal{S}}^T = \begin{bmatrix} y_1 & \ldots & y_m \end{bmatrix}_{\mathcal{S}}$. Hence, (B.28) becomes

$$y_i = (\boldsymbol{c}_i)_{\mathcal{V}}^T \cdot (\boldsymbol{x})_{\mathcal{V}} \quad i = 1, \ldots, m. \tag{B.30}$$

Rewriting the m equations of (B.30) in matrix/vector form yields a relation between the point $(\boldsymbol{x})_{\mathcal{V}}$ and its projection $\boldsymbol{y}$ given in the $\mathcal{S}$-frame:

$$(\boldsymbol{y})_{\mathcal{S}} = \boldsymbol{C}^T \cdot (\boldsymbol{x})_{\mathcal{V}}. \tag{B.31}$$

In the $\mathcal{V}$-frame, the projection $\boldsymbol{y}$ of $\boldsymbol{x}$ is then given by

$$(\boldsymbol{y})_{\mathcal{V}} = \boldsymbol{C} \cdot (\boldsymbol{y})_{\mathcal{S}} = \boldsymbol{C}\boldsymbol{C}^T \cdot (\boldsymbol{x})_{\mathcal{V}}. \tag{B.32}$$

B.1.4 Continuity

A function $\boldsymbol{f} : \mathcal{A} \to \mathcal{B}$, which maps elements of the open set $\mathcal{A}$ to $\mathcal{B}$ is

- *continuous* at $\boldsymbol{x}_0$ "if, given $\epsilon > 0$, there is a $\delta > 0$ such that

$$\|\boldsymbol{x}_0 - \boldsymbol{y}\| < \delta \to \|\boldsymbol{f}(\boldsymbol{x}_0) - \boldsymbol{f}(\boldsymbol{y})\| < \epsilon \text{ "} [96]. \tag{B.33}$$

- *continuous* on a set $\mathcal{S}$ "if it is continuous at every point of $\mathcal{S}$" [96].
- *uniformly continuous* on a set $\mathcal{S}$ "if, given $\epsilon > 0$, there is a $\delta > 0$ (dependent only on ϵ) such that the inequality (B.33) holds for all $\boldsymbol{x}, \boldsymbol{y} \in \mathcal{S}$ " [96].

- *Lipschitz* on a set $\mathcal{S}$, if $\boldsymbol{f}(\boldsymbol{x})$ satisfies the *Lipschitz condition*

$$\|\boldsymbol{f}(\boldsymbol{x}) - \boldsymbol{f}(\boldsymbol{y})\| \leq L \cdot \|\boldsymbol{x} - \boldsymbol{y}\|, \tag{B.34}$$

  with the same Lipschitz constant $L > 0$ for all points $\boldsymbol{x}, \boldsymbol{y} \in \mathcal{S}$ [96].

- *globally Lipschitz*, if $\boldsymbol{f}(\boldsymbol{x})$ satisfies the *Lipschitz condition* (B.34) with the same Lipschitz constant $L > 0$ for all $\boldsymbol{x}, \boldsymbol{y} \in \mathbb{R}^n$.

- *semi-globally Lipschitz*, if $\boldsymbol{f}(\boldsymbol{x})$ satisfies the Lipschitz condition

$$\|\boldsymbol{f}(\boldsymbol{x}) - \boldsymbol{f}(\boldsymbol{y})\| \leq L(r) \cdot \|\boldsymbol{x} - \boldsymbol{y}\|, \tag{B.35}$$

  for arbitrary $r > 0$ and for all $\|\boldsymbol{x}\| \leq r$ and all $\|\boldsymbol{y}\| \leq r$, where $L : \mathbb{R}_+ \to \mathbb{R}_+$ denotes the semi-global Lipschitz constant [87].

A function $\boldsymbol{f}(\boldsymbol{x})$, which is *Lipschitz* on some set $\mathcal{S}$, also is uniformly continuous on $\mathcal{S}$ [96]. Furthermore, a continuous function, which is continuously differentiable on $\mathbb{R}^n$, is globally Lipschitz, if its partial derivatives are uniformly bounded [96, Lemma 3.3]. Hence, any continuous function, which is continuously differentiable on $\mathbb{R}^n$ and whose partial derivatives are uniformly bounded, is uniformly continuous. This observation will be often used in proofs of stability involving Barbalat's Lemma (see Lemma C.3).

B.1.5 Linear Operators and Induced Norms

Linear operators are frequently used within this thesis to map elements of one vector space to another. Typical examples of linear operators include the matrix $\boldsymbol{A} \in \mathbb{R}^{l \times m}$ which maps an input vector $\boldsymbol{u} \in \mathbb{R}^m$ to an output vector $\boldsymbol{y} \in \mathbb{R}^l$ via the relation

$$\boldsymbol{y} = \boldsymbol{A} \cdot \boldsymbol{u}. \tag{B.36}$$

Another common example is the convolution with the impulse response $g(t)$ of a LTI Single-Input Single-Output (SISO) system

$$y(t) = g(t) * u(t) = \int_0^t g(t-\tau) \cdot u(\tau) d\tau. \tag{B.37}$$

This operator maps an input signal $u(t) \in \mathcal{L}_\infty$ to an output signal $y(t)$. It is well known from linear system theory that the convolution will lead to a bounded output signal $y \in \mathcal{L}_\infty$, if and only if the impulse response $g(t)$ satisfies $g(t) \in \mathcal{L}_1$ [110], i.e.

$$\int_0^\infty |g(t)| dt < \infty. \tag{B.38}$$

The condition $g(t) \in \mathcal{L}_1$ is satisfied if all poles of the transfer function $G(s) = \mathcal{L}\{g(t)\}$ strictly lie in the left half-plane.

For a more formal statement, let $\mathcal{U}$ and $\mathcal{Y}$ be two normed, complete vector spaces (i.e. *Banach spaces*). A mapping $\mathcal{F} : \mathcal{U} \to \mathcal{Y}$ is called a linear, bounded operator if [45]:

1. *Linearity*: $\mathcal{F}\{\alpha_1 \cdot u_1 + \alpha_2 \cdot u_2\} = \alpha_1 \cdot \mathcal{F}\{u_1\} + \alpha_2 \cdot \mathcal{F}\{u_2\}$ holds for all $u_1, u_2 \in \mathcal{U}$ and scalars $\alpha_1 \in \mathbb{F}$, $\alpha_2 \in \mathbb{F}$.

2. *Boundedness*: There exists a scalar $\kappa \in \mathbb{R}_+$, such that

$$\|\mathcal{F}\{u\}\|_{\mathcal{Y}} \leq \kappa \cdot \|u\|_{\mathcal{U}} \tag{B.39}$$

   holds for all $u \in \mathcal{U}$. Notice that $\|\cdot\|_{\mathcal{U}}$ and $\|\cdot\|_{\mathcal{Y}}$ denote the norms associated with the vector spaces $\mathcal{U}$ and $\mathcal{Y}$.

When working with a bounded, linear operator, one is often interested in the "amplification" of an input u, when it passes through the operator $\mathcal{F}\{u\}$. That is, given an input u, which is bounded in terms of the norm associated with the input vector space $\mathcal{U}$, one wants to know how large y may become at most in terms of the norm associated with the output vector space $\mathcal{Y}$. From the definition of a bounded, linear operator, it is clear that y will be bounded. The question of the "amplification" however relates to finding the smallest value of κ, for which (B.39) is satisfied. This leads to the definition of the induced (operator-) norm [45]:

$$\|\mathcal{F}\|_{\mathcal{U}\to\mathcal{Y}} \triangleq \sup_{u\in\mathcal{U}, u\neq 0} \frac{\|\mathcal{F}\{u\}\|_{\mathcal{Y}}}{\|u\|_{\mathcal{U}}}, \tag{B.40}$$

where $\|\mathcal{F}\|_{\mathcal{U}\to\mathcal{Y}}$ denotes the size (the "amplification") of the operator. The norm is called *induced* as the size of the operator $\mathcal{F}$ (its "amplification") depends on the norms of the input and output vector spaces. It may be verified that $\|\mathcal{F}\|_{\mathcal{U}\to\mathcal{Y}}$ corresponds to the smallest value of κ, for which (B.39) holds [22]. Furthermore, it may be proven that

1. any such norm $\|\mathcal{F}\|_{\mathcal{U}\to\mathcal{Y}}$ of a linear operator satisfies the norm axioms [22, p. 79];

2. any such norm is *submultiplicative* [22, p. 80], which means that the norm of the composition $y = \mathcal{F}_1\{\mathcal{F}_2\{u\}\}$ of two operators $\mathcal{F}_1 : \mathcal{W} \to \mathcal{Y}$, $\mathcal{F}_2 : \mathcal{U} \to \mathcal{W}$ is given by

$$\|\mathcal{F}_1\{\mathcal{F}_2\{u\}\}\|_{\mathcal{Y}} \leq \|\mathcal{F}_1\|_{\mathcal{W}\to\mathcal{Y}} \cdot \|\mathcal{F}_2\|_{\mathcal{U}\to\mathcal{W}} \cdot \|u\|_{\mathcal{U}}. \tag{B.41}$$

In case of the operator "matrix" (B.36), the following induced norms are commonly used:

- the *induced 1-norm*, which is induced by the 1-vector norm, which is defined in (B.4) for $p = 1$. The induced 1-norm is computed from

$$\|\boldsymbol{A}\|_{1,i} = \max_{j=1,\ldots,m} \left(\sum_{i=1}^{l} |a_{ij}| \right). \tag{B.42}$$

  Since the computation amounts to computing the largest absolute column sum, the induced 1-norm is also referred to as *column sum norm*.

- the *induced 2-norm*, which is induced by the 2-vector norm, which is defined in (B.4) for $p = 2$. The induced 2-norm is computed by

$$\|\boldsymbol{A}\|_{2,i} = \sqrt{\lambda_{\max}\left(\boldsymbol{A}^H \boldsymbol{A}\right)}, \tag{B.43}$$

  i.e. the induced 2-norm corresponds to the square root of the largest eigenvalue of $\boldsymbol{A}^H\boldsymbol{A}$. It follows from the definition of the Singular Value Decomposition (SVD) (see Section B.4.3) that $\|\boldsymbol{A}\|_{2,i}$ corresponds to the largest singular value of $\boldsymbol{A}$, i.e. $\|\boldsymbol{A}\|_{2,i} = \sigma_{\max}(\boldsymbol{A})$. The induced 2-norm is also called *spectral norm*.

- the *induced ∞-norm*, which is induced by the ∞-vector norm, which is defined in (B.5). The induced ∞-norm is computed from

$$\|\boldsymbol{A}\|_{\infty,i} = \max_{i=1,\dots,l}\left(\sum_{j=1}^{m}|a_{ij}|\right). \tag{B.44}$$

  Since the computation amounts to computing the largest absolute row sum, the induced ∞-norm is also referred to as *row sum norm*.

It may be verified that these induced matrix norms satisfy all norm axioms and furthermore, lead to the smallest value of κ in (B.39) [85, Chapter 5.6].

In case of the convolution operator (B.37), a natural choice for $\mathcal{U}$ and $\mathcal{Y}$ is $\mathcal{U} = \mathcal{Y} = \mathcal{L}_\infty^1$. In order to obtain a bounded output signal $y \in \mathcal{Y}$, the impulse response $g(t)$ must satisfy $g(t) \in \mathcal{L}_1$. The operator norm of the convolution with $g(t)$, which is induced by the $\mathcal{L}_\infty$-norm, is then given by [45]:

$$\|g(t)\|_{\mathcal{L}_\infty \to \mathcal{L}_\infty} = \int_0^\infty |g(t)|dt = \|g(t)\|_{\mathcal{L}_1}. \tag{B.45}$$

While the induced $\mathcal{L}_\infty$-norm actually derives from the convolution (i.e. a time-domain operation), it will often be treated like a transfer function norm. Hence, we define

$$\|G(s)\|_{\mathcal{L}_1} \triangleq \|g(t)\|_{\mathcal{L}_1}. \tag{B.46}$$

The norm $\|G(s)\|_{\mathcal{L}_1}$ will be referred to as $\mathcal{L}_1$-norm (of the transfer function $G(s) = \mathcal{L}\{g(t)\}$). Since the $\mathcal{L}_1$ transfer function norm is an operator norm, it is also *submultiplicative*, i.e. $\|G_1(s) \cdot G_2(s)\|_{\mathcal{L}_1} \leq \|G_1(s)\|_{\mathcal{L}_1} \cdot \|G_2(s)\|_{\mathcal{L}_1}$.

In case of a transfer function matrix $\boldsymbol{G} : \mathbb{C} \to \mathbb{C}^{l\times m}$, the impulse response matrix is defined as

$$\boldsymbol{g}(t) = \begin{bmatrix} g_{1,1}(t) & \dots & g_{1,m}(t) \\ \dots & \ddots & \dots \\ g_{l,1}(t) & \dots & g_{l,m}(t) \end{bmatrix}. \tag{B.47}$$

The $\mathcal{L}_1$-norm of $\boldsymbol{G}(s)$ is then defined as [87, Definition A.7.4]:

$$\|\boldsymbol{G}(s)\|_{\mathcal{L}_1} \triangleq \|\boldsymbol{g}(t)\|_{\mathcal{L}_1} \triangleq \max_{i=1,\dots,l}\left(\sum_{j=1}^{m}\|g_{i,j}(t)\|_{\mathcal{L}_1}\right), \tag{B.48}$$

which exists if and only if $g_{i,j}(t) \in \mathcal{L}_1$. The condition $g_{i,j}(t) \in \mathcal{L}_1$ holds, if the poles of the transfer function matrix $\boldsymbol{G}(s)$ strictly lie in the left half-plane.

B.2 Positive Definite Functions

Positive and negative (semi-) definite functions play a central role in the stability analysis of nonlinear systems using Lyapunov's second method. Their importance stems from the fact that positive definite functions generalize the idea of an energy function. Due to their high relevance, some important definitions and properties of positive and negative (semi-) definite functions are stated in this section.

Consider a scalar function $f : \mathcal{D} \to \mathbb{R}$ defined in a neighborhood $\mathcal{D} \subseteq \mathbb{R}^n$ of the origin (including the origin). Positive (semi-) definiteness of $f(\boldsymbol{x})$ is defined as follows:

Definition B.1. *A function $f(\boldsymbol{x})$ is called positive definite, if*

$$\begin{aligned} &f(\boldsymbol{x}) > 0 \quad \forall\, \boldsymbol{x} \in \mathcal{D}\backslash\mathbf{0} \quad \textit{and} \\ &f(\mathbf{0}) = 0. \end{aligned} \tag{B.49}$$

Definition B.2. *A function $f(\boldsymbol{x})$ is called positive semidefinite, if*

$$f(\boldsymbol{x}) \geq 0 \quad \forall\, \boldsymbol{x} \in \mathcal{D}. \tag{B.50}$$

Similarly, negative (semi-) definite functions are defined as:

Definition B.3. *A function $f(\boldsymbol{x})$ is called negative definite, if*

$$\begin{aligned} &f(\boldsymbol{x}) < 0 \quad \forall\, \boldsymbol{x} \in \mathcal{D}\backslash\mathbf{0} \quad \textit{and} \\ &f(\mathbf{0}) = 0. \end{aligned} \tag{B.51}$$

Definition B.4. *A function $f(\boldsymbol{x})$ is called negative semidefinite, if*

$$f(\boldsymbol{x}) \leq 0 \quad \forall\, \boldsymbol{x} \in \mathcal{D}. \tag{B.52}$$

If none of the previous definitions holds, then the function is called indefinite.

B.2.1 Quadratic Forms and Ellipsoids

In general, the problem of checking definiteness of an arbitrary function is rather involved. For example, in case of a general multivariate polynomial, checking definiteness is a NP-hard problem [128]. However, there are classes of functions, whose definiteness may be checked readily. One such class are quadratic forms

$$f(\boldsymbol{x}) = \boldsymbol{x}^T \boldsymbol{A} \boldsymbol{x}, \tag{B.53}$$

where $\boldsymbol{A} \in \mathbb{S}^n$ is symmetric and $\boldsymbol{x} \in \mathbb{R}^n$. The definiteness of the quadratic form (B.53) may be easily checked by looking at the eigenvalues $\lambda_i(\boldsymbol{A}),\ i = 1, \ldots, n$ of $\boldsymbol{A}$:

$$f(\boldsymbol{x}) \text{ positive definite} \Leftrightarrow \lambda_i(\boldsymbol{A}) > 0 \quad \forall\, i = 1, \ldots, n, \tag{B.54}$$

$$f(\boldsymbol{x}) \text{ positive semidefinite} \Leftrightarrow \lambda_i(\boldsymbol{A}) \geq 0 \quad \forall\, i = 1, \ldots, n, \tag{B.55}$$

$$f(\boldsymbol{x}) \text{ negative definite} \Leftrightarrow \lambda_i(\boldsymbol{A}) < 0 \quad \forall\, i = 1, \ldots, n, \tag{B.56}$$

$$f(\boldsymbol{x}) \text{ negative semidefinite} \Leftrightarrow \lambda_i(\boldsymbol{A}) \leq 0 \quad \forall\, i = 1, \ldots, n. \tag{B.57}$$

If none of the above relations holds, the quadratic form (B.53) is indefinite. For a proof of (B.54)-(B.57), refer to [85, Section 7.1]. Since a quadratic form is defined by the matrix $\boldsymbol{A}$, it is also common to call $\boldsymbol{A}$ a positive / negative (semi-) definite or indefinite matrix. The subsets of $\mathbb{S}^n$ of all positive definite, positive semidefinite, negative definite and negative semidefinite matrices will be denoted by $\mathbb{S}^n_{++}$, $\mathbb{S}^n_{+}$, $\mathbb{S}^n_{--}$ and $\mathbb{S}^n_{-}$, respectively.

The level sets

$$\partial\mathcal{M}_c = \left\{\boldsymbol{x} \mid \boldsymbol{x}^T\boldsymbol{A}\boldsymbol{x} = c\right\} \tag{B.58}$$

of a quadratic form are so-called *quadrics* [172]. Depending on the definiteness of $\boldsymbol{A}$, a *quadric* geometrically represents various shapes such as ellipsoids, hyperboloids and paraboloids. As positive definite functions are a central element of Lyapunov analysis, the *quadric* which results for $\boldsymbol{A} \in \mathbb{S}^n_{++}$ is of special interest. Geometrically, the latter *quadric* describes an ellipsoid in $\mathbb{R}^n$. To see this, let $c \geq 0$ and notice that every symmetric matrix $\boldsymbol{A}$ admits an eigendecomposition $\boldsymbol{A} = \boldsymbol{Q}\boldsymbol{D}\boldsymbol{Q}^T$ with a real, orthonormal matrix $\boldsymbol{Q}$ and a diagonal matrix $\boldsymbol{D}$ containing the eigenvalues [85], [23, p. 230]. Using the transformation $\bar{\boldsymbol{x}} = \boldsymbol{Q}^T\boldsymbol{x}$, the *quadric* (B.58) becomes

$$\boldsymbol{x}^T\boldsymbol{Q}\boldsymbol{D}\boldsymbol{Q}^T\boldsymbol{x} = \bar{\boldsymbol{x}}^T\boldsymbol{D}\bar{\boldsymbol{x}} = \sum_{i=1}^{n} \lambda_i(\boldsymbol{A}) \cdot \bar{x}_i^2 = c \tag{B.59}$$

with $\bar{\boldsymbol{x}}^T = \begin{bmatrix}\bar{x}_1 & \ldots & \bar{x}_n\end{bmatrix}$. In terms of the transformed coordinates $\bar{\boldsymbol{x}}$, (B.59) represents an ellipsoid

$$\frac{\bar{x}_1^2}{r_1^2} + \ldots + \frac{\bar{x}_n^2}{r_n^2} = 1 \tag{B.60}$$

with the principal axes

$$r_i = \sqrt{\frac{c}{\lambda_i(\boldsymbol{A})}}. \tag{B.61}$$

Eq. (B.61) shows that the eigenvalues determine the size of the principal axes of the ellipsoid. Since $\boldsymbol{Q}$ is orthonormal, the map $\boldsymbol{x} = \boldsymbol{Q}\bar{\boldsymbol{x}}$ only rotates the ellipsoid (B.60) but does not alter its size. Thus, the eigenvectors determine the orientation of the ellipsoid.

Similarly, the c-sublevel set of the quadratic form (B.53), given by

$$\mathcal{M}_c = \left\{\boldsymbol{x} \mid \boldsymbol{x}^T\boldsymbol{A}\boldsymbol{x} \leq c\right\}, \tag{B.62}$$

describes the interior of the ellipsoid including the boundary. Using a strict inequality instead of a non-strict inequality leads to the description of the interior of the ellipsoid excluding the boundary:

$$\mathcal{M}_c \setminus \partial\mathcal{M}_c = \left\{\boldsymbol{x} \mid \boldsymbol{x}^T\boldsymbol{A}\boldsymbol{x} < c\right\}. \tag{B.63}$$

Throughout the thesis, the term *ellipsoid* is used to denote both the boundary $\partial\mathcal{M}_c$ as well as the interior of the ellipsoid $\mathcal{M}_c$. Since it should be clear from the context whether level sets or sublevel sets are considered, no confusion arises.

Using an eigendecomposition, one may also derive the following bounds on the quadratic form (B.53), if $\boldsymbol{A}$ is positive definite:

$$\lambda_{\min}(\boldsymbol{A}) \cdot \|\boldsymbol{x}\|_2^2 \leq \boldsymbol{x}^T\boldsymbol{A}\boldsymbol{x} \leq \lambda_{\max}(\boldsymbol{A}) \cdot \|\boldsymbol{x}\|_2^2. \tag{B.64}$$

Proof. Since $\boldsymbol{A}$ is symmetric, an eigendecomposition $\boldsymbol{A} = \boldsymbol{Q}\boldsymbol{D}\boldsymbol{Q}^T$ with a real, orthonormal matrix $\boldsymbol{Q}$ and a real, diagonal matrix $\boldsymbol{D} = \operatorname{diag}\begin{bmatrix}\lambda_1(\boldsymbol{A}) & \dots & \lambda_n(\boldsymbol{A})\end{bmatrix}$ containing the eigenvalues of $\boldsymbol{A}$ exists [85, 23]. Using the transformation $\bar{\boldsymbol{x}} = \boldsymbol{Q}^T\boldsymbol{x}$, the quadratic form (B.53) becomes

$$\boldsymbol{x}^T\boldsymbol{A}\boldsymbol{x} = \sum_{i=1}^{n} \lambda_i(\boldsymbol{A}) \cdot \bar{x}_i^2. \tag{B.65}$$

From (B.65) follows

$$\lambda_{\min}(\boldsymbol{A}) \cdot \sum_{i=1}^{n} \bar{x}_i^2 \leq \sum_{i=1}^{n} \lambda_i(\boldsymbol{A}) \cdot \bar{x}_i^2. \leq \lambda_{\max}(\boldsymbol{A}) \cdot \sum_{i=1}^{n} \bar{x}_i^2, \tag{B.66}$$

as $0 < \lambda_{\min}(\boldsymbol{A}) \leq \lambda_i(\boldsymbol{A}) \leq \lambda_{\max}(\boldsymbol{A})$. Since $\boldsymbol{Q}$ is orthonormal,

$$\sum_{i=1}^{n} \bar{x}_i^2 = \bar{\boldsymbol{x}}^T\bar{\boldsymbol{x}} = \boldsymbol{x}^T \underbrace{\boldsymbol{Q}\boldsymbol{Q}^T}_{\boldsymbol{I}} \boldsymbol{x} = \|\boldsymbol{x}\|_2^2 \tag{B.67}$$

holds, which establishes (B.64). □

The bounds in (B.64) have an important geometric interpretation for the (sub)level sets associated with the quadratic form. Geometrically, the level set $\lambda_{\min}(\boldsymbol{A}) \cdot \|\boldsymbol{x}\|_2^2 = c$ associated with the lower bound in (B.64) describes the smallest sphere surrounding the ellipsoid (B.58), where surrounding means

$$\{\boldsymbol{x} \in \mathbb{R}^n |\ \boldsymbol{x}^T\boldsymbol{A}\boldsymbol{x} = c\} \subseteq \{\boldsymbol{x} \in \mathbb{R}^n |\ \lambda_{\min}(\boldsymbol{A}) \cdot \|\boldsymbol{x}\|_2^2 \leq c\}. \tag{B.68}$$

This fact follows readily from the reciprocal relation (B.61) between the principal axes of the ellipsoid and the eigenvalues of $\boldsymbol{A}$. Similarly, the level set $\lambda_{\max}(\boldsymbol{A}) \cdot \|\boldsymbol{x}\|_2^2 = c$ associated with the upper bound in (B.64) describes the largest sphere, which may be fitted into the interior of the ellipsoid (B.58), i.e.

$$\{\boldsymbol{x} \in \mathbb{R}^n |\ \lambda_{\max}(\boldsymbol{A}) \cdot \|\boldsymbol{x}\|_2^2 = c\} \subseteq \{\boldsymbol{x} \in \mathbb{R}^n |\ \boldsymbol{x}^T\boldsymbol{A}\boldsymbol{x} \leq c\}. \tag{B.69}$$

Analogous results also hold for c-sublevel sets. The c-sublevel set $\lambda_{\min}(\boldsymbol{A}) \cdot \|\boldsymbol{x}\|_2^2 \leq c$ associated with the lower bound in (B.64) describes the smallest ball surrounding the ellipsoid (B.58), i.e.

$$\{\boldsymbol{x} \in \mathbb{R}^n |\ \boldsymbol{x}^T\boldsymbol{A}\boldsymbol{x} \leq c\} \subseteq \{\boldsymbol{x} \in \mathbb{R}^n |\ \lambda_{\min}(\boldsymbol{A}) \cdot \|\boldsymbol{x}\|_2^2 \leq c\}. \tag{B.70}$$

Similarly, the c-sublevel set $\lambda_{\max}(\boldsymbol{A}) \cdot \|\boldsymbol{x}\|_2^2 \leq c$ associated with the upper bound in (B.64) describes the largest ball, which may be fitted into the interior of the ellipsoid (B.58), i.e.

$$\{\boldsymbol{x} \in \mathbb{R}^n |\ \lambda_{\max}(\boldsymbol{A}) \cdot \|\boldsymbol{x}\|_2^2 \leq c\} \subseteq \{\boldsymbol{x} \in \mathbb{R}^n |\ \boldsymbol{x}^T \boldsymbol{A} \boldsymbol{x} \leq c\}. \tag{B.71}$$

A more complex class of quadratic forms is given by

$$f(\boldsymbol{x}) = (\boldsymbol{x} - \boldsymbol{x}_c)^T \boldsymbol{A} (\boldsymbol{x} - \boldsymbol{x}_c), \tag{B.72}$$

where $\boldsymbol{A} \in \mathbb{S}_{++}^n$ is a positive definite matrix and $\boldsymbol{x}_c \in \mathbb{R}^n$ is an arbitrary vector. Geometrically, the c-sublevel set

$$\mathcal{M}_c = \left\{\boldsymbol{x} \mid (\boldsymbol{x} - \boldsymbol{x}_c)^T \boldsymbol{A} (\boldsymbol{x} - \boldsymbol{x}_c) \leq c\right\} \tag{B.73}$$

of (B.72) describes an ellipsoid centered at $\boldsymbol{x}_c$. An equivalent representation of the ellipsoid (B.73) is given by

$$\mathcal{M}_c = \left\{\boldsymbol{x} \mid \boldsymbol{x}^T \boldsymbol{A} \boldsymbol{x} + 2\boldsymbol{x}^T \boldsymbol{b} + d \leq 0\right\} \tag{B.74}$$

with

$$\boldsymbol{b}^T \boldsymbol{A}^{-1} \boldsymbol{b} - d \geq 0. \tag{B.75}$$

The additional condition (B.75) is required in order to ensure a non-negative level set constant c, as will become clear shortly. In order to transform the representation (B.74) to (B.73), the center point $\boldsymbol{x}_c$ has to be determined first. A factor comparison between the inequalities (B.73) and (B.74) yields

$$\boldsymbol{x}_c = -\boldsymbol{A}^{-1} \boldsymbol{b}. \tag{B.76}$$

The inequality (B.74) hence becomes

$$\mathcal{M}_c = \left\{\boldsymbol{x} \mid \boldsymbol{x}^T \boldsymbol{A} \boldsymbol{x} - 2\boldsymbol{x}^T \boldsymbol{A} \boldsymbol{x}_c + d \leq 0\right\}. \tag{B.77}$$

Adding and subtracting $\boldsymbol{x}_c^T \boldsymbol{A} \boldsymbol{x}_c = \boldsymbol{b}^T \boldsymbol{A}^{-1} \boldsymbol{b}$ yields

$$\mathcal{M}_c = \left\{\boldsymbol{x} \mid \boldsymbol{x}^T \boldsymbol{A} \boldsymbol{x} - 2\boldsymbol{x}^T \boldsymbol{A} \boldsymbol{x}_c + \boldsymbol{x}_c^T \boldsymbol{A} \boldsymbol{x}_c - \boldsymbol{b}^T \boldsymbol{A}^{-1} \boldsymbol{b} + d \leq 0\right\}. \tag{B.78}$$

With

$$c = \boldsymbol{b}^T \boldsymbol{A}^{-1} \boldsymbol{b} - d, \tag{B.79}$$

which is non-negative due to (B.75), one finally obtains

$$\mathcal{M}_c = \left\{\boldsymbol{x} \mid \boldsymbol{x}^T \boldsymbol{A} \boldsymbol{x} - 2\boldsymbol{x}^T \boldsymbol{A} \boldsymbol{x}_c + \boldsymbol{x}_c^T \boldsymbol{A} \boldsymbol{x}_c \leq c\right\}, \tag{B.80}$$

which is equivalent to (B.73). Thus, using (B.76) and (B.79), the ellipsoid (B.74) is transformed to the representation (B.73).

The ellipsoid (B.73) admits yet another representation. As it represents the ellipsoid centered at $\boldsymbol{x}_c$, the transformation $\bar{\boldsymbol{x}} = \boldsymbol{x} - \boldsymbol{x}_c$ implies

$$\mathcal{M}_c = \left\{ \boldsymbol{x}_c + \bar{\boldsymbol{x}} \mid \bar{\boldsymbol{x}}^T \boldsymbol{A} \bar{\boldsymbol{x}} \leq c \right\}. \tag{B.81}$$

Since $\boldsymbol{A}$ is positive definite, its matrix square root $\boldsymbol{A}^{\frac{1}{2}}$ exists (see Section B.4.2), which leads to

$$\mathcal{M}_c = \left\{ \boldsymbol{x}_c + \bar{\boldsymbol{x}} \mid \bar{\boldsymbol{x}}^T \boldsymbol{A}^{\frac{1}{2}} \cdot \boldsymbol{A}^{\frac{1}{2}} \bar{\boldsymbol{x}} \leq c \right\}. \tag{B.82}$$

By defining $\boldsymbol{z} = \boldsymbol{A}^{\frac{1}{2}} \bar{\boldsymbol{x}}$, (B.82) becomes

$$\mathcal{M}_c = \left\{ \boldsymbol{x}_c + \boldsymbol{A}^{-\frac{1}{2}} \cdot \boldsymbol{z} \mid \boldsymbol{z}^T \boldsymbol{z} \leq c \right\}. \tag{B.83}$$

Hence, (B.83) represents the ellipsoid (B.73) as an affine transformation $\boldsymbol{x} = \boldsymbol{x}_c + \boldsymbol{A}^{-\frac{1}{2}} \cdot \boldsymbol{z}$ of the ball $\boldsymbol{z}^T \boldsymbol{z} \leq c$.

Using the representation as an affine transformation, an important operation on ellipsoids can be derived, namely the orthogonal projection of an ellipsoid onto a subspace of $\mathbb{R}^n$. By projecting the ellipsoid onto a 1-dimensional subspace (i.e. a line), the largest extension of the ellipsoid in direction of the line may be easily determined. To that end, let the basis $\boldsymbol{C}$ of the subspace $\mathcal{S}$ be given by (B.22). The projection of a point in $\mathcal{V} = \mathbb{R}^n$ onto $\mathcal{S}$ is then given by (B.31). Inserting the affine transformation from (B.83) into (B.31) yields

$$(\boldsymbol{y})_{\mathcal{S}} = \boldsymbol{C}^T \left((\boldsymbol{x}_c + \boldsymbol{A}^{-\frac{1}{2}} \cdot \boldsymbol{z})_{\mathcal{V}} \right). \tag{B.84}$$

The center of the projected ellipsoid is hence given by

$$(\boldsymbol{y}_c)_{\mathcal{S}} = \boldsymbol{C}^T \cdot (\boldsymbol{x}_c)_{\mathcal{V}}, \tag{B.85}$$

leading to

$$(\boldsymbol{y})_{\mathcal{S}} = (\boldsymbol{y}_c)_{\mathcal{S}} + \boldsymbol{C}^T \cdot (\boldsymbol{A}^{-\frac{1}{2}} \cdot \boldsymbol{z})_{\mathcal{V}}. \tag{B.86}$$

In order to improve readability, the indices $\mathcal{V}$ and $\mathcal{S}$ will be dropped subsequently. Any $\boldsymbol{y}_{(\cdot)}$ will denote a quantity in the $\mathcal{S}$-frame, whereas any $\boldsymbol{z}_{(\cdot)}$ denotes a quantity in the original $\mathcal{V}$-frame. Hence, (B.86) turns into

$$\boldsymbol{y} = \boldsymbol{y}_c + \boldsymbol{C}^T \boldsymbol{A}^{-\frac{1}{2}} \cdot \boldsymbol{z}. \tag{B.87}$$

A singular value decomposition (see Section B.4.3) of the $m \times n$-matrix $\boldsymbol{C}^T \boldsymbol{A}^{-\frac{1}{2}}$ yields

$$\boldsymbol{C}^T \boldsymbol{A}^{-\frac{1}{2}} = \boldsymbol{U} \cdot \begin{bmatrix} \boldsymbol{\Sigma}_1 & \boldsymbol{0}^{m \times (n-m)} \end{bmatrix} \cdot \boldsymbol{V}^T. \tag{B.88}$$

Hence, (B.87) becomes

$$\boldsymbol{y} = \boldsymbol{y}_c + \boldsymbol{U} \cdot \begin{bmatrix} \boldsymbol{\Sigma}_1 & \boldsymbol{0}^{m \times (n-m)} \end{bmatrix} \cdot \boldsymbol{V}^T \cdot \boldsymbol{z}. \tag{B.89}$$

Since $\boldsymbol{V}$ is orthonormal, the map $\bar{\boldsymbol{w}} = \boldsymbol{V}^T \cdot \boldsymbol{z}$ preserves lengths. Hence, a ball with the radius $\sqrt{c}$ maps to a ball with the radius $\sqrt{c}$. Due to the presence of the zero

matrix $\mathbf{0}^{m\times(n-m)}$, only the first m rows of $\bar{\boldsymbol{w}}$, denoted as $\boldsymbol{w}$, influence the value of $\boldsymbol{y}$. Since $\|\boldsymbol{z}\|_2^2 \leq c$ implies $\|\boldsymbol{w}\|_2^2 \leq c$, (B.89) turns into an affine transformation of the ball $\|\boldsymbol{w}\|_2^2 \leq c$:

$$\boldsymbol{y} = \boldsymbol{y}_c + \boldsymbol{U}\boldsymbol{\Sigma}_1 \cdot \boldsymbol{w}. \tag{B.90}$$

The projected ellipsoid in the $\mathcal{S}$-frame is hence given by

$$\mathcal{M}_{c,Proj} = \left\{ \boldsymbol{y}_c + \boldsymbol{A}_{Proj}^{-\frac{1}{2}} \cdot \boldsymbol{w} \mid \boldsymbol{w}^T\boldsymbol{w} \leq c \right\} \tag{B.91}$$

with $\boldsymbol{A}_{Proj}^{-\frac{1}{2}} = \boldsymbol{U}\boldsymbol{\Sigma}_1$. Hence,

$$\boldsymbol{A}_{Proj} = \left(\boldsymbol{U}\boldsymbol{\Sigma}_1\boldsymbol{\Sigma}_1\boldsymbol{U}^T\right)^{-1} \tag{B.92}$$

holds. Since

$$\boldsymbol{C}^T\boldsymbol{A}^{-1}\boldsymbol{C} = \boldsymbol{U}\begin{bmatrix}\boldsymbol{\Sigma}_1 & \mathbf{0}^{m\times(n-m)}\end{bmatrix}\boldsymbol{V}^T\boldsymbol{V}\begin{bmatrix}\boldsymbol{\Sigma}_1 \\ \mathbf{0}^{(n-m)\times m}\end{bmatrix}\boldsymbol{U}^T = \boldsymbol{U}\boldsymbol{\Sigma}_1\boldsymbol{\Sigma}_1\boldsymbol{U}^T. \tag{B.93}$$

follows from the Singular Value Decomposition (B.88), the matrix $\boldsymbol{A}_{Proj}$ may be written as

$$\boldsymbol{A}_{Proj} = \left(\boldsymbol{C}^T\boldsymbol{A}^{-1}\boldsymbol{C}\right)^{-1}. \tag{B.94}$$

Hence, the projected ellipsoid (B.91) admits the alternative representation:

$$\mathcal{M}_{c,Proj} = \left\{ \boldsymbol{y} \mid (\boldsymbol{y}-\boldsymbol{y}_c)^T\boldsymbol{A}_{Proj}(\boldsymbol{y}-\boldsymbol{y}_c) \leq c \right\}. \tag{B.95}$$

For $\boldsymbol{x}_c = \mathbf{0}$, implying $\boldsymbol{y}_c = \mathbf{0}$, this result may also be found in [95].

B.2.2 Quadratic Forms in Terms of Traces

Throughout the proofs of stability, one often also encounters more general quadratic forms defined by

$$f(\boldsymbol{X}) = \mathrm{Tr}\left\{\boldsymbol{X}\boldsymbol{A}\boldsymbol{X}^T\right\}, \tag{B.96}$$

where $\boldsymbol{A} \in \mathbb{S}^n$ is a symmetric matrix and $\boldsymbol{X} \in \mathbb{R}^{m\times n}$ is an arbitrary real matrix with

$$\boldsymbol{X} = \begin{bmatrix}\boldsymbol{x}_1^T \\ \vdots \\ \boldsymbol{x}_m^T\end{bmatrix} \Leftrightarrow \boldsymbol{X}^T = \begin{bmatrix}\boldsymbol{x}_1 & \dots & \boldsymbol{x}_m\end{bmatrix} \tag{B.97}$$

and $\boldsymbol{x} \in \mathbb{R}^n$. In order to see that (B.96) is a quadratic form, notice first that (B.96) equals

$$f(\boldsymbol{X}) = \mathrm{Tr}\left\{\boldsymbol{A}\boldsymbol{X}^T\boldsymbol{X}\right\}. \tag{B.98}$$

due to the cyclic property (B.154). With

$$\boldsymbol{A}\boldsymbol{X}^T = \begin{bmatrix}\boldsymbol{A}\boldsymbol{x}_1 & \dots & \boldsymbol{A}\boldsymbol{x}_m\end{bmatrix}, \tag{B.99}$$

(B.98) becomes:

$$f(\boldsymbol{X}) = \mathrm{Tr}\left\{ \begin{bmatrix} \boldsymbol{A}\boldsymbol{x}_1 & \dots & \boldsymbol{A}\boldsymbol{x}_m \end{bmatrix} \cdot \begin{bmatrix} \boldsymbol{x}_1^T \\ \vdots \\ \boldsymbol{x}_m^T \end{bmatrix} \right\}. \tag{B.100}$$

Using the trace property (B.157), one finally obtains

$$f(\boldsymbol{X}) = \sum_{k=1}^{m} \boldsymbol{x}_k^T \boldsymbol{A}\boldsymbol{x}_k. \tag{B.101}$$

Clearly, (B.101) is a quadratic form. Furthermore, if $\boldsymbol{A}$ is positive / negative (semi-) definite, then the quadratic form (B.101) is positive / negative (semi-) definite as well.

If $\boldsymbol{A}$ is positive definite, then (B.101) admits the derivation of a similar bound as in the previous section:

$$\lambda_{\min}(\boldsymbol{A}) \cdot \|\boldsymbol{X}\|_F^2 \leq \mathrm{Tr}\left\{\boldsymbol{X}\boldsymbol{A}\boldsymbol{X}^T\right\} \leq \lambda_{\max}(\boldsymbol{A}) \cdot \|\boldsymbol{X}\|_F^2. \tag{B.102}$$

Proof. Since $\boldsymbol{A}$ is positive definite, the summands in (B.101) may be bounded by

$$\lambda_{\min}(\boldsymbol{A}) \cdot \boldsymbol{x}_k^T \boldsymbol{x}_k \leq \boldsymbol{x}_k^T \boldsymbol{A}\boldsymbol{x}_k \leq \lambda_{\max}(\boldsymbol{A}) \cdot \boldsymbol{x}_k^T \boldsymbol{x}_k \tag{B.103}$$

due to (B.64). Hence, the sum in (B.101) is bounded by

$$\lambda_{\min}(\boldsymbol{A}) \cdot \sum_{k=1}^{m} \boldsymbol{x}_k^T \boldsymbol{x}_k \leq \sum_{k=1}^{m} \boldsymbol{x}_k^T \boldsymbol{A}\boldsymbol{x}_k \leq \lambda_{\max}(\boldsymbol{A}) \cdot \sum_{k=1}^{m} \boldsymbol{x}_k^T \boldsymbol{x}_k. \tag{B.104}$$

Using the trace property (B.157), one obtains

$$\lambda_{\min}(\boldsymbol{A}) \cdot \mathrm{Tr}\left\{\boldsymbol{X}\boldsymbol{X}^T\right\} \leq \sum_{k=1}^{m} \boldsymbol{x}_k^T \boldsymbol{A}\boldsymbol{x}_k \leq \lambda_{\max}(\boldsymbol{A}) \cdot \mathrm{Tr}\left\{\boldsymbol{X}\boldsymbol{X}^T\right\}. \tag{B.105}$$

With the definition of the Frobenius norm in (B.9), (B.105) establishes (B.102). □

B.2.3 Sum-Of-Squares Polynomials

Sum-Of-Squares (SOS) polynomials are a special class of polynomials, whose positive (semi-)definiteness may be shown rather easily. In the subsequent introduction, some general nomenclature with respect to polynomials is introduced first. Afterwards, SOS polynomials are presented. The following introduction of polynomials and SOS polynomials is based on [128] and [151].

For $\boldsymbol{x}^T = \begin{bmatrix} x_1 & \dots & x_n \end{bmatrix} \in \mathbb{R}^n$, a monomial is defined as the scalar function

$$m_{\boldsymbol{d}}(\boldsymbol{x}) = \prod_{i=1}^{n} x_i^{d_i}, \tag{B.106}$$

where $\boldsymbol{d} = \begin{bmatrix} d_1 & \dots & d_n \end{bmatrix} \in \mathbb{N}^n$ specifies the exponents of the components of $\boldsymbol{x}$. The degree of a monomial is defined as $\deg m_{\boldsymbol{d}}(\boldsymbol{x}) \triangleq \sum_{i=1}^{n} d_i$. A polynomial in n variables then is defined as a linear combination of k monomials $m_{\boldsymbol{d}_j}(\boldsymbol{x}),\ j = 1, \dots, k$, i.e.

$$g(\boldsymbol{x}) = \sum_{j=1}^{k} c_j \cdot m_{\boldsymbol{d}_j}(\boldsymbol{x}). \tag{B.107}$$

The degree of the polynomial is defined as the largest degree of its monomials, i.e.

$$\deg g(\boldsymbol{x}) \triangleq \max_j \left(\deg m_{\boldsymbol{d}_j}(\boldsymbol{x})\right). \tag{B.108}$$

Now let the degree of the polynomial $g(\boldsymbol{x})$ be $2d$ with $d \in \mathbb{N}$. Any polynomial of degree $2d$ (or less) may be expressed in a *vector representation*:

$$g(\boldsymbol{x}) = \boldsymbol{c}^T \boldsymbol{w}(x) \tag{B.109}$$

with

$$w(\boldsymbol{x})^T = \begin{bmatrix} 1 & x_1 & \dots & x_n & x_1^2 & x_1x_2 & \dots & x_n^2 & \dots & x_n^{2d} \end{bmatrix}, \tag{B.110}$$

where $\boldsymbol{c} \in \mathbb{R}^{l_w}$ is the coefficient vector and $w(\boldsymbol{x}) \in \mathbb{R}^{l_w}$ is the monomial vector. Here, the monomial vector gathers all possible monomials up to the degree $2d$. The length of these vectors is given by $l_w = \binom{n+2d}{2d}$, which results from the combinatorial problem "drawing with replacement of $2d$ samples from an urn with $n+1$ elements". Furthermore, using $\boldsymbol{Q} \in \mathbb{S}^{l_v}$ with $l_v = \binom{n+d}{d}$, the polynomial may be expressed in a *Gram matrix representation*:

$$g(\boldsymbol{x}) = \boldsymbol{v}(\boldsymbol{x})^T \boldsymbol{Q} \boldsymbol{v}(\boldsymbol{x}) \tag{B.111}$$

with

$$\boldsymbol{v}(\boldsymbol{x})^T = \begin{bmatrix} 1 & x_1 & \dots & x_n & x_1^2 & x_1x_2 & \dots & x_n^2 & \dots & x_n^{d} \end{bmatrix}. \tag{B.112}$$

By equating the coefficients of (B.111) and (B.109), a system of linear equations may be obtained to determine $\boldsymbol{Q}$. Notice that the Gram matrix representation (B.111) usually is not unique. The relation between the representations (B.111) and (B.109) shall be illustrated by the following example:

Example B.5. *Consider the following second order polynomials in two variables:*

$$g_1(\boldsymbol{x}) = 2x_1 + 4x_2 - 2x_1x_2 + 10, \tag{B.113}$$

$$g_2(\boldsymbol{x}) = x_1^2 + 8x_1 + x_1 \cdot x_2 + 2 \cdot x_2^2 + 20. \tag{B.114}$$

In order to represent these polynomials according to (B.109)*, the monomial vector $\boldsymbol{w}(\boldsymbol{x})$ of all monomials up to the degree $2d = 2$ in $n = 2$ variables has to be determined first. The number of all monomials follows from the combinatorial problem of drawing $m = 2d$ "balls" from a urn (with replacement), which contains $l = n+1$ "balls" $\{1, x_1, x_2\}$. Since the order does not matter, the number of monomials is given by $l_w = \binom{l+m-1}{m} = \binom{n+2d}{2d} = 6$. The monomial vector is given by*

$$\boldsymbol{w}(\boldsymbol{x})^T = \begin{bmatrix} x_1 & x_2 & x_1 \cdot x_2 & x_1^2 & x_2^2 & 1 \end{bmatrix}. \tag{B.115}$$

The linear representation $\boldsymbol{c}^T\boldsymbol{w}(\boldsymbol{x})$ with $\boldsymbol{c}^T = \begin{bmatrix} c_1 & c_2 & c_3 & c_4 & c_5 & c_6 \end{bmatrix}$ is generally given by

$$\boldsymbol{c}^T \boldsymbol{w}(\boldsymbol{x}) = c_1 \cdot x_1 + c_2 \cdot x_2 + c_3 \cdot x_1x_2 + c_4 \cdot x_1^2 + c_5 \cdot x_2^2 + c_6. \tag{B.116}$$

A factor comparison of (B.116) *with the polynomials* $g_1(\boldsymbol{x})$ *and* $g_2(\boldsymbol{x})$ *leads to the following vector representations*

$$g_1(\boldsymbol{x}) = \boldsymbol{c}_1^T \cdot \boldsymbol{w}(\boldsymbol{x}) = \begin{bmatrix} 2 & 4 & -2 & 0 & 0 & 10 \end{bmatrix} \cdot \boldsymbol{w}(\boldsymbol{x}), \tag{B.117}$$

$$g_2(\boldsymbol{x}) = \boldsymbol{c}_2^T \cdot \boldsymbol{w}(\boldsymbol{x}) = \begin{bmatrix} 8 & 0 & 1 & 1 & 2 & 20 \end{bmatrix} \cdot \boldsymbol{w}(\boldsymbol{x}). \tag{B.118}$$

For a Gram matrix representation of the polynomials $g_1(\boldsymbol{x})$ *and* $g_2(\boldsymbol{x})$ *according to* (B.111)*, the monomial vector* $\boldsymbol{v}(\boldsymbol{x})$ *of all monomials up to the degree* $d = 1$ *in* $n = 2$ *variables has to be determined. It is given by*

$$\boldsymbol{v}(\boldsymbol{x})^T = \begin{bmatrix} x_1 & x_2 & 1 \end{bmatrix}. \tag{B.119}$$

The symmetric matrix $\boldsymbol{Q} \in \mathbb{S}^3$ *is generally denoted as*

$$\boldsymbol{Q} = \begin{bmatrix} q_{11} & q_{12} & q_{13} \\ q_{12} & q_{22} & q_{23} \\ q_{13} & q_{23} & q_{33} \end{bmatrix}. \tag{B.120}$$

Thus, $\boldsymbol{v}(\boldsymbol{x})^T \boldsymbol{Q} \boldsymbol{v}(\boldsymbol{x})$ *generally evaluates to*

$$\boldsymbol{v}(\boldsymbol{x})^T \boldsymbol{Q} \boldsymbol{v}(\boldsymbol{x}) = q_{11} \cdot x_1^2 + q_{22} \cdot x_2^2 + q_{33} + 2q_{13} \cdot x_1 + 2q_{23} \cdot x_2 + 2q_{12} \cdot x_1 x_2. \tag{B.121}$$

A factor comparison between (B.121) *and the polynomials* $g_1(\boldsymbol{x})$ *and* $g_2(\boldsymbol{x})$ *yields*

$$g_1(\boldsymbol{x}) = \boldsymbol{v}(\boldsymbol{x})^T \boldsymbol{Q}_1 \boldsymbol{v}(\boldsymbol{x}) = \frac{1}{2} \boldsymbol{v}(\boldsymbol{x})^T \begin{bmatrix} 0 & -2 & 2 \\ -2 & 0 & 4 \\ 2 & 4 & 2 \cdot 10 \end{bmatrix} \boldsymbol{v}(\boldsymbol{x}), \tag{B.122}$$

$$g_2(\boldsymbol{x}) = \boldsymbol{v}(\boldsymbol{x})^T \boldsymbol{Q}_2 \boldsymbol{v}(\boldsymbol{x}) = \frac{1}{2} \boldsymbol{v}(\boldsymbol{x})^T \begin{bmatrix} 2 \cdot 1 & 1 & 8 \\ 1 & 2 \cdot 2 & 0 \\ 8 & 0 & 2 \cdot 20 \end{bmatrix} \boldsymbol{v}(\boldsymbol{x}). \tag{B.123}$$

The general relation between the gram matrix representation (B.121) *and the vector representation* (B.116) *follows from factor comparison and yields the linear system of equations*

$$\begin{bmatrix} q_{11} \\ q_{12} \\ q_{13} \\ q_{22} \\ q_{23} \\ q_{33} \end{bmatrix} = \underbrace{\begin{bmatrix} 0 & 0 & 0 & 1 & 0 & 0 \\ 0 & 0 & \frac{1}{2} & 0 & 0 & 0 \\ \frac{1}{2} & 0 & 0 & 0 & 0 & 0 \\ 0 & 0 & 0 & 0 & 1 & 0 \\ 0 & \frac{1}{2} & 0 & 0 & 0 & 0 \\ 0 & 0 & 0 & 0 & 0 & 1 \end{bmatrix}}_{\boldsymbol{M}} \cdot \begin{bmatrix} c_1 \\ c_2 \\ c_3 \\ c_4 \\ c_5 \\ c_6 \end{bmatrix}. \tag{B.124}$$

A polynomial $g(\boldsymbol{x})$ of degree $2d$ (or less) in n variables is called SOS, if it may be decomposed according to:

$$g(\boldsymbol{x}) = \sum_i f_i^2(\boldsymbol{x}), \tag{B.125}$$

where $\deg f_i(\boldsymbol{x}) \leq d$. Obviously, if a polynomial is SOS, then it is positive semidefinite, i.e. $g(\boldsymbol{x}) \geq 0 \; \forall \boldsymbol{x} \in \mathbb{R}^n$. Furthermore, it has been shown in [31] that a polynomial is SOS if and only if there exists a Gram matrix representation (B.111) with a positive definite matrix $\boldsymbol{Q} \in \mathbb{S}_+^{l_v}$.

Throughout this thesis, the set of all SOS polynomials involving the variable $\boldsymbol{x}$ is denoted as $\Sigma(\boldsymbol{x})$.

B.3 Linear Matrix Inequalities and Semi-definite Programs

This section summarizes important facts about LMIs and about SDPs. For a thorough introduction, the reader is referred to [17] or [18].

B.3.1 Linear Matrix Inequalities

Given symmetric matrices $\boldsymbol{F}_i \in \mathbb{S}^n, i = 0, \ldots, q$ and decision variables $\boldsymbol{y} \in \mathbb{R}^q$, a strict LMI is defined as the linear combination

$$\boldsymbol{F}(\boldsymbol{y}) \triangleq \boldsymbol{F}_0 + \sum_{i=1}^{q} y_i \boldsymbol{F}_i > 0. \tag{B.126}$$

The inequality sign is used to indicate that the decision variables $\boldsymbol{y}^T = \begin{bmatrix} y_1 & \ldots & y_q \end{bmatrix}$ should be determined such that $\boldsymbol{F}(\boldsymbol{y})$ is positive definite, i.e. such that $\boldsymbol{x}^T \boldsymbol{F}(\boldsymbol{y}) \boldsymbol{x} > 0 \; \forall \, \boldsymbol{x} \in \mathbb{R}^n$. A non-strict LMI is defined similarly as $\boldsymbol{F}(\boldsymbol{y}) \geq 0$. The expression

$$\bar{\boldsymbol{F}}(\boldsymbol{y}) \triangleq \boldsymbol{F}_0 + \sum_{i=1}^{q} y_i \boldsymbol{F}_i < 0, \tag{B.127}$$

also represents a LMI, where the decision variables $\boldsymbol{y}$ are to be determined such that $\bar{\boldsymbol{F}}(\boldsymbol{y})$ is negative definite. Since any negative definite matrix may be turned into a positive definite matrix by $\boldsymbol{F}(\boldsymbol{y}) = -\bar{\boldsymbol{F}}(\boldsymbol{y})$, the case of negative definiteness does not require any further attention. For the solution of LMIs, powerful solvers like SeDuMi [163] or SDPT3 [166] are available.

In practice, LMIs do usually not arise in the form (B.126), but rather as

$$\begin{aligned} \boldsymbol{A}_M^T \boldsymbol{P}(\boldsymbol{y}) + \boldsymbol{P}(\boldsymbol{y}) \boldsymbol{A}_M < 0, \\ \boldsymbol{P}(\boldsymbol{y}) > 0, \end{aligned} \tag{B.128}$$

where $\boldsymbol{A}_M \in \mathbb{R}^{n \times n}$ is a given matrix and where $\boldsymbol{P} : \mathbb{R}^q \to \mathbb{S}^n$ is a matrix representation of the decision variables $\boldsymbol{y}$:

$$\boldsymbol{P}(\boldsymbol{y}) = \begin{bmatrix} y_1 & y_2 & \cdots & y_n \\ y_2 & y_{n+1} & \cdots & y_{2n-1} \\ \vdots & & \ddots & \vdots \\ y_n & y_{2n-1} & \cdots & y_q \end{bmatrix}. \tag{B.129}$$

Since the system of LMIs (B.128) is linear in the decision variables $\boldsymbol{y}$, it may transformed to the form (B.126). For that, the set of LMIs is first stacked into a single LMI:

$$\begin{bmatrix} -\boldsymbol{A}_M^T \boldsymbol{P}(\boldsymbol{y}) - \boldsymbol{P}(\boldsymbol{y}) \boldsymbol{A}_M & \boldsymbol{0}^{n\times n} \\ \boldsymbol{0}^{n\times n} & \boldsymbol{P}(\boldsymbol{y}) \end{bmatrix} > 0. \tag{B.130}$$

Stacking of LMIs is admissible since the eigenvalues of block diagonal matrices are given by the eigenvalues of the individual blocks [23, p. 209]. Afterwards, appropriate matrices $\boldsymbol{F}_i$ are determined by equating (B.130) and (B.126). For the decision variable y_2, the matrix $\boldsymbol{F}_2$ is for example given by

$$\boldsymbol{F}_2 = \begin{bmatrix} -\boldsymbol{A}_M^T \boldsymbol{P}_2 - \boldsymbol{P}_2 \boldsymbol{A}_M & \boldsymbol{0}^{n\times n} \\ \boldsymbol{0}^{n\times n} & \boldsymbol{P}_2 \end{bmatrix}, \text{ with } \boldsymbol{P}_2 = \begin{bmatrix} 0 & 1 & \dots & 0 \\ 1 & 0 & \dots & 0 \\ \vdots & & \ddots & \vdots \\ 0 & 0 & \dots & 0 \end{bmatrix}. \tag{B.131}$$

Since these transformations are cumbersome, one may resort to modeling languages such as YALMIP [108], which perform these transformations in an automated way.

Since the decision variables are usually clear from the context, the explicit notation of the dependence of $\boldsymbol{F}(\boldsymbol{y})$ or $\boldsymbol{P}(\boldsymbol{y})$ on the decision variables $\boldsymbol{y}$ will be dropped in order to improve readability.

LMIs arise naturally in the stability analysis of linear systems as shown in the next example.

Example B.6. *Consider the LTI system*

$$\dot{\boldsymbol{x}}_P(t) = \boldsymbol{A}_M \cdot \boldsymbol{x}_P(t), \tag{B.132}$$

where $\boldsymbol{A}_M \in \mathbb{R}^{n\times n}$ is Hurwitz. To analyze the stability of the system (B.132)*, consider the Lyapunov function candidate*

$$V(t) = \boldsymbol{x}_P(t)^T \boldsymbol{P} \cdot \boldsymbol{x}_P(t). \tag{B.133}$$

with $\boldsymbol{P} \in \mathbb{S}^n$. The derivative along the trajectories is given by

$$\dot{V}(t) = \boldsymbol{x}_P(t)^T \left(\boldsymbol{A}_M^T \boldsymbol{P} + \boldsymbol{P} \boldsymbol{A}_M \right) \boldsymbol{x}_P(t). \tag{B.134}$$

In order to satisfy the conditions for asymptotic stability of the Lyapunov Theorem C.2, the Lyapunov function candidate has to be positive definite, which is equivalent to requiring $\boldsymbol{P} > 0$. Furthermore, the derivative of the Lyapunov function candidate should be negative definite, which is equivalent to requiring $\boldsymbol{A}_M^T \boldsymbol{P} + \boldsymbol{P} \boldsymbol{A}_M < 0$. Hence, if there exists a solution $\boldsymbol{P} \in \mathbb{S}^n$ to the LMI

$$\begin{aligned} \boldsymbol{A}_M^T \boldsymbol{P} + \boldsymbol{P} \boldsymbol{A}_M &< 0, \\ \boldsymbol{P} &> 0, \end{aligned} \tag{B.135}$$

then the system (B.132) *is asymptotically stable. Eq.* (B.135) *is the LMI analog of the Lyapunov equation* (3.31) *and may be readily solved using any LMI solver.*

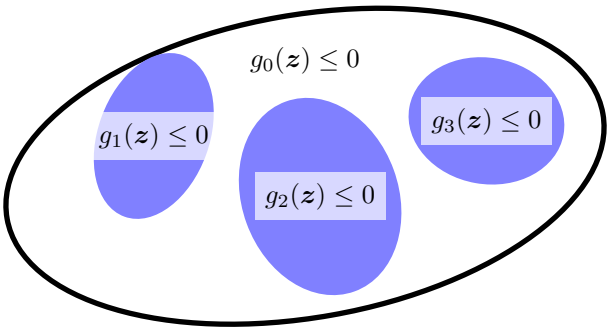

Figure B.3: Illustration of the S-Procedure: If $g_0(\boldsymbol{z}) \leq \sum_{i=1}^{3} \lambda_i g_i(\boldsymbol{z})$ holds for some $\lambda_i > 0$, then $g_0(\boldsymbol{z})$ is negative for all points, where $g_i(\boldsymbol{z}) \leq 0$ hold. Hence, these points are within the set $\mathcal{G}_0 = \{\boldsymbol{z} \mid g_0(\boldsymbol{z}) \leq 0\}$.

Another area, which gives rise to LMIs, are geometric problems involving ellipsoids [18]. Before being able to analyze these problems, an important interim result is required:

Lemma B.7 (The S-Procedure)**.** *Let* $g_0(\boldsymbol{z}) = \boldsymbol{z}^T \boldsymbol{G}_0 \boldsymbol{z},\ \boldsymbol{G}_0 \in \mathbb{S}^n$ *and* $g_i(\boldsymbol{z}) = \boldsymbol{z}^T \boldsymbol{G}_i \boldsymbol{z},\ \boldsymbol{G}_i \in \mathbb{S}^n,\ i = 1, \ldots, p$ *be quadratic forms in the variable* $\boldsymbol{z} \in \mathbb{R}^n$*. The negativity of* $g_i(\boldsymbol{z}),\ i = 1, ..., p$ *on the sublevel set* $\mathcal{G} = \{\boldsymbol{z} \mid g_i(\boldsymbol{z}) \leq 0,\ i = 1, \ldots, p\}$ *implies negativity of* $g_0(\boldsymbol{z})$ *on* $\mathcal{G}$*, if there exist non-negative multipliers* $\lambda_i \geq 0,\ i = 1, \ldots, p$*, such that*

$$\boldsymbol{G}_0 - \sum_{i=1}^{p} \lambda_i \boldsymbol{G}_i \leq 0. \tag{B.136}$$

holds.

Proof. The proof may for example be found in [17]. □

The S-Procedure is commonly used to show set containment. Let $p = 1$ and let $\mathcal{G}_0 = \{\boldsymbol{z} \mid g_0(\boldsymbol{z}) \leq 0\}$, $\mathcal{G}_1 = \{\boldsymbol{z} \mid g_1(\boldsymbol{z}) \leq 0\}$ be two sets. $\mathcal{G}_1 \subseteq \mathcal{G}_0$ holds, if the negativity of $g_1(\boldsymbol{z})$ implies negativity of $g_0(\boldsymbol{z})$ (see Figure B.3). By virtue of the S-Procedure, the implication is true if there exists a non-negative multiplier λ, such that $\boldsymbol{G}_0 - \lambda \boldsymbol{G}_1 \leq 0$ holds. Note that for $p = 1$, this condition is necessary and sufficient [18].

The use and the interpretation of the S-Procedure may be shown best with the help of an example:

Example B.8. *Consider the ellipse*

$$\mathcal{M}_c = \{x_1, x_2 \mid \begin{bmatrix} x_1 & x_2 \end{bmatrix} \cdot \begin{bmatrix} 0.25 & 0 \\ 0 & 1 \end{bmatrix} \cdot \begin{bmatrix} x_1 \\ x_2 \end{bmatrix} \leq c\} \tag{B.137}$$

with $c = 1$ *and the rectangle*

$$|x_1| \leq 1, \qquad |x_2| \leq 0.5. \tag{B.138}$$

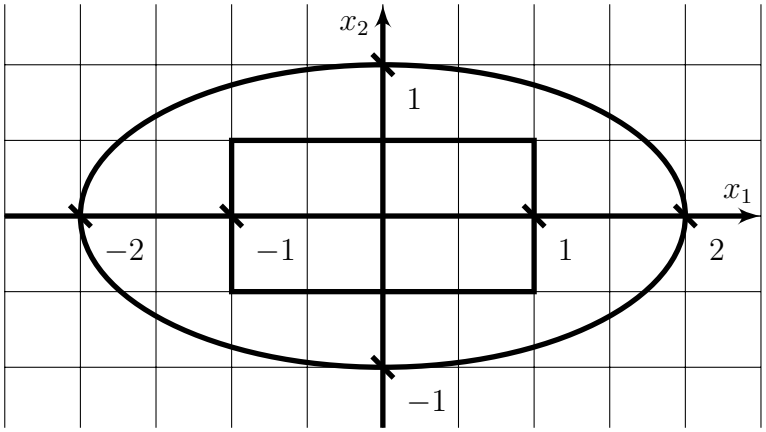

Figure B.4: Illustration of the ellipse and the rectangle from Example B.8.

For $c = 1$*, the principal axes of the ellipse are* $r_1 = 2$ *and* $r_2 = 1$*, which follows from* (B.61)*. The ellipse and the rectangle are shown in Figure B.4. The objective is to check whether the ellipse* (B.137) *surrounds the rectangle* (B.138)*. For this, the ellipse and the rectangle are reformulated to match the structure of the S-Procedure. After defining the vector*

$$\boldsymbol{z}^T \triangleq \begin{bmatrix} x_1 & x_2 & 1 \end{bmatrix} \tag{B.139}$$

the ellipse inequality (B.137) *may be rewritten as*

$$g_0(\boldsymbol{z}) = \boldsymbol{z}^T \underbrace{\begin{bmatrix} 0.25 & 0 & 0 \\ 0 & 1 & 0 \\ 0 & 0 & -c \end{bmatrix}}_{\boldsymbol{G}_0} \boldsymbol{z} \leq 0. \tag{B.140}$$

Similarly, the rectangle inequalities are rewritten as

$$g_1(\boldsymbol{z}) = \boldsymbol{z}^T \underbrace{\begin{bmatrix} 1 & 0 & 0 \\ 0 & 0 & 0 \\ 0 & 0 & -1 \end{bmatrix}}_{\boldsymbol{G}_1} \boldsymbol{z} \leq 0, \qquad g_2(\boldsymbol{z}) = \boldsymbol{z}^T \underbrace{\begin{bmatrix} 0 & 0 & 0 \\ 0 & 1 & 0 \\ 0 & 0 & -(0.5^2) \end{bmatrix}}_{\boldsymbol{G}_2} \boldsymbol{z} \leq 0. \tag{B.141}$$

A point lies within the rectangle, if it simultaneously satisfies $g_1(\boldsymbol{z}) \leq 0$ *and* $g_2(\boldsymbol{z}) \leq 0$*. If for all points within the rectangle,* $g_0(\boldsymbol{z}) \leq 0$ *holds as well, then the rectangle lies within the ellipse. In order to show that* $g_0(\boldsymbol{z}) \leq 0$ *holds, if* $g_1(\boldsymbol{z}) \leq 0$ *and* $g_2(\boldsymbol{z}) \leq 0$ *hold, it suffices to show the relation*

$$g_0(\boldsymbol{z}) \leq \lambda_1 \cdot g_1(\boldsymbol{z}) + \lambda_2 \cdot g_2(\boldsymbol{z}) \quad \forall\, \boldsymbol{z}, \tag{B.142}$$

where λ_1 *and* λ_2 *are some positive constants. The inequality* (B.142) *ensures that when* $g_1(\boldsymbol{z}) \leq 0$ *and* $g_2(\boldsymbol{z}) \leq 0$ *hold,* $g_0(\boldsymbol{z}) \leq 0$ *holds as well. Bringing all terms to the left hand side yields*

$$g_0(\boldsymbol{z}) - \lambda_1 \cdot g_1(\boldsymbol{z}) - \lambda_2 \cdot g_2(\boldsymbol{z}) \leq 0 \quad \forall\, \boldsymbol{z}. \tag{B.143}$$

Clearly, (B.143) *formulates a requirement on the negative definiteness of a function. Since* $g_0(\boldsymbol{z})$*,* $g_1(\boldsymbol{z})$ *and* $g_2(\boldsymbol{z})$ *are quadratic forms, the negative definiteness of* (B.143) *may be checked by the LMI*

$$\begin{aligned} \boldsymbol{G}_0 - \lambda_1 \cdot \boldsymbol{G}_1 - \lambda_2 \cdot \boldsymbol{G}_2 &\leq 0, \\ \lambda_1 &> 0, \\ \lambda_2 &> 0, \end{aligned} \tag{B.144}$$

where λ_1 *and* λ_2 *are the decision variables. Notice that the LMI* (B.144) *exactly corresponds to the central requirement of the S-Procedure Lemma B.7.*

Since the LMI has the solution $\lambda_1 = 0.40$*,* $\lambda_2 = 2.10$*, the rectangle lies within the ellipse, which is confirmed by Figure B.4. Conversely, for the* $c = 0.25$*, the ellipse lies within the rectangle since its principal axes become* $r_1 = 1$ *and* $r_2 = 0.5$*. In this case, the corresponding LMI is not feasible, i.e. it has no solution.*

B.3.2 Semidefinite Programs

The LMI problems of the previous two examples are commonly referred to as *feasibility problems*, since one is only interested in the existence of some solution $\boldsymbol{y}$. In case of the ellipse example from Example B.8, the computation of the smallest ellipse, which surrounds the rectangle might for example be of interest. That is, the level set constant c should be minimized. Such an optimization problem involving LMI constraints is referred to as Semidefinite Program (SDP). In general, a SDP is defined as [18]:

$$\min_{\boldsymbol{y}} \boldsymbol{c}^T \boldsymbol{y} \quad \text{s.t.} \tag{B.145}$$

$$\boldsymbol{F}_0 + \sum_{i=1}^{q} y_i \boldsymbol{F}_i < 0, \tag{B.146}$$

$$\boldsymbol{A} \cdot \boldsymbol{y} = \boldsymbol{b}. \tag{B.147}$$

A SDP aims at the minimization of the linear objective function (B.145) subject to LMI constraints (B.146) and equality constraints (B.147). For the solution of SDPs, the same powerful solvers like SeDuMi [163] or SDPT3 [166] may be used.

Now, let's return to the ellipse example:

Example B.9. *Consider the ellipse and the rectangle from Example B.8. Using a SDP, the smallest level set constant* c *of the ellipse shall be computed such that the rectangle does still lie within the ellipsoid. Obviously,* c *now is a decision variable instead of a fixed constant. In order to stress this fact, the matrix* $\boldsymbol{G}_0$ *from* (B.140)*, which defines the ellipse, is now written as* $\boldsymbol{G}_0(c)$*. Nevertheless, the containment of the rectangle within the ellipse is still ensured by the LMI* (B.144)*. Hence, the smallest level set constant*

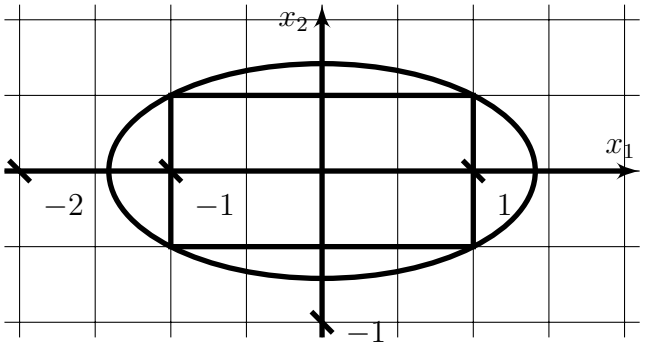

Figure B.5: Illustration of the optimized ellipse and the rectangle from Example B.9.

results from the SDP

$$\begin{aligned} &\min_{c,\lambda_1,\lambda_2} c \quad \textit{s.t.} \\ &\boldsymbol{G}_0(c) - \lambda_1 \cdot \boldsymbol{G}_1 - \lambda_2 \cdot \boldsymbol{G}_2 \leq 0, \\ &c \geq 0, \qquad \lambda_1 > 0, \qquad \lambda_2 > 0. \end{aligned} \tag{B.148}$$

Solving the SDP with some LMI solver yields $\lambda_1 = 0.25$*,* $\lambda_2 = 1$ *and* $c = 0.5$*. The principal axes of the optimized ellipse are hence given by* $r_1 = \sqrt{2}$ *and* $r_2 = 1/\sqrt{2}$*. The optimized ellipse and the rectangle are shown in Figure B.5. Clearly, the computed level set constant* c *leads to the smallest ellipse surrounding the rectangle* (B.138)*.*

Remark B.10. *In case of the simple ellipse from Example B.8, the problem of determining the smallest level set constant* c *could have been solved more easily by simply inserting all vertices of the rectangle into the ellipse equation and choosing the largest of the resulting* c*'s. However, by using the systematic formulation as a SDP, more complex tasks may also be solved.*

B.3.3 Sum-Of-Squares Programming

In Section B.2.3, SOS polynomials have been introduced. There, it has been outlined that the problem of verifying that a given polynomial with representation (B.109) is SOS may be reduced to a LMI constraint $\boldsymbol{Q} \geq 0$ and a system of linear equations. The system of linear equations relates the coefficients $\boldsymbol{Q}$ of the Gram representation (B.111) to the coefficients of the vector representation (B.109).

If furthermore a linear combination of the entries of the decision variable $\boldsymbol{Q}$ is to be minimized, the resulting optimization problem is called a SOS program. Since positive semi-definiteness may be expressed in terms of a LMI and an equality constraint, a SOS program reduces to a SDP, for which powerful solvers like SDPT3 [166] are available. To ease the process of posing such optimization problems, modeling languages like YALMIP [109] may be used.

The S-Procedure (Lemma B.7) is often used to show set containment, when the sets are defined as sublevel sets of quadratic forms. If the sets are defined as sublevel sets of SOS polynomials, the Polynomial S-Procedure [151] extends the S-Procedure. It may be stated as follows:

Lemma B.11 (The Polynomial S-Procedure)**.** *Let $g_0(\boldsymbol{x})$ and $g_i(\boldsymbol{x}),\ i = 1, \ldots, p$ with $\boldsymbol{x} \in \mathbb{R}^n$ be given polynomials. The negative semi-definiteness of $g_i(\boldsymbol{x})$ on the sublevel set $\mathcal{G} = \{\boldsymbol{x} \mid g_i(\boldsymbol{x}) \leq 0, i = 1, \ldots, p\}$ implies negative semi-definiteness of $g_0(\boldsymbol{x})$ on $\mathcal{G}$, if there exist multipliers $\lambda_i(\boldsymbol{x}) \in \Sigma(\boldsymbol{x})$, such that*

$$-g_0(\boldsymbol{x}) + \sum_{i=1}^{q} \lambda_i(\boldsymbol{x}) \cdot g_i(\boldsymbol{x}) \in \Sigma(\boldsymbol{x}) \tag{B.149}$$

holds.

Proof. If (B.149) is true, then $g_0(\boldsymbol{x}) \leq \sum_{i=1}^{p} \lambda_i(\boldsymbol{x}) \cdot g_i(\boldsymbol{x})$ is satisfied as well. By definition, $\sum_{i=1}^{p} \lambda_i(\boldsymbol{x}) \cdot g_i(\boldsymbol{x}) \leq 0\ \forall \boldsymbol{x} \in \mathcal{G}$ holds and hence, $g_0(\boldsymbol{x}) \leq 0\ \forall \boldsymbol{x} \in \mathcal{G}$. □

B.4 Matrix Facts

This section collects some important facts about matrices which are used throughout this thesis.

B.4.1 Traces

Throughout the proofs of stability of adaptive control, one often encounters the *trace* function. Subsequently, some important facts about the *trace* are collected.

The *trace* of a square matrix $\boldsymbol{A} \in \mathbb{C}^{n \times n}$ is defined as the sum of the elements on the diagonal:

$$\mathrm{Tr}\ \boldsymbol{A} = \mathrm{Tr} \begin{bmatrix} a_{11} & \ldots & a_{1n} \\ \vdots & \ddots & \vdots \\ a_{n1} & \ldots & a_{nn} \end{bmatrix} \triangleq \sum_{i=1}^{n} a_{ii}. \tag{B.150}$$

Since the transpose of a matrix does not alter the elements on the diagonal, the matrix $\boldsymbol{A}$ and its transpose have the same *trace*, i.e.

$$\mathrm{Tr}\ \boldsymbol{A} = \mathrm{Tr}\ \boldsymbol{A}^H. \tag{B.151}$$

As an immediate consequence of its definition, the *trace* is linear, i.e.

$$\mathrm{Tr}\ \{\boldsymbol{A} + \boldsymbol{B}\} = \mathrm{Tr}\ \boldsymbol{A} + \mathrm{Tr}\ \boldsymbol{B}, \tag{B.152}$$

$$\mathrm{Tr}\ \{c \cdot \boldsymbol{A}\} = c \cdot \mathrm{Tr}\ \boldsymbol{A}, \tag{B.153}$$

where $\boldsymbol{B} \in \mathbb{C}^{n \times n}$ is another square matrix of compatible dimension and $c \in \mathbb{C}$ is a scalar.

Now, let $\boldsymbol{A} \in \mathbb{C}^{n\times m}$, $\boldsymbol{B} \in \mathbb{C}^{m\times p}$ and $\boldsymbol{C} \in \mathbb{C}^{p\times n}$ be three matrices such that $\boldsymbol{ABC}$ is square. In this case, the *trace* satisfies the cyclic property:

$$\mathrm{Tr}\,\{\boldsymbol{ABC}\} = \mathrm{Tr}\,\{\boldsymbol{CAB}\}. \tag{B.154}$$

Due to the cyclic property, the trace is invariant under similarity transformations

$$\mathrm{Tr}\left\{\boldsymbol{T}^{-1}\boldsymbol{AT}\right\} = \mathrm{Tr}\left\{\boldsymbol{TT}^{-1}\boldsymbol{A}\right\} = \mathrm{Tr}\,\boldsymbol{A}, \tag{B.155}$$

where $\boldsymbol{T} \in \mathbb{C}^{n\times n}$ is a non-singular matrix. If $\boldsymbol{T}$ is unitary, i.e. $\boldsymbol{T}^{-1} = \boldsymbol{T}^H$, the latter implies $\mathrm{Tr}\left\{\boldsymbol{T}^H\boldsymbol{AT}\right\} = \mathrm{Tr}\,\boldsymbol{A}$. Furthermore, it may be readily shown using the cyclic property (B.154) that the scalar product of two vectors $\boldsymbol{a} \in \mathbb{C}^n$, $\boldsymbol{b} \in \mathbb{C}^n$ may be expressed as the trace of a dyadic product

$$\langle \boldsymbol{a}, \boldsymbol{b}\rangle = \boldsymbol{a}^H\boldsymbol{b} = \mathrm{Tr}\left\{\boldsymbol{a}^H\boldsymbol{b}\right\} = \mathrm{Tr}\left\{\boldsymbol{ba}^H\right\}. \tag{B.156}$$

More generally, the cyclic property allows representing the sum of scalar products of vectors $\boldsymbol{a}_k \in \mathbb{C}^n$, $\boldsymbol{b}_k \in \mathbb{C}^n$ as the *trace* of a matrix product

$$\sum_{k=1}^{m} \boldsymbol{a}_k^H\boldsymbol{b}_k = \sum_{k=1}^{m} \mathrm{Tr}\left\{\boldsymbol{b}_k\boldsymbol{a}_k^H\right\} = \mathrm{Tr}\left\{\sum_{k=1}^{m} \boldsymbol{b}_k\boldsymbol{a}_k^H\right\} = \mathrm{Tr}\left\{\boldsymbol{BA}^H\right\}, \tag{B.157}$$

where the fact has been used that a matrix product may be written as a sum of dyadic products:

$$\boldsymbol{BA}^H = \begin{bmatrix}\boldsymbol{b}_1 & \dots & \boldsymbol{b}_m\end{bmatrix} \cdot \begin{bmatrix}\boldsymbol{a}_1^H \\ \vdots \\ \boldsymbol{a}_m^H\end{bmatrix} = \sum_{k=1}^{m} \boldsymbol{b}_k\boldsymbol{a}_k^H. \tag{B.158}$$

B.4.2 Symmetric Matrices

This section summarizes some important facts about symmetric (positive or negative (semi-) definite) matrices $\boldsymbol{A} \in \mathbb{R}^{n\times n}$ with $\boldsymbol{A} = \boldsymbol{A}^T$.

Properties of Symmetric Matrices

If $\boldsymbol{A}$ and $\boldsymbol{B}$ are symmetric, their sum is symmetric as well, since

$$\boldsymbol{A} + \boldsymbol{B} = \boldsymbol{A}^T + \boldsymbol{B}^T = (\boldsymbol{A} + \boldsymbol{B})^T \tag{B.159}$$

holds. Furthermore, multiplying symmetric matrices with some scalar $\alpha \in \mathbb{R}$ retains symmetry. These two observations are central in proving that the set of symmetric matrices $\mathbb{S}^n \subset \mathbb{R}^{n\times n}$ forms a vector space with the conventional matrix addition and the conventional multiplication of matrices by a scalar [45].

Unlike the sum, the product of two symmetric matrices $\boldsymbol{A} \in \mathbb{S}^n$ and $\boldsymbol{B} \in \mathbb{S}^n$ is not necessarily symmetric. Consider for example

$$\boldsymbol{A} = \begin{bmatrix}1 & 1\\ 1 & 1\end{bmatrix}, \quad \boldsymbol{B} = \begin{bmatrix}1 & 1\\ 1 & 2\end{bmatrix}, \quad \boldsymbol{A}\cdot\boldsymbol{B} = \begin{bmatrix}2 & 3\\ 2 & 3\end{bmatrix}. \tag{B.160}$$

Clearly, the product $\boldsymbol{A} \cdot \boldsymbol{B}$ is not symmetric even though $\boldsymbol{A}$ and $\boldsymbol{B}$ are symmetric. In fact, the product is symmetric, if and only if the matrices $\boldsymbol{A}$ and $\boldsymbol{B}$ commute, i.e. $\boldsymbol{A} \cdot \boldsymbol{B} = \boldsymbol{B} \cdot \boldsymbol{A}$. In the latter case, one has

$$(\boldsymbol{A} \cdot \boldsymbol{B})^T = \boldsymbol{B}^T \cdot \boldsymbol{A}^T = \boldsymbol{B} \cdot \boldsymbol{A} = \boldsymbol{A} \cdot \boldsymbol{B}, \tag{B.161}$$

which satisfies the definition of symmetry.

If a symmetric matrix $\boldsymbol{A} \in \mathbb{S}^n$ is invertible, then its inverse $\boldsymbol{A}^{-1}$ is symmetric as well since

$$\left(\boldsymbol{A}^{-1}\right)^T = \left(\boldsymbol{A}^T\right)^{-1} = \boldsymbol{A}^{-1} \tag{B.162}$$

holds [185, p. 586].

For any symmetric matrix $\boldsymbol{A} \in \mathbb{S}^n$, the eigenvalues will be real [23, p. 228] and there exists an orthonormal set of eigenvectors forming a basis $\boldsymbol{Q} \in \mathbb{R}^{n \times n}$ of $\mathbb{R}^n$. Thus, $\boldsymbol{A}$ may be diagonalized by

$$\boldsymbol{A} = \boldsymbol{Q}\boldsymbol{D}\boldsymbol{Q}^T, \tag{B.163}$$

where $\boldsymbol{D} = \operatorname{diag}\begin{bmatrix}\lambda_1(\boldsymbol{A}) & \dots & \lambda_n(\boldsymbol{A})\end{bmatrix}$ is a diagonal matrix containing the eigenvalues of $\boldsymbol{A}$ [85], [23, p. 230].

Properties of Positive or Negative (Semi-) Definite Symmetric Matrices

If $\boldsymbol{A}$ and $\boldsymbol{B}$ are symmetric and positive or negative (semi-) definite, then their sum is symmetric and positive or negative (semi-) definite as well. This is an immediate consequence of the definition of positive or negative (semi-) definiteness in (B.54)-(B.57):

$$\boldsymbol{x}^T (\boldsymbol{A} + \boldsymbol{B})\, \boldsymbol{x} = \boldsymbol{x}^T \boldsymbol{A}\boldsymbol{x} + \boldsymbol{x}^T \boldsymbol{B}\boldsymbol{x}. \tag{B.164}$$

If the quadratic forms $\boldsymbol{x}^T\boldsymbol{A}\boldsymbol{x}$ and $\boldsymbol{x}^T\boldsymbol{B}\boldsymbol{x}$ are positive or negative (semi-) definite, their sum will also be positive or negative (semi-) definite. Hence, $\boldsymbol{A} + \boldsymbol{B}$ is positive or negative (semi-) definite as well. Furthermore, multiplying positive or negative (semi-) definite matrices with some positive scalar $\alpha \in \mathbb{R}_{++}$ retains positive or negative (semi-) definiteness. Unlike $\mathbb{S}^n$, the subsets $\mathbb{S}^n_{++} \subset \mathbb{S}^n$, $\mathbb{S}^n_{--} \subset \mathbb{S}^n$, $\mathbb{S}^n_{+} \subset \mathbb{S}^n$ and $\mathbb{S}^n_{-} \subset \mathbb{S}^n$ are *no* vector spaces since they are for example lacking an inverse element.

Since the product of symmetric matrices is not necessarily symmetric, the product of symmetric, positive or negative (semi-) definite is not necessarily symmetric, positive or negative (semi-) definite, either.

If the matrix $\boldsymbol{A}$ is positive (or negative) definite (i.e. $\boldsymbol{A} \in \mathbb{S}^n_{++}$ or $\boldsymbol{A} \in \mathbb{S}^n_{--}$), then it is invertible since all eigenvalues of positive (or negative) definite matrices are different from zero (see Section B.2.1). Furthermore, its inverse is positive (or negative) definite as well since

1. the inverse of a symmetric matrix is symmetric (see (B.162));
2. any eigenvalue $\lambda_i = \lambda_i(\boldsymbol{A})$ satisfies

$$\boldsymbol{A} \cdot \boldsymbol{v} = \lambda_i \cdot \boldsymbol{v}, \tag{B.165}$$

which implies that λ_i^{-1} is an eigenvalue of $\boldsymbol{A}^{-1}$ since $\boldsymbol{A}^{-1} \cdot \boldsymbol{v} = \lambda_i^{-1} \cdot \boldsymbol{v}$ follows from (B.165). Hence, $\lambda_i > 0 \; \forall \; i$ implies $\lambda_i^{-1} > 0 \; \forall \; i$ (or $\lambda_i < 0 \; \forall \; i$ implies $\lambda_i^{-1} < 0 \; \forall \; i$ in case of negative definite matrices).

Consider a symmetric, positive definite matrix $\boldsymbol{A} \in \mathbb{S}_{++}^n$. As $\boldsymbol{A}$ is symmetric, it admits the decomposition (B.163). Since $\boldsymbol{A}$ is positive definite, the diagonal matrix $\boldsymbol{D}$ of the decomposition has full rank and only contains positive entries. It does hence possess the matrix square root $\boldsymbol{D} = \boldsymbol{D}^{\frac{1}{2}} \cdot \boldsymbol{D}^{\frac{1}{2}}$. It follows from (B.163) that

$$\boldsymbol{A} = \boldsymbol{Q}\boldsymbol{D}\boldsymbol{Q}^T = \boldsymbol{Q}\boldsymbol{D}^{\frac{1}{2}} \cdot \boldsymbol{D}^{\frac{1}{2}}\boldsymbol{Q}^T = \boldsymbol{Q}\boldsymbol{D}^{\frac{1}{2}}\boldsymbol{Q}^T \cdot \boldsymbol{Q}\boldsymbol{D}^{\frac{1}{2}}\boldsymbol{Q}^T \tag{B.166}$$

holds, since $\boldsymbol{Q}$ is orthonormal. The matrix square root $\boldsymbol{A}^{\frac{1}{2}} \in \mathbb{S}_{++}^n$ satisfying $\boldsymbol{A} = \boldsymbol{A}^{\frac{1}{2}} \cdot \boldsymbol{A}^{\frac{1}{2}}$ is hence given by

$$\boldsymbol{A}^{\frac{1}{2}} = \boldsymbol{Q}\boldsymbol{D}^{\frac{1}{2}}\boldsymbol{Q}^T. \tag{B.167}$$

B.4.3 Singular Value Decomposition

A complex matrix $\boldsymbol{U} \in \mathbb{C}^{n \times n}$ is called unitary if it satisfies [23, p. 199]

$$\boldsymbol{U}^H \cdot \boldsymbol{U} = \boldsymbol{I}, \tag{B.168}$$

which implies $\boldsymbol{U}^H = \boldsymbol{U}^{-1}$. The column vectors of a unitary matrix $\boldsymbol{U}$ define an orthonormal basis of $\mathbb{C}^n$.

Now consider an arbitrary matrix $\boldsymbol{A} \in \mathbb{C}^{l \times m}$ and let $p = \min\{l, m\}$ denote the smaller dimension. Then there exist unitary matrices $\boldsymbol{U} \in \mathbb{C}^{l \times l}$ and $\boldsymbol{V} \in \mathbb{C}^{m \times m}$ such that $\boldsymbol{A}$ may be decomposed into a *Singular Value Decomposition* [45]

$$\boldsymbol{A} = \boldsymbol{U} \cdot \boldsymbol{\Sigma} \cdot \boldsymbol{V}^H, \tag{B.169}$$

where $\boldsymbol{\Sigma} \in \mathbb{R}^{l \times m}$ is real and satisfies

$$\boldsymbol{\Sigma} = \begin{bmatrix} \boldsymbol{\Sigma}_1 \\ \boldsymbol{0}^{(l-m) \times m} \end{bmatrix} \quad \text{if } l \geq m \text{ (i.e. } p = m), \tag{B.170}$$

or

$$\boldsymbol{\Sigma} = \begin{bmatrix} \boldsymbol{\Sigma}_1 & \boldsymbol{0}^{l \times (m-l)} \end{bmatrix} \quad \text{if } l < m \text{ (i.e. } p = l). \tag{B.171}$$

In either case, $\boldsymbol{\Sigma}_1 \in \mathbb{R}^{p \times p}$ is diagonal with

$$\boldsymbol{\Sigma}_1 = \operatorname{diag} \begin{bmatrix} \sigma_1 & \sigma_2 & \dots & \sigma_p \end{bmatrix} \tag{B.172}$$

and

$$\sigma_1 \geq \sigma_2 \geq \ldots \geq \sigma_p \geq 0. \tag{B.173}$$

The scalar values $\sigma_1, \ldots, \sigma_p$ are referred to as the *singular values* of the matrix $\boldsymbol{A}$ and are equivalent to the square roots of the p largest eigenvalues $\lambda_i(\boldsymbol{A}^H\boldsymbol{A})$, i.e.

$$\sigma_i(\boldsymbol{A}) = \sqrt{\lambda_i\left(\boldsymbol{A}^H\boldsymbol{A}\right)}. \tag{B.174}$$

B.4.4 Miscellaneous Relations

This section summarizes various relations, which are used in this thesis.

Block-Diagonal Matrices

Consider the block-diagonal matrix

$$\boldsymbol{A} = \begin{bmatrix} \boldsymbol{B} & \boldsymbol{0} \\ \boldsymbol{0} & \boldsymbol{C} \end{bmatrix}, \tag{B.175}$$

which is composed of the square matrices $\boldsymbol{B} \in \mathbb{C}^{n \times n}$ and $\boldsymbol{C} \in \mathbb{C}^{m \times m}$. The eigenvalues of $\boldsymbol{A}$ are given by the eigenvalues of $\boldsymbol{B}$ and $\boldsymbol{C}$ [23, p. 209]. Furthermore, if $\boldsymbol{B}$ and $\boldsymbol{C}$ are invertible, then the inverse of $\boldsymbol{A}$ is given by

$$\boldsymbol{A}^{-1} = \begin{bmatrix} \boldsymbol{B}^{-1} & \boldsymbol{0} \\ \boldsymbol{0} & \boldsymbol{C}^{-1} \end{bmatrix}. \tag{B.176}$$

This may be verified by computing $\boldsymbol{A} \cdot \boldsymbol{A}^{-1}$.

Searle Identity

Let $\boldsymbol{A} \in \mathbb{C}^{n \times n}$ and $\boldsymbol{B} \in \mathbb{C}^{n \times n}$ be arbitrary square matrices such that the inverses $(\boldsymbol{I} + \boldsymbol{A}\boldsymbol{B})^{-1}$ and $(\boldsymbol{I} + \boldsymbol{B}\boldsymbol{A})^{-1}$ exist. Then, the following relation holds [82, Eq. 20]:

$$(\boldsymbol{I} + \boldsymbol{A}\boldsymbol{B})^{-1}\boldsymbol{A} = \boldsymbol{A}(\boldsymbol{I} + \boldsymbol{B}\boldsymbol{A})^{-1} \tag{B.177}$$

In [129], this identity is called a *Searle Identity*.

Appendix C

Preliminaries of Control Theory

This section summarizes important results from control theory, which will be frequently used throughout this thesis. Section C.1 is devoted to the stability analysis of nonlinear systems using the direct method of Lyapunov. While the direct method of Lyapunov is concerned with the stability of equilibriums, Section C.2 deals with the stability (boundedness) of the input- / output map of nonlinear systems, which leads to the small-gain theorem. Finally, Section C.3 deals with the stability analysis of nonlinear, delayed systems.

C.1 Stability Analysis of Nonlinear Systems

The direct method of Lyapunov constitutes the main tool of this thesis to analyze stability of nonlinear systems. That is to say, conclusions on the boundedness of the solutions of the underlying nonlinear differential equations are drawn without actually solving the differential equations. The following introduction closely follows [96].

The stability analysis following Lyapunov's direct method is concerned with the stability of equilibriums. Consider the autonomous, nonlinear differential equation

$$\dot{\boldsymbol{x}}(t) = \boldsymbol{f}(\boldsymbol{x}(t)), \tag{C.1}$$

where $\boldsymbol{x} : \mathbb{R}_+ \to \mathcal{D}$ is the state vector and $\boldsymbol{f} : \mathcal{D} \to \mathbb{R}^n$ is a nonlinear, locally Lipschitz function. $\mathcal{D}$ denotes a domain in $\mathbb{R}^n$, that is, an open connected set in $\mathbb{R}^n$. In general, it is not known in advance whether the nonlinear differential equation (C.1) possesses a solution at all and whether this solution is unique. Throughout this thesis, the question of existence and uniqueness is however not covered. The reason for this is that once stability has been established using Lyapunov's direct method, existence and uniqueness of solutions is guaranteed as well (see Theorem 3.3 in [96]). A prerequisite for this result is the property of $\boldsymbol{f}(\boldsymbol{x}(t))$ being locally Lipschitz.

An equilibrium is a point $\boldsymbol{x}_0 \in \mathcal{D}$, which satisfies $\boldsymbol{f}(\boldsymbol{x}_0) = \boldsymbol{0}$. Without loss of generality, it will be assumed that the equilibrium lies at the origin of $\mathbb{R}^n$, i.e. $\boldsymbol{x}_0 = \boldsymbol{0}$.

Definition C.1 (Stability of an equilibrium, [96]). *The equilibrium point $\boldsymbol{x}_0 = \mathbf{0}$ of* (C.1) *is*

- *stable if, for each $\epsilon > 0$, there is a $\delta = \delta(\epsilon)$ such that*

$$\|\boldsymbol{x}(0)\| < \delta \quad \Rightarrow \quad \|\boldsymbol{x}(t)\| < \epsilon, \qquad \forall t \geq 0;$$

- *unstable if it is not stable;*
- *asymptotically stable if it is stable and δ can be chosen such that*

$$\|\boldsymbol{x}(0)\| < \delta \quad \Rightarrow \quad \lim_{t\to\infty} \boldsymbol{x}(t) = \mathbf{0}. \tag{C.2}$$

Since the above definition does not readily allow to check the stability of a nonlinear system, one usually resorts to the direct method of Lyapunov:

Theorem C.2 (Lyapunov Theorem for Autonomous Systems, [96]). *Let $\boldsymbol{x} = \mathbf{0}$ be an equilibrium point for* (C.1) *and $\mathcal{D} \subset \mathbb{R}^n$ be a domain containing $\boldsymbol{x} = \mathbf{0}$. Let $V : \mathcal{D} \to \mathbb{R}$ be a continuously differentiable function such that*

$$V(\mathbf{0}) = 0 \quad \textit{and} \quad V(\boldsymbol{x}) > 0 \textit{ in } \mathcal{D}\backslash\mathbf{0}. \tag{C.3}$$

- *If*

$$\dot{V}(\boldsymbol{x}) \leq 0 \textit{ in } \mathcal{D}, \tag{C.4}$$

  then $\boldsymbol{x} = \mathbf{0}$ is stable;
- *If*

$$\dot{V}(\boldsymbol{x}) < 0 \textit{ in } \mathcal{D}\backslash\mathbf{0}, \tag{C.5}$$

  then $\boldsymbol{x} = \mathbf{0}$ is asymptotically stable;
- *If the previous conditions hold on $\mathcal{D} = \mathbb{R}^n$ and $V(\boldsymbol{x})$ is radially unbounded, i.e.*

$$\|\boldsymbol{x}\| \to \infty \quad \Rightarrow \quad V(\boldsymbol{x}) \to \infty, \tag{C.6}$$

  then $\boldsymbol{x} = \mathbf{0}$ is globally stable or globally asymptotically stable, respectively.

Proof. See [96]. □

In case of a globally (asymptotically) stable equilibrium, the system (C.1) is sometimes said to be (asymptotically) stable. Since a system may only possess one globally (asymptotically) stable equilibrium [96], no confusion can arise.

Sometimes, Lyapunov's direct method does not allow to show asymptotic stability (of all states of the considered system). In these cases, the following lemma is useful:

Lemma C.3 (Barbalat's Lemma, [119]). *If $g : \mathbb{R}_+ \to \mathbb{R}$ is uniformly continuous for $t \geq 0$, and if the limit of the integral*

$$\lim_{t\to\infty} \int_0^t |g(\tau)| d\tau \tag{C.7}$$

exists and is finite, then

$$\lim_{t\to\infty} g(t) = 0. \tag{C.8}$$

Proof. See [119]. □

Lyapunov's direct method only considers autonomous systems. While this is sufficient in case of adaptive controllers in case of a nominal plant, non-autonomous systems have to be treated in case of off-nominal plants. A non-autonomous system is defined as

$$\dot{\boldsymbol{x}}\left(t\right) = \boldsymbol{f}\left(\boldsymbol{x}\left(t\right), t\right), \tag{C.9}$$

Due to the presence of an explicit dependence on time, (C.9) may also reflect exogenous influences such as commands and disturbances.

Sometimes, the stability of an equilibrium of a non-autonomous system can be analyzed in a similar way to the autonomous case. For this, the definition of stability and the Lyapunov theorem have to be altered appropriately [96]. However, for the non-autonomous problems, which arise within this thesis, no equilibrium may be found. For this reason, only boundedness of the solutions of the non-autonomous differential equation (C.9) is assessed.

Definition C.4 (Uniform Ultimate Boundedness, [96])**.** *The solutions of* (C.9) *are*

- *uniformly bounded if there exists a positive constant* c*, independent of* $t_0 \geq 0$*, and for every* $a \in]0, c[$*, there is* $\beta = \beta(a) > 0$*, independent of* t_0*, such that*

$$\|\boldsymbol{x}(t_0)\| \leq a \quad \Rightarrow \quad \|\boldsymbol{x}\left(t\right)\| \leq \beta, \qquad \forall\, t \geq t_0; \tag{C.10}$$

- *globally uniformly bounded, if* (C.10) *holds for arbitrary large* a*;*
- *uniformly ultimately bounded with ultimate bound* b *if there exist positive constants* b *and* c*, independent of* $t_0 \geq 0$*, and for every* $a \in]0, c[$*, there is* $T = T(a, b) \geq 0$*, independent of* t_0*, such that*

$$\|\boldsymbol{x}(t_0)\| \leq a \quad \Rightarrow \quad \|\boldsymbol{x}\left(t\right)\| \leq b, \qquad \forall\, t \geq t_0 + T(a, b); \tag{C.11}$$

- *globally uniformly ultimately bounded if* (C.11) *holds for arbitrary large* a*.*

Since the above definition does not readily allow to check Uniform Ultimate Boundedness (UUB) of a nonlinear system, one usually resorts the following Lyapunov-like theorem:

Theorem C.5 (Lyapunov Theorem for Uniform Ultimate Boundedness, [96])**.** *Let* $\mathcal{D} \subset \mathbb{R}^n$ *be an open connected set that contains the origin and* $V : [0, \infty[\times \mathcal{D} \to \mathbb{R}$ *be a continuously differentiable function such that*

$$\alpha_1\left(\|\boldsymbol{x}\|\right) \leq V(t, \boldsymbol{x}) \leq \alpha_2\left(\|\boldsymbol{x}\|\right), \tag{C.12}$$

$$\frac{\partial V(t, \boldsymbol{x})}{\partial t} + \frac{\partial V(t, \boldsymbol{x})}{\partial \boldsymbol{x}} \cdot \boldsymbol{f}(t, \boldsymbol{x}) \leq -W_3(\boldsymbol{x}), \quad \forall\, \|\boldsymbol{x}\| \geq \mu > 0 \tag{C.13}$$

$\forall\ t \geq 0$ *and* $\forall\ \boldsymbol{x} \in \mathcal{D}$*, where* $\alpha_1(\cdot)$ *and* $\alpha_2(\cdot)$ *are class* $\mathcal{K}$ *functions and* $W_3(\boldsymbol{x})$ *is a continuous positive definite function. Take* $r > 0$ *such that a ball with radius* r *satisfies* $B_r \subset \mathcal{D}$ *and suppose that*

$$\mu < \alpha_2^{-1}\left(\alpha_1\left(r\right)\right). \tag{C.14}$$

Then, there exists a class $\mathcal{KL}$ *function* $\beta(\cdot,\cdot)$ *and for every initial state* $\boldsymbol{x}(t_0)$*, satisfying* $\|\boldsymbol{x}(t_0)\| \leq \alpha_2^{-1}\left(\alpha_1\left(r\right)\right)$*, there is a* $T \geq 0$ *(dependent on* $\boldsymbol{x}(t_0)$ *and* μ*) such that the solution of* (C.9) *satisfies*

$$\|\boldsymbol{x}\left(t\right)\| \leq \beta\left(\|\boldsymbol{x}\left(t_0\right)\|, t - t_0\right), \quad \forall\ t_0 \leq t \leq t_0 + T, \tag{C.15}$$

$$\|\boldsymbol{x}\left(t\right)\| \leq \alpha_1^{-1}\left(\alpha_2\left(\mu\right)\right), \quad \forall\ t \geq t_0 + T. \tag{C.16}$$

Moreover, if $\mathcal{D} = \mathbb{R}^n$ *and* $\alpha_1(\cdot)$ *belongs to class* $\mathcal{K}_\infty$*, then* (C.15) *and* (C.16) *hold for any initial state* $\boldsymbol{x}(t_0)$*, with no restriction on how large* μ *is.*

For a definition of class $\mathcal{K}$, class $\mathcal{K}_\infty$ and class $\mathcal{KL}$ functions, the reader is referred to [96].

C.2 Input-/Output Stability

In the previous section, the trajectories of a nonlinear system have been analyzed with respect to an equilibrium. That is, it was analyzed whether the trajectories of a nonlinear system stay close to an equilibrium or even converge to an equilibrium. In this section, an alternative approach to stability analysis is taken. Instead of analyzing whether the trajectories stay close to an equilibrium, it is assessed whether the output of a nonlinear system stays bounded if the input is bounded. This stability concept is hence called *Input-/Output Stability*.

In order to measure whether the input $\boldsymbol{u}\left(t\right)$ and the output $\boldsymbol{y}\left(t\right)$ are bounded, suitable norms for the input- and output signals are required first. To that end, the $\mathcal{L}_p$-signal-norms, which have been introduced in Appendix B.1, are suited. If a signal $\boldsymbol{u}\left(t\right)$ or $\boldsymbol{y}\left(t\right)$ is an element of the function space $\mathcal{L}_p$, it is bounded in terms of the associated $\mathcal{L}_p$-norm. However, when analyzing the stability of a system, it is usually not known in advance whether the output $\boldsymbol{y}\left(t\right)$ will lie in an $\mathcal{L}_p$-space, i.e. it is not known whether $\|\boldsymbol{y}\|_{\mathcal{L}_p}$ exists and is finite. For this reason, the truncated $\mathcal{L}_p$-norms (and the truncated $\mathcal{L}_p$-spaces) are introduced first. The truncation of a signal $\boldsymbol{y}\left(t\right)$ to the interval $[0, \tau]$ is defined as

$$\boldsymbol{y}\left(t\right)_\tau = \begin{cases} \boldsymbol{y}\left(t\right) & 0 \leq t \leq \tau, \\ 0 & t > \tau \end{cases}. \tag{C.17}$$

With this definition of the truncation of a signal, the extended function spaces $\mathcal{L}_{p,e}^l$ may be defined as [96]:

$$\mathcal{L}_{p,e}^l = \left\{ \boldsymbol{y}\left(t\right) \mid \boldsymbol{y}\left(t\right)_\tau \in \mathcal{L}_p^l, \quad \forall\ \tau \in [0, \infty[\ \right\}. \tag{C.18}$$

Hence, the signal $\boldsymbol{y}(t)$ belongs to the extended space $\mathcal{L}_{p,e}^{l}$, if for any finite time τ, all of its truncations to $[0, \tau]$ belong to the respective $\mathcal{L}_{p}^{l}$ space.

With the definitions of suitable input and output vector spaces in place, the system, whose input-/output stability should be analyzed, is generally denoted as

$$\boldsymbol{y}(t) = \mathcal{F}\{\boldsymbol{u}(t)\}, \tag{C.19}$$

where $\mathcal{F} : \mathcal{L}_{e}^{m} \rightarrow \mathcal{L}_{e}^{l}$ maps input signals $\boldsymbol{u}(t) \in \mathcal{L}_{e}^{m}$ to output signals $\boldsymbol{y}(t) \in \mathcal{L}_{e}^{l}$. Notice that the $\mathcal{L}_{p}$-norms of the input- and the output signal do not have to be equivalent. Hence, the system (C.19) may map an input signal with bounded energy (i.e. $\boldsymbol{u}(t) \in \mathcal{L}_{2}^{m}$) to a bounded output signal (i.e. $\boldsymbol{u}(t) \in \mathcal{L}_{\infty,e}^{l}$). In order to keep the nomenclature simple, the respective norm (i.e. the index p) is not indicated subsequently. Furthermore, notice that even unstable systems may be represented as (C.19), since the use of extended vector spaces also admits that the input / output signals diverge to infinity for $t \rightarrow \infty$.

Throughout this thesis, only physical systems are considered that may be represented in terms of a state space model such as

$$\begin{aligned} \dot{\boldsymbol{x}}(t) &= \boldsymbol{f}(\boldsymbol{x}(t), \boldsymbol{u}(t), t), \\ \boldsymbol{y}(t) &= \boldsymbol{h}(\boldsymbol{y}(t), \boldsymbol{u}(t), t). \end{aligned} \tag{C.20}$$

The operator-notation $\boldsymbol{y}(t) = \mathcal{F}\{\boldsymbol{u}(t)\}$ from (C.19) is just a short-hand notation of the nonlinear state space model (C.20). This furthermore implies that the operator $\mathcal{F}\{\cdot\}$ is always causal since any such state space model is intrinsically causal.

Using the general definition of the nonlinear system as a mapping from one extended vector space to another, *input/output stability* may now be defined:

Definition C.6 ([96])**.** *The system described by the mapping $\mathcal{F} : \mathcal{L}_{e}^{m} \rightarrow \mathcal{L}_{e}^{l}$ is finite-gain $\mathcal{L}$ stable if there exist nonnegative constants γ and β such that*

$$\left\| \left(\mathcal{F}\left\{ \boldsymbol{u}(t) \right\} \right)_{\tau} \right\|_{\mathcal{L}_e} \leq \gamma \cdot \left\| \boldsymbol{u}(t)_{\tau} \right\|_{\mathcal{L}_e} + \beta, \tag{C.21}$$

for all $\boldsymbol{u}(t) \in \mathcal{L}_{e}^{m}$ and $\tau \in [0, \infty[$.

In (C.21), γ denotes the gain ("the amplification") of the input signal $\boldsymbol{u}(t)$ and β denotes the so called bias term. Depending on the input and output norms $\mathcal{L}_{p,e}$, the gain γ is often called $\mathcal{L}_{p}$-gain. Notice that finite-gain $\mathcal{L}$ stability is not the only notion of *input/output stability* (see for example [96] or [68] for other notions of in *input/output stability*). Nevertheless, this notion suffices for the purpose of this thesis. Hence, except when noticed otherwise, the terms *input/output stability* and *finite-gain $\mathcal{L}$ stability* are used interchangeably.

Similar to the definitions of stability in the previous section, the above definition of *input/output stability* does not readily admit to the prove stability of a given nonlinear system. In order to prove finite-gain $\mathcal{L}$ stability, one may resort to Lyapunov-like proofs,

which are conceptually similar to the proof of UUB (see [96]). In [96], several interesting results with respect to finite-gain $\mathcal{L}$ stability are presented, which may be summarized as follows:

- Under some technical assumptions, a nonlinear *state space model* with an exponentially stable equilibrium is small-signal finite-gain $\mathcal{L}_p$ stable for each $p \in [1, \infty]$. The attribute *small-signal* derives from the fact that this result only holds for input signals of a certain size. However, if the equilibrium is a global one, then the nonlinear state space model is finite-gain $\mathcal{L}_p$ stable for each $p \in [1, \infty]$ [96, Theorem 5.1].
- The above result may be used to show that if the linearization of a nonlinear *state space model* is Hurwitz, then the nonlinear system is small-signal $\mathcal{L}_p$ stable (again under some appropriate technical assumptions) [96, Corollary 5.1].
- A LTI state space model is finite-gain $\mathcal{L}_p$ stable for each $p \in [1, \infty]$, if its system matrix is Hurwitz [96, Corollary 5.2].

For the purposes of this thesis, only the notion of *finite-gain $\mathcal{L}_\infty$ stability* of LTI systems will be used in the proofs of stability of the MLESO and of $\mathcal{L}_1$-AC. In case of a LTI system and input/output signals from $\mathcal{L}_\infty$, a suitable value of the gain γ in (C.21) is given by the $\mathcal{L}_1$-norm of the transfer function $\boldsymbol{G}(s)$, which is associated with the LTI system, i.e.

$$\gamma = \|\boldsymbol{G}(s)\|_{\mathcal{L}_1}. \tag{C.22}$$

Eq. (C.22) might lead to the erroneous conclusion that the concepts of *induced transfer function norms* and *finite gain $\mathcal{L}$ stability* are equivalent. This is however not in general true as will be clarified by the subsequent discussion. While inequalities (B.39) (definition of boundedness of a linear operator) and (C.21) (definition of boundedness in case of *finite gain $\mathcal{L}$ stability*) read similar, notice that *finite-gain $\mathcal{L}$ stability* is not restricted to linear operators. Furthermore, both definitions also deviate due to the presence of the bias term β in (C.21). This bias term may account for the fact that systems may maintain a nonzero output even in the presence of a zero input. In case of a linear operator, this is not possible due to linearity. Thus, *finite gain $\mathcal{L}$ stability* represents a broader concept. Nevertheless, in case of LTI systems, the existence of an induced transfer function norm is equivalent to *finite gain $\mathcal{L}$ stability*.

When using the concept of *finite-gain $\mathcal{L}_\infty$ stability* (i.e. Bounded Input Bounded Output (BIBO) stability) to analyze the stability of state space models, it is important to recall the relation between BIBO stability and stability in the sense of Lyapunov. As mentioned before, a LTI state space model is *finite-gain $\mathcal{L}_\infty$ stable*, if its system matrix is Hurwitz. The converse is however not necessarily true. As an example, consider the

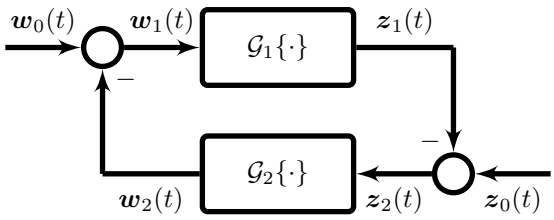

Figure C.1: Feedback Configuration for the Small-Gain Theorem.

LTI state space model

$$\begin{aligned} \begin{bmatrix} \dot{x}_1(t) \\ \dot{x}_2(t) \end{bmatrix} &= \begin{bmatrix} 2 & 1 \\ 0 & -1 \end{bmatrix} \cdot \begin{bmatrix} x_1(t) \\ x_2(t) \end{bmatrix} + \begin{bmatrix} 0 \\ 1 \end{bmatrix} \cdot u\,(t)\,, \\ y(t) &= \begin{bmatrix} 0 & 1 \end{bmatrix} \cdot \begin{bmatrix} x_1(t) \\ x_2(t) \end{bmatrix}. \end{aligned} \tag{C.23}$$

Clearly, the system (C.23) exhibits an unobservable, unstable mode, namely the state $x_1(t)$. The associated transfer function is given by

$$y(s) = \frac{1}{s+1} \cdot u(s) \tag{C.24}$$

and hence, is BIBO stable. In order to avoid these situations, the state space models, which shall be analyzed in an input-/output setting, have to be controllable and observable. This condition ensures the absence of uncontrollable and/or unobservable modes.

An important application of the concept of *finite gain $\mathcal{L}$ stability* is the *small-gain theorem*. Using the small-gain theorem, the stability of a feedback connection of two maps $\mathcal{G}_1 : \mathcal{L}_e^m \to \mathcal{L}_e^l$ and $\mathcal{G}_2 : \mathcal{L}_e^l \to \mathcal{L}_e^m$ may be analyzed. Both systems are assumed to be finite gain $\mathcal{L}$ stable, i.e.

$$\begin{aligned} \|\boldsymbol{z}_1(t)_\tau\| &\leq \gamma_1 \cdot \|\boldsymbol{w}_1(t)_\tau\| + \beta_1, \qquad \forall\, \boldsymbol{w}_1(t) \in \mathcal{L}_e^m,\ \forall\, \tau \in [0, \infty[, \\ \|\boldsymbol{w}_2(t)_\tau\| &\leq \gamma_2 \cdot \|\boldsymbol{z}_2(t)_\tau\| + \beta_2, \qquad \forall\, \boldsymbol{z}_2(t) \in \mathcal{L}_e^l,\ \forall\, \tau \in [0, \infty[. \end{aligned} \tag{C.25}$$

The considered feedback loop is shown in Figure C.1. The feedback loop is assumed to be *well defined* in the sense that for input signals $\boldsymbol{w}_0(t) \in \mathcal{L}_e^m$ and $\boldsymbol{z}_0(t) \in \mathcal{L}_e^l$, there exist unique outputs $\boldsymbol{w}_1(t), \boldsymbol{w}_2(t) \in \mathcal{L}_e^m$ and $\boldsymbol{z}_1(t), \boldsymbol{z}_2(t) \in \mathcal{L}_e^l$ [96]. The small-gain theorem may be stated as follows:

Theorem C.7 (Small-Gain Theorem, [96])**.** *Under the preceding assumptions, the feedback connection from Figure C.1 is finite-gain $\mathcal{L}$ stable, if $\gamma_1 \cdot \gamma_2 < 1$.*

Proof. The following proof is due to [96]. Assuming the existence of the solution, the signals $\boldsymbol{w}_1(t)$ and $\boldsymbol{z}_2(t)$ are given by

$$\boldsymbol{w}_1(t)_\tau = \boldsymbol{w}_0(t)_\tau - \left(\mathcal{G}_2\left\{\boldsymbol{z}_2(t)\right\}\right)_\tau, \tag{C.26}$$

$$\boldsymbol{z}_2(t)_\tau = \boldsymbol{z}_0(t)_\tau - \left(\mathcal{G}_1\left\{\boldsymbol{w}_1(t)\right\}\right)_\tau. \tag{C.27}$$

Due to the triangle inequality, it follows for $\boldsymbol{w}_1(t)$:

$$\|\boldsymbol{w}_1(t)_\tau\|_\mathcal{L} \leq \|\boldsymbol{w}_0(t)_\tau\|_\mathcal{L} + \|\left(\mathcal{G}_2\left\{\boldsymbol{z}_2(t)\right\}\right)_\tau\|_\mathcal{L}. \tag{C.28}$$

Notice that truncated norms are used here since boundedness of the closed-loop signals has not yet been ensured. Due to the finite gain $\mathcal{L}$ stability of $\mathcal{G}_2\{\cdot\}$, one obtains

$$\|\boldsymbol{w}_1(t)_\tau\|_\mathcal{L} \leq \|\boldsymbol{w}_0(t)_\tau\|_\mathcal{L} + \gamma_2 \cdot \|\boldsymbol{z}_2(t)_\tau\|_\mathcal{L} + \beta_2. \tag{C.29}$$

Inserting (C.27) and using the finite gain $\mathcal{L}$ stability of $\mathcal{G}_1\{\cdot\}$ leads to

$$\|\boldsymbol{w}_1(t)_\tau\|_\mathcal{L} \leq \|\boldsymbol{w}_0(t)_\tau\|_\mathcal{L} + \gamma_2 \cdot (\|\boldsymbol{z}_0(t)_\tau\|_\mathcal{L} + \gamma_1 \cdot \|\boldsymbol{w}_1(t)\|_\mathcal{L} + \beta_1) + \beta_2. \tag{C.30}$$

Since $\gamma_1 \cdot \gamma_2 < 1$ holds, $1 - \gamma_1 \cdot \gamma_2 > 0$ follows. Hence, (C.30) provides an upper bound for $\boldsymbol{w}_1(t)$:

$$\|\boldsymbol{w}_1(t)_\tau\|_\mathcal{L} \leq \frac{\|\boldsymbol{w}_0(t)_\tau\|_\mathcal{L} + \gamma_2 \cdot \|\boldsymbol{z}_0(t)_\tau\|_\mathcal{L} + \beta_2 + \gamma_2 \cdot \beta_1}{1 - \gamma_1 \cdot \gamma_2}, \tag{C.31}$$

which holds for all $\tau \in [0, \infty[$.

Similarly, the following bound for $\boldsymbol{z}_2(t)$ may be derived:

$$\|\boldsymbol{z}_2(t)_\tau\|_\mathcal{L} \leq \frac{\|\boldsymbol{z}_0(t)_\tau\|_\mathcal{L} + \gamma_1 \cdot \|\boldsymbol{w}_0(t)_\tau\|_\mathcal{L} + \beta_1 + \gamma_1 \cdot \beta_2}{1 - \gamma_1 \cdot \gamma_2}, \tag{C.32}$$

which holds for all $\tau \in [0, \infty[$. □

To conclude this section, notice that if (C.21) holds uniformly for all τ (since the input $\boldsymbol{u}(t)$ is an element of a non-extended vector space, i.e. $\boldsymbol{u}(t) \in \mathcal{L}^m$), then the output $\boldsymbol{y}(t)$ will lie in the corresponding non-extended vector space $\boldsymbol{y}(t) \in \mathcal{L}^l$ as well [146].

C.3 Stability Analysis of Delayed Systems

Let $C = C([-r, 0], \mathbb{R}^n)$ denote the set of continuous functions mapping the interval $[-r, 0]$ to $\mathbb{R}^n$. Furthermore, let $\boldsymbol{x}_t(\zeta) \in C$ denote $\boldsymbol{x}_t(\zeta) = \boldsymbol{x}(t+\zeta),\ -r \leq \zeta \leq 0$. Then, a RFDE is defined as

$$\dot{\boldsymbol{x}}(t) = \boldsymbol{f}(t, \boldsymbol{x}_t(\zeta)), \tag{C.33}$$

where $\boldsymbol{x} : \mathbb{R} \to \mathbb{R}^n$ and $\boldsymbol{f} :\ \mathbb{R} \times C \to \mathbb{R}^n$. In order to solve the RFDE (C.33), an initial condition $\boldsymbol{\phi} \in C$ has to be specified, i.e. a function $\boldsymbol{\phi}(\zeta) = \boldsymbol{x}(t_0 + \zeta),\ -r \leq \zeta \leq 0$. A solution of the RFDE (C.33) then is denoted as $\boldsymbol{x}(t_0, \boldsymbol{\phi}(\zeta), t)$.

Definition C.8 (Uniform Ultimate Boundedness [75])**.** *Let $\boldsymbol{x}(t_0, \boldsymbol{\phi}(\zeta), t)$ be a solution of the RFDE* (C.33)*. The solutions are UUB if there is a $b > 0$ such that for an $a > 0$, there is a constant $T(a) > 0$ such that $\|\boldsymbol{x}(t_0, \boldsymbol{\phi}(\zeta), t)\| \leq b$ for $t \geq t_0 + T(a)$ for all $t_0 \in \mathbb{R},\ \boldsymbol{\phi} \in C,\ \|\boldsymbol{\phi}(\zeta)\|_c \leq a$, where $\|\boldsymbol{\phi}(\zeta)\|_c = \sup_{-r \leq \zeta \leq 0} \|\boldsymbol{\phi}(\zeta)\|$.*

The following theorem from [75] may be used to prove UUB of a RFDE:

Theorem C.9 (Razumikhin Theorem for UUB [75])**.** *Suppose* $\boldsymbol{f} : \mathbb{R} \times C \to \mathbb{R}^n$ *takes* $\mathbb{R} \times$ *(bounded sets of* C*) into bounded sets of* $\mathbb{R}^n$ *and consider the RFDE* (C.33)*. Suppose* $u,\ v,\ w : \mathbb{R}_+ \to \mathbb{R}_+$ *are continuous nondecreasing functions,* $u(s) \to \infty$ *as* $s \to \infty$*. If there is a continuous* $V :\ \mathbb{R} \times \mathbb{R}^n \to \mathbb{R}$*, a continuous nondecreasing* $p :\ \mathbb{R}_+ \to \mathbb{R}_+$*,* $p(s) > s$ *for* $s > 0$*, and a constant* $H \geq 0$ *such that*

$$u(\|\boldsymbol{x}\,(t)\|) \leq V\,(t, \boldsymbol{x}\,(t)) \leq v(\|\boldsymbol{x}\,(t)\|), \quad t \in \mathbb{R},\ \boldsymbol{x}\,(t) \in \mathbb{R}^n \tag{C.34}$$

and

$$\dot{V}\,(t, \boldsymbol{\phi}\,(\zeta)) \leq -w(\|\boldsymbol{\phi}(0)\|), \tag{C.35}$$

if

$$\|\boldsymbol{\phi}(0)\| \geq H, \tag{C.36}$$

$$p\,(V\,(t, \boldsymbol{\phi}\,(0))) - V\,(t + \zeta, \boldsymbol{\phi}\,(\zeta)) > 0,\ \zeta \in [-r, 0], \tag{C.37}$$

then the solutions of the RFDE (C.33) *are uniformly ultimately bounded.*

Remark C.10. *Let the initial conditions satisfy* $\|\boldsymbol{\phi}\,(\zeta)\|_c \leq \bar{c}$ *for some* $\bar{c} > 0$*. Then the conditions* (C.35)*,* (C.36) *and* (C.37) *ensure that the Lyapunov function* $V(\boldsymbol{x}\,(t))$ *never leaves the set* $\mathcal{M}_c = \{\boldsymbol{x} \mid V(\boldsymbol{x}) \leq \max(v(\bar{c}), v(H))\}$*. For this reason, Theorem C.9 is also valid if the conditions are only satisfied locally.*

Appendix D

Interim Results

D.1 $\mathcal{L}_1$ Adaptive Control

Lemma D.1. *Consider the stable prediction error dynamics* (3.167)

$$\dot{\boldsymbol{e}}_P(t) = \boldsymbol{A}_M \boldsymbol{e}_P(t) + \boldsymbol{B}_P \tilde{\boldsymbol{\Theta}}_m(t)\, \boldsymbol{\omega}(\boldsymbol{x}_P(t), t)$$

and the strictly proper, stable filter (3.173)

$$\boldsymbol{C}(s) \triangleq (\boldsymbol{I} + \boldsymbol{\Lambda}\boldsymbol{K}\boldsymbol{D}(s))^{-1}\boldsymbol{\Lambda}\boldsymbol{K}\boldsymbol{D}(s).$$

Let

$$\begin{aligned} \dot{\boldsymbol{x}}_f(t) &= \boldsymbol{A}_f \boldsymbol{x}_f(t) + \boldsymbol{B}_f \boldsymbol{u}_f(t) \\ \boldsymbol{y}_f(t) &= \boldsymbol{C}_f \boldsymbol{x}_f(t) \end{aligned} \tag{D.1}$$

be a state space realization of the filter (3.173)*. If $\boldsymbol{B}_P$ has full rank, then the following relation holds*

$$\boldsymbol{C}(s) \cdot \mathcal{L}\left\{\tilde{\boldsymbol{\Theta}}_m(t)\, \boldsymbol{\omega}(\boldsymbol{x}_P(t), t)\right\} = \boldsymbol{C}_{e_P}(s) \cdot \boldsymbol{e}_P(s), \tag{D.2}$$

where

$$\boldsymbol{C}_{e_P}(s) = \boldsymbol{C}_f (s\boldsymbol{I} - \boldsymbol{A}_f)^{-1} \left(\boldsymbol{A}_f \boldsymbol{B}_f \boldsymbol{B}_P^{\#} - \boldsymbol{B}_f \boldsymbol{B}_P^{\#} \boldsymbol{A}_M\right) + \boldsymbol{C}_f \boldsymbol{B}_f \boldsymbol{B}_P^{\#} \tag{D.3}$$

is a stable and proper filter.

Proof. If $\boldsymbol{B}_P$ has full rank, i.e. $\operatorname{rank} \boldsymbol{B}_P = m$, then the error dynamics (3.167) may be solved uniquely for $\tilde{\boldsymbol{\Theta}}_m(t)\, \boldsymbol{\omega}(\boldsymbol{x}_P(t), t)$ and one obtains

$$\tilde{\boldsymbol{\Theta}}_m(t)\, \boldsymbol{\omega}(\boldsymbol{x}_P(t), t) = \boldsymbol{B}_P^{\#} \cdot (\dot{\boldsymbol{e}}_P(t) - \boldsymbol{A}_M \boldsymbol{e}_P(t)). \tag{D.4}$$

By inserting $\boldsymbol{u}_f(t) \triangleq \tilde{\boldsymbol{\Theta}}_m(t)\, \boldsymbol{\omega}(\boldsymbol{x}_P(t), t)$ from (D.4) into the state space realization (D.1) of the filter $\boldsymbol{C}(s)$, the left hand side of (D.2) becomes:

$$\begin{aligned} \dot{\boldsymbol{x}}_f(t) &= \boldsymbol{A}_f \boldsymbol{x}_f(t) + \boldsymbol{B}_f \boldsymbol{B}_P^{\#} \cdot (\dot{\boldsymbol{e}}_P(t) - \boldsymbol{A}_M \boldsymbol{e}_P(t)), \\ \boldsymbol{y}_f(t) &= \boldsymbol{C}_f \boldsymbol{x}_f(t) \end{aligned} \tag{D.5}$$

or equivalently

$$\begin{aligned} \dot{\boldsymbol{x}}_f(t) - \boldsymbol{B}_f \boldsymbol{B}_P^{\#} \cdot \dot{\boldsymbol{e}}_P(t) &= \boldsymbol{A}_f \boldsymbol{x}_f(t) - \boldsymbol{B}_f \boldsymbol{B}_P^{\#} \boldsymbol{A}_M \boldsymbol{e}_P(t), \\ \boldsymbol{y}_f(t) &= \boldsymbol{C}_f \boldsymbol{x}_f(t). \end{aligned} \tag{D.6}$$

Upon definition of $\boldsymbol{z}_f(t) = \boldsymbol{x}_f(t) - \boldsymbol{B}_f \boldsymbol{B}_P^{\#} \cdot \boldsymbol{e}_P(t)$, (D.6) becomes

$$\begin{aligned} \dot{\boldsymbol{z}}_f(t) &= \boldsymbol{A}_f \left(\boldsymbol{z}_f(t) + \boldsymbol{B}_f \boldsymbol{B}_P^{\#} \cdot \boldsymbol{e}_P(t) \right) - \boldsymbol{B}_f \boldsymbol{B}_P^{\#} \boldsymbol{A}_M \boldsymbol{e}_P(t) \\ &= \boldsymbol{A}_f \boldsymbol{z}_f(t) + \left(\boldsymbol{A}_f \boldsymbol{B}_f \boldsymbol{B}_P^{\#} - \boldsymbol{B}_f \boldsymbol{B}_P^{\#} \boldsymbol{A}_M \right) \cdot \boldsymbol{e}_P(t), \\ \boldsymbol{y}_f(t) &= \boldsymbol{C}_f \left(\boldsymbol{z}_f(t) + \boldsymbol{B}_f \boldsymbol{B}_P^{\#} \cdot \boldsymbol{e}_P(t) \right) \\ &= \boldsymbol{C}_f \boldsymbol{z}_f(t) + \boldsymbol{C}_f \boldsymbol{B}_f \boldsymbol{B}_P^{\#} \cdot \boldsymbol{e}_P(t). \end{aligned} \tag{D.7}$$

Using the definition of the filter $\boldsymbol{C}_{e_P}(s)$ in (D.3), (D.7) establishes the right hand side of (D.2). Since $\boldsymbol{A}_f$ is Hurwitz, the filter $\boldsymbol{C}_{e_P}(s)$ is Hurwitz as well. □

D.2 Analytical Solution of a Scalar Adaptive Controller in Case of Stabilization

Adaptive control approaches such as MRAC admit to construct powerful controllers for uncertain systems. However, the analysis of these controllers with respect to robustness and performance is much less mature. This is in sharp contrast to linear (and weakly nonlinear) systems, for which advanced analysis techniques such as μ-analysis [156], IQC-analysis [114] or LMI-based delay analysis [73] exist. Using these techniques, the robustness and performance with respect to parametric and non-parametric uncertainties may be thoroughly analyzed. When comparing the maturity of these tools to the available analysis techniques for nonlinear adaptive systems, one observes a significant gap.

From a higher level perspective, a potential explanation for this gap derives from the fact that no general solutions to the differential equations of nonlinear systems exist. In contrast, LTI (systems of) differential equations can be solved analytically. Furthermore, these solutions even admit a characterization in the frequency-domain, which is at the heart of many powerful analysis techniques for LTI systems.

Consequently, a reasonable approach to obtain more powerful analysis techniques for adaptive control systems is the analytical solution of the underlying differential equations. Subsequently, it will be shown how the differential equations of a scalar MRAC in case of stabilization may be solved analytically by reducing the second order differential equation to a first order Bernoulli differential equation.

Consider the scalar, direct MRAC in case of stabilization

$$\dot{x}_P(t) = A_M \cdot x_P(t) + B_P \tilde{\Theta}_x(t) \cdot x_P(t), \tag{D.8}$$

$$\dot{\tilde{\Theta}}_x(t) = -\gamma \cdot x_P^2(t) \cdot B_P, \tag{D.9}$$

which derives from (3.28) and (3.41) for $r(t) = 0$, $x_M(t) = 0$, $\phi\left(x_P\left(t\right)\right) = 0$ and $\Lambda = 1$. Differentiating (D.9) with respect to time yields

$$\ddot{\tilde{\Theta}}_x(t) = -2 \cdot \gamma \cdot B_P \cdot x_P(t) \cdot \dot{x}_P(t). \tag{D.10}$$

Upon insertion of (D.8), one obtains the second order differential equation

$$\begin{aligned} \ddot{\tilde{\Theta}}_x(t) &= -2 \cdot \gamma \cdot B_P \cdot x_P(t) \cdot \left(A_M \cdot x_P(t) + B_P \tilde{\Theta}_x(t) \cdot x_P(t)\right) \\ &= -2 \cdot \gamma \cdot B_P \cdot x_P^2(t) \cdot \left(A_M + B_P \tilde{\Theta}_x(t)\right) \\ &= 2 \cdot \dot{\tilde{\Theta}}_x(t) \cdot \left(A_M + B_P \tilde{\Theta}_x(t)\right). \end{aligned} \tag{D.11}$$

By noticing that $\frac{d}{dt}\tilde{\Theta}_x^2(t) = 2 \cdot \tilde{\Theta}_x(t) \cdot \dot{\tilde{\Theta}}_x(t)$ holds, (D.11) becomes

$$\ddot{\tilde{\Theta}}_x(t) = 2 \cdot A_M \cdot \dot{\tilde{\Theta}}_x(t) + B_P \cdot \frac{d}{dt}\tilde{\Theta}_x^2(t). \tag{D.12}$$

Integration of (D.12) then yields the Bernoulli-like first order differential equation

$$\dot{\tilde{\Theta}}_x(t) = 2 \cdot A_M \cdot \tilde{\Theta}_x(t) + B_P \cdot \tilde{\Theta}_x^2(t) + c, \tag{D.13}$$

where c is an integration constant, which has to be chosen such that the initial conditions of (D.8) and (D.9) remain valid. To that end, let the initial conditions be given by $x_P(0) = x_0$ and $\tilde{\Theta}_x(0) = \tilde{\Theta}_0$. Due to (D.9), $\dot{\tilde{\Theta}}_x(0) = -\gamma \cdot x_0^2 \cdot B_P$ has to hold at $t = 0$. Equating the latter expression with (D.13) at $t = 0$ yields the equation

$$2 \cdot A_M \cdot \tilde{\Theta}_0 + B_P \cdot \tilde{\Theta}_0^2 + c = -\gamma \cdot x_0^2 \cdot B_P. \tag{D.14}$$

Solving for c leads to the desired value of the integration constant

$$c = -B_P \cdot \left(\gamma x_0^2 + \tilde{\Theta}_0^2\right) - 2 \cdot A_M \cdot \tilde{\Theta}_0. \tag{D.15}$$

Due to the presence of the integration constant c, (D.13) is not yet a Bernoulli differential equation, but a Riccati (differential) equation. Now, consider the transformation

$$\bar{\Theta}_x(t) \triangleq \tilde{\Theta}_x(t) + k \tag{D.16}$$

with

$$k = \frac{A_M}{B_P} - \sqrt{k_0}, \tag{D.17}$$

$$k_0 = \left(\frac{A_M}{B_P}\right)^2 - \frac{c}{B_P} = \left(\frac{A_M}{B_P} + \tilde{\Theta}_0\right)^2 + \gamma \cdot x_0^2. \tag{D.18}$$

Using this transformation, the differential equation (D.13) turns into the Bernoulli differential equation

$$\dot{\bar{\Theta}}_x(t) = 2B_P\sqrt{k_0} \cdot \bar{\Theta}_x(t) + B_P \cdot \bar{\Theta}_x^2(t). \tag{D.19}$$

Hence, using the transformation $z(t) = \bar{\Theta}_x(t)^{-1}$, (D.19) is reduced to the stable, linear differential equation

$$\dot{z}(t) = -2B_P\sqrt{k_0} \cdot z(t) - B_P. \tag{D.20}$$

Let $\bar{z}(t)$ denote the analytical solution of the initial value problem (D.20) with $z(0) = 1/\bar{\Theta}_x(0) = 1/\left(\tilde{\Theta}_0 + k\right)$. Then, according to (D.16), the trajectory of the parameter error is given by:

$$\tilde{\Theta}_x(t) = \frac{1}{\bar{z}(t)} - k. \tag{D.21}$$

The trajectory of the plant state $x_P(t)$ may then either be obtained by considering (D.8) as a Linear Time Varying (LTV) system with the known parameter $\tilde{\Theta}_x(t)$ and by solving this LTV system. Or one may solve (D.9) for $x_P^2(t)$ and insert the derivative of the solution (D.21):

$$x_P^2(t) = -\frac{\dot{\tilde{\Theta}}_x(t)}{\gamma \cdot B_P} = \frac{\dot{\bar{z}}(t)}{\gamma \cdot B_P \cdot \bar{z}^2(t)}, \tag{D.22}$$

which allows conclusions on the magnitude of $x_P(t)$. Furthermore, since the solution of the adaptive controller essentially is a transformation of the solution of a first order LTI system, characteristic performance properties such as the rise time may be determined. If generalizations to higher order systems were available, such an analysis would even allow to determine eigenfrequencies and damping. Hence, it would allow a thorough analysis of the control system performance and would detect undesirable oscillations.

Appendix E

Simulation Results

This chapter presents the simulation results of the MLESO-based controller from Section 6.2 and of the Multiple-Model LQR (MM-LQR) controller from Section 6.3. Both controllers are evaluated in linear as well as nonlinear simulations at the two trim conditions $V_K^R = 35\,m/s$, $h = 1000\,m$, $m_{fuel} = 23\,kg$ and $V_K^R = 50\,m/s$, $h = 500\,m$, $m_{fuel} = 0\,kg$, for which Section 2.3 provides data.

All linear simulations and analyses consider the overall control system structure from Figure 2.4. Thus, the linear plant model includes the linearized rigid-body equations of motion (2.62), (2.63), actuator dynamics as well as control and measurement delays ($\tau_c = 50\,ms$ and $\tau_m = 20\,ms$). All linear simulations and analyses consider the uncertainties according to Table 2.5. For this reason, all time-domain and frequency-domain plots depict the nominal response and an envelope, which is the tube, wherein all uncertain responses are included. This tube is computed from 1000 simulations of the respective response with random realizations of the uncertain parameters. Notice that all analyses (e.g. open-loop Bode plot, step responses) rely on the same realizations of the uncertainties. The following analyses and simulations are conducted using the linear plant model:

- Open-loop Bode and Nichols plots;
- Box-plots of phase margin, gain margin and time-delay margin;
- Box plots of rise time, settling time and overshoot in case of a bank angle step command $\Phi_{cmd}(t)$;
- Steps of the bank angle command $\Phi_{cmd}(t)$ and of the wind disturbance $\beta_{W,cmd}(t)$;
- Closed-loop Bode plots from Φ_{cmd} and $\beta_{W,cmd}$ to the plant outputs;
- Responses to a bank angle doublet command $\Phi_{cmd}(t)$, a discrete gust command $\beta_{W,cmd}(t)$ according to Figure 6.20 (MIL-F-8785C) and to moderate Dryden turbulence[1] according to MIL-F-8785C [41].

[1] MIL-F-8785C specifies Dryden turbulence as one model for random fluctuations of the wind velocity. The turbulence is modeled as white Gaussian noise, which is passed through a specific shaping filter, which adjusts the power density spectrum of the noise. In MIL-F-8785C, the coefficients of these filters are given as functions of the turbulence intensity (light, moderate, severe), altitude and velocity.

The nonlinear plant model features the nonlinear rigid-body equations of motions from Section 2.1, a precise model of the UAS environment and of the resulting forces and moments, a detailed actuator model as well as a model of the on-board processing units. In each simulation, the UAS model is initialized to the respective trim condition. This especially includes the elevator deflection η and the thrust lever positions δT, which are held constant at their trim value throughout the simulation. Except for the doublet sweep, all nonlinear simulations include uncertainty. Hence, as in case of the linear simulations, a nominal response and an envelope are shown. However, in contrast to the linear plant model, the nonlinear simulation environment models the uncertainty of the aerodynamic data in a simplistic manner. As an example, consider the aerodynamic force in y_B-direction. The uncertainty is modeled by introducing the scalar coefficient $\lambda_{Cy} \in [0.5, 1.5]$ in the computation of the aerodynamic force:

$$(Y_A)_B = \bar{q} \cdot S \cdot \lambda_{Cy} \cdot C_Y. \tag{E.1}$$

In (E.1), $\bar{q}$ and S denote the dynamic pressure and the reference area of the wing, respectively. Furthermore, C_Y denotes the nominal dimensionless force coefficient (see Stevens & Lewis [162]). A similar model is also used for the other aerodynamic forces and moments, which result from the dimensionless force and moment coefficients C_X, C_Z, C_l, C_m, and C_n. In all cases, the scalar coefficients $\lambda_{(\cdot)}$ associated to the dimensionless coefficients vary in the interval $[0.5, 1.5]$. Although the above uncertainty model is simplistic, it allows the demonstration of the robustness of the controllers. The nonlinear plant model is used for the simulations of the responses to

- a step of the bank angle command $\Phi_{cmd}(t)$;
- a bank angle doublet sweep $\Phi_{cmd}(t)$;
- a discrete gust command $\beta_{W,cmd}(t)$ according to MIL-F-8785C [41];
- moderate Dryden turbulence according to MIL-F-8785C [41].

E.1 MLESO Control of the Lateral Motion

This section presents the simulation and analyses results of the MLESO-based controller. Sections E.1.1 and E.1.2 show the results at $V_K^R = 35\,m/s$, $h = 1000\,m$, $m_{fuel} = 23\,kg$ and $V_K^R = 50\,m/s$, $h = 500\,m$, $m_{fuel} = 0\,kg$, when using the linear plant model. Sections E.1.3 and E.1.4 then present the respective nonlinear simulation results.

E.1.1 Linear Model at 35 m/s

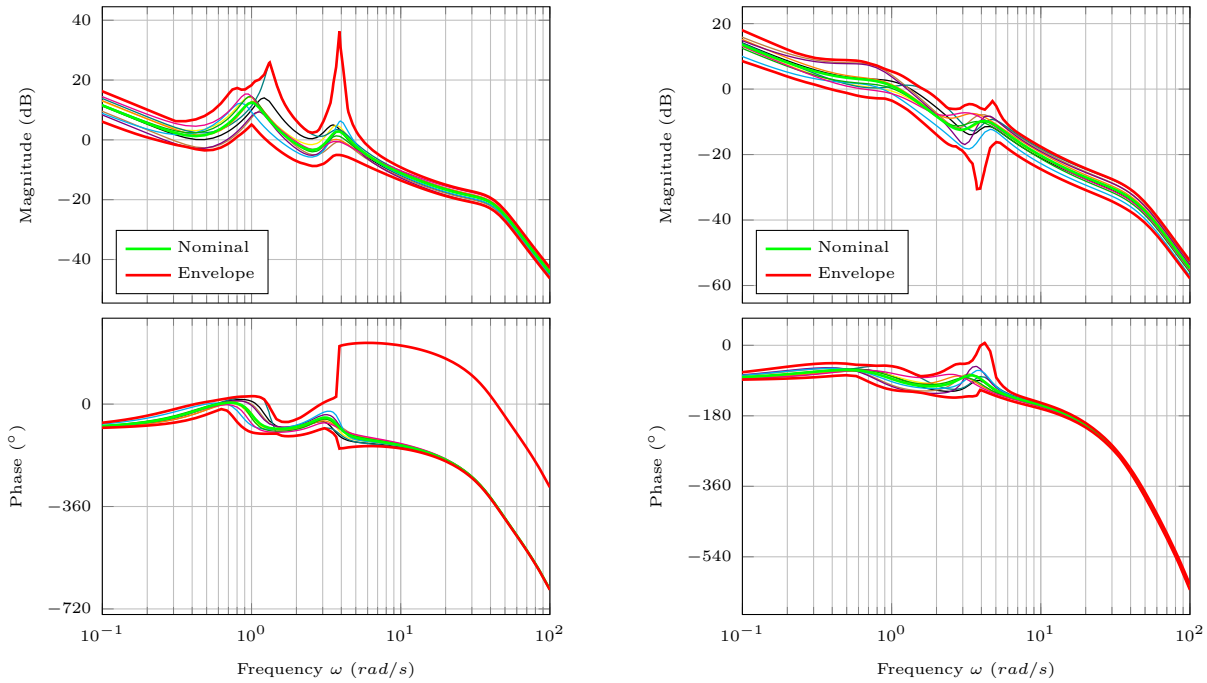

(a) Loopcut at aileron actuator input ξ

(b) Loopcut at rudder actuator input ζ

Figure E.1: Open-loop bode plots at $V_K^R = 35\,m/s$, $h = 1000\,m$, $m_{fuel} = 23\,kg$, when relying on a MLESO controller.

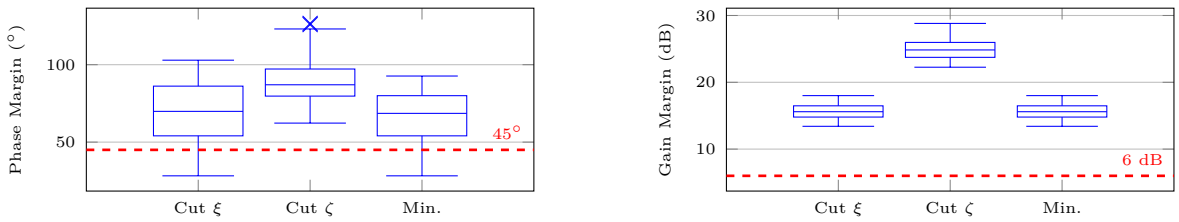

(a) Phase Margin

(b) Gain Margin

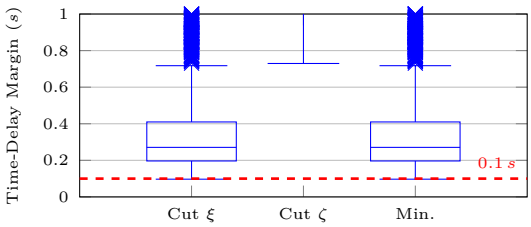

(c) Time-Delay Margin

Figure E.2: Box plots of phase, gain and time-delay margin of the MLESO controller at $V_K^R = 35\,m/s$, $h = 1000\,m$, $m_{fuel} = 23\,kg$.

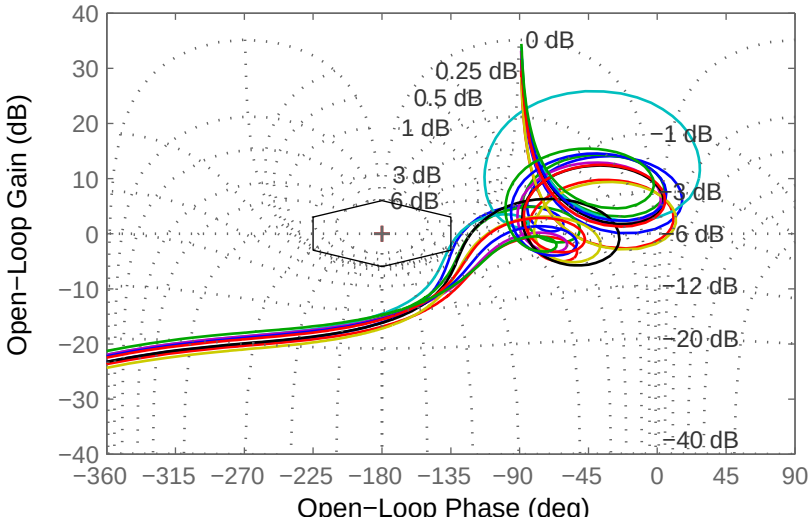

(a) Loopcut in front of the aileron control delay

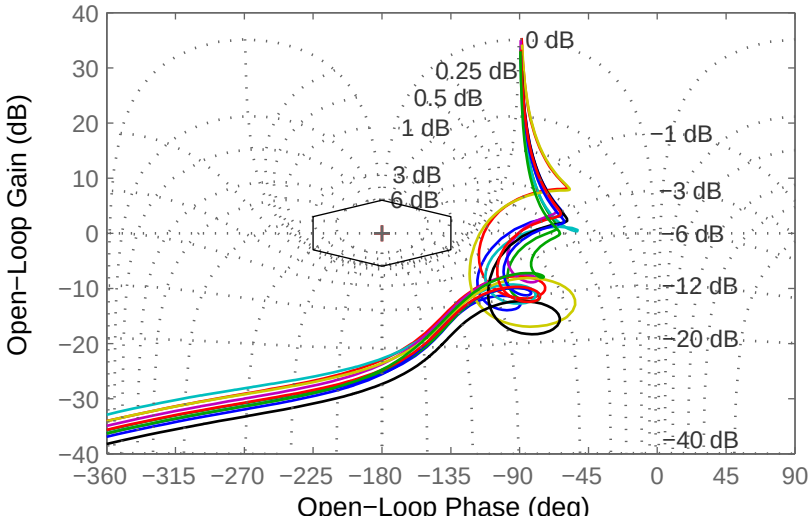

(b) Loopcut in front of the rudder control delay

Figure E.3: Nichols plots at $V_K^R = 35\,m/s$, $h = 1000\,m$, $m_{fuel} = 23\,kg$, when relying on a MLESO controller.

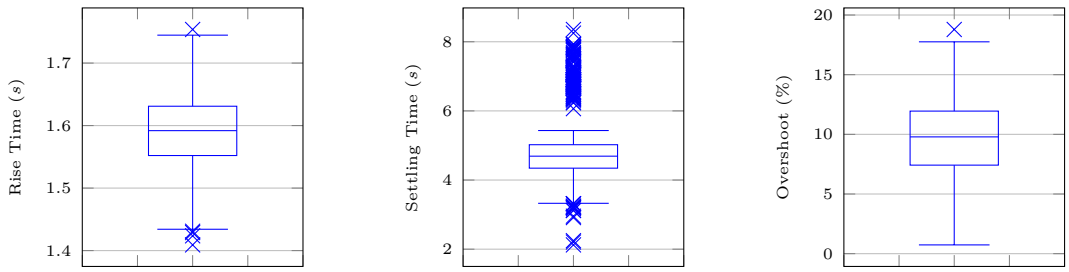

(a) Rise Time (b) Settling Time (c) Overhoot

Figure E.4: Box plots of rise time, settling time and overshoot of the LTI plant model with MLESO controller in case of a $30°$ step command $\Phi_{cmd}(t)$ at $V_K^R = 35\,m/s$, $h = 1000\,m$, $m_{fuel} = 23\,kg$.

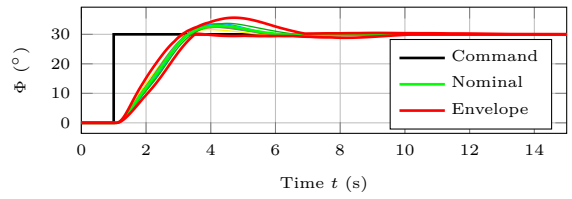

(a) Bank Angle

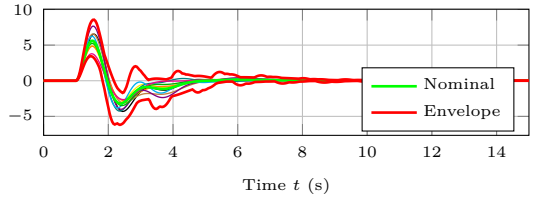

(b) Bank Angle

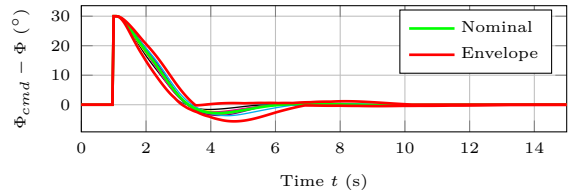

(c) Tracking Error

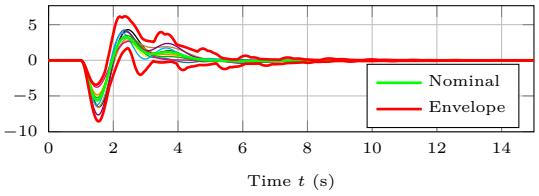

(d) Tracking Error

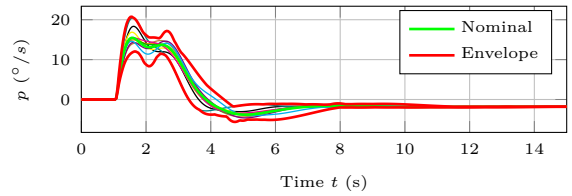

(e) Roll Rate

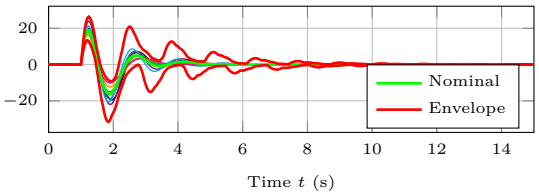

(f) Roll Rate

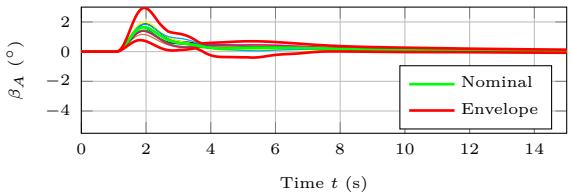

(g) Angle-of-sideslip

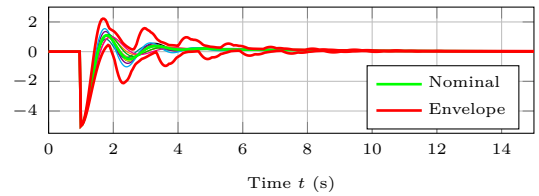

(h) Angle-of-sideslip

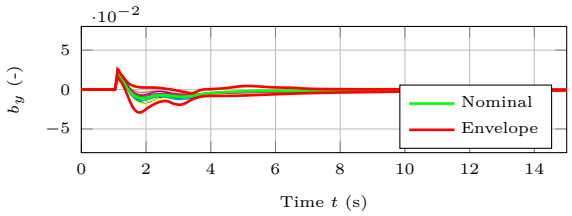

(i) Lateral Acceleration

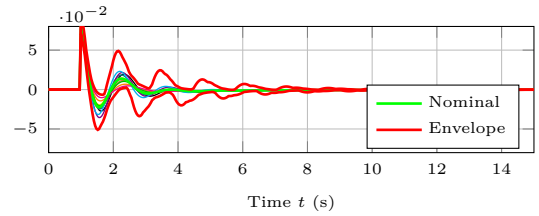

(j) Lateral Acceleration

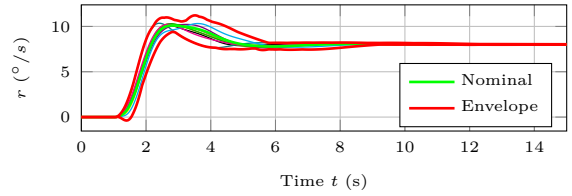

(k) Yaw Rate

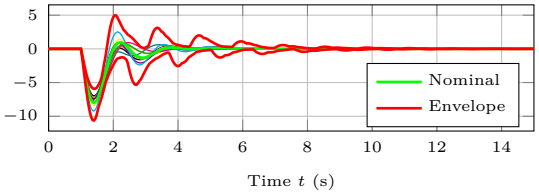

(l) Yaw Rate

Figure E.5: Rigid body states of the LTI plant model with MLESO controller in response to a $30°$ step command $\Phi_{cmd}(t)$ (left column) and to a $5°$ step command $\beta_{W,cmd}(t)$ (right column) at $V_K^R = 35\,m/s$, $h = 1000\,m$, $m_{fuel} = 23\,kg$.

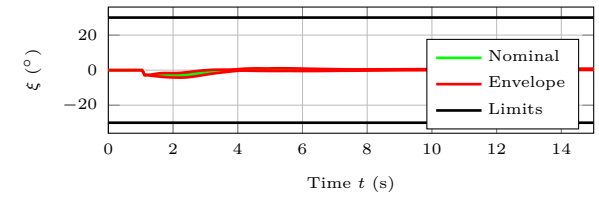

(a) Aileron Deflection

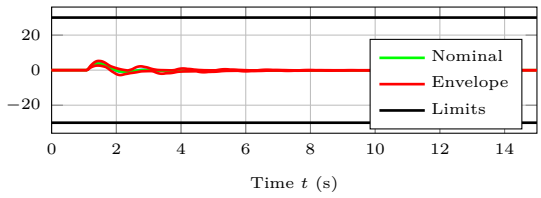

(b) Aileron Deflection

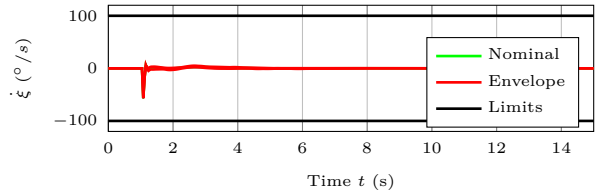

(c) Aileron Rate

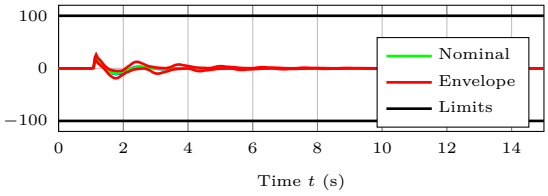

(d) Aileron Rate

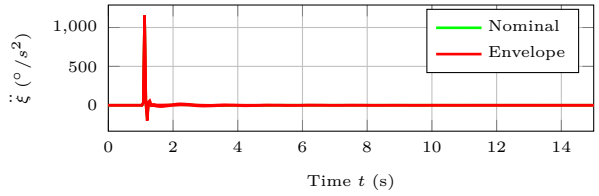

(e) Aileron Acceleration

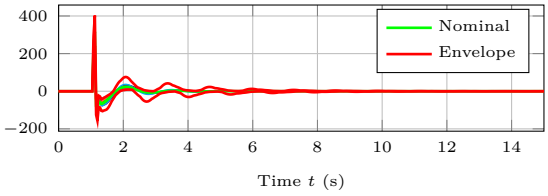

(f) Aileron Acceleration

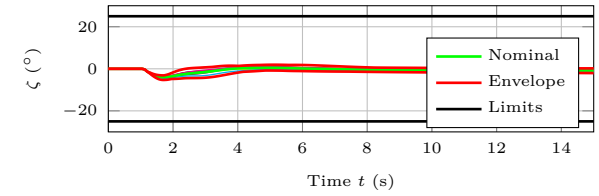

(g) Rudder Deflection

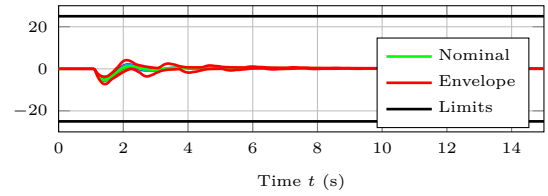

(h) Rudder Deflection

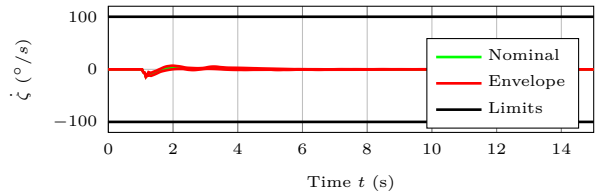

(i) Rudder Rate

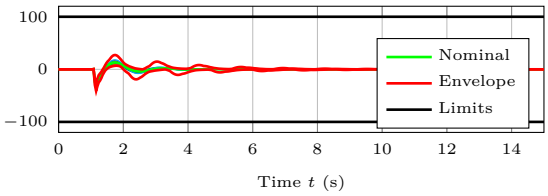

(j) Rudder Rate

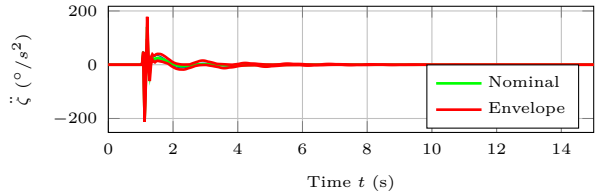

(k) Rudder Acceleration

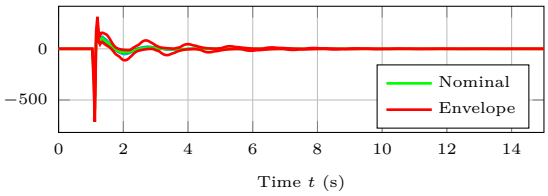

(l) Rudder Acceleration

Figure E.6: Actuator states of the LTI plant model with MLESO controller in response to a $30°$ step command $\Phi_{cmd}(t)$ (left column) and to a $5°$ step command $\beta_{W,cmd}(t)$ (right column) at $V_K^R = 35\,m/s$, $h = 1000\,m$, $m_{fuel} = 23\,kg$.

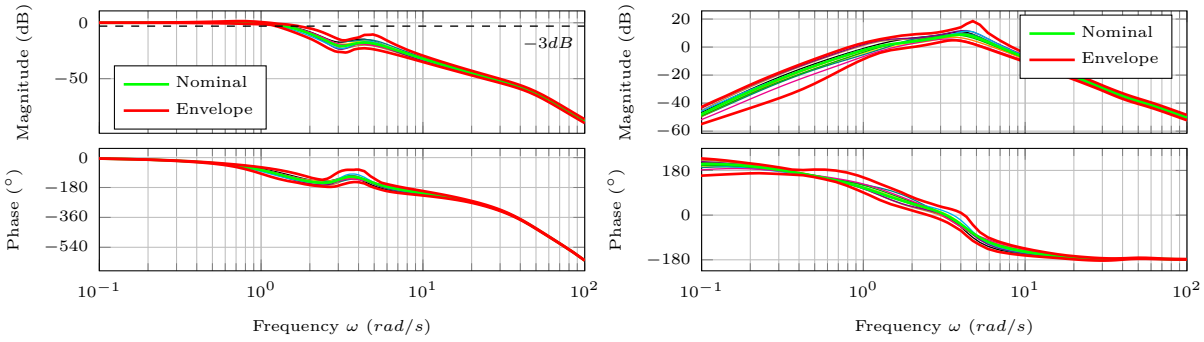

(a) Φ_{cmd} to Bank Angle Φ

(b) $\beta_{W,cmd}$ to Bank Angle Φ

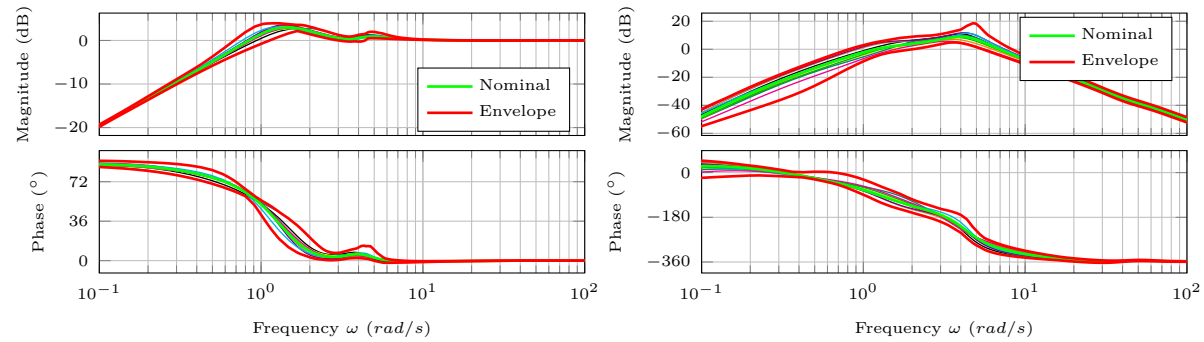

(c) Φ_{cmd} to Tracking Error $\Phi_{cmd} - \Phi$

(d) $\beta_{W,cmd}$ to Tracking Error $\Phi_{cmd} - \Phi$

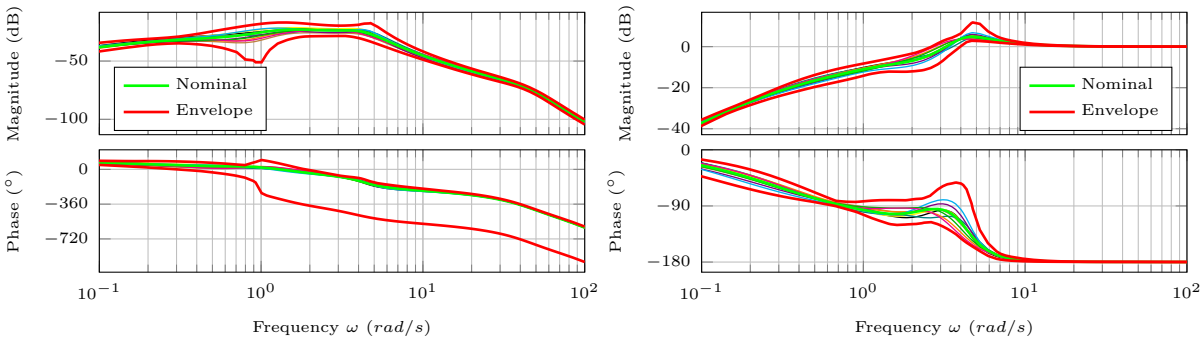

(e) Φ_{cmd} to Angle-of-sideslip β_A

(f) $\beta_{W,cmd}$ to Angle-of-sideslip β_A

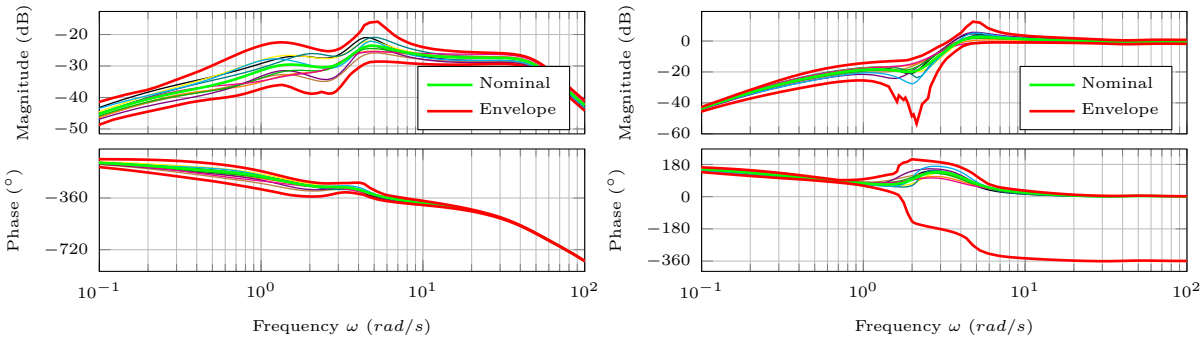

(g) Φ_{cmd} to Lateral Acceleration b_y

(h) $\beta_{W,cmd}$ to Lateral Acceleration b_y

Figure E.7: Bode plots of the closed-loop rigid-body states at $V_K^R = 35\,m/s$, $h = 1000\,m$, $m_{fuel} = 23\,kg$, when relying on a MLESO controller.

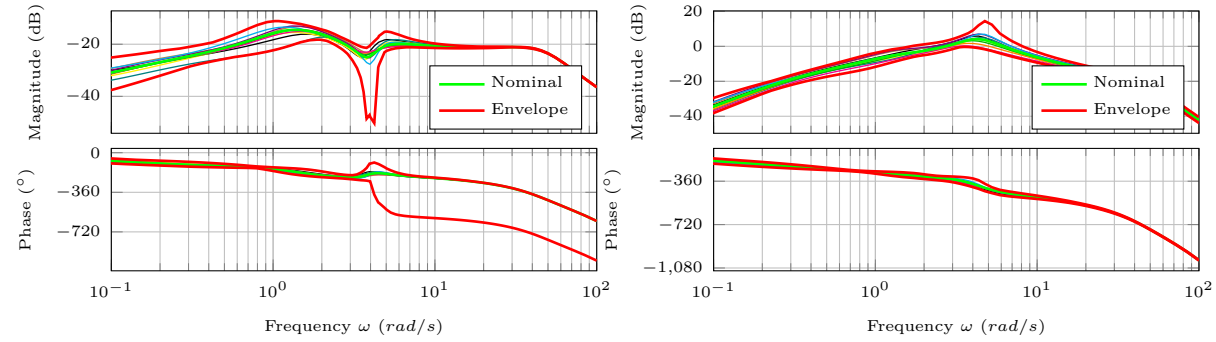

(a) Φ_{cmd} to Aileron Deflection ξ

(b) $\beta_{W,cmd}$ to Aileron Deflection ξ

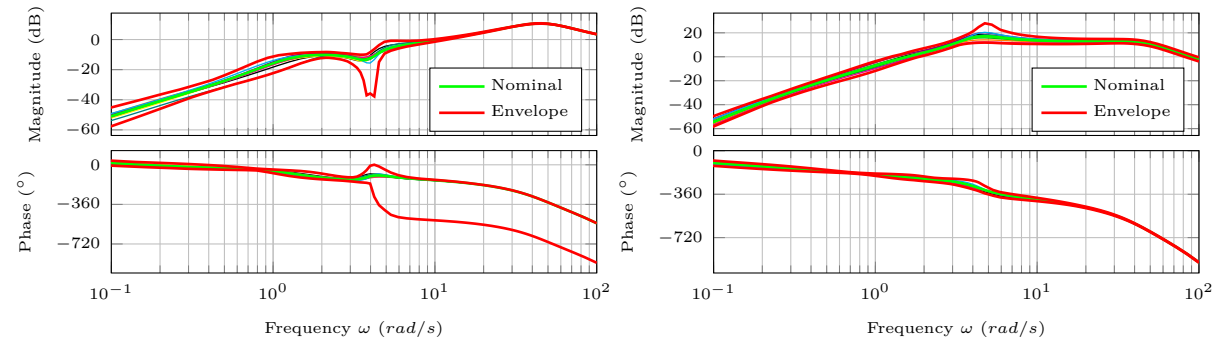

(c) Φ_{cmd} to Aileron Rate $\dot{\xi}$

(d) $\beta_{W,cmd}$ to Aileron Rate $\dot{\xi}$

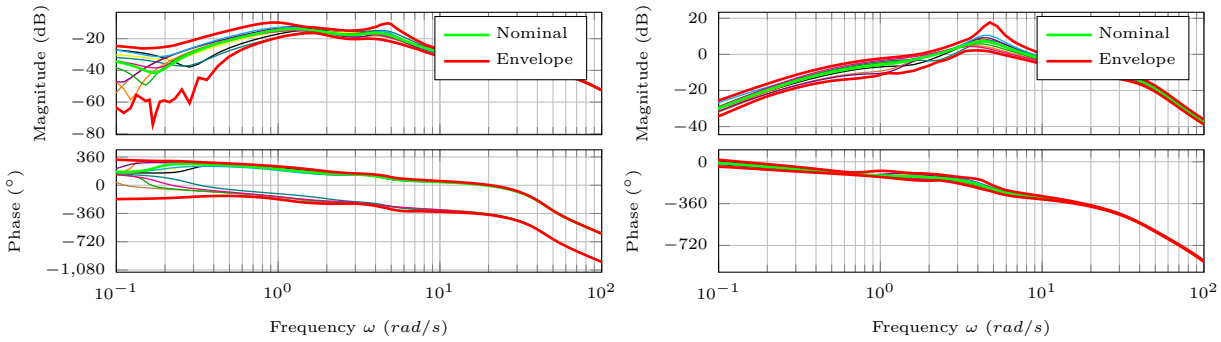

(e) Φ_{cmd} to Rudder Deflection ζ

(f) $\beta_{W,cmd}$ to Rudder Deflection ζ

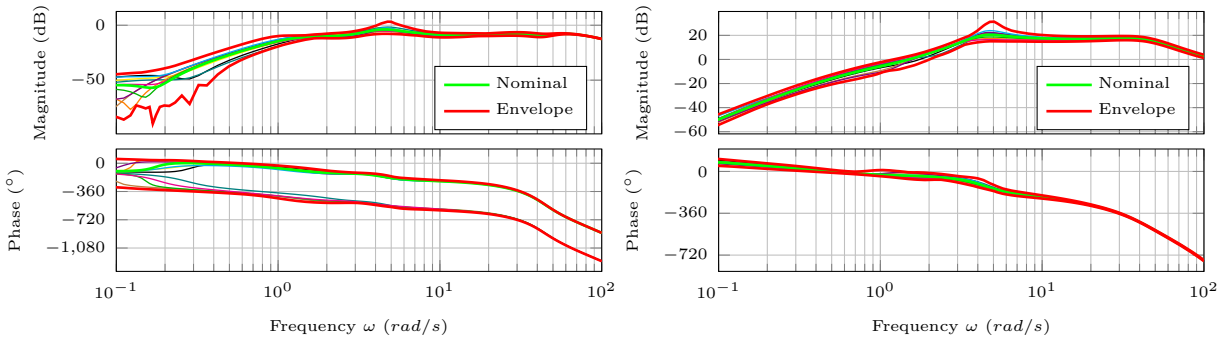

(g) Φ_{cmd} to Rudder Rate $\dot{\zeta}$

(h) $\beta_{W,cmd}$ to Rudder Rate $\dot{\zeta}$

Figure E.8: Bode plots of the closed-loop actuator states at $V_K^R = 35\,m/s$, $h = 1000\,m$, $m_{fuel} = 23\,kg$, when relying on a MLESO controller.

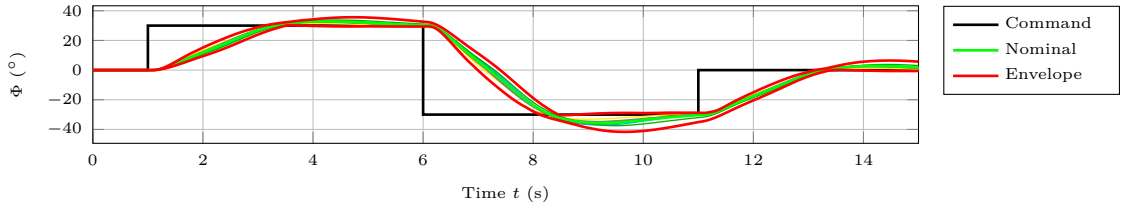

(a) Bank Angle

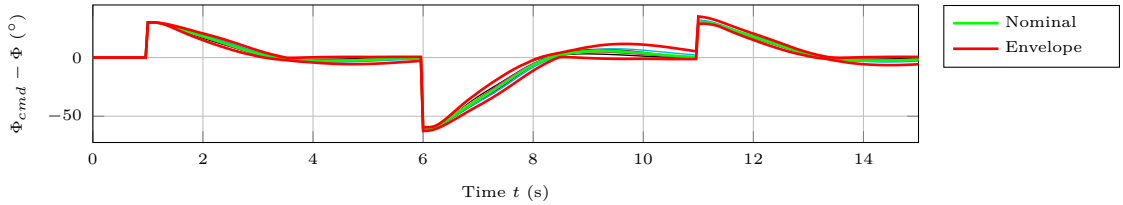

(b) Tracking Error

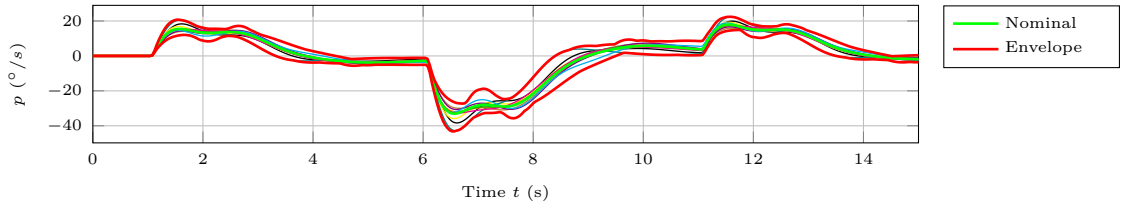

(c) Roll Rate

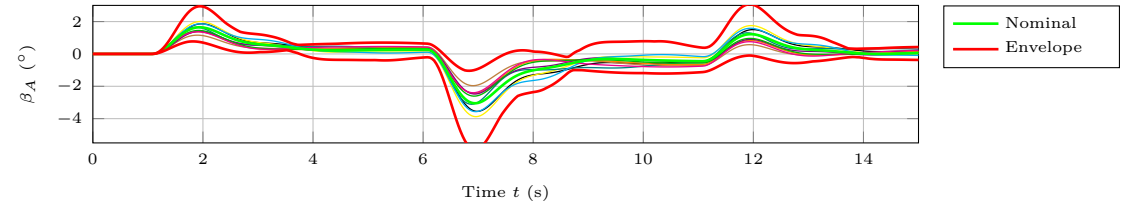

(d) Angle-of-sideslip

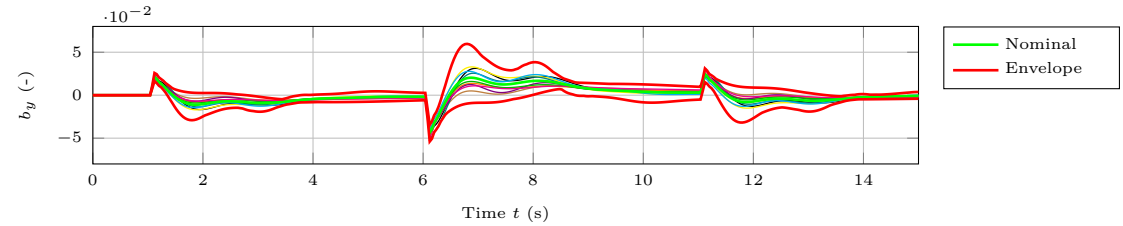

(e) Lateral Acceleration

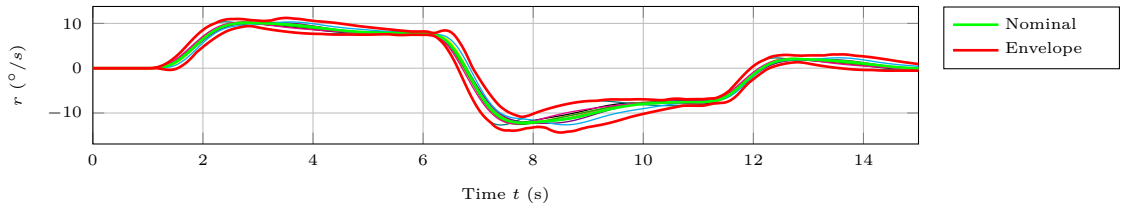

(f) Yaw Rate

Figure E.9: Rigid body states of the LTI plant model with MLESO controller in response to a $30°$ doublet command $\Phi_{cmd}(t)$ at $V_K^R = 35\,m/s$, $h = 1000\,m$, $m_{fuel} = 23\,kg$.

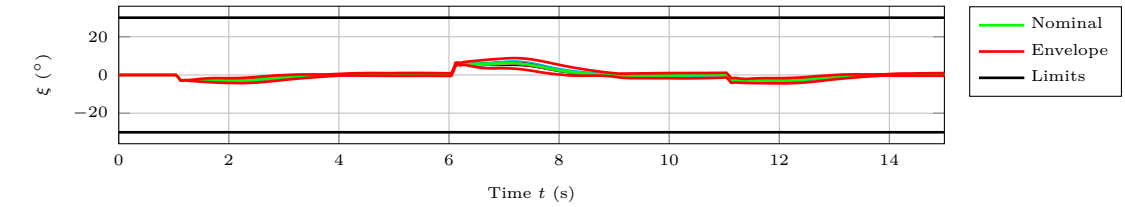

(a) Aileron Deflection

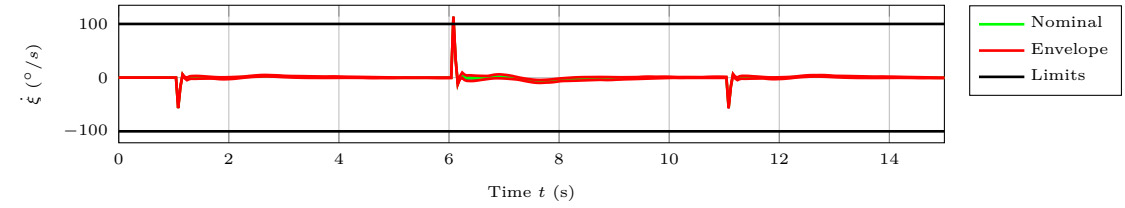

(b) Aileron Rate

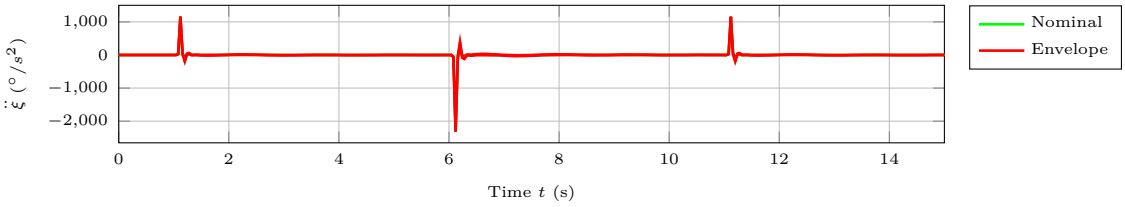

(c) Aileron Acceleration

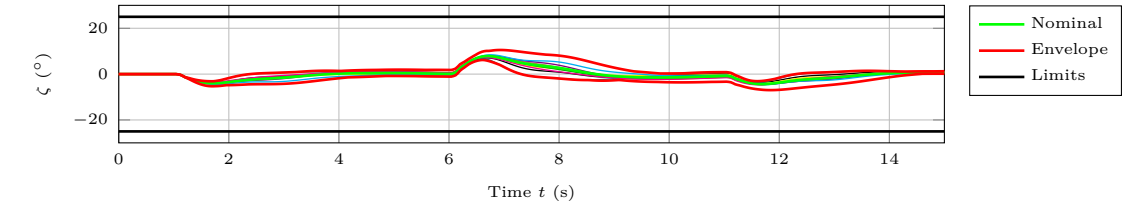

(d) Rudder Deflection

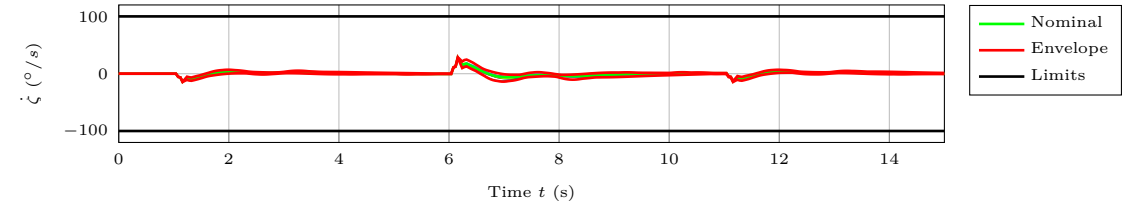

(e) Rudder Rate

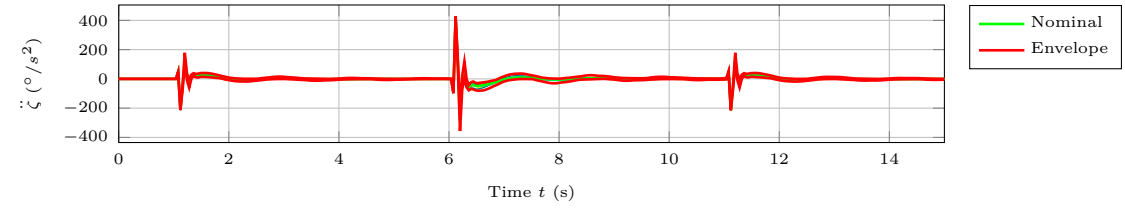

(f) Rudder Acceleration

Figure E.10: Actuator states of the LTI plant model with MLESO controller in response to a $30°$ doublet command $\Phi_{cmd}(t)$ at $V_K^R = 35\,m/s$, $h = 1000\,m$, $m_{fuel} = 23\,kg$.

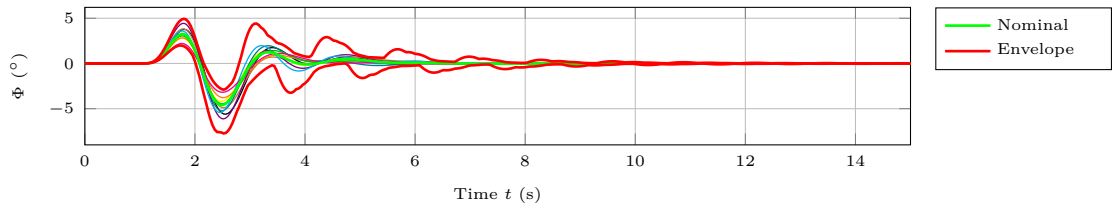

(a) Bank Angle

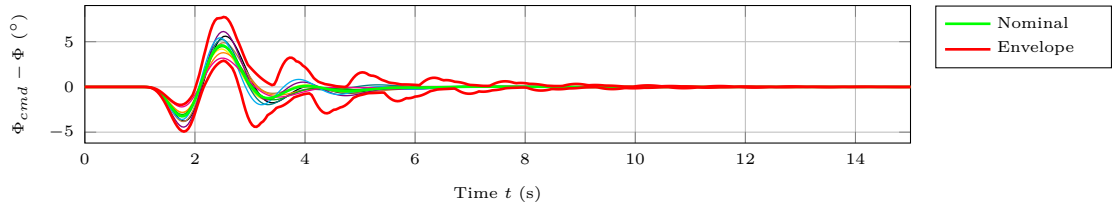

(b) Tracking Error

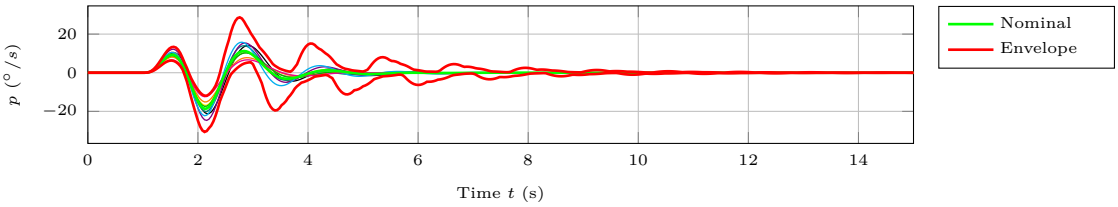

(c) Roll Rate

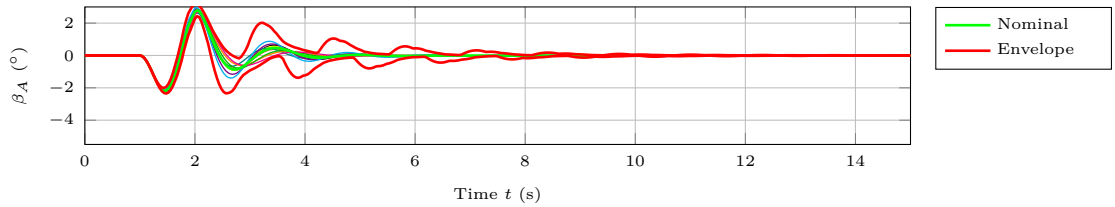

(d) Angle-of-sideslip

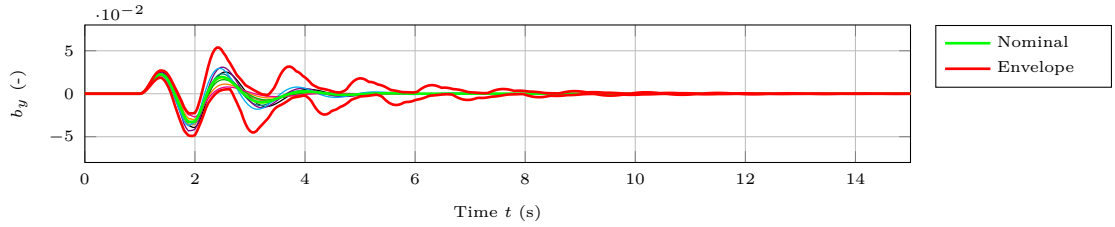

(e) Lateral Acceleration

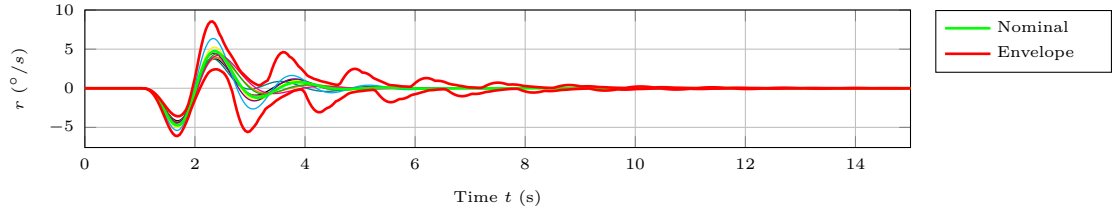

(f) Yaw Rate

Figure E.11: Rigid body states of the LTI plant model with MLESO controller in response to a $20\,m$ discrete gust at $V_K^R = 35\,m/s$, $h = 1000\,m$, $m_{fuel} = 23\,kg$.

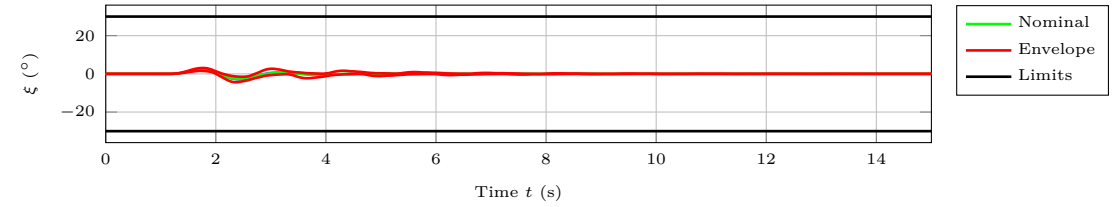

(a) Aileron Deflection

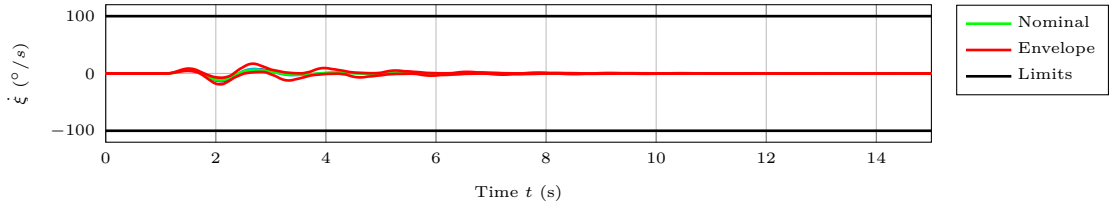

(b) Aileron Rate

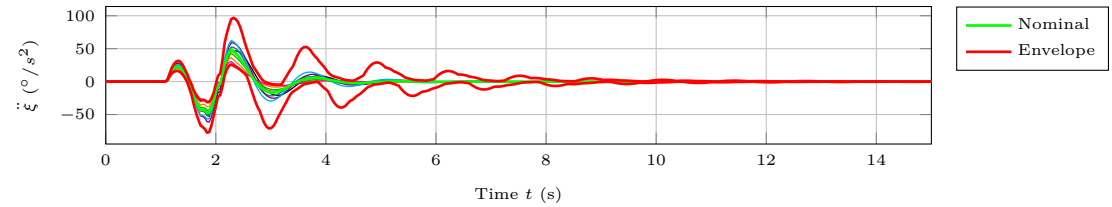

(c) Aileron Acceleration

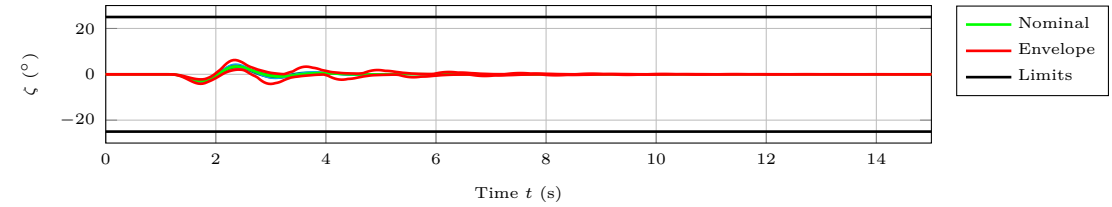

(d) Rudder Deflection

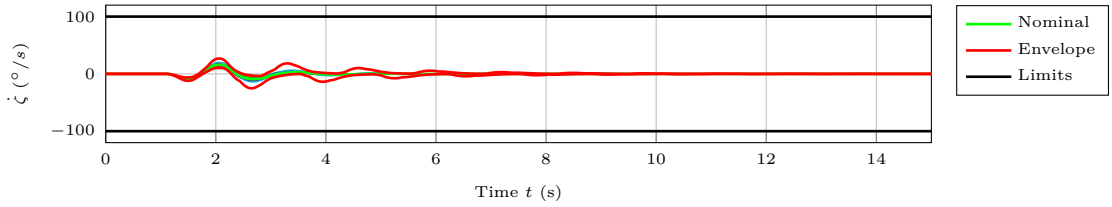

(e) Rudder Rate

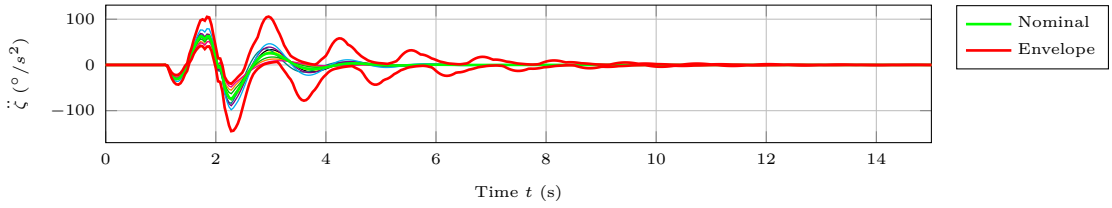

(f) Rudder Acceleration

Figure E.12: Actuator states of the LTI plant model with MLESO controller in response to a $20\,m$ discrete gust at $V_K^R = 35\,m/s$, $h = 1000\,m$, $m_{fuel} = 23\,kg$.

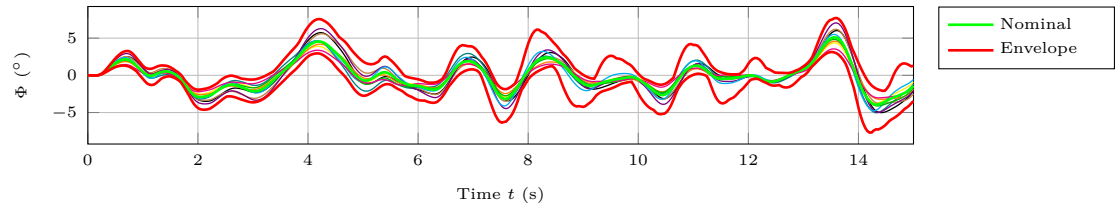

(a) Bank Angle

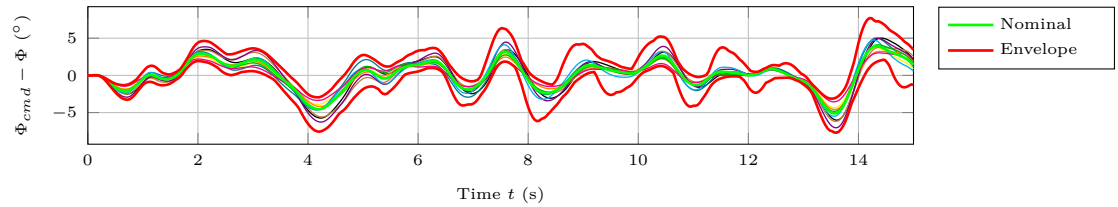

(b) Tracking Error

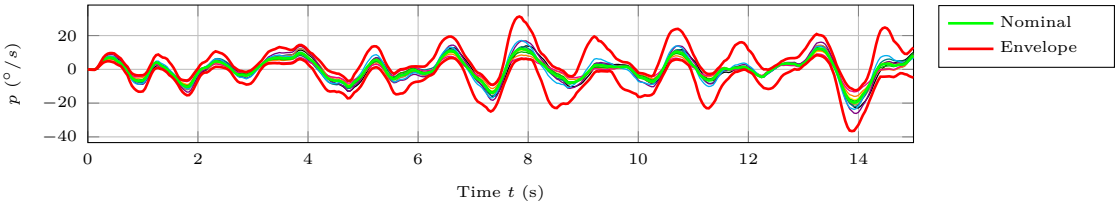

(c) Roll Rate

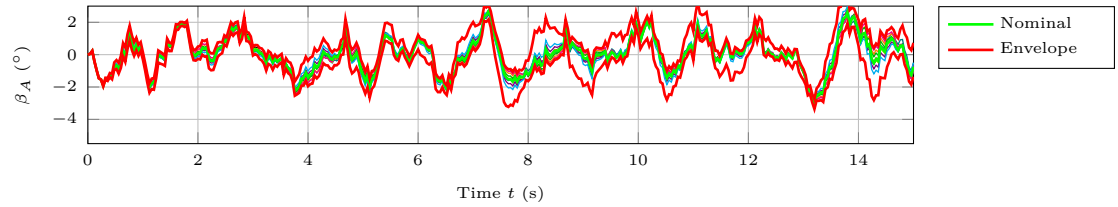

(d) Angle-of-sideslip

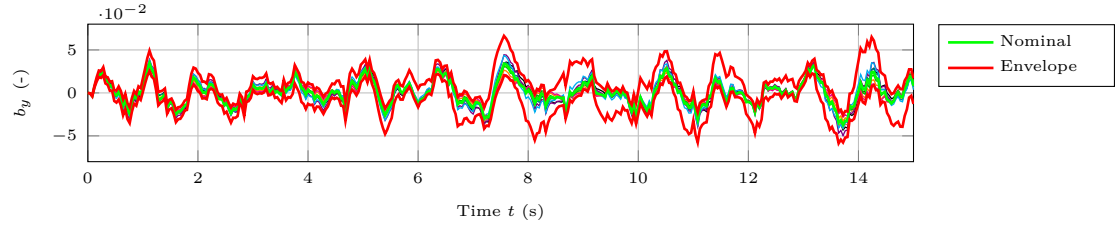

(e) Lateral Acceleration

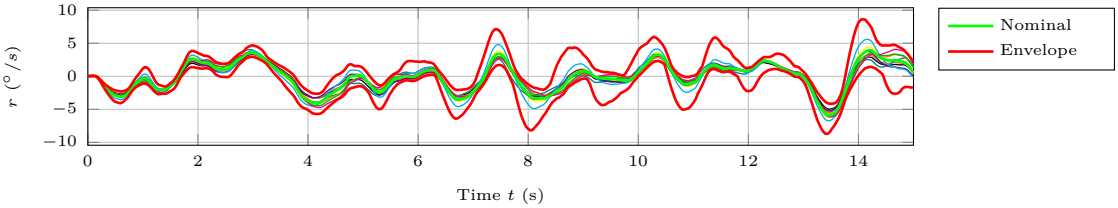

(f) Yaw Rate

Figure E.13: Rigid body states of the LTI plant model with MLESO controller in response to moderate Dryden turbulence at $V_K^R = 35\,m/s$, $h = 1000\,m$, $m_{fuel} = 23\,kg$.

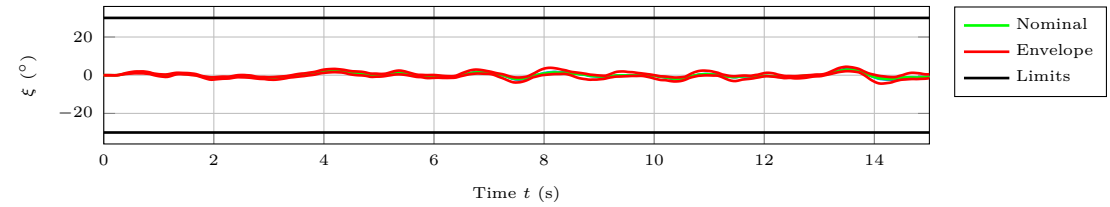

(a) Aileron Deflection

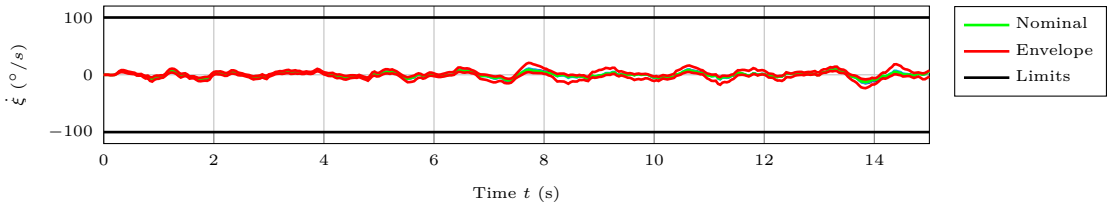

(b) Aileron Rate

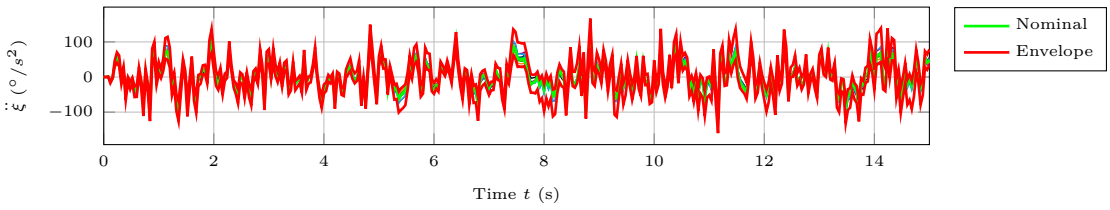

(c) Aileron Acceleration

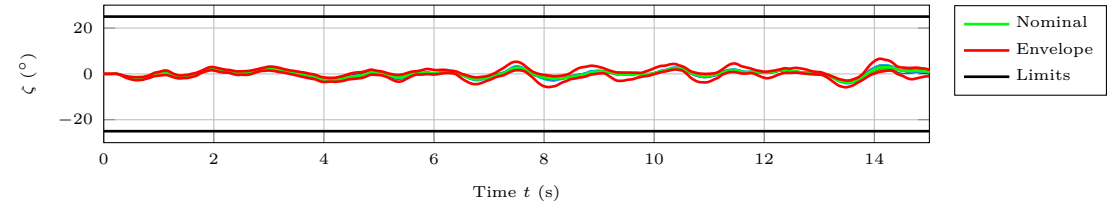

(d) Rudder Deflection

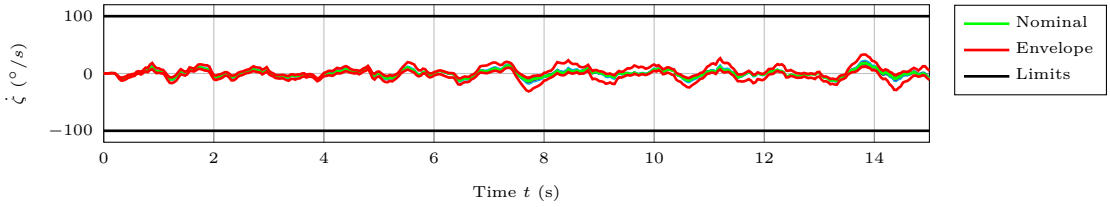

(e) Rudder Rate

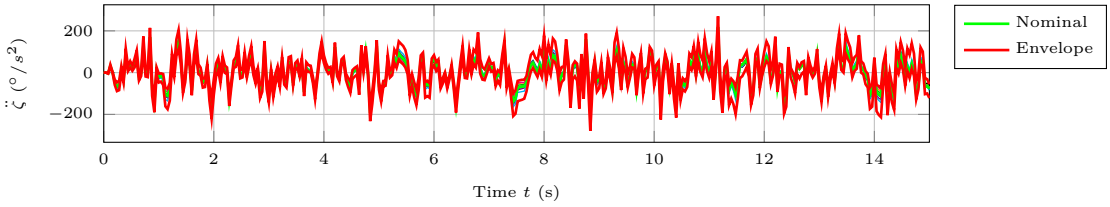

(f) Rudder Acceleration

Figure E.14: Actuator states of the LTI plant model with MLESO controller in response to moderate Dryden turbulence at $V_K^R = 35\,m/s$, $h = 1000\,m$, $m_{fuel} = 23\,kg$.

E.1.2 Linear Model at 50 m/s

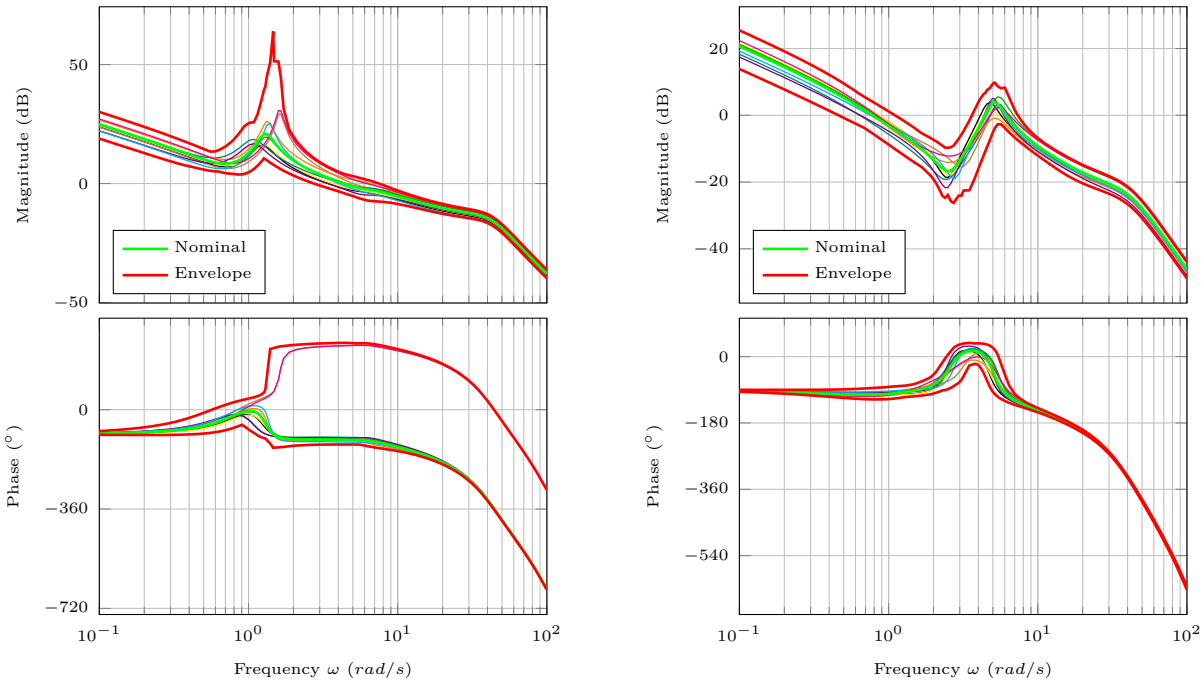

(a) Loopcut at aileron actuator input ξ

(b) Loopcut at rudder actuator input ζ

Figure E.15: Open-loop bode plots at $V_K^R = 50\,m/s$, $h = 500\,m$, $m_{fuel} = 0\,kg$, when relying on a MLESO controller.

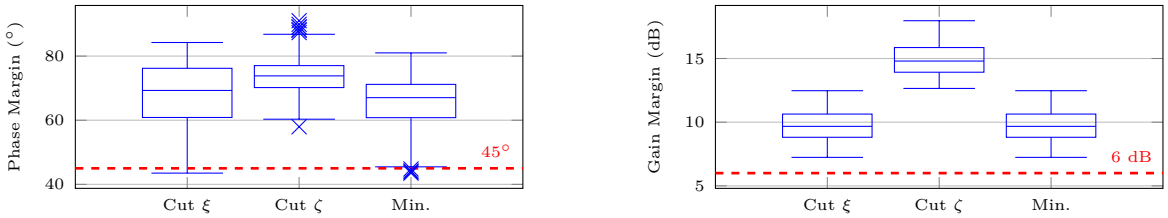

(a) Phase Margin

(b) Gain Margin

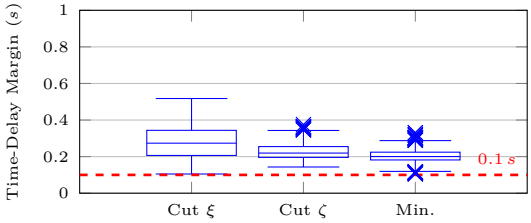

(c) Time-Delay Margin

Figure E.16: Box plots of phase, gain and time-delay margin of the MLESO controller at $V_K^R = 50\,m/s$, $h = 500\,m$, $m_{fuel} = 0\,kg$.

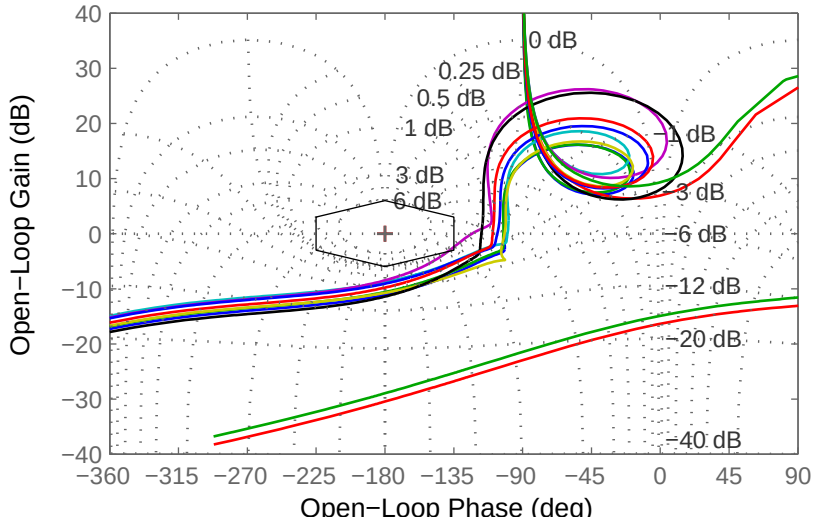

(a) Loopcut in front of the aileron control delay

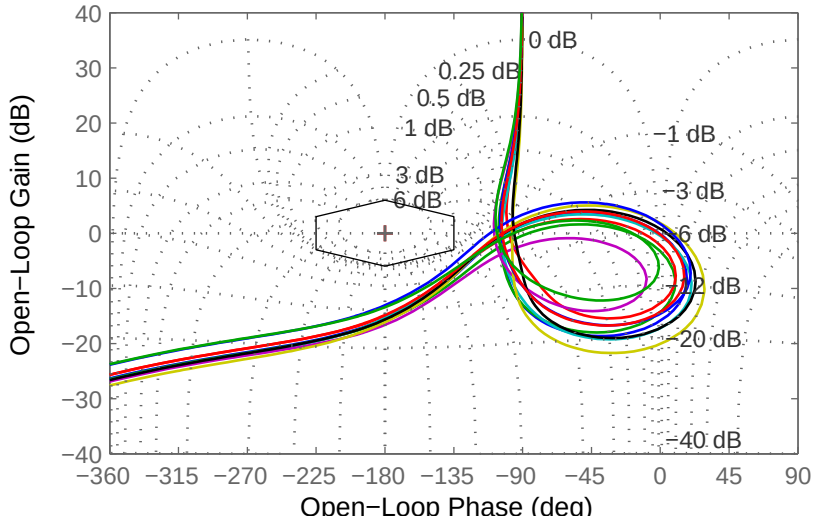

(b) Loopcut in front of the rudder control delay

Figure E.17: Nichols plots at $V_K^R = 50\,m/s$, $h = 500\,m$, $m_{fuel} = 0\,kg$, when relying on a MLESO controller.

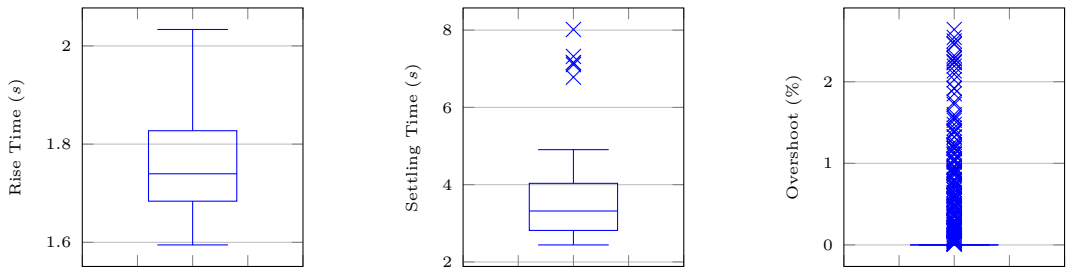

(a) Rise Time (b) Settling Time (c) Overhoot

Figure E.18: Box plots of rise time, settling time and overshoot of the LTI plant model with MLESO controller in case of a $30°$ step command $\Phi_{cmd}(t)$ at $V_K^R = 50\,m/s$, $h = 500\,m$, $m_{fuel} = 0\,kg$.

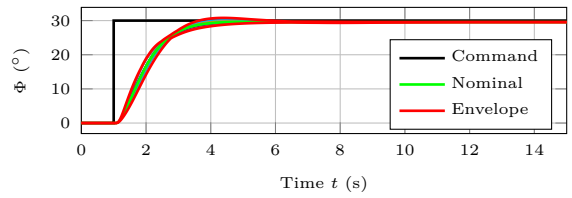

(a) Bank Angle

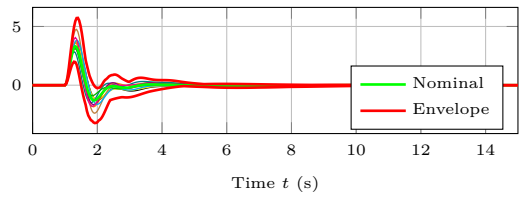

(b) Bank Angle

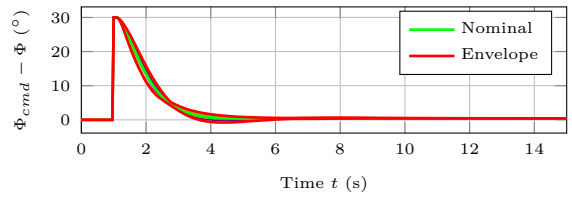

(c) Tracking Error

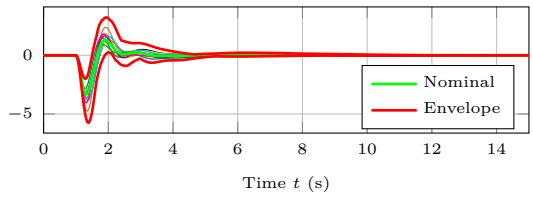

(d) Tracking Error

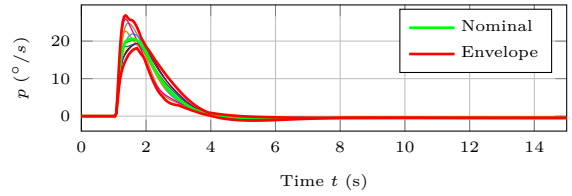

(e) Roll Rate

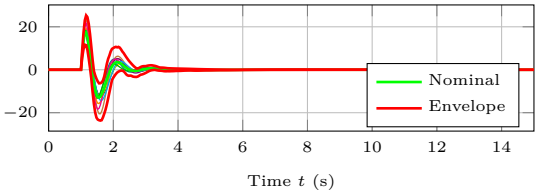

(f) Roll Rate

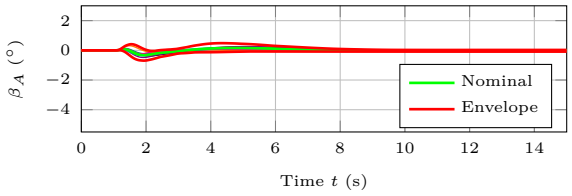

(g) Angle-of-sideslip

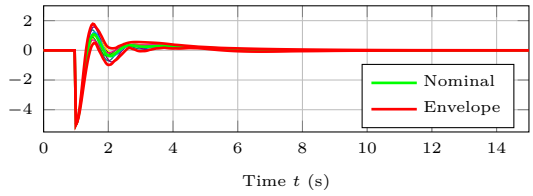

(h) Angle-of-sideslip

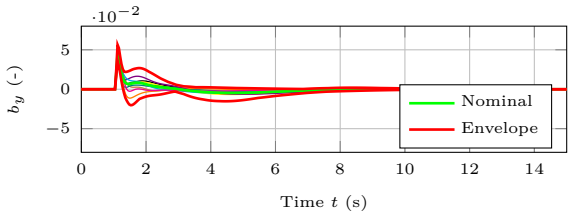

(i) Lateral Acceleration

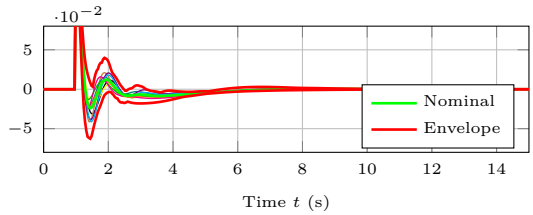

(j) Lateral Acceleration

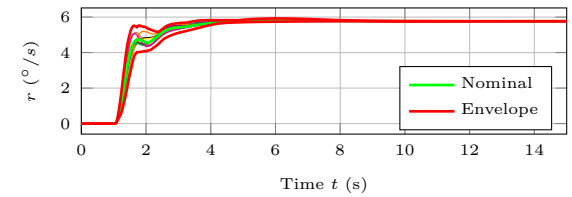

(k) Yaw Rate

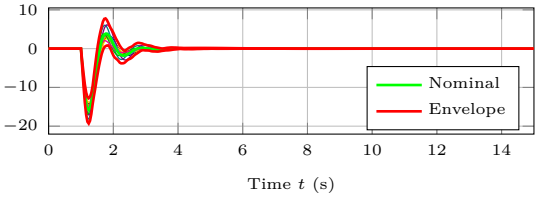

(l) Yaw Rate

Figure E.19: Rigid body states of the LTI plant model with MLESO controller in response to a $30°$ step command $\Phi_{cmd}(t)$ (left column) and to a $5°$ step command $\beta_{W,cmd}(t)$ (right column) at $V_K^R = 50\,m/s$, $h = 500\,m$, $m_{fuel} = 0\,kg$.

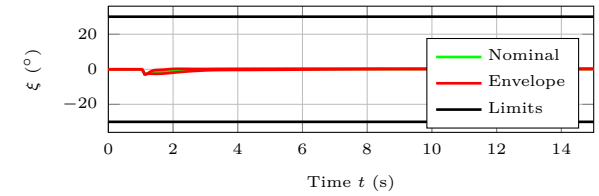

(a) Aileron Deflection

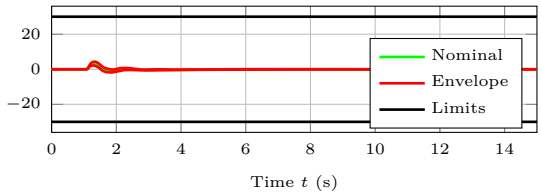

(b) Aileron Deflection

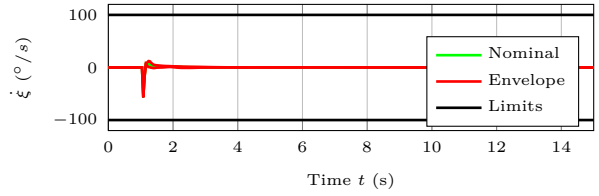

(c) Aileron Rate

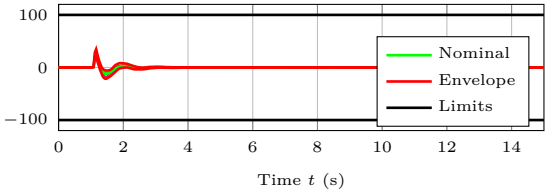

(d) Aileron Rate

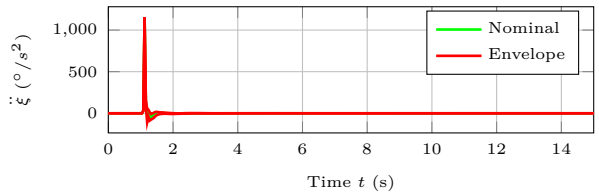

(e) Aileron Acceleration

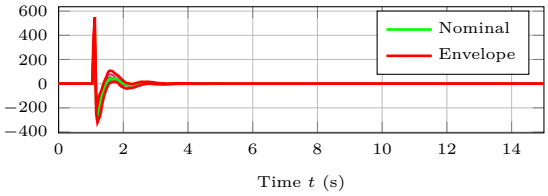

(f) Aileron Acceleration

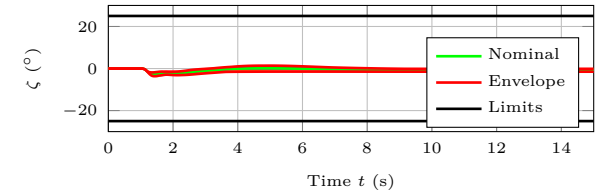

(g) Rudder Deflection

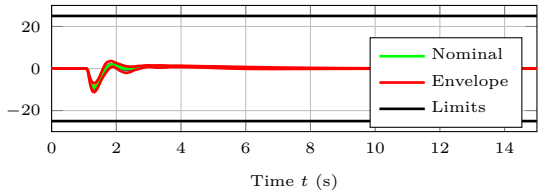

(h) Rudder Deflection

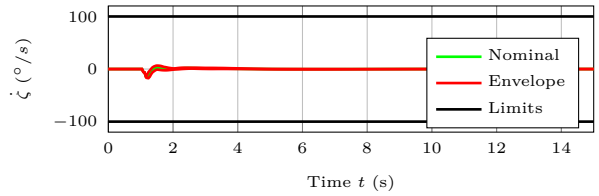

(i) Rudder Rate

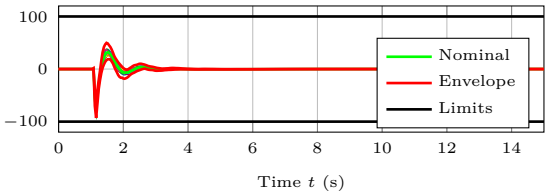

(j) Rudder Rate

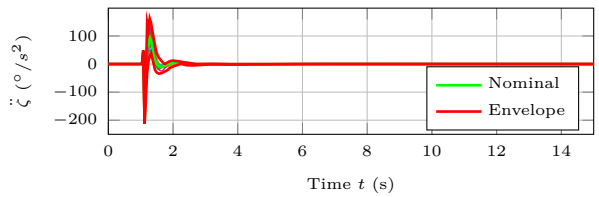

(k) Rudder Acceleration

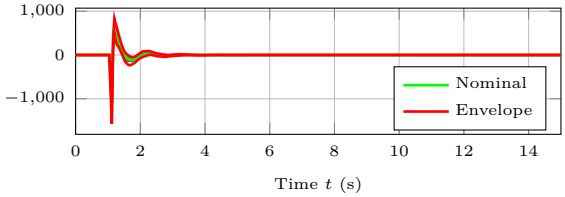

(l) Rudder Acceleration

Figure E.20: Actuator states of the LTI plant model with MLESO controller in response to a $30°$ step command $\Phi_{cmd}(t)$ (left column) and to a $5°$ step command $\beta_{W,cmd}(t)$ (right column) at $V_K^R = 50\,m/s$, $h = 500\,m$, $m_{fuel} = 0\,kg$.

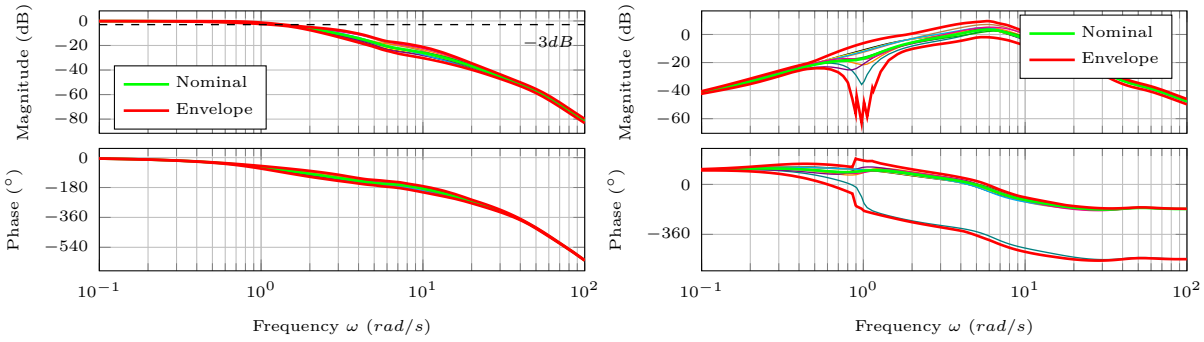

(a) Φ_{cmd} to Bank Angle Φ

(b) $\beta_{W,cmd}$ to Bank Angle Φ

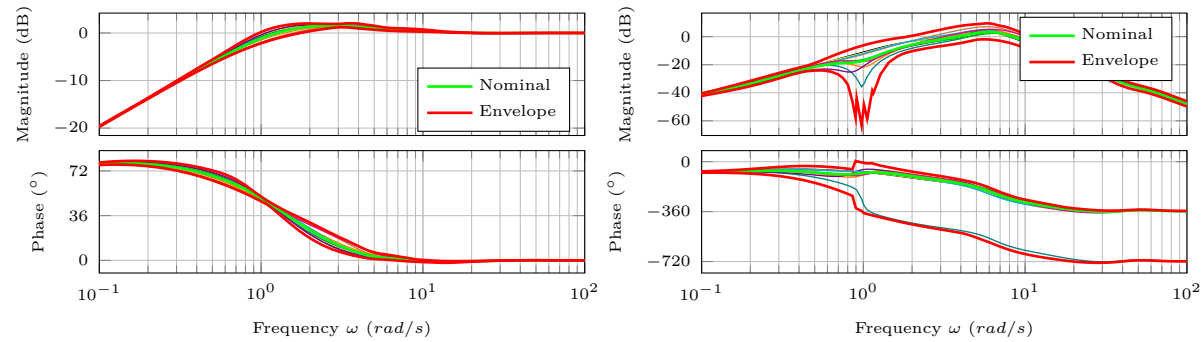

(c) Φ_{cmd} to Tracking Error $\Phi_{cmd} - \Phi$

(d) $\beta_{W,cmd}$ to Tracking Error $\Phi_{cmd} - \Phi$

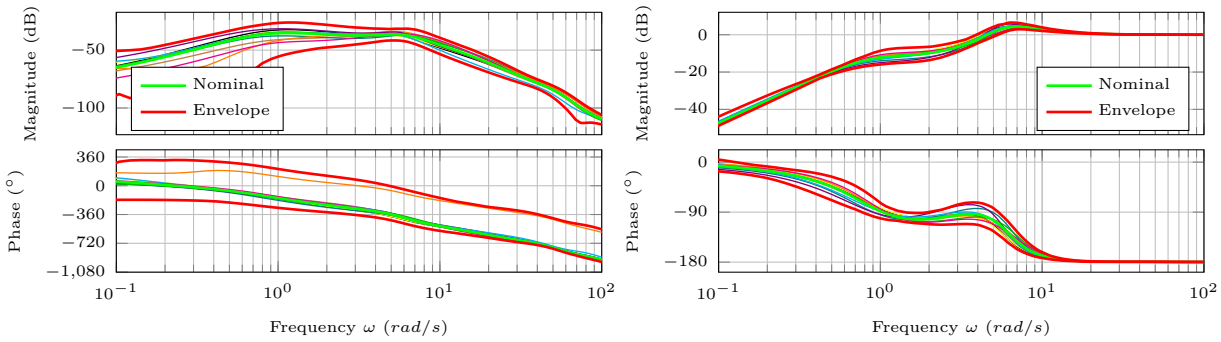

(e) Φ_{cmd} to Angle-of-sideslip β_A

(f) $\beta_{W,cmd}$ to Angle-of-sideslip β_A

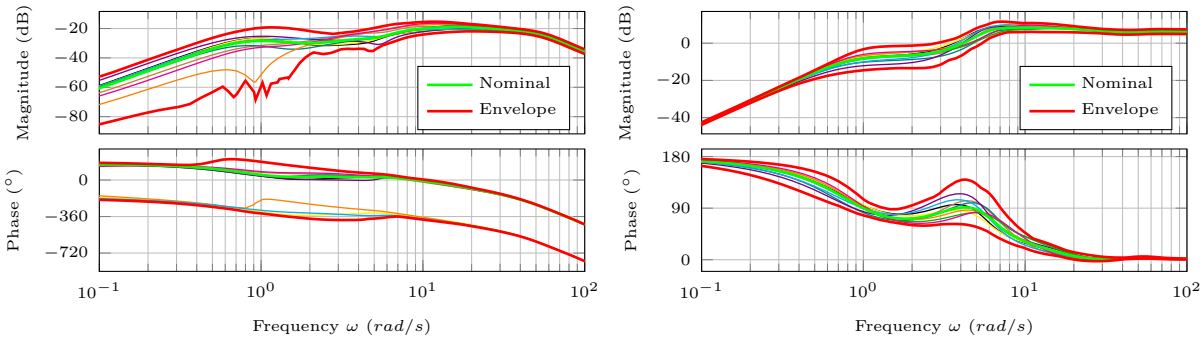

(g) Φ_{cmd} to Lateral Acceleration b_y

(h) $\beta_{W,cmd}$ to Lateral Acceleration b_y

Figure E.21: Bode plots of the closed-loop rigid-body states at $V_K^R = 50\,m/s$, $h = 500\,m$, $m_{fuel} = 0\,kg$, when relying on a MLESO controller.

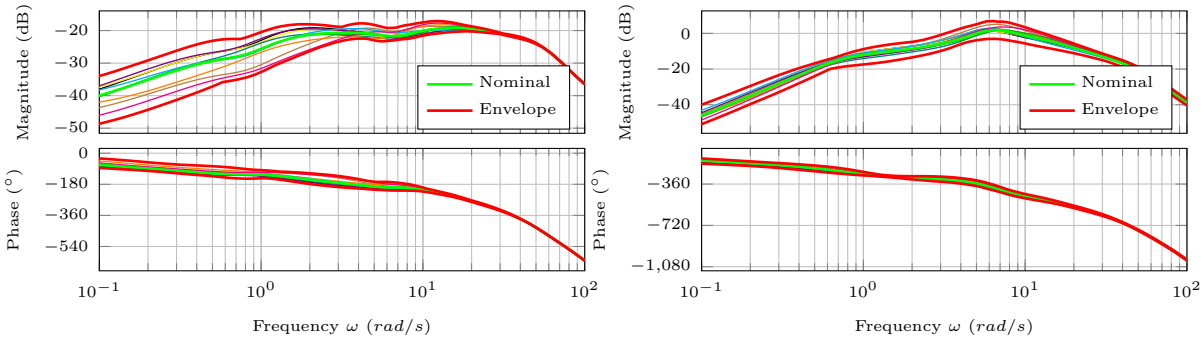

(a) Φ_{cmd} to Aileron Deflection ξ

(b) $\beta_{W,cmd}$ to Aileron Deflection ξ

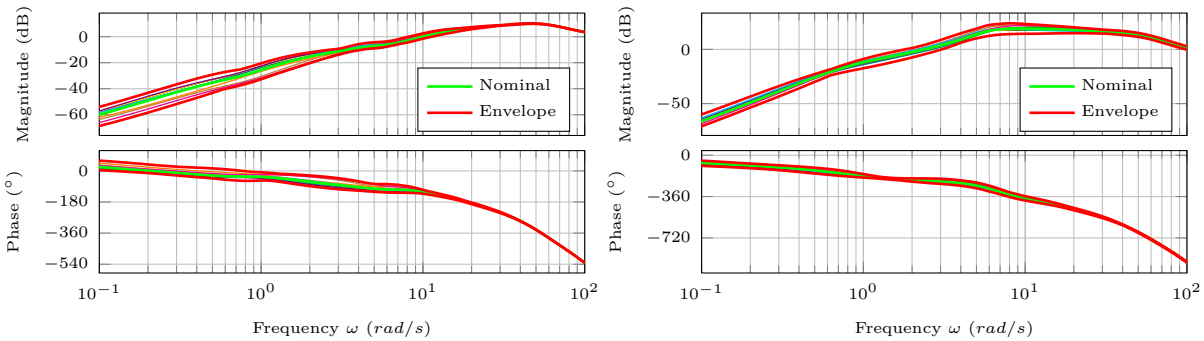

(c) Φ_{cmd} to Aileron Rate $\dot{\xi}$

(d) $\beta_{W,cmd}$ to Aileron Rate $\dot{\xi}$

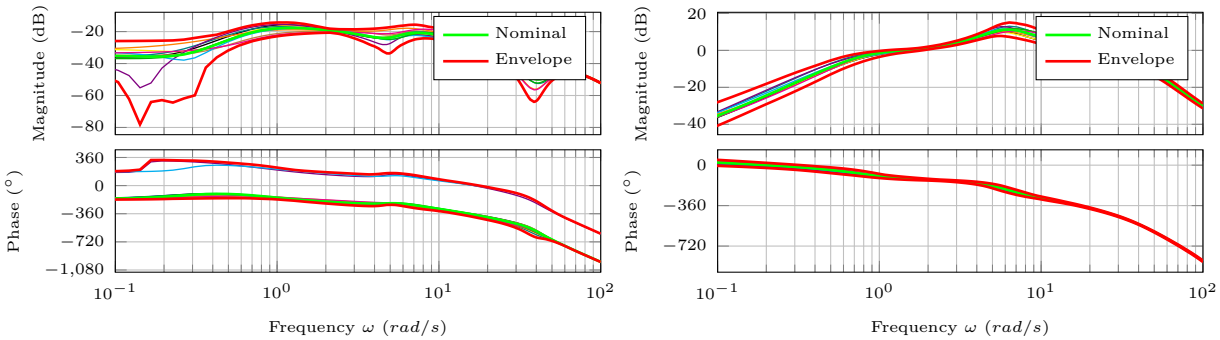

(e) Φ_{cmd} to Rudder Deflection ζ

(f) $\beta_{W,cmd}$ to Rudder Deflection ζ

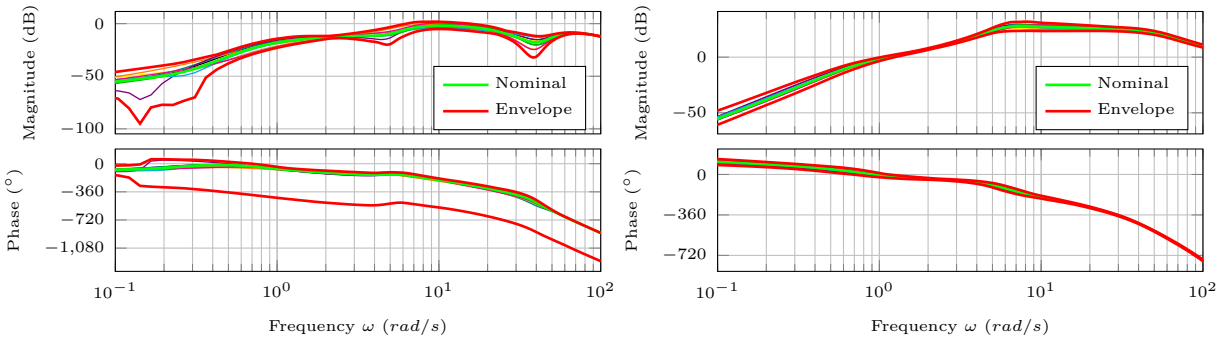

(g) Φ_{cmd} to Rudder Rate $\dot{\zeta}$

(h) $\beta_{W,cmd}$ to Rudder Rate $\dot{\zeta}$

Figure E.22: Bode plots of the closed-loop actuator states at $V_K^R = 50\,m/s$, $h = 500\,m$, $m_{fuel} = 0\,kg$, when relying on a MLESO controller.

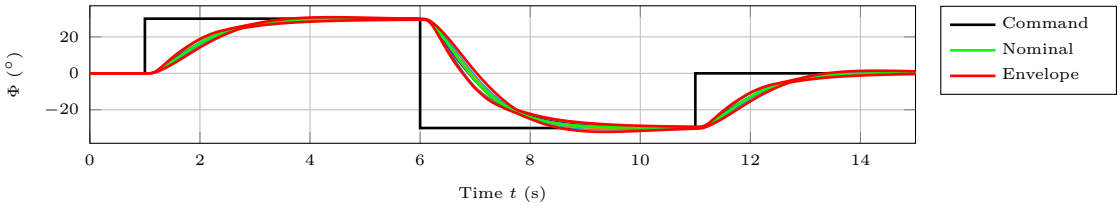

(a) Bank Angle

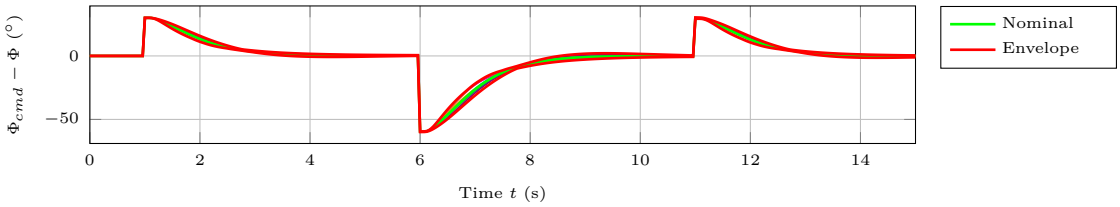

(b) Tracking Error

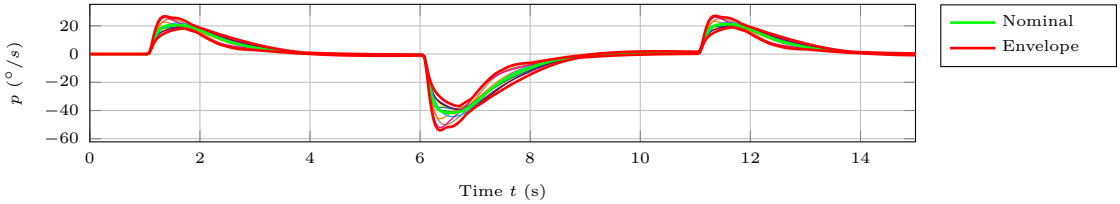

(c) Roll Rate

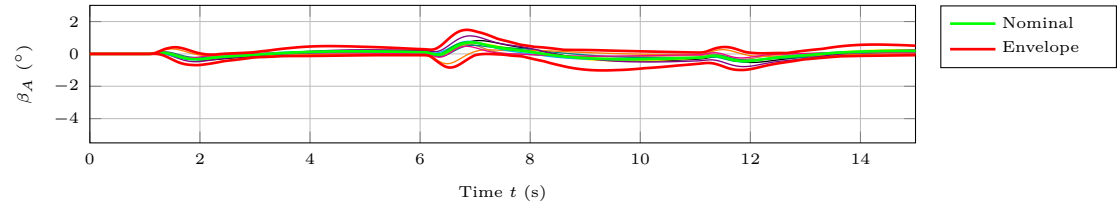

(d) Angle-of-sideslip

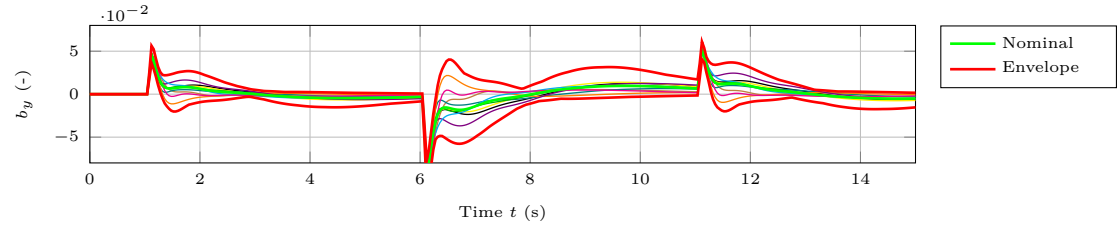

(e) Lateral Acceleration

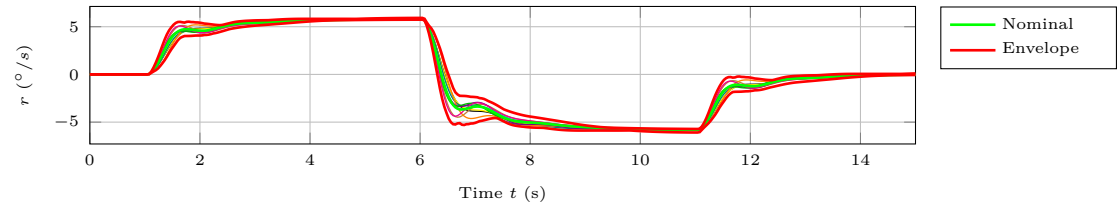

(f) Yaw Rate

Figure E.23: Rigid body states of the LTI plant model with MLESO controller in response to a $30°$ doublet command $\Phi_{cmd}(t)$ at $V_K^R = 50\,m/s$, $h = 500\,m$, $m_{fuel} = 0\,kg$.

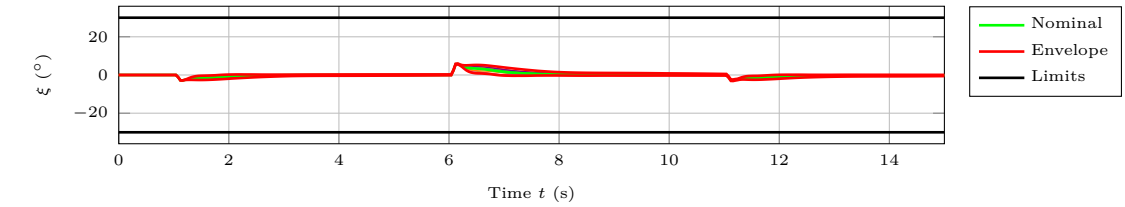

(a) Aileron Deflection

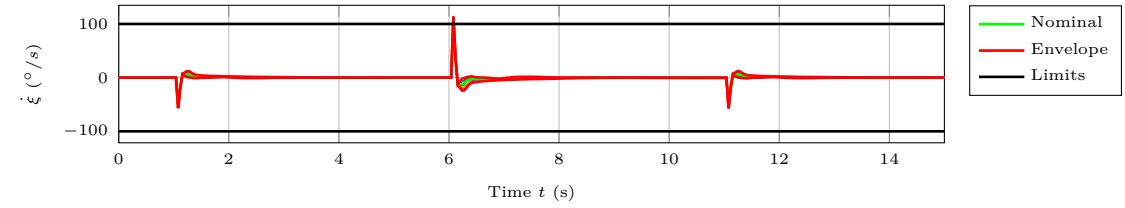

(b) Aileron Rate

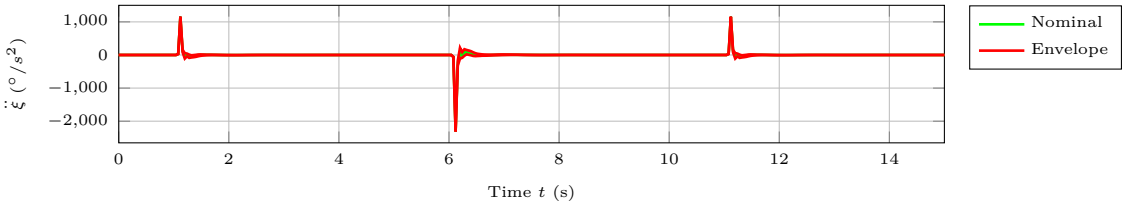

(c) Aileron Acceleration

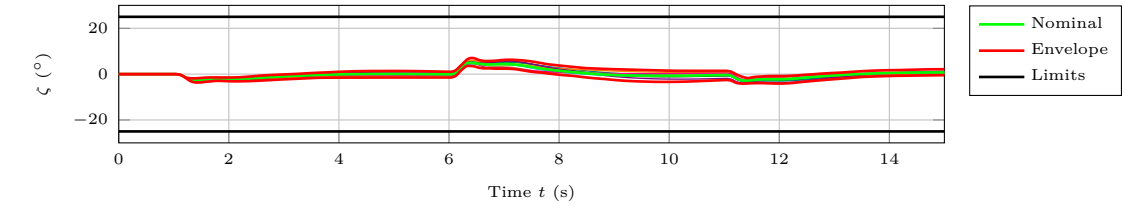

(d) Rudder Deflection

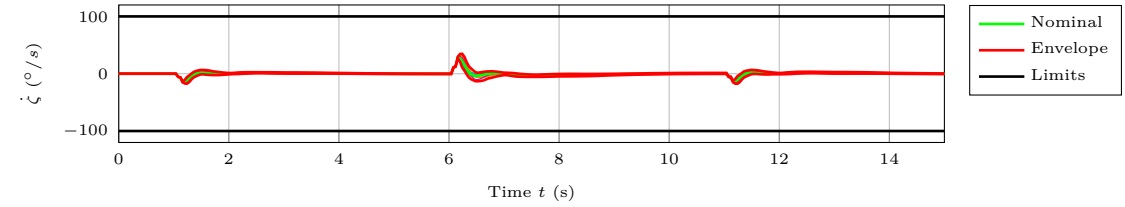

(e) Rudder Rate

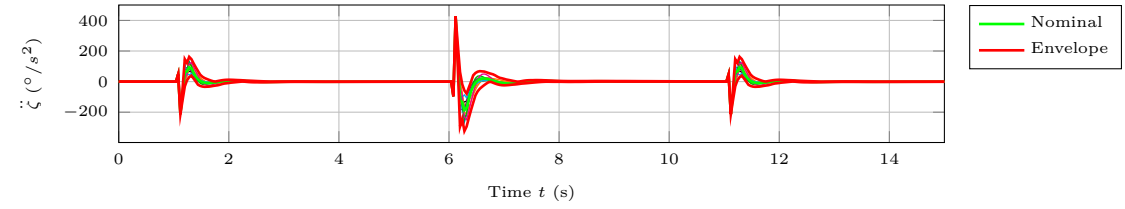

(f) Rudder Acceleration

Figure E.24: Actuator states of the LTI plant model with MLESO controller in response to a $30°$ doublet command $\Phi_{cmd}(t)$ at $V_K^R = 50\,m/s$, $h = 500\,m$, $m_{fuel} = 0\,kg$.

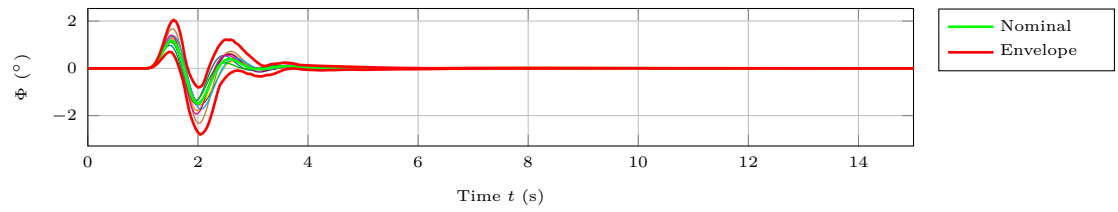

(a) Bank Angle

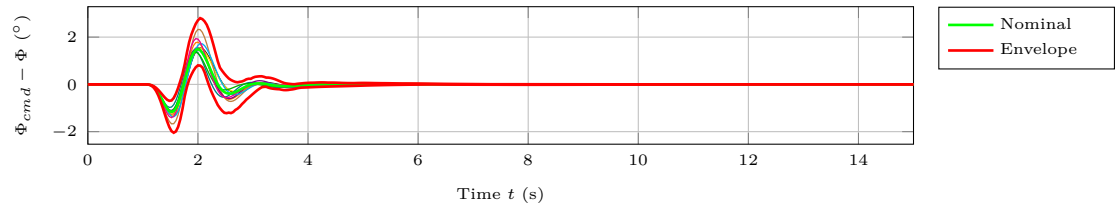

(b) Tracking Error

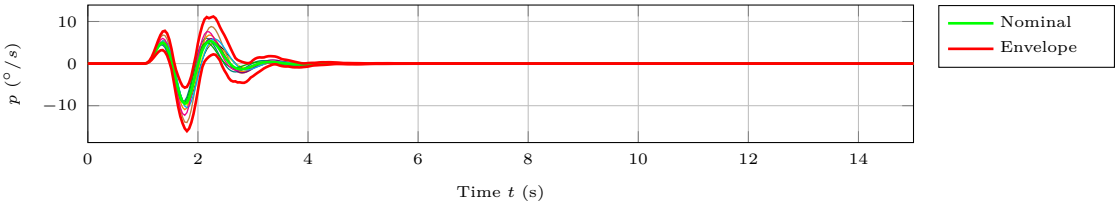

(c) Roll Rate

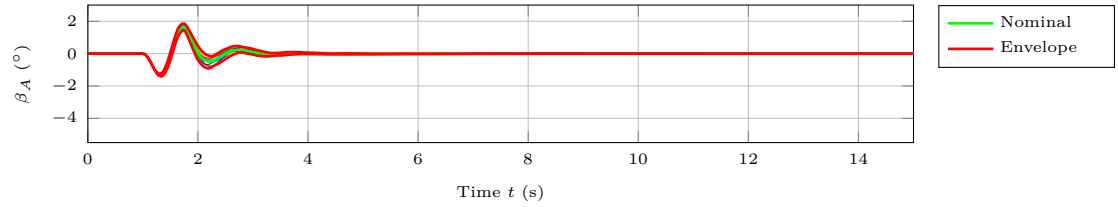

(d) Angle-of-sideslip

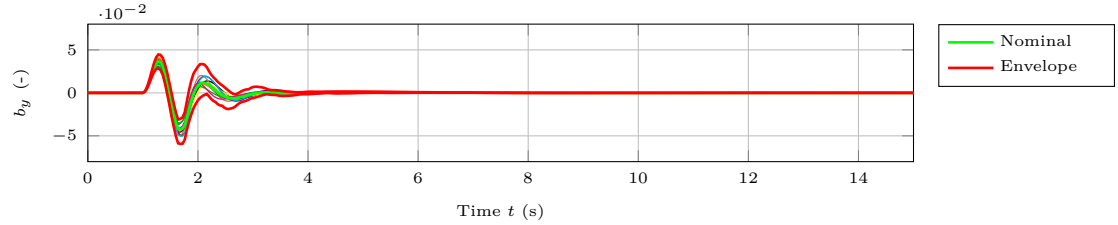

(e) Lateral Acceleration

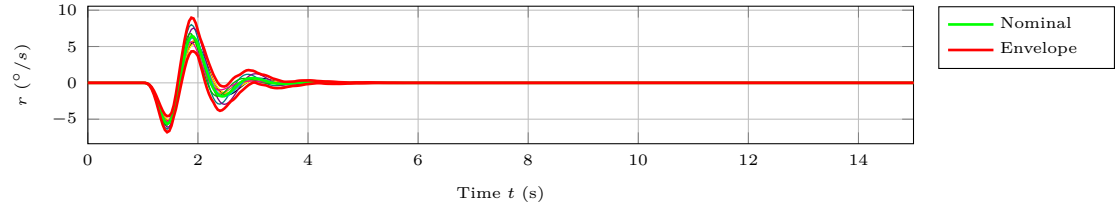

(f) Yaw Rate

Figure E.25: Rigid body states of the LTI plant model with MLESO controller in response to a $20\,m$ discrete gust at $V_K^R = 50\,m/s$, $h = 500\,m$, $m_{fuel} = 0\,kg$.

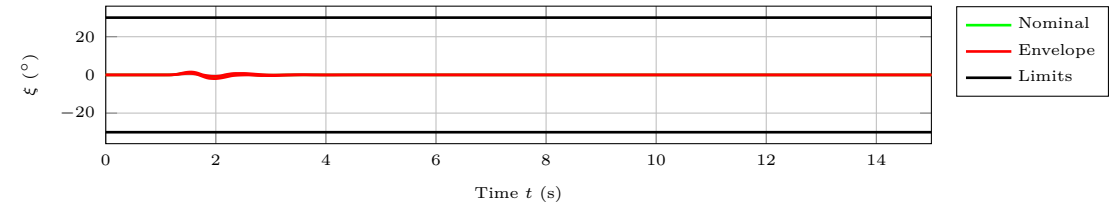

(a) Aileron Deflection

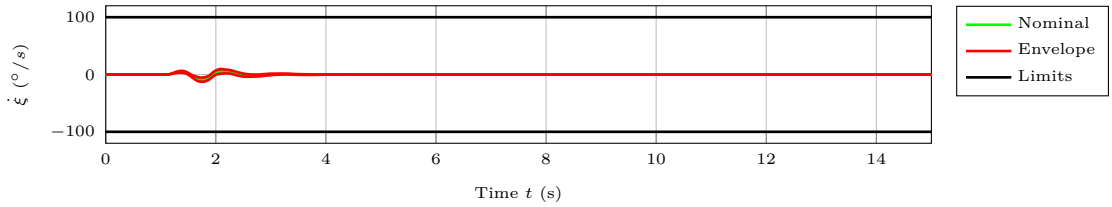

(b) Aileron Rate

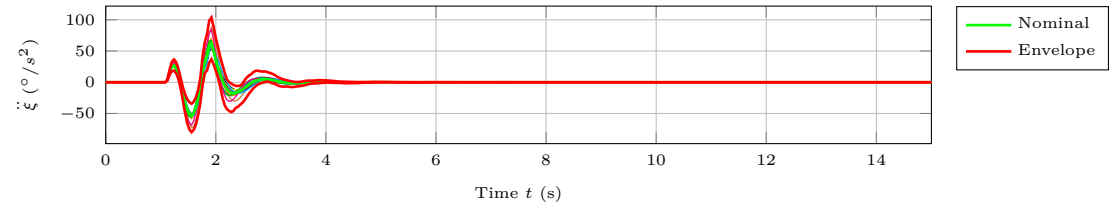

(c) Aileron Acceleration

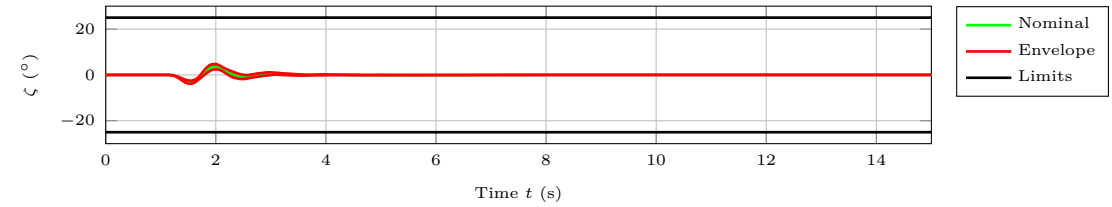

(d) Rudder Deflection

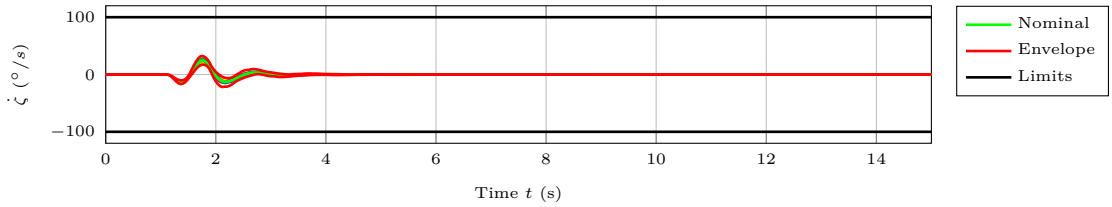

(e) Rudder Rate

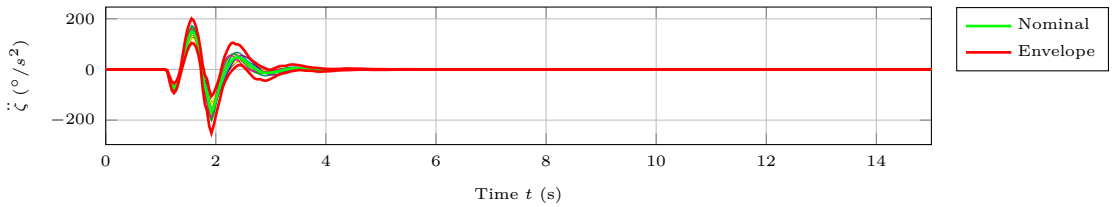

(f) Rudder Acceleration

Figure E.26: Actuator states of the LTI plant model with MLESO controller in response to a $20\,m$ discrete gust at $V_K^R = 50\,m/s$, $h = 500\,m$, $m_{fuel} = 0\,kg$.

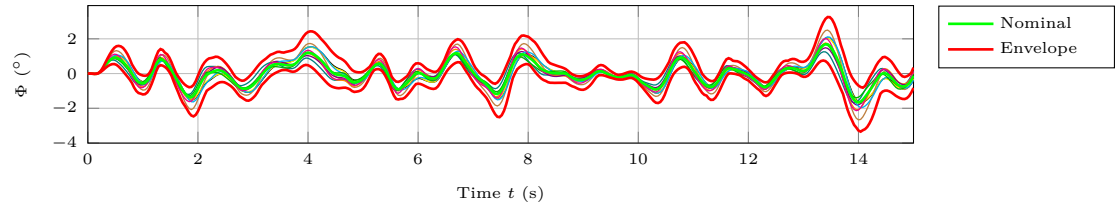

(a) Bank Angle

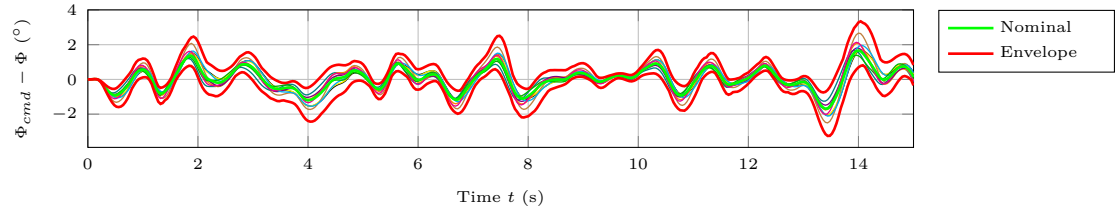

(b) Tracking Error

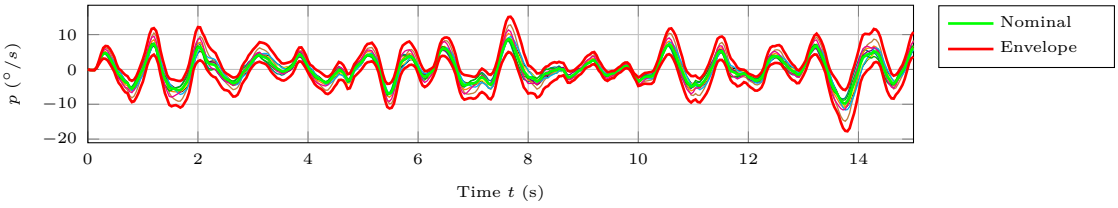

(c) Roll Rate

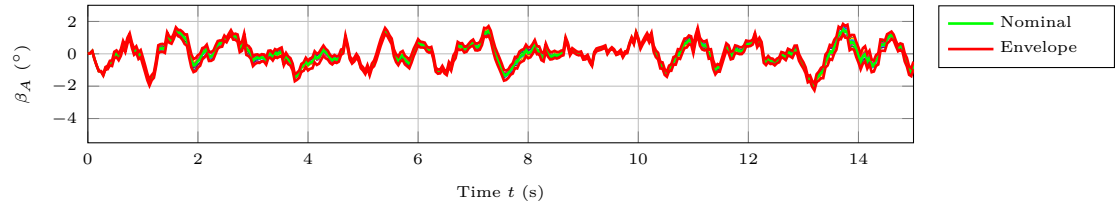

(d) Angle-of-sideslip

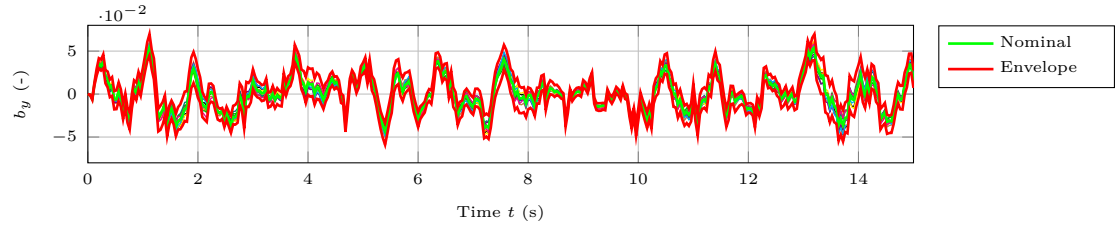

(e) Lateral Acceleration

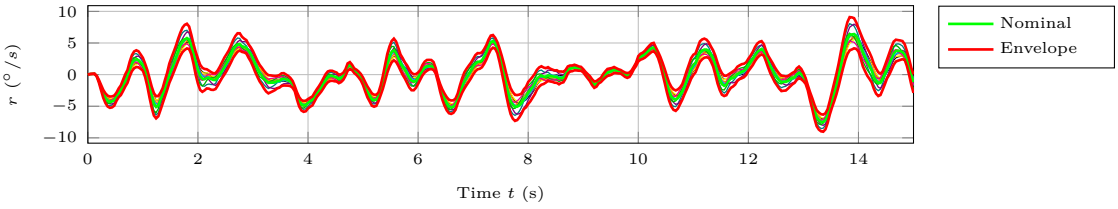

(f) Yaw Rate

Figure E.27: Rigid body states of the LTI plant model with MLESO controller in response to moderate Dryden turbulence at $V_K^R = 50\,m/s$, $h = 500\,m$, $m_{fuel} = 0\,kg$.

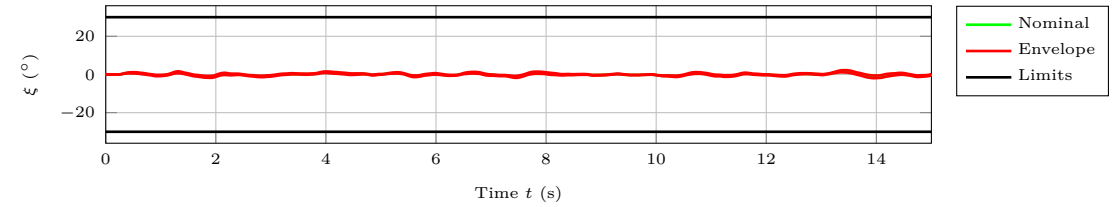

(a) Aileron Deflection

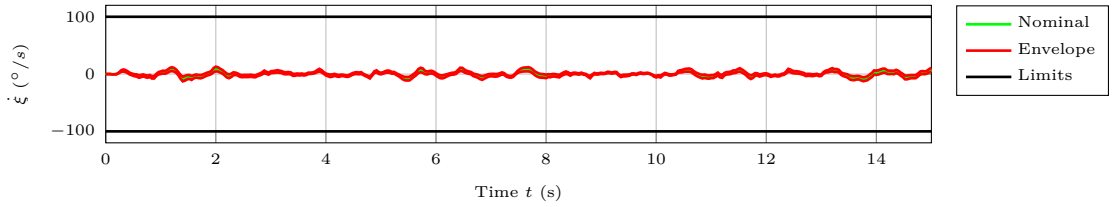

(b) Aileron Rate

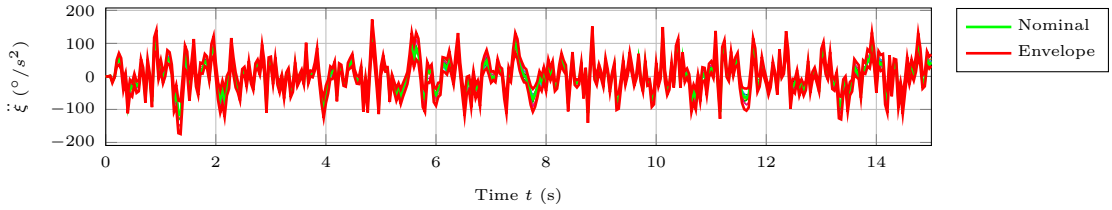

(c) Aileron Acceleration

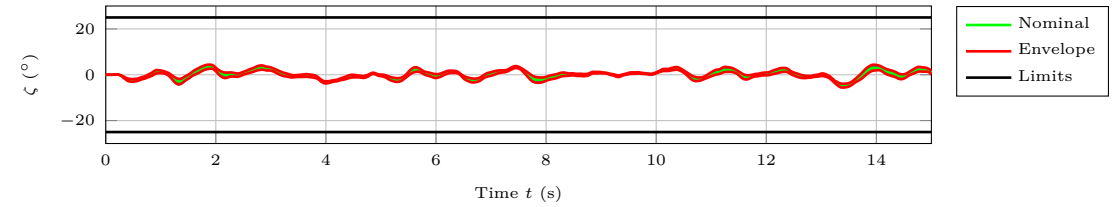

(d) Rudder Deflection

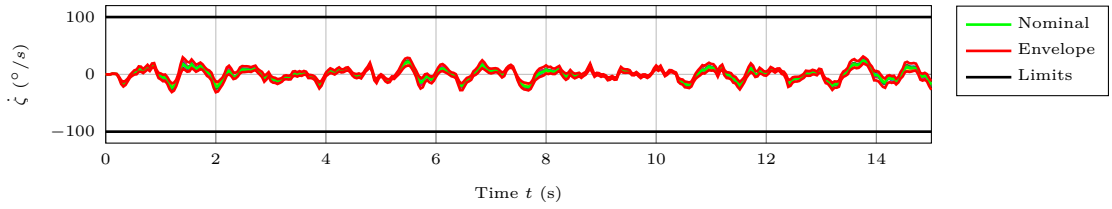

(e) Rudder Rate

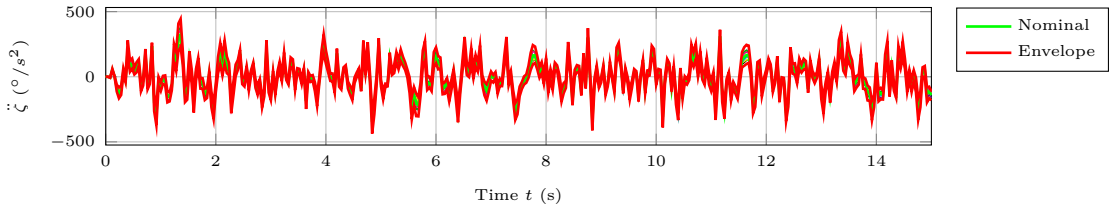

(f) Rudder Acceleration

Figure E.28: Actuator states of the LTI plant model with MLESO controller in response to moderate Dryden turbulence at $V_K^R = 50\,m/s$, $h = 500\,m$, $m_{fuel} = 0\,kg$.

E.1.3 Nonlinear Model at 35 m/s

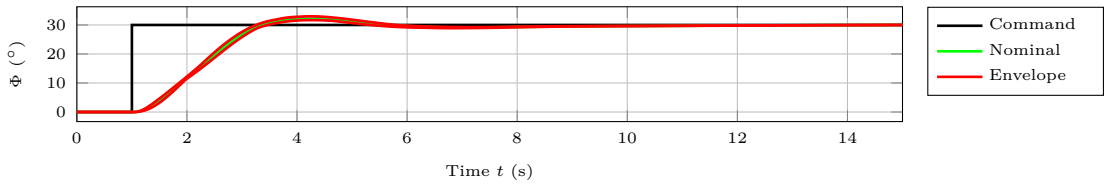

(a) Bank Angle

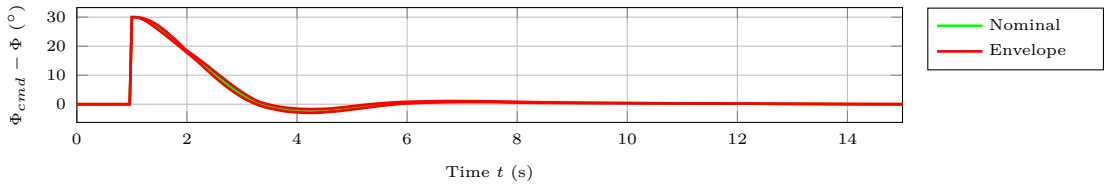

(b) Tracking Error

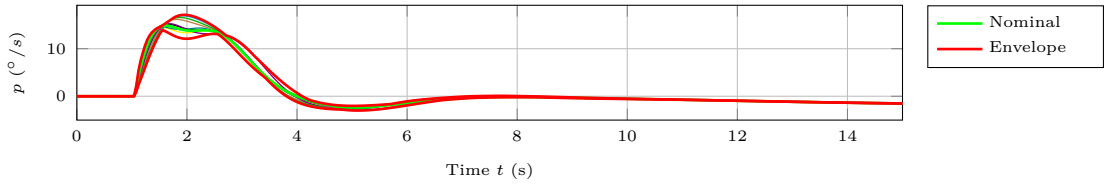

(c) Roll Rate

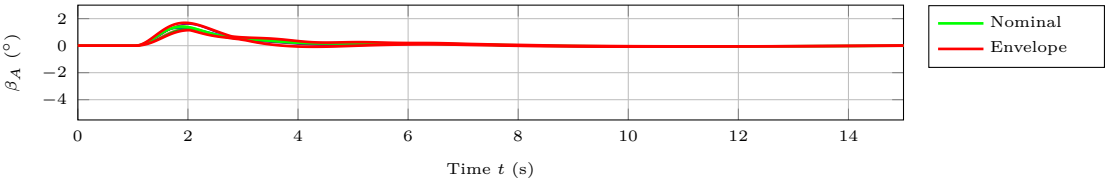

(d) Angle-of-sideslip

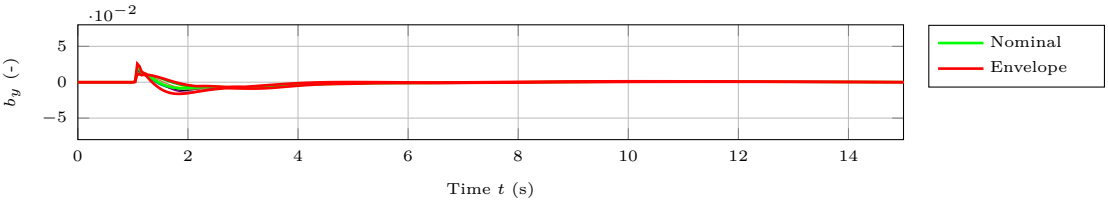

(e) Lateral Acceleration

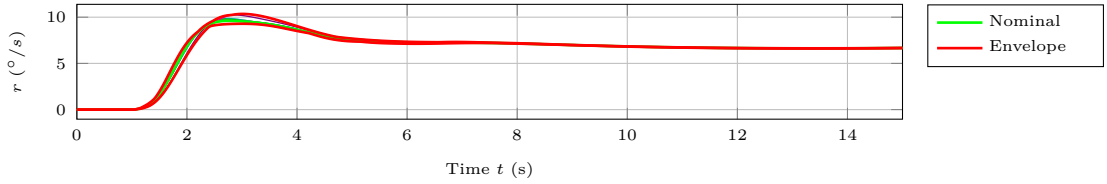

(f) Yaw Rate

Figure E.29: Rigid body states of the nonlinear plant model with MLESO controller in response to a $30°$ step command $\Phi_{cmd}(t)$ at $V_K^R = 35\,m/s$, $h = 1000\,m$, $m_{fuel} = 23\,kg$.

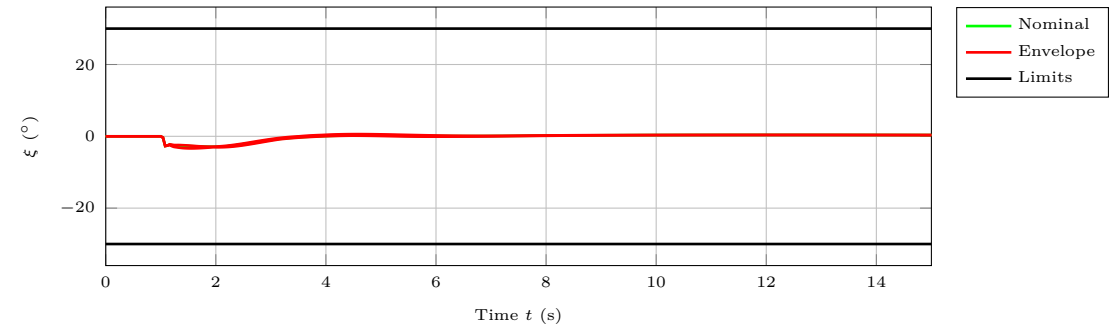

(a) Aileron Deflection

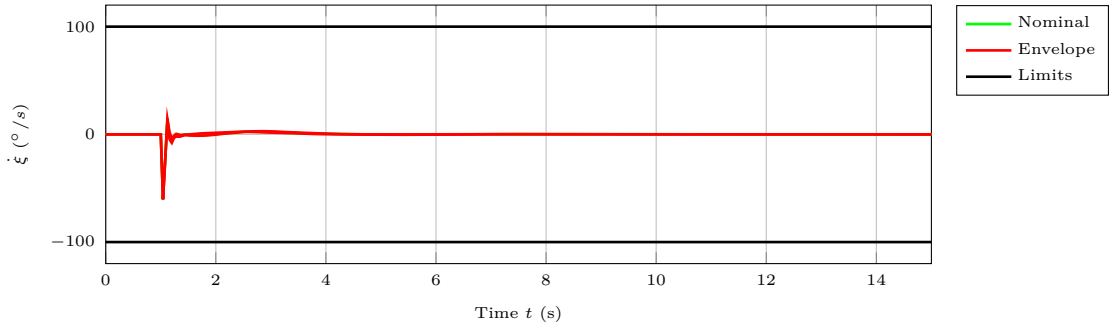

(b) Aileron Rate

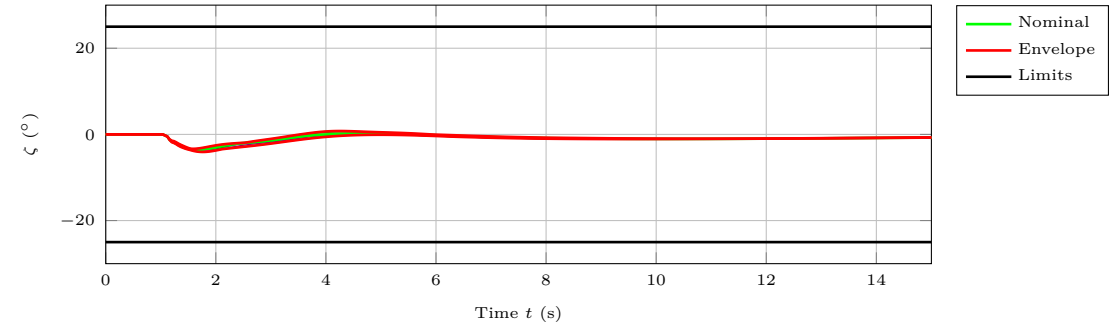

(c) Rudder Deflection

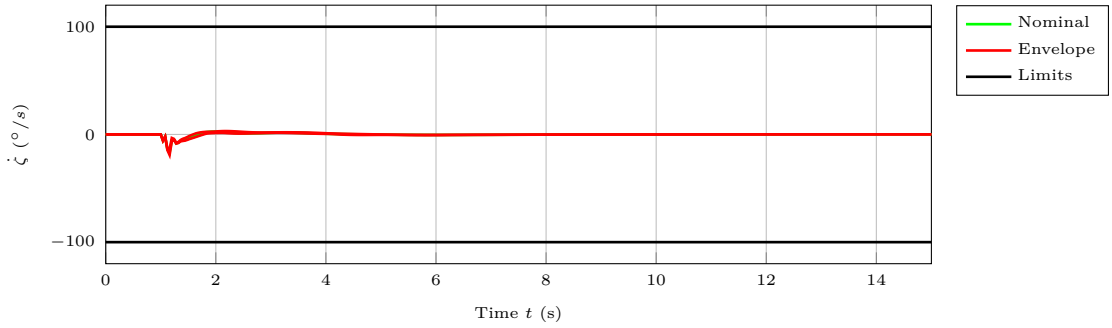

(d) Rudder Rate

Figure E.30: Actuator states of the nonlinear plant model with MLESO controller in response to a $30°$ step command $\Phi_{cmd}(t)$ at $V_K^R = 35\,m/s$, $h = 1000\,m$, $m_{fuel} = 23\,kg$.

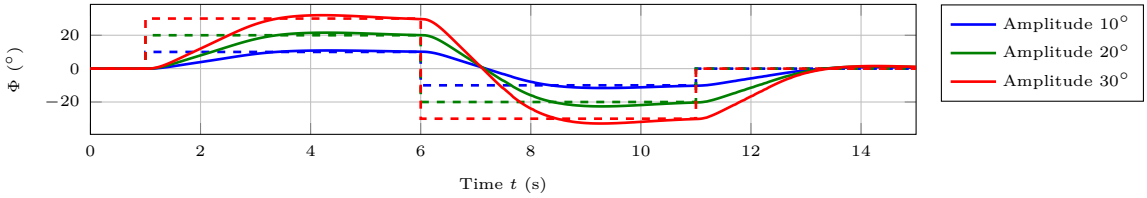

(a) Bank Angle

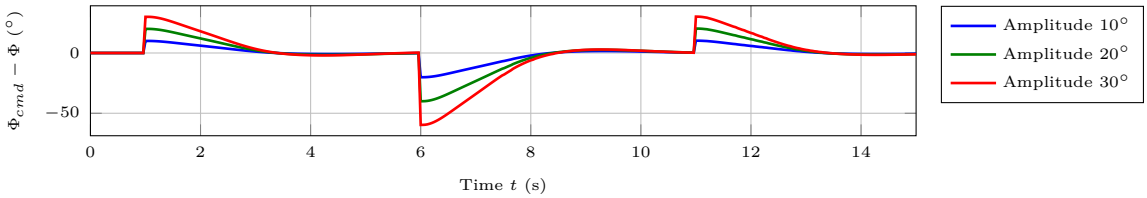

(b) Tracking Error

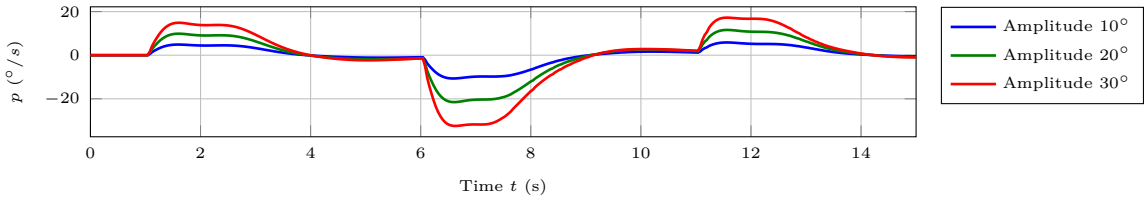

(c) Roll Rate

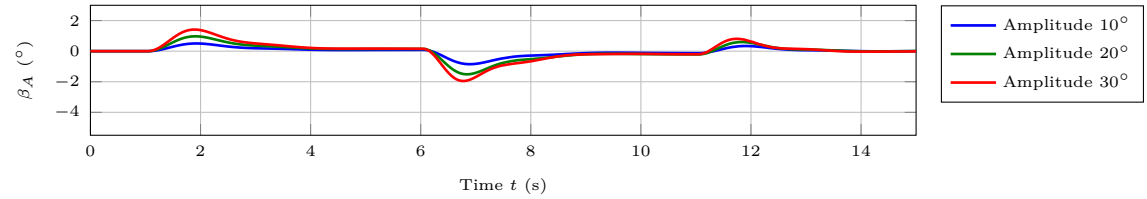

(d) Angle-of-sideslip

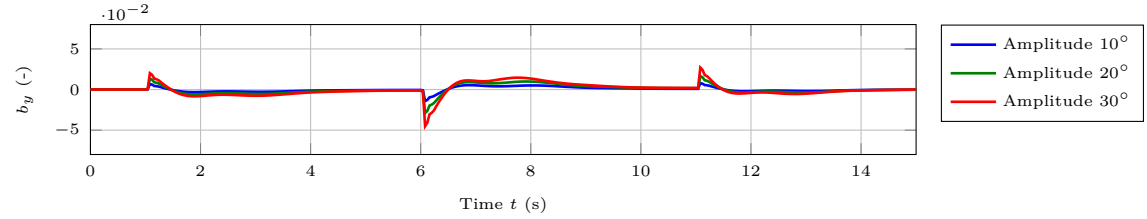

(e) Lateral Acceleration

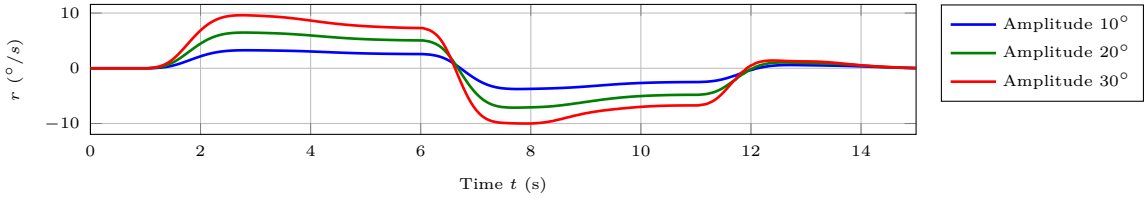

(f) Yaw Rate

Figure E.31: Rigid body states of the nonlinear plant model with MLESO controller in response to a doublet sweep at $V_K^R = 35\,m/s$, $h = 1000\,m$, $m_{fuel} = 23\,kg$.

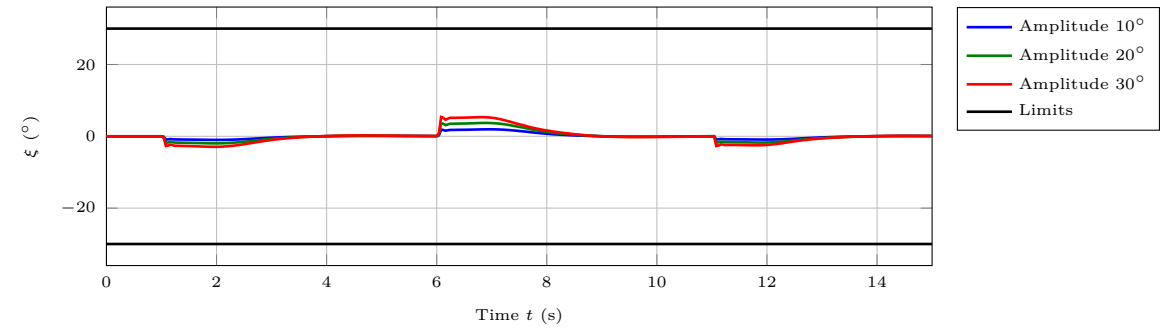

(a) Aileron Deflection

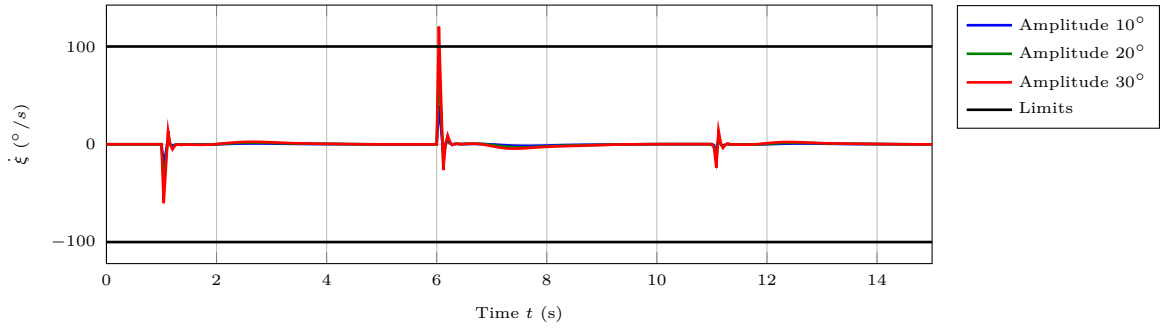

(b) Aileron Rate

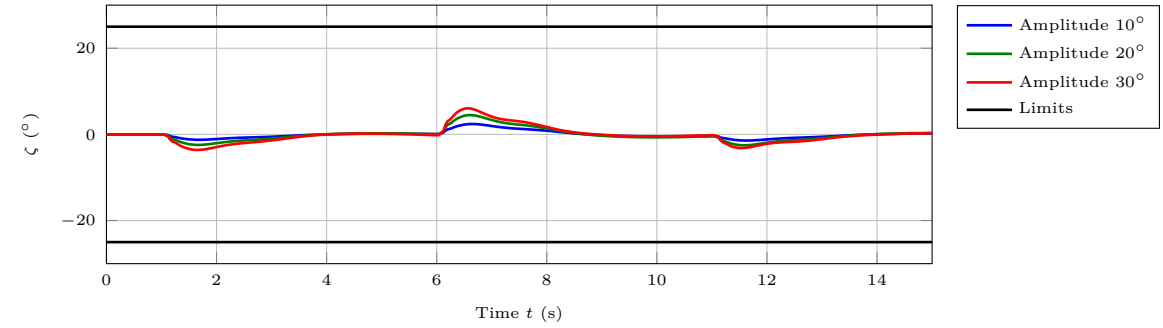

(c) Rudder Deflection

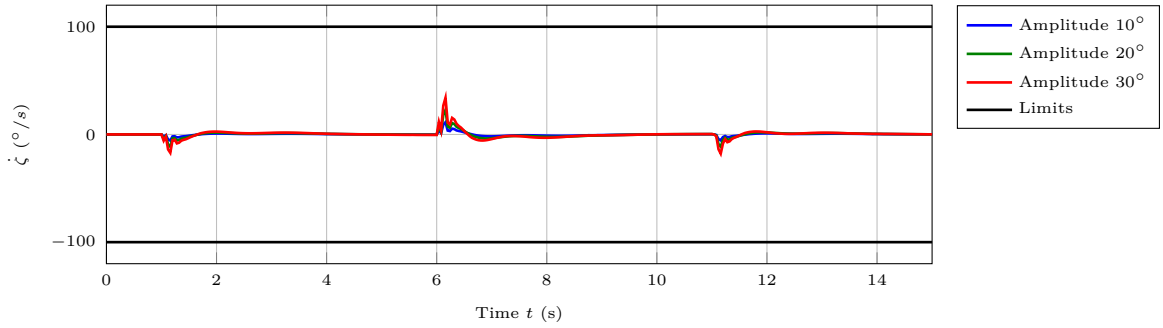

(d) Rudder Rate

Figure E.32: Actuator states of the nonlinear plant model with MLESO controller in response to a doublet sweep at $V_K^R = 35\,m/s$, $h = 1000\,m$, $m_{fuel} = 23\,kg$.

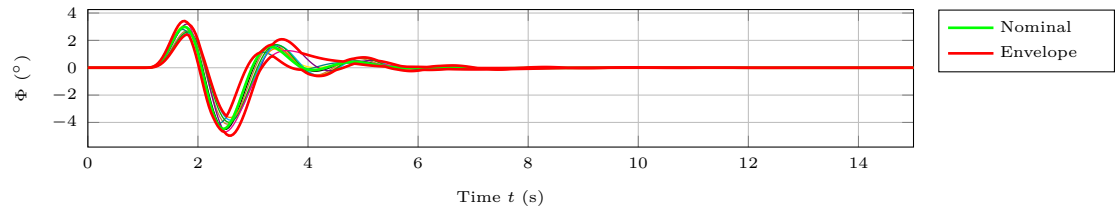

(a) Bank Angle

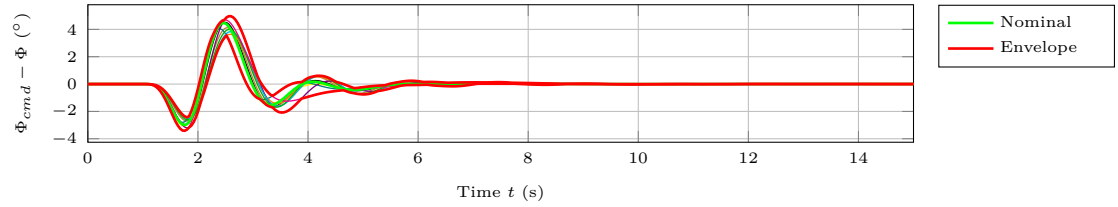

(b) Tracking Error

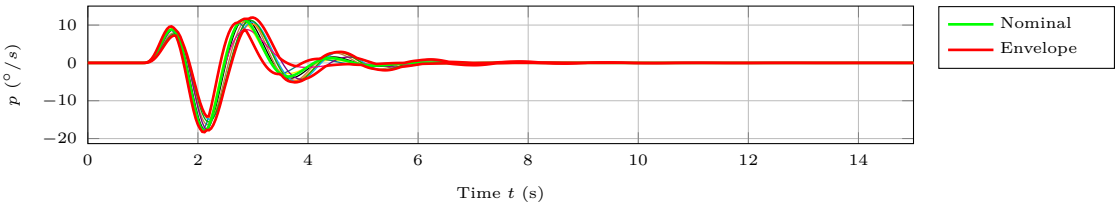

(c) Roll Rate

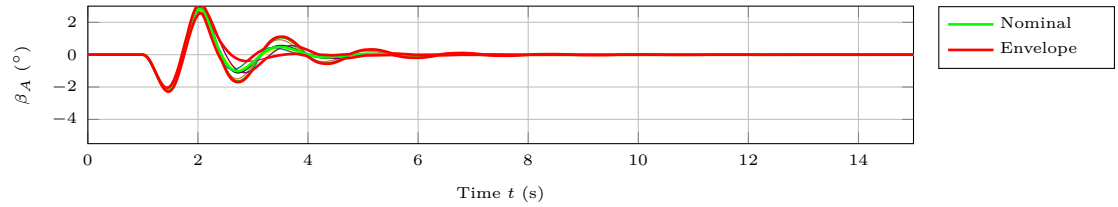

(d) Angle-of-sideslip

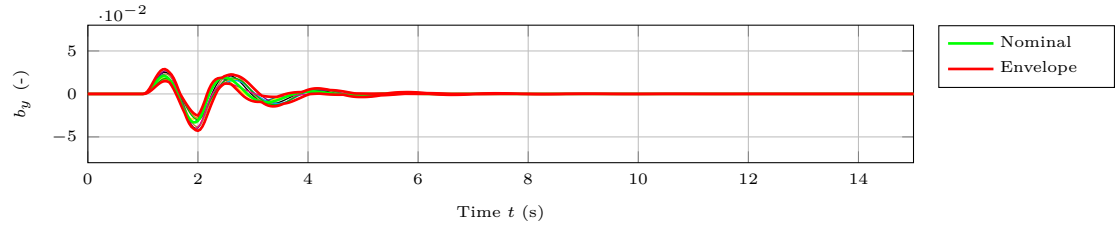

(e) Lateral Acceleration

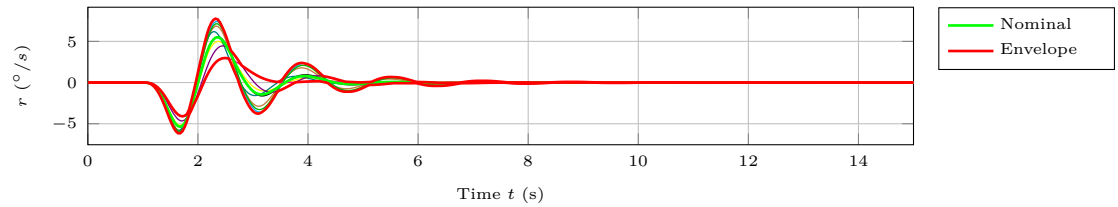

(f) Yaw Rate

Figure E.33: Rigid body states of the nonlinear plant model with MLESO controller in response to a $20\,m$ discrete gust at $V_K^R = 35\,m/s$, $h = 1000\,m$, $m_{fuel} = 23\,kg$.

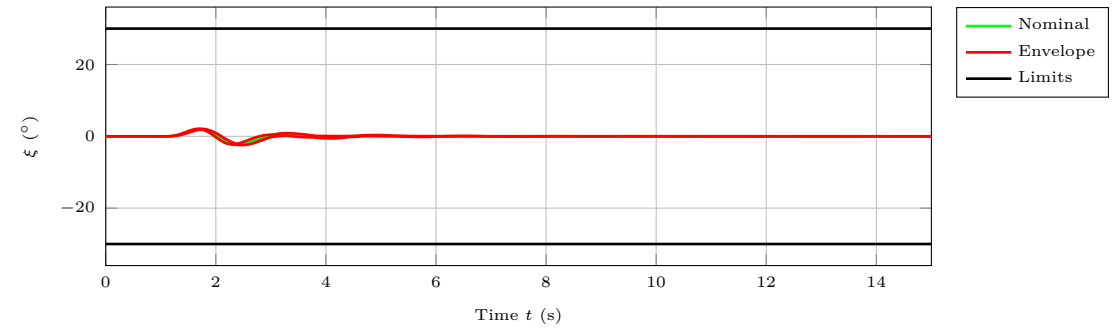

(a) Aileron Deflection

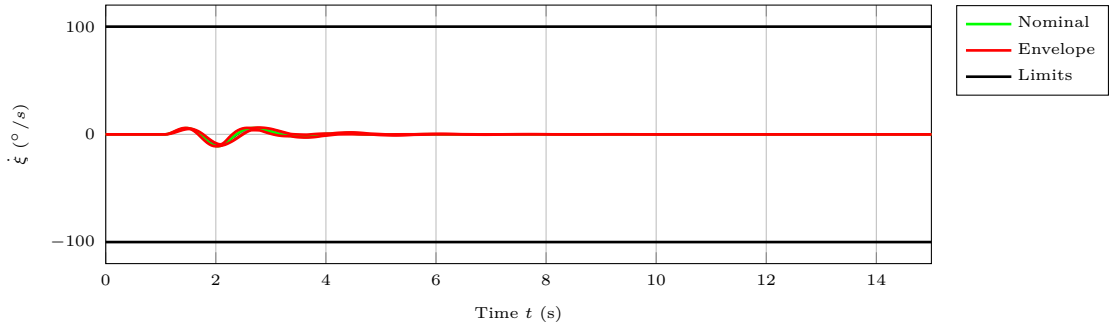

(b) Aileron Rate

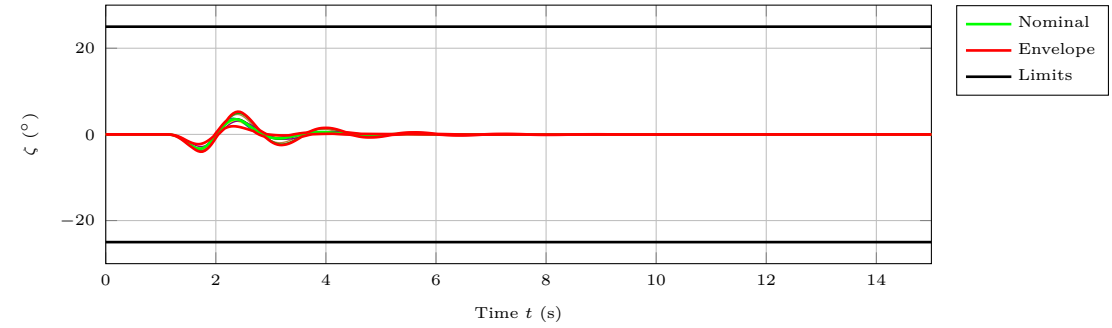

(c) Rudder Deflection

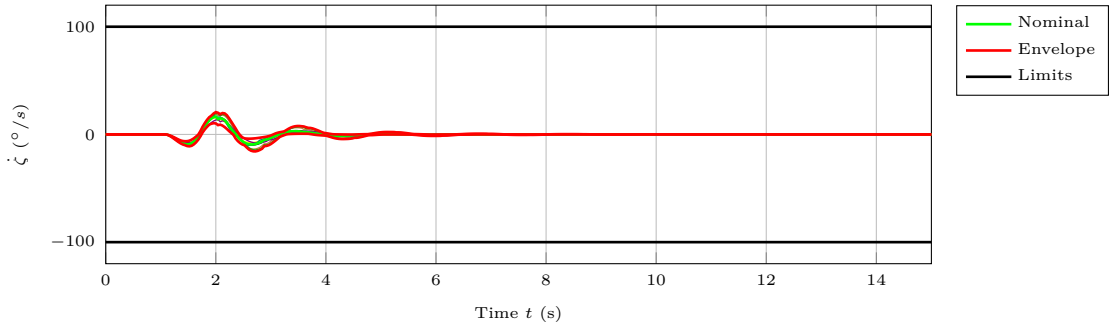

(d) Rudder Rate

Figure E.34: Actuator states of the nonlinear plant model with MLESO controller in response to a $20\,m$ discrete gust at $V_K^R = 35\,m/s$, $h = 1000\,m$, $m_{fuel} = 23\,kg$.

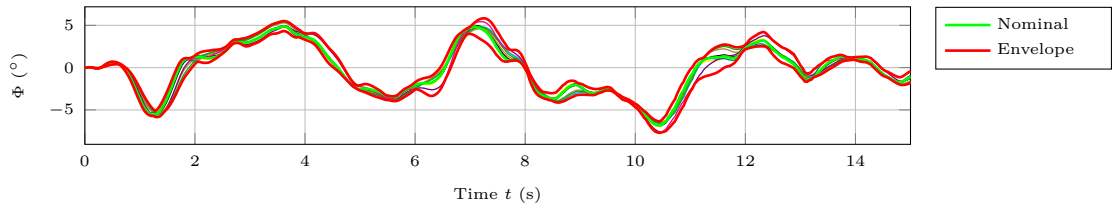

(a) Bank Angle

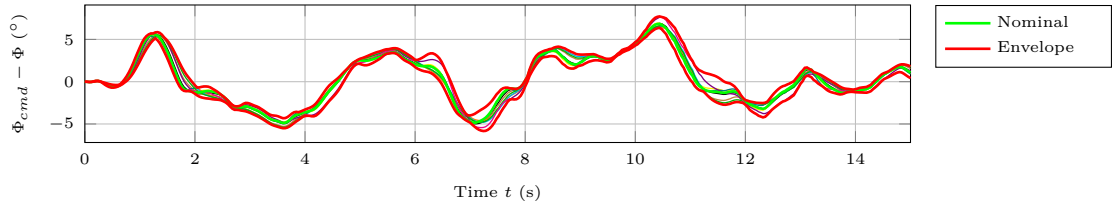

(b) Tracking Error

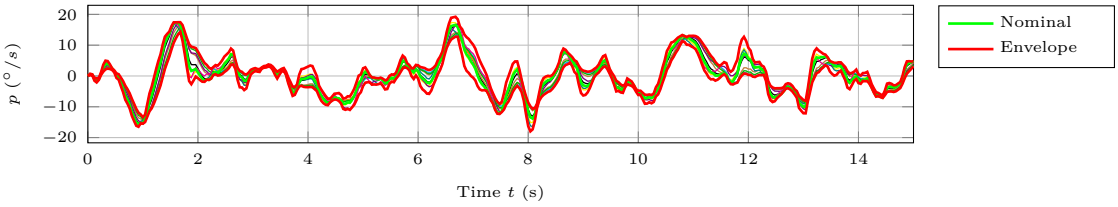

(c) Roll Rate

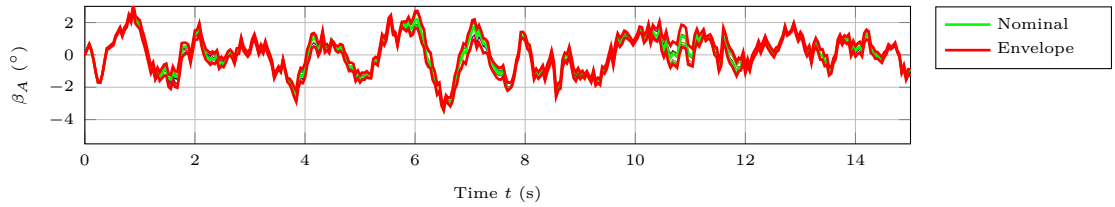

(d) Angle-of-sideslip

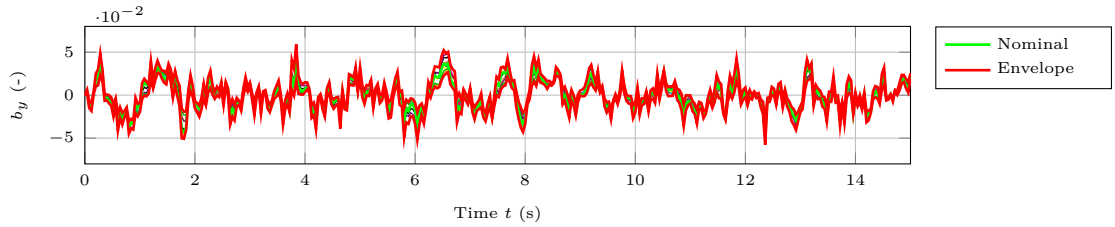

(e) Lateral Acceleration

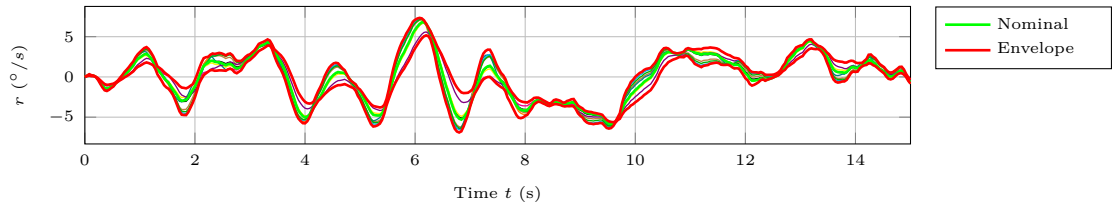

(f) Yaw Rate

Figure E.35: Rigid body states of the nonlinear plant model with MLESO controller in response to moderate Dryden turbulence at $V_K^R = 35\,m/s$, $h = 1000\,m$, $m_{fuel} = 23\,kg$.

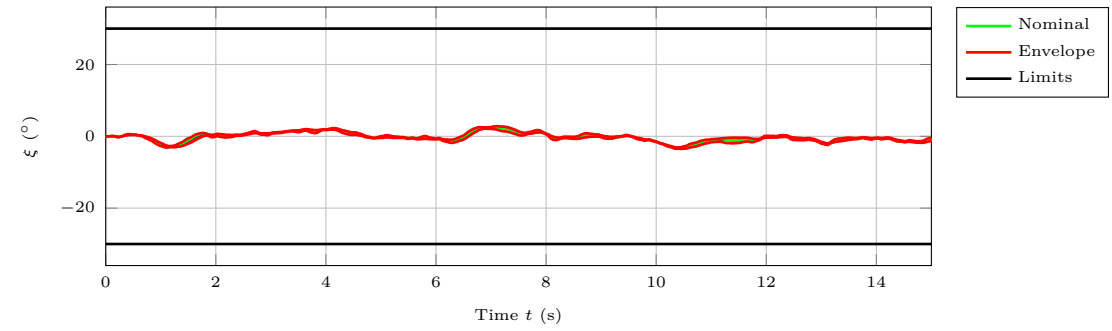

(a) Aileron Deflection

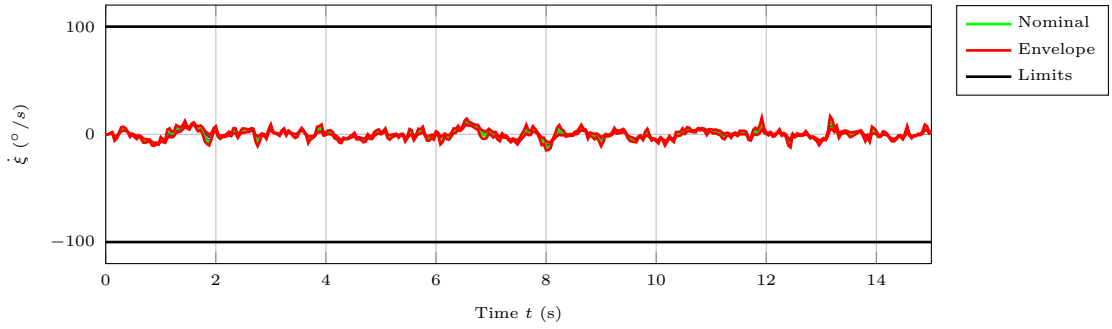

(b) Aileron Rate

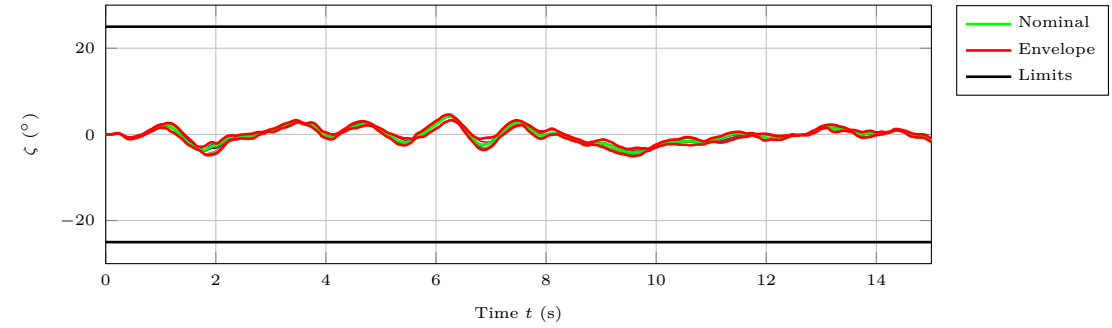

(c) Rudder Deflection

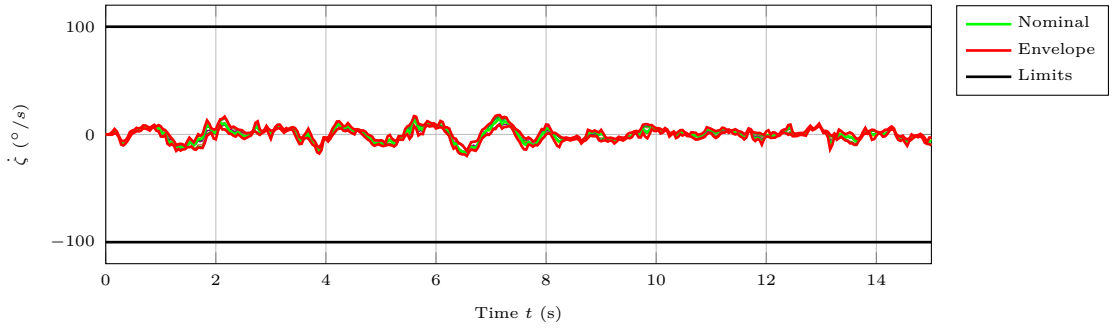

(d) Rudder Rate

Figure E.36: Actuator states of the nonlinear plant model with MLESO controller in response to moderate Dryden turbulence at $V_K^R = 35\,m/s$, $h = 1000\,m$, $m_{fuel} = 23\,kg$.

E.1.4 Nonlinear Model at 50 m/s

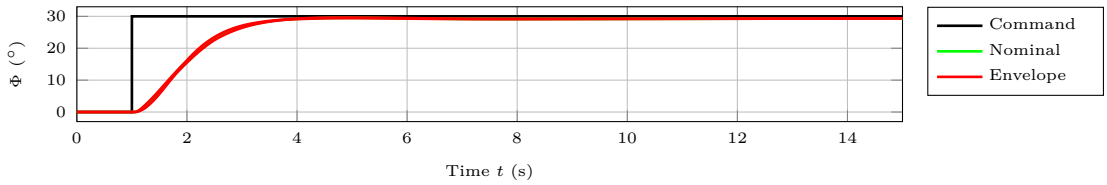

(a) Bank Angle

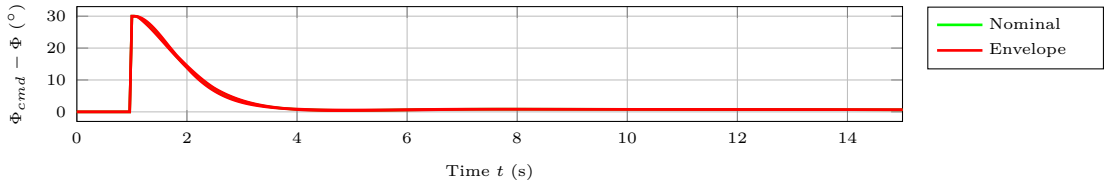

(b) Tracking Error

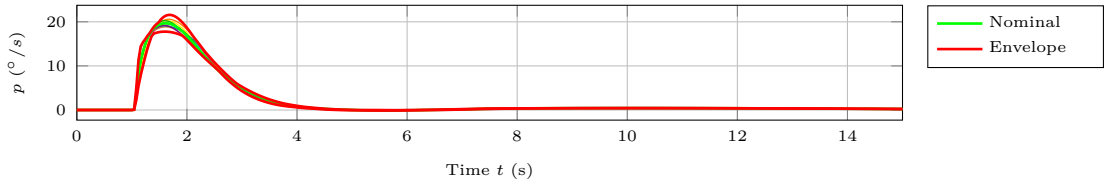

(c) Roll Rate

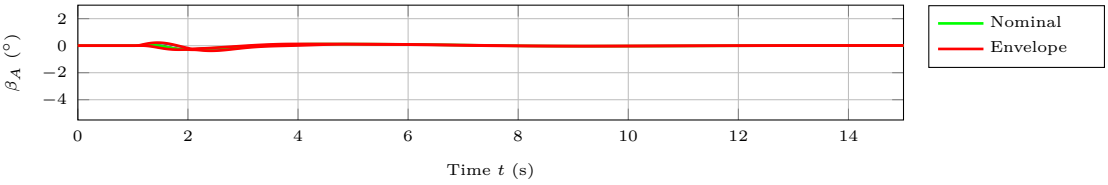

(d) Angle-of-sideslip

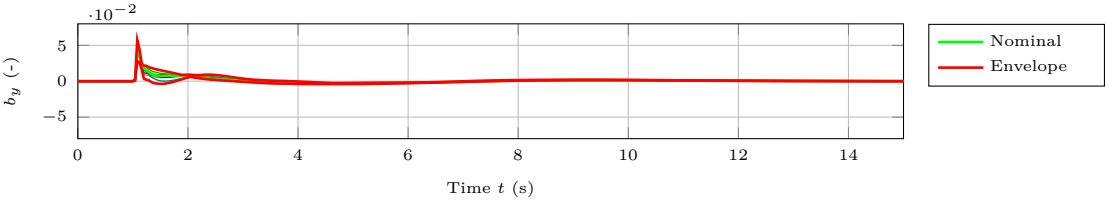

(e) Lateral Acceleration

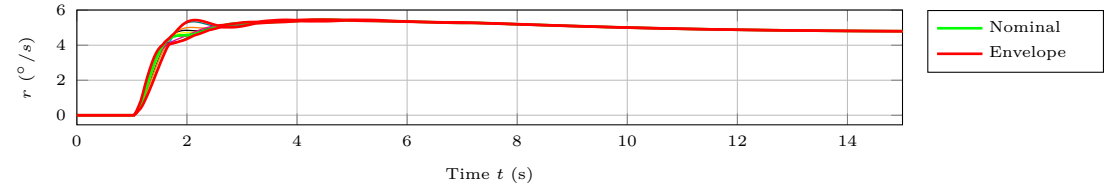

(f) Yaw Rate

Figure E.37: Rigid body states of the nonlinear plant model with MLESO controller in response to a $30°$ step command $\Phi_{cmd}(t)$ at $V_K^R = 50\,m/s$, $h = 500\,m$, $m_{fuel} = 0\,kg$.

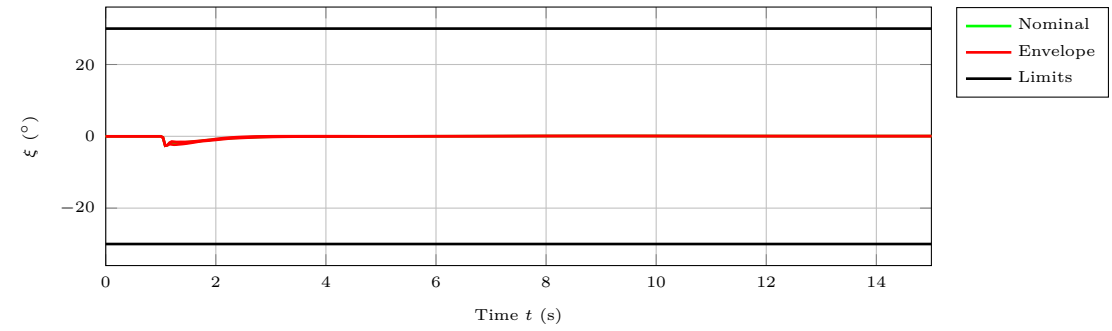

(a) Aileron Deflection

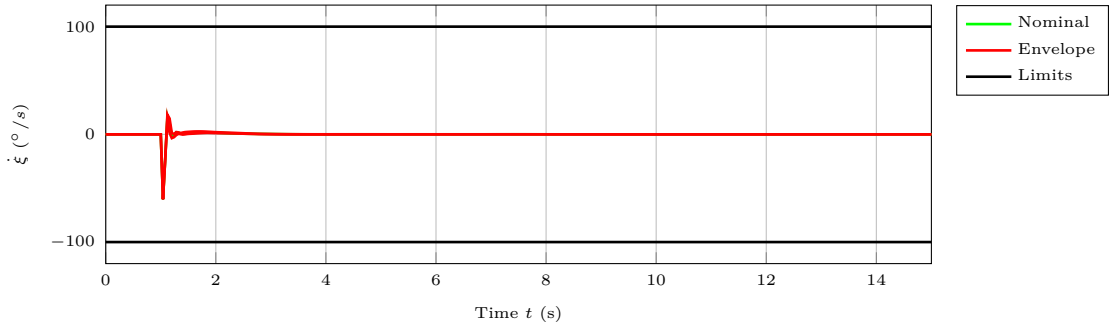

(b) Aileron Rate

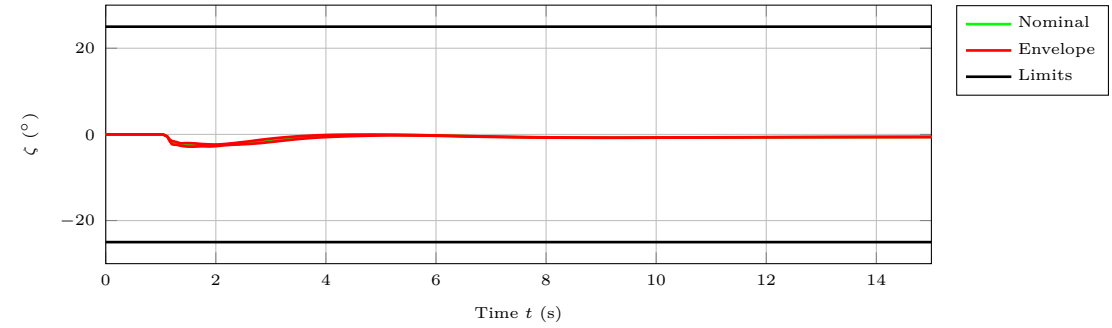

(c) Rudder Deflection

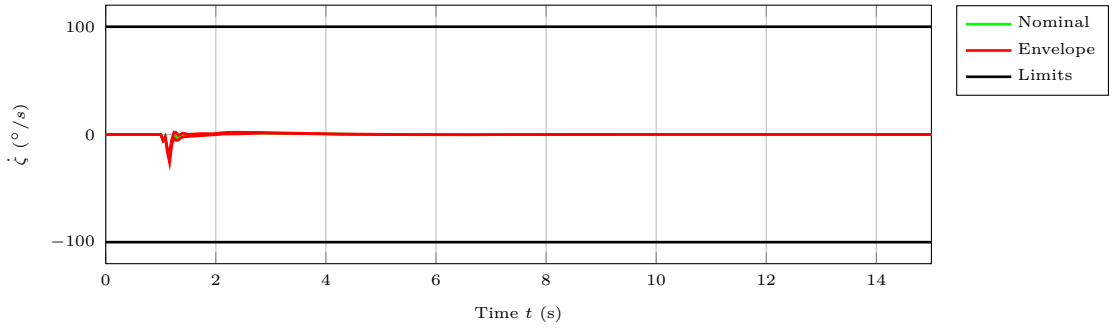

(d) Rudder Rate

Figure E.38: Actuator states of the nonlinear plant model with MLESO controller in response to a $30°$ step command $\Phi_{cmd}(t)$ at $V_K^R = 50\,m/s$, $h = 500\,m$, $m_{fuel} = 0\,kg$.

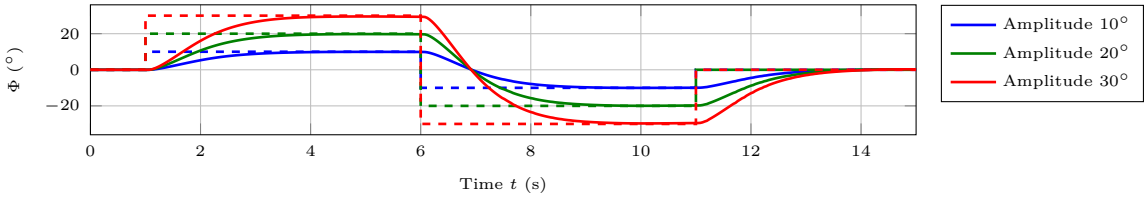

(a) Bank Angle

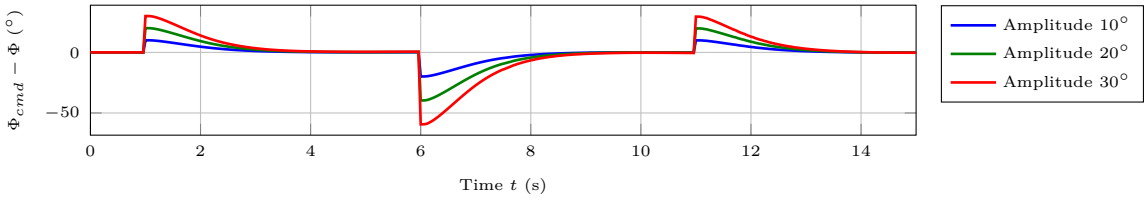

(b) Tracking Error

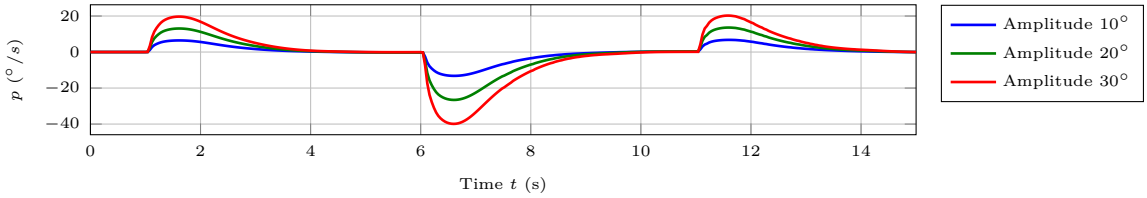

(c) Roll Rate

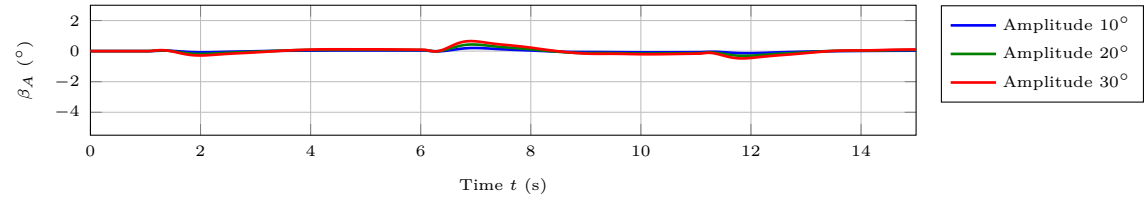

(d) Angle-of-sideslip

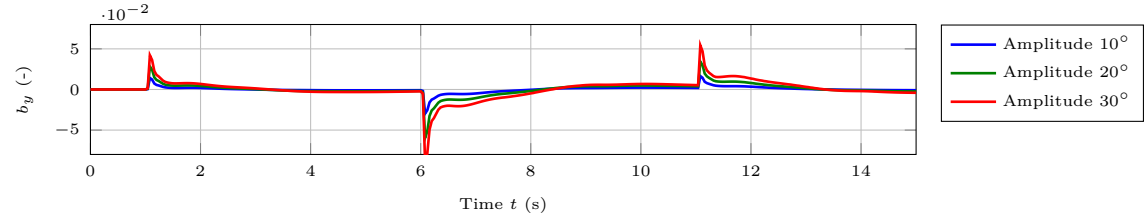

(e) Lateral Acceleration

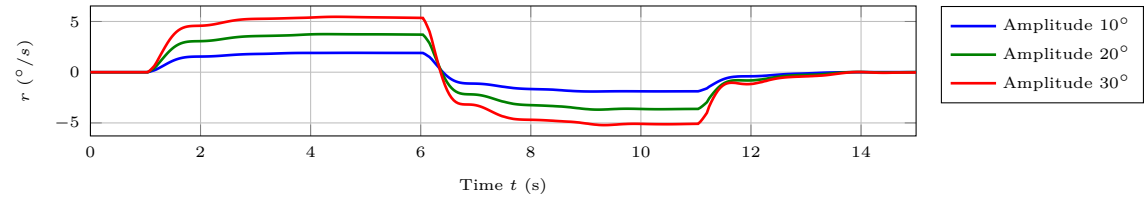

(f) Yaw Rate

Figure E.39: Rigid body states of the nonlinear plant model with MLESO controller in response to a doublet sweep at $V_K^R = 50\,m/s$, $h = 500\,m$, $m_{fuel} = 0\,kg$.

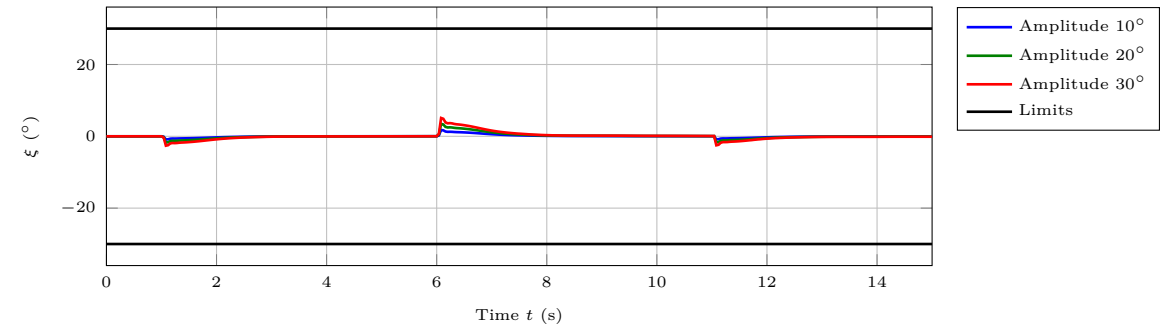

(a) Aileron Deflection

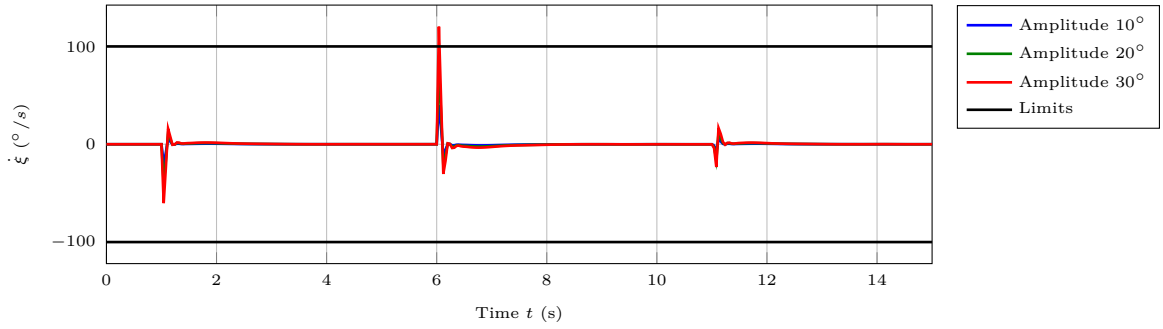

(b) Aileron Rate

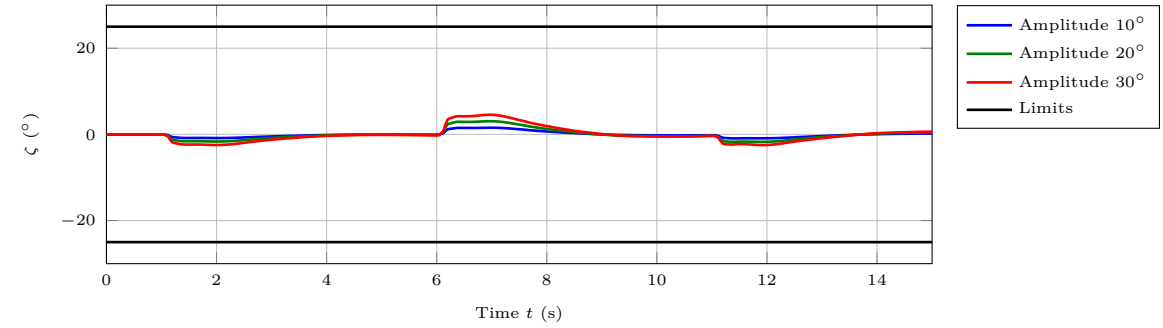

(c) Rudder Deflection

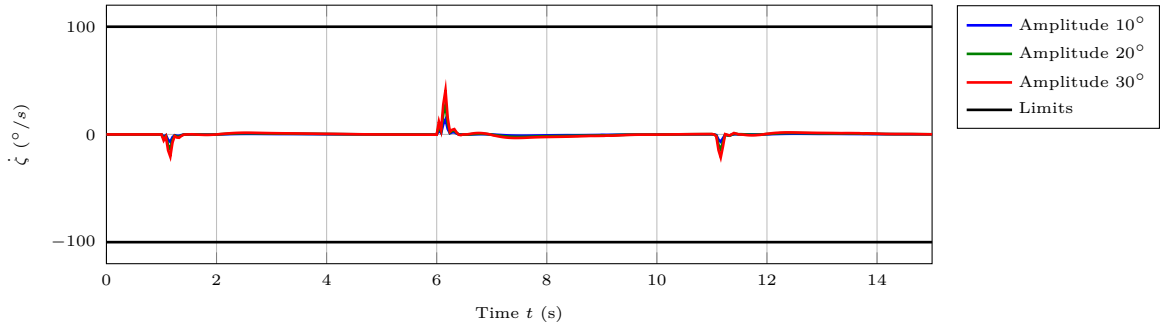

(d) Rudder Rate

Figure E.40: Actuator states of the nonlinear plant model with MLESO controller in response to a doublet sweep at $V_K^R = 50\,m/s$, $h = 500\,m$, $m_{fuel} = 0\,kg$.

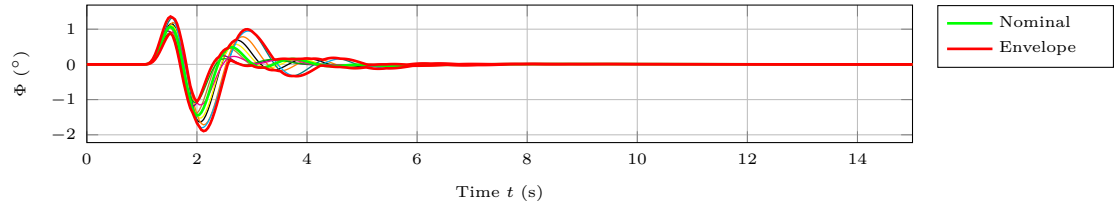

(a) Bank Angle

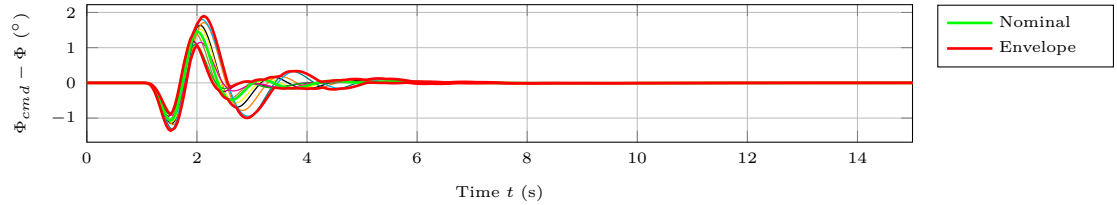

(b) Tracking Error

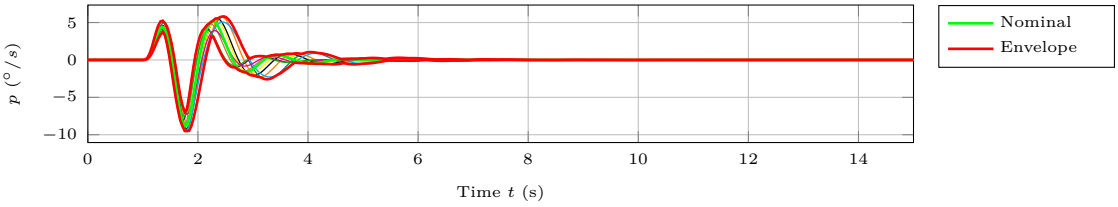

(c) Roll Rate

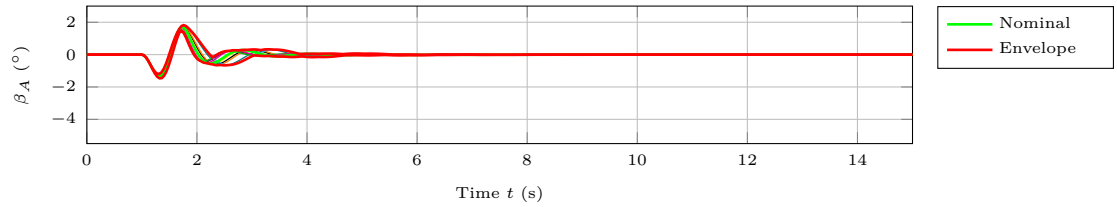

(d) Angle-of-sideslip

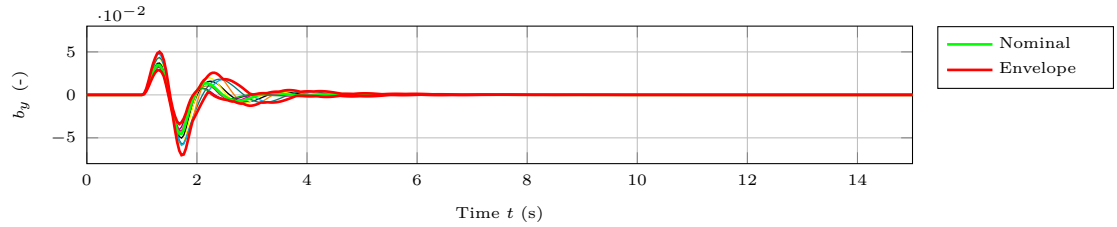

(e) Lateral Acceleration

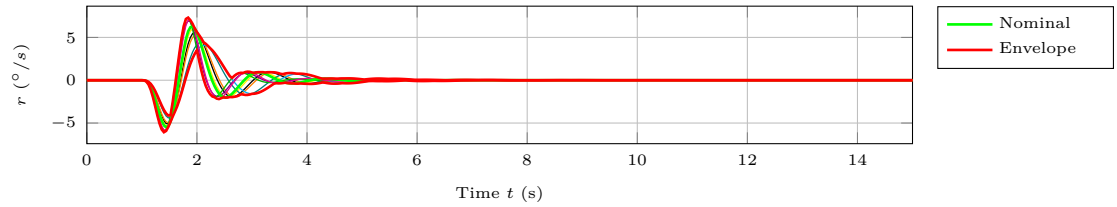

(f) Yaw Rate

Figure E.41: Rigid body states of the nonlinear plant model with MLESO controller in response to a $20\,m$ discrete gust at $V_K^R = 50\,m/s$, $h = 500\,m$, $m_{fuel} = 0\,kg$.

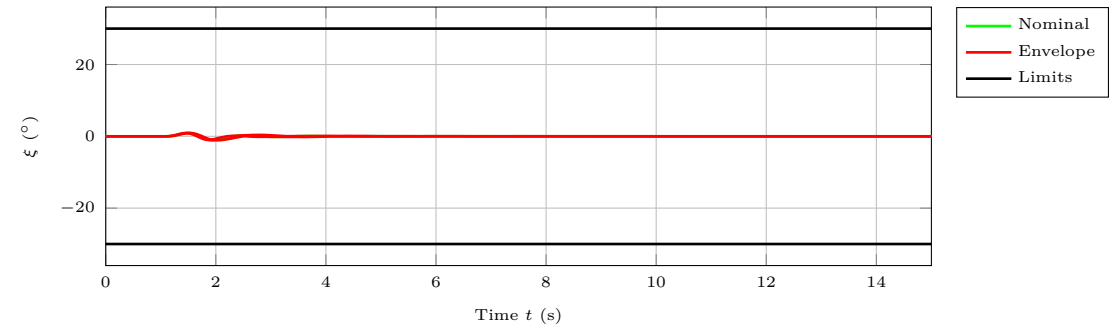

(a) Aileron Deflection

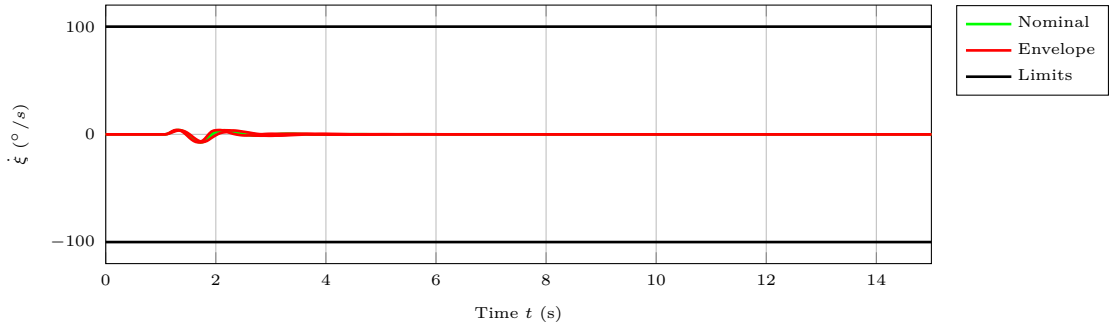

(b) Aileron Rate

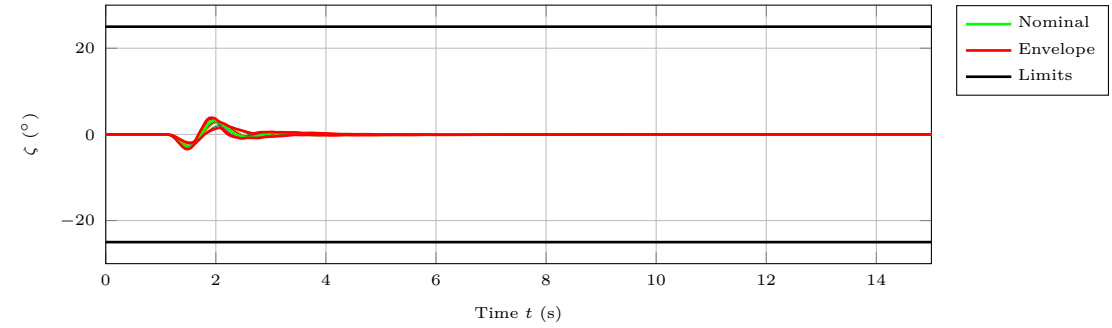

(c) Rudder Deflection

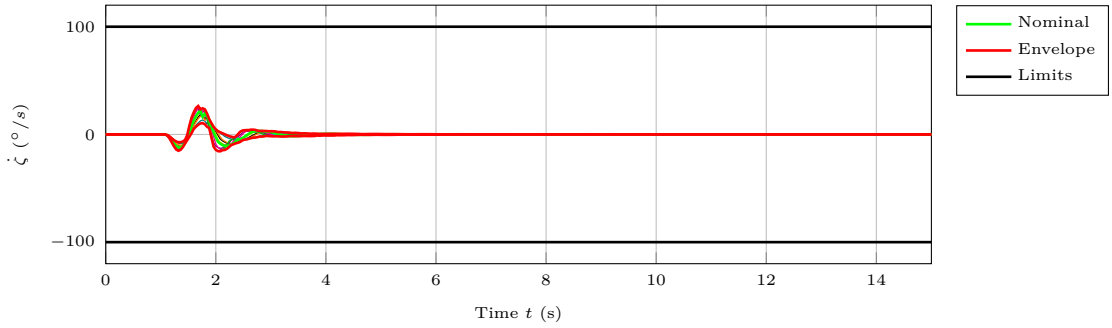

(d) Rudder Rate

Figure E.42: Actuator states of the nonlinear plant model with MLESO controller in response to a $20\,m$ discrete gust at $V_K^R = 50\,m/s$, $h = 500\,m$, $m_{fuel} = 0\,kg$.

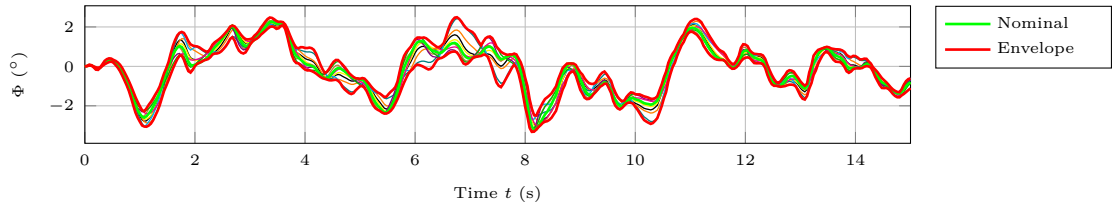

(a) Bank Angle

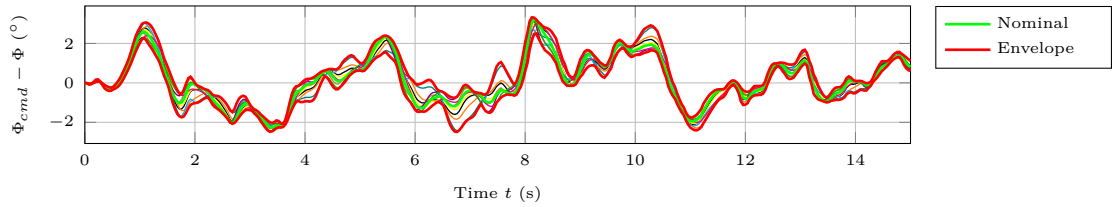

(b) Tracking Error

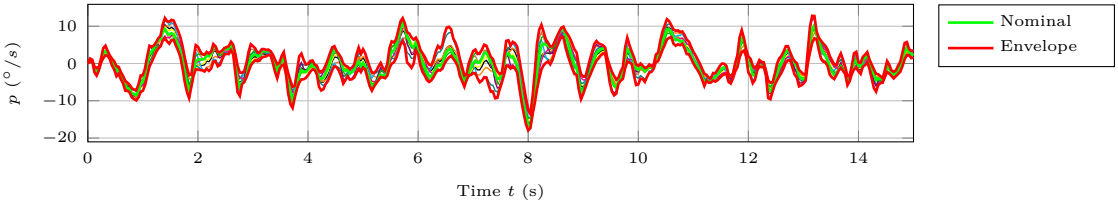

(c) Roll Rate

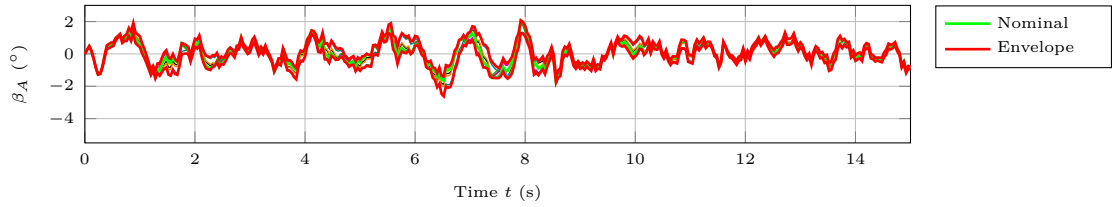

(d) Angle-of-sideslip

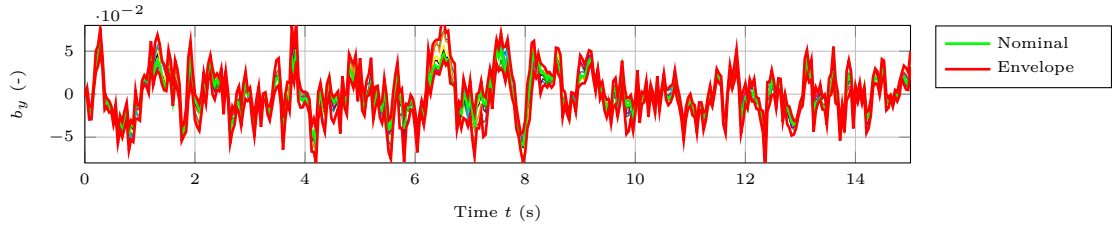

(e) Lateral Acceleration

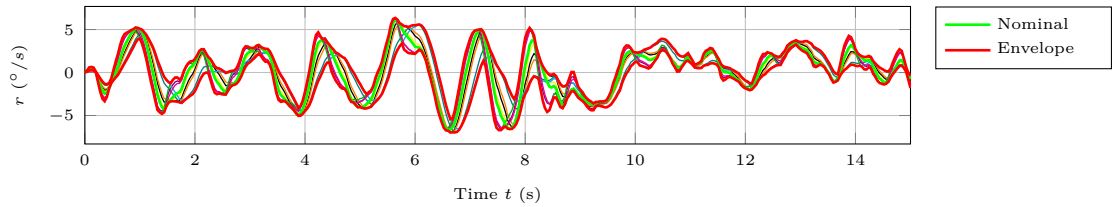

(f) Yaw Rate

Figure E.43: Rigid body states of the nonlinear plant model with MLESO controller in response to moderate Dryden turbulence at $V_K^R = 50\,m/s$, $h = 500\,m$, $m_{fuel} = 0\,kg$.

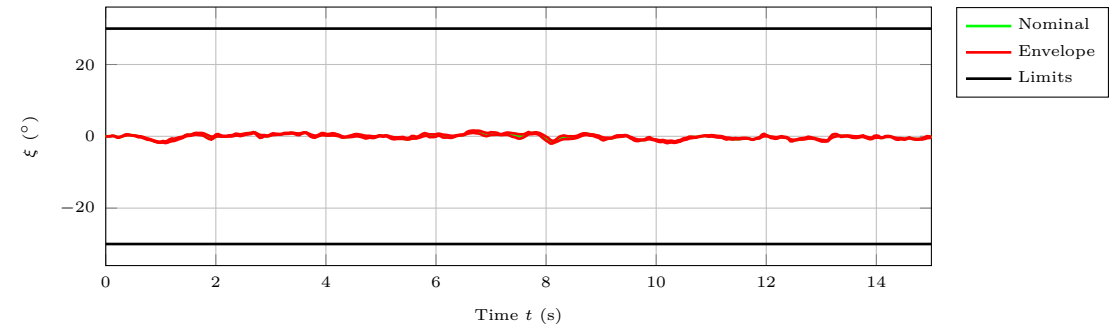

(a) Aileron Deflection

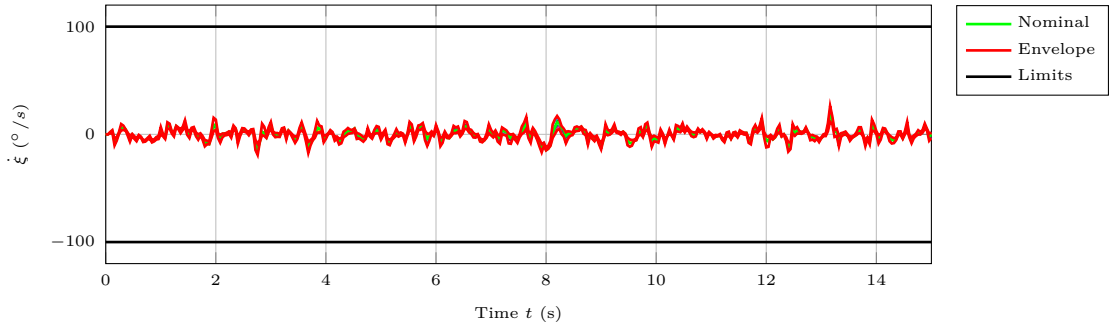

(b) Aileron Rate

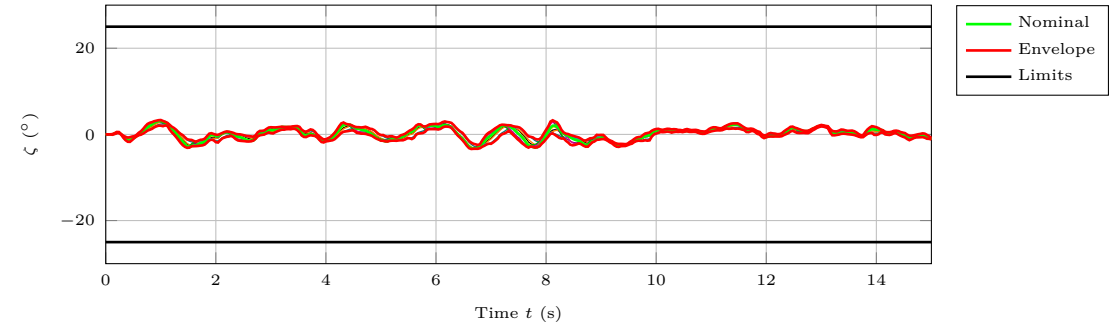

(c) Rudder Deflection

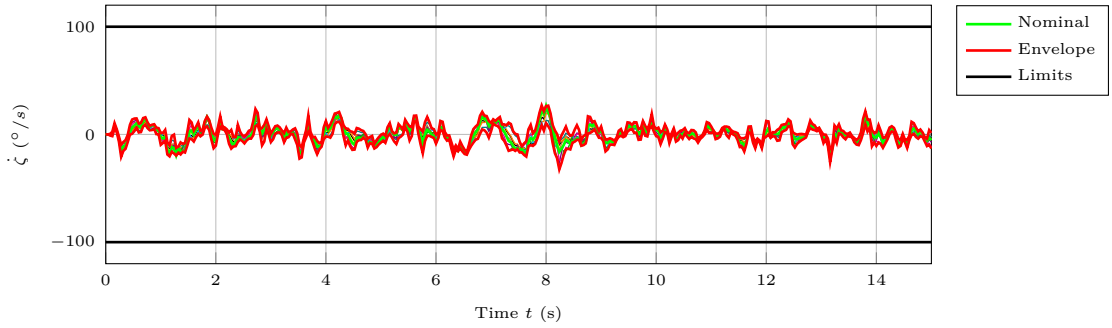

(d) Rudder Rate

Figure E.44: Actuator states of the nonlinear plant model with MLESO controller in response to moderate Dryden turbulence at $V_K^R = 50\,m/s$, $h = 500\,m$, $m_{fuel} = 0\,kg$.

E.2 LQR Control of the Lateral Motion

This section presents the simulation and analyses results of the MM-LQR-based controller. Sections E.2.1 and E.2.2 show the results at $V_K^R = 35\,m/s$, $h = 1000\,m$, $m_{fuel} = 23\,kg$ and $V_K^R = 50\,m/s$, $h = 500\,m$, $m_{fuel} = 0\,kg$, when using the linear plant model. Sections E.2.3 and E.2.4 then present the respective nonlinear simulation results.

E.2.1 Linear Model at 35 m/s

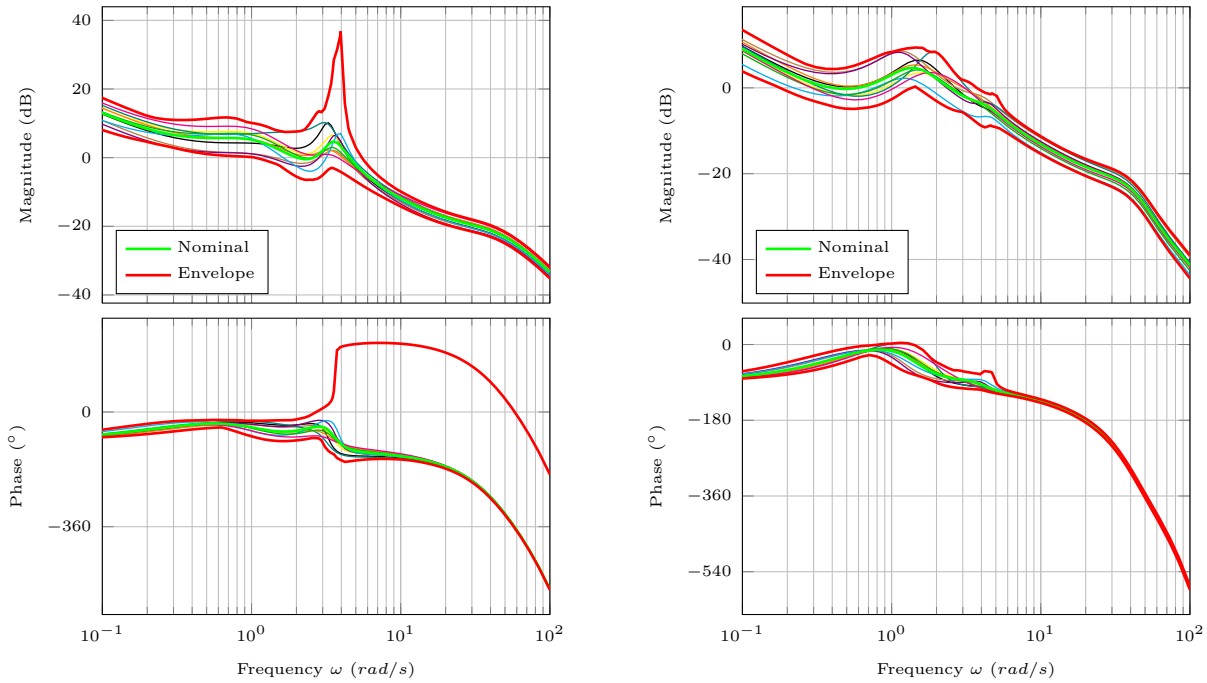

(a) Loopcut at aileron actuator input ξ

(b) Loopcut at rudder actuator input ζ

Figure E.45: Open-loop bode plots at $V_K^R = 35\,m/s$, $h = 1000\,m$, $m_{fuel} = 23\,kg$, when relying on a MM-LQR controller.

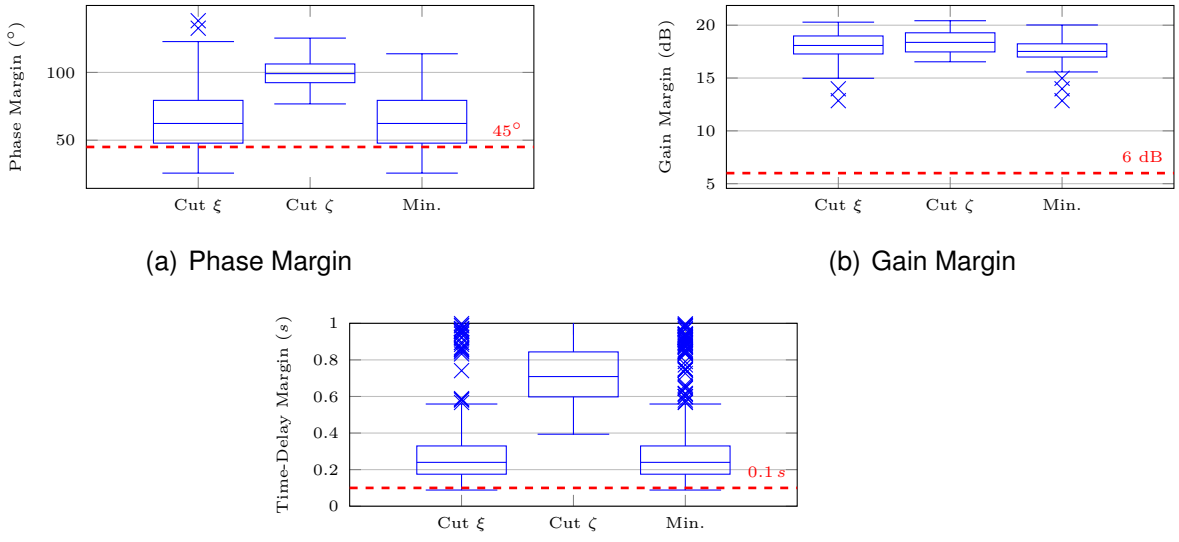

(a) Phase Margin

(b) Gain Margin

(c) Time-Delay Margin

Figure E.46: Box plots of phase, gain and time-delay margin of the MM-LQR controller at $V_K^R = 35\,m/s$, $h = 1000\,m$, $m_{fuel} = 23\,kg$.

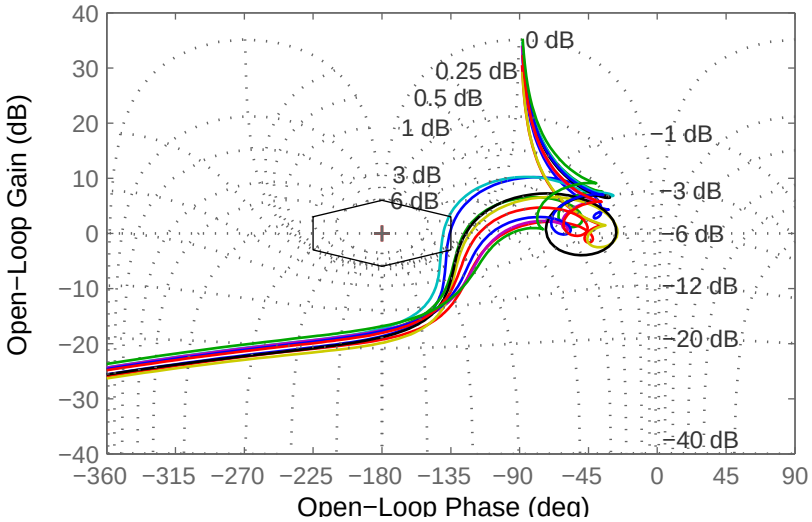

(a) Loopcut in front of the aileron control delay

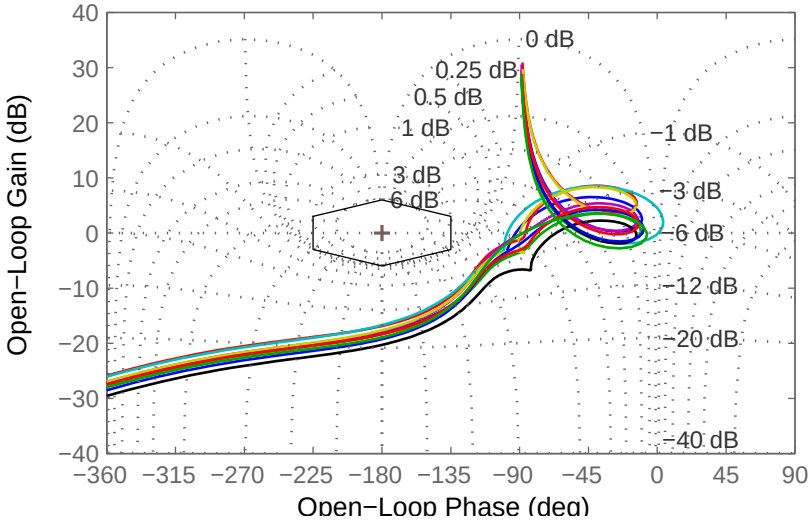

(b) Loopcut in front of the rudder control delay

Figure E.47: Nichols plots at $V_K^R = 35\,m/s$, $h = 1000\,m$, $m_{fuel} = 23\,kg$, when relying on a MM-LQR controller.

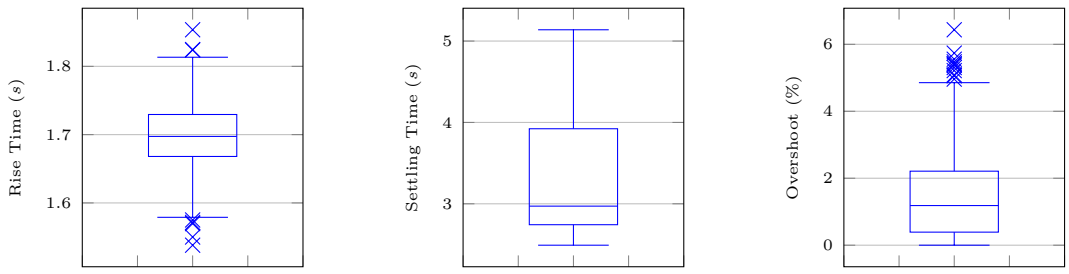

(a) Rise Time (b) Settling Time (c) Overhoot

Figure E.48: Box plots of rise time, settling time and overshoot of the LTI plant model with MM-LQR controller in case of a $30°$ step command $\Phi_{cmd}(t)$ at $V_K^R = 35\,m/s$, $h = 1000\,m$, $m_{fuel} = 23\,kg$.

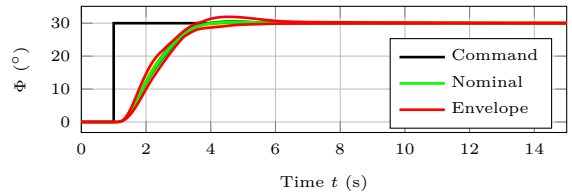

(a) Bank Angle

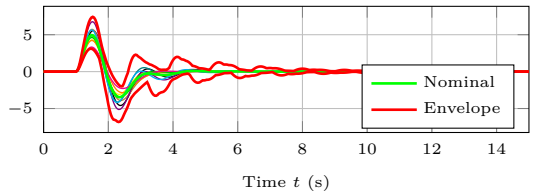

(b) Bank Angle

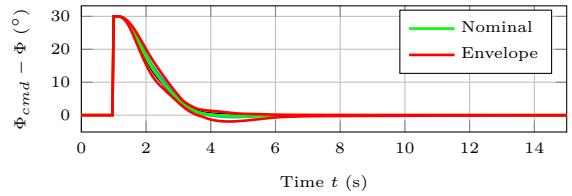

(c) Tracking Error

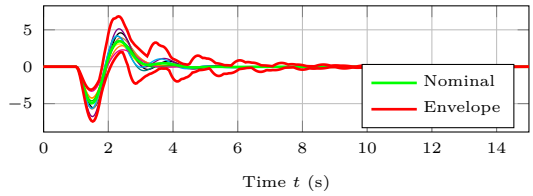

(d) Tracking Error

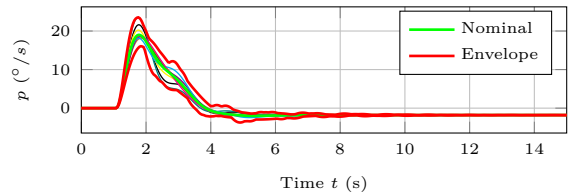

(e) Roll Rate

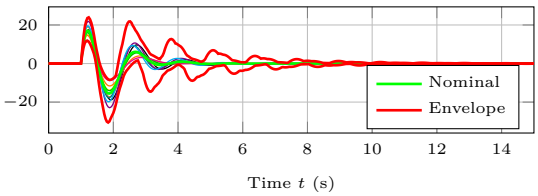

(f) Roll Rate

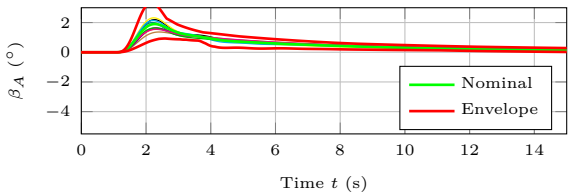

(g) Angle-of-sideslip

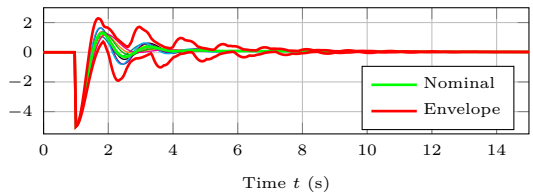

(h) Angle-of-sideslip

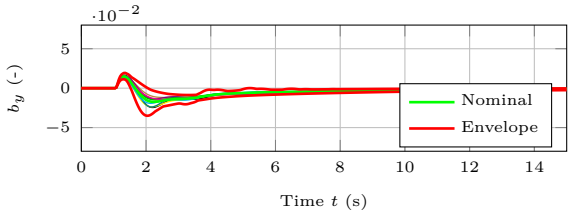

(i) Lateral Acceleration

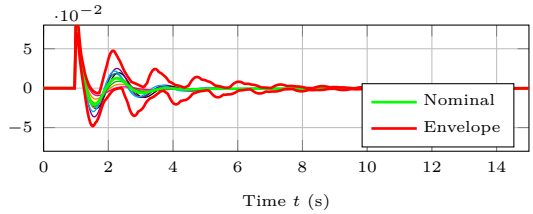

(j) Lateral Acceleration

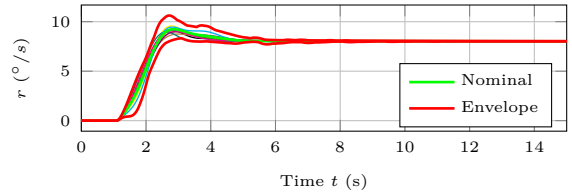

(k) Yaw Rate

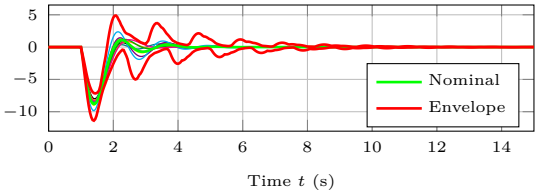

(l) Yaw Rate

Figure E.49: Rigid body states of the LTI plant model with MM-LQR controller in response to a $30°$ step command $\Phi_{cmd}(t)$ (left column) and to a $5°$ step command $\beta_{W,cmd}(t)$ (right column) at $V_K^R = 35\,m/s$, $h = 1000\,m$, $m_{fuel} = 23\,kg$.

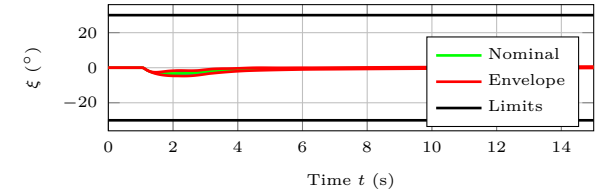

(a) Aileron Deflection

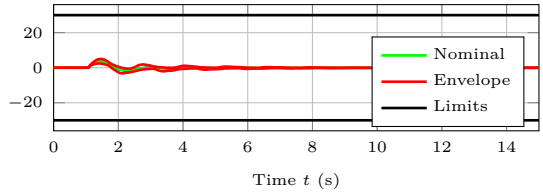

(b) Aileron Deflection

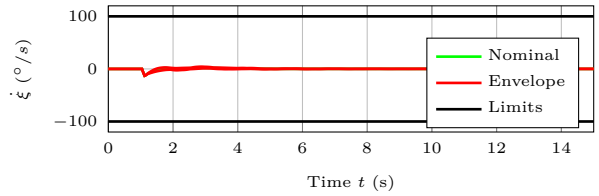

(c) Aileron Rate

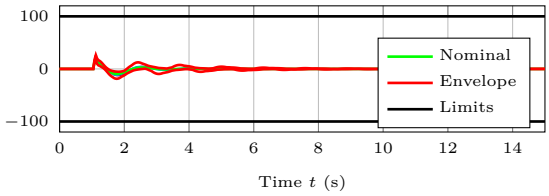

(d) Aileron Rate

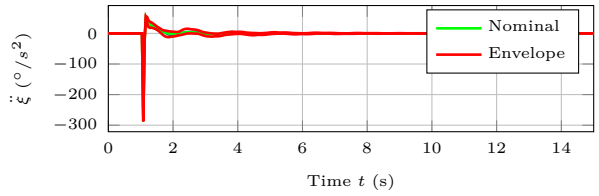

(e) Aileron Acceleration

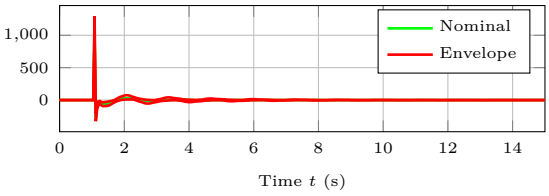

(f) Aileron Acceleration

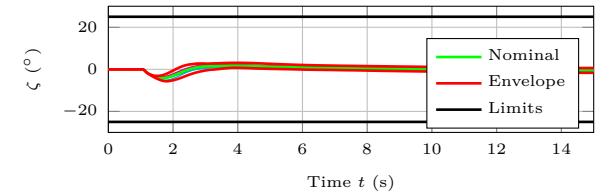

(g) Rudder Deflection

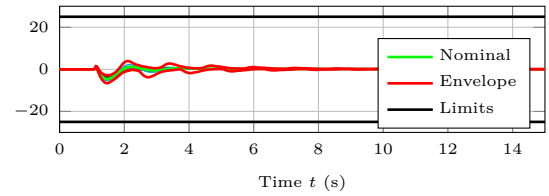

(h) Rudder Deflection

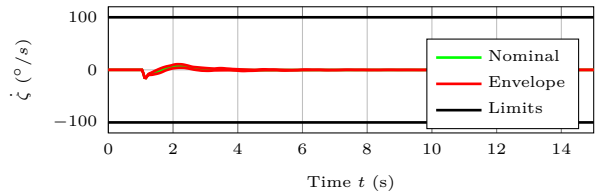

(i) Rudder Rate

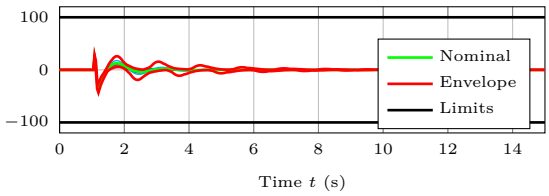

(j) Rudder Rate

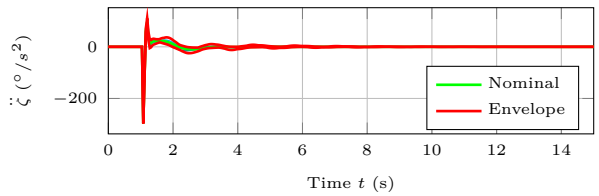

(k) Rudder Acceleration

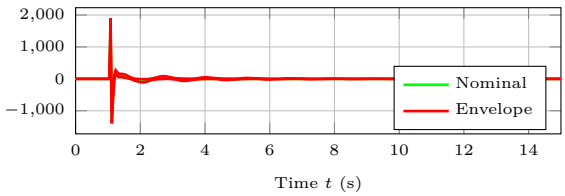

(l) Rudder Acceleration

Figure E.50: Actuator states of the LTI plant model with MM-LQR controller in response to a $30°$ step command $\Phi_{cmd}(t)$ (left column) and to a $5°$ step command $\beta_{W,cmd}(t)$ (right column) at $V_K^R = 35\,m/s$, $h = 1000\,m$, $m_{fuel} = 23\,kg$.

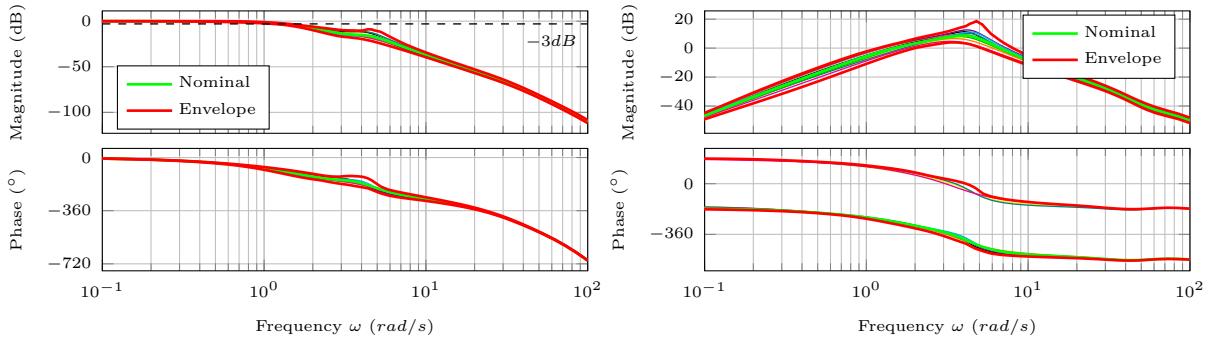

(a) Φ_{cmd} to Bank Angle Φ

(b) $\beta_{W,cmd}$ to Bank Angle Φ

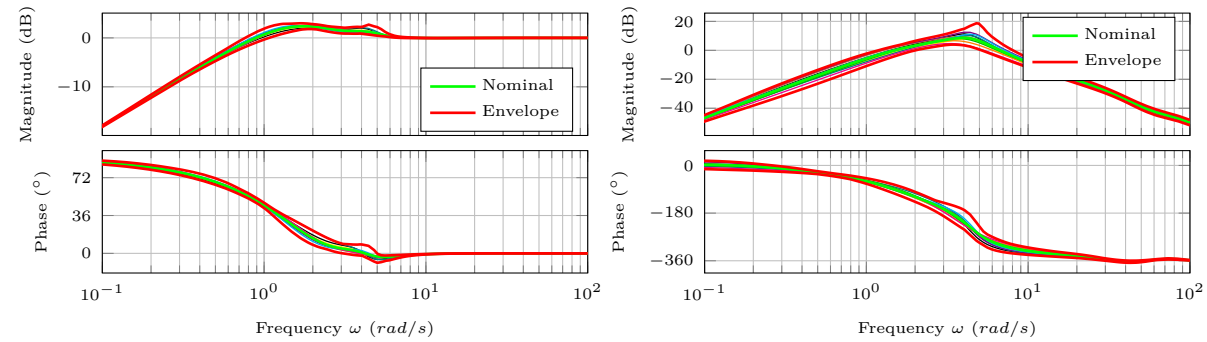

(c) Φ_{cmd} to Tracking Error $\Phi_{cmd} - \Phi$

(d) $\beta_{W,cmd}$ to Tracking Error $\Phi_{cmd} - \Phi$

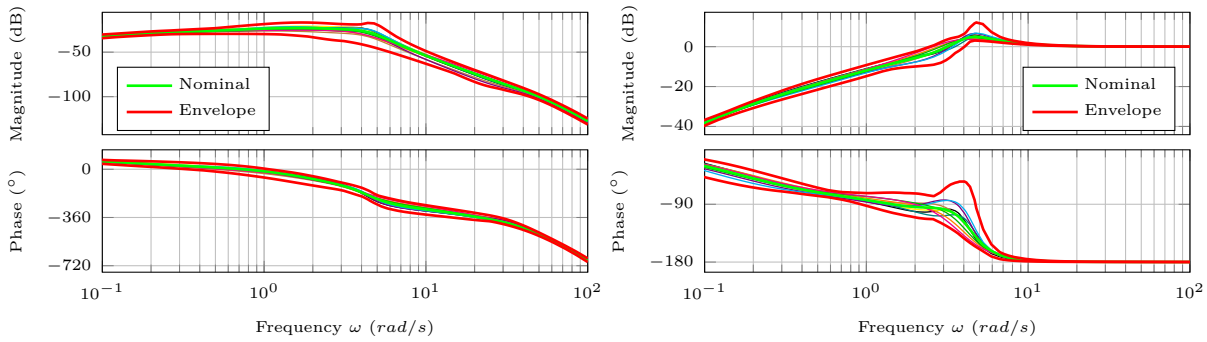

(e) Φ_{cmd} to Angle-of-sideslip β_A

(f) $\beta_{W,cmd}$ to Angle-of-sideslip β_A

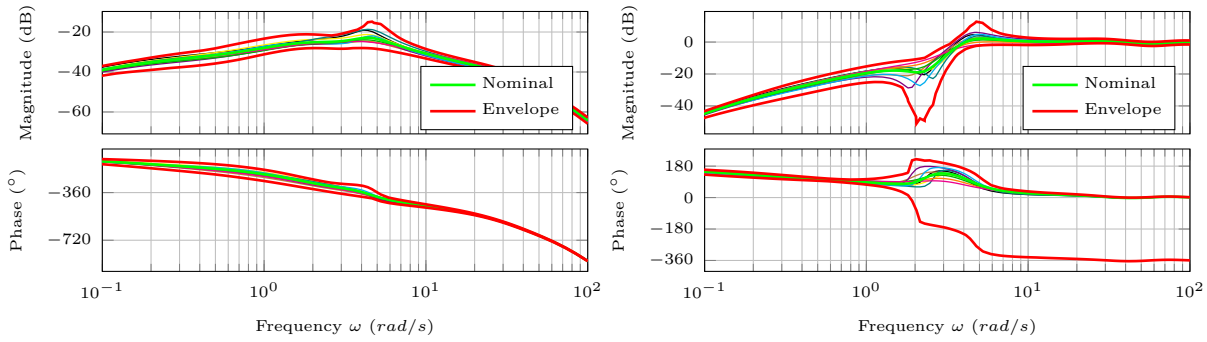

(g) Φ_{cmd} to Lateral Acceleration b_y

(h) $\beta_{W,cmd}$ to Lateral Acceleration b_y

Figure E.51: Bode plots of the closed-loop rigid-body states at $V_K^R = 35\,m/s$, $h = 1000\,m$, $m_{fuel} = 23\,kg$, when relying on a MM-LQR controller.

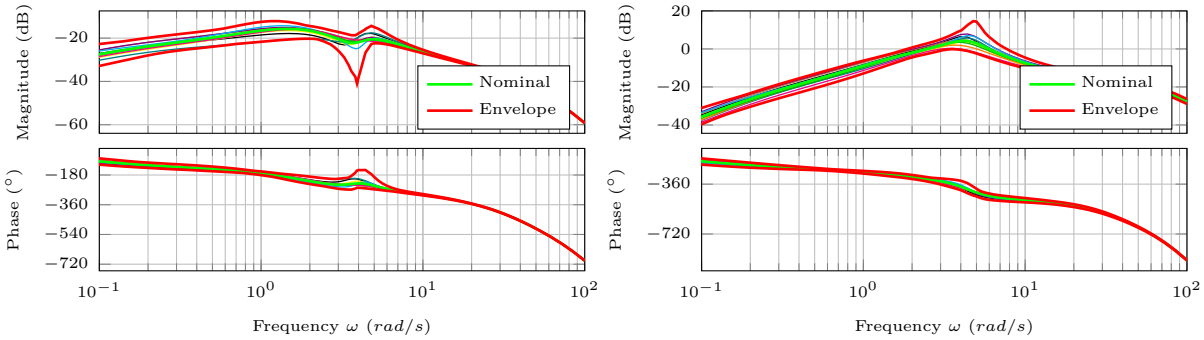

(a) Φ_{cmd} to Aileron Deflection ξ

(b) $\beta_{W,cmd}$ to Aileron Deflection ξ

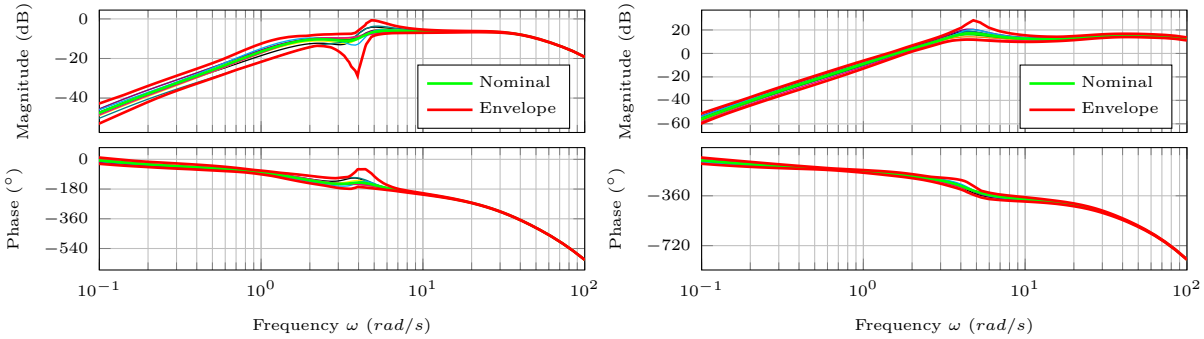

(c) Φ_{cmd} to Aileron Rate $\dot{\xi}$

(d) $\beta_{W,cmd}$ to Aileron Rate $\dot{\xi}$

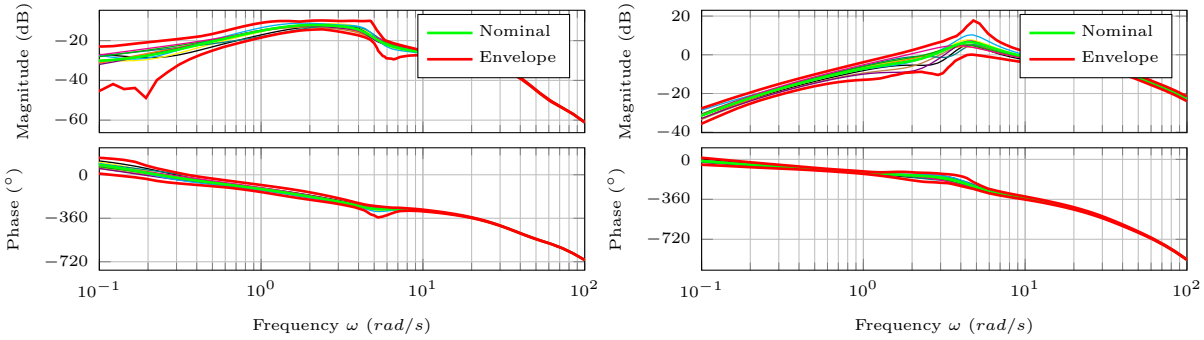

(e) Φ_{cmd} to Rudder Deflection ζ

(f) $\beta_{W,cmd}$ to Rudder Deflection ζ

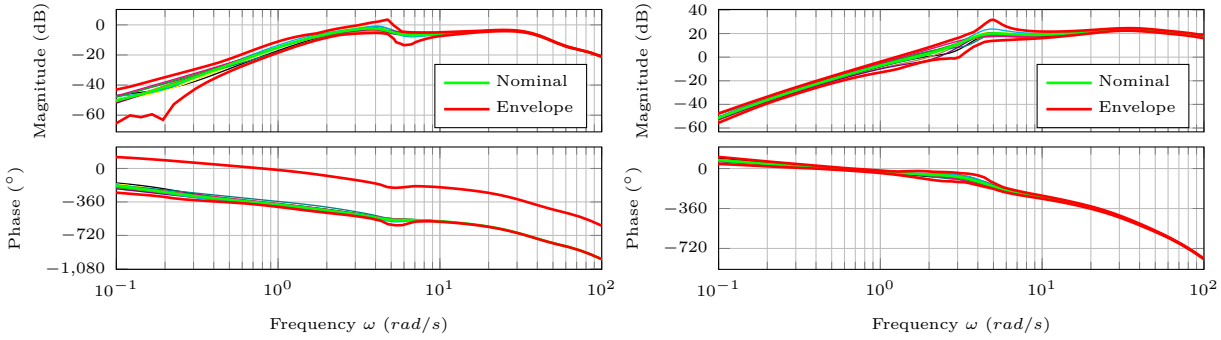

(g) Φ_{cmd} to Rudder Rate $\dot{\zeta}$

(h) $\beta_{W,cmd}$ to Rudder Rate $\dot{\zeta}$

Figure E.52: Bode plots of the closed-loop actuator states at $V_K^R = 35\,m/s$, $h = 1000\,m$, $m_{fuel} = 23\,kg$, when relying on a MM-LQR controller.

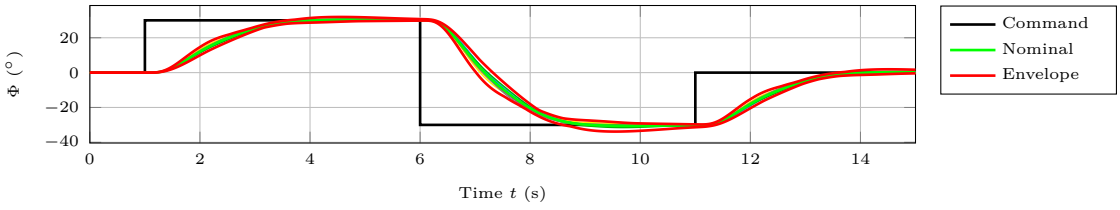

(a) Bank Angle

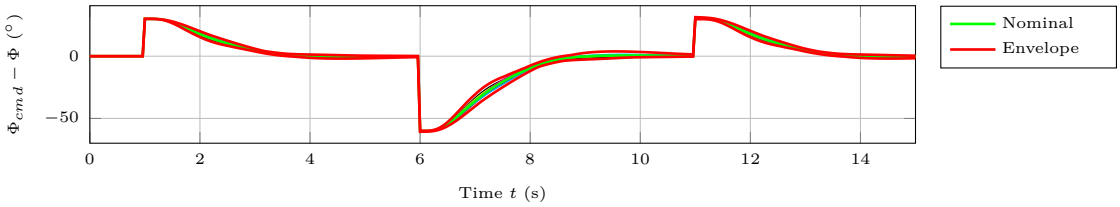

(b) Tracking Error

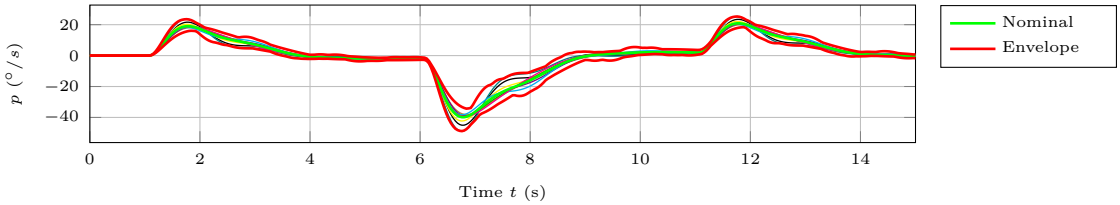

(c) Roll Rate

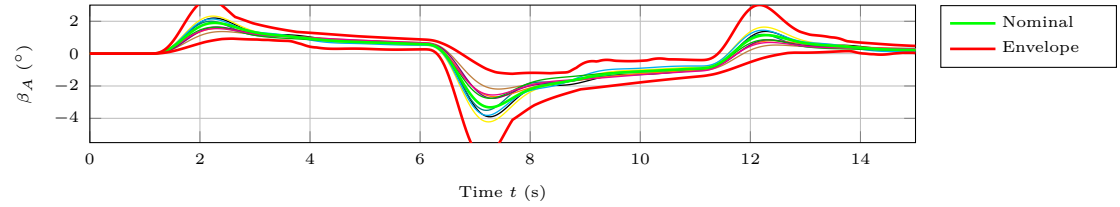

(d) Angle-of-sideslip

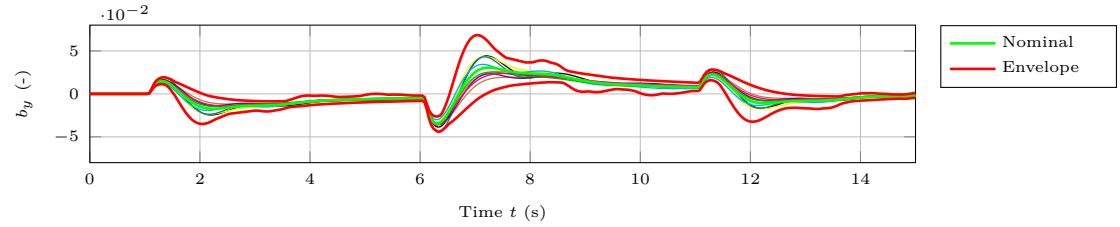

(e) Lateral Acceleration

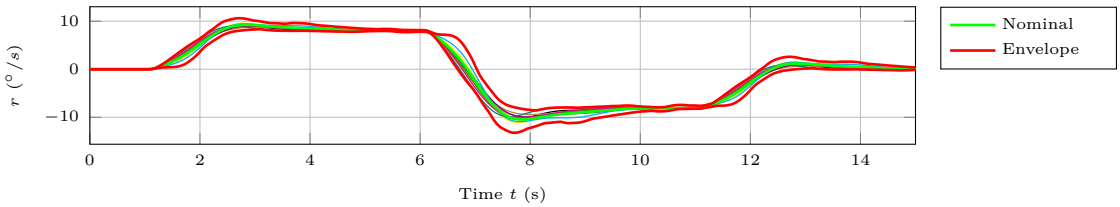

(f) Yaw Rate

Figure E.53: Rigid body states of the LTI plant model with MM-LQR controller in response to a $30°$ doublet command $\Phi_{cmd}(t)$ at $V_K^R = 35\,m/s$, $h = 1000\,m$, $m_{fuel} = 23\,kg$.

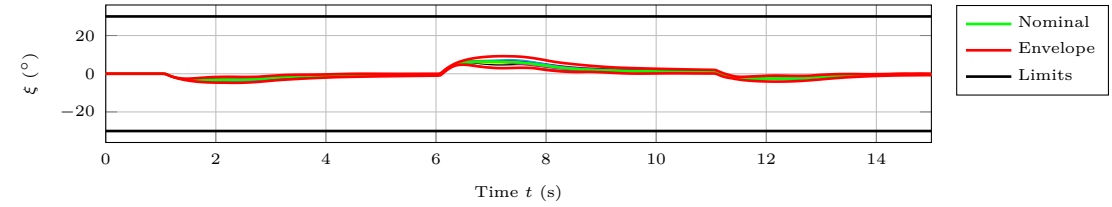

(a) Aileron Deflection

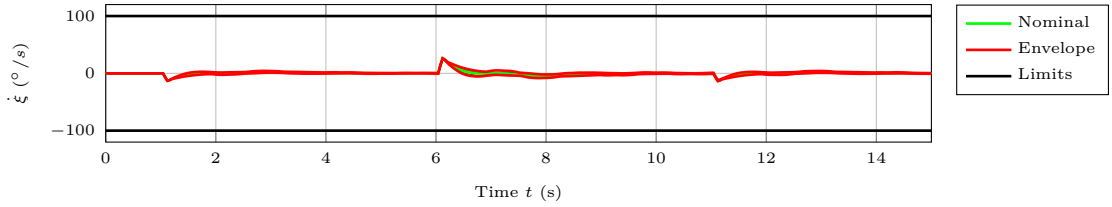

(b) Aileron Rate

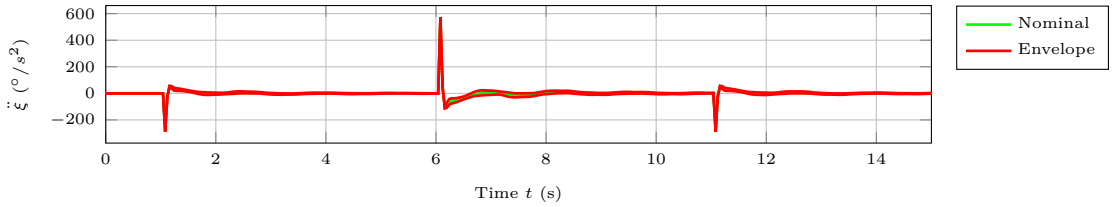

(c) Aileron Acceleration

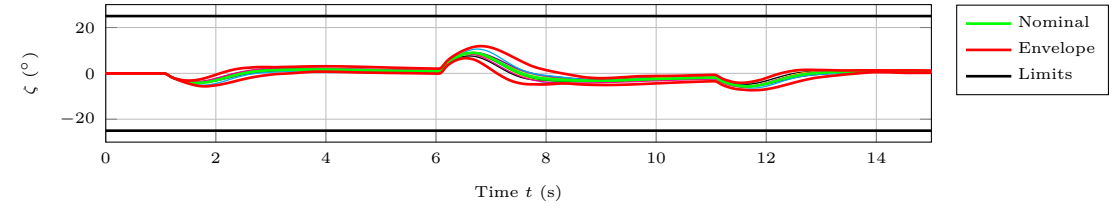

(d) Rudder Deflection

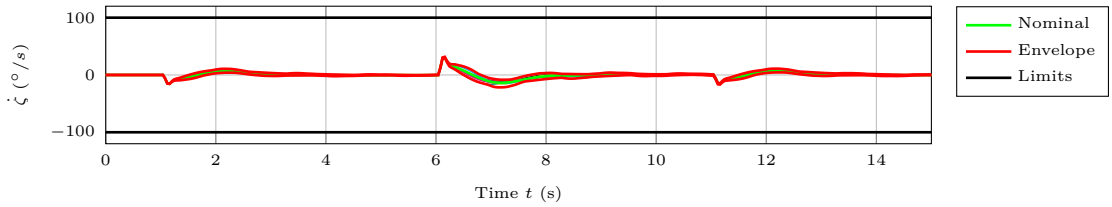

(e) Rudder Rate

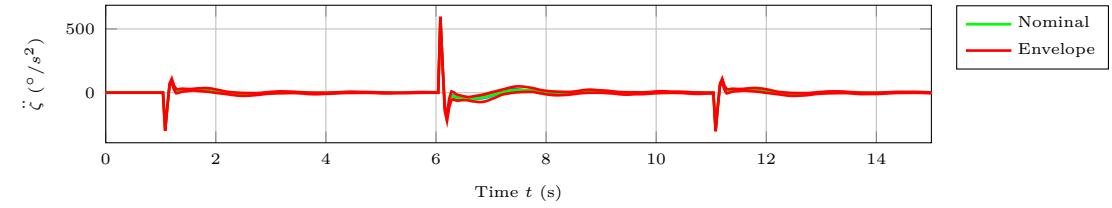

(f) Rudder Acceleration

Figure E.54: Actuator states of the LTI plant model with MM-LQR controller in response to a $30°$ doublet command $\Phi_{cmd}(t)$ at $V_K^R = 35\,m/s$, $h = 1000\,m$, $m_{fuel} = 23\,kg$.

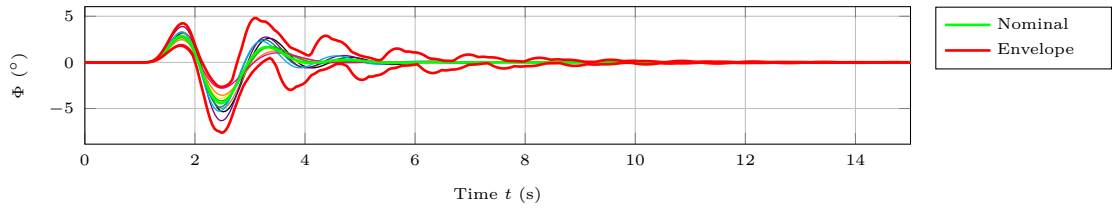

(a) Bank Angle

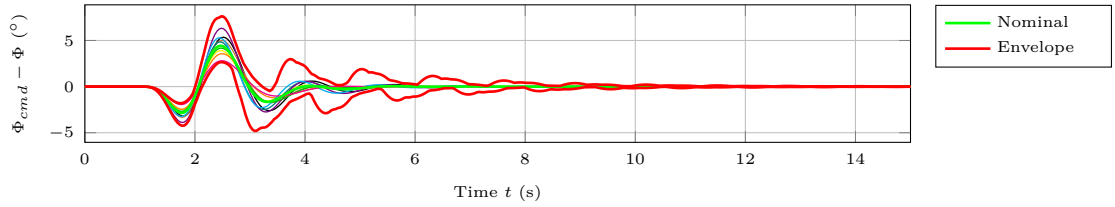

(b) Tracking Error

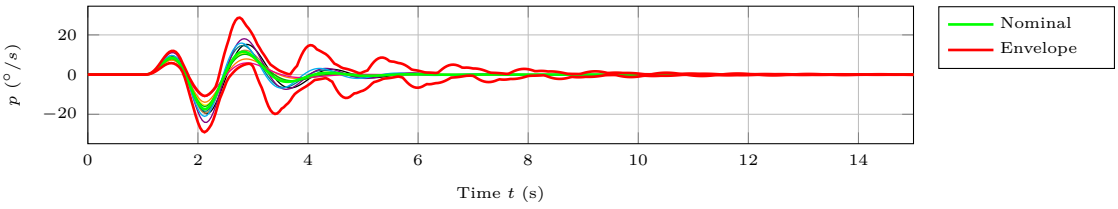

(c) Roll Rate

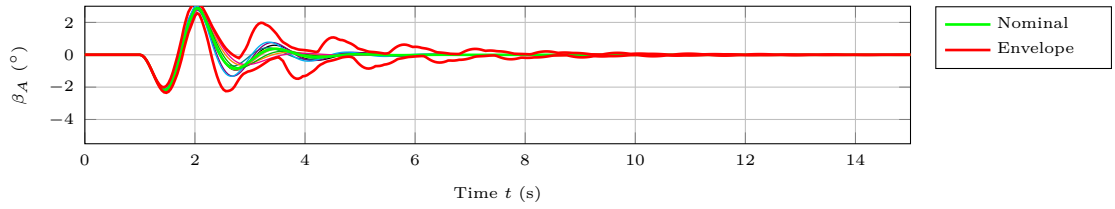

(d) Angle-of-sideslip

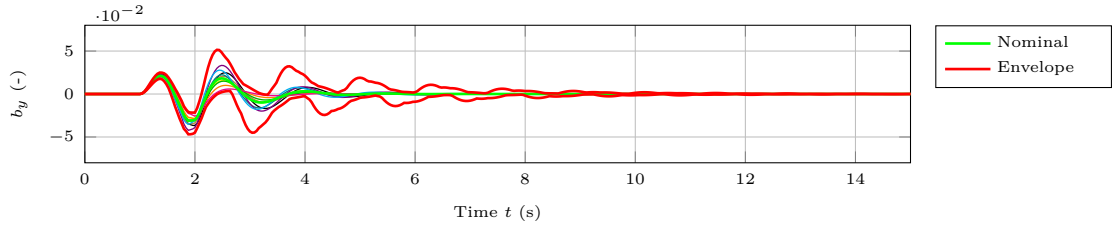

(e) Lateral Acceleration

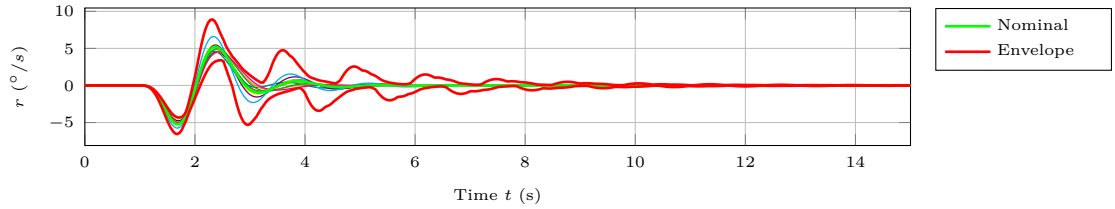

(f) Yaw Rate

Figure E.55: Rigid body states of the LTI plant model with MM-LQR controller in response to a $20\,m$ discrete gust at $V_K^R = 35\,m/s$, $h = 1000\,m$, $m_{fuel} = 23\,kg$.

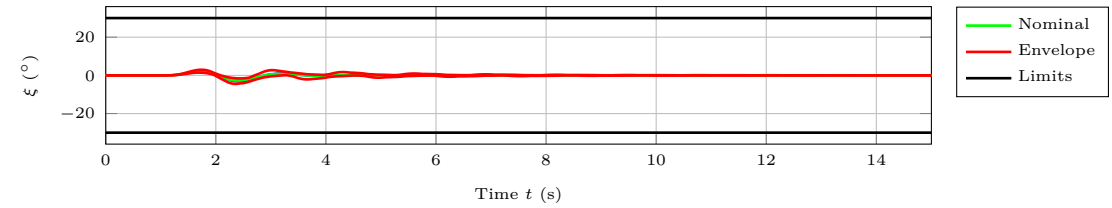

(a) Aileron Deflection

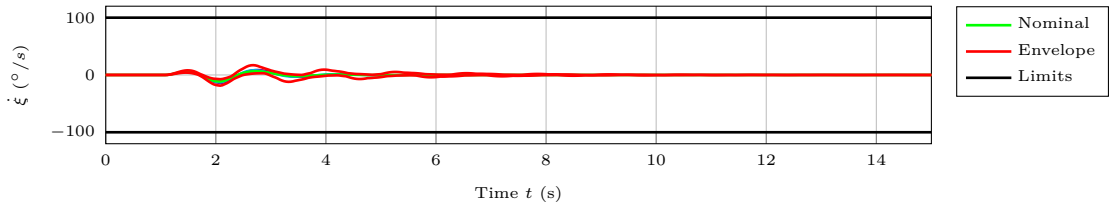

(b) Aileron Rate

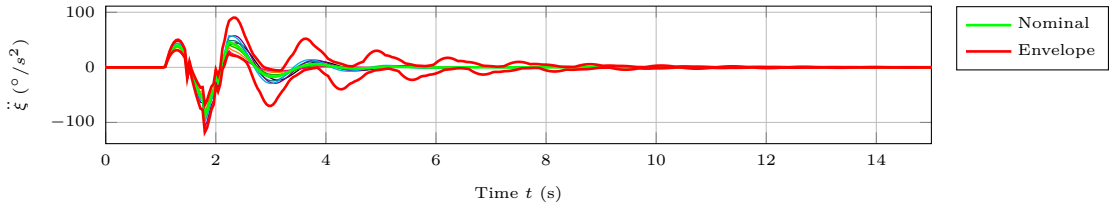

(c) Aileron Acceleration

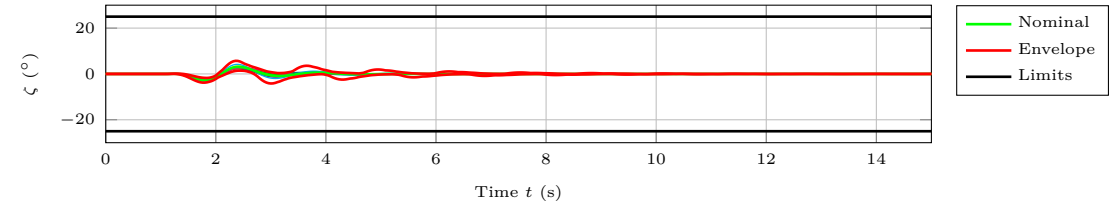

(d) Rudder Deflection

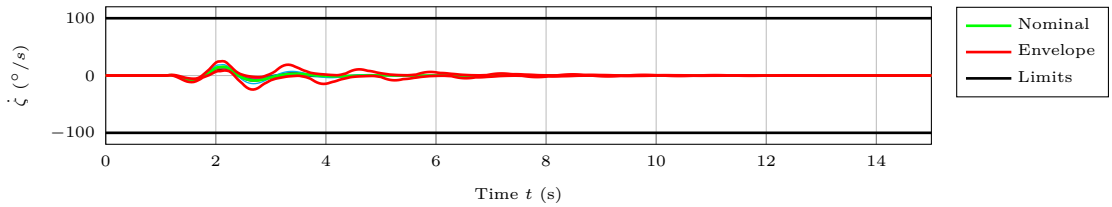

(e) Rudder Rate

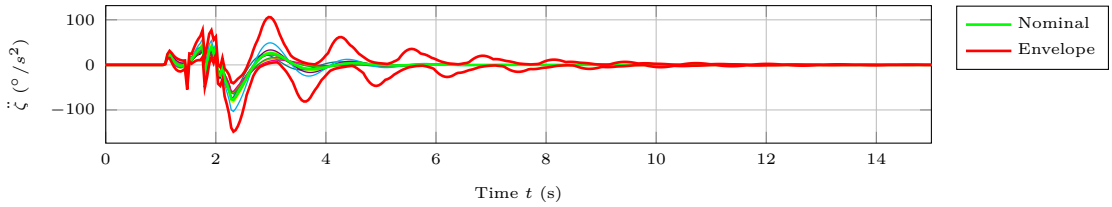

(f) Rudder Acceleration

Figure E.56: Actuator states of the LTI plant model with MM-LQR controller in response to a $20\,m$ discrete gust at $V_K^R = 35\,m/s$, $h = 1000\,m$, $m_{fuel} = 23\,kg$.

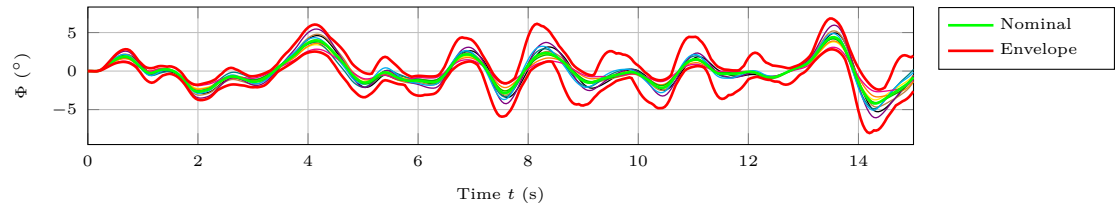

(a) Bank Angle

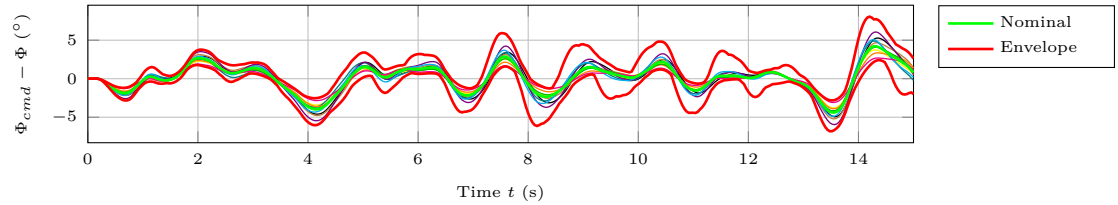

(b) Tracking Error

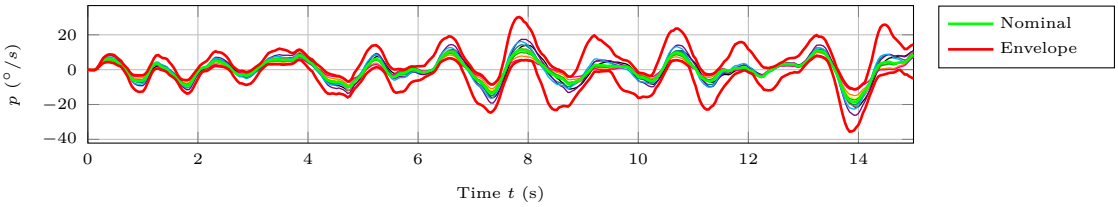

(c) Roll Rate

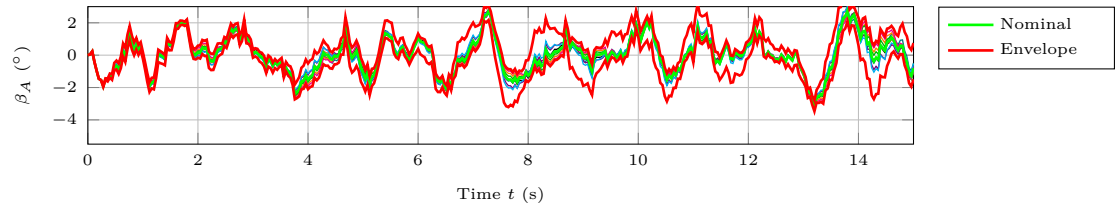

(d) Angle-of-sideslip

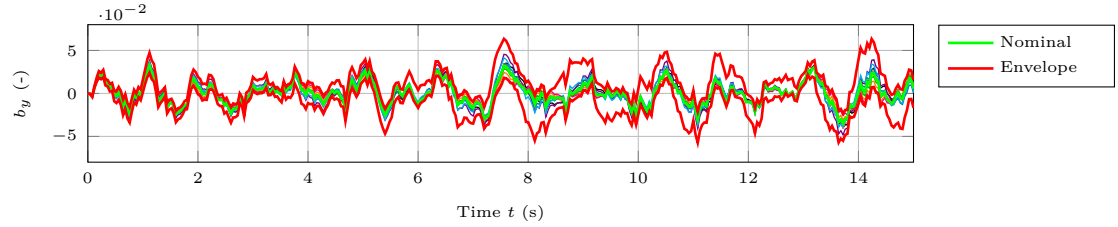

(e) Lateral Acceleration

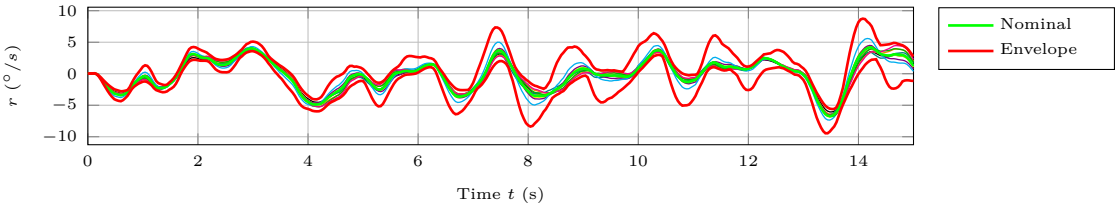

(f) Yaw Rate

Figure E.57: Rigid body states of the LTI plant model with MM-LQR controller in response to moderate Dryden turbulence at $V_K^R = 35\,m/s$, $h = 1000\,m$, $m_{fuel} = 23\,kg$.

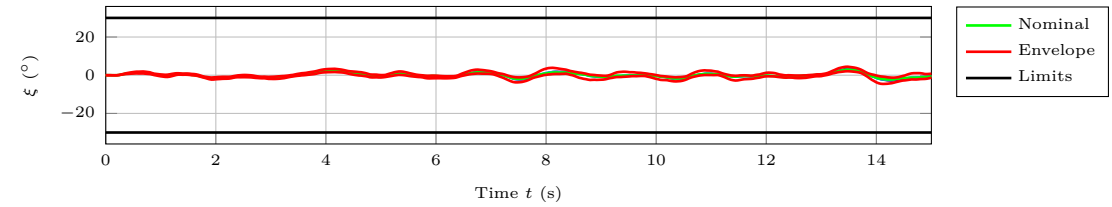

(a) Aileron Deflection

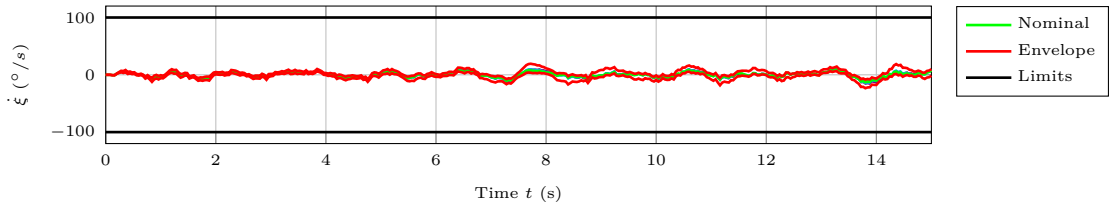

(b) Aileron Rate

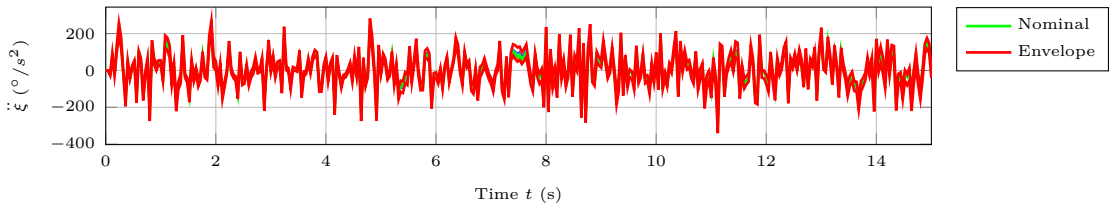

(c) Aileron Acceleration

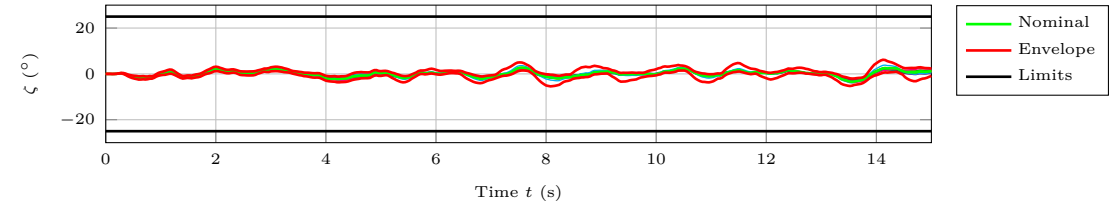

(d) Rudder Deflection

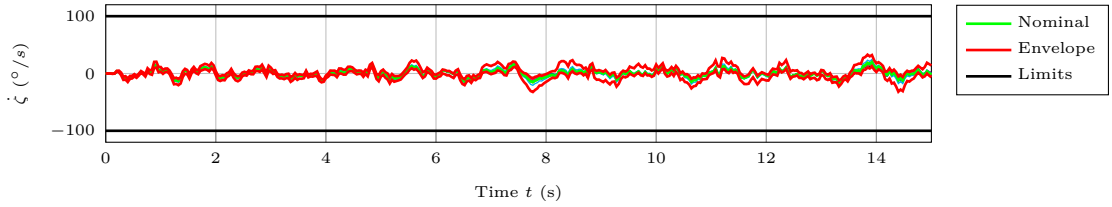

(e) Rudder Rate

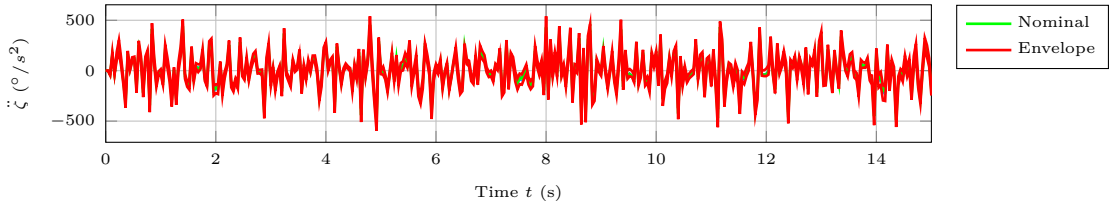

(f) Rudder Acceleration

Figure E.58: Actuator states of the LTI plant model with MM-LQR controller in response to moderate Dryden turbulence at $V_K^R = 35\,m/s$, $h = 1000\,m$, $m_{fuel} = 23\,kg$.

E.2.2 Linear Model at 50 m/s

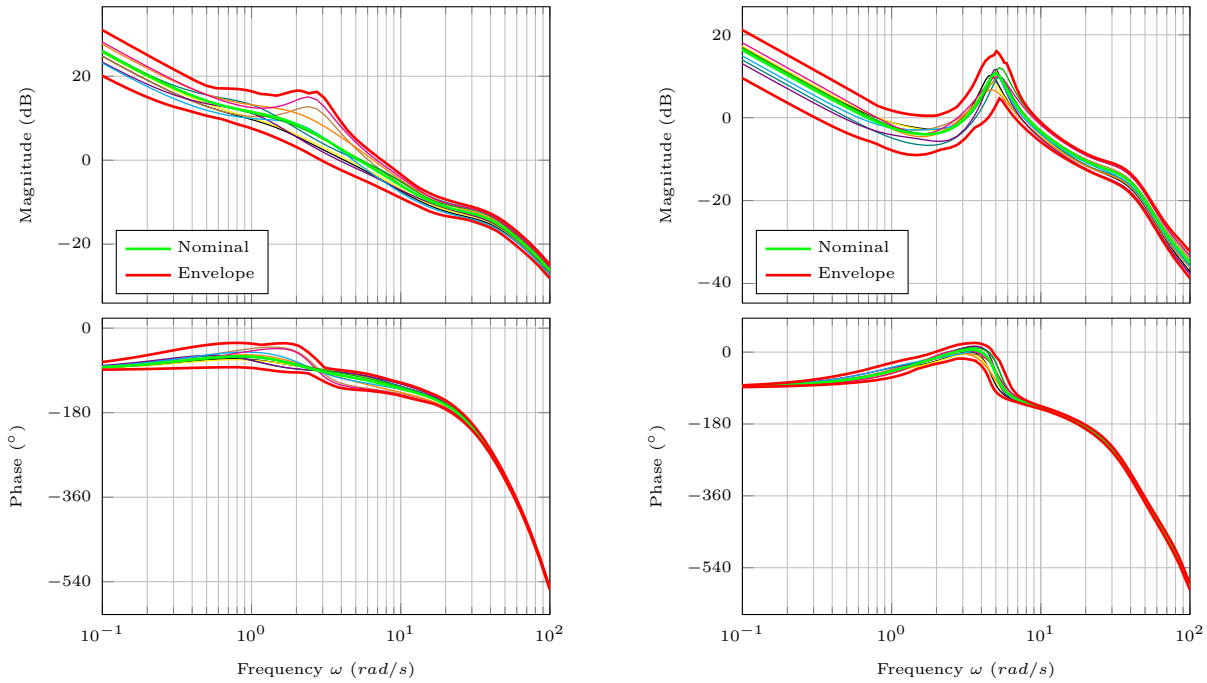

(a) Loopcut at aileron actuator input ξ

(b) Loopcut at rudder actuator input ζ

Figure E.59: Open-loop bode plots at $V_K^R = 50\,m/s$, $h = 500\,m$, $m_{fuel} = 0\,kg$, when relying on a MM-LQR controller.

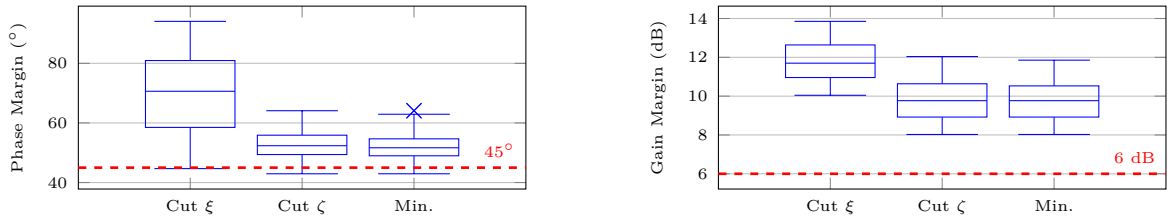

(a) Phase Margin

(b) Gain Margin

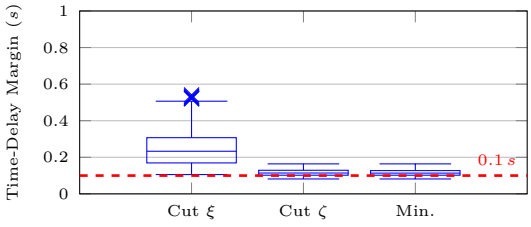

(c) Time-Delay Margin

Figure E.60: Box plots of phase, gain and time-delay margin of the MM-LQR controller at $V_K^R = 50\,m/s$, $h = 500\,m$, $m_{fuel} = 0\,kg$.

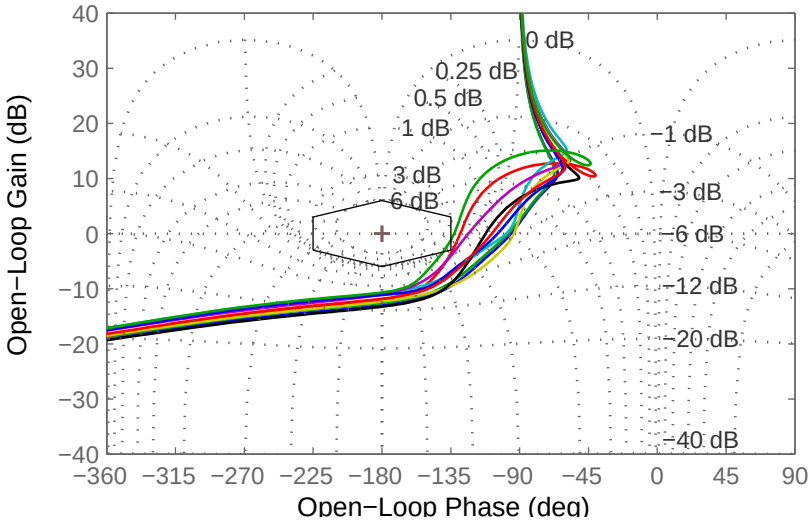

(a) Loopcut in front of the aileron control delay

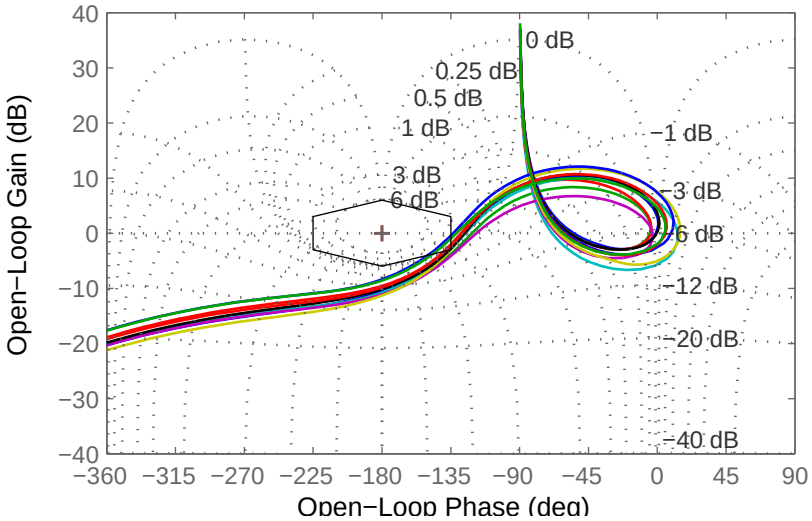

(b) Loopcut in front of the rudder control delay

Figure E.61: Nichols plots at $V_K^R = 50\,m/s$, $h = 500\,m$, $m_{fuel} = 0\,kg$, when relying on a MM-LQR controller.

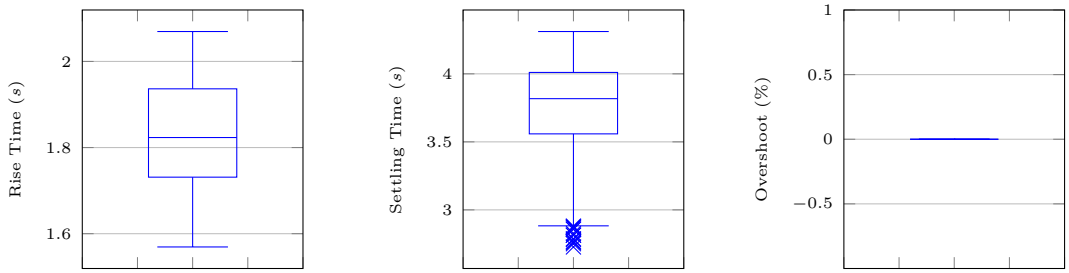

(a) Rise Time (b) Settling Time (c) Overhoot

Figure E.62: Box plots of rise time, settling time and overshoot of the LTI plant model with MM-LQR controller in case of a $30°$ step command $\Phi_{cmd}(t)$ at $V_K^R = 50\,m/s$, $h = 500\,m$, $m_{fuel} = 0\,kg$.

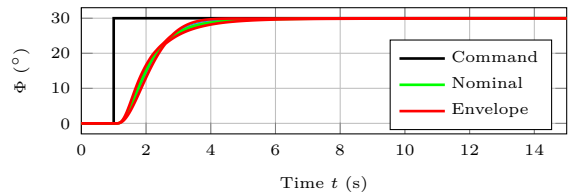

(a) Bank Angle

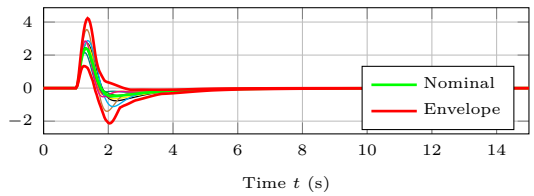

(b) Bank Angle

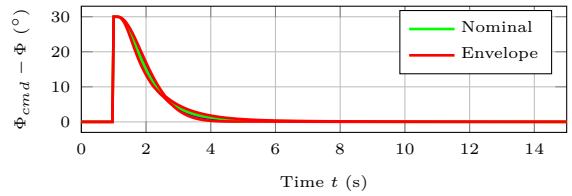

(c) Tracking Error

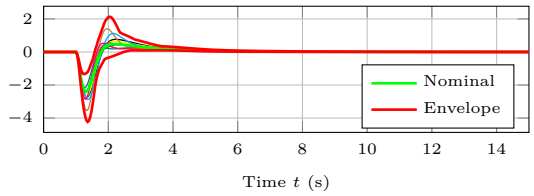

(d) Tracking Error

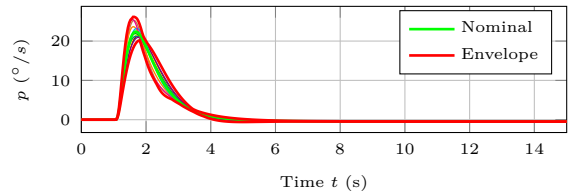

(e) Roll Rate

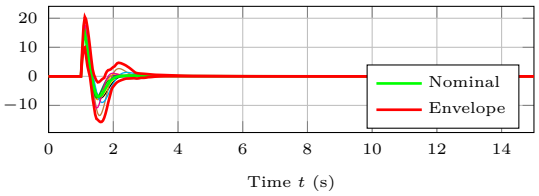

(f) Roll Rate

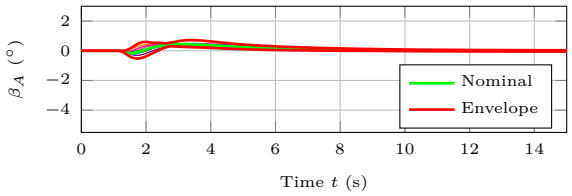

(g) Angle-of-sideslip

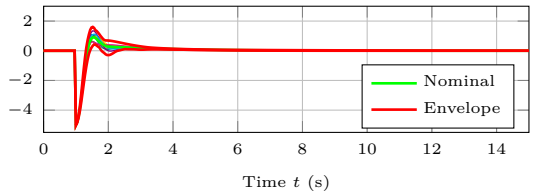

(h) Angle-of-sideslip

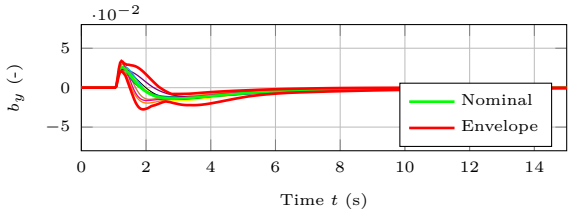

(i) Lateral Acceleration

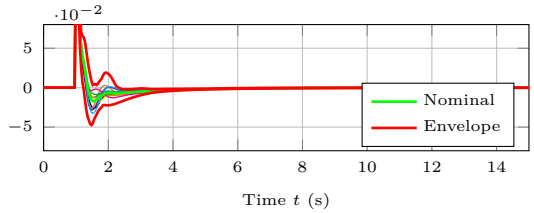

(j) Lateral Acceleration

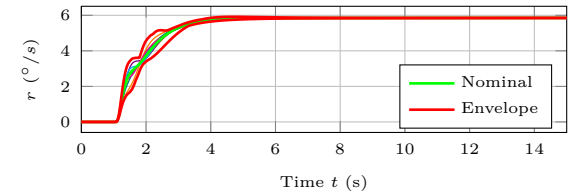

(k) Yaw Rate

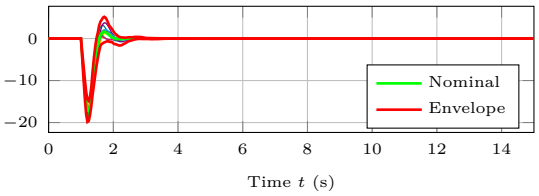

(l) Yaw Rate

Figure E.63: Rigid body states of the LTI plant model with MM-LQR controller in response to a $30°$ step command $\Phi_{cmd}(t)$ (left column) and to a $5°$ step command $\beta_{W,cmd}(t)$ (right column) at $V_K^R = 50\,m/s$, $h = 500\,m$, $m_{fuel} = 0\,kg$.

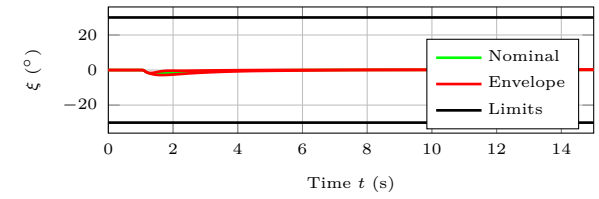

(a) Aileron Deflection

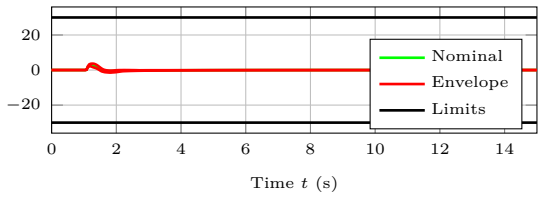

(b) Aileron Deflection

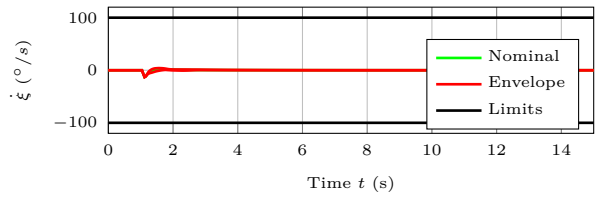

(c) Aileron Rate

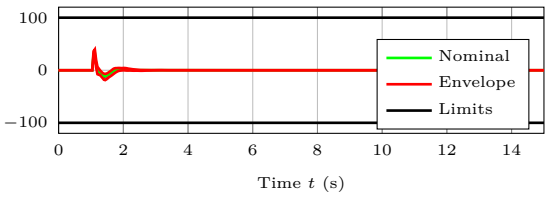

(d) Aileron Rate

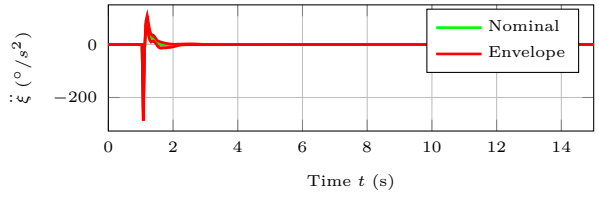

(e) Aileron Acceleration

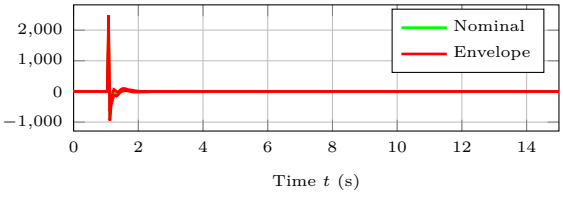

(f) Aileron Acceleration

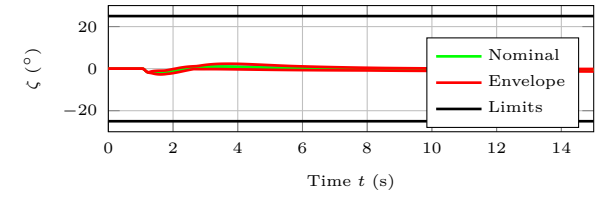

(g) Rudder Deflection

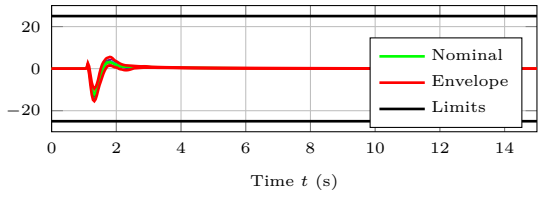

(h) Rudder Deflection

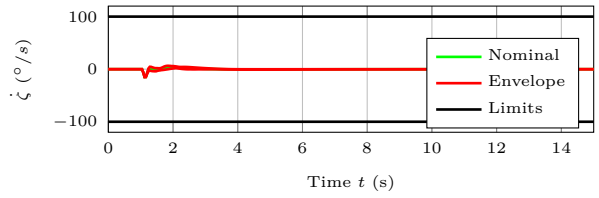

(i) Rudder Rate

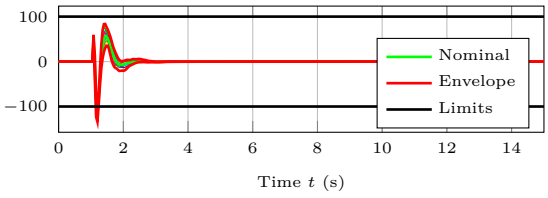

(j) Rudder Rate

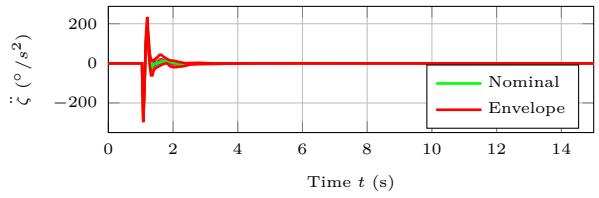

(k) Rudder Acceleration

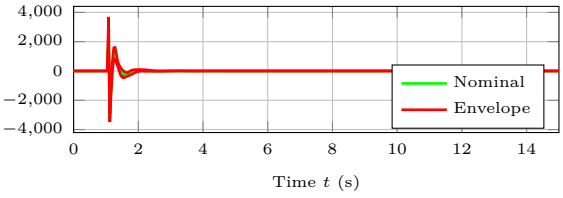

(l) Rudder Acceleration

Figure E.64: Actuator states of the LTI plant model with MM-LQR controller in response to a $30°$ step command $\Phi_{cmd}(t)$ (left column) and to a $5°$ step command $\beta_{W,cmd}(t)$ (right column) at $V_K^R = 50\,m/s$, $h = 500\,m$, $m_{fuel} = 0\,kg$.

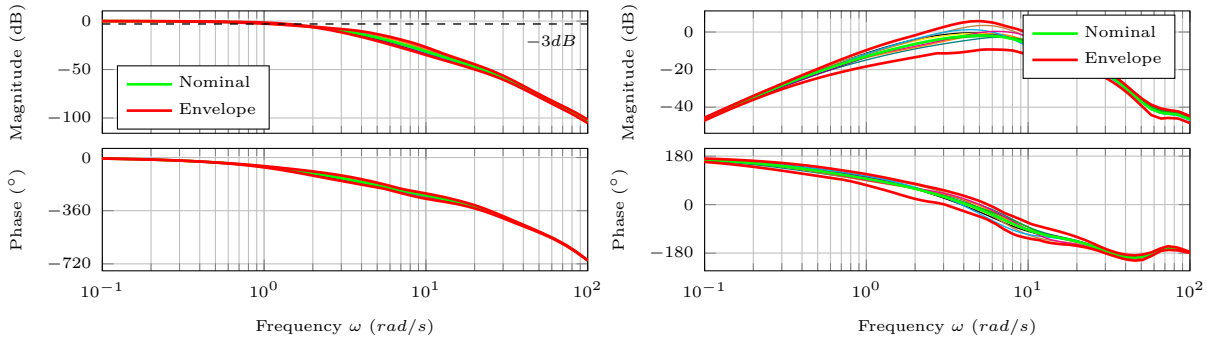

(a) Φ_{cmd} to Bank Angle Φ

(b) $\beta_{W,cmd}$ to Bank Angle Φ

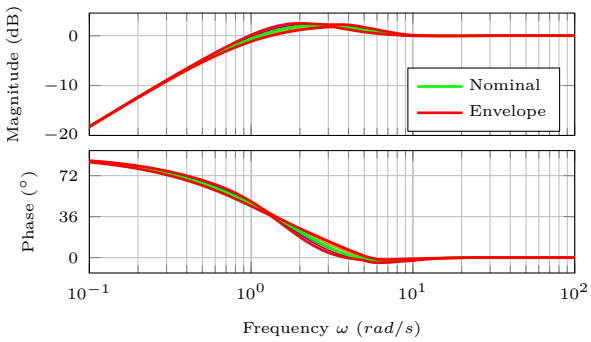

(c) Φ_{cmd} to Tracking Error $\Phi_{cmd} - \Phi$

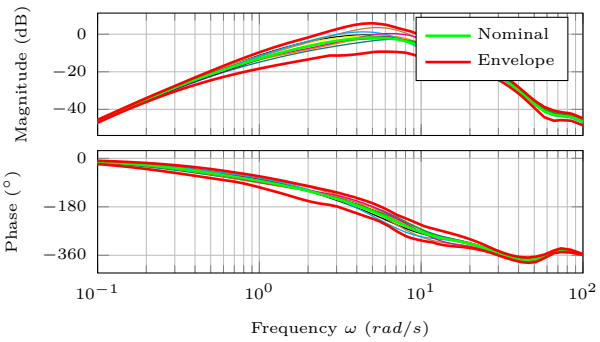

(d) $\beta_{W,cmd}$ to Tracking Error $\Phi_{cmd} - \Phi$

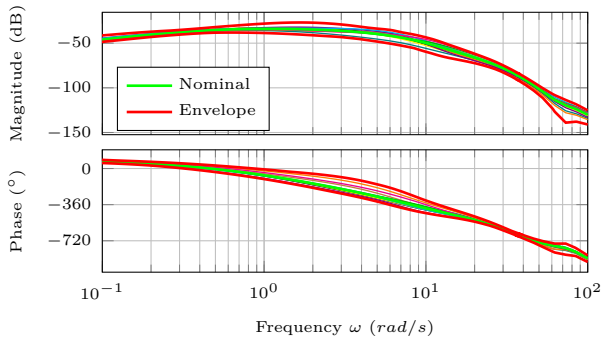

(e) Φ_{cmd} to Angle-of-sideslip β_A

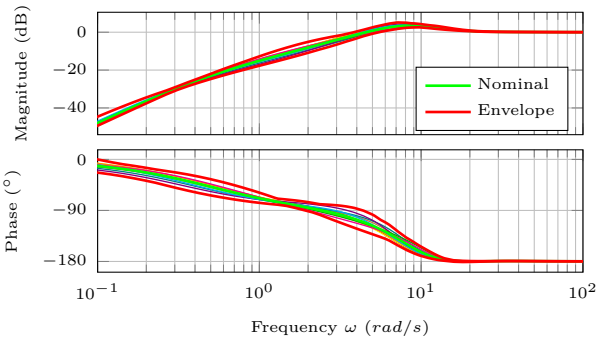

(f) $\beta_{W,cmd}$ to Angle-of-sideslip β_A

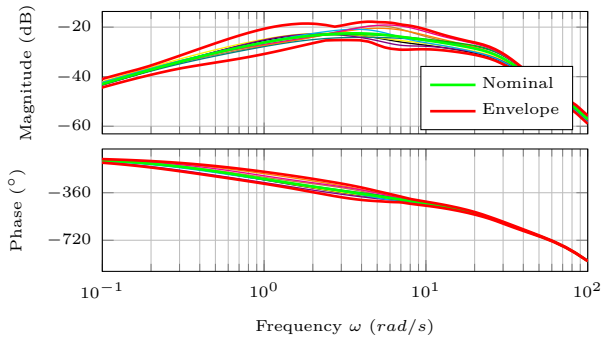

(g) Φ_{cmd} to Lateral Acceleration b_y

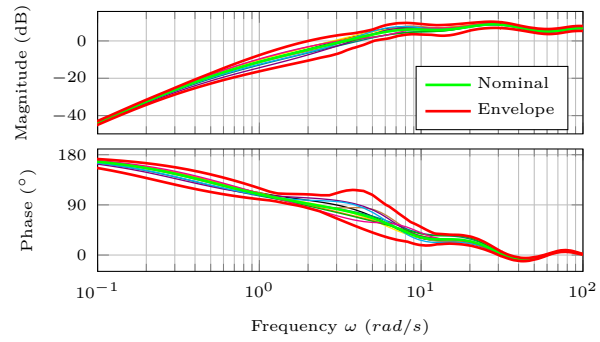

(h) $\beta_{W,cmd}$ to Lateral Acceleration b_y

Figure E.65: Bode plots of the closed-loop rigid-body states at $V_K^R = 50\,m/s$, $h = 500\,m$, $m_{fuel} = 0\,kg$, when relying on a MM-LQR controller.

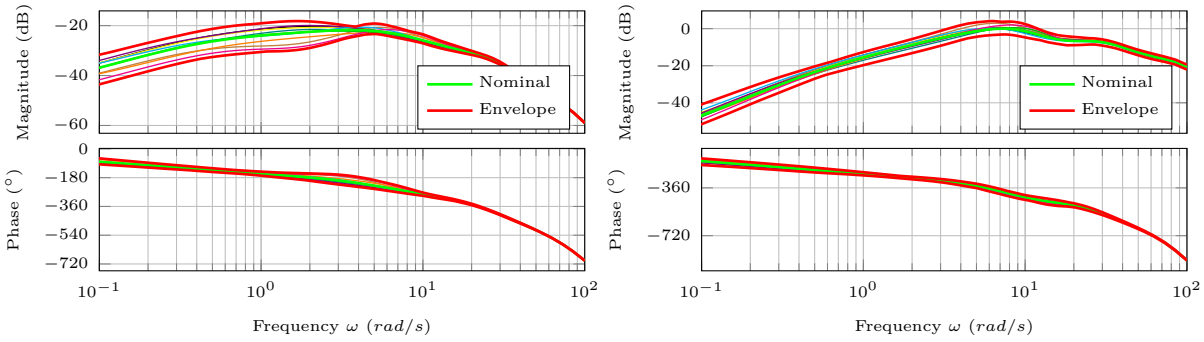

(a) Φ_{cmd} to Aileron Deflection ξ

(b) $\beta_{W,cmd}$ to Aileron Deflection ξ

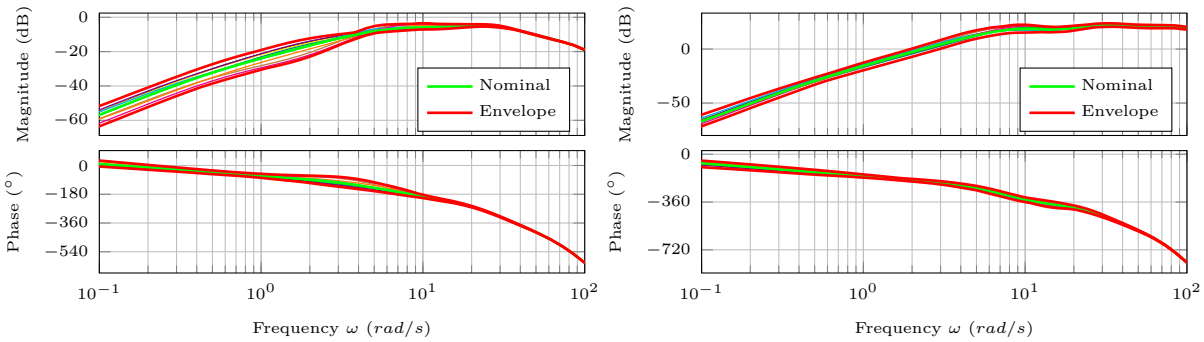

(c) Φ_{cmd} to Aileron Rate $\dot{\xi}$

(d) $\beta_{W,cmd}$ to Aileron Rate $\dot{\xi}$

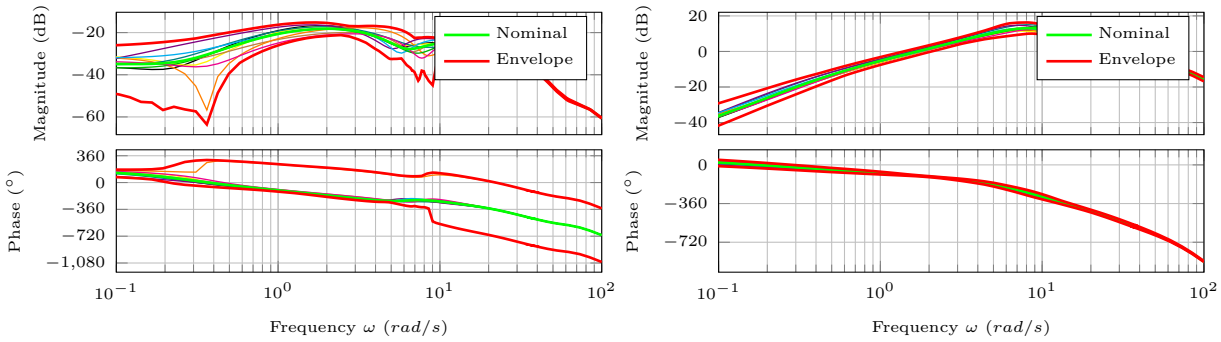

(e) Φ_{cmd} to Rudder Deflection ζ

(f) $\beta_{W,cmd}$ to Rudder Deflection ζ

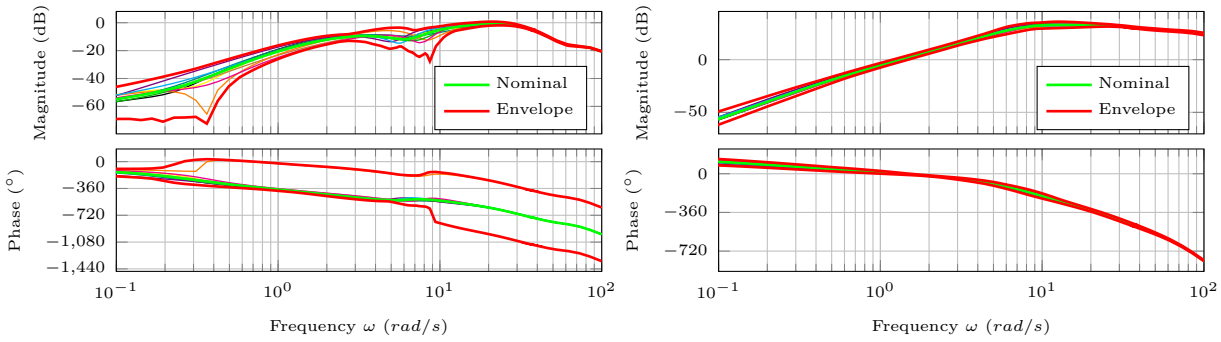

(g) Φ_{cmd} to Rudder Rate $\dot{\zeta}$

(h) $\beta_{W,cmd}$ to Rudder Rate $\dot{\zeta}$

Figure E.66: Bode plots of the closed-loop actuator states at $V_K^R = 50\,m/s$, $h = 500\,m$, $m_{fuel} = 0\,kg$, when relying on a MM-LQR controller.

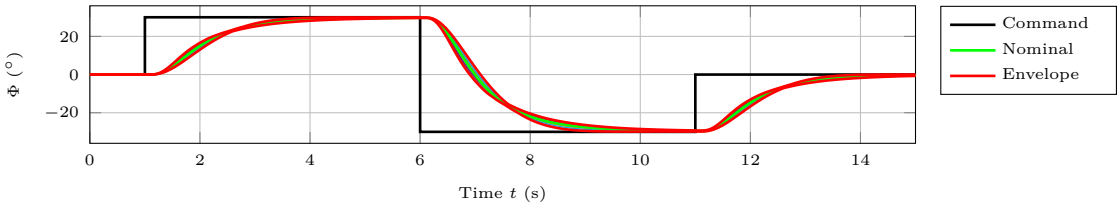

(a) Bank Angle

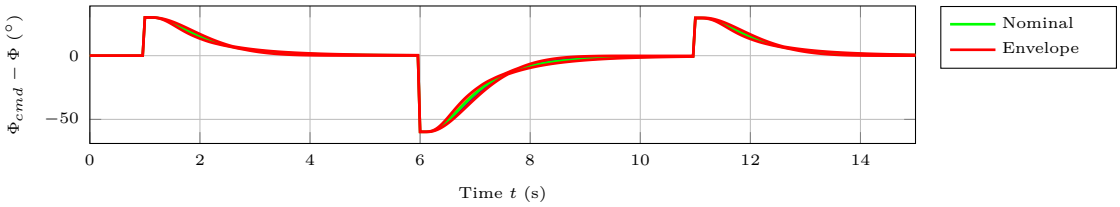

(b) Tracking Error

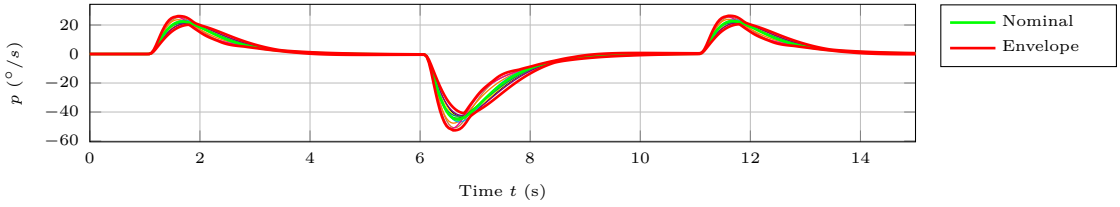

(c) Roll Rate

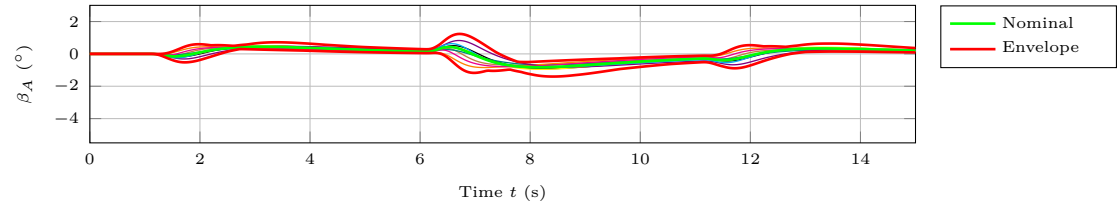

(d) Angle-of-sideslip

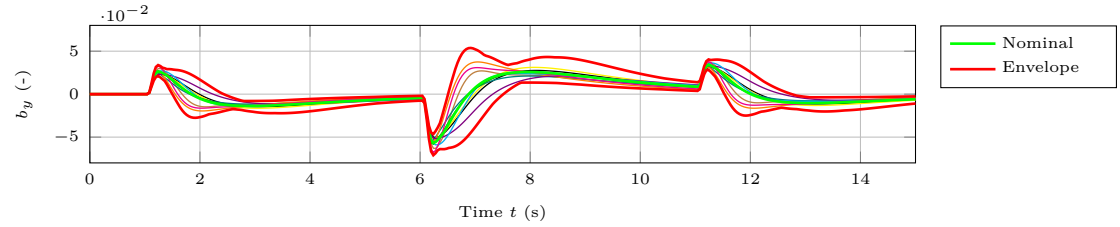

(e) Lateral Acceleration

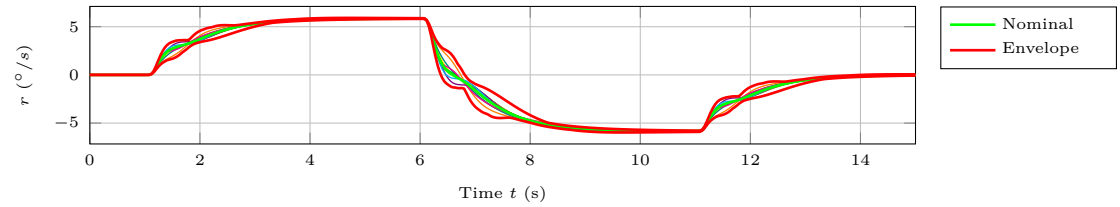

(f) Yaw Rate

Figure E.67: Rigid body states of the LTI plant model with MM-LQR controller in response to a $30°$ doublet command $\Phi_{cmd}(t)$ at $V_K^R = 50\,m/s$, $h = 500\,m$, $m_{fuel} = 0\,kg$.

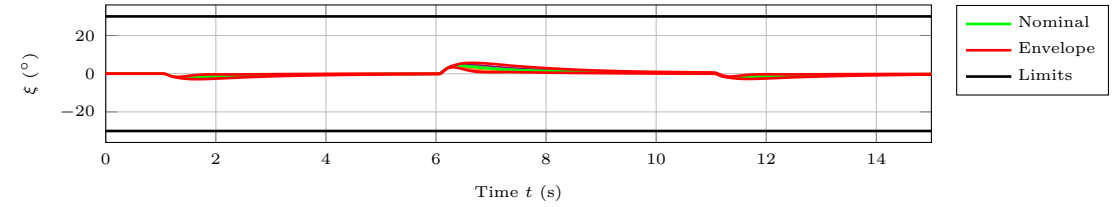

(a) Aileron Deflection

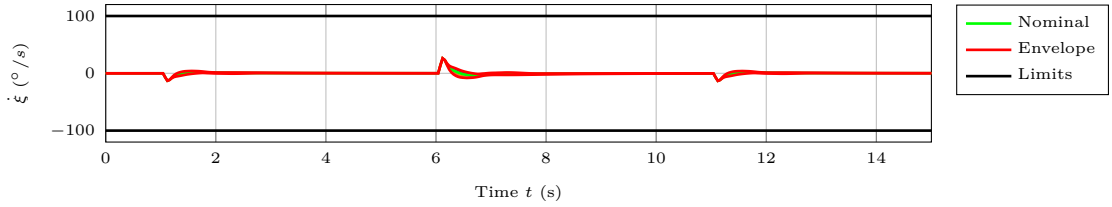

(b) Aileron Rate

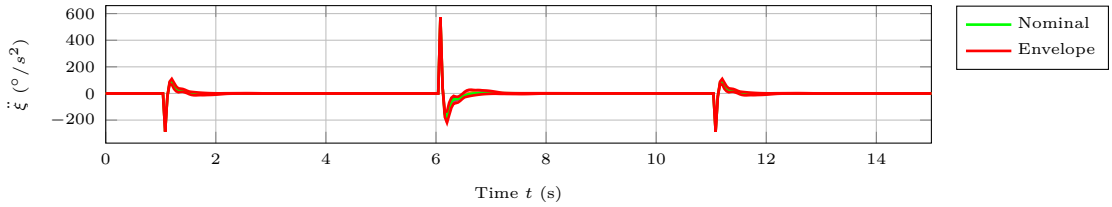

(c) Aileron Acceleration

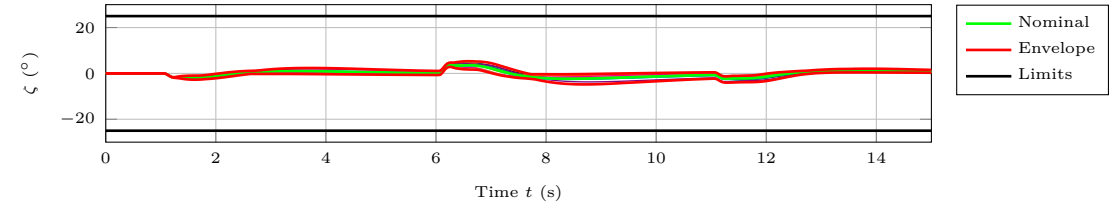

(d) Rudder Deflection

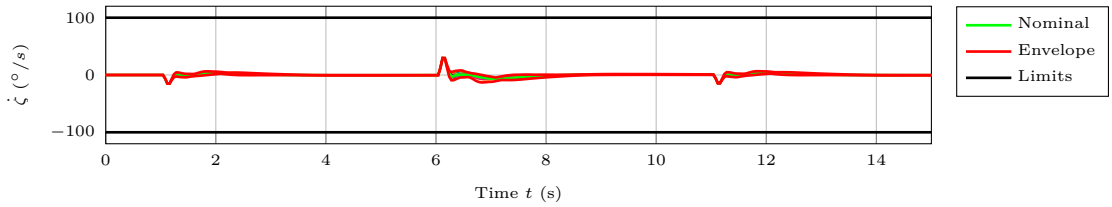

(e) Rudder Rate

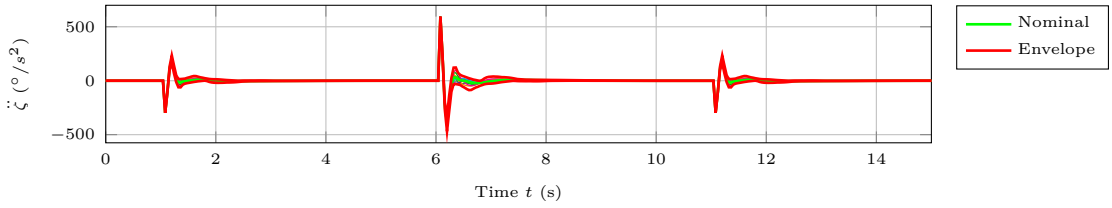

(f) Rudder Acceleration

Figure E.68: Actuator states of the LTI plant model with MM-LQR controller in response to a $30°$ doublet command $\Phi_{cmd}(t)$ at $V_K^R = 50\,m/s$, $h = 500\,m$, $m_{fuel} = 0\,kg$.

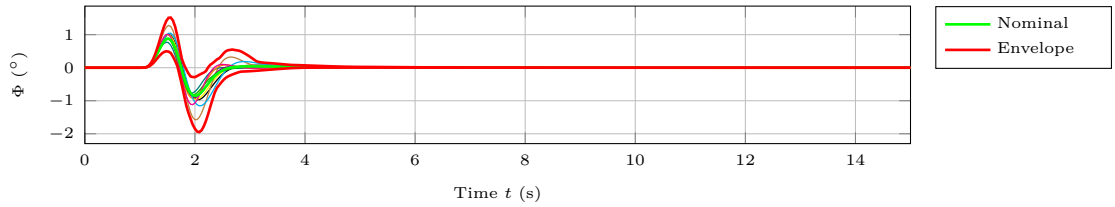

(a) Bank Angle

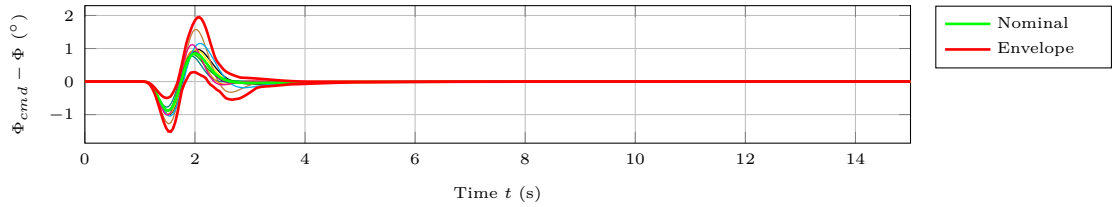

(b) Tracking Error

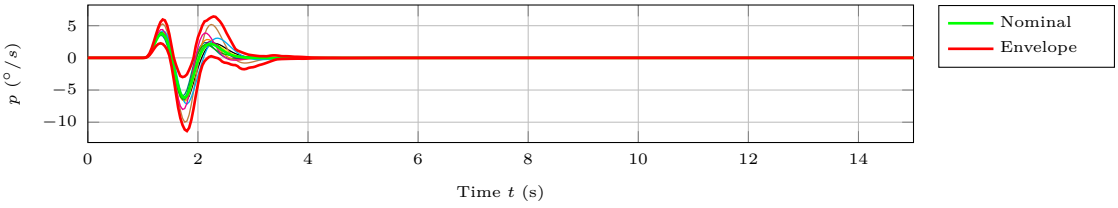

(c) Roll Rate

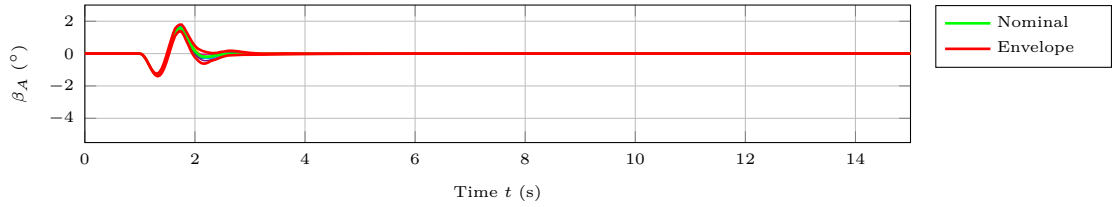

(d) Angle-of-sideslip

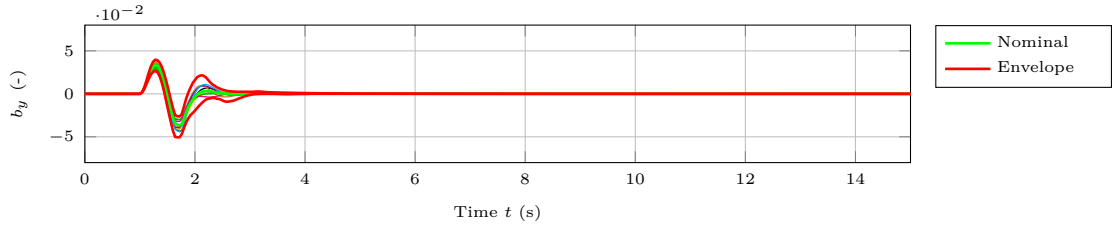

(e) Lateral Acceleration

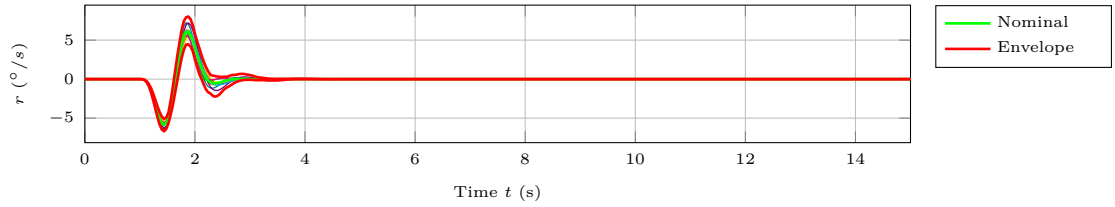

(f) Yaw Rate

Figure E.69: Rigid body states of the LTI plant model with MM-LQR controller in response to a $20\,m$ discrete gust at $V_K^R = 50\,m/s$, $h = 500\,m$, $m_{fuel} = 0\,kg$.

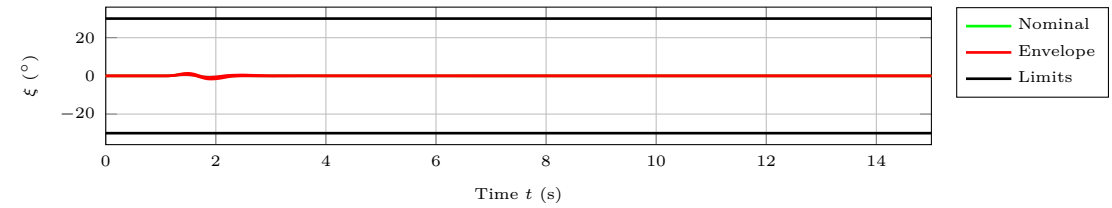

(a) Aileron Deflection

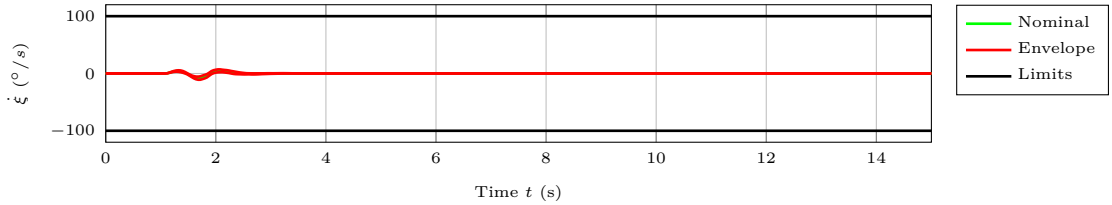

(b) Aileron Rate

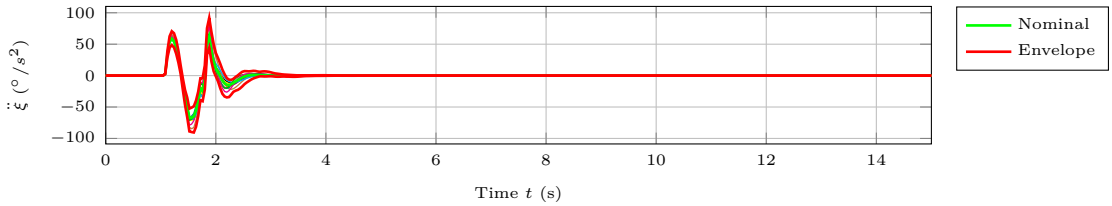

(c) Aileron Acceleration

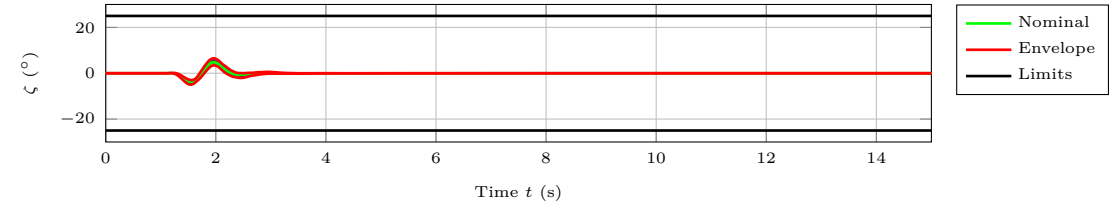

(d) Rudder Deflection

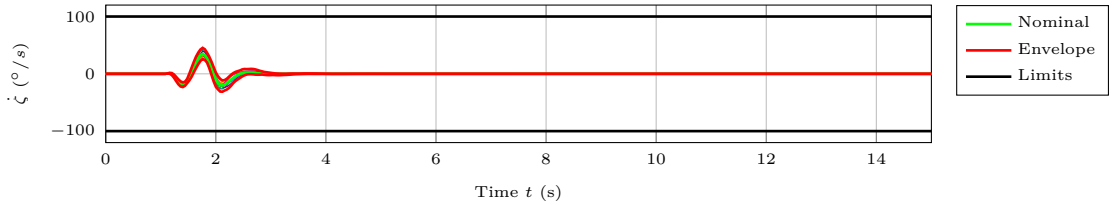

(e) Rudder Rate

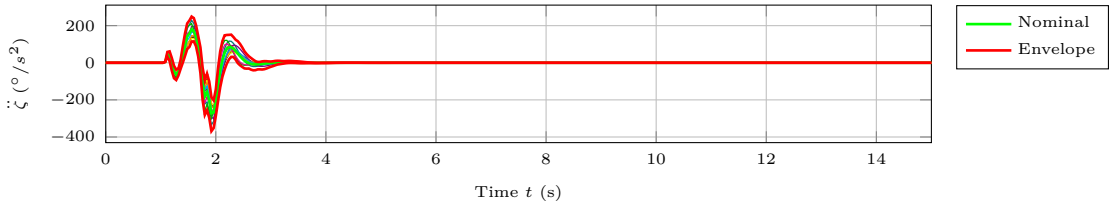

(f) Rudder Acceleration

Figure E.70: Actuator states of the LTI plant model with MM-LQR controller in response to a $20\,m$ discrete gust at $V_K^R = 50\,m/s$, $h = 500\,m$, $m_{fuel} = 0\,kg$.

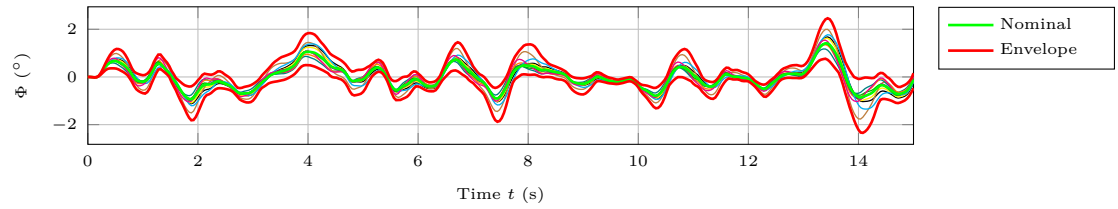

(a) Bank Angle

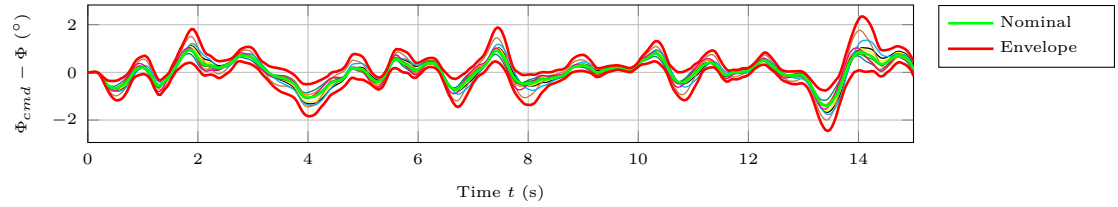

(b) Tracking Error

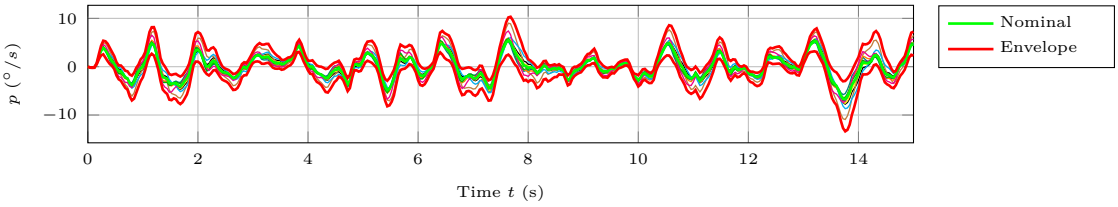

(c) Roll Rate

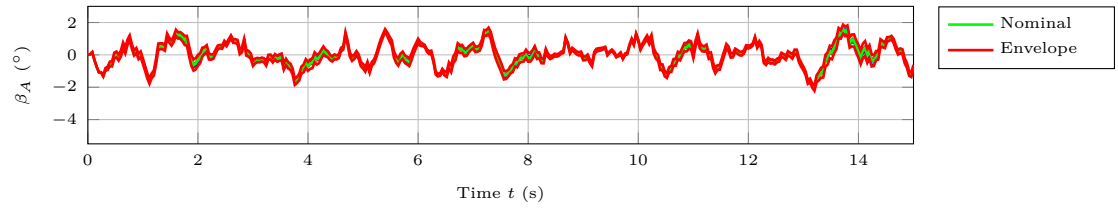

(d) Angle-of-sideslip

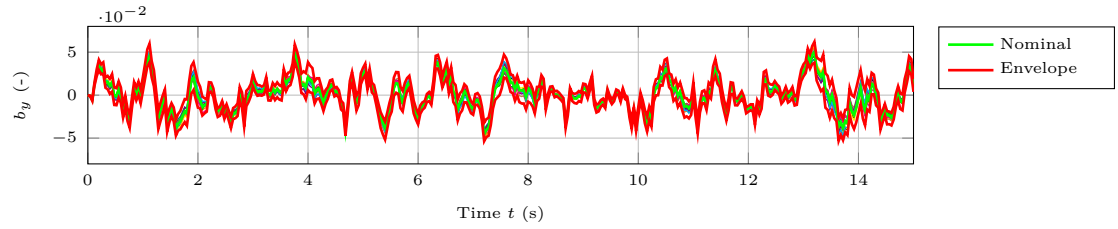

(e) Lateral Acceleration

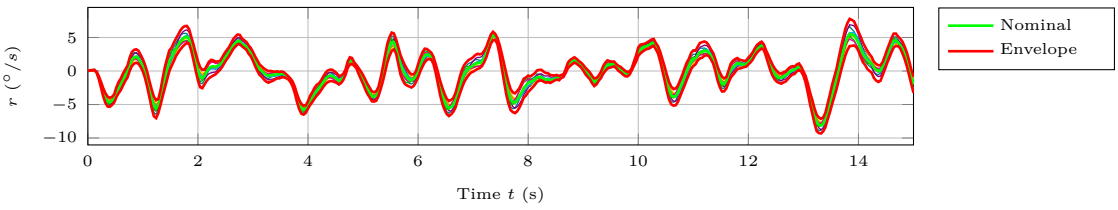

(f) Yaw Rate

Figure E.71: Rigid body states of the LTI plant model with MM-LQR controller in response to moderate Dryden turbulence at $V_K^R = 50\,m/s$, $h = 500\,m$, $m_{fuel} = 0\,kg$.

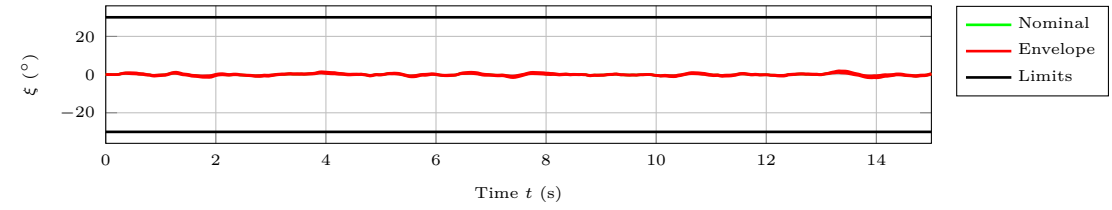

(a) Aileron Deflection

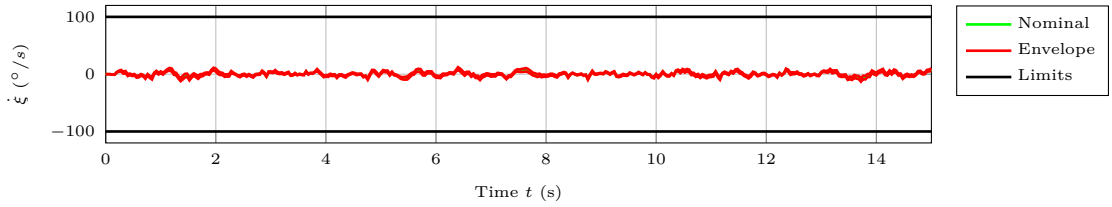

(b) Aileron Rate

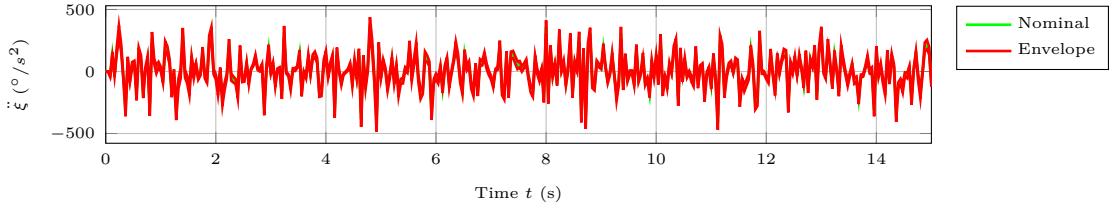

(c) Aileron Acceleration

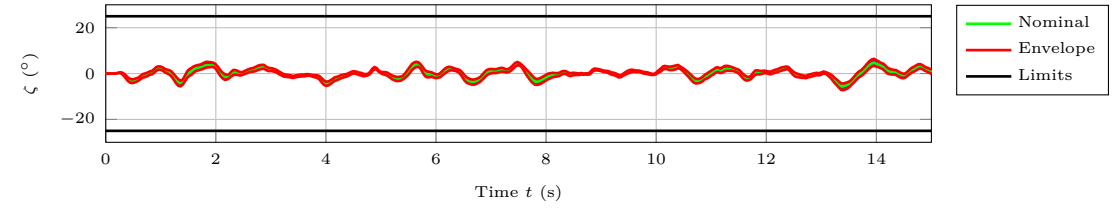

(d) Rudder Deflection

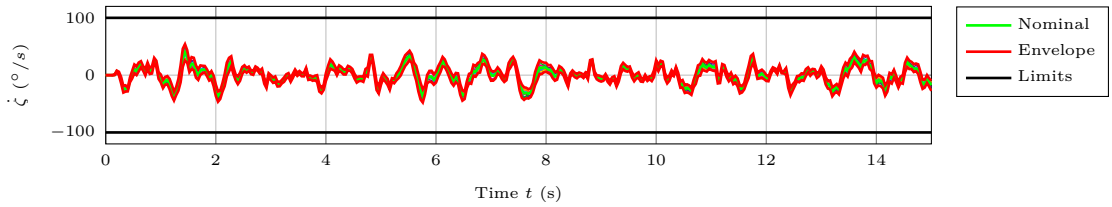

(e) Rudder Rate

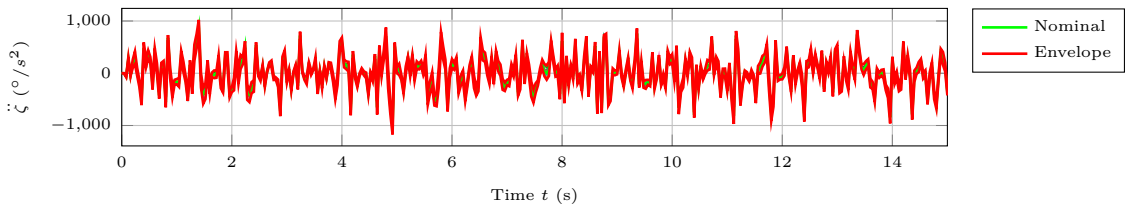

(f) Rudder Acceleration

Figure E.72: Actuator states of the LTI plant model with MM-LQR controller in response to moderate Dryden turbulence at $V_K^R = 50\,m/s$, $h = 500\,m$, $m_{fuel} = 0\,kg$.

E.2.3 Nonlinear Model at 35 m/s

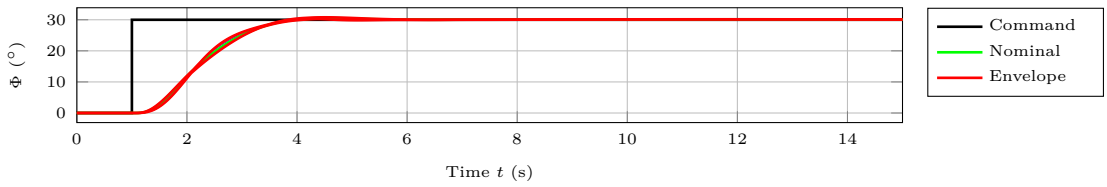

(a) Bank Angle

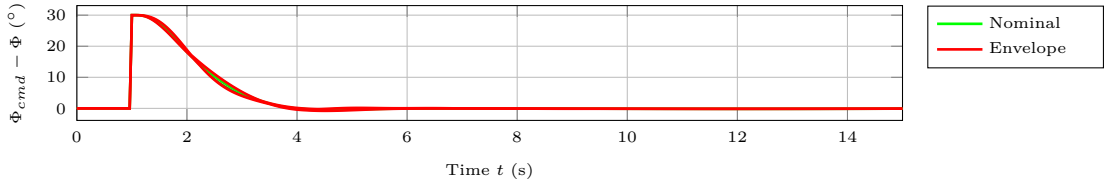

(b) Tracking Error

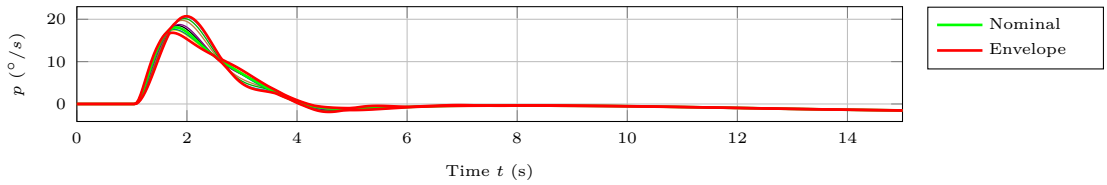

(c) Roll Rate

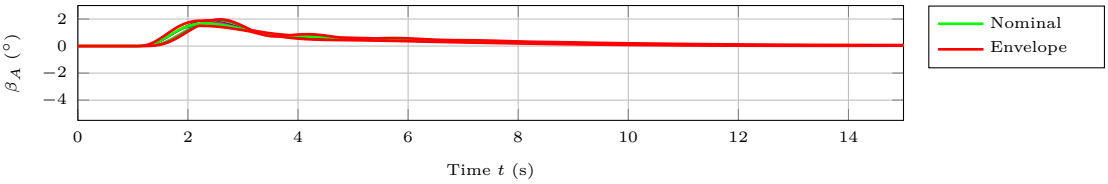

(d) Angle-of-sideslip

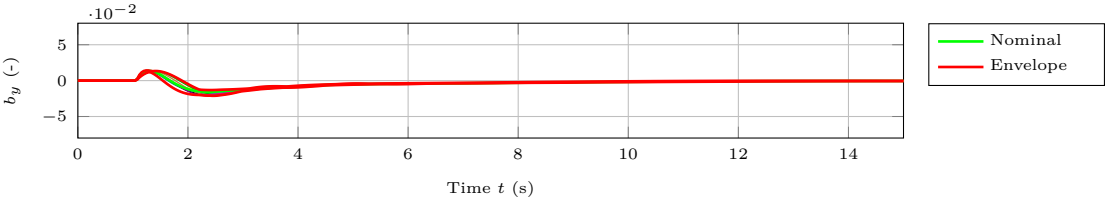

(e) Lateral Acceleration

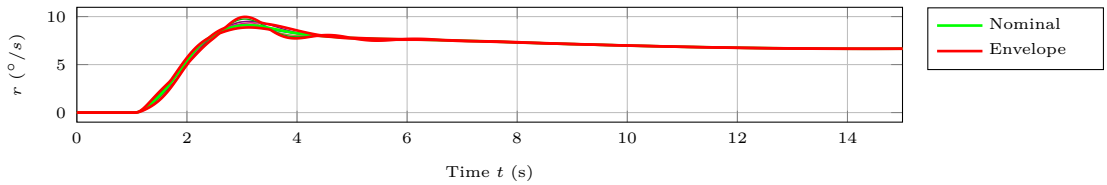

(f) Yaw Rate

Figure E.73: Rigid body states of the nonlinear plant model with MM-LQR controller in response to a $30°$ step command $\Phi_{cmd}(t)$ at $V_K^R = 35\,m/s$, $h = 1000\,m$, $m_{fuel} = 23\,kg$.

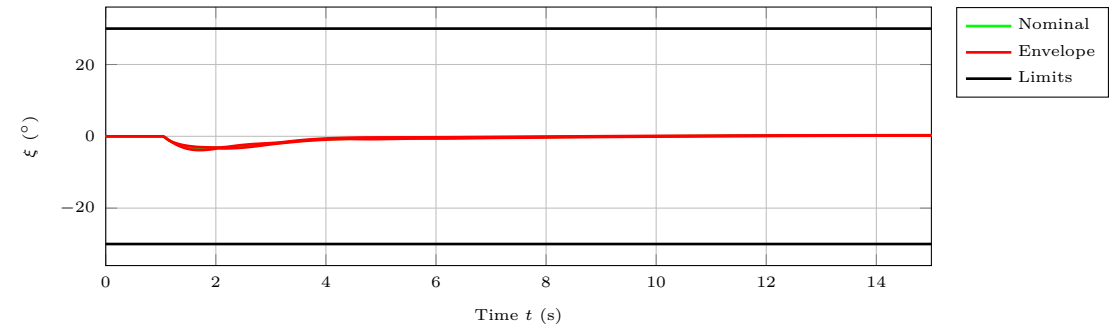

(a) Aileron Deflection

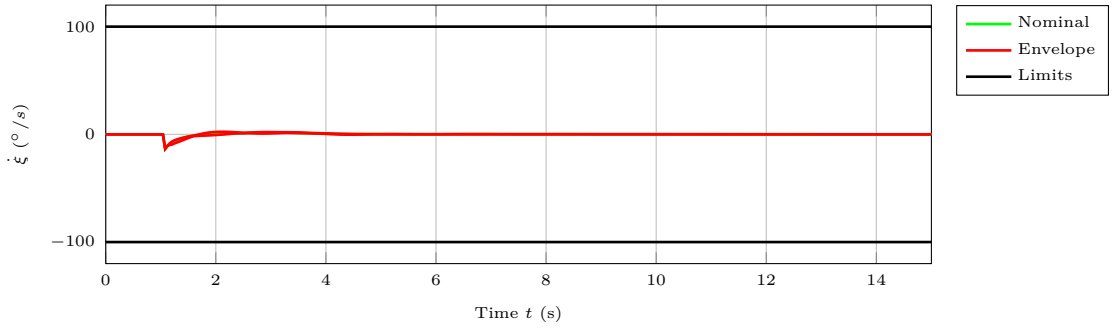

(b) Aileron Rate

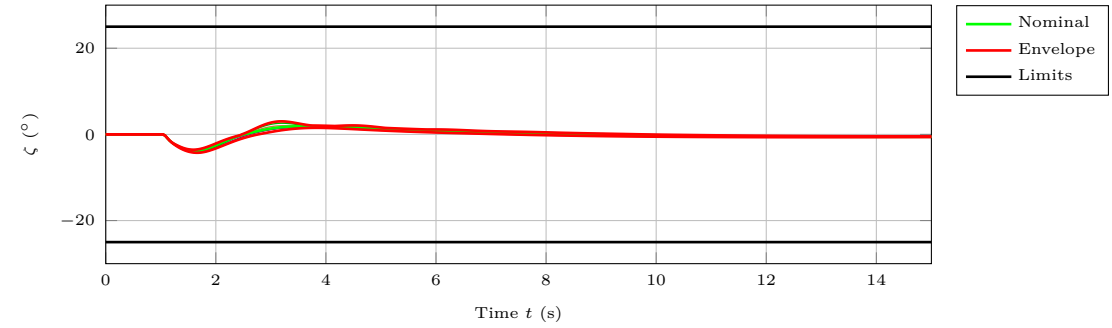

(c) Rudder Deflection

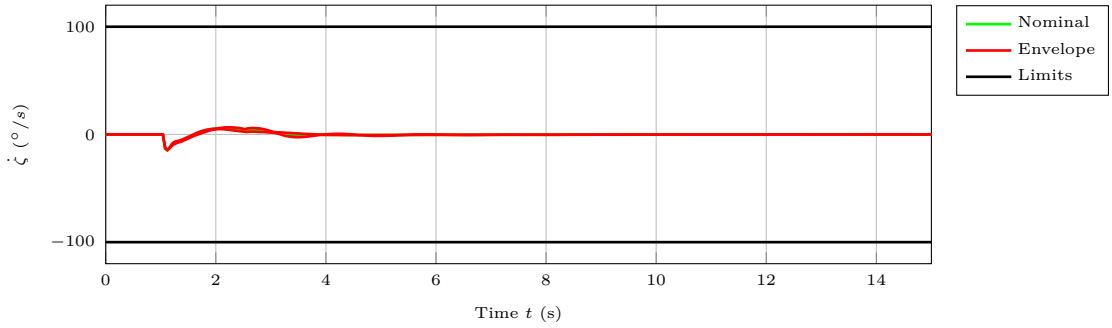

(d) Rudder Rate

Figure E.74: Actuator states of the nonlinear plant model with MM-LQR controller in response to a $30°$ step command $\Phi_{cmd}(t)$ at $V_K^R = 35\,m/s$, $h = 1000\,m$, $m_{fuel} = 23\,kg$.

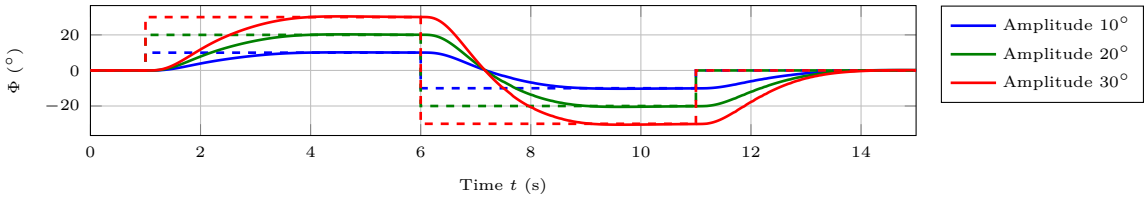

(a) Bank Angle

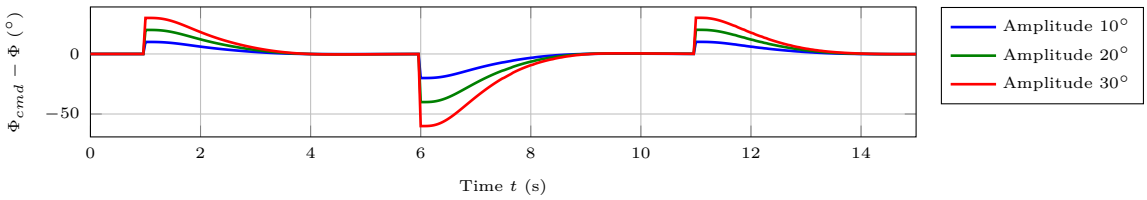

(b) Tracking Error

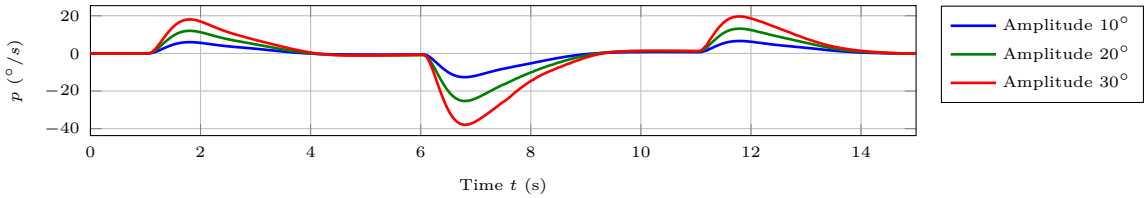

(c) Roll Rate

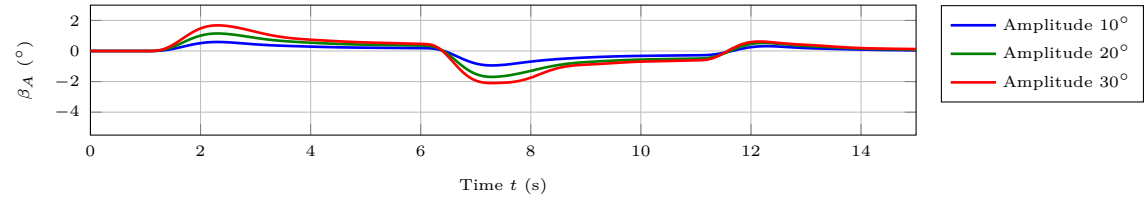

(d) Angle-of-sideslip

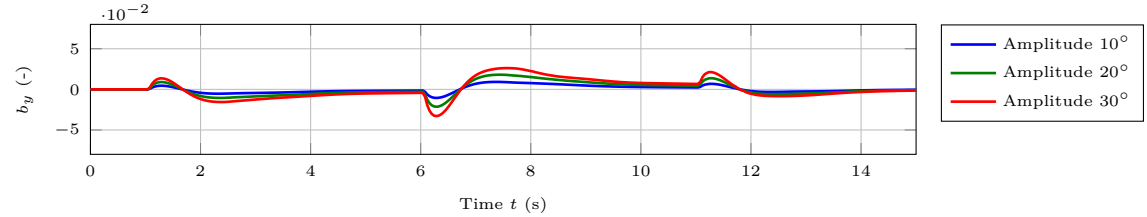

(e) Lateral Acceleration

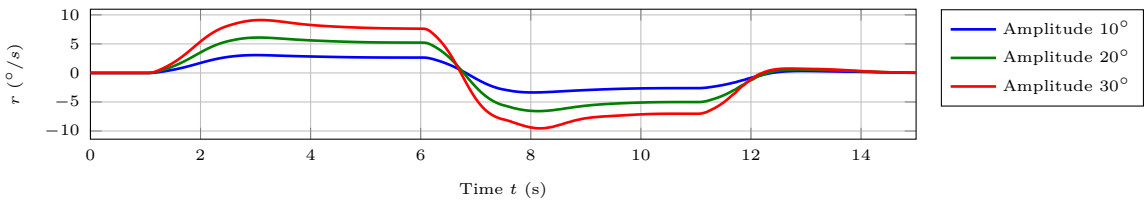

(f) Yaw Rate

Figure E.75: Rigid body states of the nonlinear plant model with MM-LQR controller in response to a doublet sweep at $V_K^R = 35\,m/s$, $h = 1000\,m$, $m_{fuel} = 23\,kg$.

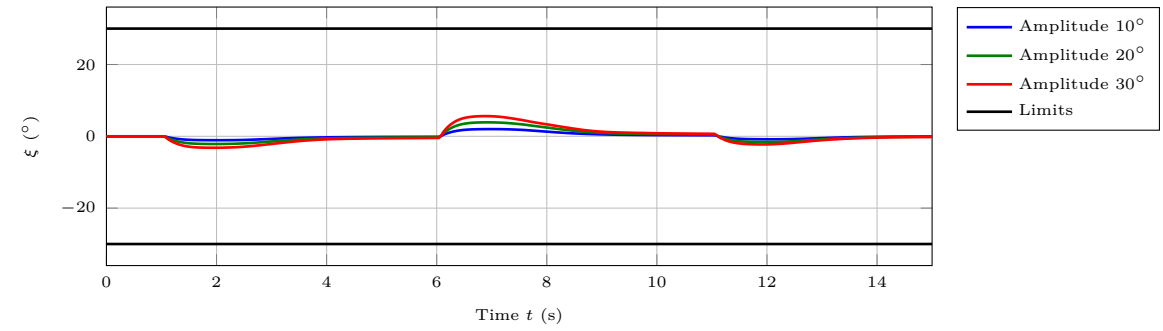

(a) Aileron Deflection

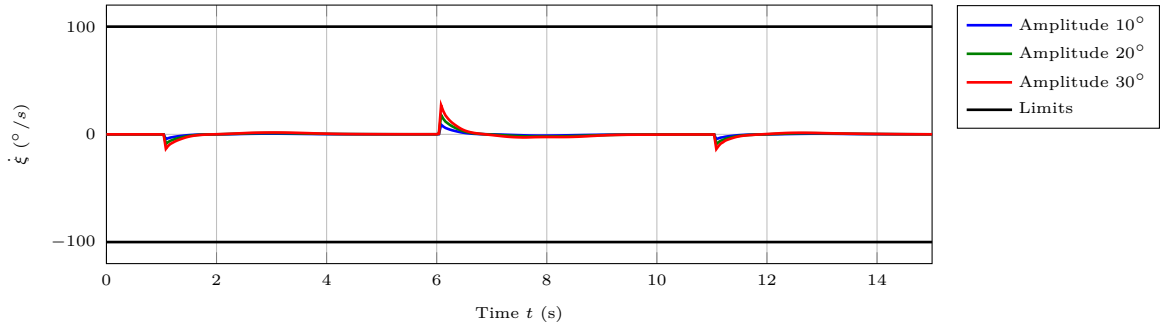

(b) Aileron Rate

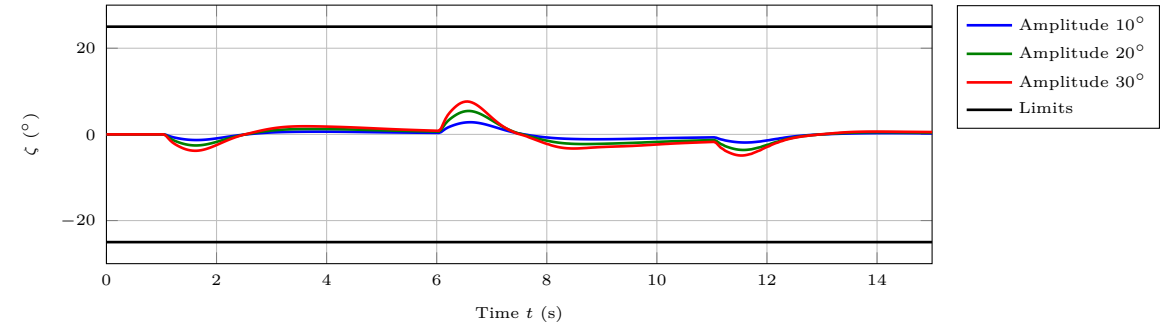

(c) Rudder Deflection

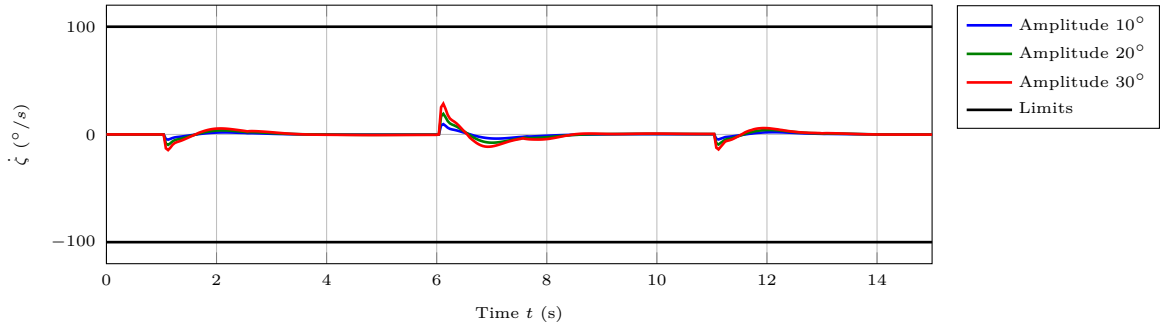

(d) Rudder Rate

Figure E.76: Actuator states of the nonlinear plant model with MM-LQR controller in response to a doublet sweep at $V_K^R = 35\,m/s$, $h = 1000\,m$, $m_{fuel} = 23\,kg$.

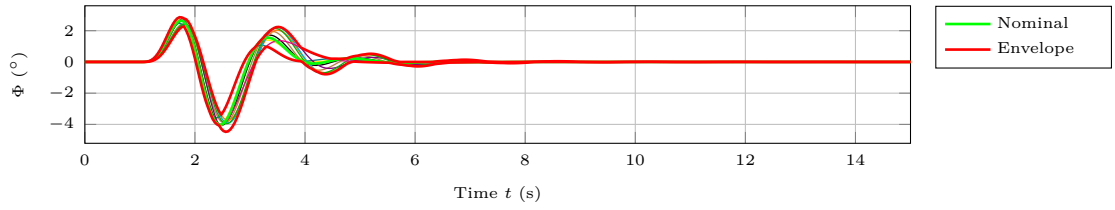

(a) Bank Angle

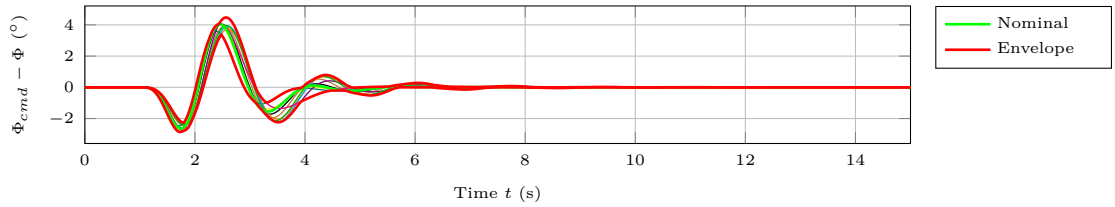

(b) Tracking Error

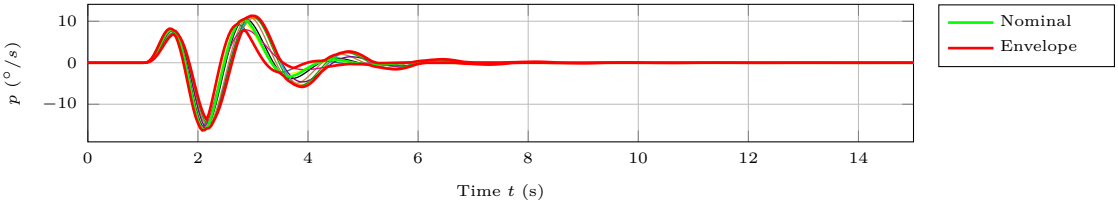

(c) Roll Rate

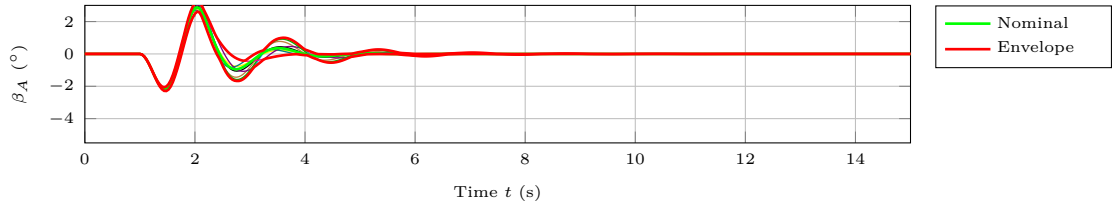

(d) Angle-of-sideslip

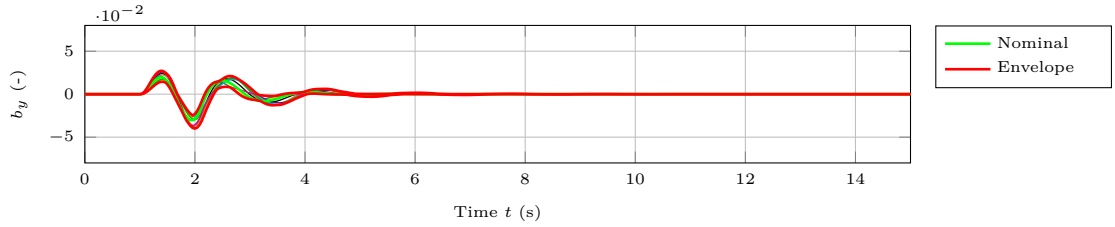

(e) Lateral Acceleration

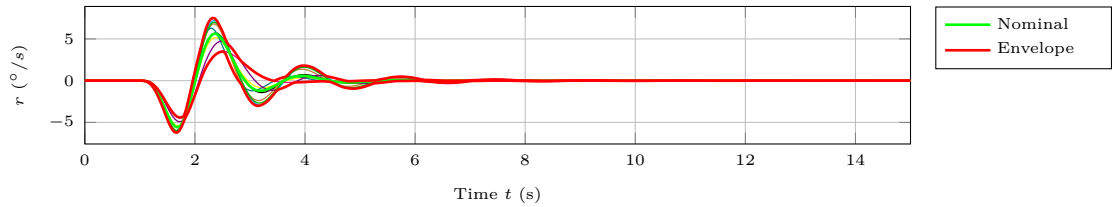

(f) Yaw Rate

Figure E.77: Rigid body states of the nonlinear plant model with MM-LQR controller in response to a $20\,m$ discrete gust at $V_K^R = 35\,m/s$, $h = 1000\,m$, $m_{fuel} = 23\,kg$.

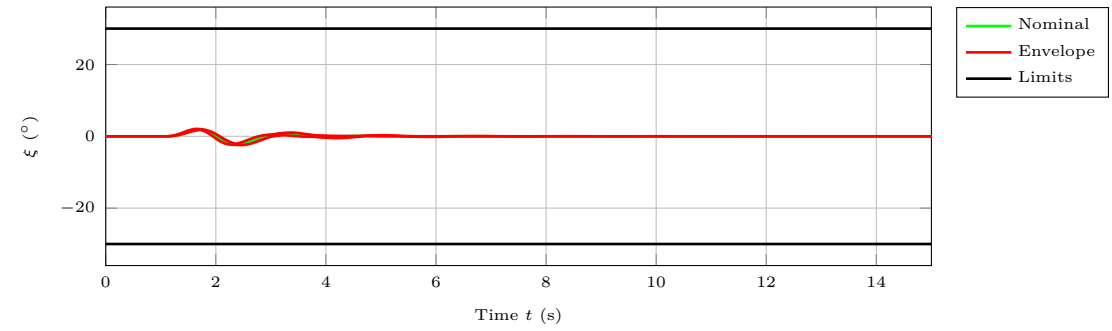

(a) Aileron Deflection

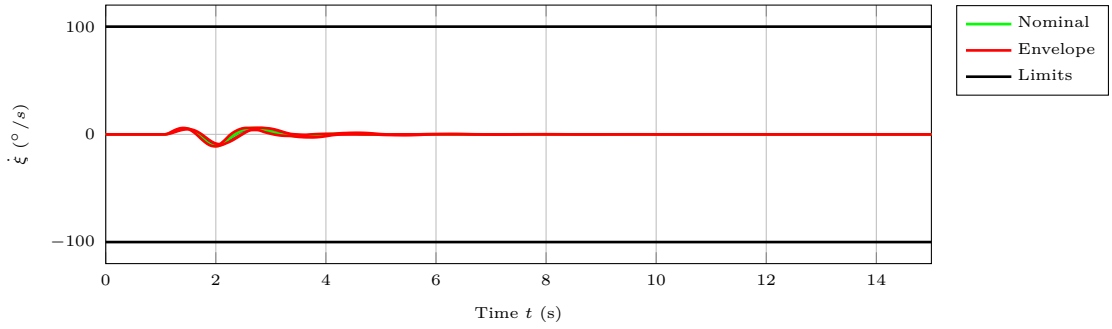

(b) Aileron Rate

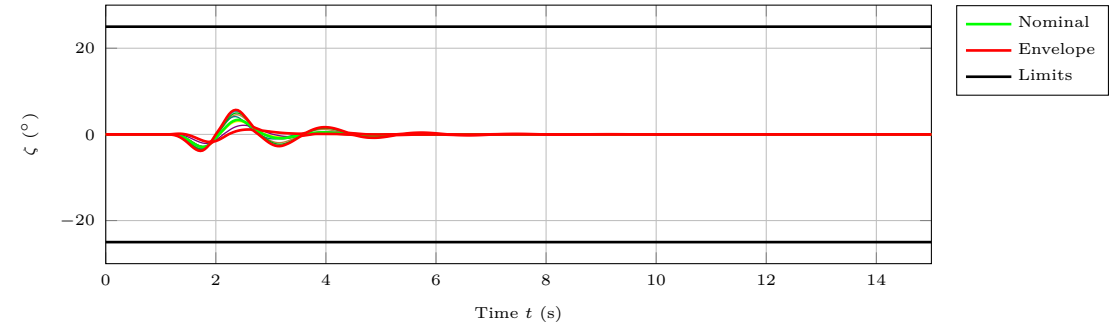

(c) Rudder Deflection

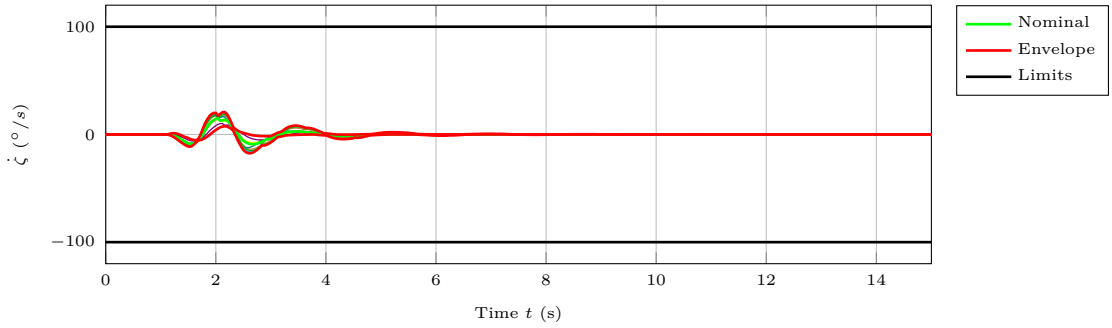

(d) Rudder Rate

Figure E.78: Actuator states of the nonlinear plant model with MM-LQR controller in response to a $20\,m$ discrete gust at $V_K^R = 35\,m/s$, $h = 1000\,m$, $m_{fuel} = 23\,kg$.

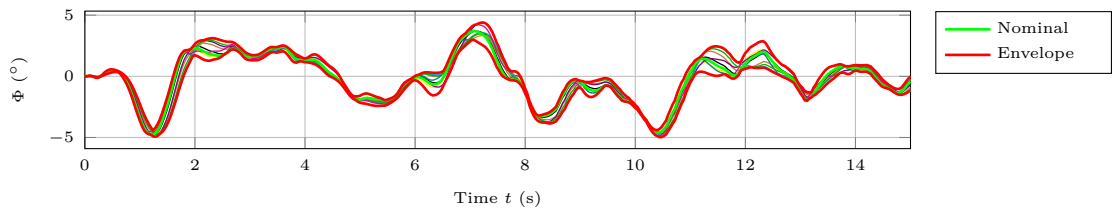

(a) Bank Angle

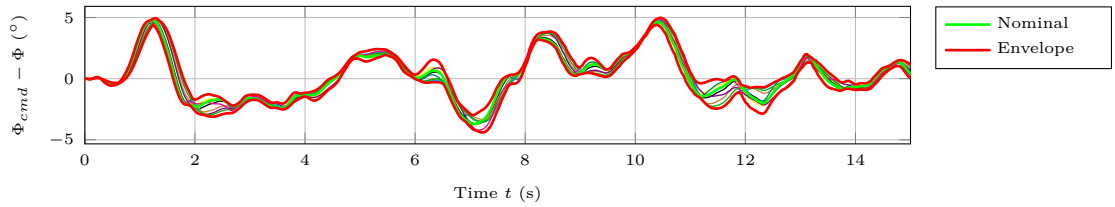

(b) Tracking Error

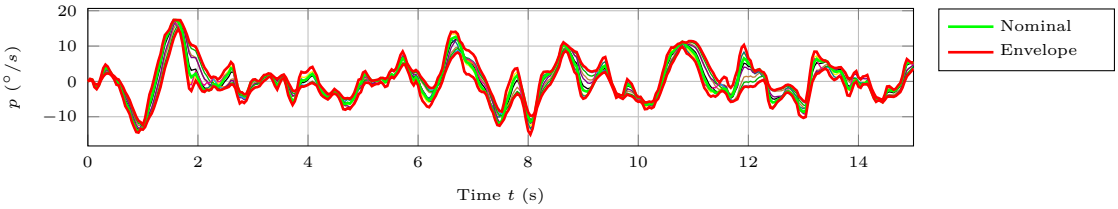

(c) Roll Rate

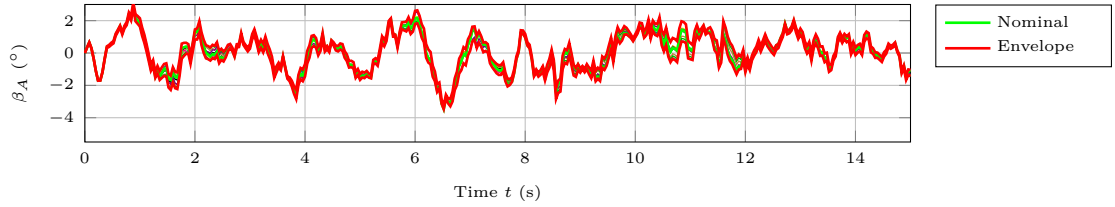

(d) Angle-of-sideslip

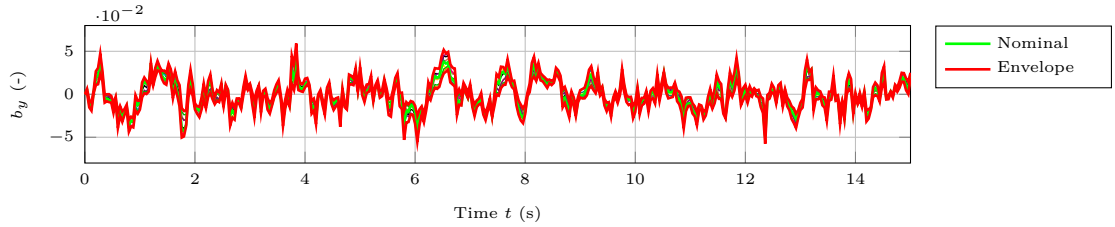

(e) Lateral Acceleration

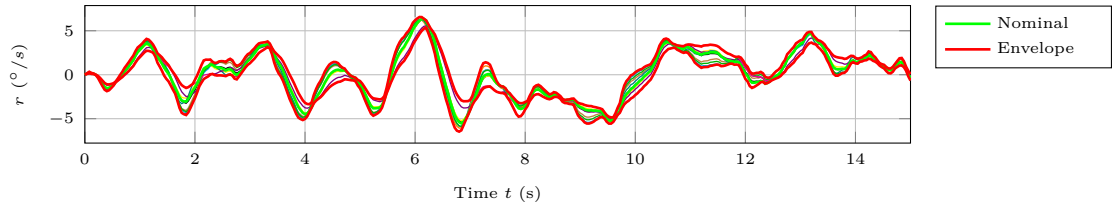

(f) Yaw Rate

Figure E.79: Rigid body states of the nonlinear plant model with MM-LQR controller in response to moderate Dryden turbulence at $V_K^R = 35\,m/s$, $h = 1000\,m$, $m_{fuel} = 23\,kg$.

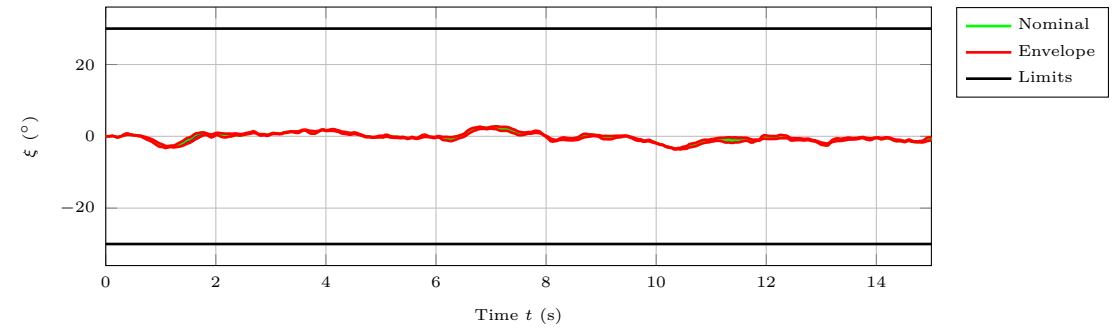

(a) Aileron Deflection

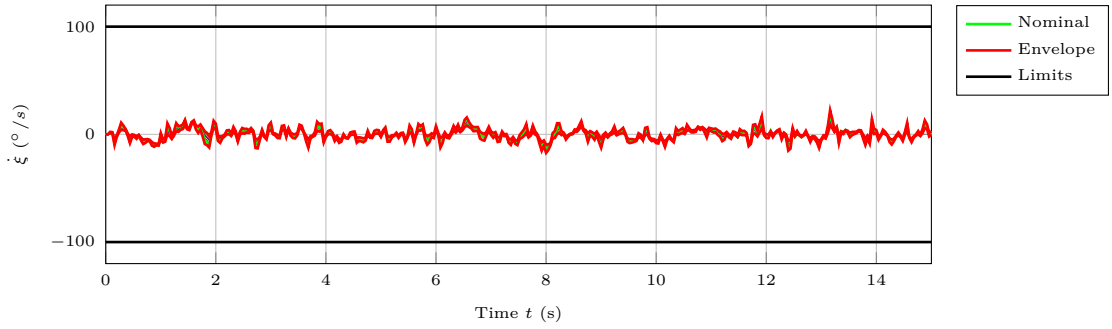

(b) Aileron Rate

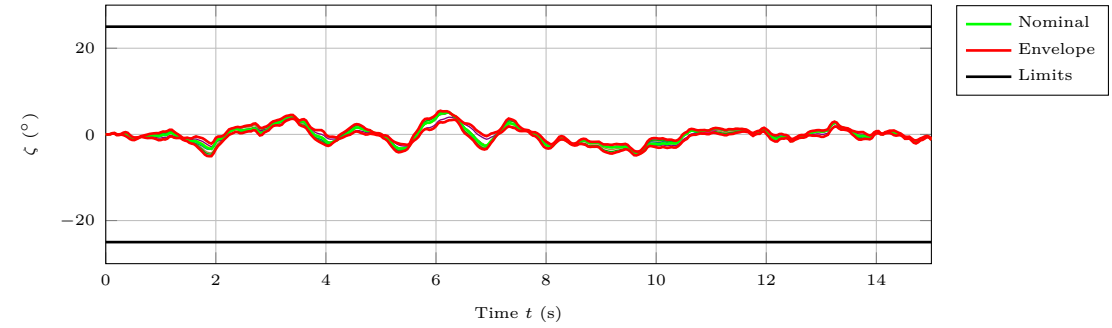

(c) Rudder Deflection

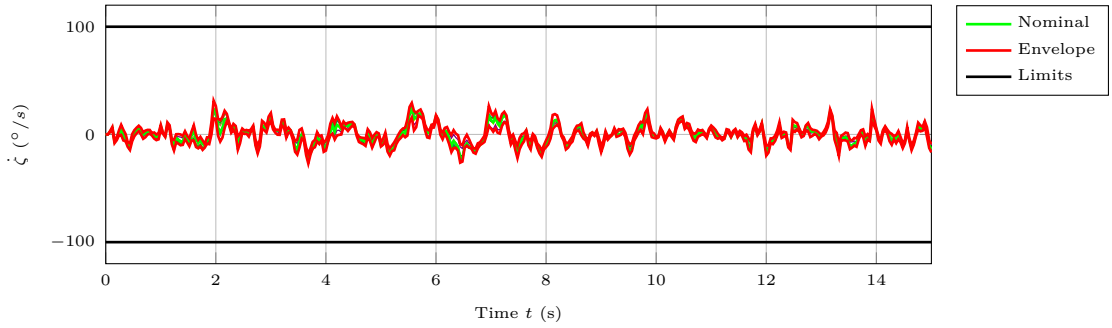

(d) Rudder Rate

Figure E.80: Actuator states of the nonlinear plant model with MM-LQR controller in response to moderate Dryden turbulence at $V_K^R = 35\,m/s$, $h = 1000\,m$, $m_{fuel} = 23\,kg$.

E.2.4 Nonlinear Model at 50 m/s

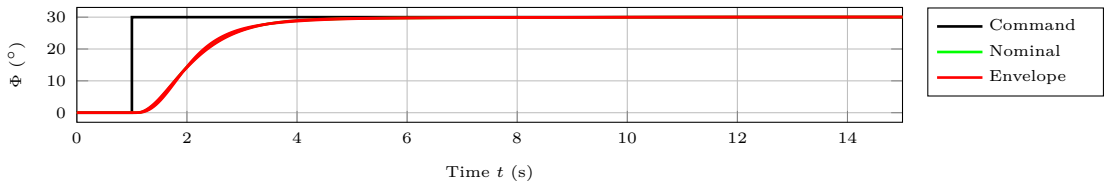

(a) Bank Angle

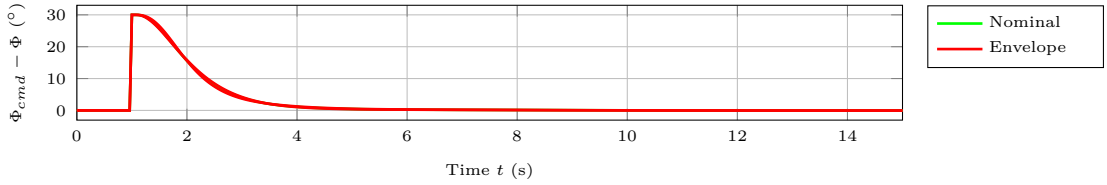

(b) Tracking Error

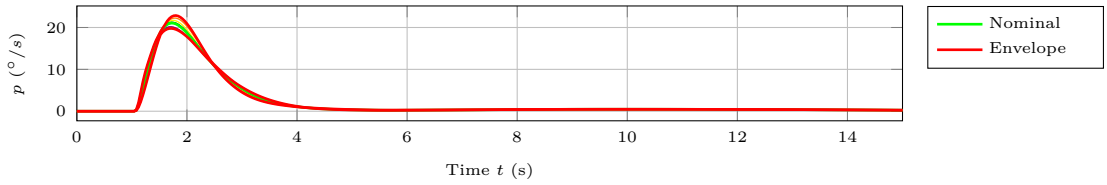

(c) Roll Rate

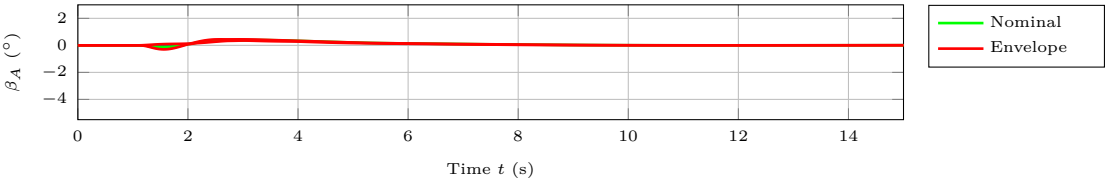

(d) Angle-of-sideslip

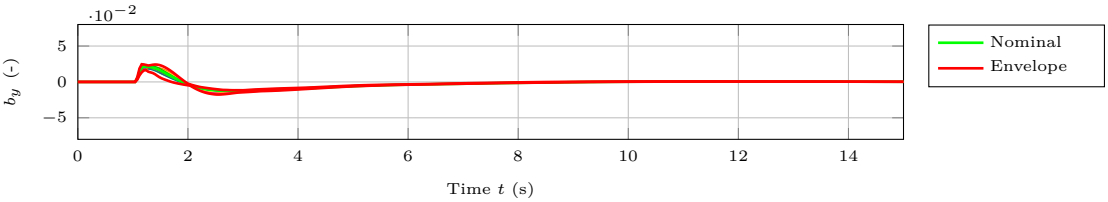

(e) Lateral Acceleration

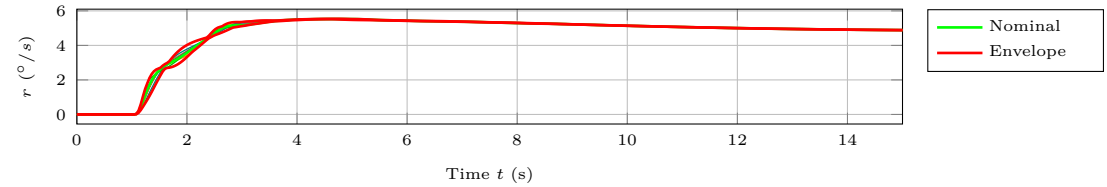

(f) Yaw Rate

Figure E.81: Rigid body states of the nonlinear plant model with MM-LQR controller in response to a $30°$ step command $\Phi_{cmd}(t)$ at $V_K^R = 50\,m/s$, $h = 500\,m$, $m_{fuel} = 0\,kg$.

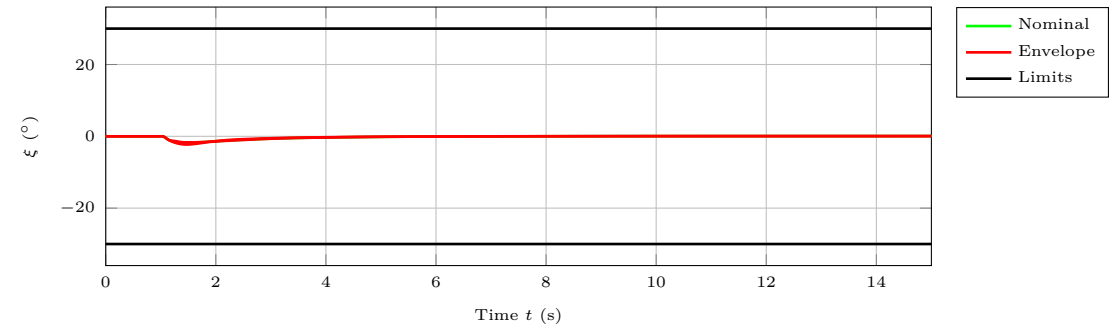

(a) Aileron Deflection

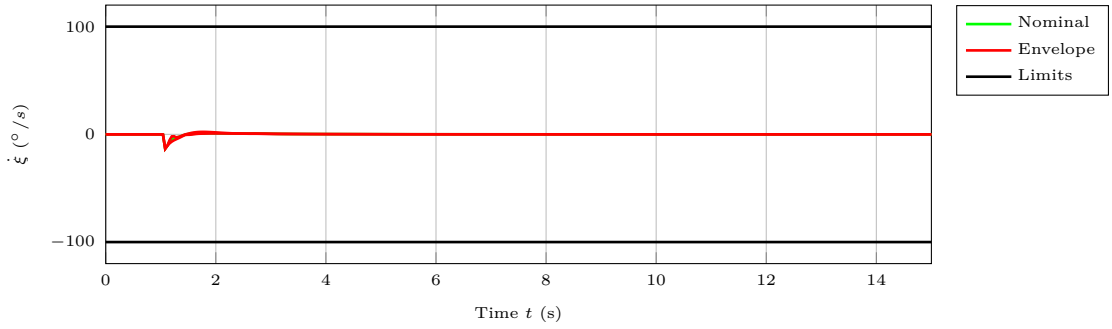

(b) Aileron Rate

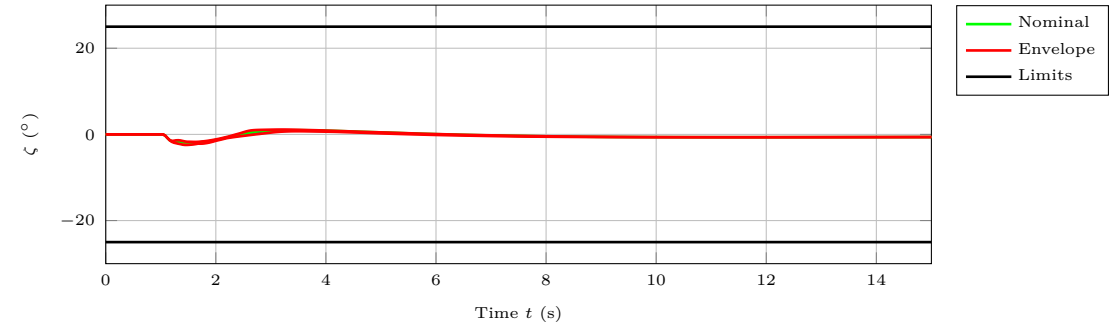

(c) Rudder Deflection

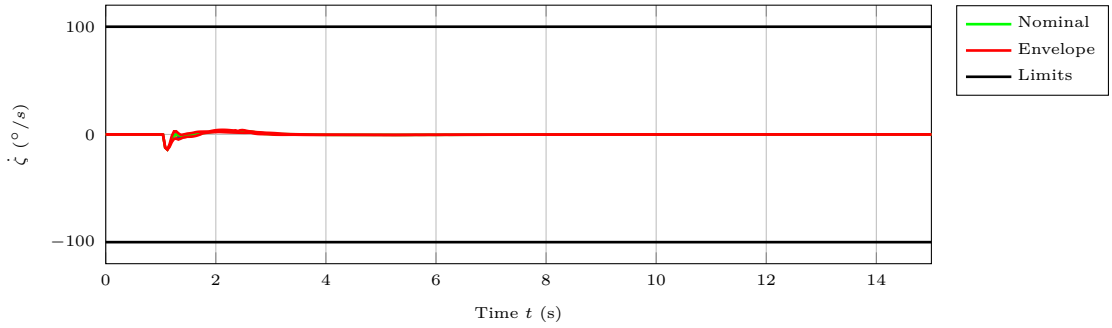

(d) Rudder Rate

Figure E.82: Actuator states of the nonlinear plant model with MM-LQR controller in response to a $30°$ step command $\Phi_{cmd}(t)$ at $V_K^R = 50\,m/s$, $h = 500\,m$, $m_{fuel} = 0\,kg$.

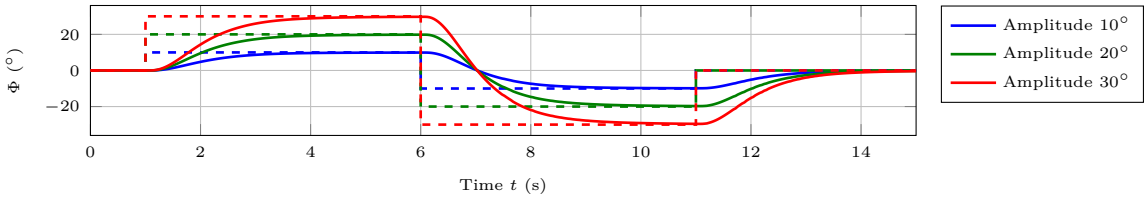

(a) Bank Angle

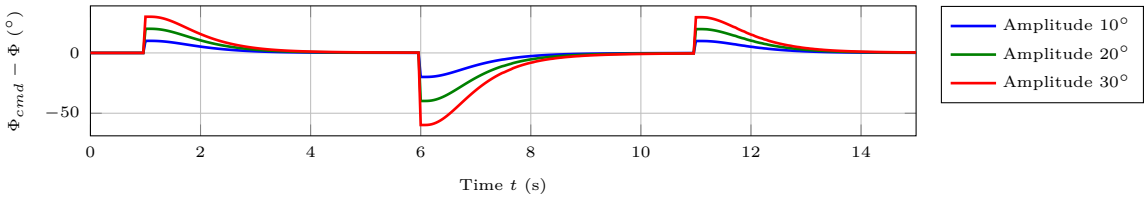

(b) Tracking Error

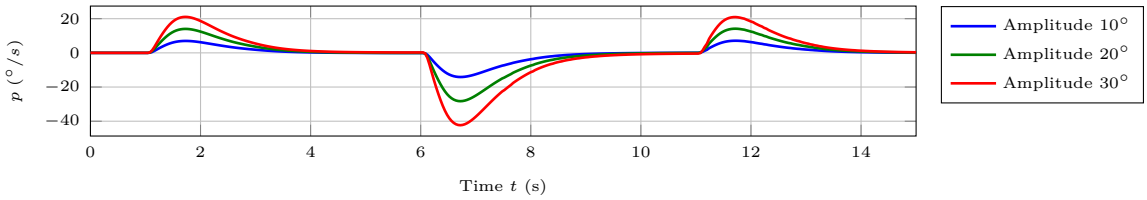

(c) Roll Rate

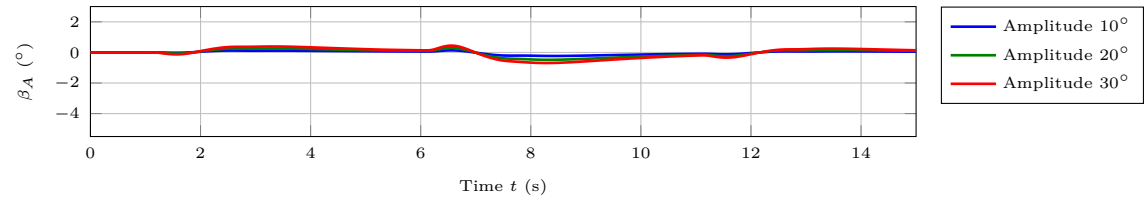

(d) Angle-of-sideslip

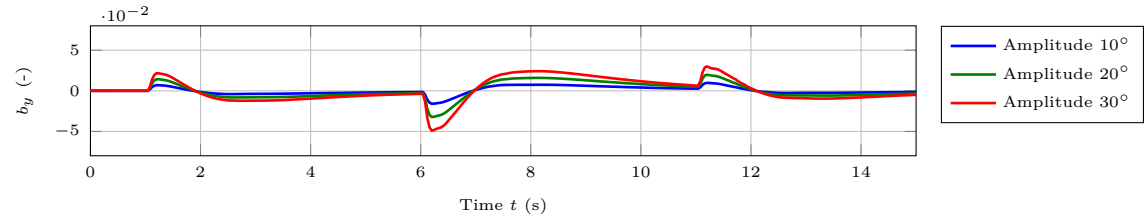

(e) Lateral Acceleration

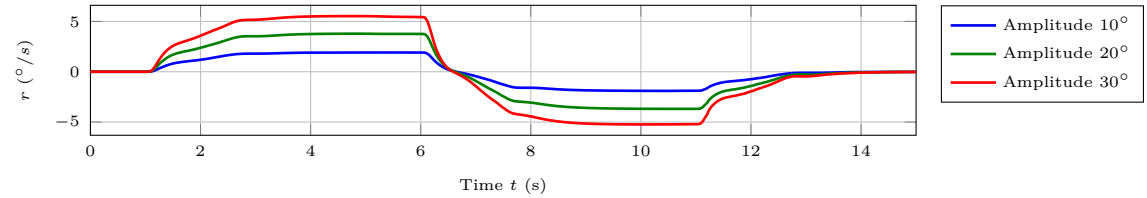

(f) Yaw Rate

Figure E.83: Rigid body states of the nonlinear plant model with MM-LQR controller in response to a doublet sweep at $V_K^R = 50\,m/s$, $h = 500\,m$, $m_{fuel} = 0\,kg$.

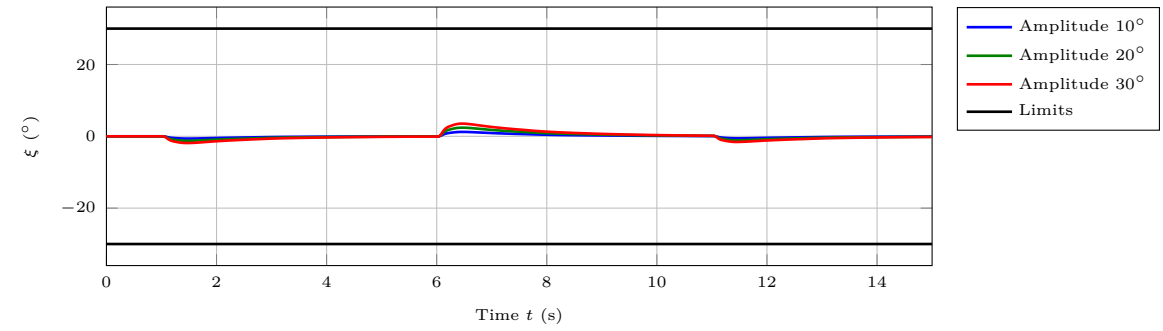

(a) Aileron Deflection

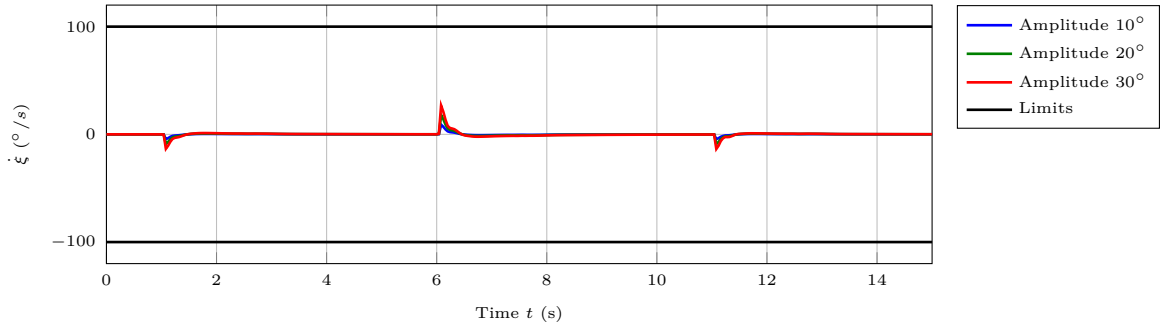

(b) Aileron Rate

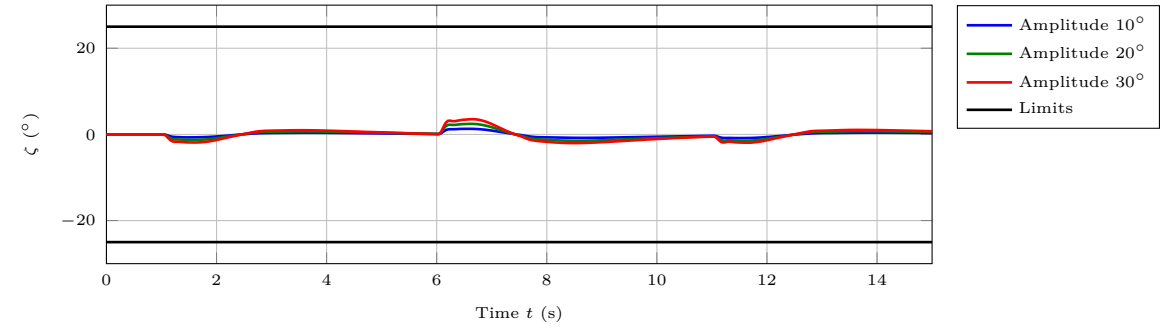

(c) Rudder Deflection

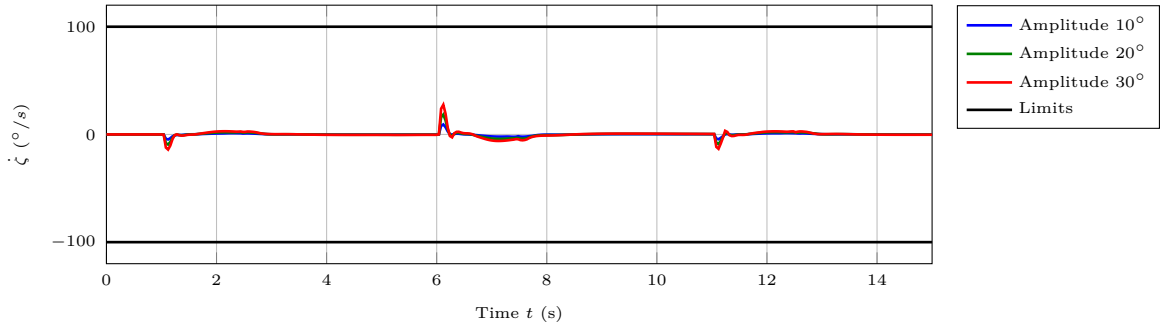

(d) Rudder Rate

Figure E.84: Actuator states of the nonlinear plant model with MM-LQR controller in response to a doublet sweep at $V_K^R = 50\,m/s$, $h = 500\,m$, $m_{fuel} = 0\,kg$.

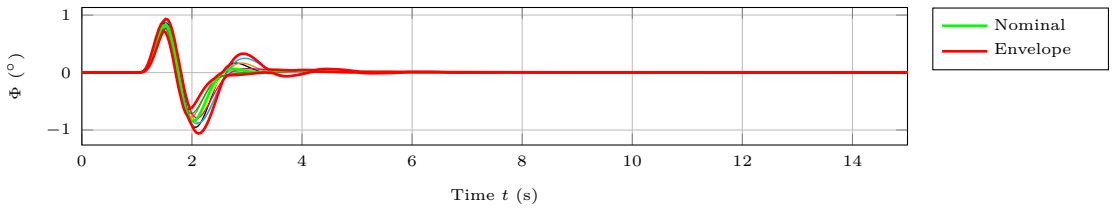

(a) Bank Angle

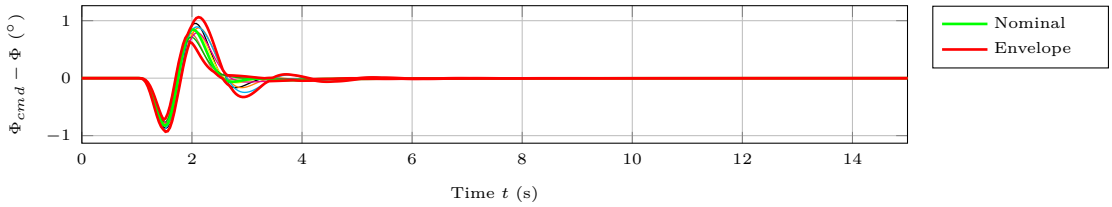

(b) Tracking Error

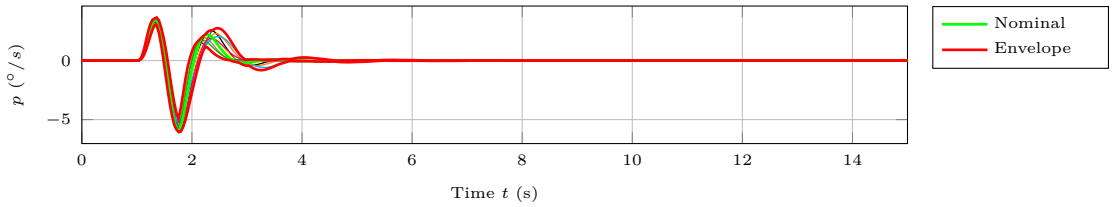

(c) Roll Rate

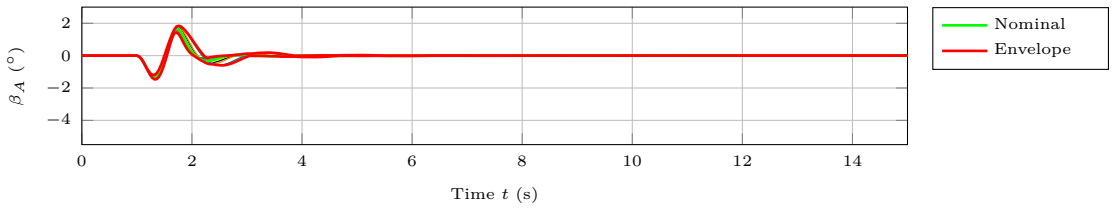

(d) Angle-of-sideslip

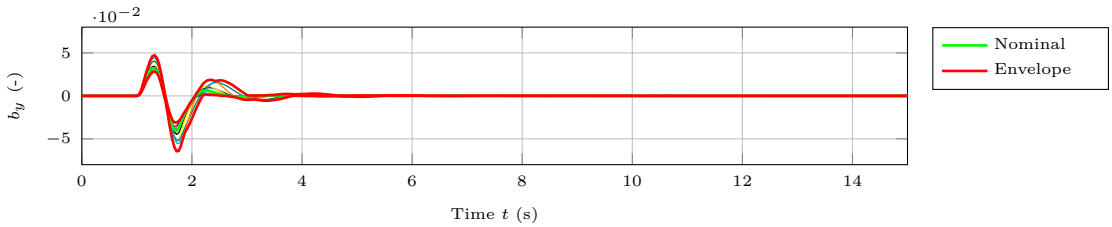

(e) Lateral Acceleration

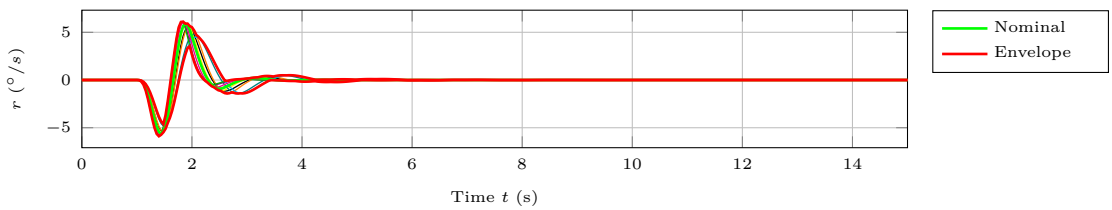

(f) Yaw Rate

Figure E.85: Rigid body states of the nonlinear plant model with MM-LQR controller in response to a $20\,m$ discrete gust at $V_K^R = 50\,m/s$, $h = 500\,m$, $m_{fuel} = 0\,kg$.

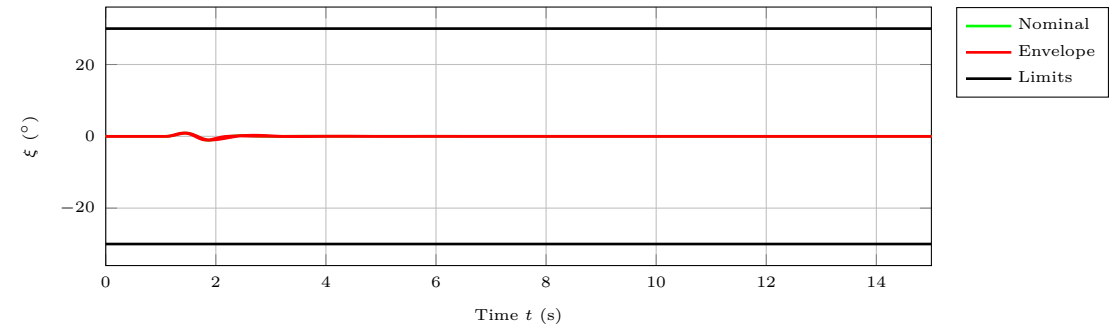

(a) Aileron Deflection

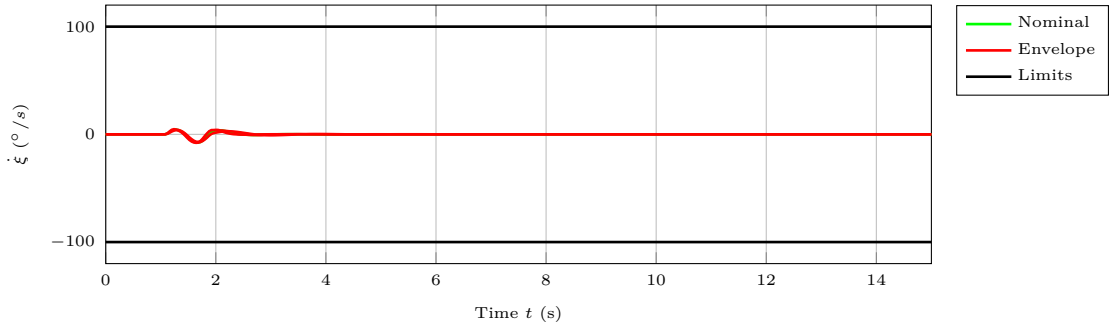

(b) Aileron Rate

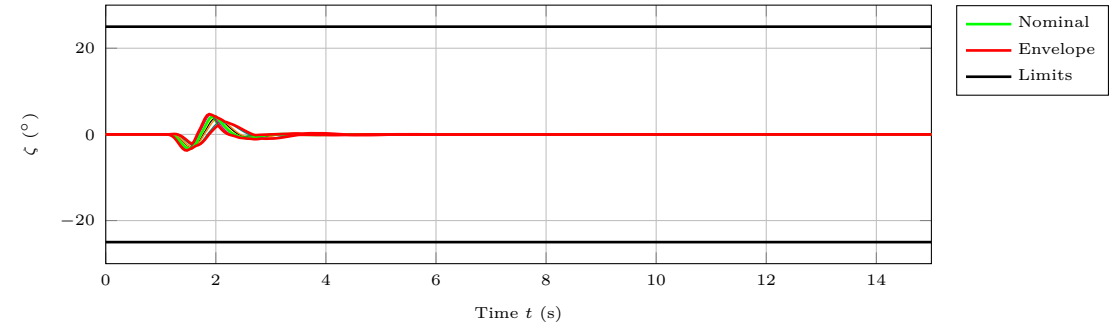

(c) Rudder Deflection

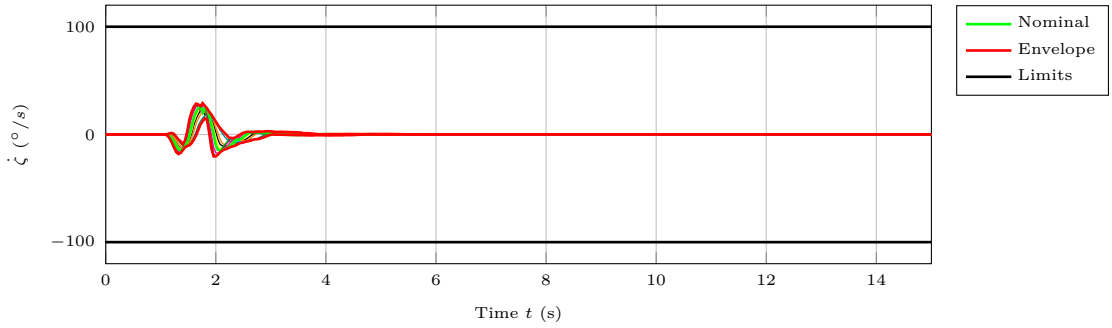

(d) Rudder Rate

Figure E.86: Actuator states of the nonlinear plant model with MM-LQR controller in response to a $20\,m$ discrete gust at $V_K^R = 50\,m/s$, $h = 500\,m$, $m_{fuel} = 0\,kg$.

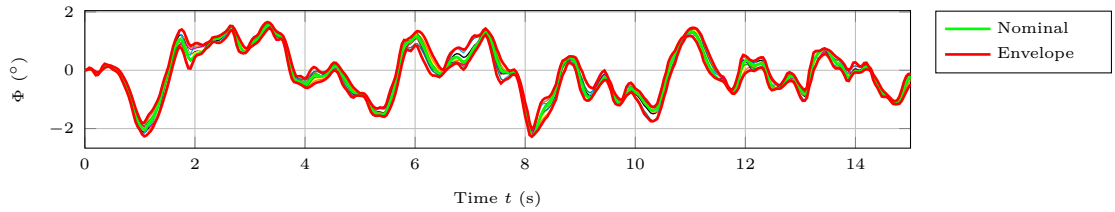

(a) Bank Angle

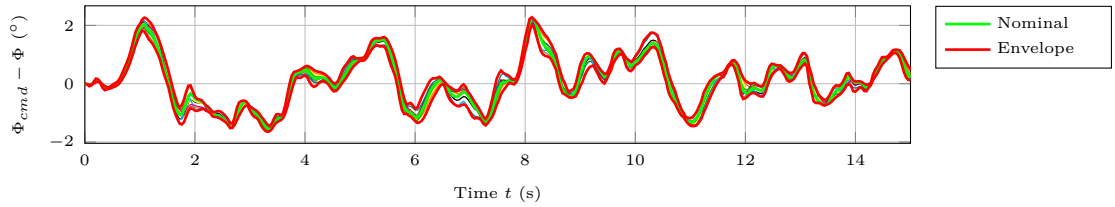

(b) Tracking Error

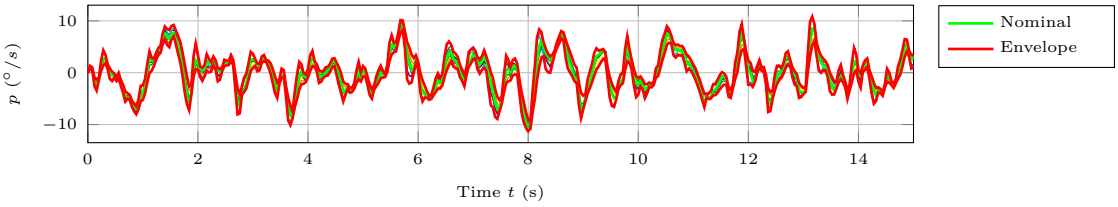

(c) Roll Rate

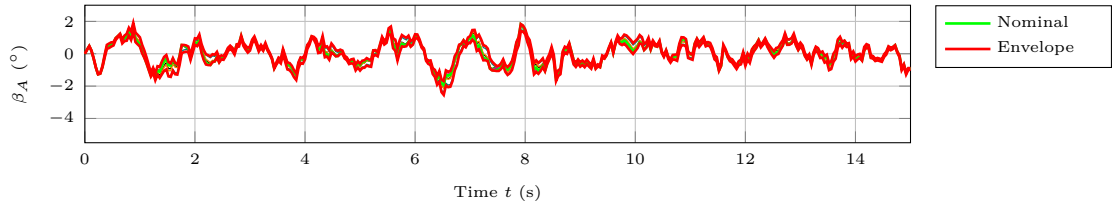

(d) Angle-of-sideslip

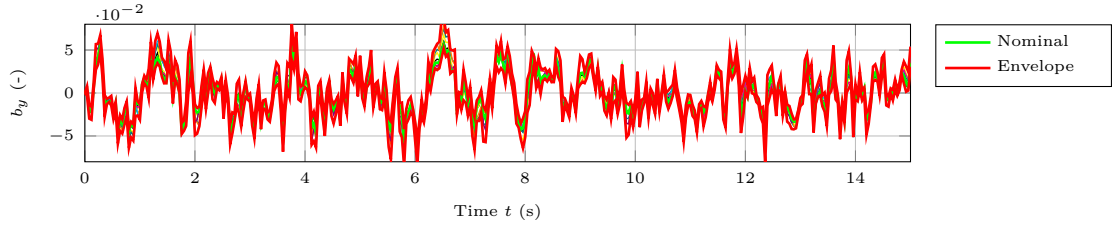

(e) Lateral Acceleration

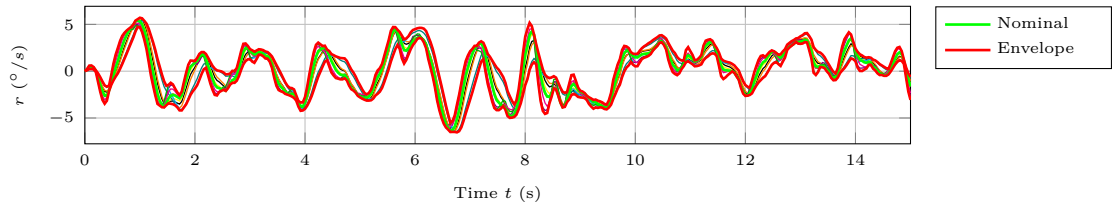

(f) Yaw Rate

Figure E.87: Rigid body states of the nonlinear plant model with MM-LQR controller in response to moderate Dryden turbulence at $V_K^R = 50\,m/s$, $h = 500\,m$, $m_{fuel} = 0\,kg$.

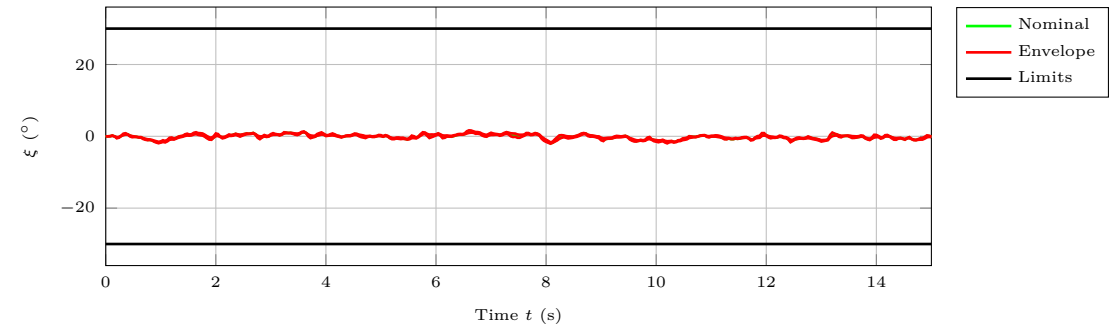

(a) Aileron Deflection

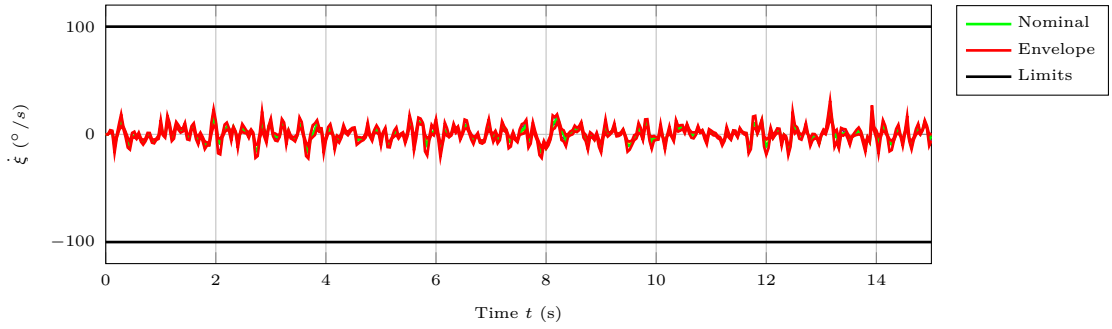

(b) Aileron Rate

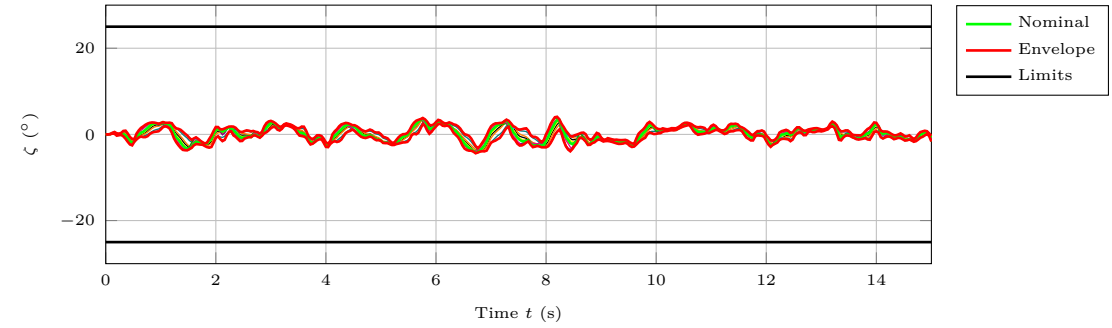

(c) Rudder Deflection

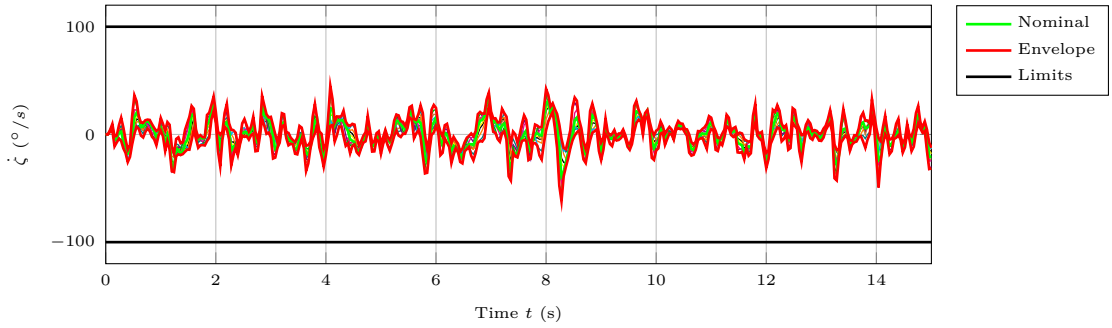

(d) Rudder Rate

Figure E.88: Actuator states of the nonlinear plant model with MM-LQR controller in response to moderate Dryden turbulence at $V_K^R = 50\,m/s$, $h = 500\,m$, $m_{fuel} = 0\,kg$.